

# METAL-ORGANIC FRAMEWORKS FOR BIOMEDICAL APPLICATIONS



Edited by  
**Masoud Mozafari**

**WP**  
WOODHEAD  
PUBLISHING

***Metal-Organic Frameworks for  
Biomedical Applications***

# ***Metal-Organic Frameworks for Biomedical Applications***

**Edited by**

Masoud Mozafari



**ELSEVIER**

**WP**

WOODHEAD  
PUBLISHING

An imprint of Elsevier

Woodhead Publishing is an imprint of Elsevier  
The Officers' Mess Business Centre, Royston Road, Duxford, CB22 4QH, United Kingdom  
50 Hampshire Street, 5th Floor, Cambridge, MA 02139, United States  
The Boulevard, Langford Lane, Kidlington, OX5 1GB, United Kingdom

Copyright © 2020 Masoud Mozafari. Published by Elsevier Inc. All rights reserved.

No part of this publication may be reproduced or transmitted in any form or by any means, electronic or mechanical, including photocopying, recording, or any information storage and retrieval system, without permission in writing from the publisher. Details on how to seek permission, further information about the Publisher's permissions policies and our arrangements with organizations such as the Copyright Clearance Center and the Copyright Licensing Agency, can be found at our website: [www.elsevier.com/permissions](http://www.elsevier.com/permissions).

This book and the individual contributions contained in it are protected under copyright by the Publisher (other than as may be noted herein).

#### **Notices**

Knowledge and best practice in this field are constantly changing. As new research and experience broaden our understanding, changes in research methods, professional practices, or medical treatment may become necessary.

Practitioners and researchers must always rely on their own experience and knowledge in evaluating and using any information, methods, compounds, or experiments described herein. In using such information or methods they should be mindful of their own safety and the safety of others, including parties for whom they have a professional responsibility.

To the fullest extent of the law, neither the Publisher nor the authors, contributors, or editors, assume any liability for any injury and/or damage to persons or property as a matter of products liability, negligence or otherwise, or from any use or operation of any methods, products, instructions, or ideas contained in the material herein.

#### **Library of Congress Cataloging-in-Publication Data**

A catalog record for this book is available from the Library of Congress

#### **British Library Cataloguing-in-Publication Data**

A catalogue record for this book is available from the British Library

ISBN: 978-0-12-816984-1 (print)

ISBN: 978-0-12-816985-8 (online)

For information on all Woodhead publications  
visit our website at <https://www.elsevier.com/books-and-journals>

*Publisher:* Matthew Deans

*Acquisitions Editor:* Glyn Jones

*Editorial Project Manager:* Joshua Mearns

*Production Project Manager:* Debasish Ghosh

*Cover Designer:* Miles Hitchen

Typeset by SPi Global, India





# Contributors

**Abbas Afkhami** Faculty of Chemistry, Bu-Ali Sina University, Hamedan, Iran

**Mazaher Ahmadi** Faculty of Chemistry, Bu-Ali Sina University, Hamedan, Iran

**Filipe A. Almeida Paz** Department of Chemistry, CICECO—Aveiro Institute of Materials, University of Aveiro, Aveiro, Portugal

**Christos Argirusis** School of Chemical Engineering, National Technical University of Athens, Athens, Greece; Clausthal Centre of Materials Technology; Institute of Energy Research and Phys. Technologies, Clausthal University of Technology, Clausthal-Zellerfeld, Germany

**Jéssica S. Barbosa** Department of Chemistry, CICECO—Aveiro Institute of Materials, University of Aveiro, Aveiro, Portugal; QOPNA & LAQV-REQUIMTE, Department of Chemistry, University of Aveiro, Campus Universitário de Santiago, Aveiro, Portugal

**Sajid Bashir** MSC161, 700 University Blvd, Kingsville, TX, United States

**Susana S. Braga** QOPNA & LAQV-REQUIMTE, Department of Chemistry, University of Aveiro, Campus Universitário de Santiago, Aveiro, Portugal

**Siddhardha Busi** Department of Microbiology, School of Life Sciences, Pondicherry University, Puducherry, India

**Sergio Carrasco** Department of Organic Chemistry, Stockholm University, Stockholm, Sweden

**Sai Raghuvver Chava** MSC161, 700 University Blvd, Kingsville, TX, United States

**Wei Chen** Institute of Medical Engineering, Department of Biophysics, School of Basic Medical Sciences, Health Science Center, Xi'an Jiaotong University, Xi'an, China

**Ioanna Christodoulou** National Center for Scientific Research (CNRS), Institute of Molecular Sciences, Paris-Sud University, Paris-Saclay University, Orsay; Institut des Matériaux Poreux de Paris, FRE 2000 CNRS, Ecole Normale Supérieure, Ecole Supérieure de Physique et de Chimie Industrielles de Paris, PSL Research University, Paris, France

**Liping Du** Institute of Medical Engineering, Department of Biophysics, School of Basic Medical Sciences, Health Science Center, Xi'an Jiaotong University, Xi'an, China

**Eddy Dumas** Lavoisier Institute of Versailles, UMR CNRS 8180, UVSQ Paris-Saclay University, Versailles, France

**Flávio Figueira** Department of Chemistry, CICECO—Aveiro Institute of Materials, University of Aveiro, Aveiro, Portugal

**Ross S. Forgan** WestCHEM School of Chemistry, University of Glasgow, Glasgow, United Kingdom

**Kranthi Kumar Gangu** Vignan's Institute of Information Technology, Visakhapatnam, India; School of Chemistry & Physics, University of KwaZulu-Natal, Durban, South Africa

**Arash Ghoorchian** Faculty of Chemistry, Bu-Ali Sina University, Hamedan, Iran

## **Contributors**

---

**Ruxandra Gref** National Center for Scientific Research (CNRS), Institute of Molecular Sciences, Paris-Sud University, Paris-Saclay University, Orsay, France

**Yuan Hu** State Key Laboratory of Fire Science, University of Science and Technology of China, Hefei, PR China

**Ihsanullah** Center for Environment and Water, Research Institute, King Fahd University of Petroleum and Minerals, Dhahran, Saudi Arabia

**Sreekantha B. Jonnalagadda** School of Chemistry & Physics, University of KwaZulu-Natal, Durban, South Africa

**Houman Kazemzadeh** Faculty of Pharmacy, Tehran University of Medical Sciences, Tehran, Iran

**Xue Li** National Center for Scientific Research (CNRS), Institute of Molecular Sciences, Paris-Sud University, Paris-Saclay University, Orsay, France

**Gang Liu** State Key Laboratory of Molecular Vaccinology and Molecular Diagnostics & Center for Molecular Imaging and Translational Medicine, School of Public Health, Xiamen University, Xiamen, China

**Jianqiang Liu** School of Pharmacy, Guangdong Medical University, Dongguan, PR China

**Jingbo Liu** MSC161, 700 University Blvd, Kingsville, TX, United States

**Tayyebeh Madrakian** Faculty of Chemistry, Bu-Ali Sina University, Hamedan, Iran

**Panagiota Markopoulou** WestCHEM School of Chemistry, University of Glasgow, Glasgow, United Kingdom

**Ricardo F. Mendes** Department of Chemistry, CICECO—Aveiro Institute of Materials, University of Aveiro, Aveiro, Portugal

**Masoud Mozafari** Cellular and Molecular Research Center; Department of Tissue Engineering & Regenerative Medicine, Faculty of Advanced Technologies in Medicine, Iran University of Medical Sciences (IUMS), Tehran, Iran

**Hafezeh Nabipour** State Key Laboratory of Fire Science, University of Science and Technology of China, Hefei, PR China

**Shamraja S. Nadar** Department of Chemical Engineering, Institute of Chemical Technology, Mumbai, India

**Majid Nasrollahi** Biomaterials Group, Faculty of Biomedical Engineering (Center of Excellence), Amirkabir University of Technology, Tehran, Iran

**Surya M. Nauli** Department of Biomedical & Pharmaceutical Sciences, Chapman University School of Pharmacy (CUSP), Harry and Diane Rinker Health Science Campus, Chapman University; Department of Medicine, University of California Irvine, Irvine, CA, United States

**Rajasekharreddy Pala** Department of Biomedical & Pharmaceutical Sciences, Chapman University School of Pharmacy (CUSP), Harry and Diane Rinker Health Science Campus, Chapman University; Department of Medicine, University of California Irvine, Irvine, CA, United States; State Key Laboratory of Molecular Vaccinology and Molecular Diagnostics & Center for Molecular Imaging and Translational Medicine, School of Public Health, Xiamen University, Xiamen, China

**Srinath Palakurthi** Texas A&M Health Science Center, Irma Lerma Rangel, Kingsville, TX, United States

**Ying Pan** School of Pharmacy, Guangdong Medical University, Dongguan, PR China

**Subhaswaraj Pattnaik** Department of Microbiology, School of Life Sciences, Pondicherry University, Puducherry, India

**Jingwen Qiu** National Center for Scientific Research (CNRS), Institute of Molecular Sciences, Paris-Sud University, Paris-Saclay University, Orsay, France

**Virendra K. Rathod** Department of Chemical Engineering, Institute of Chemical Technology, Mumbai, India

**João Rocha** Department of Chemistry, CICECO—Aveiro Institute of Materials, University of Aveiro, Aveiro, Portugal

**Sumanta Kumar Sahu** Department of Chemistry, Indian Institute of Technology (ISM), Dhanbad, Jharkhand, India

**Muhammad Sajid** Center for Environment and Water, Research Institute, King Fahd University of Petroleum and Minerals, Dhahran, Saudi Arabia

**Arpita Samui** Department of Chemistry, Indian Institute of Technology (ISM), Dhanbad, Jharkhand, India

**Alexander Schoedel** Department of Biomedical and Chemical Engineering and Sciences, Florida Institute of Technology, Melbourne, FL, United States

**Christian Serre** Institut des Matériaux Poreux de Paris, FRE 2000 CNRS, Ecole Normale Supérieure, Ecole Supérieure de Physique et de Chimie Industrielles de Paris, PSL Research University, Paris, France

**Georgia Sourkouni** Clausthal Centre of Materials Technology, Clausthal-Zellerfeld, Germany

**Nathalie Steunou** Lavoisier Institute of Versailles, UMR CNRS 8180, UVSQ Paris-Saclay University, Versailles, France

**Shunsuke Tanaka** Department of Chemical, Energy and Environmental Engineering; Organization for Research and Development of Innovative Science and Technology (ORDIST), Kansai University, Osaka, Japan

**Leena B. Vaidya** Department of Chemical Engineering, Institute of Chemical Technology, Mumbai, India

**Christos Vaitis** School of Chemical Engineering, National Technical University of Athens, Athens, Greece

**Negin Valizadeh** Biomaterials Group, Faculty of Biomedical Engineering (Center of Excellence), Amirkabir University of Technology, Tehran, Iran

**Antonio Vargas-Berenguel** Department of Chemistry and Physics, University of Almeria, Almería, Spain

**Chunsheng Wu** Institute of Medical Engineering, Department of Biophysics, School of Basic Medical Sciences, Health Science Center, Xi'an Jiaotong University, Xi'an, China

**Daqiang Yuan** State Key Laboratory of Structure Chemistry, Fujian Institute of Research on the Structure of Matter, Chinese Academy of Sciences, Fuzhou, PR China

**Yun Zeng** Department of Pharmacology, Xiamen Medical College, Xiamen, China

**Heng Zhao** Institut des Matériaux Poreux de Paris, FRE 2000 CNRS, Ecole Normale Supérieure, Ecole Supérieure de Physique et de Chimie Industrielles de Paris, PSL Research University, Paris, France

# Nomenclature of MOFs

Hafezeh Nabipour<sup>a</sup>, Masoud Mozafari<sup>b</sup>, Yuan Hu<sup>a</sup>

<sup>a</sup>State Key Laboratory of Fire Science, University of Science and Technology of China, Hefei, PR China

<sup>b</sup>Department of Tissue Engineering & Regenerative Medicine, Faculty of Advanced Technologies in Medicine, Iran University of Medical Sciences (IUMS), Tehran, Iran

## Abbreviations

|                                     |                                                                               |
|-------------------------------------|-------------------------------------------------------------------------------|
| <b>2,7-PDC</b>                      | pyrene-2,7-dicarboxylic acid                                                  |
| <b>2-Br-1,4-H<sub>2</sub>bdc</b>    | 2-bromobenzene-1,4-dicarboxylic acid                                          |
| <b>4,4'-BPY</b>                     | 4,4'-bipyridine                                                               |
| <b>ad</b>                           | adeninate                                                                     |
| <b>BBC</b>                          | 4,4',4''-(benzene-1,3,5-triyl-tris(benzene-4,1-diyl))tribenzoate)             |
| <b>bbIm</b>                         | 5(6)-bromobenzimidazole                                                       |
| <b>BDC</b>                          | benzene-1,4-dicarboxylic acid                                                 |
| <b>BDC-NH<sub>2</sub></b>           | 2-aminoterephthalic acid                                                      |
| <b>bdeppi</b>                       | <i>N,N'</i> -bis(3,5-dicarboxylphenyl)pyromellitic diimide                    |
| <b>bIm</b>                          | benzimidazole                                                                 |
| <b>bipy</b>                         | 4,4'-bipyridine                                                               |
| <b>BPDC</b>                         | biphenyl-4,4'-dicarboxylate                                                   |
| <b>bptc</b>                         | 3,3',5,5'-biphenyltetracarboxylate                                            |
| <b>BTB</b>                          | 1,4-benzenedicarboxylate                                                      |
| <b>btb</b>                          | 4,4',4''-benzene-1,3,5-triyl-tribenzoate                                      |
| <b>BTC</b>                          | 1,3,5-tricarboxylic acid                                                      |
| <b>btdd</b>                         | bis(1,2,3-triazolate-[4,5- <i>b</i> ],[4',5'- <i>i</i> ])dibenzo-[1,4]-dioxin |
| <b>BTE</b>                          | 4,4',4''-(benzene-1,3,5-triyl-tris(ethyne-2,1-diyl)) tribenzoate              |
| <b>cbIm</b>                         | 5(6)-chlorobenzimidazole                                                      |
| <b>cbIm</b>                         | 5-chlorobenzimidazole                                                         |
| <b>dcbBn</b>                        | 1,2-dihydrocyclobutabenzene-3,6-dicarboxylic acid                             |
| <b>DEF</b>                          | <i>N,N'</i> -diethylformamide                                                 |
| <b>DMF</b>                          | dimethylformamide                                                             |
| <b>dobpdc</b>                       | 4,4'-dioxido-3,3'-biphenyldicarboxylate                                       |
| <b>FIM</b>                          | 2-formylimidazole                                                             |
| <b>FIM</b>                          | 2-formylimidazole                                                             |
| <b>H(2)BPDC</b>                     | 4,4'-biphenyldicarboxylic acid                                                |
| <b>H<sub>2</sub>T<sub>2</sub>DC</b> | thieno[3,2- <i>b</i> ]thiophene-2,5-dicarboxylic acid                         |
| <b>H4dhtp</b>                       | 2,5-dihydroxyterephthalic acid                                                |
| <b>HFBB</b>                         | 4,4'-(hexafluoroisopropylidene)dibenzoate                                     |
| <b><i>m</i>-BDC</b>                 | <i>m</i> -benzenedicarboxylate                                                |

|                                        |                                                            |
|----------------------------------------|------------------------------------------------------------|
| <b>mbIm</b>                            | 5(6)-methylbenzimidazole                                   |
| <b>MIM</b>                             | 2-methylimidazole                                          |
| <b>mtz</b>                             | 5-methyl-1 <i>H</i> -tetrazole                             |
| <b>NH<sub>2</sub>-H<sub>2</sub>BDC</b> | 2-aminobenzene-1,4-dicarboxylic acid                       |
| <b>nIm</b>                             | 2-nitroimidazole                                           |
| <b>phen</b>                            | 1,10-phenanthroline                                        |
| <b>PhIm</b>                            | benzimidazole                                              |
| <b>PZDC</b>                            | pyrazine-2,3-dicarboxylate                                 |
| <b>TCPP-H2</b>                         | 4,4',4'',4'''-(porphyrin-5,10,15,20-tetrayl) tetrabenzoate |
| <b>TPDC</b>                            | <i>p</i> -terphenyl-4,4'-dicarboxylate                     |

### 1.1 Introduction

MOFs have attracted important interest from chemists and biomedical engineering scientists in the past two decades. MOF functions could be exactly tuned for biomedical applications by a building block method; some strategies to precisely control the sizes and morphologies of nanoscale MOFs are developed (nMOFs) and their applications in drug delivery investigated, as MRI contrast agents, sensing, nitrogen oxide (NO) storage, and X-ray computed tomography [1–7].

The importance of nomenclature or naming MOFs is to have a single name for a certain MOFs which is the same wherever it originates. Nomenclature and terminology should produce additional merit all the time. These are the implements to integrate new outcomes into the larger structure of science, enabling us to move from the particular to the universal. New terminology should also help us to practically argue about novel compounds, materials, and phenomena with no need to go on via limitless introductions of descriptions. Similar kinds of new materials prepared and analyzed by two or more subdisciplines of science usually lead to the development of an ad hoc nomenclature from various perspectives, which may not normally congregate into a reasonable result and are self-consistent [8]. Such double conditions exist for metal-organic frameworks (MOFs) [9] and coordination polymers (CPs) [10]; compounds produced in interdisciplinary investigational fields originating from solid state, inorganic, and coordination chemistry developed quickly throughout the past 15 years. The diverse focus and scientific background of contributing investigators have resulted in copious nomenclature propositions and applications for several subgroups therein and this group of compounds [11]; besides, a distracting amount of acronyms are used for such materials. Considering the bulk of literature in this field and their possible uses, the chemical industry is also showing interest in this subject [12]. Accordingly, a project on MOFs and CPs, viz., nomenclature guidelines and terminology, has been launched by the IUPAC division of Inorganic Chemistry [13]. The present communication summarizes the activities of the taskforce hitherto and the interplays that have been established with scientists in the area. With regard to stringent terminology, CP is an IUPAC-approved term [14], but only comprise straight-chain polymers (1D), and not 2D or 3D compounds. Therefore, the systematic terming

of these compounds would also need consideration alongside the nomenclature task. Previous research obviously indicates that logical subjects for one group of scientists might be objectionable to a different group. In here, it can be noted that the association between a substance (“the real world”) and the terms used to define it is by no means “ideally transparent.” Conversely, such an association is one of the main unresolved philosophical queries of the 20th century, with the controversial works of Ludwig Wittgenstein at the heart of the debate [15]. This communication does not aim to offer any formal propositions in due time including thinking between different groups, introduce some thoughts, and providing a schedule for additional investigation in this field. The authors seek to define the two mostly applied names, usually with overlying meanings, MOFs and CP, after a short outline on polymers and coordination compounds.

## **1.2 What is coordination compound?**

The Rules of Inorganic Nomenclature (IUPAC recommendations 2005 which is informally called the Red Book) defines “coordination entity” thus. Any of a class of substances with chemical structures in which a central usually of metallic atom or ion combined with nonmetal atoms, groups, or molecules is called ligand by coordinate bonds [16].

## **1.3 What are polymer and coordination polymer?**

J.J. Berzelius (1833) was the first to employ the term “polymer” to define all compounds which could be formulated as containing several units of a basic building block [17]. Y. Shibata (1916) [18] was the first to use “coordination polymer” to define trimers and dimers of various cobalt(II) ammine nitrates. The term has been continuously used in the scientific works as of the 1950s through apparently the pioneering review published in 1964 [19–21]. It is also notable that there is a tutorial review on “organometallic polymers” from 1981 [22]. The more traditional (organic) polymers were only nominated in 1922 when H. Staudinger suggested that the substances formerly identified as “colloids” (e.g., such as Bakelite) were actually monomers adhering jointly by covalent bonds to create materials currently recognized as (organic) polymers [17]. The continuous application of CP word as approved by the IUPAC would appear to be uncomplicated as long as properties remain because even matters normally acknowledged to be polymers (e.g., the above Bakelite, DNA, polyethylene, and cellulose) share some, if present, physical attributes. Typical polymer chemistry textbooks, e.g., Introduction to Polymer Chemistry (Carraher, 2010), also contain chapters on “CPs” [23]. Nevertheless, it can be objected that “poly-” in English means its Greek root—“more than one”; not “infinity,” as what could be reached in a properly sized crystal. An extremely polymerized organic polymer is ultrahigh-molecular-weight polyethylene, with up to 200,000 reiterating units, but typically traditional polymers have far lesser levels of polymerization. On the contrary, a 0.1 mm cubic crystal of a coordination compound



spreading limitlessly in all three directions of space by coordination bonds (a 3D coordination polymer) may simply contain 10<sup>15</sup> reiterating units (unit cell sides 10 Å, 1 molecule per cell), with 10<sup>9</sup> order of magnitude. Nonetheless, the “degree of polymerization” should be less for an equivalent 1D case corresponding to the 10th of a crystal side divided by the unit cell length; in our case 100,000, which assumes a complete, single domain, and very scarce crystal. Thus, the practical number of reiterating units will be fewer. Interestingly, a universal opinion in the initial years of crystallography stated that all crystals were polymers because lots of mainly English-speaking chemists repudiated the presence of nonmolecular crystals. For instance, the following criticisms emerged in Nature 1927: “Prof. W.L. Bragg declares that, ‘In sodium chloride apparently no molecules exist symbolized by NaCl.’ This expression is unbelievable. Whatever X-ray physics may be, chemistry is neither chess nor geometry” [24].

The present IUPAC-proposed descriptions include the following: Polymer is “a substance consisting of macromolecules” [25]. Macromolecule is “a molecule of high relative molecular mass, the structure of which basically contains several reiteration of units derived, truly or theoretically, from molecules of low relative molecular mass” [26].

### 1.4 What is a CP?

It is arguable that AgCl<sub>(s)</sub> is a CP as the coordination objects, and probably polynuclear species as well, are separately existent in solution. Despite this, the compound hardly fulfills the standard of having the composition of macromolecules. From another standpoint, is it possible to consider the materials produced in this way as having the composition of macromolecules by changing the chlorides for 4,40-bipyridine or 1,3-benzenedicarboxylate,? About another theoretical level in which polymers are identified with such properties as plasticity, it can be argued that such polymers hardly exist in crystalline systems. This can contradict the subgroup of CPs named “soft.” Furthermore, if crystallinity is an incompatible standard for a polymer, how do we deal with the well-known amorphous vanadium tetracyanoethylene radical magnetic materials [27] from the Miller group? Therefore, it is generally obvious that a crystalline material is not essentially a polymer; yet, an easy discrimination may not always be possible.

### 1.5 Metal-organic framework

The term has rather originated recently [28], taking a plurality of means for which many scientists have proposed more or less overlapping descriptions.

Here, it is not proposed that terminology problems are best resolvable by a public voting; yet, some points are worthy of note. A relatively considerable minor group, 21 out of 91, consider that MOFs should be confirmed proliferous by determining gas sorption isotherms; however, this is not agreed upon by any of the scientists affiliated with the journals

CrystEngComm, Dalton Transactions, and Crystal Design & Growth. The work group also believes that this stringent meaning might be problematic to apply and, additionally, could indispose numerous substances categorized as MOFs' previous surveys concerned with this class. In addition, this is considered to be unworthy that merely 8% of the responses show that carboxylate is a determining fragment of a MOF. Meanwhile, no one is rejecting the significance and the crucial emergence for the whole field once these substances began to launch.

## 1.6 “Organic” in metal-organic

There is no awareness of an IUPAC description of organic, and it may be useful that there are still few fairly blurry terms. Thus, no attempt is made to alter this condition, so either diethyl triamine, acetylacetonate, aminopolycarboxylic acids, cyclopentadienyl, glycinate, oxalates, cyanides, and triazacyclononane are regarded as organic or inorganic will be assigned to the discernment of individual chemists.

## 1.7 Nomenclature of MOFs

Worthy of note is the term porous structures, or open structures (frameworks), suggesting that disordered unbound solvent molecules are able to infiltrate cavities of a certain structure (framework) and simply get it out. The term MOF infers not only the presence of a porous structure, but also robust bonds rendering a rigid framework with a clear-cut geometry in which joining structural units can be substituted during the production [10]. Otherwise stated, such materials should have a clearly pronounced crystal construct being a basic standard for creating a perfect configuration—property associations [29–31]. The acronym MOF is regularly employed as a global term for this group of compounds; however, it means a distinct metal-organic structure if an ordinal number follows the MOF (Table 1.1, lines 1–11). Analyzing a multitude of constructs and MOF attributes allows to establish standards for designing framework structures with preferred features as [32], for instance, in the class of MOFs with a similar symmetry IRMOF-1 and IRMOF-2 (isoreticular metal-organic frameworks) (see Table 1.1, lines 12–20) [33]. A large number of descriptions exist equivalent to the grouping of the investigational classes which manufactured these MOFs, for instance, CPL, F-MOF-1, MOP-1, (see Table 1.1, lines 21–23), and so forth. Investigators from Russia [34–38] and China [39,40] mostly apply the term “metal-organic coordination polymers” with identified conformation. Plenty of MOFs are integrated into groups with similar letter denomination not in accordance with the resemblance of their structures (as noted by the above instances), but based on the location of their detection. These categories, for instance, include MIL, UiO, UAC, UTSA, HKUST, LIC, and so on (see Table 1.1, lines 24–43). The zeolite topology comprises another great class of MOFs. Tetrahedra consisting of nitrogen atoms encompass metal ions (Fe, Co, Cu, Zn, etc.) and are linked via imidazole rings which may come with various activities. The acronym ZIF (zeolite imidazolate framework) introduces these MOFs by a number (see Table 1.1, lines 44–52). Apart from organic polymers for which the functional, physical, and

Table 1.1: Examples of typical MOF names and their composition.

| No. | Designation                 | Formula                                                          | Abbreviation interpretation                                  |                                       |
|-----|-----------------------------|------------------------------------------------------------------|--------------------------------------------------------------|---------------------------------------|
| 1   | MOF-5                       | $Zn_4O(BDC)_2$                                                   | Metal-organic framework                                      |                                       |
| 2   | MOF-11                      | $Co_2(ad)_2(CO_2CH_3)_2$                                         |                                                              |                                       |
| 3   | MOF-177                     | $Zn_4O(BTB)_2$                                                   |                                                              |                                       |
| 4   | MOF-74-Zn                   | $Zn_2(H_4dhtp)$                                                  |                                                              |                                       |
| 5   | MOF-101                     | $Cu_2(BDC-Br)_2(H_2O)_2$                                         |                                                              |                                       |
| 6   | MOF-505                     | $Cu_2(bptc)(H_2O)_3(DMF)_3$                                      |                                                              |                                       |
| 7   | MOF-525                     | $Zr_6O_4(OH)_4(TCPP-Fe)_3$                                       |                                                              |                                       |
| 8   | MOF-200                     | $Zn_4O(BBC)_2$                                                   |                                                              |                                       |
| 9   | MOF-210                     | $(Zn_4O)_3(BTE)_4(BPDC)_3$                                       |                                                              |                                       |
| 10  | MOF-235                     | $[Fe_3O(BDC)_3(DMF)_3][FeCl_4] \cdot (DMF)_3$                    |                                                              |                                       |
| 11  | MOF-253                     | $Al(OH)(BPYDC)$                                                  |                                                              |                                       |
| 12  | IRMOF-1 (MOF-5)             | $Zn_4O(BDC)_3 \cdot 7DEF \cdot 3H_2O$                            |                                                              | Isorecticular metal-organic framework |
| 13  | IRMOF-2                     | $Zn_4O(2-Br-1,4-H_2bdc)_3$                                       |                                                              |                                       |
| 14  | IRMOF-3                     | $Zn_4O(NH_2-H_2BDC)_3$                                           |                                                              |                                       |
| 15  | IRMOF-6                     | $Zn_4O(dcbBn)_3$                                                 |                                                              |                                       |
| 16  | IRMOF-9                     | $Zn_4O(H(2)BPDC)_3$                                              |                                                              |                                       |
| 17  | IRMOF-13                    | $Zn_4O(2,7-PDC)_3$                                               |                                                              |                                       |
| 18  | IRMOF-16                    | $Zn_4O(TPDC)_3 \cdot 17DEF \cdot 2H_2O$                          |                                                              |                                       |
| 19  | IRMOF-20                    | $Zn_4O(H_2T_2DC)_3$                                              |                                                              |                                       |
| 20  | Mg-IRMOF-74                 | $Mg_2(dobpdc)$                                                   | Coordination polymer with pillared layer structure           |                                       |
| 21  | CPL-2                       | $Cu_2(PZDC)_2(4,4'-BPY)$                                         |                                                              |                                       |
| 22  | F-MOF-1                     | $[Cu(HFBBA)(phen)_2](H_2HFBBA)_2(H_2O)(HCO_2)$                   |                                                              | Fluorinated metal-organic framework   |
| 23  | MOP-1                       | $Cu_{24}(m-BDC)_{24}(DMF)_{14}(H_2O)_{10}$                       | Metal-organic polyhedra                                      |                                       |
| 24  | MIL-53-Al                   | $Al(OH)(BDC)$                                                    | Materials of Institut Lavoisier                              |                                       |
| 25  | MIL-53(Al)-NH <sub>2</sub>  | $Al(OH)(BDC-NH_2)$                                               |                                                              |                                       |
| 26  | MIL-100-Fe                  | $[Fe_3(\mu_3-O)(\mu_6-BTC)_2F(H_2O)_2]_n$                        |                                                              |                                       |
| 27  | MIL-101                     | $Cr_3O(H_2O)_2F(BDC)_3 \cdot nH_2O$                              |                                                              |                                       |
| 28  | MIL-88B-4CH <sub>3</sub>    | $2Fe_3O(OH)(H_2O)_2(BDC-Me_2)_3$                                 |                                                              |                                       |
| 29  | MIL-88-Fe                   | $Fe_3O(MeOH)_3(O_2C(CH_2)_2CO_2)_3 \cdot AcO \cdot (MeOH)_{4,5}$ |                                                              |                                       |
| 30  | MIL-88A                     | $Fe_3O(MeOH)_3(O_2CCH=CHCO_2)_3 \cdot MeCO_2 \cdot nH_2O$        |                                                              |                                       |
| 31  | MIL-125-NH <sub>2</sub> -Ti | $Ti_8O_8(OH)_4(BDC-NH_2)_6$                                      |                                                              |                                       |
| 32  | UiO-66                      | $Zr_6O_6(BDC)_6$                                                 | Universitetet i Oslo                                         |                                       |
| 33  | UiO-67                      | $Zr_6O_6(BPDC)_6$                                                |                                                              |                                       |
| 34  | UiO-68                      | $Zr_6O_6(TPDC)_6$                                                |                                                              |                                       |
| 35  | UAC-1                       | $(Al_4(OH)_2(OCH_3)_4(BDC-NH_2)_3 \cdot xH_2O$                   |                                                              |                                       |
| 36  | UTSA-49                     | $Zn(mtz)_2$                                                      | Chung Ang University-1<br>University of Texas at San Antonio |                                       |
| 37  | HKUST-1                     | $Cu_3(BTC)_2$                                                    | Hong Kong University of Science and Technology               |                                       |

Table 1.1: Examples of typical MOF names and their composition—cont'd

| No. | Designation | Formula                                                                                    | Abbreviation interpretation                     |
|-----|-------------|--------------------------------------------------------------------------------------------|-------------------------------------------------|
| 38  | LIC-1       | $\text{Gd}_2(\text{BDC-NH}_2)_3(\text{DMF})_4$                                             | Leiden Institute of Chemistry                   |
| 39  | NNU-28      | $\text{Zr}_6\text{O}_4(\text{OH})_4(\text{L})_6$                                           | Northwestern University                         |
| 40  | MFU-4l      | $\text{Zn}_5\text{Cl}_4(\text{btdd})_3$                                                    | Metal-organic framework<br>Ulm University       |
| 41  | SNU-51      | $[\text{Zn}_2(\text{bdcppi})(\text{DMF})_3] \cdot 6 \text{ DMF} \cdot 4\text{H}_2\text{O}$ | Seoul National University                       |
| 42  | SUMOF-1     | $\text{M}_6(\text{btb})_4(\text{bipy})_3$                                                  | Stockholm University<br>Metal-Organic Framework |
| 43  | UMCM-1      | $\text{Zn}_4\text{O}(\text{BDC})(\text{BTB})_{4/3}$                                        | University of Michigan<br>Crystalline Material  |
| 44  | ZIF-7       | $\text{Zn}(\text{PhIm})_2$                                                                 | Zeolite imidazolate<br>framework                |
| 45  | ZIF-8       | $\text{Zn}(\text{MIM})_2$                                                                  |                                                 |
| 46  | ZIF-67      | $\text{Co}(\text{MIM})_2$                                                                  |                                                 |
| 47  | ZIF-68      | $\text{Zn}(\text{blm})(\text{nIm})$                                                        |                                                 |
| 48  | ZIF-69      | $\text{Zn}(\text{cblm})(\text{nIm})$                                                       |                                                 |
| 49  | ZIF-90      | $\text{Zn}(\text{FIM})_2$                                                                  |                                                 |
| 50  | ZIF-300     | $\text{Zn}(2\text{-mlm})_{0.86}(\text{bblm})_{1.14}$                                       |                                                 |
| 51  | ZIF-301     | $\text{Zn}(2\text{-mlm})_{0.94}(\text{cblm})_{1.06}$                                       |                                                 |
| 52  | ZIF-302     | $\text{Zn}(2\text{-mlm})_{0.67}(\text{mblm})_{1.33}$                                       |                                                 |

optical properties are, by foremost, characterized by the characteristics and the amount of monomeric units in the chain, the interconnection of constructing units in the framework mainly determines the characteristics of metal-organic frameworks. Hence, fabrication of MOFs implies not only the selection of structural blocks of the framework, but also their characteristic organization in the solid phase [41].

### 1.8 CP versus MOF

According to some of the responses to our investigation, the whole possible cases are covered by 1D, 2D or 3D CPs, and that the MOF is a supernumerary word and could be excluded from use. However, the IUPAC workgroup does not believe in this. “MOF” is currently a commonly used word so that it would not vanish due to a paper in Pure and Applied Chemistry. It is also advantageous as being close to a self-description. Accordingly, “coordination polymer” and “porous coordination polymer” are perhaps easily grasped by chemists. But, coordination chemistry is typically an unfamiliar subject to academics in closely liked fields of study, including biochemists, physicists, and even biologists, not to mention the scientifically educated in the general population. In this class, however, many can develop an instinctive apprehension of things obtained provided metal ions and organic molecules are combined to any type of structure. More practically, another problem is that a bulk of

individuals, mainly those going about the present topic from the solid state inorganic aspect, do not use the term coordination chemists and “coordination polymer” and many do not apply the term “metal-organic framework,” rendering a more challenging literature review. Furthermore, one can notice that other generic terms including “hybrid inorganic-organic materials” are used in related communications, which, to the authors’ views, are considered to be insufficient as they denote few general configuration of the substance merely in a wide-ranging, indeterminate manner [8].

## References

- [1] S. Keskin, S. Kızılel, Biomedical applications of metal organic frameworks, *Ind. Eng. Chem. Res.* 50 (4) (2011) 1799–1812.
- [2] M.A. Chowdhury, Metal-organic-frameworks for biomedical applications in drug delivery, and as MRI contrast agents, *J. Biomed. Mater. Res. A* 105 (4) (2017) 1184–1194.
- [3] W. Chena, C. Wu, Synthesis, functionalization, and applications of metal–organic frameworks in biomedicine, *Dalton Trans.* 47 (2018) 2114–2133.
- [4] P. Horcajada, R. Gref, T. Baati, P.K. Allan, G. Maurin, P. Couvreur, G. Férey, R.E. Morris, C. Serre, Metal–organic frameworks in biomedicine, *Chem. Rev.* 112 (2) (2012) 1232–1268.
- [5] M.X. Wu, Y.W. Yang, Metal–organic framework (MOF)-based drug/cargo delivery and cancer therapy, *Adv. Mater.* 29 (2017) 1606134.
- [6] H. Cai, Y. Liang, H. DanLi, Biological metal–organic frameworks: structures, host–guest chemistry and bio-applications, *Coord. Chem. Rev.* 378 (2019) 207–221.
- [7] A.C. McKinlay, R.E. Morris, P. Horcajada, G. Férey, P. Couvreur, C. Serre, BioMOFs: metal–organic frameworks for biological and medical applications, *Angew. Chem. Int. Ed.* 49 (36) (2010) 6260–6266.
- [8] S.R. Batten, N.R. Champness, X.-M. Chen, J. Garcia-Martinez, S. Kitagawa, L. Öhrström, M. O’Keeffe, M.P. Suh, J. Reedijk, Coordination polymers, metal–organic frameworks and the need for terminology guidelines, *CrystEngComm* 14 (2012) 3001–3004.
- [9] (a)J.L.C. Rowsell, O.M. Yaghi, Metal-organic frameworks: a new class of porous materials, *Microporous Mesoporous Mater.* 73 (2004) 3–14; (b)J.R. Long, O.M. Yaghi, The pervasive chemistry of metal–organic frameworks, *Chem. Soc. Rev.* 38 (2009) 1213–1214.
- [10] S.R. Batten, D.R. Turner, M.S. Neville, *Coordination Polymers: Design, Analysis and Application*, RSC, Cambridge, 2009.
- [11] K. Biradha, A. Ramana, J.J. Vittal, Coordination polymers versus metal – organic frameworks, *Cryst. Growth Des.* 9 (2009) 2969–2970.
- [12] (a)M. Jacoby, Heading to market with MOFs for metal-organic frameworks, lab-scale research is brisk as commercialization begins, *Chem. Eng. News* 86 (34) (2008) 13–16. (b) A.U. Czaja, N. Trukhan, U. Muller, Industrial applications of metal–organic frameworks, *Chem. Soc. Rev.* 38 (2009) 1284–1293.
- [13] (a)Coordination Polymers and Metal Organic Frameworks: Terminology and Nomenclature Guidelines, <http://www.iupac.org/web/ins/2009-012-2-200>. (b) L. Öhrström, Chemistry International, IUPAC, 2010. January–February, 23.
- [14] L.G. Donaruma, B.P. Block, K.L. Loening, N. Plate, T. Tsuruta, K.C. Buschbeck, W.H. Powell, J. Reedijk, Nomenclature for regular single-strand and quasi-single-strand inorganic and coordination polymers 1984, *Pure Appl. Chem.* 57 (1985) 149–168.
- [15] L. Wittgenstein, *Tractatus Logico-Philosophicu*, Harcourt, New York, 1922.
- [16] N.G. Connelly, T. Damhus, R.M. Hartshorn, A.T. Hutton (Eds.), *Nomenclature of Inorganic Chemistry IUPAC Recommendations 2005*, International Union of Pure and Applied Chemistry by The Royal Society of Chemistry, Cambridge, 2005.
- [17] A.J. Ihde, *The Development of Modern Chemistry*, Dover Publications, New York, 1984.

- [18] Y. Shibata, *CAN* 11:5339, *J. Coll. Sci. Imp. Univ. Tokyo* 37 (1916) 1–17.
- [19] B. Moulton, M.J. Zaworotko, *Coordination polymers: toward functional transition metal sustained materials and supermolecules*, *Curr. Opin. Solid State Mater. Sci.* 6 (2002) 117.
- [20] S.V. Vinogradova, O.V. Vinogradova, *Coordination polymers with inorganic main chains*, *Russ. Chem. Rev.* 44 (1975) 510.
- [21] S. Subramanian, M.J. Zaworotko, *Porous solids by design: [Zn(4,4'-bpy)<sub>2</sub>(SiF<sub>6</sub>)<sub>n</sub>·xDMF, a single framework octahedral coordination polymer with large square channels*, *Angew. Chem. Int. Ed. Engl.* 34 (1995) 2127–2129.
- [22] J.C.J. Bailar, *Coordination polymers*, in: W.L. Jolly (Ed.), *Preparative Inorganic Reactions*, vol. 1, Interscience Publishers, John Wiley & Sons, New York, 1964, pp. 1–27.
- [23] C.E. Carraher, *Organometallic polymers*, *J. Chem. Educ.* 58 (1981) 921–934.
- [24] C.E. Carraher Jr., *Introduction to Polymer Chemistry*, second ed., CRC Press, Inc., 2010.
- [25] H.E. Armstrong, *Poor common salt!* *Nature* 120 (1927) 478.
- [26] A.D. Jenkins, P. Kratochvil, R.F.T. Stepto, U.W. Suter, *Polymer division commission on macromolecular nomenclature*, *Pure Appl. Chem.* 68 (1996) 2287–2311.
- [27] M. Nic, J. Jirat, B. Kosata, *The IUPAC Compendium of Chemical Terminology (Gold Book)*, International Union of Pure and Applied Chemistry, 2009.
- [28] K.I. Pokhodnya, A.J. Epstein, J.S. Miller, *Thin-film V[TCNE]<sub>x</sub> magnets*, *Adv. Mater.* 12 (2000) 410–413.
- [29] O.M. Yaghi, H.L. Li, *Hydrothermal synthesis of a metal-organic framework containing large rectangular channels*, *J. Am. Chem. Soc.* 117 (1995) 10401–10402.
- [30] L.R. MacGillivray (Ed.), *Metal–Organic Frameworks: Design and Application*, Wiley, New York, 2010.
- [31] A.D. Burrows, J. Holman, A. Parsons, G. Pilling, G. Price, *Chemistry*, vol. 3, Oxford University Press, Oxford, 2009.
- [32] M. O’Keeffe, M.A. Peskov, S. Ramsden, O.M. Yaghi, *The reticular chemistry structure resource (RCSR) database of, and symbols for, crystal nets*, *Acc. Chem. Res.* 41 (12) (2008) 1782–1789.
- [33] O.M. Yaghi, M. O’Keeffe, N.W. Ockwig, H.K. Chae, M. Eddaoudi, J. Kim, *Reticular synthesis and the design of new materials*, *Nature (London)* 423 (2003) 705–714.
- [34] M. Eddaoudi, J. Kim, N. Rosi, D. Vodak, J. Wachter, M. O’Keeffe, O.M. Yaghi, *Systematic design of pore size and functionality in isorecticular MOFs and their application in methane storage*, *Science* 295 (2002) 469–472.
- [35] M.P. Yutkin, M.S. Zavakhina, D.G. Samsonenko, D.N. Dybtsev, V.P. Fedin, *Porous homo- and heterochiral cobalt(II) aspartates with high thermal stability of the metal-organic framework*, *Russ. Chem. Bull. Int. Ed.* 59 (2010) 733–740 (*Izv. Akad. Nauk, Ser. Khim.* 719 (2010)).
- [36] M.P. Yutkin, M.S. Zavakhina, D.G. Samsonenko, D.N. Dybtsev, V.P. Fedin, *Synthesis and characterization of expected and unexpected topologies of homochiral porous metal(II) malate frameworks*, *Inorg. Chim. Acta* 394 (2013) 367–372.
- [37] M.S. Zavakhina, D.G. Samsonenko, A.V. Virovets, D.N. Dybtsev, V.P. Fedin, *Homochiral Cu(II) and Ni(II) malates with tunable structural features*, *J. Solid State Chem.* 210 (2014) 125–129.
- [38] M.S. Zavakhina, M.P. Yutkin, D.G. Samsonenko, D.N. Dybtsev, V.P. Fedin, *Synthesis and structure of homochiral polymeric praseodymium tartrate*, *Russ. Chem. Bull. Int. Ed.* 60 (2011) 2425–2428 (*Izv. Akad. Nauk, Ser. Khim.* 2378 (2011)).
- [39] J.S. Hu, Z. Lei, C.L. Pan, J. He, *A new 2D → 3D polythreaded framework constructed on an N-centered tripodal linker and copper(i)*, *Mendeleev Commun.* 24 (2014) 290–292.
- [40] J.S. Hu, X.M. Zhang, H.L. Xing, J. He, J.J. Shi, *Construction of an unusual 3D framework based on V-shaped imidazolyl and oxalate ligands*, *Mendeleev Commun.* 23 (2013) 231.
- [41] V.V. Butova, M.A. Soldatov, A.A. Guda, K.A. Lomachenko, C. Lamberti, *Metal-organic frameworks: structure, properties, methods of synthesis and characterization*, *Russ. Chem. Rev.* 85 (3) (2016) 280.



# *Secondary building units of MOFs*

**Alexander Schoedel**

*Department of Biomedical and Chemical Engineering and Sciences, Florida Institute of Technology,  
Melbourne, FL, United States*

## **2.1 Introduction**

Metal-organic crystals composed of single metal ions and functional linkers were discovered in earnest in the late 1950s, but their enormous potential has long remained unnoticed [1–3]. Such 1D, 2D, and 3D structures are crystalline and therefore enabled the characterization at the atomic level by means of single-crystal X-ray diffraction. They were later termed coordination polymers, a class of materials that gained momentum in the 1990s, mainly due to their simple, yet intriguing structures and newly emerging properties. However, in many cases, the weakness of the coordination bond stalled efforts to establish permanent porosity due to framework collapse. The quest for permanently porous materials, especially with respect to gas storage and separation, then led to the development of highly robust architectures based upon metal-carboxylate clusters. Such metal cluster entities, often referred to as secondary building units (SBUs) [4], are joined together with multifunctional organic molecules, the linkers, to produce metal-organic frameworks (MOFs). Since metal ions and linkers sustain one coordination mode within the SBUs, the overall coordination geometry leads to the formation of predictable framework structures by virtue of crystal engineering [5] or reticular chemistry [6]. These concepts provide many opportunities for creating robust metal-organic crystals by design and for translating molecular functionality and reactivity into the solid state [7]. In contrast to inorganic zeolites [8], mesoporous silica [9], and porous carbon [10], the modular nature of MOFs, and their amenability to fine-tuning of properties, has led to growing scientific interest over the past 20 years.

## **2.2 Concept**

Unlike with conventional porous materials, knowledge about the topology of MOFs provides fast opportunity to designed synthesis. The concept of reticular chemistry is the simplification of MOF structures by deconstruction into their underlying nets, i.e., the atoms are the vertices

(or nodes) and are linked together by the bonds (edges). For example, in the diamond (**dia**) structure, each carbon atom is a tetrahedral vertex, the bonds in between are the edges. This concept can be adapted to larger, porous inorganic structures, such as zeolites, where the  $\text{TO}_4$  ( $T = \text{Si}, \text{Al}$ ) building unit is the tetrahedra and the  $-\text{O}-$  linker between them serves as the edge of the net. In coordination polymers, the single metal ion serves as the vertex and the organic linkers serve as the edges, joining the vertices together.

In MOFs constructed from multiatomic SBUs, usually their center of gravity (barycenter) serves as a vertex and the organic linker as an edge. SBUs are usually classified according to their points of extension (POE), the number of possible connections between them through organic linkers. We tend to introduce this concept on the example of the famous HKUST-1 [11]. Each of the  $\text{Cu}_2(-\text{COO})_4$  clusters contains two Cu ions, coordinated in a square planar geometry by four carboxylate O (Fig. 2.1). The four carboxylate C then serve as POE in a square planar-shaped SBU (shown in green). Simplification of this multiatomic SBU to its barycenter renders it into a 4-c node. The tritopic BTC linker ( $\text{H}_3\text{BTC} = 1,3,5$ -benzene tricarboxylic acid) corresponds to a 3-c node as shown. The topology of the resulting (3,4)-c net is twisted boracite (**tbo**). For illustration purposes the augmented version of the net, here **tbo-a**, is often used by replacing the nodes by coordination figures (4-c squares and 3-c triangles). The augmented net directly illustrates the shapes of the vertex figures with nodes sustained by the POE. Moreover, in the ideal or maximum symmetry embedding, the edges within and between the vertex figures are equal and unity.

In all SBUs, the minimum number of POE is three, a triangular-shaped building unit. Terminal and 2-coordinated metal clusters exist in MOFs; however, they have no influence on the underlying net topology. To the best of our knowledge, the maximum number of POE for discrete metal-carboxylate clusters is 24, creating a rhombicuboctahedron. Augmented and often porous metal-containing building units are termed metal-organic polyhedra (MOPs), which can serve as highly connected nodes in MOFs. The barycenter of the whole MOP represents the vertex of the net, linked together by the organic moieties. These nets are amenable to further deconstruction into multinodal ones, based on metal-oxide SBUs and branched organic linkers. Another class of SBUs are infinite in one dimension and sustain

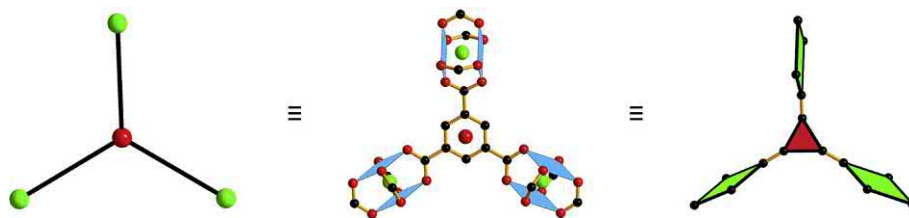


Fig. 2.1

Deconstruction of  $\text{Cu}_2(-\text{COO})_4$  and triangular-shaped building units. Color code: black, C; red, O; blue polyhedra, Cu. Hydrogen atoms are omitted for clarity.

so-called rod MOFs. The lack of a well-defined barycenter in these rod SBUs prevents the determination of an “un-augmented” version of the rod pattern. Therefore, the topology of rod MOFs is always based upon the POEs as nodes (Figs. 2.2 and 2.3).

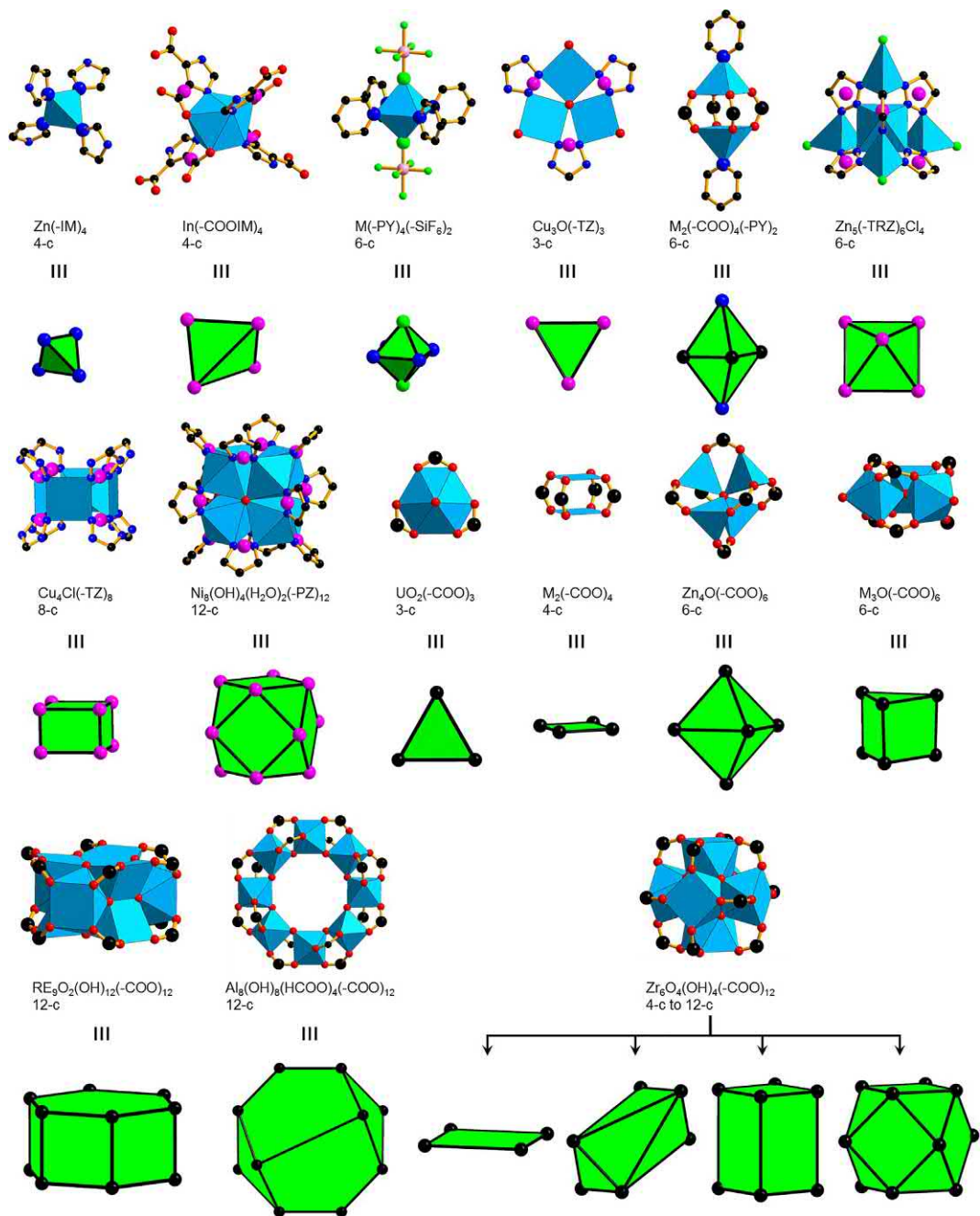
Herein, we present each of the building units together with a different MOF structure that is considered prototypical for an isorecticular (of the same net topology) class of MOFs [12]. These prototypes are not always the default nets, i.e., the linear connection of such SBUs; however, they often represent the most well-known MOF. Properties and potential application of some of these materials are briefly described to familiarize the reader with the importance of a particular SBU and the framework (Fig. 2.3).

Regardless of the nature of MOFs, the pattern of POE defines the shape of the metal cluster SBU. Therefore, it is important to assign POE properly in the organic functional groups bound to the metal clusters. Fig. 2.4 illustrates the placement of POE for such functional groups. As mentioned earlier, the carboxylate C is a POE as well as the pyridine N atom. In imidazoles (-IM), the POE is the N atom bound to the metal. However, in imidazole-carboxylates, we prefer the assignment of the POE as a fictive atom between the C—C bond of the five-membered ring. In pyrazoles (-PZ) and tetrazoles (-TZ), with two N atoms linked to metals, we use a fictive atom at the center of the N—N bond as POE. For triazoles (-TRZ) with three N atoms linked, the POE is located at the center of the five-membered ring. For pairs of —OH groups such as in catechol, the POE is a fictive atom in the C-C bond. Pyridine-2-ol is handled similar to carboxylate and the POE is placed on the C atom in the (—OCN) group.

First, we briefly introduce single metal nodes but mainly focus on metal-carboxylate SBUs, since their architectural stability allows for achieving permanent porosity. The difference of metal-carboxylate MOFs and metal-pyridine coordination polymers arises from the bond energy between the building units, i.e., the bond of a neutral nitrogen moiety compared to an anionic carboxylate to a charged metal cation. However, the bond energy still needs to be low enough to enable reversible reactions and facilitate the growth of single crystals [13].

In particular, metal-carboxylate MOFs have gained traction by the end of the 1990s following seminal contributions of Yaghi, Williams, and Kitagawa [11, 14, 15]. The first report on a microporous (pore diameter <2.0 nm) material, termed MOF-2, established the determination of surface area and pore volume. After synthesis the guest molecules were removed and reversible type I gas sorption isotherms using nitrogen at 77 K were collected. This method has since become the gold standard for proof of porosity.

High symmetry building units allow exquisite control over the coordination environment, which makes them highly desirable for the rational design of new frameworks. Although there are many different decorated clusters reported as discrete entities [16], only a dozen of them have thus far been utilized in the construction of MOFs.



**Fig. 2.2**

M-O and M-N building units utilized in the construction of metal-organic frameworks. The coordination ranges from 3 to 24. Color code: black, C; red, O; blue, N; light blue, metal; pink, points of extension. Hydrogen atoms are omitted for clarity.

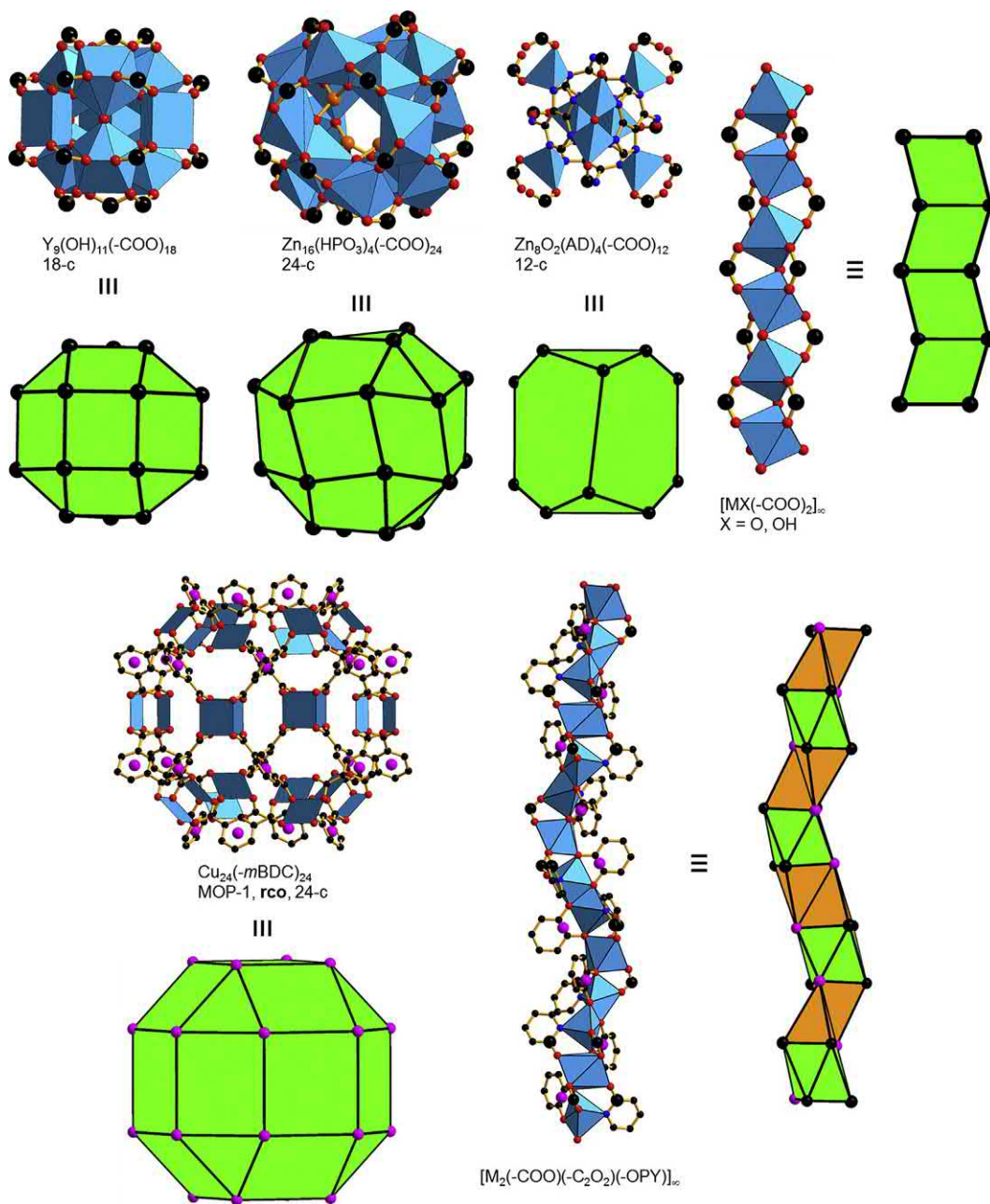


Fig. 2.3

Highly coordinated M-O and M-N building units, as well as MOPs and rod-like SBUs, utilized in the construction of metal-organic frameworks. The coordination ranges from 12 to  $\infty$ . Color code: black, C; red, O; blue, N; light blue, metal; pink, points of extension. Hydrogen atoms are omitted for clarity.

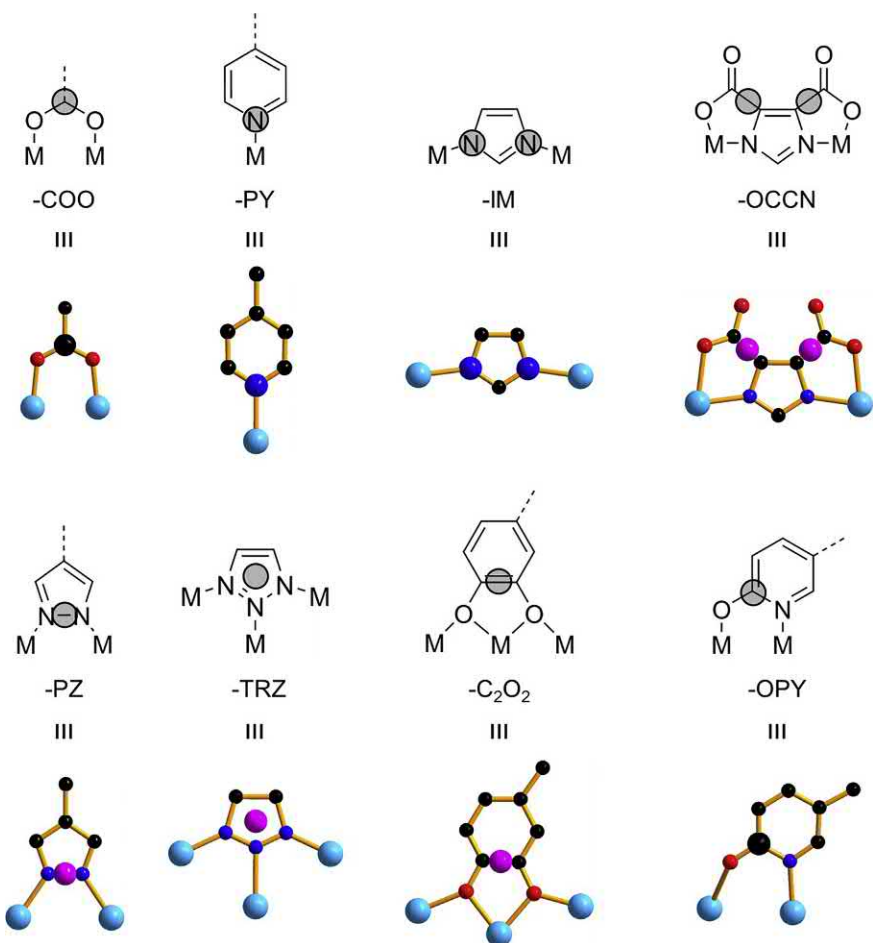


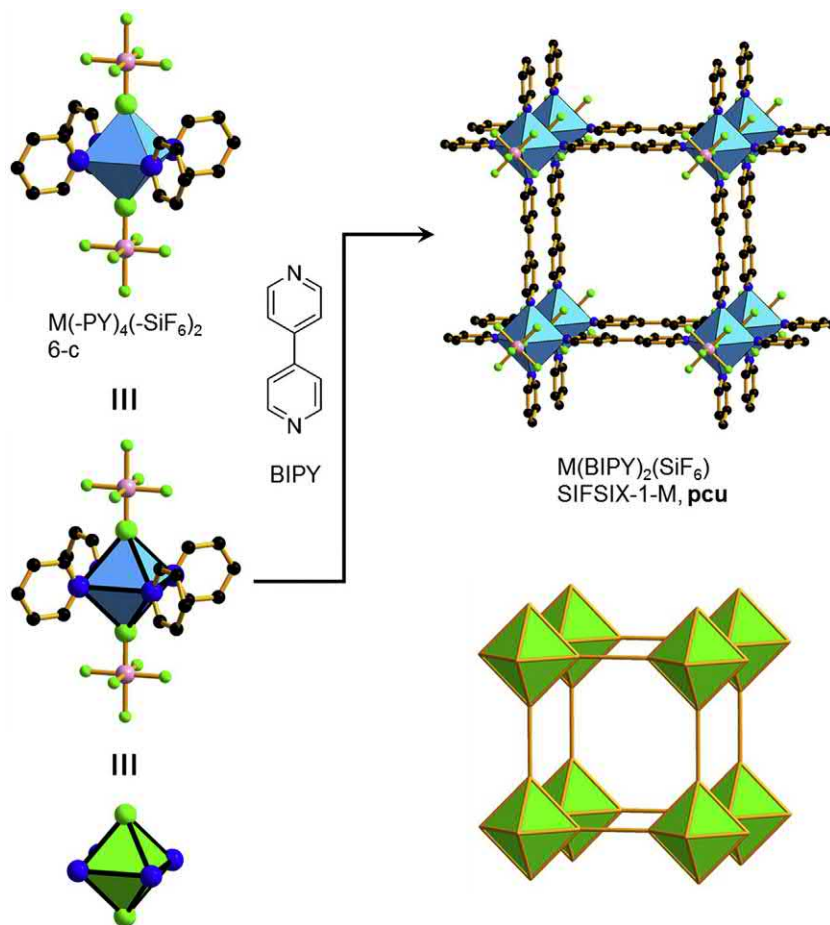
Fig. 2.4

Positions of points of extension (POE) in different functional groups. Color code: black, C; red, O; blue, N; light blue, metal; pink, points of extension. Hydrogen atoms are omitted for clarity.

### 2.3 Single metal nodes—Pillared square grids, ZMOFs, and ZIFs

Single metal nodes as building units were explored in the early 1990s, since many discrete pyridine-based structures had previously been made and crystallized. The first 2-dimensional square grid framework with formula  $\text{Cd}(\text{BIPY})_2(\text{NO}_3)_2$  (BIPY = 4,4'-bipyridine) was synthesized in 1994 [17]. It is composed of  $\text{Cd}(-\text{PY})_4$  nodes, where each  $\text{Cd}^{2+}$  cation is octahedrally coordinated by four pyridines in the equatorial plane and two charge-balancing nitrate ions on the axial positions. These counterions are not a part of the building unit since they are exchangeable without alteration of the framework structure or topology. A closely related molecular material, in which square planar  $\text{Pd}^{2+}$  cations are coordinated by ethylenediamine in a *cis*-fashion, inspired the framework design.  $\text{Cd}(\text{BIPY})_2(\text{NO}_3)_2$  contains





**Fig. 2.5**

The octahedral 6-c  $M(-PY)_4(-SiF_6)_2$  building unit produces a pillared square grid framework of formula  $M(BIPY)_2(SiF_6)_2$  with rectangular channels, termed SIFSIX-1-M. Color code: black, C; blue, N; green, F; rose, Si; blue polyhedra, metal. Hydrogen atoms are omitted for clarity.

large guest-filled voids and was the first coordination polymer to perform catalytic cyanosilylation reactions of benzaldehyde and imines. Contributions during the mid-1990s on  $M(BIPY)_2$  and related frameworks were crucial for the development of MOFs up until today. Some of these coordination polymers fall under the stricter definition of MOFs (having permanent porosity) and will be discussed here based on their metal nodes. In particular, we focus on the octahedral  $M(-PY)_4(-SiF_6)_2$  building unit (Fig. 2.5) [18].

Each building unit contains a six coordinated, octahedral  $M^{2+}$  cation ( $M = Cu, Zn, Ni, Co$ ), where four pyridine nitrogen and two fluorine of hexafluorosilicate act as POE. These  $M(BIPY)_2(SiF_6)_2$  frameworks are charge balanced and often described as pillared square grid, due to the anionic  $SiF_6^{2-}$  in the axial positions. Depending on the synthetic conditions and the

nature of M,  $M(\text{BIPY})_2(\text{SiF}_6)$  crystallize as noninterpenetrated, permanently porous frameworks with a 6-c primitive cubic (**pcu**) topology. The large square channels along the crystallographic [001] axis have dimensions of  $8 \times 8 \text{ \AA}$ , and the empty space is about 50% of the total unit cell volume. Materials of composition  $M(\text{BIPY-}n)_2(\text{SiF}_6)$  (BIPY-*n* generally represents 4,4'-bipyridine or its derivatives, i.e., linear linkers with two terminal aromatic nitrogen donor moieties) are exceptional with respect to adsorption and separation of gases. Remarkably, they can be fine-tuned in many ways by replacing both the organic linker and the inorganic anion [19–22].

Other single metal building units are observed in a class termed zeolite-like metal-organic frameworks (ZMOFs), first described in 2006 [23]. Zeolites are porous aluminosilicates composed of 4-c  $\text{TO}_4$  tetrahedra, where the T—O—T bond angles (average  $145^\circ$ ) play a significant role in their large structural diversity. ZMOFs are based on the same principles; however, the building units are augmented to  $\text{MN}_4\text{O}_2$  or  $\text{MN}_4\text{O}_4$ . Therefore each metal cation (mostly  $\text{In}^{3+}$  or  $\text{Cd}^{2+}$ ) is either eight coordinated by four pyridine, or pyrrole N and four carboxylate O, or six coordinated by four pyridine, or pyrrole N and two carboxylate O. Herein, we highlight the synthesis of **rho**-ZMOF from *1H*-imidazole-4,5-dicarboxylic acid and  $\text{In}^{3+}$  (Fig. 2.6).

Each indium is eight coordinated in a dodecahedron geometry by four linkers through an N-, O-hetero-chelation. Thus, the four POE can be placed between the middle carbons of these five-membered rings. Linking of these augmented building units through the organic moiety results in frameworks with zeolite topology (here: 4-c **rho**), depending on the angle of the linker. This strategy toward ZMOFs was further explored and other topologies such as sodalite (**sod**) were obtained from, e.g., 4,6-pyrimidinedicarboxylic acid. The bond strength of the hetero-chelation to the single metal produced stable, permanently porous materials that were utilized for encapsulation and catalysis, as well as gas adsorption [24–26].

Another class of zeolitic MOF structures was introduced in 2006 by combination of tetrahedral metal nodes, such as  $\text{Zn}(\text{-IM})_4$  and imidazolate linkers [27, 28]. Therefore, the name zeolitic imidazolate frameworks (ZIFs) was coined. Although structures based on tetrahedral coordinated metal cations and imidazolate linkers had been known for quite some time, the synthetic strategy to produce a plethora of structures had not been discovered. A series of 12 ZIFs were reported using differently functionalized imidazolate linkers and different metal salts. The obtained zeolite topologies were BCT, DFT, GIS, SOD, MER, and RHO [8]. Herein, we highlight the synthesis of ZIF-8 with **sod** topology (Fig. 2.7). All ZIF structures are based on nets of linked  $\text{MN}_4$  tetrahedra. In this context, the M—IM—M angle between the tetrahedral building units plays an important role, and thus allows for the generation of zeolitic structures. The topological diversity arises from the different functionalities at the imidazolate linker. ZIF-8, together with ZIF-67, was used in UV-lithography techniques for bio-grafting of enzymes onto their surfaces and subsequent catalysis reactions [29].

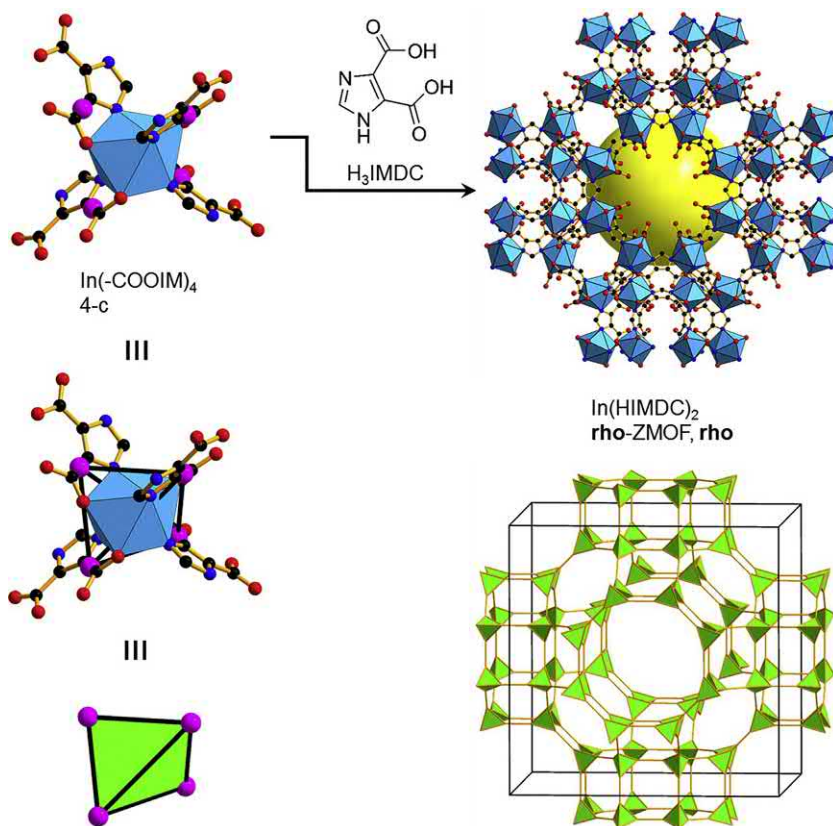


Fig. 2.6

The dodecahedral building unit  $\text{In}(-\text{COOIM})_4$  serves as a 4-c node to construct zeolite-like MOF structures, such as **rho-ZMOF**. Color code: black, C; red, O; blue, N; blue polyhedra, In; pink, POE. The *yellow sphere* represents the empty space in the framework. Hydrogen atoms are omitted for clarity.

## 2.4 Traditional carboxylate based (metal-oxide) SBUs

In comparison to the majority of MOFs made from single metal nodes, the use of metal-carboxylate clusters provides a roadmap toward robust MOFs showing permanent porosity. First, we introduce 3-c carboxylate SBUs  $\text{UO}_2(-\text{COO})_3$  that have recently regained popularity due to their predictable geometry and high stability. Usually, uranium(VI) exists as a linear uranyl cation  $[\text{UO}_2]^{2+}$  and coordinates three carboxylate groups in the equatorial plane to generate a hexagonal bipyramid. The first uranyl coordination compound of this geometry was sodium uranyl acetate,  $\text{NaUO}_2(\text{CH}_3\text{COO})_3$ , which was reported in the early 1930s [30]. The default net for linking triangles of formula  $(\text{UO}_2)_2(\text{BDC})_3$  ( $\text{H}_2\text{BDC}$  = 1,4-benzenedicarboxylic acid, Fig. 2.8) was obtained in 2006 through a hydrothermal reaction [31]. The compound crystallizes in a 2-D 3-c honeycomb net (**hcb**) with a twofold interpenetration.

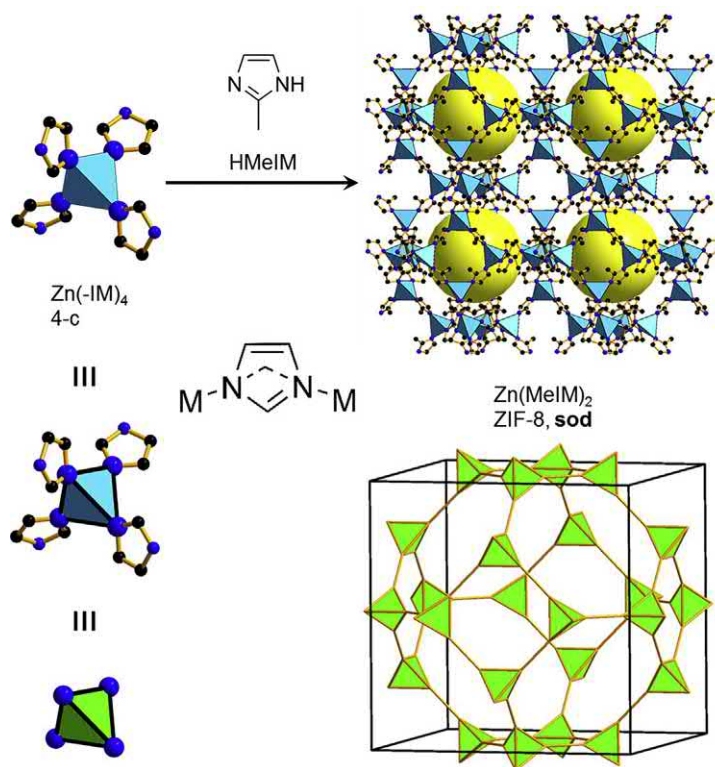


Fig. 2.7

Linking of tetrahedral  $M(-IM)_4$  building units produces a variety of ZIF structures (here: ZIF-8, using 2-methyl-imidazole). The crucial  $M-IM-M$  bond angle is highlighted. Color code: black, C; blue, N; blue polyhedra, Zn. The *yellow spheres* represent the empty space in the framework. Hydrogen atoms are omitted for clarity.

Recently, the combination of  $UO_2(-COO)_3$  with  $Me_3-BTB$  ( $Me_3-H_3BTB =$  Trimethyl benzenetri benzoic acid) produced a framework with formula  $(UO_2)(Me_3-BTB)$  [32]. The methyl groups cause a distortion in the benzoate moieties, and therefore the formation of the default 3-c **hcb** topology is impossible. The obtained MOF, termed NU-1301, shows a previously unreported multinodal 3-c **nun** topology with an  $a = 173.3 \text{ \AA}$  cubic unit cell, the largest reported thus far for nonbiological materials. The cavities of the structure measure 5.0 and 6.2 nm in diameter, and NU-1301 shows the lowest density of any MOF to date ( $0.124 \text{ g cm}^{-3}$ ). NU-1301 exemplifies that there are still many highly porous materials to be discovered, even by combination of relatively simple building units.

Square paddlewheels of formula  $M_2(-COO)_4$  are among the most commonly known SBUs in MOFs and contain four POE. The molecular structure is well known as it is found in copper(II) acetate hydrate with formula  $Cu_2(CH_3COO)_4(H_2O)_2$ . Each copper ion is coordinated in a square pyramidal fashion by four carboxylate O and one water molecule. Paddlewheels can be

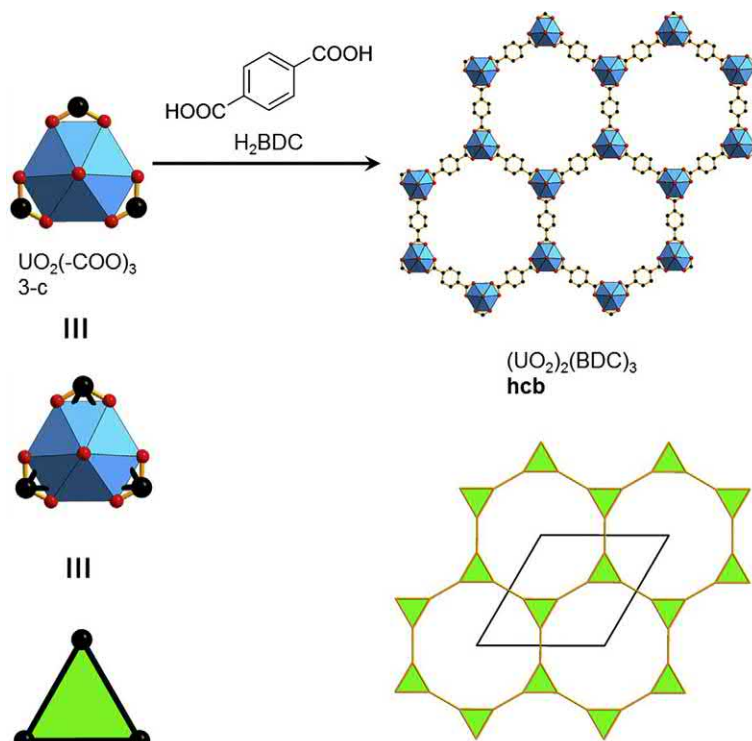


Fig. 2.8

$(\text{UO}_2)_2(\text{BDC})_3$  crystallizes in the default 3-c **hcb** topology. Color code: black, C; red, O; blue polyhedra, U. Hydrogen atoms and interpenetrated nets are omitted for clarity.

linked to a variety of multitopic organic molecules to produce functional frameworks. Especially copper and zinc variants readily crystallize under mild synthetic conditions, leading to predictable structure outcomes.

HKUST-1, or MOF-199, is probably the most well-known MOF built from  $\text{Cu}_2(-\text{COO})_4$  paddlewheel clusters (Fig. 2.9) [11]. When linked to tritopic BTC linkers ( $\text{H}_3\text{BTC}$  = benzene-1,3,5-tricarboxylic acid),  $\text{Cu}_3(\text{BTC})_2$  is produced. It crystallizes in a cubic structure with the binodal (3,4)-c **tbo** (twisted boracite) topology. This framework is prototypical and facile to prepare. Measurements of BET surface area after full activation have revealed around  $1800 \text{ m}^2 \text{ g}^{-1}$ . HKUST-1 was used as bioreactor by shaping it into hollow capsules with selective permeability [33]. Many variants of HKUST-1 were synthesized, including the use of different metal cations and isorecticular variants by using longer linkers. MOF-399 of formula  $\text{Cu}_3(\text{BBC})_2$  ( $\text{H}_3\text{BBC}$  = 4,4',4''-(benzene-1,3,5-triyl-tris(benzene-4,1-diyl))tribenzoic acid) had long been known for having the lowest crystal density in MOFs ( $0.126 \text{ g cm}^{-3}$ ) before NU-1301 was reported [34].



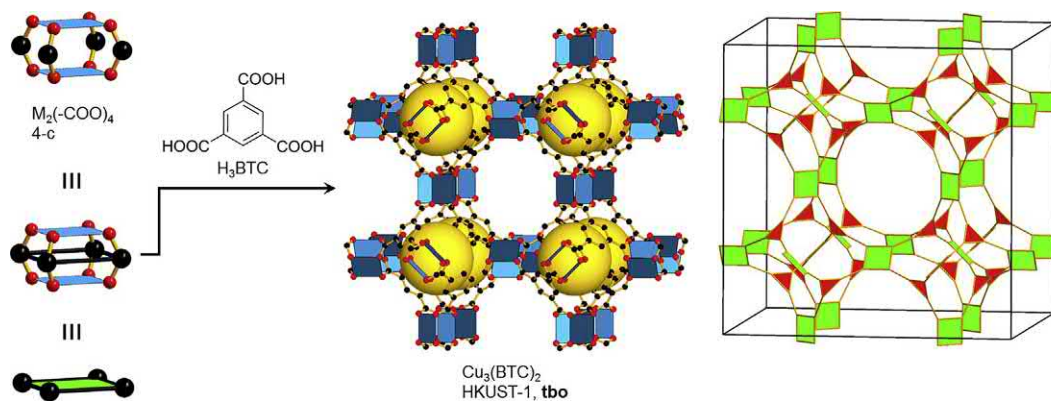


Fig. 2.9

HKUST-1 composed of square paddlewheel  $\text{Cu}_2(-\text{COO})_4$  SBUs and triangular BTC linkers. Color code: black, C; red, O; blue polyhedra, Cu. The *yellow spheres* represent the empty space in the framework. Hydrogen atoms are omitted for clarity.

An important property of the  $\text{Cu}_2(-\text{COO})_4$  SBU was subsequently discovered in MOF-11 with formula  $\text{Cu}_2(\text{ATC})$  ( $\text{H}_4\text{ATC}$  = adamantane-1,3,5,7-tetracarboxylic acid) [35]. The framework is made from square paddlewheel SBUs and tetratopic, tetrahedral-shaped ATC linkers. Therefore, the underlying net is composed of linking square and tetrahedral building units, leading to a binodal 4-c **pts** topology. Although the SBU is generally described as  $\text{Cu}_2(-\text{COO})_4$ , it contains two axial water/solvent molecules in its as-synthesized form  $\text{Cu}_2(-\text{COO})_4(\text{H}_2\text{O})_2$ . MOF-11 marks the discovery of open metal sites (OMS) in a framework after removal of such water/solvent molecules for the first time. It was shown that OMS are crucial for catalysis, gas adsorption, or postsynthetic modifications.

$\text{Zn}_4\text{O}(-\text{COO})_6$  represented the first type of a 6-c SBU, showing an octahedral geometry. The structure of basic zinc acetate  $\text{Zn}_4\text{O}(\text{CH}_3\text{COO})_6$  is known as a molecular compound since the 1950s [36]. It consists of a single  $\mu_4\text{-O}$  in the middle bound to four  $\text{Zn}^{2+}$  to form a  $\text{Zn}_4\text{O}$  tetrahedron. Each tetrahedron is then coordinated by three bridging carboxylates to the other  $\text{Zn}_4\text{O}$  tetrahedra. The carboxylate carbons, i.e., the POE, form the overall octahedron (Fig. 2.10). Besides Zn, this structure has also been observed for Co and Be, as well as mixed metals.

The first MOF containing the  $\text{Zn}_4\text{O}(-\text{COO})_6$  SBU,  $\text{Zn}_4\text{O}(\text{BDC})_3$ , was synthesized in the late 1990s and termed MOF-5, in reminiscence of the famous zeolite ZSM-5 [37]. The framework shows the default topology for linear connection of octahedra, 6-c **pcu** (primitive cubic). The robustness of the SBU allowed for activation of the framework through guest removal and nitrogen gas adsorption (77 K) experiments. They revealed an estimated Langmuir surface area of  $2900 \text{ m}^2 \text{ g}^{-1}$  and a pore volume of  $1.04 \text{ cm}^3 \text{ g}^{-1}$ . These values exceeded by far all conventional porous materials known at the time such as zeolites, silicates, or porous carbon [8–10]. Therefore, the utilization of strong bonds from the metal-cluster SBUs to the linkers



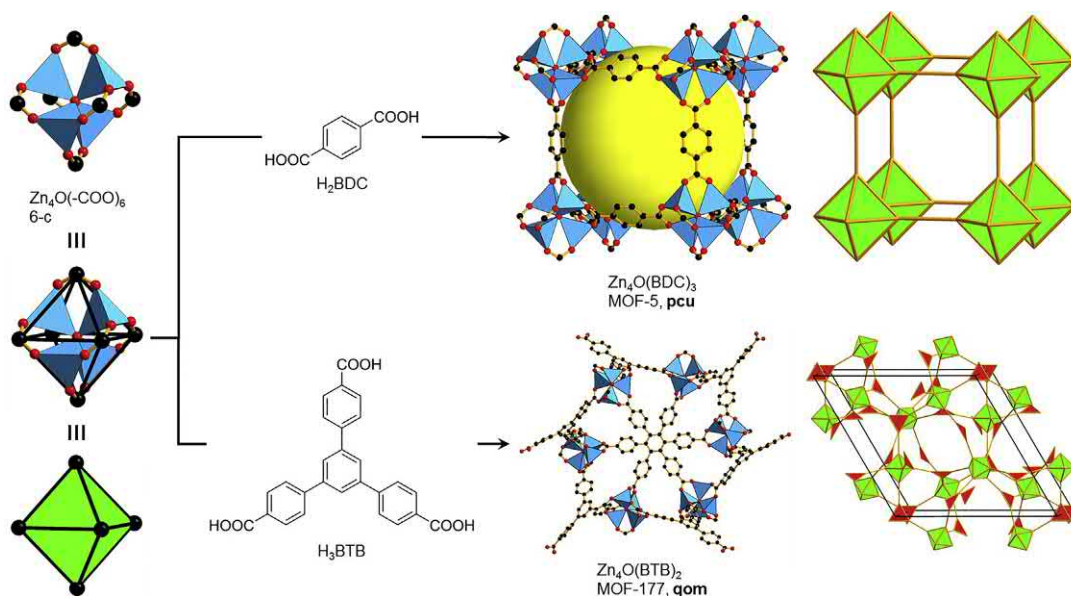


Fig. 2.10

$Zn_4O(-COO)_6$  as a 6-c node in MOF-5 and MOF-177. Color code: black, C; red, O; blue polyhedra, Zn. The *yellow sphere* represents the empty space in the framework. Hydrogen atoms are omitted for clarity.

represented a turning point in the field, from metal-pyridine bonds toward more robust metal-carboxylate bonds. This strategy then enabled the synthesis of many framework materials with structural integrity, permanent porosity, and high surface areas.

However, since the  $pcu$  topology is self-dual, interpenetration can occur at a certain linker length, which is detrimental to achieving high surface areas [12]. In 2004, a new design approach was introduced based on  $Zn_4O(-COO)_6$  SBUs and triangular BTB linkers ( $H_3BTB = 4,4',4''$ -benzene-1,3,5-triyl-tribenzoate) [38]. The highly porous framework  $Zn_4O(BTB)_2$ , MOF-177, was produced consisting of linked octahedra and triangles in a 5-nodal (3,6)-c  $qom$  net. In contrast to the other possible (3,6)-c nets,  $rtl$  (rutile) and  $pyr$  (pyrite),  $qom$  is not self-dual and therefore interpenetration is inherently precluded. Porosity measurements using  $N_2$  at 77 K revealed a Langmuir surface area of  $4500 \text{ m}^2 \text{ g}^{-1}$  and a pore volume of  $1.59 \text{ cm}^3 \text{ g}^{-1}$ . The importance of the  $Zn_4O(-COO)_6$  SBU is underlined by numerous reports on robust and highly porous frameworks. For example, the use of mixed linkers—a linear ( $H_2BPDC = 4,4$ -biphenyldicarboxylic acid) and a triangular ( $H_3BTE$ )—enabled the synthesis of MOF-210 with a previously unknown (3,6)-c  $toz$  topology. At the time, this material held the world record in BET area with a value of  $6240 \text{ m}^2 \text{ g}^{-1}$  and also shows a large pore volume of  $3.60 \text{ cm}^3 \text{ g}^{-1}$ .

Another large class of 6-c nets is composed of a very common metal-oxide cluster, the  $M_3O(-COO)_6$  trigonal prism. It consists of a central  $\mu_3$ -O bound to three  $M^{2+/3+}$  to form an  $M_3O$  triangle. Each of the four equatorial positions at the  $MO_6$ -octahedra is coordinated by

carboxylates, where the carbons, i.e., the POE, form an overall trigonal prism. A water/solvent molecule or a charge-balancing anion occupies the remaining coordination sites in the as-synthesized cluster. Basic chromium(III)-acetate,  $[\text{Cr}_3\text{O}(\text{CH}_3\text{COO})_6(\text{H}_2\text{O})_3]\text{Cl}$ , was first synthesized around 100 years ago and its structure was elucidated by single-crystal X-ray diffraction in 1965 [39].

Linking of  $\text{M}_3\text{O}(\text{—COO})_6$  SBUs was initially explored through the use of linear dicarboxylates, producing a series of frameworks, termed MIL-88 (MIL = Materials of Institute Lavoisier) as well as MOF-235 (Fig. 2.11) [40, 41]. The trigonal prismatic SBUs were mainly based on chromium(III) and iron(III) and resulted in many isorecticular structures. MOF-235 and -236 were afforded by linear linking of trigonal prisms with BDC and *m*BDC, and the default topology was identified as 6-c **acs** [41]. The framework of MOF-235 is identical to the

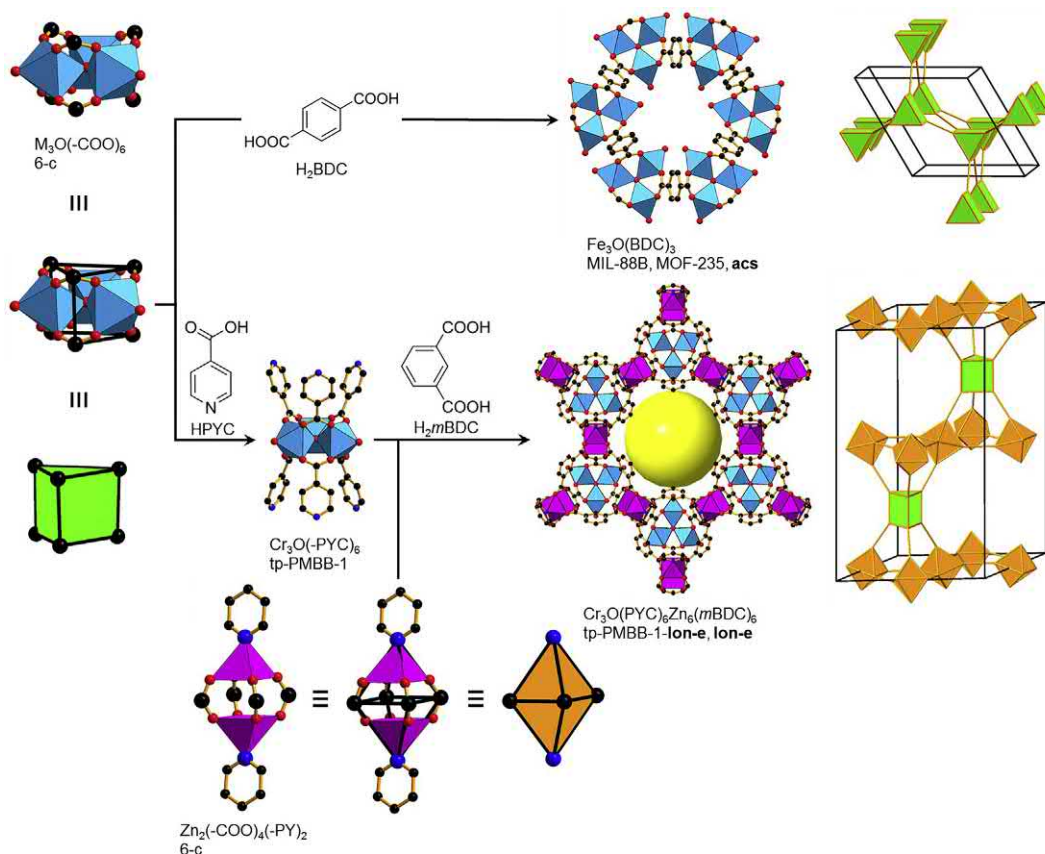


Fig. 2.11

$\text{M}_3\text{O}(\text{—COO})_6$  trigonal prismatic SBUs with linear linkers to produce the default 6-c **acs** net, and with two linkers as well as an octahedral  $\text{Zn}_2(\text{—COO})_4(\text{—PY})_2$  SBU to produce the complex tp-PMBB-1-**lon-e** framework. Color code: black, C; red, O; blue, N; blue polyhedra, Cr; pink polyhedra, Zn. The *yellow sphere* represents the empty space in the framework. Hydrogen atoms are omitted for clarity.

reported MIL-88B, although containing different guest molecules. The isorecticular MIL-88 series consists of linkers having different length such as H<sub>2</sub>EDC (ethene-1,2-dicarboxylic acid = fumaric acid, MIL-88A), H<sub>2</sub>BDC (MIL-88B), H<sub>2</sub>NDC (1,4-naphthalenedicarboxylic acid, MIL-88C), and H<sub>2</sub>BPDC (4,4-biphenyldicarboxylic acid, MIL-88D) [42]. MIL-88A represents the parent compound and was studied in terms of nitric oxide adsorption and delivery in biomedical applications [43, 44]. All MOFs undergo large structural changes, when exposed to different guest molecules [45]. In the MIL-88 series, these reversible breathing phenomena might reach high amplitudes of up to 270% of the original unit cell volumes, without loss of crystallinity. MIL-88 variants were also investigated as nanoscale carriers for antitumor and retroviral drug delivery and imaging [46].

A higher complexity in MOFs can be obtained if two SBUs are combined with two linkers. In 2013, we utilized a two-step approach to address a strategy that leads to a variety of 3-D MOFs with **lon-e** (lonsdaleite-e) topology based on 6-c trigonal prismatic M<sub>3</sub>O(—COO)<sub>6</sub> and 6-c octahedral Zn<sub>2</sub>(—COO)<sub>4</sub>(—PY)<sub>2</sub> SBUs [47]. The two-step approach relies on preformation of a decorated Cr<sub>3</sub>O(—PCA)<sub>6</sub> SBU (HPCA = 4-pyridine carboxylic acid, tp-PMBB-1), which is isolated in the first step. The highly soluble cluster is then dissolved and subsequently connected to the axial positions of Zn<sub>2</sub>(—COO)<sub>4</sub>(—PY)<sub>2</sub>. This SBU is in turn part of an in situ formed undulating 4-c **kgm** (kagome) net when reacted together with *m*BDC. It was shown that a versatile class of MOFs could be obtained using nine different angular linkers. The series was systematically studied in terms of gas sorption performance with respect to carbon dioxide and methane.

## 2.5 Highly coordinated carboxylate-based (metal-oxide) SBUs

In the context of metal-carboxylate MOFs, we would like to highlight the special role of Zr<sub>6</sub>-carboxylate clusters since they can serve as 4-c, up to 12-c nodes, depending on the linker and the synthetic conditions. Zr<sub>6</sub>O<sub>4</sub>(OH)<sub>4</sub>(—COO)<sub>12</sub> SBUs were in earnest discovered in a 12-c **fcu** topology framework termed UiO-66 [48]. Following this seminal contribution, Zr-MOFs gained traction in 2011 and are nowadays widely investigated due to their high stability and low toxicity. Close to 100 crystal structures are reported per year, as revealed by a search in the Cambridge Structural Database [49]. We herein introduce a handful of Zr-clusters with different numbers of POE (Fig. 2.12).

Only very recently, a 4-c Zr<sub>6</sub>O<sub>4</sub>(OH)<sub>6</sub>(HCOO)<sub>6</sub>(—COO)<sub>4</sub> SBU was obtained through the reaction of zirconium(IV) salts with a rectangular-shaped TPTC linker (H<sub>4</sub>TPTC = [1,1',4',1''-terphenyl]-3,3'',5,5''-tetracarboxylic acid) [50]. The 3-D framework termed NU-1400 of formula Zr<sub>6</sub>O<sub>4</sub>(OH)<sub>6</sub>(HCOO)<sub>6</sub>(TPTC) shows rhombic-shaped pores. The topology is reported as 4-c **lvt** that is predetermined to flexibility and comparable by oversimplification to 4-c **sra**. However, since the linker geometry is rectangular, rather than square, we prefer to deconstruct it into two joint triangular nodes according to a well-established deconstruction

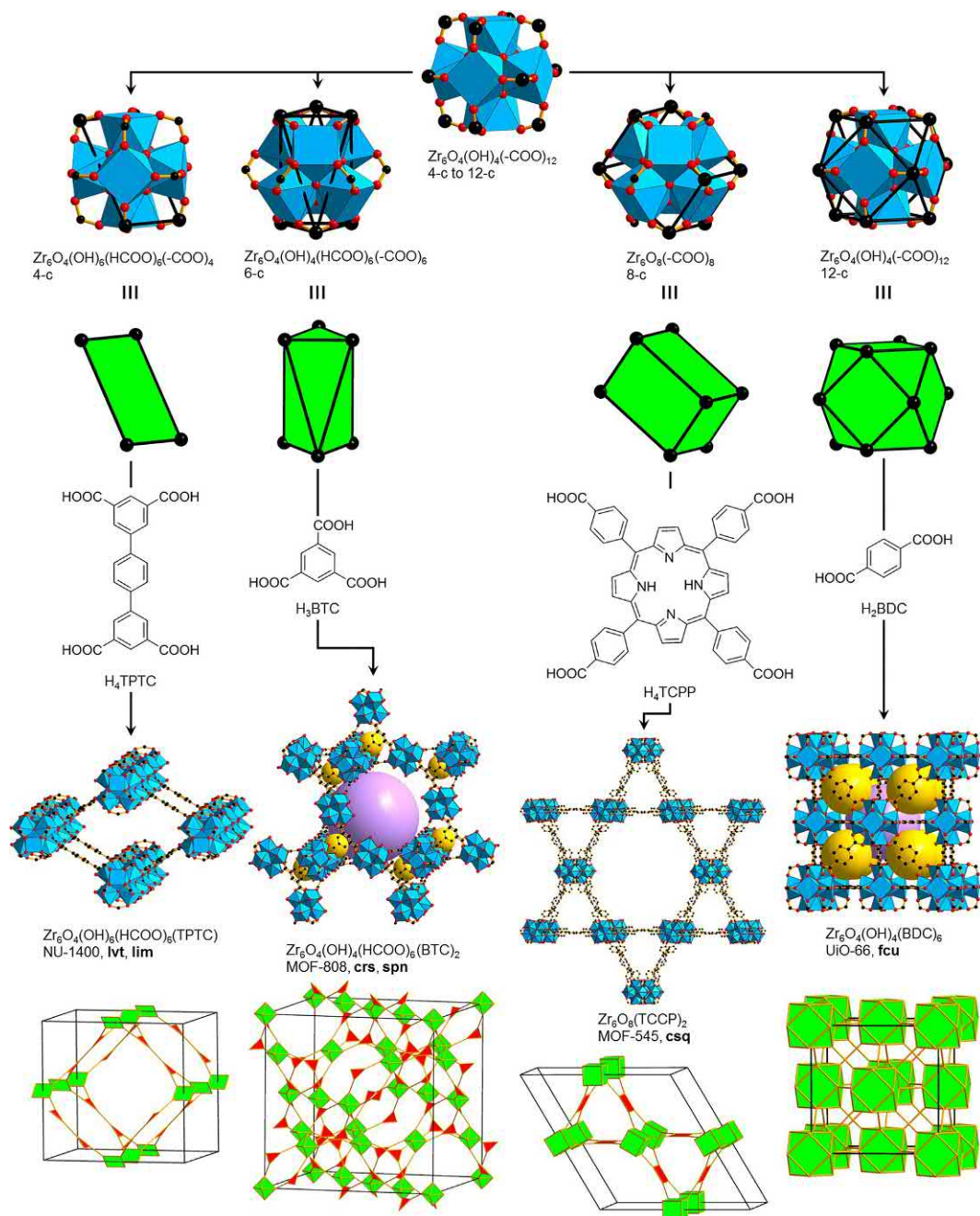


Fig. 2.12

$Zr_6$ -SBUs with different number of points of extension. Rectangle or square (4-c), trigonal antiprism or octahedron (6-c), rectangular prism or cube (8-c), and cuboctahedron (12-c). Color code: black, C; red, O; blue, N; blue polyhedra, Zr. The *yellow and purple spheres* represent the empty space in the framework. Hydrogen atoms are omitted for clarity.



approach [51]. It thus renders the 4-c **lvt** into a (3,4)-c **lim** topology which is amenable to isorecticular synthesis

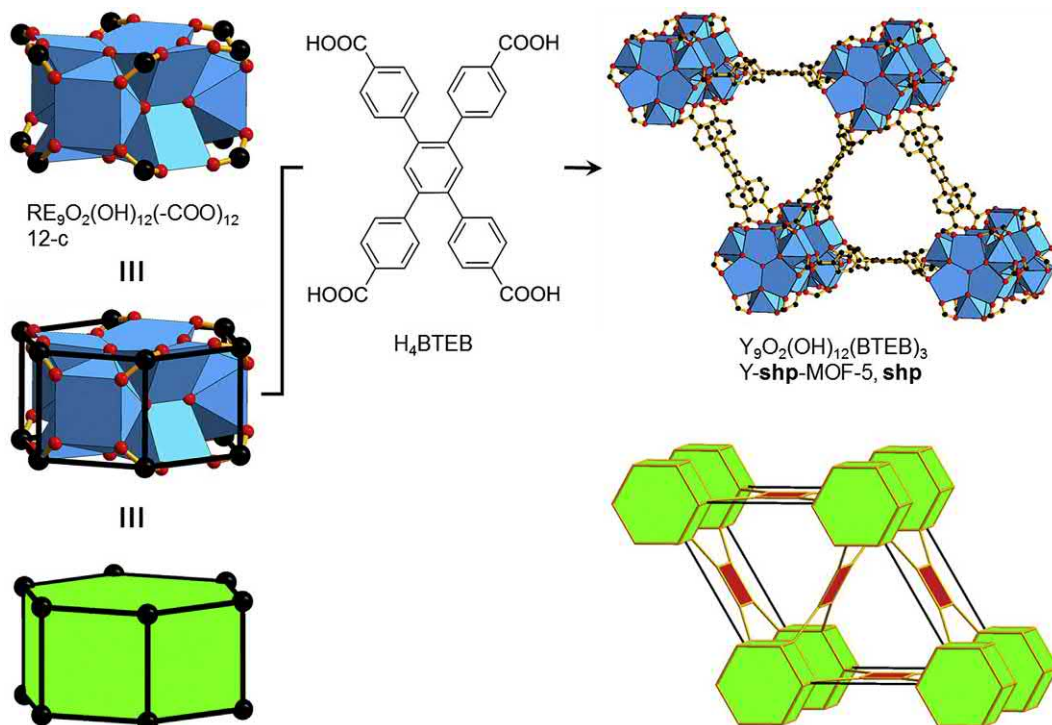
If two OH groups are substituted by two linker carboxylates ( $-\text{COO}$ ), a 6-c  $\text{Zr}_6\text{O}_4(\text{OH})_4(\text{HCOO})_6(-\text{COO})_6$  SBU is obtained. An early example of such SBUs can be found in MOF-808 with a formula of  $\text{Zr}_6\text{O}_4(\text{OH})_4(\text{BTC})_2(\text{HCOO})_6$  [52]. The 6-c Zr-cluster shows an overall trigonal antiprismatic ( $D_{3d}$ ) geometry and therefore leads to a (3,6)-c **spn** topology. We would like to note here that in the maximum symmetry embedding of the **spn** net, the 6-c node is an ideal octahedron ( $O_h$ ). MOF-808 has an internal pore diameter of 18.4 Å and the high thermal and chemical stability of the SBU allowed for the first demonstration of superacidity in MOFs [53]. In particular, the sulfate anions are grafted on the SBUs by replacing formate anions in aqueous sulfuric acid.

A higher coordination of the SBU is observed in a framework termed MOF-545. It is composed of 8-c  $\text{Zr}_6\text{O}_8(-\text{COO})_8$  SBUs, which, when combined with tetratopic TCPP linkers ( $\text{H}_4\text{TCPP}$  = tetrakis(4-carboxyphenyl)porphyrin), produce  $\text{Zr}_6\text{O}_8(\text{TCPP})_2$  [54]. Eight  $\mu_3\text{-O}$  are located on the faces of the  $\text{Zr}_6$ -octahedron, eight of the twelve edges are decorated with bidentate carboxylate groups, and water molecules occupy the remaining coordination sites. The POE, which are all the carboxylate C in the structure, form a rectangular prism. Therefore, the vertex figure in the maximum symmetry embedding is a cube. A critical element regarding the topology are the bond angles at the SBU, which, together with the square planar TCPP linker, facilitate the formation of a (4,8)-c **csq** net. MOF-545 shows a pore diameter of 36 Å, and exhibits a BET surface area of 2260  $\text{m}^2 \text{g}^{-1}$ . Desymmetrization of the square planar TCCP by replacement with TBAPy ( $\text{H}_4\text{TBAPy}$  = 1,3,6,8-tetrakis(*p*-benzoic acid)pyrene) produces  $\text{Zr}_6(\text{OH})_{16}(\text{TBAPy})_2$  (NU-1000) [55]. Herein, the longer axis of the pyrene core is aligned with the hexagonal [001] axis, which suggests a deconstruction into two 3-c triangles, leading to a binodal (3,8)-c **xly** topology [56]. The topology of the stable NU-1000 allowed for the postsynthetic linker exchange with TCPP to produce a MOF for photodynamic therapy [57].

MOFs based on clusters with 12 POE were very rare until about 10 years ago, when the first zirconium MOF UiO-66 was discovered [48]. The  $\text{Zr}_6\text{O}_4(\text{OH})_4(-\text{COO})_{12}$  SBU is decorated with 12 carboxylate groups in a cuboctahedral geometry and, when linked with  $\text{H}_2\text{BDC}$ , produces  $\text{Zr}_6\text{O}_4(\text{OH})_4(\text{BDC})_6$ . The default net for linking cuboctahedra is 12-c **fcu**. UiO-66 shows small tetrahedral and larger octahedral cavities, and exhibits a Langmuir surface area of 1187  $\text{m}^2 \text{g}^{-1}$ . The high coordination of the SBU, together with the strong nature of the Zr-oxygen bond, contributes to the high thermal and chemical stability. Isorecticular MOFs with  $\text{H}_2\text{BPDC}$  (UiO-67) and  $\text{H}_2\text{TPDC}$  (UiO-68) were synthesized and exhibit surface areas of 3000 and 4170  $\text{m}^2 \text{g}^{-1}$ , respectively. Others utilized shorter linkers such as ( $\text{H}_2\text{EDC}$  = ethene-1,2-dicarboxylic acid, fumaric acid) to produce Zr-*fum*-MOF [58]. Such MOFs were later shaped into nanoparticles for diagnostic and therapeutic applications [59]. The occurrence

and characterization of defects on the molecular level of UiO-66 were also the subject of many studies, but will not be further discussed in this review [60].

Another 12-c SBU was reported in a series of (4,12)-c **shp** topology MOFs. Rare earth metal salts were reacted with tetratopic, square-shaped TCPP linkers ( $H_4TCPP =$  tetrakis(4-carboxyphenyl) porphyrin), in the presence of 2-fluorobenzoic acid modulators, to produce  $RE_9O_2(OH)_{12}(TCPP)_3$  ( $RE = Y, Tb$ ), **Y-shp-MOF-1** and **Tb-shp-MOF-1** [61]. In the  $RE_9O_2(OH)_{12}(-COO)_{12}$  SBU, three of the nine rare earth metal ions are each coordinated to four  $\mu_3$ -OH and four carboxylate oxygen. A water molecule occupies the remaining coordination site. The other six rare earth metals are bound to a  $\mu_3$ -oxygen, four  $\mu_3$ -OH, two carboxylate oxygen, and a water ligand. The anionic ( $-5$ ) charge of the cluster is balanced by in situ generated dimethylammonium (DMA) cations. The 12 POE form an overall hexagonal prismatic (d6R) geometry. Together with tetratopic linkers such as BTEB ( $H_4BTEB = 1,2,4,5$ -tetrakis(4-carboxyphenyl)benzene), a framework of formula  $RE_9O_2(OH)_{12}(BTEB)_3$ , termed **Y-shp-MOF-5**, was afforded (Fig. 2.13) [62]. The hexagonal structure ( $P6/mmm$ ) contains triangular channels with a diameter of 11 Å, and a hexagonal prismatic cage with 9.9 Å in



**Fig. 2.13**

Schematic of the (4,12)-c **Y-shp-MOF-5** based on the 12-c hexagonal prismatic (d6R)  $RE_9O_2(OH)_{12}(-COO)_{12}$  SBU. Color code: black, C; red, O; blue polyhedra, Y. Hydrogen atoms are omitted for clarity.

diameter (including v. d. W. radii). It has a slightly lower apparent BET surface area and a pore volume of  $1550 \text{ m}^2 \text{ g}^{-1}$  and  $0.61 \text{ cm}^3 \text{ g}^{-1}$ , respectively, when compared to the parent compounds.

SBUs with high coordination (12-c, 16-c) are also sustained by ring-like SBUs of formula  $\text{Al}_8(\text{OH})_8(\text{—COO})_{16}$  and, when linked with BTB, produce MOF-519 and MOF-520 (Fig. 2.14) [63]. The Al-cluster can potentially serve as a 16-c SBU. It is composed of eight octahedrally coordinated  $\text{Al}^{3+}$  cations that are each bound by two  $\mu_3\text{—OH}$  and four bidentate carboxylate groups. In MOF-520 four of the total 16 carboxylate binding sites are occupied by terminal formate ligands, producing a 12-c  $\text{Al}_8(\text{OH})_8(\text{HCOO})_4(\text{—COO})_{12}$  SBU. The topology of both frameworks was earlier observed in  $\text{Be}_{12}(\text{OH})_{12}(\text{BTB})_4$  crystallizing in a (3,12)-c **sum** net [64]. However, we believe that the later reassignment to (3,12)-c **fon** is more suitable since it takes the whole ring-like SBU into account. In MOF-519, the SBU contains partially uncoordinated BTB linkers instead of formate, which narrows the pore space compared to MOF-520.

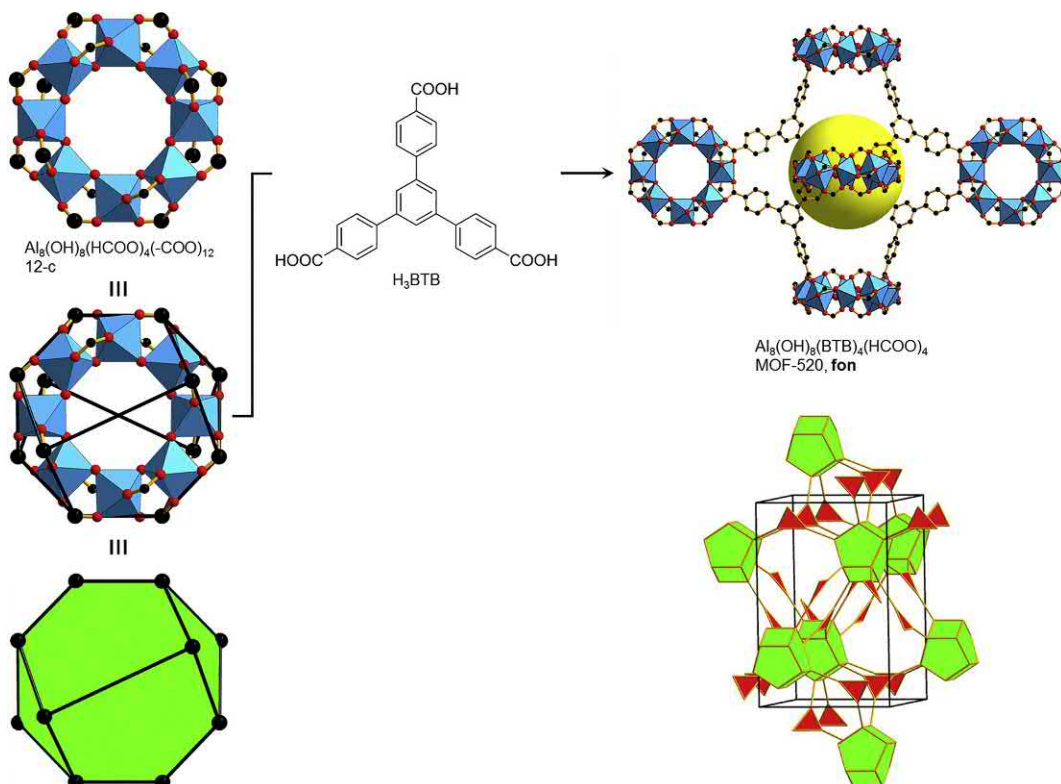


Fig. 2.14

MOF-520 composed of an  $\text{Al}_8(\text{OH})_8(\text{—COO})_{16}$  SBU that shows 12 points of extension. Color code: black, C; red, O; blue polyhedra, Al. The *yellow sphere* represents the empty space in the framework. Hydrogen atoms are omitted for clarity.



MOF-519 shows a BET surface area of  $2400 \text{ m}^2 \text{ g}^{-1}$  and can adsorb  $259 \text{ cm}^3 \text{ cm}^{-3}$  methane with a deliverable capacity of  $210 \text{ cm}^3 \text{ cm}^{-3}$  between 5 and 65 bar and 298 K. In MOF-520, the four coordination sites occupied with formate anions at the  $\text{Al}_8(\text{OH})_8(-\text{COO})_{16}$  SBU have allowed for the binding and alignment of molecules with varying size, complexity, and functionality [65]. These molecules are highly ordered and could be refined with atomic precision using single-crystal X-ray diffraction. It was also demonstrated that racemic mixtures can be separated in chiral MOF-520 crystals and that structure determination of complex molecules is feasible.

To the best of our knowledge, the only MOF sustained by an 18-c SBU was discovered in 2014, when yttrium nitrate was reacted with  $\text{H}_3\text{BTB}$ , in the presence of a 2-fluorobenzoic acid modulator. The anionic  $\text{Y}_9(\text{OH})_{11}(-\text{COO})_{18}$  SBU is linked to triangular BTB to produce  $\text{Y}_9(\text{OH})_{11}(\text{BTB})_6$ , **gea**-MOF-1 (Fig. 2.15) [66]. The metal-oxide cluster contains nine metal ions forming a tricapped trigonal prism. Each of the six yttrium ions at the trigonal prism is

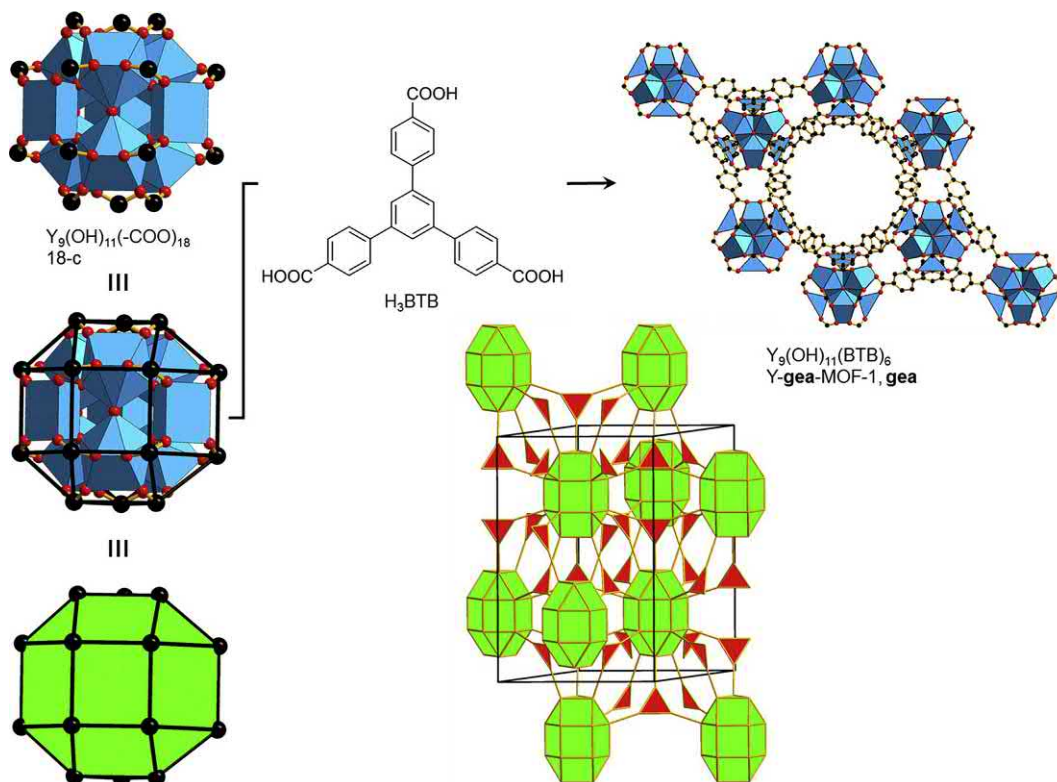
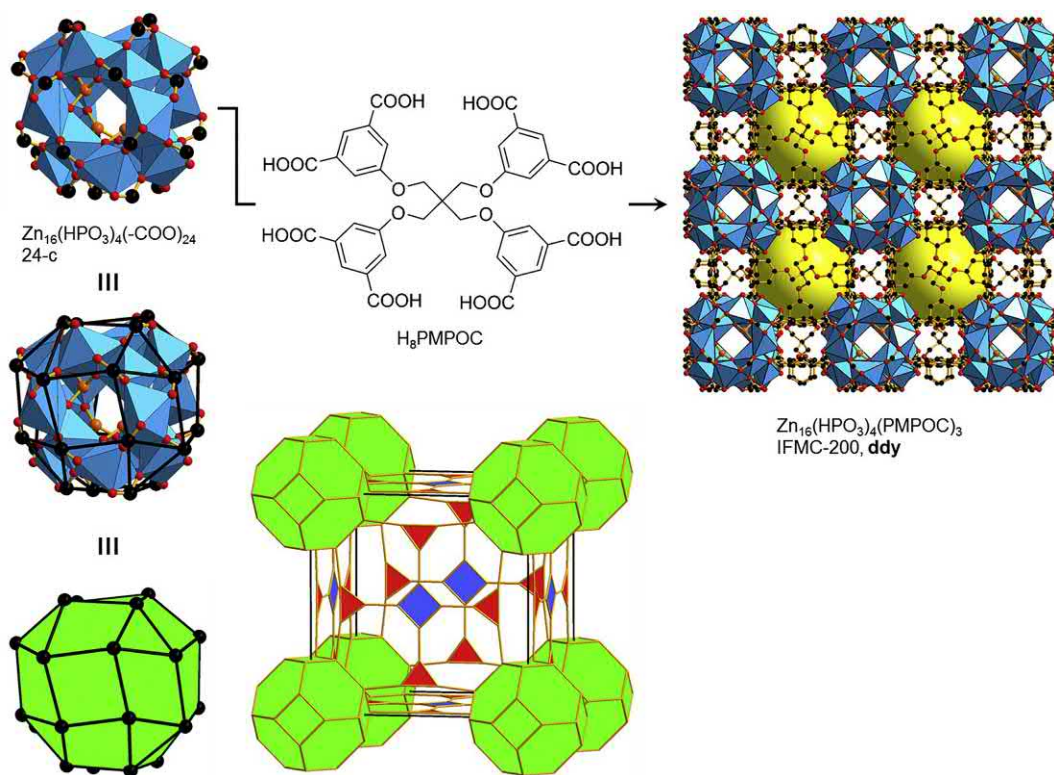


Fig. 2.15

A (3,18)-c **gea** topology MOF composed of an anionic  $\text{Y}_9(\text{OH})_{11}(-\text{COO})_{18}$  SBU with 18 points of extension in the shape of an **eto** polyhedron. Color code: black, C; red, O; blue polyhedra, Y. Hydrogen atoms are omitted for clarity.

coordinated to four carboxylate O, three  $\mu_3$ -OH, and a  $\mu_2$ -OH. The three remaining Y ions are coordinated by four carboxylate O and two  $\mu_3$ -OH. The overall negative charge of the SBU is balanced by DMA generated in situ from DMF solvent molecules. The 18 POE sit at the vertices of an **eto** polyhedron which can be viewed as the regular 12-c cuboctahedron (**cuo**) with six additional POE. Its formation is a direct consequence of the incompatibility of 12-c and 3-c building units in terms of edge-transitive nets. Viewed along the [001] axis, the (3,18)-c **gea** topology can be understood as a pillared **hxl** net. The structure of **gea**-MOF-1 exhibits three types of cavities with diameters 22.4, 14.6, and 5.6 Å, respectively. It shows an apparent BET surface area of 1490 m<sup>2</sup> g<sup>-1</sup> and a pore volume of 0.58 cm<sup>3</sup> g<sup>-1</sup>. Y-**gea**-MOF-1 was also used as a catalyst in the coupling of carbon dioxide and epoxides.

In contrast to the MOPs discussed below, the unprecedented Zn<sub>16</sub>(HPO<sub>3</sub>)<sub>4</sub>(-COO)<sub>24</sub> is the only metal-oxide cluster SBU with 24 POE (Fig. 2.16) [67]. Twelve Zn cations are each tetrahedrally coordinated by three carboxylate O, and one  $\mu_2$ -O of HPO<sub>3</sub>. The four remaining Zn ions show an octahedral geometry, with three carboxylate O in a facial coordination and three  $\mu_2$ -O of HPO<sub>3</sub>.



**Fig. 2.16**

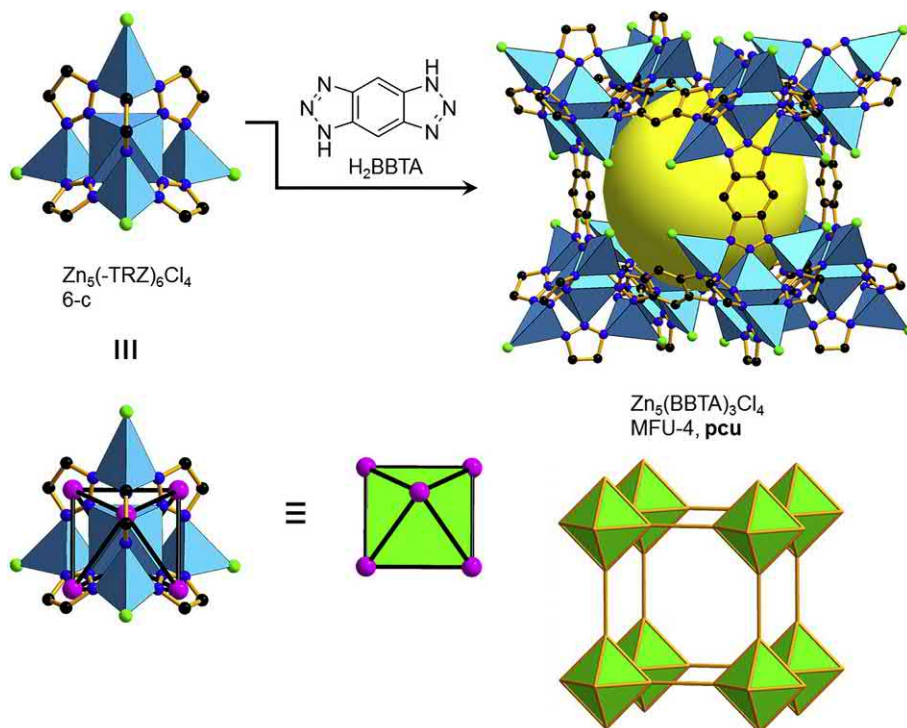
The highly coordinated Zn<sub>16</sub>(HPO<sub>3</sub>)<sub>4</sub>(-COO)<sub>24</sub> SBU produces a (3,4,24)-c **ddy** topology MOF, termed IFMC-200. Color code: black, C; red, O; orange, P; blue polyhedra, Zn. The *yellow spheres* represent the empty space in the framework. Hydrogen atoms are omitted for clarity.

The carboxylate C that serves as POE forms an overall 24-c rhombicuboctahedron. When the SBU is linked with PMPOC ( $H_8PMPOC = 5,5'-((2,2-bis((3,5-dicarboxyphenoxy)methyl)propane-1,3-diyl)bis(oxy))diisophthalic\ acid$ ), containing a 3-c and a 4-c node, IFMC-200 of formula  $Zn_{16}(HPO_3)_4(PMPOC)_4$  is produced. The overall topology (3,4,24)-c **ddy** in its maximum symmetry embedding consists of truncated octahedra, squares, and triangles. IFMC-200 is stable over a wide range of pH values and was utilized as a heterogeneous Lewis acid catalyst for esterification of fatty acids with alcohols to produce biodiesel.

## 2.6 Nitrogen-containing SBUs—Pyrazoles, triazoles, tetrazoles, and bio-MOFs

Nitrogen-containing SBUs are either based on neutral N-donor ligands such as pyridine (-PY) or anionic N-donor ligands such as pyrazole, triazole, or tetrazole (-PZ, -TRZ, -TZ).

A triazole-based framework MFU-4 of formula  $Zn_5(BBTA)_3Cl_4$  [ $H_2BBTA = 1,5-dihydrobenzo[1,2-d:4,5-d']bis([1,2,3]triazole)$ ], with a simple 6-c **pcu** net, was reported in 2009 (Fig. 2.17) [68].

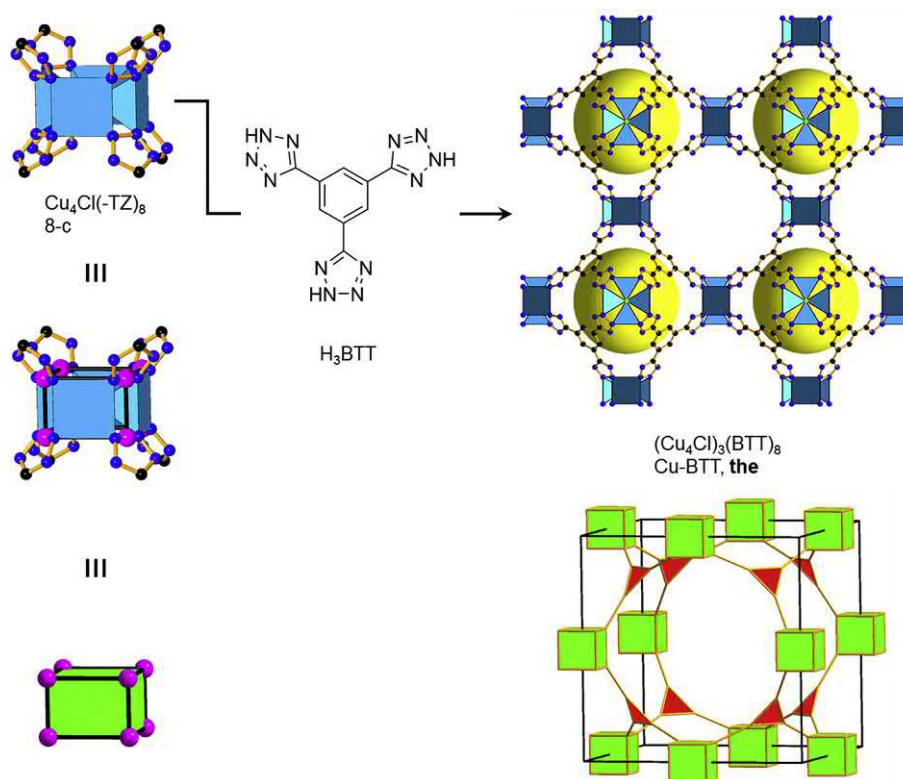


**Fig. 2.17**

Structure of the  $Zn_5(BBTA)_3Cl_4$  (MFU-4), which crystallizes in a simple 6-c **pcu** topology. Color code: black, C; blue, N; green, Cl; blue polyhedra, Zn. The *yellow ball* represents the open space in the framework. Hydrogen atoms are omitted for clarity.

The  $Zn_5(-TRZ)_3Cl_4$  SBU contains two differently coordinated Zn atoms. The central Zn is coordinated in an octahedral fashion to six triazolate N. The four remaining Zn are tetrahedrally coordinated to three triazolate N and one terminal Cl. Therefore, the overall vertex figure is an octahedron, when imaginary POE are placed in the middle of the triazolate moieties. The cluster SBU allows for solvent removal at temperatures above 250°C, and a high water stability as proven by water adsorption isotherms.

In 2006, a (3,8)-c **the** topology MOF was produced from a 8-c  $Mn_4Cl(-TZ)_8$  SBU together with BTT ( $H_3BTT = 1,3,5$ -benzenetristetrazole) (Fig. 2.18) [69]. Mn-BTT is an anionic MOF that contains solvated manganese(II) cations to balance the charge. In the SBU, each manganese atom is coordinated to a central  $\mu_4$ -Cl and additionally by four tetrazole N. The isostructural Cu-BTT variant of formula  $(Cu_4Cl)_3(BTT)_8$  shows a higher stability than the Mn variant as reflected by their experimental BET surface areas of 1100 and 2100  $m^2 g^{-1}$ , respectively [70]. The higher number of OMS in Cu-BTT accounts for a higher hydrogen uptake of 2.42 wt% at



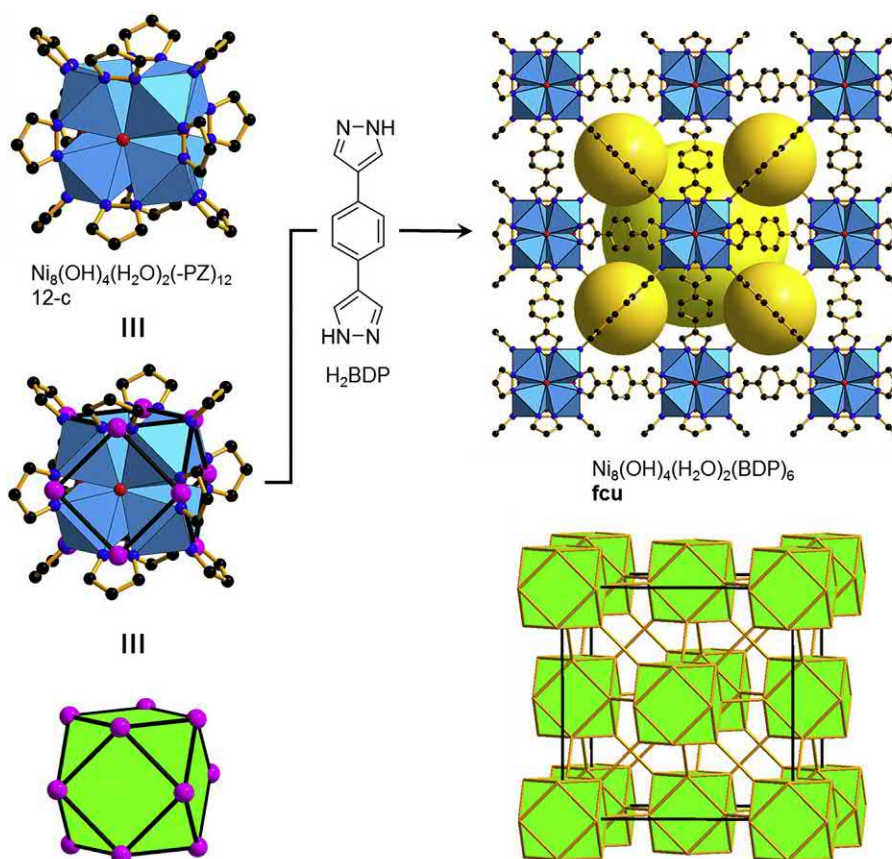
**Fig. 2.18**

Structure of the  $Cu_4Cl(-TZ)_8$  SBUs that produce Cu-BTT. The 3,8-c **the** topology is composed of cubes and triangles. Color code: black, C; blue, N; green, Cl; blue polyhedra, Cu. The *yellow ball* represents the open space in the framework. Hydrogen atoms are omitted for clarity.



77 K. In 2011, a (3,8)-c **the** topology framework based on a closely related  $\text{Cu}_4\text{Cl}(\text{COO})_8$  SBU was reported [71].

Another M-N cluster SBU with even higher coordination was reported in 2013 [72]. The 12-c  $\text{Ni}_8(\text{OH})_4(\text{H}_2\text{O})_2(-\text{PZ})_{12}$  contains eight octahedrally coordinated Ni atoms and each of them is bound to three  $\mu_4$ -OH or  $\mu_4$ -OH<sub>2</sub>, respectively, in addition to three pyrazolate N. The overall geometry of the SBU is a cuboctahedron and as the direct consequence of the linear linking,  $\text{Ni}_8(\text{OH})_4(\text{H}_2\text{O})_2(\text{BDP})_6$  ( $\text{H}_2\text{BDP}$  = 1,4-di(1H-pyrazol-4-yl)benzene) the default 12-c **fcu** net is observed (Fig. 2.19). In analogy to UiO-66 the framework contains small tetrahedral and larger octahedral cavities, and shows a BET surface area of  $1770 \text{ m}^2 \text{ g}^{-1}$ . An isorecticular series of expanded and functionalized frameworks was reported. They have high hydrolytic stability,

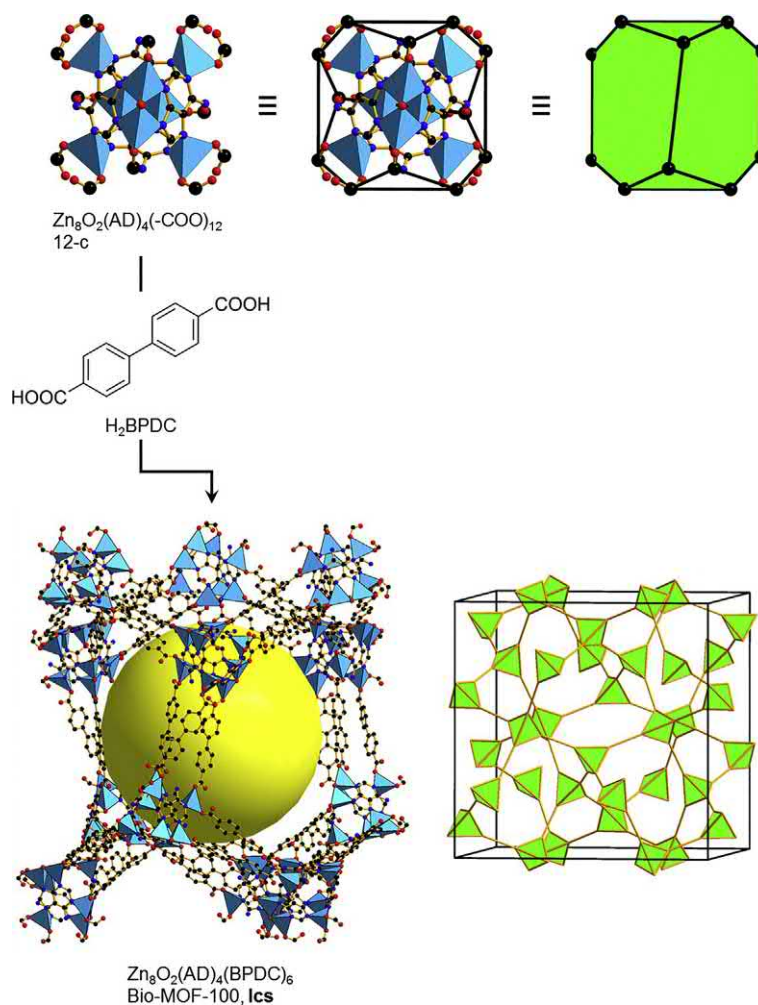


**Fig. 2.19**

The 12-c  $\text{Ni}_8(\text{OH})_4(\text{H}_2\text{O})_2(-\text{PZ})_{12}$  SBUs are directly linked with BDP to produce  $\text{Ni}_8(\text{OH})_4(\text{H}_2\text{O})_2(\text{BDP})_6$  with 12-c **fcu** topology. Color code: black, C; red, O; blue, N; blue polyhedra, Ni; pink, points of extension. The *yellow spheres* represent the empty space in the framework. Hydrogen atoms are omitted for clarity.

due to the strong metal-azolate bonds. Fluoro-functionalized variants showed increased hydrophobicity and were used for capturing volatile organic compounds such as chemical warfare agents.

In 2012, a complex 12-c adenine-containing SBU was reported for the construction of a mesoporous framework,  $\text{Zn}_8\text{O}_2(\text{AD})_4(\text{BPDC})_6$  (HAD = adenine), termed bio-MOF-100 (Fig. 2.20) [73]. The SBU of formula  $\text{Zn}_8\text{O}_2(\text{AD})_4(-\text{COO})_{12}$ , specified by the authors as a ZABU (zinc-adeninate building unit), contains 8 tetrahedrally coordinated  $\text{Zn}^{2+}$  and 4 AD as well as 12 carboxylates. The SBU shows the overall geometry of a truncated tetrahedron (**tte**), based on



**Fig. 2.20**

The 12-c  $\text{Zn}_8\text{O}_2(\text{AD})_4(-\text{COO})_{12}$  SBU is triple cross-linked with BPDC to afford bio-MOF-100 with 4-c **lcs** topology. Color code: black, C; red, O; blue, N; blue tetrahedra, Zn. The *yellow sphere* represents the empty space in the framework. Hydrogen atoms are omitted for clarity.



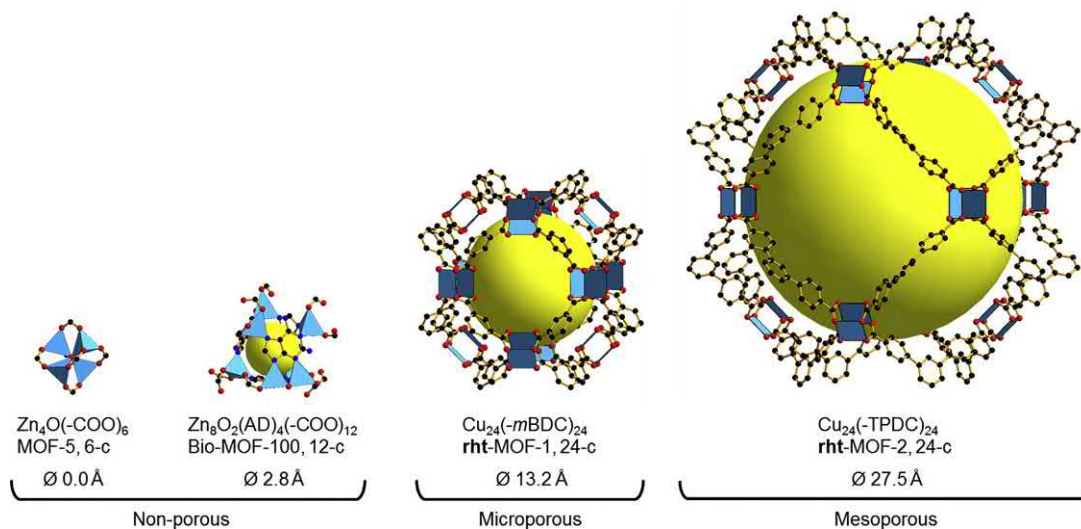
the carboxylate C as POE. Three POE on a tetrahedral vertex are linked through BPDC to a next neighboring SBU, which renders bio-MOF-100 into a 4-c **lcs** net. This topology is different from the default net for 4-c nodes **dia** because of the different conformation of the six-membered rings. Cubic crystals of bio-MOF-100 show a large cell parameter and contain only mesopores of 28 Å in diameter. An anionic framework termed bio-MOF-1, with a closely related SBU, was utilized to host and release cationic drug molecules [74].

## 2.7 Metal-organic polyhedra

Thus far, M-O- and M-N-based clusters were introduced as SBUs in MOFs since they serve as prerequisites toward design of topology and structure. Augmentation of such SBUs into larger clusters facilitated higher coordination and thus higher porosity, as exemplified by bio-MOF-100. In addition, such polyhedra are generally sustained by relatively simple building units and can be isolated as discrete structures [75]. The most important one in this class is termed MOP-1  $\text{Cu}_{24}(\text{mBDC})_{24}$  with a rhombicuboctahedral (**rco**) shape (Fig. 2.21, middle) [76, 77].

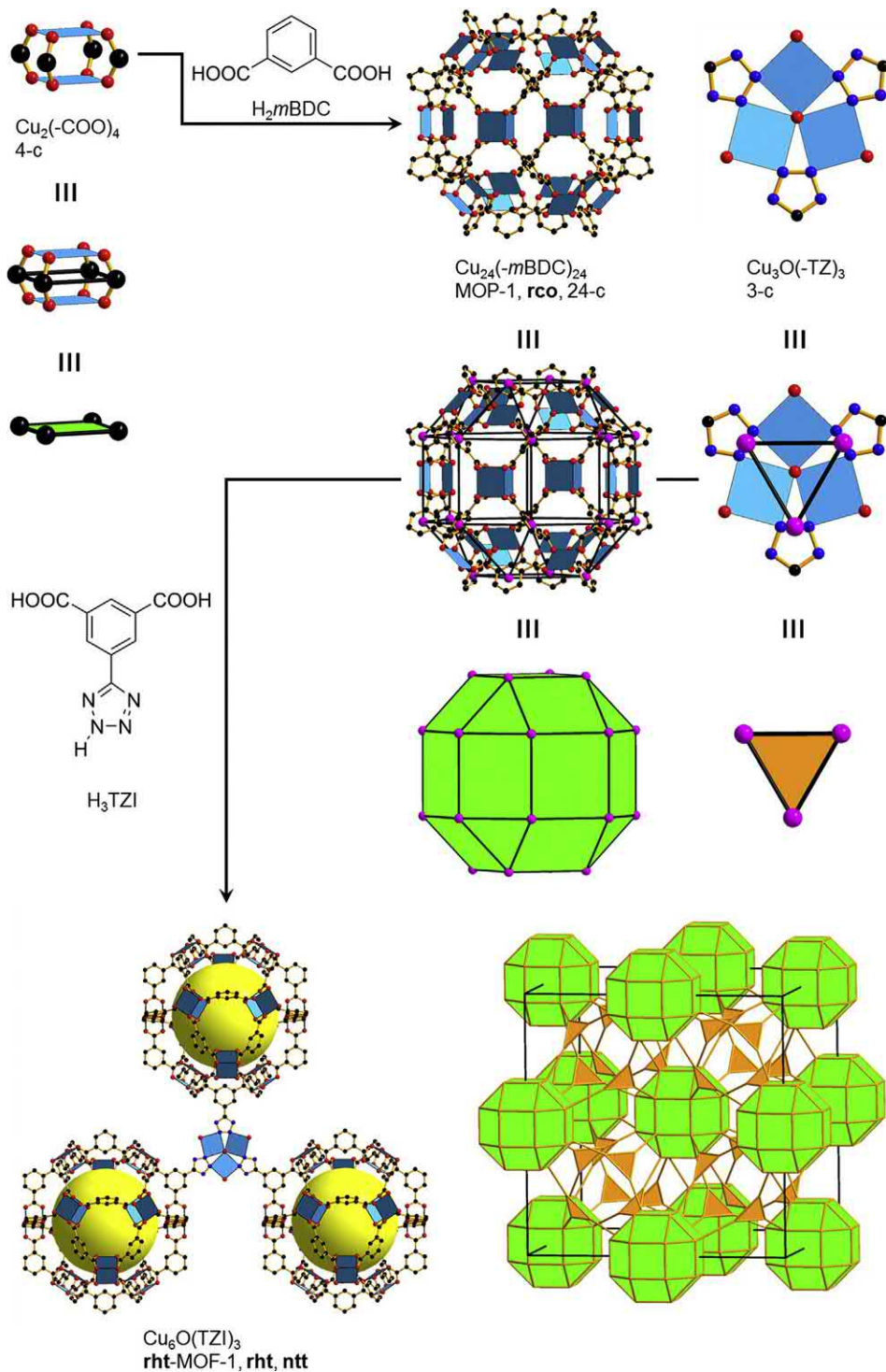
MOP-1 is composed of 12  $\text{Cu}_2(\text{—COO})_4$  square paddlewheel SBUs and 24 *m*BDC linkers and can serve as a 24-c building unit. For the first time, linking these so-called nanoballs with a 3-c  $\text{Cu}_3\text{O}(\text{—TZ})_3$  SBU produced a (3,24)-c **rht** MOF (Fig. 2.22) [78].

The **rht** topology is the only mathematical possibility of combining 3-c and 24-c nodes. However, it is the subject of an ongoing discussion, whether **rht** should be deconstructed into a



**Fig. 2.21**

Different levels of porosity in MOF building units. Color code: gray, C; red, O; blue, N; and blue polyhedra, metal. The colored spheres represent the empty space in the polyhedral building units, including v. d. Waals radii. Hydrogen atoms are omitted for clarity.



**Fig. 2.22**

Schematic of **rht-MOF-1** sustained by a  $\text{Cu}_{24}(-m\text{BDC})_{24}$  building unit together with a triangular  $\text{Cu}_3\text{O}(-\text{PZ})_3$  SBU. Color code: black, C; red, O; blue, N; blue polyhedra, Cu; pink, points of extension. The *yellow spheres* represent the empty space in the framework. Hydrogen atoms are omitted for clarity.

trinodal (3,4)-c **ntt** topology [51]. The derived **ntt** net takes into account that both the MOP and the triangular, functionalized *m*BDC linker can be subjected to reticular chemistry approaches. After discovery of **rht**-MOF-1, many functionalized and expanded hexacarboxylate linkers were utilized to produce isorecticular **rht** frameworks. These reticular chemistry approaches mostly rely on increasing the linker length and introduce functionality. In particular, **rht**-MOFs can be expanded in two directions: First, the elongation of the triangular linker by introduction of phenylene or acetylene units [79]. Second, the augmentation of the MOP by elongation of the *m*BDC moiety [80]. Therefore, the use of MOPs represents an elegant strategy toward modular structures showing very high porosity.

## 2.8 Infinite rod like SBUs

A metal-cluster SBU is generally built of metal atoms (M) bound to other metal atoms in the same SBU either by M-X-M links (X is a nonmetal) or through a common point of extension, such as M-O-C-O-M in carboxylates or M-N-N-M in pyrazolates. In rod SBUs the metal atoms are linked by the same patterns into infinite rods. Principles of reticular chemistry apply to rod MOFs in the same manner as to MOFs built from discrete SBUs. We tend to introduce our description of rod MOFs using the well-known MIL-53 [81]. Isorecticular frameworks are MOF-71 and MIL-47 [82, 83]. We detail the deconstruction of MIL-53 with formula Cr(OH)(BDC) and a rod SBU composition of  $[\text{Cr}(\text{OH})(-\text{COO})_2]_\infty$  (Fig. 2.23). As in discrete SBUs, the pattern of POE (carboxylate C) defines the shape of the metal SBU. However, the rod SBU lacks a well-defined barycenter, which in turn means that there is no “un-augmented” net.

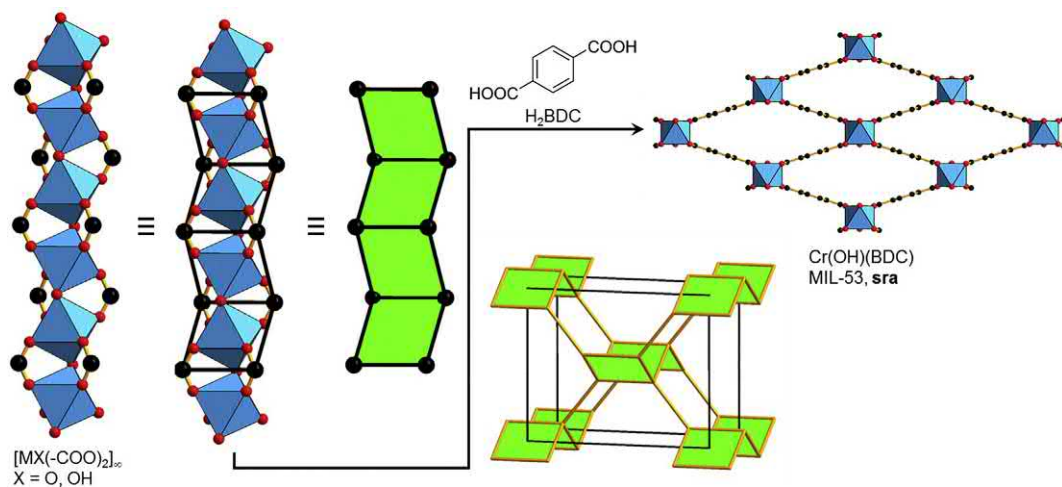


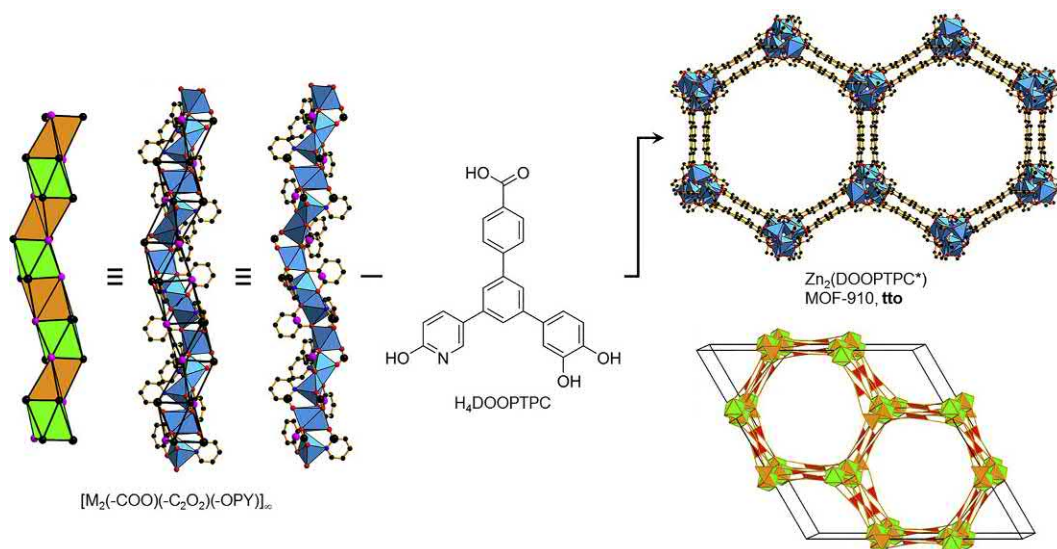
Fig. 2.23

MIL-53 having a 4-c **sra** topology framework based upon zigzag ladders of general formula  $[\text{MX}(-\text{COO})_2]_\infty$  ( $X = \text{O}, \text{OH}$ ). Color code: black, C; red, O; blue polyhedra, Cr. Hydrogen atoms are omitted for clarity.

Therefore, the SBUs in MIL-53 are zigzag ladders that are directly linked by ditopic BDC into a 3-D framework. MIL-53 is a flexible framework and was utilized for the controlled, long-term delivery of ibuprofen under physiological conditions [84].

The 4-c **sra** net is one of the most common topologies in MOF chemistry. The symbol **sra** is derived from the positions of the Al net in  $\text{SrAl}_2$ . The same topology is found in zeolites, denoted as the zeolite framework type **ABW**.

Rod MOFs can also be composed of two or more vertex figures, as observed in MOF-910 with formula  $\text{Zn}_3(\text{DOOPTPC}^*)_2$ , ( $\text{H}_4\text{DOOPTPC} = 3'',4''$ -dihydroxy-5'-(6-hydroxypyridin-3-yl)-[1,1':3',1''-terphenyl]-4-carboxylic acid). The unique rod SBU of general formula  $[\text{M}_2(-\text{COO})(-\text{C}_2\text{O}_2)(-\text{OPY})]_\infty$  contains octahedra and tetrahedra in a ratio of 1:2 (Fig. 2.24) [85]. DOOPTPC\* refers to a semiquinonate produced by an in situ one-electron oxidation from a catechol. This oxidation changes the overall charge of the linker to  $-3$ . The topology of MOF-910 is (3,6)-c **tto**. The rod SBU contains three distinct bidentate coordinating groups: carboxylates ( $-\text{COO}$ ), benzosemiquinonate ( $-\text{C}_2\text{O}_2$ ), and pyridonate ( $-\text{OPY}$ ). The three coordinating groups are not interchangeable due to the asymmetry of the tritopic linker. The angular portion of the linker,  $-\text{C}_2\text{O}_2$ , and  $-\text{OPY}$  that coordinate to the same rod are crucial for the formation of a helical SBU. Moreover, the distance between the functional groups defines the pitch of this threefold helix. The different functional groups would also allow for reticular



**Fig. 2.24**

Three coordination modes are present in the complex rod SBU of MOF-910. The POE form octahedra and tetrahedra in a ratio of 1:2. Color code: black, C; red, O; blue, N; blue polyhedra, metal; pink, points of extension. Hydrogen atoms are omitted for clarity.

chemistry approaches through expansion of the benzoate moiety without altering the underlying **tto** topology.

Other rod MOFs, such as the famous MOF-74 and its isoreticular frameworks, were used for the adsorption of large biomolecules [86]. Their large pore openings, up to 9.8 nm, enabled the adsorption of Vitamin B<sub>12</sub>, myoglobin, and green fluorescent protein. A detailed review has been published on the deconstruction and topology of MOF-74, among other rod MOFs [87].

## 2.9 Concluding remarks

In summary, we highlighted the importance of the SBU approach in MOF chemistry. The formation of many robust metal clusters and their linkage with organic moieties through strong bonds have provided unprecedented stability to metal-organic structures. Moreover, through variable coordination and high symmetry, SBUs facilitate the design and synthesis of frameworks using reticular chemistry approaches. The ever-growing number of SBUs, together with linker design by virtue of synthetic organic chemistry, enables custom design of MOFs nearly at will, amenable for any specific application. In this chapter, some material properties are detailed to highlight the importance of crystalline MOFs that preserve structural integrity and thus permanent porosity. The controlled SBU approach, which is unique to reticular chemistry, is already producing porous crystals that are superior to many traditional porous materials. In addition, their low toxicity and high stability make them perfect candidates for a variety of biomedical applications. Thus, MOFs are expected to have an even larger scientific and economic impact in the near future.

## Acknowledgment

Funding of MOF research in the Schoedel group is supported by startup funds from the Florida Institute of Technology.

## References

- [1] Y. Kinoshita, I. Matsubara, Y. Saito, The crystal structure of bis(glutaronitrilo)copper(I) nitrate, *Bull. Chem. Soc. Jpn.* 32 (1959) 1216.
- [2] Y. Kinoshita, I. Matsubara, Y. Saito, The crystal structure of bis(succinonitrilo)copper(I) nitrate, *Bull. Chem. Soc. Jpn.* 32 (1959) 741.
- [3] Y. Kinoshita, I. Matsubara, T. Higuchi, Y. Saito, The crystal structure of bis(adiponitrilo)copper(I) nitrate, *Bull. Chem. Soc. Jpn.* 32 (1959) 1221.
- [4] M. Eddaoudi, D.B. Moler, H. Li, B. Chen, T.M. Reineke, M. O’Keeffe, O.M. Yaghi, Modular chemistry: secondary building units as a basis for the design of highly porous and robust metal-organic carboxylate frameworks, *Acc. Chem. Res.* 34 (2001) 319.
- [5] B. Moulton, M. Zaworotko, From molecules to crystal engineering: supramolecular isomerism and polymorphism in network solids, *J. Chem. Rev.* 101 (2001) 1629.
- [6] O.M. Yaghi, M. O’Keeffe, N.W. Ockwig, H.K. Chae, M. Eddaoudi, J. Kim, Reticular synthesis and the design of new materials, *Nature* 423 (2003) 705.



- [7] H. Furukawa, K.E. Cordova, M. O’Keeffe, O.M. Yaghi, The chemistry and applications of metal-organic frameworks, *Science* 341 (2013) 1230444.
- [8] C. Baerlocher, L.B. McCusker, D.H. Olson, Atlas of Zeolite Framework Types, sixth revised ed., Elsevier Science, Amsterdam, 2007.
- [9] D. Zhao, J. Feng, Q. Huo, N. Melosh, G.H. Fredrickson, B.F. Chmelka, G.D. Stucky, Triblock copolymer syntheses of mesoporous silica with periodic 50 to 300 angstrom pores, *Science* 279 (1998) 548.
- [10] A.A. Zakhidov, R.H. Baughman, Z. Iqbal, C. Cui, I. Khayrullin, S.O. Dantas, J. Marti, V.G. Ralchenko, Carbon structures with three-dimensional periodicity at optical wavelengths, *Science* 282 (1998) 897.
- [11] S.S.-Y. Chui, S.M.F. Lo, J.P.H. Charmant, A.G. Orpen, I.D. Williams, A chemically functionalizable nanoporous material  $[\text{Cu}_3(\text{TMA})_2(\text{H}_2\text{O})_3]_n$ , *Science* 283 (1999) 1148.
- [12] M. Eddaoudi, J. Kim, N. Rosi, D. Vodak, J. Wachter, M. O’Keeffe, O.M. Yaghi, Systematic design of pore size and functionality in isorecticular MOFs and their application in methane storage, *Science* 295 (2002) 469.
- [13] J. Jiang, Y. Zhao, O.M. Yaghi, Covalent chemistry beyond molecules, *J. Am. Chem. Soc.* 138 (2016) 3255.
- [14] H. Li, M. Eddaoudi, T.L. Groy, O.M. Yaghi, Establishing microporosity in open metal-organic frameworks: gas sorption isotherms for Zn(BDC) (BDC = 1,4-benzenedicarboxylate), *J. Am. Chem. Soc.* 120 (1998) 8571.
- [15] M. Kondo, T. Yoshitomi, H. Matsuzaka, S. Kitagawa, K. Seki, Three-dimensional framework with channeling cavities for small molecules:  $\{[\text{M}_2(4,4'\text{-bpy})_3(\text{NO}_3)_4] \cdot x\text{H}_2\text{O}\}_n$  (M = Co, Ni, Zn), *Angew. Chem. Int. Ed. Engl.* 36 (1997) 1725.
- [16] D.J. Tranchemontagne, J.L. Mendoza-Cortés, M. O’Keeffe, O.M. Yaghi, Secondary building units, nets and bonding in the chemistry of metal-organic frameworks, *Chem. Soc. Rev.* 38 (2009) 1257.
- [17] M. Fujita, J. Yazaki, K. Ogura, Preparation of a macrocyclic polynuclear complex,  $[(\text{en})\text{Pd}(4,4'\text{-bpy})_4(\text{NO}_3)_8]$  (en = ethylenediamine, bpy = bipyridine), which recognizes an organic molecule in aqueous media, *J. Am. Chem. Soc.* 112 (1990) 5645.
- [18] S. Subramanian, M.J. Zaworotko, Porous solids by design:  $[\text{Zn}(4,4'\text{-bpy})_2(\text{SiF}_6)]_n \cdot x\text{DMF}$ , a single framework octahedral coordination polymer with large square channels, *Angew. Chem. Int. Ed. Engl.* 34 (1995) 2127.
- [19] P. Nugent, Y. Belmabkhout, S.D. Burd, A.J. Cairns, R. Luebke, K. Forrest, T. Pham, S. Ma, B. Space, L. Wojtas, M. Eddaoudi, M.J. Zaworotko, Porous materials with optimal adsorption thermodynamics and kinetics for  $\text{CO}_2$  separation, *Nature* 495 (2013) 80.
- [20] A. Kumar, D.G. Madden, M. Lusi, K.-J. Chen, E.A. Daniels, T. Curtin, J.J. Perry, M.J. Zaworotko, Direct air capture of  $\text{CO}_2$  by physisorbent materials, *Angew. Chem. Int. Ed.* 54 (2015) 14372.
- [21] P.M. Bhatt, Y. Belmabkhout, A. Cadiau, K. Adil, O. Shekhat, A. Shkurenko, L. J. Barbour, M. Eddaoudi, A fine-tuned fluorinated MOF addresses the needs for trace  $\text{CO}_2$  removal and air capture using physisorption, *J. Am. Chem. Soc.* 138 (2016) 9301.
- [22] K. Adil, Y. Belmabkhout, R.S. Pillai, A. Cadiau, P.M. Bhatt, A.H. Assen, G. Maurin, M. Eddaoudi, Gas/vapour separation using ultra-microporous metal-organic frameworks: insights into the structure/separation relationship, *Chem. Soc. Rev.* 46 (2017) 3402.
- [23] Y. Liu, V.C. Kravtsov, R. Larsen, M. Eddaoudi, Molecular building blocks approach to the assembly of zeolite-like metal-organic frameworks (ZMOFs) with extra-large cavities, *Chem. Commun.* (2006) 1488.
- [24] M.H. Alkordi, Y. Liu, R.W. Larsen, J.F. Eubank, M. Eddaoudi, Zeolite-like metal-organic frameworks as platforms for applications: on metalloporphyrin-based catalysts, *J. Am. Chem. Soc.* 130 (2008) 12639.
- [25] D.F. Sava, V.C. Kravtsov, F. Nouar, L. Wojtas, J.F. Eubank, M. Eddaoudi, Quest for zeolite-like metal-organic frameworks: on pyrimidinecarboxylate bis-chelating bridging ligands, *J. Am. Chem. Soc.* 130 (2008) 3768.
- [26] F. Nouar, J. Eckert, J.F. Eubank, P. Forster, M. Eddaoudi, Zeolite-like metal-organic frameworks (ZMOFs) as hydrogen storage platform: lithium and magnesium ion-exchange and  $\text{H}_2$ -(rho-ZMOF) interaction studies, *J. Am. Chem. Soc.* 131 (2009) 2864.
- [27] K.S. Park, Z. Ni, A.P. Côté, J.Y. Choi, R. Huang, F.J. Uribe-Romo, H.K. Chae, M. O’Keeffe, O.M. Yaghi, Exceptional chemical and thermal stability of zeolitic imidazolate frameworks, *Proc. Natl. Acad. Sci. U. S. A.* 103 (2006) 10186.
- [28] X.-C. Huang, Y.-Y. Lin, J.-P. Zhang, X.-M. Chen, Ligand-directed strategy for zeolite-type metal-organic frameworks: zinc(II) imidazolates with unusual zeolitic topologies, *Angew. Chem. Int. Ed.* 45 (2006) 1557.



- [29] C.M. Doherty, G. Greci, R. Riccò, J.I. Mardel, J. Reboul, S. Furukawa, S. Kitagawa, A. J. Hill, P. Falcaro, Combining UV lithography and an imprinting technique for patterning metal-organic frameworks, *Adv. Mater.* 25 (2013) 4701.
- [30] I. Fankuchen, Crystal structure of sodium uranyl acetate, *Zeitschrift für Kristallographie—Crystalline Materials*, vol. 91, 1935 p.473.
- [31] Y.B. Go, X. Wang, A.J. Jacobson, (6,3)-Honeycomb structures of uranium(VI) benzenedicarboxylate derivatives: the use of noncovalent interactions to prevent interpenetration, *Inorg. Chem.* 46 (2007) 6594.
- [32] P. Li, N.A. Vermeulen, C.D. Malliakas, D.A. Gómez-Gualdrón, A.J. Howarth, B.L. Mehdi, A. Dohnalkova, N.D. Browning, M. O’Keeffe, O.K. Farha, Bottom-up construction of a superstructure in a porous uranium-organic crystal, *Science* (2017).
- [33] R. Ameloot, F. Vermoortele, W. Vanhove, M.B.J. Roeffaers, B.F. Sels, D.E. De Vos, Interfacial synthesis of hollow metal-organic framework capsules demonstrating selective permeability, *Nat. Chem.* 3 (2011) 382.
- [34] H. Furukawa, Y.B. Go, N. Ko, Y.K. Park, F.J. Uribe-Romo, J. Kim, M. O’Keeffe, O.M. Yaghi, Isoreticular expansion of metal-organic frameworks with triangular and square building units and the lowest calculated density for porous crystals, *Inorg. Chem.* 50 (2011) 9147.
- [35] B. Chen, M. Eddaoudi, T.M. Reineke, J.W. Kampf, M. O’Keeffe, O.M. Yaghi,  $\text{Cu}_2(\text{ATC})\cdot 6\text{H}_2\text{O}$ : design of open metal sites in porous metal-organic crystals (ATC: 1,3,5,7-adamantane tetracarboxylate), *J. Am. Chem. Soc.* 122 (2000) 11559.
- [36] H. Koyama, Y. Saito, The crystal structure of zinc oxyacetate,  $\text{Zn}_4\text{O}(\text{CH}_3\text{COO})_6$ , *Bull. Chem. Soc. Jpn.* 27 (1954) 112.
- [37] H. Li, M. Eddaoudi, M. O’Keeffe, O.M. Yaghi, Design and synthesis of an exceptionally stable and highly porous metal-organic framework, *Nature* 402 (1999) 276.
- [38] H.K. Chae, D.Y. Siberio-Perez, J. Kim, Y. Go, M. Eddaoudi, A.J. Matzger, M. O’Keeffe, O.M. Yaghi, A route to high surface area, porosity and inclusion of large molecules in crystals, *Nature* 427 (2004) 523.
- [39] B.N. Figgis, G.B. Robertson, Crystal-molecular structure and magnetic properties of  $\text{Cr}_3(\text{CH}_3\text{COO})_6\text{O}\cdot 1.5\text{H}_2\text{O}$ , *Nature* 205 (1965) 694.
- [40] C. Mellot-Draznieks, C. Serre, S. Surblé, N. Audebrand, G. Férey, Very large swelling in hybrid frameworks: a combined computational and powder diffraction study, *J. Am. Chem. Soc.* 127 (2005) 16273.
- [41] A.C. Sudik, A.P. Côté, O.M. Yaghi, Metal-organic frameworks based on trigonal prismatic building blocks and the new “acs” topology, *Inorg. Chem.* 44 (2005) 2998.
- [42] S. Surblé, C. Serre, C. Mellot-Draznieks, F. Millange, G. Férey, A new isoreticular class of metal-organic-frameworks with the MIL-88 topology, *Chem. Commun.* (2006) 284.
- [43] C. Serre, F. Millange, S. Surblé, G. Férey, A route to the synthesis of trivalent transition-metal porous carboxylates with trimeric secondary building units, *Angew. Chem. Int. Ed.* 43 (2004) 6285.
- [44] A.C. McKinlay, J.F. Eubank, S. Wuttke, B. Xiao, P.S. Wheatley, P. Bazin, J.C. Lavalley, M. Daturi, A. Vimont, G. De Weireld, P. Horcajada, C. Serre, R.E. Morris, Nitric oxide adsorption and delivery in flexible MIL-88(Fe) metal-organic frameworks, *Chem. Mater.* 25 (2013) 1592.
- [45] C. Serre, C. Mellot-Draznieks, S. Surblé, N. Audebrand, Y. Filinchuk, G. Férey, Role of solvent-host interactions that lead to very large swelling of hybrid frameworks, *Science* 315 (2007) 1828.
- [46] P. Horcajada, T. Chalati, C. Serre, B. Gillet, C. Sebrie, T. Baati, J.F. Eubank, D. Heurtaux, P. Clayette, C. Kreuz, J.-S. Chang, Y.K. Hwang, V. Marsaud, P.-N. Bories, L. Cynober, S. Gil, G. Férey, P. Couvreur, R. Gref, Porous metal-organic-framework nanoscale carriers as a potential platform for drug delivery and imaging, *Nat. Mater.* 9 (2010) 172.
- [47] A. Schoedel, W. Boyette, L. Wojtas, M. Eddaoudi, M.J. Zaworotko, A family of porous lonsdaleite-e networks obtained through pillaring of decorated kagomé lattice sheets, *J. Am. Chem. Soc.* 135 (2013) 14016.
- [48] J.H. Cavka, S. Jakobsen, U. Olsbye, N. Guillou, C. Lamberti, S. Bordiga, K.P. Lillerud, A new zirconium inorganic building brick forming metal organic frameworks with exceptional stability, *J. Am. Chem. Soc.* 130 (2008) 13850.
- [49] F. Allen, The Cambridge Structural Database: a quarter of a million crystal structures and rising, *Acta Crystallogr. Sect. B* 58 (2002) 380.

- [50] Y. Zhang, X. Zhang, J. Lyu, K.-i. Otake, X. Wang, L.R. Redfern, C.D. Malliakas, Z. Li, T. Islamoglu, B. Wang, O.K. Farha, A flexible metal–organic framework with 4-connected  $Zr_6$  nodes, *J. Am. Chem. Soc.* 140 (2018) 11179.
- [51] M. O’Keeffe, O.M. Yaghi, Deconstructing the crystal structures of metal–organic frameworks and related materials into their underlying nets, *Chem. Rev.* 112 (2012) 675.
- [52] H. Furukawa, F. Gándara, Y.-B. Zhang, J. Jiang, W.L. Queen, M.R. Hudson, O.M. Yaghi, Water adsorption in porous metal–organic frameworks and related materials, *J. Am. Chem. Soc.* 136 (2014) 4369.
- [53] J. Jiang, F. Gándara, Y.-B. Zhang, K. Na, O.M. Yaghi, W.G. Klemperer, Superacidity in sulfated metal–organic framework-808, *J. Am. Chem. Soc.* 136 (2014) 12844.
- [54] W. Morris, B. Voloskiy, S. Demir, F. Gándara, P.L. McGrier, H. Furukawa, D. Cascio, J.F. Stoddart, O.M. Yaghi, Synthesis, structure, and metalation of two new highly porous zirconium metal–organic frameworks, *Inorg. Chem.* 51 (2012) 6443.
- [55] J.E. Mondloch, W. Bury, D. Fairen-Jimenez, S. Kwon, E.J. DeMarco, M.H. Weston, A.A. Sarjeant, S. T. Nguyen, P.C. Stair, R.Q. Snurr, O.K. Farha, J.T. Hupp, Vapor-phase metalation by atomic layer deposition in a metal–organic framework, *J. Am. Chem. Soc.* 135 (2013) 10294.
- [56] M. Li, D. Li, M. O’Keeffe, O.M. Yaghi, Topological analysis of metal–organic frameworks with polytopic linkers and/or multiple building units and the minimal transitivity principle, *Chem. Rev.* 114 (2014) 1343.
- [57] X. Zhao, Z. Zhang, X. Cai, B. Ding, C. Sun, G. Liu, C. Hu, S. Shao, M. Pang, Postsynthetic ligand exchange of metal–organic framework for photodynamic therapy, *ACS Appl. Mater. Interfaces* 11 (2019) 7884.
- [58] G. Zahn, H.A. Schulze, J. Lippke, S. König, U. Sazama, M. Fröba, P. Behrens, A water-born Zr-based porous coordination polymer: modulated synthesis of Zr-fumarate MOF, *Microporous Mesoporous Mater.* 203 (2015) 186.
- [59] A. Zimpel, N. Al Danaf, B. Steinborn, J. Kuhn, M. Höhn, T. Bauer, P. Hirschle, W. Schrimpf, H. Engelke, E. Wagner, M. Barz, D.C. Lamb, U. Lächelt, S. Wuttke, Coordinative binding of polymers to metal–organic framework nanoparticles for control of interactions at the biointerface, *ACS Nano* 13 (2019) 3884.
- [60] C.A. Trickett, K.J. Gagnon, S. Lee, F. Gándara, H.-B. Bürgi, O.M. Yaghi, Definitive molecular level characterization of defects in UiO-66 crystals, *Angew. Chem. Int. Ed.* 54 (2015) 11162.
- [61] Z. Chen, Ł.J. Weseliński, K. Adil, Y. Belmabkhout, A. Shkurenko, H. Jiang, P.M. Bhatt, V. Guillermin, E. Dauzon, D.-X. Xue, M. O’Keeffe, M. Eddaoudi, Applying the power of reticular chemistry to finding the missing alb-MOF platform based on the (6,12)-coordinated edge-transitive net, *J. Am. Chem. Soc.* 139 (2017) 3265.
- [62] R.G. AbdulHalim, P.M. Bhatt, Y. Belmabkhout, A. Shkurenko, K. Adil, L.J. Barbour, M. Eddaoudi, A fine-tuned metal–organic framework for autonomous indoor moisture control, *J. Am. Chem. Soc.* 139 (2017) 10715.
- [63] F. Gándara, H. Furukawa, S. Lee, O.M. Yaghi, High methane storage capacity in aluminum metal–organic frameworks, *J. Am. Chem. Soc.* 136 (2014) 5271.
- [64] K. Sumida, M.R. Hill, S. Horike, A. Dailly, J.R. Long, Synthesis and hydrogen storage properties of  $Be_{12}(OH)_{12}(1,3,5\text{-benzenetribenzoate})_4$ , *J. Am. Chem. Soc.* 131 (2009) 15120.
- [65] S. Lee, E.A. Kapustin, O.M. Yaghi, Coordinative alignment of molecules in chiral metal–organic frameworks, *Science* 353 (2016) 808.
- [66] V. Guillermin, J. WeselińskiŁukasz, Y. Belmabkhout, A.J. Cairns, V. D’Elia, Ł. Wojtas, K. Adil, M. Eddaoudi, Discovery and introduction of a (3,18)-connected net as an ideal blueprint for the design of metal–organic frameworks, *Nat. Chem.* 6 (2014) 673.
- [67] D.-Y. Du, J.-S. Qin, Z. Sun, L.-K. Yan, M. O’Keeffe, Z.-M. Su, S.-L. Li, X.-H. Wang, X.-L. Wang, Y.-Q. Lan, An unprecedented (3,4,24)-connected heteropolyoxozincate organic framework as heterogeneous crystalline Lewis acid catalyst for biodiesel production, *Scientific Rep.* 3 (2013) 2616.
- [68] S. Biswas, M. Grzywa, H.P. Nayek, S. Dehnen, I. Senkowska, S. Kaskel, D. Volkmer, A cubic coordination framework constructed from benzobistriazolone ligands and zinc ions having selective gas sorption properties, *Dalton Trans.* (2009) 6487.

- [69] M. Dincă, A. Dailly, Y. Liu, C.M. Brown, D.A. Neumann, J.R. Long, Hydrogen storage in a microporous metal–organic framework with exposed Mn<sup>2+</sup> coordination sites, *J. Am. Chem. Soc.* 128 (2006) 16876.
- [70] M. Dincă, W.S. Han, Y. Liu, A. Dailly, C.M. Brown, J.R. Long, Observation of Cu<sup>2+</sup>-H<sub>2</sub> interactions in a fully desolvated sodalite-type metal–organic framework, *Angew. Chem. Int. Ed.* 46 (2007) 1419.
- [71] Y.-X. Tan, Y.-P. He, J. Zhang, Pore partition effect on gas sorption properties of an anionic metal-organic framework with exposed Cu<sup>2+</sup> coordination sites, *Chem. Commun.* 47 (2011) 10647.
- [72] N.M. Padial, E. Quartapelle Procopio, C. Montoro, E. López, J.E. Oltra, V. Colombo, A. Maspero, N. Masciocchi, S. Galli, I. Senkowska, S. Kaskel, E. Barea, J.A.R. Navarro, Highly hydrophobic isorecticular porous metal–organic frameworks for the capture of harmful volatile organic compounds, *Angew. Chem. Int. Ed.* 52 (2013) 8290.
- [73] J. An, O.K. Farha, J.T. Hupp, E. Pohl, J.I. Yeh, N.L. Rosi, Metal-adeninate vertices for the construction of an exceptionally porous metal-organic framework, *Nat. Commun.* 3 (2012) 604.
- [74] J. An, S.J. Geib, N.L. Rosi, Cation-triggered drug release from a porous zinc–adeninate metal–organic framework, *J. Am. Chem. Soc.* 131 (2009) 8376.
- [75] J.J. Perry IV, J.A. Perman, M.J. Zaworotko, Design and synthesis of metal–organic frameworks using metal–organic polyhedra as supermolecular building blocks, *Chem. Soc. Rev.* 38 (2009) 1400.
- [76] M. Eddaoudi, J. Kim, J.B. Wachter, H.K. Chae, M. O’Keeffe, O.M. Yaghi, Porous metal–organic polyhedra: 25 Å cuboctahedron constructed from 12 Cu<sub>2</sub>(CO<sub>2</sub>)<sub>4</sub> paddle-wheel building blocks, *J. Am. Chem. Soc.* 123 (2001) 4368.
- [77] B. Moulton, J. Lu, A. Mondal, M.J. Zaworotko, Nanoballs: nanoscale faceted polyhedra with large windows and cavities, *Chem. Commun.* (2001) 863.
- [78] F. Nouar, J.F. Eubank, T. Bousquet, L. Wojtas, M.J. Zaworotko, M. Eddaoudi, Supermolecular building blocks (SBBs) for the design and synthesis of highly porous metal-organic frameworks, *J. Am. Chem. Soc.* 130 (2008) 1833.
- [79] O.K. Farha, I. Eryazici, N.C. Jeong, B.G. Hauser, C.E. Wilmer, A.A. Sarjeant, R.Q. Snurr, S.T. Nguyen, A.Ö. Yazaydin, J.T. Hupp, Metal–organic framework materials with ultrahigh surface areas: is the sky the limit? *J. Am. Chem. Soc.* 134 (2012) 15016.
- [80] J.F. Eubank, F. Nouar, R. Luebke, A.J. Cairns, L. Wojtas, M. Alkordi, T. Bousquet, M.R. Hight, J. Eckert, J.P. Embs, P.A. Georgiev, M. Eddaoudi, On demand: the singular rht net, an ideal blueprint for the construction of a metal–organic framework (MOF) platform, *Angew. Chem. Int. Ed.* 51 (2012) 10099.
- [81] C. Serre, F. Millange, C. Thouvenot, M. Noguès, G. Marsolier, D. Louër, G. Férey, Very large breathing effect in the first nanoporous chromium(III)-based solids: MIL-53 or Cr<sup>III</sup>(OH)·{O<sub>2</sub>C–C<sub>6</sub>H<sub>4</sub>–CO<sub>2</sub>}·{HO<sub>2</sub>C–C<sub>6</sub>H<sub>4</sub>–CO<sub>2</sub>H}<sub>x</sub>·H<sub>2</sub>O<sub>y</sub>, *J. Am. Chem. Soc.* 124 (2002) 13519.
- [82] N.L. Rosi, J. Kim, M. Eddaoudi, B. Chen, M. O’Keeffe, O.M. Yaghi, Rod packings and metal–organic frameworks constructed from rod-shaped secondary building units, *J. Am. Chem. Soc.* 127 (2005) 1504.
- [83] K. Barthelet, J. Marrot, D. Riou, G. Férey, A breathing hybrid organic–inorganic solid with very large pores and high magnetic characteristics, *Angew. Chem. Int. Ed.* 41 (2002) 281.
- [84] P. Horcajada, C. Serre, G. Maurin, N.A. Ramsahye, F. Balas, M.A. Vallet-Regí, M. Sebban, F. Taulelle, G.R. Férey, Flexible porous metal-organic frameworks for a controlled drug delivery, *J. Am. Chem. Soc.* 130 (2008) 6774.
- [85] Catarineu, N.; Schoedel, A.; Urban, P.; Morla, M.; Yaghi, O.M., Reticular synthesis of a complex metal-organic framework from a heterotritopic linker, Unpublished results, 2016.
- [86] H. Deng, S. Grunder, K.E. Cordova, C. Valente, H. Furukawa, M. Hmadeh, F. Gándara, A.C. Whalley, Z. Liu, S. Asahina, H. Kazumori, M. O’Keeffe, O. Terasaki, J.F. Stoddart, O.M. Yaghi, Large-pore apertures in a series of metal-organic frameworks, *Science* 336 (2012) 1018.
- [87] A. Schoedel, M. Li, D. Li, M. O’Keeffe, O.M. Yaghi, Structures of metal–organic frameworks with rod secondary building units, *Chem. Rev.* 116 (2016) 12466.

# Mixed-metal systems for the synthesis of MOFs

Jianqiang Liu, Ying Pan

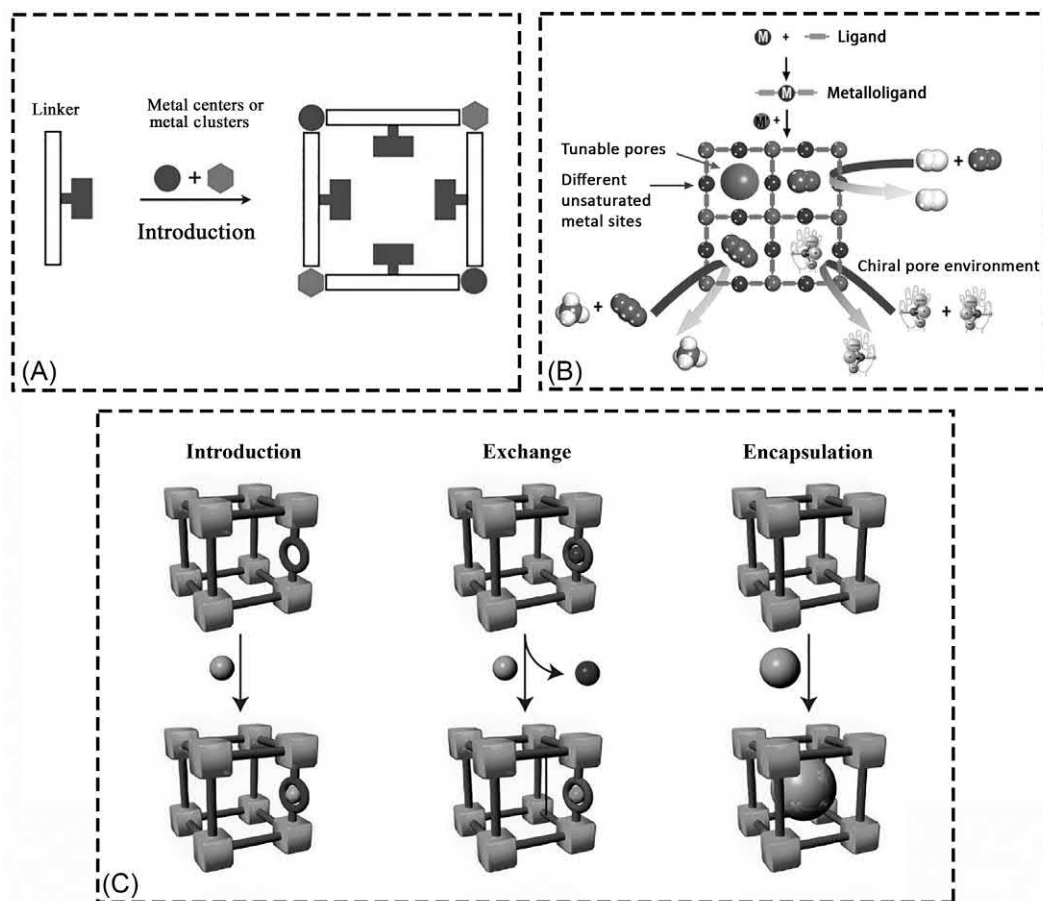
*School of Pharmacy, Guangdong Medical University, Dongguan, PR China*

## 3.1 Introduction

Metal-organic frameworks (MOFs) are a novel type of crystalline porous materials, which are governed by the precise combination of metal atoms with the organic struts [1–4]. The multiple coordination chemistry of the metal cations, coupled with the availability of diverse organic ligands, enables MOFs to be an attractive platform to integrate various functional building blocks into one MOF system for multifunctional applications [5–7]. Therefore, the selection of the metal resources and organic ligands is crucial for the design and synthesis of novel functionalized MOF materials for specific applications in many fields [8]. Due to the versatility and flexibility in MOF design and synthesis, the developed mixed-metal strategy over MOFs allows for the incorporation of more than one types of metal center within the same skeleton to afford heterometallic-organic frameworks [9, 10].

Mixed-metal-organic frameworks (MM-MOFs), in which two or more types of metal ions are periodically arrayed throughout the framework, endow them with an additional degree of structural diversity and a variety of advanced applications [10–13]. Dramatically, in comparison to MOFs constructed with a single metal, heterometallic MOFs based on diverse metal-containing building units have the following advantages: (i) exhibit a characteristic and novel topological network; (ii) effectively improve the type and density of active metal sites; (iii) easily facilitate the formation of ionic skeletons; (iv) facilitate the construction of a hierarchical channel, which can strengthen and boost the interaction forces of the host and guest molecules. In view of the above situation, kinds of novel heterometallic MOFs have been reasonably designed, which have been used in many fields (such as high-efficiency gas capture and separation) because of synergetic or cooperative effects of different metals within one structure [14–17]. However, the systematic research and exploration on the synthetic methodology and applications of heterometallic MOFs are still immature.

One common methodology for the building of heterometallic MOFs is to incorporate more than one type of metal cations to react with multicoordinated sites linkers in self-assembly. In other words, heterometallic MOFs were constructed by more than two building blocks (e.g., two metals plus linkers), which usually combined with N-donor and O-donor coligand (Fig. 3.1A). From the processes of chemical synthesis, these heterometallic MOFs are generally obtained by the solvothermal conditions through the mixtures of the suitable metal salts and the organic linker in highly polar solvents [18–20]. The second approach is to introduce metal-organic complexes as precursors to further bind to the metal cations (Fig. 3.1B). The metalloligands are



**Fig. 3.1**

Routes for syntheses of heterometallic MOFs: (A) direct self-assembly; (B) metalloligand as precursor; (C) postsynthetic metalation (PSMet). Copyright from A.D. Burrows, *Mixed-component metal-organic frameworks (MC-MOFs): enhancing functionality through solid solution formation and surface modifications*, *CrystEngComm* 13 (2011) 3623–3642; D.J. Evans, C.J. Sumby, C.J. Doonan, *Post-synthetic metalation of metal-organic frameworks*, *Chem. Soc. Rev.* 43 (2014) 5933–5951; C.D. Madhab, S.C. Xiang, Z.J. Zhang, B.L. Chen, *Functional mixed metal-organic frameworks with metalloligands*, *Angew. Chem. Int. Ed.* 50 (2011) 10510–10520.

utilized to bind with the second metal ions or metal clusters to form the heterometallic MOFs. This approach will tune the pore sizes and curvatures and rationally immobilize different metal sites (such as open metal sites, catalytically active metal sites, and photoactive metal sites). The third method is postsynthetic metalation of MOFs; postsynthetic metalation (PSMet) can be categorized into three pathways (Fig. 3.1C) [17]: (a) metal introduction in the functional groups; (b) ion exchange in charged frameworks; or, (c) host-guest encapsulation of metal-containing molecules within the pores. Six general strategies have been exploited for the postsynthetic metal introduction to frameworks, including direct introduction to noncoordinated functional groups; construction of a binding site at the linker; liberating binding groups by an orthogonal deprotection step; formation of a coordinating site at a node; outright linker exchange; and direct framework addition during the formation of a new organometallic entity. The ion exchange in charged frameworks was developed and mainly contained two approaches, exchange of metals coordinated to organic linkers and exchange of extra-framework cations. However, the encapsulation of various metal-based guests from the MOF host matrix has been employed and categorized as guest introduction, nanoparticle formation, and “ship-in-a-bottle” self-assembly.

In fact, the feature of the integrating heterometallic MOFs is also an effective way of increasing structural variation, which can result in the synergetic or cooperative effects [21–24]. It is foreseen that a variety of heterometallic MOFs will exhibit great promise in gas storage and separation, enantioselective separation, heterogeneous catalysis, sensing, and as photoactive and nanoscale drug delivery and biomedical imaging materials in the near future.

In this chapter, we summarized the synthetic strategy and structural diversity of the mixed-metal MOFs system. A short discussion of the still remaining challenges in this new domain of research is also proposed at the end of this chapter.

## **3.2 Mixed-metal MOFs**

### **3.2.1 Mixed-metal MOFs with alkali metals**

Alkaline cations can serve as favorable components in MOFs assembly because of their versatile coordinative geometry, low polarizability, and unique affinity for various linkers [25]. Some documents have indicated that the introduction of  $\text{Na}^+/\text{K}^+$  cations can be taken as a feasible heterometallic strategy to change the size and geometry of the clusters, which will induce the functional properties of MOFs [26]. Thus, the incorporation of alkali-metal ions into the heterometallic framework is attractive because the alkali cations are related to the active adsorption sites in the context of adsorbents. It is very necessary to understand the role of alkali-metal cations in modulating the assemblies of MOFs with unique architectures and excellent properties.



Du et al. reported two isostructural heterometallic MOFs,  $\{[\text{Cd}_3\text{M}_6(\text{TDPAT})_2(\text{H}_2\text{O})_9] \cdot x\text{solvent}\}$  ( $\text{M} = \text{K}$  and  $\text{Rb}$ ,  $\text{H6TDPAT} = 2,4,6\text{-tris}(3,5\text{-dicarboxylphenylamino})\text{-}1,3,5\text{-triazine}$ ) [27], which were synthesized via solvothermal reaction. Both of them are 3D chiral frameworks constructed by interpenetration of two identical 3D cage nets, which feature a giant double-walled heterometallic cage  $\text{M}_{36}\text{Cd}_{24}(\text{TDPAT})_8 @ \text{M}_{54}\text{Cd}_{24}(\text{TDPAT})_8$  (Fig. 3.2). Later, they also have obtained series of heterometallic MOFs using the reactions of  $\text{Pb}(\text{OAc})_2 \cdot 3\text{H}_2\text{O}$ ,  $\text{MNO}_3$  ( $\text{M} = \text{K}$ ,  $\text{Rb}$ , and  $\text{Cs}$ ) with  $m\text{-H}_2\text{BDC}$  ( $1,3\text{-H}_2\text{BDC} = 1,3\text{-benzenedicarboxylic acid}$ ) in a mixed-solvent of DMF and methanol ( $v/v = 2/1$ ). They show 3D coordination frameworks built by a novel 12-metal heterometallic  $\text{Pb}_6\text{-M}_6$  cage [28]. A heterometallic layered complex of  $\{[\text{Eu}_2\text{Na}(\text{Hpddb})(\text{pddb})_2(\text{CH}_3\text{COO})_2] \cdot 2.5(\text{DMA})\}$  was designed and synthesized. It has been used to detect the nitrofurant antibiotics and toxic

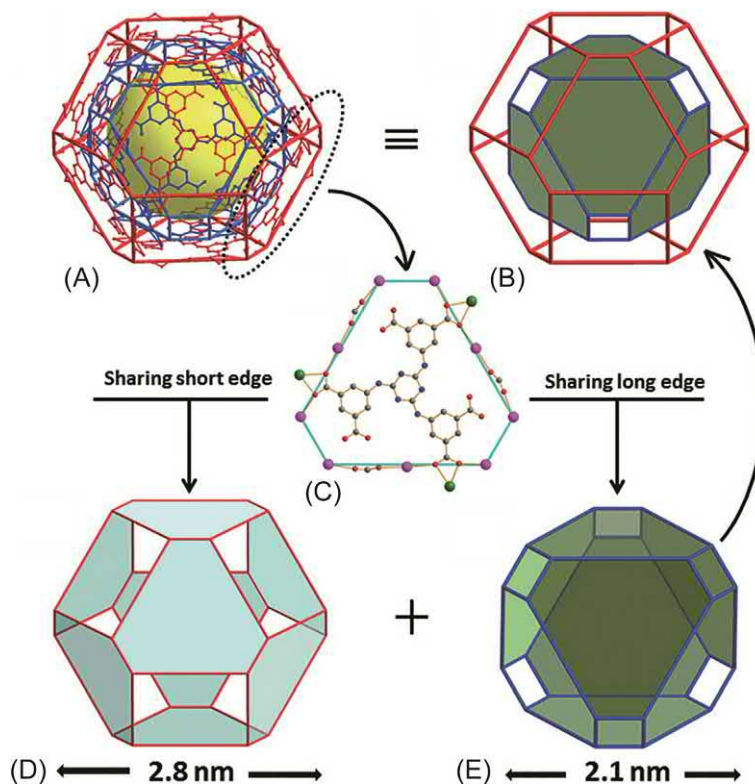


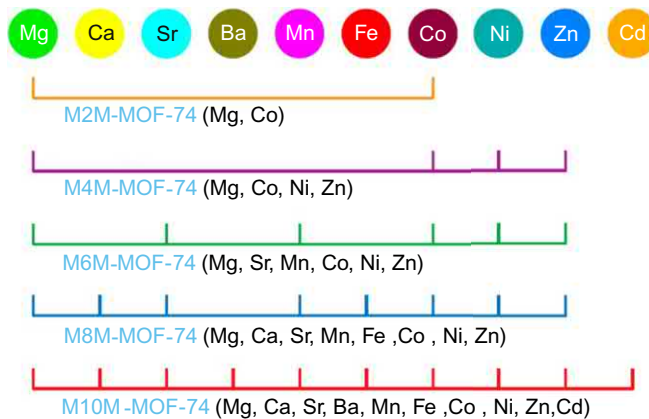
Fig. 3.2

(A,B) The cage-within-cage network. (C) The hexagonal face constructed from 1 TDPAT ligand, 9  $\text{K}^+$  and 3  $\text{Cd}^{2+}$  ions ( $\text{Cd}$ , green;  $\text{K}$ , pink;  $\text{C}$ , gray;  $\text{O}$ , red;  $\text{N}$ , dark blue). (D) The outer tetrakaidecahedral cage  $\text{K}_{54}[\text{Cd}_3(\text{TDPAT})]_8$ . (E) The inner tetrakaidecahedral cage  $\text{K}_{36}[\text{Cd}_3(\text{TDPAT})]_8$ . Copyright from X.W. Xu, C.B. Tian, S.W. Du, *Synthesis, structure and luminescence properties of two  $\text{Cd}(\text{II})/\text{M}(\text{I})$  ( $\text{M} = \text{K}$ ,  $\text{Rb}$ ) interpenetrated heterometallic frameworks based on giant double-walled cages*, *CrystEngComm* 19 (2017) 4269–4272.

inorganic anions. These interesting results indicate that heterometallic materials can serve as favorable multiple-responsive luminescence sensors to selectively recognize different kinds of contaminants [29]. Ptak et al. had synthesized two heterometallic perovskite-type metal-organic frameworks (MOFs) containing the ammonium cation ( $\text{NH}_4^+$ ,  $\text{Am}^+$ ):  $[\text{NH}_4][\text{Na}_{0.5}\text{Cr}_{0.5}(\text{HCOO})_3]$  ( $\text{AmNaCr}$ ) and  $[\text{NH}_4][\text{Na}_{0.5}\text{Al}_{0.475}\text{Cr}_{0.025}(\text{HCOO})_3]$  ( $\text{AmNaAlCr}$ ). The optical properties show that both of these two materials exhibit  $\text{Cr}^{3+}$ -based emission characteristic of intermediate ligand field strength [30]. Du have tried to design and synthesize a series of novel MOFs assembled from  $\text{Pb}^{\text{II}}$  and 2,3,5,6-tetrachloro-1,4-benzenedicarboxylic acid by simply adding different alkali-metal ions as templates. Some of their structures showed 3D rod-packing  $\text{Pb}^{\text{II}}$ -carboxylate framework and a  $3\text{DNa}^{\text{I}}$ -BDC- $\text{Cl}_4$  (or  $\text{Li}^{\text{I}}$ -BDC- $\text{Cl}_4$ ) network. The results illustrate the powerful effect of the alkali-metal templates in MOFs assemblies [25].

### 3.2.2 Mixed-metal MOFs with alkaline earth metals

Earth abundant alkaline earth metal centers (Mg, Ca, Sr, Ba), which possess several unique attributes such as low-weight, low-cost as well as low-toxic, etc., serve as good candidates to construct multifunctional heterometallic MOFs. As an archetypical alkaline earth metal ion,  $\text{Mg}^{2+}$  is most commonly used to build MM-MOFs. The typical example is MOF-74.  $\text{Mg}^{2+}$  is the cation present in the “original” MOF-74 [31], which can coexist with several metal ions in a single-crystal structure. For example, Yaghi and coworkers reported the syntheses and characterization of a series of isostructural MM-MOFs, containing 2 (Mg, Co), 4 (Mg, Co, Ni, Zn), 6 (Mg, Sr, Mn, Co, Ni, Zn), 8 (Mg, Ca, Sr, Mn, Fe, Co, Ni, Zn), and 10 (Mg, Ca, Sr, Ba, Mn, Fe, Co, Ni, Zn, Cd),



**Fig. 3.3**

Combination of metal ions used to synthesize MM-MOF-74. Copyright from S.R. Caskey, A.G. Wong-Foy, A.J. Matzger, *Dramatic tuning of carbon dioxide uptake via metal substitution in a coordination polymer with cylindrical pores*, *J. Am. Chem. Soc.* 130 (2008) 10870–10871.

Fe, Co, Ni, Zn, Cd) divalent metals (Fig. 3.3). These materials were obtained through a one-pot solvothermal reaction. H<sub>4</sub>DOT (DOT = 2,5-dioxidoterephthalate) and the equimolar amounts of specific metal salts (nitrate salts of Mg, Ca, Sr, Ba, Mn, Co, Ni, Zn and acetate salts of Fe and Cd) were dissolved in a [10:0.6:0.6 (v/v/v)] mixture of DMF-ethanol-water, while the mixture was placed in a vial and heated at 120°C for 20–24 h to yield crystalline MM-MOF-74 samples [32]. Interestingly, the EDS results implied that each of these MM-MOF-74 crystals contains all of the expected metals, but the distribution of these metals in MOFs may be different. It is worth noting that the final molar ratio of the metal ions in a single-crystal is influenced by many factors, including the reactivity, solubility, and coordination environment of the metal ions and the pH of the reaction system.

Besides the aforementioned strategy for the synthesis of alkaline earth mixed-metal MOFs in a single step, a different stepwise synthetic strategy has also been commonly explored, which uses the appropriate metal complexes as “ligands”, i.e., one type of the metal ion first assembled with the ligand, leaving other coordination sites to combine the second kind of metal ions. Chen et al. reported a series of transition/alkaline earth MM-MOFs from 1D to 3D by selected  $[\text{Cu}^{\text{II}}(\text{pzdc})_2]^{2-}/[\text{M}^{\text{II}}(\text{Hpzdc})_2]$  ( $\text{M} = \text{Co}$  or  $\text{Ni}$ ) ( $\text{H}_2\text{pzdc} = \text{pyrazine 2,3-dicarboxylic acid}$ ,  $\text{ampy} = 2\text{-amino-4-methylpyridine}$ ) as “metalloligands” to connect with the alkaline earth cations ( $\text{Ca}^{2+}$ ,  $\text{Sr}^{2+}$ ,  $\text{Ba}^{2+}$ ) [33]. In general, different “metalloligands”  $[\text{Co}(\text{Hpzdc})_2(\text{H}_2\text{O})_2]$  ( $L_{\text{Co}}$ ),  $[\text{Ni}(\text{Hpzdc})_2(\text{H}_2\text{O})_2]$  ( $L_{\text{Ni}}$ ), and  $[\text{Cu}(\text{pzdc})_2(\text{H}_2\text{O})_2] \cdot 2\text{ampy} \cdot 6\text{H}_2\text{O}$  ( $L_{\text{Cu}}$ ) were first synthesized through a simple reaction. Typically, 1 mmol of ( $L_{\text{Co}}$ ,  $L_{\text{Ni}}$ , or  $L_{\text{Cu}}$ ) was dissolved in 20 mL of ethanol, then 2 mmol of the alkaline earth salts ( $\text{Ca}(\text{NO}_3)_2$ ,  $\text{SrCl}_2$ , or  $\text{BaCl}_2$ ) was added to the mixture with stirring at room temperature for half an hour. After the filtrate slowly evaporates at room temperature, the rod crystals were obtained. The above results indicated that the ionic radii of the alkaline earth cations and the different types of the alkaline earth metal salts anions have a significant influence on the structural diversities. Pombeiro et al. developed a new 2D heterometallic  $\text{Cu}^{\text{II}}/\text{Mg}$  coordination polymer by using  $\text{Cu}(\text{NO}_3)_2$  and  $\text{H}_3\text{tea}$  (triethanolamine) as a main ligand source, then added  $\text{Mg}(\text{OH})_2$  (pH regulator and building block) to the alkalization of the obtained mixture, followed by the addition of lithium pyromellitate as spacer source to in situ generated  $\text{LiOH}$  and  $\text{H}_4\text{pma}$  (1,2,4,5-benzenetetracarboxylic acid) self-assembly to form the  $[\text{Cu}_2\text{Mg}_2(\mu\text{-Htea})_2(\mu_6\text{-pma})(\text{H}_2\text{O})_6]_n \cdot 6n\text{H}_2\text{O}$ . The crystal structure of these  $\text{Cu}/\text{Mg}$ -MOFs is composed by infinite interdigitated 2D metal-organic layers, which extend to an intricate 3D supramolecular framework via H-bonds, demonstrating an unprecedented  $[\text{Cu}_2\text{Mg}(\mu\text{-O})_2(\mu\text{-COO})_2]^-$  core and a specific net topology [34].

Alkaline earth and lanthanide ions possess large radius, rich coordination geometries, and coordination numbers, which have great potential in the design and synthesis of these novel heterometallic alkaline earth-lanthanide MOFs with intriguing functional properties. For instance, Li and coworkers reported a unique 2D microporous alkaline earth-lanthanide MOFs  $\{[\text{Ba}_3\text{La}_{0.5}(\mu_3\text{-L})_{2.5}(\text{H}_2\text{O})_3(\text{DMF})] \cdot (3\text{DMF})\}_n$ , which is constructed by rigid asymmetrical

*p*-terphenyl-3,4'',5-tricarboxylic acid (H<sub>3</sub>L) tricarboxylate ligand Ba(NO<sub>3</sub>)<sub>2</sub> and Ln(NO<sub>3</sub>)<sub>3</sub>·6H<sub>2</sub>O under solvothermal conditions. A 1D microporous channel with window size of 9.151 Å × 10.098 Å can be detected along the crystallographic *a* axis [35]. Cheng et al. have been successfully synthesized by ten novel Ln<sup>III</sup>-Ba<sup>II</sup> MM-MOFs (Ln = Pr, Sm, Eu, Gd, Tb, Dy, Lu) under the hydrothermal reaction of H<sub>2</sub>PDA (PDA = pyridine-2,6-dicarboxylic anion), Ba(OH)<sub>2</sub>·3H<sub>2</sub>O, and Ln(NO<sub>3</sub>)<sub>3</sub>·6H<sub>2</sub>O in a mixture of water [36]. The varieties of these 10 topological structures originated from two aspects: (i) the lanthanide contraction effect, which solely depend on the size of lanthanide ions; (ii) depending on the amount of Ba(OH)<sub>2</sub> added in the synthesis systems. Constructing alkaline earth metal-containing heterometallic coordination networks with intriguing structures and outstanding properties gives rise to a new perspective of crystallographic engineering.

### 3.2.3 Mixed-metal MOFs with *d*<sup>10</sup> metals

MOFs with polynuclear *d*<sup>10</sup> configurational metal (Cu<sup>I</sup>, Ag<sup>I</sup>, Au<sup>I</sup>, Zn<sup>II</sup>, or Cd<sup>II</sup>) have attracted intense interest over the past decade; these novel *d*<sup>10</sup>-MOFs not only possess appealing structures, but also exhibit unique photoluminescent properties [37–39]. In recent years, there has been a growing interest to investigate the new mixed-metal MOFs with *d*<sup>10</sup> metals, which provide abundant probabilities for structural design and property modulation. Using metal-oxo anions (such as CrO<sub>4</sub><sup>2-</sup>, Cr<sub>2</sub>O<sub>7</sub><sup>2-</sup>) as secondary ligands to bind the other metal cations opens up new opportunities to develop novel heterometallic MOFs [40, 41]. Wang and coworkers reported the preparation of two heterometallic MOFs based on Ag<sup>+</sup> and Cr<sub>2</sub>O<sub>7</sub><sup>2-</sup> through solvent-mediated anion-induced crystal-to-crystal transformations using a monometallic cationic MOF as a precursor. The inorganic Cr<sub>2</sub>O<sub>7</sub><sup>2-</sup> anions act as secondary ligand to form effective Ag—O—Cr bonds in the formation of Ag/Cr bimetallic MOFs. When immersing monometallic MOF Ag<sub>2</sub>(btr)<sub>2</sub>·2ClO<sub>4</sub>·3H<sub>2</sub>O, [btr = 4,4'-bis(1,2,4-triazole)] in the aqueous solutions of NaBF<sub>4</sub>·K<sub>2</sub>Cr<sub>2</sub>O<sub>7</sub> and KPF<sub>6</sub>·K<sub>2</sub>Cr<sub>2</sub>O<sub>7</sub>, respectively, red crystals of Ag<sub>9</sub>(btr)<sub>6</sub>(Cr<sub>2</sub>O<sub>7</sub>)<sub>4</sub>·PF<sub>6</sub>·6H<sub>2</sub>O and yellow crystals of Ag<sub>2</sub>(btr)<sub>2</sub>Cr<sub>2</sub>O<sub>7</sub>·0.5H<sub>2</sub>O were successfully synthesized. Interestingly, the presence of noncoordination KPF<sub>6</sub> and NaBF<sub>4</sub> in K<sub>2</sub>Cr<sub>2</sub>O<sub>7</sub> solution serves as structure-directing agents during the solvent-mediated structural transformations; the preparation of these Ag/Cr MOFs was fruitless under the same conditions without BF<sub>4</sub><sup>-</sup>/PF<sub>6</sub><sup>-</sup> anions [42]. This work provides a new strategy for the formation of novel heterometallic MOFs which cannot be obtained through conventional methods. Recently, Guo et al. successfully synthesized a CuTCPP MOFs materials by using Cu(NO<sub>3</sub>)<sub>2</sub>·3H<sub>2</sub>O and TCPP (5,10,15,20-tetrakis(4-carboxyphenyl)porphyrin) through the solvothermal reaction. Subsequently, the as-synthesized CuTCPP MOFs act as the carriers which were used to load the Ag nanoparticles and successfully prepared Ag-CuTCPP MOFs. Choosing an effective MOFs carrier to encapsulate the Ag nanoparticles not only maintains the activity of the Ag, but also controls the release of Ag ions and prevents the long-term direct contact between Ag ions and the normal tissues [43].

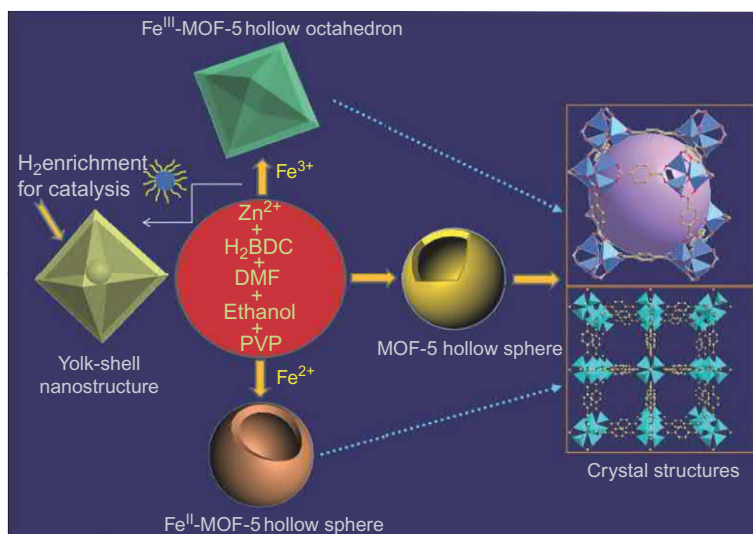
Currently, choosing an appropriate organic ligand as structural directing is an effective approach agent to synthesis new heterometallic MOFs. Zheng et al. using a tripodal alcohol ligands ( $H_3L$ , 2-(hydroxymethyl)-2-(pyridin-4-yl)-1,3-propanediol) as structural directing agent to in situ formed two 4-connected heterometallic supertetrahedral SBUs with high-nuclearity metal clusters. Two 3D novel zeolite-like MM-MOF,  $Cu[Cd_4Cu_6(L)_4(H_2O)_{18}](Ac)_9 \cdot DMA \cdot 3H_2O$  and  $Cu[Mn_4Cu_6(L)_4(Ac)_3(H_2O)_{12}](Ac)_6 \cdot CH_3CN \cdot 13H_2O$ , have been successfully synthesized by solvothermal reaction, which represent the first cases of zeolite-like cluster organic frameworks based on Cd-Cu and Mn-Cu heterometallic supertetrahedral building units. Although both of them are composed by similar SBUs, they exhibit entirely different framework topologies, indicating the tunability flexible structure of these materials [44]. In brief, choosing an appropriate linker as structural directing agent to construct unique clusters is an effective way to explore zeolite-like organic-inorganic hybrid heterometallic frameworks.

Zinc is one of the most classic  $d^{10}$  metals to construct MOFs. As the increasing research on MOFs, the mixed-metal MOFs containing  $Zn^{2+}$  have been widely studied. For instance, Zou and coworkers investigated the reaction kinetics for Zn and Co ions in a bimetallic MOF system, employing the typical ZIF-8/67 ( $M(2-mIM)_2$ ,  $M = Zn$  for ZIF-8, and  $Co$  for ZIF-67,  $2-mIM = 2$ -methylimidazole) as a proof-of-concept model. By substituting the single metal salt solutions with the mixtures of two metal salts following the same steps, a series of Co/Zn mixed-metal ZIFs were prepared (denoted as  $Co_xZn_{100-x}$ -ZIF, where  $x$  is the molar percentage of cobalt in total metals). When both Zn and Co ions are present in the starting solution, Co-rich cores to Zn-rich shells can be observed at low Co/Zn ratio concentration gradient, while at high Co/Zn ratio homogeneous distributions of the two metals can be achieved. What's more, by adding these two metals in sequence, more sophisticated structures are presented. Particularly, when first added the  $Co^{2+}$ , ZIF-67@ZIF-8/67 core-shell nanocrystals are obtained with controllable core/shell thickness ratio; when first added the  $Zn^{2+}$ , due to the weak nucleation ability of  $Zn^{2+}$ , only agglomerates of irregular shape can be observed [45].

Metal partial substitution has been employed as effective strategy to generate heterometallic MOFs which contain different types of metal ion. Li et al. successfully synthesized water-stable metal MM-MOFs by simply doping metal ions ( $Cu^{2+}$ ,  $Cd^{2+}$ , or  $Fe^{2+}$ ) into the STU-1s ( $Zn(BIm)$ ) frameworks via a direct synthetic route. To improve the stability of MOFs, metal-ion metathesis was employed by altering the existing metal ions (e.g.,  $Zn^{2+}$ ) with more inert metal species (e.g.,  $Cu^{2+}$ ,  $Cd^{2+}$ , and  $Fe^{2+}$ ), thereby reforming the thermodynamic stability factors of the MOF skeleton. Five synthesis methods have been explored to achieve  $Cu^{2+}$  doped STU-1s, including direct heating, solvothermal, slow diffusion, microwave, and mechanical synthesis. Four different  $Cu^{2+}$  doped STU-1 samples (denoted as  $Cu_{0.01}$ -STU-1,  $Cu_{0.05}$ -STU-1,  $Cu_{0.10}$ -STU-1, and  $Cu_{0.167}$ -STU-1) can be obtained by

adjusting the Zn/Cu mole ratios (Zn/Cu: 99/1, 95/5, 90/10, and 5/1, respectively). Likewise,  $\text{Cd}^{2+}$  doped  $\text{Cd}_{0.6}$ -STU-1 and  $\text{Fe}^{2+}$  doped  $\text{Fe}_{0.10}$ -STU-1 samples were also successfully synthesized [46].

A typical and common representative MOFs, MOF-5, consists of  $\text{Zn}_4$  O-clusters and  $\text{H}_2\text{BDC}$  (benzene-1,4-dicarboxylate) linkers forming a cubic network [47]. Recently, Wang et al. prepared a series of well-defined bimetallic MOF nanocages ( $\text{Fe}$ -substituted MOF-5, denoted as  $\text{Fe}^{\text{II}}$ -MOF-5 and  $\text{Fe}^{\text{III}}$ -MOF-5) through a facile one-step solvothermal method, where zinc and ferric ions serve as metallic nodes,  $\text{H}_2\text{BDC}$  as organic ligands, PVP (poly(vinylpyrrolidone)) as stabilizing reagent, and DMF (*N,N*-dimethylformamide)/DMAC (*N,N*-dimethylacetamide)-ethanol as mixed solvent (Fig. 3.4) [48]. Significantly, when  $(\text{NH}_4)_2\text{SO}_4 \cdot \text{FeSO}_4 \cdot 6\text{H}_2\text{O}$  is added into the reaction system of MOF-5 hollow nanospheres,  $\text{Fe}^{\text{II}}$ -MOF-5 hollow nanospheres were yielded, indicating the coordination flexibility of the polymeric architectures. Impressively, when  $\text{Fe}(\text{acac})_3$  (iron(III) acetylacetonate) instead of  $(\text{NH}_4)_2\text{SO}_4 \cdot \text{FeSO}_4 \cdot 6\text{H}_2\text{O}$ ,  $\text{Fe}^{\text{III}}$ -MOF-5 could also be acquired, the PXRD pattern would be in accordance with the simulation of MOF-5. Interestingly, it is worth noting that the addition of PVP in the MOF-5 synthesis system leads to the formation of homogeneous  $\text{Fe}^{\text{III}}$ -MOF-5 with hollow octahedral nanostructures. What's more, it is also found that the solvent played a crucial role in determining the morphology of the obtained  $\text{Fe}^{\text{III}}$ -MOF-5. When DMAC is used as a solvent instead of DMF, abundant well-defined hollow octahedral



**Fig. 3.4**

A series of well-defined MOF hollow nanocages. Copyright from Z. Zhang, Y. Chen, X. Xu, J. Zhang, G. Xiang, W. He, X. Wang, Well-defined metal-organic framework hollow nanocages, *Angew. Chem. Int. Ed.* 53 (2014) 429–433.



nanostructures of Fe<sup>III</sup>-MOF-5 could be produced. Impressively, by prolonging the reaction time, the morphology evolution process from homogeneous MOF nanocrystals with high-energy facets and concave into hollow nanocages can be observed.

In recent years, lanthanide-d<sup>10</sup> heterometallic MOFs have attracted considerable interests because of their aesthetical structures and potential applications in different areas. Cao and coworkers reported three pillared-layer 4d-4f Ag(I)-Ln(III) MOFs with the formula of [Ln<sub>2</sub>Ag(hma)<sub>2</sub>(ina)(H<sub>2</sub>O)<sub>2</sub>]<sub>n</sub>·nH<sub>2</sub>O [Ln = La, Pr, Nd] under hydrothermal conditions by using H<sub>3</sub>hma (hemimellitic acid) and Hina (isonicotinic acid) as co-ligands and silver nitrate and lanthanide oxide/hydroxide as metal sources. In this pillared-layer architecture, H<sub>3</sub>hma have three neighboring carboxylate groups, which endow more versatile coordination modes between d<sup>10</sup> metal and lanthanide ions, while Hina is an excellent linear ligand containing both N and O heteroatoms, where N atom can readily coordinate with Ag(I) ion, generating Ag-ina pillars. This pillared-layer heterometallic structure construct by the alternate arrangement of lanthanide-organic layers and [Ag(ina)] pillars and the layers and pillars are connected by the Ln-O and Ag-O coordination bonds [49]. Other researchers have also used similar hydrothermal methods to prepare novel Ln-Ag MOFs as promising functional materials. For example, Cheng et al. synthesized two isostructural Ag(I)-Ln(III) heterometallic-organic frameworks {[Ln<sub>3</sub>Ag<sub>3</sub>(BPDC)<sub>5</sub>(OX)(H<sub>2</sub>O)<sub>7</sub>·7H<sub>2</sub>O]<sub>n</sub> (Ln = Tb, Gd) by employing H<sub>2</sub>BPDC (2,2'-bipyridine-3,3'-dicarboxylic acid) and H<sub>2</sub>OX (oxalic acid) as mixed-ligand under hydrothermal conditions [50]. As the 4d metal ion, the coordination numbers of Ag<sup>+</sup> can vary from two to six and different coordination geometries such as linear, trigonal, tetrahedral, trigonal pyramidal, and octahedral can be obtained, which may provide numerous opportunities to form 4d-4f heterometallic-organic frameworks.

Recently, many d<sup>10</sup>-Ln mixed-metal MOFs have been reported by researchers. For instance, two 3D solvent-stable Zn(II)-Ln(III) heterometallic MOFs {[ (CH<sub>3</sub>)<sub>2</sub>NH<sub>2</sub>]<sub>2</sub>[Zn<sub>2</sub>Ln<sub>2</sub>(FDA)<sub>6</sub>(DMF)<sub>2</sub>·2DMF]<sub>n</sub> (Ln = Eu and Tb) assembled with Zn<sub>2</sub>Ln<sub>2</sub>(COO)<sub>10</sub> tetrametallic clusters and H<sub>2</sub>FDA (furan-2,5-dicarboxylic acid) have been successfully prepared by Cui and coworkers. These two yellow block crystals can be obtained by zinc nitrates and lanthanide nitrates with H<sub>2</sub>FDA in DMF at 120°C [51]. Zhao and coworkers successfully synthesized a 4d-4f heterometallic Yb-Cd MOF {[Yb<sub>2</sub>(L)<sub>6</sub>Cd<sub>2</sub>][Cd(H<sub>2</sub>O)<sub>6</sub>·6H<sub>2</sub>O]<sub>n</sub> (H<sub>2</sub>L = oxidiacetic acid) under hydrothermal conditions. In detail, the mixture of Yb<sub>2</sub>O<sub>3</sub>, Cd(NO<sub>3</sub>)<sub>2</sub>·4H<sub>2</sub>O, H<sub>2</sub>L, and H<sub>2</sub>O were heated at 180°C for 3 days to afford Yb-Cd crystals. In this structure, each L coordinates with one Yb<sup>3+</sup> center and chelates with two Cd<sup>2+</sup> ions in an anti-anti configuration, where the Yb and Cd atoms are connected by O—C—O bridges and arranged alternatively to form a cubic octahedral cage secondary building unit. Interestingly, the [Cd(H<sub>2</sub>O)<sub>6</sub>]<sup>2+</sup> cations staying in the porosity of the anionic Yb-Cd MOFs serve as the thermodynamically stable species to balance the negative [Yb<sub>2</sub>(L)<sub>6</sub>Cd<sub>2</sub>]<sup>2-</sup> in structure. Even more intriguing, when using these Yb-Cd as a precursor immersed in the aqueous solution of Mn(ClO<sub>4</sub>)<sub>2</sub>·6H<sub>2</sub>O or Zn(ClO<sub>4</sub>)<sub>2</sub>·6H<sub>2</sub>O, a reversible transformation process

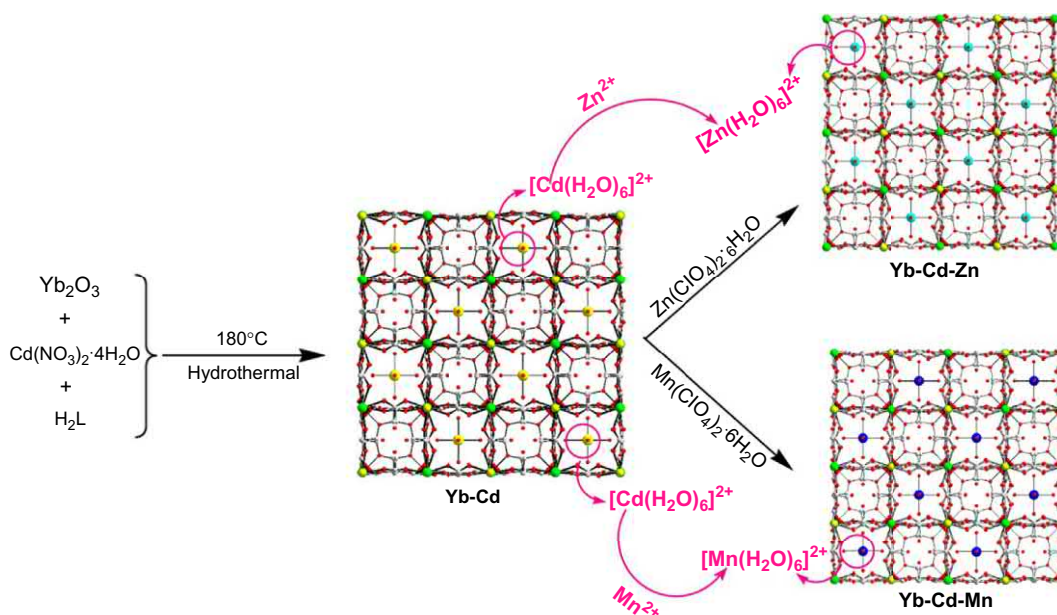


Fig. 3.5

Synthesis of Yb-Cd, Yb-Cd-Mn, and Yb-Cd-Zn. Copyright from Y. Wang, X.-G. Wang, B. Yuan, C.-Y. Shao, Y.-Y. Chen, B.-B. Zhou, M.-S. Li, X.-M. An, P. Cheng, X.-J. Zhao, Cation-exchange porosity tuning in a dynamic 4d-4f-3d framework for NiII ion-selective luminescent probe, *Inorg. Chem.* 54 (2015) 4456–4465.

from single-crystal to single-crystal driven by  $[\text{Cd}(\text{H}_2\text{O})_6]^{2+}$  cations can be observed, generating two 4d-4f-3d heterotrimetallic coordination polymer Yb-Cd-Mn ( $\{[\text{Yb}_2(\text{L})_6\text{Cd}_2][\text{Mn}(\text{H}_2\text{O})_6] \cdot 6\text{H}_2\text{O}\}_n$ ) or Yb-Cd-Zn ( $\{[\text{Yb}_2(\text{L})_6\text{Cd}_2][\text{Zn}(\text{H}_2\text{O})_6] \cdot 6\text{H}_2\text{O}\}_n$ ) (Fig. 3.5) [52]. In this regard, postsynthetic cation-exchange strategy is effective to obtain different heterotrimetallic MOFs.

Up to now, extensive efforts have been devoted to synthesize  $d^{10}$ -Ln MOFs with attractive features. Sun et al. synthesized a series of 3d-4f heterometallic coordination polymers ( $\{[\text{NH}_2(\text{CH}_2)_2]_2\text{LnCu}_2\text{Br}(\text{IN})_6 \cdot (\text{DMA})_2\}_n$  ( $\text{Ln} = \text{Sm}, \text{Eu}, \text{Gd}, \text{Tb}, \text{Dy}$ ), and  $[\text{LnCu}(\text{IN})_4 \cdot \text{DMA}]_n$  ( $\text{Ln} = \text{Er}, \text{Yb}$ )) under solvothermal condition based on a linear ligand HIN (isonicotinic acid), CuBr (cuprous halide), and lanthanide nitrate [53]. Zhang and coworkers developed a 3D heterometallic MOF  $[\text{Eu}_6\text{Zn}(\mu_3\text{-OH})_8(\text{NDC})_6(\text{H}_2\text{O})_6]_n$  by the reaction of electron-rich  $\pi$ -conjugated  $\text{H}_2\text{NDC}$  (1,4-naphthalenedicarboxylic acid),  $\text{Zn}(\text{NO}_3)_2$ , and  $\text{Eu}(\text{NO}_3)_3$  under solvothermal conditions [54]. Su's group obtained a family of isostructural 2D Cd(II)-lanthanide(III) heterometallic  $[\text{CdCl}(\text{L})\text{Eu}_x\text{Tb}_y(\text{H}_2\text{O})(\text{DMA})](\text{NO}_3) \cdot 3\text{DMA}$  frameworks by taking advantage of diverse molar ratios of Ln(III) and metalloligands through solvothermal reaction [55]. It's worth noting that metalloligands as metal-containing complexes have many advantages over the traditional organic ligands, such as metalloligands are more flexible to construct MOFs with diverse topologies; metalloligands with extra

coordination binding sites can further coordinate with the second metal ions and/or metal clusters, which is ideal candidates to construct heterometallic-organic frameworks through self-assembly and stepwise synthesis.

### 3.2.4 Mixed-metal MOFs with transition metals

Although numerous homometallic transition MOF structures have been reported, there has been relatively little progress in the synthesis and uses of heterometallic MOFs. In fact, some pioneering researches have already shown that the heterometallic MOFs exhibited superior properties to their counterpart monometallic MOFs and, in some cases, it can even endow new functionalities due to the introduction of the extra metal ions. Pombeiro and coworkers prepared two new stable heterometallic  $\text{Cu}^{\text{II}}/\text{Fe}^{\text{II}}$  MOFs  $[\text{Cu}_6(\text{H}_2\text{tea})_6\text{Fe}(\text{CN})_6]_n(\text{NO}_3)_{2n} \cdot 6n\text{H}_2\text{O}$  and  $[\text{Cu}_6(\text{Hmdea})_6\text{Fe}(\text{CN})_6]_n(\text{NO}_3)_{2n} \cdot 7n\text{H}_2\text{O}$  by facile aqueous-medium self-assembly reactions of  $\text{Cu}(\text{NO}_3)_2 \cdot 2.5\text{H}_2\text{O}$  with  $\text{H}_3\text{tea}/\text{H}_2\text{mdea}$  (triethanolamine/*N*-methyldiethanolamine),  $\text{K}_3[\text{Fe}(\text{CN})_6]$ , and  $\text{NaOH}$  under ambient conditions (Fig. 3.6) [56].

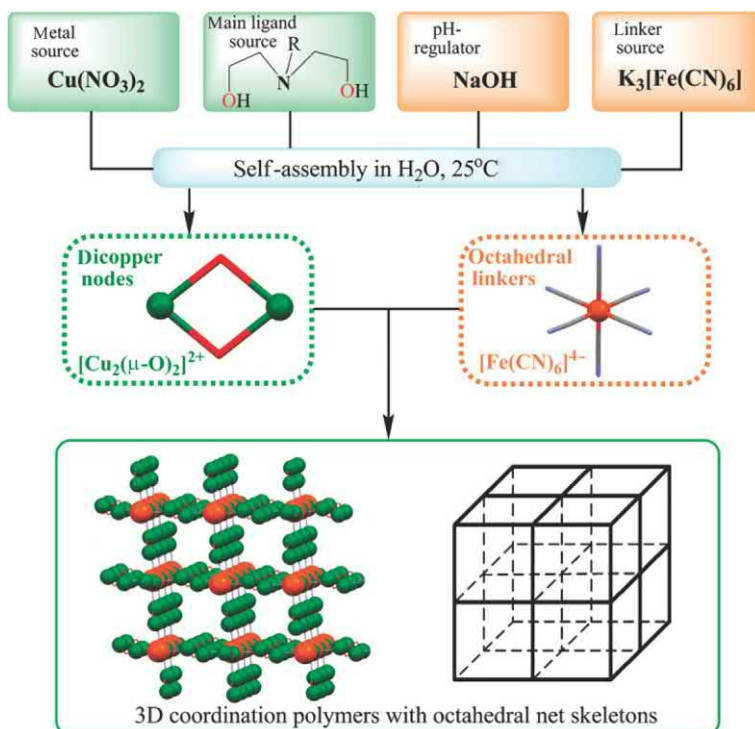


Fig. 3.6

Aqueous-medium self-assembly synthesis of heterometallic  $\text{Cu}^{\text{II}}/\text{Fe}^{\text{II}}$  metal-organic frameworks. Copyright from Y.Y. Karabach, M.F.C. Guedes da Silva, M.N. Kopylovich, B. Gil-Hernandez, J. Sanchiz, A.M. Kirillov, A.J.L. Pombeiro, *Self-assembled 3D heterometallic  $\text{Cu}^{\text{II}}/\text{Fe}^{\text{II}}$  coordination polymers with octahedral net skeletons: structural features, molecular magnetism, thermal and oxidation catalytic properties*, *Inorg. Chem.* 49 (2010) 11097–11105.

These 3D frameworks are constructed by the  $[\text{Cu}_2(\mu\text{-H}_2\text{tea})_2]^{2+}$  or  $[\text{Cu}_2(\mu\text{-Hmdea})_2]^{2+}$  nodes and the octahedral  $[\text{Fe}(\text{CN})_6]^{4-}$  linkers, featuring regular (1) or distorted (2) octahedral net skeletons, suggesting that a slight modification of the main ligand source leads to different structures.

Ohba and coworkers developed 3D pillared-layer trimetallic MOFs  $[\text{Co}_2\text{Ln}(\text{L})_2(\text{H}_2\text{O})_4][\text{Cr}(\text{CN})_6] \cdot n\text{H}_2\text{O}$  (Ln = La, Gd;  $\text{H}_2\text{L}$  = 2,6-di(acetoacetyl)pyridine) by stepwise aggregation of trinuclear  $\text{Co}(\text{II})\text{Ln}(\text{III})\text{Co}(\text{II})$  complexes (Ln = La and Gd) and mononuclear  $[\text{Cr}(\text{CN})_6]^{3-}$  [57]. The as-obtained trinuclear  $\text{Co}(\text{II})\text{Ln}(\text{III})\text{Co}(\text{II})$  complexes were mixed with  $\text{K}_3[\text{Cr}(\text{CN})_6]$  in 1:1 molar ratio to give reddish-orange  $\text{Co}_2\text{Ln}(\text{L})_2(\text{H}_2\text{O})_4[\text{Cr}(\text{CN})_6] \cdot n\text{H}_2\text{O}$  crystals in aqueous solution. The asymmetric pillared-layer structure consists of two crystallographically independent  $[\text{Co}_2\text{Ln}(\text{L})_2(\text{H}_2\text{O})_4]^{3+}$  and  $[\text{Cr}(\text{CN})_6]^{3-}$  units. The trinuclear moieties have a linear  $\text{Co}(\text{II})\text{Ln}(\text{III})\text{Co}(\text{II})$  core between two  $\text{L}^{2-}$  ligands, which is held by four enolate-bridges, and the Ln(III) ion located at the 2,6-diacylpyridine site exhibits a ten-coordinate geometry with four  $\text{H}_2\text{O}$  molecules above and below the  $\{\text{Co}_2\text{Ln}(\text{L})_2\}$  plane. The  $\{\text{Co}_2\text{Ln}(\text{L})_2\}$  trinuclear units serve as good precursors for the construction of trimetallic assemblies.

Martí-Gastaldo et al. reported the one-pot synthesis of mixed-metal NiFe-MOF-74 solids under anaerobic conditions by reaction of variable amounts of anhydrous  $\text{FeCl}_2$  and  $\text{Ni}(\text{NO}_3)_2 \cdot 6\text{H}_2\text{O}$  with  $\text{H}_4\text{dhtp}$  (2,5-dihydroxyterephthalic acid) in a mixture of anhydrous DMF and anhydrous MeOH refluxed at  $120^\circ\text{C}$  for 18 h in a glovebox [58]. The as-obtained solids exhibit as green microcrystalline powders, while increasing the iron content in the synthesis systems produced crystals with a smaller particle size and rounder shape. Compared to the monometallic MOF-74, the as-synthesized NiFe-MOF-74 displayed the combination of porosity with ferromagnetic ordering. The amount of Fe doping can be simply tuned by rational adjustment of the metals ratios in the synthesis systems. This one-step controllable doping strategy provides more opportunities to design new mixed-metal materials which may not be accessible by conventional synthesis.

On the other hand, Li et al. prepared partial Co-substituted Ni-MOF-74 via a postsynthetic metal exchange strategy. Co-substituted Ni-MOF-74 ( $\text{Co}/\text{Ni}$ -MOF-74- $x$ , where  $x$  represents the exchange time) was prepared by immersing the as-synthesized Ni-MOF-74 in a DMF solution of  $\text{Co}(\text{NO}_3)_2 \cdot 6\text{H}_2\text{O}$  for different times (Fig. 3.7) [59]. A gradual color change from *yellow-green* to *brown* of the solid evidenced the successful metal-exchange process. In the same time, the *pink*  $\text{Co}(\text{NO}_3)_2 \cdot 6\text{H}_2\text{O}$  solution gradually faded with the reaction time, further confirming the metathesis between the  $\text{Co}^{2+}$  in solution and the  $\text{Ni}^{2+}$  in the MOF framework. Interestingly, the amount of the incorporated  $\text{Co}^{2+}$  can be tuned by carefully adjusting the incubation time of Ni-MOF-74 in  $\text{Co}(\text{NO}_3)_2 \cdot 6\text{H}_2\text{O}$  solution. The exchange degree can be enhanced by appropriately prolonging the immerse time; it's worth noting that when the metal-exchange achieves saturation, prolonging the reaction time can only slightly influence the incorporated amount of Co. This demonstrated that not all of the  $\text{Ni}^{2+}$  in Ni-MOF-74 framework can be replaced by  $\text{Co}^{2+}$ ; the access of  $\text{Co}^{2+}$  in solution to  $\text{Ni}^{2+}$  in the framework can

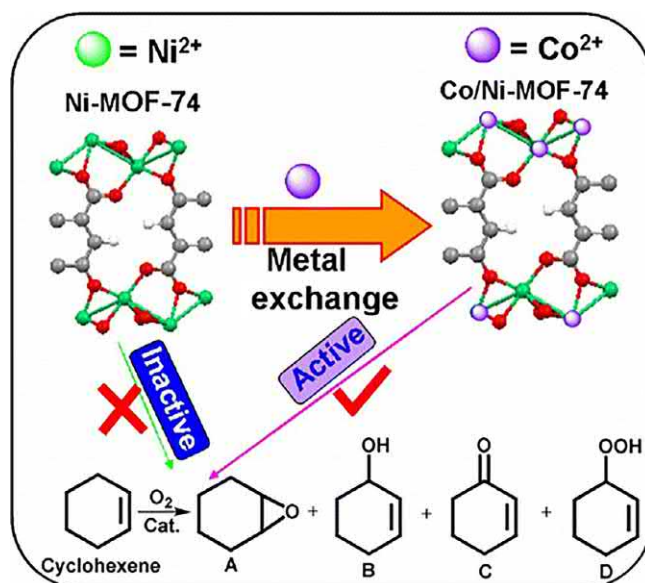


Fig. 3.7

Synthesis of Co-substituted Ni-MOF-74 via a postsynthetic metal exchange strategy. Copyright from D. Sun, F. Sun, X. Deng, Z. Li, *Mixed-metal strategy on metal–organic frameworks (MOFs) for functionalities expansion: Co substitution induces aerobic oxidation of cyclohexene over inactive Ni-MOF-74*. *Inorg. Chem.* 54 (2015) 8639–8643.

be restricted by the diffusional limitations of the honeycomb-like network of MOF-74. The facile postsynthetic metal exchange strategy present in this research has great potential for the development of mixed-metal MOFs with intriguing functionalities.

A series of  $[\text{Ni}_6^{\text{II}}\text{Ln}^{\text{III}}]$  heptanuclear complex have been reported by Milios and coworkers. The brown plate-like crystals  $[\text{Ni}_6^{\text{II}}\text{Dy}^{\text{III}}(\text{L})_4(\text{Htea})_4](\text{ClO}_4)_{2.5}(\text{NO}_3)_{0.5} \cdot 5.5\text{MeCN} \cdot \text{H}_2\text{O}$  was synthesized based on the solvothermal reaction of  $\text{Dy}(\text{NO}_3)_3 \cdot 6\text{H}_2\text{O}$ ,  $\text{Ni}(\text{ClO}_4)_2 \cdot 6\text{H}_2\text{O}$ ,  $\text{H}_3\text{tea}$  (triethanolamine),  $\text{N}(\text{Et})_3$ , and HL (1H-indeno[1,2-b]quinoxalin-11-one) in MeCN for 12 h, while using  $\text{Gd}(\text{NO}_3)_3 \cdot 6\text{H}_2\text{O}$  or  $\text{Y}(\text{NO}_3)_3 \cdot 6\text{H}_2\text{O}$  as the starting lanthanide salts, the isostructural  $[\text{Ni}_6^{\text{II}}\text{Gd}^{\text{III}}(\text{L})_4(\text{Htea})_2(\text{tea})_2](\text{ClO}_4) \cdot 4\text{MeCN} \cdot \text{H}_2\text{O}$  or  $[\text{Ni}_6^{\text{II}}\text{Y}^{\text{III}}(\text{L})_4(\text{Htea})_2(\text{tea})_2](\text{ClO}_4)_{0.5}(\text{NO}_3)_{0.5} \cdot 2.5\text{H}_2\text{O} \cdot 1.4\text{MeCN}$  crystals can be obtained. All of these complexes exhibit the same  $[\text{Ni}_6^{\text{II}}\text{Ln}^{\text{III}}]$  metallic core [60].

Based on the theory of hard-soft acid-base, lanthanide ions act as hard acids which are preferring oxygen to nitrogen donors, while the transition ion serves as a borderline acid which has a strong tendency to bind N as well as O atoms [61]. Bai et al. one-pot synthesized a family of 3D homochiral Mn(II)-Ln(III) frameworks  $\{\text{MnLn}(\text{D-cam})_2(\text{D-Hcam})(2,2'\text{-bpy})\}_n$  (Ln = Nd, Dy, Eu, and La) assembled from  $\text{Ln}(\text{NO}_3)_3 \cdot 6\text{H}_2\text{O}$ , D-camphoric acid,  $\text{MnCl}_2 \cdot 4\text{H}_2\text{O}$  and 2,2'-bipy under solvothermal conditions [62]. D-Camphoric acid acts as a bridge to construct heterometallic centers as well as a chiral source for the formation of multidimensional

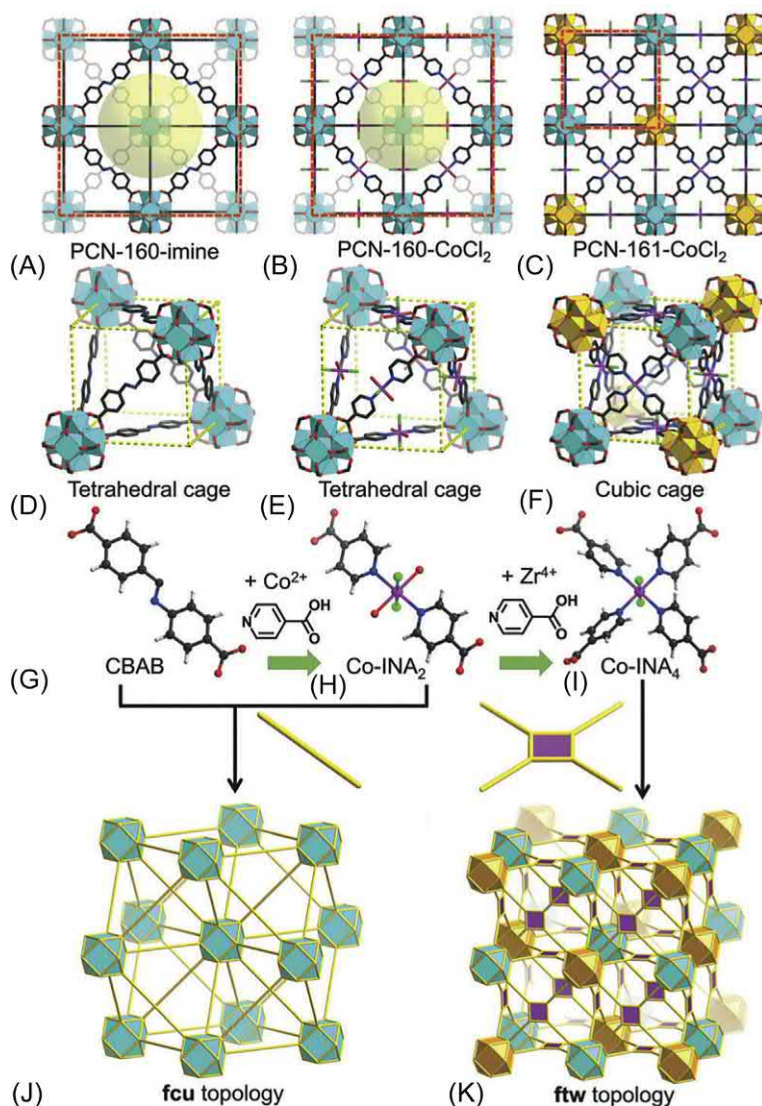


MOFs. Interestingly, the D-camphoric acids unprecedentedly unfold three coordination modes with proper degree in one structure. Very recently, the “one-pot” approach was further developed by Rosi and coworkers in a systematical work [11]. They used the bifunctional H<sub>2</sub>ina (isonicotinic acid) linker and its derivatives connected with one oxophilic of the hard-acid metal cations (Zr<sup>4+</sup>, Hf<sup>4+</sup>, Dy<sup>3+</sup>) as well as second soft metal cations (Co<sup>2+</sup>, Cu<sup>+</sup>, Cu<sup>2+</sup>, Ni<sup>2+</sup>, Fe<sup>3+</sup>, Cd<sup>2+</sup>) to construct diverse classes of bimetallic MOFs with well-established coordination complexes and controlled topologies. These general one-pot assembly strategies can furnish more flexible coordination modes in multicomponent heterometallic MOFs system.

Postsynthetic ion metathesis is quite effective to prepare multimetal MOFs which cannot be obtained by one-pot solvothermal synthesis. For instance, Dinca and coworkers synthesized a series of Ti<sup>3+</sup>-, V<sup>2+/3+</sup>-, Cr<sup>2+/3+</sup>-, Mn<sup>2+</sup>-, and Fe<sup>2+</sup>-substituted MOF-5 by postsynthetic ion metathesis [63]. The as-prepared divalent metal ions inserted MOF-5 was denoted as M-MOF-5, while the trivalent metal ions inserted denoted as CIM-MOF-5. To prepare M-MOF-5 or CIM-MOF-5 by direct reaction of the Zn(NO<sub>3</sub>)<sub>2</sub> and Ti<sup>3+</sup>, V<sup>2+/3+</sup>, Cr<sup>2+/3+</sup>, Mn<sup>2+</sup>, or Fe<sup>2+</sup> salts with BDC (terephthalic acid) were unsuccessful. On the contrary, soaking the as-obtained MOF-5 in concentrated solution of VCl<sub>2</sub>(pyridine)<sub>4</sub>, CrCl<sub>2</sub>, MnCl<sub>2</sub>, and Fe(BF<sub>4</sub>)<sub>2</sub>·6H<sub>2</sub>O in DMF for 7 days afforded M-MOF-5 (M = V<sup>2+</sup>, Cr<sup>2+</sup>, Mn<sup>2+</sup>, or Fe<sup>2+</sup>), while identical conditions involving TiCl<sub>3</sub>·3THF, VCl<sub>3</sub>·3THF, or CrCl<sub>3</sub>·3THF in DMF resulted in CIM-MOF-5 (M = Ti<sup>3+</sup>, V<sup>3+</sup>, or Cr<sup>3+</sup>). The MZn<sub>3</sub>O(O<sub>2</sub>C)<sub>6</sub> clusters in MOF-5 provide electronically unique and structurally flexible pseudotrigonal bipyramidal or dianionic pseudotetrahedral all-oxygen coordination conditions. Liu et al. reported the synthesis of titanium incorporated UiO-66 (UiO-66(Ti)) through a facile modified postgrafting method. In a typical process, the as-synthesized UiO-66 was mixed with certain amount of Ti(OBu)<sub>4</sub> in toluene; thereafter the mixture was heated at 100°C for 24 h under N<sub>2</sub> atmosphere to obtain the UiO-66(Ti) with various ratio of Ti/Zr [64]. This study demonstrated that the Ti species are not simply confined or grafted in the UiO-66 framework. Inversely, the Ti species might be incorporated with Zr for the formation of oxo-bridged hetero-Zr-Ti clusters, which serve as the skeleton of the UiO-66(Ti).

Recently, Zhou and co-workers demonstrated a series of heterometallic MOFs with MX<sub>2</sub>(ina)<sub>4</sub> moieties (where ina = isonicotinate; M = Co<sup>2+</sup> or Fe<sup>2+</sup>; X = OH<sup>-</sup>, Cl<sup>-</sup>, Br<sup>-</sup>, I<sup>-</sup>, NCS<sup>-</sup>, or NCSe<sup>-</sup>) based on the stepwise synthetic methods [65]. In this study, they introduced the MX<sub>2</sub>(py)<sub>4</sub> units (py = pyridine) into Zr-MOFs (PCN-160-imine). In a typical preparation process, PCN-160-imine frameworks were first composed by Zr<sub>6</sub> clusters and CBAB (4-carboxybenzylidene-4-aminobenzoate) linker (Fig. 3.8G). Subsequently, the CBAB linker among PCN-160-imine was substituted by Co-ina moiety (Co-ina<sub>2</sub>, Fig. 3.8H) to afford PCN-160-CoCl<sub>2</sub>. The Co<sup>2+</sup> center in PCN-160-CoCl<sub>2</sub> was binding with two ina ligands, Cl<sup>-</sup>, and solvent molecules in an opposite direction, and the solvent molecules coordinated with the Co<sup>2+</sup> center was further substituted by a couple of ina ligands and resulted in a square planar metaloligand (Co-ina<sub>4</sub>, Fig. 3.8I). Then, the leaving carboxylates poised binding with Zr<sup>4+</sup>,





**Fig. 3.8**

Single-crystal structures of (A) PCN-160-imine, (B) PCN-160-CoCl<sub>2</sub>, and (C) PCN-161-CoCl<sub>2</sub> with small tetrahedral cages (D, E) and cubic cages (F), respectively. (G–I) Linkers and their topological representations. The transformation of **fcu** topology (J) into **ftw** topology (K). Copyright from S. Yuan, J.-S. Qin, J. Su, B. Li, J. Li, W. Chen, H.F. Drake, P. Zhang, D. Yuan, J. Zuo, H.-C. Zhou, *Sequential transformation of zirconium(IV)-MOFs into heterobimetallic MOFs bearing magnetic anisotropic obalt(II)centers*, *Angew. Chem. Int. Ed.* 57 (2018) 1–7.

12-connected Zr<sub>6</sub> cluster was accommodated in a pocket, forming 12 uncoordinated carboxylate groups of the skeleton. Thus, a new Zr<sub>6</sub> cluster was formed at the center of the octahedral cage of PCN-160-CoCl<sub>2</sub>. The present research not only provides an approach for the synthesis of heterometallic MOFs, but also opens up an avenue for the interconversion of

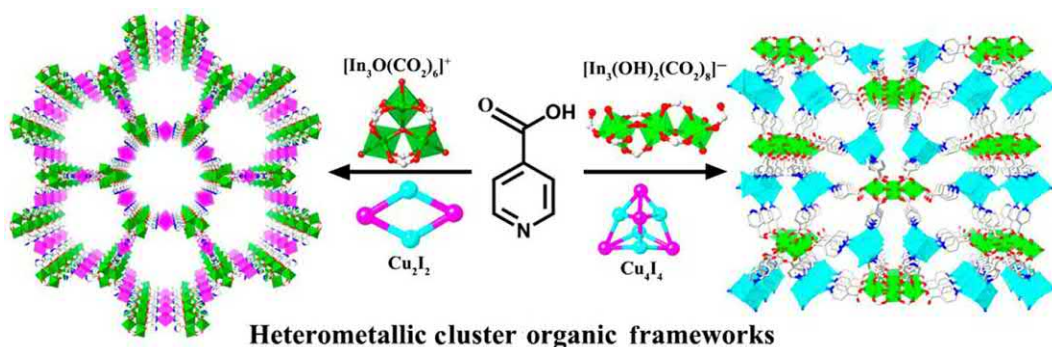


Fig. 3.9

Schematic illustrations of 3D cationic framework with hexagonal channels of  $23.0 \times 23.0 \text{ \AA}$  and polyhedral view of the 3D negative motif with irregular hexagonal channels. Copyright from J.H. Liu, Y.J. Qi, D. Zhao, H.H. Li, S.T. Zheng, *Heterometallic-organic frameworks built from trinuclear indium and cuprous halide clusters: ligand-oriented assemblies and iodine adsorption behavior*, *Inorg. Chem.* 58 (2019) 516–523.

two different frameworks through sequential modifications. As we know, Hina contains pyridyl nitrogen-donor and carboxylate oxygen-donor groups, which is selected as a common synthon for the preparation of heterometallic cluster-based organic frameworks according to HSAB theory. Recently, two novel heterometallic-organic frameworks built from trinuclear indium and cuprous halide clusters,  $[(\text{In}_3\text{O})_2(\text{Cu}_2\text{I}_2)_3(\text{ina})_{12}(\text{H}_2\text{O})_6](\text{NO}_3)_2 \cdot \text{solvent}$  and  $[\text{NH}_2(\text{CH}_3)_2][\text{In}_3(\text{OH})_2(\text{H}_2\text{O})_2(\text{ina})_8(\text{Cu}_4\text{I}_4)_2] \cdot \text{solvent}$ , where Hina = isonicotinic acid, have been successfully synthesized with the orientation of the ina ligand. They exhibit a highly porous honeycomb-like 3D cationic framework with a trigonal-bipyramid-type cage based on a planar  $[\text{In}_3\text{O}(\text{CO}_2)_6]^+$  trimer and a rhombohedral  $\text{Cu}_2\text{I}_2$  cluster and displays a 3D negative motif with irregular hexagonal channels constructed from a  $[\text{In}_3(\text{OH})_2(\text{CO}_2)_8]^-$  trimer and a cubane-like  $\text{Cu}_4\text{I}_4$  cluster, respectively (Fig. 3.9) [20].

### 3.2.5 Mixed-metal MOFs with rare earth metals

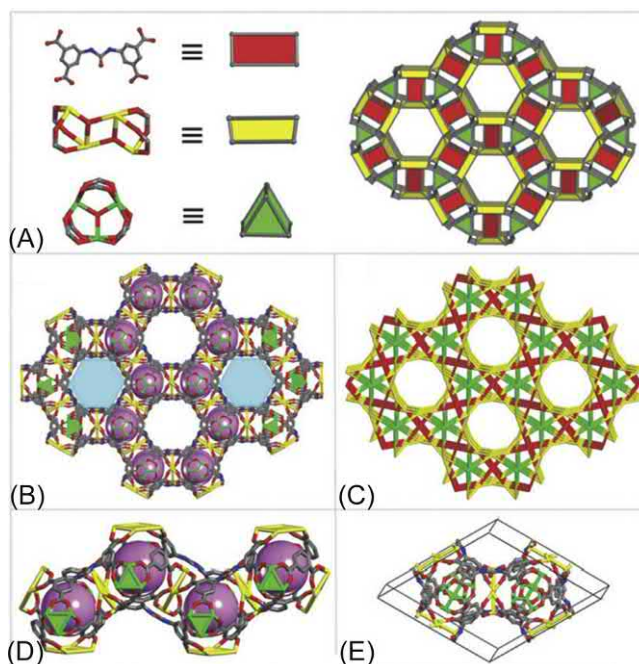
As multifunctional metal centers, rare earth metals have attracted increasing attention from researchers for their intriguing coordination properties and interesting chemical characteristics resulted from 4f electrons and the tendency to form isostructural complexes. Numbers of monometallic coordination polymers based on rare earth metals have been synthesized. Nevertheless, the flexible coordination geometry and high coordination number of the rare earth ions make it difficult to prepare rare earth heterometallic MOFs.

As is well-known, rare earth metal ions have high affinity to hard donor ligands containing oxygen or nitrogen atoms, especially carboxylate ligands, which are usually employed to construct mixed-lanthanide metal coordination polymers. Chen and coworkers reported the synthesis of mixed-lanthanide MOFs  $(\text{Eu}_x\text{Tb}_{1-x})_2(\text{DMBDC})_3(\text{H}_2\text{O})_4 \cdot \text{DMF} \cdot \text{H}_2\text{O}$

(Eu<sub>x</sub>Tb<sub>1-x</sub>-DMBDC) ( $x = 0.0011, 0.0046, \text{ and } 0.0069$ ) (DMBDC = 2,5-dimethoxy-1,4-benzenedicarboxylate) by reacting H<sub>2</sub>DMBDC with varying molar ratios of Eu(NO<sub>3</sub>)<sub>3</sub> to Tb(NO<sub>3</sub>)<sub>3</sub> through a solvothermal reaction in the mixed solvents of DMF, ethanol, and water to yield the colorless rod-like crystals [66]. As expected, these as-obtained mixed-lanthanide MOFs are isostructural to the monometallic Tb-DMBDC and Eu-DMBDC. Shortly afterwards, Chen group successfully prepared another series of new mixed-lanthanide MOFs Tb<sub>1-x</sub>Eu<sub>x</sub>(C<sub>13</sub>H<sub>7</sub>O<sub>4</sub>N)(C<sub>13</sub>H<sub>8</sub>O<sub>4</sub>N)(H<sub>2</sub>O)<sub>2.5</sub> (Tb<sub>1-x</sub>Eu<sub>x</sub>PIA) (H<sub>2</sub>PIA = 5-(pyridin-4-yl) isophthalic acid) based on a mixture of Tb(NO<sub>3</sub>)<sub>3</sub> and Eu(NO<sub>3</sub>)<sub>3</sub>, H<sub>2</sub>PIA under similar hydrothermally conditions [67]. A series of Eu and Tb codoped Ln-MOFs: Eu<sub>x</sub>Tb<sub>1-x</sub>L ( $x = 0.1\text{--}0.9$ ) (H<sub>2</sub>L = 1,3-bis(4-carboxyphenyl)imidazolium) was synthesized by Zhang and coworkers [68]. With judicious modulation of the relative concentration of the different lanthanide ions, a family of isostructural mixed-Ln-MOFs can be obtained. Therefore, due to the isostructural features of these monometallic LnMOFs, it can straightforwardly prepare a series of mixed-LnMOFs in which various types of lanthanide ions with variable molar ratios can be systematically comprised into the frameworks.

Recently, Lin et al. reported thermal and chemical stable heterometallic MOFs by a tetra-carboxylic ligand CBDA (5,5'-(carbonylbis(azanediyl))-diisophthalic acid) with In and Tb nitrate salts give rise to a porous In/Tb-CBDA under solvothermal conditions [69]. The framework of In/Tb-CBDA is formed by cooperatively assembling the rarely reported tetra-nuclear In<sub>4</sub>O<sub>2</sub>(COO)<sub>4</sub> and trinuclear Tb<sub>3</sub>O(COO)<sub>6</sub> clusters and a tetra-carboxylate ligand (CBDA) with the urea group (Fig. 3.10). It is worth noting that forming multinuclear metal clusters promotes the framework to maintain high stability under different conditions including heating, exposure to air, and soaking in basic and acidic aqueous solutions.

As a versatile class of cyanide-based metalloligand, [M(CN)<sub>8</sub>]<sup>3-/4-</sup> (M = Mo, W) serves as a suitable platform to combine lanthanide ions with higher coordination numbers, which will afford more complicated topologies and magnetic behaviors. For example, a new isomorphous family of neutral cyanido-bridged Ln<sup>III</sup>-W<sup>V</sup> heterometallic complexes [Ln<sup>III</sup>(pym)<sub>2</sub>(i-PrOH)(H<sub>2</sub>O)<sub>2</sub>(μ-CN)W<sup>V</sup>(CN)<sub>7</sub>] (where Ln = Gd<sup>III</sup>, Tb<sup>III</sup>, Dy<sup>III</sup>, Ho<sup>III</sup> and Er<sup>III</sup>, pym = 2-(1H-imidazol-2-yl)-pyridine), i-PrOH = isopropyl alcohol) has been prepared by one-step reaction of [Ln(pym)<sub>2</sub>]<sup>2+</sup> and (NH<sub>3</sub>Bu)<sub>3</sub>[W(CN)<sub>8</sub>] [NH<sub>3</sub>Bu<sup>3+</sup> = tri-*n*-butylammonium cation] complexes [70], in which the [Ln(pym)<sub>2</sub>]<sup>2+</sup> was generated in situ by mixing 1 equiv. of the corresponding Ln<sup>III</sup> nitrate salts and 2 equiv. of the pym ligand in water/2-propanol solution. In this structure, both tungsten(V) and lanthanide(III) ions are eight-coordinated, in distorted square antiprism (W<sup>V</sup>) and distorted trigonal dodecahedron (Ln<sup>III</sup>) surrounding, respectively. Each lanthanide (III) ion is chelating by two pym molecules, where these two pym molecules act as capping ligands toward the lanthanide (III) ions. An extended 3D supramolecular network is well-developed through the interplay of hydrogen bonds and π-π stacking interactions induced between the binuclear entities. Moreover, Ohkoshi et al. synthesized a series of Ln<sup>III</sup>(bis-oxazoline)[Mo<sup>V</sup>(CN)<sub>8</sub>] (Ln = Ce-Yb) complexes based on the



**Fig. 3.10**

Single-crystal structure of In/Tb-CBDA: (A) polyhedron view of the net: the organic linker and tetranuclear cluster  $[\text{In}_4\text{O}_2(\text{COO})_4]$  simplified as a square and trinuclear cluster  $[\text{Tb}_3\text{O}(\text{COO})_6]$  viewed as a triangular prism geometry, respectively; (B) ball-stick model of the framework; (C) topology view of the net; (D) 1D chain assembled by cages; (E) the unit cell structure. Copyright from D. Wang, Z. Liu, L. Xu, C. Li, D. Zhao, G. Ge, Z. Wang, J. Lin, *A heterometallic metal-organic framework based on multi-nuclear clusters exhibiting high stability and selective gas adsorption*, *Dalton Trans.* 48 (2019) 278–284.

cyanide-based metalloligand of  $[\text{Mo}^{\text{V}}(\text{CN})_8]^{3-}$  [71]. The combination of  $\text{Ln}^{\text{III}}$  with box (2,2'-bis(2-oxazoline) ligand and  $[\text{Mo}^{\text{V}}(\text{CN})_8]^{3-}$  via solvothermal reaction resulted in  $\{[\text{Ln}^{\text{III}}(\text{box})_n(\text{DMF})_m][\text{Mo}^{\text{V}}(\text{CN})_8]\} \cdot x(\text{solvent})$ .

As a result, many heterometal-organic frameworks containing lanthanide ions have been well-established, including systems associated with  $[\text{Ln}-\text{M}]$  ( $\text{M} = \text{Ag}, \text{Cu}, \text{Mn}, \text{Fe}, \text{Co}, \text{W}, \text{Mo}, \text{etc.}$ ) [72–77].

### 3.3 Conclusions and perspectives

The past decade has witnessed the explosive development of heterometallic MOFs, not only due to their intriguing varieties of molecular architectures and topologies, but also their potential applications. However, heterometallic MOFs remain relatively unexplored due to complications that arise more than two building blocks in one system; the most reported work has been more empirical than systematic, especially the first approach. The metalloligand

approach has enabled us to rationally immobilize a variety of different functional sites, but it is still difficult to predesign precursors and retain microporosity. PSMet is a versatile and effective strategy for modulating and tailoring the functionality of the heterometallic MOFs; it is still a challenge in improving the efficiency of metalation and establishing protocols. It should be noted that the number of literature that reported heterometallic MOFs for biomedical applications are very limited and, certainly, an increasing number of examples will appear in the near future, which will exploit the full potential of these mixed-metal MOFs in biomedical field.

## Acknowledgments

This project received partial support from the project of outstanding young and middle-aged teachers training objects of Guangdong Medical University and Dongguan Science and Technology Bureau.

## References

- [1] H. Furukawa, K.E. Cordova, M. O’Keeffe, O.M. Yaghi, The chemistry and applications of metal-organic frameworks, *Science* 341 (2013) 1230444.
- [2] B. Li, H.-M. Wen, Y. Cui, W. Zhou, G. Qian, B. Chen, Emerging multifunctional metal-organic framework materials, *Adv. Mater.* 28 (2016) 8819–8860.
- [3] J. Liu, G. Liu, C. Gu, W. Liu, J. Xu, B. Li, W. Wang, Rational synthesis of a novel 3,3,5-c polyhedral metal-organic framework with high thermal stability and hydrogen storage capability, *J. Mater. Chem. A* 4 (2016) 11630–11634.
- [4] S. Qiu, G. Zhu, Molecular engineering for synthesizing novel structures of metal-organic frameworks with multifunctional properties, *Coord. Chem. Rev.* 253 (2009) 2891–2911.
- [5] Y. Cui, B. Li, H. He, W. Zhou, B. Chen, G. Qian, Metal-organic frameworks as platforms for functional materials, *Acc. Chem. Res.* 49 (2016) 483–493.
- [6] H.-C. Zhou, J.R. Long, O.M. Yaghi, Introduction to metal-organic frameworks, *Chem. Rev.* 112 (2012) 673–674.
- [7] H.-L. Jiang, T.A. Makal, H.-C. Zhou, Interpenetration control in metal-organic frameworks for functional applications, *Coord. Chem. Rev.* 257 (2013) 2232–2249.
- [8] A. Dhakshinamoorthy, A.M. Asiri, H. Garcia, Mixed-metal or mixed-linker metal organic frameworks as heterogeneous catalysts, *Catal. Sci. Technol.* 6 (2016) 5238–5261.
- [9] Z. Wang, S.M. Cohen, Postsynthetic modification of metal-organic frameworks, *Chem. Soc. Rev.* 38 (2009) 1315–1329.
- [10] A.D. Burrows, Mixed-component metal-organic frameworks (MC-MOFs): enhancing functionality through solid solution formation and surface modifications, *CrystEngComm* 13 (2011) 3623–3642.
- [11] P.F. Muldoon, C. Liu, C.C. Miller, S.B. Koby, A.G. Jarvi, T.Y. Luo, S. Saxena, M. O’Keeffe, N.L. Rosi, Programmable topology in new families of heterobimetallic metal-organic frameworks, *J. Am. Chem. Soc.* 140 (2018) 6194–6198.
- [12] Q.-G. Zhai, X. Bu, C. Mao, X. Zhao, P. Feng, Systematic and dramatic tuning on gas sorption performance in heterometallic metal-organic frameworks, *J. Am. Chem. Soc.* 138 (2016) 2524–2527.
- [13] S.-T. Zheng, T. Wu, C. Chou, A. Fuhr, P. Feng, X. Bu, Development of composite inorganic building blocks for MOFs, *J. Am. Chem. Soc.* 134 (2012) 4517–4520.
- [14] G. Ferey, F. Millange, M. Morcrette, C. Serre, M.-L. Doublet, J.M. Greneche, J.-M. Tarascon, Mixed-valence Li/Fe-based metal-organic frameworks with both reversible redox and sorption properties, *Angew. Chem. Int. Ed.* 46 (2007) 3259–3263.



- [15] S.K. Elsaidi, M.H. Mohamed, L. Wojtas, A.J. Cairns, M. Eddaoudiac, M.J. Zaworotko, Two-step crystal engineering of porous nets from  $[\text{Cr}_3(\mu_3\text{-O})(\text{RCO}_2)_6]$  and  $[\text{Cu}_3(\mu_3\text{-Cl})(\text{RNH}_2)_6\text{Cl}_6]$  molecular building blocks, *Chem. Commun.* 49 (2013) 8154–8156.
- [16] J. Qian, F. Jiang, K. Su, J. Pan, Z. Xue, L. Liang, P.P. Baga, M. Hong, Heterometallic cluster-based indium-organic frameworks, *Chem. Commun.* 50 (2014) 15224–15227.
- [17] D.J. Evans, C.J. Sumbly, C.J. Doonan, Post-synthetic metalation of metal-organic frameworks, *Chem. Soc. Rev.* 43 (2014) 5933–5951.
- [18] Y. Han, H. Zheng, K. Liu, H. Wang, H. Huang, L.-H. Xie, L. Wang, J.-R. Li, In-situ ligand formation-driven preparation of a heterometallic metal-organic framework for highly selective separation of light hydrocarbons and efficient mercury adsorption, *ACS Appl. Mater. Interfaces* 8 (2016) 23331–23337.516.
- [19] C.D. Madhab, S.C. Xiang, Z.J. Zhang, B.L. Chen, Functional mixed metal-organic frameworks with metalloligands, *Angew. Chem. Int. Ed.* 50 (2011) 10510–10520.
- [20] J.H. Liu, Y.J. Qi, D. Zhao, H.H. Li, S.T. Zheng, Heterometallic-organic frameworks built from trinuclear indium and cuprous halide clusters: ligand-oriented assemblies and iodine adsorption behavior, *Inorg. Chem.* 58 (2019) 516–523.
- [21] C. Wang, C. Liu, X. He, Z.M. Sun, A cluster-based mesoporous Ti-MOF with sodalite supercages, *Chem. Commun.* 53 (2017) 11670–116073.
- [22] Y.-X. Tan, X. Yang, B.-B. Li, D.Q. Yuan, Rational design of a Flu-type heterometallic cluster-based Zr-MOF, *Chem. Commun.* 52 (2016) 13671–13674.
- [23] Y. Okano, H. Ohara, A. Kobayashi, M. Yoshida, M. Kato, Systematic introduction of aromatic rings to diphosphine ligands for emission color tuning of dinuclear copper(I) iodide complexes, *Inorg. Chem.* 55 (2016) 5227–5236.
- [24] W. Liu, Y. Fang, G.Z. Wei, G.S.J. Teat, K. Xiong, Z. Hu, W.P. Lustig, J. Li, A family of highly efficient CuI-based lighting phosphors prepared by a systematic, bottom-up synthetic approach, *J. Am. Chem. Soc.* 137 (2015) 9400–9408.
- [25] S.C. Chen, Z.H. Zhang, Y.S. Zhou, W.Y. Zhou, Y.Z. Li, M.Y. He, Q. Chen, M. Du, Alkali-metal-templated assemblies of new 3D lead(II) tetrachloroterephthalate coordination frameworks, *Cryst. Growth Des.* 11 (2011) 4190–4197.
- [26] X.N. Chen, W.X. Zhang, Y.Y. Lin, Y.Z. Zheng, X.M. Chen, A dynamic porous magnet exhibiting reversible guest-induced magnetic behavior modulation, *Adv. Mater.* 19 (2007) 1494–1498.
- [27] X.W. Xu, C.B. Tian, S.W. Du, Synthesis, structure and luminescence properties of two Cd(II)/M(I) (M = K, Rb) interpenetrated heterometallic frameworks based on giant double-walled cages, *CrystEngComm* 19 (2017) 4269–4272.
- [28] X.Q. Li, H.B. Zhang, S.T. Wu, J.D. Lin, P. Lin, Z.H. Li, S.W. Du, Synthesis, structures and luminescent properties of new Pb(II)/M(I) (M = K, Rb and Cs) frameworks based on dicarboxylic acids: a novel icosahedral  $\text{Pb}_6\text{-M}_6$  SBU, *CrystEngComm* 14 (2012) 936–944.
- [29] S. Xu, J.J. Shi, B. Ding, Z.Y. Liu, X.G. Wang, X.J. Zhao, E.C. Yang, A heterometallic sodium(I)–europium (III)-organic layer exhibiting dual-responsive luminescent sensing for nitrofurantoin antibiotics,  $\text{Cr}_2\text{O}_7^{2-}$  and  $\text{MnO}_4^-$  anions, *Dalton Trans.* 48 (2019) 1823–1834.
- [30] M. Ptak, D. Stefańska, A. Gagor, K.L. Svane, A. Walsh, W. Paraguassu, Heterometallic perovskite-type metal-organic framework with an ammonium cation: structure, phonons, and optical response of  $[\text{NH}_4]\text{Na}_{0.5}\text{Cr}_x\text{Al}_{0.5-x}(\text{HCOO})_3$  ( $x = 0, 0.025$  and  $0.5$ ), *Phys. Chem. Chem. Phys.* 20 (2018) 22284–22295.
- [31] S.R. Caskey, A.G. Wong-Foy, A.J. Matzger, Dramatic tuning of carbon dioxide uptake via metal substitution in a coordination polymer with cylindrical pores, *J. Am. Chem. Soc.* 130 (2008) 10870–10871.
- [32] L.J. Wang, H. Deng, H. Furukawa, F. Gándara, K.E. Cordova, D. Peri, O.M. Yaghi, Synthesis and characterization of metal-organic framework-74 containing 2, 4, 6, 8, and 10 different metals, *Inorg. Chem.* 53 (2014) 5881–5883.
- [33] S. Zhang, X. Liu, Q. Yang, Q. Wei, G. Xie, S. Chen, Mixed-metal-organic frameworks (M'MOFs) from 1D to 3D based on the “organic”connectivity and the inorganic connectivity: syntheses, structures and magnetic properties, *CrystEngComm* 17 (2015) 3312–3324.



- [34] A.M. Kirillov, Y.Y. Karabach, M.V. Kirillova, M. Haukka, A.J. Pombeiro, Topologically unique 2D heterometallic Cu<sup>II</sup>/Mg coordination polymer: synthesis, structural features, and catalytic use in alkane hydrocarboxylation, *Cryst. Growth Des.* 12 (2012) 1069–1074.
- [35] B. Ding, S.X. Liu, Y. Cheng, C. Guo, X.X. Wu, J.H. Guo, Y.Y. Liu, Y. Li, Heterometallic alkaline earth-lanthanide Ba<sup>II</sup>-La<sup>III</sup> microporous metal-organic framework as bifunctional luminescent probes of Al<sup>3+</sup> and MnO<sup>4-</sup>, *Inorg. Chem.* 55 (2016) 4391–4402.
- [36] X.Q. Zhao, Y. Zuo, D.L. Gao, B. Zhao, W. Shi, P. Cheng, Syntheses, structures, and luminescence properties of a series of Ln<sup>III</sup>-Ba<sup>II</sup> heterometal-organic frameworks, *Cryst. Growth Des.* 9 (2009) 3948–3957.
- [37] X. Wang, C. Qin, E. Wang, Y. Li, N. Hao, C. Hu, L. Xu, Syntheses, structures, and photoluminescence of a novel class of d<sup>10</sup> metal complexes constructed from pyridine-3,4-dicarboxylic acid with different coordination architectures, *Inorg. Chem.* 43 (2004) 1850–1856.
- [38] C. Yue, C. Yan, R. Feng, M. Wu, L. Chen, F. Jiang, M. Hong, A polynuclear d<sup>10</sup>-d<sup>10</sup> metal complex with unusual near-infrared luminescence and high thermal stability, *Inorg. Chem.* 48 (2009) 2873–2879.
- [39] H.L. Jiang, B. Liu, Q. Xu, Rational assembly of d<sup>10</sup> metal-organic frameworks with helical nanochannels based on flexible v-shaped ligand, *Cryst. Growth Des.* 10 (2010) 806–811.
- [40] X.Y. Chen, B. Zhao, P. Cheng, B. Ding, D.Z. Liao, S.P. Yan, Z.H. Jiang, Multi-dimensional systems built from dichromate anions-syntheses, crystal structures, and magnetic properties, *Eur. J. Inorg. Chem.* 3 (2004) 562–569.
- [41] L. Pan, N. Ching, X.Y. Huang, J. Li, An unprecedented two-fold interpenetrated heterometallic 4664 network constructed by five-connected copper metal nodes, *Chem. Commun.* 12 (2001) 1064–1065.
- [42] X. Li, Y. Gong, H. Zhao, R. Wang, Solvent-mediated crystal-to-crystal transformations from a cationic homometallic metal-organic framework to heterometallic frameworks, *CrystEngComm* 16 (2014) 8818–8824.
- [43] X. Guo, B. Guo, Y. Wang, S. Guan, Preparation of spherical metal-organic frameworks encapsulating Ag nanoparticles and study on its antibacterial activity, *Mater. Sci. Eng. C* 80 (2017) 698–707.
- [44] L.-D. Lin, C.-C. Deng, D. Zhao, X.-X. Li, S.-T. Zheng, Construction of zeolite-like cluster organic frameworks from 3d-4d/3d-3d heterometallic supertetrahedral secondary building units: syntheses, structures, and properties, *Chem. Eur. J.* 24 (2018) 251–258.
- [45] W. Guo, W. Xia, K. Cai, Y. Wu, B. Qiu, Z. Liang, C. Qu, R. Zou, Kinetic-controlled formation of bimetallic metal-organic framework hybrid structures, *Small* 13 (2017) 1702049.
- [46] X.-W. Zhu, X.-P. Zhou, D. Li, Exceptionally water stable heterometallic gyroidal MOFs: tuning the porosity and hydrophobicity by doping metal ions, *Chem. Commun.* 52 (2016) 6513–6516.
- [47] H. Li, M. Eddaoudi, M. O’Keeffe, O.M. Yaghi, Design and synthesis of an exceptionally stable and highly porous metal-organic framework, *Nature* 402 (1999) 276–279.
- [48] Z. Zhang, Y. Chen, X. Xu, J. Zhang, G. Xiang, W. He, X. Wang, Well-defined metal-organic framework hollow nanocages, *Angew. Chem. Int. Ed.* 53 (2014) 429–433.
- [49] X. Li, R. Cao, Syntheses, structure and properties of three-dimensional pillared-layer Ag(I)-Ln(III) heterometallic coordination polymers based on mixed isonicotinate and hemimellitate ligands, *J. Solid State Chem.* 196 (2012) 182–186.
- [50] H. Ma, L. Wang, J. Chen, X. Zhang, L. Wang, N. Xu, G. Yang, P. Cheng, A multi-responsive luminescent sensor for organic small-molecule pollutants and metal ions based on a 4d-4f metal-organic framework, *Dalton Trans.* 46 (2017) 3526–3534.
- [51] L. Li, J.-Y. Zou, S.-Y. You, H.-M. Cui, G.-P. Zeng, J.-Z. Cui, Tuning the luminescence of two 3d-4f metal-organic frameworks for the fast response and highly selective detection of aniline, *Dalton Trans.* 46 (2017) 16432–16438.
- [52] Y. Wang, X.-G. Wang, B. Yuan, C.-Y. Shao, Y.-Y. Chen, B.-B. Zhou, M.-S. Li, X.-M. An, P. Cheng, X.-J. Zhao, Cation-exchange porosity tuning in a dynamic 4d-4f-3d framework for Ni<sup>II</sup> ion-selective luminescent probe, *Inorg. Chem.* 54 (2015) 4456–4465.
- [53] G. Xiong, D. Qi, Y. He, L. You, B. Ren, Y. Sun, Lanthanide contraction and anion-controlled structure diversity in two types of novel 3d-4f heterometallic coordination polymers: crystal structure and magnetic properties, *Inorg. Chim. Acta* 483 (2018) 299–304.

- [54] Q. Zhang, M. Lei, H. Yan, J. Wang, Y. Shi, A water-stable 3D luminescent metal-organic framework based on heterometallic [Eu<sup>III</sup>Zn<sup>II</sup>] clusters showing highly sensitive, selective, and reversible detection of ronidazole, *Inorg. Chem.* 56 (2017) 7610–7614.
- [55] S.-R. Zhang, D.-Y. Du, J.-S. Qin, S.-L. Li, W.-W. He, Y.-Q. Lan, Z.-M. Su, 2D Cd(II)-lanthanide(III) heterometallic-organic frameworks based on metalloligands for tunable luminescence and highly selective, sensitive, and recyclable detection of nitrobenzene, *Inorg. Chem.* 53 (2014) 8105–8113.
- [56] Y.Y. Karabach, M.F.C. Guedes da Silva, M.N. Kopylovich, B. Gil-Hernandez, J. Sanchiz, A.M. Kirillov, A.J. L. Pombeiro, Self-assembled 3D heterometallic Cu<sup>II</sup>/Fe<sup>II</sup> coordination polymers with octahedral net skeletons: structural features, molecular magnetism, thermal and oxidation catalytic properties, *Inorg. Chem.* 49 (2010) 11097–11105.
- [57] T. Shiga, H. Okawa, S. Kitagawa, M. Ohba, Stepwise synthesis and magnetic control of trimetallic magnets [Co<sub>2</sub>Ln(L)<sub>2</sub>(H<sub>2</sub>O)<sub>4</sub>][Cr(CN)<sub>6</sub>] $\cdot$ *n*H<sub>2</sub>O (Ln = La, Gd; H<sub>2</sub>L = 2,6-di(acetoacetyl)pyridine) with 3-D pillared-layer structure, *J. Am. Chem. Soc.* 128 (2006) 16426–16427.
- [58] V. Rubio-Giménez, J.C. Waerenborgh, J.M. Clemente-Juan, C. Martí-Gastaldo, Spontaneous magnetization in heterometallic NiFe-MOF-74 microporous magnets by controlled iron doping, *Chem. Mater.* 29 (2017) 6181–6185.
- [59] D. Sun, F. Sun, X. Deng, Z. Li, Mixed-metal strategy on metal–organic frameworks (MOFs) for functionalities expansion: Co substitution induces aerobic oxidation of cyclohexene over inactive Ni-MOF-74, *Inorg. Chem.* 54 (2015) 8639–8643.
- [60] A.B. Canaj, D.I. Tzimopoulos, D.A. Kalofolias, M. Siczek, T. Lis, M. Murrie, C.J. Milios, Heterometallic lanthanide-centred [Ni<sub>6</sub>Ln<sup>III</sup>] rings, *Dalton Trans.* 47 (2018) 12863–12867.
- [61] B. Drahos, J. Kotek, I. Cisarova, P. Hermann, L. Helm, I. Lukes, E. Toth, Mn<sup>2+</sup> complexes with 12-membered pyridine based macrocycles bearing carboxylate or phosphonate pendant arm: crystallographic, thermodynamic, kinetic, redox, and 1H/17O relaxation studies, *Inorg. Chem.* 50 (2011) 12785–12801.
- [62] D.-B. Dang, B. An, Y. Bai, G.-S. Zheng, J.-Y. Niu, Three-dimensional homochiral manganese-lanthanide frameworks based on chiral camphorates with multi-coordination modes, *Chem. Commun.* 49 (2013) 2243–2245.
- [63] C.K. Brozek, M. Dinca, Ti<sup>3+</sup>-, V<sup>2+/3+</sup>-, Cr<sup>2+/3+</sup>-, Mn<sup>2+</sup>-, and Fe<sup>2+</sup>-substituted MOF-5 and redox reactivity in Cr- and Fe-MOF-5, *J. Am. Chem. Soc.* 135 (2013) 12886–12891.
- [64] A. Wang, Y. Zhou, Z. Wang, M. Chen, L. Sun, X. Liu, Titanium incorporated with UiO-66(Zr)-type metal-organic framework (MOF) for photocatalytic application, *RSC Adv.* 6 (2016) 3671–3679.
- [65] S. Yuan, J.-S. Qin, J. Su, B. Li, J. Li, W. Chen, H.F. Drake, P. Zhang, D. Yuan, J. Zuo, H.-C. Zhou, Sequential transformation of zirconium(IV)-MOFs into heterobimetallic mOFs bearing magnetic anisotropic cobalt(II) centers, *Angew. Chem. Int. Ed.* 57 (2018) 12578–12583.
- [66] Y. Cui, H. Xu, Y. Yue, Z. Guo, J. Yu, Z. Chen, J. Gao, Y. Yang, G. Qian, B. Chen, A luminescent mixed-lanthanide metal-organic framework thermometer, *J. Am. Chem. Soc.* 134 (2012) 3979–3982.
- [67] X.T. Rao, T. Song, J.K. Gao, Y.J. Cui, Y.Y. Yang, C.D. Wu, B.L. Chen, G.D. Qian, A highly sensitive mixed lanthanide metal-organic framework self-calibrated luminescent thermometer, *J. Am. Chem. Soc.* 135 (2013) 15559–15564.
- [68] S.N. Zhao, L.J. Li, X.Z. Song, M. Zhu, Z.M. Hao, X. Meng, L.L. Wu, J. Feng, S.Y. Song, C. Wang, H. J. Zhang, Lanthanide ion codoped emitters for tailoring emission trajectory and temperature sensing, *Adv. Funct. Mater.* 25 (2015) 1463–1469.
- [69] D. Wang, Z. Liu, L. Xu, C. Li, D. Zhao, G. Ge, Z. Wang, J. Lin, A heterometallic metal-organic framework based on multi-nuclear clusters exhibiting high stability and selective gas adsorption, *Dalton Trans.* 48 (2019) 278–284.
- [70] M.-G. Alexandru, D. Visinescu, S. Shova, F. Lloret, M. Julve, Cyanido-bridged {Ln<sup>III</sup>W<sup>V</sup>} heterobinuclear complexes: synthesis and magneto-structural study, *Inorg. Chem.* 56 (2017) 12594–12605.
- [71] S. Chorazy, M. Arczynski, K. Nakabayashi, B. Sieklucka, S. Ohkoshi, Visible to near-infrared emission from Ln<sup>III</sup>(Bis-oxazoline)[Mo<sup>V</sup>(CN)<sub>8</sub>] (Ln = Ce–Yb) magnetic coordination polymers showing unusual lanthanide-dependent sliding of cyanido-bridged layers, *Inorg. Chem.* 54 (2015) 4724–4736.

- [72] N.-N. Sun, B. Yan, A fluorescent probe based on a Tb<sup>3+</sup>/Cu<sup>2+</sup> co-functionalized MOF for urinary sarcosine detection, *Analyst* 143 (2018) 2349–2355.
- [73] G. Xiong, L. You, B. Ren, Y. He, S. Wang, Y. Sun, Structure and magnetocaloric effect of two kinds of Ln-Mn<sup>II</sup> heterometallic coordination polymers produced by fractional crystallization, *Eur. J. Inorg. Chem.* 24 (2016) 3969–3977.
- [74] X. He, W. Cheng, Q. Lin, Y. Dong, Y. Xu, Syntheses, structures, luminescence, and magnetic properties of a series of novel coordination polymers constructed by nanosized [Ln<sub>8</sub>Fe<sub>4</sub>] rings, *Cryst. Growth Des.* 17 (2017) 347–354.
- [75] W.-Y. Wu, R.-F. Zhang, X.-J. Zhang, P. Cheng, Two novel 3d-4f heterometallic coordination polymers with infinite [Ln<sub>4</sub>(OH)<sub>4</sub>]<sub>n</sub><sup>8n+</sup> chains involving *in situ* decarboxylation, *Dalton Trans.* 44 (2015) 7144–7147.
- [76] S. Chorazy, K. Nakabayashi, M. Arczynski, R. Pełka, S. Ohkoshi, B. Sieklucka, Multifunctionality in bmetallic Ln<sup>III</sup>[W<sup>V</sup>(CN)<sub>8</sub>]<sub>3</sub><sup>-</sup> (Ln = Gd, Nd) coordination helices: optical activity, luminescence, and magnetic coupling, *Chem. Eur. J.* 20 (2014) 7144–7159.
- [77] S.-Y. Qian, H. Zhou, Y. Zhang, A.-H. Yuan, Three octacyanometallate-based Ln<sup>III</sup>-M<sup>V</sup> (Ln = La, Ce; M = Mo, W) bimetallic assemblies with a one-dimensional rope-ladder chain structure, *Z. Anorg. Allg. Chem.* 636 (2010) 2671–2674.

# Metal-organic frameworks for biomedical applications: The case of functional ligands

Jéssica S. Barbosa<sup>a,b</sup>, Flávio Figueira<sup>a</sup>, Susana S. Braga<sup>b</sup>, Filipe A. Almeida Paz<sup>a</sup>

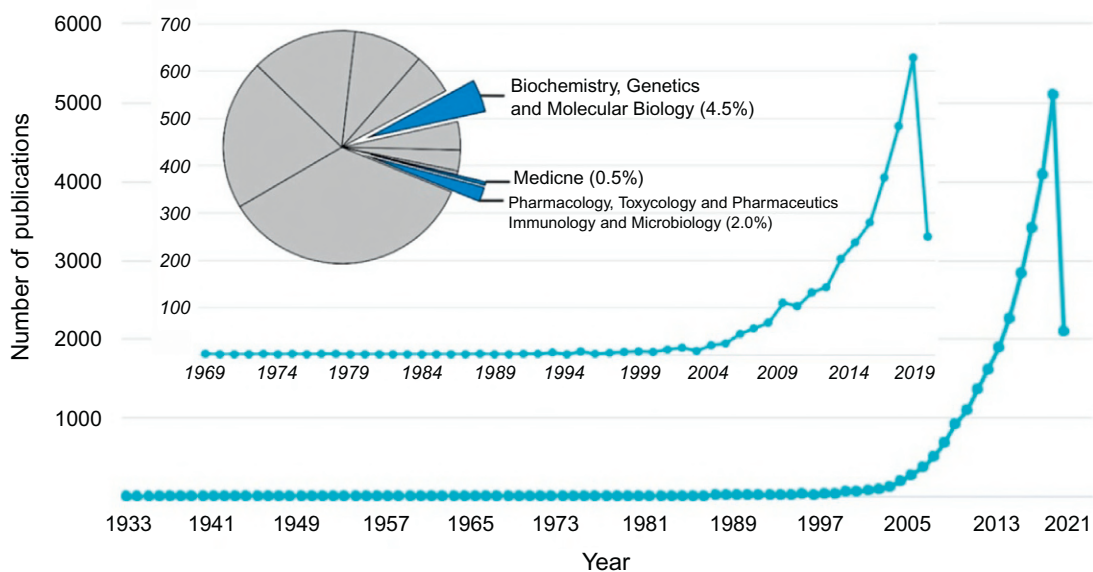
<sup>a</sup>Department of Chemistry, CICECO—Aveiro Institute of Materials, University of Aveiro, Aveiro, Portugal <sup>b</sup>QOPNA & LAQV-REQUIMTE, Department of Chemistry, University of Aveiro, Campus Universitário de Santiago, Aveiro, Portugal

## Abbreviations

|                 |                                        |
|-----------------|----------------------------------------|
| <b>Ade/ad</b>   | adenine                                |
| <b>alen</b>     | alendronate                            |
| <b>APIs</b>     | active pharmaceutical ingredients      |
| <b>Az bz-TC</b> | 3,3',5,5'-azobenzenetetracarboxylate   |
| <b>bioMOFs</b>  | biocompatible MOFs                     |
| <b>BPDC</b>     | biphenyldicarboxylate                  |
| <b>BPOs</b>     | bisphosphonic acids                    |
| <b>Ca-zol</b>   | calcium-zoledronate                    |
| <b>DNA</b>      | deoxyribonucleic acid                  |
| <b>FFA</b>      | free fatty acids                       |
| <b>Fol</b>      | folate                                 |
| <b>FR</b>       | folate receptors                       |
| <b>Gal</b>      | gallate                                |
| <b>Hdfp/dfp</b> | deferiprone                            |
| <b>MOF</b>      | metal-organic framework                |
| <b>Olz</b>      | olsalazine                             |
| <b>pam</b>      | pamidronate                            |
| <b>PBS</b>      | phosphate buffered solution            |
| <b>Pzdc</b>     | 3,5-pyrazoledicarboxylic acid          |
| <b>qPCR</b>     | quantitative polymerase chain reaction |
| <b>RDA</b>      | recommended dietary allowance          |
| <b>RNA</b>      | ribonucleic acid                       |
| <b>ROS</b>      | reactive oxygen species                |
| <b>SBF</b>      | simulated body fluid                   |
| <b>SLBs</b>     | single lipid bilayers                  |
| <b>TAC</b>      | total antioxidant capacity             |
| <b>zol</b>      | zoledronate                            |

## 4.1 Introduction

Metal-Organic Frameworks (MOFs) have been attracting the attention of several research and industry groups, as it can be seen by the notorious increase in the number of publications in this field (see Fig. 4.1). MOFs are a class of hybrid materials with the remarkable ability to combine the properties of different organic ligands and metallic centres in a coordination-based network [1–5]. Depending on the specific functionalities of both components, it is possible to obtain materials with unique properties, which grant them applications in the most diversified areas, such as catalysis, photoluminescence, protonic conductivity, magnetic studies, gas storage, and separation, among others [6–19]. More recently, MOFs found their way into biomedical applications where their physical and chemical characteristics make them promising candidates for drug storage, drug delivery, nitric oxide storage/delivery, bioimaging, and biosensing [20–23]. This evolution throughout time is depicted in Fig. 4.1, with highlight to the number of publications on MOFs with biological relevance and their massive growth in the last 10 years [4, 24, 25].



**Fig. 4.1**

Evolution of published work on MOFs over time. Within the several areas of research, the increasing interest on biological applications is highlighted. *Build with data from Scopus database. Consulted in April 15th 2019. Scopus. (2019). Scopus – Analyze search results: Metal-organic Frameworks. Available at: <https://www.scopus.com> (Accessed 15 April 2019).*

## 4.2 Building blocks for MOFs

When envisioning the design of MOFs towards a specific application, it is easy to come across endless possibilities. In fact, besides the tremendous amount of different metallic centres and organic ligands available, there is also a plethora of different possible combinations between these building blocks (see Fig. 4.2).

In the field of biomedical applications, the design of MOFs is mainly based on two different approaches: (i) the selection of building blocks that convey the MOF with the ability to adsorb guest molecules with biological properties or (ii) the use of biologically active organic building blocks. MOFs prepared using the first approach are typically employed as delivery systems, in which different drugs are impregnated into the pores of the network to be released later under a specific stimulus. Most of the MOFs reported for biomedical applications follow this concept [26, 27]. The second type of networks is considered the new generation of biocompatible MOFs, also called bioMOFs. In this case, the building blocks (organic ligands) are chosen according to their intrinsic biological properties and therapeutic action [28]. In either case, the requirements for biological applications, particularly medical applications *in vivo*, are very demanding and imply a large investment in order to meet the regulatory

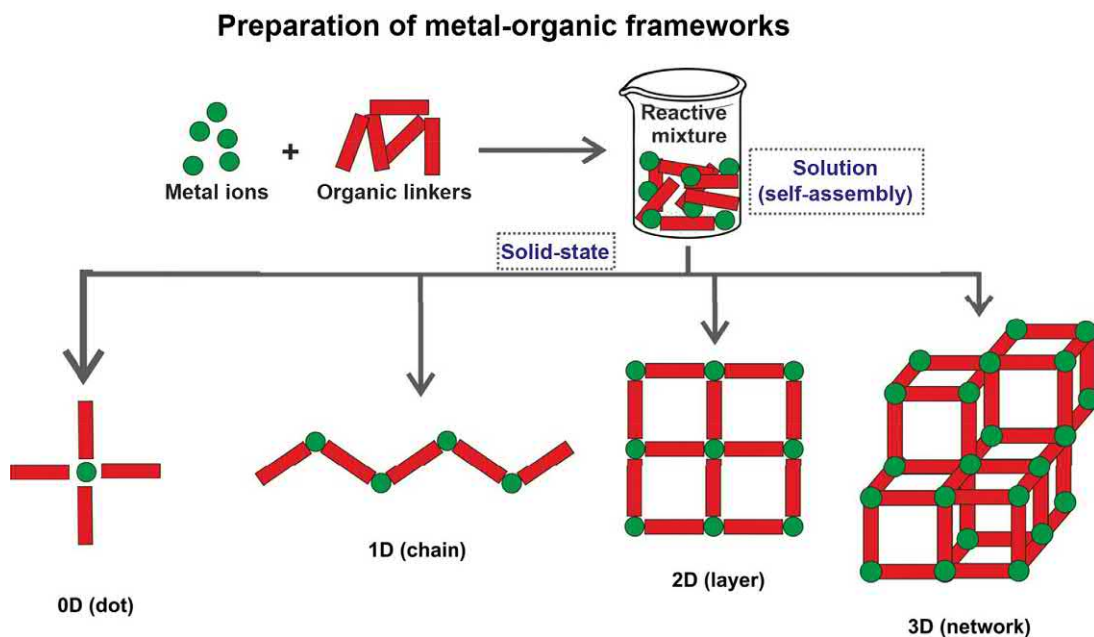


Fig. 4.2

Schematic representation of the composition (● metallic centres and — organic ligands) and assemble of Metal-Organic Frameworks with different dimensionalities: 0D (left), 1D chain (middle left), 2D layer (middle right), and 3D network (right).



requirements associated with their approval for human and animal use. These MOFs have to be effective and their production method must be easy and reproducible [29]. Toxicological safety is another very important condition to fulfil. Examples of MOFs with low toxicity are MIL88A, MIL88B, and MIL100—three different MOFs containing carboxylate ligands (with different structures and organic configurations) that exhibited no harmful effects following intravenous administration to rats at very high doses [30, 31].

The use of biologically relevant ligands or biomolecules in the preparation of MOFs plays a paramount role, while the network presents, on its own, the desired properties for a given application/therapy [24, 28, 32, 33]. At this point, the therapeutic potential is no longer dependent on the porosity of the network (volume and pore size) or the ability to establish host–guest interactions (which sometimes hinders the application of some materials), but on the combination of organic ligands (biomolecules) and/or metals that can at a certain stage be released by dissociation of the network until complete dissolution [28]. Of course, this statement may appear somewhat controversial since it is often stated that the lack of stability hampers the potential use of MOFs. If the MOF remains intact long enough to complete its function, it can then degrade in situ and the degradation products are dealt by the body's own systems. Herein, depending on the crystalline structure, composition, particle size, and formulation, the degradation of MOFs can be modulated from some days to several weeks (up to 3 weeks) under simulated physiological conditions [24, 28, 31, 33].

### ***4.3 Ligands as the core to access biomedical applications***

The careful selection of the building blocks and their combination with biocompatible metal nodes is the fundamental step to build capable bioMOFs. There are a wide variety of compounds that may act as constitutive organic ligands for the rational design of bioMOFs, including amino acids, peptides, proteins, nucleobases, carboxylic acids, phosphonic acids, or even active pharmaceutical ingredients (APIs) and supplements (Fig. 4.3).

Some interesting MOFs based on these bioactive molecules are reported, along with data on their physico-chemical properties. Nevertheless, their biological properties are poorly studied, with insufficient data on their biodistribution and biodegradability in vivo, cell uptake pathways, and even on their actual therapeutic activity.

This chapter intends to provide the reader with information about the organic ligands used in the construction of bioMOFs, as well as their biological applicability, emphasizing a few examples on how bioactive molecules can be used to construct coordination-based networks. Compounds relevant for use as organic ligands must contain complexing groups such as polycarboxylates, phosphonates, sulfonates, imidazolates, amines, pyridyl, phenolates, and/or heterocycles [24, 31].

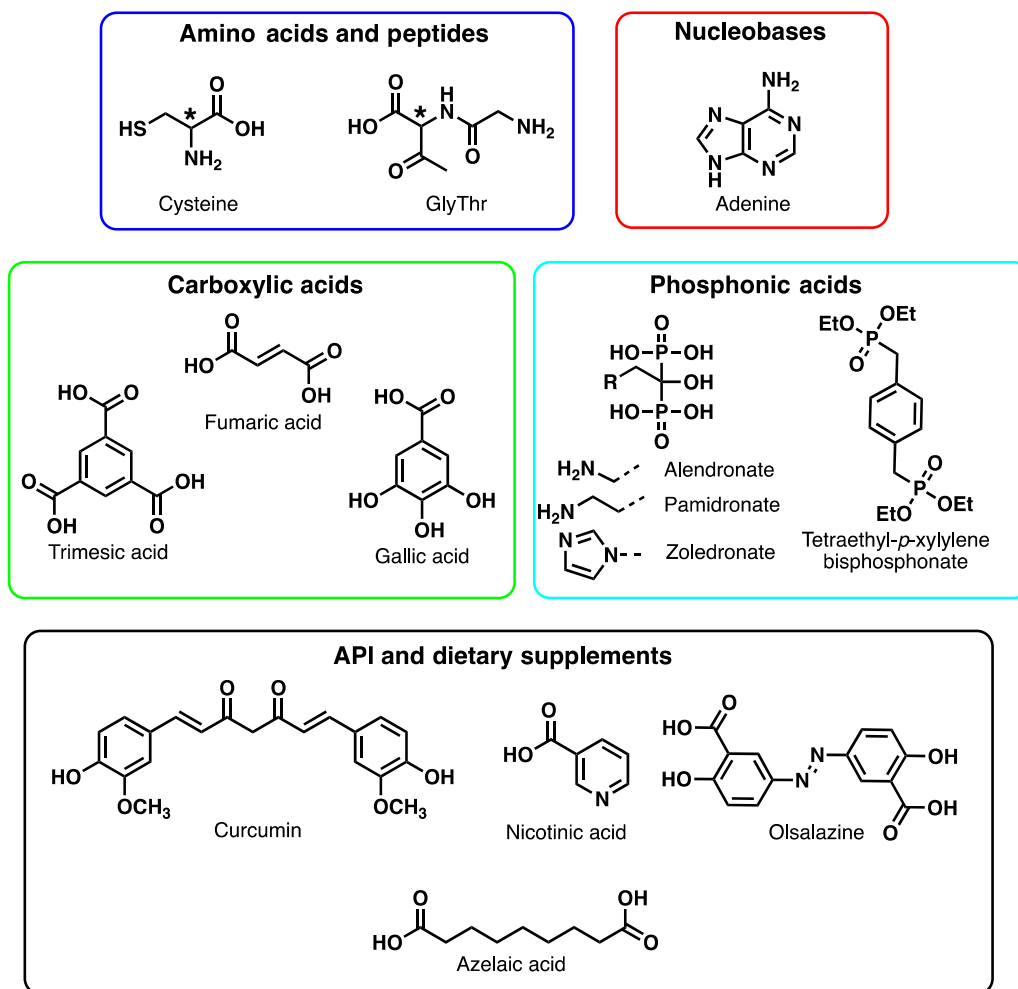


Fig. 4.3

Bioactive compounds used in the preparation of biocompatible MOFs.

#### 4.3.1 Amino acids and peptides

Amino acids are important biomolecules composed of an amino and a carboxylic terminal group ( $-\text{NH}_2$  and  $-\text{COOH}$ ), as well as an R side-chain, specific to each amino acid. The various amino acids can establish amide bonds between their terminal groups to form peptides, while maintaining in the final molecule the free  $-\text{NH}_2$  and  $-\text{COOH}$  groups. In fact, these terminals are the structural feature that enables amino acids and peptides to coordinate with metallic centres and form bioMOFs [28, 34]. The carboxylic groups in the amino acids provide a series of strong coordination modes due to their large negative charge density. Moreover, adjacent carboxylic and amino groups are able to coordinate with metallic centres in specific

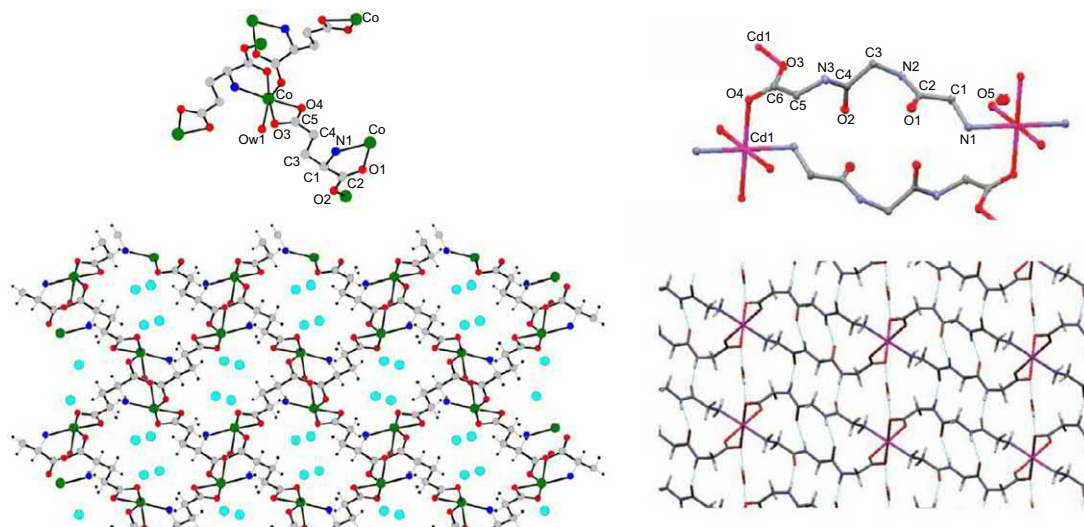
angles and directions (O,N—chelating modes), which is of utmost importance to obtain extended network structures.

Additional coordination modes are possible when the side-chain of the amino acid has groups that bind to metals, such as a carboxylic, imidazole, thioether, or phenol ring. In these cases, the formation of networks with higher degrees of dimensionality can be promoted [34, 35]. One prolific example of the use of an amino acid having a side-chain that provides additional coordination is the amino acid-based Zr-MOF, denoted as MIP-202(Zr), in which the 12-connected  $Zr_6(\mu_3-O)_4(\mu_3-OH)_4$  node and the *L*-aspartate spacer are assembled in water to generate a 3D microporous framework with a UiO66 type structure [36]. MIP-202(Zr) not only features a green and scalable synthesis, but also possesses very high hydrolytic and chemical stability. While a high degree of dimensionality is a strongly demanded quality in a MOF structure, the use of amino acid-based chirality within these networks is essentially the most appealing feature associated with their use as ligands.

Two recent approaches have been particularly successful in the synthesis of chiral MOFs, both relying on the use of chiral amino acids to form the framework of the material. The first method, used by Morris et al., uses a chiral co-ligand (in this specific case, *L*-aspartate) that does not bridge the metal centres, but forces chirality by coordinating to the metal centre [36]. On the other hand, the most common method uses a chiral organic bridging ligand to link the metal centres in the framework. The resulting homochiral/enantiomerically pure networks can display interesting properties for further applications in the fields of asymmetric catalysis, enantioselective separation, circular dichroism sensors, and magnetism [37–41]. As so, nowadays, numerous amino acid-based MOFs are reported [42]. For instance, Rosseinsky et al. and Jacobson et al. prepared two distinctive homochiral MOFs from aspartic acid in combination with different metallic centres (zinc and nickel, respectively). On both networks, the three-dimensionality was enabled by three possible coordination modes of the amino acid to the metallic centre [43, 44]. Another chiral three-dimensional network was designed by Bernal et al., where glutamic acid was used as ligand mixed with cobalt metallic centres (Fig. 4.4, left) [45].

On a different perspective, Marsh et al. described a series of four different networks, in which peptides were used as organic ligands: either a tripeptide of alanine or glycine; or a dipeptide of alanine or alanine-threonine— $Cd(L-Ala_3)_2$ ,  $Cd(Gly_3)_2 \cdot H_2O$ ,  $Cd(L-Ala_2)_2$ , and  $Cd(L-Ala,L-Thr)_2 \cdot 4H_2O$ , respectively (Fig. 4.4, right) [46].

It is important to notice that most of these reports emphasize mainly the description of the synthesis and crystalline structure characterization [47, 48]. Very few papers report application studies of the materials, which are focused on magnetism and gas adsorption [44, 45]. In fact, although amino acids and peptides are the most widespread ligands used in the preparation of MOFs, not all the MOFs made from them are designed for biocompatible purposes and therefore they cannot be used as bioMOFs. Using metals as zirconium and nickel, for instance,



**Fig. 4.4**

Chiral three-dimensional MOFs. Co-Glutamic acid-based MOFs (left); Cd MOFs prepared by Marsh et al. (right). Based on Zhang, Y., Saha, M., Bernal, I., 2003. *[Cobalt(II)L-glutamate(H<sub>2</sub>O)·H<sub>2</sub>O]<sub>∞</sub>: a new 3D chiral metal-organic interlocking network with channels. CrystEngComm. 5, 34–37; Lee, H.-Y., et al., 2008. Covalent metal–peptide framework compounds that extend in one and two dimensions. Cryst. Growth Des. 8 (1), 296–303.*

increases network stability, but it also increases the inherent toxicity. Moreover, the use of such metals completely disregards the rationale behind the preparation of bioMOFs, where the slow release of the MOFs constituents for a given treatment is the core concept. However, it is possible to find a few examples in the literature focused on understanding the biomedical potential of bioMOFs. In one of these few examples, Terzyk et al. studied the antioxidant potential of a bioMOF composed by cysteine and magnesium. In vitro studies of the bioMOF showed an increase in the intracellular levels of cysteine over time, interpreted as the result of network disintegration over time with release of its building blocks to the culture medium and their subsequent uptake by human lung epithelial cells (A549 cell line). Given that this ligand contains sulfhydryl groups in its structure, the authors expected it to be able to lower the antioxidant activity within the cells. This was measured through a total antioxidant capacity (TAC) test, which showed an ability to reduce Cu ions. Adding to the promising results on the antioxidant capacity, this bioMOF also presented low toxicity on healthy cells [49]. In a prior study, Ueda et al. prepared a coordination polymer constructed by the glycine-threonine peptide and zinc, denominated  $[Zn(\text{glythr})_2(\text{H}_2\text{O})_2] \cdot n\text{H}_2\text{O}$ . This material was analyzed concerning its ability to inhibit the adrenalin-induced release of free fatty acids (FFA) from isolated rat adipocytes. The results showed a high insulinomimetic activity for the MOF when compared with standard  $\text{ZnSO}_4$ , with  $\text{IC}_{50}$  values of  $0.96 \pm 0.05$  and  $1.58 \pm 0.05$  mmol L, respectively [50].

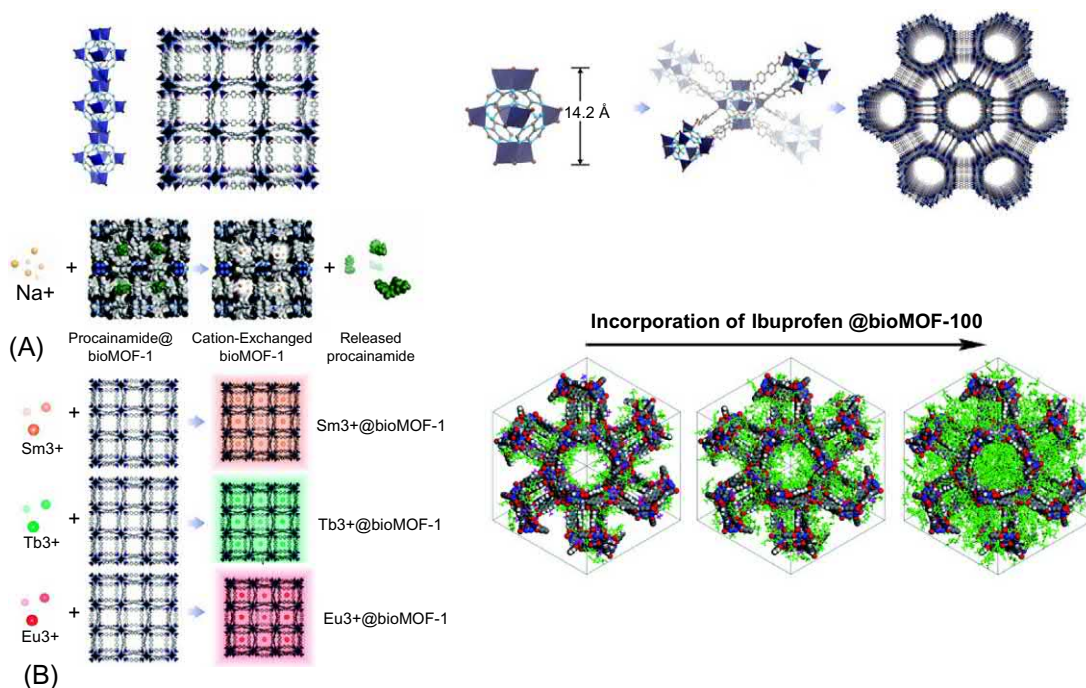
### 4.3.2 Nucleobases

Nucleobases, the key constituents of nucleic acids (deoxyribonucleic acid, DNA and ribonucleic acid, RNA), have been explored as ligands for the construction of MOF-based materials. The structural feature that turns these molecules into suitable ligands is the presence of multiple coordination sites by (i) accessible nitrogen and oxygen lone pairs and/or (ii) by strong hydrogen bonds [28, 34, 35, 51]. Adenine (ade/ad), having five potential metal-binding sites (Fig. 4.3), is thus the most frequently used nucleobase [28, 34]. Despite the several coordination possibilities, it is important to notice that the low symmetry and limited length of adenine molecules (and other nucleosides) restrict their ability to afford three-dimensional MOFs [52]. When porosity is a desired property, the use of a secondary auxiliary ligand is crucial to construct 3D networks [35].

A significant amount of literature reports addresses the design and preparation of nucleoside-based bioMOFs [24, 28]. As described below, the applications of such materials are varied, with some of them directed to CO<sub>2</sub> capture opposing a surprising handful of them that are focused on biomedical applications. For instance, Rosi et al. and Rosseinsky et al. described two adenine-based MOFs with different compositions and crystalline structures:

$[\text{Zn}_8(\text{ade})_4(\text{BPDC})_6\text{O}]\cdot 2\text{Me}_2\text{NH}_2$  and  $[\text{Ni}_3(\text{pzdc})_2(7\text{Hade})_2(\text{H}_2\text{O})_4]\cdot (\text{H}_2\text{O})_{2.18}$ , respectively [53, 54]. Both materials are 3D networks and were efficiently applied on CO<sub>2</sub> adsorption, the last one showing a good selectivity of CO<sub>2</sub> over CH<sub>4</sub>. In fact, for this specific application, the three-dimensionality and inherent porosity of the network were imperative and could only be achieved with the use of secondary ligands (as previously mentioned): either the biphenyldicarboxylate (BPDC) or the 3,5-pyrazoledicarboxylic acid (pzdc), respectively [53, 54]. In the first case, BPDC interconnects one-dimensional chains of Zn-adenine, which results in a 3D structure with large 1D channels. In the second case, pzdc established a bridge between dimeric units of Ni-adenine, forming a one-dimensional chain along the *c* axis. The porosity of the material was then achieved due to interactions between parallel chains, by means of strong and weak hydrogen bonds (from the adenine amino group N10) to two carboxylate oxygen (from the carboxylic acid) and via  $\pi$ - $\pi$  interactions (between the pyrimidine rings of adenine).

Further developments on nucleobase-based MOFs include the pioneer work of Rosi et al. with the development of  $[\text{Zn}_8(\text{ad})_4(\text{BPDC})_6\text{O}]\cdot 2\text{Me}_2\cdot\text{NH}_2$ , a MOF suitable both for CO<sub>2</sub> capture and for cationic drug delivery [53, 55]. The promptly denominated bioMOF-1 has a three-dimensional structure with channels containing an intrinsic anionic nature balanced by the presence of dimethylammonium cations (a product of DMF decomposition as well as DMF and water molecules). This cationic nature proved to be a crucial characteristic, when the authors loaded cationic drugs into the channels via cation exchange with the dimethylammonium cations. This was performed with procainamide-HCl (an antiarrhythmic drug), without changing the crystalline integrity,  $[\text{Zn}_8(\text{ad})_4(\text{BPDC})_6\text{O}]\cdot 3.5(\text{procainamide-H})\cdot$



**Fig. 4.5**

Examples of adenine-based bioMOFs. (A) Adsorption and release mechanism of procainamide from bioMOF-1; (B) bioMOF-1 doped with lanthanides; (C) Incorporation of ibuprofen in bioMOF-100. Based on An, J., Geib, S.J., Rosi, N.L., 2009. Cation-triggered drug release from a porous zinc-adeninate metal-organic framework. *J. Am. Chem. Soc.* 131 (24), 8376–8377; An, J., et al., 2011. Zinc-adeninate metal-organic framework for aqueous encapsulation and sensitization of near-infrared and visible emitting lanthanide cations. *J. Am. Chem. Soc.* 133 (5), 1220–1223; An, J., et al., 2012. Metal-adeninate vertices for the construction of an exceptionally porous metal-organic framework. *Nat. Commun.* 3, 604; Bernini, M.C., et al., 2014. Screening of bio-compatible metal-organic frameworks as potential drug carriers using Monte Carlo simulations. *J. Mater. Chem. B.* 2 (7), 766–774.

1.5Cl·16.5H<sub>2</sub>O. Furthermore, the controlled release of procainamide·HCl, over the course of 72 h, was possible when exogenous cations from biological fluids (e.g., Na<sup>+</sup>) were used to trigger its release (Fig. 4.5A). These results show that it is possible to circumvent the short half-life of procainamide in vivo, making way for ingenious new strategies of delivering this drug to patients in a controlled fashion. Nevertheless, it would be recommended to use another metallic centre because of the high doses of procainamide needed. In its current dosage forms, procainamide needs to be taken every 3–4 h to maintain the therapeutic seric levels, with total daily doses of 500–1000 mg. Given the high amounts of zinc in its composition, the direct application of the bioMOF-1 to deliver procainamide would imply an intake of c.a. 600 mg Zn for each 1000 mg of the API. This makes the bioMOF-1 unlikely to be approved for human use, because of zinc-related toxicity. Indeed, the Recommended Dietary Allowance



(RDA) of zinc is as low as 8 mg per day for women and 11 mg per day for men and pregnant women [56]. Acute toxicity is associated with gastrointestinal complications, while chronic intake of excess zinc induces copper deficiency, altered iron function, and reduced immune function [56, 57].

BioMOF-1 was further demonstrated to serve as a luminescent and prospect sensing material when visible and near-infrared emitting lanthanide cations are encapsulated in its pores (Fig. 4.5B) [58]. When loaded with  $\text{Yb}^{3+}$ , bioMOF-1 showed a luminescence signal dependent on the presence of  $\text{O}_2$  gas. Upon excitation with 340 nm light and exposure to pure  $\text{O}_2$  gas for at least 5 min, the luminescence signal of the material decreased by approximately 40%; luminescence intensity could then be restored after exposure to  $\text{N}_2$  gas.

The zinc-adenine building units that are the base of construction of bioMOF-1 can also be employed as discrete metal-organic vertices for the assembly of new bioMOFs with larger pores. To this end, the reaction conditions used to prepare bioMOF-1 are optimized to avoid the growth of monodimensional zinc-adenine chains and form discrete clusters instead. These clusters comprise eight zinc cations in coordination with four adenine ligands, thus being significantly larger in size than their well-known zinc-carboxylate equivalents (14.3 Å versus  $\sim 10.5$  Å in diameter). As a result of this exceptionally large size, each cluster connects to a neighbor unit via three auxiliary BPDC ligands (instead of one, as in the bioMOF-1), being also connected to a total of four neighboring zinc-adenine clusters. The periodical repetition of this connectivity over an extended three-dimensional framework results in a new material with incredibly large cavities,  $[\text{Zn}_8(\text{ad})_4(\text{BPDC})_6\text{O}_2] \cdot 4\text{Me}_2\text{NH}_2 \cdot 49\text{DMF} \cdot 31\text{H}_2\text{O}$ , also known as bioMOF-100 [59]. With a pore volume of  $4.3 \text{ cm}^3 \text{ g}^{-1}$ , bioMOF-100 presents an extraordinary potential for biological applications, either in drug delivery systems or for the immobilization of large biomolecules. In fact, a later work, focused on Monte Carlo simulations, showed that bioMOF-100 could store an outstanding 2 g of ibuprofen ( $\alpha$ -*p*-isobutylphenylpropionic acid) per gram of material (Fig. 4.5C). Moreover, the presence of dimethylammonium cations on the channels of bioMOF-100 helps reinforce the interactions between the network and the ibuprofen molecule, which in turn allows a slow release of kinetics [60].

### 4.3.3 Carboxylic acids

Carboxylic acids and their carboxylate salts are abundant in the organism and participate in many biochemical processes of cell machinery; some of them even have more than one carboxyl group. The best example is the Krebs cycle, a sequence of metabolic reactions crucial for the production of energy, in which the intermediates are carboxylic acids (e.g., fumaric, malic, and succinic acids). The COOH functional group of these molecules, besides the biochemical reactivity, also conveys them with the ability to bind metallic centres under different modes of coordination, which makes them promising ligands to be incorporated in bioMOFs [34].

Yaghi et al. recently reported MOF-1201 and MOF-1203, two porous chiral MOFs comprising L-lactate and calcium ions and capable of encapsulating and delaying the release of *cis*-1,3-dichloropropene, a pesticide used as a preplant soil fumigant to control nematodes and other pests in soils [61]. The carrier materials decompose naturally in water, decreasing their environmental impact. Although not yet used in biomedical applications, these two materials have a biocompatible composition and degradation profile, thus being a good example of safe, eco-friendly MOF with potential interdisciplinary integration.

Carboxylic-based MOFs with demonstrated application in medicine are also known (see Fig. 4.3). Serre et al. reported BioMIL-3 or  $[\text{Ca}_2(\text{azbz-TC})(\text{H}_2\text{O})(\text{DMF})] \cdot x\text{H}_2\text{O} \cdot y\text{DMF}$  ( $x \cong 0.4$  and  $y \cong 0.2$ ), a porous network constructed with 3,3',5,5'-azobenzenetetracarboxylate (azbz-TC) as a ligand in coordination with calcium metallic centres. When dried, BioMIL-3 can adsorb NO into its pores. The pores of BioMIL-3 bear unsaturated  $\text{Ca}^{2+}$  sites that interact with gaseous NO gas and allow it to be slowly released from the network over a period of more than 10 h. BioMIL-3 is, according to the authors, an interesting approach for the delivery of NO gas in biomedical applications [62]. It is important to notice that, in this case, even though the carboxylic-based MOF may be applied in biological functions, the carboxylic acid does not have a direct role in this application. As a ligand, its relevance was merely towards the construction of a network with adequate porosity and geometry for the mentioned application. Nonetheless, there are also a few studies in which the carboxylic acid as a ligand has a more active function.

In the work of Gref et al., a series of porous MOFs was prepared with iron as the metallic centre and various carboxylic acids as the ligands. MIL-53, MIL-88A, and MIL-100 contain terephthalic, fumaric, and trimesic acids, respectively. As a result, the different frameworks present pores with distinct dimensions, the larger being MIL-100 (25–29 Å) followed by MIL-88A (8.6 Å) and finally MIL-53 (6 Å). In vitro studies on the degradation of these materials under physiological conditions showed that the networks of MIL-88A and MIL-100 disintegrated during 7 days at 37°C and released large amounts of the respective carboxylic acids (fumaric and trimesic acid). Note that these molecules are endogenous in the body and present low toxicity (fumaric acid,  $\text{LD}_{50} = 10.7 \text{ g kg}^{-1}$ ; trimesic acid,  $\text{LD}_{50} = 8.4 \text{ g kg}^{-1}$ ), thus they could be further used by the organism or excreted without posing a threat. The loading capacity of these MOFs was tested with a wide range of anticancer and antiviral drugs. Efficient loading and release occurred for the combinations of MIL-53 with cidofovir (cytosine phosphate analogue, antiviral), of MIL-88A with busulfan (1,4-butanediol dimethanesulfonate, antitumoural), and of MIL-100 with cidofovir and azidothymidine triphosphate, an antiretroviral (Fig. 4.6, left). The release of azidothymidine triphosphate from MIL-100 occurred over 3 days of immersion in simulated physiological conditions (phosphate buffered solution, PBS at 37°C) [30]. The versatility of MIL-100 is evidenced by numerous literature reports, in which further surface engineering improved its stability without disrupting its porosity, crystallinity, structure, and adsorption/release abilities [63–65].

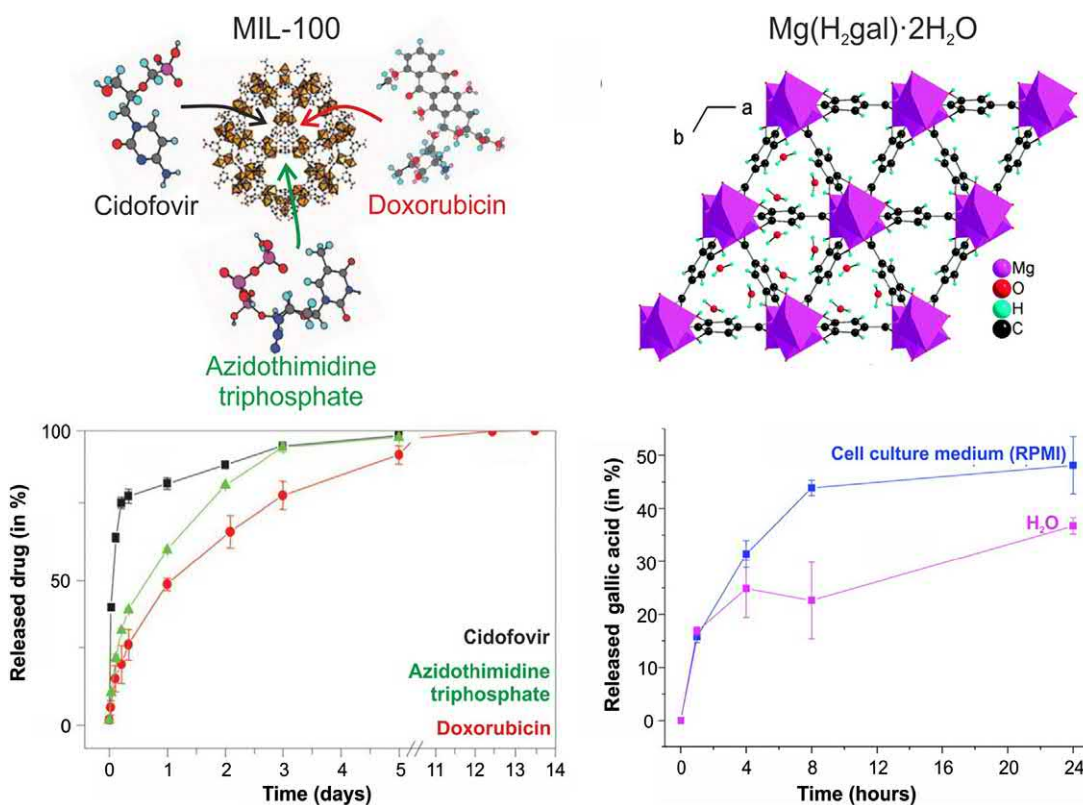


Fig. 4.6

MIL-100 structure adsorption (*top left*); MIL-100 adsorption and release of three APIs (*bottom left*); Mg(H<sub>2</sub>gal)·2H<sub>2</sub>O structure (*top right*); released gallic acid over time in H<sub>2</sub>O and cell culture medium (*bottom right*). Based on Horcajada, P., et al., 2009. Porous metal–organic-framework nanoscale carriers as a potential platform for drug delivery and imaging. *Nat. Mater.* 9, 172; Cooper, L., et al., 2015. A biocompatible porous Mg-gallate metal-organic framework as an antioxidant carrier. *Chem. Commun.* 51 (27), 5848–5851.

Another microporous carboxylic-based MOF was prepared by Devic et al., having gallate as the ligand and coordinated magnesium as the metallic centre. Studies on the stability at 37°C of Mg(H<sub>2</sub>gal)·2H<sub>2</sub>O in both water and RPMI cell culture medium showed that the network slowly disintegrates and releases the ligand, gallic acid, into the solution (Fig. 4.6, right).

The degradation is faster in RPMI, with ca. 48 ± 5% of the carboxylic acid being released to medium after 24 h, versus 37 ± 1% when it is in pure water. Gallic acid also has antioxidant properties, being further demonstrated that Mg(H<sub>2</sub>gal)·2H<sub>2</sub>O lowers the production of Reactive Oxygen Species (ROS) by cells of the human promyelocytic leukemia line (HL-60) [66].

In follow-up studies, two novel 3-D bioMOFs, MIL-155 and MIL-156, were built from calcium and the same ligand [67]. These solids present different inorganic subunits: MIL-155 or [Ca<sub>2</sub>(H<sub>2</sub>O)(H<sub>2</sub>gal)<sub>2</sub>]·2H<sub>2</sub>O has infinite chains of edge-sharing dimers of CaO<sub>7</sub> polyhedra linked

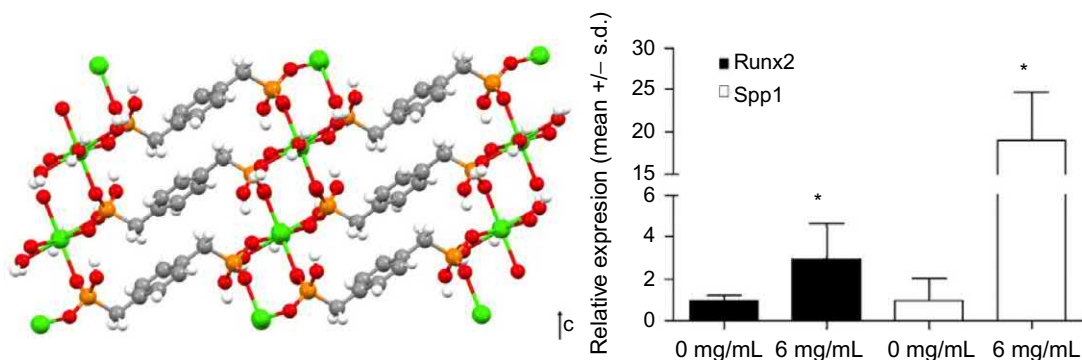
through partially deprotonated gallate ligands and MIL-156 or  $[\text{Ca}_3\text{K}_2(\text{H}_2\text{O})_2(\text{gal})_2] \cdot n\text{H}_2\text{O}$  ( $n \sim 5$ ) is made from ribbon-like inorganic subunits containing both eight-fold and six-fold coordinated calcium ions linked through fully deprotonated gallate ligands. While made from the same constituents, the two materials exhibit very distinct solubility profiles in relevant simulated biological media. MIL-156 does not present any antioxidant effect because of its high chemical stability, while the progressive release of the gallate ligand from the less stable MIL-155 leads to a remarkable antioxidant effect, which is even higher than that previously reported for  $\text{Mg}(\text{H}_2\text{gal}) \cdot 2\text{H}_2\text{O}$ . Taken together, these results demonstrate how carboxylic acids can be successfully applied in the design of bioMOFs having interesting therapeutic properties that can be further explored for future applications.

#### 4.3.4 Phosphonic acids

MOFs with phosphonic acids as ligands are characterized by the presence of strong metal to  $\text{O}_3\text{P}-\text{C}$  bonds. Along with the high stability of  $\text{P}-\text{C}$  bonds to elevated temperatures, this allows the preparation of MOF materials with high chemical and thermal stabilities [9]. With such favorable characteristics, it is not surprising to find numerous examples of MOFs with phosphonic acids as ligands in the literature. Nonetheless, only a few of these are designed and prepared with ligands holding interesting biomedical properties. Highlighted is a very specific class of bioMOFs that contain bisphosphonic acids (BPOs) as ligands.

BPOs are a class of compounds composed by two phosphonate groups linked by nonhydrolysable phosphoether bonds to a central carbon atom (a  $\text{P}-\text{C}-\text{P}$  core, Fig. 4.3). [68]. The  $\text{P}-\text{C}-\text{P}$  bonds in the core give BPOs the ability to bind strongly and selectively to bone tissue and to modulate bone growth and remodeling [68–74]. Nowadays, the drug class of BPOs comprises a broad set of commercially available molecules, employed in the treatment and prevention of osteoporosis and other several bone-related disorders [75–79]. The medicinal properties of BPOs, allied with the availability of several coordination sites in their structures, make them very attractive ligands for the preparation of MOFs. A wide variety of BPO-MOFs is already reported, with the main focus on the structural description and physical properties [80–86]. The reported applications cover a variety of fields, but biological and medicinal uses are strongly unexplored. Nonetheless, there are still a few reports on the therapeutic potential of the prepared BPO-based MOFs (Fig. 4.7) [87–89].

A network composed by calcium metallic centres in coordination with the BPO ligand alendronate,  $[\text{Ca}(\text{H}_3\text{alen}) \cdot \text{H}_2\text{O}]$ , was recently reported to promote in vitro osteoblast differentiation along with the inhibition of the proliferation and differentiation of osteoclasts [88]. Another study, by Alvarez et al., reports a material obtained from the same calcium and alendronate precursors, but having inert behavior, i.e., no bioactive properties were observed in simulated body fluid (SBF) [87]. Since different approaches were used to study the biological properties of both materials, a practical direct comparison of the results is



**Fig. 4.7**

Structure and activity of two BPO-based MOFs: on the left, the structure of an alendronate-containing bioMOF; on the right, the structure of CaP1 bioMOF and its effect on the activity of MG63 osteosarcoma cell line. Cells were treated with CaP1 for 15 days, followed by extraction and quantification of the levels of Runx2 and Spp1 mRNA by qPCR (quantitative polymerase chain reaction). Runx2 is a multifunctional transcription factor that controls skeletal development by regulating the differentiation of osteoblasts and the expression of many extracellular matrix protein genes. During osteoblast differentiation, Runx2 upregulates the expression of bone matrix protein gene Spp1. Based on Boanini, E., et al., 2013. *Crystalline calcium alendronate obtained by octacalcium phosphate digestion: a new chance for local treatment of bone loss diseases?* *Adv. Mater.* 25 (33), 4605–4611; Shi, F.N., et al., 2015. *Calcium phosphonate frameworks for treating bone tissue disorders.* *Inorg. Chem.* 54 (20), 9929–9935.

impossible. However, given that both present the same composition  $[\text{Ca}(\text{H}_3\text{alen})]\cdot\text{H}_2\text{O}$ , we can postulate that the different biological activity results from different crystallographic structures. While the first crystallizes on the spatial group  $\text{P}2_1/\text{n}$ , the latter belongs to the  $\text{P}2_12_12_1$  spatial group [87, 88]. The different spatial arrangements of the atoms could have an influence on their interaction with the surrounding medium.

Starting from two different BPOs, pamidronate (pam) and zoledronate (zol), Lin et al. prepared two interesting cytotoxic bioMOFs. Both feature calcium metallic centres and they are named Ca-pam  $[\text{Ca}(\text{H}_2\text{-pam})(\text{H}_2\text{O})]\cdot\text{H}_2\text{O}$  and Ca-zol  $[\text{Ca}(\text{H}_2\text{-zol})(\text{H}_2\text{O})]$ . Following the preparation step, the MOFs were coated with single lipid bilayers (SLBs) and further conjugated with anisamide to improve the network stability and enable them to target cancer cells. In vitro studies showed that both MOFs were able to induce apoptosis on H460 human nonsmall lung cancer cells (with  $\text{IC}_{50}$  values of  $1.0 \pm 0.1 \mu\text{M}$  and  $0.84 \pm 0.2 \mu\text{M}$ , for Ca-pam and Ca-zol, respectively), while only Ca-zol revealed a cytotoxic effect on AsPC-1 human pancreatic cancer cells (with  $\text{IC}_{50}$  values of  $3.6 \pm 2.3 \mu\text{M}$ ) [89].

Using a similar approach, Wang et al. developed a new bio-resorbable sub-100 nm diameter pH-responsive MOF of calcium zoledronate (Ca-zol) as a potential cytotoxic anticancer agent [90]. Folate (Fol) was also incorporated in the MOF, because folate receptors (FR)

are known to be overexpressed in several tumors and thus this ligand may facilitate tumor uptake. The MOF had excellent chemical and colloidal stability under physiological conditions, and it was able to encapsulate more zol than any other existing drug delivery system. It outperformed pure zoledronate regarding the in vitro ability to inhibit cell proliferation and induce apoptosis in two tumor cell lines (FR-overexpressing nonsmall-cell lung carcinoma line, H460, and prostate cancer line, PC3). In vivo studies using mouse xenograft models of H460 and PC3 confirmed the superior activity of the MOF, which is 80%–85% more active than pure zoledronate.

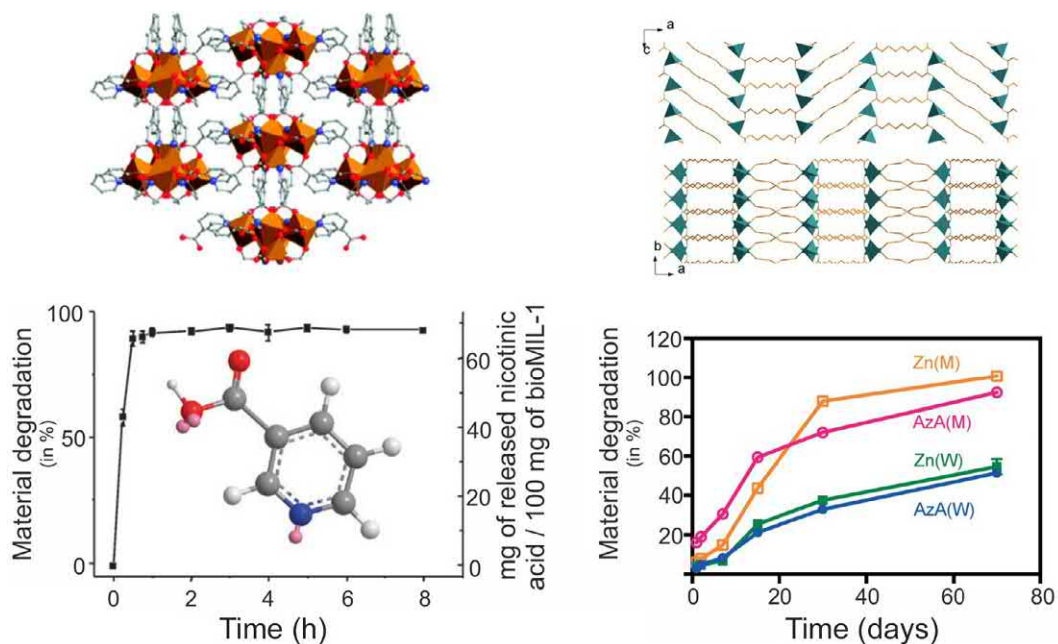
BioMOFs with other BPOs, besides the commercially available ones, are very rare. To the best of our knowledge, there is only a single study in which a noncommercial BPO was used to prepare MOFs directed towards biomedical applications. Using calcium as metallic centre and the BPO tetraethyl-*p*-xylylenebisphosphonate as ligand, Rocha et al. obtained two distinct MOFs,  $[\text{Ca}(\text{H}_2\text{O})_3(\text{HPXBP})]$  (CaP1) and  $[\text{Ca}_2(\text{H}_2\text{O})_2(\text{HPXBP})_{1.5}]$  (CaP2) (Fig. 4.7, top right), which are organized into three-dimensional networks. The differences in their crystalline structures, with different spatial arrangement of the components, may account for the different bioactivities of these materials: CaP1 promotes the formation of bone-precursor phases (calcium phosphates and hydroxyapatite) and stimulates the activity of osteoblasts, while CaP2 does not show any bioactive behavior [91].

#### 4.3.5 Active pharmaceutical ingredients and dietary supplements

Until recently, MOFs developed with the intended application of drug delivery would be regarded only as carriers. Such application requires, as mentioned before, a framework with three-dimensionality and large pores, along with additional characteristics to ease the incorporation of the desired drug (such as the ability to establish host-guest interactions). Moreover, the whole process for the encapsulation and release of the drug is strongly dependent on diffusion rates and matrix degradation kinetics, which in turn could also be associated with the release of exogenous ligands with added toxicity issues [24, 28, 31, 92]. An alternative is to use APIs or other actives as endogenous ligands to construct bioactive networks, similar to the majority of the bioMOFs described this far. In fact, a strong and preponderant factor that propels the design and preparation of such materials is that most of the drugs in the market already possess multiple coordinating groups in their structure (e.g., carboxylic and phosphonic acids) (see Fig. 4.8) [93].

In 2010, Serre et al. reported the first bioMOF containing pyridine-3-carboxylic acid, also known as niacin or vitamin B3. As an essential nutrient, vitamin B3 deficiency induces a skin disease called pellagra, and its regular intake is needed to maintain adequate cellular metabolism, intestinal and brain functions, and the regulation of lipoproteins. The vitamin B3-based material, named bioMIL 1 by the team that developed it, contains iron as metal centre [90]. The stability of bioMIL-1 is relatively low and studies show it decomposes in





**Fig. 4.8**

Structure and decomposition profile of bioMIL-1 (left); structure and decomposition profile of Zn-Azolate bioMOF (right). Based on Miller, S.R., et al., 2010. *Biodegradable therapeutic MOFs for the delivery of bioactive molecules*. *Chem. Commun.* 46 (25), 4526–4528; Tamames-Tabar, C., et al., 2015. *A Zn azelate MOF: combining antibacterial effect*. *CrystEngComm.* 17 (2), 456–462.

approximately 1 h under simulated physiological conditions (PBS, pH = 7.4, 37°C, Fig. 4.8, left). It should be further noted that the use of iron as a metal centre for bioMOFs is not recommended due to the daily intake limit associated with elemental iron, that is, iron should not be taken at doses higher than 20 mg kg<sup>-1</sup> day<sup>-1</sup> [94]. Furthermore, iron is to be taken only in case of deficiency, since it is known to bioaccumulate in the body due to the lack of active physiological excretion pathways making iron loss very low (estimated around 1–2 mg per day) [93, 95, 96]. A second bioMOF, bioMIL-2, was obtained using calcium and glutaric (propane-1,3-dicarboxylic) acid as a ligand, but it also decomposes rapidly in aqueous medium [97]. These two reports, although describing bioMOFs that decompose quite rapidly, can be regarded as a driving force towards similar studies in the future, in which the degradation profiles will be modulated to meet the length of the treatment.

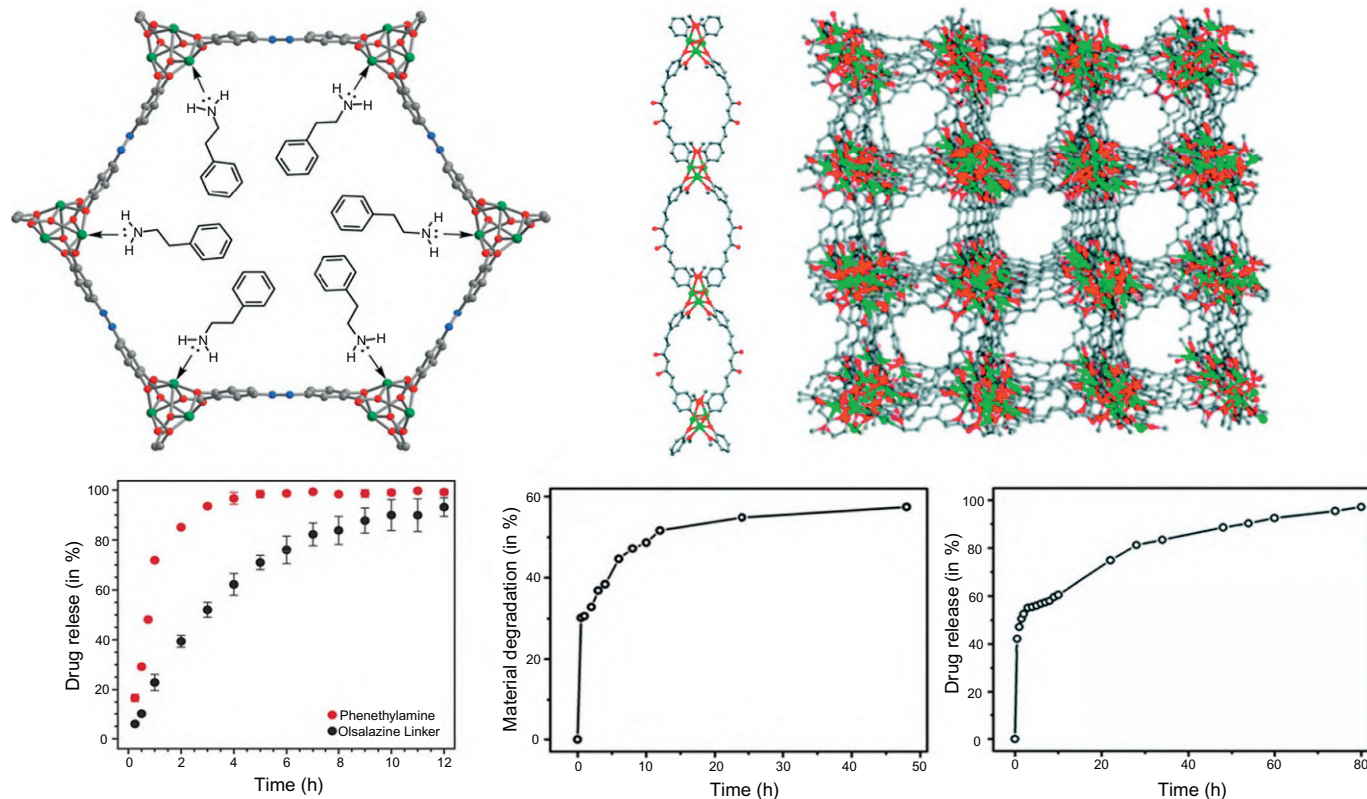
A series of bioMOFs with deferiprone (Hdfp) was reported in 2013 by Spencer et al. [98]. Deferiprone is a second-line iron-chelating agent used in the treatment of patients with transfusional iron overload due to thalassemia syndromes (when current chelation therapy is inadequate) [99, 100]. In these networks, the drug was coordinated with zinc metallic centres. One of these MOFs, [Zn<sub>3</sub>(bdc)<sub>2</sub>(dhp)<sub>2</sub>]<sub>2</sub>·2DMF, does not release the drug when

suspended in DMSO or methanol; however, when suspended in phosphate buffered saline (PBS buffer), HCl-PBS buffer (pH 5.5), 1 N HCl, or saturated citric acid solution, the network rapidly decomposes into the corresponding components and the drug was released.

Blanco-Prieto et al. reported a material constituted by azelaic (1,7-heptanedicarboxylic) acid as a ligand in coordination with zinc metallic centres (Fig. 4.8, right). With this approach, the authors intended to combine the therapeutic effects of the network components: azelaic acid is approved for the topical treatment of rosacea [101], being also popular in acne products, and cationic zinc ( $Zn^{2+}$ ) also exhibits some antibacterial action [102]. Additionally, the controlled release of azelaic acid from the network would be expected to help curb the low solubility and bioavailability issues. The new three-dimensional bioMOF [ $Zn(C_9O_4H_{14})$ ] was called bioMIL-5. Studies on its decomposition profile showed two different rates in MilliQ water and MHCA bacteria broth. After 70 days, only 55% had decomposed in water, whereas in MHCA broth almost all the material had decomposed (95%). This was attributed to differences in the pH of the medium (pH of water is lower than of the MHCA) and to the presence of several amino acids, sugars, and salts in the MHCA broth, which could compete for the zinc metallic centre sites. The antibacterial activity of bioMIL-5 was tested on two Gram-positive bacteria (*Staphylococcus aureus* and *Staphylococcus epidermidis*), and the material maintained the biological activity of its components. More importantly, it was showed that, at long-term, bioMIL-5 can control the growth of *S. epidermidis* in a suspension. All together, these results showed the potential of bioMIL-5 to be further used as an antibacterial agent for further applications, such as skin care or cosmetics [92].

MOFs can be further optimized for the delivery of combination therapy, by building networks that bear a bioactive molecule as ligand and loading them with a second active molecule in the pores (Fig. 4.9). This way, upon diffusion and further dissociation of the network, two bioactive compounds are released, and by controlling the properties of the pores and the stability of the network, the release profile of the two substances can be adjusted to different kinetic profiles.

Following this concept, Zhu et al. [102a] designed a new bioMOF with curcumin as the ligand and zinc as the metallic centre. Stability studies of [ $Zn_3(\text{curcumin})_2 \cdot 7(\text{DMA}) \cdot 3(\text{ethanol})$ ] in PBS showed a two-stage decomposition kinetics, with degradation starting in the first hour to release 30.5% of the ligand, and a slower rate of decomposition over the next 10 h, with only 21% of the curcumin being released (most likely due to saturation associated with the low solubility of curcumin in aqueous media). Afterwards, [ $Zn_3(\text{curcumin})_2 \cdot 7(\text{DMA}) \cdot 3(\text{ethanol})$ ] was loaded with ibuprofen and tested as sustained release system in PBS (pH = 7.4) at 37°C. Interestingly, 97% of ibuprofen was released in around 80 h and again a two-stage kinetics was observed; in the first 2 h, ca. 52.5% of the loaded-drug was released, while the remaining was released more gradually. [ $Zn_3(\text{curcumin})_2 \cdot 7(\text{DMA}) \cdot 3(\text{ethanol})$ ] was further evaluated regarding its growth inhibition properties on the BxPC-3 pancreatic adenocarcinoma cell line,



**Fig. 4.9**

Structure of Mg-Olsalazine bioMOF (*top left*) with release and decomposition profile (*bottom left*); Structure of Zn-curcumin bioMOF (*top right*) with drug release and decomposition profiles (*bottom right*). Based on Levine, D.J., et al., 2016. Olsalazine-based metal-organic frameworks as biocompatible platforms for H<sub>2</sub> adsorption and drug delivery. *J. Am. Chem. Soc.* 138 (32), 10143–10150; Su, H., et al., 2015. A highly porous medical metal-organic framework constructed from bioactive curcumin. *Chem. Commun.* 51 (26), 5774–5777.

but results show that the activities of curcumin and the MOF are similar. At the highest concentration tested,  $50 \text{ mg L}^{-1}$  (or a mass equivalent to the mass of curcumin, in the case of the MOF), both curcumin and the MOF, reduced the viability of BxPC-3 cells by 60% [95]. The use of zinc as metal centre was, most likely, not innocent, since one of the specificities of pancreatic adenocarcinoma ductal and acinar epithelium cells is a uniform and marked decrease in the zinc levels [103]. Zinc was, however, unable to create a synergic effect with the curcumin regarding the cytotoxic performance of this MOF. A word of caution is also required on the use of zinc in MOFs aiming at medicinal use on human patients, given its aforementioned low dietary allowance (RDA).

In 2016, Long et al. reported a series of new mesoporous MOFs that follow the same rationale of double drug loading. The networks have as ligand the drug olsalazine (used in the treatment of ulcerative colitis, other gastrointestinal diseases, and colorectal cancer) and different metal centres, namely Mg, Fe, Co, Ni, and Zn.  $[\text{Mg}_2(\text{olz})]$ , was chosen as model MOF because it contains magnesium, an essential element. The stability of  $[\text{Mg}_2(\text{olz})]$  in PBS (pH 7.4) at  $37^\circ\text{C}$  was evaluated, showing the release of 80% of olsalazine in the first 4 h, and the remaining 20% over the next 6 h. The high surface area and porosity of  $[\text{Mg}_2(\text{olz})]$  allowed including phenethylamine as a guest to form  $[\text{Mg}_2(\text{olz})(\text{PEA})_2]$ . Phenethylamine, a neurotransmitter, is also sold as dietary supplement for improving mood. Upon immersion of  $[\text{Mg}_2(\text{olz})(\text{PEA})_2]$  in PBS with shaking at  $37^\circ\text{C}$ , PEA release was faster than that of olsalazine. After 3 h, ca. 95% of PEA was released when compared to 50% of the olsalazine. This was attributed to rapid displacement of PEA from the pores upon soaking, which happens prior to network disassembly [104]. This work is a great example of how drug-based MOFs can be useful tools for the delivery of combination therapy, with the added advantage of featuring two kinds of release kinetics: a fast one for the drug in the pores, and a slower one for the drug that forms the network.

#### **4.4 Concluding remarks**

This field of research, which has emerged only very recently, has focused on the use of selected MOFs for a few given applications. Thus, considering the large number of existing MOFs and the wide range of possible bio-applications, there is still a lot to do in this domain.

For instance, in terms of bio-application, many practical problems of bioMOF materials warrant serious consideration, such as toxicity, morphology, machinability, dissolvability, and the preparation of homogeneous nanocrystals. Their biosafety, bio-distribution, and efficacy *in vitro* and/or *in vivo* still need to be revised and adjusted before real biomedical applications.

Most of these problems arise because the preparation and prediction of new structures from biomolecules are still demanding due to the low symmetry of bio-ligands, the chemical stability of bioMOFs does not yet meet the requirements of traditional biomaterials, and the

development of practical and stable formulations meeting the requirements of a given administration is still complex.

Nonetheless, some results show that MOFs have some significant advantages over existing bioorganic or inorganic systems, and throughout this chapter, we intended to direct the reader to these advancements.

Importantly, it is possible to perceive that a significant structural progress has been made in the preparation of MOFs with the prerequisites to act as a bioMOF. Characteristics such as the use of metals and ligands with low toxicity as well as their degradability under *in vitro* physiological conditions can be used as an advantage since a combination of bioactive molecules and metals is used as the MOFs constituents. Thus, these can provide the therapeutic capabilities without any complex third-party biomolecules load and release mechanisms for a therapeutic delivery. However, these studies are scarce and should be standardized for all MOFs composed of biocompatible ligands and metal centres.

In this regard, it seems that a judicious selection of the metal centres and ligands based on their charges, geometries, and bioactive sites is key to engineering bioMOF architectures. We firmly believe that bioMOFs, especially those with bio-ligands of the phosphonate family with calcium or magnesium metal centres, have a promising future once the structures are unveiled as well as the degradation profiles are thoroughly studied.

## Acknowledgments

This work was developed within the scope of the project CICECO-Aveiro Institute of Materials (FCT Ref. UID/CTM/50011/2019), financed by national funds through the FCT/MCTES. Thanks are also due to FCT/MCT for the financial support for the QOPNA research Unit (FCT Ref. UID/QUI/00062/2019) through national funds and, where applicable, cofinanced by the FEDER, within the PT2020 Partnership Agreement, and to the Portuguese NMR Network. JSB gratefully acknowledges FCT for the Ph.D. grant No. PD/BD/135104/2017. The research contracts of F. Figueira (REF. -168-89-ARH/2018) is funded by national funds (OE), through FCT—Fundação para a Ciência e a Tecnologia, I.P., in the scope of the framework contract foreseen in the numbers 4, 5, and 6 of the article 23, of the Decree-Law 57/2016, of August 29, changed by Law 57/2017, of July 19.

## References

- [1] P. Silva, et al., Multifunctional metal–organic frameworks: from academia to industrial applications, *Chem. Soc. Rev.* 44 (19) (2015) 6774–6803.
- [2] A.U. Czaja, N. Trukhan, U. Muller, Industrial applications of metal-organic frameworks, *Chem. Soc. Rev.* 38 (5) (2009) 1284–1293.
- [3] R.F. Mendes, F.A. Almeida Paz, Transforming metal-organic frameworks into functional materials, *Inorg. Chem. Front.* 2 (6) (2015) 495–509.
- [4] Scopus, Scopus – Analyze search results: Metal-organic Frameworks, Available at: <https://www.scopus.com>, 2019. (Accessed 15 April 2019).
- [5] S. Kitagawa, Metal–organic frameworks (MOFs), *Chem. Soc. Rev.* 43 (16) (2014) 5415–5418.
- [6] R.F. Mendes, et al., A lamellar coordination polymer with remarkable catalytic activity, *Chem. Eur. J.* 22 (37) (2016) 13136–13146.



- [7] R.F. Mendes, et al., Sustainable synthesis of a catalytic active one-dimensional lanthanide-organic coordination polymer, *Chem. Commun.* 51 (54) (2015) 10807–10810.
- [8] A. Dhakshinamoorthy, Z. Li, H. Garcia, Catalysis and photocatalysis by metal organic frameworks, *Chem. Soc. Rev.* 47 (22) (2018) 8134–8172.
- [9] A.D. Firmino, et al., Microwave synthesis of a photoluminescent metal-organic framework based on a rigid tetrakisphosphonate linker, *Inorg. Chim. Acta* 455 (2017) 584–594.
- [10] J. Zhang, et al., Topological diversities and luminescent properties of lanthanide metal-organic frameworks based on a tetracarboxylate ligand, *Cryst. Growth Des.* 14 (5) (2014) 2394–2400.
- [11] S.M. Vilela, et al., Photoluminescent layered lanthanide-organic framework based on a novel trifluorotriphosphonate organic linker, *CrystEngComm* 16 (3) (2014) 344–358.
- [12] P. Ramaswamy, N.E. Wong, G.K.H. Shimizu, MOFs as proton conductors – challenges and opportunities, *Chem. Soc. Rev.* 43 (16) (2014) 5913–5932.
- [13] M. Bazaga-Garcia, et al., Guest molecule-responsive functional calcium phosphonate frameworks for tuned proton conductivity, *J. Am. Chem. Soc.* 136 (15) (2014) 5731–5739.
- [14] D. Maspoch, et al., A nanoporous molecular magnet with reversible solvent-induced mechanical and magnetic properties, *Nat. Mater.* 2 (3) (2003) 190–195.
- [15] M. Kurmoo, Magnetic metal-organic frameworks, *Chem. Soc. Rev.* 38 (5) (2009) 1353–1379.
- [16] D. Maspoch, D. Ruiz-Molina, J. Veciana, Old materials with new tricks: multifunctional open-framework materials, *Chem. Soc. Rev.* 36 (5) (2007) 770–818.
- [17] Y. He, et al., Microporous metal-organic frameworks for storage and separation of small hydrocarbons, *Chem. Commun.* 48 (97) (2012) 11813–11831.
- [18] D. Kim, A. Coskun, Template-directed approach towards the realization of ordered heterogeneity in bimetallic metal-organic frameworks, *Angew. Chem. Int. Ed.* 56 (2017) 5071–5076.
- [19] A. Kirchon, et al., From fundamentals to applications: a toolbox for robust and multifunctional MOF materials, *Chem. Soc. Rev.* 47 (23) (2018) 8611–8638.
- [20] M.-X. Wu, Y.-W. Yang, Metal-organic framework (MOF)-based drug/cargo delivery and cancer therapy, *Adv. Mater.* 29 (23) (2017) 1606134.
- [21] W. Chen, C. Wu, Synthesis, functionalization, and applications of metal-organic frameworks in biomedicine, *Dalton Trans.* 47 (7) (2018) 2114–2133.
- [22] S.T. Gregg, et al., Functionalised solids delivering bioactive nitric oxide gas for therapeutic applications, *Mater. Today Commun.* 12 (2017) 95–105.
- [23] Y. Cui, et al., Photonic functional metal-organic frameworks, *Chem. Soc. Rev.* 47 (15) (2018) 5740–5785.
- [24] P. Horcajada, et al., Metal-organic frameworks in biomedicine, *Chem. Rev.* 112 (2) (2012) 1232–1268.
- [25] J. Della Rocca, D. Liu, W. Lin, Nanoscale metal-organic frameworks for biomedical imaging and drug delivery, *Acc. Chem. Res.* 44 (10) (2011) 957–968.
- [26] S. Beg, et al., Nanoporous metal organic frameworks as hybrid polymer-metal composites for drug delivery and biomedical applications, *Drug Discov. Today* 22 (4) (2017) 625–637.
- [27] L. Wang, M. Zheng, Z. Xie, Nanoscale metal-organic frameworks for drug delivery: a conventional platform with new promise, *J. Mater. Chem. B* 6 (5) (2018) 707–717.
- [28] S. Rojas, T. Devic, P. Horcajada, Metal organic frameworks based on bioactive components, *J. Mater. Chem. B* 5 (14) (2017) 2560–2573.
- [29] M. Giménez-Marqués, et al., Nanostructured metal-organic frameworks and their bio-related applications, *Coord. Chem. Rev.* 307 (2016) 342–360.
- [30] P. Horcajada, et al., Porous metal-organic-framework nanoscale carriers as a potential platform for drug delivery and imaging, *Nat. Mater.* 9 (2009) 172.
- [31] A.C. McKinlay, et al., BioMOFs: metal-organic frameworks for biological and medical applications, *Angew. Chem. Int. Ed.* 49 (36) (2010) 6260–6266.
- [32] F. Novio, et al., Coordination polymer nanoparticles in medicine, *Coord. Chem. Rev.* 257 (19–20) (2013) 2839–2847.
- [33] C. Tamames-Tabar, et al., MOFs in pharmaceutical technology, in: *Bio- and Bioinspired Nanomaterials*, Wiley, 2014.
- [34] I. Imaz, et al., Metal-biomolecule frameworks (MBioFs), *Chem. Commun.* 47 (26) (2011) 7287–7302.

- [35] H. Cai, Y.-L. Huang, D. Li, Biological metal–organic frameworks: structures, host–guest chemistry and bio-applications, *Coord. Chem. Rev.* 378 (2019) 207–221.
- [36] Z. Lin, A.M.Z. Slawin, R.E. Morris, Chiral induction in the ionothermal synthesis of a 3-D coordination polymer, *J. Am. Chem. Soc.* 129 (16) (2007) 4880–4881.
- [37] L. Ma, C. Abney, W. Lin, Enantioselective catalysis with homochiral metal–organic frameworks, *Chem. Soc. Rev.* 38 (5) (2009) 1248–1256.
- [38] J.-H. Zhang, et al., Homochiral metal-organic frameworks based on amino acid ligands for HPLC separation of enantiomers, *Electrophoresis* 38 (19) (2017) 2513–2520.
- [39] J. Navarro-Sánchez, et al., Peptide metal–organic frameworks for enantioselective separation of chiral drugs, *J. Am. Chem. Soc.* 139 (12) (2017) 4294–4297.
- [40] Y.-W. Zhao, Y. Wang, X.-M. Zhang, Homochiral MOF as circular dichroism sensor for enantioselective recognition on nature and chirality of unmodified amino acids, *ACS Appl. Mater. Interfaces* 9 (24) (2017) 20991–20999.
- [41] E. Yang, et al., Zeolitic metal–organic frameworks based on amino acid, *Inorg. Chem.* 53 (19) (2014) 10027–10029.
- [42] Y. Xie, et al., Rational design of MOFs constructed from modified aromatic amino acids, *Chem. Eur. J.* 13 (33) (2007) 9399–9405.
- [43] J.A. Gould, et al., A homochiral three-dimensional zinc aspartate framework that displays multiple coordination modes and geometries, *Chem. Commun.* 46 (16) (2010) 2793–2795.
- [44] E.V. Anokhina, et al., Chiral three-dimensional microporous nickel aspartate with extended Ni–O–Ni bonding, *J. Am. Chem. Soc.* 128 (30) (2006) 9957–9962.
- [45] Y. Zhang, M. Saha, I. Bernal, [Cobalt(II)L-glutamate(H<sub>2</sub>O)-H<sub>2</sub>O] $\infty$ : a new 3D chiral metal-organic interlocking network with channels, *CrystEngComm* 5 (2003) 34–37.
- [46] H.-Y. Lee, et al., Covalent metal–peptide framework compounds that extend in one and two dimensions, *Cryst. Growth Des.* 8 (1) (2008) 296–303.
- [47] C. Li, et al., Twisted metal–amino acid nanobelts: chirality transcription from molecules to frameworks, *J. Am. Chem. Soc.* 132 (23) (2010) 8202–8209.
- [48] M. Mizutani, et al., An infinite chiral single-helical structure formed in Cu (II)-L-/D-glutamic acid system, *Inorg. Chim. Acta* 283 (1) (1998) 105–110.
- [49] M. Wiśniewski, et al., Cystine-based MBioF for maintaining the antioxidant-oxidant balance in airway diseases, *ACS Med. Chem. Lett.* 9 (12) (2018) 1280–1284.
- [50] E. Ueda, et al., New bioactive zinc(II) complexes with peptides and their derivatives: synthesis, structure, and in vitro insulinomimetic activity, *Bull. Chem. Soc. Jpn.* 77 (2004) 981–986.
- [51] S. Sivakova, S.J. Rowan, Nucleobases as supramolecular motifs, *Chem. Soc. Rev.* 34 (1) (2005) 9–21.
- [52] P. Amo-Ochoa, F. Zamora, Coordination polymers with nucleobases: from structural aspects to potential applications, *Coord. Chem. Rev.* 276 (2014) 34–58.
- [53] J. An, N.L. Rosi, Tuning MOF CO<sub>2</sub> adsorption properties via cation exchange, *J. Am. Chem. Soc.* 132 (16) (2010) 5578–5579.
- [54] K.C. Stylianou, et al., CO<sub>2</sub> selectivity of a 1D microporous adenine-based metal–organic framework synthesised in water, *Chem. Commun.* 47 (12) (2011) 3389–3391.
- [55] J. An, S.J. Geib, N.L. Rosi, Cation-triggered drug release from a porous zinc-adeninate metal-organic framework, *J. Am. Chem. Soc.* 131 (24) (2009) 8376–8377.
- [56] Medicine, I.o, Dietary Reference Intakes for Vitamin A, Vitamin K, Arsenic, Boron, Chromium, Copper, Iodine, Iron, Manganese, Molybdenum, Nickel, Silicon, Vanadium, and Zinc, The National Academies Press, Washington, DC, 2001, P. 800.
- [57] R.I. Spain, T.P. Leist, E.A. De Sousa, When metals compete: a case of copper-deficiency myeloneuropathy and anemia, *Nat. Clin. Pract. Neurol.* 5 (2009) 106.
- [58] J. An, et al., Zinc-adeninate metal-organic framework for aqueous encapsulation and sensitization of near-infrared and visible emitting lanthanide cations, *J. Am. Chem. Soc.* 133 (5) (2011) 1220–1223.
- [59] J. An, et al., Metal-adeninate vertices for the construction of an exceptionally porous metal-organic framework, *Nat. Commun.* 3 (2012) 604.

- [60] M.C. Bernini, et al., Screening of bio-compatible metal-organic frameworks as potential drug carriers using Monte Carlo simulations, *J. Mater. Chem. B* 2 (7) (2014) 766–774.
- [61] J. Yang, et al., Calcium l-lactate frameworks as naturally degradable carriers for pesticides, *J. Am. Chem. Soc.* 139 (24) (2017) 8118–8121.
- [62] S.R. Miller, et al., A rare example of a porous Ca-MOF for the controlled release of biologically active NO, *Chem. Commun.* 49 (71) (2013) 7773–7775.
- [63] V. Agostoni, et al., A “green” strategy to construct non-covalent, stable and bioactive coatings on porous MOF nanoparticles, *Sci. Rep.* 5 (2015) 7925.
- [64] E. Bellido, et al., Heparin-engineered mesoporous iron metal-organic framework nanoparticles: toward stealth drug nanocarriers, *Adv. Healthcare Mater.* 4 (8) (2015) 1246–1257.
- [65] T. Hidalgo, et al., Chitosan-coated mesoporous MIL-100(Fe) nanoparticles as improved bio-compatible oral nanocarriers, *Sci. Rep.* 7 (2017) 43099.
- [66] L. Cooper, et al., A biocompatible porous Mg-gallate metal-organic framework as an antioxidant carrier, *Chem. Commun.* 51 (27) (2015) 5848–5851.
- [67] T. Hidalgo, et al., Crystal structure dependent *in vitro* antioxidant activity of biocompatible calcium gallate MOFs, *J. Mater. Chem. B* 5 (15) (2017) 2813–2822.
- [68] R. Russell, et al., Mechanisms of action of bisphosphonates: similarities and differences and their potential influence on clinical efficacy, *Osteoporos. Int.* 19 (6) (2008) 733–759.
- [69] D. Goltzman, Discoveries, drugs and skeletal disorders, *Nat. Rev. Drug Discov.* 1 (2002) 784.
- [70] R.G.G. Russell, Bisphosphonates: the first 40 years, *Bone* 49 (1) (2011) 2–19.
- [71] R. Russell, M. Rogers, Bisphosphonates: from the laboratory to the clinic and back again, *Bone* 25 (1) (1999) 97–106.
- [72] S.D. Vasikaran, Bisphosphonates: an overview with special reference to alendronate, *Ann. Clin. Biochem.* 38 (6) (2001) 608–623.
- [73] G.H. Nancollas, et al., Novel insights into actions of bisphosphonates on bone: differences in interactions with hydroxyapatite, *Bone* 38 (5) (2006) 617–627.
- [74] J.E. Dunford, et al., Structure-activity relationships for inhibition of farnesyl diphosphate synthase *in vitro* and inhibition of bone resorption *in vivo* by nitrogen-containing bisphosphonates, *J. Pharmacol. Exp. Ther.* 296 (2) (2001) 235–242.
- [75] N.B. Watts, D.L. Diab, Long-term use of bisphosphonates in osteoporosis, *J. Clin. Endocrinol. Metab.* 95 (4) (2010) 1555–1565.
- [76] I.R. Reid, et al., Comparison of a single infusion of zoledronic acid with risedronate for Paget’s disease, *N. Engl. J. Med.* 353 (9) (2005) 898–908.
- [77] D. Hosking, et al., Long-term control of bone turnover in Paget’s disease with zoledronic acid and risedronate, *J. Bone Miner. Res.* 22 (1) (2007) 142–148.
- [78] D.K. Wysowski, P. Greene, Trends in osteoporosis treatment with oral and intravenous bisphosphonates in the United States, 2002–2012, *Bone* 57 (2) (2013) 423–428.
- [79] G.A. Rodan, T.J. Martin, Therapeutic approaches to bone diseases, *Science* 289 (5484) (2000) 1508–1514.
- [80] D. Fernandez, D. Vega, A. Goeta, Alendronate zwitterions bind to calcium cations arranged in columns, *Acta Crystallogr. Sect. C: Cryst. Struct. Commun.* 59 (Pt 12) (2003) m543–m545.
- [81] D. Fernandez, D. Vega, A. Goeta, The calcium-binding properties of pamidronate, a bone-resorption inhibitor, *Acta Crystallogr. Sect. C: Cryst. Struct. Commun.* 58 (Pt 10) (2002) m494–m497.
- [82] D. Fernandez, et al., The Zn<sup>2+</sup> salt of pamidronate: a role for water in the metal-cation binding properties of bisphosphonates, *Acta Crystallogr. Sect. C: Cryst. Struct. Commun.* 60 (Pt 2) (2004) m73–m75.
- [83] Z.-C. Zhang, S.-S. Bao, L.-M. Zheng, Ladder-like metal diphosphonates exhibiting field-induced magnetic transitions, *Inorg. Chem. Commun.* 10 (9) (2007) 1063–1066.
- [84] J. Hu, et al., Syntheses, structures and fluorescence studies of two new cadmium(II) pyridyl-diphosphonates, *Inorg. Chem. Commun.* 11 (10) (2008) 1110–1112.
- [85] Y. Gong, et al., Transformation from a low-dimensional framework to a high-dimensional architecture based on different metal ions: syntheses, structures, and photoluminescences, *Inorg. Chem.* 45 (13) (2006) 4987–4995.

- [86] K.-R. Ma, et al., Three M(II)-diphosphonate coordination polymers with N-heterocyclic group (M=Ni, Fe, Mg): synthesis, characterization and magnetic properties, *Synth. Met.* 182 (2013) 40–48.
- [87] E. Alvarez, et al., A biocompatible calcium bisphosphonate coordination polymer: towards a metal-linker synergistic therapeutic effect? *CrystEngComm* 15 (46) (2013) 9899–9905.
- [88] E. Boanini, et al., Crystalline calcium alendronate obtained by octacalcium phosphate digestion: a new chance for local treatment of bone loss diseases? *Adv. Mater.* 25 (33) (2013) 4605–4611.
- [89] D. Liu, et al., Coercing bisphosphonates to kill cancer cells with nanoscale coordination polymers, *Chem. Commun.* 48 (21) (2012) 2668–2670.
- [90] K.M. Au, et al., Folate-targeted pH-responsive calcium zoledronate nanoscale metal-organic frameworks: turning a bone antiresorptive agent into an anticancer therapeutic, *Biomaterials* 82 (2016) 178–193.
- [91] F.N. Shi, et al., Calcium phosphonate frameworks for treating bone tissue disorders, *Inorg. Chem.* 54 (20) (2015) 9929–9935.
- [92] C. Tamames-Tabar, et al., A Zn azelate MOF: combining antibacterial effect, *CrystEngComm* 17 (2) (2015) 456–462.
- [93] S.R. Miller, et al., Biodegradable therapeutic MOFs for the delivery of bioactive molecules, *Chem. Commun.* 46 (25) (2010) 4526–4528.
- [94] T. Madiwale, E. Liebelt, Iron: not a benign therapeutic drug, *Curr. Opin. Pediatr.* 18 (2) (2006) 174–179.
- [95] M.C.R. Symons, J.M.C. Gutteridge, *Free Radicals and Iron: Chemistry, Biology, and Medicine*, The Quarterly Review of Biology, vol. 75, Oxford University Press, 1998.
- [96] M.V. Peto, Aluminium and Iron in humans: bioaccumulation, pathology, and removal, *Rejuvenation Res.* 13 (5) (2010) 589–598.
- [97] S.R. Miller, P. Horcajada, C. Serre, Small chemical causes drastic structural effects: the case of calcium glutarate, *CrystEngComm* 13 (6) (2011) 1894–1898.
- [98] A.D. Burrows, et al., Incorporation by coordination and release of the iron chelator drug deferiprone from zinc-based metal-organic frameworks, *Chem. Commun.* 49 (96) (2013) 11260–11262.
- [99] ApoPharma USA, Ferriprox (deferiprone). Highlights of Prescribing Information, Available at: [https://www.accessdata.fda.gov/drugsatfda\\_docs/label/2011/021825lbl.pdf](https://www.accessdata.fda.gov/drugsatfda_docs/label/2011/021825lbl.pdf), 2011. (Accessed 20 May 2019).
- [100] Apotex Europe, Ferriprox Product Information, Available at: [https://www.ema.europa.eu/en/documents/product-information/ferriprox-epar-product-information\\_en.pdf](https://www.ema.europa.eu/en/documents/product-information/ferriprox-epar-product-information_en.pdf), 2019. (Accessed 20 May 2019).
- [101] U.S. Food and Drug Administration, Finacea, Azelaic acid 15% Topical Gel. FDA Approved Drug Products, Available at: <https://www.accessdata.fda.gov/scripts/cder/daf/index.cfm?event=overview.process&ApplNo=021470#collapseApproval>, 2002. (Accessed 20 May 2019).
- [102] J. Pasquet, et al., The contribution of zinc ions to the antimicrobial activity of zinc oxide, *Colloids Surf. A Physicochem. Eng. Asp.* 457 (2014) 263–274.
- [102a] H. Su, et al., A highly porous medical metal-organic framework constructed from bioactive curcumin, *Chem. Commun.* 51 (26) (2015) 5774–5777.
- [103] L.C. Costello, R.B. Franklin, A review of the current status and concept of the emerging implications of zinc and zinc transporters in the development of pancreatic cancer, *Pancreat. Disord. Ther. Suppl* 4 (2013) 002.
- [104] D.J. Levine, et al., Olsalazine-based metal-organic frameworks as biocompatible platforms for H<sub>2</sub> adsorption and drug delivery, *J. Am. Chem. Soc.* 138 (32) (2016) 10143–10150.

# *The role of flexibility in MOFs*

Majid Nasrollahi<sup>a</sup>, Hafezeh Nabipour<sup>b</sup>, Negin Valizadeh<sup>a</sup>, Masoud Mozafari<sup>c</sup>

<sup>a</sup>*Biomaterials Group, Faculty of Biomedical Engineering (Center of Excellence), Amirkabir University of Technology, Tehran, Iran* <sup>b</sup>*State Key Laboratory of Fire Science, University of Science and Technology of China, Hefei, PR China* <sup>c</sup>*Department of Tissue Engineering & Regenerative Medicine, Faculty of Advanced Technologies in Medicine, Iran University of Medical Sciences (IUMS), Tehran, Iran*

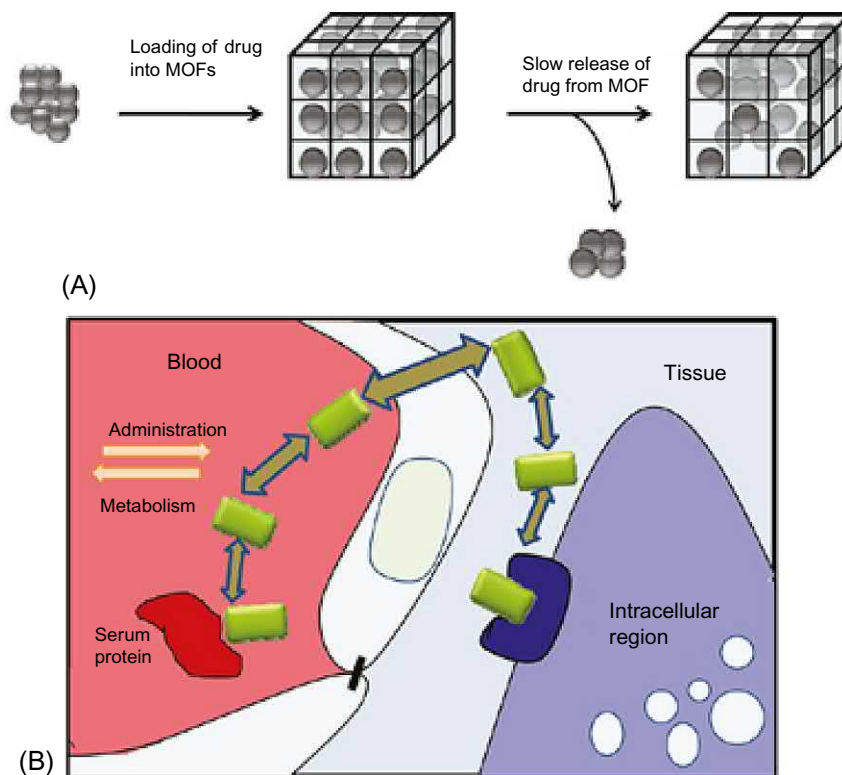
## **5.1 Introduction**

MOFs can be subjectively categorized as rigid or flexible. Rigid MOFs have permanent porosity and robust porous frameworks similar to inorganic porous materials. Flexible MOFs are known to have dynamics and respond external factors in nature such as temperature, pressure, and light [1–3]. Structural flexibility makes these MOFs able to reversibly modulate their pore size according to the situation; hence these MOFs are promising in applications of molecular sensing and sieving. In the literatures, because of flexible frameworks and lack the rigidity, they are known as flexible MOFs, soft porous crystal [4], spongelike MOFs [5], dynamic MOFs [6], or springlike [7]. The structure of flexible MOFs is capable of transforming through different ways like gate opening or a phase change [8, 9]. Such flexibility is more possible to be seen during the adsorption-desorption process, where the interaction between the pore surface and adsorbed molecules is believed to be the origin of flexibility [10]. A large number of flexible MOFs with different applications have been reported these years. They are also so popular in nanobiotechnology advances such as specific gas separations [11, 12], sensing for detecting traces of organic molecules [13], and slow release of drugs for long-release single-injection therapies [14].

The efficiency of drug delivery in the body by using nontoxic nanocarriers is the most significant challenge in this research field. Some important requirements for an efficient therapy with nanocarriers include biocompatibility, controlling the release and avoiding the “burst effect,” controlling matrix degradation and engineering its surface, being detectable by various imaging techniques, and efficiently entrapping drugs with high loading capacity. As MOFs contain transition metal ions, toxicology is another important property of MOFs that must be taken into consideration, particularly when these materials are used in health-related applications: biomedical or biological. Hinks et al. employed a research into toxicology of

iron(II) fumarate that has the same chemical composition as the MOF designated Fe-MIL-88A [15]. They reported that iron fumarate can be consumed as an oral iron supplement. This approval supported the optimistic view about toxicology of MOFs. Fe-MIL-88 and Fe-MIL-101 also showed similar results [15]. Due to the ability to adapt their porosity to the shape of the guest molecule and adjust the framework's functional groups, flexible MOFs are considered as optimal drug delivery materials [16, 17]. The capacity to be generated as controlled localized delivery of drugs may well contribute to the effective treatment and reducing side effects (Fig. 5.1) [18].

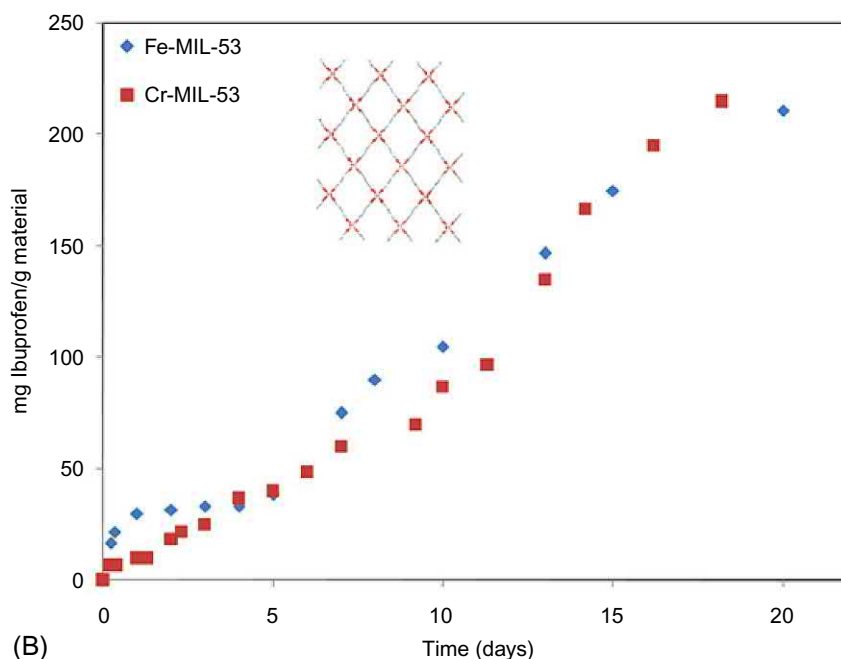
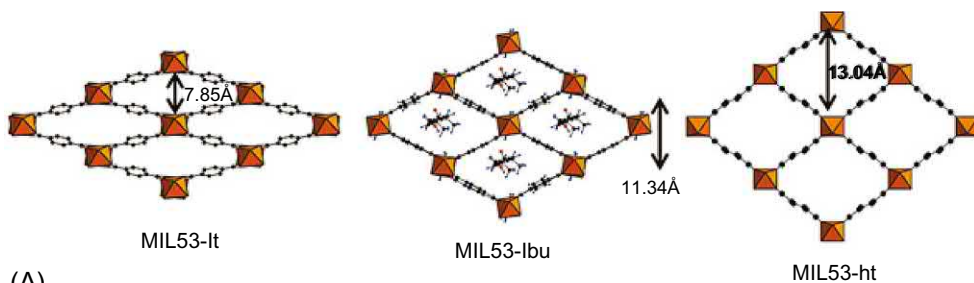
Horcajada et al. [19] also studied the structure of a flexible MOF, MIL-53, upon heating to investigate the delivery of ibuprofen. It showed expansion upon dehydration-hydration (Fig. 5.2A). It is also found that the chromium (Cr) and aluminum (Al) MIL-53t (t = low temperature) solids could show a reversible pore opening, involving atomic displacements by 5.2 Å during dehydration [18], while the iron analogue [20, 21] opened the pores over the adsorption of molecules. In fact, formation of hydrogen bonds between the inorganic



**Fig. 5.1**

(A) Generalized scheme for the use of MOFs as drug delivery vehicles. (B) In vivo conditions involved in the slow release of drugs [18].





**Fig. 5.2**

(A) Schematic representation of the breathing effect of the Cr-MIL-53 hybrid solid upon dehydration-hydration. (B) Ibuprofen delivery from Cr-MIL-53 and Fe-MIL-53 [18].

hydrophilic parts of the pore and the water molecules explains that Cr and Al solids experience structural change over dehydration. The complete process of delivering ibuprofen from MIL-53 took about 3 weeks (Fig. 5.2B). It was explained that the flexibility of the material led to bending around the drug molecules, resulting in such long duration of delivery [19].

The concept of stress-induced chemical detection was studied through integration of a thin film of HKUST-16, a MOF composed of Cu(II) ions linked by 1,4-benzenedicarboxylate (BTC) ligand  $[\text{Cu}_3\text{BTC}_2(\text{H}_2\text{O})_3]_n$  [22]. It was expected that the greater structural flexibility, the higher sensitivities would be achieved. It was shown that the energy of guest adsorption in MOF structure could be transformed to mechanical energy. The energy might be used in creating a reversible, selective, and responsive sensor.

## 5.2 General aspects of framework flexibility

Different modes of framework flexibility are described by Coudert et al. (Fig. 5.3) [23]. Supramolecular host-guest interactions are the most common origin of framework flexibility. However, MOFs are also able to show framework flexibility without desorption and adsorption phenomena. Flexibility is a desired response to external force fields, ranging from mechanical stress to temperature and interactions with light.

### 5.2.1 Breathing, swelling, linker rotation, and subnetwork displacement

The breathing phenomenon allows MOFs to make reversible transitions, which lead to a change in unit cell volume ( $\Delta V \neq 0$ ). Angles and characteristic distances of the unit cell change, and two distinct phases of crystallographic space groups (np and lp) may be different. The MIL-53(M) family ( $[M(\text{BDC})(\text{OH})]_n$  with BDC = 1,4-benzenedicarboxylate and M = Al, Fe, Cr, Sc, Ga, In)

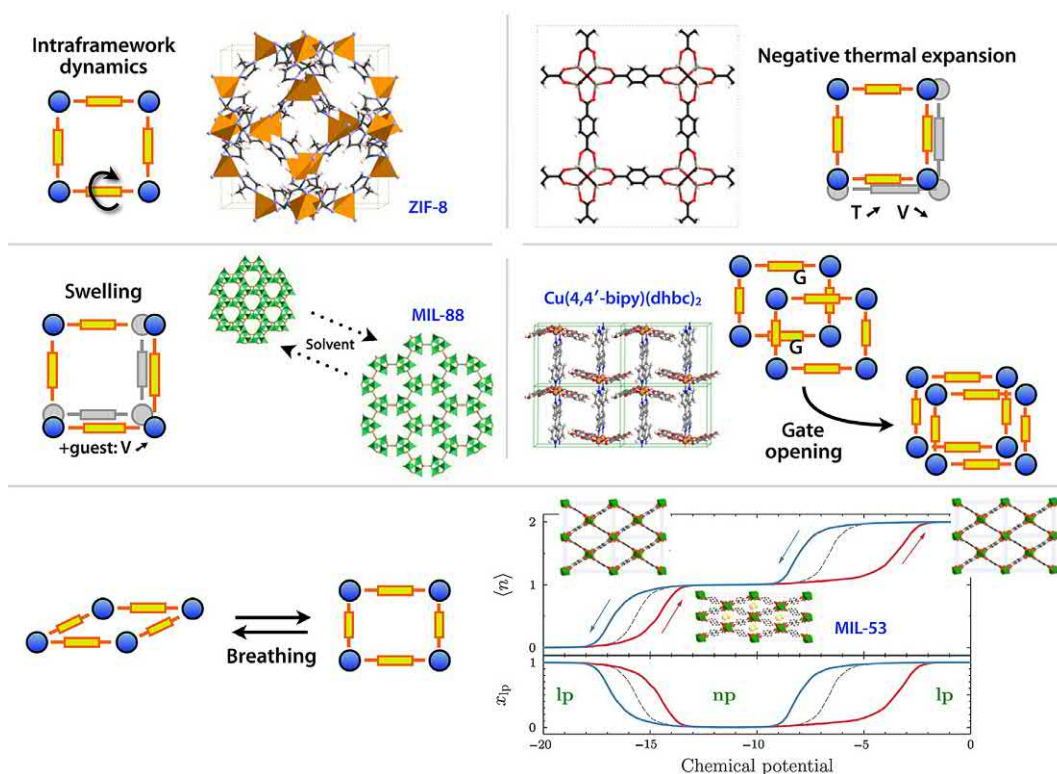


Fig. 5.3

Different categories of dynamic MOFs, each illustrated by a material displaying the phenomenon. The lower panel also depicts the typical hysteretic two-step adsorption-desorption isotherms of breathing materials (red and blue, respectively, upper half), along with evolution of phase composition (lower half) [23].

is a typical instance for this kind of flexibility. The impact of distinctive structure building units on the framework flexibility has been broadly studied, theoretical and experimental, due to the various kinds of linker derivatives and structure forming metals.

The swelling mode is also known by a rather small expansion of the MOF unit cell volume ( $\Delta V \neq 0$ ), although the unit cell shape and space group do not change. MIL-88 might be one of the most representative materials having the swelling mode of flexibility that is based on a trimeric iron(III) subunits [24]. The changes in the cell volume and unit cell parameters are guest dependent to a large extent. For example, in the case of MIL-88A, the unit cell grows from 1135 to 1840 Å<sup>3</sup> after adsorption of n-butanol, to 1970 Å<sup>3</sup> for the ethanol filled material, to 2090 Å<sup>3</sup> in methanol, and to 2110 Å<sup>3</sup> after soaking in water [24]. Shrinking in the absence of guest molecules (or not triggered by guest adsorption/desorption) or thermal expansion are also a flexibility mode linked to swelling. Some of archetypal “rigid” MOFs such as MOF-5 are known flexible because of these features [25].

Linker rotation is regarded as a continuous transition, meaning that the spatial alignment of a linker turns around a rotational axis continuously. Zeolitic imidazolate framework (ZIF-8, [Zn(mIm)<sub>2</sub>]<sub>n</sub>, mIm = 2-methylimidazole) may be a typical type of this flexibility mode [26]. To explain this phenomenon, pore window size with the adsorption properties of the material is determined.

The theoretical and experimental studies have concluded that the rotational linker movements lead to the expansion of the pore windows, and thus MOFs absorb guest molecules more than expected. Framework flexibility based on linker rotation is used for special engineering functions such as selectivity in adsorption of certain guest molecules [27].

Another phenomenon that includes some MOFs in flexible category is subnetwork displacement. This is limited to such systems that are connected to each other by relatively weak forces (van der Waals interactions), not strong chemical bonds. In these frameworks, subnets are able to relocate, drift, or shift. Subnetwork displacement includes interdigitated and stacked two-dimensional (2-D) frameworks as well as interpenetrated three-dimensional (3-D) frameworks [28]. The 2-D MOF [Cu(dhbc)<sub>2</sub>(bipy)] (Hdhbc = 2,5-dihydroxybenzoic acid, 4,4'-bipy = 4,4'-bipyridine), for example, can respond to a certain threshold pressure of methane oxygen, or nitrogen is applied via a gate opening/closing [29].

### 5.2.2 Photoinduction

Photoinduction means that molecules can respond to the light through changing their conformation or structure. If this feature is implemented into MOFs, the shape and size of pores could be controlled by light irradiation, leading to the ability to adsorb certain guests. Adding a functional side group to the linker may be the most widely used method to produce photoswitches. In most cases the prototypical azobenzene groups are incorporated into MOFs.

Dangling in the pores, azobenzene photoswitches change their conformations from *trans* to *cis* after light exposure (365 nm), accompanying generally by a variation in the accessibility of the pore size. Modrow et al. used an azobenzene-functionalized bipyridine derivative in the synthesis of the pillared layer-based framework  $[\text{Zn}_2(2,6\text{-ndc})2\text{-(azo-bipy)}]_n$  (azo-bipy = 3-azo-phenyl-4,4'-bipyridine), which was the first usage of a photoswitchable linker [30]. Material's exposure to light of a wavelength of 365 nm causes the linker transits from the *trans*- (thermodynamically stable) to the *cis*-isomer. By either thermal treatment or irradiation with light of a wavelength of 440 nm, a reversible switching back can be achieved. Other groups pursued the concept over the past 10 years. Park et al. used azobenzene-functionalized bdc-type linker to prepare an IRMOF-1 derivative containing [31]. Then, Brown et al. [32] developed an azobenzene-functionalized linker in order to introduce it into IRMOF-74-III  $[\text{Mg}_2(\text{C}_{26}\text{H}_{16}\text{O}_6\text{N}_2)]_n$ , expanding from 8.3 to 10.3 Å by switching from *trans* to *cis*. The light-induced release of adsorbed dye was also demonstrated by adjusting the conformation of the azobenzene with the light wavelength. It also should be noted that we can uptake much more  $\text{CO}_2$  if the azobenzene is in the *trans*-conformation.

Yanai and coworkers undertook a different approach [33]. As guest molecules, they used azobenzene photoswitches and loaded them with  $[\text{Zn}_2(\text{bdc})_2(\text{DABCO})]_n$  (bdc, 1,4-benzenedicarboxylate; DABCO, 1,4-diazabicyclo [2.2.2]octane) framework. The  $[\text{Zn}_2(\text{bdc})_2(\text{DABCO})]_n$  frameworks are also able to show the behavior of the photoswitch, and upon exposure to different solvents, they perform minor changes in the crystal structure. These materials transform between open pore and closed pore (cp), or narrow pore (np) and large pore (lp) forms. That is why the MOF is contracted around the azobenzene guest, when azobenzene in the *cis* form and after contact to light, the conformation of the guest changes to *trans* and the framework expands to the lp form [34].

### 5.2.3 Thermal-induction

It is a feature of those MOFs that are able to show a reversible change in their lattice parameters after exposure to an extent temperature without alteration of the molecular composition. That is why materials containing solvent guests are categorized in this class. In this case, higher temperature would only result in a phase transition induced by guest desorption [35]. It is needed to make a distinction between two phenomena in such MOFs based on their structures at room temperature. The first one is those systems that are present in their large pore form after activation. And the second one is those that are contracted and possess narrow pores after activation. The former are most likely to undergo a phase transition when cooled, and the latter undergo a reversible phase transition when heated. Before the complete phase transition occurs, the expansion or shrinkage of a framework is described by positive or negative thermal expansion (PTE or NTE, respectively). In other words, PTE and NTE are continuous processes [36]. In order to compare PTE and NTE of materials, we usually compare their thermal expansion coefficients ( $\alpha$ ).

MIL-53 system is a clear example for describing that. At around 125 K, a lp-np phase transition is observed via cooling down to low temperatures [37]. Material transforms gradually turn into the lp form above 325 K, and a relatively large hysteresis is observed. Phase transition is finished at approximately 375 K. Decreasing the benzene ring motion is assumed to be responsible for this behavior, and their fast rotation is believed to help span the diamond-shaped channels of MIL-53(Al). A closer look at the origins of the thermally induced flexibility of MIL-53 was taken, finding that dispersive interactions stabilize the np at low temperatures [38]. The higher entropy of the rotating linker molecules was seen at higher temperature, resulting in the formation of the lp phase. A functionalized analogue of the  $[\text{Zn}_2(\text{bdc})_2(\text{DABCO})]_n$  62 system, namely,  $[\text{Zn}_2(\text{BME-bdc})_2(\text{DABCO})]_n$  (BME-bdc, 2,5-bis(2-methoxyethoxy) benzenedicarboxylate) also shows a np-lp transformation [39].

DeVries et al. [40] presented other example of thermoresponsive MOF named hinged metal-organic framework (HMOF), which is prepared from a meso-tetra(4-pyridyl)porphine linker (MTPP) and  $\text{CdI}_2$ . Each cadmium (Cd) ion possesses an octahedral coordination sphere, with four pyridyl groups of different porphine linkers coordinating to the Cd in the equatorial position and two iodines coordinating in the axial position. A 2-D sheet is formed by contribution of two equatorially coordinating porphines. The two other porphines of the second grid skew to the first grid, leading to a lattice fence-like topology. This form let the coordinating iodine ions be close. However, after a certain temperature, the lattice fence-like structure starts dangling due to repulsing neighboring iodine molecules, which is an inevitable result of rising in iodines' thermal movement.

Some materials have another feature called thermal amorphization that allows them be categorized in flexible MOFs. A series of ZIF-like materials are amorphous at 300°C, but increasing temperature to 450°C generates a new and dense phase. The new phase and the amorphous one are reversible at room temperature [41].

### 5.3 Origins of flexibility in MOFs

Many parameters have effect on the flexibility of MOFs. The noticeable factors are known as secondary building units (SBUs) and the organic ligand that affect the contraction and/or expansion of MOFs. Through having impact on the pore shape and the nature and strength of the bonds of the framework, aforementioned parameters could noticeably affect the flexibility in MOF structures.

#### 5.3.1 Secondary building units (SBUs)

It is obvious that not every SBU is able to show proper response like expansion or contraction in specific circumstances. Although some researches have formulated empirical rules that ought to be provided simultaneously to let the structure breathe [42], there has hitherto been no full

theory established that provides full understanding and predicting of the key flexibility parameters of MOFs. Some of these rules concern metal clusters: the inorganic brick should have a mirror plane with the carboxylates ordered in symmetrical positions around it. This was detected in MIL-88 (Fe and Cr) framework [43]. Another rule is based on the number of carbon atoms of the carboxylic groups surrounding the cluster and number of metallic atoms within the cluster. These rules were seen in many flexible MOFs such as  $[\text{Zn}_2(\text{bdc})_2(\text{DABCO})]_n$  [44] and MIL-88 (Fe and Cr) [43]. Schneemann et al. [45] reviewed the effect of the metal nodes on the flexibility of MOFs. For instance, the MIL-53(M) family  $[\text{M}(\text{bdc})(\text{OH})]_n$  (M = Al [20], Fe [46], Cr [8], Sc [46], Ga [47], In [48]) showed different flexibility behavior based on the metal center nature. The Al, Ga, and Cr analogues of MIL-53 behaved the same, where after reaching the activation temperature (300°C), the expansion of the pore was seen. The Fe and Sc analogues, however, behaved completely different. These flexible MOFs showed pore contraction (narrow pore to closed pore transition) after activation.

Férey and Serre announced another approach, which proposed that using some SBUs can directly result in the flexibility of the structure and then allow breathing [42]. For example, MOFs with trigonal prismatic SBUs,  $\text{M}_3\text{O}(\text{COO})_6(\text{H}_2\text{O})_2\cdot\text{X}$  (M = Cr, Fe, Al; X =  $\text{F}^-$ ,  $\text{OH}^-$ ), because of their rotation around O—O axis of the carboxylate groups (kneecap-like rotational axis), can show a change in the orientation of the metal trimer and the phenyl rings [43]. A metal paddle wheel SBU is another SBU that allows the breathing of the structure [49]. A paddle wheel, also known as “soft SBU” [50], is composed of a metal dimer interconnected by four carboxylic groups, representing a pseudosquare SBU. They function as an inorganic element for most flexible MOFs [51]. Their connection to linear linkers creates  $[\text{M}_2\text{L}_2]_n$  planar grids, which are generally connected to pillar ligands (like DABCO or bipy) in the third direction, making a 3-D  $\alpha$ -Po topology framework. A typical example of them is  $[\text{M}_2(\text{bdc})_2(\text{DABCO})]_n$  (M = Zn, Co, Cu) [52, 53]. Linkers (bdc) and paddle wheels build the planar grid in which the paddle wheels are interconnected by DABCO and form the 3-D network.  $[\text{Zn}_2(\text{bdc})_2(\text{DABCO})]_n$  is another example of these flexible MOFs that show a phase transition during the activation process [53]. The paddle wheel deformation in them plays an important role in the transformation when the particular SBU cannot get involved in the breathing process, in contrast to MIL-53. After guest molecule adsorption, the angle of O-Zn-O adjacent was originally 90 degree in the lp phase and changes to 87 degree in the np structure. Simultaneously, the “kneecap” O-Zn-Zn-O and O-C-O dihedral angle, which is breathing cause in MIL-53, changes from 0 degree in the lp phase to 9.81 degree in the np structure. Isomorphous compound  $[\text{Co}_2(\text{bdc})_2(\text{DABCO})]_n$  also showed the same transition [54]. All these observations supplementary emphasize how the metal nodes/SBUs can affect the flexibility of the framework.

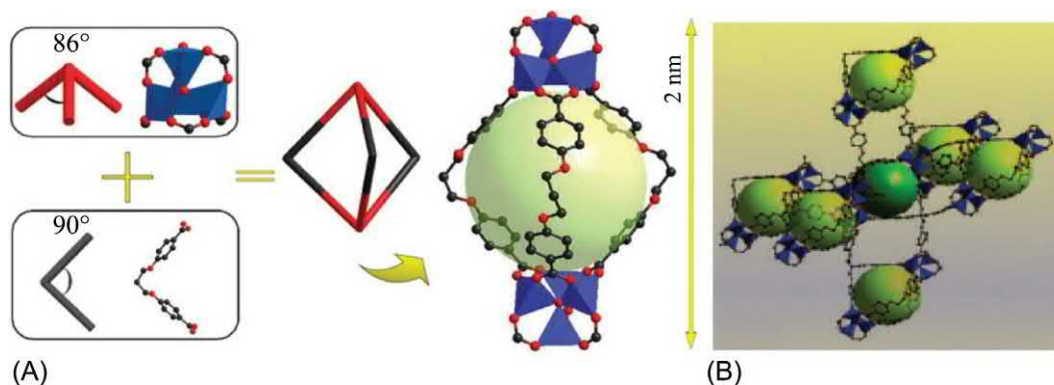
### 5.3.2 The impact of organic ligand

Structural diversity is another important structural feature of flexible MOFs. The syntheses, design and applications of MOFs based on flexible ligands (FL-MOFs) are now really distinguished. In principle, versatile conformations resulted from the ability of the metal



ligating functional groups in a flexible ligand, which is rotating around the single bond. This couples with coordination preferences of metal ions (clusters), providing a method to generate structural diversity. A clear instance is ligand 5-(3,5-dicarboxybenzyloxy)isophthalic acid. This can act as tetrahedral nodes and planar with two special conformations that correspond to the two phenyl rings in the ligand coplanar [55]. By contrast, those rigid ligands with two similar phenyl rings, such as 1,1'-azobenzene-3,3',5,5'-tetracarboxylic acid and 3,3',5,5'-biphenyltetracarboxylate, are always coplanar and categorize as four-connected planar nodes in nbo-type MOF materials [56]. A wide variety of FL-MOFs have been synthesized, and some reviews studying the structural diversity of FL-MOFs have been reported [57]. Having *cis*- or *trans*-conformation can have significant effect on the produced MOF. Assembling, for instance, the *trans*-H<sub>2</sub>CDC and Al(III) produced a MIL-53-like porous network, but that of the *cis*-H<sub>2</sub>CDC (1,4-cyclohexanedicarboxylate acid) generated a layered structure [58]. A self-casemated and interdigitated layered framework was synthesized by using 4,4'-oxybis(benzoic acid) (H<sub>2</sub>obb) ligands and Co(II) [59]. As the number of various flexible ligands used in FL-MOFs is really huge, it might be too difficult to review all of the reported FL-MOF structures. Various conformations can be achieved when the four arms rotate around -O-CH<sub>2</sub>-moieties, altering relative orientation. Carbon atoms in carboxylic group, C<sub>carboxyl</sub>, facilitate, distinguishing the conformations of H<sub>4</sub>tcm by a tetrahedron (known as carboxyl tetrahedra). H<sub>4</sub>tcm has been used in more than one hundred FL-MOF structures. Almost all H<sub>4</sub>tcm conformations in these FL-MOFs are similar. Isomorphous conformation is an exaptation in this area. The carboxyl-core-carboxyl angle is completely various, ranging from 41° to 174°. This pattern is also seen in the distance of carboxyl-carboxyl, changing from 5.176 Å to 15.341 Å. That is why geometries of the carboxyl tetrahedron could be regular, irregular, or closely flattened. Responding to diverse coordination environments of metal ions is possible because of these various conformations of H<sub>4</sub>tcm, bringing about a wide range of FL-MOF structures.

Even though numerous examples of such FL-MOFs were recognized, preparing noncentrosymmetric FL-MOFs with H<sub>4</sub>tcm was somehow unexpected, meaning that no matter which H<sub>4</sub>tcm conformations were used, most final FL-MOFs of H<sub>4</sub>tcm were centrosymmetric. For instance, under solvothermal conditions, a centrosymmetric FL-MOF with Zn<sub>4</sub>O(CO<sub>2</sub>)<sub>6</sub> building units, {[Zn<sub>4</sub>O(tcm)<sub>1,5</sub>]-4DMA·10DEF·10H<sub>2</sub>O}<sub>n</sub> (DEF = N,N'-diethylformamide), was synthesized [60]. In this case, the tcm<sup>4-</sup> ligand is seen at C<sub>2</sub> axis and belongs to C<sub>2</sub> point group. Three carboxylic groups of Zn<sub>4</sub>O(CO<sub>2</sub>)<sub>6</sub> cluster function as a tritopic subunit with angles of 86 degree and the carboxyl-core-carboxyl angles in the tcm<sup>4-</sup> ligand are nearly 90° (Fig. 5.4A). Finally, three carboxyl-core-carboxyl edges from three ligands and two Zn<sub>4</sub>O(CO<sub>2</sub>)<sub>6</sub> vertices form a nanoscale trigonal bipyramidal cage with a diameter of ca. 2.0 nm. Rotation of -O-CH<sub>2</sub>-moieties provides the curvature needed at the vertices. The remaining two arms from each ligand link the neighboring cages so that each nanocage is doubly cross-linked to six adjacent nanocages (Fig. 5.4B). A pcu network is generated through the above cage-to-cage connections by considering the cages as nodes. A specific affinity to polar molecules can be seen in this FL-MOF due to the O-rich



**Fig. 5.4**

(A) Trigonal bipyramidal cage built by  $tcm^{4-}$  and  $Zn_4O(CO_2)_6$  cluster. (B) Representation of nanoscale cages covalently linked into a FL-MOF with **pcu** network in order to form intersecting channels [60].

environment at molecular cavity walls. The adsorption amounts of ethanol, water, and methanol vary incrementally from 5.12 to 12.3 wt%. In contrast the cyclohexane uptake is nearly zero even at the high pressure (0.007 wt%).

### 5.3.3 Biomedical applications of flexible MOFs

Today, flexible MOFs are considered as one of the useful materials in the field of environmental remediation. For example, flexible MIL-53(Cr) is used for the adsorption of two typical pharmaceuticals: clofibrac acid (CA) and carbamazepine (CBZ) [61]. CA is the metabolite and active principle of blood lipid regulators, which is one of the most persistent drug residues detected in aqueous environment. CBZ is described as an anticonvulsant medication that is used primarily in the treatment of epilepsy and neuropathic pain. CBZ is also a high environmental risk in the aquatic environment worldwide. Regarding the flexible MIL-53(Cr), the breathing effect was accompanied by a modification of the hydrophobicity/hydrophilicity to absorb these pharmaceuticals. After the adsorption of CBZ, the form of MIL-53(Cr), in the lp version, is identical, while at the initial stage of adsorption, the np version with partial opening of the pores and relatively small free volume accessible to guest molecules was seen in the diffraction pattern (Fig. 5.5).

Recently, polysaccharide-based metal-organic frameworks (polysaccharide-MOFs), which are mostly flexible, as a self-assembled highly ordered functional nanostructure, have drawn great attention. Polysaccharide-MOFs have shown several promising and outstanding biological properties such as biocompatibility, bioavailability, and biosafety. These exceptional properties are providing a new field of a wide range of biological applications. They are categorized in green, renewable framework material composite [62]. In flexible bio-MOFs, biomolecules such as

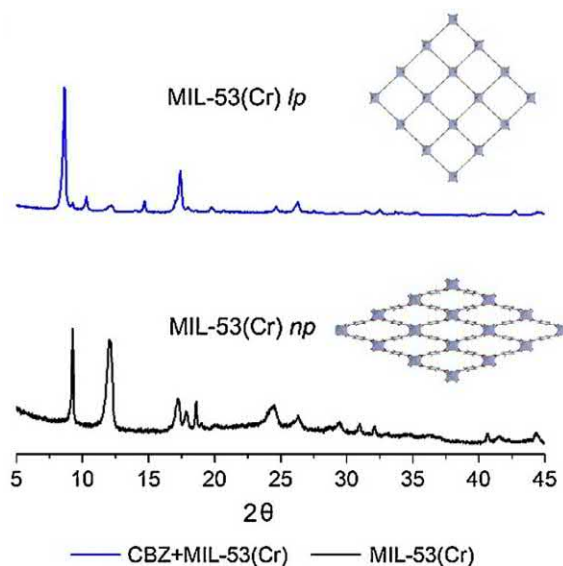


Fig. 5.5

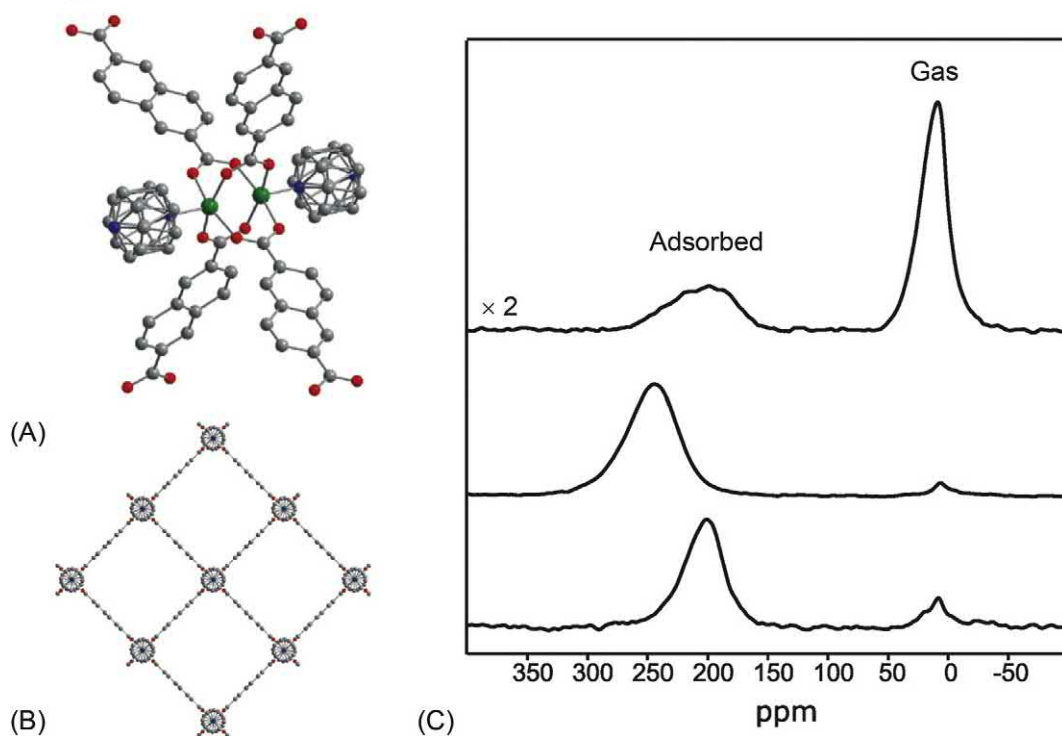
XRD pattern of MIL53(Cr) before and after adsorption [61].

peptides, amino acids, nucleobases, and saccharides are presented as building units of MOFs produced from renewable raw materials, which are generally biodegradable and nontoxic [63]. In comparison with conventional ligands in MOFs, polysaccharide-based ligands could have access to substantial conformational space via low-energy rotations, which highly differ from the classical rigid aromatic-based MOFs. They also contain varied functional groups, suitable for binding metal ions [64]. These bioligands also bring about other benefits like ease of synthesis, easy availability, multiple reactive sites, tailor-made structure, and preexisting chirality [65]. It should be noted that the incorporation of such ligands not only does improve the biocompatibility of MOF but also results in functional composites, which is in itself a motivation factor. Thus, not surprisingly, the scientific community have greatly noticed the properties of bio-MOFs such as sensing, gas storing, separating, catalyzing, and providing new openings for applications in biomedicines [66, 67]. Kim et al. [68] clarified how interactions between cellulosic material and MOFs can affect the properties of MOFs. The flexible bonds make the MOF mechanically robust for various environmental remediation applications in biomechanical applications. The presence of hydroxyl groups of cellulose undergoes chemical modifications that help in the incorporation of MOF on the surface of cellulose. The presence of cellulose provides some additional features such as low density, hydrophilicity, biodegradability, and significantly higher surface area compared with pure MOF.

Another use of flexible MOFs is xenon (Xe) and krypton (Kr) selectivity. Xe is a noble gas with substantial usages in the medical industries, semiconductors, lighting, and ion propulsion. It plays an important role as a probe molecule to examine the chemistry of biomolecules like

proteins. In addition, numerous research have been conducted into the use of Xe as part of theoretical or experimental studies on ligand–protein binding due to the “simplistic” nature of Xe as a probe. Pure Xe can be difficult to produce because of its rarity; thus absorption of it has attracted great attention today. Kaskel and coworkers conducted on the activation-induced flexibility in a flexible porous MOF, namely,  $\text{Ni}_2(2,6\text{-ndc})_2(\text{DABCO})$  (DUT-8(Ni); 2,6-ndc = 2,6-naphthalenedicarboxylate), to examine the absorption of Xe by this MOF (Fig. 5.6) [69].

Another research was carried out by Witman et al. [70] to show the ability of flexible MOFs to selectivity of Xe and Kr in comparison with rigid MOFs. They used a rare-earth polymeric framework and a microporous calcium dicarboxylate, denoted as BioMIL-2, to do so. It should be noted that flexibility somewhat enhances selectivity. Owing to the ring rotation and large pore shifts to a higher mean value, pore can essentially be blocked. Ring rotation and pore shifts both aid to decline the Henry coefficients in the flexible structure but in such a way as to overall increase the selectivity. BioMIL-2 [71] is known to be Kr selective under the rigid pore



**Fig. 5.6**

(A) The paddle wheel unit. (B) View along the crystallographic [001] direction of  $\text{Ni}_2(2,6\text{-ndc})_2(\text{DABCO})$ . (C)  $^{129}\text{Xe}$  NMR spectra showing the phase change: (top) narrow pore at room temperature, (middle) large pore state at 200 K, and (bottom) large pore state at room temperature after sample cooling and subsequent heating [69].

approximation. However, when flexibility is considered, it is Xe selective as a result of an overall rise in pore size. BioMIL-2 is just one of the several MOFs that are able to show this phenomenon. Xe can also induce strong cardioprotection through a range of mechanisms [72]. It can be possible by activating protein kinase C-epsilon and downstream p38 mitogen-activated protein kinases [73]. Detailed discussion on the biological role of Xe has been reviewed in a recent study [74]. According to the literature and clinical studies, it is clear that Xe offers a safer anesthetic solution than existing technology [72, 74, 75]. Such recovery and recycling of Xe gas within a closed system would likely involve pressure swing adsorption (PSA) or vacuum swing adsorption (VSA) type of porous materials as adsorbents (Fig. 5.7) [76].

Li et al. [77] studied the effect of flexibility in MOFs in inducing the nitric oxide (NO) forming decomposition of S-nitrosothiols (RSNOs [R denotes some organic group]), a class of NO-donating compounds that stands unique in biological applications. A group of NO synthase enzymes endogenously produce NO, which contributes to the neurotransmission, immune response, and regulation of vascular tone [78]. In addition, the production of biological NO is vital for wound-healing process, promoting accelerated wound closure [79, 80]. These properties emphasize the importance of inducing the release of NO directly from RSNOs. As RSNOs can naturally be found present in blood, this function is hypothesized to permit the controlled production of NO through the use of MOF-based blood-contacting materials. Li [77] suggested that free copper ions in solution are able to interact with an initial RSNO molecule to form a Cu-S bond, accompanied by the release of NO. It is a repeatable process with a second RSNO molecule to form a  $\text{CH}_3\text{S-Cu-SCH}_3^+$ , consequently results in disulfide formation and copper regeneration. Li also proved that this specific reaction could merely be possible for a flexible MOF that allows for distortion around the copper center to accommodate the additional RSNO molecule [77].

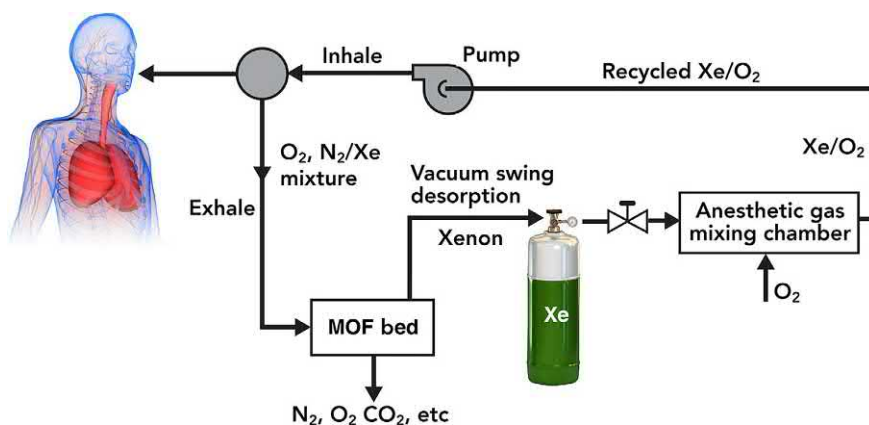


Fig. 5.7

Schematic representation of Xe recycling and recovery using MOFs at room temperature. Reprinted with permission from D. Banerjee, C.M. Simon, S.K. Elsaidi, M. Haranczyk, P.K. Thallapally, Xenon gas separation and storage using metal-organic frameworks, *Chem 4* (2018) 466–94.

In another work, Farha et al. [81] described a new class of metal-adeninate MOFs containing adenine biomolecular linkers. They explained how controlling the coordination mode of adenine can impact the structure and function of these materials. Due to the size and flexibility of the structure in bio-MOF-100, distance restraints were applied with standard values for the adenine taken from the Nucleic Acid Database. Rosi et al. [82] also reported a significant encapsulation of the cationic antiarrhythmic drug, procainamide, into an anionic zinc-adeninate framework  $Zn_8(\text{adeninate})_4(\text{biphenyldicarboxylate})_6O_2Me_2NH_2 \cdot 8DMF \cdot 11H_2O$ . Due to the short in vivo half-life of procainamide, it is needed to control this compound every 3–4 h, and this MOF has enabled us to achieve a controlled release of this drug, meaning that the loading process was accomplished through a slow ionic exchange by single suspension of the solid in a drug solution, leading to a loading up to 22 wt% after 15 days.

## 5.4 Conclusion

Flexibility is a unique physical phenomenon in MOFs. Flexible MOFs possess properties that can be rare in rigid MOFs. The most common method to synthesize and design a flexible MOF is probably the use of flexible linkers. However, other parameters, like types of secondary building unit (SBU), can also play a role to be flexible in nature. The flexibility causes MOF to show proper response to external stimuli such as pressure, temperature, and light. These properties have made flexible MOFs remarkably useful biomedical applications. Flexible MOFs through their structure, tunable composition, pore size, volume, flexible network and/or accessible metal sites, and easy functionalization have many benefits for the adsorption and release of biomolecules. Their biodegradable character can also be modified through an adequate choice of the metal, linker, and structure, which results in a degradation in body fluid from a few minutes up to weeks. An alternative method of releasing high amounts of drugs consists in making a bioactive MOF based on the drug itself as the linker and release it through the degradation of the MOF itself, or use a bioactive metal (Ag, Fe, Zn, Sc, Mn, In, Gd, ...) as the inorganic cation, to introduce additional properties such as antibacterial activity or imaging properties. Research on biomedical applications of MOFs is gaining momentum, and this emerging new class of porous materials is likely to replace the traditional nanoporous materials in drug delivery and storage in the future. Early studies of toxicology and degree of biocompatibility of MOFs are encouraging, and these fascinating materials may be suitable for further trials in different medical applications. Finally, the MOF research community has made a great progress in the past decade, and the future of the field seems very bright with the new opportunities that will become available for MOFs.

## References

- [1] K. Uemura, R. Matsuda, S. Kitagawa, Flexible microporous coordination polymers, *J. Solid State Chem.* 178 (2005) 2420–2429, <https://doi.org/10.1016/j.jssc.2005.05.036>.



- [2] F.-X. Coudert, Responsive metal–organic frameworks and framework materials: Under pressure, taking the heat, in the spotlight, with friends, *Chem. Mater.* 27 (2015) 1905–1916, <https://doi.org/10.1021/acs.chemmater.5b00046>.
- [3] Hazra A, van Heerden DP, Sanyal S, Lama P, Esterhuysen C, Barbour LJ. CO<sub>2</sub>-induced single-crystal to single-crystal transformations of an interpenetrated flexible MOF explained by in situ crystallographic analysis and molecular modeling. *Chem. Sci.* 2019;2. <https://doi.org/10.1039/C9SC04043A>.
- [4] S. Horike, S. Shimomura, S. Kitagawa, Soft porous crystals, *Nat. Chem.* 1 (2009) 695–704, <https://doi.org/10.1038/nchem.444>.
- [5] G. Férey, A selective magnetic sponge, *Nat. Mater.* 2 (2003) 136–137, <https://doi.org/10.1038/nmat837>.
- [6] K. Uemura, S. Kitagawa, M. Kondo, K. Fukui, R. Kitaura, H.C. Chang, et al., Novel flexible frameworks of porous cobalt(II) coordination polymers that show selective guest adsorption based on the switching of hydrogen-bond pairs of amide groups, *Chem A Eur J* 8 (2002) 3586–3600, [https://doi.org/10.1002/1521-3765\(20020816\)8:16<3586::AID-CHEM3586>3.0.CO;2-K](https://doi.org/10.1002/1521-3765(20020816)8:16<3586::AID-CHEM3586>3.0.CO;2-K).
- [7] K. Biradha, M. Fujita, A springlike 3D-coordination network that shrinks or swells in a crystal-to-crystal manner upon guest removal or readsorption, *Angew. Chem. Int. Ed.* 41 (2002) 3392–3395, [https://doi.org/10.1002/1521-3773\(20020916\)41:18<3392::AID-ANIE3392>3.0.CO;2-V](https://doi.org/10.1002/1521-3773(20020916)41:18<3392::AID-ANIE3392>3.0.CO;2-V).
- [8] C. Serre, F. Millange, C. Thouvenot, M. Nogue, D. Loue, Very large breathing effect in the first nanoporous chromium(III)-based solids MIL-53 or Cr(III)(OH) x [O(2)C-C(6)H(4)-CO(2)] x [HO(2)C-C(6)H(4)-CO(2)H](x) x H(2)O(y), *J. Am. Chem. Soc.* 124 (2002) 13519–13526.
- [9] K. Barthelet, J. Marrot, D. Riou, G. Férey, A breathing hybrid organic-inorganic solid with very large pores and high magnetic characteristics, *Angew. Chem. Int. Ed.* 41 (2002) 281–284, [https://doi.org/10.1002/1521-3773\(20020118\)41:2<281::AID-ANIE281>3.0.CO;2-Y](https://doi.org/10.1002/1521-3773(20020118)41:2<281::AID-ANIE281>3.0.CO;2-Y).
- [10] T. Devic, P. Horcajada, C. Serre, F. Salles, G. Maurin, B. Moulin, et al., Functionalization in flexible porous solids: Effects on the pore opening and the host-guest interactions, *J. Am. Chem. Soc.* 132 (2010) 1127–1136, <https://doi.org/10.1021/ja9092715>.
- [11] R. Babarao, J. Jiang, Molecular screening of metal-organic frameworks for CO<sub>2</sub> storage, *Langmuir* 24 (12) (2008) 6270–6278.
- [12] M. Liu, K. Xie, M.D. Nothling, P.A. Gurr, S.S.L. Tan, Q. Fu, et al., Ultrathin metal-organic framework Nanosheets as a gutter layer for flexible composite gas separation membranes, *ACS Nano* 12 (2018) 11591–11599, <https://doi.org/10.1021/acsnano.8b06811>.
- [13] T. Düren, Y.S. Bae, R.Q. Snurr, Using molecular simulation to characterise metal-organic frameworks for adsorption applications, *Chem. Soc. Rev.* 38 (2009) 1237–1247, <https://doi.org/10.1039/b803498m>.
- [14] S.S. Han, J.L. Mendoza-Cortés, W.A. Goddard, Recent advances on simulation and theory of hydrogen storage in metal-organic frameworks and covalent organic frameworks, *Chem. Soc. Rev.* 38 (2009) 1460–1476, <https://doi.org/10.1039/b802430h>.
- [15] N.J. Hinks, A.C. McKinlay, B. Xiao, P.S. Wheatley, R.E. Morris, Metal organic frameworks as NO delivery materials for biological applications, *Microporous Mesoporous Mater.* 129 (2010) 330–334, <https://doi.org/10.1016/j.micromeso.2009.04.031>.
- [16] Serre C, Mellot-Draznieks C, Surlé S, Audebrand N, Filinchuk Y, Férey G. Role of solvent-host interactions that lead to very large swelling of hybrid frameworks. *Science* (80- ) 2007;315:1828–31. <https://doi.org/10.1126/science.1137975>.
- [17] J.G. Vitillo, C. Atzori, B. Civalleri, N. Barbero, C. Barolo, F. Bonino, Design and Characterization of MOFs (Metal-Organic Frameworks) for Innovative Applications, (2017). <https://doi.org/10.1002/9783527807130.ch10>.
- [18] S. Keskin, S. Kızılel, Biomedical applications of metal organic frameworks, *Ind. Eng. Chem. Res.* 50 (2011) 1799–1812, <https://doi.org/10.1021/ie101312k>.
- [19] P. Horcajada, C. Serre, G. Maurin, N.A. Ramsahye, F. Balas, M. Vallet-Regí, et al., Flexible porous metal-organic frameworks for a controlled drug delivery, *J. Am. Chem. Soc.* 130 (2008) 6774–6780, <https://doi.org/10.1021/ja710973k>.
- [20] T. Loiseau, C. Serre, C. Huguenard, G. Fink, F. Taulelle, M. Henry, et al., A rationale for the large breathing of the porous aluminum terephthalate (MIL-53) upon hydration, *Chem A Eur J* 10 (2004) 1373–1382, <https://doi.org/10.1002/chem.200305413>.

- [21] T.R. Whitfield, X. Wang, L. Liu, A.J. Jacobson, Metal-organic frameworks based on iron oxide octahedral chains connected by benzenedicarboxylate dianions, *Solid State Sci.* 7 (2005) 1096–1103, <https://doi.org/10.1016/j.solidstatesciences.2005.03.007>.
- [22] M.D. Allendorf, R.J.T. Houk, L. Andruszkiewicz, A.A. Talin, J. Pikarsky, A. Choudhury, et al., Stress-induced chemical detection using flexible metal-organic frameworks, *J. Am. Chem. Soc.* 130 (2008) 14404–14405, <https://doi.org/10.1021/ja805235k>.
- [23] F.X. Coudert, A. Boutin, A.H. Fuchs, A.V. Neimark, Adsorption deformation and structural transitions in metal-organic frameworks: From the unit cell to the crystal, *J. Phys. Chem. Lett.* 4 (2013) 3198–3205, <https://doi.org/10.1021/jz4013849>.
- [24] C. Mellot-Draznieks, C. Serre, S. Surblé, N. Audebrand, G. Férey, Very large swelling in hybrid frameworks: A combined computational and powder diffraction study, *J. Am. Chem. Soc.* 127 (2005) 16273–16278, <https://doi.org/10.1021/ja054900x>.
- [25] S.S.-Y. Chui, A chemically functionalizable nanoporous material [Cu<sub>3</sub>(TMA)<sub>2</sub>(H<sub>2</sub>O)<sub>3</sub>]<sub>n</sub>, *Science* 283 (80) (1999) 1148–1150, <https://doi.org/10.1126/science.283.5405.1148>.
- [26] D. Fairen-Jimenez, S.A. Moggach, M.T. Wharmby, P.A. Wright, S. Parsons, T. Düren, Opening the gate: Framework flexibility in ZIF-8 explored by experiments and simulations, *J. Am. Chem. Soc.* 133 (2011) 8900–8902, <https://doi.org/10.1021/ja202154j>.
- [27] J. Seo, R. Matsuda, H. Sakamoto, C. Bonneau, S. Kitagawa, A pillared-layer coordination polymer with a rotatable pillar acting as a molecular gate for guest molecules, *J. Am. Chem. Soc.* 131 (2009) 12792–12800, <https://doi.org/10.1021/ja904363b>.
- [28] S. Bureekaew, H. Sato, R. Matsuda, Y. Kubota, R. Hirose, J. Kim, et al., Control of interpenetration for tuning structural flexibility influences sorption properties, *Angew. Chem. Int. Ed.* 49 (2010) 7660–7664, <https://doi.org/10.1002/anie.201002259>.
- [29] R. Kitaura, K. Seki, G. Akiyama, S. Kitagawa, Porous coordination-polymer crystals with gated channels specific for supercritical gases, *Angew. Chem. Int. Ed.* 42 (2003) 428–431, <https://doi.org/10.1002/anie.200390130>.
- [30] A. Modrow, D. Zargarani, R. Herges, N. Stock, The first porous MOF with photoswitchable linker molecules, *Dalton Trans.* 40 (2011) 4217, <https://doi.org/10.1039/c0dt01629b>.
- [31] J. Park, D. Yuan, K.T. Pham, J.-R. Li, A. Yakovenko, H.-C. Zhou, Reversible alteration of CO<sub>2</sub> adsorption upon photochemical or thermal treatment in a metal-organic framework, *J. Am. Chem. Soc.* 134 (2012) 99–102, <https://doi.org/10.1021/ja209197f>.
- [32] J.W. Brown, B.L. Henderson, M.D. Kiesz, A.C. Whalley, W. Morris, S. Grunder, et al., Photophysical pore control in an azobenzene-containing metal-organic framework, *Chem. Sci.* 4 (2013) 2858, <https://doi.org/10.1039/c3sc21659d>.
- [33] N. Yanai, T. Uemura, M. Inoue, R. Matsuda, T. Fukushima, M. Tsujimoto, et al., Guest-to-host transmission of structural changes for stimuli-responsive adsorption property, *J. Am. Chem. Soc.* 134 (2012) 4501–4504, <https://doi.org/10.1021/ja2115713>.
- [34] J.H. Lee, S. Jeoung, Y.G. Chung, H.R. Moon, Elucidation of flexible metal-organic frameworks: Research progresses and recent developments, *Coord. Chem. Rev.* 389 (2019) 161–188, <https://doi.org/10.1016/j.ccr.2019.03.008>.
- [35] J.M. Ogborn, I.E. Collings, S.A. Moggach, A.L. Thompson, A.L. Goodwin, Supramolecular mechanics in a metal-organic framework, *Chem. Sci.* 3 (2012) 3011, <https://doi.org/10.1039/c2sc20596c>.
- [36] I. Grobler, V.J. Smith, P.M. Bhatt, S.A. Herbert, L.J. Barbour, Tunable anisotropic thermal expansion of a porous zinc(II) metal-organic framework, *J. Am. Chem. Soc.* 135 (2013) 6411–6414, <https://doi.org/10.1021/ja401671p>.
- [37] Y. Liu, J.-H. Her, A. Dailly, A.J. Ramirez-Cuesta, D.A. Neumann, C.M. Brown, Reversible structural transition in MIL-53 with large temperature hysteresis, *J. Am. Chem. Soc.* 130 (2008) 11813–11818, <https://doi.org/10.1021/ja803669w>.
- [38] A.M. Walker, B. Civalieri, B. Slater, C. Mellot-Draznieks, F. Corà, C.M. Zicovich-Wilson, et al., Flexibility in a metal-organic framework material controlled by weak dispersion forces: The Bistability of MIL-53(Al), *Angew. Chem. Int. Ed.* 49 (2010) 7501–7503, <https://doi.org/10.1002/anie.201002413>.

- [39] C. Yang, X. Wang, M.A. Omary, Crystallographic observation of dynamic gas adsorption sites and thermal expansion in a breathable Fluorous metal-organic framework, *Angew. Chem. Int. Ed.* 48 (2009) 2500–2505, <https://doi.org/10.1002/anie.200804739>.
- [40] L.D. DeVries, P.M. Barron, E.P. Hurley, C. Hu, W. Choe, “Nanoscale lattice fence” in a metal-organic framework: Interplay between hinged topology and highly anisotropic thermal response, *J. Am. Chem. Soc.* 133 (2011) 14848–14851, <https://doi.org/10.1021/ja2032822>.
- [41] R.E. Morris, L. Brammer, Coordination change, lability and hemilability in metal-organic frameworks, *Chem. Soc. Rev.* 46 (2017) 5444–5462, <https://doi.org/10.1039/C7CS00187H>.
- [42] G. Férey, C. Serre, Large breathing effects in three-dimensional porous hybrid matter: Facts, analyses, rules and consequences, *Chem. Soc. Rev.* 38 (2009) 1380, <https://doi.org/10.1039/b804302g>.
- [43] K.J. Gagnon, C.M. Beavers, A. Clearfield, MOFs under pressure: The reversible compression of a single crystal, *J. Am. Chem. Soc.* 135 (2013) 1252–1255, <https://doi.org/10.1021/ja311613p>.
- [44] A.L. Goodwin, D.A. Keen, M.G. Tucker, Large negative linear compressibility of Ag<sub>3</sub>[co(CN)<sub>6</sub>], *Proc. Natl. Acad. Sci.* 105 (2008) 18708–18713.
- [45] A. Schneemann, V. Bon, I. Schwedler, I. Senkowska, S. Kaskel, R.A. Fischer, Flexible metal-organic frameworks, *Chem. Soc. Rev.* 43 (2014) 6062–6096, <https://doi.org/10.1039/c4cs00101j>.
- [46] J.P.S. Mowat, V.R. Seymour, J.M. Griffin, S.P. Thompson, A.M.Z. Slawin, D. Fairen-Jimenez, et al., A novel structural form of MIL-53 observed for the scandium analogue and its response to temperature variation and CO<sub>2</sub> adsorption, *Dalton Trans.* 41 (2012) 3937–3941, <https://doi.org/10.1039/C1DT11729G>.
- [47] C. Volkringer, T. Loiseau, N. Guillou, G. Férey, E. Elkaïm, A. Vimont, XRD and IR structural investigations of a particular breathing effect in the MOF-type gallium terephthalate MIL-53(Ga), *Dalton Trans.* (2009) 2241, <https://doi.org/10.1039/b817563b>.
- [48] E.V. Anokhina, M. Vougo-Zanda, X. Wang, A.J. Jacobson, In(OH)BDC·0.75BDCH 2 (BDC = Benzenedicarboxylate), a Hybrid inorganic-organic vernier structure, *J. Am. Chem. Soc.* 127 (2005) 15000–15001, <https://doi.org/10.1021/ja055757a>.
- [49] W.-Y. Gao, M. Chrzanowski, S. Ma, Metal-metalloporphyrin frameworks: A resurging class of functional materials, *Chem. Soc. Rev.* 43 (2014) 5841–5866.
- [50] J. Seo, C. Bonneau, R. Matsuda, M. Takata, S. Kitagawa, Soft secondary building unit: Dynamic bond rearrangement on multinuclear core of porous coordination polymers in gas media, *J. Am. Chem. Soc.* 133 (2011) 9005–9013.
- [51] A. Pichon, C.M. Fierro, M. Nieuwenhuyzen, S.L. James, A pillared-grid MOF with large pores based on the Cu<sub>2</sub>(O<sub>2</sub>CR)<sub>4</sub> paddle-wheel, *CrstEngComm* 9 (2007) 449–451.
- [52] K. Seki, W. Mori, Syntheses and characterization of microporous coordination polymers with open frameworks, *J. Phys. Chem. B* 106 (2002) 1380–1385.
- [53] D.N. Dybtsev, H. Chun, K. Kim, Rigid and flexible: A highly porous metal-organic framework with unusual guest-dependent dynamic behavior, *Angew. Chem. Int. Ed.* 43 (2004) 5033–5036.
- [54] R. Kitaura, K. Fujimoto, S. Noro, M. Kondo, S. Kitagawa, A pillared-layer coordination polymer network displaying hysteretic sorption:[Cu<sub>2</sub>(pzdc)<sub>2</sub>(dpyg)]<sub>n</sub> (pzdc = Pyrazine-2, 3-dicarboxylate; dpyg = 1, 2-Di(4-pyridyl) glycol), *Angew. Chem. Int. Ed.* 41 (2002) 133–135.
- [55] Z.-J. Lin, L.-W. Han, D.-S. Wu, Y.-B. Huang, R. Cao, Structure versatility of coordination polymers constructed from a semirigid tetracarboxylate ligand: Syntheses, structures, and photoluminescent properties, *Cryst. Growth Des.* 13 (2012) 255–263.
- [56] Y. Liu, J.F. Eubank, A.J. Cairns, J. Eckert, V.C. Kravtsov, R. Luebke, et al., Assembly of metal-organic frameworks (MOFs) based on indium-trimer building blocks: A porous MOF with soc topology and high hydrogen storage, *Angew. Chem. Int. Ed.* 46 (2007) 3278–3283.
- [57] N.N. Adarsh, P. Dastidar, Coordination polymers: What has been achieved in going from innocent 4,4'-bipyridine to bis-pyridyl ligands having a non-innocent backbone? *Chem. Soc. Rev.* 41 (2012) 3039–3060.
- [58] F. Niekel, M. Ackermann, P. Guerrier, A. Rothkirch, N. Stock, Aluminum-1, 4-cyclohexanedicarboxylates: High-throughput and temperature-dependent in situ EDXRD studies, *Inorg. Chem.* 52 (2013) 8699–8705.
- [59] D.P. Martin, R.M. Supkowski, R.L. LaDuca, Self-catenated and interdigitated layered coordination polymers constructed from kinked dicarboxylate and organodiamine ligands, *Inorg. Chem.* 46 (2007) 7917–7922.

- [60] T.-F. Liu, J. Lü, X. Lin, R. Cao, Construction of a trigonal bipyramidal cage-based metal–organic framework with hydrophilic pore surface via flexible tetrapodal ligands, *Chem. Commun.* 46 (2010) 8439–8441.
- [61] Y. Gao, K. Liu, R. Kang, J. Xia, G. Yu, S. Deng, A comparative study of rigid and flexible MOFs for the adsorption of pharmaceuticals: Kinetics, isotherms and mechanisms, *J. Hazard. Mater.* 359 (2018) 248–257, <https://doi.org/10.1016/j.jhazmat.2018.07.054>.
- [62] Z. Ajoyan, P. Marino, A.J. Howarth, Green applications of metal–organic frameworks, *CrstEngComm* 20 (2018) 5899–5912.
- [63] S.L. Anderson, K.C. Stylianou, Biologically derived metal organic frameworks, *Coord. Chem. Rev.* 349 (2017) 102–128.
- [64] H. Cai, Y.-L. Huang, D. Li, Biological metal–organic frameworks: Structures, host–guest chemistry and bio-applications, *Coord. Chem. Rev.* 378 (2019) 207–221.
- [65] R.S. Forgan, Metal-organic frameworks: Edible frameworks, *Encycl Inorg. Bioinorg. Chem.* (2011) 1–13.
- [66] S.S. Nadar, V.K. Rathod, Encapsulation of lipase within metal-organic framework (MOF) with enhanced activity intensified under ultrasound, *Enzyme Microb. Technol.* 108 (2018) 11–20.
- [67] T. Rajkumar, D. Kukkar, K.-H. Kim, J.R. Sohn, A. Deep, Cyclodextrin-metal–organic framework (CD-MOF): From synthesis to applications, *J. Ind. Eng. Chem.* (2019).
- [68] M.L. Kim, E.H. Otal, J.P. Hinestroza, Cellulose meets reticular chemistry: Interactions between cellulosic substrates and metal–organic frameworks, *Cellul.* 26 (2019) 123–137.
- [69] N. Klein, C. Herzog, M. Sabo, I. Senkowska, J. Getzschmann, S. Paasch, et al., Monitoring adsorption-induced switching by  $^{129}\text{Xe}$  NMR spectroscopy in a new metal–organic framework Ni<sub>2</sub>(2, 6-ndc)2 (dabco), *Phys. Chem. Chem. Phys.* 12 (2010) 11778–11784.
- [70] M. Witman, S. Ling, S. Jawahery, P.G. Boyd, M. Haranczyk, B. Slater, et al., The influence of intrinsic framework flexibility on adsorption in nanoporous materials, *J. Am. Chem. Soc.* 139 (2017) 5547–5557.
- [71] S.R. Miller, P. Horcajada, C. Serre, Small chemical causes drastic structural effects: The case of calcium glutarate, *CrstEngComm* 13 (2011) 1894–1898, <https://doi.org/10.1039/C0CE00450B>.
- [72] T. Goto, Y. Nakata, Y. Ishiguro, Y. Niimi, K. Suwa, S. Morita, Minimum alveolar concentration-awake of xenon alone and in combination with isoflurane or sevoflurane, *Anesthesiology* 93 (2000) 1188–1193.
- [73] I.C. Umana, C.A. Daniele, D.S. McGehee, Neuronal nicotinic receptors as analgesic targets: it’s a winding road, *Biochem. Pharmacol.* 86 (2013) 1208–1214.
- [74] D.A. Winkler, A. Thornton, G. Farjot, I. Katz, The diverse biological properties of the chemically inert noble gases, *Pharmacol. Ther.* 160 (2016) 44–64.
- [75] R.D. Sanders, D. Ma, M. Maze, Xenon: Elemental anaesthesia in clinical practice, *Br. Med. Bull.* 71 (2005) 115–135.
- [76] D. Banerjee, C.M. Simon, S.K. Elsaidi, M. Haranczyk, P.K. Thallapally, Xenon gas separation and storage using metal-organic frameworks, *Chem* 4 (2018) 466–494.
- [77] T. Li, K. Taylor-Edinbyrd, R. Kumar, A computational study of the effect of the metal organic framework environment on the release of chemically stored nitric oxide, *Phys. Chem. Chem. Phys.* 17 (2015) 23403–23412.
- [78] F.-Q. Guo, M. Okamoto, N.M. Crawford, Identification of a plant nitric oxide synthase gene involved in hormonal signaling, *Science* 302 (80) (2003) 100–103.
- [79] M.B. Witte, A. Barbul, Role of nitric oxide in wound repair, *Am. J. Surg.* 183 (2002) 406–412.
- [80] A. Schmidt, T. von Woedtke, B. Vollmar, S. Hasse, S. Bekeschus, Nrf2 signaling and inflammation are key events in physical plasma-spurred wound healing, *Theranostics* 9 (2019) 1066.
- [81] J. An, O.K. Farha, J.T. Hupp, E. Pohl, J.I. Yeh, N.L. Rosi, Metal-adeninate vertices for the construction of an exceptionally porous metal–organic framework, *Nat. Commun.* 3 (2012) 604.
- [82] J. An, S.J. Geib, N.L. Rosi, Cation-triggered drug release from a porous zinc-adeninate metal-organic framework, *J. Am. Chem. Soc.* 131 (2009) 8376–8377.

# *Surface modification of metal-organic frameworks for biomedical applications*

Kranthi Kumar Gangu<sup>a,b</sup>, Sreekantha B. Jonnalagadda<sup>b</sup>

<sup>a</sup>Vignan's Institute of Information Technology, Visakhapatnam, India <sup>b</sup>School of Chemistry & Physics, University of KwaZulu-Natal, Durban, South Africa

## **6.1 Introduction**

The production of biologically potential molecules or intermediates is of prime significance in pharmaceutical industry, especially in the R&D in pursuit of developing new drugs [1–3]. Many of the organic moieties possess antibacterial and other activities and medicinal advantages. Often, the synthesis to bring forward the best active compounds and to introduce unique features to the medicinal drugs is a cumbersome task [4–6]. Pharmaceutical applications like drug specimen and drug membrane interactions, crystal growth, and lipid studies are imperative to afford good biological activities [7–9]. Few specimens have acted as pioneering chemicals or intermediates for pharmaceutical applications and their synthesis has revolutionized the pharmaceutical and fine chemical industries. Safer, flexible, and cheaper procedures are in demand for the synthesis of drugs as well as for further advancement in treatment of diseases. Certain chemical intermediates are very essential in the synthesis of final drug molecules and pharmaceutical companies are investing huge amounts for their production. Significant efforts were made for reducing such burden on pharmaceutical industries and in such scenario, facilitation of reactions by appropriate catalyst has been proposed [10–13]. The introduction of catalyst materials has alleviated the time taken with tedious synthetic procedures as appropriate catalyst substantially reduces the reaction time and enhances the yield of desired product with energy efficiency [14–16]. Homogeneous catalysis is one of such criterion, which was adopted frequently to gain advantages of catalysis chemistry, but setbacks in difficult separation and reusability problems restrain their utilization [17–19]. Moreover, prolonged exposure to the reaction causes toxicity to the target/desired organic molecules. Thus, the development of heterogeneous solid catalysts facilitated to overcome the limitations with homogeneous catalysts while gaining full benefits of catalyzed reactions [20–23].

Heterogeneous catalysts have received ample attention in the past decades and their utilization in value-added organic transformations is becoming a major field. Besides easy separation and recyclability, heterogeneous catalysts have many advantages that can enable organic reactions with enhanced selectivity and specificity [24–28]. The advent of heterogeneous solid catalysts avoided the cumbersome conventional organic reactions. C-C bond formation and C-C bond coupling are the utmost-priority organic reactions in the medicinal chemistry and these reactions become flexible and achievable with the introduction of heterogeneous catalysts. Heterogeneous catalysts in general offer wider scope in applications and benefits and provide sustainable solutions for challenges faced in multistep organic synthesis [29–34]. Transition metals such as Pd, Rh, Pt, and so on are viable heterogeneous catalysts and have immense potential for displaying superb catalytic activities, but the only implications are that they needed suitable support material as host to achieve appropriate surface properties for showcasing their efficiency in catalysis [35–38]. Porous materials like activated carbon, zeolites, and carbon nanotubes are some of such support materials for designing transition metal impregnated heterogeneous solid catalysts [39, 40]. Chemical stability, recyclability, and leaching of harmful chemicals pose challenges to seek the ways for exploring other alternative outstanding materials.

Metal-organic frameworks (MOFs) are the emerging class of advanced materials containing metal ions coordinated with mono-, bi-, and multi-dentate organic linkers resulting in porous structured framework material with unique of physical, chemical, and mechanical properties. Framework rigidity, tunability of pores, high surface area, and scope for dispersion/anchoring/impregnating of various functional groups are added advantages of MOFs [41–45]. MOFs could also revolutionize the field of heterogeneous catalysis as these remarkable materials can be used to create better and stronger catalysts, which are cheaper and easier to produce than the other porous/solid catalysts. There are a variety of MOFs as support or inherent sole catalysts even for the same element or compound, differing in size and atomic arrangement, which can have very diverse properties [46, 47]. MOFs and surface-modified MOFs in the organic reactions as catalysts have received recognition as excellent materials that have been performing brilliantly, while maintaining the quality and delivery of services [48–50]. Depending on the size, shape, surface, and defect properties, the MOFs show different catalytic activities in terms of reaction time and yields of product. The versatile MOFs can be accommodated as active centers in many approaches for effective catalysis. Inside the pores side group linker functionalization with active metal complexes and mixed-linker MOFs is probable location/strategy for embedding specialized catalytically active substances into the framework [51–53].

This chapter deals with various works reported by researchers for the modification of MOFs and their functionalities as heterogeneous catalysts in value-added organic transformations. The dispersion of various transition metals and mixed linker bonding are appropriate strategies in the transformation of MOFs into coveted materials in heterogeneous catalysis. Knoevenagel



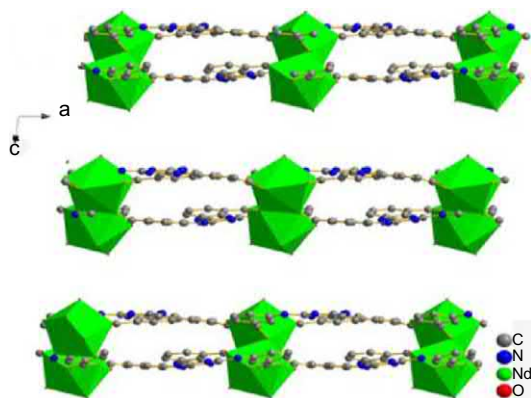
condensation, Heck reaction, Suzuki reaction, and Sonogashira reactions are prominent organic transformations in pharmaceutical industries and their reaction products are important chemical intermediates and precursors for synthesizing biologically active drug molecules. This review details the works of different authors on the above mentioned reactions and the modification of MOFs in order to achieve enhanced catalytic activities.

## 6.2 Modified MOFs for Knoevenagel condensation

Reaction between carbonyl and active methylene groups is achievable through Knoevenagel condensation, and different researchers have carried out this reaction by using various modified MOFs as catalysts.  $\alpha,\beta$ -Unsaturated compounds obtained from this condensation reaction are widely used as precursors in the synthesis of perfumes, pharmaceuticals, fine chemicals, functional polymers, and agrochemicals. Various homogeneous catalysts like amines, ionic liquids, alkali salts, and others are used for Knoevenagel condensation. Although, microwave irradiation and sonification techniques have also been developed, no homogeneous catalyst or synthesis technique has met the green principles for large-scale production. To avoid these shortfalls, researchers have put concerted efforts for alternate materials like MOF rigid solids as catalysts for making flexibility in Knoevenagel condensation [54–56]. On these lines, Guo et al. [57] have reported two-dimensional metal-organic framework (2D-MOF) with Nd(III) and 4,4,4'-*s*-triazine-1,3,5-triyltri-*m*-aminobenzoate as precursor metal ion and tritopic semirigid ligand, respectively. They have prepared MOF, namely  $[(\text{Nd}_2(\text{TATMA})_2 \cdot 4\text{DMF} \cdot 4\text{H}_2\text{O})_n (\text{NdTATMA})]$  that possesses Lewis basic sites, which help in heterogeneous catalysis. Particularly, triazine molecules in the structure of MOF acted as high-density Lewis basic sites with elevated performance in the synthesis of biological active substances. In the structure of MOF, inorganic cluster of  $\{\text{Nd}_2(\text{COO})_6\}$  connected with six different coordination modes of ligands form a 2D layer structure as shown in Fig. 6.1. In the catalytic reaction, 100 mg of NdTATMA was employed in the reaction between aldehyde and malononitrile for Knoevenagel condensation. After reaction the resultant NdTATMA was separated and reused. Inductively coupled plasma analysis revealed that no Nd(III) traces were identified in the separated catalyst material.

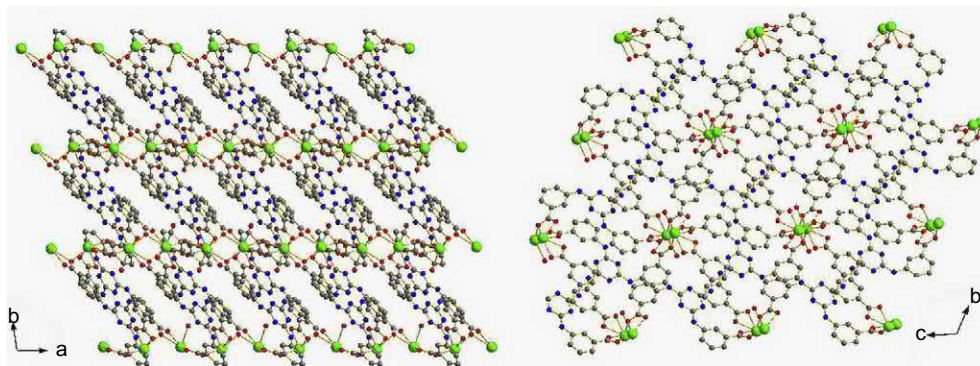
In similar lines, Zhao [58] have reported a three-dimensional (3D) MOF structure, namely,  $\{[\text{Eu}(\text{TATMA})(\text{H}_2\text{O}) \cdot 2\text{H}_2\text{O}]_n\}$ , using same ligand as reported by Feng et al., but with Eu(III) as metal ion. This MOF was utilized in the base-catalytic reactions owing to the availability of more Lewis basic sites. A significant  $\text{C}=\text{C}$  bond formation could be achieved easily by the use of this MOF. This MOF withstood four times reuse without any damage to framework structure as per the powder XRD (X-ray diffraction) studies. As shown in Fig. 6.2, one-dimensional (1D) Eu(II) chains were linked with fully deprotonated ligands and finally forms a 3D structure.

In another study, Yang et al. [59] have reported dual acid-base catalytic characteristic MOF, namely, UiO-66-NH<sub>2</sub> with Zr(IV) and 2-aminoterephthalate precursors. The possibility of



**Fig. 6.1**

Schematic representation of the 2D framework. Reprinted with permissions from F. Guo, B. Yuan, W. Shi, A novel 2D metal-organic framework with Lewis basic sites as a heterogeneous base catalysis, *Inorg. Chem. Commun.* 86 (2017) 285–289.



**Fig. 6.2**

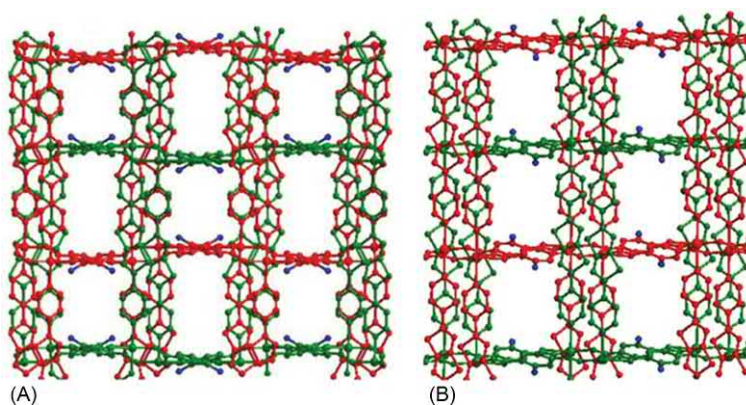
Schematic representation of the 3D framework. Reprinted with permissions from S. Zhao, A novel 3D MOF with rich Lewis basic sites as a base catalysis toward Knoevenagel condensation reaction, *J. Mol. Struct.* 1167 (2018) 11–15.

surface modifications of MOFs tends to complimentary or alternative to many other solid catalysts. Here in this study, the bare MOF, UiO-66 [metal: Zr(IV) and ligand: 1,4-benzenedicarboxylate (BDC)] has been altered with amino group ( $-\text{NH}_2$ ) attached to ligand, 2-amine-1,4-benzenedicarboxylate instead of BDC, creating a more catalytic active sites. Zr (IV), Lewis acid sites, and  $-\text{NH}_2$  basic sites enhance the catalytic nature of MOF. The acid-base bifunctional character of MOF can be utilized in the significant C-C bond coupling

reactions. The study stated that the introduction of amino group into the structure of ligand increases the basicity, which is lacking in the amino-free ligand. The study proposed that the increase in basicity due to interactions of intramolecular hydrogen bonding between carboxylate oxygen and amino group.

Almasi et al. [60] have used +2 oxidation state central metal ion, Pb and methanetetra benzoate (MTB) linker in the preparation of MOF,  $\{[\text{Pb}_4(\mu_8\text{-MTB})_2(\text{H}_2\text{O})_4]\cdot 5\text{DMF}\cdot \text{H}_2\text{O}\}_n$ . The development of coordinatively unsaturated metal centers of Pb(II) upon activation (removal of solvent molecules) served as Lewis acidic sites for organic reactions. In this study, the basic sites of MOFs were speculated from carboxylate oxygen atoms linked to the Pb(II) ions. This MOF showed highest BET (Brunauer-Emmett-Teller) surface area of  $980\text{ m}^2/\text{g}$  compared to other MOFs, when MTB was used as ligand. Due to good textural characteristics, author suggested the occurrence of catalytic activity within the pore system of MOF. In another study, Almasi et al. [61] have reported 3D fluorite ( $\text{CaF}_2$ )-like structured MOF,  $\{[\text{Ni}_4(\mu_6\text{-MTB})_2(\mu_2\text{-H}_2\text{O})_4(\text{H}_2\text{O})_4]\cdot 10\text{DMF}\cdot 11\text{H}_2\text{O}\}_n$ . The removal of entrapped solvent molecules in the cages facilitate in raising the void volume. BET specific surface area of  $700\text{ m}^2/\text{g}$  of this MOF led to applications in catalysis. This compound exhibited acid-catalyzed Knoevenagel condensation with impressed yields (c.100%). As analogous to  $\text{CaF}_2$  structure, MOF has gained more stability and restrict hydrolysis, even if MOF was immersed in water for several days. Post-synthetic modification of MOFs with amino groups ( $1^\circ$ ,  $2^\circ$ , and  $3^\circ$ ) has been reported by Poonam et al. As these MOFs were sensitive toward exposure to humidity, solvent, and high temperatures ( $>200^\circ\text{C}$ ), their operations in catalysis were limited. Functionalization of MOFs is one of the strategies to improve the performance of the MOFs. The introduction of desired functional groups in post-synthetic approach is more advantages than direct synthetic approach. Post-synthetic modification of MOFs facilitates the incorporation of functional groups into MOF structures without damaging the basic framework structure. Three amines, viz., *N*-butylamine, diethylamine, and 4-dimethylaminopyridine (DMAP), were grafted to the parent MOF, Zr-BDC through post-synthetic method in this work. Along with Lewis acidity of Zr-BDC MOF, the grafted amino group provides basic nature, resulting in a bifunctional acid-base character. More availability of lone-pair electrons on nitrogen in the DMAP-based Zr-BDC MOF having high basicity has subsequently exhibited more catalytic activity. The study revealed that surface modification of MOFs with desired components as solid catalyst is the driving force responsible for biological potent reactions [62].

Zhi et al. have reported the synthesis of two amino-functionalized MOFs,  $\{[\text{Zn}(\text{Py}_2\text{TTz})(2\text{-NH}_2\text{-BDC})]\cdot (\text{DMF})\}_n$  and  $\{[\text{Cd}(\text{Py}_2\text{TTz})(2\text{-NH}_2\text{-BDC})]\cdot (\text{DMF})\cdot 0.5(\text{H}_2\text{O})\}_n$ , using 2-NH<sub>2</sub>-BDC = 2-amino-1,4-benzenedicarboxylate and Py<sub>2</sub>TTz = 2,5-bis(4-pyridyl)thiazolo[5,4-*d*]thiazole as linker and auxiliary linker, respectively. In both structures, nitrogen atoms of thiazole and amino groups are present in the channels, which are openly accessible and afford to



**Fig. 6.3**

Schematic representation of (A) a twofold interpenetrated 3D framework of Zn-based MOF along the c-axis; blue represents the  $-\text{NH}_2$  group, (B) a twofold interpenetrated 3D framework of Cd(II)-based MOF along the b-axis; blue represents the amino group. Reprinted with permissions from Z.-W. Zhai, S.-H. Yang, Y.-R. Lv, C.-X. Du, L.-K. Li, S.-Q. Zang, *Amino functionalized Zn/Cd-metal-organic frameworks for selective  $\text{CO}_2$  adsorption and Knoevenagel condensation reactions*, *Dalton Trans.* 48 (2019) 4007–4014.

base-oriented catalyzed reactions (Fig. 6.3). A study has been carried out to investigate the importance of 2- $\text{NH}_2$ -BDC and  $\text{Py}_2\text{TTz}$  components. The study revealed that with 2- $\text{NH}_2$ -BDC as catalyst only 1% conversion rate was observed, whereas with function of  $\text{Py}_2\text{TTz}$  as catalyst, 72% conversion was observed. When both 2- $\text{NH}_2$ -BDC and  $\text{Py}_2\text{TTz}$  simultaneously employed in the reaction, the conversion rate was lower than that of  $\text{Py}_2\text{TTz}$ . This experiment evidentially proved that nitrogen atoms present in the  $\text{Py}_2\text{TTz}$  played a significant role in the catalysis. In another experiment conducted to study the nitrogen atoms that are more prominent in the  $\text{Py}_2\text{TTz}$  ligand disclosed that both pyridine and thiozole groups were catalytic active sites in  $\text{Py}_2\text{TTz}$  linker. Overall, the study revealed that one or more substances in the structure of MOFs promote the catalytic activity. In many cases, synergic effect plays a significant role in enhancing catalytic activities [63].

Amarajothi et al. [64] have reported Al-based MOF for catalytic studies in the Knoevenagel condensation reaction between benzaldehyde and malononitrile. MOF CAU-1- $\text{NH}_2$ ,  $[\text{Al}_4(\text{OH})_2(\text{OCH}_3)_4(\text{p-BDC-NH}_2)_3]$ , where  $(\text{p-BDC-NH}_2)^{2-} = 2\text{-aminoterephthalate}$  was prepared by microwave-assisted synthesis. CAU-1- $\text{NH}_2$  was utilized in the catalytic reaction, where amino group leads to Brønsted-base-catalytic reactions and formed desired benzylidene malononitrile product, whereas under same experimental conditions, unfunctionalized/free amino group Al-MOF tend to undesired benzaldehyde diethyl acetal product through Lewis-acid catalysis. The same MOF, CAU-1- $\text{NH}_2$ , when compared with MIL-101 catalysts showed low catalytic activity (25% yields), this was ascribed to lower pore dimensions of CAU-1- $\text{NH}_2$

compared to those of MIL-101 solid catalysts. Overall, the study enlightened the pore dimensions and the nature of active sites decides the conversion as well as product selectivity. Depending on the requirements of certain target organic products, the tuning of MOFs should be carried out. When the pores of the reactant substrates fit with the MOF catalyst pore size, the reaction takes place without any diffusion limitations.

In another study, Valentina et al. have compared various MOFs for higher catalytic activity [65]. In this study, authors have disclosed that the introduction of basic sites in MOFs have showed higher catalytic performance compared to that of bare MOFs. In this regard, they have studied  $\text{Cu}_3(\text{BTC})_2 \cdot (\text{H}_2\text{O})_3$ , MIL-100(Al), UiO-66, and UiO-66- $\text{NH}_2$  on their catalytic performance toward C-C bond formation. The IR (infrared) spectroscopy with  $\text{CDCl}_3$  as probe molecule was used to study the basic properties of MOFs. In earlier studies, insertion of  $\text{NH}_2$  groups showed effect on basicity. The strength of basicity of  $\text{Cu}_3(\text{BTC})_2 \cdot (\text{H}_2\text{O})_3$ , MIL-100(Al), and UiO-66 were in the range of 830–839 kJ/mol but for UiO-66- $\text{NH}_2$ , the strength of basicity raised to 867 kJ/mol. Lewis acid-base pair of  $\text{M}^{n+}-\text{O}^{2-}$  of metal carboxylate component of MOFs also are important in catalysis. Thus, along with base functional groups, the length of M-O bond also plays a pivotal role in activating the reactants on the surface of metal-carboxylate entities of MOF catalysts.

Gangu et al. have reported alkaline Mg-based MOF,  $[\text{Mg}_3(\text{NDC})_3(\text{DMF})_4] \cdot \text{H}_2\text{O}$  with 2,6-naphthalenedicarboxylic acid (NDC) as linker. A 3D network structure was formed with trinuclear Mg secondary building units with six NDC molecules. MOF showed superb catalytic performance with the creation of coordinatively unsaturated Mg(II) centers [66]. The Lewis acidic character of MOF acts as a heterogeneous catalyst in the synthesis of 4H-pyrans scaffolds, which have wide utilization in the pharmaceutical industry for developing anti-HIV, anticancer, antimalarial, anti-inflammatory, cytotoxic, antihyperglycemic, antimicrobial, and antidiabetic drugs [67, 68]. Ample of void spaces in the framework and  $\text{Mg}^{2+}$  open metal sites were advantageous in the catalyzed organic transformation reactions (Fig. 6.4). In another study, Gangu et al. [69] have prepared 3D supramolecular structures of  $[\text{Co}(4,5\text{-Imdc})_2(\text{H}_2\text{O})_2]$  (1) and  $[\text{Cd}(4,5\text{-Imdc})_2(\text{H}_2\text{O})_3] \cdot \text{H}_2\text{O}$  hydrothermally using 4,5-Imidazolecarboxylic acid (4,5-Imdc) as ligand. Upon activation of water molecules, open metal sites of Co(II) and Cd(II) were generated. Biologically active pyrano pyrazole derivatives have been synthesized with Co(II)- and Cd(II)-based MOFs as catalysts. Among MOFs, Co(II) MOF showed superior performance than Cd(II) MOF. The reason attributed to this is that soft Lewis acidic character of Cd(II) metal ions diminishes the interactions of catalyst with reactive substrates.

In an attempt to develop efficient catalysts, Gangu et al. [70] have reported MOF,  $[\text{Ni}_2(2,6\text{-pydc})_2(\mu\text{-}4,4'\text{bpy})(\text{H}_2\text{O})_4] \cdot 2\text{H}_2\text{O}$  with supramolecular network structure. Catalytic active sites of Lewis Ni(II) acid centers were developed during the bonding with labile 2,6-pydc and 4,4'bpy ligands (Fig. 6.5). Here in this report, unlike classic MOFs, due to lack of void space



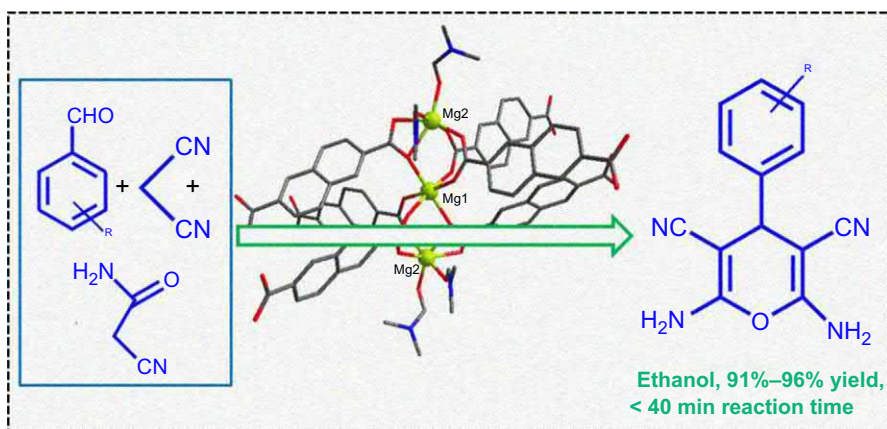


Fig. 6.4

Catalyzed organic reaction in the presence of  $[Mg_3(NDC)_3(DMF)_4] \cdot H_2O$ . Reprinted with permissions from K.K. Gangu, S. Maddila, S.B. Mukkamala, S.B. Jonnalagadda, *Synthesis, structure, and properties of new Mg(II)-metal-organic framework and its prowess as catalyst in the production of 4H-pyrans*, *Ind. Eng. Chem. Res.* 56 (2017) 2917-2924.

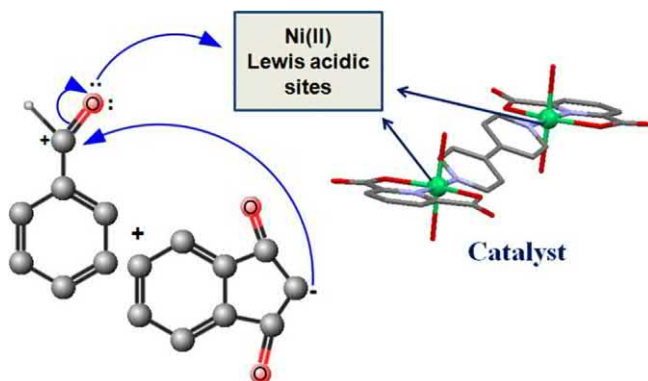


Fig. 6.5

A schematic representation of electronic transformation in the presence of Ni(II) coordination complex. Reprinted with permissions from K.K. Gangu, S. Maddila, S.B. Mukkamala, S.B. Jonnalagadda, *Catalytic activity of supra molecular self-assembled nickel (II) coordination complex in synthesis of indeno-pyrimidine derivatives*, *Polyhedron* 158 (2019) 464-470.

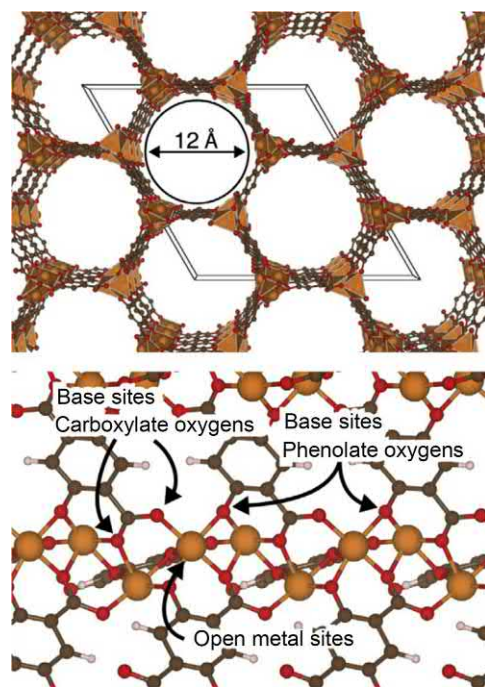
available in the structure, the catalytic reactions were carried out on the surfaces of catalyst. Indeno-pyrimidine derivatives have been synthesized by employing this compound as catalyst and target organic substrate was obtained in short intervals of time (<20 min) in excellent yields (up to 97%). Reusability of catalyst up to six times is another added advantage of it. The study revealed that catalytic nature of MOFs is not restricted to void space available in the structure, external/internal surfaces of MOFs are also one of the possibilities for delivering catalyzed reactions.



Good recyclability and high stability heterogeneous catalyst are paramount to synthesize important chemical intermediates through C-C coupling reactions. In these efforts, Fan et al. [71] have reported rare Ba(II)-based MOF,  $[\text{Ba}_2(\text{L})(\text{DMF})(\text{H}_2\text{O})(\text{NO}_3)_{1/3}]\cdot\text{DMF}\cdot\text{EtOH}\cdot 2\text{H}_2\text{O}$  (UPC-33), where L = 4,4'-((2-amino-5-carboxy-1,3-phenylene)bis(ethyne-2,1-diyl))-dibenzoic acid. An amino group functionalized ligand "L" is synthesized primarily and thus MOF, UPC-33 was prepared. This is the first 12 barium nuclear clusters obtained from amino-functionalized ligand. Stability to heat, Lewis basic  $-\text{NH}_2$  decorated channels, and optimization of pores meet the prerequisites for heterogeneous catalyst. With UPC-33 as catalyst, C-C bond formation has been achieved in 5 h when aldehyde and malononitrile were employed in the reaction medium. Study revealed that MOF-based catalysis is related to cavity centric reactions that was asserted with the experiment where bulky aromatic aldehydes were used as reactants. Due to bulkiness of aldehydes, size does not fit for the size of the MOF cavities, thus variation in reaction time as well as yield was observed.

Jiijia et al. have studied the morphological influences of MOFs on catalytic activity. Micro- and nano-sized MOFs exhibit unique physical and chemical properties compared to bulk MOFs [72]. Capping agents/additives were widely used for the controlled synthesis of MOFs to obtain micro-/nano-sized crystals. Tuning of morphology along with nucleation rate and crystal growth process can be achieved with the introduction of definite capping agents [73, 74]. In this study, the authors tried to produce MOFs micro crystals with specific morphology with the application of monocarboxylates as capping agents. MOF,  $\{\text{Zn}_2(\text{oba})_4(3\text{-bpdh})_2\}_\alpha\cdot 4\text{H}_2\text{O}$  (**1Zn**) where oba = 4,4'-oxybis(benzoic acid and bpdh = *N,N'*-bis-(1-pyridine-3-yl-ethylidene)-hydrazine were prepared solvothermally. Acetic acid and water were used as crystal growth modifiers and acquired rod-, plate-, and plate cluster-like morphologies of **1Zn** micro crystals. Spindle-like morphology crystals of **1Zn** was obtained, when capping agent was absent. Catalytic activity of spindle and plate cluster-like morphologies have exhibited 100% conversion of reactants in Knoevenagel condensation process, whereas rod- and plate-like morphologies showed lower catalytic activities. The reason attributed was that higher surface area of spindle and plate-like cluster morphologies of **1Zn** enhance interaction of reactants and catalyst. Study explicitly interpreted that catalytic activity of MOFs was size and morphology specific. Unlike functionalization of MOF with amino groups in the previous studies, Valvekens et al. [75] have reported intrinsic basicity characteristic of MOF, namely,  $\text{M}_2\text{dobdc}$ , where  $\text{M}^{2+}$  = metal ion and  $\text{dobdc}^{4-}$  = 2,5-dioxidoterephthalate. Due to the presence of phenolate oxygen atoms bonding with metal ions, coordinatively unsaturated catalytic sites were generated. Honeycomb-like structure was formed from the bonding of metal oxide ions with  $\text{dobdc}^{4-}$  linkers as shown in Fig. 6.6. Developed pores of 1.2 nm in diameter and intrinsically available basic sites were fit for the catalyzed Knoevenagel condensation reactions.

Nanostructured Co(II) MOF has been reported by Joharian et al. [76] using sonication method. MOF,  $[\text{Co}_2(\text{ppda})(4\text{-bpdh})_2(\text{NO}_3)_2]_n$ , where, ppda = *p*-phenylenediacrylic acid and



**Fig. 6.6**

(Top) Pores in the M<sub>2</sub>dobdc MOF; a sphere with a diameter of 1.2 nm fits inside the pores (brown = carbon; orange = metal; red = oxygen); (bottom) representation of the potential base sites and open metal sites in the framework. Reprinted with permissions from P. Valvekens, M. Vandichel, M. Waroquier, V. Van Speybroeck, D. De Vos, *Metal-dioxidoterephthalate MOFs of the MOF-74 type: microporous basic catalysts with well-defined active sites*, *J. Catal.* 317 (2014) 1–10.

4-bpdh = 2,5-bis(4-pyridyl)-3,4-diaza-2,4-hexadiene possessed supramolecular self-assembled network having different size and morphology depending on starting reagents concentration and irradiation power in environmentally friendly sonication technique. Nano-sized particle of this MOF with surface area higher than bulk MOF was utilized as heterogeneous catalyst for Knoevenagel condensation. Lewis basic characteristics of a zinc group in catalyst provide good interaction with substrates and produced yield of 98%. Same MOFs when prepared using mechanochemical and solvothermal methods showed low catalytic activity, and yields dropped to 68% and 63%, respectively. The study enlightens the relevance of particle size and method for preparation of catalyst as prerequisites for getting unparalleled properties in catalysis.

Tan and Zeng [77] have reported nanocomposite material comprising noble metal nanoparticles and MOFs. Ion-exchange process in MOFs is one of the alternative strategies to achieve diverse functionalities particularly in catalysis. Charged framework MOFs can undergo ion exchange with ease. Negatively charged scaffolds of MOFs are replaceable with charge

balancing positively charged cations, thus creating specific properties to MOFs. In another way, defective sites of MOFs can be integrated with metal nanoparticles, thus developing hybrid catalytic systems with improved functionalities, compared with pristine MOFs.

Overall Knoevenagel condensation can be achieved in a facile manner with the employment of modified MOF solid catalyst. In some cases MOF themselves possessed active sites and in some cases post-modification of MOFs was carried out to introduce catalytic active sites inside the pores or on the surfaces. Improved yields of desired products were obtained compared to other porous supports.

### 6.3 Modified MOFs for Heck reaction

Like Knoevenagel condensation, Heck reaction for C-C bond formation through cross-coupling reaction having an extra mileage in the modern organic synthesis. Immobilization of Pd ions on solid supports like carbon nanofibers, carbon nanotubes, magnetic  $\text{Fe}_3\text{O}_4$ , metal oxides, and polymers have been investigated extensively [78–80]. Owing to high surface area and numerous possibilities on surface modification MPFs are considered as suitable supports for immobilization [81–83]. The following studies enlighten the formation of C-C cross-coupling product with an aid of functionalized solid MOFs as heterogeneous catalyst.

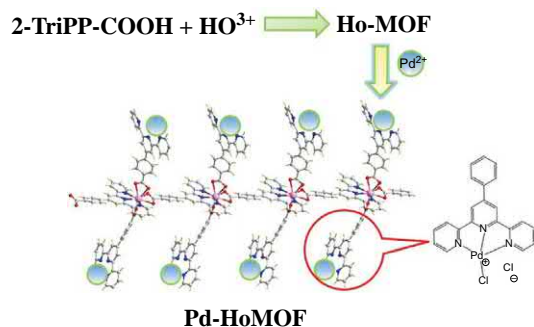
Surface modification of copper-coordinated terephthalic acid (BDC) has been reported by Alamgholiloo et al. [84]. Open metal sites of Cu(BDC) MOF were grafted with Pd complexation Schiff-base[pyridyl salicylimine (2-Py-SI)] through solvothermal technique. The synthesized  $\text{Pd}^{\text{II}}@ \text{Cu}(\text{BDC})/2\text{-Py-SI}$  MOF is used as efficient heterogeneous catalyst for Heck coupling reactions. Immobilization of palladium ions on different support materials was reported earlier, but in this study, authors have attempted to justify that MOFs are suitable candidates for immobilization of Pd(II)-like metal ions. The terminal positioned DMF molecules in the structure of Cu(BDC) allow the easy replacement with other kinds of groups.  $\text{Pd}^{\text{II}}@ \text{Cu}(\text{BDC})/2\text{-Py-SI}$  catalyzed the C-C coupling reaction between aryl halides and alkenes. As per the yields and selectivity,  $\text{Pd}^{\text{II}}@ \text{Cu}(\text{BDC})/2\text{-Py-SI}$  showed results better than other heterogeneous catalysts. The study has enlightened that the introduced Schiff-base could be used as good stabilizer for Pd(II) ions and increased the catalytic performance of MOF. In another study, Brown et al. [85] integrated Pd(II) ions into multivariate MOF,  $\text{Zn}_4\text{O}(\text{BDC-NH}_2)_n(\text{BDC})_{(3-n)}$ . 1,4-Benzenedicarboxylate (BDC) and 2-amino-1,4-benzenedicarboxylate ( $\text{BDC-NH}_2$ ) were two linkers incorporated in the structure of MOF. The inherent tendency of MOFs is to implant various catalytic units into their cages without disturbing their framework structure. In this study variation in the proportion of BDC- $\text{NH}_2$  provided information regarding the amount of metal catalyst that the pores occupy and its relative catalytic activity. Of the available various metalation experiments, lower metal loading MOF structure showed high selectivity to trans-isomer of target molecule. Increased BDC- $\text{NH}_2$  loadings enhanced Pd(II) sites for catalysis, but the experimental results showed that catalytic

activity rapidly declined, which is attributed to increased loading of BDC-NH<sub>2</sub> blocking the pores for entering the substrate to interact with Pd sites. Overall the study interpreted that interplay of porosity and metalation affect the catalytic activity and their optimization process was needed for efficient catalytic activity.

Transition metal complexes have wider applications in catalysis as homogeneous catalysts, but with constraints in recovery and reusability of catalyst materials. These limitations associated with metal complexes as homogeneous catalysts, particularly in separation after reaction was overcome by the encapsulation of such complexes immobilized on solid supports like MOFs [86, 87]. In this connection, Rezaei et al. [88] have reported Pd(II) complex encapsulated into MIL-Cr MOF. The resulting Pd complex@MIL-Cr is used as a solid catalyst in Heck coupling reactions. As mentioned earlier unique properties of MOFs like porosity, abundant surface area, and resistant to moisture can prompt them as suitable hosts for various other species of interest. In the earlier studies, Pd(II) nanoparticles were encapsulated into MOFs via post-modification methods or direct methods, but such hybrid MOFs suffered from some disadvantages like agglomeration of incorporated metal particles, which diminish their catalytic activity [89, 90]. Unlike such attempts, in this study instead of Pd(II) nanoparticles, Pd(II) complex was incorporated into MIL-Cr MOF. A 0.5 mol% of Pd complex@MIL-Cr in DMF at 80°C was optimized condition for obtaining high yield of target product. The high catalytic activity of this MOF was ascribed to conversion of Pd(II) complex into Pd(II) nanoparticles in the pores of MIL-Cr. The attractiveness of this study was encapsulation of Pd(II) complex achieved without damage to the structure of MIL-Cr and Pd complex@MIL-Cr framework was analogous to the parent MIL-Cr. Study has brought new vista to Pd(II) centric catalyzed value-added organic transformations.

In another study, Dong et al. [91] have reported Ho(III)-based MOF (Ho-MOF), namely [Ho(2-TriPP-COO)<sub>3</sub>] where 4'-(4-carboxyphenyl)-2,2':6',2''-terpyridine (2-TriPP-COOH) was ligand. Pd(II) catalyzed C-C coupling reactions is of great significance in pharmaceutical and fine chemical industries, but one of the serious problem of it is the leaching of Pd(II) ions from the so far utilized heterogeneous supports. To surmount this problem, free polypyridine groups available in this Ho-MOF structure reasonably played a crucial role for integration and direct binding of Pd<sup>2+</sup> species in the skeleton of MOF after post-synthetic modification as shown Fig. 6.7. This single site MOF has displayed good catalytic activity with negligible leaching of Pd(II) ions. However, parent Ho-MOF exhibited no catalytic activity (yield in traces), which indicate that the coupling reaction achieved in this study was due to Pd-HoMOF.

Huang et al. [92] have reported mixed linker MOF (MIXMOF) supported Pd(II) nanoparticles for efficient, recyclable, and stable heterogeneous catalyst. The incorporation of Pd(II) nanoparticles into porous MOFs still remains complex owing to their dispersion into the solution. In this regard, authors have attempted to prepare amine-functionalized mixed linker MOF, MIL-53(Al)-NH<sub>2</sub> (Al(OH)[H<sub>2</sub>N-BDC] for efficient grafting of Pd nanoparticles. Amino



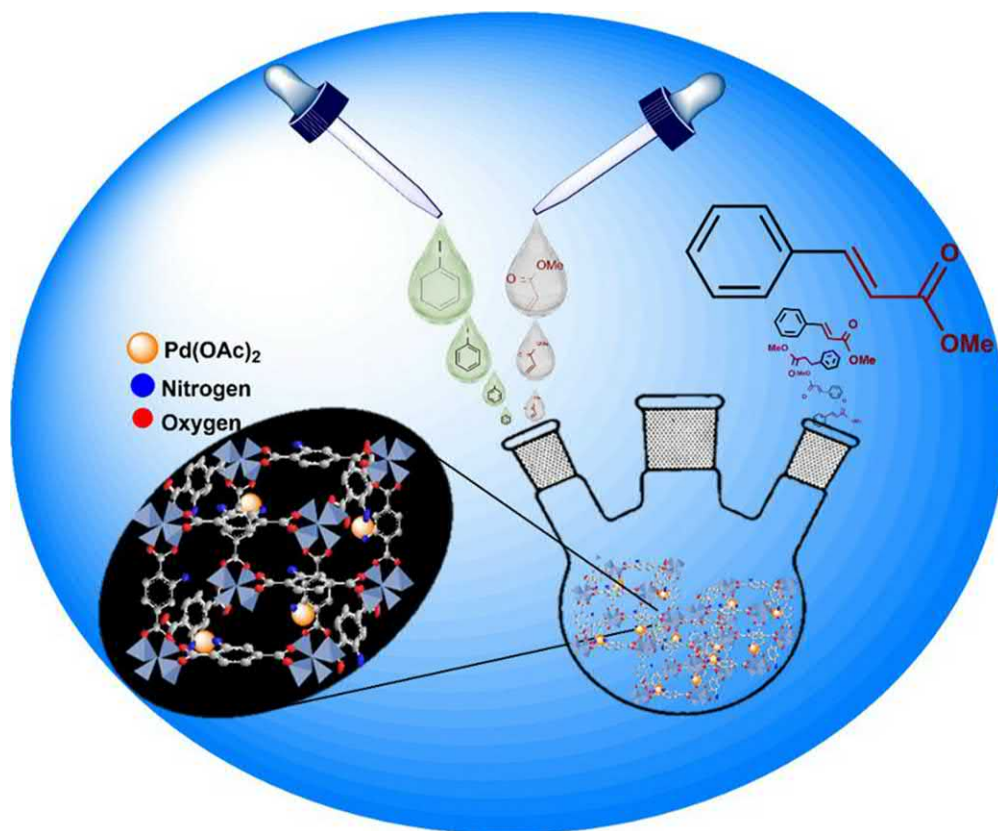
**Fig. 6.7**

Schematic representation of the synthetic route for Pd-HoMOF catalyst. The structure model (down) of Pd-HoMOF shows the incorporation of palladium(II) ions into the MOF framework. Atomic scheme: holmium, *rose*; palladium, *azure*; oxygen, *red*; nitrogen, *blue*; carbon, *gray*. Reprinted with permissions from D. Dong, Z. Li, D. Liu, N. Yu, H. Zhao, H. Chen, J. Liua, D. Liu, *Postsynthetic modification of single Pd sites into uncoordinated polypyridine groups of a MOF as the highly efficient catalyst for Heck and Suzuki reactions*, *New J. Chem.* 42 (2018) 9317–9323.

groups present in the structure can be used for post-modification of mix linker MIL-53(Al)-NH<sub>2</sub>. Loading of Pd caused no apparent loss in the crystallinity as per powder XRD studies and framework integrity was well maintained. A certain amount of amino groups on the functionalized ligand in the structure of this MOF are beneficial for the exact immobilization of Pd nanoparticles. About 50% of the NH<sub>2</sub> groups contained Pd/MIL-53(Al)-NH<sub>2</sub> MOF produced 93% yield of target molecule in the Heck reaction between bromobenzene and styrene. About 50% of the amino groups on MOF structure showed higher catalytic activity. The amount of amine in the support was also important for higher activity of Pd nanoparticles. The study revealed that instead of sole ligand, addition of functionalized ligand in appropriate proportions become an added advantage for good dispersion of metal nanoparticles.

Nuri et al. [93] have chosen one of the MOF-5-based IRMOF for surface modification with deposition Pd(II) particles. IRMOF series are obtained from Zn<sub>4</sub>O tetrahedron-shaped entities bonded with six carboxylate ions giving 3D porous framework. In general, various metals viz. rhodium, magnesium, copper, zinc, ruthenium, tin, and in particular palladium was often utilized in the C-C bond coupling reactions. Among various types of IRMOFs series, amino-functionalized IRMOF-3 was used for the Pd(II) particle deposition in this study. A total of 50 mg of Pd(OAc)<sub>2</sub> was added to 1 g IRMOF-3 activated particles dispersed in CH<sub>2</sub>Cl<sub>2</sub> resulting in IRMOF-3-Pd catalyst. When compared the prepared catalyst with other kinds of catalysts including support-free Pd(OAc)<sub>2</sub> that showed poorer results in terms of reaction time and yield of target molecule, the recyclable IRMOF-3-Pd produced 100% yield of product in 25 min of reaction time (Fig. 6.8). The characteristic results of SEM (scanning electron microscopy), TEM (transmission electron microscopy), powder XRD, and X-ray photoelectron spectroscopy (XPS) have demonstrated that IRMOF-3 is suitable support among IRMOF series for grafting palladium particles.





**Fig. 6.8**

IRMOF-3-Pd as solid catalyst in Heck reaction. Reprinted with permissions from A. Nuri, N. Vucetic, J.-H. Smatt, Y. Mansoori, J.-P. Mikkola, D.Y. Murzin, Pd supported IRMOF-3: heterogeneous, efficient and reusable catalyst for Heck reaction, *Catal. Lett.* 149 (2019) 1941–1951.

In the similar lines, Bagherzadeh et al. [94] have reported surface-modified Mn-based MOF, Pd/MnBDC. Like previous studies, Pd(II) nanoparticles were supported on MnBDC MOF to avoid environmental and health impact on work-up process and to gain good dispersion of the catalytic active sites. Several approaches such as impregnation, chemical vapor deposition, and co-precipitation for loading Pd nanoparticles onto different supports have their own limitations like leaching of metal ions [95, 96]. In this work, the authors have described solution impregnation method, where orange colored Pd solution was added to the prepared MnBDC in the presence of hydrazine hydrate, resulting in a gray powder after drying. Electronic spectroscopy results revealed that Pd nanoparticles attached on the surface of the MnBDC and active sites of Pd particles catalyze the coupling reaction. Li et al. [97] have reported tandem catalysis by Pd(II) encapsulated Zr-based MOF. UiO-66-NH<sub>2</sub> was prepared from a combination of [Zr<sub>6</sub>O<sub>4</sub>(OH)<sub>4</sub>(CO<sub>2</sub>)<sub>12</sub>] clusters and 2-aminoterephthalic acid linkers. Authors in this study have reported bifunctional activity to the MOF, where uncoordinated



zirconium sites acted as Lewis acid sites. Oxidation activity of nano-Pd particles encapsulated into MOF structure led to Pd@UiO-66-NH<sub>2</sub> with tandem catalytic nature. Both oxidation and acetalization can be achieved in one reactor without transfer of intermediates. This multifunctional catalyst overcomes the multistep reactions and reduces the by-product/waste production so as to meet Green Chemistry principles. In another study, Ashouri et al. [98] have studied the effect of framework functionality on the catalytic activation of supported Pd in coupling reactions. Two functional and nonfunctional MOFs, namely, Pd/CoBDCNH<sub>2</sub> and Pd/Co BDC were prepared and their influence on Pd nanoparticles dispersion was examined. Functionalized MOF possessed the tendency to inhibit the Pd nanoparticle aggregation. Functional, [Co<sub>3</sub>(BDCNH<sub>2</sub>)<sub>3</sub>(DMF)<sub>2</sub>(H<sub>2</sub>O)<sub>2</sub>]<sub>n</sub>, and nonfunctional, [Co<sub>3</sub>(BDC)<sub>3</sub>(DMF)<sub>2</sub>(H<sub>2</sub>O)<sub>2</sub>]<sub>n</sub>, MOFs were used for the Pd nanoparticles dispersion.

Even though, Pd(II) individually and in anchored form with support materials exhibit good catalytic nature, these catalyzed reactions are expensive for commercial processes. Keeping this point, Rani and Srivastava [99] have reported Cu(I)-based MOF namely [Cu<sub>4</sub>L<sub>4</sub>(DABCO)<sub>2</sub>] (Cu-MOF) by using DABCO (1,4-diazabicyclo[2.2.2]octane) as ligand. As per the reports, Cu(I) were active catalyst species in the coupling reactions based on these encouraging results in which Cu-MOF was prepared. Cu-MOF was prepared in acetonitrile and KI media, and highest catalytic activity was observed in terms of yield and selectivity with KI medium. Cu(I) sites in Cu-MOF were more accessible to reactants compared to Cu(I) in cluster form. Study has revealed that Cu sites more isolated in MOF structure propagate the relevance of MOFs in heterogeneous catalysis.

Overall amino-functionalized linkers or mixed linkers in MOFs are probably assisting the dispersion/immobilization of metal nanoparticles. The creation of catalytic active sites with various attempts on MOFs is expected to enable the enhanced catalytic activity and provide solutions to synthetic organic reactions.

#### **6.4 Modified MOFs for Suzuki-Miyaura and Sonogashira reactions**

As discussed in previous sections, C-C bond formation is a crucial step in the drug design and employment of appropriate heterogeneous system produces enhanced yields of organic product using appropriately designed catalyst materials. This section establishes explicit knowledge on the development of suitable solid systems.

MOFs are solid matrices to support various metal nanoparticles for efficient catalytic applications. The probable pore sizes of MOFs are sometimes not suitable to the dispersed metal nanoparticles for getting into channels/pores of MOF [100–102]. Other options to place metal nanoparticles on external surface of MOFs were also worthy to get good catalytic activity. Zhang et al. [103] have reported novel MOF support materials in nanoscale range to alleviate the problems with uncontrollable impregnation of metal nanoparticles into pores of

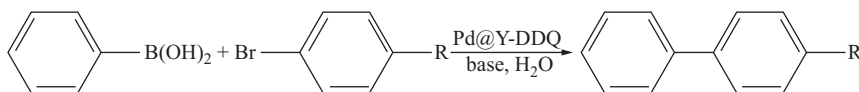


Fig. 6.9

Suzuki-Miyaura coupling reactions catalyzed by Pd@Y-DDQ. Reprinted with permissions from Y. Zhu, M. Zhu, L. Xia, Y. Wu, H. Hua, J. Xie, *Lanthanide metal-organic frameworks with six-coordinated Ln(III) ions and free functional organic sites for adsorptions and extensive catalytic activities*, *Sci. Rep.* 6 (2016) 29728.

MOFs. Scandium(III) and trimesic acid-based MOF denoted as ScBTC is synthesized in nanoscale dimensions by using surfactant-assisted microwave irradiation approach and further palladium nanoparticles were impregnated with same technique. Higher loading of Pd nanoparticles into ScBTC was achieved, that is, about 4.5 wt% compared to other works reported in the literature, that is, not exceeding 3 wt%. This reveals that lower loading could be obtained only when particles are surface loaded. In this study Pd nanoparticles were penetrated into channels/pores of host material. High yields of target molecule were obtained at room temperature in a short time. Even if the studies are in early stages, the nanoscale MOFs proved advantageous and more competitive over the bulk MOFs. In another study, Zhu et al. [104] have studied the modification of MOFs for efficient catalytic activity. In this study, authors have examined two active sites, open metal sites (OMSs) and free functional organic sites (FOSs) created in the structures of Ln(III)-based MOFs, namely Y-DDQ, Dy-DDQ and Eu-DDQ where DDQ = *N,N'*-dibenzoic acid-2,3-diaminoquinoxaline. Availability of FOSs in the structures and immobilization of palladium nanoparticles were done using post-synthetic modification. Grafting of —NH, —SH, and —OH onto the surfaces of porous materials opened up flexibility for immobilization of heavy metal precursors, viz., Pd, Ru, Au, Pt, etc., through post-synthetic method. Without the loss of crystallinity, Pd metal ions were immobilized to supported Y-DDQ with chelating amino group interactions, resulting in Pd@Y-DDQ. >96% of the yield obtained in the Suzuki reaction as shown in Fig. 6.9 is due to free amino groups facilitating the Pd metal ions coordination without aggregation on MOFs. These results were substantiated by other MOFs, Pd/MIL-101Cr-NH<sub>2</sub> and Pd/MIL-53(Al)-NH<sub>2</sub>, which also showed excellent catalytic activity (yields >95%).

As we discussed about the ethnicity of IRMOF-3 for grafting catalytic active metal ions into their surfaces/pores, Saha et al. [105] have reported in the similar lines, the immobilization of Pd ions on IRMOF-3 for Suzuki C-C coupling reaction. Basically, IRMOF-3 was constructed from Zn-(NO<sub>3</sub>)<sub>2</sub>·4H<sub>2</sub>O and 2-amino-1,4-benzene dicarboxylic acid and the existing free amino groups undergo a variety of catalyzed organic transformations. In this study, a bidentate Schiff base was developed upon condensation of amino group containing IRMOF-3 with pyridine-2-aldehyde, thereafter Pd(II) ion were anchored with help of Schiff base moieties, resulting in [Zn<sub>4</sub>O(ATA)<sub>3-x</sub>(PITA-PdCl<sub>2</sub>)<sub>x</sub>] (IRMOF-3-PI-Pd), where ATA = 2-aminoterephthalate and PITA = 2-pyridyl-imine terephthalate (Fig. 6.10).

Under mild reaction conditions (80°C, ethanol/H<sub>2</sub>O as solvent and K<sub>2</sub>CO<sub>3</sub> as base), IRMOF-3-PI-Pd catalyzed C-C coupling reaction between bromobenzene and phenylboronic acid gave

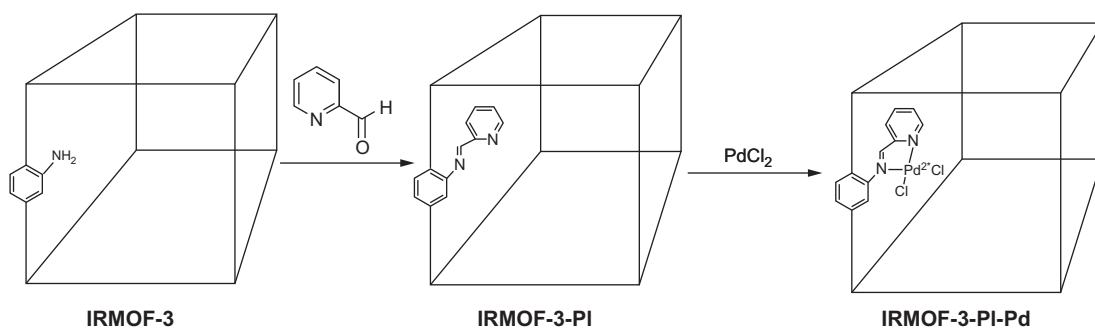


Fig. 6.10

Post-synthesis modification procedure for obtaining MOFs containing the Pd(II) Schiff base complex. Reprinted with permissions from D. Saha, R. Sen, T. Maity, S. Koner, *Anchoring of palladium onto surface of porous metal-organic framework through post-synthesis modification and studies on Suzuki and Stille coupling reactions under heterogeneous condition*, *Langmuir* 29 (2013) 3140–3151.

biphenyl target molecule in 100% yield in 2 h. Study has revealed that target specific surface modification of MOFs ultimately generates eco-friendly potent catalysts for synthesizing organic molecules with good biomedical applications. In furtherance of study, Panahi et al. [106] have reported Pd-loaded MOF (Pd@Cu-MOF),  $\text{Cu}_2(\text{NH}_2\text{-BDC})_2(\text{DABCO})$  where, BDC = 1,4-benzenedicarboxylic acid and DABCO = diazabicyclooctane for sustainable catalytic organic transformation. Pd@Cu-MOF was prepared by solvent-free ball-milling method. Thereafter, Pd particles were dispersed in it. Suzuki-Miyaura coupling reaction was carried out by employing Pd@Cu-MOF solid catalyst through environmentally benign ultrasound irradiation. In free  $-\text{NH}_2$  and Pd particle MOF,  $\text{Cu}_2(\text{BDC})_2(\text{DABCO})$  possessed surface area of  $1496 \text{ m}^2/\text{g}$ , but drastically dropped to 873 and  $226 \text{ m}^2/\text{g}$  upon the introduction of Pd nanoparticles and amino groups, respectively. The surface area of Pd@Cu-MOF was higher upon loading of Pd nanoparticles. It was attributed to the absence of Pd nanoparticles, amino groups associated with hydrogen bonding with carboxylate oxygen atoms led to the MOF aggregation (surface area reduction), whereas in the presence of Pd particles, amino groups substantially bonded with introduced Pd particles and diminished the hydrogen bonding. The total development lessened the agglomeration of MOF particles and increased the surface area. Different derivatives of biaryl compounds were synthesized with insignificant leaching of Pd in Pd@Cu-MOF heterogeneous catalyst. Tahmasebi et al. [107] have reported Pd nanoparticle-encapsulated  $\text{Cu}_2(\text{BDC})_2(\text{DABCO})$  MOF, where Pd nanoparticles were introduced as a one-step protocol into pores of MOF with the use of temperature controlling program without the involvement of any external reducing agent. Temperature programming control ranges from 80 to  $130^\circ\text{C}$  for 20-h reduces Pd(II) ions to Pd(0) nanoparticles and make the encapsulation into the cavities of  $\text{Cu}_2(\text{BDC})_2(\text{DABCO})$  MOF simpler.

The introduction of metal centers in general onto MOFs and particularly onto amino-functionalized MOFs was useful in the coupling reactions. In another way the use of mixed linker in the construction of MOFs was an added advantage for tuning the catalytic activity via

varying the mixed linker MOF composition [59, 105, 108, 109]. Considering these points, Sun et al. [110] reported two mixed-linker MOFs, UiO-66-Mix and UiO-67-Mix with various ratios of 2-amino-1,4-benzenedicarboxylate/1,4-benzenedicarboxylate and 2-amino-biphenyl-4,4'-dicarboxylic acid/4,4'-biphenyldicarboxylic acid by using Zr(II) metal centers. In post-synthetic modification (PSM), two MOFs were treated with pyridine-2-carboxaldehyde and further with Pd ions to afford Pd heterogeneous catalysts, UiO-66-Mix-PI-Pd and UiO-67-Mix-PI-Pd, where PI = pyridylimine (PI formed by the reaction of pendant amino groups and pyridine-2-carboxaldehyde). This study revealed that PI role was prominent to promote C-C coupling reactions, because when free PI Pd-loaded UiO-67 catalyst was tested, low conversion percentage was recorded. When UiO-67 and UiO-67-PI were tested with no Pd amount, no reaction occurred, but the addition of 6 mg of Pd to UiO-67-PI speeds up the reaction forming coupling product in 2 h with complete conversion. The advantages of solid MOF modifications such as catalysts and optimization methods in view of reaction time and conversion finally led to the Pd-catalyzed Suzuki reaction in environmentally benign system. The selection of appropriate support as well as nature of ligand are key for Pd-grafted heterogeneous catalyst. In this direction, Rostamnia et al. [111] have prepared commercially cheap metal and ligand-based bifunctional open metal site MOF, namely Cu-BDC (BDC = benzene-1,4-dicarboxylate = terephthalate). Cu-BDC thereby grafted with Pd coordinated pyridyl-salicylimine led to Pd@Cu-BDC/Py-SI MOF, where Py-SI = pyridyl-salicylimine). Pd@Cu-BDC/Py-SI-promoted coupling reaction led to product biaryls in high yields without any by-products. Moreover, this catalyst was chemoselective toward Suzuki reaction. Carson et al. [112] have studied the influence of bases on the Pd-loaded MOF catalyzed Suzuki reactions. Authors chose four bases, such as  $K_2CO_3$ ,  $Cs_2CO_3$ , KF, and CsF and MOF catalyst Pd@MIL-101-NH<sub>2</sub>(Cr) for investigating the effect of bases on the reduction of decomposition of MOF catalyst. Chemical stability of catalyst was of utmost importance for their wide spread utilization. Reaction conditions are largely influenced by the stability of MOF-based catalysts in the construction of MOF-sensitive coordination bonds existing between metal ion/cluster and linkers. In the presence of  $K_2CO_3$ ,  $Cs_2CO_3$  bases, yields of products are high in short reaction times, but decomposition was rapid compared to fluorides (KF and CsF). Fluoride bases maintained the crystallinity and porous nature for longer time, which is apt for the Suzuki coupling reactions. Compared to potassium, caesium bases significantly increased the catalytic activity. The migration of palladium and redeposition onto the external surfaces of MOF was possible with Cs bases. In order to improve the half-life period, reduction of waste, and cost, the optimization of reaction conditions is vital, particularly in pharmaceuticals and fine chemical industries. Late transition metals like Pd, Rh, and Pt have shown superb catalytic activity in C-C coupling reactions. Due to low availability of these metals, early earth-abundance metals like nickel as catalyst is sustainable alternative to late transition metals. In this direction, Elumalai et al. [113] have reported Ni-deposited UiO-66 (made up of Zr clusters and 1,4-benzo dicarboxylic acid) MOF. Catalyst was used up to seven times without detrimental to yield and amount of catalyst recovered. No leaching of Ni metal ions into the reaction solution was observed.

Nanoporous carbons (NPCs) are emergent materials with unique features like high surface area and porosity. NPCs are ideally used in the support materials in heterogeneous catalysis. The preparation of NPCs is quite complex and often encounter many shortcomings like disordered structures of carbon materials [114–117]. To avoid this, Dong et al. [118] have reported versatile and facile strategy for the preparation of NPCs. As method suggested, authors derived the NPCs from direct carbonization of MOFs without the use of additional carbon precursors. Of various flexible MOFs, UiO-66,21 MIL-100,22 and Al-PCP widely popular MOF-5( $\text{Zn}_4\text{O}(\text{H-BDC})_3$ , BDC = 1,4-benzenedicarboxylate) were used for the carbonization for NPC preparation. Obtained MOF-5-NPC when further immobilized with Pd nanoparticles by using impregnation method followed by reduction with  $\text{NaBH}_4$  finally results in MOF-5-NPC-Pd. In order to get Zn-free MOF-5-NPC-Pd, treatment with 10% HCl was carried out as shown in Fig. 6.11. High surface area of Zn-free MOF-5-NPC-Pd leads to high dispersion of Pd and subsequently exhibited high catalytic activity.

A carbonylative (introduction of CO at 10 bar) assisted Suzuki coupling reaction was reported by Augustyniak et al. [119] with Pd embedded on Ni(II) ion and pyrazolate ligand containing MOF  $\text{Ni}(\text{H}_2\text{BDP-SO}_3)_2$ ,  $[\text{Ni}(2,5\text{-di}(1\text{H-pyrazol-4-yl})\text{benzenesulfonate})_2]$ . Study indicated that Ni(II) cations and 2,5-di(1H-pyrazol-4-yl)benzenesulfonate linker MOF were suitable support for  $\text{Pd}^{2+}$  and Pd nanoparticles. The so-formed  $\text{Pd}@\text{Ni}(\text{H}_2\text{BDP-SO}_3)_2$  as catalyst formed coupling product diaryl ketone of 21% at 1 bar CO pressure and 51% at 5 bar CO, finally sole product was obtained at 10 bar CO. This study revealed that carbonylative-aided heterogeneous catalytic activity was an alternative approach for the efficient Suzuki coupling reaction than other counterpart catalysts. In another study, the introduction of open metal-binding sites into MOF provides extra mileage in terms of properties and applications especially in catalysis. Keeping this point, Fei and Cohen [120] have reported the incorporation of free 2,2'-bipyridine



Fig. 6.11

The preparation process of the catalyst and the Suzuki coupling reaction. Reprinted with permissions from W. Dong, L. Zhang, C. Wang, C. Feng, N. Shang, S. Gao, C. Wang, Palladium nanoparticles embedded in metal-organic framework derived porous carbon: synthesis and application for efficient Suzuki-Miyaura coupling reactions, *RSC Adv.* 6 (2016) 37118–37123.

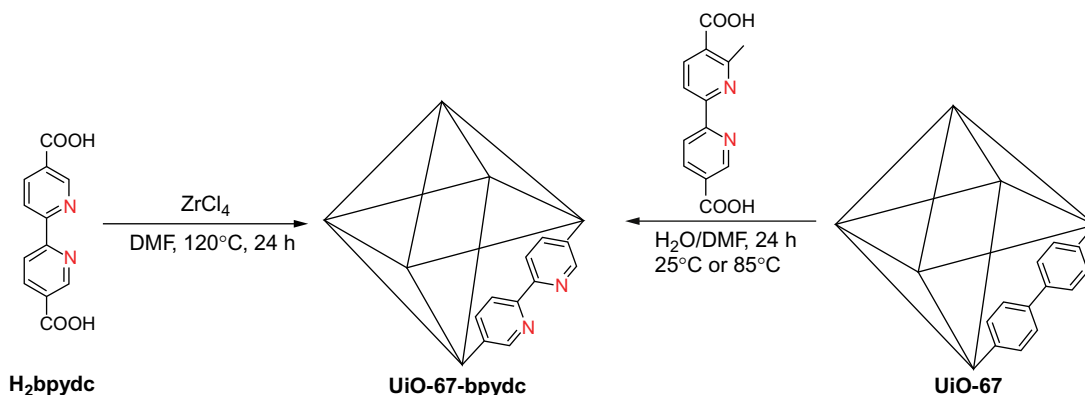


Fig. 6.12

Synthesis of UiO-67-bpydc using direct synthesis and post-synthetic exchange. Reprinted with permissions from H. Fei, S.M. Cohen, *A robust, catalytic metal-organic framework with open 2,2'-bipyridine sites*, *Chem. Commun.* 50 (2014) 4810–4812.

(bpy) into MOFs, which develop open metal sites. Bidentate chelator, bpy is the widely used auxiliary ligand in coordination chemistry and renders special properties to MOF structure. Direct solvothermal method and post-synthetic method were proposed to incorporate bpy into selected highly robust UiO-67 platform as shown in Fig. 6.12. The resulting UiO-67-bpydc exhibited high porous nature after activation and Pd metalation was simply achieved through complex formation. Low palladium leaching and low catalyst loading are another advantages of this porous solid catalyst for commercially worthy C-C coupling reaction.

Li et al. [121] have reported the impacts of linker substitution on the heterogeneous catalysis of MOFs in Suzuki coupling reactions. 2,2'-bipyridyl-substituted UiO-67 (Zr-terephthalic acid) MOF were selected judiciously for the encapsulation of Pd nanoparticles. Uncoordinated 2,2'-bipyridyl moieties make easy the anchoring of loading and stabilizing Pd complexes. Isorecticular bipyridyl MOF series, namely m-bpy-MOF-Pd, m-6,6'-Me<sub>2</sub>bpy-MOF-Pd, and m-4,4'-Me<sub>2</sub>bpy-MOF-Pd were used in the investigation of the effect of mixed linker substitution in the coupling reaction. Remarkably, m-6,6'-Me<sub>2</sub>bpy-MOF-Pd catalyst has showed enhanced catalytic activity compared to other MOF series. The reason ascribed to electronic and steric effects that existed between bipyridyl and palladium sites, which is high for m-6,6'-Me<sub>2</sub>bpy-MOF-Pd. This study unveils the deeper understanding in the influence of various factors like linker engineering and surrounding chemical environment of modified MOFs on heterogeneous catalytic sites.

As discussed earlier, without appropriate stabilization, metal nanoparticles especially Pd particles are prone to aggregation and lose their catalytic activity. In this way, Roya et al. [122] have chosen Co(II)-Salicylate containing MOF as support material for the immobilization of Pd nanoparticles. The uncoordinated oxygen atoms in this framework were used for the stabilization of entered Pd nanoparticles. Pd-catalyzed alkynylation of aryl halides was carried out in the absence of copper co-catalyst, which tends to form by-product oxidative



homocoupling that can be avoided by employing this designed catalyst. Pd(0) played a prominent role in the promotion of reaction, this was confirmed with Hg(0) poisoning test. During the reaction time 1.0 mL of mercury was added and the progress of reaction was observed. Due to the formation of Pd-Hg amalgamate, catalytic reactive tendency of Pd was quenched and coupling reaction becomes inactive. Eco-friendly, mild reaction conditions with this modified MOF pave the way for other kinds of biologically valued organic transformations.

Annapurna et al. [123] reported MIL-101-supported nano-sized Pd particles for coupling reaction between heteroaryl/aryl bromide and alkynes.  $\text{Cr}_3(\text{F},\text{OH})(\text{H}_2\text{O})_2\text{O}[(\text{O}_2\text{C})\text{-C}_6\text{H}_4\text{-}(\text{CO}_2)]_3 \cdot n\text{H}_2\text{O}$  (MIL-101) is congenial support because it possessed high surface area c.4000  $\text{m}^2/\text{g}$  and pore size c.30 Å to accommodate metal particle insertion. Furthermore, unsaturated chromium sites present about 3.0 mmol/g acted as Lewis acid sites after the removal of water molecules. Sonogashira coupling reaction was carried out between 202 mg of 4-bromonitrobenzene, 204 mg of phenylacetylene, 3.5 wt% Pd/MIL-101, and 276 mg of  $\text{K}_2\text{CO}_3$  in DMF- $\text{H}_2\text{O}$  system at 130°C. The yield of the desired product increases with changing reaction time from 3 to 6 h. The encouraged results with a series of aryl bromides prompted for examining hetero aryl bromide and heteroarylalkynes substrates also. No considerable coupling product was identified with the use of heteroarylalkynes. The study enlighten even if efficient solid catalyst is employed in the reaction, the selection of substrates is also imperative to get the desired product in high yields.

Bifunctional  $\text{Cu}_3(\text{BTC})_2$  (BTC = benzene-1,3,5-tricarboxylate) MOF with Pd functionalization has been reported by Arnanz and group [124]. MOF-Cu(BTC)-[Pd] has been prepared as shown in Fig. 6.13, which develops stable MOF with additional functional moieties. The introduction of Pd complex into the pores of  $\text{Cu}_3(\text{BTC})_2$  was confirmed by X-ray studies. Change of intensity in the XRD peaks confirms the entering of complex into pores. Both Cu and Pd sites in the same structure are adequate heterogeneous bi-functional catalyst for Sonogashira C-C coupling reaction. Surface modification of MOFs with different organic molecules and transition metal complexes renders the development of multifunctional MOF solid catalysts to preserve sustainability and stability of catalytic activity.

The quality of bare MOFs can be augmented with systematic functionalization of metal nodes and organic linkers by the incorporation of various multiple functional units into them. *N*-Heterocyclic carbene (NHC) is an example of such a kind of ligand [125–127]. Possible electronic transitions between  $\sigma/\pi$  and d-donations make feasible the bonding with metal. To take advantage of these traits, Ezugwu et al. [128] have reported *N*-heterocyclic carbene-based MOF for efficient Sonogashira cross-coupling reaction. 1,3-bis(4-carboxyphenyl) imidazolium chloride ( $\text{H}_2\text{L}^+\text{Cl}^-$ ) ligand has been prepared previously by treating with  $\text{Zn}(\text{NO}_3)_2 \cdot 6\text{H}_2\text{O}$  to get MOF with active imidazolium moieties. NHCs can be achieved by the treatment of imidazolium-containing framework with  $\text{Pd}(\text{OAc})_2$  in THF as solvent under an inert atmosphere. Carbene carbon generating Pd-NHC is evidenced by NMR (nuclear magnetic

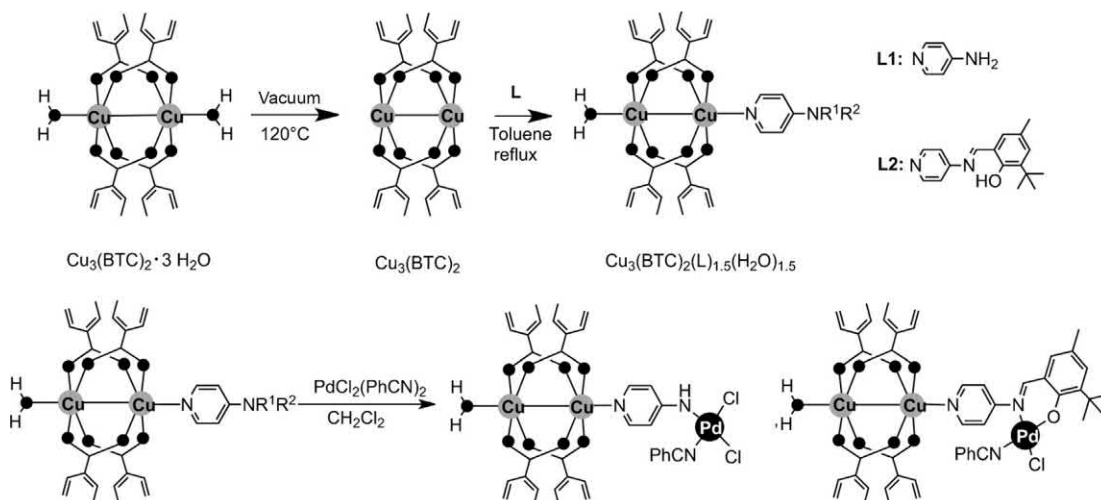


Fig. 6.13

Functionalization of  $\text{Cu}_3(\text{BTC})_2$  with palladium complexes. Reprinted with permissions from A. Arnanz, M. Pintado-Sierra, A. Corma, M. Iglesias, F. Sanchez, Bifunctional metal organic framework catalysts for multistep reactions: MOF-cu(BTC)-[Pd] catalyst for one-pot heteroannulation of acetylenic compounds, *Adv. Synth. Catal.* 354 (2012) 1347–1355.

resonance) studies. This study emancipated the carbene carbon containing ligands useful for the grafting of various metal nanoparticles.

Hetero-bimetal, that is, Pd(II) and Y(III) connected with 2,2'-bipyridine-5,5'-dicarboxylate acid (bpydc) MOF has been reported by Huang et al. [129] for Sonogashira reaction. The synergistic effect of Pd(II) and Y(III) in Pd/Y-MOF exhibited enhanced catalytic activity than Pd(bpydc)Cl<sub>2</sub> MOF. The author has suggested that the immobilization/dispersion of Pd(II) onto the surfaces/pores showed catalytic competence lower than the Pd(II) coordinated into the structure. The coordination of two metals in this MOF was achieved with suitability of chosen bpydc ligand. Two Cl and two N atoms in bpydc initially coordinated Pd(II) ions thereby linking the available carboxylic groups in bpydc to the Y(III) ions, resulting in a 3D framework structure. Catalytic activity of Pd/Y-MOF for small-sized reactant molecules was almost tantamount/comparable with homogeneous Pd(OAc)<sub>2</sub> owing to well accessibility and dispersion propensity afforded in the designed Pd/Y-MOF. Moreover, the coordination of Pd(II) ions and N atoms in bpydc hamper the leaching of Pd(II) sites under reaction conditions.

Overall most of the Pd ions and other transition metal immobilization or dispersion was conducted by impregnation, co-precipitation, solvothermal, and post-synthetic approaches. Electronic effects, steric effects, and auxiliary ligands like bipyridyls and inclusion of appropriate base in the reaction conditions are responsible for the functioning of catalysts. In most of the cases solvent, temperature, and other parameters also play a pivotal role in deciding the selectivity and conversion rates of final products.

## 6.5 Conclusions

In summary, C-C bond formation is highly anticipated reaction in pharmaceutical/fine chemical industry to design and construct novel drug molecules with emergent biological activities. In most of the cases, these C-C bond/coupling intermediates are key components and critical step toward the synthesis of final drug entities. Considering economic and environmental contexts of this reaction it is of crucial importance. Tedious multistep and work-up procedures are increasingly fostering the development new systems. In recent years most of the researchers have adopted varied technologies in organic transformations, one thing that seems to restrain all technologies is the use of heterogeneous/solid MOFs as catalysts. MOFs as heterogeneous catalysis are revolutionizing the next advancement in the field of catalysis. The objective of embedding specialized catalytic active substances on their surfaces or into pores is to make a new catalytic system that will function as environmentally viable and alienate the cumbersome methodologies, which industries are implementing. Many studies have reported using bare MOFs or modified MOFs for enhanced catalysis in Knoevenagel, Heck, Suzuki and Sonogashira, and multicomponent reactions. The flexibility for modifying and designing the MOFs according to the requirement is an added advantage of MOFs. The enhancement in catalytic performance is attributed to the alloying of nano-structured transition metals like Pd, which make the interaction with organic reactants stronger than the individual Pd ions. Mixed linker combination, immobilization of active catalytic substances using MOFs as host materials, and so on are some of the strategies followed by many researchers for productive catalytic efficiency. MOF catalytic systems have efficiently overcome the deficits such as leaching, separation, and recyclability that occur in the homogeneous system. In most of the cases even the selection of reactants and reaction conditions also play a pivotal role in improving the yields, even if suitable catalyst was employed in the reaction. This chapter enlightens the development of suitable solid MOF heterogeneous catalysts and structure-property relationships in catalysis in providing value-added organic moieties of pharmaceutical and other industrial importance.

## References

- [1] B. Louage, O. De Wever, W.E. Hennink, B.G. De Geest, Developments and future clinical outlook of taxane nanomedicines, *J. Control. Release* 253 (2017) 137–152, <https://doi.org/10.1016/j.jconrel.2017.03.027>.
- [2] P. Horcajada, C. Serre, M. Vallet-Regí, M. Sebban, F. Taulelle, G. Férey, Metal-organic frameworks as efficient materials for drug delivery, *Angew. Chem. Int. Ed.* 45 (2006) 5974–5978.
- [3] V.L. Rechac, F.G. Cirujano, A. Corma, F.X. Llabres, Diastereoselective synthesis of pyranoquinolines on zirconium-containing UiO-66 metal-organic frameworks, *Eur. J. Inorg. Chem.* (2016) 4512–4516.
- [4] Z. Liu, L. Lv, Y. He, Y. Feng, An anionic metal-organic framework constructed from a triazole-functionalized diisophthalate featuring hierarchical cages for selective adsorptive C<sub>2</sub>H<sub>2</sub>/CH<sub>4</sub> and CO<sub>2</sub>/CH<sub>4</sub> separation, *CrystEngComm* 19 (2017) 2795–2801.
- [5] X. Gao, M. Zhai, W. Guan, J. Liu, Z. Liu, A. Damirin, Controllable synthesis of a smart multifunctional Nanoscale metal-organic framework for magnetic resonance/optical imaging and targeted drug delivery, *ACS Appl. Mater. Interfaces* 9 (2017) 3455–3462.

- [6] M. Yu, D. You, J. Zhuang, S. Lin, L. Dong, S. Weng, B. Zhang, K. Cheng, W. Weng, H. Wang, Controlled release of naringin in metal-organic framework-loaded mineralized collagen coating to simultaneously enhance osseointegration and antibacterial activity, *ACS Appl. Mater. Interfaces* 9 (2017) 19698–19705, <https://doi.org/10.1021/acsami.7b05296>.
- [7] I. Erucar, S. Keskin, Efficient storage of drug and cosmetic molecules in biocompatible metal organic frameworks: a molecular simulation study, *Ind. Eng. Chem. Res.* 55 (7) (2016) 1929–1939, <https://doi.org/10.1021/acs.iecr.5b04556>.
- [8] N. Stock, S. Biswas, Synthesis of metal-organic frameworks (MOFs): routes to various MOF topologies, morphologies, and composites, *Chem. Rev.* 112 (2) (2012) 933–969, <https://doi.org/10.1021/cr200304e>.
- [9] T.L. Easun, F. Moreau, Y. Yan, S. Yang, M. Schroder, Structural and dynamic studies of substrate binding in porous metal-organic frameworks, *Chem. Soc. Rev.* 46 (2017) 239–274.
- [10] G. Maurin, C. Serre, A. Cooper, G. Ferey, The new age of MOFs and of their porous-related solids, *Chem. Soc. Rev.* 46 (2017) 3104–3107.
- [11] J.Y. Lee, O.K. Farha, J. Roberts, K.A. Scheidt, S.T. Nguyen, J.T. Hupp, Metal-organic framework materials as catalysts, *Chem. Soc. Rev.* 38 (2009) 1450–1459.
- [12] S.L. James, Metal-organic frameworks, *Chem. Soc. Rev.* 32 (2003) 276–288.
- [13] Z. Wang, G. Chen, K. Ding, Self-supported catalysts, *Chem. Rev.* 109 (2009) 322–359.
- [14] A. Dhakshinamoorthy, M. Alvaro, H. Garcia, Metal-organic frameworks (MOFs) as heterogeneous catalysts for the chemoselective reduction of carbon-carbon multiple bonds with hydrazine, *Adv. Synth. Catal.* 351 (2009) 2271–2276.
- [15] S. Opelt, S. Turk, E. Dietzsch, A. Henschel, S. Kaskel, E. Klemm, Preparation of palladium supported on MOF-5 and its use as hydrogenation catalyst, *Catal. Commun.* 9 (2008) 1286–1290.
- [16] D. Farrusseng, S. Aguado, C. Pinel, Metal-organic frameworks: opportunities for catalysis, *Angew. Chem. Int. Ed.* 48 (2009) 7502–7513.
- [17] S. Horike, M. Dinca, K. Tamaki, J.R. Long, Size-selective Lewis-acid catalysis in a microporous metal-organic framework with exposed Mn<sup>2+</sup> coordination sites, *J. Am. Chem. Soc.* 130 (2008) 5854–5855.
- [18] L. Ma, C. Abney, W. Lin, Enantioselective catalysis with homochiral metal-organic frameworks, *Chem. Soc. Rev.* 38 (2009) 1248–1256.
- [19] R.Q. Zou, H. Sakurai, X.Q. Preparation, Adsorption properties, and catalytic activity of 3D porous metal-organic frameworks composed of cubic building blocks and alkali-metal ions, *Angew. Chem. Int. Ed. Engl.* 45 (2006) 2542–2546.
- [20] Y.K. Hwang, D.Y. Hong, J.S. Chang, S.H. Jung, Y.K. Seo, J. Kim, et al., Amine grafting on coordinatively unsaturated metal centers of MOFs: consequences for catalysis and metal encapsulation, *Angew. Chem. Int. Ed. Engl.* 47 (2008) 4144.
- [21] L. Dandan, X. Hai-Qun, J. Long, J. Hai-Long, Metal-organic frameworks for catalysis: state of the art, challenges, and opportunities, *Energy Chem.* 1 (2019) 100005.
- [22] L. Jiao, J.Y. RuSeow, W.S. Skinner, Z.U. Wang, H.-L. Jiang, Metal-organic frameworks: structures and functional applications, *Mater. Today* 27 (2019) 43–68.
- [23] J. Liang, Y.-B. Huang, R. Cao, Metal-organic frameworks and porous organic polymers for sustainable fixation of carbon dioxide into cyclic carbonates, *Coord. Chem. Rev.* 378 (2019) 32–65.
- [24] Z. Hu, Y. Peng, K.M. Tan, D. Zhao, Enhanced catalytic activity of a hierarchical porous metal-organic framework CuBTC, *CrystEngComm* 17 (2015) 7124–7129.
- [25] C.J. Doonan, C.J. Sumbly, Metal-organic framework catalysis, *CrystEngComm* 19 (2017) 4044–4048.
- [26] H.V. Dang, Y.T.N. Le, D.T.M. Tran, A.N.Q. Phan, N.T.S. Phan, Synthesis of benzo[1,4]thiazines via ring expansion of 2-aminobenzothiazoles with terminal alkynes under metal-organic framework catalysis, *Catal. Lett.* 148 (2018) 1383–1395.
- [27] S.H. Doan, N.K.Q. Tran, P.H. Pham, V.H.H. Nguyen, N.N. Nguyen, P.T.M. Ha, S. Li, H.V. Le, N.T.H. Le, T. N. Tu, N.T.S. Phan, A new synthetic pathway to triphenylpyridines via cascade reactions utilizing a new iron-organic framework as a recyclable heterogeneous catalyst, *Eur. J. Org. Chem.* 2019 (2019) 2382–2389.
- [28] B. Parmar, P. Patel, V. Murali, Y. Rachuri, R.I. Kureshy, N.-u.H. Khanad, E. Suresh, Efficient heterogeneous catalysis by dual ligand Zn(II)/cd(II) MOFs for the Knoevenagel condensation reaction: adaptable synthetic

- routes, characterization, crystal structures and luminescence studies, *Inorg. Chem. Front.* 5 (2018) 2630–2640.
- [29] A. Dhakshinamoorthy, A.M. Asiric, H. Garcia, Metal-organic frameworks catalyzed C–C and C–heteroatom coupling reactions, *Chem. Soc. Rev.* 44 (2015) 1922–1947.
- [30] J. Liu, L. Chen, H. Cui, J. Zhang, L. Zhang, C.-Y. Su, Applications of metal-organic frameworks in heterogeneous supramolecular catalysis, *Chem. Soc. Rev.* 43 (2014) 6011–6061.
- [31] Y.Y. Xiong, J.Q. Li, C.S. Yan, H.Y. Gao, J.P. Zhou, L.L. Gong, M.B. Luo, L. Zhang, P.P. Meng, F. Luo, MOF catalysis of FeII-to-FeIII reaction for an ultrafast and one-step generation of the Fe<sub>2</sub>O<sub>3</sub>@MOF composite and uranium(VI) reduction by iron(II) under ambient conditions, *Chem. Commun.* 52 (2016) 9538–9541.
- [32] P. Garcia-Garcia, M. Muller, A. Corma, MOF catalysis in relation to their homogeneous counterparts and conventional solid catalysts, *Chem. Sci.* 5 (2014) 2979–3007.
- [33] T.L.N. Lien, C.V. Nguyenb, G.H. Danga, K.K.A. Lea, N.T.S. Phan, Towards applications of metal-organic frameworks in catalysis: Friedel-Crafts acylation reaction over IRMOF-8 as an efficient heterogeneous catalyst, *J. Mol. Catal. A Chem.* 349 (2011) 28–35.
- [34] N.T.S. Phan, K.K.A. Le, T.D. Phan, MOF-5 as an efficient heterogeneous catalyst for Friedel-Crafts alkylation reactions, *Appl. Catal. A Gen.* 382 (2010) 246–253.
- [35] L.T.L. Nguyen, T.T. Nguyen, K.D. Nguyen, N.T.S. Phan, Metal-organic framework MOF-199 as an efficient heterogeneous catalyst for the aza-Michael reaction, *Appl. Catal. A Gen.* 425–426 (2012) 44–52.
- [36] I.W. Davies, L. Matty, D.L. Hughes, P.J. Reider, Are heterogeneous catalysts precursors to homogeneous catalysts? *J. Am. Chem. Soc.* 123 (2001) 10139–10140.
- [37] K. Pirkanniemi, M. Sillanpaa, Heterogeneous water phase catalysis as an environmental application: a review, *Chemosphere* 48 (2002) 1047–1060.
- [38] Y.-Z. Chen, R. Zhang, L. Jiao, H.-L. Jiang, Metal-organic framework-derived porous materials for catalysis, *Coord. Chem. Rev.* 362 (2018) 1–23.
- [39] K. Yamamoto, Y. Sakata, Y. Nohara, Y. Takahashi, T. Tatsumi, Organic-inorganic hybrid zeolites containing organic frameworks, *Science* 300 (2003) 470–472.
- [40] K. Kim, T. Lee, Y. Kwon, Y. Seo, J. Song, J.K. Park, H. Lee, J.Y. Park, H. Ihee, S. J. Cho, R. Ryoo, Lanthanum-catalysed synthesis of microporous 3D graphene-like carbons in a zeolite template, *Nature* 535 (2016) 131–135.
- [41] K.K. Gangu, S. Maddila, S.B. Mukkamala, S.B. Jonnalagadda, A review on contemporary metal-organic framework materials, *Inorg. Chim. Acta* 446 (2016) 61–74.
- [42] H.-C.J. Zhou, S. Kitagawa, Metal-organic frameworks (MOFs), *Chem. Soc. Rev.* 43 (2014) 5415–5418.
- [43] O.M. Yaghi, M. O’Keeffe, N.W. Ockwig, H.K. Chae, M. Eddaoudi, J. Kim, Reticular synthesis and the design of new materials, *Nature* 423 (2003) 705–714.
- [44] R.M. Christopher, C.H. Brianna, L. Zheng, M.J. David, Approaches for synthesizing breathing MOFs by exploiting dimensional rigidity, *Coord. Chem. Rev.* 258 (2014) 119–136.
- [45] H. Furukawa, K.E. Cordova, M. O’Keeffe, O.M. Yaghi, The chemistry and applications of metal-organic frameworks, *Science* 341 (2013) 1230444.
- [46] R.J. Kuppler, D.J. Timmons, Q.R. Fang, J.R. Li, T.A. Makal, M.D. Young, D. Yuan, D. Zhao, W. Zhuang, H. C. Zhou, Potential applications of metal-organic frameworks, *Coord. Chem. Rev.* 253 (2009) 3042–3066.
- [47] H.X. Deng, C.J. Doonan, H. Furukawa, R.B. Ferreira, J. Towne, C.B. Knobler, B. Wang, O. M. Yaghi, Multiple functional groups of varying ratios in metal-organic frameworks, *Science* 327 (2010) 846–850.
- [48] P. Falcaro, R. Ricco, A. Yazdi, I. Imaz, S. Furukawa, D. Maspoch, R. Ameloote, J.D. Evansf, C. J. Doonanf, Application of metal and metal oxide nanoparticles@MOFs, *Coord. Chem. Rev.* 307 (2016) 237–254.
- [49] S.N. Shamraja, L. Vaidya, S. Maurya, K.R. Virendra, Polysaccharide based metal organic frameworks (polysaccharide-MOF): a review, *Coord. Chem. Rev.* 396 (2019) 1–21.
- [50] K. Pawan, A. Bhaskar, F.T. Yiu, K. Ki-Hyun, S. Khullar, B. Wang, Regeneration, degradation, and toxicity effect of MOFs: opportunities and challenges, *Environ. Res.* 176 (2019) 108488.
- [51] Z. Fangcai, Y. Zhichen, X. Shihao, Z. Yuanguang, Formation of Co<sub>3</sub>O<sub>4</sub> hollow polyhedrons from metal-organic frameworks and their catalytic activity for CO oxidation, *Mater. Lett.* 182 (2016) 214–217.

- [52] A.H. Chughtai, N. Ahmad, H.A. Younus, A. Laypkovc, F. Verpoort, Metal-organic frameworks: versatile heterogeneous catalysts for efficient catalytic organic transformations, *Chem. Soc. Rev.* 44 (2015) 6804–6849.
- [53] Z. Miao, Y. Luan, C. Qi, D. Ramella, The synthesis of a bifunctional copper metal organic framework and its application in the aerobic oxidation/Knoevenagel condensation sequential reaction, *Dalton Trans.* 45 (2016) 13917–13924.
- [54] X.S. Wang, J. Liang, L. Li, Z.J. Lin, P.P. Bag, S.Y. Gao, Y.B. Huang, R. Cao, An anion metal-organic framework with Lewis basic sites-rich toward charge exclusive cationic dyes separation and size-selective catalytic reaction, *Inorg. Chem.* 55 (2016) 2641–2649.
- [55] U.P.N. Tran, K.K.A. Le, N.T.S. Phan, Expanding applications of metal-organic frameworks: zeolite imidazolate framework ZIF-8 as an efficient heterogeneous catalyst for the Knoevenagel reaction, *ACS Catal.* 1 (2011) 120–127.
- [56] D. Rambabu, M. Ashraf, Pooja, A. Gupta, A. Dhir, Mn-MOF@pi composite: synthesis, characterisation and an efficient catalyst for the Knoevenagel condensation reaction, *Tetrahedron Lett.* 58 (2017) 4691–4694.
- [57] F. Guo, B. Yuan, W. Shi, A novel 2D metal-organic framework with Lewis basic sites as a heterogeneous base catalysis, *Inorg. Chem. Commun.* 86 (2017) 285–289.
- [58] S. Zhao, A novel 3D MOF with rich Lewis basic sites as a base catalysis toward Knoevenagel condensation reaction, *J. Mol. Struct.* 1167 (2018) 11–15.
- [59] Y. Yang, H.-F. Yao, F.-G. Xi, E.-Q. Gao, Amino-functionalized Zr(IV) metal-organic framework as bifunctional acid-base catalyst for Knoevenagel condensation, *J. Mol. Catal. A Chem.* 390 (2014) 198–205.
- [60] M. Almasi, V. Zelenak, M.V. Opanasenko, J. Cejka, Efficient and reusable Pb(II) metal-organic framework for Knoevenagel condensation, *Catal. Lett.* 148 (2018) 2263–2273.
- [61] M. Almasi, V. Zelenak, M. Opanasenkob, J. Cejka, A novel nickel metal-organic framework with fluorite-like structure: gas adsorption properties and catalytic activity in Knoevenagel condensation, *Dalton Trans.* 43 (2014) 3730–3738.
- [62] P. Rani, R. Srivastava, Tailoring the catalytic activity of metal organic frameworks by tuning the metal center and basic functional sites, *New J. Chem.* 41 (41) (2017) 8166–8177.
- [63] Z.-W. Zhai, S.-H. Yang, Y.-R. Lv, D. Chen-Xia, L.-K. Li, S.-Q. Zang, Amino functionalized Zn/Cd-metal-organic frameworks for selective CO<sub>2</sub> adsorption and Knoevenagel condensation reactions, *Dalton Trans.* 48 (2019) 4007–4014.
- [64] D. Amarajothi, H. Niclas, L. Dirk, N. Stock, Knoevenagel condensation reaction catalysed by Al-MOFs with CAU-1 and CAU-10-type structures, *CrystEngComm* 19 (2017) 4187–4193.
- [65] N.P. Valentina, M.M. Maria, J. Jeon, J.W. Jun, M.N. Timofeeva, S.H. Jhung, Catalytic behavior of metal-organic frameworks in the Knoevenagel condensation reaction, *J. Catal.* 316 (2014) 251–259.
- [66] K.K. Gangu, S. Maddila, S.B. Mukkamala, S.B. Jonnalagadda, Synthesis, structure, and properties of new Mg(II)-metal-organic framework and its prowess as catalyst in the production of 4H-pyrans, *Ind. Eng. Chem. Res.* 56 (2017) 2917–2924.
- [67] R.M. Mohareb, M.Y. Zaki, N.S. Abbas, Synthesis, anti-inflammatory and anti-ulcer evaluations of thiazole, thiophene, pyridine and pyran derivatives derived from androstenedione, *Steroids* 98 (2015) 80–91.
- [68] R.P. Queiroz, R.C. Calhella, L.A. Silva, E. Pinto, S.J. Nascimento, Synthesis of novel 3-(aryl)benzothieno [2,3-c]pyran-1-ones from Sonogashira products and intramolecular cyclization: antitumoral activity evaluation, *Eur. J. Med. Chem.* 44 (2009) 1893–1899.
- [69] K.K. Gangu, S. Maddila, S.B. Mukkamala, S.B. Jonnalagadda, Synthesis, characterisation and catalytic activity of 4,5-imidazoledicarboxylate ligated Co(II) and Cd(II) metal-organic coordination complexes, *J. Mol. Struct.* 1143 (2017) 153–162.
- [70] K.K. Gangu, S. Maddila, S.B. Mukkamala, S.B. Jonnalagadda, Catalytic activity of supra molecular self-assembled nickel (II) coordination complex in synthesis of indeno-pyrimidine derivatives, *Polyhedron* 158 (2019) 464–470.
- [71] W. Fan, Y. Wang, Q. Zhang, A. Kirchon, Z. Xiao, L. Zhang, F. Dai, R. Wang, D. Sun, An amino-functionalized metal-organic framework, based on a rare Ba<sub>12</sub>(COO)<sub>18</sub>(NO<sub>3</sub>)<sub>2</sub> cluster, for efficient C3/C2/C1 separation and preferential catalytic performance, *Chem. Eur. J.* 24 (2018) 2137–2143.



- [72] J. Wang, X. Wang, H. Xu, X. Zhao, Z. Zheng, Z.-l. Xu, A new Zn (II) porous metal-organic framework and the catalytic properties in Knoevenagel condensation controlled by its morphology, *ChemPlusChem* 82 (2017) 1182–1187.
- [73] T. Rhauderwiek, S. Waitschat, S. Wuttke, H. Reinsch, T. Bein, N. Stock, Nanoscale synthesis of two porphyrin-based MOFs with gallium and indium, *Inorg. Chem.* 55 (2016) 5312–5419.
- [74] M. Pang, A.J. Cairns, Y. Liu, Y. Belmabkhout, H.C. Zeng, M. Eddaoudi, Highly monodisperse MIII-based soc-MOFs (M = In and Ga) with cubic and truncated cubic morphologies, *J. Am. Chem. Soc.* 134 (2012) 13176–13179.
- [75] P. Valvekens, M. Vandichel, M. Waroquier, V. Van Speybroeck, D. De Vos, Metal-dioxidoterephthalate MOFs of the MOF-74 type: microporous basic catalysts with well-defined active sites, *J. Catal.* 317 (2014) 1–10.
- [76] M. Joharian, S. Abedi, A. Morsali, Sonochemical synthesis and structural characterization of a new nanostructured co(II) supramolecular coordination polymer with Lewis base sites as a new catalyst for Knoevenagel condensation, *Ultrason. Sonochem.* 39 (2017) 897–907.
- [77] Y.C. Tan, H.C. Zeng, Lewis basicity generated by localised charge imbalance in noble metal nanoparticle-embedded defective metal-organic frameworks, *Nat. Commun.* 9 (2018) 4326.
- [78] D. Kurandina, M. Rivas, M. Radzhabov, V. Gevorgyan, Heck reaction of electronically diverse tertiary alkyl halides, *Org. Lett.* 20 (2018) 357–360.
- [79] H. Go, I. Shun, U. Yasuhiro, A palladium NNC-pincer complex as an efficient catalyst precursor for the Mizoroki-Heck reaction, *Adv. Synth. Catal.* 360 (2018) 1833–1840.
- [80] T.-H. Park, A.J. Hickman, K. Koh, S. Martin, A.G. Wong-Foy, M.S. Sanford, A.J. Matzger, Highly dispersed palladium(II) in a defective metal-organic framework: application to C–H activation and functionalization, *J. Am. Chem. Soc.* 133 (2011) 20138–20141.
- [81] A. Minatti, X. Zheng, S.L. Buchwald, Synthesis of chiral 3-substituted indanones via an enantioselective reductive-Heck reaction, *J. Org. Chem.* 72 (2007) 9253–9258.
- [82] J. Gao, W. Wang, S. Zhang, S. Xiao, C. Zhan, M. Yang, X. Lu, W. You, Distinction between PTB7-Th samples prepared from Pd (PPh<sub>3</sub>)<sub>4</sub> and Pd<sub>2</sub> (dba)<sub>3</sub>/P (o-tol)<sub>3</sub> catalysed stille coupling polymerization and the resultant photovoltaic performance, *J. Mater. Chem. A* 6 (2018) 179–188.
- [83] S. Shi, K.S. Nawaz, M.K. Zaman, Z. Sun, Advances in enantioselective C–H activation/Heck reaction and Suzuki reaction, *Catalysts* 8 (2018) 90.
- [84] H. Alamgholiloo, S. Rostamnia, A. Hassankhani, J. Khalafy, M.M. Baradarani, G. Mahmoudi, X. Liu, Stepwise post-modification immobilization of palladium Schiff-base complex on to the OMS-Cu (BDC) metal-organic framework for Mizoroki-Heck cross-coupling reaction, *Appl. Organomet. Chem.* 32 (2018) e4539.
- [85] J.W. Brown, N.N. Jarenwattananon, T. Otto, J.L. Wang, S. Glöggler, L.S. Bouchard, *Catal. Commun.* 65 (2015) 105–107.
- [86] P. Panster, S. Wieland, in: B. Cornils, W.A. Herrmann (Eds.), *Applied Homogeneous Catalysis with Organometallic Compounds*, vol. 2, VCH, Weinheim, 1996, p. 605.
- [87] C. Torborg, M. Beller, Recent applications of palladium-catalyzed coupling reactions in the pharmaceutical, agrochemical, and fine chemical industries, *Adv. Synth. Catal.* 351 (2009) 3027–3043.
- [88] S. Rezaei, A. Landarani-Isfahani, M. Moghadam, S. Tangestaninejad, V. Mirkhani, I. Mohammadpoor-Baltork, Mono- and multifold C–C coupling reactions catalyzed by a palladium complex encapsulated in MIL-Cr as a three dimensional nano reactor, *RSC Adv.* 6 (2016) 92463–92472.
- [89] D. Liu, T.F. Liu, Y.P. Chen, L. Zou, D. Feng, K. Wang, Q. Zhang, S. Yuan, C. Zhong, H.C. Zhou, A reversible crystallinity-preserving phase transition in metal-organic frameworks: discovery, mechanistic studies, and potential applications, *J. Am. Chem. Soc.* 137 (2015) 7740–7746.
- [90] J. Canivet, S. Aguado, Y. Schuurman, D. Farrusseng, MOF-supported selective ethylene dimerization single-site catalysts through one-pot postsynthetic modification, *J. Am. Chem. Soc.* 135 (2013) 4195.
- [91] D. Dong, Z. Li, D. Liu, N. Yu, H. Zhao, H. Chen, J. Liua, D. Liu, Postsynthetic modification of single Pd sites into uncoordinated polypyridine groups of a MOF as the highly efficient catalyst for Heck and Suzuki reactions, *New J. Chem.* 42 (2018) 9317–9323.

- [92] Y. Huang, S. Gao, T. Liu, L. Jian, X. Lin, H. Li, R. Cao, Palladium nanoparticles supported on mixed-linker metal-organic frameworks as highly active catalysts for Heck reactions, *ChemPlusChem* 77 (2012) 106–112.
- [93] A. Nuri, N. Vucetic, J.-H. Smatt, Y. Mansoori, J.-P. Mikkola, D.Y. Murzin, Pd supported IRMOF-3: heterogeneous, efficient and reusable catalyst for Heck reaction, *Catal. Lett.* 149 (2019) 1941–1951.
- [94] M. Bagherzadeh, F. Ashouri, L. Hashemi, A. Morsali, Supported Pd nanoparticles on Mn-based metal-organic coordination polymer: efficient and recyclable heterogeneous catalyst for Mizoroki-Heck cross coupling reaction of terminal alkenes, *Inorg. Chem. Commun.* 44 (2014) 10–14.
- [95] F. Zhao, M. Shirai, Y. Ikushima, M. Arai, The leaching and re-deposition of metal species from and onto conventional supported palladium catalysts in the Heck reaction of iodobenzene and methyl acrylate in N-methylpyrrolidone, *J. Mol. Catal. A* 180 (2002) 211–219.
- [96] M. Dams, L. Drijkoningen, B. Pauwels, G.V. Tendeloo, D.E. De Vos, P.A. Jacobs, Pd-zeolites as heterogeneous catalysts in heck chemistry, *J. Catal.* 209 (2002) 225–236.
- [97] X. Li, Z. Guo, C. Xiao, T.W. Goh, D. Tesfagaber, W. Huang, Tandem catalysis by palladium nanoclusters encapsulated in metal-organic frameworks, *ACS Catal.* 4 (2014) 3490–3497.
- [98] F. Ashouri, M. Zare, M. Bagherzadeh, The effect of framework functionality on the catalytic activation of supported Pd nanoparticles in the Mizorokie Heck coupling reaction, *C.R. Chim.* (2016) 1–9.
- [99] P. Rani, R. Srivastava, Cu(I) metal organic framework catalyzed C-C and C-N coupling reactions, *Tetrahedron Lett.* 55 (2014) 5256–5260.
- [100] P.Z. Li, K. Aranishi, Q. Xu, ZIF-8 immobilized nickel nanoparticles: highly effective catalysts for hydrogen generation from hydrolysis of ammonia borane, *Chem. Commun.* 48 (2012) 3173–3175.
- [101] H.L. Jiang, B. Liu, T. Akita, M. Haruta, H. Sakurai, Q. Xu, Au@ZIF-8: CO oxidation over gold nanoparticles deposited to metal-organic framework, *J. Am. Chem. Soc.* 131 (2009) 11302–11303.
- [102] S. Gao, N. Zhao, M. Shu, S. Che, Palladium nanoparticles supported on MOF-5: a highly active catalyst for a ligand- and copper-free Sonogashira coupling reaction, *Appl. Catal. A* 388 (2010) 196–201.
- [103] L. Zhang, Z. Su, F. Jiang, Y. Zhou, W. Xu, M. Hong, Catalytic palladium nanoparticles supported on nanoscale MOFs: a highly active catalyst for Suzuki-Miyaura cross-coupling reaction, *Tetrahedron* 69 (2013) 9237–9244.
- [104] Z. Yu, M. Zhu, L. Xia, Y. Wu, H. Hua, J. Xie, Lanthanide metal-organic frameworks with six-coordinated Ln(III) ions and free functional organic sites for adsorptions and extensive catalytic activities, *Sci. Rep.* 6 (2016) 29728.
- [105] D. Saha, R. Sen, T. Maity, S. Koner, Anchoring of palladium onto surface of porous metal-organic framework through post-synthesis modification and studies on Suzuki and Stille coupling reactions under heterogeneous condition, *Langmuir* 29 (2013) 3140–3151.
- [106] L. Panahi, M.R. Naimi-Jamal, J. Mokhtari, Ultrasound-assisted Suzuki-Miyaura reaction catalyzed by Pd@Cu<sub>2</sub>(NH<sub>2</sub>-BDC)<sub>2</sub>(DABCO), *J. Organomet. Chem.* 868 (2018) 36–46.
- [107] S. Tahmasebi, J. Mokhtari, M.R. Naimi-Jamal, A. Khosravi, L. Panahi, One-step synthesis of Pd-NPs@Cu<sub>2</sub>(BDC)<sub>2</sub>DABCO as efficient heterogeneous catalyst for the Suzuki-Miyaura cross-coupling reaction, *J. Organomet. Chem.* 853 (2017) 35–41.
- [108] S.M. Chavan, G.C. Shearer, S. Svelle, U. Olsbye, F. Bonino, J. Ethiraj, K.P. Lillerud, S. Bordiga, Synthesis and characterization of amine-functionalized mixed-ligand metal-organic frameworks of UiO-66 topology, *Inorg. Chem.* 53 (2014) 9509–9515.
- [109] M. Arici, O.Z. Yesilel, M. Tas, Coordination polymers assembled from 3,3',5,5'-azobenzenetetracarboxylic acid and different bis(imidazole) ligands with varying flexibility, *Cryst. Growth Des.* 15 (2015) 3024–3031.
- [110] R. Sun, B. Liu, B.-G. Li, S. Jie, Palladium(II)@zirconium-based mixed-linker metal-organic frameworks as highly efficient and recyclable catalysts for Suzuki and Heck cross-coupling reactions, *ChemCatChem* 8 (2016) 1–12.
- [111] S. Rostamnia, H. Alamgholiloo, X. Liu, Pd-grafted open metal site copper-benzene-1,4-dicarboxylate metal organic frameworks (Cu-BDC MOF's) as promising interfacial catalysts for sustainable Suzuki coupling, *J. Colloid Interface Sci.* 469 (2016) 310–317.
- [112] F. Carson, V. Pascanu, A.B. Gumez, Y. Zhang, A.E. Platero-Prats, X. Zou, B. Martin-Matute, Influence of the base on Pd@MIL-101-NH<sub>2</sub>(Cr) as catalyst for the Suzuki-Miyaura cross-coupling reaction, *Chem. Eur. J.* 21 (2015) 10896–10902.

- [113] P. Elumalai, H. Mamlouk, W. Yiming, L. Feng, S. Yuan, H.-C. Zhou, S. Madrahimov, Recyclable and reusable heteroleptic nickel catalyst immobilized on MOF for Suzuki-Miyaura coupling, *ACS Appl. Mater. Interfaces* (2018).
- [114] S.J. Yang, T. Kim, K. Lee, Y.S. Kim, J. Yoon, C.R. Park, Solvent evaporation mediated preparation of hierarchically porous metal organic framework-derived carbon with controllable and accessible large-scale porosity, *Carbon* 71 (2014) 294–302.
- [115] H.L. Jiang, B. Liu, Y.Q. Lan, K. Kuratani, T. Akita, H. Shioyama, F.Q. Zong, Q. Xu, From metal-organic framework to nanoporous carbon: toward a very high surface area and hydrogen uptake, *J. Am. Chem. Soc.* 133 (2011) 11854–11857.
- [116] R.R. Salunkhe, Y. Kamachi, N.L. Torad, S.M. Hwang, Z.Q. Sun, S.X. Dou, J. H. Kim, Y. Yamauchi, Fabrication of symmetric supercapacitors based on MOF-derived nanoporous carbons, *J. Mater. Chem. A* 2 (2014) 19848–19854.
- [117] B. Harshitha, P.P. Aiyappa, R. Banerjee, S. Kurungo, Porous carbons from nonporous MOFs: influence of ligand characteristics on intrinsic properties of end carbon, *Cryst. Growth Des.* 13 (2013) 4195–4199.
- [118] W. Dong, L. Zhang, C. Wang, C. Feng, N. Shang, S. Gao, C. Wang, Palladium nanoparticles embedded in metal-organic framework derived porous carbon: synthesis and application for efficient Suzuki-Miyaura coupling reactions, *RSC Adv.* 6 (2016) 37118–37123.
- [119] A.W. Augustyniak, W. Zawartka, J.A.R. Navarro, A.M. Trzeciak, Palladium nanoparticles supported on a nickel pyrazolate metal organic framework as a catalyst for Suzuki and carbonylative Suzuki couplings, *Dalton Trans.* 45 (2016) 13525–13531.
- [120] H. Fei, S.M. Cohen, A robust, catalytic metal-organic framework with open 2,2'-bipyridine sites, *Chem. Commun.* 50 (2014) 4810–4812.
- [121] X. Li, B. Zhang, R. Van Zeeland, L. Tang, Y. Pei, Z. Qi, T.W. Goh, L.M. Stanley, W. Huang, Unveiling the effects of linker substitution in Suzuki coupling with palladium nanoparticles in metal-organic frameworks, *Catal. Lett.* 148 (2018) 940–945.
- [122] A.S. Roy, J. Mondal, B. Banerjee, P. Mondal, A. Bhaumik, S.M. Islam, Pd-grafted porous metal-organic framework material as an efficient and reusable heterogeneous catalyst for C–C coupling reactions in water, *Appl. Catal. A Gen.* 469 (2014) 320–327.
- [123] M. Annapurna, T. Parsharamulu, P. Vishnuvardhan Reddy, M. Suresh, P.R. Likhari, M.L. Kantam, Nano palladium supported on high-surface area metal-organic framework MIL-101: an efficient catalyst for Sonogashira coupling of aryl and heteroaryl bromides with alkynes, *Appl. Organomet. Chem.* 29 (2015) 234–239.
- [124] A. Arnanz, M. Pintado-Sierra, A. Corma, M. Iglesias, F. Sanchez, Bifunctional metal organic framework catalysts for multistep reactions: MOF-cu(BTC)-[Pd] catalyst for one-pot heteroannulation of acetylenic compounds, *Adv. Synth. Catal.* 354 (2012) 1347–1355.
- [125] L. Oehninger, R. Rubbiani, I. Ott, N-Heterocyclic carbene metal complexes in medicinal chemistry, *Dalton Trans.* 42 (2013) 3269–3284.
- [126] A. Burgun, R.S. Crees, M.L. Cole, C.J. Doonan, C.J. Sumbly, A 3-D diamondoid MOF catalyst based on in situ generated [Cu(L)2] N-heterocyclic carbene (NHC) linkers: hydroboration of CO<sub>2</sub>, *Chem. Commun.* 50 (2014) 11760–11763.
- [127] G.C. Fortman, S.P. Nolan, N-Heterocyclic carbene (NHC) ligands and palladium in homogeneous cross-coupling catalysis: a perfect union, *Chem. Soc. Rev.* 40 (2011) 5151–5169.
- [128] C.I. Ezugwu, B. Mousavi, M.A. Asrafa, A. Mehta, H. Vardhan, F. Verpoort, An N-heterocyclic carbene based MOF catalyst for Sonogashira cross-coupling reaction, *Cat. Sci. Technol.* 6 (2016) 2050–2054.
- [129] J. Huang, W. Wang, H. Li, Water-medium organic reactions catalyzed by active and reusable Pd/Y heterobimetal-organic framework, *ACS Catal.* 37 (2013) 1526–1536.

# Hydrothermal synthesis of MOFs

Wei Chen, Liping Du, Chunsheng Wu

*Institute of Medical Engineering, Department of Biophysics, School of Basic Medical Sciences, Health Science Center, Xi'an Jiaotong University, Xi'an, China*

## 7.1 Introduction to the hydrothermal method

The term *hydrothermal* is purely of geological origin. It was first used by the British Geologist, Sir Roderick Murchison (1792–1871), to describe the action of water at elevated temperature and pressure in bringing about changes in the earth's crust, leading to the formation of various rocks and minerals [1]. Hydrothermal method, also termed “hydrothermal synthesis,” refers to various techniques of crystallizing substances from high-temperature aqueous solutions at high vapor pressures. The hydrothermal method is a method of synthesis of single crystals which depends on the solubility of minerals in hot water under high pressure. Although the thermal technique has made tremendous progress, there is no unanimity about its definition. The term *hydrothermal* usually refers to any heterogeneous reaction in the presence of aqueous solvents or mineralizers under high pressure and temperature conditions to dissolve and recrystallize materials which are relatively insoluble under ordinary conditions [1]. There is no definite lower limit for the pressure and temperature conditions as there are vast numbers of publications under mild hydrothermal conditions. Specifically, the term *solvothermal* refers to any chemical reaction in the presence of a solvent in supercritical or near supercritical conditions. Under hydrothermal conditions, the reactions are occurred at the interface of solid and liquid. Therefore, the hydrothermal reactions are also defined as special cases of chemical transport reactions. The beginning of hydrothermal research is associated with the study of natural systems, e.g., the genesis of various rocks, minerals, and ore deposits through the laboratory simulations. The first report of the hydrothermal growth of crystals was by German geologist, Karl Emil von Schafhäütl in 1845 [2]. Until 1881, all the early hydrothermal experiments were carried out in simple glass tubes with sealed ends. H. De Senarmont, the founder of hydrothermal synthesis in geoscience, used glass tubes containing gel, SiO<sub>2</sub> and H<sub>2</sub>O, HCl, or CO<sub>2</sub>, enclosed in steel tubes, which could be heated to 200–300°C. Daurree (1857), who introduced the pressure balance in the hydrothermal synthesis, used a steel tube to synthesis quartz and wollastonite at 400°C with water as a solvent. Besides, he also attempted to use natural hot spring water from Plombières as

the mineralizer. With the discovery of hydrothermal activity in the deep sea on Galapagos during 1970s, the research on hydrothermal vent fluid to study the origin of life is sparking. In 1873, von Chroustchoff proposed that gold lining of steel autoclaves could prevent the corrosion. After that, the tendency to reach higher pressure-temperature conditions than the usual 5–10 atm began. In 1880, Hannay claimed to have synthesized artificial diamond through the hydrothermal technique. Moissan also claimed to have synthesized diamond as large as 0.5 mm from charcoal. The first ever large size crystals obtained by the earliest scientists was hydrated potassium silicate with the size of 2–3 mm long, reported by Friedel and Sarasin in 1881. During 19th century, including quartz, feldspars, mica, leucite, nephelite, epidote, etc., over 80 mineral species are supposed to have been synthesized. Spezia (1896) found that plates of quartz kept at 27°C for several months with water under a pressure 1750–1850 atm did not lose its weight and no etch figures were found. When  $\text{Na}_2\text{SiO}_3$  was introduced,  $\text{SiO}_2$  separated out as quartz and the rhombohedral faces of the quartz were easily attacked. Toward the turn of the 19th century, the science of hydrothermal technology moved from Europe to North America, assisted by the American Industrial Revolution. The establishment of the Geophysical Laboratory at the Carnegie Institute of Washington, USA, was the most important milestone in the history of hydrothermal technology. In the geophysical laboratory, Bowen established a fine hydrothermal research laboratory dedicated to the major contributions to the field of hydrothermal research for USA in the early 20th century. In 1920s, he framed the most important petrologic principle, viz., *Bowen's Reaction Principle*. Morey first designed a simple, gasketed, sealed steel autoclave of 25–100 mL volume which became very popular for its simplicity and ease to handle. With the development of the autoclave, an even higher pressure and temperature could be achieved. In 1931, Goranson carried out a systematic study to explore the solubility of water in a liquid having the composition of the Stone Mountain Granite, which was regarded as the most outstanding advancement in the hydrothermal technique to the petrologic problems. The hydrothermal research spread to Eastern Europe and Asia on a small scale, and much later to China and India after the Second World War. Specifically, the first hydrothermal work in Japan was conducted by Dr. Tominosuke Katsurai in 1926. He worked on the soda treatment of aluminum ore through hydrothermal extraction.

Hydrothermal materials synthesis was becoming a popular field of research after the development of ceramic process technology during 1970s. A growing interest to enhance the hydrothermal reaction kinetics by microwave, acoustic wave simulations, mechanical mixing, and electrochemical reactions was followed. With these processes, the duration of the experiments was reduced by two orders of magnitude, making the technique more economic. The hydrothermal technique offered an excellent facility for coating of various compounds on metals and ceramics. For example, coating of apatite layers on chemically treated Ti metals and organic polymers on metals have been reported. Compared with HAP whiskers prepared by other methods, whiskers synthesized by the hydrothermal method had

a more controlled and even morphology and purity in composition. Hydrothermal technique has shown many new advantages such as homogeneous precipitation with metal chelates, decomposition of hazardous and/or refractory chemical substances, and monomerization of high polymers. Based on these features, the hydrothermal technique has attracted great attentions from various fields, involving materials scientist, earth scientist, materials engineers, physicists, chemists, biologists, and others. At last, the future of the hydrothermal synthesis is toward lowering the pressure and temperature conditions, which will facilitate the in situ observation. As the design and cost of autoclave become simpler and cheaper, the hydrothermal method will be more attractive to the scientists and industries.

## 7.2 Basic mechanism and general protocols

The free energy is represented as a function of temperature, pressure, and mol numbers:

$$G = f(T, P, n_1, n_2, \dots, n_i) \quad (7.1)$$

$$DG = \left(\frac{\delta G}{\delta T}\right)_{P,n} dT + \left(\frac{\delta G}{\delta P}\right)_{T,n} dP + \left(\frac{\delta G}{\delta n_1}\right)_{P,T,n} dn_1 + \left(\frac{\delta G}{\delta n_2}\right)_{P,T,n} dn_2 \quad (7.2)$$

where  $n_i$  = constant mol number of all components,  $n_j$  = constant number of components except one.

The variation in the free energy can be expressed in terms of the chemical potential:

$$\left(\frac{\delta G}{\delta n_i}\right)_{P,T,n} = \mu_i \quad (7.3)$$

When  $P$  and  $T$  are kept constant, Eq. (7.2) becomes

$$dG_{P,T} = \mu_i dn_1 + \mu_i dn_2 + \dots + \mu_i dn_i \quad (7.4)$$

$$G_{P,T} = \sum_i n_i \mu_i \quad (7.5)$$

Differentiation of Eq. (7.5)

$$dG_{P,T} = n_1 d\mu_1 + n_2 d\mu_2 + \dots + n_i d\mu_i + \mu_i d n_1 + \dots + \mu_i d n_i = \sum_{n_i} d\mu_i + \sum_{\mu_i} dn_i \quad (7.6)$$

By equating Eqs. (7.4), (7.6),

$$\sum_{n_i} d\mu_i = 0 \quad (7.7)$$

Eq. (7.7) is considered as the overall equilibrium condition under constant  $P$  and  $T$ .

In a hydrothermal system,  $n_A$  mol of solid A,  $n_{1A}$  mol of partially soluble A, and  $n_B$  mol solvent, the free energy of the system corresponds to Eq. (7.5)

$$G = n_A \mu_A + n_{1A} \mu_{1A} + n_B \mu_B \quad (7.8)$$



The free energy  $dG$  becomes

$$G + dG = (n_A - dn)\mu_A + (n_{1A} + dn)\mu_{1A} + n_B\mu_B \quad (7.9)$$

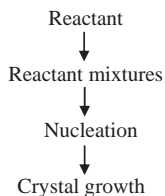
Under constant  $P$  and  $T$ ,

$$dG = (\mu_{1A} - \mu_A)dn \quad (7.10)$$

If  $\mu_{1A} < \mu_A$ , the free energy decreases, then  $dG/dn$  is negative and the process occurs on its own; if  $\mu_{1A} > \mu_A$ , the chemical potential decreases, the crystallization of the substance from solution B takes place; if  $\mu_{1A} = \mu_A$ , the process reaches the equilibrium state. The phase transition stops when the chemical potential of the component reaches equal in both phases. This mechanism is realized only when the changes of  $dG$  do not depend on the chemical potential and concentration of other components of the solution. Consideration of these relationships may help in understanding the physico-chemical principles of the hydrothermal process.

The importance of kinetics of crystallization was studied since the commercialization of the zeolites by the hydrothermal method. Based on the experience, the growth of the crystals in aqueous solutions shows the relationship between the anisotropy of the rates of process: temperature, supersaturation, and the presence of “foreign” components. These parameters can be varied over a wide range. The influence of the solvent to the crystal growth is different to each crystal. For example, the present of  $\text{NH}_4^+$  ions in the solution produces an obvious increase in the rate of growth of the prismatic faces, in contrast to the slow rate of growth in the ordinary condition. Pressure does not have a direct effect on the rate of growth of crystals, but it could have an effluence through other parameters: mass transfer and solubility. Therefore, in some cases, the increase in pressure could lead to the increase of rate of growth.

Hydrothermal synthesis of metal-organic frameworks (MOFs) is generally made by mixing solutions of metal ions salts and organic ligands in the solvent and by maintaining the mixture at high temperature (higher than  $100^\circ\text{C}$ ) at specific periods. The synthesis of MOFs involves several steps, as shown below:



The process of MOFs synthesis takes place at elevated temperatures in order to achieve a high yield of crystals in an acceptable period of time. The variables in the synthesis are temperature, pH, and chemical composition of the reactants. To achieve a nano-sized particle, surfactants or molecule templates are usually applied in the synthesis process. For example, in the presence of cetyltrimethylammonium bromide (CTAB), the ZIF-8 crystals could turn into the cubes [3].

With the increasing of acetic acid concentration, the morphology of Fe-MIL-88B-NH<sub>2</sub> turned from microsized to nanosized crystals [4].

Adjusting the metal ions and organic linkers, the pore volume and size of MOFs could be modulated to benefit the loading of varied drugs. Because the drug delivery is physical interaction, the drug could remain its biological activity and delivery via concentration diffusion. Furthermore, the controlled and targeted release (pH-response, light-response, cancer cells targeted, etc.) could be achieved by the functionalization of MOFs. The combination of drug delivery with bioimaging, photothermal therapy, photodynamic therapy, etc. makes the MOFs multifunctional. In the biosensors' application, MOFs and hybrid MOFs could detect biomolecules by the fluorescent and electrochemical methods with high selectivity and low detection limit.

### 7.3 Synthesis of MOFs by the hydrothermal approach

Various MOFs were synthesized by the hydrothermal methods with different size, morphology, and crystalline structure. Although thousands of MOFs are reported until now, there are still many issues which must be considered before it is applied in the biomedical applications, such as size, surface charge, shape, stability, and toxicity. These parameters are not individual, affecting each other. For the understanding of this toxicity of MOFs, there are several comprehensive reviews [5–7]. The toxicity of MOFs depends on many parameters including the kinetics of degradation, bio-distribution, accumulation in tissues and organs, and excretion from the body. Until now, the data are rare. The evaluation of metals and linkers individually might be the first considerable solution. Most acceptable metals for biomedical application are Ca, Mg, Zn, Zr, Fe, Ti, whose oral LD<sub>50</sub> are 1, 8.1, 0.35, 4.1, 0.45, and 25, respectively [8]. For the linkers, most reported linkers are exogenous ligands like imidazolate, terephthalic, trimesic, et al. Rat oral doses of terephthalic, trimesic, 2,6 naphthalendicarboxylic acid, and 1-methylimidazole are 1.13, 5.5, and 8.4 g kg<sup>-1</sup>, respectively [8, 9]. Therefore, in this chapter, Fe, Zr, Cu, and Zn-based MOFs will be illustrated in detail based on their potential biomedical applications.

#### 7.3.1 Synthesis of Fe-MOFs

P. Horcajada et al. synthesized a series of iron-based MOFs, including MIL-53, MIL-88A, MIL-88Bt, MIL-100, and MIL-101-NH<sub>2</sub> (MIL = Materials of Institut Lavoisier) through hydrothermal or solvothermal method (Fig. 7.1) [10]. The ligands for MIL-53, MIL-88A, MIL-88Bt, MIL-100, and MIL-101-NH<sub>2</sub> are terephthalate, fumarate, tetramethylterephthalate, trimesate, and aminoterephthalate, respectively. In vitro degradation under physiological conditions indicated that MIL-88A and MIL-100 had a major degradation occurred after seven days in incubation at 37°C. The ligand of MIL-88A was endogenous and had low toxicity values (LD<sub>50</sub> (fumarate) = 10.7 g kg<sup>-1</sup>). The absence of immune or inflammatory reactions after the injection of nanoMOFs indicated the low toxicity in vivo. Besides, the nanoMOFs had

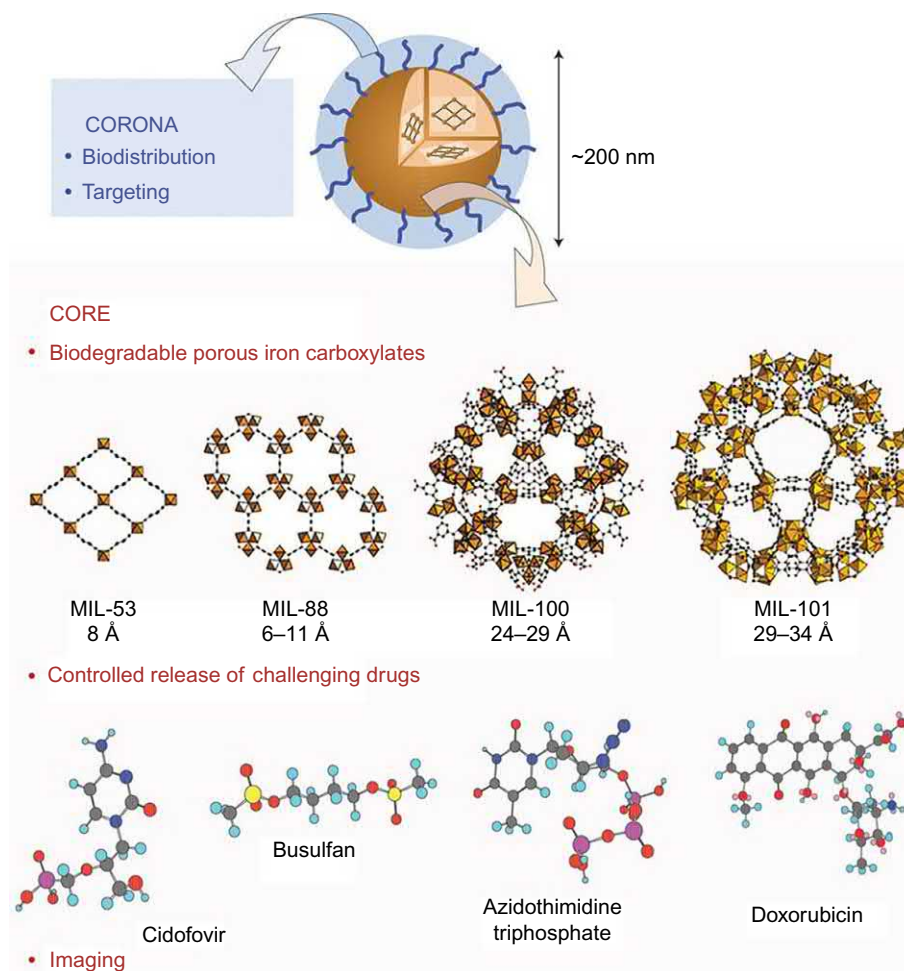


Fig. 7.1

Scheme of engineered core-corona porous iron carboxylates for drug delivery and imaging (the ligands for MIL-53, MIL-88, MIL-100, and MIL-101 terephthalic acid, fumaric acid, trimesic acid, and terephthalic acid). Reprinted with permission from

P. Horcajada, T. Chalati, C. Serre, B. Gillet, C. Sebrie, T. Baati, J.F. Eubank, D. Heurtaux, P. Clayette, C. Kreuz, J.-S. Chang, Y.K. Hwang, V. Marsaud, P.-N. Bories, L. Cynober, S. Gil, G. Férey, P. Couvreur, R. Gref, *Porous metal-organic-framework nanoscale carriers as a potential platform for drug delivery and imaging*, *Nat. Mater.* 9 (2009) 172. Copyright (2011) American Chemical Society.

no significant differences in comparison with the control groups. Four anticancer or antiviral drugs (busulfan (Bu), azidothymidine triphosphate (AZT-TP), cidofovir (CDV), and doxorubicin (Doxo)) were used as the object to test the loading efficiency of nanoMOFs. Bu entrapment in microporous MOFs (MIL-88A, MIL-53, and MIL-89) was lower than that for MIL-100, but significantly larger than that for the existing materials. In case of AZP-TP and CDV, a simply soaking method could achieve high drug loading efficiency; in most cases, higher than 80%. Due to the existence of iron atoms, the nanoMOFs could be applied as contrast

agents. Relaxivity value  $\gamma_1$  of MIL-88A nanoparticles was of the order of  $50 \text{ s}^{-1} \text{ mM}^{-1}$ , which was sufficient for in vivo use. Besides, MIL-100(Fe) could also be applied as a novel nanocarrier for delivering docetaxel (DTX) to the breast cancer cells [11]. The GraftFast reaction was applied in the surface modification of microwave-assisted hydrothermal-synthesized mesoporous iron trimesate nanMOF MIL-100(Fe) [12]. The method could obtain a homogeneous and chemically stable coating of PEG with enhanced colloidal and chemical robustness under physiological conditions, associated to a shielding effect. The PEG-coated MIL-100(Fe) nanoMOFs induced a lower immune response compared with naked one. Additionally, the polyethyleneglycol (PEG)-modified MIL-53(Fe) was prepared by an ultrasonication method [13]. Functionalized modification of PEG on the surface of MIL-53 reduced the size of the crystals and increased the surface area of the materials from 35 to  $40.85 \text{ m}^2$ . The modified nanoMOFs revealed high uptake of 5-FU drug and showed slow release of drug under in vitro conditions, which released only 31% of drug after 3 h and 100% after 6 days. When MIL-53 was used to deliver the oridonin, it exhibited a pH dependence behavior [14]. During the drug release at pH 5.5, a Weibull distribution was found, in contrast to first-order kinetics at pH 7.2. A solvothermal-synthesized MIL-53(Fe) could catalyze the oxidation of 3,3,5,5-tetramethylbenzidine (TMB) to produce a blue-colored 3,3,5,5'-tetramethylbenzidine diamine which could be inhibited by biothiols. Therefore, the cellular biothiols could be detected by the MIL-53(Fe) using a colorimetric analytical method [15].

MIL-88-NH<sub>2</sub>(Fe) with hydrogen-rich organic ligands and amino groups could form hydrogen bonds with intrinsic carboxyl and hydroxyl groups of mucin [16]. Besides, the hydrogen bonding generated a mucoadhesive property to increase the precocular retention of nanoparticles. Therefore, the MIL-88-NH<sub>2</sub>(Fe) could be used to improve the drug efficiency of brimonidine. The nanoMOFs were synthesized by a solvothermal method and the brimonidine was loaded by the physical absorption approach. In vivo evaluations showed that MIL-88-NH<sub>2</sub>(Fe)/brimonidine could remain on the precocular surface for a prolonged period, leading to a prolonged duration of intraocular pressure reduction and promoting the ocular bioavailability of brimonidine. It was found that by altering the concentration of concentration of triblock copolymer F127 and acetic acid, the size and aspect ratio of Fe-MIL-88B-NH<sub>2</sub> MOFs could be managed correspondingly (Fig. 7.2) [4]. Iron ions were first coordinated with F127 to form a complex. If the ligand were added, the nanocrystals were formed. However, if the acetic acid and ligand were added at the same time, the larger nanocrystals would be formed. The different size and aspect ratio of MOFs had different proton relativity and contrast enhancement in MRI [17]. With the increasing of surface area and pore volume, a significant enhancement in  $\gamma_2$  will be followed.

### 7.3.2 Synthesis of Zr-MOFs

The zirconium MOF UiO-66 (UiO stands for Universitetet i Oslo) is biocompatible and has a half maximal inhibitory concentration (IC<sub>50</sub>) of  $1.50 \pm 0.15 \text{ mg mL}^{-1}$  against the HeLa cell line after 24 h of exposure [18]. UiO-66 was constructed by 1,4-benzenedicarboxylate

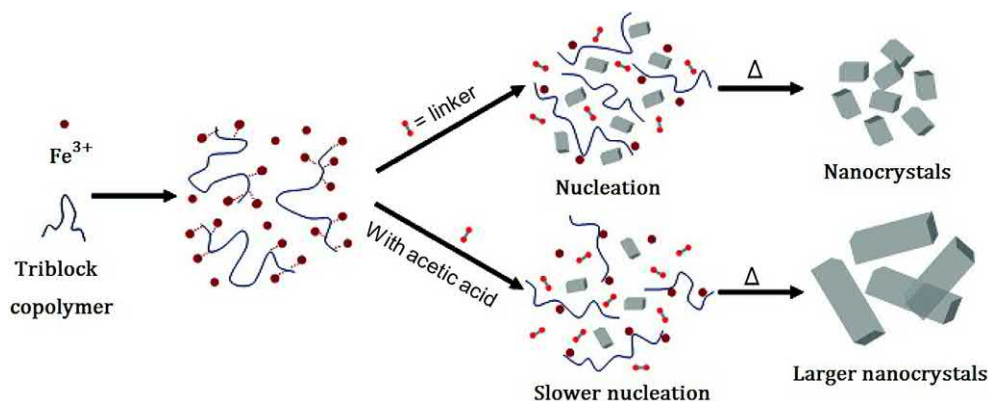


Fig. 7.2

Schematic representation of the size-controlled fabrication of Fe-MIL-88B-NH<sub>2</sub> nanocrystals. Reprinted with permission from M.-H. Pham, G.-T. Vuong, A.-T. Vu, T.-O. Do, Novel route to size-controlled Fe-MIL-88B-NH<sub>2</sub> metal-organic framework nanocrystals, *Langmuir* 27 (2011) 15261–15267. Copyright (2011) American Chemical Society.

(BDC) ligand and Zr<sub>6</sub>O<sub>4</sub>(OH)<sub>4</sub> clusters through a thermal method. When the trimethylamine (TEA) was added as the modulator, the pore size of the MOFs could be enlarged which will be suitable for protein delivery [19]. Besides BDC, other ligands could also be used to synthesize Zr-MOFs. The Zr-MOFs composed by the naphthalene-2,6-dicarboxylic acid and 4,4-biphenyldicarboxylic acid ligands promoted entry through the caveolin-pathway, avoiding lysosomal degradation and enhancing the therapeutic activity of encapsulated drug [20]. With *p*-azidomethylbenzoic acid, *p*-propargyloxybenzoic, and acetic acid as the modulators, surface functionalized UiO-66 was synthesized under solvothermal conditions [21]. A click chemistry reaction would be applied to modify the surface of the nanoMOFs (Fig. 7.3). After PEGylation, the stability of the nanoparticles in the biological solution was improved. The PEGylated UiO-66 exhibited pH-responsive release, mirroring the change in conditions from blood-stream circulation to cancer cellular internalization to allow stimuli-responsive drug delivery. Coating UiO-66 with PEG-2000 enhanced caveolae-mediated endocytosis, allowing the nanoMOFs to partially escape the lysosome, which will avoid the degradation of the drug and improve the possibility of reaching other cellular organelles. Compared with unmodified one, the PEGylated nanoparticles loading dichloroacetic acid (DCA) exhibited significant cytotoxicity, enhancing the therapeutic effect. For the caffeine loading the release, MIL-100(Fe) and UiO-66(Zr) appeared spectacular cosmetic payloads and progressive releases, being a promising carrier [22]. Zr-fum (fumarate) was more efficient at transporting the drug mimic calcein into HeLa cells, and DCA-loaded, PEGylated Zr-fum was more effective at reducing HeLa and MCF-7 cell proliferation than the analogous UiO-66 sample [23]. The smaller size of DCA-loaded Zr-MOFs (around 20 nm) exhibited greater cytotoxicity toward MCF-7 cells than their larger (around 100 nm) analogues [24]. The partial internalization of the smaller MOFs through passive diffusion allowed DCA release directly into the cytosol to enhance its therapeutic effects.

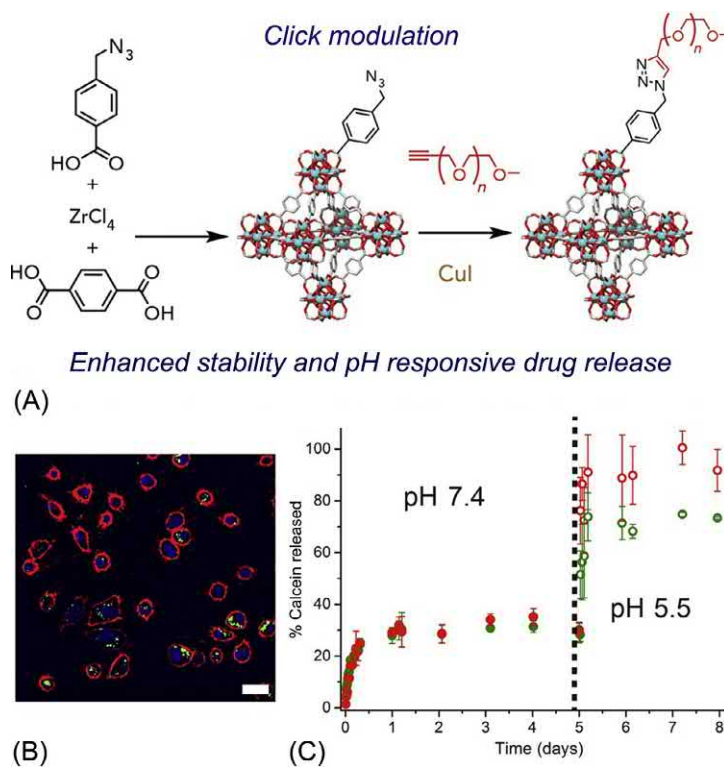


Fig. 7.3

The PEGylation of UiO-66: (A) schematic of the click modulation protocol in the preparation of UiO-66-L1-dodecane; (B) confocal microscopy images of HeLa cells incubated with calcein@ UiO-66-L1-dodecane; (C) pH-responsive release of calcein from the PEGylated MOFs [21]. Reprinted with permission from I. Abánades Lázaro, S. Haddad, S. Sacca, C. Orellana-Tavra, D. Fairen-Jimenez, R.S. Forgan, Selective surface PEGylation of UiO-66 nanoparticles for enhanced stability, cell uptake, and pH-responsive drug delivery, *Chem* 2 (2017) 561–578. Copyright (2017) Elsevier.

Due to the strong Zr-O-P chemical complexation between the Zr-MOFs and phospholipid, lipid bilayer-encapsulated Zr-based nanoMOFs exhibited enhanced phosphatic-resistance in phosphate buffer solution and exceptional stability in harsh chemical environments (Fig. 7.4) [25]. Moreover, the modified nanoMOFs showed enhanced cellular uptake efficiency and real biostability. The anticancer drugs (paclitaxel and cisplatin)-loaded Zr-MOFs UiO-66 and UiO-67 were encapsulated inside a modified poly( $\epsilon$ -caprolactone) with D- $\alpha$ -tocopheryl polyethylene glycol succinate polymeric matrix, in the form of microparticles [26]. Cytotoxicity studies indicated that the microparticles had better anticancer activity compared with free drugs. An in situ polymerization of aniline on the surface of UiO-66 could form a PAN@UiO-66 composite nanoparticles [27]. Due to the photothermal effect of PAN, the composite could be used as an effective photothermal agent for colon cancer. Immobilized Ag nanoparticles in UiO-66 exhibited a strong inhibitory effect on the growth of SMMC-7721 and HeLa cells in a dose-dependent manner through the apoptosis-inducing effect [28].



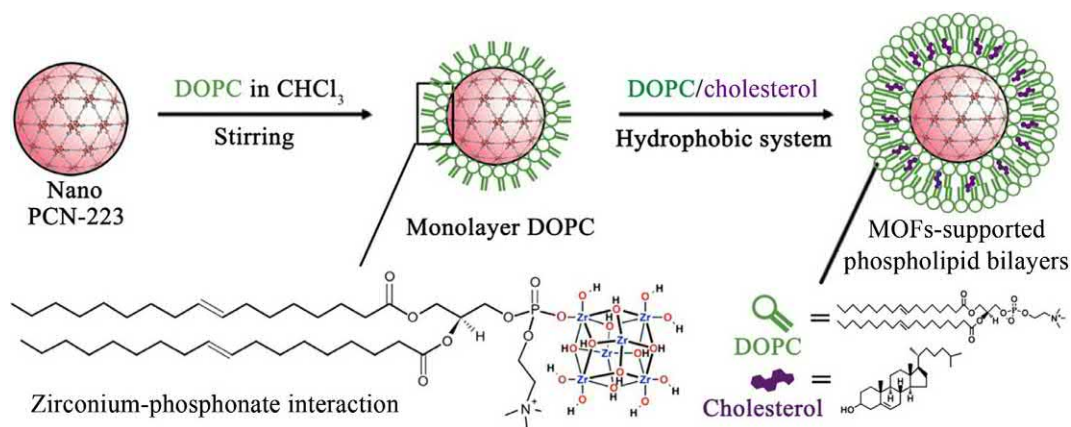


Fig. 7.4

The formation of MOFs-supported phospholipid bilayers on Zr-based MOFs through the strong Zr-O-P interaction between the Zr<sub>6</sub> clusters and 1,2-dioleoyl-sn-glycero-3-phosphocholine (DOPC) molecules, which significantly enhanced its stability in phosphate buffer solution (PBS). *Reprinted with permission from J. Yang, X. Chen, Y. Li, Q. Zhuang, P. Liu, J. Gu, Zr-based MOFs shielded with phospholipid bilayers: improved biostability and cell uptake for biological applications, Chem. Mater. 29 (2017) 4580–4589. Copyright (2017) American Chemical Society.*

### 7.3.3 Synthesis of Cu-MOFs

MOFs have attracted more and more attention due to their highly porous structure with tunable pores and high surface area, which have been widely applied in many fields such as catalysis, gas storage, and drug delivery. One of the most important properties of MOF is their tunable structures by tailoring the solution chemistry toward diverse particular applications. For example, the conductivity of MOFs has been reported to be enhanced significantly by molecular doping of iodine [29, 30]. More recently, Cu-MOFs have been reported to be synthesized via the equal volume mixture of Cu(NO<sub>3</sub>)<sub>2</sub>·3H<sub>2</sub>O in deionized water (solution A) and benzene-1,3,5-tricarboxylic acid (trimesic acid) dissolved in ethanol (solution B), which was stirred for 30 min and heated under hydrothermal conditions to 383 K for 18 h [31]. The synthesized Cu-MOFs were deposited on an FTO-coated glass covered with a very thin TiO<sub>2</sub> layer using a layer-by-layer (LBL) technique to sensitize a doctor-bladed TiO<sub>2</sub> nanoparticle film, which was used as a light-absorbing layer in TiO<sub>2</sub>-based solar cells. It is reported that the electrical conductivity of the MOF film can be increased drastically by iodine doping. In addition, the iodine doping of MOF is crucial for the reduction of the charge-transfer resistance of the TiO<sub>2</sub>/MOF/electrolyte interface. Another work reported that TiO<sub>2</sub> nanoparticle and multiwalled carbon nanotubes composite powder can be prepared hydrothermally, which was then sensitized with Cu-MOFs using a layer-by-layer deposition technique [32]. It is demonstrated that the electron transfer can be accelerated significantly by the introduction of carbon nanotubes, which can increase the power conversion efficiency by enhancing the photovoltaic performance of the cell.

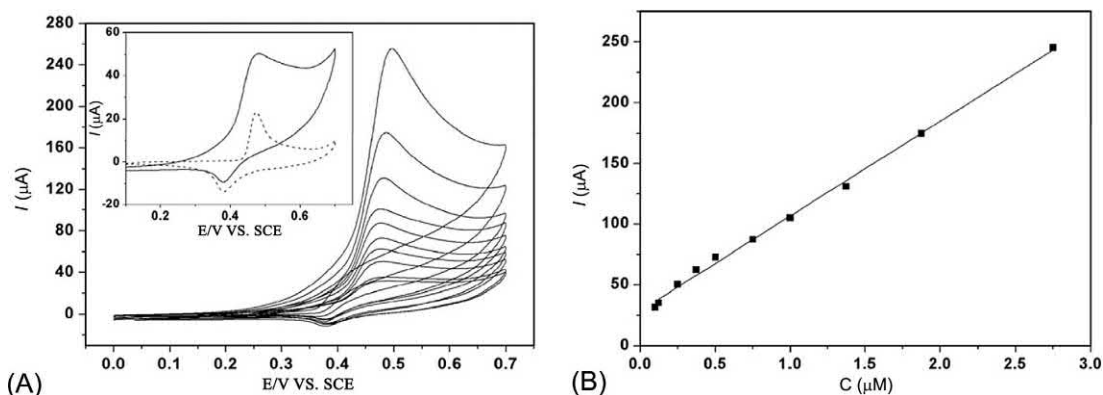


Fig. 7.5

(A) CV curves of  $[\text{Cu}(\text{adp})(\text{BIB})(\text{H}_2\text{O})]_n$  modified electrode in 0.1 M NaOH solution at different concentration of  $\text{H}_2\text{O}_2$ . Scan rate:  $100 \text{ mV s}^{-1}$ . Inset: CVs of  $[\text{Cu}(\text{adp})(\text{BIB})(\text{H}_2\text{O})]_n$  film modified GCE in 0.1 M NaOH solution in the absence (dotted line) and presence (solid line) of  $0.25 \mu\text{M}$   $\text{H}_2\text{O}_2$  at scan rate of  $100 \text{ mV s}^{-1}$ . (B) Plot of electrocatalytic peak currents versus  $\text{H}_2\text{O}_2$  concentrations at  $[\text{Cu}(\text{adp})(\text{BIB})(\text{H}_2\text{O})]_n/\text{GC}$  electrode in 0.1 M NaOH solution. Reprinted with permission from C.Y. Zhang, M.Y. Wang, L. Liu, X.J. Yang, X.Y. Xu, *Electrochemical investigation of a new Cu-MOF and its electrocatalytic activity towards  $\text{H}_2\text{O}_2$  oxidation in alkaline solution*, *Electrochem. Commun.* 33 (2013) 131–134. Copyright (2013) Elsevier.

In addition to energy harvesting and energy-storing devices, electrocatalytic activity of Cu-MOFs have also been investigated toward  $\text{H}_2\text{O}_2$  oxidation in alkaline solution (Fig. 7.5) [33]. This work described the hydrothermal synthesis of a new Cu-MOFs, i.e.,  $[\text{Cu}(\text{adp})(\text{BIB})(\text{H}_2\text{O})]_n$  (BIB = 1,4-bisimidazolebenzene;  $\text{H}_2\text{adp}$  = adipic acid). The synthesized Cu-MOFs were then used to modify the electrochemical electrode for cyclic voltammogram (CV) measurement. The results show a pair of redox peaks at ca. 0.43 V in 0.1 M NaOH solution corresponding to  $\text{Cu}^{\text{III}}(\text{OH})\text{-MOF}/\text{Cu}^{\text{II}}(\text{H}_2\text{O})\text{-MOF}$  couple. In addition, the Cu-MOF-modified electrode also shows high electrocatalytic activity toward  $\text{H}_2\text{O}_2$  oxidation in a dose-dependent manner at the concentrations ranging from 0.1 to  $2.75 \mu\text{M}$ . The detection limit is as low as  $0.068 \mu\text{M}$ . It is demonstrated that Cu-MOF could be a promising material for  $\text{H}_2\text{O}_2$  detection.

A typical Cu-MOF, HKUST-1 ( $\text{Cu}_3(\text{BTC})_2$ , BTC = 1,3,5-benzenetricarboxylic acid; HKUST = Hong Kong University of Science and Technology), was incorporated with graphite oxide in order to improve its hydrothermal stability and catalytic activity [34]. The resulting Cu-MOF/graphite oxide composites show enhanced porosity with high surface areas and some meso/macropores due to the growth of MOF between the graphene layers or their thin agglomerates, which could overcome their inherent shortcomings. For example, the access of reactant molecules to active sites and mass transfer in channels are facilitated by the high surface areas and meso/macropores. The hydrophobic environment surrounding metallic sites provided by the graphite oxide was able to protect the coordination bonds from

attack by water molecules and presents better affinity of active sites to organic reactants. All this could contribute to the improvement in the hydrothermal stability and the catalytic activity of Cu-MOF/graphite oxide composites, which make it more suitable for practical applications in heterogeneous catalysis.

#### 7.3.4 Synthesis of Zn-MOFs

Zn-MOFs have also been reported to be synthesized by the hydrothermal method. For example, a report described the synthesis of three Zn-MOFs using a dual-ligand approach with a basic N-donor ligand and carboxylate ligands under hydrothermal conditions [35]. It is indicated that all the three synthesized Zn-MOFs show distinct solvent-dependent photoluminescence emissions as demonstrated by the photoluminescent spectra analyses, which enable the highly sensitive detection of nitroaromatics via fluorescence quenching effect. It is assumed that the electron-donating MOF framework to the highly electron-withdrawing nitro group in the nitro compounds is contributed to the fluorescence quenching effect. This provides an approach for the synthesis of more electron-rich MOFs with luminescence property toward the potential applications of sensing nitro-substituted compounds.

MOF-5, which is a kind of MOFs with  $\text{Zn}^{2+}$  as central metal ions, has been reported to be synthesized using an optimized hydrothermal procedure starting from terephthalic acid and zinc nitrate, and diethylformamide as the organic solvent [36]. Hydrogen adsorption in MOF-5 was demonstrated to be pure physical adsorption. Hydrogen uptake is found to be correlated with the specific surface area for crystalline microporous materials and MOF-5 shows pretty high storage capacity which is promising for potential applications of hydrogen storage.

The design and synthesis of efficient fluorescence MOFs have also attracted more and more attention. Recently, some luminescent MOFs have been developed for the sensing of ions and small molecules. For instance, a robust bright salmon pink luminescent Zn-MOF for sensing of small molecules has been reported [37]. The synthesized Zn-MOFs show extraordinary photoluminescence behavior resulting from two emission modes and the magnitude of the fluorescence intensity change was found to be depended on the different interactions with solvents from each other. It is suggested that Zn-MOFs with multifunctional luminescence could be promising candidates to serve as sensitive elements in sensors for the detection of small molecules. Another report synthesized three 3D Zn-MOFs featured with different topological structures based on a tetracarboxylate ligand to investigate their fluorescent selectivity for the detection of small molecules [38]. It is indicated that the structures of 3D Zn-MOFs are related to the choice of reaction solvent, where DMF results in a diamond topology, DMA facilitates the formation of Zn-MOFs with lonsdaleite network, and DMF/DMA (1:1) generates the structure of Zn-MOFs with an NbO net. The fluorescent measurement results show that all the synthesized 3D Zn-MOFs were able to detect a

series of aromatic compounds, which exhibit the highest quenching behavior upon adding in a solvent of 1,4-DNB compounds. These Zn-MOFs provide promising candidates for the sensing organic molecule and pollutants.

### 7.3.5 Synthesis of other MOFs

In addition to Fe-MOFs, Zr-MOFs, Cu-MOFs, and Zn-MOFs, MOFs based on other metal ions have also been synthesized by hydrothermal method for different purposes. For example, four interpenetrating frameworks have been synthesized by a hydrothermal reaction using different central metal ions and connectivity coefficient between bpea<sup>2-</sup> anions and long heterocyclic aromatic ligands, which include  $[\text{Ni}(\text{bpea})(\text{L1})(\text{H}_2\text{O})]_n$ ,  $[\text{Ni}(\text{bpea})(\text{L2})]_n$ ,  $\{[\text{Ni}(\text{bpea})(\text{L3})_{1.5}(\text{H}_2\text{O})] \cdot (\text{L3})\}_n$ , and  $[\text{Co}(\text{bpea})(\text{L3})]_n$  ( $\text{H}_2\text{bpea}$  = biphenylethene-4',4'-dicarboxylic acid, L1 = 1,3-di(4-pyridyl)propane, L2 = 1,4-bis-(imidazol-1-yl-methylene) benzene, L3 = 1,4-bis(1-imidazolyl)benzene) [39]. It is indicated that all the synthesized MOFs have different structure features and topology due to the different flexibility and rigidity of ligands used for the synthesis of MOFs (i.e., L1, L2, and L3). It is suggested that the versatile coordination modes of carboxyl groups have an important impact on the final frameworks.

Another report described the synthesis of four kinds of MOFs using partially or wholly deprotonated 5,5'-(1,4-phenylenebis(methylene))bis(oxy)diisophthalic acid (H4L1) and 5,5'-(1,3-phenylenebis(methylene))bis(oxy)diisophthalic acid (H4L2) in the presence or absence of auxiliary bipy ligand (Fig. 7.6) [40], which include  $\{[\text{Co}(\text{L1})_{0.5}] \cdot (\text{H}_2\text{O})_2\}_n$  (1),  $\{[\text{Mn}(\text{L1})_{0.5}] \cdot (\text{H}_2\text{O})_2\}_n$  (2),  $\{[\text{Cu}(\text{H}_2\text{L1})](\mu_2\text{-bipy})\}_n$  (bipy = 4,4'-bipyridyl) (3), and  $\{[\text{Zn}_2(\text{L2})] \cdot \text{H}_2\text{O}\}_n$  (4). It is indicated that all the four MOFs have the structure of three-dimensional (3D) networks, although the underlying formation mechanisms are different to some extent. In addition, compounds 1 and 2 exhibit antiferromagnetic coupling between adjacent Co(II) ions and Mn(II) ions. Compound 4 exhibits strong violet emissions, which could be a good candidate for violet-light-emitting materials.

## 7.4 Conclusions and prospects

Since discovered in 1989 by Robson, MOFs have attracted increasing attention due to their decisive advantages and unique physical properties, which include tunable pore sizes, flexible networks, various compositions, and easy functionalization. MOFs have been utilized as key components for the development of various functional systems and have been widely applied in many fields such as biomedicine, catalysis, gas storage, and biosensing applications. Since the synthesis of MOFs by reticular design in 1999, a number of approaches for the synthesis of MOFs have emerged, which include conventional synthesis, microwave synthesis, and electrochemical synthesis. Among them, hydrothermal method is one of the most basic and conventional approaches, which has been used extensively in

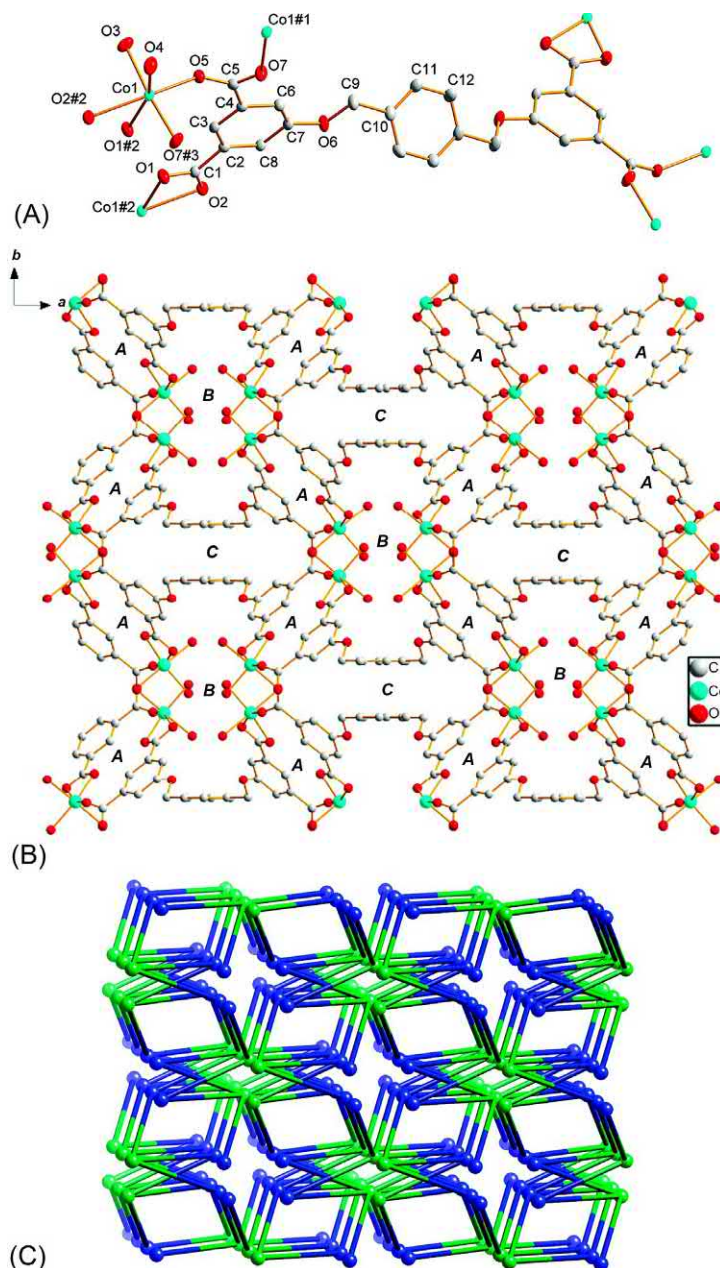


Fig. 7.6

(a) Thermal ellipsoid plot (ORTEP) drawing of 1 showing 30% ellipsoid probability (hydrogen atoms are omitted for clarity). Symmetry codes: #1 =  $x, -y, 0.5 + z$ ; #2 =  $0.5 - x, 0.5 - y, -z$ ; #3 =  $x, -y, -0.5 + z$ . (b) A view of three kinds of channels of compound 1 along the  $c$  axis (hydrogen atoms are omitted for clarity). (c) Schematic representation of the topology of compound 1. *Blue nodes* represent Co atoms and *green nodes* represent  $L1^{4-}$  ligands. Reprinted with permission from Z.R. Pan, H.G. Zheng, T.W. Wang, Y. Song, Y.Z. Li, Z.J. Guo, S.R. Batten, *Hydrothermal synthesis, structures, and physical properties of four new flexible multicarboxylate ligands-based compounds*, *Inorg. Chem.* 47 (2008) 9528–9536. Copyright (2018) American Chemical Society.



many fields and show promising prospects after functionalized with various groups and molecules via covalent or noncovalent bonding. For example, with proper functionalization, MOFs have been widely applied in drug delivery and biosensing purposes.

Although promising, hydrothermal method for the synthesis of MOFs also faces major challenges. The proper functionalization of MOFs with demanding properties suitable for different biomedical applications is one of the major challenges. For example, for the biosensing applications, it usually requires endowing the MOFs with functional sensing elements that are sensitive to target molecules or signals, which is rather difficult in some cases. In the future, the surface functionalization of nanoscale MOFs should be systemically investigated. Another major challenge is how to control the key properties of MOFs such as toxicity, size and shape, and biological stability. However, the structure and properties of MOFs can be easily manipulated by the adjustment of the metal ions and organic ligands. For instance, the applications of MOFs in the biomedical field usually need to comprehensively consider many properties such as toxicity, stability, size, and shape, which are not isolated, but interact with each other and other environmental variables including solution pH and cellular microenvironments. In the future, the determination of the toxicity of MOFs should be based on a vast database, which takes a long time and requires enormous *in vivo* experiments. Although many challenges existed, and improvements are still required for practical applications, MOFs still have a brighter future and promising applications in many fields due to their unique properties and decisive advantages.

## Acknowledgments

This work was supported by the National Natural Science Foundation of China (Grant No. 51861145307, 31700859, 31661143030, 31470956), the Doctoral Fund of Education Ministry of China (Grant No. 2016M602832), and the Fundamental Research Funds for the Central Universities.

## References

- [1] K. Byrappa, M. Yoshimura, Hydrothermal technology—principles and applications, in: K. Byrappa, M. Yoshimura (Eds.), *Handbook of Hydrothermal Technology*, William Andrew Publishing, Norwich, NY, 2001, pp. 1–52.
- [2] K. Byrappa, M. Yoshimura, History of hydrothermal technology, in: K. Byrappa, M. Yoshimura (Eds.), *Handbook of Hydrothermal Technology*, William Andrew Publishing, Norwich, NY, 2001, pp. 53–81.
- [3] Y. Pang, D. Heryadi, F. Zhou, L. Zhao, G. Lestari, H. Su, Z. Lai, Tuning the crystal morphology and size of zeolitic imidazolate framework-8 in aqueous solution by surfactants, *CrystEngComm* 13 (23) (2011) 6937–6940.
- [4] M.-H. Pham, G.-T. Vuong, A.-T. Vu, T.-O. Do, Novel route to size-controlled Fe–MIL-88B–NH<sub>2</sub> metal–organic framework nanocrystals, *Langmuir* 27 (24) (2011) 15261–15267.
- [5] M. S.-Y. Teresa, C.P. Angelika, S. Christian, Nanoparticles of metal-organic frameworks: on the road to *in vivo* efficacy in biomedicine, *Adv. Mater.* 30 (37) (2018) 1707365.
- [6] W. Chen, C. Wu, Synthesis, functionalization, and applications of metal-organic frameworks in biomedicine, *Dalton Trans.* 47 (7) (2018) 2114–2133.



- [7] C.T. Tabar, D. Cunha, D.E. Imbuluqueta, F. Ragon, C. Serre, M.J.B. Prieto, P. Horcajada, Cytotoxicity of nanoscaled metal-organic frameworks, *J. Mater. Chem. B* 2 (2014) 262–271.
- [8] P. Horcajada, R. Gre, T. Baati, P. Allan, G. Maurin, P. Couvreur, G. Férey, R.E. Morris, C. Serre, Metal-organic frameworks in biomedicine, *Chem. Rev.* 112 (2) (2012) 1232–1268.
- [9] C.Y. Sun, C. Qin, X.L. Wang, Z.M. Su, Metal-organic frameworks as potential drug delivery systems, *Expert Opin. Drug Deliv.* 10 (1) (2013) 89–101.
- [10] P. Horcajada, T. Chalati, C. Serre, B. Gillet, C. Sebrie, T. Baati, J.F. Eubank, D. Heurtaux, P. Clayette, C. Kreuz, J.-S. Chang, Y.K. Hwang, V. Marsaud, P.-N. Bories, L. Cynober, S. Gil, G. Férey, P. Couvreur, R. Gref, Porous metal-organic-framework nanoscale carriers as a potential platform for drug delivery and imaging, *Nat. Mater.* 9 (2009) 172.
- [11] M. Rezaei, A. Abbasi, R. Varshochian, R. Dinarvand, M. Jeddi-Tehrani, NanoMIL-100(Fe) containing docetaxel for breast cancer therapy, *Artif. Cells Nanomed. Biotechnol.* 46 (2018) 1390–1401.
- [12] M. Giménez-Marqués, E. Bellido, T. Berthelot, T. Simón-Yarza, T. Hidalgo, R. Simón-Vázquez, Á. González-Fernández, J. Avila, M.C. Asensio, R. Gref, P. Couvreur, C. Serre, P. Horcajada, GraftFast surface engineering to improve MOF nanoparticles furtiveness, *Small* 14 (2018) 1801900.
- [13] H.P. Nguyen Thi, H.D. Ninh, C.V. Tran, B.T. Le, S.V. Bhosale, D.D. La, Size-control and surface modification of flexible metal-organic framework MIL-53(Fe) by polyethyleneglycol for 5-fluorouracil anticancer drug delivery, *ChemistrySelect* 4 (2019) 2333–2338.
- [14] X. Leng, X. Dong, W. Wang, N. Sai, C. Yang, L. You, H. Huang, X. Yin, J. Ni, Biocompatible Fe-based micropore metal-organic frameworks as sustained-release anticancer drug carriers, *Molecules* 23 (2018).
- [15] Y. Jiang, Q.-M. Yang, Q.-J. Xu, S.-Y. Lu, L.-Y. Hu, M.-W. Xu, Y.-S. Liu, Metal organic framework MIL-53 (Fe) as an efficient artificial oxidase for colorimetric detection of cellular biothiols, *Anal. Biochem.* 577 (2019) 82–88.
- [16] S.-N. Kim, C.G. Park, B.K. Huh, S.H. Lee, C.H. Min, Y.Y. Lee, Y.K. Kim, K.H. Park, Y.B. Choy, Metal-organic frameworks, NH<sub>2</sub>-MIL-88(Fe), as carriers for ophthalmic delivery of brimonidine, *Acta Biomater.* 79 (2018) 344–353.
- [17] S. Dehghani, N.R. Alam, S. Shahriarian, T. Mortezaadeh, S. Haghgoo, A. Golmohamadpour, B. Majidi, M. Khoobi, The effect of size and aspect ratio of Fe-MIL-88B-NH<sub>2</sub> metal-organic frameworks on their relaxivity and contrast enhancement properties in MRI: in vitro and in vivo studies, *J. Nanopart. Res.* 20 (2018) 278.
- [18] C. Orellana-Tavra, E.F. Baxter, T. Tian, T.D. Bennett, N.K.H. Slater, A.K. Cheetham, D. Fairen-Jimenez, Amorphous metal-organic frameworks for drug delivery, *Chem. Commun.* 51 (2015) 13878–13881.
- [19] W. Zhe, H. Shuanggang, Y. Jian, L. Ajuan, L. Yongsheng, Z. Qixin, G. Jinlou, Nanoscale Zr-based MOFs with tailorable size and introduced mesopore for protein delivery, *Adv. Funct. Mater.* 28 (2018) 1707356.
- [20] C. Orellana-Tavra, S. Haddad, R.J. Marshall, I. Abánades Lázaro, G. Boix, I. Imaz, D. Maspoch, R.S. Forgan, D. Fairen-Jimenez, Tuning the endocytosis mechanism of Zr-based metal-organic frameworks through linker functionalization, *ACS Appl. Mater. Interfaces* 9 (2017) 35516–35525.
- [21] I. Abánades Lázaro, S. Haddad, S. Sacca, C. Orellana-Tavra, D. Fairen-Jimenez, R.S. Forgan, Selective surface PEGylation of UiO-66 nanoparticles for enhanced stability, cell uptake, and pH-responsive drug delivery, *Chem* 2 (2017) 561–578.
- [22] D. Cunha, M. Ben Yahia, S. Hall, S.R. Miller, H. Chevreau, E. Elkaïm, G. Maurin, P. Horcajada, C. Serre, Rationale of drug encapsulation and release from biocompatible porous metal-organic frameworks, *Chem. Mater.* 25 (2013) 2767–2776.
- [23] I. Abánades Lázaro, S. Haddad, J.M. Rodrigo-Muñoz, R.J. Marshall, B. Sastre, V. del Pozo, D. Fairen-Jimenez, R.S. Forgan, Surface-functionalization of Zr-fumarate MOF for selective cytotoxicity and immune system compatibility in nanoscale drug delivery, *ACS Appl. Mater. Interfaces* 10 (2018) 31146–31157.
- [24] I.A. Lazaro, S.A. Lazaro, R.S. Forgan, Enhancing anticancer cytotoxicity through bimodal drug delivery from ultrasmall Zr MOF nanoparticles, *Chem. Commun.* 54 (2018) 2792–2795.
- [25] J. Yang, X. Chen, Y. Li, Q. Zhuang, P. Liu, J. Gu, Zr-based MOFs shielded with phospholipid bilayers: improved biostability and cell uptake for biological applications, *Chem. Mater.* 29 (2017) 4580–4589.

- [26] M. Filippousi, S. Turner, K. Leus, P.I. Sifaka, E.D. Tseligka, M. Vandichel, S.G. Nanaki, I.S. Vizirianakis, D.N. Bikiaris, P. Van Der Voort, G. Van Tendeloo, Biocompatible Zr-based nanoscale MOFs coated with modified poly( $\epsilon$ -caprolactone) as anticancer drug carriers, *Int. J. Pharm.* 509 (2016) 208–218.
- [27] W. Wang, L. Wang, Y. Li, S. Liu, Z. Xie, X. Jing, Nanoscale polymer metal–organic framework hybrids for effective photothermal therapy of colon cancers, *Adv. Mater.* 28 (2016) 9320–9325.
- [28] C. Han, J. Yang, J. Gu, Immobilization of silver nanoparticles in Zr-based MOFs: induction of apoptosis in cancer cells, *J. Nanopart. Res.* 20 (2018) 7.
- [29] M.-H. Zeng, Q.-X. Wang, Y.-X. Tan, S. Hu, H.-X. Zhao, L.-S. Long, M. Kurmoo, Rigid pillars and double walls in a porous metal-organic framework: single-crystal to single-crystal, controlled uptake and release of iodine and electrical conductivity, *J. Am. Chem. Soc.* 132 (2010) 2561–2563.
- [30] Y. Kobayashi, B. Jacobs, M.D. Allendorf, J.R. Long, Conductivity, doping, and redox chemistry of a microporous dithiolene-based metal-organic framework, *Chem. Mater.* 22 (2010) 4120–4122.
- [31] D.Y. Lee, D.V. Shinde, S.J. Yoon, K.N. Cho, W. Lee, N.K. Shrestha, S.H. Han, Cu-based metal-organic frameworks for photovoltaic application, *J. Phys. Chem. C* 118 (2013) 16328–16334.
- [32] D.Y. Lee, C.Y. Shin, S.J. Yoon, H.Y. Lee, W. Lee, N.K. Shrestha, J.K. Lee, S.H. Han, Enhanced photovoltaic performance of Cu-based metal-organic frameworks sensitized solar cell by addition of carbon nanotubes, *Sci. Rep.* 4 (2014) 3930.
- [33] C.Y. Zhang, M.Y. Wang, L. Liu, X.J. Yang, X.Y. Xu, Electrochemical investigation of a new Cu-MOF and its electrocatalytic activity towards  $H_2O_2$  oxidation in alkaline solution, *Electrochem. Commun.* 33 (2013) 131–134.
- [34] D.-D. Zu, L. Lu, X.-Q. Liu, D.-Y. Zhang, L.-B. Sun, Improving hydrothermal stability and catalytic activity of metal-organic frameworks by graphite oxide incorporation, *J. Phys. Chem. C* 118 (2014) 19910–19917.
- [35] H. Wang, W.T. Yang, Z.M. Sun, Mixed-ligand Zn-MOFs for highly luminescent sensing of nitro compounds, *Chem. Asian J.* 8 (2013) 982–989.
- [36] B. Panella, M. Hirscher, H. Pütter, U. Müller, Hydrogen adsorption in metal–organic frameworks: Cu-MOFs and Zn-MOFs compared, *Adv. Funct. Mater.* 16 (2006) 520–524.
- [37] J.H. Cui, Z.Z. Lu, Y.Z. Li, Z.J. Guo, H.G. Zheng, A microporous metal–organic framework with FeS<sub>2</sub> topology based on [Zn<sub>6</sub>(16-O)] cluster for reversible sensing of small molecules, *Chem. Commun.* 48 (2012) 7967–7969.
- [38] J. Yang, L.L. Zhang, X.Q. Wang, R.M. Wang, F.N. Dai, D.F. Sun, Fluorescent selectivity for small molecules of three Zn-MOFs with different topologies based on a tetracarboxylate ligand, *RSC Adv.* 5 (2015) 62982–62988.
- [39] L. Zhang, Y.-L. Yao, Y.-X. Che, J.-M. Zheng, Hydrothermal synthesis of a series of interpenetrated metal-organic frameworks based on long multicarboxylate and long heterocyclic aromatic ligands, *Cryst. Growth Des.* 10 (2010) 528–533.
- [40] Z.R. Pan, H.G. Zheng, T.W. Wang, Y. Song, Y.Z. Li, Z.J. Guo, S.R. Batten, Hydrothermal synthesis, structures, and physical properties of four new flexible multicarboxylate ligands-based compounds, *Inorg. Chem.* 47 (2008) 9528–9536.

# Microwave synthesis of metal-organic frameworks

Ricardo F. Mendes, João Rocha, Filipe A. Almeida Paz

*Department of Chemistry, CICECO—Aveiro Institute of Materials, University of Aveiro, Aveiro, Portugal*

## Abbreviations

|                             |                                                                                |
|-----------------------------|--------------------------------------------------------------------------------|
| <b>4,4'-bpy</b>             | 4,4'-bipyridyl                                                                 |
| <b>ALD</b>                  | atomic layer deposition                                                        |
| <b>APTES</b>                | 3-aminopropyltriethoxysilane                                                   |
| <b>Boc</b>                  | tertbutyloxycarbonyl                                                           |
| <b>Dcbpy<sup>2-</sup></b>   | 2,2'-bipyridine-4,4'-dicarboxylate                                             |
| <b>DMF</b>                  | dimethylformamide                                                              |
| <b>H<sub>2</sub>abdc</b>    | 2-amino-1,4-dicarboxylic acid                                                  |
| <b>H<sub>2</sub>bdc</b>     | benzene-1,4-dicarboxylic acid                                                  |
| <b>H<sub>2</sub>dhbdc</b>   | 1,2-dihydroxibenzene-1,4-dicarboxylic acid                                     |
| <b>H<sub>2</sub>oba</b>     | 4,4'-oxydibenzoic acid                                                         |
| <b>H<sub>2</sub>pydc</b>    | 2,5-pyridinedicarboxylic acid                                                  |
| <b>H<sub>2</sub>TDC</b>     | 9,10-triptycenedicarboxylic acid                                               |
| <b>H<sub>3</sub>btc</b>     | benzene-1,3,5-tricarboxylic acid                                               |
| <b>H<sub>4</sub>DH3PhDC</b> | 2',5'-dimethyl-3,3''-dihydroxy-[1,1':4',1''-terphenyl]-4,4''-dicarboxylic acid |
| <b>H<sub>6</sub>bmt</b>     | benzene-1,3,5-triyltris(methylene)triphosphonic acid                           |
| <b>H<sub>6</sub>nmp</b>     | nitrilotrinethylphosphonic acid                                                |
| <b>HKUST</b>                | Hong Kong University of Science and Technology                                 |
| <b>HT</b>                   | hydro(solvo)thermal                                                            |
| <b>Imda</b>                 | imidazole-4,5-dicarboxylic acid                                                |
| <b>IRMOF</b>                | isoreticular metal-organic framework                                           |
| <b>MeIm</b>                 | 2-methylimidazolate                                                            |
| <b>MIL</b>                  | Materials of Institute Lavoisier                                               |
| <b>MITD</b>                 | microwave-induced thermal deposition                                           |
| <b>MOF</b>                  | metal-organic framework                                                        |
| <b>MWAS</b>                 | microwave-assisted synthesis                                                   |
| <b>OP</b>                   | one-pot heating batch                                                          |
| <b>PSM</b>                  | postsynthetic modification                                                     |
| <b>PXRD</b>                 | powder X-ray diffraction                                                       |
| <b>UiO</b>                  | University of Oslo                                                             |
| <b>ZIF</b>                  | zeolitic imidazolate framework                                                 |

## 8.1 Introduction

As the field of metal-organic frameworks (MOFs) is coming of age, research is progressively moving out from the academic laboratories into industrial applications [1]. This move calls for the development of practical and cost-effective synthesis routes for the preparation of MOF materials. Syntheses based on conventional heating, namely hydro(solvo)thermal (HT) and one-pot heating batch (OP) synthesis, are still widely used. Most reported materials have indeed been prepared using these routes, which require high reaction times (up to several days) and large equipment (ovens), resulting in higher overall energy consumption. Additionally, these methods have other limitations, such as the need for large volumes of solvent, poor reproducibility between batches, and nonuniform particle size and morphology. In this context, microwave-assisted synthesis (MWAS) has emerged as a promising alternative approach.

MWAS is widely used in both organic and inorganic chemistry, providing an efficient way to synthesize new compounds with short crystallization times, narrow particle size distribution, easy morphology control, phase selectivity, and close control of the reaction parameters (i.e. pressure, power, reaction time, and temperature). In MWAS, electromagnetic radiations (microwaves) are generated by a magnetron, which converts the high-voltage current into high-frequency radiation. It relies on the solvent or substrate ability to convert to heat the microwave energy absorbed, via the interaction of electromagnetic waves with molecules having a dipole moment (permanent or induced), such as water or  $N,N'$ -dimethylformamide. In the presence of microwave radiation, the molecules attempt to align with the oscillating electric field, leading to rotation. At the appropriate frequency, the collisions between molecules increase their kinetic energy and, thus, temperature. This, however, does not mean that only solvents with a dipole moment can efficiently be used in MWAS reactions. With the significant technical improvements, (see next section) virtually any pure solvent can now be used.

Because, in MWAS, the radiation interacts with individual solvent molecules and the heating of the reaction mixture is more uniform. In contrast to conventional heating where energy is transferred to the reaction mixture by conductive heat, in microwave heating the reaction mixture interacts with an alternating electric field. This means that the energy is generated across the reaction mixture, instead of simple conduction from an external source (Fig. 8.1). Note this figure features an unstirred reaction heated for 60 s. With efficient stirring, temperature gradients can be mitigated. The MWAS method is one of the most energy efficient methods for preparing MOFs, exhibiting several following advantages:

- (i) Rapid heating of the reaction mixtures, leading to short reaction times.
- (ii) Controlled and rapid cooling, ensuring a precise control of the synthetic procedure.
- (iii) Uniform products concerning crystal sizes and composition.

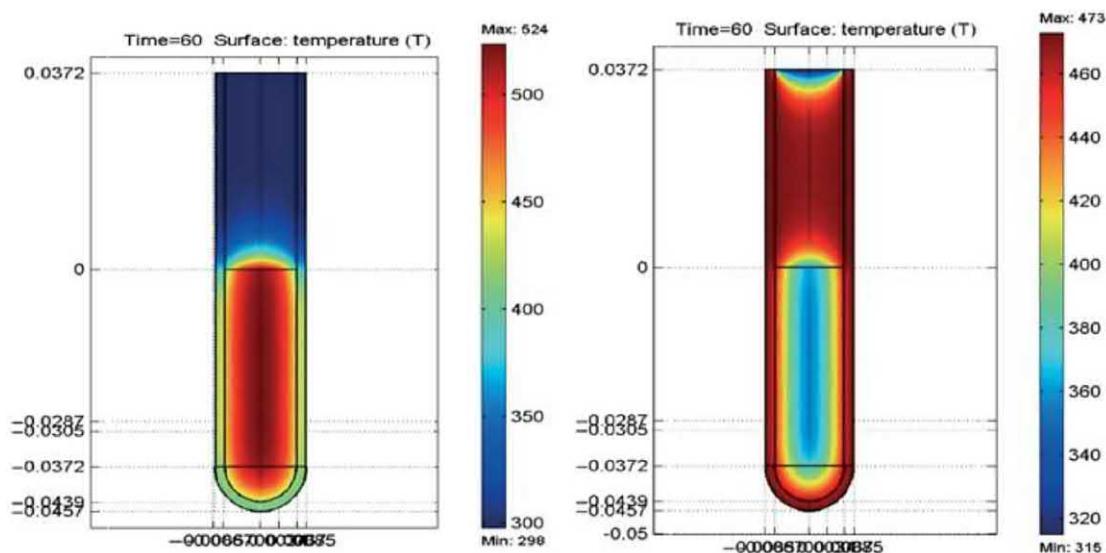


Fig. 8.1

Temperature profile after 60 s under microwave irradiation (left) compared to treatment in an oil-bath (right). Microwave irradiation raises the temperature of the whole reaction volume simultaneously, whereas in the oil-heated tube the reaction mixture in contact with the vessel wall is heated first. Temperature scale in K. “0” on the vertical scale indicates the position of the meniscus. *Reproduced with permission from J.-S. Schanche, Microwave synthesis solutions from personal chemistry, Mol. Divers. 7(2) (2003) 291–298.*

- (iv) Low energy consumption and high efficiency (50%–60% cf. 20%–30% of thermal heating).
- (v) The microwave energy is applied only to solvents, while the reactor and the remaining reagents are not affected by the radiation.

In order to transpose the MOFs MWAS method from the laboratory to industrial processes, a better understanding of the effect of microwave radiation is required. This chapter aims to both summarize the efforts developed in the last decade on the use of MWAS in the preparation of MOFs and to highlight its use in MOFs’ postsynthetic modification and in film/membrane preparation.

## 8.2 Commercial microwave equipment

Conventional domestic microwave ovens are not suitable to be used in a chemical laboratory because the generated microwaves will move and bounce off walls, generating pockets of high and low energy, ultimately compromising reproducibility. Moreover, such ovens are not fitted with temperature sensors and are not built to handle safely hot and flammable organic solvents. For these reasons, scientific microwave ovens were developed to withstand

explosions of the reaction vessel, as well as to control temperature, pressure, and reaction stirring velocity. In this section, a brief overview of the commercially available microwave equipment is presented, with a focus on small-scale devices. For a more detailed description, the reader is referred to the websites of the manufacturers: Anton Paar (<http://www.anton-paar.com>), Biotage (<http://www.biotage.com>), CEM Corporation (<http://www.cem.com>), and Milestone (<http://www.milestonesrl.com>). We stress that the equipment specifications detailed in the following paragraphs are at the moment of the writing up of the current chapter and details may change in the coming months after publication.

**Anton-Parr** manufactures the Monowave 400 and Monowave 200 (main difference between two models is the temperature and pressure range), which are high-performance microwave reactors specially designed for small-scale synthesis (Fig. 8.2A). This equipment utilizes 850 W magnetrons, reaching the maximum temperature of 300°C and 435 psi pressure (260°C and 290 psi for Monowave 200). Temperature is monitored via an infrared detector or, alternatively, a fiber-optic probe is immersed in the reaction vessel. Reactions can be performed in 4, 10, and 30 mL vessels. The autosampler MAS 24 allows for unattended sequential processing of up to 24 experiments. For scale-up work, this manufacturer also has made available the Masterwave BTR, a benchtop reactor for reactions in the kilogram range.

**Biotage** manufactures the Biotage Initiator+, a new generation of synthesis instruments for organic, medicinal, materials, nano, and polymer chemistry (Fig. 8.2B). Temperature and pressure up to 300°C and 435 psi can be attained using a 400 W magnetron. With a “regulate on pressure” system, low boiling point solvents can be used enabling the reaction to achieve the highest possible temperature during the run. Temperature is also monitored via an infrared detector, with a fiber-optic probe being also available. Larger volumes can be used, with four different vial sizes from 0.2 to 20 mL.



(A)



(B)

**Fig. 8.2**

Two of the small-scale dedicated microwave units: (A) Anton Paar Monowave and (B) Biotage Initiator. Reproduced with permission from (A) Anton Paar; (B) Biotage.



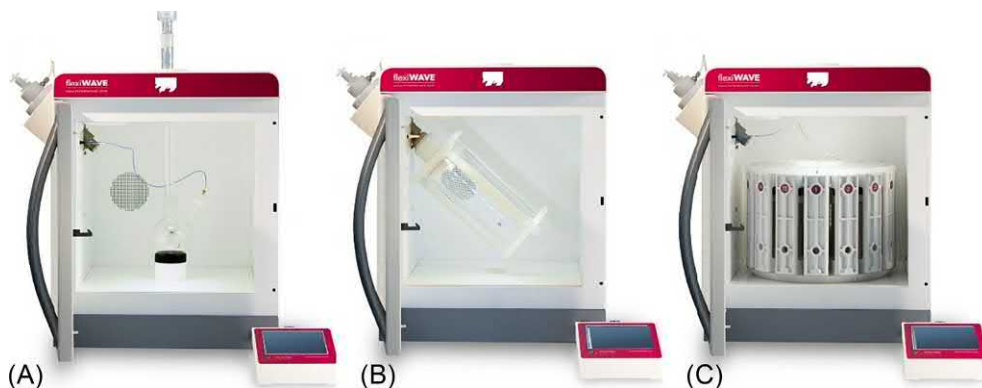


**Fig. 8.3**

Small-scale microwave units from CEM: (A) Discover SP and (B) MARS 6. *Reproduced with permission from CEM.*

**CEM** manufactures two main microwave equipments for chemical synthesis, Discover SP and MARS 6 (Fig. 8.3). The former uses a 300 W magnetron, with maximum reaction temperature of 300°C and pressure 300 psi. Activent vessel caps automatically relieve gaseous by-products, providing safety by minimizing overpressurization. The 300 mL single-mode microwave cavity allows a higher flexibility in terms of reaction vessel sizes, in both pressurized and open vessel modes. In pressurize mode, 10, 30, and 80 mL vessels can be used, while in open mode glassware up to 125 mL is available. MARS 6 is a multimode microwave system which provides parallel reaction processing under uniform conditions. It uses 1800 W magnetron and allows multiple reaction vessels to run simultaneously, only taking up 30 min to complete a set of 36 vessels, with the ability to accommodate multiple pressurized vessels, or up to a 5 L open flask.

**Milestone** has made available two microwave systems: FlexiWAVE and SynthWAVE. The equipment uses two 950 W magnetrons, being the most powerful commercial microwave system available. The large microwave cavity has a volume in excess of 70 L, which allows the chemist to easily configure many different reaction setups in a very flexible environment (Fig. 8.4), namely: (i) classic glassware—it allows synthetic reactions under reflux; (ii) high pressure—can replace reflux devices, moving from high boiling solvents to low boiling solvents; high temperature reactions (up to 300°C) can be performed; up to 15 high-pressure vessels may be used simultaneously in parallel synthesis; (iii) solid-phase—capable of physically rotating the reaction vessel, to achieve very homogenous bulk heating of slurries, viscous, and solid reaction mixtures media and temperature control by a contactless infrared sensor. Furthermore, this setup allows operations under normal atmosphere, inert gas, and vacuum.

**Fig. 8.4**

Small-scale microwave flexi WAVE unit from Milestone: (A) classic glassware, (B) solid-phase, and (C) high-pressure models. *Reproduced with permission from Milestone.*

All systems can be controlled directly or interfaced with a PC (except the CEM MARS 6). Pressure, temperature, power, and stirring velocity can be monitored and controlled in real time. Reaction vessel cooling is also controlled by pressurized air.

### 8.3 Microwave synthesis of MOFs

The first MWAS of MOFs was reported by Jhung et al. for the preparation of the chromium trimesate MIL-100 [2]. The material was obtained at 220°C; the same temperature as for the HT method, but with a considerable decrease in the reaction time from 4 days to 4 h, maintaining the 44% crystal yield. Liang and coworkers showed that MWAS may also improve the crystallinity and purity of zirconium-bearing MOFs (MIL-140A and MIL-140B) [3]. The reactions were performed in DMF at 220°C, and the materials obtained after a reaction time of 15 min. This swift reaction, when compared to the HT method (16 h for MIL-140A and 6 h for MIL-140B), prevents the formation of a secondary phase present even after 18 h of conventional heating. The same problem was reported by Wang et al. for the two-dimensional paddle wheel framework  $[\text{Cu}_2(\text{oba})_2(\text{DMF})_2] \cdot 5.25\text{DMF}$  (MCF-23), where  $\text{H}_2\text{oba} = 4,4'$ -oxydibenzoic acid [4]. In the HT preparation of MCF-23, an impurity was always observed.

The synthesis of other well-known MOFs using MWAS has also been reported over the last decade (Table 8.1). At first, this method was employed as an alternative for the preparation of MOFs in a more cost-efficient and rapid way. Although this main motivation is still used [17–19], with time it has evolved to the possibility of screening and study the influence of different synthesis variables in the preparation of the same and new materials.

Table 8.1 Composition and microwave conditions used in the preparation of selected MOFs.

| MOF                      | Formula <sup>a</sup>                                                        | Microwave conditions |                  |                         | Refs. |
|--------------------------|-----------------------------------------------------------------------------|----------------------|------------------|-------------------------|-------|
|                          |                                                                             | Power (W)            | Temperature (°C) | Reaction time (minutes) |       |
| MOF-5                    | [Zn <sub>4</sub> O(bdc) <sub>3</sub> ]                                      | –                    | 95–135           | 10–60                   | [5]   |
| HKUST-1                  | [Cu <sub>3</sub> (btc) <sub>2</sub> ]                                       | 300                  | 150–220          | 1–240                   | [6]   |
| MIL-101                  | [Cr <sub>3</sub> OH<br>(H <sub>2</sub> O) <sub>2</sub> (bdc) <sub>3</sub> ] | 300                  | 220              | 15                      | [7]   |
| NH <sub>2</sub> -MIL-101 | [Fe <sub>3</sub> O(OH)(abdc) <sub>3</sub> ]                                 | –                    | 150              | 15                      | [8]   |
| MIL-100                  | [Cr <sub>3</sub> O(OH)(btc) <sub>2</sub> ]                                  | –                    | 220              | 240                     | [2]   |
| MIL-53(Al)               | [Al(OH)(bdc)]                                                               | –                    | 200              | 150                     | [9]   |
| MIL-53(Cr)               | [Cr(OH)(bdc)]                                                               | –                    | 210              | 120                     | [9]   |
| MIL-53(Fe)               | [Fe(OH)(bdc)]                                                               | 300                  | 100              | 60                      | [10]  |
| MIL-147(V)               | [V(OH)(bdc)]                                                                | –                    | 175              | 120                     | [9]   |
| MIL-140A                 | [ZrO(bdc)]                                                                  | –                    | 220              | 1                       | [11]  |
| MIL-88B                  | [Fe <sub>3</sub> O(bdc) <sub>3</sub> ]                                      | 200                  | 150              | 15                      | [12]  |
| NH <sub>2</sub> -MIL-88B | [Fe <sub>3</sub> O(abdc) <sub>3</sub> ]                                     | 200                  | 150              | 15                      | [12]  |
| ZIF-8                    | [Zn(Melm) <sub>2</sub> ]                                                    | 80                   | 243              | 180                     | [13]  |
| MOF-74(Co)               | [Co <sub>4</sub> O(dhbdc) <sub>3</sub> ]                                    | 300                  | 130              | 60                      | [14]  |
| CPO-27                   | [Co <sub>2</sub> (DHTP)(H <sub>2</sub> O) <sub>2</sub> ]                    | 400                  | 70               | 44–180                  | [15]  |
| UiO-66                   | [Zr <sub>6</sub> O <sub>4</sub> (OH) <sub>4</sub> (bdc) <sub>6</sub> ]      | –                    | 120              | 15                      | [16]  |

<sup>a</sup>H<sub>2</sub>bdc, benzene-1,4-dicarboxylic acid; H<sub>3</sub>btc, benzene-1,3,5-tricarboxylic acid; H<sub>2</sub>dhbdc, 1,2-dihydroxybenzene-1,4-dicarboxylic acid; H<sub>2</sub>abdc, 2-amino-1,4-dicarboxylic acid; Melm, 2-methylimidazolate; H<sub>2</sub>DHTP, 1,5-dihydroxyterephthalic acid.

### 8.3.1 Influence of reaction conditions

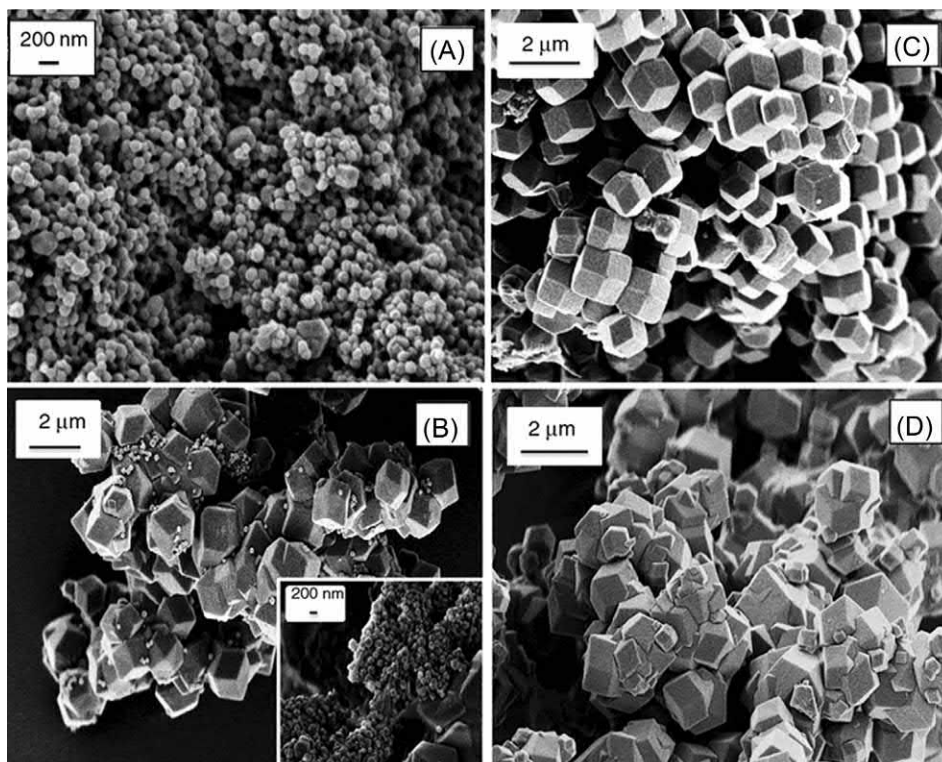
Microwave activation of the reaction mixture is an effective way to promote the nucleation of the entire volume of the reactor, especially when compared to conventional heating methods. Because heat is evenly distributed, a complete dissolution of the reagents is achieved in a short time, resulting in a high nucleation density. These factors contribute to the short reaction times and reduced crystal size (by promoting nucleation over crystal growth). In this section we give examples of how MWAS parameters affect the preparation of MOFs. For a comprehensive review of the subject, the reader is referred to the work of Thomas-Hillman et al. [17].

Reaction time decrease prompted by MWAS when compared with other conventional heating methods is well-known and viewed as one of its main assets. As presented previously, the first reported synthesis using MWAS by Jung et al. [2] allowed a considerable reduction of reaction time of MIL-100 from 4 days (using HT synthesis) to just 4 h, maintaining the same reaction yield. Recently, Pourebrahimi and Kazemeini reported that the HT synthesis of MIL-101(Cr) at 220°C took 8 h, and less than 1 h by MWAS [18]. Jurcic et al. obtained [Zn(dcbpy)(DMF)]·DMF (H<sub>2</sub>dcbpy = 2,2'-bipyridine-4,4'-dicarboxylic acid) in just 2 min (four 30s cycles), a considerable reduction when compared with 6 days at 100°C using conventional heating [19].

Reaction time reduction is achieved because, under microwave radiation, nucleation is favored over crystal growth. It is, thus, not surprising that one of the consequences of using MWAS is the concomitant reduction of crystal size. This is one of the reasons why conventional heating methods have been extensively used for preparing MOFs: relatively large crystals are required for single-crystal X-ray diffraction. The advent of nanotechnology and the improvement of the new single-crystal diffractometers made MWAS more appealing. Chen et al. have reported the size reduction and morphology change in the MWAS preparation of a moisture-stable MOF, Co-PL-1 ([Co(Imda)(4,4'-bpy)] (where Imda = imidazole-4,5-dicarboxylic acid and 4,4'-bpy = co-ligand 4,4'-bipyridyl) [20]. MWAS reduced the reaction time from 3 days (conventional HT) to just 30 min. Crystals obtained by HT presented a nanorod shape (size  $\sim 350$  nm), while those obtained by MWAS were cubic-shaped with size  $\sim 100$  nm. The size decrease resulted in an increase in CO<sub>2</sub> adsorption. Similar results were reported by He et al. [21]: MOF-74 synthesized with nickel was obtained using OP, HT, and MWAS; while the decrease of reaction time was evident (from 32 h by OP to 1 h), the products obtained by MWAS had a smaller size with a more uniform distribution and presented a better CO<sub>2</sub> capture even in a humid environment. Chalati et al., on the other hand, studied the HT and MWAS conditions to obtain MIL-88A (prepared by the self-assembly of Fe<sup>3+</sup> ions with fumaric acid) with different sizes [22]. In the case of MWAS, different temperatures (50°C, 80°C, and 100°C for 2 min) and different reaction times (1, 2, 5, and 10 min at 80°C) were tested. The MOF crystal size (10 to 150 nm) increased with both the increase of reaction time and temperature.

The crystal size of MOFs may also be tuned from the micro to nanometer range. Marti et al. reported the MWAS synthesis of a substituted imidazolate material (SIM-1) at 85°C and different reaction times (15 min, 1, 2, and 3 h) [23]. At 15 min of reaction time, ca. 240 nm agglomerates of cubic-shaped material are obtained. With increasing reaction time, the morphology is preserved, but the cubic crystal size ranges from ca. 1.49 to 2.5  $\mu\text{m}$  (Fig. 8.5). A similar result was recently reported concerning the synthesis of the nanosized medi-MOF-1 (Zn<sup>2+</sup>-curcumin) [24]. While temperature has a small effect on the crystal size (synthesis temperatures in the range 100–180°C), increasing the reaction time (from 5 to 10 min at 130°C) increases the crystal size (Fig. 8.6).

The preparation of pure-phase MOFs is often a challenge. Because different crystalline phases can be obtained using the same precursors (and in some cases very similar experimental conditions), it is very common to obtain mixtures of two or more compounds. MWAS offers the possibility to quickly test a range of experimental conditions and optimize the synthesis process. For example, Babu et al. reported UMCM-15 which contains three different organic linkers: 1,4-benzenedicarboxylic acid, 2,6-naphthalenedicarboxylic acid, and 4,4'-bipyridine, self-assembled with Zn<sup>2+</sup> ions [25]. While the pure-phase could be obtained under solvothermal conditions at 85°C for 32 h, MWAS afforded UMCM-15 in just 5 min, albeit with some impurity. Increasing the reaction time to 20 min provided the pure MOF. Jhung et al. showed



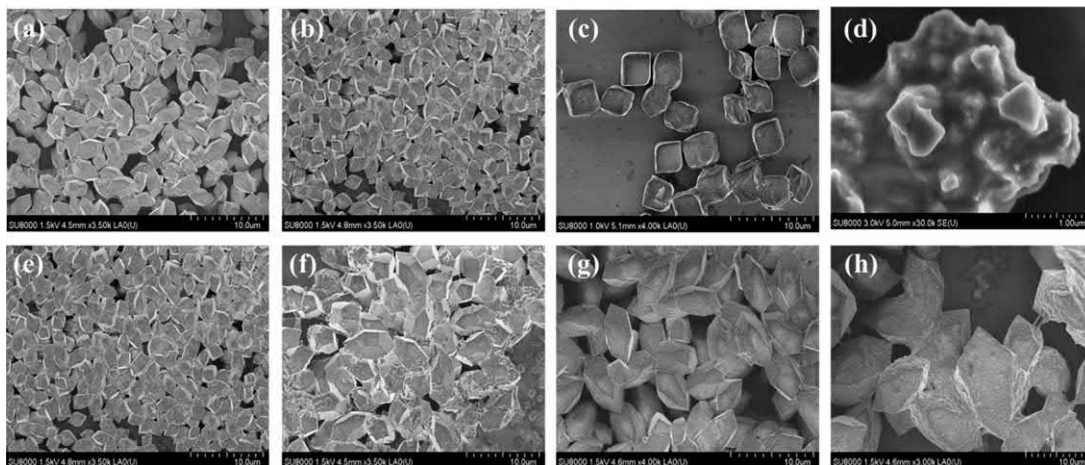
**Fig. 8.5**

SEM images of SIM-1 synthesized by MWAS at different reaction times: (A) 15 min, (B) 1 h, (C) 2 h, and (D) 3 h. Reproduced with permission from A.M. Marti, M. Van, K.J. Balkus, *Tuning the crystal size and morphology of the substituted imidazole material, SIM-1*, *J. Porous. Mater.* 21(6) (2014) 889–902.

that MWAS may be an efficient tool to prepare new MOFs, not previously obtained by conventional HT synthesis [26]. Under MWAS, a nickel glutarate MOF,  $[\text{Ni}_{22}(\text{C}_5\text{H}_6\text{O}_4)_{20}(\text{OH})_4(\text{H}_2\text{O})_{10}] \cdot 38\text{H}_2\text{O}$ , is obtained by MWAS, while  $[\text{Ni}_{20}(\text{C}_5\text{H}_6\text{O}_4)_{20}(\text{H}_2\text{O})_8] \cdot 40\text{H}_2\text{O}$  (MIL-77) is obtained using similar HT conditions. The former material is thought to be so thermodynamically stable that MIL-77 is preferentially obtained at short reaction time. In fact, even in MWAS conditions, as the temperature and reaction time increase, a mixture of the two materials is obtained. Similar results were obtained by Khan et al. in the preparation of a series of Al-benzenetricarboxylic acid MOFs [27]. Two porous MOFs, MIL-100 and MIL-96, were obtained by MWAS: MIL-100 was obtained after only 1 min, contaminated with a small amount of MIL-96; increasing the reaction time to 30–60 min, MIL-96 is instead isolated as a pure-phase.

Although MWAS allows screening the optimal experimental conditions, only few research groups have effectively explored this possibility. Silva et al. studied the synthesis of  $[\text{Ce}_2(\text{pydc})_3(\text{H}_2\text{O})_2]$  (where  $\text{H}_2\text{pydc} = 2,5\text{-pyridinedicarboxylic acid}$ ) and screened different

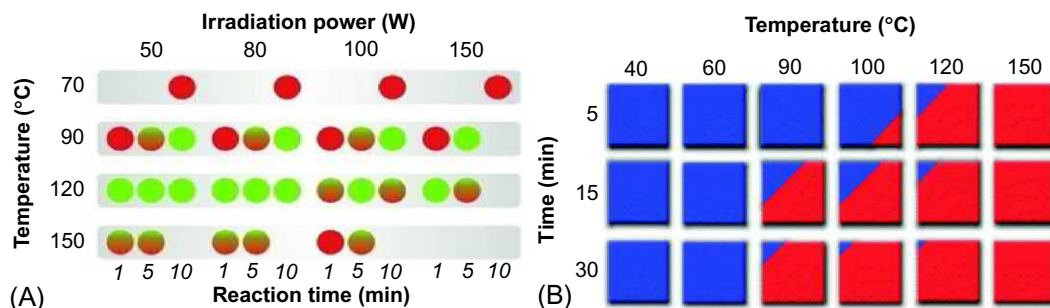




**Fig. 8.6**

SEM images of medi-MOF-1 obtained by MWAS at different temperatures: (A) 100°C, (B) 130°C, (C) 150°C, (D) 180°C, for 5 min, and at 130°C for (E) 5 min, (F) 6 min, (G) 7 min, (H) 10 min, respectively. *Reproduced with permission from X. Feng, Y. Wang, F. Muhammad, F. Sun, Y. Tian, G. Zhu, Size, shape, and porosity control of Medi-MOF-1 via growth modulation under microwave heating, Cryst. Growth Des. 19(2) (2019) 889–895.*

conditions of temperature (70°C, 90°C, 120°C, and 150°C), reaction time (1, 5, and 10 min), and irradiation power (50, 80, 100, and 150 W) [28]. Pure  $[\text{Ce}_2(\text{pydc})_3(\text{H}_2\text{O})_2]$  could be obtained using two different sets of conditions: 120°C and 1 min reaction time (irradiation power < 100W); or 90°C and 10 min of reaction (Fig. 8.7A). The same group later reported



**Fig. 8.7**

(A) Diagram for MWAS optimization of the synthesis of  $[\text{Ce}_2(\text{pydc})_3(\text{H}_2\text{O})_2]$ . *red*: absence of the desired material or amorphous phase; *green*: pure  $[\text{Ce}_2(\text{pydc})_3(\text{H}_2\text{O})_2]$ . (B) MWAS optimization of the reaction temperature and time to obtain  $[\text{La}_2(\text{H}_3\text{bmt})(\text{H}_5\text{bmt})(\text{H}_2\text{O})_2] \cdot 3\text{H}_2\text{O}$  (*blue*) and  $[\text{La}_2(\text{H}_3\text{bmt})_2(\text{H}_2\text{O})_2] \cdot \text{H}_2\text{O}$  (*red*). *Reproduced with permission from P. Silva, D. Ananias, S.M. Bruno, A.A. Valente, L.D. Carlos, J. Rocha, F.A. A. Paz, Photoluminescent metal-organic frameworks—rapid preparation, catalytic activity, and framework relationships, Eur. J. Inorg. Chem. 2013(32) (2013) 5576–5591; S.M.F. Vilela, A.D.G. Firmino, R.F. Mendes, J.A. Fernandes, D. Ananias, A.A. Valente, H. Ott, L.D. Carlos, J. Rocha, J.P.C. Tomé, F.A.A. Paz, Lanthanide-polyphosphonate coordination polymers combining catalytic and photoluminescence properties, Chem. Commun. 49(57) (2013) 6400–6402.*



similar results in the preparation of a lamellar compound,  $[\text{La}(\text{H}_6\text{nmp})]$  (where  $\text{H}_6\text{nmp}$  = nitrilotrimethylphosphonic acid) [29]. A mixture of this compound and  $[\text{La}(\text{H}_3\text{nmp})]\cdot 1.5\text{H}_2\text{O}$  [30] or other unknown materials was obtained at  $120^\circ\text{C}$ . A pure compound was isolated by either increasing the irradiation power (from 50 to 70 W, 10 min reaction time) or by increasing the temperature (to  $140^\circ\text{C}$ ). Vilela et al. investigated the influence of temperature on the MWAS of  $[\text{La}(\text{H}_4\text{bmt})(\text{H}_5\text{bmt})(\text{H}_2\text{O})_2]\cdot 3\text{H}_2\text{O}$  and  $[\text{La}_2(\text{H}_3\text{bmt})_2(\text{H}_2\text{O})_2]\cdot \text{H}_2\text{O}$  (where  $\text{H}_6\text{bmt}$  = benzene-1,3,5-triyltris(methylene)triphosphonic acid) [31]. As depicted in Fig. 8.7B, despite the reaction time used,  $[\text{La}(\text{H}_4\text{bmt})(\text{H}_5\text{bmt})(\text{H}_2\text{O})_2]\cdot 3\text{H}_2\text{O}$  can be obtained at  $40^\circ\text{C}$  or  $60^\circ\text{C}$ , while pure  $[\text{La}_2(\text{H}_3\text{bmt})_2(\text{H}_2\text{O})_2]\cdot \text{H}_2\text{O}$  is preferentially obtained at  $150^\circ\text{C}$ . It is also possible to observe a transition of one compound to the other upon temperature increase.

Although the preparation of MOFs by MWAS has incremented in the last decade, a long road still lies ahead. A better understanding regarding the influence of each synthesis parameter, namely the temperature, reaction time, and pressure, needs to be gained if we are to use the full potential of MWAS in MOF synthesis.

### 8.3.2 Postsynthetic modifications

The biomedical applications of MOFs are attracting increasing interest, partially because their large nanoporosity endows them with drug-delivery properties [32, 33]. In this context, challenges arise concerning controlling the drug amounts delivered and the release rates, and one way of dealing with these issues is using postsynthetic modifications [34–37]. In this process, certain MOFs' components are modified after the material is prepared. Microwave heating has been used, for example, to incorporate nanoparticles (to increasing the catalytic performance) [38, 39], to modify the organic linkers (to incorporate new active groups for detection or catalysis) [40], or to exchange cations [41].

Most functionalization by microwave radiation normally targets organic reactions performed on the organic linkers. For instance, the group of Yaghi used this approach to deprotect certain amino-bearing linkers: Mg-bearing IRMOF-74-III was prepared with 2',5'-dimethyl-3,3''-dihydroxy-[1,1':4',1''-terphenyl]-4,4''-dicarboxylic acid. The latter was functionalized with six different substituents by conventional HT synthesis [42], but, as an example, we will here focus only on the functionalization with  $-\text{CH}_2\text{NHBoc}$  and  $-\text{CH}_2\text{NMeBoc}$  (Boc = tertbutyloxycarbonyl). The Boc protecting group was used to introduce  $-\text{CH}_2\text{NH}_2$  and  $-\text{CH}_2\text{NHMe}$  into IRMOF-74-III, as unprotected amines react with magnesium. While the synthesis of the MOFs used hydrothermal conditions at  $120^\circ\text{C}$  for 20 h, the deprotection of the amine group was achieved via microwave irradiation ( $230^\circ\text{C}$ , 10 min), with no need for drastic conditions (strong acids for example), which may lead to MOFs' framework collapse [43, 44]. More recently, the same approach was used to deprotect the amine group of Boc, allowing the continuous postfunctionalization of IRMOF-74-III with different amino acids (Fig. 8.8) [45]. This incorporation of several amino acids was only possible using this microwave approach, which preserves the

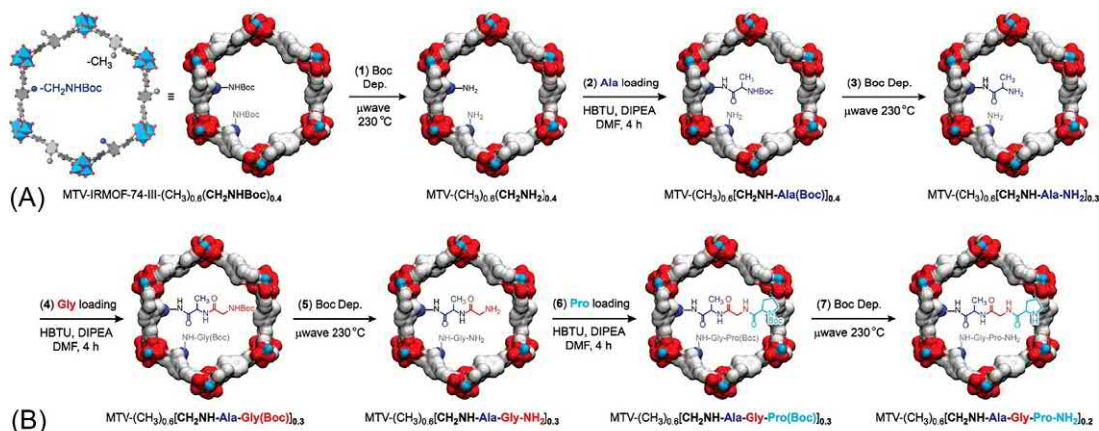


Fig. 8.8

(A) Polyhedral representation of the —CH<sub>2</sub>NHBoc functionalized IRMOF-74-III pore.

(B) Postsynthetic modifications (1)–(7) are illustrated using a van der Waals surface: thermal Boc deprotections using microwave radiation for (1), (3), (5), and (7); amino acid loading steps for (2), (4), and (6) (Ala, Gly, and Pro, respectively). The evolution of one potential reaction by-product (dipeptide H<sub>2</sub>N-Pro-Gly-CONHL) is represented in gray. Due to incomplete postsynthetic transformations, these by-products also affect the molecular formula of the compounds.

Reproduced with permission from A.M. Fracaroli, P. Siman, D.A. Nagib, M. Suzuki, H. Furukawa, F.D. Toste, O.M. Yaghi, Seven post-synthetic covalent reactions in tandem leading to enzyme-like complexity within metal-organic framework crystals, *J. Am. Chem. Soc.* 138(27) (2016) 8352–8355.

material crystallinity even after 4 cycles of deprotection/amino acid incorporation.

In another report, this deprotection was used to improve CO<sub>2</sub> adsorption under dry and humid conditions [46].

Another striking example of amine-bearing MOF functionalized using MWAS is that of NH<sub>2</sub>-MIL-53. This material was functionalized with various alkyl halides, with the aim of being used as a catalyst in the cycloaddition of epoxides and CO<sub>2</sub> under solvent-free conditions [47]. Kim et al. adopted the microwave method for the postfunctionalization of a UiO-66 analog, prepared using the 1,4-benzenedicarboxylate bromide functionalized linker instead [48]. The MOF was then functionalized via a nucleophilic substitution with a cyano group. Although this modification could be performed by conventional HT synthesis at 140°C for 24 h, with 40 % of yield, MWAS surpasses this benchmark after only 10 min at 170°C, with an impressive yield of 90%.

Postsynthetic modification of auxiliary MOFs linker can also be accomplished.

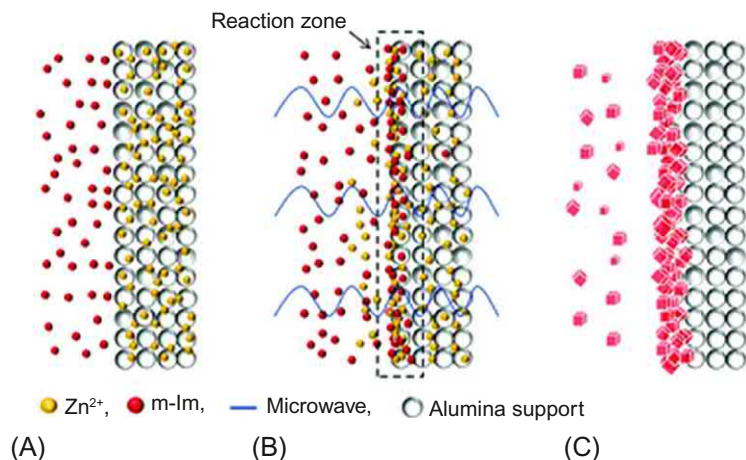
Hindelang et al. prepared a Zn-bearing MOF using 9,10-triptycenedicarboxylic acid and 3,3'-dimethyl-4,4'-bipyridine (the latter acting as a pillar linker) under microwave conditions (60°C, 10 min) [49]. After a postsynthetic epoxidation to introduce oxirane groups, a nucleophilic ring-opening with ethyl mercaptan was carried out by microwave radiation (140°C, 6 h).

Although many of these postsynthetic modifications of MOFs are directed to improvements in the areas of gas sorption, with the continuous improvement of synthetic organic reactions, more specifically in organic reactions with bio-molecules (amino acids, proteins, etc.), it is evident that microwave radiation will be an important tool in the future to functionalize MOFs.

### 8.3.3 MOF film/membrane preparation

The large number of MOFs reported and their proof-of-concept applications are translating research efforts into real-world industrial applications. In this context, research into the preparation of thin films and membranes of MOFs gained a considerable momentum in the last 5 years.

ZIF-8 has been the most used MOF in thin films and membranes, mainly due to the great potential of this material for gas adsorption and separation. Kwon et al. have successfully grown a thin film of ZIF-8 on a porous alumina ( $\alpha$ -Al<sub>2</sub>O<sub>3</sub>) support through a seeding method (Fig. 8.9). The support was immersed in a solution containing the metal precursor (zinc nitrate) and transferred to a solution of the organic linker. Rapid crystal formation was promoted by microwave radiation (100 W, 1.5 min) [50]. According to the authors, a high concentration of the precursors near the support should be maintained by soaking the support with the metal ions prior to the application of microwave radiation. Moreover, the metal ions readily absorb the microwave radiation, leading to a localized temperature increase which promotes the rapid



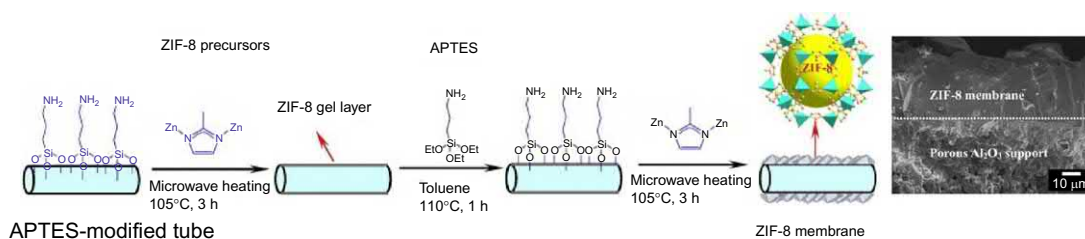
**Fig. 8.9**

Schematic representation of a microwave-assisted seeding process: (A) support saturated with a Zn<sup>2+</sup> solution in a ligand solution; (B) formation of a reaction zone at the interface under microwave irradiation; and (C) heterogeneous nucleation near the support's surface. Reproduced with permission from H.T. Kwon, H.K. Jeong, Highly propylene-selective supported zeolite-imidazolate framework (ZIF-8) membranes synthesized by rapid microwave-assisted seeding and secondary growth, *Chem. Commun.* 49(37) (2013) 3854–3856.

formation of ZIF-8 nanocrystals. The same group used this approach, called microwave-induced thermal deposition, in which an electrically conductive layer of MOF-5 (also known as IRMOF-1) forms on the surface of the support. The resulting thin film acts as seeds for a membrane produced by secondary growth, under conventional hydrothermal conditions [51]. However, the seeding and growth method using microwave radiation (first case) is advantageous because no conductive surface layers are required, increasing the number of different MOFs that may be deposited and improving the membrane's mechanical stability. The increase of the localized temperature, caused by the interaction of the metal ions with the microwave radiation, leads to a better attachment of the seed crystals onto the support, resulting in more homogeneous and reproducible films and membranes than those attained by conventional seeding methods. The method was also employed to other MOFs, such as ZIF-7 and SIM-1, ultimately proving its wider applicability.

ZIF-8 membranes were reported by Zhu et al. [52]. Alumina tubes were modified with 3-aminopropyltriethoxysilane (APTES) which formed a monolayer on the surface of the support. The modified alumina tubes were then immersed in a methanol solution containing the two precursors and heated at 105°C under microwave radiation for 3 h (Fig. 8.10). To obtain a denser and more uniform ZIF-8 membrane, APTES modification and microwave synthesis may be repeated. These membranes show potential for high hydrogen permselectivity (preferential permeation of certain ionic species through ion-exchange membranes), with mixture separation factors for  $H_2/CH_4$  and  $H_2/C_3H_8$  of *ca.* 44 and 329, some of the highest values reported for MOFs membranes. The same group reported materials for  $CO_2/CH_4$  separation using this membrane preparation method [53].

A different approach for preparing thin films of ZIF-8 and MIL-53 was proposed by Bechelany et al. [54]. Polymer nanofibers were used as support and, instead of immersing the fibers in the metal solution, a zinc oxide film was deposited by atomic layer deposition. The coated fibers were immersed in the linker solution at 100°C for 1.5 h under microwave radiation.



**Fig. 8.10**

Schematic representation of the preparation and a field emission scanning electron microscopy (FESEM) cross-section image of a tubular ZIF-8 membrane by repeated APTES modification and microwave synthesis on alumina tube. Adapted with permission from Y.Q. Zhu, Q. Liu, J. Caro, A.S. Huang, *Highly hydrogen-permselective zeolitic imidazolate framework ZIF-8 membranes prepared on coarse and macroporous tubes through repeated synthesis*, *Sep. Purif. Technol.* 146 (2015) 68–74.

This approach led to the formation of a layer of large ZIF-8 crystals which homogeneously covers the entire nanofibers. A similar approach was reported by Li et al., which used a zinc plate as a sacrificial template for the formation of  $[\text{Zn}_3(\text{BTC})_2]$  [55]. The thin films were obtained by MWAS and film thickness was controlled by the reaction time, with higher reaction times (5–30 min) originating crystals with larger sizes (200 nm–100  $\mu\text{m}$ ).

## 8.4 Concluding remarks

Microwave-assisted synthesis has seen a considerable development in recent years. Although this method has been much used for promoting organic and inorganic reactions, other areas of synthetic chemistry are ripping the benefits that a microwave apparatus may bring, such as shorter reaction times, increased product yield and purity, and smaller particle size. The interest of this methodology for the preparation of metal-organic frameworks has also been shown. It allows screening a large number of experimental conditions in a relatively short time, affording a precise control of purity and crystal size and morphology. Microwave-assisted synthesis also opens up new avenues for MOF postsynthetic modification and the fabrication of films and membranes using mild conditions that preserve the framework's integrity.

The range of commercially available microwave synthesis equipment allows the precise control of temperature, pressure, and reaction time, enabling rapid heating and decreased energy costs. It is, thus, no surprise that the number of studies reporting its use is ever increasing considerably.

## Acknowledgments

This work was developed within the scope of the project CICECO-Aveiro Institute of Materials, FCT Ref. UID/CTM/50011/2019, financed by national funds through the FCT/MCTES, and the project "Smart Green Homes—BOSCH" (POCI-010247-FEDER-007678). RFM gratefully acknowledges FCT for a Junior Research Position (CEECIND/00553/2017).

## References

- [1] P. Silva, S.M.F. Vilela, J.P.C. Tomé, F.A.A. Paz, Multifunctional metal-organic frameworks: from academia to industrial applications, *Chem. Soc. Rev.* 44 (19) (2015) 6774–6803.
- [2] S.H. Jung, J.H. Lee, J.S. Chang, Microwave synthesis of a nanoporous hybrid material, chromium trimesate, *Bull. Kor. Chem. Soc.* 26 (6) (2005) 880–881.
- [3] W.B. Liang, D.M. D'Alessandro, Microwave-assisted solvothermal synthesis of zirconium oxide based metal-organic frameworks, *Chem. Commun.* 49 (35) (2013) 3706–3708.
- [4] X.F. Wang, Y.B. Zhang, H. Huang, J.P. Zhang, X.M. Chen, Microwave-assisted solvothermal synthesis of a dynamic porous metal-carboxylate framework, *Cryst. Growth Des.* 8 (12) (2008) 4559–4563.
- [5] J.S. Choi, W.J. Son, J. Kim, W.S. Ahn, Metal-organic framework MOF-5 prepared by microwave heating: factors to be considered, *Microporous Mesoporous Mater.* 116 (1–3) (2008) 727–731.
- [6] N.A. Khan, S.H. Jung, Facile syntheses of metal-organic framework  $\text{Cu}_3(\text{BTC})_2(\text{H}_2\text{O})_3$  under ultrasound, *Bull. Kor. Chem. Soc.* 30 (12) (2009) 2921–2926.



- [7] L. Bromberg, Y. Diao, H.M. Wu, S.A. Speakman, T.A. Hatton, Chromium(III) terephthalate metal organic framework (MIL-101): HF-free synthesis, structure, polyoxometalate composites, and catalytic properties, *Chem. Mater.* 24 (9) (2012) 1664–1675.
- [8] K.M.L. Taylor-Pashow, J. Della Rocca, Z.G. Xie, S. Tran, W.B. Lin, Postsynthetic modifications of iron-carboxylate nanoscale metal-organic frameworks for imaging and drug delivery, *J. Am. Chem. Soc.* 131 (40) (2009) 14261.
- [9] N.A. Khan, J.W. Jun, J.H. Jeong, S.H. Jung, Remarkable adsorptive performance of a metal-organic framework, vanadium-benzenedicarboxylate (MIL-47), for benzothiophene, *Chem. Commun.* 47 (4) (2011) 1306–1308.
- [10] J. Jia, F.J. Xu, Z. Long, X.D. Hou, M.J. Sepaniak, Metal-organic framework MIL-53(Fe) for highly selective and ultrasensitive direct sensing of MeHg<sup>+</sup>, *Chem. Commun.* 49 (41) (2013) 4670–4672.
- [11] W.B. Liang, R. Babarao, D.M. D’Alessandro, Microwave-assisted solvothermal synthesis and optical properties of tagged MIL-140A metal-organic frameworks, *Inorg. Chem.* 52 (22) (2013) 12878–12880.
- [12] M.Y. Ma, A. Betard, I. Weber, N.S. Al-Hokbany, R.A. Fischer, N. Metzler-Nolte, Iron-based metal-organic frameworks MIL-88B and NH<sub>2</sub>-MIL-88B: high quality microwave synthesis and solvent-induced lattice “breathing” *Cryst. Growth Des.* 13 (6) (2013) 2286–2291.
- [13] Y.R. Lee, M.S. Jang, B.Y. Cho, H.J. Kwon, S. Kim, W.S. Ahn, ZIF-8: a comparison of synthesis methods, *Chem. Eng. J.* 271 (2015) 276–280.
- [14] H.Y. Cho, D.A. Yang, J. Kim, S.Y. Jeong, W.S. Ahn, CO<sub>2</sub> adsorption and catalytic application of Co-MOF-74 synthesized by microwave heating, *Catal. Today* 185 (1) (2012) 35–40.
- [15] E. Haque, S.H. Jung, Synthesis of isostructural metal-organic frameworks, CPO-27s, with ultrasound, microwave, and conventional heating: effect of synthesis methods and metal ions, *Chem. Eng. J.* 173 (3) (2011) 866–872.
- [16] M. Taddei, P.V. Dau, S.M. Cohen, M. Ranocchiari, J.A. van Bokhoven, F. Costantino, S. Sabatini, R. Vivani, Efficient microwave assisted synthesis of metal-organic framework UiO-66: optimization and scale up, *Dalton Trans.* 44 (31) (2015) 14019–14026.
- [17] I. Thomas-Hillman, A. Laybourn, C. Dodds, S.W. Kingman, Realising the environmental benefits of metal-organic frameworks: recent advances in microwave synthesis, *J. Mater. Chem. A* 6 (25) (2018) 11564–11581.
- [18] S. Pourebrahimi, M. Kazemini, A kinetic study of facile fabrication of MIL-101(Cr) metal-organic framework: effect of synthetic method, *Inorg. Chim. Acta* 471 (2018) 513–520.
- [19] M. Jurcic, W.J. Peveler, C.N. Savory, D.O. Scanlon, A.J. Kenyon, I.P. Parkin, The vapour phase detection of explosive markers and derivatives using two fluorescent metal-organic frameworks, *J. Mater. Chem. A* 3 (12) (2015) 6351–6359.
- [20] C. Chen, Q.B. Jiang, H.F. Xu, Z. Lin, Highly efficient synthesis of a moisture-stable nitrogen-abundant metal-organic framework (MOF) for large-scale CO<sub>2</sub> capture, *Ind. Eng. Chem. Res.* 58 (4) (2019) 1773–1777.
- [21] C.W. Chen, X.B. Feng, Q. Zhu, R. Dong, R. Yang, Y. Cheng, C. He, Microwave-assisted rapid synthesis of well-shaped MOF-74 (Ni) for CO<sub>2</sub> efficient capture, *Inorg. Chem.* 58 (4) (2019) 2717–2728.
- [22] T. Chalati, P. Horcajada, R. Gref, P. Couvreur, C. Serre, Optimisation of the synthesis of MOF nanoparticles made of flexible porous iron fumarate MIL-88A, *J. Mater. Chem.* 21 (7) (2011) 2220–2227.
- [23] A.M. Marti, M. Van, K.J. Balkus, Tuning the crystal size and morphology of the substituted imidazole material, SIM-1, *J. Porous Mater.* 21 (6) (2014) 889–902.
- [24] X. Feng, Y. Wang, F. Muhammad, F. Sun, Y. Tian, G. Zhu, Size, shape, and porosity control of Medi-MOF-1 via growth modulation under microwave heating, *Cryst. Growth Des.* 19 (2) (2019) 889–895.
- [25] R. Babu, S.H. Kim, A.C. Kathalikkattil, R.R. Kuruppathparambil, D.W. Kim, S.J. Cho, D.W. Park, Aqueous microwave-assisted synthesis of non-interpenetrated metal-organic framework for room temperature cycloaddition of CO<sub>2</sub> and epoxides, *Appl. Catal. A Gen.* 544 (2017) 126–136.
- [26] S.H. Jung, J.H. Lee, P.M. Forster, G. Férey, A.K. Cheetham, J.S. Chang, Microwave synthesis of hybrid inorganic-organic porous materials: phase-selective and rapid crystallization, *Chem. Eur. J.* 12 (30) (2006) 7899–7905.



- [27] N.A. Khan, J.S. Lee, J. Jeon, C.H. Jun, S.H. Jung, Phase-selective synthesis and phase-conversion of porous aluminum-benzenetricarboxylates with microwave irradiation, *Microporous Mesoporous Mater.* 152 (2012) 235–239.
- [28] P. Silva, D. Ananias, S.M. Bruno, A.A. Valente, L.D. Carlos, J. Rocha, F.A.A. Paz, Photoluminescent metal-organic frameworks—rapid preparation, catalytic activity, and framework relationships, *Eur. J. Inorg. Chem.* 2013 (32) (2013) 5576–5591.
- [29] P. Silva, F. Vieira, A.C. Gomes, D. Ananias, J.A. Fernandes, S.M. Bruno, R. Soares, A.A. Valente, J. Rocha, F.A.A. Paz, Thermal transformation of a layered multifunctional network into a metal-organic framework based on a polymeric organic linker, *J. Am. Chem. Soc.* 133 (38) (2011) 15120–15138.
- [30] L. Cunha-Silva, L. Mafra, D. Ananias, L.D. Carlos, J. Rocha, F.A.A. Paz, Photoluminescent lanthanide-organic 2D networks: a combined synchrotron powder X-ray diffraction and solid-state NMR study, *Chem. Mater.* 19 (14) (2007) 3527–3538.
- [31] S.M.F. Vilela, A.D.G. Firmino, R.F. Mendes, J.A. Fernandes, D. Ananias, A.A. Valente, H. Ott, L.D. Carlos, J. Rocha, J.P.C. Tomé, F.A.A. Paz, Lanthanide-polyphosphonate coordination polymers combining catalytic and photoluminescence properties, *Chem. Commun.* 49 (57) (2013) 6400–6402.
- [32] S. Beg, M. Rahman, A. Jain, S. Saini, P. Midoux, C. Pichon, F.J. Ahmad, S. Akhter, Nanoporous metal organic frameworks as hybrid polymer-metal composites for drug delivery and biomedical applications, *Drug Discov. Today* 22 (4) (2017) 625–637.
- [33] L. Wang, M. Zheng, Z.G. Xie, Nanoscale metal-organic frameworks for drug delivery: a conventional platform with new promise, *J. Mater. Chem. B* 6 (5) (2018) 707–717.
- [34] S.M. Cohen, Modifying MOFs: new chemistry, new materials, *Chem. Sci.* 1 (1) (2010) 32–36.
- [35] K.K. Tanabe, S.M. Cohen, Postsynthetic modification of metal-organic frameworks—a progress report, *Chem. Soc. Rev.* 40 (2) (2011) 498–519.
- [36] Z.Q. Wang, S.M. Cohen, Postsynthetic modification of metal-organic frameworks, *Chem. Soc. Rev.* 38 (5) (2009) 1315–1329.
- [37] Z. Yin, S. Wan, J. Yang, M. Kurmoo, M.H. Zeng, Recent advances in post-synthetic modification of metal-organic frameworks: new types and tandem reactions, *Coord. Chem. Rev.* 378 (2019) 500–512.
- [38] M.S. El-Shall, V. Abdelsayed, A. Khder, H.M.A. Hassan, H.M. El-Kaderi, T.E. Reich, Metallic and bimetallic nanocatalysts incorporated into highly porous coordination polymer MIL-101, *J. Mater. Chem.* 19 (41) (2009) 7625–7631.
- [39] M. Montazerolghaem, S.F. Aghamiri, S. Tangestaninejad, M.R. Talaie, A metal-organic framework MIL-101 doped with metal nanoparticles (Ni & Cu) and its effect on CO<sub>2</sub> adsorption properties, *RSC Adv.* 6 (1) (2016) 632–640.
- [40] J. Bonnefoy, A. Legrand, E.A. Quadrelli, J. Canivet, D. Farrusseng, Enantiopure peptide-functionalized metal-organic frameworks, *J. Am. Chem. Soc.* 137 (29) (2015) 9409–9416.
- [41] J.P. Tu, X.L. Zeng, F.J. Xu, X. Wu, Y.F. Tian, X.D. Hou, Z. Long, Microwave-induced fast incorporation of titanium into UiO-66 metal-organic frameworks for enhanced photocatalytic properties, *Chem. Commun.* 53 (23) (2017) 3361–3364.
- [42] A.M. Fracaroli, H. Furukawa, M. Suzuki, M. Dodd, S. Okajima, F. Gandara, J.A. Reimer, O.M. Yaghi, Metal-organic frameworks with precisely designed interior for carbon dioxide capture in the presence of water, *J. Am. Chem. Soc.* 136 (25) (2014) 8863–8866.
- [43] G.L. Stahl, R. Walter, C.W. Smith, General procedure for synthesis of mono-N-acylated 1,6-diaminohexanes, *J. Org. Chem.* 43 (11) (1978) 2285–2286.
- [44] M. Prashad, D. Har, B. Hu, H.Y. Kim, M.J. Girgis, A. Chaudhary, O. Repic, T.J. Blacklock, Process development of a large-scale synthesis of TKA731: a tachykinin receptor antagonist, *Org. Process Res. Dev.* 8 (3) (2004) 330–340.
- [45] A.M. Fracaroli, P. Siman, D.A. Nagib, M. Suzuki, H. Furukawa, F.D. Toste, O.M. Yaghi, Seven post-synthetic covalent reactions in tandem leading to enzyme-like complexity within metal-organic framework crystals, *J. Am. Chem. Soc.* 138 (27) (2016) 8352–8355.

- [46] R.W. Faig, T.M.O. Popp, A.M. Fracaroli, E.A. Kapustin, M.J. Kalmutzki, R.M. Altamimi, F. Fathieh, J.A. Reimer, O.M. Yaghi, The chemistry of CO<sub>2</sub> capture in an amine-functionalized metal-organic framework under dry and humid conditions, *J. Am. Chem. Soc.* 139 (35) (2017) 12125–12128.
- [47] H.G. Seok, D.W. Kim, J.G. Yang, M.I. Kim, D.W. Park, Catalytic performance of microwave functionalized NH<sub>2</sub>-MIL-53 for cyclic carbonate synthesis from CO<sub>2</sub> and epoxides, *J. Nanosci. Nanotechnol.* 16 (5) (2016) 4612–4619.
- [48] M. Kim, S.J. Garibay, S.M. Cohen, Microwave-assisted cyanation of an aryl bromide directly on a metal-organic framework, *Inorg. Chem.* 50 (3) (2011) 729–731.
- [49] K. Hindelang, S.I. Vagin, C. Anger, B. Rieger, Tandem post-synthetic modification for functionalized metal-organic frameworks via epoxidation and subsequent epoxide ring-opening, *Chem. Commun.* 48 (23) (2012) 2888–2890.
- [50] H.T. Kwon, H.K. Jeong, Highly propylene-selective supported zeolite-imidazolate framework (ZIF-8) membranes synthesized by rapid microwave-assisted seeding and secondary growth, *Chem. Commun.* 49 (37) (2013) 3854–3856.
- [51] Y. Yoo, Z.P. Lai, H.K. Jeong, Fabrication of MOF-5 membranes using microwave-induced rapid seeding and solvothermal secondary growth, *Microporous Mesoporous Mater.* 123 (1–3) (2009) 100–106.
- [52] Y.Q. Zhu, Q. Liu, J. Caro, A.S. Huang, Highly hydrogen-permselective zeolitic imidazolate framework ZIF-8 membranes prepared on coarse and macroporous tubes through repeated synthesis, *Sep. Purif. Technol.* 146 (2015) 68–74.
- [53] Y.Q. Zhu, Q. Liu, A.S. Huang, Microwave synthesis of tubular zeolitic imidazolate framework ZIF-8 membranes for CO<sub>2</sub>/CH<sub>4</sub> separation, *Sep. Sci. Technol.* 51 (5) (2016) 883–891.
- [54] M. Bechelany, M. Drobek, C. Vallicari, A. Abou Chaaya, A. Julbe, P. Miele, Highly crystalline MOF-based materials grown on electrospun nanofibers, *Nanoscale* 7 (13) (2015) 5794–5802.
- [55] Z.Q. Li, M. Zhang, B. Liu, C.Y. Guo, M. Zhou, Rapid fabrication of metal-organic framework thin films using in situ microwave irradiation and its photocatalytic property, *Inorg. Chem. Commun.* 36 (2013) 241–244.

### ***Further reading***

J.-S. Schanche, Microwave synthesis solutions from personal chemistry, *Mol. Divers.* 7 (2) (2003) 291–298.

# Electrochemical synthesis of MOFs

Arash Ghoorchian, Abbas Afkhami, Tayyebeh Madrakian, Mazaher Ahmadi

Faculty of Chemistry, Bu-Ali Sina University, Hamedan, Iran

## Abbreviations

|                             |                                                                    |
|-----------------------------|--------------------------------------------------------------------|
| <b>1,3-H<sub>2</sub>BDC</b> | isophthalic acid                                                   |
| <b>BPDC</b>                 | 2,2'-bipyridine-5,5'-dicarboxylate                                 |
| <b>BPES</b>                 | bipolar electrosynthesis                                           |
| <b>BTC</b>                  | 1,3,5-benzenetricarboxylate (benzenetricarboxylate, trimesic acid) |
| <b>EASA</b>                 | electrochemically assisted self-assembly                           |
| <b>FTO</b>                  | fluorine-tin-oxide                                                 |
| <b>GCE</b>                  | glassy carbon electrode                                            |
| <b>H<sub>3</sub>BTC</b>     | 1,3,5-benzenetricarboxylate acid                                   |
| <b>H<sub>3</sub>TATB</b>    | 4,4',4''-s-triazine-2,4,6-triyl-tribenzoic                         |
| <b>H<sub>4</sub>BTEC</b>    | 1,2,4,5-benzenetetracarboxylate acid                               |
| <b>HBZIM</b>                | benzimidazole                                                      |
| <b>IDEs</b>                 | interdigitated electrodes                                          |
| <b>ITO</b>                  | indium tin oxide                                                   |
| <b>MOFs</b>                 | metal-organic frameworks                                           |
| <b>MTBS</b>                 | tributylmethylphosphonium methyl sulfate                           |

## 9.1 Introduction

Metal-organic frameworks (MOFs) are crystalline materials of high porosity and versatility. MOFs are formed through coordination of organic linkers around metal ions or their clusters; hence, are also known as porous coordination networks or porous coordination polymers [1]. Their structure in terms of the size of the microporous channels and moieties can be well-controlled using bottom-up synthesis approaches [2]. With proper selection of linkers, microporous channels of <2 nm in diameter can be synthesized, making them tunable molecular sieves with the ability of selective pass of certain molecules in a mixture [1]. These coordination polymers have been widely investigated since the late 1950s and early 1960s [1]. However, the MOFs field was practically relaunched at the end of the last century [1]. Since then, many efforts have been devoted to synthesis MOFs of super-high surface areas of several thousands of square of meters per gram of the material. In addition to their high

surface areas and small pores size, MOFs provide other interesting properties such as high stability, tunable structure, and functionality. By far, these porous structures have gained high attention of researchers in the development of catalysts [3], electrocatalysts [4], molecular sieves [5], and gas cargos [6] where high surface areas and tunable pore size properties are desired. Moreover, the final structure of MOFs can be tuned through appropriately choosing the metal ion and the functionalized linker, leading to a wide application of MOFs in the fields of solar cells [7], fuel cells [8], biomedicine [9], and electrochemistry [10]. For example, photoactive and conductive MOFs have been synthesized using light-harvesting linkers [11] and conductive linkers [12], respectively.

Traditionally, MOFs are synthesized using the hydrothermal method. In this method, the precursors (i.e., linker and metal ion source) are dissolved in water or an organic solvent (in solvothermal methods). Optionally, certain sacrificial templates are also dissolved in the solvent. Then, the solution is placed in an autoclave for further heating above the solvent boiling point under elevated pressures for a period of time, ranging from few hours to days to form the desired MOF structure [13]. In addition to the hydrothermal synthesis method, other alternative methods such as microwave-assisted synthesis [14–17], spray-drying method [18–21], sonochemical synthesis [22, 23], and mechanochemical method [24] have also been utilized for the synthesis of MOFs. Recently, electrochemical methods have gained high attention in the synthesis of MOFs [1]. Electrosynthesis provides some advantages over traditional methods such as mild synthesis conditions, short synthesis times, real-time alteration of the MOFs' structure, no need for metal salts and therefore separation of anions is not needed, and direct deposition of MOFs on the desired substrates [25, 26].

Although usually MOFs are synthesized in bulk form using conventional methods for certain applications such as gas storage and separation purposes, in recent years, MOFs' application has been expanded to sensors, membranes, and electronic devices where thin films of the materials are needed. Practically, MOFs should be deposited on certain substrates as thin films or coatings where their homogeneities, high porosities, and tunable thicknesses are desired in electric devices and catalytic coatings of reactors [27]. The available methods for the preparation of thin films of MOFs such as the in situ growth of MOF on bare or modified substrates [28–30], seeded growth or secondary growth [31, 32], dip-coating method [33], and layer-by-layer approach [34–36] face some drawbacks such as the occurrence of substrate corrosion and lacking control for obtaining a homogeneous coating, requirement of nano-sized MOF seeds, and complicated and time-consuming process, respectively [27]. On the other hand, the electrochemical methods enable the synthesis of thin films of MOFs on desired substrates with controllable final characteristics which can overcome the above-mentioned drawbacks. Historically, HKUST-1 was the first electrochemically synthesized MOF [37]. In this method, the metal ions were provided by anodic dissolution of a metallic electrode and thus no salt precursor was needed for the synthesis of the HKUST-1 MOF, which facilitates large-scale production of the MOF by the elimination of the anions produced by the metal salt.

Since then, there have been many developments in electrosynthesis of MOFs in terms of methodologies and electrochemical designs.

In this chapter, we will summarize the frequently used methods for the electrochemical synthesis of different MOFs on various substrates. Different electrochemical methods such as anodic dissolution, cathodic electrosynthesis, galvanic displacement, and electrophoretic deposition have been discussed in terms of the mechanisms and their strengths and shortcomings. Furthermore, different substrates such as metallic and conductive glass substrates used for electrochemical synthesis of MOFs have been discussed.

## 9.2 Electrochemical synthesis routes of thin films of MOFs

Thin films of MOFs can be synthesized and deposited on substrates of interest directly or indirectly. In the case of direct electrosynthesis methods such as anodic dissolution and reductive electrosynthesis, the MOFs are synthesized using electrochemical reaction which occurs on the surface of the electrode. In these methods, the electrochemical reaction directly results in the desired MOF. However, in the case of indirect methods such as galvanic displacement, electrophoretic deposition, and self-templated synthesis, the MOFs are synthesized using certain procedures of which the electrochemical reaction is one of the procedure steps. The main advantage of the direct methods over the indirect methods is the possibility of controlling the synthesis procedure through real-time tuning electrochemical parameters and conditions. Table 9.1 summarizes the recent application of electrochemical methods for the synthesis of MOFs. In the following section, some frequently used methods for direct or indirect electrochemical synthesis of MOFs are discussed (Fig. 9.1).

### 9.2.1 Anodic dissolution

Anodic dissolution, so-called anodic electrosynthesis, is the most well-known electrochemical synthesis route for the preparation of MOFs [71]. In anodic dissolution, an electrode is immersed in a solution containing a supporting electrolyte and the organic linker. When an oxidation voltage or current is applied, the electrode (anode) dissolves and consequently, the metal ions are rapidly released near the electrode surface. This metal ions then chemically react with the organic ligands to form the MOF layer on the electrode surface. A schematic overview of the anodic dissolution method is shown in Fig. 9.1A. This approach was first introduced by Mueller and coworkers [27]. The most significant advantage of anodic dissolution in comparison with other synthesis methods is independence of MOF characteristics to the source of metal ion precursors (e.g.,  $\text{Cu}(\text{NO}_3)_2$  vs  $\text{CuCl}_2$ ) [72]. For example, the surface area of HKUST-1, an MOF containing  $\text{Cu}^{2+}$ -paddlewheel-type nodes and 1,3,5-benzenetricarboxylate (BTC), prepared by anodic dissolution, was doubled compared to samples synthesized solvothermally. In the chemical synthesis of MOFs, counter ions (from the precursor) block the pores [73–75].

**Table 9.1: Summary of the substrates used for the electrochemical synthesis of MOFs (methods and applications).**

| Substrate type    | Substrate                | MOF                                | Electrochemical method      | Applications                                                                  | References |
|-------------------|--------------------------|------------------------------------|-----------------------------|-------------------------------------------------------------------------------|------------|
| Conductive glass  | Cu-coated ITO            | HKUST-1 and CBBr                   | Anodic dissolution          | –                                                                             | [38]       |
|                   | Zn-coated ITO            | Zn-BTC, Zn-BPDC                    | Anodic dissolution          | –                                                                             | [38]       |
| Metallic          | Cu-coated ITO            | HKUST-1                            | Anodic dissolution          | –                                                                             | [39]       |
|                   | ITO                      | Zn-BTC                             | EASA                        | –                                                                             | [40]       |
|                   | Cu plate                 | HKUST-1                            | Anodic dissolution          | Capacitive humidity sensor                                                    | [41]       |
|                   | Ni foam                  | Ni <sub>3</sub> (BTC) <sub>2</sub> | Anodic dissolution          | Electrocatalyst for the hydrogen evolution reaction                           | [42]       |
|                   | Zn plate                 | Zn(1,3-BDC) <sub>0.5</sub> (BZIM)  | Anodic dissolution          | Ibuprofen adsorption                                                          | [43]       |
|                   | Al plate                 | MIL-53(Al) modified with Fe, V, Ti | Anodic dissolution          | Olefin epoxidation                                                            | [44]       |
|                   | Cu plate                 | HKUST-1                            | Anodic dissolution          | Electrocatalyst for oxygen reduction                                          | [45]       |
|                   | Zn plate                 | IRMOF-3                            | Anodic dissolution          | Fluorescence determination of 2,4,6-trinitrophenol                            | [46]       |
|                   | Cu plate                 | Cu <sub>3</sub> (BTC) <sub>2</sub> | Anodic dissolution          | CO <sub>2</sub> and CH <sub>4</sub> separation                                | [47]       |
|                   | Al plate                 | MIL-53(Al)                         | Anodic dissolution          | Catalyst for the direct conversion of methane to methanol                     | [48]       |
|                   | Zn plate                 | Zn <sub>3</sub> (BTC) <sub>2</sub> | Anodic dissolution          | Ibuprofen slow-release                                                        | [49]       |
|                   | Cu plate                 | NENU-3                             | Anodic dissolution          | –                                                                             | [50]       |
|                   | Cu rod                   | HKUST-1                            | Anodic dissolution          | Catalytic hydrolysis of carbonyl sulfide                                      | [51]       |
|                   | Cu plate                 | HKUST-1                            | Anodic dissolution          | Electrodeposition of functional gold nanostructures                           | [52]       |
|                   | Stainless steel fibers   | E-MOF-5                            | Reductive electro-synthesis | Solid-phase microextraction and analysis of trace exogenous estrogens in milk | [53]       |
|                   | Cu plate                 | HKUST-1                            | Anodic dissolution          | Determination of ethanol and methanol vapors                                  | [54]       |
|                   | Macroporous Cu electrode | HKUST-1                            | Anodic dissolution          | –                                                                             | [55]       |
| Co-coated Ni foam | 2D-layered Ni-Co-BTC MOF | Anodic dissolution                 | –                           | [56]                                                                          |            |
| Cu plate          | HKUST-1                  | Anodic dissolution                 | –                           | [57]                                                                          |            |
| Cu mesh           | HKUST-1                  | Anodic dissolution                 | –                           | [58]                                                                          |            |
| Cu plate          | HKUST-1                  | Anodic dissolution                 | –                           | [58]                                                                          |            |



|              |                                      |                                                          |                             |                                                                                    |      |
|--------------|--------------------------------------|----------------------------------------------------------|-----------------------------|------------------------------------------------------------------------------------|------|
| Carbonaceous | Cu mesh                              | Cu-BTC and Cu-TATB                                       | Anodic dissolution          | –                                                                                  | [59] |
|              | Cu plate                             | Cu <sub>3</sub> (BTC) <sub>2</sub>                       | Anodic dissolution          | Catalyst for the reduction of <i>p</i> -nitrophenol to <i>p</i> -aminophenol       | [60] |
|              | Zn plate                             | Zn-(acrylamide-co-acrylic acid) MOF                      | Anodic dissolution          | –                                                                                  | [61] |
|              | Tb foil                              | Tb-BTC                                                   | Anodic dissolution          | Luminescent sensor for the detection of 2,4-dinitrotoluene                         | [62] |
|              | Gd foil                              | Gd-BTC                                                   | Anodic dissolution          | Luminescent sensor for the detection of 2,4-dinitrotoluene                         | [62] |
|              | Zn tablet                            | MOF-5                                                    | Anodic dissolution          | Electrocatalytic application to the hydrogen evolution reaction                    | [63] |
|              | Fe plate                             | MIL-100 (Fe)                                             | Anodic dissolution          | –                                                                                  | [64] |
|              | Cu plate                             | HKUST-1                                                  | Anodic dissolution          | –                                                                                  | [64] |
|              | Cu tracks on a printed circuit board | Cu <sub>3</sub> (BTC) <sub>2</sub>                       | Anodic dissolution          | –                                                                                  | [25] |
|              | Zn tablet                            | MOF-5                                                    | Anodic dissolution          | Improving the photocatalytic activity of BiOBr                                     | [65] |
|              | Custom-fabricated Cu IDEs            | Cu-BTC                                                   | Anodic dissolution          | Determination of methanol and water vapor                                          | [66] |
|              | GCE                                  | HKUST-1                                                  | Reductive electrosynthesis  | Organic molecules sensor                                                           | [67] |
|              | GCE                                  | Tris(bipyridine) ruthenium(II) functionalized Zn-BTC MOF | EASA                        | Electrochemiluminescent immunoassay of human heart-type fatty-acid-binding protein | [68] |
|              | Cu-coated GCE                        | HKUST-1 (Cu <sub>3</sub> (BTC) <sub>2</sub> )            | Self-templated synthesis    | Nonenzymatic glucose sensing platform                                              | [69] |
|              | GCE                                  | Zn-BTC                                                   | EASA                        | –                                                                                  | [40] |
| Carbon plate | Zn-BTC                               | EASA                                                     | –                           | [40]                                                                               |      |
| Graphite     | Cu(BTEC) <sub>0.5</sub> DMF          | Reductive electrosynthesis                               | Capacitive pseudocapacitors | [70]                                                                               |      |

*CBBr*, [Cu(C<sub>10</sub>H<sub>8</sub>N<sub>2</sub>)<sup>2+</sup>]Br<sub>2</sub>; *BTC*, benzene tricarboxylate; *BPDC*, 2,2'-bipyridine-5,5'-dicarboxylate; *1,3-H<sub>2</sub>BDC*, isophthalic acid; *HBZIM*, benzimidazole; *E-MOF-5*, (Et<sub>3</sub>NH)<sub>2</sub>Zn<sub>3</sub>(BDC)<sub>4</sub>; *H<sub>3</sub>TATB*, 4,4',4''-s-triazine-2,4,6-triyl-tribenzoic; *H<sub>4</sub>BTEC*, 1,2,4,5-benzenetetracarboxylate acid; *IDEs*, interdigitated electrodes; *EASA*, electrochemically assisted self-assembly; *GCE*, glassy carbon electrode.

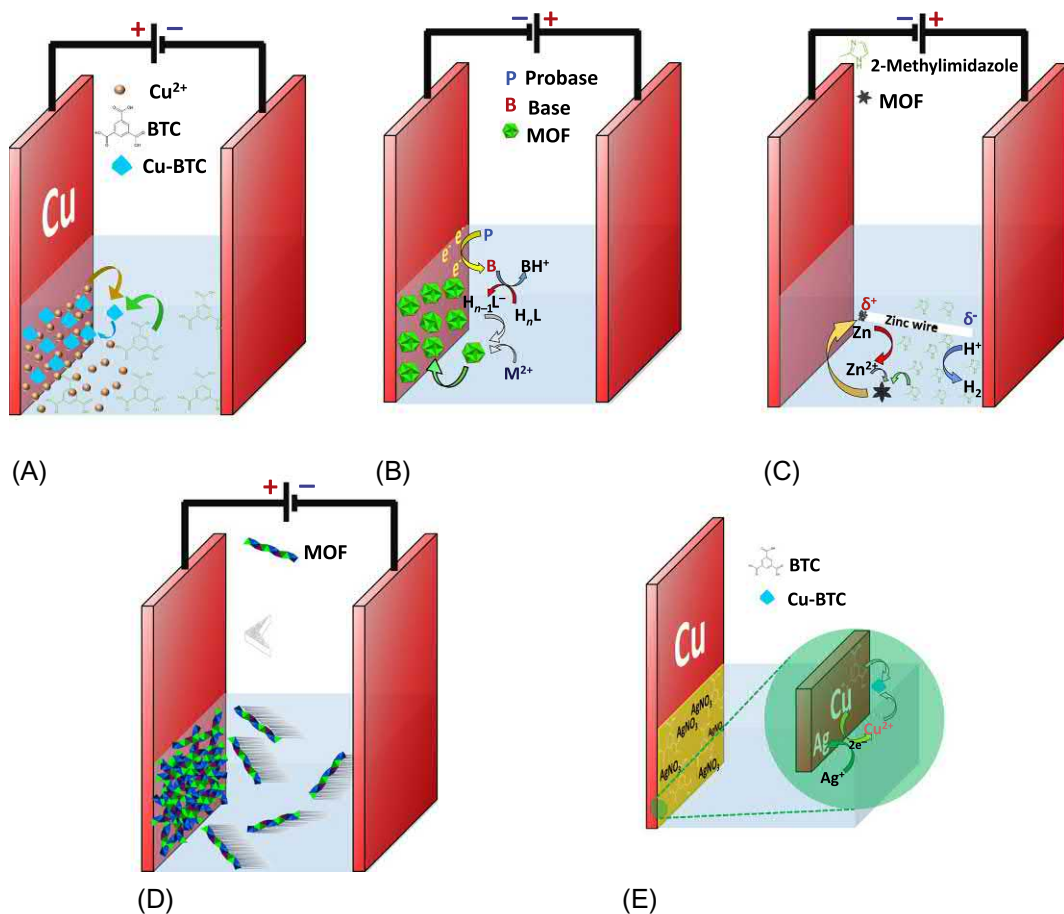


Fig. 9.1

Electrochemical synthesis of MOFs. (A) Anodic dissolution; (B) reductive electrosynthesis; (C) bipolar electrosynthesis; (D) electrophoretic deposition; (E) galvanic displacement.

In addition, control over MOF properties is easier for anodic dissolution due to the possibility of various oxidation states of the metal by applying suitable electrochemical conditions.

In 1999, Chui and coworkers were among the first to examine the formation of HKUST-1 thin films, as one of the most studied MOFs, on Cu electrode based on anodic dissolution method [73]. The electrosynthesis was performed in a two-electrode configuration. As an anodic voltage is applied, the elemental copper is oxidized to copper ion ( $\text{Cu}^{2+}$ ) and released into the solution containing BTC.

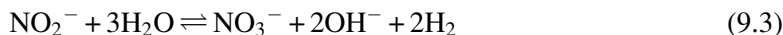
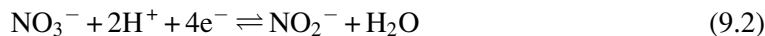
The mechanism of anodic electrosynthesis of MOFs can be deduced by four steps: nucleation, growth, intergrowth, and finally detachment [76]. First, metal ions are introduced in a solution containing the linker. Nucleation process occurs at a critical concentration of metal

ions close to the electrode surface. Then, micrometric-sized crystals are formed by the growth of the nuclei. The crystal islands are formed by the intergrowth of the nuclei. In the detachment step, the electrode under the as-formed crystals dissolves further.

Solvent, electrolyte concentration, applied potential (or current density), electrodeposition time, and the distance between the electrodes are important parameters which govern the property of the resulting MOF. In the anodic dissolution method, the use of protic solvents is preferred due to the hydrogen evolution reaction. In fact, this method is performed in protic solvents to avoid the electro-reduction of metal ions at the cathode surface [71]. Generally, an increase in the concentration of supporting electrolyte, electrosynthesis time, and applied potential leads to a high yield of the material synthesis [60]. Also, the applied potential plays a critical role in the crystal size. The rate of dissolution is increased at high applied potentials and leads to a higher nucleation rate [25]. In addition, as the amount of water increases, the larger crystals are formed. In other words, water molecules hydrate the metal ions and thus nucleation rate is decreased [77].

### 9.2.2 Reductive electrosynthesis

Unlike the anodic dissolution method, a solution containing all the starting materials is necessary for reductive electrosynthesis of MOFs. This method is based on the electrochemical generation of a “probase” agent at the cathode surface such as nitrate or perchlorate ions (Fig. 9.1B). A reaction mechanism is proposed for synthesis of copper MOFs as following [78, 79]:



where M and  $H_nL$  are metal and protonated linker, respectively.

By applying cathodic potentials, the electrode can be covered by a metal coating (Eq. 9.1). The electrochemical generation of hydroxide ions occurs by the reduction of oxoanions (Eqs. 9.2 and 9.3). The next step is the deprotonation of the linker in the alkaline conditions (Eq. 9.4). In fact, the use of an electrochemical stimulation is to bring a rise in solution pH and deprotonation of the organic linker. Finally, the deprotonated ligand rapidly reacts with the metal ions (Eq. 9.5) [78, 79]. Since the  $OH^{-}$  species are produced in situ at the working electrode, MOF film was predominantly electrodeposited on the electrode surface.

A clever selection of the probase agent is critical to suppress the need for high applied potential values and unwanted side reactions. It should be noted that the reductive electrosynthesis is not applicable for the preparation of MOFs containing easily reducible metals. Hence, the anodic dissolution method can be complementary to the reductive electrosynthesis in the MOF synthesis. The difference between the reduction potential of probase and the low reduction potentials of oxidizable metals (e.g., Zn) constitutes a serious obstacle for electrochemical synthesis of MOFs. Consequently, the oxidizable metal and an MOF film were co-deposited onto the working electrode (Fig. 9.1B). Therefore, it is necessary to find new ways to develop the reductive electrosynthesis of MOFs. In order to solve the problem, triethylammonium was used as a probase agent [80]. It requires less negative potential. This approach enables the control of the electrosynthesis conditions, and as a result, the absence of metal ion deposition on the substrate. Other probase agent can be used in the reductive electrosynthesis of MOFs. Zeolitic imidazolate structures were electrodeposited on the ITO surface using an oxygen-assisted reductive electrosynthesis [80]. This oxygen-assisted electrochemical synthesis allows the formation of frameworks without the plating of reduced metals (Zn and Co).

In reductive electrosynthesis of MOFs, the electrochemical properties of as-prepared MOF films can be easily tuned by the selection of the reduction potentials. Very recently, Cu-BTC thin films are successfully electrodeposited on the FTO at different cathodic potentials [67]. The morphology, electrocatalytic activity, electronic states of metal, and sensing ability of Cu-BTC frameworks are regulated by the variation of electrosynthesis potential.

### 9.2.3 Bipolar electrosynthesis

Bipolar electrosynthesis (BPES) is an electrodeposition technique in which a conductive object is located in a supporting electrolyte under a potential gradient. In the BPES, a polarization occurs between two sides of the conductive object where different redox reactions can simultaneously occur [81]. HKUST-1 and ZIF-8 structures were electrodeposited on the zinc wire by site-selective BPES [82]. MOF film at the hemisphere of the conductive object was deposited where potential gradient generates the metal ions. The intrinsic site selectivity of BPES makes it a helpful technique of choice to fabricate MOFs in a controllable way. The  $\text{Zn}^{2+}$  ions are generated at the positive side of the zinc wire. Then, 2-methylimidazole as organic linker chemically reacts with the metal ions (Fig. 9.1C). In addition, conductive organic single crystals were used as bipolar electrodes to prepare a new generation of MOFs [83]. Compared to anodic dissolution and reductive electrosynthesis methods, MOF films are site-selectively grown on the substrate through the BPES technique.

### 9.2.4 Electrophoretic deposition

In the electrophoretic deposition method, colloidal or charged particles in a nonpolar solvent move towards a conductive substrate of opposite charge due to the presence of a high electric field [84]. This electrochemical method has the benefit that it allows the deposition

of MOF films on a variety of known conductive substrates (metallic substrates, glassy carbon, and conductive glass electrode) [27]. The candidate MOF should present some surface defects to generate partial charges on the MOF surface. Hupp and coworkers employed the electrophoretic deposition for the first time in the synthesis of several well-known MOF thin films (HKUST-1, ZIF-8, NU-1000, and UiO-66) [85–88]. Intrinsic surface defects result in partial negative charges on the MOF lattice. Two electrodes are inserted into the solution containing defective MOFs and a fixed electric potential is applied. As expected, the MOF particles were deposited on the positively charged substrates. To use the electrophoretic deposition for the preparation of MOFs, the presence of stable colloidal suspensions seems to be necessary. This electrochemical synthesis route is outlined in an idealized scheme in Fig. 9.1D. Furthermore, Eu-BTC and Tb<sub>0.55</sub>Eu<sub>0.45</sub>-BTC MOF films on the ITO, FTO, and zinc plate substrates were coated by the electrophoretic deposition method [89]. First, Tb<sub>0.55</sub>Eu<sub>0.45</sub>-BTC MOF is chemically synthesized. In order to coat Tb<sub>0.55</sub>Eu<sub>0.45</sub>-BTC film on the electrode, the as-prepared Tb<sub>0.55</sub>Eu<sub>0.45</sub>-BTC is dispersed in dichloromethane solvent. Then, a DC potential is fixed at 90 V for 5 min between two ZnO plates. The deposited MOF was successfully employed for the determination of 2,4,6-trinitrotoluene and nitrobenzene in a gaseous media.

### 9.2.5 Galvanic displacement

In galvanic displacement, an active metallic substrate (e.g., copper) is in contact with a solution containing metal ions of a relatively noble metal (e.g., silver). Due to the difference between the reduction potential of noble and active metals, the noble metal is reduced and deposited on the electrode. In other words, the active metal is oxidized and provide electrons for a cathodic reaction [90, 91]. The released metal ions can be used as a metal source in the synthesis of MOFs. Galvanic displacement differs from electrodeposition methods because an external voltage or current necessary in electrodeposition is not required. This method has been employed for the deposition of HKUST-1 on a conductive glass [90]. A solution of BTC ligand and silver nitrate was spin-coated a copper modified glass electrode. The oxidation of copper and the reduction of Ag<sup>+</sup> ions simultaneously occur to form of HKUST-1 (Fig. 9.1E). After evaporation of the solvent, a uniform HKUST-1 thin film is achieved.

The galvanic displacement method enables the preparation of interesting MOF films. In 2017, Jang et al. introduced MOF-derived n-type SnO<sub>2</sub> porous hollow polyhedron nanocubes functionalized with discrete p-type Co<sub>3</sub>O<sub>4</sub> islands [92]. When the dissolution of Co<sub>3</sub>O<sub>4</sub> on the surface of polyhedron structures has occurred, meso- and macro-sized pores are formed. Meanwhile, PdO nanoparticles and Co<sub>3</sub>O<sub>4</sub> islands are successfully functionalized on SnO<sub>2</sub> porous nanocubes. A 21.9-fold increase in the detection of acetone vapor in the presence of the as-prepared composite is achieved due to the formation of macro- and meso-sized pores in the MOF-templated oxides.

### 9.2.6 Miscellaneous methods

As an alternative to the above-mentioned methods for synthesizing MOF thin films, “self-templated synthesis” [93] and “covalent electrografting” [94] have been introduced.

Self-templated synthesis is perhaps the simplest method for preparation of MOFs, which involves a couple of facile conversion steps. In this technique, the synthesis of MOF can be done by the electrochemical fabrication of metal oxides, which afterward are converted to a framework by a chemical reaction. The metal oxide has two important roles: first, the supply of metal ions and, second, nucleation site for the growth of MOFs. For example, the HKUST-1 was prepared on a copper electrode by a two-step synthesis method [95]. First, copper hydroxide is obtained by electro-oxidation and, then, converted into HKUST-1 in the presence of the corresponding organic ligands.

Covalent electrografting, known as anchoring of a linker, is a simple procedure to prepare MOF films. Linker molecules can be attached on the electrode surface and then act as a nucleation site for formation of MOFs. Balakrishnan et al. have developed an electrochemical method which produces HKUST-1 on conductive carbon substrates. Generally, aryl radicals are generated by reduction of 4-carboxybenzenediazonium cation. This standard procedure resulted in the grafting of a 4-carboxyphenyl radicals onto a glassy carbon electrode. Copper (II) ions can interact with grafted layer on the electrode surface and HKUST-1 grow in the presence of H<sub>3</sub>BTC [94].

## 9.3 Electrochemical synthesis of MOFs on various conductive substrates

Substrates play an important role in MOFs' electrochemical synthesis. The final application of the synthesized MOFs relies on the characteristics of the used substrates [96]. For example, for gas/liquid separation purposes, porous substrates can be used [97]. For sensors, the MOFs are deposited on signal transduction surfaces. Frequently used substrates in the synthesis of MOFs are metallic substrates, electrically conductive glass substrates, and carbonaceous electrodes (Table 9.1).

### 9.3.1 Deposition of MOFs on metallic substrates

Metallic substrates in forms of plates, meshes, and foams have been used as electrodes for electrochemical synthesis of MOFs. In these methods, the metallic electrode usually is the source for the metal ions for the formation of the MOF. However, in some synthesis strategies (e.g., reductive electrosynthesis), the metal ions are not provided by the electrode. Also in some cases, the material used for the construction of the electrodes is different from the metal ion used for the synthesis of MOFs [98]. Where the metal ions are provided by the electrode (e.g., anodic dissolution), upon applying a potential to the metallic electrode,



the metal is oxidized to the desired metal ions at anode electrode and release to the reaction medium. The cathode electrode can be the same as the anode or other conductive electrodes. The formation of MOF starts near to the anode electrode where the metal ions are presented to the reaction medium containing the linker. Various parameters can affect the final MOF characteristics such as the geometry of the electrode, applied voltage (magnitude and applying method), reaction time, type of the electrolyte and its concentration, the solvent, and temperatures and pressures.

Since most of MOFs are not electrically conductive, the geometry of the electrodes plays an important role in the synthesis of MOF layers of high thickness. The formation of MOFs starts with nucleation of MOF crystals on, usually, anode electrode through the reaction between the linker and the released metal ions. Then the crystal growth can further the dominant process until the electrode surface is completely covered with the MOF layer. Therefore, when insulating linkers are used for the preparation of MOFs, the preparation of thick MOF layers is not practically possible. However, by using electrode meshes, this issue can be addressed to some extent. It has been reported that using Cu mesh as the anode and Cu plate as the cathode, HKUST-1 films can be synthesized electrochemically [99]. The optimum condition used for the preparation of HKUST-1 films were the potential of 2.7 V, the reaction time of 20–30 min, reaction temperature of 50°C, the supporting electrolyte of MTBS (tributylmethylphosphonium methyl sulfate), and the solvent of ethanol: water (65:35). Under the optimum conditions, HKUST-1 layer of 10  $\mu\text{m}$  in thickness with an average crystal size of 6  $\mu\text{m}$  was synthesized. The findings showed that applying higher or lower voltages destroyed the mesh electrode by increasing asymmetric oxidation of the electrode mainly from the edge and center locations. Furthermore, the results indicate that the pore size of the mesh electrode affects the film thickness. It has been reported that finer mesh sizes lead to thinner layers [99]. The authors indicated that the smaller pores size meshes can be more rapidly filled with microcrystals than the larger pores size meshes.

The applied voltage magnitude has a critical impact on the MOFs synthesis. When the electrode provides the metal ions, the applied voltage must be high enough to enable electro-oxidation of the metallic electrode to metal ions. Increasing the voltage to very high voltages is not beneficial since the rate of releasing the metal increases and achievement of homogenous films could be difficult. On the other hand, the application of very low voltages increases the reaction time. Therefore, the applied voltage magnitude should be optimized for the synthesis of dense and thick MOF films [100]. The voltage applying method is also an important parameter. The applying method could be in continuous or pulsed modes such as square wave voltammetry, cyclic voltammetry, and differential pulse voltammetry. It has been reported that pulsed modes are more desirable since they prevent the electrode polarization [101].

The reaction time also is important in the electrochemical synthesis of MOFs since short reaction times lead to MOF layers of poor density and thickness, while longer reaction times

may lead to the electrode polarization and its destruction. It has been reported that extending the reaction time leads to thicker MOF films and also affects the roughness of the synthesized layers [100]. Furthermore, it has been reported that extending the reaction time decreases the intergrown microcrystals gap [101].

The type of the electrolyte and its concentration also play an important role in the physical characteristics of the deposited MOF layer and the reaction kinetics. Usually, the presence of the supporting electrolyte at high concentrations accelerates the reaction kinetically and thus shortens the reaction time [99, 102]. However, the electrolyte's high concentration may interfere in the MOF polymer formation and affect the homogeneity of the deposited layer. It has been reported that the presence of a certain supporting electrolyte can increase the current density, leading to thicker films while the synthesized films are cracked at the anode electrode [64]. This problem may lead to detachment of the MOF crystals from the electrode surface, which causes the growth of crystals in the solution medium.

The solvent type also affects the MOF layer properties. When the metal ions are provided through electro-oxidation of metallic electrodes, the use of protic solvents is preferred due to the hydrogen evolution reaction. In fact, this method is performed in protic solvents to avoid the reduction of metal ions at the cathode [71]. It has been reported that when the water content of a mixed solvent of water: ethanol is increased from 10% to 35%, the crystal size of HKUST-1 increases from 2 to 11  $\mu\text{m}$  since hydrogen evolution of the solution is altered and furthermore the chemistry of the linker may be altered [102, 103].

Although there are some reports on the synthesis of MOFs at low temperatures and pressures [100, 101], some of MOFs cannot be synthesized at low temperatures or atmospheric pressures using electrochemical methods. The reason behind this could be the high energy barriers of nucleation of certain MOFs. Recently, a novel setup has been developed for electrochemical deposition of MOFs at high temperatures and high pressures [64]. As an example, MIL-101(Fe) MOF, which cannot be synthesized electrochemically at room temperature, was synthesized using the developed setup and the effect of reaction temperature on the MOF crystal size and shape was evaluated. The results showed that, at high temperatures (170–190°C), monodispersed small crystallites of  $\sim 50$  nm in diameter could be synthesized, while lower temperatures (110–130°C) lead to polydisperse crystals of 50 nm to 1  $\mu\text{m}$ . The authors indicated that, at high temperatures, the nucleation of crystals was faster than their growth, hence resulting in a thin layer of uniform nano-sized crystals.

### **9.3.2 Deposition of MOFs on conductive glass substrates**

MOFs can be deposited on transparent substrates as photocatalysts in sensors and photoelectric devices. In this case, usually, electrically conductive glass substrates are used. However, to deposit MOFs of high quality and high density on these sorts of substrates, it is difficult to use conventional methods due to the weak bonding of MOFs on glass substrates [101]. Fortunately,

in recent years, it has been enabled to deposit MOFs directly or indirectly on electrically conductive glass substrate using electrochemical methods. In this regard, electrically conductive glasses such as indium tin oxide (ITO), fluorine-tin-oxide (FTO), and patterned deposited glass substrates have been utilized to deposit MOFs. In these cases, different electrochemical methods such as reductive electrosynthesis, electrophoretic deposition, and galvanic displacement have been successfully utilized for deposition of desired MOFs on electrically conductive glass substrates.

Galvanic displacement method has been utilized for deposition of HKUST-1 MOF on a glass support [90]. To this end, the glass support is coated with Cu metallic pattern by a thermal evaporation method. Then, the MOF was deposited on the created shadow mask of copper. Consequently, HKUST-1 MOF was synthesized using galvanic displacement method. In other studies, FTO was used as an electrode for reductive electrosynthesis of MOF-5 thin films [79, 104]. The electrophoretic deposition method has been utilized for deposition of NU-1000, UiO-66, HKUST-1, and MIL-53 on FTO electrodes [85–88]. In these studies, the MOFs were deposited on positively charged FTO electrodes.

### **9.3.3 Deposition of MOF on carbonaceous substrates**

Carbonaceous substrates also have been used for electrochemical deposition of MOF films. The modified electrodes usually have been as electrochemical and electrochemiluminescent sensors, and for electrochemical characterization of the deposited MOF films. Furthermore, they can be used for studying the MOFs upon applying a voltage, which causes oxidation or reduction of the electrochemically active elements or functional group in the MOF layer structure [40, 67–70]. Frequently used carbonaceous substrates for electrochemical synthesis of MOFs comprise glassy carbon electrode (GCE) and carbon plates including graphite electrode (Table 9.1). HKUST-1 has been electrodeposited on GCE using reductive electrosynthesis method [67]. The electrodeposited MOF thin film was used as the sensing material in the electrode structure for the determination of nicotine amide adenine dinucleotide. Further, the potential application of the prepared sensor was evaluated for monitoring some other organic compounds. In another study,  $\text{Cu}_3(\text{BTC})_2$  MOF has been deposited on GCE using a self-templated synthesis method. To this end, first, metallic copper is electrodeposited on the GCE. Then the Cu layer is oxidized to copper hydroxide nanotubes [69]. Finally, the nanotubes are converted to HKUST-1 in the presence of  $\text{H}_3\text{BTC}$  linker.

## **9.4 Conclusions and future perspectives**

In this chapter, the advances in several electrochemical synthesis routes of MOFs were discussed. The anodic dissolution is the most likely approach to fabricate MOFs using electrochemical methods. For MOFs, electrochemical synthesis methods hold several advantages such as shorter synthesis times, controlling the thickness and morphology by

altering current or voltage, as well as mild synthesis conditions compared to conventional methods. They can be fabricated as thin films on various substrates. Furthermore, new MOF structures can be synthesized using electrochemical methods, which were not previously possible to be synthesized using traditional methods. To turn this fantasy into a reality, it is necessary to first reveal more detailed mechanisms of electrosynthesis of MOFs and also to comprehensively evaluate the effects of electrosynthesis parameters on the growth of these materials.

Although, as it can be seen in [Table 9.1](#), HKUST-1 is the most frequently electrochemically synthesized MOF, the application of electrochemical methods in the synthesis of other MOFs which are difficult to synthesize is growing. In future years, most probably, researchers will focus on the design of electrochemical reactors which can be operated under high temperatures and high pressures. Furthermore, for the utilization of MOFs as electrochemical sensors, it is necessary to develop electrically conductive MOFs. To this end, various conductive linkers should be synthesized and be utilized for the synthesis of conductive MOFs.

## References

- [1] H. Al-Kutubi, J. Gascon, E.J.R. Sudhölter, L. Rassaei, Electrosynthesis of metal-organic frameworks: challenges and opportunities, *ChemElectroChem* 2 (2015) 462–474.
- [2] N. Stock, S. Biswas, Synthesis of metal-organic frameworks (MOFs): routes to various MOF topologies, morphologies, and composites, *Chem. Rev.* 112 (2012) 933–969.
- [3] J. Liu, L. Chen, H. Cui, J. Zhang, L. Zhang, C.-Y. Su, Applications of metal-organic frameworks in heterogeneous supramolecular catalysis, *Chem. Soc. Rev.* 43 (2014) 6011–6061.
- [4] K.F. Babu, M.A. Kulandainathan, I. Katsounaros, L. Rassaei, A.D. Burrows, P.R. Raithby, F. Marken, Electrocatalytic activity of Basolite™ F300 metal-organic-framework structures, *Electrochem. Commun.* 12 (2010) 632–635.
- [5] J.-R. Li, J. Sculley, H.-C. Zhou, Metal-organic frameworks for separations, *Chem. Rev.* 112 (2012) 869–932.
- [6] S. Ma, H.-C. Zhou, Gas storage in porous metal-organic frameworks for clean energy applications, *Chem. Commun.* 46 (2010) 44–53.
- [7] Y. Li, C. Chen, X. Sun, J. Dou, M. Wei, Metal-organic frameworks at interfaces in dye-sensitized solar cells, *ChemSusChem* 7 (2014) 2469–2472.
- [8] G.K.H. Shimizu, J.M. Taylor, S. Kim, Proton conduction with metal-organic frameworks, *Science* 341 (2013) 354–355.
- [9] J. Della Rocca, D. Liu, W. Lin, Nanoscale metal-organic frameworks for biomedical imaging and drug delivery, *Acc. Chem. Res.* 44 (2011) 957–968.
- [10] A. Morozan, F. Jaouen, Metal organic frameworks for electrochemical applications, *Energy Environ. Sci.* 5 (2012) 9269–9290.
- [11] J.-L. Wang, C. Wang, W. Lin, Metal-organic frameworks for light harvesting and photocatalysis, *ACS Catal.* 2 (2012) 2630–2640.
- [12] C.H. Hendon, D. Tian, A. Walsh, Conductive metal-organic frameworks and networks: fact or fantasy? *Phys. Chem. Chem. Phys.* 14 (2012) 13120–13132.
- [13] T. Rodenas, I. Luz, G. Prieto, B. Seoane, H. Miro, A. Corma, F. Kapteijn, I.X.F.X. Llabres, J. Gascon, Metal-organic framework nanosheets in polymer composite materials for gas separation, *Nat. Mater.* 14 (2015) 48–55.

- [14] Z. Ni, R.I. Masel, Rapid production of metal–organic frameworks via microwave-assisted solvothermal synthesis, *J. Am. Chem. Soc.* 128 (2006) 12394–12395.
- [15] K.M.L. Taylor-Pashow, J. Della Rocca, Z. Xie, S. Tran, W. Lin, Postsynthetic modifications of iron-carboxylate nanoscale metal–organic frameworks for imaging and drug delivery, *J. Am. Chem. Soc.* 131 (2009) 14261–14263.
- [16] P. Horcajada, T. Chalati, C. Serre, B. Gillet, C. Sebrie, T. Baati, J.F. Eubank, D. Heurtaux, P. Clayette, C. Kreuz, J.-S. Chang, Y.K. Hwang, V. Marsaud, P.-N. Bories, L. Cynober, S. Gil, G. Férey, P. Couvreur, R. Gref, Porous metal–organic-framework nanoscale carriers as a potential platform for drug delivery and imaging, *Nat. Mater.* 9 (2009) 172.
- [17] A. Centrone, Y. Yang, S. Speakman, L. Bromberg, G.C. Rutledge, T.A. Hatton, Growth of metal–organic frameworks on polymer surfaces, *J. Am. Chem. Soc.* 132 (2010) 15687–15691.
- [18] A. Garcia Marquez, P. Horcajada, D. Grosso, G. Férey, C. Serre, C. Sanchez, C. Boissiere, Green scalable aerosol synthesis of porous metal–organic frameworks, *Chem. Commun.* 49 (2013) 3848–3850.
- [19] A. Carné-Sánchez, I. Imaz, M. Cano-Sarabia, D. Maspoch, A spray-drying strategy for synthesis of nanoscale metal–organic frameworks and their assembly into hollow superstructures, *Nat. Chem.* 5 (2013) 203.
- [20] H. Furukawa, U. Müller, O.M. Yaghi, “Heterogeneity within order” in metal–organic frameworks, *Angew. Chem. Int. Ed.* 54 (2015) 3417–3430.
- [21] Z. Wang, D. Ananias, A. Carné-Sánchez, C.D.S. Brites, I. Imaz, D. Maspoch, J. Rocha, L.D. Carlos, Lanthanide–organic framework nanothermometers prepared by spray-drying, *Adv. Funct. Mater.* 25 (2015) 2824–2830.
- [22] W.-J. Son, J. Kim, J. Kim, W.-S. Ahn, Sonochemical synthesis of MOF-5, *Chem. Commun.* (2008) 6336–6338.
- [23] L.-G. Qiu, Z.-Q. Li, Y. Wu, W. Wang, T. Xu, X. Jiang, Facile synthesis of nanocrystals of a microporous metal–organic framework by an ultrasonic method and selective sensing of organoamines, *Chem. Commun.* (2008) 3642–3644.
- [24] M. Klimakow, P. Klobes, A.F. Thünemann, K. Rademann, F. Emmerling, Mechanochemical synthesis of metal–organic frameworks: a fast and facile approach toward quantitative yields and high specific surface areas, *Chem. Mater.* 22 (2010) 5216–5221.
- [25] R. Ameloot, L. Stappers, J. Fransaer, L. Alaerts, B.F. Sels, D.E. De Vos, Patterned growth of metal-organic framework coatings by electrochemical synthesis, *Chem. Mater.* 21 (2009) 2580–2582.
- [26] A. Bétard, R.A. Fischer, Metal–organic framework thin films: from fundamentals to applications, *Chem. Rev.* 112 (2012) 1055–1083.
- [27] W.-J. Li, M. Tu, R. Cao, R.A. Fischer, Metal–organic framework thin films: electrochemical fabrication techniques and corresponding applications & perspectives, *J. Mater. Chem. A* 4 (2016) 12356–12369.
- [28] D. Nagaraju, D.G. Bhagat, R. Banerjee, U.K. Kharul, In situ growth of metal-organic frameworks on a porous ultrafiltration membrane for gas separation, *J. Mater. Chem. A* 1 (2013) 8828–8835.
- [29] X. Gao, G. Ji, R. Cui, J. Liu, Z. Liu, In situ growth of metal–organic frameworks (MOFs) on the surface of other MOFs: a new strategy for constructing magnetic resonance/optical dual mode imaging materials, *Dalton Trans.* 46 (2017) 13686–13689.
- [30] R. Guo, X. Cai, H. Liu, Z. Yang, Y. Meng, F. Chen, Y. Li, B. Wang, In situ growth of metal–organic frameworks in three-dimensional aligned lumen arrays of wood for rapid and highly efficient organic pollutant removal, *Environ. Sci. Technol.* 53 (2019) 2705–2712.
- [31] V.V. Guerrero, Y. Yoo, M.C. McCarthy, H.-K. Jeong, HKUST-1 membranes on porous supports using secondary growth, *J. Mater. Chem.* 20 (2010) 3938–3943.
- [32] R. Ranjan, M. Tsapatsis, Microporous metal organic framework membrane on porous support using the seeded growth method, *Chem. Mater.* 21 (2009) 4920–4924.
- [33] A. Demessence, C. Boissière, D. Grosso, P. Horcajada, C. Serre, G. Férey, G.J.A.A. Soler-Illia, C. Sanchez, Adsorption properties in high optical quality nanoZIF-8 thin films with tunable thickness, *J. Mater. Chem.* 20 (2010) 7676–7681.
- [34] J.G. Hinman, J.G. Turner, D.M. Hofmann, C.J. Murphy, Layer-by-layer synthesis of conformal metal–organic framework shells on gold nanorods, *Chem. Mater.* 30 (2018) 7255–7261.

- [35] M.C. So, S. Jin, H.-J. Son, G.P. Wiederrecht, O.K. Farha, J.T. Hupp, Layer-by-layer fabrication of oriented porous thin films based on porphyrin-containing metal–organic frameworks, *J. Am. Chem. Soc.* 135 (2013) 15698–15701.
- [36] O. Shekhah, Layer-by-layer method for the synthesis and growth of surface mounted metal-organic frameworks (SURMOFs), *Materials* 3 (2010) 1302–1315.
- [37] Y. Sun, H.C. Zhou, Recent progress in the synthesis of metal-organic frameworks, *Sci. Technol. Adv. Mater.* 16 (2015) 54202–54213.
- [38] J.L. Hauser, M. Tso, K. Fitchmun, S.R.J. Oliver, Anodic electrodeposition of several metal organic framework thin films on indium tin oxide glass, *Cryst. Growth Des.* 19 (2019) 2358–2365.
- [39] L.L. Jiang, X. Zeng, M. Li, M.Q. Wang, T.Y. Su, X.C. Tian, J. Tang, Rapid electrochemical synthesis of HKUST-1 on indium tin oxide, *RSC Adv.* 7 (2017) 9316–9320.
- [40] S. Alizadeh, D. Nematollahi, Electrochemically assisted self-assembly technique for the fabrication of mesoporous metal-organic framework thin films: composition of 3D hexagonally packed crystals with 2D honeycomb-like mesopores, *J. Am. Chem. Soc.* 139 (2017) 4753–4761.
- [41] M.S. Hosseini, S. Zeinali, Capacitive humidity sensing using a metal–organic framework nanoporous thin film fabricated through electrochemical in situ growth, *J. Mater. Sci. Mater. Electron.* 30 (2019) 3701–3710.
- [42] S. Jabarian, A. Ghaffarinejad, Electrochemical synthesis of NiBTC metal organic framework thin layer on nickel foam: an efficient electrocatalyst for the hydrogen evolution reaction, *J. Inorg. Organomet. Polym. Mater.* 29 (2019) 1565–1574.
- [43] O.J. De Lima Neto, A.C.D.O. Frós, B.S. Barros, A.F. De Farias Monteiro, J. Kulesza, Rapid and efficient electrochemical synthesis of a zinc-based nano-MOF for ibuprofen adsorption, *New J. Chem.* 43 (2019) 5518–5524.
- [44] D.E. Kravchenko, I.A. Tyablikov, P.A. Kots, B.A. Kolozhvari, D.A. Fedosov, I.I. Ivanova, Olefin epoxidation over metal-organic frameworks modified with transition metals, *Pet. Chem.* 58 (2018) 1255–1262.
- [45] S. Jabarian, A. Ghaffarinejad, H. Kazemi, Electrochemical and solvothermal syntheses of HKUST-1 metal organic frameworks and comparison of their performances as electrocatalyst for oxygen reduction reaction, *Anal. Bioanal. Electrochem.* 10 (2018) 1611–1619.
- [46] J.Z. Wei, X.L. Wang, X.J. Sun, Y. Hou, X. Zhang, D.D. Yang, H. Dong, F.M. Zhang, Rapid and large-scale synthesis of irmoF-3 by electrochemistry method with enhanced fluorescence detection performance for tnp, *Inorg. Chem.* 57 (2018) 3818–3824.
- [47] K. Pirzadeh, A.A. Ghoreyshi, M. Rahimnejad, M. Mohammadi, Electrochemical synthesis, characterization and application of a microstructure  $\text{Cu}_3(\text{BTC})_2$  metal organic framework for  $\text{CO}_2$  and  $\text{CH}_4$  separation, *Korean J. Chem. Eng.* 35 (2018) 974–983.
- [48] D.Y. Osadchii, A.I. Olivos-Suarez, Á. Szécsényi, G. Li, M.A. Nasalevich, I.A. Dugulan, P.S. Crespo, E.J. M. Hensen, S.L. Veber, M.V. Fedin, G. Sankar, E.A. Pidko, J. Gascon, Isolated Fe sites in metal organic frameworks catalyze the direct conversion of methane to methanol, *ACS Catal.* 8 (2018) 5542–5548.
- [49] W.W. Lestari, M. Arvinawati, R. Martien, T. Kusumaningsih, Green and facile synthesis of MOF and nano MOF containing zinc(II) and benzen 1,3,5-tri carboxylate and its study in ibuprofen slow-release, *Mater. Chem. Phys.* 204 (2018) 141–146.
- [50] F. Zhang, T. Zhang, X. Zou, X. Liang, G. Zhu, F. Qu, Electrochemical synthesis of metal organic framework films with proton conductive property, *Solid State Ionics* 301 (2017) 125–132.
- [51] L. Shen, G. Wang, X. Zheng, Y. Cao, Y. Guo, K. Lin, L. Jiang, Tuning the growth of Cu-MOFs for efficient catalytic hydrolysis of carbonyl sulfide, *Cuihua Xuebao/Chinese J. Catal.* 38 (2017) 1373–1381.
- [52] S.D. Worrall, M.A. Bissett, P.I. Hill, A.P. Rooney, S.J. Haigh, M.P. Attfield, R.A.W. Dryfe, Metal-organic framework templated electrodeposition of functional gold nanostructures, *Electrochim. Acta* 222 (2016) 361–369.
- [53] H. Lan, D. Pan, Y. Sun, Y. Guo, Z. Wu, Thin metal organic frameworks coatings by cathodic electrodeposition for solid-phase microextraction and analysis of trace exogenous estrogens in milk, *Anal. Chim. Acta* 937 (2016) 53–60.



- [54] M.S. Hosseini, S. Zeinali, M.H. Sheikhi, Fabrication of capacitive sensor based on Cu-BTC (MOF-199) nanoporous film for detection of ethanol and methanol vapors, *Sensors Actuators B Chem.* 230 (2016) 9–16.
- [55] C. Warakulwit, S. Yadnum, C. Boonyuen, C. Wattanakit, A. Karajic, P. Garrigue, N. Mano, D. Bradshaw, J. Limtrakul, A. Kuhn, Elaboration of metal organic framework hybrid materials with hierarchical porosity by electrochemical deposition-dissolution, *CrystEngComm* 18 (2016) 5095–5100.
- [56] X. Zhang, J. Luo, P. Tang, X. Ye, X. Peng, H. Tang, S.G. Sun, J. Fransaer, A universal strategy for metal oxide anchored and binder-free carbon matrix electrode: a supercapacitor case with superior rate performance and high mass loading, *Nano Energy* 31 (2017) 311–321.
- [57] N.T. Phuong, C. Buess-Herman, N.T. Thom, P.T. Nam, T.D. Lam, D.T.M. Thanh, Synthesis of Cu-BTC, from Cu and benzene-1,3,5-tricarboxylic acid (H<sub>3</sub>BTC), by a green electrochemical method, *Green Process. Synth.* 5 (2016) 537–547.
- [58] T.R.C. Van Assche, N. Campagnol, T. Muselle, H. Terryn, J. Fransaer, J.F.M. Denayer, On controlling the anodic electrochemical film deposition of HKUST-1 metal-organic frameworks, *Microporous Mesoporous Mater.* 224 (2016) 302–310.
- [59] S. Sachdeva, A. Pustovarenko, E.J.R. Sudhölter, F. Kapteijn, L.C.P.M. De Smet, J. Gascon, Control of interpenetration of copper-based MOFs on supported surfaces by electrochemical synthesis, *CrystEngComm* 18 (2016) 4018–4022.
- [60] R. Senthil Kumar, S. Senthil Kumar, M. Anbu Kulandainathan, Efficient electrosynthesis of highly active Cu<sub>3</sub>(BTC)<sub>2</sub>-MOF and its catalytic application to chemical reduction, *Microporous Mesoporous Mater.* 168 (2013) 57–64.
- [61] H. Yang, H. Du, L. Zhang, Z. Liang, W. Li, Electrosynthesis and electrochemical mechanism of Zn-based metal-organic frameworks, *Int. J. Electrochem. Sci.* 10 (2015) 1420–1433.
- [62] N. Campagnol, E. Rezende Souza, D.E. De Vos, K. Binnemans, J. Fransaer, Luminescent terbium-containing metal-organic framework films: new approaches for the electrochemical synthesis and application as detectors for explosives, *Chem. Commun.* 50 (2014) 12680–12683.
- [63] H.M. Yang, X.L. Song, T.L. Yang, Z.H. Liang, C.M. Fan, X.G. Hao, Electrochemical synthesis of flower shaped morphology MOFs in an ionic liquid system and their electrocatalytic application to the hydrogen evolution reaction, *RSC Adv.* 4 (2014) 15720–15726.
- [64] N. Campagnol, T. Van Assche, T. Boudewijns, J. Denayer, K. Binnemans, D. De Vos, J. Fransaer, High pressure, high temperature electrochemical synthesis of metal-organic frameworks: films of MIL-100 (Fe) and HKUST-1 in different morphologies, *J. Mater. Chem. A* 1 (2013) 5827–5830.
- [65] H.M. Yang, X. Liu, X.L. Song, T.L. Yang, Z.H. Liang, C.M. Fan, In situ electrochemical synthesis of MOF-5 and its application in improving photocatalytic activity of BiOBr, *Trans. Nonferrous Metals Soc. China (English Edition)* 25 (2015) 3987–3994.
- [66] S. Sachdeva, M.R. Venkatesh, B.E. Mansouri, J. Wei, A. Bossche, F. Kapteijn, G.Q. Zhang, J. Gascon, L.C.P. M. de Smet, E.J.R. Sudhölter, Sensitive and reversible detection of methanol and water vapor by in situ electrochemically grown CuBTC MOFs on interdigitated electrodes, *Small* 13 (2017) 1604150–1604156.
- [67] L. Ji, J. Hao, K. Wu, N. Yang, Potential-tunable metal-organic frameworks: electrosynthesis, properties, and applications for sensing of organic molecules, *J. Phys. Chem. C* 123 (2019) 2248–2255.
- [68] X. Qin, X. Zhang, M. Wang, Y. Dong, J. Liu, Z. Zhu, M. Li, D. Yang, Y. Shao, Fabrication of tris (bipyridine)ruthenium(II)-functionalized metal-organic framework thin films by electrochemically assisted self-assembly technique for electrochemiluminescent immunoassay, *Anal. Chem.* 90 (2018) 11622–11628.
- [69] S. Shahrokhian, E. Khaki Sanati, H. Hosseini, Direct growth of metal-organic frameworks thin film arrays on glassy carbon electrode based on rapid conversion step mediated by copper clusters and hydroxide nanotubes for fabrication of a high performance non-enzymatic glucose sensing platform, *Biosens. Bioelectron.* 112 (2018) 100–107.
- [70] M. Naseri, L. Fotouhi, A. Ehsani, S. Dehghanpour, Facile electrosynthesis of nano flower like metal-organic framework and its nanocomposite with conjugated polymer as a novel and hybrid electrode material for highly capacitive pseudocapacitors, *J. Colloid Interface Sci.* 484 (2016) 314–319.
- [71] U. Müller, H. Pütter, M. Hesse, H. Wessel, BASF-Aktiengesellschaft, WO, 49892, A1, (2005).

- [72] E. Stavitski, M. Goesten, J. Juan-Alcañiz, A. Martinez-Joaristi, P. Serra-Crespo, A.V. Petukhov, J. Gascon, F. Kapteijn, Kinetic control of metal–organic framework crystallization investigated by time-resolved in situ X-ray scattering, *Angew. Chem. Int. Ed.* 50 (2011) 9624–9628.
- [73] S.S.-Y. Chui, S.M.-F. Lo, J.P. Charmant, A.G. Orpen, I.D. Williams, A chemically functionalizable nanoporous material  $[\text{Cu}_3(\text{TMA})_2(\text{H}_2\text{O})_3]_n$ , *Science* 283 (1999) 1148–1150.
- [74] K. Schlichte, T. Kratzke, S. Kaskel, Improved synthesis, thermal stability and catalytic properties of the metal-organic framework compound  $\text{Cu}_3(\text{BTC})_2$ , *Microporous Mesoporous Mater.* 73 (2004) 81–88.
- [75] Q.M. Wang, D. Shen, M. Bülow, M.L. Lau, S. Deng, F.R. Fitch, N.O. Lemcoff, J. Semanscin, Metallo-organic molecular sieve for gas separation and purification, *Microporous Mesoporous Mater.* 55 (2002) 217–230.
- [76] T. Van Assche, J.F. Denayer, K. Binnemans, D.E. De Vos, J. Fransaer, On the Electrochemical Deposition Mechanism of Metal-Organic Frameworks, Meeting Abstracts, The Electrochemical Society, 2014, p. 558.
- [77] M.G. Goesten, P.C. Magusin, E.A. Pidko, B. Mezari, E.J. Hensen, F. Kapteijn, J. Gascon, Molecular promoting of aluminum metal–organic framework topology MIL-101 by N,N-dimethylformamide, *Inorg. Chem.* 53 (2014) 882–887.
- [78] H. Liu, H. Wang, T. Chu, M. Yu, Y. Yang, An electrodeposited lanthanide MOF thin film as a luminescent sensor for carbonate detection in aqueous solution, *J. Mater. Chem. C* 2 (2014) 8683–8690.
- [79] M. Li, M. Dincă, Reductive electrosynthesis of crystalline metal–organic frameworks, *J. Am. Chem. Soc.* 133 (2011) 12926–12929.
- [80] Q. Zhang, Z. Wu, Y. Lv, Y. Li, Y. Zhao, R. Zhang, Y. Xiao, X. Shi, D. Zhang, R. Hua, J. Yao, J. Guo, R. Huang, Y. Cui, Z. Kang, S. Goswami, L. Robison, K. Song, X. Li, Y. Han, L. Chi, O.K. Farha, G. Lu, Oxygen-assisted cathodic deposition of zeolitic imidazolate frameworks with controlled thickness, *Angew. Chem. Int. Ed.* 58 (2019) 1123–1128.
- [81] G. Loget, J.R. Roche, E. Gianessi, L. Bouffier, A. Kuhn, Indirect bipolar electrodeposition, *J. Am. Chem. Soc.* 134 (2012) 20033–20036.
- [82] S. Yadnum, J. Roche, E. Lebraud, P. Négrier, P. Garrigue, D. Bradshaw, C. Warakulwit, J. Limtrakul, A. Kuhn, Site-selective synthesis of Janus-type metal-organic framework composites, *Angew. Chem. Int. Ed.* 53 (2014) 4001–4005.
- [83] I. Malyska, C. Mézière, M. Kielar, L. Hirsch, G. Wantz, N. Avarvari, A. Kuhn, L. Bouffier, Bipolar electrochemistry with organic single crystals for wireless synthesis of metal–organic Janus objects and asymmetric photovoltage generation, *J. Phys. Chem. C* 121 (2017) 12921–12927.
- [84] P. Sarkar, P.S. Nicholson, Electrophoretic deposition (EPD): mechanisms, kinetics, and application to ceramics, *J. Am. Ceram. Soc.* 79 (1996) 1987–2002.
- [85] I. Hod, W. Bury, D.M. Karlin, P. Deria, C.W. Kung, M.J. Katz, M. So, B. Klahr, D. Jin, Y.W. Chung, T.W. Odom, O.K. Farha, J.T. Hupp, Directed growth of electroactive metal-organic framework thin films using electrophoretic deposition, *Adv. Mater.* 26 (2014) 6295–6300.
- [86] I. Stassen, M. Styles, T. Van Assche, N. Campagnol, J. Fransaer, J. Denayer, J.-C. Tan, P. Falcaro, D. De Vos, R. Ameloot, Electrochemical film deposition of the zirconium metal–organic framework UiO-66 and application in a miniaturized sorbent trap, *Chem. Mater.* 27 (2015) 1801–1807.
- [87] X. Kang, Q. Zhu, X. Sun, J. Hu, J. Zhang, Z. Liu, B. Han, Highly efficient electrochemical reduction of  $\text{CO}_2$  to  $\text{CH}_4$  in an ionic liquid using a metal–organic framework cathode, *Chem. Sci.* 7 (2016) 266–273.
- [88] H. Zhu, H. Liu, I. Zhitomirsky, S. Zhu, Preparation of metal–organic framework films by electrophoretic deposition method, *Mater. Lett.* 142 (2015) 19–22.
- [89] J.-f. Feng, X. Yang, S.-y. Gao, J. Shi, R. Cao, Facile and rapid growth of nanostructured In-BTC metal–organic framework films by electrophoretic deposition for explosives sensing in gas and  $\text{Cr}^{3+}$  detection in solution, *Langmuir* 33 (2017) 14238–14243.
- [90] R. Ameloot, L. Pandey, M. Van der Auweraer, L. Alaerts, B.F. Sels, D.E. De Vos, Patterned film growth of metal–organic frameworks based on galvanic displacement, *Chem. Commun.* 46 (2010) 3735–3737.
- [91] A. Gutes, C. Carraro, R. Maboudian, Silver dendrites from galvanic displacement on commercial aluminum foil as an effective SERS substrate, *J. Am. Chem. Soc.* 132 (2010) 1476–1477.

- [92] J.-S. Jang, W.-T. Koo, S.-J. Choi, I.-D. Kim, Metal organic framework-templated chemiresistor: sensing type transition from P-to-N using hollow metal oxide polyhedron via galvanic replacement, *J. Am. Chem. Soc.* 139 (2017) 11868–11876.
- [93] H. Guo, G. Zhu, I.J. Hewitt, S. Qiu, “Twin copper source” growth of metal–organic framework membrane:  $\text{Cu}_3(\text{BTC})_2$  with high permeability and selectivity for recycling  $\text{H}_2$ , *J. Am. Chem. Soc.* 131 (2009) 1646–1647.
- [94] S. Balakrishnan, A.J. Downard, S.G. Telfer, HKUST-1 growth on glassy carbon, *J. Mater. Chem.* 21 (2011) 19207–19209.
- [95] K. Okada, R. Ricco, Y. Tokudome, M.J. Styles, A.J. Hill, M. Takahashi, P. Falcaro, Copper conversion into  $\text{Cu}(\text{OH})_2$  nanotubes for positioning  $\text{Cu}_3(\text{BTC})_2$  MOF crystals: controlling the growth on flat plates, 3d architectures, and as patterns, *Adv. Funct. Mater.* 24 (2014) 1969–1977.
- [96] D. Zacher, O. Shekhah, C. Wöll, R.A. Fischer, Thin films of metal–organic frameworks, *Chem. Soc. Rev.* 38 (2009) 1418–1429.
- [97] S. Qiu, M. Xue, G. Zhu, Metal–organic framework membranes: from synthesis to separation application, *Chem. Soc. Rev.* 43 (2014) 6116–6140.
- [98] N. Campagnol, E.R. Souza, D.E. De Vos, K. Binnemans, J. Fransaer, Luminescent terbium-containing metal–organic framework films: new approaches for the electrochemical synthesis and application as detectors for explosives, *Chem. Commun.* 50 (2014) 12545–12547.
- [99] T.R.C. Van Assche, G. Desmet, R. Ameloot, D.E. De Vos, H. Terryn, J.F.M. Denayer, Electrochemical synthesis of thin HKUST-1 layers on copper mesh, *Microporous Mesoporous Mater.* 158 (2012) 209–213.
- [100] W.-J. Li, J. Lü, S.-Y. Gao, Q.-H. Li, R. Cao, Electrochemical preparation of metal–organic framework films for fast detection of nitro explosives, *J. Mater. Chem. A* 2 (2014) 19473–19478.
- [101] C. Hou, Q. Xu, J. Peng, Z. Ji, X. Hu, (110)-oriented ZIF-8 thin films on ITO with controllable thickness, *Chemphyschem* 14 (2013) 140–144.
- [102] A. Martinez Joaristi, J. Juan-Alcañiz, P. Serra-Crespo, F. Kapteijn, J. Gascon, Electrochemical synthesis of some archetypical  $\text{Zn}^{2+}$ ,  $\text{Cu}^{2+}$ , and  $\text{Al}^{3+}$  metal organic frameworks, *Cryst. Growth Des.* 12 (2012) 3489–3498.
- [103] R. Pech, J. Pickardt, catena-Triaqua- $\mu$ -[1,3,5-benzenetricarboxylato(2-)]-copper(II), *Acta Crystallogr. Sect. C* 44 (1988) 992–994.
- [104] M. Li, M. Dincă, Selective formation of biphasic thin films of metal–organic frameworks by potential-controlled cathodic electrodeposition, *Chem. Sci.* 5 (2014) 107–111.

# Mechanochemical synthesis of MOFs

**Shunsuke Tanaka**

*Department of Chemical, Energy and Environmental Engineering, Kansai University, Osaka, Japan;  
Organization for Research and Development of Innovative Science and Technology (ORDIST), Kansai  
University, Osaka, Japan*

## 10.1 Introduction

Ordered nanoporous materials offer many interesting opportunities in both academia and industry, because of their high specific surface area and remarkable tunability of the structure and surface characteristics. Crystalline materials in which metal complexes are orderly assembled have been synthesized based on complexation reaction of metal ions which act as coordination centers and organic ligands which act as linkers between metal centers. Such a family of materials is called metal-organic frameworks (MOFs) and is known as one of the most exciting recent developments in ordered nanoporous material science [1–14]. MOFs are based on a combination of coordination chemistry and supramolecular engineering. MOFs possess high surface area far exceeding that of zeolites and their pore size can be tuned by varying the size of organic ligands and/or a modification that can be associated to the change in functional groups in the ligands [15]. Because the structure of MOFs is crystalline, their nanopores ensure structural arrangement and size equalization. In addition, one of the greatest features lies in the framework flexibility, which is different from the rigid framework of zeolites. Systematic combinations of metal and organic components enable an unprecedented rational design of framework structures, resulting in the development of framework flexibility properties (Fig. 10.1) [16–19]. New applications that could not be achieved with conventional ordered nanoporous materials are being developed by engineering such properties.

### 10.1.1 Comparison between zeolites and MOFs

MOFs are often compared to zeolites which are representative of the crystalline ordered nanoporous materials. The characteristics of MOFs are summarized in Table 10.1 as differences from zeolites.

- (1) Zeolites synthesis mostly uses organic structure-directing agent (OSDA) to form the crystalline structure [20–23], while MOFs synthesis does not require OSDA.

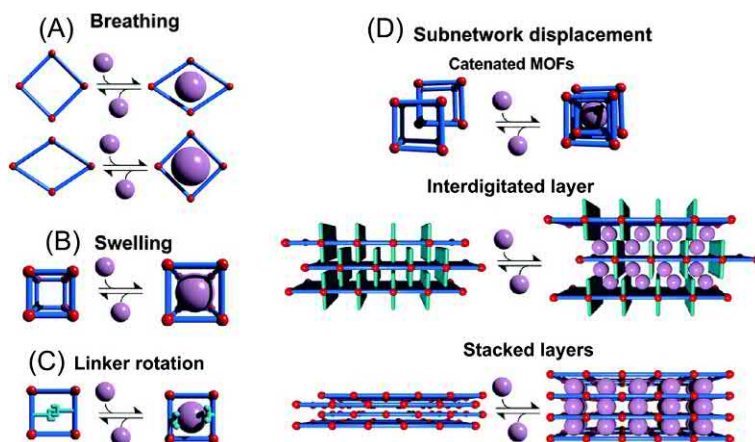


Fig. 10.1

Classification of different flexibility modes of MOFs. *Reproduced with permission from A. Schneemann, V. Bon, I. Schwedler, I. Senkovska, S. Kaskel, R.A. Fischer, Chem. Soc. Rev. 43 (2014) 6062–6096. Copyright 2014 Royal Society of Chemistry.*

Table 10.1: The main differences between zeolites and MOFs.

|                          | MOFs                                                                               | Zeolites                                                                      |
|--------------------------|------------------------------------------------------------------------------------|-------------------------------------------------------------------------------|
| (1) Structure formation  | Typically, MOF synthesis does not require organic structure-directing agent (OSDA) | OSDA is used to guide the formation of particular types of pores and channels |
| (2) Activation           | Removal of the solvent under relatively mild conditions                            | Removal of OSDA by high-temperature calcination                               |
| (3) Synthesis conditions | Under mild conditions<br>Some can be synthesized at RT                             | Hydrothermal synthesis                                                        |
| (4) Pore size            | Flexible framework with discriminatory gate-opening effect                         | Rigid pore structure with homogeneous distribution                            |
| (5) Crystal size         | Crystal size can be varied over a wide range of values                             | Wide-range control is hard to achieve with classical porous aluminosilicates  |

- (2) Zeolites synthesis requires a calcination step to pyrolyze and remove OSDA from the inside of their pores, while the pores of MOFs can be relatively easily activated by removal of the reaction solvents and unreacted starting materials because of OSDA-free synthesis.
- (3) Zeolites are hydrothermally synthesized under high temperature and pressure conditions, while MOFs are synthesized under relatively mild conditions, often at room temperature and ordinary pressure.

- (4) Zeolites possess rigid frameworks, while MOFs possess flexible framework, resulting in pore size of the MOFs be changed by the framework flexibility.
- (5) The crystal size of zeolites is generally in the range of several hundred of nm to several of  $\mu\text{m}$ , while the crystal size of MOFs can be relatively easily varied in a wide range of several tens of nm to several tens of  $\mu\text{m}$  [24–30].

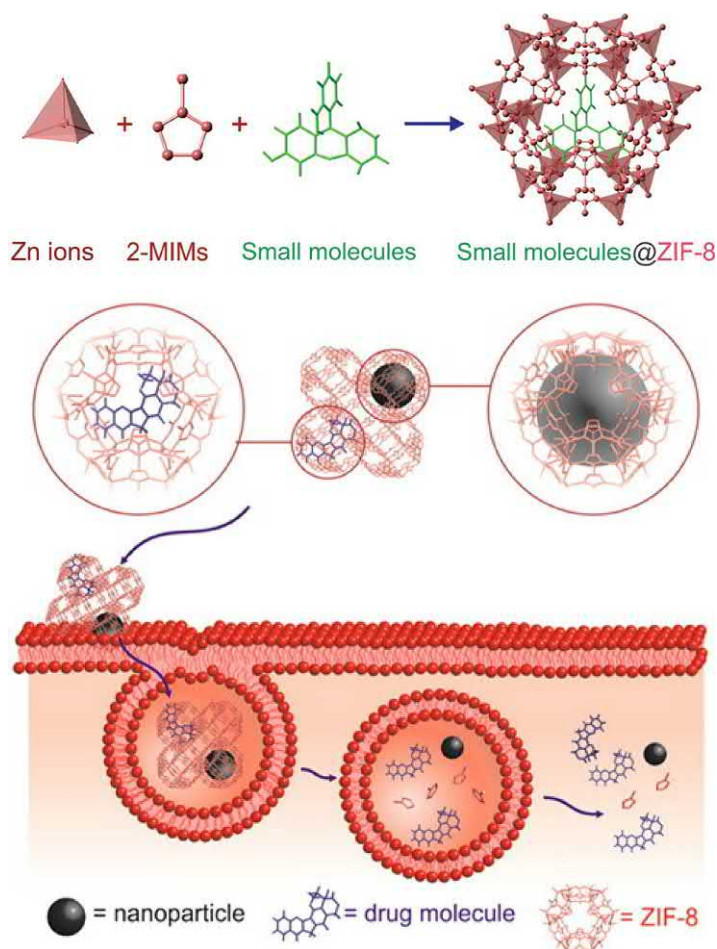
### 10.1.2 Representative example of MOFs for bio-applications

Two families of MOFs, MILs (materials of Institute Lavoisier) [31,32] and CPOs (coordination polymers from Oslo) [33] were the first studied for their potential biomedical applications. The main focus was on the use of MOFs as a drug delivery, paying particular attention to metal center toxicity. An understanding of MOFs' toxicity is an important concern not only for the safe use of them for humans, but also for nature environment, leading to the research for biodegradable MOFs. Horcajada prepared MIL-100 and MIL-101 applied for the delivery of ibuprofen in the gastrointestinal tract and demonstrated high drug-loading capacity and complete control of drug release under physiological conditions [31]. Less toxic system using iron and more flexible MILs were studied. The structural flexibility of MILs, so-called “breathing” behavior [32], exhibited another particularly interesting feature for potential applications in drug delivery.

On the other hand, another family of MOFs, ZIFs (zeolitic imidazolate frameworks) [34–37], recognized as one of the most structurally stable MOFs, have been explored for pharmaceutical purposes. Biologically active molecules such as caffeine [38,39] and anticancer drugs, 5-fluorouracil [40,41] and doxorubicin [42,43], were incorporated into ZIFs. Only a few relevant examples demonstrated that these systems can be controlled drug release. Among the many ZIFs, ZIF-8 ( $\text{Zn}$  (2-methylimidazole)<sub>2</sub>) is undoubtedly the most extensively studied due to its facile synthesis coupled with its high structural stability [44]. ZIF-8 crystallizes into the sodalite topology, forming the large cages (diameter of 1.16 nm) interconnected via narrow 6-ring windows (0.34 nm). Such framework structure gives ZIF-8 particularly interesting “gate-opening” functionality. Numerous experimental and computational studies have revealed that the pore apertures swing open by reorientation of imidazolate linkers and expand when probed with guest molecules [45–51]. In addition, our group revealed that “gate-opening” functionality and transport property of ZIF-8 are strongly affected by crystal size [52,53]. The doxorubicin-loaded ZIF-8 complex, which aims to treat mucoepidermoid carcinoma of the human lung, human colorectal adenocarcinoma (HT-29), and human promyelocytic leukemia (HL-60) cell lines, exhibited lower toxicity rather than pure doxorubicin, due to the slow release of the drug that is achieved by inclusion in the ZIF-8 [42]. Ren et al. further demonstrated that nanoparticles composed of polyacrylic acid and ZIF-8 possess ultrahigh doxorubicin loading capacity and can be used as pH-responsive



drug delivery [43]. The use of pH-responsive drug deliveries is effective in reduction of undesired drug release during its transport in blood circulation and improvement of the effective drug release in the tumor tissue or within tumor cells. Zheng et al. successfully developed a one-pot process which combines ZIFs synthesis and encapsulation of anticancer drugs [54]. In addition, the doxorubicin-loaded ZIF-8 complex demonstrated to be efficient pH-responsive drug delivery systems. Further studies involving ZIFs with encapsulated anticancer drugs revealed that they have potential for fluorescence imaging. Zhuang et al. demonstrated the encapsulation of fluorescein and camptothecin inside ZIF-8 frameworks during ZIF-8 synthesis (Fig. 10.2) [55]. Liu et al. successfully fabricated carbon



**Fig. 10.2**

Encapsulation of small molecules into the frameworks during synthesis. Schematic illustration shows that nanoparticles are endocytosed by cells and the pH-triggered disintegration of the ZIF-8 framework in these acidic compartments results in drug release. *Reproduced with permission from J. Zhuang, C.H. Kuo, L.Y. Chou, D.Y. Liu, E. Weerapana, C.K. Tsung, ACS Nano 8 (2014) 2812–2819. Copyright 2014 American Chemical Society.*

nanodots@ZIF-8 nanoparticles, which exhibit green fluorescence and microporosity, and demonstrated the potential platforms for simultaneous pH-responsive anticancer drug delivery and fluorescence imaging in cancer cells [41].

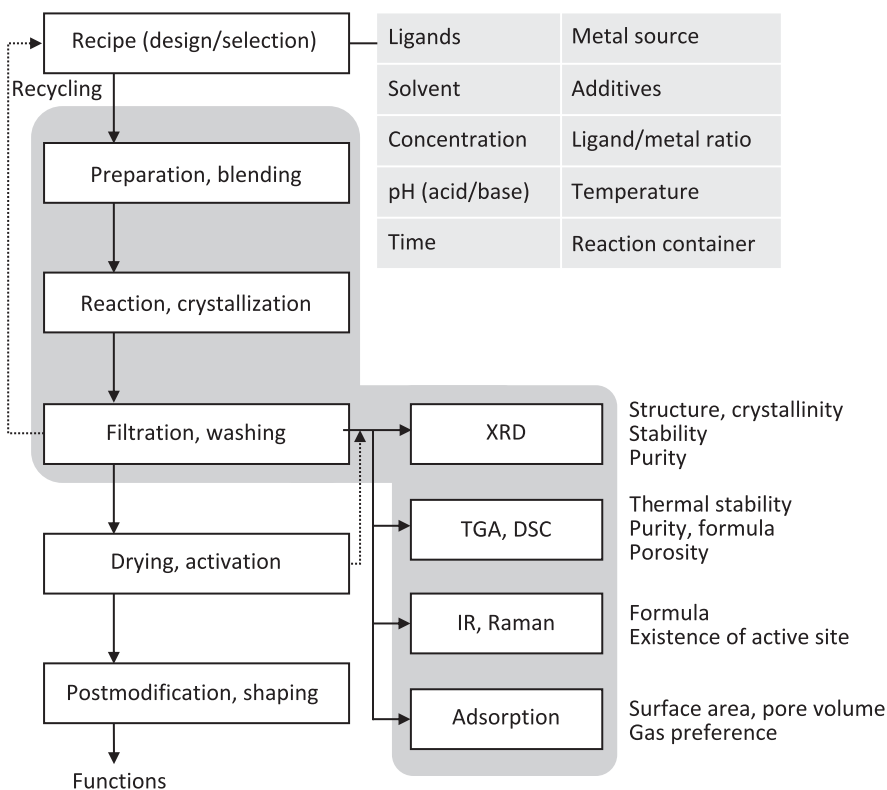
### **10.1.3 Engineering greener and more economical manufacturing process and control**

Given the rapid advances in the development of MOFs applications in the fields of chemistry, bio/chemical engineering, electronics, and medication, the commercial availability of MOFs should be pursued. One of the obstacles in developing MOF-based technologies is the lack of stability of most MOFs toward temperature, humidity, and acid-base solvents [37,56]. Even more important issues are the high cost of the starting materials (in particular, organic ligands), the limited availability and the high cost of commercial MOFs, and above all, the difficulty of scaling up the synthesis in a cost-effective way with maintaining the product quality. As of this writing, most MOFs are retailed in relatively small quantities at prices that are never cheap, delaying academic and industrial developments. Aside from the fact that cost is the dominant factor in the commercialization of MOFs, environmental impact and safety are recognized as significant concerns for large-scale production and practical application. Reducing the environmental impact of synthesis is an interrelated concern with lowering manufacturing costs. In production of MOFs, the process is as important as material design and property. The steps mainly consist of (1) making recipe (design/selection), (2) preparation and blending, (3) reaction and crystallization, (4) filtration and washing, (5) drying and activation, and (6) postmodification and shaping (Fig. 10.3). The challenges in developing manufacturing process are not only associated with improving and enhancement of reaction efficiency and yield, but also related to the environmental impact of the synthesis, as well as the properties of the final product.

The following outlines the synthesis routes developed to date for the purpose of reducing environmental impact and manufacturing costs. In particular, this review focuses on the mechanochemical synthesis of MOFs and outlines the characteristics of the MOFs obtained in that way.

## **10.2 Production of MOFs**

Of great importance to translating MOFs into practical technologies is the ability to manufacture MOFs with the scale, purity, and cost required for implementation. Normally, the synthesis of MOFs relies on the solution and solvothermal techniques, whereby metal salts and organic ligands are dissolved in appropriate organic solvents and exposed to elevated temperatures. Then, the products are crystallized to give single crystals in the organic solution. In the laboratory, MOFs are most commonly synthesized in milligram scales, with reaction of multiple days in expensive organic solvents [57]. However, the potential applications would require kiloton scale production rather than kilogram scale far beyond milligram scale.



**Fig. 10.3**

General block flow diagram of MOFs synthesis and evaluation processes.

The synthesis conditions are generally the balance of competition between kinetic and thermodynamic factors, resulting in a narrow range of reaction conditions for a successful synthesis.

Recently, a great deal of effort has been made to develop a method of synthesizing MOFs, including solvothermal, microwave-assisted [58–63], sonochemical [64–68], microfluidic [69–73], spray-drying [74–76], thermochemical [77], and mechanochemical [78–81] techniques. Solvent-minimization methodologies have been investigated as alternatives for solution and solvothermal techniques.

There are several common challenges for prospective scale-up production as follows:

- (1) Solvent-minimization process: Organic solvents are not only expensive, but also might cause environmental issues and there is some risk resulting from their toxicity and in some cases flammability. The significant issues would arise from the use of organic solvents on a larger scale.

- (2) Even easier activation: Although the MOFs' activation is easier than zeolites, removal of the reaction solvents and unreacted starting materials from the inside of their pores is required. This would be a major consideration on a larger scale.
- (3) Preferable alternative of metal sources: Normally, metal salts such as nitrates and chlorides are used as a metal source. However, nitrates create a safety hazard and chlorides cause corrosion on passive materials. Oxide and hydroxide metal precursors would be preferred on a larger scale.

All these challenges make the synthesis of MOFs more complicated than zeolites, because they are unique to each MOF due to their different composition, coordination nature, and pore structure. Therefore, a custom synthesis procedure suitable for each MOF is required.

A number of strategies for addressing these challenges have been demonstrated, including electrochemical, microfluidic, spray-drying, thermochemical, and mechanochemical techniques. Electrochemical synthesis of MOFs has succeeded in eliminating anions by using a metal electrode as a metal source. Microfluidic and spray-drying synthesis allow for continuous production. However, these methods share the liquid phase coordination reaction with the conventional method. Thermochemical and mechanochemical approaches achieved a solvent-free synthesis of MOFs from metal oxide or hydroxide. The mechanochemical reaction has potential advantages of large-scale production, producing quantitative yields and avoiding large quantities of solvent and high temperatures.

### **10.3 Mechanochemical synthesis**

Mechanochemistry, i.e., chemical synthesis enabled by mechanical force, is well-known in metallurgy and mineral processing, but within the last few decades it is experiencing an exciting period of rediscovery in the fields of catalysis, inorganic chemistry, and pharmaceutical synthesis [82]. The key idea behind this synthesis method is to promote chemical reactions by milling or grinding solid starting materials with minimal amounts of solvents or without solvent at all. Normally, the synthesis of MOFs relies on the liquid phase coordination reaction, whereby metal salts and organic ligands are dissolved in appropriate solvents. On the other hand, the application of mechanochemistry enables a solvent-minimization access for MOFs production. The solid-solid reaction has potential advantages for ease of handling and large-scale production, producing directly the products in powder form with quantitative yields. However, a major drawback lies in the scale-up of mechanosynthesis, which is essentially a batch processing technique with relatively low production rates. In addition, note that purification step using solvents may be still required despite the “solvent-free” or “solventless” mechanochemical reaction. Nevertheless, mechanosynthesis is the most environmentally friendly methodology, and therefore, expected as an economically promising production process for MOFs.

### 10.3.1 Three classifications of mechanochemical method

There are three different mechanochemical approaches used for MOFs production [83]. The simplest and most direct approach is neat grinding which is truly solvent-free grinding, in which the powdery starting materials are ground without the use of any solvents and/or additives. The solvent-free grinding evolved into liquid-assisted grinding which adds catalytic amounts of liquid phases to improve the mobility of the materials, enabling more versatile and quicker process. This technique is demonstrated to be effective for the synthesis of new compounds which could not be achieved by neat grinding, while still avoiding excessive use of solvents. Finally, ion- and liquid-assisted grinding is successful in promoting solid-state reactions by using catalytic liquids with salt additives to accelerate the MOFs formation. In the mechanochemical treatment, ball milling is generally performed in the same manner as grinding with a mortar and pestle, with emphasis on quantitative yields and reproducibility of the process. In the mechanochemical synthesis of MOFs, the metal sources can be diverse as pure metals, metal oxides, metal hydroxides, metal carbonates, or metal salts. Using these techniques, the rapid and quantitative synthesis of almost all major MOFs families has been successfully demonstrated, including MOF-5 [84], HKUST-1 [85–88], MOF-74 [89,90], pillared MOFs [91,92], ZIFs [93–97], and UiO-66 [98].

### 10.3.2 Pioneering studies of MOFs mechanosynthesis

James et al. demonstrated, for the first time, MOFs synthesis by mechanochemical reaction (Fig. 10.4) [99]. The neat grinding of a dry mixture of copper acetate and isonicotinic acid resulted in the formation of copper(II) isonicotinate MOF,  $\text{Cu}(\text{INA})_2$  (INA = isonicotinate), with acetic acid and water by-products partially occluded in the pores. The conventional solvothermal methods reported for the synthesis of  $\text{Cu}(\text{INA})_2$  required high temperature (150°C) and long reaction times (48 h). The same compound could be obtained in high yield within 10 min at room temperature by mechanochemical reaction without the use of solvents. This work revealed that mechanochemistry is effective for a fast, convenient, and less expensive synthesis of MOFs. A similar approach provided the industrially relevant HKUST-1 or  $\text{Cu}_3(\text{btc})_2$  (btc = 1,3,5-benzentricarboxylate).

The pioneering effort toward mechanosynthesis of MOFs from metal oxide was made by Frisčić et al. [92–94,100]. It is notable that ZnO can be used in a solid-solid reactions. They have demonstrated that liquid-assisted grinding or ion- and liquid-assisted grinding can be utilized to prepare MOFs with moderate porosity using ZnO. The addition of minute amounts of solvents, such as *N,N*-dimethylformamide, and salt catalysts, such as sodium and ammonium salts, has been indispensable to accelerate the MOFs construction. Furthermore, an additional posttreatment may be needed for activation in certain cases because the reaction of ZnO with organic ligands leads to nonporous products.

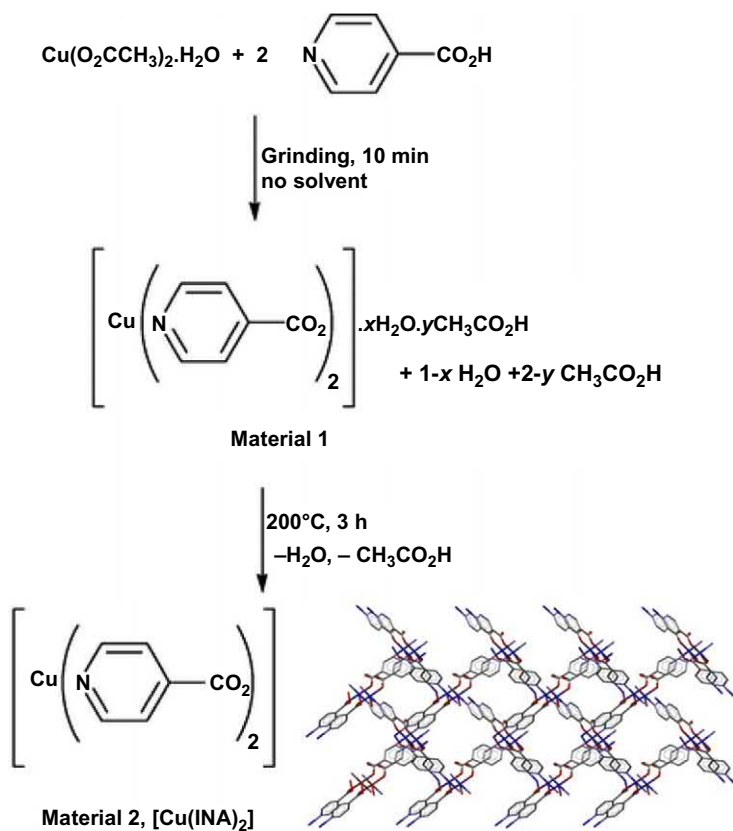


Fig. 10.4

Mechanochemical reaction between copper acetate and isonicotinic acid, resulting in the formation of copper(II) isonicotinate MOF, Cu(INA)<sub>2</sub> MOF. The initial form of the product (material 1) still contains some water and acetic acid by-products. These can be driven off by heating to give material 2, which is the empty porous framework. *Reproduced with permission from A. Pichon, A. Lazuen-Garay, S.L. James, CrystEngComm 8 (2006) 211–214. Copyright 2006 Royal Society of Chemistry.*

### 10.3.3 Mechanochemical dry conversion of metal source to MOFs

Given these findings, Balema et al. and our group presented the neat grinding synthesis of yttrium-based MIL-78 [101] and zinc-based ZIF-8 [96], respectively. The solvent-free mechanosynthesis of MIL-78 used a metal hydride as a metal source, forming hydrogen as a by-product. On the other hand, ZIF-8 was converted from ZnO and an imidazole ligand, forming water as a by-product. This approach is a very simple operation of mechanically mixing a powder mixture of ZnO and imidazole ligand at the stoichiometric ratio under normal temperature and pressure. No solvent is required, and ZIF-8 can be synthesized only by mechanically mixing ZnO and imidazole ligand at the stoichiometric ratio. The use of nanosized ZnO powder made it possible to accelerate such reaction without the use of any



solvent and salt. Avoiding the use of any solvents and salts in synthesis can reduce environmental contamination and impurity incorporation into the crystal lattice. In addition, since the by-product is only water and does not require solid-liquid separation, the loss of the product is small. The process was investigated for reaction times of 3–240 h, yielding highest specific surface area of 1480 m<sup>2</sup>/g at 96 h. The experimentally determined surface areas reported for ZIF-8 range from ~530 to 1700 m<sup>2</sup>/g, whereas the majority of values are around 1200 m<sup>2</sup>/g [24,26,27,34,63,102–106]. Therefore, the pore structure of the mechanochemically dry converted ZIF-8 is comparable to that of conventional ZIF-8. Whereas the reaction rate of ZnO with imidazole ligand estimated from TGA was increasing, the surface area and micropore volume took a downward turn after milling for 96 h due to the formation of amorphous domains. In our first effort, a tumbling ball mill was used. The tumbling ball mill is simple in structure, inexpensive and easy to scale up to a large-scale apparatus, and is suitable for large-scale production of fine powder. On the other hand, the reaction takes a long time due to the gravity mixing of the ball and the starting materials. In a planetary ball mill, a centrifugal acceleration occurs due to the two rotation axes, which are rotation of the reaction vessel and the revolution of the turntable, resulting in shortening of the reaction time. Although some research has been performed with the use of larger industrial ball mills and planetary ball mills, the apparatus still holds disadvantages such as low production volume, long equipment shutdown times, and difficulties associated with recovery of the products.

#### **10.3.4 Porosification (volume expansion and density depletion) associated with crystal conversion**

So far, although mechanochemical approach has also been used for the synthesis of zeolites, it was only a pretreatment grinding to improve the reactivity of the starting materials, or to make zeolite crystals into nanoparticles. In both cases, after mechanochemical treatment, the recrystallization process of zeolite under hydrothermal conditions is indispensable because the mechanochemical treatment causes amorphization of zeolite crystals. On the other hand, mechanochemical treatment in the synthesis of MOFs is a direct formation route of crystalline nanoporous structure (Fig. 10.5). Of particular interest is that crystal transformation of nonporous metal precursors to porous MOFs occurs with accompanying density depletion which is volume expansion. Taking the ZnO-to-ZIF-8 crystal transformation as an example, the volume expansion can be estimated as follows [96,107]:

$$\text{volume expansion} = \frac{M_{\text{ZIF-8}} \rho_{\text{ZnO}}}{M_{\text{ZnO}} \rho_{\text{ZIF-8}}}$$

where  $M$  is molecular weight and  $\rho$  is physical density. A volume change of 16.5 times ZnO may occur during the ZnO-to-ZIF-8 crystal transformation due to the difference in their



Fig. 10.5

Mechanochemical dry conversion of ZnO-to-ZIF-8 with accompanying volume expansion. A 16.5-fold in volume change is estimated during the ZnO-to-ZIF-8 crystal transformation.

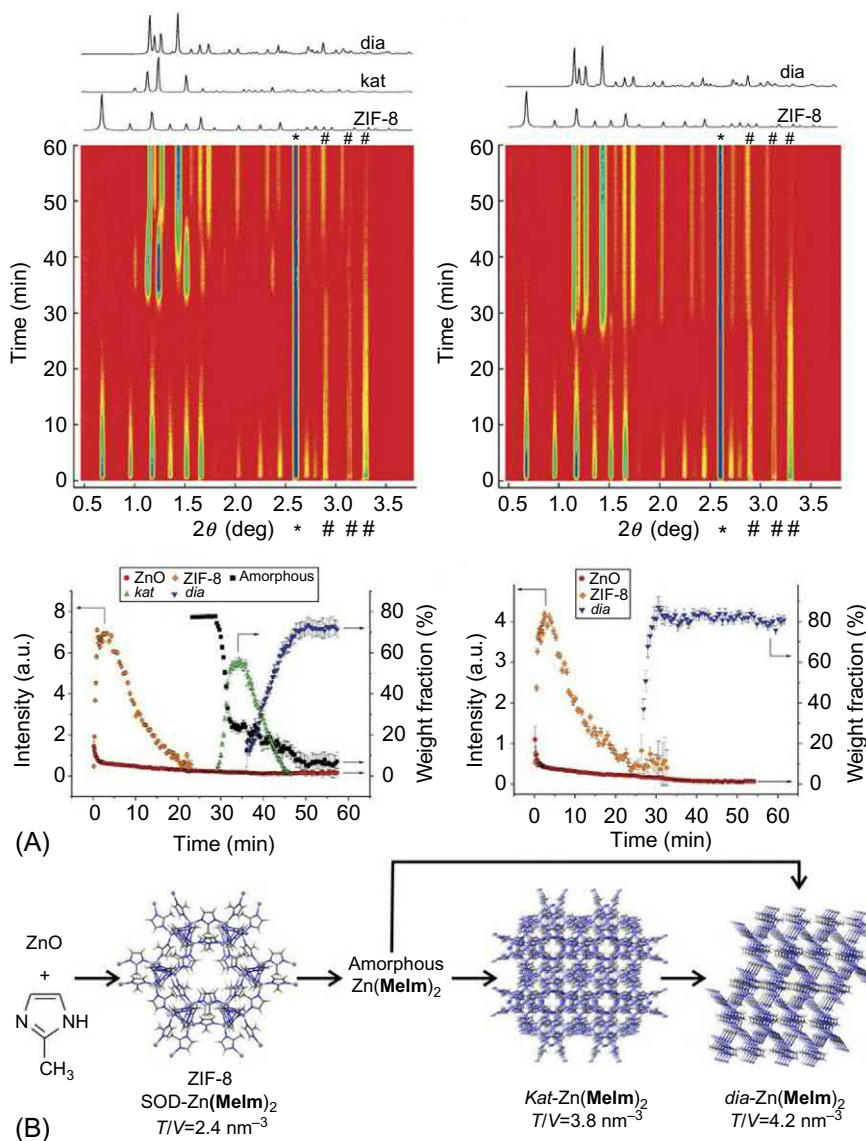
molecular weight (81.38 g/mol for ZnO and 227.58 g/mol for ZIF-8) and physical density (5.61 g/cm<sup>3</sup> for ZnO and 0.95 g/cm<sup>3</sup> for ZIF-8).

### 10.3.5 Acceleration of mechanochemical reaction

It is well-recognized that the presence of solvents provides necessary mobility for the metal ions and the organic ligands to complete the desired coordination reactions. In the neat grinding process, it is not possible to cause the reaction to occur naturally only by physical mixing of the metal sources and the organic ligands. In order to trigger the reaction, additional energy must be supplied in certain ways, such as strong mechanical force on ball milling, addition of liquid and salt catalysts, heating, and extrusion.

While neat grinding is simplest in operation which consists of grinding a dry mixture of starting materials, the synthetic range is more limited, resulting in incomplete conversion and product amorphization (Fig. 10.6) [108]. Bennett et al. revealed that neat grinding causes the amorphization of activated open MOFs [109,110]. In contrast, the presence of the liquid proved to enable not only the improvement of reactivity, but also the inhibition of amorphization due to the acting as a space-filling agent. Frisčić et al. synthesized pillared MOFs, which is designated by Hupp et al. [111], by liquid-assisted grinding from ZnO with fumaric acid and 4,4'-bipyridyl or 1,2-di(4-pyridyl)ethylene as dual ligands in the presence of a space-filling liquid agent such as *N,N*-dimethylformamide, methanol, ethanol, or 2-propanol (Fig. 10.7) [92]. Klimakow et al. synthesized HKUST-1 and its benzenetribenzoate-based analogue MOF-14 by liquid-assisted grinding from copper acetate [87]. However, the by-product acetic acid blocked the micropores, resulting in lower surface area compared to other synthetic methods.

In a recent study by Xu et al., the mechanochemical-assisted synthesis of MIL-101(Cr) was demonstrated without the use of solvent and hydrofluoric acid, but with postgrind heat



**Fig. 10.6**

(A) Time-resolved diffractograms of mechanochemical amorphization and recrystallization. (B) Crystal structure transformation. *Reproduced with permission from A.D. Katsenis, A. Puskaric, V. Strukil, C. Mottillo, P.A. Julien, K. Uzarevic, M.H. Pham, T.O. Do, S.A.J. Kimber, P. Lazic, O. Magdysyuk, R.E. Dinnebier, I. Halasz, T. Friscic, Nat. Commun 6 (2015) 6662. Copyright 2015 Springer Nature.*

treatment at 220°C for 4 h [112]. On the other hand, in a study by Frisčić et al., the gram-scale synthesis of UiO-66 and UiO-66-NH<sub>2</sub> was demonstrated with postgrind organic vapor treatment at 45°C for 3 days and 1 week, respectively [98]. As ion- and liquid-assisted grinding successfully accelerate the formation of large-pore pillared MOFs, it was also applied to ZIFs synthesis [100]. A variety of ZIFs with different structures were obtained

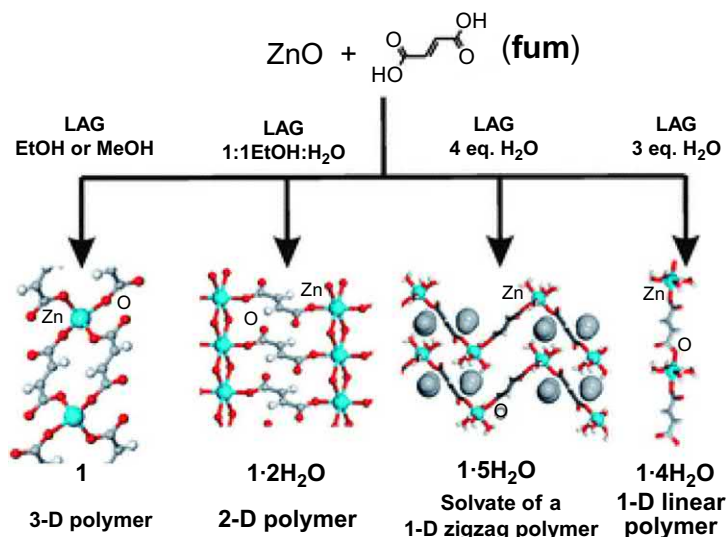
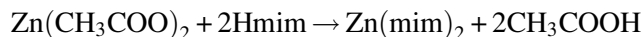


Fig. 10.7

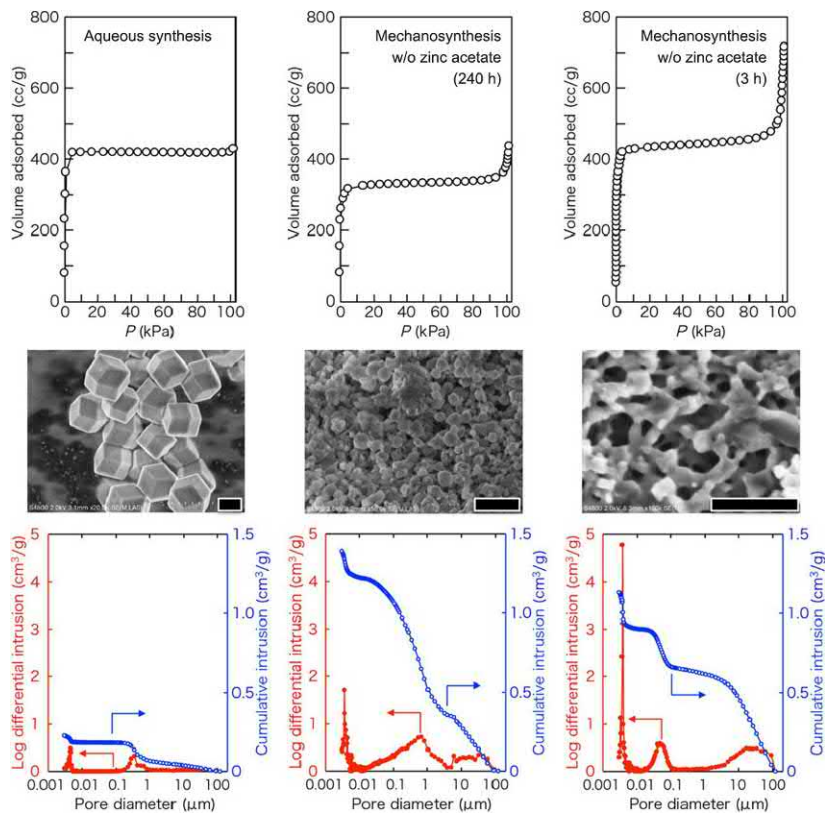
Mechanochemical reaction between ZnO and fumaric acid by liquid-assisted grinding. Guest water molecules acting as a space-filling agent are shown in gray. Reproduced with permission from T. Friščić, L. Fabian, *CrystEngComm* 11 (2009) 743–745. Copyright 2009 Royal Society of Chemistry.

quantitatively by the ion- and liquid-assisted grinding using alkali metal, ammonium nitrate, or ammonium sulfate [93]. The control of structure could be achieved by either the organic solvent and/or salt additives for grinding.

More recently, our group demonstrated that a simple salt-assisted mechanochemical synthesis can accelerate the reaction of ZnO with organic ligand and construction of ZIF-8 [113]. It is notable that the synthesis strategy is the addition of zinc salt, zinc acetate dihydrate, as both a zinc source and a catalyst. This upgraded version of solvent-free grinding enables not only large-scale and high-yield production, but also formation of unique polycrystalline micron-size particles with hierarchical superstructure (Fig. 10.8). In this approach, added zinc acetate reacts with imidazole ligands and then release acetic acid as follows:

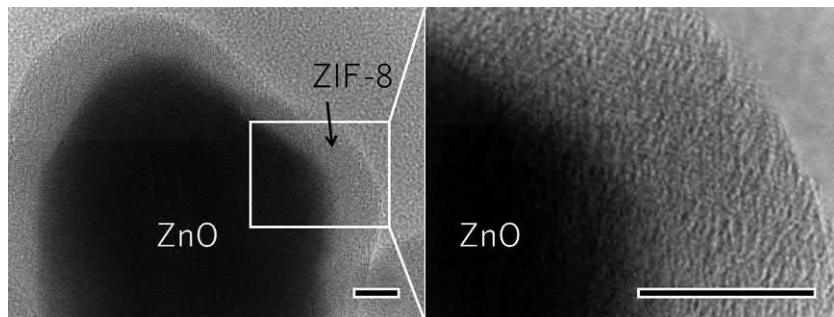


where Hmim is 2-methylimidazole and mim is deprotonated 2-methylimidazole. Our synthesis strategy is based on the expectation that the acid dissolution of ZnO and mass transfer by the autogenous acetic acid and hydrated water promote the complex forming reaction between ionized Zn and Hmim. In contrast, using neat grinding, large ZnO particles poorly reacted with imidazole ligands. The lower conversion is not surprising because the mechanochemical dry conversion, a solid-solid reaction, is dominated by a surface reaction. The reacted interface thickness was at most tens of nanometers, producing the core-shell materials with unreacted residual ZnO cores and microporous ZIF shells (Fig. 10.9). The upgraded solvent-free grinding



**Fig. 10.8**

Hierarchical pore structure of ZIF-8 prepared by simple salt-assisted mechanosynthesis. (Upper)  $N_2$  adsorption isotherms, (middle) FESEM images (scale bar: 500 nm), and mercury intrusion porosimetry of (left) conventional monocrystalline ZIF-8 and mechanosynthesized ZIF-8 powders prepared using nanosized ZnO (right) with and (center) without the addition of zinc acetate dihydrate. *Reproduced with permission from S. Tanaka, T. Nagaoka, A. Yasuyoshi, Y. Hasegawa, J.F. M. Denayer, Cryst. Growth Des. 18 (2018) 274–279. Copyright 2017 American Chemical Society.*



**Fig. 10.9**

Solvent-free mechanochemical synthesized core-shell particle with unreacted ZnO core and microporous ZIF-8 shell. When using large ZnO particles with small external surface area, surface-controlled solid-solid reactions result in low conversion only near the surface. *Reproduced with permission from S. Tanaka, K. Kida, T. Nagaoka, T. Ota, Y. Miyake, Chem. Commun. 49 (2013) 7884–7886. Copyright 2013 Royal Society of Chemistry.*





**Fig. 10.10**

Twin-screw extruder for continuous flow system of MOFs mechanosynthesis. *Reproduced with permission from D. Crawford, J. Casaban, R. Haydon, N. Giri, T. McNally, S.L. James, Chem. Sci. 6 (2015) 1645–1649. Copyright 2015 Royal Society of Chemistry.*

using solid catalysts only uses powdery starting materials for ease of handling, resulting in formation of a hierarchical trimodal architecture with interconnected porosity throughout the micro-, meso-, and macroporous regions.

### 10.3.6 Continuous flow system of MOFs mechanosynthesis

Crawford et al. applied an extrusion process to mechanochemical synthesis of MOFs, including HKUST-1, ZIF-8, and aluminum fumarate [78,88,114]. The extrusion is a continuous processing technique used in industries such as metallurgy, plastics, food, and pharmaceuticals [115]. A typical extrusion line has a single or twin-screw feeder and a heatable barrel, conveying the materials. The materials to be extruded are subjected to shear and mixing forces inside the barrel. Thus, the extrusion technique can be easily integrated or adopted into a continuous manufacturing process. HKUST-1 was synthesized by extruding copper hydroxide and 1,3,5-benzentricarboxylate in the presence of methanol (Fig. 10.10) [88]. ZIF-8 was synthesized by extruding zinc carbonate and 2-methylimidazole at 200°C without any additives. Aluminum fumarate was synthesized by extruding aluminum sulfate, sodium hydroxide, and fumaric acid at 150°C. The extrusion process is an efficient way to produce MOFs with high space-time-yields. This green chemistry continuous process is significantly promising for the convenient MOFs production.

## 10.4 Conclusions and perspectives

Despite the recent efforts in MOFs research, commercially available MOFs for their large-scale applications including biotech areas are still limited by their commercial availability [57], costs [116], stability [37,56], and safety and effectiveness. On the other hand, many



Table 10.2: MOFs manufacturer.

| Manufacturer<br>(Location)                           | MOFs (sales catalogue)                                                                                                                                        | Comment                                    | References |
|------------------------------------------------------|---------------------------------------------------------------------------------------------------------------------------------------------------------------|--------------------------------------------|------------|
| Atomis<br>(Kyoto, Japan)                             |                                                                                                                                                               | Spin-off from Kyoto University             | [117]      |
| BASF<br>(Germany)                                    | Fe-BTC (BasoliteF300)<br>HKUST-1 (BasoliteC300)<br>MOF-177 (BasoliteZ377)                                                                                     | Sold by Sigma-Aldrich                      | [118]      |
| MOFapps<br>(Oslo, Norway)                            | MIL-53(Al)<br>(BasoliteA100)<br>ZIF-8 (BasoliteZ1200)<br>Aluminum fumarate<br>HKUST-1<br>MIL-100(Fe)<br>MIL-68<br>MIL-101<br>ZIF-8<br>ZIF-67<br>UiO-66 series | Linked to ProfMOF                          | [119]      |
| MOF Technologies<br>(Belfast, Ireland)               | Aluminum fumarate<br>HKUST-1<br>MOF-74(Mg)<br>ZIF-8<br>ZIF-67                                                                                                 | Partnered with Decco to develop TruPick    | [120]      |
| NuMat<br>(Chicago, IL, United States)                |                                                                                                                                                               | ION-X for electronic gas delivery platform | [121]      |
| Promethean Particles<br>(Nottingham, United Kingdom) | MIL-53(Al)<br>ZIF-8                                                                                                                                           |                                            | [122]      |
| Strem Chemicals                                      | MIL-100(Fe)<br>PCN-250(Fe)<br>ZIF-8                                                                                                                           |                                            | [123]      |

international companies involving university spinout companies are energetically leading development, such as BASF via Sigma-Aldrich (Germany), MOF Technologies (Ireland), Johnson Matthey (United Kingdom), MOFgen (United Kingdom), Immaterial (United Kingdom), Axel'One (France), MOFapps (Norway), ProfMOF (Norway), NuMat (United States), STREM Chemicals (United States), mosaic (United States), ACSYNAM (Canada), Atomis (Japan), and so on (Table 10.2). Sigma-Aldrich provides MOF Constructor Tool which offers access to the portfolio of organic linkers and metal precursors including inorganic secondary building units suitable for the preparation of MOFs on the web [118]. Anyone can easily explore the tool to learn about the properties of different MOFs and their promising applications such as gas adsorption, storage, separations, catalysis, sensors, drug delivery, and more.

### 10.4.1 World's first commercial use of MOFs

While MOFs have long been expected for gas storage, separation, and catalysis applications, the first product transition from the laboratory was in packaging applications where MOFs were used as storage materials to release plant growth regulator that slows down ripening of fruits and vegetables. In 2016, MOF Technologies teamed up with fruit and vegetable supplier Decco Worldwide Post-Harvest Holdings to develop the MOFs usable for that next-generation packaging called TruPick [124]. The packaging works by releasing 1-methylcyclopropane, a plant growth regulator that slows down ripening. Although MOF Technologies has not released any details regarding the MOFs within the TruPick, MOF Technologies was founded based on patented mechanochemical manufacturing technique, which was invented at Queen's University in Belfast [125,126]. It is unknown how many MOFs are synthesized by mechanochemical process, though a wide catalogue for commercial MOFs is available from MOF Technologies [120]. As mentioned above, MOFs are normally synthesized in organic solvents, which poses food and bio-safety concern. Solvent-free synthesis has advantages in both such safety concerns and efficient manufacturing.

### 10.4.2 Commercial developments

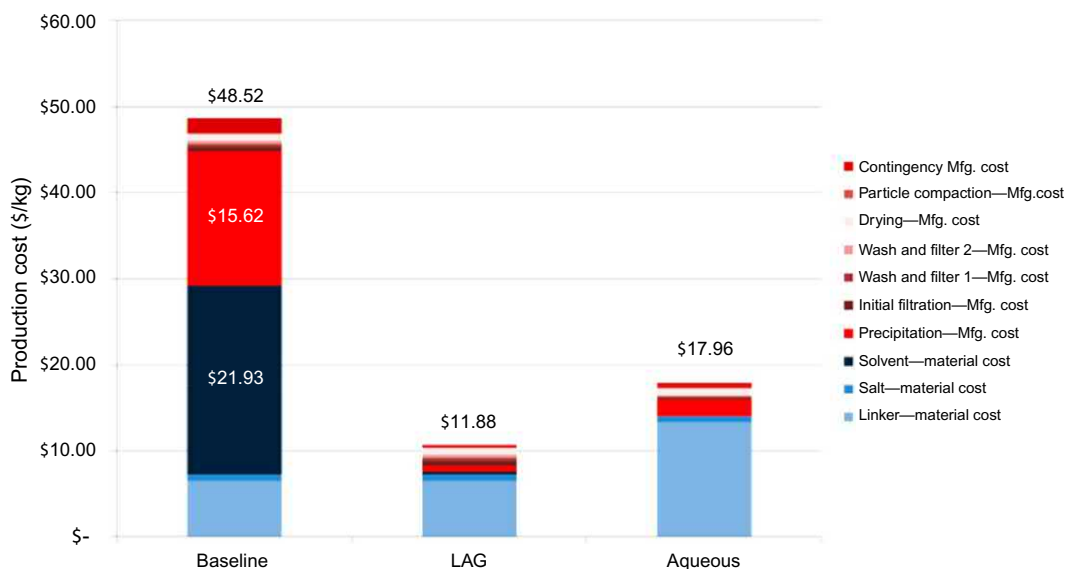
Many other companies are working toward the commercialization of MOFs. MOFgen was founded based on patented technology invented at the School of Chemistry at St Andrews [127]. MOFgen is exploiting its intellectual property in a number of applications including infection control, wound-healing, and consumer healthcare. ACSYNAM is a spinout company from the McGill University Department of Chemistry and developing a platform of energetic materials as next-generation solid fuel components for rocket and spacecraft propulsion using MOFs [128]. The group of Frisčić at the McGill University Department of Chemistry is leading the research on solvent-free methodologies for clean synthesis of MOFs. NuMat released MOF-filled dopant gas cylinders called ION-X (Fig. 10.11). The ION-X offers high capacity storage and safe delivery of dopant gases such as arsine, phosphine, and boron trifluoride for the electronics industry [129,130]. The pressure in the filled ION-X cylinder is less than 1 atm, significantly reducing the health and environmental impact of accidental gas releases. NuMat have explored multiple manufacturing processes including solvothermal, mechanochemical, and continuous flow methods [121]. MOFapps aims to develop and offer commercially viable applications in the field of gas storage, industrial cooling, toxic gas protection, and healthcare, in particular using the exclusive licensee for UiO-66 and the zirconium-based family of MOFs [119]. Atomis is a venture company from Kyoto University and aims to apply MOFs to gas storage, batteries, and analysis of trace substances for development of new pharmaceuticals [117]. Atomis has succeeded in palletization and tableting by combining MOFs and activated carbon in collaboration with Ohara Paragium Chemical. Atomis is developing a platform of “gas medicine” which is direct



**Fig. 10.11**

ION-X technology developed by NuMat for safe storage and delivery of hazardous gases. *Reproduced with permission from Nat. Chem. 8 (2016) 987. Copyright 2016 Springer Nature.*

delivery of gases such as carbon monoxide and nitric oxide to organs such as brain, heart, and liver without passing through the lungs, helping prevent and treat various diseases such as cancer. Above all, more recently, the movement toward the industrialization of MOFs has accelerated in Europe. In the framework of a Horizon 2020 project, “PROduction, control and Demonstration of structured hybrid nanoporous materials for Industrial adsorption Applications (ProDIA)” has been granted through the European Commission [131]. ProDIA focuses on the development of reliable production methods of nanoporous materials including activation and shaping processes. In the project, MOF Technologies, Johnson Matthey, and Axel One take the lead in mechanosynthesis, water-based synthesis, and spray dry synthesis, respectively, for pilot-scale production. Recently, DeSantis et al. reported techno-economic analysis for manufacture of four MOFs, MOF-5, MOF-74(Ni), MOF-74(Mg), and HKUST-1 [116]. This analysis evaluated and compared the cost breakdowns for materials and manufacturing for the three industrial-scale synthesis methods, including solvothermal, liquid-assisted grinding mechanochemical, and water-based synthesis, at 92% yield. Although material costs (primarily organic ligand and metal precursor) are lowered by increased yield, gains are modest due to the high reactant recycle rates assumed in the baseline process. Manufacturing costs are further reduced significantly by increased yield due to the lower capital expenditures for a given production rate. For promising production at a scale of



**Fig. 10.12**

A cost breakdown for the synthesis of Mg-MOF-74 by the baseline industrial-scale solvothermal, liquid-assisted grinding mechanochemical, and water-based processes with reported yields. Material costs are represented by shades of *blue*, while manufacturing costs are represented by shades of *red*. Reproduced with permission from D. DeSantis, J.A. Mason, B.D. James, C. Houchins, J.R. Long, M. Veenstra, *Energy Fuels* 31 (2017) 2024–2032. Copyright 2017 American Chemical Society.

2.5 Mkg/year, the analysis suggests that both liquid-assisted grinding mechanochemical and water-based processes reduce production costs significantly (Fig. 10.12).

### 10.4.3 Challenges to the mainstream adoption of mechanochemical synthesis

The above-mentioned recent research progress has proved that mechanochemistry can offer advantages as an alternative to traditional solvent-based synthesis. Table 10.3 shows the main examples of combining MOFs with pharmaceutically relevant organic molecules using mechanochemical techniques. For efficient control of drug delivery and release, biologically active molecules have been successfully incorporated into the framework of MOFs as building blocks, and/or encapsulated into the nanopores of MOFs as a guest. However, some challenges to the mainstream adoption of mechanochemical synthesis for MOFs still remain. In addition, the growing markets will continue to require further cost-efficiency, environmental sustainability, safety, and differentiation and advantage from other nanoporous materials.

Even if mechanochemical reaction itself is solvent-free, solvents may still be required for purification and activation processes. Even though the solvent-minimization process could be achieved in mechanochemistry, it would not be practical to use no solvent at all from the

**Table 10.3: Composite compounds of biologically active molecules and MOFs synthesized by mechanochemical reactions.**

| Metal                 | Bioactive molecule (comment)                                                                                | References |
|-----------------------|-------------------------------------------------------------------------------------------------------------|------------|
| Ag                    | 4-Aminosalicylic acid (antibiotic)                                                                          | [132]      |
| Bi                    | Salicylic acid (antiphlogistic analgetic)                                                                   | [133]      |
| Cu                    | Isonicotinic acid                                                                                           | [99]       |
| Mg                    | Ibuprofen (nonsteroidal antiphlogistic analgetic), naproxen (nonsteroidal antiinflammatory), salicylic acid | [134]      |
| Zn                    | Fumaric acid (food additive, supplement)                                                                    | [92]       |
| Zn, Cu                | Gabapentin (antiepilepticum)                                                                                | [135]      |
| La, Y, Er, Ce, Nd, Mn | Gabapentin (antiepilepticum)                                                                                | [136]      |

perspective of the whole manufacturing process. Note that mechanochemistry can provide distinct advantages over the other approaches when avoiding the use of particularly undesirable solvents such as toxicity and carcinogenicity, when reducing the energy consumption, when simplifying the subsequent production steps, and when obtaining specific reactivities not achieved by conventional other approaches.

Most of the mechanosyntheses performed in the laboratory have been performed in the range of hundreds of milligrams to several grams. The scalability issues in mechanosynthesis have not been addressed yet. The recent demonstration of continuous flow system using extruder points to interesting new directions for scalable processing of MOFs mechanosynthesis.

This review discusses the recent developments in mechanochemical methodology for MOFs synthesis. Recent mechanochemistry is rapidly expanding in the field of chemistry and materials science, changing its focus from metallurgy, size reduction, and resource recycling to pharmaceuticals, self-assembly, and supramolecular synthesis. Now, the challenge of mechanochemistry is to move away from the qualitative and often intuitive interpretations and to become a quantitative and well-understood area of chemistry. Clearly, in addition to understanding the chemical reaction itself, engineering aspects such as mass and heat transfer, scalability, and reactor design must also be understood. This links the fields of chemistry and engineering, and researchers involved in such development will be required to pay careful attention to green chemistry/engineering.

## Acknowledgments

S. Tanaka acknowledges JSPS Challenging Research (Exploratory), #19146448, and JST A-STEP, #18066368.

## References

- [1] M. Kondo, T. Yoshitomi, H. Matsuzaka, S. Kitagawa, K. Seki, Three-dimensional framework with channeling cavities for small molecules:  $\{[M_2(4,4'\text{-bpy})_3(\text{NO}_3) \cdot x\text{H}_2\text{O}]_n\}$  ( $M = \text{Co}, \text{Ni}, \text{Zn}$ ), *Angew. Chem. Int. Ed.* 36 (1997) 1725–1727.
- [2] H. Li, M. Eddaoudi, M. O’Keeffe, O.M. Yaghi, Design and synthesis of an exceptionally stable and highly porous metal-organic framework, *Nature* 402 (1999) 276–279.
- [3] S.S.Y. Chui, S.M.F. Lo, J.P.H. Charmant, A.G. Orpen, I.D. Williams, A chemically functionalizable nanoporous material  $[\text{Cu}_3(\text{TMA})_2(\text{H}_2\text{O})_3]_n$ , *Science* 283 (1999) 1148–1150.
- [4] M. Eddaoudi, D.B. Moler, H. Li, B. Chen, T.M. Reinecke, M. O’Keeffe, O.M. Yaghi, Modular chemistry: secondary building units as a basis for the design of highly porous and robust metal-organic carboxylate frameworks, *Acc. Chem. Res.* 34 (2001) 319–330.
- [5] O.M. Yaghi, M. O’Keeffe, N.W. Ockwig, H.K. Chae, M. Eddaoudi, J. Kim, Reticular synthesis and the design of new materials, *Nature* 423 (2003) 705–714.
- [6] S.L. James, Metal-organic frameworks, *Chem. Soc. Rev.* 32 (2003) 276–288.
- [7] S. Kitagawa, R. Kitaura, S. Noro, Functional porous coordination polymers, *Angew. Chem. Int. Ed.* 43 (2004) 2334–2375.
- [8] M. Fujita, M. Tominaga, A. Hori, B. Therrien, Coordination assemblies from a Pd(II)-cornered square complex, *Acc. Chem. Res.* 38 (2005) 369–378.
- [9] J.L. Rowsell, O.M. Yaghi, Strategies for hydrogen storage in metal-organic frameworks, *Angew. Chem. Int. Ed.* 44 (2005) 4670–4679.
- [10] C. Serre, C. Mellot-Draznieks, S. Surble, N. Audebrand, Y. Filinchuk, G. Férey, Role of solvent-host interactions that lead to very large swelling of hybrid frameworks, *Science* 315 (2007) 1828–1831.
- [11] D. Maspoch, D. Ruiz-Molina, J. Veciana, Old materials with new tricks: multifunctional open-framework materials, *Chem. Soc. Rev.* 36 (2007) 770–818.
- [12] G. Férey, Hybrid porous solids: past, present, future, *Chem. Soc. Rev.* 37 (2008) 191–214.
- [13] J.R. Li, R.J. Kuppler, H.C. Zhou, Selective gas adsorption and separation in metal-organic frameworks, *Chem. Soc. Rev.* 38 (2009) 1477–1504.
- [14] S. Horike, S. Shimomura, S. Kitagawa, Soft porous crystals, *Nat. Chem.* 1 (2009) 695–704.
- [15] H. Furukawa, K.E. Cordova, M. O’Keeffe, O.M. Yaghi, The chemistry and applications of metal-organic frameworks, *Science* 341 (2013) 974–986.
- [16] A. Schneemann, V. Bon, I. Schwedler, I. Senkovska, S. Kaskel, R.A. Fischer, Flexible metal-organic frameworks, *Chem. Soc. Rev.* 43 (2014) 6062–6096.
- [17] A.J. Fletcher, K.M. Thomas, M.J. Rosseinsky, Flexibility in metal-organic framework materials: impact on sorption properties, *J. Solid State Chem.* 178 (2005) 2491–2510.
- [18] H. Kajiro, A. Kondo, K. Kaneko, H. Kanoh, Flexible two-dimensional square-grid coordination polymers: structures and functions, *Int. J. Mol. Sci.* 11 (2010) 3803–3845.
- [19] S.M.J. Rogge, M. Waroquier, V. Van Speybroeck, Reliably modeling the mechanical stability of rigid and flexible metal-organic frameworks, *Acc. Chem. Res.* 51 (2018) 138–148.
- [20] M.E. Davis, R.F. Lobo, Zeolite and molecular sieve synthesis, *Chem. Mater.* 4 (1992) 756–768.
- [21] C.S. Cundy, P.A. Cox, The hydrothermal synthesis of zeolites: history and development from the earliest days to the present time, *Chem. Rev.* 103 (2003) 663–702.
- [22] X. Meng, F. Xiao, Green routes for synthesis of zeolites, *Chem. Rev.* 114 (2014) 1521–1543.
- [23] J. Li, A. Corma, J. Yu, Synthesis of new zeolite structures, *Chem. Soc. Rev.* 44 (2015) 7112–7127.
- [24] J. Cravillon, S. Munzer, S.J. Lohmeier, A. Feldhoff, K. Huber, M. Wiebcke, Rapid room-temperature synthesis and characterization of nanocrystals of a prototypical zeolitic imidazolate framework, *Chem. Mater.* 21 (2009) 1410–1412.
- [25] T. Tsuruoka, S. Furukawa, Y. Takashima, K. Yoshida, S. Isoda, S. Kitagawa, Nanoporous nanorods fabricated by coordination modulation and oriented attachment growth, *Angew. Chem. Int. Ed.* 48 (2009) 4739–4743.



- [26] Y. Pan, Y. Liu, G. Zeng, L. Zhao, Z. Lai, Rapid synthesis of zeolitic imidazolate framework-8 (ZIF-8) nanocrystals in an aqueous system, *Chem. Commun.* 47 (2011) 2071–2073.
- [27] S. Tanaka, K. Kida, M. Okita, Y. Ito, Y. Miyake, Size-controlled synthesis of zeolitic imidazolate framework-8 (ZIF-8) crystals in an aqueous system at room temperature, *Chem. Lett.* 41 (2012) 1337–1339.
- [28] K. Zhang, R.P. Lively, C. Zhang, W.J. Koros, R.R. Chance, Investigating the intrinsic ethanol/water separation capability of ZIF-8: an adsorption and diffusion study, *J. Phys. Chem. C* 117 (2013) 7214–7225.
- [29] A. Schaate, P. Roy, A. Godt, J. Lippke, F. Waltz, M. Wiebcke, P. Behrens, Modulated synthesis of Zr-based metal-organic frameworks: from nano to single crystals, *Chem. Eur. J.* 17 (2011) 6643–6651.
- [30] H. Chevreau, A. Permyakova, F. Nouar, P. Fabry, C. Livage, F. Ragon, A. Garcia-Marquez, T. Devic, N. Steunou, C. Serre, P. Horcajada, Synthesis of the biocompatible and highly stable MIL-127(Fe): from large scale synthesis to particle size control, *CrystEngComm* 18 (2016) 4094–4101.
- [31] P. Horcajada, C. Serre, M. Vallet-Regí, M. Sebban, F. Taulelle, G. Férey, Metal-organic frameworks as efficient materials for drug delivery, *Angew. Chem. Int. Ed.* 45 (2006) 5974–5978.
- [32] P. Horcajada, C. Serre, G. Maurin, N.A. Ramsahye, F. Balas, M. Vallet-Regi, M. Sebban, F. Taulelle, G. Férey, Flexible porous metal-organic frameworks for a controlled drug delivery, *J. Am. Chem. Soc.* 130 (2008) 6774–6780.
- [33] P.D.C. Dietzel, R. Blom, H. Fjellvåg, Base-induced formation of two magnesium metal-organic framework compounds with a bifunctional tetratopic ligand, *Eur. J. Inorg. Chem.* (2008) 3624–3632.
- [34] K.S. Park, Z. Ni, A.P. Cote, J.Y. Choi, R.D. Huang, F.J. Uribe-Romo, H.K. Chae, M. O’Keeffe, O.M. Yaghi, Exceptional chemical and thermal stability of zeolitic imidazolate frameworks, *Proc. Natl. Acad. Sci. U. S. A.* 103 (2006) 10186–10191.
- [35] R. Banerjee, A. Phan, B. Wang, C. Knobler, H. Furukawa, M. O’Keeffe, O.M. Yaghi, High-throughput synthesis of zeolitic imidazolate frameworks and application to CO<sub>2</sub> capture, *Science* 319 (2008) 939–943.
- [36] A. Phan, C.J. Doonan, F.J. Uribe-Romo, C.B. Knobler, M. O’Keeffe, O.M. Yaghi, Synthesis, structure, and carbon dioxide capture properties of zeolitic imidazolate frameworks, *Acc. Chem. Res.* 43 (2010) 58–67.
- [37] J.J. Low, A.I. Benin, P. Jakubczak, J.F. Abrahamian, S.A. Faheem, R.R. Willis, Virtual high throughput screening confirmed experimentally: porous coordination polymer hydration, *J. Am. Chem. Soc.* 131 (2009) 15834–15842.
- [38] N. Liédana, A. Galve, C. Rubio, C. Téllez, J. Coronas, CAF@ZIF-8: one-step encapsulation of caffeine in MOF, *ACS Appl. Mater. Interfaces* 4 (2012) 5016–5021.
- [39] L. Paseta, G. Potier, S. Abbott, J. Coronas, Using Hansen solubility parameters to study the encapsulation of caffeine in MOFs, *Org. Biomol. Chem.* 13 (2015) 1724–1731.
- [40] C.Y. Sun, C. Qin, X.L. Wang, G.S. Yang, K.Z. Shao, Y.Q. Lan, Z.M. Su, P. Huang, C.G. Wang, E.B. Wang, Zeolitic imidazolate framework-8 as efficient pH-sensitive drug delivery vehicle, *Dalton Trans.* 41 (2012) 6906–6909.
- [41] L. He, T. Wang, J. An, X. Li, L. Zhang, L. Li, G. Li, X. Wu, Z. Su, C. Wang, Carbon nanodots@zeolitic imidazolate framework-8 nanoparticles for simultaneous pH-responsive drug delivery and fluorescence imaging, *CrystEngComm* 16 (2014) 3259–3263.
- [42] I.B. Vasconcelos, T.G. da Silva, G.C.G. Militão, T.A. Soares, N.M. Rodrigues, M.O. Rodrigues, N.B. da Costa Jr., R.O. Freire, S.A. Junior, Cytotoxicity and slow release of the anti-cancer drug doxorubicin from ZIF-8, *RSC Adv.* 2 (2012) 9437–9442.
- [43] H. Ren, L. Zhang, J. An, T. Wang, L. Li, X. Si, L. He, X. Wu, C. Wang, Z. Su, Polyacrylic acid@zeolitic imidazolate framework-8 nanoparticles with ultrahigh drug loading capability for pH-sensitive drug release, *Chem. Commun.* 50 (2014) 1000–1002.
- [44] C. Zhang, W.J. Koros, Zeolitic imidazolate framework-enabled membranes: challenges and opportunities, *J. Phys. Chem. Lett.* 6 (2015) 3841–3849.
- [45] J. Pérez-Pellitero, H. Amrouche, F.R. Siperstein, G. Pirngruber, C. Nieto-Draghi, G. Chaplais, A. Simon-Masseron, D. Bazer-Bachi, D. Peralta, N. Bats, Adsorption of CO<sub>2</sub>, CH<sub>4</sub>, and N<sub>2</sub> on zeolitic imidazolate frameworks: experiments and simulations, *Chem. Eur. J.* 16 (2010) 1560–1571.

- [46] M.T. Luebbers, T.J. Wu, L.J. Shen, R.I. Masel, Effects of molecular sieving and electrostatic enhancement in the adsorption of organic compounds on the zeolitic imidazolate framework ZIF-8, *Langmuir* 26 (2010) 15625–15633.
- [47] D. Fairen-Jimenez, S.A. Moggach, M.T. Wharmby, P.A. Wright, S. Parsons, T. Düren, Opening the gate: framework flexibility in ZIF-8 explored by experiments and simulations, *J. Am. Chem. Soc.* 133 (2011) 8900–8902.
- [48] S.A. Moggach, T.D. Bennett, A.K. Cheetham, The effect of pressure on ZIF-8: increasing pore size with pressure and the formation of a high-pressure phase at 1.47 GPa, *Angew. Chem. Int. Ed.* 48 (2009) 7087–7089.
- [49] C.O. Ania, E. García-Pérez, M. Haro, J.J. Gutiérrez-Sevillano, T. Valdés-Solís, J.B. Parra, S. Calero, Understanding gas-induced structural deformation of ZIF-8, *J. Phys. Chem. Lett.* 3 (2012) 1159–1164.
- [50] L. Zhang, Z. Hu, J. Jiang, Sorption-induced structural transition of zeolitic imidazolate framework-8: a hybrid molecular simulation study, *J. Am. Chem. Soc.* 135 (2013) 3722–3728.
- [51] H. Tanaka, S. Ohsaki, S. Hiraide, D. Yamamoto, S. Watanabe, M.T. Miyahara, Adsorption-induced structural transition of ZIF-8: a combined experimental and simulation study, *J. Phys. Chem. C* 118 (2014) 8445–8454.
- [52] S. Tanaka, K. Fujita, Y. Miyake, M. Miyamoto, Y. Hasegawa, T. Makino, S. Van Der Perre, J.C.S. Remi, T. Van Assche, G.V. Baron, J.F.M. Denayer, Adsorption and diffusion phenomena in crystal size engineered ZIF-8 MOF, *J. Phys. Chem. C* 119 (2015) 28430–28439.
- [53] S. Tanaka, K. Okubo, K. Kida, M. Sugita, T. Takewaki, Grain size control of ZIF-8 membranes by seeding-free aqueous synthesis and their performances in propylene/propane separation, *J. Membr. Sci.* 544 (2017) 306–311.
- [54] H. Zheng, Y. Zhang, L. Liu, W. Wan, P. Guo, A.M. Nystrom, X. Zou, One-pot synthesis of metal-organic frameworks with encapsulated target molecules and their applications for controlled drug delivery, *J. Am. Chem. Soc.* 138 (2016) 962–968.
- [55] J. Zhuang, C.H. Kuo, L.Y. Chou, D.Y. Liu, E. Weerapana, C.K. Tsung, Optimized metal-organic-framework nanospheres for drug delivery: evaluation of small-molecule encapsulation, *ACS Nano* 8 (2014) 2812–2819.
- [56] A.J. Howarth, Y. Liu, P. Li, Z. Li, T.C. Wang, J. Hupp, O.K. Farha, Chemical, thermal and mechanical stabilities of metal-organic frameworks, *Nat. Rev. Mater.* 1 (2016) 15018.
- [57] M. Rubio-Martinez, C. Avci-Camur, A.W. Thornton, I. Imaz, D. Maspoch, M.R. Hill, New synthetic routes towards MOF production at scale, *Chem. Soc. Rev.* 46 (2017) 3453–3480.
- [58] S.H. Jung, J.H. Lee, J.S. Chang, Microwave synthesis of a nanoporous hybrid material, chromium trimesate, *Bull. Kor. Chem. Soc.* 26 (2005) 880–881.
- [59] S.H. Jung, J.H. Lee, J.W. Yoon, C. Serre, G. Férey, J.S. Chang, Microwave synthesis of chromium terephthalate MIL-101 and its benzene sorption ability, *Adv. Mater.* 19 (2007) 121–124.
- [60] Z. Ni, R.I. Masel, Rapid production of metal-organic frameworks via microwave-assisted solvothermal synthesis, *J. Am. Chem. Soc.* 128 (2006) 12394–12395.
- [61] J.S. Choi, W.J. Son, J. Kim, W.S. Ahn, Metal-organic framework MOF-5 prepared by microwave heating: factors to be considered, *Micropor. Mesopor. Mater.* 116 (2008) 727–731.
- [62] K.M.L. Taylor-Pashow, J.D. Rocca, Z. Xie, S. Tran, W. Lin, Postsynthetic modifications of iron-carboxylate nanoscale metal-organic frameworks for imaging and drug delivery, *J. Am. Chem. Soc.* 131 (2009) 14261–14263.
- [63] H. Bux, F.Y. Liang, Y.S. Li, J. Cravillon, M. Wiebcke, J. Caro, Zeolitic imidazolate framework membrane with molecular sieving properties by microwave-assisted solvothermal synthesis, *J. Am. Chem. Soc.* 131 (2009) 16000–16001.
- [64] N.A. Khan, S.H. Jung, Facile syntheses of metal-organic framework  $\text{Cu}_3(\text{BTC})_2(\text{H}_2\text{O})_3$  under ultrasound, *Bull. Kor. Chem. Soc.* 30 (2009) 2921–2926.
- [65] D.W. Jung, D.A. Yang, J. Kim, J. Kim, W.S. Ahn, Facile synthesis of MOF-177 by a sonochemical method using 1-methyl-2-pyrrolidinone as a solvent, *Dalton Trans.* 39 (2010) 2883–2887.

- [66] N.A. Khan, I.J. Kang, H.Y. Seok, S.H. Jung, Facile synthesis of nano-sized metal-organic frameworks, chromium-benzenedicarboxylate, MIL-101, *Chem. Eng. J.* 166 (2011) 1152–1157.
- [67] E. Haque, S.H. Jung, Synthesis of isostructural metal-organic frameworks, CPO-27s, with ultrasound, microwave, and conventional heating: effect of synthesis methods and metal ions, *Chem. Eng. J.* 173 (2011) 866–872.
- [68] H.Y. Cho, J. Kim, S.N. Kim, W.S. Ahn, High yield 1-L scale synthesis of ZIF-8 via a sonochemical route, *Micropor. Mesopor. Mater.* 169 (2013) 180–184.
- [69] R. Ameloot, F. Vermoortele, W. Vanhove, M.B.J. Roeyffers, B.F. Sels, D.E. De Vos, Interfacial synthesis of hollow metal-organic framework capsules demonstrating selective permeability, *Nat. Chem.* 3 (2011) 382–387.
- [70] M. Faustini, J. Kim, G.Y. Jeong, J.Y. Kim, H.R. Moon, W.S. Ahn, D.P. Kim, Microfluidic approach toward continuous and ultrafast synthesis of metal-organic framework crystals and hetero structures in confined microdroplets, *J. Am. Chem. Soc.* (2013) 14619–14626.
- [71] A. Polyzoidis, T. Altenburg, M. Schwarzer, S. Loebbecke, S. Kaskel, Continuous microreactor synthesis of ZIF-8 with high space-time-yield and tunable particle size, *Chem. Eng. J.* 283 (2016) 971–977.
- [72] S. Tai, W.Q. Zhang, J. Zhang, G. Luo, Y. Jia, M. Deng, Y. Ling, Facile preparation of UiO-66 nanoparticles with tunable sizes in a continuous flow microreactor and its application in drug delivery, *Micropor. Mesopor. Mater.* 220 (2016) 148–154.
- [73] S. Watanabe, S. Ohsaki, A. Fukuta, T. Hanafusa, K. Takada, H. Tanaka, T. Maki, K. Mae, M.T. Miyahara, Characterization of mixing performance in a microreactor and its application to the synthesis of porous coordination polymer particles, *Adv. Powder Technol.* 28 (2017) 3104–3110.
- [74] A. Carné-Sánchez, I. Imaz, M. Cano-Sarabia, D. Maspoch, A spray-drying strategy for synthesis of nanoscale metal-organic frameworks and their assembly into hollow superstructures, *Nat. Chem.* 5 (2013) 203–211.
- [75] L. Garzón-Tovar, M. Cano-Sarabia, A. Carné-Sánchez, C. Carbonell, I. Imaz, D. Maspoch, A spray-drying continuous-flow method for simultaneous synthesis and shaping of microspherical high nuclearity MOF beads, *React. Chem. Eng.* 1 (2016) 533–539.
- [76] S. Tanaka, R. Miyashita, Aqueous-system-enabled spray-drying technique for the synthesis of hollow polycrystalline ZIF-8 MOF particles, *ACS Omega* 2 (2017) 6437–6445.
- [77] J.B. Lin, R.B. Lin, X.N. Cheng, J.P. Zhang, X.M. Chen, Solvent/additive-free synthesis of porous/zeolitic metal azolate frameworks from metal oxide/hydroxide, *Chem. Commun.* 47 (2011) 9185–9187.
- [78] S.L. James, C.J. Adams, C. Bolm, D. Braga, P. Collier, T. Friscič, F. Grepioni, K.D.M. Harris, G. Hyett, W. Jones, A. Krebs, J. Mack, L. Maini, A.G. Orpen, I.P. Parkin, W.C. Shearouse, J.W. Steed, D.C. Waddell, Mechanochemistry: opportunities for new and cleaner synthesis, *Chem. Soc. Rev.* 41 (2012) 413–447.
- [79] P.A. Julien, C. Mottillo, T. Friscič, Metal-organic frameworks meet scalable and sustainable synthesis, *Green Chem.* 19 (2017) 2729–2747.
- [80] J.L. Do, T. Friscič, Mechanochemistry: a force of synthesis, *ACS Cent. Sci.* 3 (2017) 13–19.
- [81] Y.R. Miao, K.S. Suslick, Mechanochemical reactions of metal-organic frameworks, *Adv. Inorg. Chem.* 71 (2018) 403–434.
- [82] L. Takacs, The historical development of mechanochemistry, *Chem. Soc. Rev.* 42 (2013) 7649–7659.
- [83] T. Friscič, New opportunities for materials synthesis using mechanochemistry, *J. Mater. Chem.* 20 (2010) 7599–7605.
- [84] D. Lv, Y. Chen, Y. Li, R. Shi, H. Wu, X. Sun, J. Xiao, H. Xi, Q. Xia, Z. Li, Efficient mechanochemical synthesis of MOF-5 for linear alkanes adsorption, *J. Chem. Eng. Data* 62 (2017) 2030–2036.
- [85] A. Pichon, S.L. James, An array-based study of reactivity under solvent-free mechanochemical conditions—insights and trends, *CrystEngComm* 10 (2008) 1839–1847.
- [86] M. Schlesinger, S. Schulze, M. Hietschold, M. Mehning, Evaluation of synthetic methods for microporous metal-organic frameworks exemplified by the competitive formation of  $[\text{Cu}_2(\text{btc})_3(\text{H}_2\text{O})_3]$  and  $[\text{Cu}_2(\text{btc})(\text{OH})(\text{H}_2\text{O})]$ , *Micropor. Mesopor. Mater.* 132 (2010) 121–127.
- [87] M. Klimakow, P. Klobes, A.F. Thunemann, K. Rademann, F. Emmerling, Mechanochemical synthesis of metal-organic frameworks: a fast and facile approach toward quantitative yields and high specific surface areas, *Chem. Mater.* 22 (2010) 5216–5221.

- [88] D. Crawford, J. Casaban, R. Haydon, N. Giri, T. McNally, S.L. James, Synthesis by extrusion: continuous, large-scale preparation of MOFs using little or no solvent, *Chem. Sci.* 6 (2015) 1645–1649.
- [89] Y. Jia, C. Sun, Y. Peng, W. Fang, X. Yan, D. Yang, J. Zou, S.S. Mao, X. Yao, Metallic Ni nanocatalyst in situ formed from a metal-organic-framework by mechanochemical reaction for hydrogen storage in magnesium, *J. Mater. Chem. A* 3 (2015) 8294–8299.
- [90] P.A. Julien, K. Užarević, A.D. Katsenis, S.A.J. Kimber, T. Wang, O.K. Farha, Y. Zhang, J. Casaban, L.S. Germann, M. Etter, R.E. Dinnebier, S.L. James, I. Halasz, T. Friščić, In situ monitoring and mechanism of the mechanochemical formation of a microporous MOF-74 framework, *J. Am. Chem. Soc.* 138 (2016) 2929–2932.
- [91] I. Halasz, T. Friščić, S.A.J. Kimber, K. Užarević, A. Puškarić, C. Mottillo, P. Julien, V. Štrukil, V. Honkimäki, R.E. Dinnebier, Quantitative in situ and real-time monitoring of mechanochemical reactions, *Faraday Discuss.* 170 (2014) 203–221.
- [92] T. Friščić, L. Fabian, *CrystEngComm* 11 (2009) 743–745.
- [93] P.J. Beldon, L. Fábíán, R.S. Stein, A. Thirumurugan, A.K. Cheetham, T. Friščić, *Angew. Chem. Int. Ed.* 49 (2010) 9640–9643.
- [94] M.J. Cliffe, C. Mottillo, R.S. Stein, D.K. Bučarb, T. Friščić, *Chem. Sci.* 3 (2012) 2495–2500.
- [95] C. Mottillo, Y. Lu, M.H. Pham, M.J. Cliffe, T.O. Do, T. Friščić, *Green Chem.* 15 (2013) 2121–2131.
- [96] S. Tanaka, K. Kida, T. Nagaoka, T. Ota, Y. Miyake, *Chem. Commun.* 49 (2013) 7884–7886.
- [97] K. Imawaka, M. Sugita, T. Takewaki, S. Tanaka, Mechanochemical synthesis of bimetallic CoZn-ZIFs with sodalite structure, *Polyhedron* 158 (2019) 290–295.
- [98] K. Užarević, T.C. Wang, S.Y. Moon, A.M. Fidelli, J.T. Hupp, O.K. Farha, T. Friščić, Mechanochemical and solvent-free assembly of zirconium-based metal-organic frameworks, *Chem. Commun.* 52 (2016) 2133–2136.
- [99] A. Pichon, A. Lazuen-Garay, S.L. James, Solvent-free synthesis of a microporous metal-organic framework, *CrystEngComm* 8 (2006) 211–214.
- [100] T. Friščić, D.G. Reid, I. Halasz, R.S. Stein, R.E. Dinnebier, M.J. Duer, Ion- and liquid-assisted grinding: improved mechanochemical synthesis of metal-organic frameworks reveals salt inclusion and anion templating, *Angew. Chem. Int. Ed.* 49 (2010) 712–715.
- [101] N.K. Singh, M. Hardi, V.P. Balema, Mechanochemical synthesis of an yttrium based metal-organic framework, *Chem. Commun.* 49 (2013) 972–974.
- [102] X.C. Huang, Y.Y. Lin, J.P. Zhang, X.M. Chen, Ligand-directed strategy for zeolite-type metal-organic frameworks: Zinc(II) imidazolates with unusual zeolitic topologies, *Angew. Chem. Int. Ed.* 45 (2006) 1557–1559.
- [103] S.R. Venna, J.B. Jasinski, M.A. Carreon, Structural evolution of zeolitic imidazolate framework-8, *J. Am. Chem. Soc.* 132 (2010) 18030–18033.
- [104] P.Y. Moh, P. Cubillas, M.W. Anderson, M.P. Atfield, Revelation of the molecular assembly of the nanoporous metal organic framework ZIF-8, *J. Am. Chem. Soc.* 133 (2011) 13304–13307.
- [105] D. Peralta, G. Chaplais, A. Simon-Masseron, K. Barthelet, C. Chizallet, A.A. Quoineaud, G.D. Pirngruber, Comparison of the behavior of metal-organic frameworks and zeolites for hydrocarbon separations, *J. Am. Chem. Soc.* 134 (2012) 8115–8126.
- [106] K. Kida, M. Okita, K. Fujita, S. Tanaka, Y. Miyake, Formation of high crystalline ZIF-8 in an aqueous solution, *CrystEngComm* 15 (2013) 1794–1801.
- [107] S. Tanaka, K. Sakamoto, H. Inada, M. Kawata, G. Takasaki, K. Imawaka, Vapor-phase synthesis of ZIF-8 MOF thick film by conversion of ZnO nanorod array, *Langmuir* 34 (2018) 7028–7033.
- [108] T.D. Bennett, S. Cao, J.C. Tan, D.A. Keen, E.G. Bithell, P.J. Beldon, T. Friščić, A.K. Cheetham, Facile mechanosynthesis of amorphous zeolitic imidazolate frameworks, *J. Am. Chem. Soc.* 133 (2011) 14546–14549.
- [109] T.D. Bennett, A.K. Cheetham, Amorphous metal-organic frameworks, *Acc. Chem. Res.* 47 (2014) 1555–1562.
- [110] A.D. Katsenis, A. Puskarić, V. Štrukil, C. Mottillo, P.A. Julien, K. Užarević, M.H. Pham, T.O. Do, S.A.J. Kimber, P. Lazic, O. Magdysyuk, R.E. Dinnebier, I. Halasz, T. Friščić, In situ X-ray diffraction monitoring of a mechanochemical reaction reveals a unique topology metal-organic framework, *Nat. Commun.* 6 (2015) 6662.

- [111] B.Q. Ma, K.L. Mulfort, J.T. Hupp, Microporous pillared paddle-wheel frameworks based on mixed-ligand coordination of zinc ions, *Inorg. Chem.* 44 (2005) 4912–4914.
- [112] K.Y. Leng, Y.Y. Sun, X.L. Li, S. Sun, W. Xu, Rapid synthesis of metal-organic frameworks MIL-101(Cr) without the addition of solvent and hydrofluoric acid, *Cryst. Growth Des.* 16 (2016) 1168–1171.
- [113] S. Tanaka, T. Nagaoka, A. Yasuyoshi, Y. Hasegawa, J.F.M. Denayer, Hierarchical pore development of ZIF-8 MOF by simple salt-assisted mechanosynthesis, *Cryst. Growth Des.* 18 (2018) 274–279.
- [114] D.E. Crawford, J. Casaban, Recent developments in mechanochemical materials synthesis by extrusion, *Adv. Mater.* 28 (2016) 5747–5754.
- [115] J.R. Wagner Jr., E.M. Mount III, H.F. Giles Jr., *Extrusion: The Definitive Processing Guide and Handbook*, second ed., Elsevier, Oxford, UK, 2014.
- [116] D. DeSantis, J.A. Mason, B.D. James, C. Houchins, J.R. Long, M. Veenstra, Techno-economic analysis of metal-organic frameworks for hydrogen and natural gas storage, *Energy Fuel* 31 (2017) 2024–2032.
- [117] Atomis, Available from: <http://www.atomis.co.jp/en/>. (Accessed 1 June 2019).
- [118] MOF Constructor Tool of Sigma-Aldrich, Available from: <https://www.sigmaaldrich.com/materials-science/learning-center/mof-constructor.html>. (Accessed 1 June 2019).
- [119] MOFapps, Available from: <http://www.mofapps.com/>. (Accessed 1 June 2019).
- [120] MOF Technologies, Available from: <https://www.moftechnologies.com/>. (Accessed 1 June 2019).
- [121] NuMat, Available from: <https://www.numat-tech.com/>. (Accessed 1 June 2019).
- [122] Promethean Particles, Available from: <https://www.prometheanparticles.co.uk/>. (Accessed 1 June 2019).
- [123] Strem Chemicals, Available from: <https://www.strem.com/>. (Accessed 1 June 2019).
- [124] MOF Technologies Announces World's First Commercial Application of Metal Organic Framework Technology by Decco Worldwide at MOF 2016, MOF Technologies, 2016.
- [125] S.L. James, A. Lazuen-Garay, A. Pichon, Chemical Synthesis, EP1928831 B1 European Patent, 2006.
- [126] S.L. James, A. Lazuen-Garay, A. Pichon, Use of Grinding in Chemical Synthesis, US8466285 B2 United States Patent, 2007.
- [127] MOFgen, Available from: <http://www.mofgen.com/>. (Accessed 1 June 2019).
- [128] ACSYNAM, Available from: <http://www.acsynam.com/>. (Accessed 1 June 2019).
- [129] Editorial: Frameworks for commercial success. *Nat. Chem.* 8 (2016) 987.
- [130] ION-X of NuMat, Available from: <https://www.chemistryworld.com/news/mofs-offer-safer-toxic-gas-storage-/1017610.article>. (Accessed 1 June 2019).
- [131] ProDIA, Available from: <http://prodia-mof.eu/>. (Accessed 1 June 2019).
- [132] D. Braga, F. Grepioni, V. André, M.T. Duarte, Drug-containing coordination and hydrogen bonding networks obtained mechanochemically, *CrystEngComm* 11 (2009) 2618–2621.
- [133] V. André, A. Hardeman, I. Halasz, R.S. Stein, G.J. Jackson, D.G. Reid, M.J. Duer, C. Curfs, M. T. Duarte, T. Frišćić, Mechanochemical synthesis of the metallodrug bismuth subsalicylate from  $\text{Bi}_2\text{O}_3$  and structure of bismuth salicylate without auxiliary organic ligands, *Angew. Chem. Int. Ed.* 50 (2011) 7858–7861.
- [134] T. Frišćić, I. Halasz, F.C. Strobridge, R.E. Dinnebier, R.S. Stein, L. Fábíán, C. Curfs, A rational approach to screen for hydrated forms of the pharmaceutical derivative magnesium naproxen using liquid-assisted grinding, *CrystEngComm* 13 (2011) 3125–3129.
- [135] D. Braga, F. Grepioni, L. Maini, R. Brescello, L. Cotarca, Simple and quantitative mechanochemical preparation of the first zinc and copper complexes of the neuroleptic drug gabapentin, *CrystEngComm* 10 (2008) 469–471.
- [136] S. Quaresma, V. André, A.M.M. Antunes, L. Cunha-Silva, M.T. Duarte, Gabapentin coordination networks: mechanochemical synthesis and behavior under shelf conditions, *Cryst. Growth Des.* 13 (2013) 5007–5017.

# Sonochemical synthesis of MOFs

Christos Vaitsis<sup>a</sup>, Georgia Sourkouni<sup>b</sup>, Christos Argiris<sup>a,b,c</sup>

<sup>a</sup>School of Chemical Engineering, National Technical University of Athens, Athens, Greece

<sup>b</sup>Clausthal Centre of Materials Technology, Clausthal-Zellerfeld, Germany <sup>c</sup>Institute of Energy Research and Phys. Technologies, Clausthal University of Technology, Clausthal-Zellerfeld, Germany

## 11.1 Introduction

Over the last 40 years, sonochemistry has become a well-defined technique, which revolves around the ultrasound effect and acoustic cavitation. Ultrasounds include frequencies above the audible limit of human hearing (20 kHz). In chemistry and synthesis, the typical values are up to 1 MHz, while in medicine, devices operate to a maximum of 20 Mhz. This technology has been expanded in a wide spectrum of areas, ranging from chemical synthesis, biology (microbial/enzyme (in)activation), and medicine to environmental protection (water treatment, soil decontamination), food industries, and cosmetics (e.g., emulsification) [1, 2]. Some of the ultrasound applications in (bio)medicine include ultrasonic computed tomography (UCT), where acoustic waves can replace X-rays in CT scanners, with good results for breast imaging for tumor detection, lithotripsy for the removal of kidney stones, bone surgery, and more [3–5].

The effects of ultrasound derive primarily from the acoustic cavitation. The pressure fluctuations generated by the ultrasounds in a liquid medium lead to the formation, growth, and implosive collapse of bubbles. More specifically, the liquid continuously expands (negative pressure) and compresses (positive pressure) until it reaches a critical diameter, which depends on the nature of the liquid and the ultrasound frequency (Fig. 11.1). The collapse of the bubble is almost an adiabatic process and it results in the massive buildup of energy within the bubble. The microscopic cavitations bubbles can also collapse near the surface of the solid substrate and activate it or split larger particles to smaller ones or deagglomerate nanoparticles. Other than the elevated temperature and pressure, those localized hot-spots can result in powerful cavitation-generated shock waves and microjets which can cause effective stirring/mixing of the adjusted layer of liquid [2, 6].

Sonochemical reactions can occur in three distinct regions. The first region is the interior of the bubble itself, which can be visualized as a micro/nanoreactor, dictated by extreme



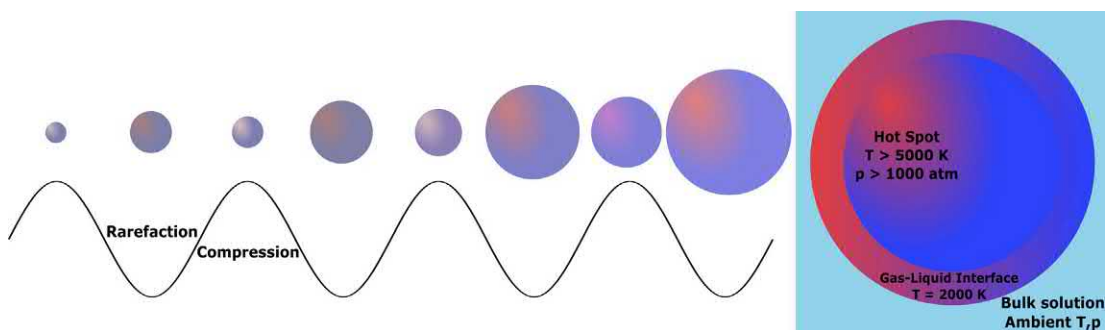


Fig. 11.1

Schematic illustration of bubble growth.

temperature ( $>5000$  K) and pressure conditions ( $>1000$  atm). The second one is the interface between the bubble and the bulk solvent. The relative efficiencies of nonvolatile solutes to react in this region depend on their hydrophobicity which determines their ability to accumulate at the gas-liquid interface [7]. The third one is the vicinity of the bubble, where the bulk solution is at the ambient temperature and free radicals form in the hot regions.

Furthermore, there are several external parameters, which can affect the yield and direction of sonochemical processes. Those processes can benefit from dissolved gas bubbles, like helium and argon, since they act as a nucleus for cavitation. By increasing the frequency, the production and intensity of cavitation in liquids decrease. The rarefaction/compression cycles are very short at high frequency to permit a bubble to grow at a size sufficient for cavitation. It is important to add that during sonication, due to extreme conditions, highly reactive radical species are generated, such as  $\text{H}_2\text{O}_2$  and  $\text{OH}\cdot$ . The amount of  $\text{H}_2\text{O}_2$  at low frequencies is lower, since a higher temperature can be maintained for a long time, inducing  $\text{H}_2\text{O}_2$  dissociation to  $\text{OH}\cdot$  [8]. Higher ultrasonic intensity can deliver more powerful sonochemical effects, but not indefinitely because the time available for the bubble collapse at high amplitudes could be insufficient. It could also result in liquid agitation instead of cavitation and poor transmission of the ultrasound in liquid media. However, an increase in temperature can allow the cavitation to be achieved at lower acoustic intensity, which is a direct consequence of the rise in vapor pressure associated with the heating of the liquid. Finally, the properties of the selected solvent can heavily affect the cavitation, since surface tension and viscosity can inhibit the formation of voids [2].

Over the past decades, sonochemistry has been widely used in organic synthesis, due to its convenience. A large array of organic reactions has been repeated under ultrasound irradiation with high yields and shorter reaction times [9]. Mild conditions have become possible and many reactions can now be performed at lower temperatures or alternative pathways with

the same or better efficiency. Selectivity has been another great advantage, since some reactions can lead to different products under the effect of US by favoring, for example, the substitution products; an effect called “sonochemical switching” [10, 11].

The extensive use of ultrasounds in various aspects of chemical processes, along with the tremendous increase in MOFs research, has brought the sonochemical synthesis of MOFs one step closer, in order to achieve shorter reaction times, phase-selectivity, and shape control. In 2008, the first sonochemical synthesis of MOFs took place by Qiu et al. with  $(\text{Zn}_3\text{BTC}_2)\cdot 12\text{H}_2\text{O}$  [12], while later that year, MOF-5 [13] and ZnBDC [14] were also successfully constructed.

## 11.2 Use of ultrasounds in MOFs

The implementation of ultrasounds in the MOF research has narrowed the gap to smaller particle size with milder conditions, as opposed to the conventional methods, mainly dictated by their need for high temperatures and long reaction times. For a more direct way to compare the different synthesis techniques, Table 11.1 has been compiled and additional information is available as well [29].

### 11.2.1 Comparison with conventional studies

To better understand the differences among the different synthesis methods, Haque et al. have performed a kinetic study in 2010, where they elucidated the determining factors by comparing conventional heating, microwaves, and ultrasounds [30]. The mild conditions synthesis of Fe-MIL-53 has made it an ideal candidate for this comparison. The average reaction time needed to obtain the product is 1.5–3 days at 70–80°C for the conventional heating, 1.5–2.5 h at 60–70°C for microwaves, and 0.5–1 h at 50–70°C for the ultrasounds. The crystallization curves have given an estimate of the nucleation and crystal growth rates, while the activation energies and preexponential factors were calculated with the Arrhenius equation.

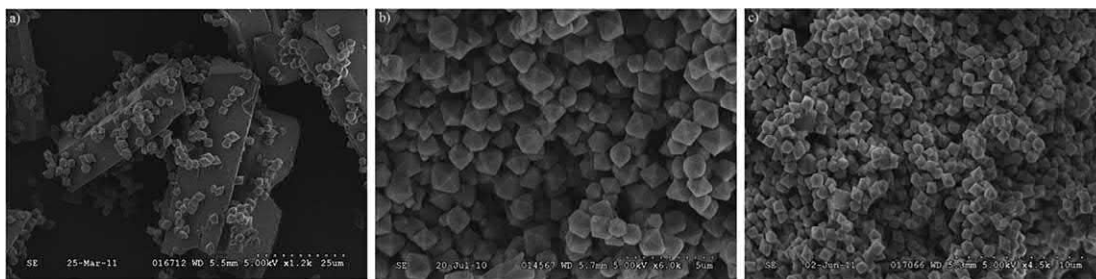
In general, chemical reactions can be accelerated either by reducing the activation energy or by increasing the preexponential factor. In this case, the increased rates (Ultrasounds > Microwaves > Conventional) are a result of increased preexponential factors. A similar study of MIL-53 was also done in 2012, where Gordon et al. tested the effect of reaction time, temperature, power (either microwave or ultrasound), and vessel type (round bottom flask and sealed pressurized glass) on the crystallinity and yield [27]. Based on the investigation, during the microwave synthesis, nucleation was visually observed after 30 s and crystalline materials could be received after 10 min, with better crystallinity after 30 min, while during sonochemical preparation, nucleation was observed after 5 min and maximum crystallinity was achieved after 7 min, pointing out that reaction time had

Table 11.1: Comparison among different synthesis methods of known MOFs.

| MOF name            | Method    | Temperature-power | Reaction time | Particle size | BET/<br>Langmuir<br>surface<br>area<br>(m <sup>2</sup> /g) | Pore<br>volume<br>(cm <sup>3</sup> /g) | Yield (%) | Morphology                              | References<br>(year) |
|---------------------|-----------|-------------------|---------------|---------------|------------------------------------------------------------|----------------------------------------|-----------|-----------------------------------------|----------------------|
| HKUST-1<br>(Cu-BTC) | ST-reflux | 150°C             | 12 h          | <30 μm        | 1239/–                                                     | 0.62                                   | 65        | Octahedral                              | [15] (2006)          |
|                     | MC        | 30 Hz             | 20 min        | –             | 1119/–                                                     | 0.59                                   | –         | –                                       | [16] (2010)          |
|                     | MW        | 140°C             | 30 min        | ~10 μm        | 1392/–                                                     | 0.56                                   | 88        | Mainly<br>octahedral                    | [17] (2009)          |
|                     | US        | 60 W              | 30 min        | 10–200 nm     | 1075/–                                                     | 0.662                                  | >62.6     | –                                       | [18] (2009)          |
|                     |           |                   |               |               |                                                            |                                        |           |                                         |                      |
|                     | US-EC     | 60%               | 15 min        | <500 nm       | 403/541                                                    | 0.332                                  | 92        | Quasi-<br>spherical and<br>octahedral   | [19] (2016)          |
| Zn-MOF-5            | RT        | RT                | 2.5 h         | –             | –/3909                                                     | –                                      | 63        | –                                       | [20] (2008)          |
|                     | ST        | 105°C             | 24 h          | ~900 μm       | –/3200                                                     | 1.21                                   | –         | Cubic                                   | [13, 21]<br>(2008)   |
|                     | MW        | 105°C<br>600 W    | 30 min        | 20–25 μm      | –/3008                                                     | 1.13                                   | –         | Cubic                                   | [21] (2008)          |
|                     | US        | 155°C<br>30%      | 10 min        | 5–25 μm       | –/3208                                                     | 1.26                                   | –         | Cubic                                   | [13] (2008)          |
| Mg-MOF-74           | RT        | RT                | 20 h          | –             | 1007/–                                                     | 0.65                                   | –         | –                                       | [22] (2014)          |
|                     | ST        | 125°C             | 24 h          | 14 μm         | 1564/–                                                     | 0.76                                   | –         | Cauliflower–<br>agglomerated<br>needles | [23] (2012)          |
|                     | MW        | 125°C<br>5°C/min  | 90 min        | 3–5 μm        | 1416/<br>2085                                              | 0.682                                  | –         | Column-like                             | [24] (2013)          |
|                     | US        | 500 W<br>(100%)   | 60 min        | 0.6 μm        | 1690/–                                                     | 0.93                                   | –         | Uniform<br>spherical                    | [23] (2012)          |

|            |    |                |        |                                                      |               |     |       |                                                                                                        |                            |
|------------|----|----------------|--------|------------------------------------------------------|---------------|-----|-------|--------------------------------------------------------------------------------------------------------|----------------------------|
| Zn-MOF-177 | RT | RT             | 3 h    | –                                                    | –/4944        | –   | 60    | –                                                                                                      | [20] (2008)                |
|            | ST | 85°C           | 48 h   | 0.5–1 mm                                             | 4833/<br>5403 | 1.9 | –     | –                                                                                                      | [25] (2010)                |
|            | MW | 105°C<br>800 W | 35 min | 15–50 µm                                             | 4197/<br>4807 | 1.7 | –     | –                                                                                                      | [26] (2007)<br>[25] (2010) |
| Fe-MIL-53  | US | 300 W<br>(60%) | 40 min | 5–20 µm                                              | 4898/<br>6210 | 2.3 | –     | –                                                                                                      |                            |
|            | ST | 150°C          | 15 h   | 25–250 µm<br>(prisms)<br>and 2.5 µm<br>(bipyramidal) | –             | –   | 56.1  | Elongated<br>triangular<br>prism-shaped<br>and<br>hexagonal<br>bipyramidal<br>Hexagonal<br>bipyramidal | [27] (2012)                |
|            | MW | 150°C<br>150 W | 30 min | 0.5–1.5 µm                                           | –             | –   | 57.6  |                                                                                                        |                            |
| Fe-MIL-88A | US | 300 W<br>(60%) | 15 min | 0.5–1.5 µm                                           | –             | –   | 30.2  |                                                                                                        |                            |
|            | HT | 65°C           | 2 h    | 550 nm                                               | –             | –   | 71.2  | –                                                                                                      | [28] (2011)                |
|            | ST | 100°C          | 24 h   | >1200 nm                                             | –             | –   | 91.7  | –                                                                                                      |                            |
|            | MW | 65–80°C        | 2 min  | 110–160 nm                                           | –             | –   | 48–59 | –                                                                                                      |                            |
|            | US | 50°C           | 15 min | >1200 nm                                             | –             | –   | 22.5  | –                                                                                                      |                            |

*RT*, room temperature; *ST*, solvothermal; *HT*, hydrothermal; *MW*, microwaves; *EC*, electrochemical; *MC*, mechanochemical; *US*, ultrasound.



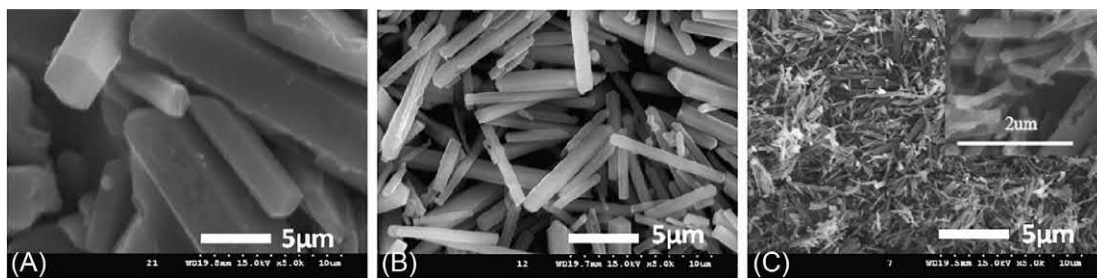
**Fig. 11.2**

SEM images of Fe-MIL-53 synthesized by (A) conventional heating at 150°C for 18 h, (B) microwaves at 150°C for 30 min, (C) ultrasounds at 60% power (VCX 500W) for 15 min [27].

greater influence on yield than power (Fig. 11.2). A recent study of Cr-MIL-101 has also confirmed the above kinetics [31].

Another essential parameter of a MOF design process is the choice of the metal center. Different metals need different approaches regarding synthesis methods and conditions, due to their physicochemical properties. Especially in biomedicine, toxicity is an important factor, along with stability and the flexibility of accepting the biomolecule. In 2011, zinc, cobalt, and nickel were compared during the sonochemical synthesis of CPO-27 (also known as MOF-74) (Fig. 11.3) [32]. Zn reactivity was shown to be higher based on the crystallization curves, in the order of  $Zn > Co > Ni$ . This behavior can be explained if the lability of metal ions, which follows the previous order, is considered. On the other hand, ligand field stabilization energy (LFSE) follows the reverse order, thus Zn has the lowest LFSE [33]. More specifically, the lability is related to the linker deprotonation, affecting the reaction rate. Hence, when labile ions are used, mild conditions are sufficient for the MOF crystallization.

Other popular synthetic approaches involve mechanochemistry and electrochemistry. Mechanochemical synthesis can be easily carried out by grinding the MOF precursors together manually in a mortar or by utilizing a ball mill [34–36]. It is a strict mechanical synthesis without



**Fig. 11.3**

SEM images of Co-CPO-27 synthesized at 70°C by (A) conventional heating for 24 h, (B) microwaves for 3 h, (C) ultrasounds for 75 min [32].

the need of any external conditions, since the temperature is increased by the friction only and the use of solvents can be avoided as well. Cu-BTC was prepared by grinding copper acetate and H<sub>3</sub>BTC for 15 min [37]. The largest portion of the particles had a size of over 60 nm, whereas the ultrasound technique led to a particle size of less than 65 nm. Surprisingly, surface area measurements revealed better values for the mechanochemical MOF (M-MOF) (BET: 1034 vs 371 m<sup>2</sup>/g, Langmuir: 1205 vs 545 m<sup>2</sup>/g, pore volume: 0.5 vs 0.386 cm<sup>3</sup>/g), but the dye adsorption experiments showed that the ultrasound one (U-MOF) had better efficiency for methylene blue (MB) and crystal violet (CV). Within 2 h, 12.5% and 7.2% have been adsorbed by M-MOF, 13.5% and 18.9% by U-MOF, while after 24 h the percentages are increased to 19.5% and 10.9% for M-MOF and 31.9% and 27.4% for U-MOF, respectively. Cu-BTC has shown a better efficiency toward MB, which could be explained due to its smaller size. In other words, MB can be captured inside the square-shaped pores easier than CV.

Cu-BTC (or HKUST-1) has been one of the most popular MOFs. It has been constructed by various methods, including attempts for scale-up continuous production and it is suitable for catalysis, gas adsorption, and other applications [38–40]. Most of its sonochemical synthesis parameters, such as ultrasound power, temperature, reaction time, solvent ratio, and sonotrode tip size, have been examined by Armstrong et al. [41]. In an attempt to divulge the crystallization mechanisms, they have studied the effects of these parameters and also compared the resulting crystals with the conventional synthesis. Variations in amplitude form an inverse parabola reaching maximum particle size at 80% power, while keeping the temperature at 10°C with an ice bath does not lead to a reaction. Particle size can be slightly decreased by increasing the reaction time with an immediate boost on yield. So, based on the above results and kinetic rates, it is suggested that the shockwave region of the bubble is involved in the crystal initiation, since in general crystal initiation can either take place in the shockwave or the implosion region [42]. Sonofragmentation is another phenomenon that should be taken into consideration during sonochemical synthesis [43, 44], which can be noticed via SEM analysis.

It has also been tested for its efficiency to adsorb the antibiotic drug rifampicin [45]. HKUST-1 was prepared by both a bulk conventional method by heating at 80°C for 24 h and under ultrasound irradiation for 1 h without external heating. Almost half of the sonochemically synthesized particles have a size of 60–100 nm, and 20% has less than 60 nm, whereas the majority of the conventional have a size above 150 nm. Regarding the uptake properties of HKUST-1 (13 mg of MOF in 50 mL aqueous solution of 0.17 mmol rifampicin), the ultrasound one can adsorb 26.6% within 3 h and 98% after 48 h, while the conventional reaches 19% and 59.6%, respectively. On the other hand, the bulk can achieve a steep release of rifampicin in dry ethanol (34.2% within 30 min) and reaches 64.9% after 120 h, whereas the sonochemical one follows a more gradual release over the course of 72 h (32.4%) and ultimately spiking up to 78.5% at 120 h, something that might make it more suitable for a controlled delivery. Imatinib was yet another candidate to investigate Cu-BTC as an adsorbent [46]. With the same



MOFs and synthesis conditions, 96.7% and 81.1% of this anticancer drug (50 mL aqueous solution of 0.085 mmol imatinib) was adsorbed after 144 h by the ultrasound and bulk MOF, respectively. However, the former cannot be fully released and around 59% is observed after 240 h, while the latter can reach 90.7%.

### 11.2.2 Alternative US methods

Another interesting approach for sonochemical synthesis is the use of a metal substrate instead of the usual nitrate or acetate form. Two zinc (MOF-5, ZIF-8) and two copper-based MOFs (Cu-BTC, Cu-BDC) were prepared as thin films by using a Cu clad and a Zn strip [47]. Before mixing them with the linkers, they were treated in an oxidizing solution of NaOH,  $(\text{NH}_4)_2\text{S}_2\text{O}_8$ , and water to receive nanowires and nanostrands. The thin films were grown in situ after a 60-min irradiation in an ultrasound bath, although the first crystals appeared at the 5-min mark. It is important to note that the ultrasonic irradiation was necessary, since the MOFs could not be obtained without it under the same conditions ( $T = 22\text{--}45^\circ\text{C}$ ).

Microemulsions are thermodynamically stable systems which consist of a water phase, an oil phase, and a surfactant. They can be considered as many nanoreactors that can be used in the synthesis of nanomaterials. With appropriate control of the synthesis parameters, they can produce tailor-made materials down to the nanoscale level. Aside from oil in water systems, water in oil microemulsions exist as well and they are referred as reverse micelles. This method has been used in 2016 for the synthesis of two zeolitic imidazolate frameworks (ZIFs) at ambient conditions [48]. In 2018, a thorium MOF was prepared with an ultrasound-assisted reverse micelle technique [49]. More specifically, an aqueous solution of thorium nitrate and a pyridine-based linker along with *n*-hexane as an oil phase and sodium dodecyl sulfate as a surfactant was introduced in an ultrasound bath for 21 min at  $40^\circ\text{C}$ . These conditions gave the optimum results with a mean particle size of 27 nm, uniform morphology, and thermal stability of  $354^\circ\text{C}$ . Without the ultrasounds, even with increased temperature ( $85^\circ\text{C}$ ) and reaction time (60 min), the product could not reach the previous results, while the crystals were prone to agglomeration and lacked uniformity.

Combinations of techniques are certainly possible and sonoelectrochemical synthesis can be such an example. This combination can be either achieved by using those two techniques independently at the same time or by incorporating the sonotrode into the electrochemical setup as a working electrode [50–52]. HKUST-1 was simply prepared by introducing the  $\text{NaNO}_3$  and  $\text{H}_3\text{BTC}$  into an electrochemical cell containing the DMF/water mixture and two copper electrodes partially submerged, which play the role of metal source [19]. The solution was kept under ultrasound irradiation, while at the same time the anodic dissolution ( $\text{Cu}_{(\text{aq})}^0 \rightleftharpoons \text{Cu}_{(\text{aq})}^{2+} + 2\text{e}^-$ ) took place by applying a potential difference. The particles had octahedral and quasi-spherical shapes and their size was under 500 nm, while the crystallite size ranged from 22.28 to 47.05 nm depending on the selected parameters. The smallest crystallite size was achieved after

3.5 min with a concentration of 24 mM H<sub>3</sub>BTC, 60% amplitude, and current density of 69 mA/cm<sup>2</sup>, but the yield was low (21%). In order to gain maximum yield (92%), duration increased to 15 min, current density to 135.5 mA/cm<sup>2</sup>, and concentration was doubled.

### 11.2.3 Effects of synthesis parameters on final product

Sonochemical synthesis can take place either into an ultrasound bath or with the use of an ultrasonic probe. Probes can generally be used in a continuous mode or a pulsed mode. Amaro-Gahete and coworkers have observed the differences among the above modes during the preparation of Fe-MIL-88A [53]. They have tested an ultrasound bath for 1 and 2 h, as well as pulsed mode for 5 and 10 min (10 s pulse duration) and a continuous mode for 10 min. By using the probes, they managed to receive smaller particles, but with lower surface areas.

It is certain that for general use, such as homogenizations, emulsifications, deagglomerations, etc., a probe is much more efficient, due to a focused and uniform input. Of course, the sonotrode diameter should always be selected by taking into consideration the solution volume, since a small tip into a large beaker would not result into a uniform process.

#### 11.2.3.1 Effect of solvents

Some of the most used solvents in the preparation of MOFs are DMF, ethanol, and water either as sole solvents or as mixtures. However, not every solvent used for a solvothermal synthesis is suitable for an ultrasound synthesis. Before selecting a solvent, it is important to consider its properties based on its type and whether it is polar or nonpolar, protic, or aprotic. Polar aprotic solvents can increase the activation energy if anionic species are involved in the system, due to the strong hydrogen bonding between the polar aprotic solvent and the anion [54].

Cu-BTC can be prepared in polar protic solvents even at room temperature with a mixture of ethanol and water after stirring for 6 h [55]. The adjustment of ethanol ratio in water can affect the final size and surface area of the crystals. If water is used as the sole solvent or even at a ratio of 75%, the MOF network collapses. This can be explained by the nature of this MOF, since large amounts of water prevent the coordination between the copper center and the carboxyl groups of BTC. Ethanol is necessary at a content of at least 33% in order to receive a crystalline structure and its use as the sole solvent can further reduce the particle size. BET surface area achieves its maximum value at 3:1 ratio of ethanol to water, so the use of water cannot be avoided when the goal is large surface areas for potential gas adsorption applications. On the other hand, when ultrasounds are used, DMF is preferred as a solvent and the particle size can be increased when the DMF content in water is decreased, although ratios with massive DMF or water parts do not form a crystalline product [41].

The effects of solvents have been illustrated by Israr and coworkers. For example, the attempt of Ni-BTC synthesis was not successful when water and/or ethanol was used under

sonication [56]. On the contrary, the same system during a solvothermal preparation can lead to crystal formation, even if it took days. However, if DMF replaces the above solvents, the effect of ultrasounds is enough to receive a crystalline product after 2 h. Similarly, good results with high BET surface area and pore volume can be achieved during the Cu-BTC sonochemical preparation with the same solvent [57]. If a mixture of water and ethanol is used, the addition of a base, such as NaOH, NH<sub>4</sub>OH, or pyridine, is essential for the acceleration of deprotonation, but the surface area is reduced.

DMF has been one of the most popular solvents for the synthesis of MOFs. With a high boiling point of ~153°C, evaporation losses are avoided at the usual operating temperatures of 80–120°C. If activation energy is taken into account, it is increased due to hydrogen bonding of negative ions and polar-protic solvents (e.g., water, ethanol), which in turn prevents the reaction between the cation and the linkers. On the other hand, DMF, as a polar aprotic solvent, can guide the negative linker anions towards the reaction with the metal cation. However, it is not certain why the intensity of this effect is so high during sonochemistry, although the reaction rate can be explained by heating uniformity, increase of heating rate, or enhancement of the precursor gel dissolution [32, 56, 58].

DEF (b.p. ~176°C) and NMP (b.p. ~202°C) have also been used for the fabrication of MOFs and specifically for the synthesis of Zn-MOF-5 (among others). DEF has been used for the conventional methods [59, 60], but NMP was introduced later in order to compare it with DEF for the sonochemical synthesis. NMP could lead to superior quality of crystals and reduced formation time (from 30 to 8 min) [13]. Its lower cost and higher boiling point have also made it attractive for the synthesis of MOF-177 [25, 26].

Conventional organic solvents are massively used in the synthesis of MOFs due to high solubility and boiling points. However, their toxicity increases the risks of environmental and health problems, turning researchers to green chemistry and alternative solvents, such as ionic liquids (IL) and deep eutectic solvents (DES). A choline chloride/dimethylurea (1:2) DES with a eutectic temperature of 70°C and almost zero vapor pressure has been successfully used as a solvent for the sonochemical synthesis of Cu-BTC [61]. Various reaction times (from 30 to 120 min) and power levels were tested with VCX 500W. By increasing the power from 20% to 40%, the temperature rises from 100°C to 167°C, with optimal results in terms of crystal quality and BET surface area at 30% power (145°C). The use of DES had also made the process of washing and evacuating the DES from the MOF pores more difficult. In other words, in order to access the maximum of the pore volume and surface area, washing with water and ethanol was necessary immediately after the synthesis and before cooling down to a temperature lower than the eutectic one, since once solidified, the surface area could only be partially recovered. Nevertheless, caution is needed when ionic liquids are tested in ultrasound synthesis, and problems can emerge due to inadequate stability and degradation upon irradiation [62].

### 11.2.3.2 Effect of US power and temperature

Generally, the ultrasound amplitude is directly linked with the reaction temperature, thus increasing the power leads to an increase in heating rate and/or maximum temperature. Of course, temperature can be adjusted to a desired level by utilizing a heating immersion circulator bath, but forcing the reaction to a lower temperature may negatively affect the yield [63] or obstruct the whole process despite the attempts for high intensities and longer reaction times [13].

During the study of Ni-BTC synthesis, the increase from 40/60% to 80% power promotes a different product, since the agitation effect can be stronger [56]. In detail, at 80% of the VCX 750W,  $C_{26}H_{44}O_8Ni_2N_8$  is collected, as opposed to  $C_{16}H_{41}O_7Ni_4N_{17}$  at 40/60%. They both belong to the same crystal system (monoclinic) and space group, but their lattice parameters, as well as their compositions, are different. A range of 50–80°C was tested as the operating temperature and 60°C gave the best results in terms of yield, which is also increased when the power level rises (29%, 78%, 88% yield at 40%, 60%, and 80% power, respectively).

Different temperatures can also lead to different morphologies. Mehrani and coworkers have studied how can they alter the morphology of  $[Cu(BDT)(DMF)\cdot CH_3OH\cdot 0.25DMF]_n$  by testing 10°C, 40°C, and 70°C [64]. More specifically, the irradiation of the mixture for 2 h with Tecna 6 ultrasonic bath can lead to rice-like at 10°C, laminate-like at 40°C, and pellet-like crystals at 70°C. Their particle size with a frequency above 50% varies from 60 to 90 nm for rice, 65–95 nm for laminate, and 100–120 nm for pellet morphology.

### 11.2.3.3 Effect of reaction time

The typical durations of sonochemical synthesis are up to 2 h, while durations less than 1 h are not uncommon, depending on the ultrasound intensity and temperature, something that makes this technique ideal compared to prolonged reaction times (12–24 h) of solvothermal methods.

Within 5 and 10 min ( $Zn_3BTC_2$ ),  $12H_2O$  nanoparticles of 50–100 nm can be collected, whereas increasing the time to 30 or 90 min, size is increased to 100–200 and 700–900 nm [12].

$Cu_2(BDC)_2(dabco)\cdot 2DMF\cdot 2H_2O$ , TMU-5, and TMU-7 particles can uniformly grow with an increased size after 90 min, compared to agglomerated particles when reaction proceeds for no further than 30 or 60 min [65–67]. Changes in size can affect morphology as well.

For example, within 10 min, Zn (BDC)( $H_2O$ ) nanobelts are being formed with a width of 150–300 nm and length of 2–5  $\mu m$ , while after 20 min quadrate nanosheets of 500 nm to 2  $\mu m$  appear and after 60 min size can go up to 10  $\mu m$  [14]. Lastly, at the 90 min mark, nanosheets attain irregular shapes. Similarly,  $[Tb(BTC)(H_2O)_6]_n$  nanorods can be prepared after 30 or 60 min with a diameter of 30–50 nm and length of 300–500 nm, which can be converted to nanowires if duration exceeds 90 min [68].  $[Zn(tptz)(fum)\cdot DMF]_n$  loses its rod morphology when doubling the reaction time from 15 to 30 min and particle size is reduced by a factor of 30 at 0.001 M [69].

Surface area can be heavily affected by reaction time, along with other parameters. For instance, MOF-177 is defined by its high surface area, so optimizations have been made in order to improve this trait. An increase in sonication time from 40 to 50 min can “push” surface area (BET) from 3322 to 4136 m<sup>2</sup>/g when ultrasound power is kept at 50% (VCX 500W) [25]. If amplitude is raised to 60%, the same kind of boost is observed when duration is increased from 30 (3710 m<sup>2</sup>/g) to 40 min (4898 m<sup>2</sup>/g).

#### 11.2.3.4 Effect of concentration

The morphology and particle size are directly associated with the initial concentration values. Various studies have been conducted regarding the optimal concentrations and the general consensus is that decreasing the reagents’ concentration can lead to the reduction of particle size. Additionally, the usual problems of agglomeration and absence of uniformity can also arise from wrong choices of initial concentrations.

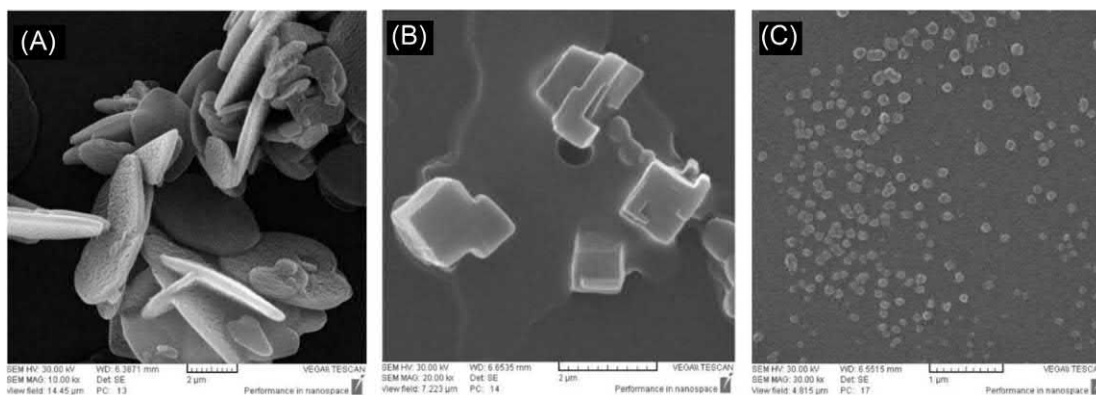
With a concentration of 0.05 M (1:1 molar ratio), the particle size of [Zn<sub>2</sub>(btec)(DMF)<sub>2</sub>]<sub>n</sub> ranges from 50 to 230 nm, where 40% of crystals are less than 140 nm [70]. Changing the concentration to 0.02 M, the range decreases to 40–160 nm, with a 45% having a particle size less than 80 nm, while with 0.001 M even smaller particles (30–105 nm) appear, where half of them are less than 60 nm. Similarly, the size of [[Na<sub>16</sub>(Ni<sub>8</sub>L<sub>12</sub>)(H<sub>2</sub>O)<sub>20</sub>(H<sub>3</sub>O)<sub>4</sub>](CH<sub>3</sub>CN)(H<sub>2</sub>O)<sub>18.5</sub>]<sub>∞</sub> (H<sub>3</sub>L = 4,5 imidazoledicarboxylic acid) can be reduced in half after reducing the initial concentrations in half [71]. With a molar ratio of 1:1.5 (metal:linker), most crystals have a size of 70–100 nm at [Ni<sup>2+</sup>] = 0.05 M, while at 0.025 M the largest part (85%) grow to a size of 30–50 nm. Higher concentrations (0.01 M) yield larger [Cd(L1)(DMF)<sub>3</sub>] (L1 = 4,4-(carbonylbis(azanediyl)) dibenzoic acid) particles in the range of 80–160 nm, while at 0.001 and 0.005 M they are reduced to 40–120 nm [72] (Fig. 11.4).

Changes in concentration can alter the morphology of TMU-31 [74]. Within 15 or 30 min, uniform TMU-31 plates could be collected for 0.01 M, uniform cubic plates for 0.005 M, and spheres for 0.001 M (Fig. 11.5). HTMU-55 was tested as a catalyst for the Henry reaction



Fig. 11.4

SEM images of sonochemically synthesized TMU-16-NH<sub>2</sub> (15 min) with concentrations of (A) 0.01 M, (B) 0.02 M, (C) 0.04 M [73].



**Fig. 11.5**

SEM images of sonochemically synthesized TMU-31 (30 min) with concentrations of (A) 0.01 M, (B) 0.005 M, (C) 0.001 M [74].

(benzaldehyde and nitromethane) [75]. It has a sphere morphology at 0.005 M (15 min) and any increase in concentration (0.01 and 0.05 M) leads to a larger size of rod particles. TMU-23 nanoplates can be received for 0.01 M, while agglomerated particles appear for 0.03 and 0.06 M [76]. By reducing the concentration, TMU-7 and TMU-21 can lose their uniformity and unique shape [67, 77]. During a 15-min experiment, particle size of  $[\text{Zn}(\text{tptz})(\text{fum})\text{-DMF}]_n$  is increased from 500 nm to 6  $\mu\text{m}$  by changing the concentration from 0.05 to 0.001 M, while at 30 min it increases from 70 to 500 nm [69].

#### 11.2.3.5 Effect of modulators and additives

Triethylamine has been widely used as an additive in order to initiate or accelerate the deprotonation of the functional (carboxylic) groups of the organic linker [20, 78]. As a vital step to the final MOF preparation, the time needed for this process can affect the whole reaction duration, and many times, depending on the agent and linker, the solvent cannot achieve this as fast or at all. The work of Yang et al. can be a simple example to demonstrate the effect of TEA [23]. During the conventional synthesis of Mg-MOF-74, the mixture is heated at 125°C. However, for the sonochemical synthesis at full power of VCX 500 W, without using an external heating source, the autogenous temperature is limited to 95°C. When TEA is added to the solution, the temperature rises to 125°C and uniform crystals can be received.

Instead of a simple addition of TEA into the solution, there is also an alternative way to introduce it by implementing a vapor-phase diffusion technique. Taking as an example the preparation of  $[\text{Cd}_2(\text{BTC})_2(\text{H}_2\text{O})_2]$ , a vial containing TEA and DMF is placed inside the beaker, which contains the main mixture [79]. The beaker gets sealed with a plastic film and placed in the ultrasonic bath. MOF nanorods with an average diameter of 30–50 nm and a length



of 300–500 nm can be collected after 5 min in the presence of TEA vapors. However, when the vial is removed from the beaker but the ultrasounds are still in effect, the nanorod templates are dissolved from the inside and MOF nanotubes are formed. The diameter of the nanorods can be increased to 50–100 nm after 5 min of the vial removal, a small number of nanotubes appear after 10 min, and a large number of nanotubes with inner diameters of 50–100 nm and outer diameter of 100–300 nm appear after the 20 min mark. Tb-BTC was also prepared with the same method [80]. Its yield of 0.6%–7.2% (based on Tb) is much lower than similar MOFs, like Cu-BTC [18], Zn-BTC [12], and Zn-BDC [14], but with a TEA presence even for 2 min, the yield manages to rise to 65.7%.

Acetic acid can be used as a modulator to block two dimensions and force the crystal growth to another. To better explain this mechanism, the conventional synthesis of [Cu(ndc)(dabco)<sub>0.5</sub>] 1D nanorods is described [81]. CH<sub>3</sub>COOH has the same functionality as the linkers, so it can hinder the coordination interaction between the metal ions and the linkers, which generates a competitive situation that regulates the rate of framework extension and crystal growth. More specifically, the crystal growth takes place in the [0 0 1] direction (dabco-Cu) instead of the [1 0 0] (ndc-Cu). In other words, due to the same carboxylate functionality of ndc and acetate, acetic acid can block the other path. By following the same mechanism, Cu<sub>2</sub>(BDC)<sub>2</sub>(dabco)·2DMF·2H<sub>2</sub>O [65] and [[Cu<sub>2</sub>(BDC-NH<sub>2</sub>)<sub>2</sub>(dabco)]DMF·3H<sub>2</sub>O] [82] were prepared in 40 kHz ultrasound bath.

DUT-32[Zn<sub>4</sub>O(BPDC)(BTCTB)<sub>4/3</sub>(DEF)<sub>39.7</sub>(H<sub>2</sub>O)<sub>11.3</sub>] synthesis parameters have been studied along with acetic acid and pyridine effect [83]. At the optimal reaction time of 60 min, where irregular structures and agglomerated particles can be avoided, it is observed that higher reagents' concentrations lead to less regular plate shapes, while with lower concentrations more spherical particles can be obtained. A higher frequency of 60 kHz was tested as well, which resulted into larger agglomerated particles, thus 40 kHz frequency was preferred. Regarding the modulator effects, the addition of pyridine led to a more uniform size with plate-like morphology and smaller thickness, while the mixture of pyridine and acetic acid yielded larger nonuniform particles. The amoxicillin removal efficiency of the ultrasound samples was investigated and values above 92% (conventional method (100°C, 48 h) threshold) were observed for the fully optimized sample. The anticancer drug doxorubicin release profile gave sufficient results at pH 7.4 (54%). Modifications in pH managed to increase the percentage to 83% (pH = 6) and 98% (pH = 4.5) over the course of 4 days. The *in vitro* cytotoxicity studies showed that both the MOF and the doxorubicin-loaded MOF had low impact to healthy cells, while the drug-loaded DUT-32 was efficient to kill prostate and cervical cancer cells.

During the sonochemical synthesis of Zn(TDC)(4-BPMH)]<sub>*n*</sub>·*n*(H<sub>2</sub>O) 1, 2, and 3 mL of pyridine were tested to examine the differences in morphology [84]. The addition of 2 mL was proven to give better results with uniform sheet-shaped nano-plates rather than nanoparticles without order. The nano-plates were also more efficient at the adsorption of 2,4-dichlorophenol and amoxicillin compared to the crystals prepared without pyridine.

### 11.2.4 MOF composites

Combining materials with other substances can be fundamental for their improvement. In other words, weak points can be ignored and new physicochemical properties can be gained with enhanced functionalities, like better stability, synthesis kinetics, and a wider range of potential applications. In a usual preparation of composites, all the reagents (MOF precursors and composite materials) are mixed together. An alluring technique, for situations where composing materials need to be trapped into the MOF cage, is called “bottle around ship”. During this *in situ* synthesis, the MOF is being built around the composing materials which will occupy the MOF pores after the formation is completed [85]. Various active species have been used for MOF composites fabrication, such as carbon allotropes, oxides, and polymers, but only a handful have been sonochemically synthesized.

Countless carbon forms have been developed through the years, including nanotubes (CNTs), fullerene, graphite, and graphene, gaining a lot of attention due to their dimensionality (0D to 3D) and degrees of graphitization [86]. Their phenomenal attributes, such as chemical and thermal robustness, mechanical strength, low toxicity, etc., can shroud the possibly low chemical stability and electrical conductivities of MOFs [87]. Two of the most interesting materials are graphene and graphene oxide (GO). Graphite consists of millions of graphene layers, where the carbon atoms are arranged in 2D hexagonal-honeycomb lattice. The graphite structure can make the material hydrophilic and expand the layer separation, when oxidizing agents are used. Thus, graphite oxide can be dispersed and exfoliated, resulting in the extraction of monolayer sheets, which is graphene oxide [88].

One of the MOFs that have been combined with GO is TMU-23 [89]. Inside an ultrasound bath, zinc acetate is added into a well-dispersed DMF solution of graphene oxide. The metal is added before the linker, in order to achieve a complete exchange of  $Zn^{2+}$  with the oxygen functional groups on the surface of GO. Subsequently, the linkers are added and GO-TMU-23 (10% GO) is prepared within 1 h. The composite was tested as a dye removal agent and a 10 ppm aqueous solution of methylene blue was used. TMU-23 and GO were also tested for comparison purposes. After only 2 min, 30 mg of GO-TMU-23 had an efficiency of 89% removal, and after 15 min, adsorption rises to 97%. At the same time, 3 mg of GO and 27 mg TMU-23 lead to efficiency rates of 48% and 50% within 2 min, while after 15 min they increase to 90% and 78%, respectively.

GO-Ni-BTC was fabricated via an ultrasound-assisted ball milling technique with water as the sole solvent [90]. The coupling effect of ultrasonic waves and mechanical force can promote the reaction without the need of organic solvents. The difference between Ni-BTC and GO-Ni-BTC was tested by measuring the adsorption efficiency in an aqueous Congo Red solution, resulting in capacities of 2046 and 2489 mg/g, respectively.

TMU-4 and TMU-5 were grown on a silk substrate and were studied for morphine adsorption [91]. A layer-by-layer deposition method was used to develop those zinc MOFs on the silk

fibers in combination with ultrasounds for homogenous coating. The fibers were treated with a NaOH solution (pH = 9) prior to MOF growth in order to deprotonate the carboxylic group on the fibers' surface. The layers were created by sequential dipping of the silk (for 90 s) in an aqueous solution of zinc nitrate and alternating with a DMF solution, which contained the linker, both of which were placed in an ultrasound bath. By skipping the ultrasound bath, the average particle size was higher while the thickness can be directly associated with the number of dipping cycles. Regarding the adsorption studies, the MOFs can fully preserve morphine after around 48 h (TMU-4) and 72 h (TMU-5) and fully release it after 12 and 14 days, respectively, with an initial average of 20% after 7 min. The same synthesis method had also been followed for Cu-BTC, which was tested for its antibacterial activity against *Escherichia coli* and *Staphylococcus aureus* [92]. A larger number of dipping cycles resulted in slightly better efficiency, but still, Cu-BTC@silk was inferior to popular drugs, such as gentamicin. Similarly, Co-BTC@silk was fabricated for the above studies, as well as for iodine adsorption [93]. HKUST-1, prepared with a combination of ultrasound and solvothermal methods, has been also combined with active carbon and tested against methicillin-resistant *S. aureus* (MRSA) and *Pseudomonas aeruginosa* [94]. Additionally, the optimization of various parameters (dye concentration, composite mass, pH, sonication time) for the adsorption of 3 dyes (crystal violet, disulfine blue, quinoline yellow) was carried out by Taguchi statistical method.

Abazari et al. have recently tested the effect of a magnetic bio-MOF (MBMOF) ( $\text{Zn}_8(\text{Ad})_4(\text{BPDC})_6\text{O}\cdot 2(\text{NH}_2(\text{CH}_3)_2)^+\cdot 8\text{DMF}\cdot 11\text{H}_2\text{O}$ ) on *Leishmania major* parasites under in vitro and in vivo conditions [95]. After the preparation of the mercapto-acetic acid functionalized  $\text{Fe}_3\text{O}_4$  nanoparticles, those were added in a DMF, water and nitric acid solution containing zinc acetate dehydrate, adenine, and BPDC in a molar ratio of 1:1:1 (0.02 M). The mixture was kept in a 40 kHz ultrasound bath for 2 h. Shorter reaction times and higher concentrations were studied as well, but agglomerated and nonuniform crystals appear. For the in vivo tests, mice subcutaneously infected with *L. major* promastigotes were used. The  $\text{Fe}_3\text{O}_4$ @MBMOF was topically applied to the lesions in an ointment form (vaseline base) with concentrations of 12.5 and 25  $\mu\text{g}/\text{mL}$ . Due to toxic impact on macrophage cells under in vitro conditions, no other form was utilized on mice. Additionally, there were three control groups, which were treated with the antimony-based drug glucantime, vaseline, and ethanol, respectively, and the last control group received no treatment. The mice were topically treated three times a week for 21 days. After the 3 weeks, the lesion size was slightly reduced in the two test groups and glucantime group. Also, the number of parasites in liver and spleen of the above groups was lower than the number of the control groups, while the higher dose of 25  $\mu\text{g}/\text{mL}$  has given the best results.

Core-shell nanoparticles have attracted a lot of attention to the biomedical field, due to their benefits to bio-imaging and drug delivery. Their properties can be modified by adjusting the core-shell ratio or changing the constituting materials, leading to better functionality and

stability, as well as controlled release of the core [96–99]. SiO<sub>2</sub> was used as a shell during the preparation of Cu-BTC [100]. In a mixture of DMF, ethanol, and water, containing the MOF precursors and NaOH, tetraethylorthosilicate is added dropwise, while the system is kept under ultrasound irradiation. Depending on the reaction time, the silica shell thickness can be controlled ranging from 12 nm (90 min) to 60 nm (150 min). The core-shell structures were deposited on glass slides with a sol-gel spin coating technique (2000 rpm) and they were tested for their photocatalytic activity of phenol decomposition under visible light, along with TiO<sub>2</sub>, pure Cu-BTC, and silica. The results showed high efficiency rates of 92% within 45 min and indicated that a thicker silica shell can improve degradation.

Abdpour et al. have attempted the decoration of Fe-MIL-53 with Fe-MIL-100 [101]. In detail, the sonochemically synthesized MIL-53 was decorated with the conventionally synthesized MIL-100, under ultrasound irradiation. The nanoparticles were deposited on the hexagonal bipyramidal crystals as a result of the electrostatic self-assembly process due to the positively charged MIL-53 surface and negatively charged MIL-100 particles and the composite was tested for its photocatalytic activity. MIL-100@MIL-53 showed enhanced performance compared to the pure MIL-53 during the degradation of methyl orange and it has improved the activity at visible light spectrum.

Fe-MIL-53 has been prepared with the addition of phosphotungstic acid (PTA) [102]. General uses of PTA include catalysis [103] and staining (in histology) [104]. In this case, PTA has managed to increase thermal stability of the MOF from 300°C to 420°C, but surface area and pore volume have been reducing due to pores being filled with PTA. The composite was evaluated as a catalyst for the esterification of oleic acid under ultrasound irradiation. The used solvent (ethanol or *n*-butanol) during this process did not have a significant impact on the yield, but modifying other parameters to the optimal values, such as PTA loading, catalyst amount, and ultrasound amplitude, increased the yield from around 20% to 97%.

## References

- [1] H. Feng, G. Barbosa-Canovas, J. Weiss, *Ultrasound Technologies for Food and Bioprocessing*, Springer, New York, 2010.
- [2] T.J. Mason, J.P. Lorimer, *Applied Sonochemistry: The Uses of Power Ultrasound in Chemistry and Processing*, Wiley-VCH, Weinheim, Germany, 2002 ix, 303 p.
- [3] G.H. Glover, J.C. Sharp, Reconstruction of ultrasound propagation speed distributions in soft tissue: time-of-flight tomography, *IEEE Trans. Sonics Ultrason.* 24 (4) (1977) 229–234.
- [4] J.F. Greenleaf, R.C. Bahn, Clinical imaging with transmissive ultrasonic computerized tomography, *IEEE Trans. Biomed. Eng.* 28 (2) (1981) 177–185.
- [5] A.L. Scherzinger, R.A. Belgam, P.L. Carson, C.R. Meyer, J.V. Sutherland, F.L. Bookstein, T.M. Silver, Assessment of ultrasonic computed tomography in symptomatic breast patients by discriminant analysis, *Ultrasound Med. Biol.* 15 (1) (1989) 21–28.
- [6] K.S. Suslick, Sonochemistry, *Science* 247 (4949) (1990) 1439–1445.
- [7] A. Henglein, Sonochemistry: historical developments and modern aspects, *Ultrasonics* 25 (1) (1987) 6–16.

- [8] J.C. Colmenares, G. Chatel, *Sonochemistry: From Basic Principles to Innovative Applications*, Springer International Publishing, 2017.
- [9] L. da Silveira Pinto, M. de Souza, Sonochemistry as a general procedure for the synthesis of coumarins, including multigram synthesis, *Synthesis* 49 (12) (2017) 2677–2682.
- [10] T. Ando, S. Sumi, T. Kawate, J. Ichihara, T. Hanafusa, Sonochemical switching of reaction pathways in solid–liquid two-phase reactions, *J. Chem. Soc., Chem. Commun.* (7) (1984) 439–440.
- [11] T. Ando, P. Bauchat, A. Foucaud, M. Fujita, T. Kimura, H. Sohmiya, Sonochemical switching from ionic to radical pathways in the reactions of styrene and trans- $\beta$ -methylstyrene with lead tetraacetate, *Tetrahedron Lett.* 32 (44) (1991) 6379–6382.
- [12] L.G. Qiu, Z.Q. Li, Y. Wu, W. Wang, T. Xu, X. Jiang, Facile synthesis of nanocrystals of a microporous metal–organic framework by an ultrasonic method and selective sensing of organoamines, *Chem. Commun.* 31 (2008) 3642–3644.
- [13] W.J. Son, J. Kim, J. Kim, W.S. Ahn, Sonochemical synthesis of MOF-5, *Chem. Commun.* 47 (2008) 6336–6338.
- [14] Z.-Q. Li, L.-G. Qiu, W. Wang, T. Xu, Y. Wu, X. Jiang, Fabrication of nanosheets of a fluorescent metal–organic framework  $[\text{Zn}(\text{BDC})(\text{H}_2\text{O})]_n$  (BDC = 1,4-benzenedicarboxylate): ultrasonic synthesis and sensing of ethylamine, *Inorg. Chem. Commun.* 11 (11) (2008) 1375–1377.
- [15] P. Krawiec, M. Kramer, M. Sabo, R. Kunschke, H. Fröde, S. Kaskel, Improved hydrogen storage in the metal–organic framework  $\text{Cu}_3(\text{BTC})_2$ , *Adv. Eng. Mater.* 8 (4) (2006) 293–296.
- [16] M. Schlesinger, S. Schulze, M. Hietschold, M. Mehring, Evaluation of synthetic methods for microporous metal–organic frameworks exemplified by the competitive formation of  $[\text{Cu}_2(\text{btc})_3(\text{H}_2\text{O})_3]$  and  $[\text{Cu}_2(\text{btc})(\text{OH})(\text{H}_2\text{O})]$ , *Microporous Mesoporous Mater.* 132 (1–2) (2010) 121–127.
- [17] Y.-K. Seo, G. Hundal, I.T. Jang, Y.K. Hwang, C.-H. Jun, J.-S. Chang, Microwave synthesis of hybrid inorganic–organic materials including porous  $\text{Cu}_3(\text{BTC})_2$  from Cu(II)-trimesate mixture, *Microporous Mesoporous Mater.* 119 (1–3) (2009) 331–337.
- [18] Z.-Q. Li, L.-G. Qiu, T. Xu, Y. Wu, W. Wang, Z.-Y. Wu, X. Jiang, Ultrasonic synthesis of the microporous metal–organic framework  $\text{Cu}_3(\text{BTC})_2$  at ambient temperature and pressure: An efficient and environmentally friendly method, *Mater. Lett.* 63 (1) (2009) 78–80.
- [19] G.G. da Silva, C.S. Silva, R.T. Ribeiro, C.M. Ronconi, B.S. Barros, J.L. Neves, S.A. Júnior, Sonoelectrochemical synthesis of metal–organic frameworks, *Synth. Met.* 220 (2016) 369–373.
- [20] D.J. Tranchemontagne, J.R. Hunt, O.M. Yaghi, Room temperature synthesis of metal–organic frameworks: MOF-5, MOF-74, MOF-177, MOF-199, and IRMOF-0, *Tetrahedron* 64 (36) (2008) 8553–8557.
- [21] J.-S. Choi, W.-J. Son, J. Kim, W.-S. Ahn, Metal–organic framework MOF-5 prepared by microwave heating: factors to be considered, *Microporous Mesoporous Mater.* 116 (1–3) (2008) 727–731.
- [22] M. Díaz-García, Á. Mayoral, I. Díaz, M. Sánchez-Sánchez, Nanoscaled M-MOF-74 materials prepared at room temperature, *Cryst. Growth Des.* 14 (5) (2014) 2479–2487.
- [23] D.-A. Yang, H.-Y. Cho, J. Kim, S.-T. Yang, W.-S. Ahn,  $\text{CO}_2$  capture and conversion using Mg-MOF-74 prepared by a sonochemical method, *Energy Environ. Sci.* 5 (4) (2012) 6465–6473.
- [24] X. Wu, Z. Bao, B. Yuan, J. Wang, Y. Sun, H. Luo, S. Deng, Microwave synthesis and characterization of MOF-74 (M = Ni, Mg) for gas separation, *Microporous Mesoporous Mater.* 180 (2013) 114–122.
- [25] D.W. Jung, D.A. Yang, J. Kim, J. Kim, W.S. Ahn, Facile synthesis of MOF-177 by a sonochemical method using 1-methyl-2-pyrrolidinone as a solvent, *Dalton Trans.* 39 (11) (2010) 2883–2887.
- [26] H. Furukawa, M.A. Miller, O.M. Yaghi, Independent verification of the saturation hydrogen uptake in MOF-177 and establishment of a benchmark for hydrogen adsorption in metal–organic frameworks, *J. Mater. Chem.* 17 (30) (2007) 3197–3204.
- [27] J. Gordon, H. Kazemian, S. Rohani, Rapid and efficient crystallization of MIL-53(Fe) by ultrasound and microwave irradiation, *Microporous Mesoporous Mater.* 162 (2012) 36–43.
- [28] T. Chalati, P. Horcajada, R. Gref, P. Couvreur, C. Serre, Optimisation of the synthesis of MOF nanoparticles made of flexible porous iron fumarate MIL-88A, *J. Mater. Chem.* 21 (7) (2011) 2220–2227.
- [29] C. Vaitsis, G. Sourkouni, C. Argiris, Metal organic frameworks (MOFs) and ultrasound: a review, *Ultrason. Sonochem.* 52C (2019) 105–118.

- [30] E. Haque, N.A. Khan, J.H. Park, S.H. Jung, Synthesis of a metal-organic framework material, iron terephthalate, by ultrasound, microwave, and conventional electric heating: a kinetic study, *Chem. Eur. J.* 16 (3) (2010) 1046–1052.
- [31] S. Pourebrahimi, M. Kazemeini, A kinetic study of facile fabrication of MIL-101(Cr) metal-organic framework: effect of synthetic method, *Inorg. Chim. Acta* 471 (2018) 513–520.
- [32] E. Haque, S.H. Jung, Synthesis of isostructural metal-organic frameworks, CPO-27s, with ultrasound, microwave, and conventional heating: effect of synthesis methods and metal ions, *Chem. Eng. J.* 173 (3) (2011) 866–872.
- [33] A.L.R. Sekaly, J. Murimboh, N.M. Hassan, R. Mandal, M.E. Ben Younes, C.L. Chakrabarti, M.H. Back, D. C. Grégoire, Kinetic speciation of Co(II), Ni(II), Cu(II), and Zn(II) in model solutions and freshwaters: lability and the d electron configuration, *Environ. Sci. Technol.* 37 (1) (2003) 68–74.
- [34] A. Pichon, A. Lazuen-Garay, S.L. James, Solvent-free synthesis of a microporous metal-organic framework, *CrystEngComm* 8 (3) (2006) 211–214.
- [35] W. Yuan, A.L. Garay, A. Pichon, R. Clowes, C.D. Wood, A.I. Cooper, S.L. James, Study of the mechanochemical formation and resulting properties of an archetypal MOF:  $\text{Cu}_3(\text{BTC})_2$  (BTC = 1,3,5-benzenetricarboxylate), *CrystEngComm* 12 (12) (2010) 4063–4065.
- [36] M. Klimakow, P. Klobes, A.F. Thünemann, K. Rademann, F. Emmerling, Mechanochemical synthesis of metal-organic frameworks: a fast and facile approach toward quantitative yields and high specific surface areas, *Chem. Mater.* 22 (18) (2010) 5216–5221.
- [37] A.R. Abbasi, M. Karimi, K. Daasbjerg, Efficient removal of crystal violet and methylene blue from wastewater by ultrasound nanoparticles Cu-MOF in comparison with mechanosynthesis method, *Ultrason. Sonochem.* 37 (2017) 182–191.
- [38] J.J. Gutiérrez-Sevillano, J.M. Vicent-Luna, D. Dubbeldam, S. Calero, Molecular mechanisms for adsorption in Cu-BTC metal organic framework, *J. Phys. Chem. C* 117 (21) (2013) 11357–11366.
- [39] A. Vishnyakov, P.I. Ravikovitch, A.V. Neimark, M. Bülow, Q.M. Wang, Nanopore structure and sorption properties of Cu-BTC metal-organic framework, *Nano Lett.* 3 (6) (2003) 713–718.
- [40] C. McKinsty, E.J. Cussen, A.J. Fletcher, S.V. Patwardhan, J. Sefcik, Scalable continuous production of high quality HKUST-1 via conventional and microwave heating, *Chem. Eng. J.* 326 (2017) 570–577.
- [41] M.R. Armstrong, S. Senthilnathan, C.J. Balzer, B. Shan, L. Chen, B. Mu, Particle size studies to reveal crystallization mechanisms of the metal organic framework HKUST-1 during sonochemical synthesis, *Ultrason. Sonochem.* 34 (2017) 365–370.
- [42] S.L. Hem, The effect of ultrasonic vibrations on crystallization processes, *Ultrasonics* 5 (4) (1967) 202–207.
- [43] S. Doktycz, K. Suslick, Interparticle collisions driven by ultrasound, *Science* 247 (4946) (1990) 1067–1069.
- [44] B.W. Zeiger, K.S. Suslick, Sonofragmentation of molecular crystals, *J. Am. Chem. Soc.* 133 (37) (2011) 14530–14533.
- [45] A.R. Abbasi, M. Rizvandi, Influence of the ultrasound-assisted synthesis of Cu-BTC metal-organic frameworks nanoparticles on uptake and release properties of rifampicin, *Ultrason. Sonochem.* 40 (Pt A) (2018) 465–471.
- [46] A.R. Abbasi, M. Rizvandi, A. Azadbakht, S. Rostamnia, Controlled uptake and release of imatinib from ultrasound nanoparticles  $\text{Cu}_3(\text{BTC})_2$  metal-organic framework in comparison with bulk structure, *J. Colloid Interface Sci.* 471 (2016) 112–117.
- [47] O. Abuzalat, D. Wong, M. Elsayed, S. Park, S. Kim, Sonochemical fabrication of Cu(II) and Zn(II) metal-organic framework films on metal substrates, *Ultrason. Sonochem.* 45 (2018) 180–188.
- [48] W. Sun, X. Zhai, L. Zhao, Synthesis of ZIF-8 and ZIF-67 nanocrystals with well-controllable size distribution through reverse microemulsions, *Chem. Eng. J.* 289 (2016) 59–64.
- [49] G. Sargazi, D. Afzali, A. Mostafavi, A novel synthesis of a new thorium (IV) metal organic framework nanostructure with well controllable procedure through ultrasound assisted reverse micelle method, *Ultrason. Sonochem.* 41 (2018) 234–251.
- [50] V. Saez, T.J. Mason, Sonoelectrochemical synthesis of nanoparticles, *Molecules* 14 (10) (2009) 4284–4299.
- [51] P. Sakkas, O. Schneider, S. Martens, P. Thanou, G. Sourkouni, C. Argiris, Fundamental studies of sonoelectrochemical nanomaterials preparation, *J. Appl. Electrochem.* 42 (9) (2012) 763–777.



- [52] D.S. Karousos, K.I. Desdenakis, P.M. Sakkas, G. Sourkouni, B.G. Pollet, C. Argirusis, Sonoelectrochemical one-pot synthesis of Pt – carbon black nanocomposite PEMFC electrocatalyst, *Ultrason. Sonochem.* 35 (Pt B) (2017) 591–597.
- [53] J. Amaro-Gahete, R. Klee, D. Esquivel, J.R. Ruiz, C. Jimenez-Sanchidrian, F.J. Romero-Salguero, Fast ultrasound-assisted synthesis of highly crystalline MIL-88A particles and their application as ethylene adsorbents, *Ultrason. Sonochem.* 50 (2019) 59–66.
- [54] J. Smith, *Organic Chemistry*, McGraw-Hill Education, 2010.
- [55] B. Zhang, J. Zhang, C. Liu, X. Sang, L. Peng, X. Ma, T. Wu, B. Han, G. Yang, Solvent determines the formation and properties of metal–organic frameworks, *RSC Adv.* 5 (47) (2015) 37691–37696.
- [56] F. Israr, D. Chun, Y. Kim, D.K. Kim, High yield synthesis of Ni-BTC metal-organic framework with ultrasonic irradiation: role of polar aprotic DMF solvent, *Ultrason. Sonochem.* 31 (2016) 93–101.
- [57] F. Israr, D.K. Kim, Y. Kim, S.J. Oh, K.C. Ng, W. Chun, Synthesis of porous Cu-BTC with ultrasonic treatment: effects of ultrasonic power and solvent condition, *Ultrason. Sonochem.* 29 (2016) 186–193.
- [58] M. Gharibeh, G.A. Tompsett, W.C. Conner, K.S. Yngvesson, Microwave synthesis of SAPO-11 and AlPO-11: aspects of reactor engineering, *ChemPhysChem* 9 (17) (2008) 2580–2591.
- [59] U. Mueller, M. Schubert, F. Teich, H. Puetter, K. Schierle-Arndt, J. Pastré, Metal–organic frameworks—prospective industrial applications, *J. Mater. Chem.* 16 (7) (2006) 626–636.
- [60] M. Eddaoudi, J. Kim, N. Rosi, D. Vodak, J. Wachter, M. O’Keeffe, O.M. Yaghi, Systematic design of pore size and functionality in isoreticular MOFs and their application in methane storage, *Science* 295 (5554) (2002) 469–472.
- [61] S.-H. Kim, S.-T. Yang, J. Kim, W.-S. Ahn, Sonochemical synthesis of  $\text{Cu}_3(\text{BTC})_2$  in a deep eutectic mixture of choline chloride/dimethylurea, *Bull. Kor. Chem. Soc.* 32 (8) (2011) 2783–2786.
- [62] J.D. Oxley, T. Prozorov, K.S. Suslick, Sonochemistry and sonoluminescence of room-temperature ionic liquids, *J. Am. Chem. Soc.* 125 (37) (2003) 11138–11139.
- [63] C.G. Carson, A.J. Brown, D.S. Sholl, S. Nair, Sonochemical synthesis and characterization of submicrometer crystals of the metal–organic framework  $\text{Cu}[(\text{hfi}(\text{pbb}))(\text{H}2\text{hfi}(\text{pbb}))0.5]$ , *Cryst. Growth Des.* 11 (10) (2011) 4505–4510.
- [64] A. Mehrani, A. Morsali, Y. Hanifehpour, S.W. Joo, Sonochemical temperature controlled synthesis of pellet-, laminate- and rice grain-like morphologies of a Cu(II) porous metal-organic framework nano-structures, *Ultrason. Sonochem.* 21 (4) (2014) 1430–1434.
- [65] M.A. Alavi, A. Morsali, Ultrasound assisted synthesis of  $\{[\text{Cu}_2(\text{BDC})_2(\text{dabco})] \cdot 2\text{DMF} \cdot 2\text{H}_2\text{O}\}$  nanostructures in the presence of modulator; new precursor to prepare nano copper oxides, *Ultrason. Sonochem.* 21 (2) (2014) 674–680.
- [66] M.Y. Masoomi, M. Bagheri, A. Morsali, High adsorption capacity of two Zn-based metal-organic frameworks by ultrasound assisted synthesis, *Ultrason. Sonochem.* 33 (2016) 54–60.
- [67] M.Y. Masoomi, M. Bagheri, A. Morsali, Porosity and dye adsorption enhancement by ultrasonic synthesized Cd(II) based metal-organic framework, *Ultrason. Sonochem.* 37 (2017) 244–250.
- [68] S.-M. Hu, H.-L. Niu, L.-G. Qiu, Y.-P. Yuan, X. Jiang, A.-J. Xie, Y.-H. Shen, J.-F. Zhu, Facile synthesis of highly luminescent nanowires of a terbium-based metal–organic framework by an ultrasonic-assisted method and their application as a luminescent probe for selective sensing of organoamines, *Inorg. Chem. Commun.* 17 (2012) 147–150.
- [69] P. Abdolalian, A. Morsali, G. Bruno, Sonochemical synthesis and characterization of microrod to nanoparticle of new mixed-ligand zinc(II) fumarate metal-organic polymer, *Ultrason. Sonochem.* 37 (2017) 654–659.
- [70] F.Z. Karizi, V. Safarifard, S.K. Khani, A. Morsali, Ultrasound-assisted synthesis of nano-structured 3D zinc(II) metal-organic polymer: precursor for the fabrication of ZnO nano-structure, *Ultrason. Sonochem.* 23 (2015) 238–245.
- [71] A. Tahmasian, A. Morsali, Ultrasonic synthesis of a 3D Ni(II) metal–organic framework at ambient temperature and pressure: new precursor for synthesis of nickel(II) oxide nano-particles, *Inorg. Chim. Acta* 387 (2012) 327–331.

- [72] L. Esrafil, A.A. Tehrani, A. Morsali, L. Carlucci, D.M. Proserpio, Ultrasound and solvothermal synthesis of a new urea-based metal-organic framework as a precursor for fabrication of cadmium(II) oxide nanostructures, *Inorg. Chim. Acta* 484 (2019) 386–393.
- [73] V. Safarifard, A. Morsali, Facile preparation of nanocubes zinc-based metal-organic framework by an ultrasound-assisted synthesis method; precursor for the fabrication of zinc oxide octahedral nanostructures, *Ultrason. Sonochem.* 40 (Pt A) (2018) 921–928.
- [74] L. Esrafil, A. Azhdari Tehrani, A. Morsali, Ultrasonic assisted synthesis of two urea functionalized metal organic frameworks for phenol sensing: a comparative study, *Ultrason. Sonochem.* 39 (2017) 307–312.
- [75] M. Joharian, A. Morsali, Ultrasound-assisted synthesis of two new fluorinated metal-organic frameworks (F-MOFs) with the high surface area to improve the catalytic activity, *J. Solid State Chem.* 270 (2019) 135–146.
- [76] M. Gharib, V. Safarifard, A. Morsali, Ultrasound assisted synthesis of amide functionalized metal-organic framework for nitroaromatic sensing, *Ultrason. Sonochem.* 42 (2018) 112–118.
- [77] F. Bigdeli, H. Ghasempour, A. Azhdari Tehrani, A. Morsali, H. Hosseini-Monfared, Ultrasound-assisted synthesis of nano-structured zinc(II)-based metal-organic frameworks as precursors for the synthesis of ZnO nano-structures, *Ultrason. Sonochem.* 37 (2017) 29–36.
- [78] L. Peng, J. Zhang, Z. Xue, B. Han, X. Sang, C. Liu, G. Yang, Highly mesoporous metal-organic framework assembled in a switchable solvent, *Nat. Commun.* 5 (2014) 4465.
- [79] R. Li, Y.P. Yuan, L.G. Qiu, W. Zhang, J.F. Zhu, A rational self-sacrificing template route to metal-organic framework nanotubes and reversible vapor-phase detection of nitroaromatic explosives, *Small* 8 (2) (2012) 225–230.
- [80] J.-D. Xiao, L.-G. Qiu, F. Ke, Y.-P. Yuan, G.-S. Xu, Y.-M. Wang, X. Jiang, Rapid synthesis of nanoscale terbium-based metal-organic frameworks by a combined ultrasound-vapour phase diffusion method for highly selective sensing of picric acid, *J. Mater. Chem. A* 1 (31) (2013) 8745–8752.
- [81] T. Tsuruoka, S. Furukawa, Y. Takashima, K. Yoshida, S. Isoda, S. Kitagawa, Nanoporous nanorods fabricated by coordination modulation and oriented attachment growth, *Angew. Chem. Int. Ed. Engl.* 48 (26) (2009) 4739–4743.
- [82] M.A. Alavi, A. Morsali, S.W. Joo, B.K. Min, Ultrasound and modulation assisted synthesis of  $\{[\text{Cu}_2(\text{BDC-NH}_2)_2(\text{dabco})]\text{DMF}\cdot 3\text{H}_2\text{O}\}$  nanostructures: new precursor to prepare nanorods and nanotubes of copper(II) oxide, *Ultrason. Sonochem.* 22 (2015) 349–358.
- [83] R. Abazari, A. Reza Mahjoub, A.M.Z. Slawin, C.L. Carpenter-Warren, Morphology- and size-controlled synthesis of a metal-organic framework under ultrasound irradiation: an efficient carrier for pH responsive release of anti-cancer drugs and their applicability for adsorption of amoxicillin from aqueous solution, *Ultrason. Sonochem.* 42 (2018) 594–608.
- [84] R. Abazari, A.R. Mahjoub, Ultrasound-assisted synthesis of Zinc(II)-based metal organic framework nanoparticles in the presence of modulator for adsorption enhancement of 2,4-dichlorophenol and amoxicillin, *Ultrason. Sonochem.* 42 (2018) 577–584.
- [85] I. Ahmed, S.H. Jung, Composites of metal-organic frameworks: preparation and application in adsorption, *Mater. Today* 17 (3) (2014) 136–146.
- [86] X.-W. Liu, T.-J. Sun, J.-L. Hu, S.-D. Wang, Composites of metal-organic frameworks and carbon-based materials: preparations, functionalities and applications, *J. Mater. Chem. A* 4 (10) (2016) 3584–3616.
- [87] Q.L. Zhu, Q. Xu, Metal-organic framework composites, *Chem. Soc. Rev.* 43 (16) (2014) 5468–5512.
- [88] X. Huang, X. Qi, F. Boey, H. Zhang, Graphene-based composites, *Chem. Soc. Rev.* 41 (2) (2012) 666–686.
- [89] M. Tanhaei, A.R. Mahjoub, V. Safarifard, Sonochemical synthesis of amide-functionalized metal-organic framework/graphene oxide nanocomposite for the adsorption of methylene blue from aqueous solution, *Ultrason. Sonochem.* 41 (2018) 189–195.
- [90] S. Zhao, D. Chen, F. Wei, N. Chen, Z. Liang, Y. Luo, Removal of Congo red dye from aqueous solution with nickel-based metal-organic framework/graphene oxide composites prepared by ultrasonic wave-assisted ball milling, *Ultrason. Sonochem.* 39 (2017) 845–852.
- [91] A.R. Abbasi, M. Yousefshahi, A. Azadbakht, Synthesis and characterization of azine-functionalized zinc cation metal-organic frameworks nanostructures upon silk fibers under ultrasound irradiation, study of pores effect on morphine adsorption affinity, *Colloid Surface A* 498 (2016) 58–65.

- [92] A.R. Abbasi, K. Akhbari, A. Morsali, Dense coating of surface mounted CuBTC metal-organic framework nanostructures on silk fibers, prepared by layer-by-layer method under ultrasound irradiation with antibacterial activity, *Ultrason. Sonochem.* 19 (4) (2012) 846–852.
- [93] S. Shamaei, A.R. Abbasi, N. Noori, E. Rafiee, A. Azadbakht, Ultrasound-assisted coating of silk yarn with nano-porous  $\text{Co}_3(\text{BTC})_2 \cdot 12\text{H}_2\text{O}$  with iodine adsorption affinity, *Colloids Surf. A Physicochem. Eng. Asp.* 431 (2013) 66–72.
- [94] F.N. Azad, M. Ghaedi, K. Dashtian, S. Hajati, V. Pezeshkpour, Ultrasonically assisted hydrothermal synthesis of activated carbon-HKUST-1-MOF hybrid for efficient simultaneous ultrasound-assisted removal of ternary organic dyes and antibacterial investigation: Taguchi optimization, *Ultrason. Sonochem.* 31 (2016) 383–393.
- [95] R. Abazari, A.R. Mahjoub, S. Molaie, F. Ghaffarifar, E. Ghasemi, A.M.Z. Slawin, C.L. Carpenter-Warren, The effect of different parameters under ultrasound irradiation for synthesis of new nanostructured  $\text{Fe}_3\text{O}_4@$ bio-MOF as an efficient anti-leishmanial in vitro and in vivo conditions, *Ultrason. Sonochem.* 43 (2018) 248–261.
- [96] X. Yang, S. Yuan, L. Zou, H. Drake, Y. Zhang, J. Qin, A. Alsalmeh, H.C. Zhou, One-step synthesis of hybrid core-shell metal-organic frameworks, *Angew. Chem. Int. Ed. Engl.* 57 (15) (2018) 3927–3932.
- [97] M.B. Gawande, A. Goswami, T. Asefa, H. Guo, A.V. Biradar, D.L. Peng, R. Zboril, R.S. Varma, Core-shell nanoparticles: synthesis and applications in catalysis and electrocatalysis, *Chem. Soc. Rev.* 44 (21) (2015) 7540–7590.
- [98] W.J. Rieter, K.M. Pott, K.M. Taylor, W. Lin, Nanoscale coordination polymers for platinum-based anticancer drug delivery, *J. Am. Chem. Soc.* 130 (35) (2008) 11584–11585.
- [99] R. Ghosh Chaudhuri, S. Paria, Core/shell nanoparticles: classes, properties, synthesis mechanisms, characterization, and applications, *Chem. Rev.* 112 (4) (2012) 2373–2433.
- [100] Z.Q. Li, A. Wang, C.Y. Guo, Y.F. Tai, L.G. Qiu, One-pot synthesis of metal-organic framework@ $\text{SiO}_2$  core-shell nanoparticles with enhanced visible-light photoactivity, *Dalton Trans.* 42 (38) (2013) 13948–13954.
- [101] S. Abdpour, E. Kowsari, M.R.A. Moghaddam, Synthesis of MIL-100(Fe)@MIL-53(Fe) as a novel hybrid photocatalyst and evaluation photocatalytic and photoelectrochemical performance under visible light irradiation, *J. Solid State Chem.* 262 (2018) 172–180.
- [102] A. Nikseresht, A. Daniyali, M. Ali-Mohammadi, A. Afzalnia, A. Mirzaie, Ultrasound-assisted biodiesel production by a novel composite of Fe(III)-based MOF and phosphotungstic acid as efficient and reusable catalyst, *Ultrason. Sonochem.* 37 (2017) 203–207.
- [103] M.H. Bhure, C.V. Rode, R.C. Chikate, N. Patwardhan, S. Patil, Phosphotungstic acid as an efficient solid catalyst for intramolecular rearrangement of benzyl phenyl ether to 2-benzyl phenol, *Catal. Commun.* 8 (2) (2007) 139–144.
- [104] G. Mazzucco, B. Basolo, G. Monga, The use of mallory’s phosphotungstic acid-hematoxylin (PTAH) stain in renal pathology, *Pathol.– Res. Pract.* 175 (4) (1982) 380–391.

# *Postsynthetic modification of MOFs for biomedical applications*

**Panagiota Markopoulou, Ross S. Forgan**

*WestCHEM School of Chemistry, University of Glasgow, Glasgow, United Kingdom*

## **12.1 Introduction**

Metal-organic frameworks [1–5], commonly referred to as MOFs or porous coordination polymers [6], are a family of hybrid, often highly porous, network structures comprising metal ions or clusters connected by organic linkers [3]. The ability to form nanosized particles of highly crystalline materials with high porosity and the possibility of tuning their properties by choosing appropriate metals and linkers are a few features of MOFs [6–11] that make them advantageous for biomedical applications [12–19]. There is no surprise that the ability to introduce complex chemical functionalities is essential in order to obtain specialized materials tailored for targeted applications. The ability to tune the chemical environment of their pore spaces can lead to very effective encapsulation of desired molecules [20, 21] (i.e., drugs), while functionalization of their outer surface [22–24] can lead to improved stability and biocompatibility, while targeting groups can also be introduced [25].

The most direct way to introduce functional groups to the structure of MOFs is by using functionalized organic linkers as building blocks during the framework synthesis [26, 27]. However, this route is often limited by the fact that the solvothermal conditions that are most commonly used for the fabrication of MOFs are quite harsh (high temperature, high pressure) and many chemical functional groups cannot survive them [28]. Moreover, even if the functional groups can tolerate the conditions, there is a high chance of unwanted side reactivity yielding undesired and unpredictable products [29].

Given the limitations of direct introduction of functional groups, the functionalization of already made materials can offer a more attractive alternative. The term postsynthetic modification (PSM) is used to describe the chemical alterations that are used in order to introduce new functionalities to an already fabricated framework [30, 31], a term inspired from the biological process of posttranslational modification of proteins [32]. As in nature, where

new chemical functionalities are introduced to an intact peptide/protein [33, 34], PSM takes place in a similar way on the final material instead of its monomers (linker/metal). It is important to note that the conditions required to achieve the modification must be tolerated by the material and typically the crystallinity of the lattice is maintained. Significantly, the fact that MOFs are porous gives the ability to postsynthetically functionalize not only their outer surfaces, but their inner surface area as well, as reagents have the ability to penetrate the interior of the materials through their pores. This is something that cannot be achieved with other types of materials like quantum dots (QDs), gold nanoparticles (AuNPs), and superparamagnetic iron nanoparticles (SPIONs) where only the exterior is available and can be modified [35].

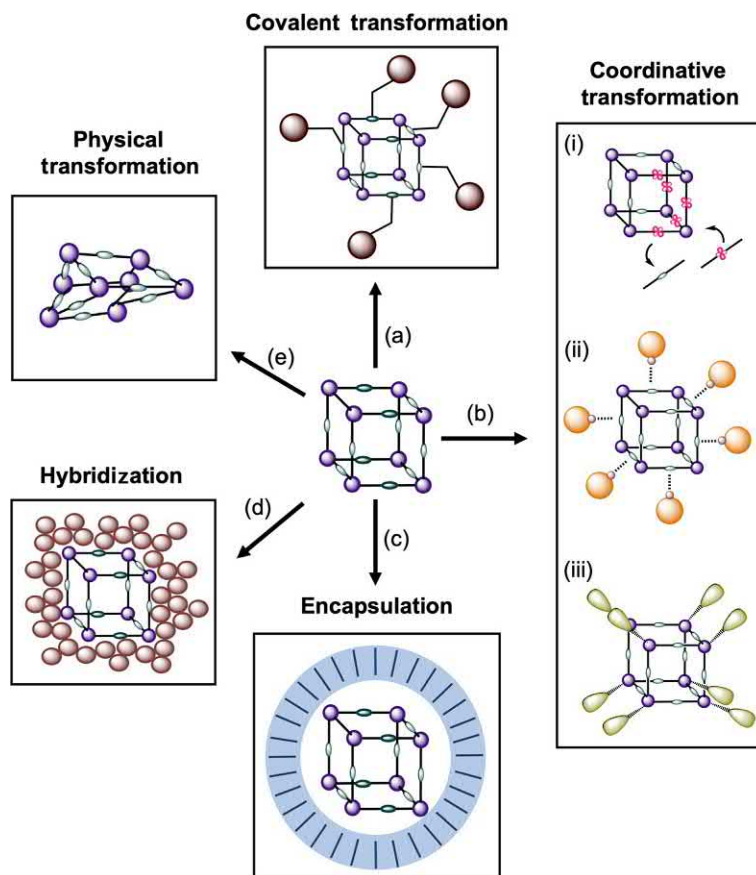
## 12.2 Types of postsynthetic modification (PSM)

In general, the PSM methods used for the functionalization of MOFs can be divided into five main groups, (i) covalent transformation, (ii) coordinative transformation, (iii) noncovalent/encapsulation, (iv) hybridization with other materials, and (v) physical changes (e.g., through application of heat or pressure) (Fig. 12.1). While most types of PSM applied for biomedical applications are chemical in nature and aim to maintain the crystallinity of the materials, there are some recent examples of physical postsynthetic modifications of MOFs where the aim is to alter the crystal structure of the materials in order to achieve desired properties like controlled drug release. The coming sections will describe some brief examples of each strategy in the context of drug delivery.

### 12.2.1 Covalent postsynthetic modification

In covalent PSM, a reagent is used to modify a component of the framework (most usually the organic linker) by forming a new covalent bond. At first glance, covalent PSM may seem more challenging than noncovalent coordinative functionalization. However, MOFs can exhibit exceptional thermal and chemical stability [36], making this a very viable technique. Many types of covalent PSM have been employed by several groups to functionalize MOFs, including amide bond coupling [37–40], urea formation [40, 41], bromination [42–44], so-called click reactions [45–48], imine condensation [40, 49, 50], and alkylation [51].

While covalent PSM is typically carried out on pendant functional groups attached to the MOF linkers, Forgan et al. [47] developed a covalent surface functionalization protocol via a copper-catalyzed azide-alkyne cycloaddition (CuAAC) to convert functionalized modulators and selectively surface functionalize Zr-based nanoparticles of the Zr MOF UiO-66 ( $\text{Zr}_6\text{O}_4(\text{OH})_4(\text{RCO}_2)_{12}$  oxoclusters connected via terephthalate linkers, UiO standing for Universitetet i Oslo) with a variety of polymers. Modulators are capping ligands that are added during MOF synthesis which can control both particle size and surface chemistry; in this case, *p*-azidomethylbenzoic acid was introduced to particle surfaces during one-pot syntheses.



**Fig. 12.1**

Schematic illustrations of various postsynthetic modification protocols: (a) covalent transformation; (b) coordinative transformation, separated into (i) linker exchange, (ii) coordination to ligand donor sites, and (iii) coordination to inorganic secondary building units; (c) encapsulation; (d) hybridization with other materials, and (e) physical transformation, such as pressure or heat.

Alkyne-functionalized poly(ethylene) glycol (PEG) chains of different molecular weights were covalently attached to the azide-modulated UiO-66 nanoparticles (Fig. 12.2A), with thermogravimetric analysis (TGA) showing an addition of  $\sim 21.7\%$  (w/w) organic matter. Critically, covalent bond formation was confirmed by mass spectrometry, while controls using no catalyst showed no evidence of PEGylation. Moreover, as it was shown from degradation studies, the PEGylated materials showed significantly improved stability toward phosphate degradation, thus enhancing their potential for use as drug delivery systems. As a proof of concept, prior to surface functionalization, the nanoparticles were loaded with calcein, a fluorescent model drug molecule. The release of the cargo was observed to be significantly delayed at pH 7.4 (Fig. 12.2B) compared to unfunctionalized analogs, with only around 25% of the drug being released after 50 h. When the pH was changed to 5.5, the release of the cargo was



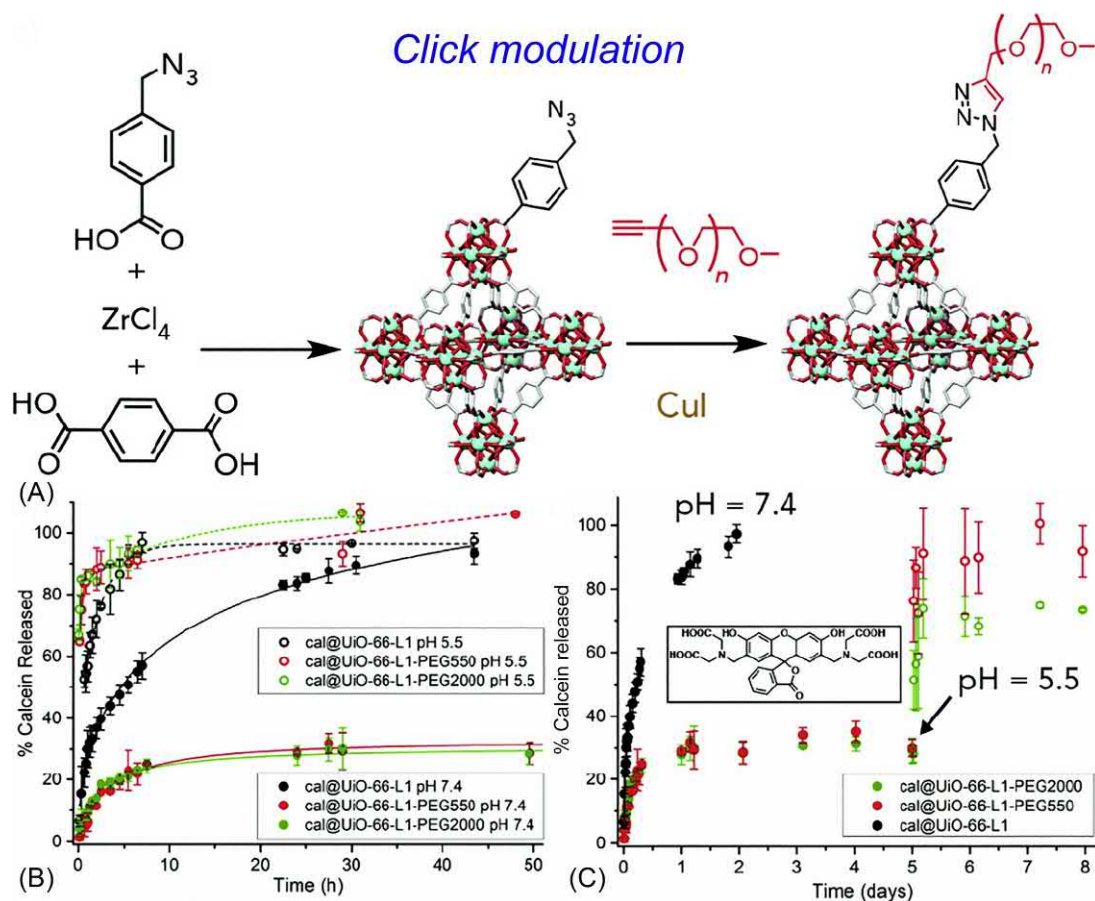


Fig. 12.2

(A) Schematic of the click modulation protocol, whereby azide-functionalized modulators are installed on UiO-66 surfaces during synthesis and then postsynthetically transformed by copper-catalyzed azide-alkyne cycloaddition (CuAAC). (B) Calcein release profiles of surface-functionalized MOFs and their nonfunctionalized analogs in PBS (1×) pH 7.4. (C) pH-responsive calcein release from the PEGylated MOFs in PBS (1×). Modified from I. Abánades Lázaro, S. Haddad, S. Sacca, C. Orellana-Tavra, D. Fairen-Jimenez, R.S. Forgan, *Chem* 2 (2017) 561–578. Copyright (2017) Elsevier.

almost immediate and reached 90% within only a few hours (Fig. 12.2C). This makes these PEGylated particles very promising candidates for use as pH-responsive drug delivery systems.

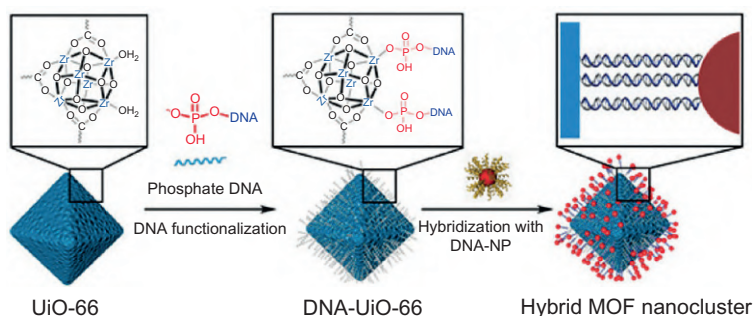
### 12.2.2 Coordinative postsynthetic modification

When a reagent forms a dative bond with a MOF building block in a heterogenous postsynthetic manner, the term coordinative or dative PSM is used. In principle, there are three types of coordinative PSM. First, an organic molecule is added and forms a dative bond with unsaturated

metal sites at the MOF secondary building units (SBUs), for example, at missing linker defects, low nuclearity clusters, or surface sites [52–55]. In some cases, it is possible to entirely exchange the initial linker, which is often termed postsynthetic ligand exchange or solvent-assisted linker exchange [56–61]. In the third class, a metal is introduced to the MOF structure and attached to the linker via coordinative bonding [62–64]. A variety of MOF structures have been shown to be able to release auxiliary ligands under certain conditions [65]; this way unsaturated metal clusters are available for further functionalization.

Mirkin et al. developed a general method to coordinatively functionalize unsaturated metal sites on the outer surfaces of MOFs with terminal phosphate-modified oligonucleotides [66]. To prove the true potential and generality of their method, nine MOFs containing four different metals (Zr, Cr, Fe, and Al) were functionalized. The functionalization of the materials was straightforward and was achieved through coordinative bonding of the terminal phosphate of the oligonucleotide to the unsaturated metal cluster of the MOF (Fig. 12.3).

By calculating the DNA coverage of three isorecticular MOFs of the UiO-66 family, it was proven that surface coverage shows a linear correlation to the density of surface metal nodes. Moreover, it was observed that in MOFs with higher SBU coordination numbers (i.e., higher connected nodes) a greater DNA surface coverage was achieved, due to MOFs with higher SBU connectivity having more defective surfaces and therefore more unsaturated metal sites. Furthermore, by varying the metal in MOFs but retaining the same ligand and topology, it was noticed that stronger metal-phosphate bonds favor higher DNA surface coverage. By taking advantage of the single-strand DNA (ssDNA) coverage, surface functionalized UiO-66 nanoparticles were hybridized (see Section 12.2.4) with AuNPs bearing complimentary ssDNA. By varying the AuNP:MOF ratio it was observed that, at high ratios, the formation of MOF-NP satellite structures is favored, where at low ratios polymeric structures are observed. Finally, the cytotoxicity of UiO-66-AuNP was assessed with 3-(4,5-dimethylthiazol-2-yl)-2,5-diphenyltetrazolium bromide (MTT) metabolic



**Fig. 12.3**

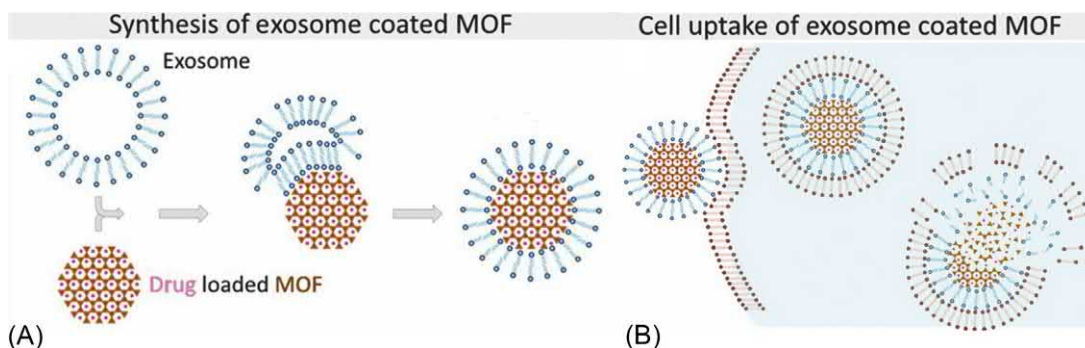
Schematic functionalization of the Zr MOF UiO-66 with phosphate terminated DNA. Reproduced with permission from S. Wang, C.M. McGuirk, M.B. Ross, S. Wang, P. Chen, H. Xing, Y. Liu, C.A. Mirkin, *J. Am. Chem. Soc.* 139 (2017) 9827–9830. Copyright (2017) American Chemical Society.

assay where no cytotoxic effect was observed for concentrations up to 20 pM after 24 h of incubation against human ovarian cancer cells (SK-OV-3).

### 12.2.3 Noncovalent postsynthetic modification/encapsulation

Another route by which modification can be performed is through noncovalent interactions. This can variously be encapsulation of a cargo molecule like a drug into the pores of the framework, physisorption of functionality onto the outer surface, or even complete encapsulation of the material itself into a protecting capsule in order to improve its stability, enhance its properties, and control leakage of the cargo and burst release.

A good example of this type of modification is the work carried out by Engelke et al. [67] where MOFs were coated with exosomes in order to improve their stability, prevent burst release of loaded drugs, and protect both the nanoparticles and the drugs from enzymatic degradation. Exosomes are more advantageous compared to synthetic lipid bilayers, as they are endogenous liposomes generated from the cells for communication reasons [68, 69]. Engelke et al. employed MOFs in order to overcome the challenge of loading drugs into exosomes. Nanoparticles of MIL-88A(Fe), a flexible iron MOF where fumarate is linked by  $\text{Fe}_3\text{O}(\text{RCO}_2)_6(\text{H}_2\text{O})_2\text{OH}$  clusters, were loaded with cargo and then coated with exosomes derived from the cervical cancer HeLa cell line, using the fusion method (Fig. 12.4A). Control experiments with calcein-loaded MOFs showed that there was no leakage of calcein from the exosome-coated particles for up to 10 h. The lysosomal environment was simulated with artificial lysosomal fluid and the stability profile of the exosome-coated particles was vastly different in this environment, where the fluorescence intensity increased dramatically in only a few hours. This was attributed to the fact that the MOFs are decomposing in the lysosomal



**Fig. 12.4**

Schematic representation of (A) the postsynthetic encapsulation of MOF nanoparticles by exosomes, and (B) their cellular uptake and proposed cargo release mechanism. Modified from B. Illes, P. Hirsche, S. Barnert, V. Cauda, S. Wuttke, H. Engelke, *Chem. Mater.* 29 (2017) 8042–8046. Copyright (2017) American Chemical Society.

environment and the increase of the osmotic pressure due to the decomposition leads to the destruction of the exosome bilayer (Fig. 12.4B). Finally, in order to investigate the potential use of their materials as drug delivery systems, Engelke et al. loaded the MIL-88A(Fe) nanoparticles with the chemotherapeutic drug suberohydroxamic acid and evaluated the effect on the cell viability of HeLa cells via the MTT assay. Interestingly, the empty exosome-coated nanoparticles caused no adverse effect on the cell viability, but the drug-loaded ones significantly decreased the cell viability with an  $IC_{50}$  value of  $4.78 \mu\text{g mL}^{-1}$  after 3 days of incubation, proving the hypothesis of the use of the exosome-coated materials as efficient drug carriers.

#### **12.2.4 Hybridization with other materials**

A common type of modification for MOFs is their hybridization with other materials such as silica, quantum dots, and metal nanoparticles. This way their stability can be improved, and also new interesting properties can be introduced.

Lin and his team [18] synthesized mixed-linker amino-functionalized MIL-101(Fe) nanoparticles (a large pore polymorph of the MIL-88 family where  $\text{Fe}_3\text{O}(\text{RCO}_2)_6(\text{H}_2\text{O})_2\text{OH}$  nodes are connected by terephthalate linkers) by introducing a small percentage of 2-aminoterephthalic acid along with the terephthalic acid linker during synthesis. This way, due to the amino functionalities, they were able to further functionalize the materials by attaching the ethoxysuccinato-cisplatin (ESCP) prodrug through covalent amide bond formation, achieving conversions up to 40%. Similarly, the particles were loaded with Br-BODIPY (1,3,5,7-tetramethyl-4,4-difluoro-8-bromomethyl-4-bora-3a,4a-diaza-s-indacene) (Fig. 12.5A) to test their efficacy as an optical imaging contrast agent, achieving BODIPY incorporation yields of 5.6%–11.6% (w/w). After the synthesis and functionalization of the materials, their stability in simulated biological conditions was tested, where both the drug and optical agent-functionalized nanoparticles showed poor stability under those conditions having half-lives of approximately 1.2 and 2.5 h, respectively. In order to improve stability, they were coated with a thin silica layer by exposure to  $\text{Na}_2\text{SiO}_3$  (Fig. 12.5B), achieving a Si/Fe molar ratio of 1.4 and no alteration of the morphology of the nanoparticles according to scanning electron microscopy (SEM) and powder X-ray diffraction (PXRD). Interestingly, when testing the release of ESCP and BODIPY from the silica-covered nanoparticles, their half-lives were vastly increased to 14 and 16 h, respectively, establishing their appropriateness for biomedical applications. After the silica functionalization and stability studies, the corresponding biological efficiency of the nanoparticles was investigated *in vitro*. Confocal microscopy on human colon adenocarcinoma cells HT-29 treated with the BODIPY-loaded materials showed internalization of the particles in a dose-dependent manner (Fig. 12.5C–E). Interestingly, treatment of the cells with free BODIPY did not show any fluorescence due to its inability to cross the cell membrane, proving that the nanoparticles are needed for successful cellular internalization of the imaging agent.

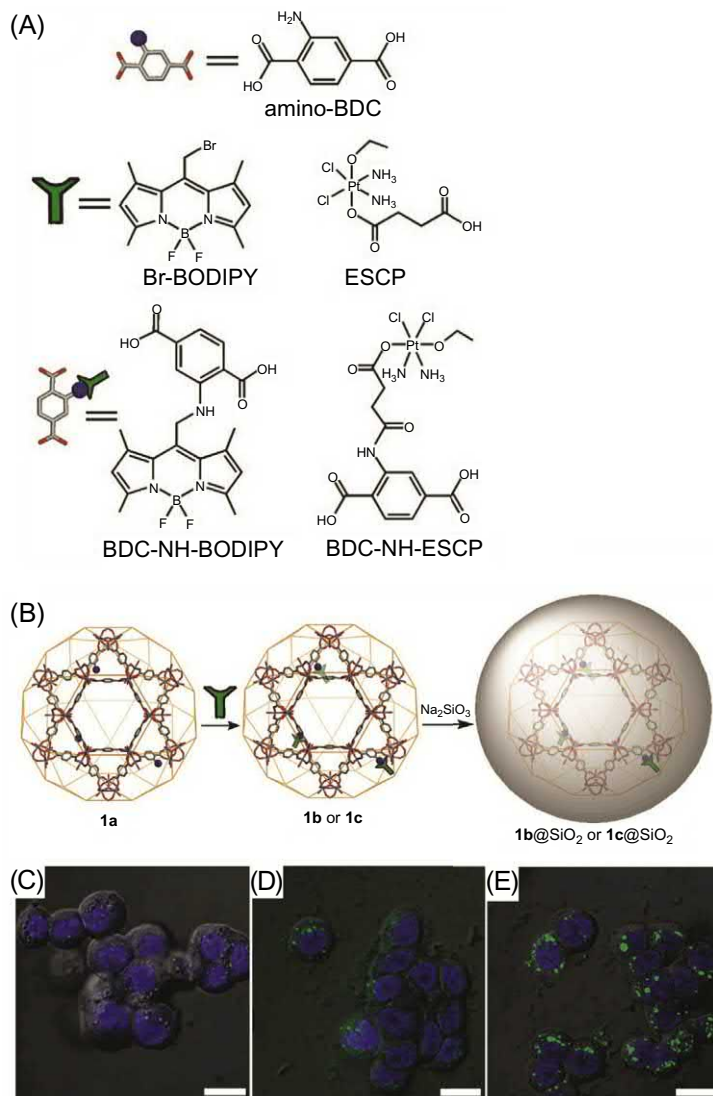


Fig. 12.5

(A) Chemical structures of differing components used in (B) the postsynthetic hybridization of cargo-loaded MOF nanoparticles with silica. Overlay of DIC and confocal microscopy images of *blue* and *green* channels of HT-29 cells with (C) no nanoparticles, (D) 1.19 mgmL<sup>-1</sup> of the silica-functionalized BODIPY particles and, (E) 0.38 mgmL<sup>-1</sup>. The scale bars represent 25  $\mu$ m. Modified from K.M. Taylor-Pashow, J. Della Rocca, Z. Xie, S. Tran, W. Lin, *J. Am. Chem. Soc.* 131 (2009) 14261–14263. Copyright (2009) American Chemical Society.

The anticancer efficacy of the ESCP-loaded nanoparticles was evaluated by employing 3-(4,5-dimethylthiazol-2-yl)-5-(3-carboxymethoxyphenyl)-2-(4-sulfophenyl)-2H-tetrazolium (MTS) cell metabolic activity assays. The IC<sub>50</sub> of the drug-loaded nanoparticles was 29  $\mu$ M, less cytotoxic than free cisplatin under the same conditions which has an IC<sub>50</sub> of 20  $\mu$ M. In order to further improve the cytotoxicity of their materials, Lin et al. employed additional



postsynthetic modification of their nanoparticles [18]. They functionalized the silica shell of the ESCP-loaded nanoparticles with silyl-functionalized c(RGDfK), cyclo[arginine-glycine-aspartic acid-phenylalanine-lysine], a cyclic peptide which has the ability to target the  $\alpha_v\beta_3$  integrin, which is known to be overexpressed in most angiogenic tumors [70]. This way, they managed to achieve similar  $IC_{50}$  values to the free drug, 21  $\mu\text{M}$ , and showed that multiple orthogonal postsynthetic modification steps can be utilized to optimize properties for drug delivery.

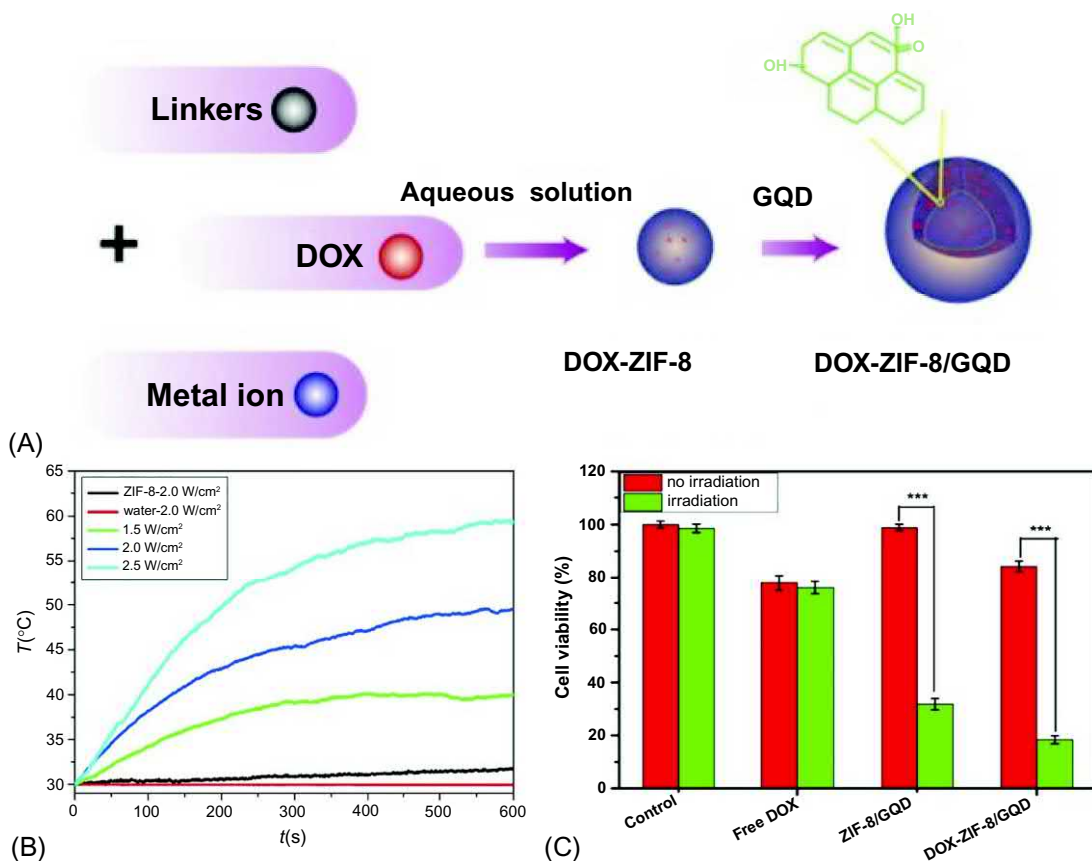
Zhao et al. [71] synthesized 2D copper-based metal-organic framework nanosheets which were then postsynthetically hybridized with iron and gold nanoparticles. More specifically, they managed to synthesize rectangular Cu(HBTC)-1 nanosheets (Cu clusters connected by 1,3,5-benzenetricarboxylate linkers in two dimensions) with a diameter between 1 and 4  $\mu\text{M}$ , and consecutively, in a postsynthetic manner, they introduced gold and iron nanoparticles to the surface of the MOF nanosheets via coprecipitation. The successful incorporation of the bimetallic nanoparticles at the surface of the MOF nanosheets was established by both PXRD and X-ray photoelectron spectroscopy (XPS), while transmission electron microscopy (TEM) and energy-dispersive X-ray spectroscopy (EDS) elemental mapping revealed that a large number of gold and iron nanoparticles were supported on the surface of Cu(HBTC)-1. After the successful synthesis and characterization of the materials, their ability to simulate peroxidase enzyme activity and degrade  $\text{H}_2\text{O}_2$  to form hydroxyl radicals that could oxidize a substrate was evaluated, by monitoring the formation of oxidized 3,3',5,5'-tetramethylbenzidine (TMB- $\text{H}_2\text{O}_2$ ) as it has a characteristic absorbance peak at 652 nm. When the substrate was incubated with the bimetal-functionalized MOF nanosheets, a strong absorbance at 652 nm was observed, establishing the ability of the hybrid materials to catalyze the substrate. Control experiments of incubating the nanoparticles by themselves with TMB showed no absorbance. Incubation of the nanosheets with the substrate showed some absorbance which was, however, very weak compared to that yielded from the hybrid materials, establishing that the connection of the nanoparticles and the nanosheets is essential in order for the system to perform properly. In the final part of the study, Zhao et al. investigated the ability of DNA to regulate the peroxidase-like activity of their materials. Single-stranded DNA (ssDNA) was efficiently absorbed through  $\pi$ - $\pi$  stacking (noncovalent PSM) to the terephthalic acid linker, showing that multiple PSM protocols are often used in tandem. It was observed that the strength of the peroxidase-like behavior of the materials correlates with the concentration of the absorbed ssDNA. The potential applications of the bimetallic materials were tested, with the first one being the colorimetric detection of  $\text{H}_2\text{O}_2$  and glucose, with obvious importance for diabetes sufferers. Since the absorbance at 652 nm intensifies as the concentration of  $\text{H}_2\text{O}_2$  increases, it was hypothesized that Cu(HBTC)-1/ $\text{Fe}_3\text{O}_4$ -AuNPs could be used for the detection of glucose, as the most commonly used mechanism for its detection is monitoring the generation of  $\text{H}_2\text{O}_2$ . Indeed, the experimental investigation revealed that this would be possible as the absorbance increase correlated with the increase of the glucose concentration. The limit of quantification of the technique was 12.86  $\mu\text{M}$  and the limit of



detection was 12.2  $\mu\text{M}$  (38/s). Given that the range of glucose levels in the blood serum of healthy and diabetic individuals ranges from 3 to 8 nM and 9–40 nM, respectively, it is clear that these bimetallic nanosheets have real potential in this type of application.

Zhu et al. [72] hybridized ZIF-8 (Zeolitic Imidazolate Framework, tetrahedral zinc(II) ions connected by 2-methylimidazolate ring linkers) nanoparticles with graphene quantum dots (GQD) for efficient simultaneous drug delivery and photothermal therapy by near IR irradiation. More specifically, the anticancer drug doxorubicin (DOX) was loaded in situ to the pores of the metal-organic framework nanoparticles; weak coordination bonds between the DOX molecules and zinc allow the attachment of the drug to the MOF. Subsequently, the drug-loaded particles were covered with GQDs, which were absorbed to the surface of the ZIF-8 nanoparticles through hydrogen bonding between the NH groups of the MOF linker and the carboxyl, hydroxyl, and epoxy groups of the quantum dots (Fig. 12.6A). The hybrid DOX-ZIF-8/GQD materials showed very promising results in photothermal therapy, with the temperature increase correlating to the irradiation time and the concentration of the suspension. Even at the low concentration of 5  $\text{mgmL}^{-1}$  and a low irradiation power of 2.0  $\text{Wcm}^{-2}$ , the nanoparticles increased the temperature of their suspension from 30°C to 40°C after 10 min of irradiation (Fig. 12.6B). The cytotoxicity and cellular uptake of the materials were evaluated in vitro against the breast cancer cell line 4T1. Empty ZIF-8/GQD nanoparticles were proven to be biocompatible even at the highest concentration tested (200  $\text{mgmL}^{-1}$ ) by Cell Counting Kit-8 (CCK-8) assay, establishing that they are safe to be used as drug delivery carriers. The uptake of the DOX-loaded nanoparticles was investigated with confocal microscopy where it was seen that both the free drug and the drug-loaded materials were internalized by the cells at a good level. Finally, the synergistic effect of the chemotherapeutic and photothermal therapy efficacy of the nanoparticles was tested by incubation of the cells with DOX-ZIF-8/GQD for 8 h followed by 3 min of NIR irradiation. The results were very promising; both free DOX and DOX-ZIF-8/GQD decreased the cell viability of the cells to a similar extent (approximately 75% cell viability was obtained), but DOX-ZIF-8/GQD managed to decrease it even further after NIR irradiation (approximately 32% cell viability, Fig. 12.6C), demonstrating the strong synergistic effect of chemo- and photo-therapy and highlighting the strong potential of those materials for this type of applications.

In these examples, incorporation of other materials into the existing MOF is achieved through unselective surface adsorption. Greater control can be achieved using the strong, selective recognition characteristic of DNA hybridization. Zhao et al. [73] tested the possibility of further functionalization via DNA hybridization with a complementary strand after the successful attachment of single-stranded DNA (ssDNA) to the outer surface of PCN-224 (tetrakis (4-carboxyphenyl)porphyrin (TCPP) linkers coordinated with  $\text{Zr}_6(\text{OH})_8(\text{RCO}_2)_6$  clusters). Incubation of the functionalized A30-PCN-224 (30-mer poly-adenine sequence, A30) with gold nanoparticles (AuNPs) functionalized with a complementary poly-thymine 30-mer



**Fig. 12.6**

(A) Schematic representation of the method used for the hybridization of doxorubicin-loaded ZIF-8 nanoparticles with graphene quantum dots. (B) Temperature increase induced by DOX-ZIF-8/GQD nanoparticles after NIR irradiation ( $\lambda = 808$  nm) of various intensities for 10 min. (C) Cell viability of 4 T1 cells after 8 h of incubation with and without laser irradiation. Modified from Z. Tian, X. Yao, K. Ma, X. Niu, J. Grothe, Q. Xu, L. Liu, S. Kaskel, Y. Zhu, *ACS Omega*, 2 (2017) 1249–1258. Copyright (2017) American Chemical Society. Further permissions related to the material excerpted should be directed to the American Chemical Society.

(T30) strand yielded satellite assemblies (confirmed by TEM) and control experiments where the MOFs were incubated with noncomplimentary A30-AuNPs did not show efficient assembly. Subsequently, they hybridized the DNA strands of A30-PCN-224 with the antinucleolin DNA aptamer AS1411 [74, 75], which was functionalized with 24 extra T bases at its 5' terminus. Nucleolin is overexpressed on the surface of MDA-MB-231 breast cancer cells and, therefore, served as a receptor for the aptamer-functionalized NMOFs (Apt-NMOFs). The internalization of Apt-NMOFs was further investigated with confocal microscopy and flow cytometry and was found to be significantly higher than in the case of NMOFs functionalized

with random DNA strands, showcasing the effectiveness of the aptamer to the targeting effect. Finally, the possibility of using their protocol for attachment of therapeutic DNA strands was tested. For this purpose, CpG ONDs (cytosine-guanine oligonucleotides, the “p” stands for the phosphodiester bond between nucleotides) were chosen for their properties as immune modulators [76]. CpG ONDs-functionalized with a T30 chain were successfully coordinated to A30-NMOs through the established DNA hybridization protocol. Flow cytometry experiments showed improved internalization of the CpG-NMOFs by macrophage cells and minimal internalization of free CpG strands. Moreover, compared to free CpG, CpG NMOFs were more efficient at increasing the levels of secreted cytokines. Preliminary *in vivo* studies of the biocompatibility of nonfunctionalized NMOFs and CpG-NMOFs on ICR male mice showed no negative effect for either of the materials tested, making them promising candidates for further biomedical applications.

### 12.2.5 Physical postsynthetic modification

A recent type of postsynthetic modification of MOFs involves mechanical or physical modification of the crystalline materials in order to introduce new advantageous properties. Fairen-Jimenez [77, 78] developed a new protocol that involves mechanical amorphization of drug-loaded Zr-based MOFs in order to achieve controlled release and minimize the burst release effect. They studied a wide range of nanoparticles from the UiO family and efficiently loaded them with the fluorescent molecule calcein and the anticancer drug  $\alpha$ -cyano-4-hydroxycinnamic acid ( $\alpha$ -CHC), achieving loadings as high as 15.2% (w/w) and 20.3% (w/w), respectively. After the drug loading, they amorphized the materials by ball milling, causing a partial collapse of the crystal lattice around the guest molecules; the metal-ligand connectivity was maintained, but the bulk of the material lost its long-range order (Fig. 12.7A). The effect of the amorphization on drug release depended on the cargo. In the case of  $\alpha$ -CHC, there was no difference between the crystalline and amorphous materials, but, in the case of the calcein-loaded particles, the results varied between different materials. For all of the crystalline materials, calcein was fully released in about 3 days with a significant burst effect over the first hours (Fig. 12.7B). The amorphous MOFs showed a more controlled drug release. In the cases of UiO-66-Br and UiO-66-NO<sub>2</sub>, (analogs linked by 2-bromo and 2-nitroterephthalate, respectively) even after 15 days only 63% and 68% of calcein was released, respectively, due to entrapment of the molecule into the partially decomposed framework. In a separate study, amorphizing UiO-66 nanoparticles prolonged calcein release for up to 30 days (Fig. 12.7C). Finally, the cellular uptake of the nanoparticles from HeLa cells was established using confocal microscopy, where a strong signal was detected and the internalization of the nanoparticles was established.

The same group also demonstrated [79] controlled drug release after postsynthetic thermal treatment of crystalline NU-1000 (Zr<sub>6</sub>(OH)<sub>8</sub>O<sub>4</sub>(OH<sub>2</sub>)<sub>4</sub>(RCO<sub>2</sub>)<sub>8</sub> nodes connected with

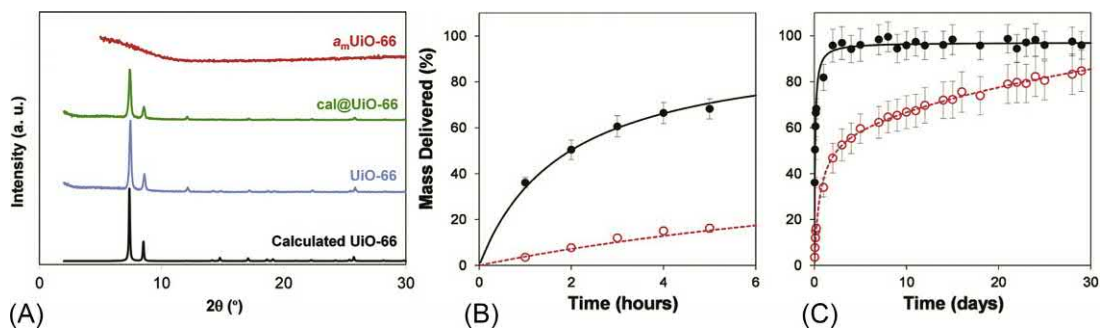


Fig. 12.7

(A) Stacked PXRD patterns of UiO-66 nanoparticles; predicted (*black*), as synthesized (*blue*), after calcein loading (*green*), and after postsynthetic amorphization (*red*). Calcein release profiles from cal@UiO-66 (*black*, crystalline) and a<sub>m</sub>cal@UiO-66 (*red*, amorphized) over the time course of (B) 5 h and (C) 30 days. Modified from C. Orellana-Tavra, E.F. Baxter, T. Tian, T.D. Bennett, N.K.H. Slater, A.K. Cheetham, D. Fairen-Jimenez, *Chem. Commun.* 51 (2015) 13878–13881. Copyright (2015) Royal Society of Chemistry.

1,3,6,8-tetrakis(*p*-benzoate)pyrene linkers, **csq** topology, NU standing for Northwestern University) and NU-901 (a related structure where the same nodes and linkers exhibit **scu** topology) nanoparticles. After successful synthesis and characterization, the materials were loaded with calcein and  $\alpha$ -CHC and then treated at 180°C, to cause partial decomposition of the crystal lattice and trap the guest molecules into the framework. It is worth noting that, on the contrary to the ball-milling approach of their previous studies, the temperature treatment does not cause complete amorphization of the materials. Regarding the drug release studies, the delay was not as prominent as in the case of the ball-milling-induced amorphization of the nanoparticles, but, nevertheless, in the case of NU-1000, the temperature-treated sample had a delayed release for up to 7 days compared to the nontreated analog, confirming the hypothesis that this treatment can prove useful to induce controlled drug release and improve the efficiency of MOFs as drug delivery systems. The endocytosis of the calcein-loaded nanoparticles was visualized with optical sectioning structured illumination microscopy (SIM), allowing 3D visualization of the internalization of the nanoparticles. It was observed that, after 30 min of incubation, the nanoparticles were gathered around the cells with none being internalized, and over the course of 24 h, the cells gradually take up a large number of nanoparticles.

These examples show that a large range of protocols are available to the synthetic chemist to postsynthetically modify MOFs both chemically and physically, often with multiple methodologies used in tandem, allowing highly complex hybrid materials to be prepared. The following section will focus on the different types of functionalities typically postsynthetically incorporated into MOFs and the subsequent biological application(s).

### 12.3 Typical functionalities added

There is a great variety of functionalities that are postsynthetically added to MOFs with biomedical applications in mind. The most common ones can be divided into three categories based on their type and the goal that aims to be achieved: polymers, biomolecules, and photodynamic therapy and imaging agents.

#### 12.3.1 Polymers

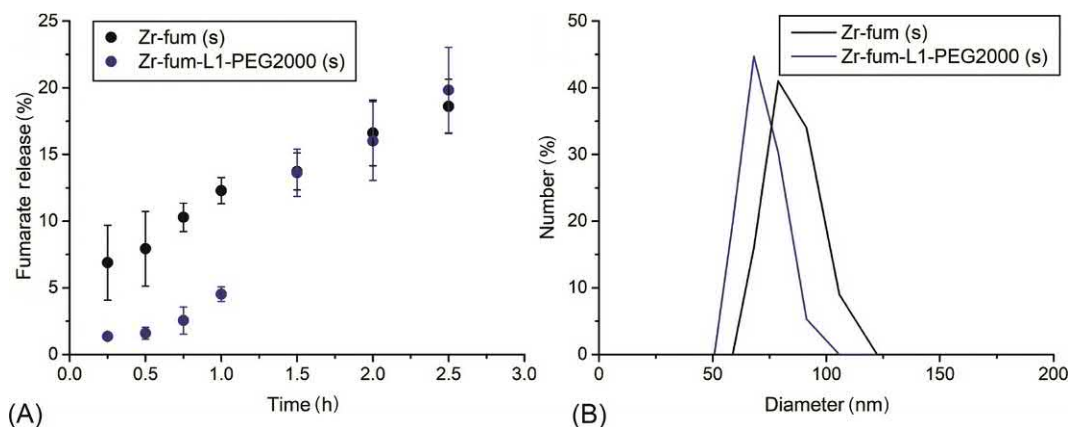
A major challenge that needs to be overcome for MOFs to be used as drug delivery systems is improvement of their colloidal stability [77, 80]. It is essential for nanoparticles used as drug delivery systems to have a monodisperse size distribution and the colloidal dispersion of the system needs to be stable over time. Attachment of polymers or macromolecules—both endogenous and exogenous—to the surface of the MOFs helps to improve their colloidal stability and additionally protects them from degradation [81–83]. Polymer attachment to the surface of the drug carriers can also help to avoid burst release of the loaded cargo, improve the biocompatibility and dispersity of the nanoparticles, and induce passive or active targeting effects, making the drug delivery system more efficient and, in some cases, achieve stimuli-responsive drug release.

One of the most common polymers used for postsynthetic modification of MOF nanoparticles for these purposes is poly(ethylene glycol) (PEG) [12, 47, 84]. There are many properties of PEG chains that make the tactic of using them to decorate nanomaterials very advantageous. PEG-appended drugs have improved pharmacokinetic properties [75], they show prolonged blood circulation times [85–87] and, therefore, have improved chances of reaching their target. Moreover, the mass increase due to functionalization helps to avoid renal excretion [88], and due to the drug/carrier being covered, its recognition by the immune system is delayed [89, 90]. The use of PEG chains improves the colloidal stability of drug nanocarriers and minimizes their aggregation [47, 88].

Given the abovementioned advantages of PEG as well as the fact that it is Food and Drug Administration (FDA) approved [91], there is no surprise that it is widely used for the surface functionalization of a variety of MOFs. Horcajada et al. [12] used PEG chains to surface-functionalize the iron(III)-based porous nanoparticles, MIL-100(Fe) and MIL-88A(Fe) (MIL-100(Fe) contains  $\text{Fe}_3\text{O}(\text{RCO}_2)_6(\text{OH}_2)_2\text{OH}$  clusters connected by 1,3,5-benzenetricarboxylate linkers). The postsynthetic surface functionalization was carried out with  $\text{CH}_3\text{O-PEG-NH}_2$  chains that are coordinatively attached to the metal sites of the MOF from the amino functionality. It was proven by *in vivo* experiments on Wistar female rats that the PEGylated samples had slightly less accumulation in the liver and spleen when compared to their non-PEGylated counterparts. Moreover, after establishing that the iron MOFs are promising candidates for use as contrast agents due to their successful detection *in vivo*, they measured their  $r_2$  relaxivities to assess potential applications in magnetic resonance imaging (MRI).

It was found that the PEGylated materials yielded larger values than the bare ones, and this was attributed to the PEG coating affecting the  $r_2$  values in two opposite ways; firstly, increasing the size of the individual particles, and secondly, reducing their aggregation.

Having previously described the protocol for PEGylation of UiO-66 (see Section 12.2.1), Forgan et al. [48] have subsequently applied their click chemistry route to surface functionalize Zr-fum (a structural analog of UiO-66 linked by fumarate, also known as MOF-801) nanoparticles, also with PEG chains. Again, the PEGylated samples demonstrated enhanced stability against phosphate degradation (Fig. 12.8A) and improved colloidal stability (Fig. 12.8B). Moreover, the internalization efficiency of the functionalized materials was tested against HeLa and J774 macrophage cells. It was shown that the PEGylation process slightly decreased the internalization efficacy against HeLa cells, but improved it in the case of J774. The nanoparticles were loaded with the anticancer probe molecule dichloroacetic acid (DCA) and it was observed that the PEGylated, drug-loaded nanoparticles had significantly higher cytotoxicity levels, likely due to inducing enhanced caveolae-mediated endocytosis, proving that MOF surface functionalization can improve their drug delivery capabilities. The same group has also used this protocol to surface-functionalize UiO-66 nanoparticles with poly-L-lactide and poly-*N*-isopropylacrylamide (PNIPAM) [92]. In both cases, the surface-functionalized materials again exhibited enhanced stability and improved colloidal suspension, while also enhancing the uptake of the nanoparticles from HeLa cells. It should be noted that DCA-loaded surface-functionalized materials induced significant toxicity toward macrophages and lymphocytes, healthy components of the immune system, highlighting the need for careful choice of polymer coating when preparing MOFs for drug delivery.



**Fig. 12.8**

(A) Stability of bare and PEGylated Zr-fum samples, measured spectroscopically by release of fumarate, in PBS 10 × (pH 7.4). (B) Dynamic light scattering profiles of PEGylated and uncoated Zr-fum nanoparticles in water. Modified from I. Abánades Lázaro, S. Haddad, J.M. Rodrigo-Muñoz, R.J. Marshall, B. Sastre, V. del Pozo, D. Fairen-Jimenez, R.S. Forgan, *ACS Appl. Mater. Interfaces* 10 (2018) 31146–31157. Copyright (2018) American Chemical Society.



Sada et al. [93] developed a controlled cargo release protocol by functionalizing UiO-66-NH<sub>2</sub> (a structural analog of UiO-66 linked by 2-aminoterephthalate) with the thermoresponsive polymer PNIPAM, in this case by amide coupling. PNIPAM is known to be soluble in water at temperatures below 32°C, but it forms aggregates at higher temperatures. Sada et al. took advantage of this property and suggested that UiO-66 coated with PNIPAM would retain its loaded cargo at temperatures higher than 32°C, but release it at the lower temperatures where PNIPAM uncoils. To achieve covalent surface functionalization, they performed amide coupling between the amino group of the amino-terephthalate of UiO-66-NH<sub>2</sub> and a terminal NHS-ester functionality of the modified PNIPAM polymer (Fig. 12.9A).

Following the coupling, the surface-functionalized material was loaded with cargo; three different guest molecules were tested, resorufin, caffeine, and procainamide, and the release of

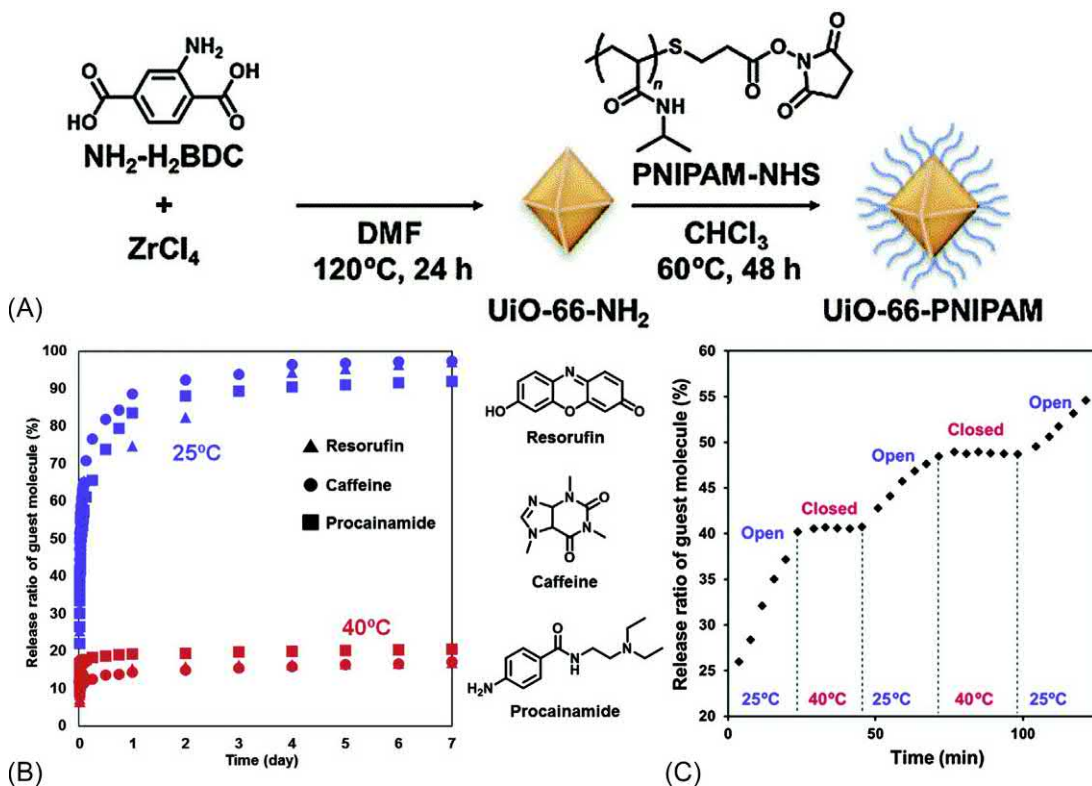


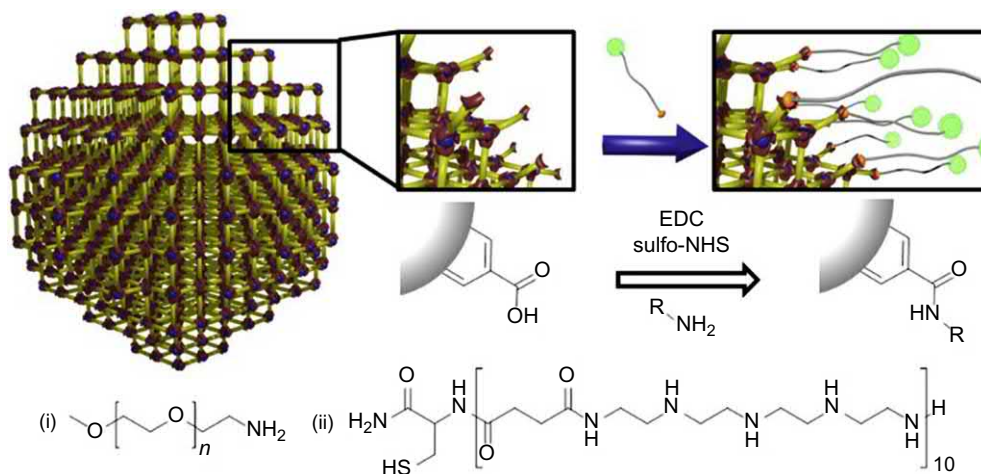
Fig. 12.9

(A) Schematic illustration of the synthesis of UiO-66-NH<sub>2</sub> nanoparticles and their postsynthetic surface functionalization with PNIPAM through NHS-activated amide coupling. (B) Cargo release profiles from surface-functionalized nanoparticles in high and low temperatures. (C) Step-wise cargo release of resorufin from PNIPAM-functionalized UiO-66 representing the exceptional temperature response of the material. Modified from S. Nagata, K. Kokado, K. Sada, *Chem. Commun.* 51 (2015) 8614–8617. Copyright (2015) Royal Society of Chemistry.

the loaded molecules was studied at 25°C and at 40°C. It was observed that, at the lower temperature, where PNIPAM is unfolded, the release of the guest molecules was almost immediate with 80% of the cargo escaping within the first 24 h. When the analogous experiment was carried out at 40°C, only about 20% of the loaded amount was released within a week (Fig. 12.9B). Finally, Sada et al. performed step-wise release experiments where they alternated the temperature from high to low and observed fast cargo release at low temperature and immediate arrest of the release at high temperature, showcasing the excellent external stimuli response and controlled cargo release of their material (Fig. 12.9C).

Wuttke et al. [94] took advantage of the mild conditions used in peptide synthesis for amide bond formation, using 1-ethyl-3-(3-dimethylaminopropyl) carbodiimide (EDC) as a coupling reagent, and applied this methodology to covalently attach two model polymers to the outer surface of MIL-100(Fe) nanoparticles. The polymers chosen were an amino-terminated PEG chain and Stp10-C, a bifunctional polymer having both an amino group to achieve the attachment to the nanoparticles, via amide coupling with free carboxylates at terminal linker sites, but also a thiol group for further functionalization with the fluorescent label Cy5 (Fig. 12.10). After successfully coupling the polymers to the outer surface of the nanoparticles and proving that functionalization of the nanoparticles significantly improved their colloidal stability, the biocompatibility and uptake of the fluorescent material were tested. Fluorescence microscopy proved the internalization of the nanoparticles by murine neuroblastoma N2A cells after as little as 7 h of treatment and significantly higher uptake after 24 h of treatment was observed. MTT metabolic assays showed that the surface-functionalized material was fully biocompatible up to 300  $\mu\text{g mL}^{-1}$ , having an almost identical profile as the unfunctionalized material. To test the materials for potential use in MRI, both the longitudinal and transverse relaxations were measured for the two polymer-functionalized materials and for the unfunctionalized precursor. It was found that both MIL-100(Fe)-PEG and MIL-100(Fe)-Stp10-C had lower  $r_1$  and  $r_2$  values than the unfunctionalized MIL-100(Fe) and this was attributed to minimized water exchange due to the polymer coating. Despite this, the relaxivity values were still high enough to achieve visualization by MRI.

Bellido et al. [81] covered MIL-100(Fe) nanoparticles with heparin, a naturally occurring polymer known for its anticoagulant properties [95]. Through FT-IR studies, it was found that the attachment of the biomolecule to the surface of the MOF was achieved by coordination of the heparin sulfate groups to the iron sites (Fig. 12.11A). It was estimated that around 6500 heparin chains were surrounding each NP, which corresponds to 0.1 heparin chains per  $\text{nm}^2$ . No significant difference was observed in the Brunauer-Emmett-Teller (BET) surface areas of the coated and noncoated materials, suggesting that the pores of the MOF are still accessible after heparin coating and the biomolecule is attached only to the outer surface of the materials. Caffeine was loaded to Hep-MIL-100(Fe), and as expected, its release both in water (Fig. 12.11B) and in PBS pH 7.4 (Fig. 12.11C) was found to be slower in the case of the heparin-coated material. The coated materials showed improved colloidal stability in both PBS



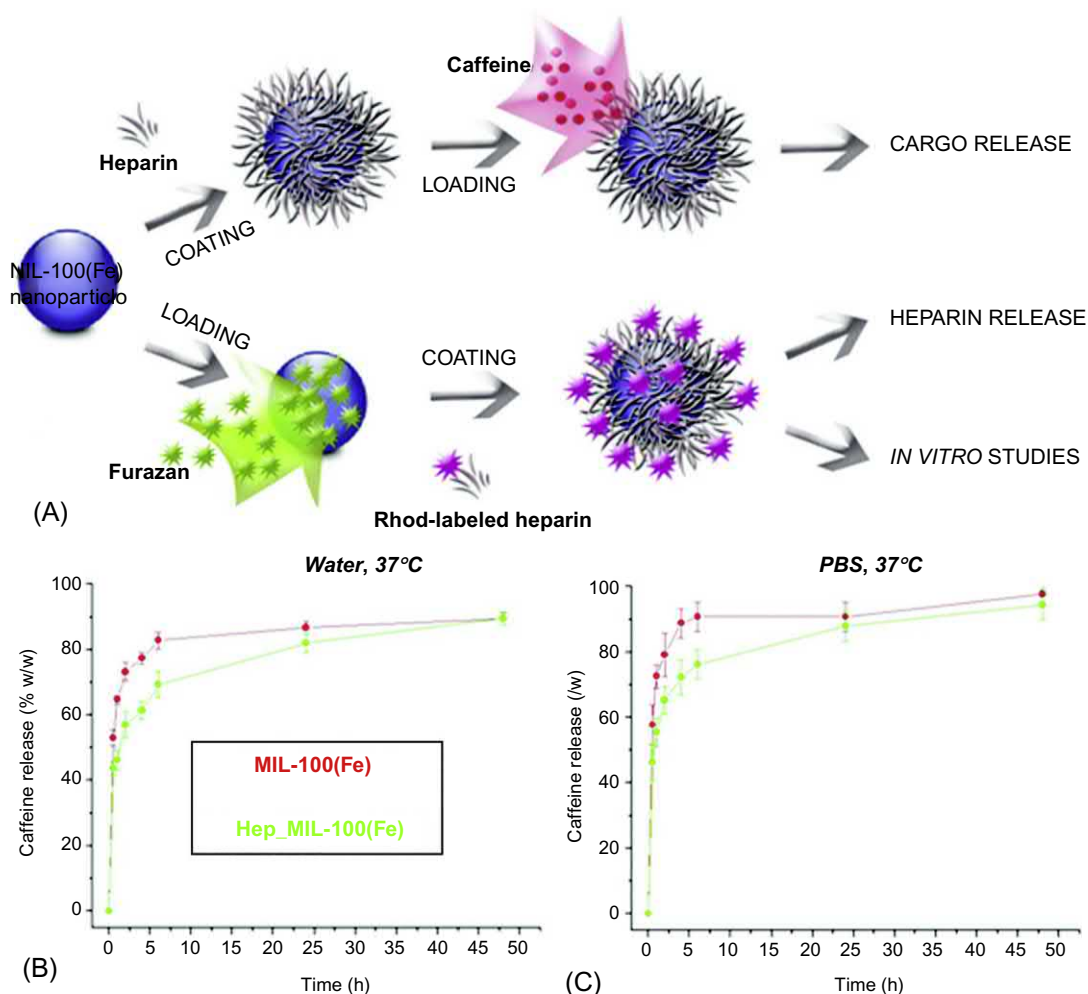
**Fig. 12.10**

Schematic representation of the postsynthetic functionalization of MIL-100(Fe) nanoparticles with PEG-NH<sub>2</sub> and Stp10-C-NH<sub>2</sub> chains through amide coupling. Modified from A. Zimpel, T. Preiß, R. Röder, H. Engelke, M. Ingrisich, M. Peller, J.O. Rädler, E. Wagner, T. Bein, U. Lächelt, S. Wuttke, *Chem. Mater.* 28 (2016) 3318–3326. Copyright (2016) American Chemical Society.

spiked with albumin to simulate blood serum and in Roswell Park Memorial Institute (RPMI) cell growth medium, proving that the surface functionalization improved the properties of the nanoparticles. Finally, it was proven that the heparin coating confers significant stealth properties to MIL-100(Fe) with slower uptake of the heparin-coated NPs into macrophage cells in contrast to the faster uptake of the noncoated analogs. Also, the cellular response (cytokine production) was found to be much less activated in the case of Hep-MIL-100(Fe) compared to MIL-100(Fe), making the heparin-coated material a very promising candidate for a drug delivery system as it has improved half-life that will prolong its circulation and also exhibits properties that allows it to escape the immune system.

In a similar way, Forgan et al. [92] surface-functionalized zirconium UiO-66 nanoparticles with heparin chains. The postsynthetic modification managed to improve the colloidal stability and aggregation levels of the material, but the stability of the material against phosphate degradation (PBS, pH 7.4) was not significantly improved, perhaps suggestive of heparin release over time. However, when the HeLa cell internalization efficiency of the materials was tested, it was observed that cells took up significantly higher quantities than the bare UiO-66. Finally, the cytotoxicity of UiO-66-Hep as well as DCA@UiO-66-Hep was tested against HeLa cells and it was found that both were very well-tolerated and did not cause any cytotoxic effect for concentrations even as high as 1 mgmL<sup>-1</sup>.

Liu et al. [96] synthesized Hf-TCPP nanoMOFs (a MOF with formula Hf<sub>6</sub>(OH)<sub>4</sub>O<sub>4</sub>(TCPP)<sub>3</sub> that has the structure of the Zr analog MOF-525) in an attempt to combine the advantageous


**Fig. 12.11**

(A) Schematic representation of the postsynthetic modification and cargo loading of MIL-100(Fe) nanoparticles. Caffeine release profile of heparin-functionalized and nonfunctionalized MIL-100(Fe) nanoparticles in (B) water and (C) PBS at 37°C. Modified from E. Bellido, T. Hidalgo, M.V. Lozano, M. Guillevic, R. Simon-Vazquez, M.J. Santander-Ortega, A. Gonzalez-Fernandez, C. Serre, M.J. Alonso, P. Horcajada, *Adv. Healthc. Mater.* 4 (2015) 1246–1257. Copyright (2015) John Wiley and Sons.

properties of the porphyrin as a photosensitizer and the high X-ray attenuation of Hf, which could make the MOFs promising candidates for use both in photodynamic therapy (PDT) and radiotherapy (RT) (Fig. 12.12A). After the synthesis, the nanoMOFs were postsynthetically surface-functionalized with poly(maleic anhydride-*alt*-1-tetradecene) chains that had been grafted with PEG using 3-(dimethylamino)-1-propylamine poly(ethylene glycol) via encapsulation of the MOF materials. MTT metabolic activity assays against three cell lines,

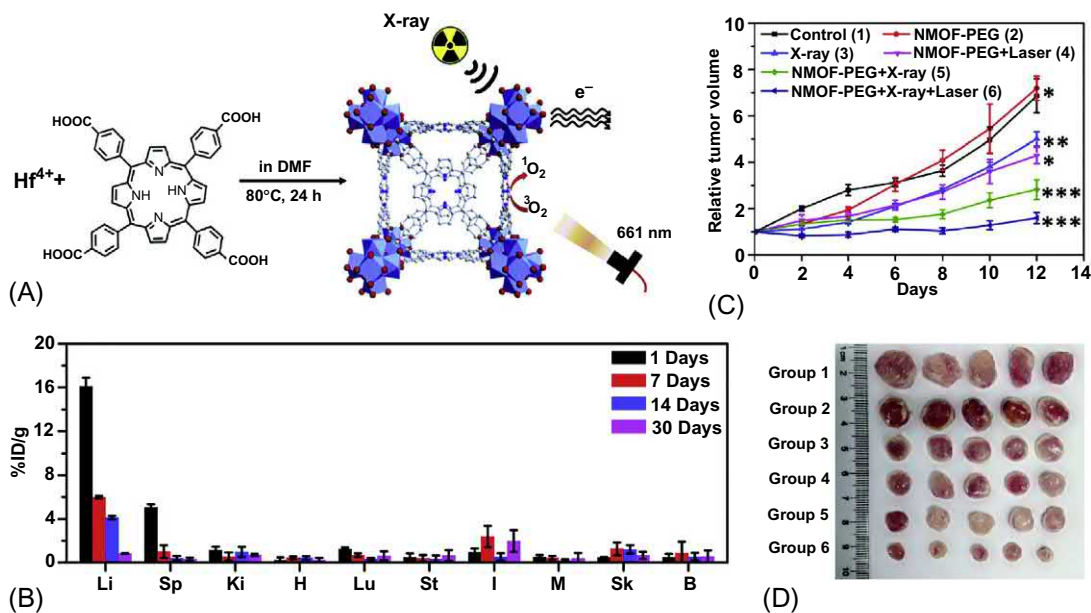


Fig. 12.12

(A) Schematic of Hf-TCCP MOF synthesis which is subsequently PEGylated by immersion in a  $\text{CHCl}_3$  solution. (B) Biodistribution of PEGylated nanoparticles in healthy mice at the time course of 30 days at various organs (Li) liver, (Sp) spleen, (Ki) kidneys, (H) heart, (Lu) lung, (St) stomach, (I) intestine, (M) muscle, (Sk) skin, and (B) bone. (C) Tumor growth graphs after various treatments and controls. (D) Images of the mice tumors on day 14 after various treatments. Modified from J. Liu, Y. Yang, W. Zhu, X. Yi, Z. Dong, X. Xu, M. Chen, K. Yang, G. Lu, L. Jiang, Z. Liu, *Biomaterials* 97 (2016) 1–9. Copyright (2016) Elsevier.

HeLa cervical cancer, NIH3T3 mouse embryonic fibroblasts and 4T1 mouse breast carcinoma, showed no cytotoxicity from both coated and noncoated MOFs toward the cells, while lactate dehydrogenase (LDH) and reactive oxygen species (ROS) generation assays further indicated that none of the materials, at any of the concentrations tested, caused any damage to the cells. In vitro testing against the 4T1 mouse breast cancer cells showed that PEG-Hf-TCCP had significantly better PDT performance compared to free TCCP, which was attributed to improved singlet oxygen generation from the nanoMOFs under laser exposure. Radiotherapy testing also showed that the PEGylated nanoMOFs could cause significant DNA damage under X-ray irradiation compared to untreated control experiments. In vivo experiments on mice bearing 4 T1 tumors showed that the PEGylated material had a half-life of approximately 3.27 h in blood circulation and, even though the bioaccumulation in the liver and spleen was initially very high, rapid decrease indicated biodegradation and clearance of the material out of the body (Fig. 12.12B), which was confirmed by concurrently tracking Hf levels in the urine and feces. Evaluation of the efficiency of the material for combinatory RT and PDT treatment was very promising, showing significant decreases in the size of tumors with



either laser irradiation or X-ray irradiation after the intravenous administration of MOFs. More importantly, when the tumor was treated both with X-rays and laser, the shrinkage was significantly higher than in the separate cases (Fig. 12.12C and D).

### 12.3.2 Biomolecules

Another key strategy for postsynthetically modifying MOFs for use in biomedicine is incorporation of biomolecules, in order to improve the biocompatibility of the materials and also confer them with desirable biological properties such as active targeting. We have chosen to include oligonucleotides within this section rather than with the polymers in Section 12.3.1, as they are isolated as defined, monodisperse single molecule sequences.

Folic acid is commonly incorporated into MOFs postsynthetically, as many types of cancer cells have overexpressed folate receptors on their cell membrane surface, and therefore, folic acid-functionalized nanoMOFs are expected to exhibit targeting and enhanced permeability in those cancer cells. Forgan et al. surface-functionalized both Zr-fum [48] and UiO-66 [92] nanoparticles with folic acid by postsynthetic coordination of the carboxylic acid moieties of the folic acid molecule to the zirconium sites of the MOFs. Functionalization did not alter the crystallinity of the MOFs and, in both cases, improved the colloidal stability while decreasing the aggregation levels of the materials. However, mixed results were obtained regarding the stability of the surface-functionalized MOFs against phosphate deterioration. In the case of UiO-66, the stability was indeed improved after surface functionalization with folic acid against the nonfunctionalized material, but, in the case of Zr-fum, the folic acid-functionalized nanoparticles degraded significantly faster than the nonfunctionalized ones. The uptake of the materials by cervical cancer HeLa cells and by J774 macrophage cells was studied with flow cytometry after synthesizing materials loaded with the fluorescent probe calcein. In the case of HeLa cells, which overexpress the folate receptor, it was found that folate coating increased the internalization by  $58 \pm 5\%$  compared to the uncoated analog, but no significant difference was observed in uptake by J774 macrophage cells, suggestive of a targeting effect. In the case of folate-coated UiO-66, only the internalization by HeLa cells was studied, and it was again found to be higher than that of the nonfunctionalized material.

Subsequently, the cytotoxicity of Zr-fum-FA was tested against J774 macrophage cells and peripheral blood lymphocytes; in both cases, the MOF nanoparticles were very well-tolerated for concentrations up to  $0.5 \text{ mg mL}^{-1}$ . The immune system response to Zr-fum and Zr-fum-FA was also investigated. Specifically, both materials induced ROS production in J774 cells, with the folate covered MOF inducing a less severe effect compared to the bare Zr-fum. Neither of the materials activated the immune system, tested by C3 and C4 complement cascade activation, where both samples did not have any effect and their behavior matched untreated control experiments.



Li et al. [97] developed MOF-based nanoprobes for sensitive and selective DNA detection. More specifically, they synthesized UiO-66-NH<sub>2</sub> nanoparticles, then introduced sulfosuccinimidyl 4-(*N*-maleimidomethyl)cyclohexane-1-carboxylate (sulfo-SMCC), a maleimide containing cross-linker, which covalently conjugated with the pendant amine groups. The nanoparticles were loaded with the fluorescent dye fluorescein and, after that, by taking advantage of the previously introduced cross-linker, the surface of the nanoparticles was covered with thiolated hairpin DNA strands in order to prevent burst release of the cargo (Fig. 12.13A). Dye release experiments showed minimal leakage, suggesting the effective protection of the cargo from the surface DNA hairpins. When a complimentary DNA strand target was introduced to the material, the hairpin surface oligonucleotides hybridized with it, leading to disassociation from the surface of the MOF and therefore release of the loaded dye. As such, the developed materials showed excellent sensitivity as DNA probes with detection limits as low as 20 fM. To test multiple oligonucleotide strand detection, the probes were loaded with three different fluorescent dyes and surface-functionalized with three different sequences of single-strand DNA. Equal amounts of each probe were mixed together in

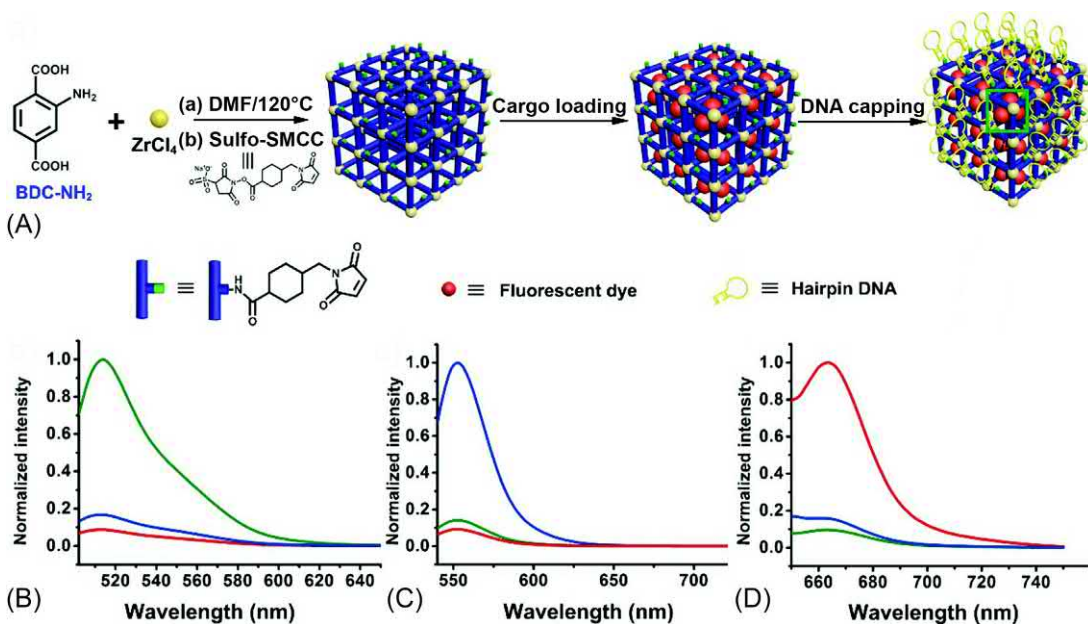


Fig. 12.13

(A) Schematic representation of the synthesis, cargo loading, and surface functionalization of UiO-66-NH<sub>2</sub> nanoparticles with hairpin DNA. Fluorescence spectra illustrating the selective DNA detection from the MOF probes. Three MOF probes were mixed together and then exposed to different targets; (B) T1 green (494/513 nm), (C) T2 blue (525/553 nm), and (D) T3 red (646/664 nm). Modified from S. Wu, C. Li, H. Shi, Y. Huang, G. Li, *Anal. Chem.* 90 (2018) 9929–9935. Copyright (2018) American Chemical Society.

a suspension and experiments were carried out where only one target complementary DNA strand was introduced to the suspension at a time. The probes showcased outstanding selectivity with only the corresponding dye being released each time (Fig. 12.13B), showing the very promising properties of the probes for simultaneous multiplex sensing.

Zhao and Li [73] collaboratively developed a versatile, straightforward method for postsynthetic modification of Zr MOFs with DNA strands. More specifically, they took advantage of the high affinity of phosphates to Zr and postsynthetically attached oligonucleotide single strands, through their phosphate groups, to unsaturated Zr centers of the porphyrin-based Zr MOF PCN-224, which was chosen due to its good stability and advantageous imaging properties [98]. The DNA strand attached to the MOFs (a 30-mer polyadenine sequence, A30) was labeled with Cy3 dye and this way the amount of the attached DNA to the MOF nanoparticles was quantified and was found to be 9.7 mmol of DNA per mg of nanoparticles. Further experiments showed that the crystallinity, morphology, stability, colloidal suspension, and aggregation of the nanoparticles did not change after the functionalization.

In a similar mindset, Lächelt et al. [99] developed a method of postsynthetic surface functionalization of MOFs via coordinative attachment of oligohistidine-tagged (His-tag) molecules to the unsaturated metal sites of the frameworks. In order to prove its versatility, they tested their protocol on three different MOFs, HKUST-1 (Hong Kong University of Science and Technology,  $\text{Cu}_2(\text{RCO}_2)_4$  paddlewheels connecting 1,3,5-benzenetricarboxyate linkers), MIL-88A, and Zr-fum, and used a variety of histidine-tagged polymers, peptides and proteins. The stability of the Zr-fum His-tag conjugates in suspension was investigated, and while stable at pH 7.4, it was observed that acidification led to partial disassociation of the functionalities, attributed to protonation of the histidine moieties. However, a His-tag-Zr-fum suspension was stable in Dulbecco's modified eagle cell culture medium (DMEM) spiked with fetal bovine serum, establishing its advantageous properties for use under biological conditions. By employing two different His-tagged fluorescent proteins, the simultaneous binding of two different functionalities to the MOF nanoparticles was established, showing the advantage of the protocol for multimodal surface functionalization of MOFs, proving that simultaneous attachment of more than one functionality of interest (i.e. drug and targeting or protective groups) is possible. The protocol was used to deliver pro-apoptotic peptides into cells, dramatically enhancing their cell uptake and cytotoxicity.

Zhang et al. [100] took advantage of the selective binding of mercury(II) to thymine-thymine (T-T) mismatched base pairs [101–103] and developed a hybrid system consisting of the zirconium analog of UiO-66-NH<sub>2</sub> and T-rich single-stranded fluorescence-labeled DNA as a sensor for mercury(II). In the absence of mercury ions, the DNA probe binds to the MOF nanoparticles through  $\pi$ - $\pi$  stacking and hydrogen bonding, and the fluorescence is quenched with an efficiency of 75% due to photoinduced energy transfer [104] (Fig. 12.14). When

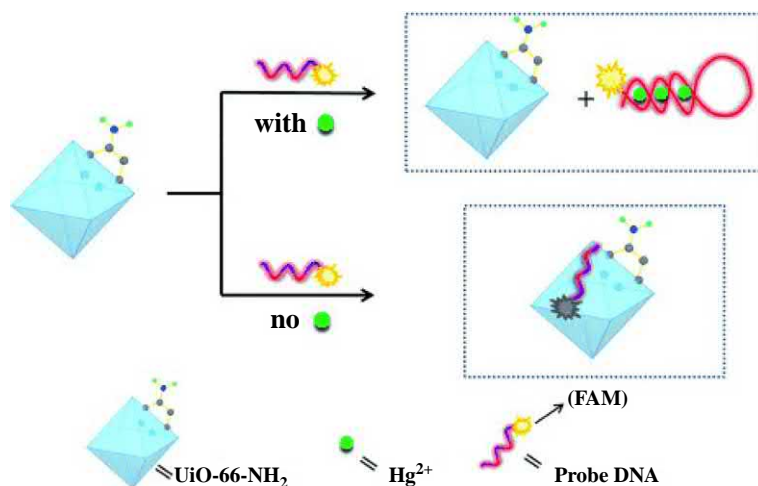


Fig. 12.14

Schematic illustration of the postsynthetic modification of UiO-66-NH<sub>2</sub> with DNA and its proposed Hg<sup>2+</sup> detection mechanism. Modified from L.-L. Wu, Z. Wang, S.-N. Zhao, X. Meng, X.-Z. Song, J. Feng, S.-Y. Song, H.-J. Zhang, *Chem. Eur. J.* 22 (2016) 477–480. Copyright (2016) John Wiley and Sons.

mercury ions are present, however, they bind to the DNA probe due to their affinity to the T-T pairs and the DNA probe fluoresces. The limit of detection of this sensing system was calculated to be 17.6 nM, which is lower than the limit of Hg<sup>2+</sup> in drinking water (30 nM) set by the World Health Organisation (WHO), proving the sensors' outstanding sensitivity. In order to test the selectivity of the sensor system, the fluorescence levels were measured against various other metal ions, where only Hg managed to give very enhanced fluorescence signals with the rest of the ions giving minimal to no response.

### 12.3.3 Photodynamic therapy and imaging units

Due to its noninvasive nature and minimal collateral tissue damage, photodynamic therapy (PDT) has gained interest in research for cancer treatment [72, 105, 106]. Under irradiation of the appropriate wavelength photosensitisers (PS), the PDT active molecules can transfer their excited state energy to nearby oxygen and form reactive oxygen species (ROS) that irreversibly damage cancer cells [107, 108]. Even though PDT has many advantageous properties for cancer therapy, such as precise treatment localization, there are still limitations, and one of the main ones is that photosensitisers are usually large organic molecules with poor aqueous selectivity and high levels of aggregation [109].

In order to overcome the poor bioavailability of PS molecules, the employment of MOFs as nanocarriers has been investigated. Typically, PS molecules are anchored to the particle surface to minimize the diffusion distance required for ROS to leave the MOF interior. As an example, Dong's group [110] suggested the surface functionalization of UiO-66 nanoparticles

with S-ethylthiol ester monosubstituted metal-free porphyrin (TPP-SH) under mild conditions, aiming to exploit the advantages of porphyrin-based PS, efficient singlet oxygen production and broad absorption spectrum [111, 112], and overcome its limitations; the high levels of aggregation, and poor tumor localization [109]. The postsynthetic functionalization of UiO-66 with TPP-SH was based on the known property of S-ethylthiol binding metal cations, including  $Zr^{4+}$ , to form a five membered ring [113–115] (Fig. 12.15A). The binding of the S-ethylthiol-substituted porphyrin to the Zr sites of the UiO-66 nanoparticles was confirmed by XPS. The amount of porphyrin incorporated was calculated by UV-Vis spectroscopy and was found to be 2.9% (w/w), while energy-dispersive X-ray spectra showed uniform coverage of the surface from the porphyrin units. When the  $^1O_2$  generation efficiency of UiO-66-TPP-SH was tested compared to free TPP-SH, the surface-functionalized nanoparticles proved to be more efficient, and this was attributed to the different location of the porphyrin on the nanoparticulate platform. UiO-66-TPP-SH proved to be very membrane-penetrative for HeLa cells, as proven by fluorescent cell imaging. Finally, the cytotoxicity of UiO-66-TPP-SH and free TPP-SH were evaluated before (Fig. 12.15B) and after (Fig. 12.15C) light irradiation by MTT assays. Both compounds were not cytotoxic prior to irradiation for any of the concentrations tested; however, after irradiation, UiO-66-TPP-SH proved to be much more efficient at killing the cancer cells compared to free TPP-SH even at  $5 \mu\text{g mL}^{-1}$  which was the lowest concentration tested. At the lowest concentration, UiO-66-TPP-SH gave around 45% cell viability after irradiation where the free TPP-SH sample had a cell viability of approximately 90%, proving the excellent phototoxicity properties of UiO-66-TPP-SH for use in PDT.

Zheng et al. [116] suggested a different approach to utilize MOFs for PDT. They suggested that epitaxial growth of porous organic polymers [117, 118] (POPs) on MOFs could prove useful at improving their properties and facilitate their use in biomedicine. More specifically, they employed solvent-assisted ligand exchange to incorporate  $\text{NH}_2\text{-BDC}$  into already-synthesized UiO-66 nanoparticles, before utilizing those NMOFs to synthesize photoactive porphyrin-POP-MOF nanocomposites by growing the porphyrin POPs on the surface of the amino-functionalized UiO-66. Polymerization of tetrakis(4-aminophenyl)-21H,23H-porphine and terephthalaldehyde in the presence of amino-functionalized UiO-66 yielded the POP-MOF composites, and the crystallinity, porosity, and stability of the MOF were maintained after hybridization with POPs. The POP-MOF nanocomposites proved very efficient at ROS production, established both by UV-Vis spectroscopy with the use of ROS indicators, as well as inside HeLa cells by confocal microscopy. The phototoxicity of the composites was tested by MTT metabolic activity assay against hepatocellular carcinoma (HepG2) and cervical cancer (HeLa) cells. In both cases, no cytotoxicity is present prior to irradiation, but after irradiation for times as low as 5 min, the POP-MOF composites show exceptional toxicity, with cell viability values reaching 50% after 5 min of irradiation and going as low as 20% after 15 min for the HepG2 cells. In the case of HeLa cells, the effect is even more prominent with cell viability being 30% after 5 min of irradiation and reaching a low of 10% after 15 min

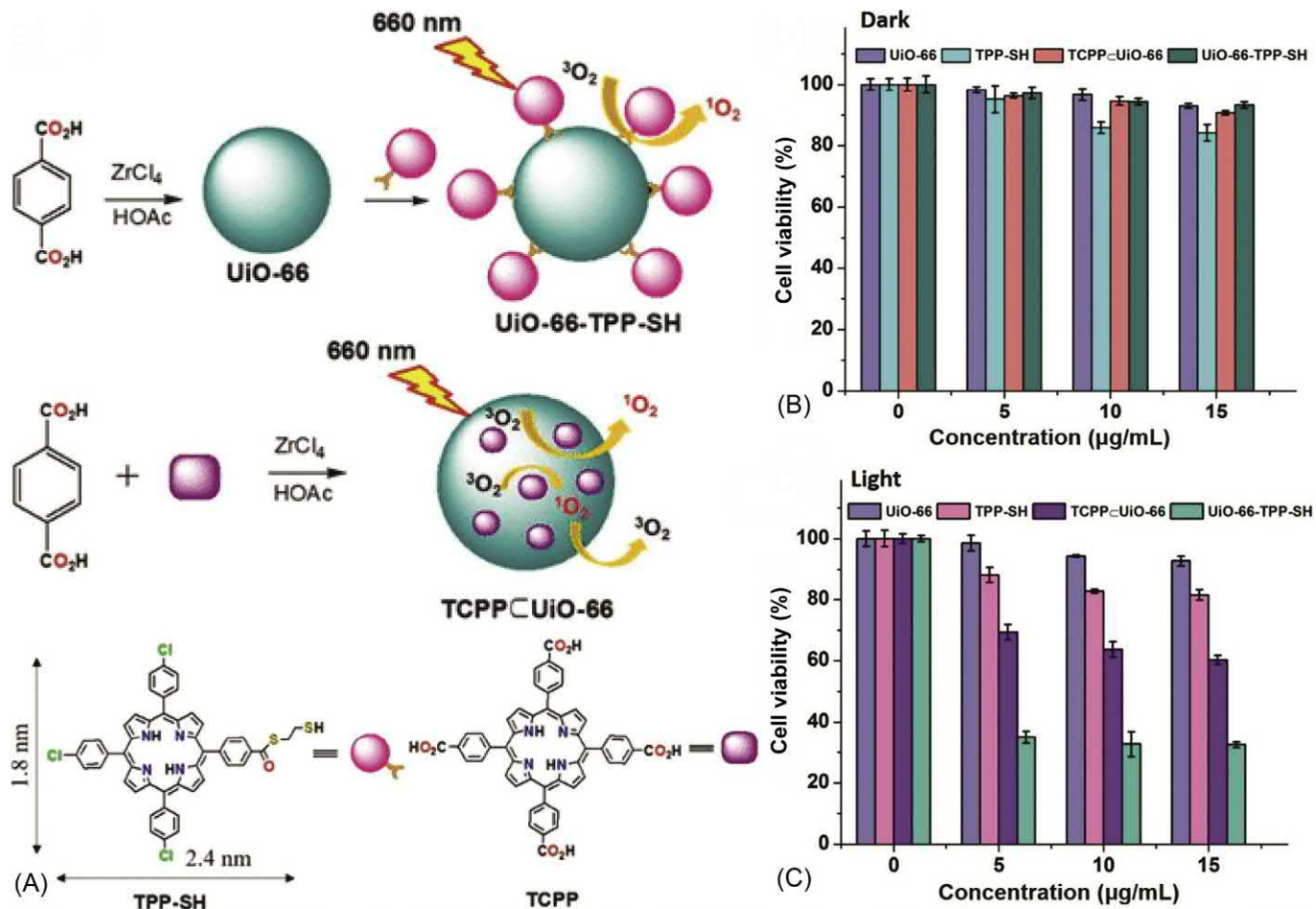


Fig. 12.15

(A) Schematic representation of the synthesis of UiO-66-TPP-SH and its proposed mechanism for  $^1\text{O}_2$  generation. Cell viability after the various treatments (B) before and (C) after laser irradiation ( $100 \text{ mWcm}^{-2}$ , 10 min). Modified from J.-L. Kan, Y. Jiang, A. Xue, Y.-H. Yu, Q. Wang, Y. Zhou, Y.-B. Dong, *Inorg. Chem.* 57 (2018) 5420–5428. Copyright (2018) American Chemical Society.

irradiation. The above results were also confirmed by flow cytometry, establishing the efficiency of POP-MOF nanocomposites for use in PDT.

Xie et al. [119] surface-functionalized UiO-66 nanoparticles with carboxyl-functionalized I<sub>2</sub>-BODIPY (3-(2',6'-diiodo-1',3',5',7'-tetramethyl-4',4'-difluoro-4'-bora-3'a, 4'a-diaza-sindacen-8'-yl) propanoic acid) using solvent-assisted ligand exchange in order to maintain the UiO-66 crystallinity and topology [57, 120] (Fig. 12.16A). Indeed, characterization of the functionalized materials showed that their crystallinity was intact and BODIPY incorporation was calculated to be approximately 30% (w/w) by <sup>1</sup>H NMR spectroscopy. The cell uptake of the functionalized nanoparticles was observed with confocal microscopy and flow cytometry experiments, where it was seen that both the BODIPY-functionalized UiO-66 NPs and free BODIPY were able to cross the cell membrane and be internalized from B16F10 mouse melanoma cells, but with the nanoparticles being more efficient and yielding higher fluorescence values than the free BODIPY. When the singlet oxygen production abilities of UiO-66-BODIPY and free BODIPY were tested, the results showed that the free BODIPY was more efficient than UiO-66-BODIPY; the reduced activity was attributed to the heterogenous nature of the MOF NPs. Subsequently, the cytotoxicity of the functionalized UiO-66 and free BODIPY before and after irradiation was tested with MTT assays. Both materials did not show any significant cytotoxicity prior irradiation; however, after irradiation, they both proved very efficient at killing the cells, with the viability decreasing to less than 20% for the highest concentration tested (6.25 μg mL<sup>-1</sup>).

Following this work, Xie and co-workers tested the potential of their UiO-66-BODIPY nanoparticles as agents for computed tomography(CT) [121]. The Hounsfield Unit (HU) maximum of UiO-66-BODIPY is 236 HU, meaning that the samples are visible under CT. Firstly, the biocompatibility of UiO-66-BODIPY was tested in vivo on healthy Kunming male mice, by monitoring the body weight of tested mice after administration of UiO-66-BODIPY as well as examining histological images of the heart, liver, spleen, lung, and kidneys. No difference compared to the control was observed in any of the cases, even at the highest administrated dose of 100 mgkg<sup>-1</sup>. The efficiency of UiO-66-BODIPY as an imaging agent was tested in vivo in mice with orthotopic hepatoma tumors (Fig. 12.16B). At 24 h after administration, the CT value reaches its maximum of 200 HU and there is clear distinction between tumor and healthy tissue (Fig. 12.16C and D). The tumor signal remains at very high levels for another 12 h and after that it gradually reduces due to natural metabolism until it vanishes 72 h after administration (Fig. 12.16E). The significant accumulation of UiO-66-BODIPY in the tumor for several hours makes it a promising candidate for use in computed tomography.



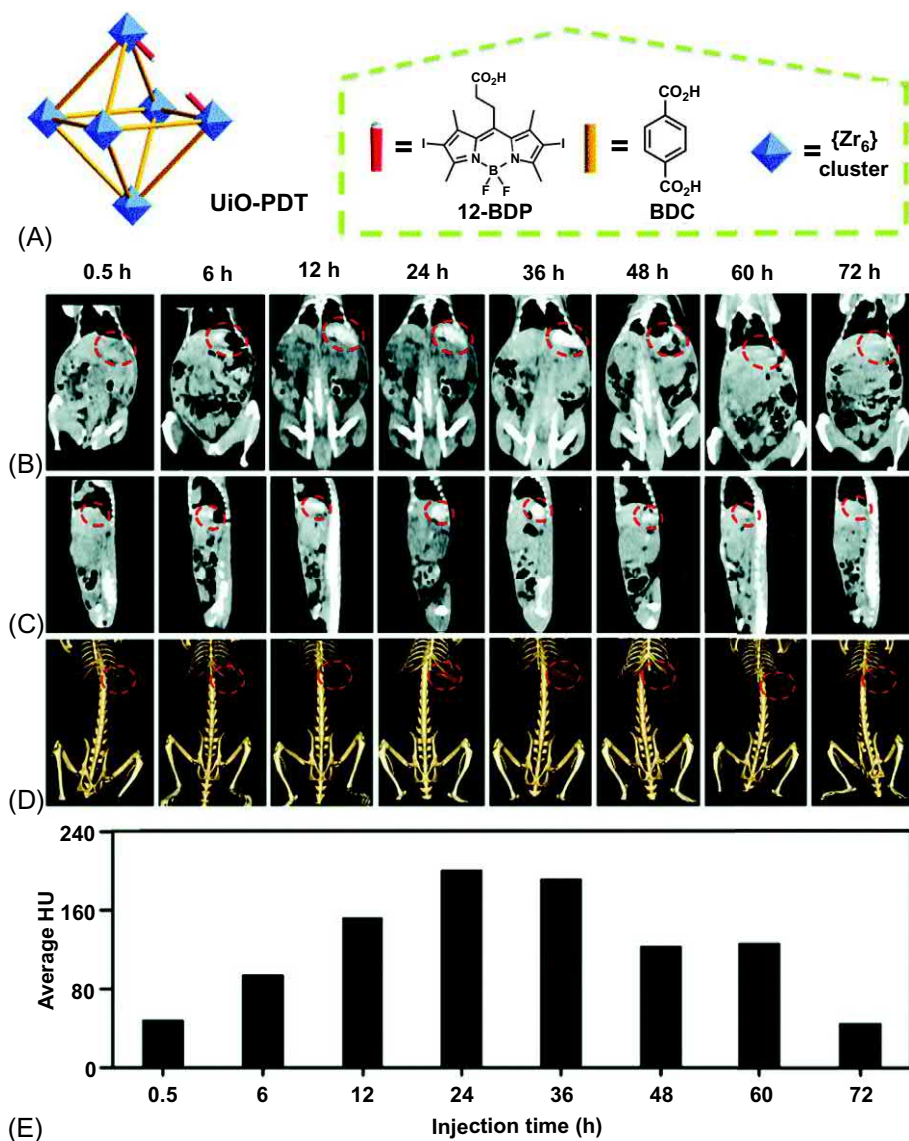


Fig. 12.16

(A) Schematic representation of the UiO-PDT synthesis. CT images in vivo of rats after treatment with UiO-PDT nanoparticles ( $0.1 \text{ mg g}^{-1}$  body weight); (B) images for the ventral sides, (C) images for the lateral sides, and (D) 3D-reconstruction of the CT images show the ventral sides of the hepatic tumors (red circles). (E) Change of the HU values for the UiO-66-PDT nanoparticles over the time course of 72 h after injection. Modified from T. Zhang, L. Wang, C. Ma, W. Wang, J. Ding, S. Liu, X. Zhang, Z. Xie, *J. Mater. Chem. B* 5 (2017) 2330–2336. Copyright (2017) Royal Society of Chemistry.

## 12.4 Conclusions

In general, postsynthetic modification of metal-organic frameworks is a very powerful method to improve the properties of MOFs. A large number of general protocols now exist to incorporate new functionality or change physical properties of already-synthesized MOFs, and this chapter has provided pertinent examples for a number of these approaches in the context of nanomedicine. In general, the drive to prepare highly functionalized nanoparticles has meant that a majority of these approaches are now being applied toward selective surface functionalization of MOFs, as opposed to the bulk functionalization that is common for applications such as gas storage.

The various different approaches of PSM compose a useful toolkit for scientists in order to (i) maintain and complement the already promising attributes of MOFs that have made them highly desirable for biomedical applications (nanoparticle size, monodispersity, crystallinity, thermal stability, high cargo loading), (ii) improve or mask the nondesirable ones (poor colloidal stability, aggregation, stability under biological conditions), but also (iii) attribute new ones (targeting, controlled cargo release, imaging, and photodynamic agents) in an effort to synthesize a new set of improved materials that can prove to be useful in a wide variety of biomedical applications from controlled and targeted drug delivery to imaging and photodynamic therapy.

## References

- [1] G. Férey, *Chem. Soc. Rev.* 37 (2008) 191–214.
- [2] J.R. Long, O.M. Yaghi, *Chem. Soc. Rev.* 38 (2009) 1213–1214.
- [3] H.-C. Zhou, J.R. Long, O.M. Yaghi, *Chem. Rev.* 112 (2012) 673–674.
- [4] M. Kondo, T. Yoshitomi, H. Matsuzaka, S. Kitagawa, K. Seki, *Angew. Chem. Int. Ed.* 36 (1997) 1725–1727.
- [5] H. Furukawa, K.E. Cordova, M. O’Keeffe, O.M. Yaghi, *Science* 341 (2013) 1230444.
- [6] O.M. Yaghi, H. Li, *J. Am. Chem. Soc.* 117 (1995) 10401–10402.
- [7] M. Eddaoudi, J. Kim, N. Rosi, D. Vodak, J. Wachter, M. O’Keeffe, O.M. Yaghi, *Science* 295 (2002) 469–472.
- [8] H.K. Chae, D.Y. Siberio-Perez, J. Kim, Y. Go, M. Eddaoudi, A.J. Matzger, M. O’Keeffe, O.M. Yaghi, *Nature* 427 (2004) 523–527.
- [9] G. Férey, C. Mellot-Draznieks, C. Serre, F. Millange, J. Dutour, S. Surble, I. Margiolaki, *Science* 309 (2005) 2040–2042.
- [10] K. Koh, A.G. Wong-Foy, A.J. Matzger, *Angew. Chem. Int. Ed.* 47 (2008) 677–680.
- [11] P.Z. Moghadam, A. Li, S.B. Wiggin, A. Tao, A.G.P. Maloney, P.A. Wood, S.C. Ward, D. Fairen-Jimenez, *Chem. Mater.* 29 (2017) 2618–2625.
- [12] P. Horcajada, T. Chalati, C. Serre, B. Gillet, C. Sebrie, T. Baati, J.F. Eubank, D. Heurtaux, P. Clayette, C. Kreuz, J.-S. Chang, Y.K. Hwang, V. Marsaud, P.-N. Bories, L. Cynober, S. Gil, G. Férey, P. Couvreur, R. Gref, *Nat. Mater.* 9 (2010) 172–178.
- [13] R. Bian, T. Wang, L. Zhang, L. Li, C. Wang, *Biomater. Sci.* 3 (2015) 1270–1278.
- [14] R.C. Huxford, J. Della Rocca, W. Lin, *Curr. Opin. Chem. Biol.* 14 (2010) 262–268.
- [15] S. Beg, M. Rahman, A. Jain, S. Saini, P. Midoux, C. Pichon, F.J. Ahmad, S. Akhter, *Drug Discov. Today* 22 (2017) 625–637.
- [16] J. Della Rocca, D. Liu, W. Lin, *Acc. Chem. Res.* 44 (2011) 957–968.

- [17] P. Horcajada, C. Serre, M. Vallet-Regi, M. Sebban, F. Taulelle, G. Ferey, *Angew. Chem. Int. Ed.* 45 (2006) 5974–5978.
- [18] K.M. Taylor-Pashow, J. Della Rocca, Z. Xie, S. Tran, W. Lin, *J. Am. Chem. Soc.* 131 (2009) 14261–14263.
- [19] S. Rojas, T. Devic, P. Horcajada, *J. Mater. Chem. B* 5 (2017) 2560–2573.
- [20] J. Zhuang, C.-H. Kuo, L.-Y. Chou, D.-Y. Liu, E. Weerapana, C.-K. Tsung, *ACS Nano* 8 (2014) 2812–2819.
- [21] D. Cunha, M. Ben Yahia, S. Hall, S.R. Miller, H. Chevreau, E. Elkaïm, G. Maurin, P. Horcajada, C. Serre, *Chem. Mater.* 25 (2013) 2767–2776.
- [22] C.V. McGuire, R.S. Forgan, *Chem. Commun.* 51 (2015) 5199–5217.
- [23] D. Zacher, R. Schmid, C. Woll, R.A. Fischer, *Angew. Chem. Int. Ed.* 50 (2011) 176–199.
- [24] W.J. Rieter, K.M.L. Taylor, W. Lin, *J. Am. Chem. Soc.* 129 (2007) 9852–9853.
- [25] A.R. Chowdhuri, D. Laha, S. Chandra, P. Karmakar, S.K. Sahu, *Chem. Eng. J.* 319 (2017) 200–211.
- [26] R. Custelcean, M.G. Gorbunova, *J. Am. Chem. Soc.* 127 (2005) 16362–16363.
- [27] D. Maspoch, D. Ruiz-Molina, K. Wurst, N. Domingo, M. Cavallini, F. Biscarini, J. Tejada, C. Rovira, J. Veciana, *Nat. Mater.* 2 (2003) 190–195.
- [28] X.-C. Yi, F.-G. Xi, Y. Qi, E.-Q. Gao, *RSC Adv.* 5 (2015) 893–900.
- [29] R.S. Forgan, R.J. Marshall, M. Struckmann, A.B. Bleine, D.-L. Long, M.C. Bernini, D. Fairen-Jimenez, *CrystEngComm* 17 (2015) 299–306.
- [30] Z. Wang, S.M. Cohen, *Chem. Soc. Rev.* 38 (2009) 1315–1329.
- [31] S.M. Cohen, *Chem. Rev.* 112 (2012) 970–1000.
- [32] C.T. Walsh, S. Garneau-Tsodikova, G.J. Gatto Jr., *Angew. Chem. Int. Ed.* 44 (2005) 7342–7372.
- [33] R.L. Soffer, *Mol. Cell. Biochem.* 2 (1973) 3–14.
- [34] R. Uy, F. Wold, *Science* 198 (1977) 890–896.
- [35] R.A. Sperling, W.J. Parak, *Phil. Trans. Royal Soc. A* 368 (2010) 1333–1383.
- [36] K.S. Park, Z. Ni, A.P. Cote, J.Y. Choi, R. Huang, F.J. Uribe-Romo, H.K. Chae, M. O’Keeffe, O.M. Yaghi, *Proc. Natl. Acad. Sci. USA* 103 (2006) 10186–10191.
- [37] Z. Wang, S.M. Cohen, *J. Am. Chem. Soc.* 129 (2007) 12368–12369.
- [38] K.K. Tanabe, Z. Wang, S.M. Cohen, *J. Am. Chem. Soc.* 130 (2008) 8508–8517.
- [39] Z. Wang, K.K. Tanabe, S.M. Cohen, *Inorg. Chem.* 48 (2009) 296–306.
- [40] T. Kawamichi, T. Kodama, M. Kawano, M. Fujita, *Angew. Chem. Int. Ed.* 47 (2008) 8030–8032.
- [41] E. Dugan, Z. Wang, M. Okamura, A. Medina, S.M. Cohen, *Chem. Commun.* (2008) 3366–3368.
- [42] Z. Wang, S.M. Cohen, *Angew. Chem. Int. Ed.* 47 (2008) 4699–4702.
- [43] R.J. Marshall, S.L. Griffin, C. Wilson, R.S. Forgan, *J. Am. Chem. Soc.* 137 (2015) 9527–9530.
- [44] R.J. Marshall, S.L. Griffin, C. Wilson, R.S. Forgan, *Chem. Eur. J.* 22 (2016) 4870–4877.
- [45] T. Gadzikwa, G. Lu, C.L. Stern, S.R. Wilson, J.T. Hupp, S.T. Nguyen, *Chem. Commun.* (2008) 5493–5495.
- [46] Y. Goto, H. Sato, S. Shinkai, K. Sada, *J. Am. Chem. Soc.* 130 (2008) 14354–14355.
- [47] I. Abánades Lázaro, S. Haddad, S. Sacca, C. Orellana-Tavra, D. Fairen-Jimenez, R.S. Forgan, *Chem* 2 (2017) 561–578.
- [48] I. Abánades Lázaro, S. Haddad, J.M. Rodrigo-Muñoz, R.J. Marshall, B. Sastre, V. del Pozo, D. Fairen-Jimenez, R.S. Forgan, *ACS Appl. Mater. Interfaces* 10 (2018) 31146–31157.
- [49] W. Morris, C.J. Doonan, H. Furukawa, R. Banerjee, O.M. Yaghi, *J. Am. Chem. Soc.* 130 (2008) 12626–12627.
- [50] A.D. Burrows, C.G. Frost, M.F. Mahon, C. Richardson, *Angew. Chem. Int. Ed.* 47 (2008) 8482–8486.
- [51] J.S. Seo, D. Whang, H. Lee, S.I. Jun, J. Oh, Y.J. Jeon, K. Kim, *Nature* 404 (2000) 982.
- [52] S.S. Chui, S.M. Lo, J.P. Charmant, A.G. Orpen, I.D. Williams, *Science* 283 (1999) 1148–1150.
- [53] H. Li, M. Eddaoudi, T.L. Groy, O.M. Yaghi, *J. Am. Chem. Soc.* 120 (1998) 8571–8572.
- [54] S. Ma, H.-C. Zhou, *J. Am. Chem. Soc.* 128 (2006) 11734–11735.
- [55] M. Dincă, A. Dailly, Y. Liu, C.M. Brown, D.A. Neumann, J.R. Long, *J. Am. Chem. Soc.* 128 (2006) 16876–16883.
- [56] M. Kim, J.F. Cahill, H. Fei, K.A. Prather, S.M. Cohen, *J. Am. Chem. Soc.* 134 (2012) 18082–18088.

- [57] O. Karagiari, M.B. Lalonde, W. Bury, A.A. Sarjeant, O.K. Farha, J.T. Hupp, *J. Am. Chem. Soc.* 134 (2012) 18790–18796.
- [59] S. Takaishi, E.J. DeMarco, M.J. Pellin, O.K. Farha, J.T. Hupp, *Chem. Sci.* 4 (2013) 1509–1513.
- [59] S. Jeong, D. Kim, X. Song, M. Choi, N. Park, M.S. Lah, *Chem. Mater.* 25 (2013) 1047–1054.
- [60] O. Karagiari, W. Bury, A.A. Sarjeant, C.L. Stern, O.K. Farha, J.T. Hupp, *Chem. Sci.* 3 (2012) 3256–3260.
- [61] H.G.T. Nguyen, M.H. Weston, O.K. Farha, J.T. Hupp, S.T. Nguyen, *CrystEngComm* 14 (2012) 4115–4118.
- [62] S. Proch, J. Herrmannsdörfer, R. Kempe, C. Kern, A. Jess, L. Seyfarth, J. Senker, *Chem. Eur. J.* 14 (2008) 8204–8212.
- [63] K.L. Mulfort, J.T. Hupp, *Inorg. Chem.* 47 (2008) 7936–7938.
- [64] K.L. Mulfort, J.T. Hupp, *J. Am. Chem. Soc.* 129 (2007) 9604–9605.
- [65] D. Sun, S. Ma, Y. Ke, D.J. Collins, H.-C. Zhou, *J. Am. Chem. Soc.* 128 (2006) 3896–3897.
- [66] S. Wang, C.M. McGuirk, M.B. Ross, S. Wang, P. Chen, H. Xing, Y. Liu, C.A. Mirkin, *J. Am. Chem. Soc.* 139 (2017) 9827–9830.
- [67] B. Illes, P. Hirschle, S. Barnert, V. Cauda, S. Wuttke, H. Engelke, *Chem. Mater.* 29 (2017) 8042–8046.
- [68] C. Bang, T. Thum, *Int. J. Biochem. Cell Biol.* 44 (2012) 2060–2064.
- [69] A.-K. Ludwig, B. Giebel, *Int. J. Biochem. Cell Biol.* 44 (2012) 11–15.
- [70] J.W. Lee, R.L. Juliano, *Mol. Biol. Cell* 11 (2000) 1973–1987.
- [71] B. Tan, H. Zhao, W. Wu, X. Liu, Y. Zhang, X. Quan, *Nanoscale* 9 (2017) 18699–18710.
- [72] Z. Tian, X. Yao, K. Ma, X. Niu, J. Grothe, Q. Xu, L. Liu, S. Kaskel, Y. Zhu, *ACS Omega* 2 (2017) 1249–1258.
- [73] W. Ning, Z. Di, Y. Yu, P. Zeng, C. Di, D. Chen, X. Kong, G. Nie, Y. Zhao, L. Li, *Small* 14 (2018) e1703812.
- [74] J.H. Lee, M.V. Yigit, D. Mazumdar, Y. Lu, *Adv. Drug Deliv. Rev.* 62 (2010) 592–605.
- [75] S. Soundararajan, W. Chen, E.K. Spicer, N. Courtenay-Luck, D.J. Fernandes, *Cancer Res.* 68 (2008) 2358–2365.
- [76] D.M. Klinman, *Nat. Rev. Immunol.* 4 (2004) 249–258.
- [77] C. Orellana-Tavra, R.J. Marshall, E.F. Baxter, I.A. Lázaro, A. Tao, A.K. Cheetham, R.S. Forgan, D. Fairen-Jimenez, *J. Mater. Chem. B* 4 (2016) 7697–7707.
- [78] C. Orellana-Tavra, E.F. Baxter, T. Tian, T.D. Bennett, N.K.H. Slater, A.K. Cheetham, D. Fairen-Jimenez, *Chem. Commun.* 51 (2015) 13878–13881.
- [79] M.H. Teplensky, M. Fantham, P. Li, T.C. Wang, J.P. Mehta, L.J. Young, P.Z. Moghadam, J.T. Hupp, O.K. Farha, C.F. Kaminski, D. Fairen-Jimenez, *J. Am. Chem. Soc.* 139 (2017) 7522–7532.
- [80] C. Orellana-Tavra, S. Haddad, R.J. Marshall, I. Abánades Lázaro, G. Boix, I. Imaz, D. MasPOCH, R. S. Forgan, D. Fairen-Jimenez, *ACS Appl. Mater. Interfaces* 9 (2017) 35516–35525.
- [81] E. Bellido, T. Hidalgo, M.V. Lozano, M. Guillevic, R. Simon-Vazquez, M.J. Santander-Ortega, A. Gonzalez-Fernandez, C. Serre, M.J. Alonso, P. Horcajada, *Adv. Healthc. Mater.* 4 (2015) 1246–1257.
- [82] S. Sene, M.T. Marcos-Almaraz, N. Menguy, J. Scola, J. Volatron, R. Rouland, J.-M. Grenèche, S. Miraux, C. Menet, N. Guillou, F. Gazeau, C. Serre, P. Horcajada, N. Steunou, *Chem* 3 (2017) 303–322.
- [83] E. Bellido, M. Guillevic, T. Hidalgo, M.J. Santander-Ortega, C. Serre, P. Horcajada, *Langmuir* 30 (2014) 5911–5920.
- [84] Z. Shi, X. Chen, L. Zhang, S. Ding, X. Wang, Q. Lei, W. Fang, *Biomater. Sci.* 6 (2018) 2582–2590.
- [85] R. Gref, Y. Minamitake, M.T. Peracchia, V. Trubetsky, V. Torchilin, R. Langer, *Science* 263 (1994) 1600–1603.
- [86] A. Abuchowski, T. van Es, N.C. Palczuk, F.F. Davis, *J. Biol. Chem.* 252 (1977) 3578–3581.
- [87] A. Abuchowski, J.R. McCoy, N.C. Palczuk, T. van Es, F.F. Davis, *J. Biol. Chem.* 252 (1977) 3582–3586.
- [88] K. Knop, R. Hoogenboom, D. Fischer, U.S. Schubert, *Angew. Chem. Int. Ed.* 49 (2010) 6288–6308.
- [89] D.D. Lasic, D. Needham, *Chem. Rev.* 95 (1995) 2601–2628.
- [90] V.P. Torchilin, *Nat. Rev. Drug Discov.* 4 (2005) 145–160.
- [91] J.M. Harris, *J. Macromol. Sci. Part C* 25 (1985) 325–373.
- [92] I. Abánades Lázaro, S. Haddad, J.M. Rodrigo-Muñoz, C. Orellana-Tavra, V. del Pozo, D. Fairen-Jimenez, R. S. Forgan, *ACS Appl. Mater. Interfaces* 10 (2018) 5255–5268.

- [93] S. Nagata, K. Kokado, K. Sada, *Chem. Commun.* 51 (2015) 8614–8617.
- [94] A. Zimpel, T. Preiß, R. Röder, H. Engelke, M. Ingrisich, M. Peller, J.O. Rädler, E. Wagner, T. Bein, U. Lächelt, S. Wuttke, *Chem. Mater.* 28 (2016) 3318–3326.
- [95] J. Hirsh, S.S. Anand, J.L. Halperin, V. Fuster, *Circulation* 103 (2001) 2994–3018.
- [96] J. Liu, Y. Yang, W. Zhu, X. Yi, Z. Dong, X. Xu, M. Chen, K. Yang, G. Lu, L. Jiang, Z. Liu, *Biomaterials* 97 (2016) 1–9.
- [97] S. Wu, C. Li, H. Shi, Y. Huang, G. Li, *Anal. Chem.* 90 (2018) 9929–9935.
- [98] Y. Bai, Y. Dou, L.-H. Xie, W. Rutledge, J.-R. Li, H.-C. Zhou, *Chem. Soc. Rev.* 45 (2016) 2327–2367.
- [99] R. Röder, T. Preiß, P. Hirschle, B. Steinborn, A. Zimpel, M. Höhn, J.O. Rädler, T. Bein, E. Wagner, S. Wuttke, U. Lächelt, *J. Am. Chem. Soc.* 139 (2017) 2359–2368.
- [100] L.-L. Wu, Z. Wang, S.-N. Zhao, X. Meng, X.-Z. Song, J. Feng, S.-Y. Song, H.-J. Zhang, *Chem. Eur. J.* 22 (2016) 477–480.
- [101] H. Urata, E. Yamaguchi, T. Funai, Y. Matsumura, S. Wada, *Angew. Chem. Int. Ed.* 49 (2010) 6516–6519.
- [102] Y. Miyake, H. Togashi, M. Tashiro, H. Yamaguchi, S. Oda, M. Kudo, Y. Tanaka, Y. Kondo, R. Sawa, T. Fujimoto, T. Machinami, A. Ono, *J. Am. Chem. Soc.* 128 (2006) 2172–2173.
- [103] N. Dave, M.Y. Chan, P.-J.J. Huang, B.D. Smith, J. Liu, *J. Am. Chem. Soc.* 132 (2010) 12668–12673.
- [104] X. Zhu, H. Zheng, X. Wei, Z. Lin, L. Guo, B. Qiu, G. Chen, *Chem. Commun.* 49 (2013) 1276–1278.
- [105] L. Gao, R. Liu, F. Gao, Y. Wang, X. Jiang, X. Gao, *ACS Nano* 8 (2014) 7260–7271.
- [106] B.C. Wilson, M.S. Patterson, *Phys. Med. Biol.* 53 (2008) R61–109.
- [107] K. Han, S.-B. Wang, Q. Lei, J.-Y. Zhu, X.-Z. Zhang, *ACS Nano* 9 (2015) 10268–10277.
- [108] P. Agostinis, K. Berg, K.A. Cengel, T.H. Foster, A.W. Girotti, S.O. Gollnick, S.M. Hahn, M. R. Hamblin, A. Juzeniene, D. Kessel, M. Korbelik, J. Moan, P. Mroz, D. Nowis, J. Piette, B. C. Wilson, J. Golab, *CA Cancer J. Clin.* 61 (2011) 250–281.
- [109] M.A. Rajora, J.W.H. Lou, G. Zheng, *Chem. Soc. Rev.* 46 (2017) 6433–6469.
- [110] J.-L. Kan, Y. Jiang, A. Xue, Y.-H. Yu, Q. Wang, Y. Zhou, Y.-B. Dong, *Inorg. Chem.* 57 (2018) 5420–5428.
- [111] M. Lismont, L. Dreesen, S. Wuttke, *Adv. Funct. Mater.* 27 (2017) 1606314.
- [112] M.C. DeRosa, R.J. Crutchley, *Coord. Chem. Rev.* 233–234 (2002) 351–371.
- [113] C.P. Rao, J.R. Dorfman, R.H. Holm, *Inorg. Chem.* 25 (1986) 428–439.
- [114] R. Hart, W. Levason, B. Patel, G. Reid, *J. Chem. Soc. Dalton Trans.* (2002) 3153–3159.
- [115] A. Cohen, A. Yeori, I. Goldberg, M. Kol, *Inorg. Chem.* 46 (2007) 8114–8116.
- [116] X. Zheng, L. Wang, Q. Pei, S. He, S. Liu, Z. Xie, *Chem. Mater.* 29 (2017) 2374–2381.
- [117] N.B. McKeown, P.M. Budd, *Chem. Soc. Rev.* 35 (2006) 675–683.
- [118] P.J. Waller, F. Gándara, O.M. Yaghi, *Acc. Chem. Res.* 48 (2015) 3053–3063.
- [119] W. Wang, L. Wang, Z. Li, Z. Xie, *Chem. Commun.* 52 (2016) 5402–5405.
- [120] O. Karagiari, W. Bury, J.E. Mondloch, J.T. Hupp, O.K. Farha, *Angew. Chem. Int. Ed.* 53 (2014) 4530–4540.
- [121] T. Zhang, L. Wang, C. Ma, W. Wang, J. Ding, S. Liu, X. Zhang, Z. Xie, *J. Mater. Chem. B* 5 (2017) 2330–2336.

### **Further reading**

- T. Tejada-Berges, C.O. Granai, M. Gordinier, W. Gajewski, *Expert Rev. Anticancer Ther.* 2 (2002) 143–150.

# Characterizations of MOFs for biomedical application

Arpita Samui, Sumanta Kumar Sahu

*Department of Chemistry, Indian Institute of Technology (ISM), Dhanbad, Jharkhand, India*

## 13.1 Introduction

Metal organic frameworks (MOFs) are a new class of hybrid material where organic molecule binds up with inorganic molecule (generally high nuclearity metal clusters or transition metal ions) through coordinate linkage and formed framework or cage-like structure. So, the MOFs are one type of coordinate polymers (CPs). Periodic arrangement of metal and organic linkers offers the high crystallinity of MOFs, which allow to differentiate from noncrystalline CPs. Depending on crystalline morphology and synthetic strategies, MOFs are generally divided as crystalline, amorphous, luminescent, nano-, and bio-MOFs [1]. In crystalline MOFs, the linkers are arranged in infinitely regular way to form highly ordered solid porous framework. In amorphous MOFs, the basic building block as in crystalline is retained, but the infinite arrangement is not observed. The luminescent MOFs give an emission light when excited at a particular wavelength due to presence of luminescent organic ligand or metal ion. The nanosized or nanoparticulate structure MOFs are called nano-MOFs (NMOFs). In bio-MOFs, the biomolecules are incorporated by trapping into the porous cavities of MOFs or by incorporating during the synthesis of MOFs. Simultaneously, the bio-MOFs are synthesized by using biomolecules as linkers and bioactive metal as inorganic counterpart.

All these MOFs have unique characteristic features like microporosity and can be easily functionalized by surface modification or properly choosing the organic ligand. Surface modification using polymer or peptide can also provide the functionalization of MOFs. Due to all these properties, MOFs have attracted much more attention in various fields like gas or fuel storage, heterogeneous catalysis, sensing and molecular separation, etc. [2–6]. Due to small size with high surface area and facile synthetic procedure, NMOFs have drawn much more attention in biomedical field like drug delivery, biosensors, cancer treatment, biogas storage, enzyme immobilization, bio-imaging and magnetic resonance imaging (MRI), etc. [7–12]. Stability of NMOFs in various solvents including water and also over a wide range of temperature is a significant feature for biomedical application.



Microporous NMOFs can be used as a biomimetic mineralization for the coating of cells and viruses. The tunable pore size of NMOFs builds up a selective barrier to allow the passing of biologically relevant substrate toward cell or virus [9]. Very high surface area with effective pore size and pore volume of NMOFs provides effective enzyme or drug encapsulation [12,13]. Generally, NMOFs are massively used in drug delivery because of its high drug loading with controllable release efficiency, adequate colloidal stability, and also the degradation rate. The NMOFs can be efficiently internalized into the cell due to their small size. Most importantly, NMOFs possess major criteria, biocompatibility and nontoxicity, for biomedical application. Magnetic resonance imaging (MRI) is an enormous 3D imaging method and generally used in clinic for noninvasive imaging to detect tumor or to assess chemotherapy response [11]. The NMOFs formed by or composited with MRI contrast agent like paramagnetic Gadolinium ( $Gd^{3+}$ ) or superparamagnetic  $Fe^{2+}$  or  $Fe^{3+}$  oxides or sometime  $Mn^{2+}$  are generally used in clinical field for medical theragnostic study.

So, after synthetization, the NMOFs should be properly characterized to be used in biomedical field. As the NMOFs have several unique characteristics properties, there are also numerous techniques for analysis of these features. This chapter is discussing about almost all these characterization techniques which are generally used to detect the properties of NMOFs.

## **13.2 Characterizations**

MOFs are regularly arranged coordinated polymer like highly notorious with unique characteristics compound. In recent days, all these unique properties are properly characterized by using several modern advanced techniques. Some of these techniques which are mostly crucial are explained in this following chapter.

### **13.2.1 Structural characterization**

The MOF is formed by regular arrangement of organic linkers and inorganic metal ions. So, several types of plane or crystalline structural arrangement can be possible, which are investigated by X-ray diffraction method (XRD). As both the organic and inorganic types of molecules are present in the MOFs, atomic composition is studied by energy dispersive X-ray (EDX) analysis. The functionality after MOF formation is investigated by several procedure like Fourier-transform infrared spectroscopy (FTIR) analysis, nuclear magnetic resonance (NMR) spectroscopy, X-ray photoelectron spectroscopy (XPS), etc. These techniques are discussed with some explanation in the following section.

### 13.2.1.1 Phase purity and structure modeling

MOFs are formed by regular attachment of metal and organic linkers. So, the MOFs have a particular crystalline arrangement. This crystallinity can be studied using XRD method. Generally, two types of XRD analyses can be performed depending on sample condition. First one is single crystal XRD (SC-XRD), which is a nondestructive analytical technique and provides the detailed information about the crystal including bond length, bond angle, cell dimension, etc. For SC-XRD, sample size should be in the range 30–300  $\mu\text{m}$  with crystal size 150–250  $\mu\text{m}$ . Another one is powder X-ray diffraction (PXRD) where powder sample is used to study the crystallographic analysis. Generally, nano materials which have size  $<200$  nm are used for biomedical application. So, SC-XRD analysis is not feasible for nano-MOFs analysis. So, phase purity and crystalline structure are determined by using PXRD method.

In PXRD, a diffraction pattern is obtained due to interaction of the incident X-ray beam and powder sample. The X-rays are produced in a cathode tube where electron is produced by heating the filament, and then accelerated toward target material by applying voltage, to bombard the target material with electron. When the electron has sufficient energy to dislodge an inner electron of the target material, the X-rays are produced from the target material. The X-rays are collimated and directed toward the powder sample, after filtering with crystal monochromators to produce monochromatic X-rays. The instrumentation of PXRD is present in Fig. 13.1. Cu is the most common used target material and  $K_{\alpha}$  radiation of wavelength

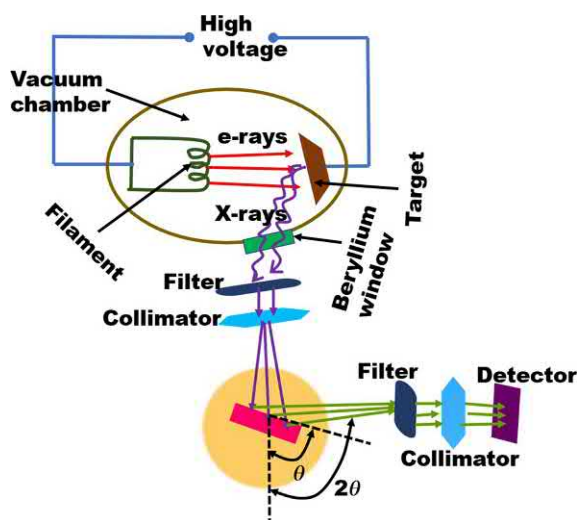


Fig. 13.1

Schematic instrumentation of PXRD technique.

1.5418 Å is used to bombard the powder sample. The intensity of reflected X-rays is recorded into the rotated detector.

Constructive interference is produced from the reflected X-rays when the condition satisfied the Bragg's law. This law correlates the wavelength of incident X-rays ( $\lambda$ ), the incident angle of the X-ray beam ( $\theta$ ), and the spacing between the plane of crystal lattice ( $d$ ). The Bragg's equation is

$$n\lambda = 2d \sin\theta$$

Where  $n$  is an integer (1, 2, 3, ...). So, constructive interference occurs when the path length of the incident X-rays is equal to the integer multiple of the wavelength of the X-ray beam.

The diffraction pattern produced from XRD analysis gives sharp, well-defined, narrow, and significant peak for crystalline compound. However, for amorphous compound, the diffraction pattern consists of noise signal with messy peak or with some sort order of bumps. The PXRD can be used to measure the crystallinity of the compounds by comparing the integrated intensity of sharp peak and background noise. Till now different methods are reported to calculate the crystallinity and crystallinity index.

Crystal structure can be determined by using this powder X-ray diffraction [14–17]. But, sometimes it becomes difficult in case of PXRD due to overlapping of the reflection beam generated from the powder sample. A number of methods like simulated annealing and charge flipping are developed for structural determination of the crystal compound. Unknown structure of powder sample can be determined by using Rietveld refinement method. It is full pattern analysis technique. Structure modeling can also be performed from PXRD diffraction pattern using various softwares like TOPAS Program or material studio software.

Fujii et al. developed the structure elucidation from the PXRD pattern of mixed ligand metal organic framework. For determination of the structure of the MOF, GSAS program is used to perform the Rietveld refinement on the PXRD diffractogram using a reference sample as shown in Fig. 13.2C. The final refinement is used to predict the crystal structure of the mixed ligand MOFs shown in Fig. 13.2A and B [18].

Yakovenko et al. constructed a method for structure envelope (SE) of a MOF from the PXRD pattern. To envelope the structure, the intensities of reflection intensities are used in SUPERFLIP software, from where charge-flipping (CF) structure can also be resolved, shown in Fig. 13.3 [19].

Yakovenko et al. then developed a new method, difference envelope density (DED) analysis, to study the guest molecule into the MOFs. From the PXRD data, this DED analysis provides many information about guest molecule inside the MOF like solvent location, activation process, gas loading, etc. So, using this analysis, structure determination can be performed for MOF with any guest molecule using PXRD pattern, shown in Fig. 13.4 [20].

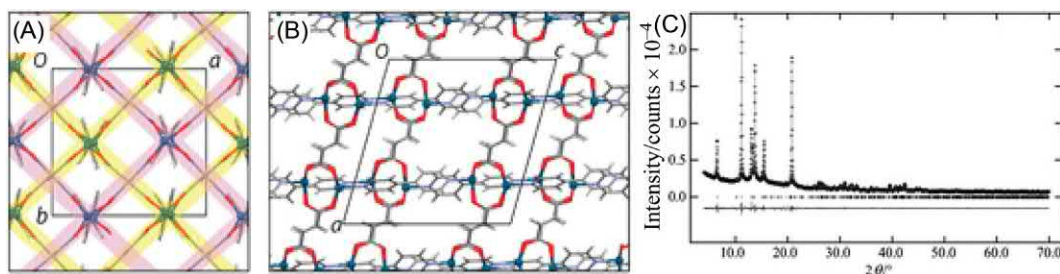


Fig. 13.2

Crystal structure of MOF (A) along C-axis (B) along b-axis; (C) Rietveld refinement of PXRD diffraction pattern for the MOF. Reproduced from K. Fujii, A.L. Garay, J. Hill, E. Sbircea, Z. Pan, M. Xu, D.C. Apperley, S.L. James, K.D.M. Harris, *Direct structure elucidation by powder X-ray diffraction of a metal–organic framework material prepared by solvent-free grinding*, *Chem. Commun.* 46 (2010) 7572–7574, with permission from The Royal Society of Chemistry, Copyright 2019.

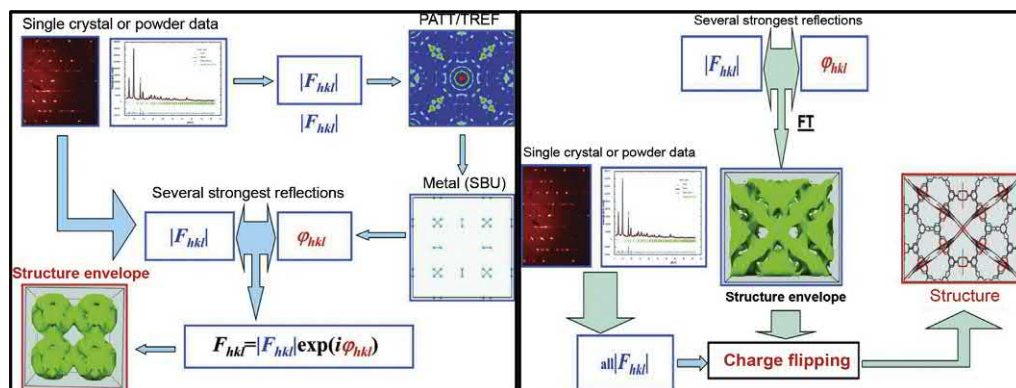


Fig. 13.3

Diagram illustrating the algorithm for structure envelope (left side) and charge flipping (right side). Reproduced from A.A. Yakovenko, J.H. Reibenspies, N. Bhuvanesh, H.-C. Zhou, *Generation and applications of structure envelopes for porous metal–organic frameworks*, *J. Appl. Crystallogr.* 46 (2013) 346–353, with permission from IUCr, Copyright 2019.

### 13.2.1.2 Elemental and functionality analysis

MOFs are synthesized by mixing a metal salt and one or more type of organic linker in a solvent or without solvent by grinding procedure. So, after the formation of MOFs, the elements present in the MOFs are analyzed using energy dispersive X-ray (EDX) analysis.

In this analysis, at first an electron beam hits the sample and transfers energy to an atom of the sample. Using this energy, an electron of the atom “jumps” to a higher energy level or is “knocked out” from the sample leaving behind a hole. In second step, negatively charged

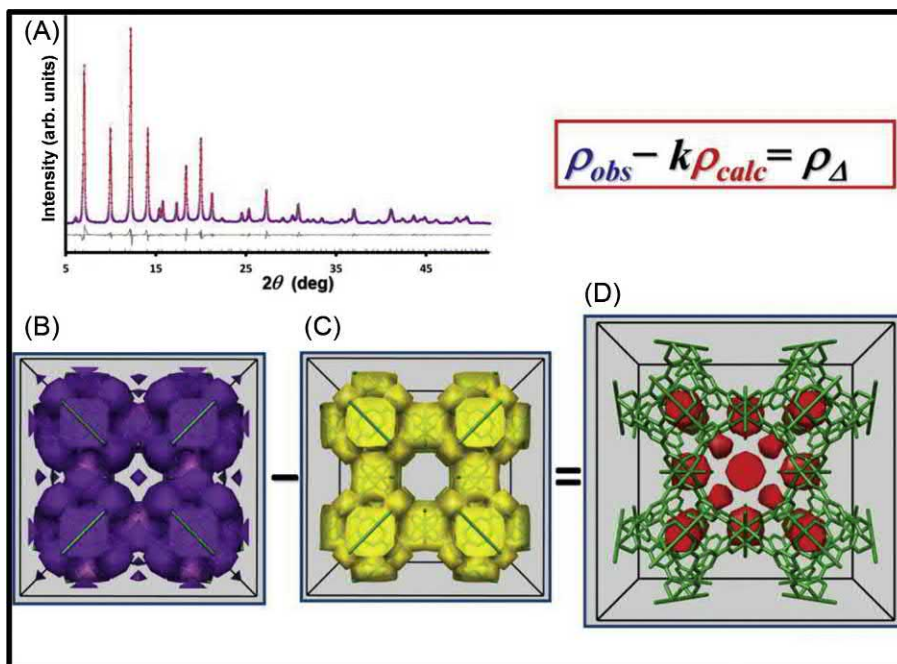


Fig. 13.4

(A) Final Pawley whole pattern decomposition plot of HKUST-1, (B) its observed structure envelope based on  $\rho_{obs}$ , (C) its calculated structure envelope based on  $\rho_{calc}$ , and (D) its difference envelope density  $\rho_{\Delta}$  overlapped with its structural model. *Reproduced from A.A. Yakovenko, Z. Wei, M. Wriedt, J.-R. Li, G.J. Halder, H.-C. Zhou, Study of guest molecules in metal–organic frameworks by powder X-ray diffraction: analysis of difference envelope density, Cryst. Growth Des. 14 (2014) 5397–5407, with permission from The American Chemical Society, Copyright 2019.*

electron from higher energy level fills the positively charged hole of lower energy. The energy difference of this transition is released as X-rays whose characteristic energy depends only upon the atomic number of an element and is captured by a detector for EDX analysis. So, this analysis is the fingerprint to identify elements (generally atomic number  $>5$ ) or atom present in the MOFs. So, after the synthesis, the composition of NMOFs is investigated using EDX analysis. But, for organic linkers, only the element present can be studied using this analysis. The functionality of the organic linkers is studied using FTIR, NMR, Raman, and XPS studied.

Ray Chowdhuri et al. synthesized multifunctional upconversion NMOFs for targeted antitumoral drug delivery application and have used EDX analysis to prove proper elemental composition in the targeted particle. The EDX spectrum of only upconversion nanoparticles (UCNP), only UIO-66-NH<sub>2</sub> MOFs, are compared with the targeted MOFs for confirmation of successful synthesis and elemental composition of the designed UCNP-embedded NMOFs [21].

Fourier-transform infrared spectroscopy (FTIR) analysis is performed to analysis the functional group present in the compound. So, the FTIR analysis is used to identify the functionality of the MOFs, as well as it performed to recognize the presence and binding status of guest molecules like drug, enzyme, etc. into the MOFs.

FTIR analysis can be performed by two modes, one attenuated total reflection (ATR) mode and another is diffuse reflectance (DRIFTS) mode. ATR mode is generally performed for strongly adsorbing or thick sample or for liquid sample. The solid or liquid sample is directly used to measure the reflected IR beam from which the detector records and produces the IR spectrum. DRIFTS mode can be used for both organic and inorganic solid materials which can be ground as fine powder and mixed with ground KBr to form a pallet. The detectors record the transmitted IR beam which scattered from the pallet and produced IR spectrum by following the Fourier-transform equation. These IR spectra are used to analysis the functional group present in the MOFs or biomolecule-embedded NMOFs.

As a preliminary proof for proper synthesise and conjugation, FTIR spectroscopy is used in all research works. For example, magnetic-IRMOF-3 is synthesized and targeted by conjugating with folic acid (FA) for targeted anticancer drug delivery [22]. FTIR is used here for confirmation of proper synthesise and conjugation. In general, carbonyl group in the range  $1800\text{--}1500\text{ cm}^{-1}$ , amine group in the range  $3600\text{--}3300\text{ cm}^{-1}$ , and metal oxygen linkage in the range  $600\text{--}400\text{ cm}^{-1}$  are used to detect from FTIR analysis MOFs applied in the biomedical field.

Nuclear magnetic resonance (NMR) spectroscopy is also used for further confirmation of the status of organic linkers and the presence of guest molecule.  $^{13}\text{C}$  NMR spectra for Organic linkers, drug or enzyme, can be performed in solution phase as they are soluble in  $\text{D}_6\text{-DMSO}$  or  $\text{CDCl}_3$ . As the MOFs are not soluble in any organic solvent, solid-state NMR spectroscopy is performed for MOFs and guest molecule like drug- or enzyme-loaded MOFs.

NMR is a physical phenomenon in which nuclei of the compound are perturbed by weak oscillating magnetic field in a strong static magnetic field and produced an electromagnetic signal which has characteristic frequency depending on individual compound. So, these spectra give the detailed information about the structure of the material. So, the solid-state NMR spectroscopy allows to study the structural formulation of NMOFs as well as performs to identify any guest molecule like protein, drug, etc. present in the MOFs. A broadened line spectrum is resulted for NMOFs from the solid-state  $^{13}\text{C}$  NMR spectrophotometer, whereas for organic compound dissolved in NMR solvent, a single peak type spectrum is observed in liquid-state  $^{13}\text{C}$  NMR. This line broadening is obtained due to different types of interaction, clearly described by Brückner et al. [23].

X-ray photoelectron spectroscopy (XPS) is also used to properly analyze empirical formula or chemical state of MOFs and also to study the electronic state of the metal ion. Generally,



transition metal ions are used to synthesize a MOF and the transition metal ion has several numbers of electronic states. So, XPS is an obligatory characterization technique to find the proper ionic state of the metal ion.

XPS is a surface characterization technique where soft X-ray source ( $AlK\alpha$  or  $MgK\alpha$ ) is used to ionize the electron from surface of the solid sample. When a sample is bombarded by sufficient energy X-ray, the inner shell electron transfers to an excited state or ejects from the atom. In XPS, sufficient energy X-ray is used for breaking the photoelectron away from the nuclear attraction force from the element. Some of these photo-ejected electrons are scattered inelastically, while others undergo prompt emission from the solid surface to the vacuum. These ejected electrons are collected by an electron analyzer and measure the kinetic energy to produce an energy spectrum of intensity of ejected electron versus binding energy of the electron. XPS can detect all the elements with an atomic number greater than three by measuring the binding energy of the electron. Hydrogen and helium are possible to detect from XPS. From the area calculation under a peak, the element percentage in a sample can also be obtained from the XPS spectra. By further studying one peak deconvolution, all the possible bonds correspond to that element present in a sample can also be identified.

Ke et al. had studied the XPS spectrum of fumarate (Fu)-MOFs to analysis the ionization state of the metal ion and also to confirm the selective fluoride ion removal by MOFs [24]. The XPS spectrum of Zr-MOF confirms the presence of C, O, and Zr element present in the MOF. The high-resolution spectrum of Zr3d confirms the Zr(IV) is present in the MOF-801. They also study the XPS spectrum of CaFu MOFs and confirm the presence of Ca(II) ion in the MOFs. The CaFu MOFs are used to selectively remove fluoride ion. It is also approved from XPS spectrum of before and after treatment of fluoride ion.

### **13.2.2 Surface characterization**

Characterization of surface property for NMOFs can be possible by several techniques. The surface morphology of the particles is studied by using scanning electron microscope (SEM) or field emission scanning electron microscope (FESEM) analysis. The detailed inner structure can be visualized by transmission electron microscopy (TEM) analysis. The hydrodynamic particle size and the surface charge of the particles can be investigated by dynamic light scattering (DLS) technique and zeta potential analysis, respectively. Surface area and pore size distribution of NMOFs are studied by Brunauer-Emmett-Teller (BET) analysis. All these techniques are explained in the following section.

#### **13.2.2.1 Surface morphology analysis**

Investigation of surface morphology of MOFs is required for confirmation of successful synthetization of MOFs or effect of any target molecule, drug, or enzyme on the material. SEM and FESEM imaging are used to study the morphology of the particle. Principle for both these

analyses is the use of focused electron beam to produce high magnification of surface topography, which perform visual analysis of surface morphology. In SEM, the electron beam generated by thermionic process, i.e., from heated tungsten filament, has lower energy. So, SEM could not give the clear image for nanoscale materials. But for biomedical application, the used material or MOF should have size in the range 200–50 nm as the pore size of shell is in nano range. So, FESEM imaging is used for morphology study of NMOFs in biomedical application. FESEM is field emission scanning electron microscope where a thin sharp needle shape tungsten is used to generate the electron beam by electro magnetization. The produced beam has sharp high electron density and produced high-resolution image for the particle. Dried samples are used for FESEM imaging after making the conducting surface by thin layer coating of gold or platinum under high vacuum. The overall microscope, used in FESEM, is kept under high vacuum. The surface of object is scanned by electron in zig-zag pattern. The secondary electron beam generated from the surface of the scanned object is caught by detector and transformed into digital image which is seen on the screen of monitor.

Generally, MOFs have a particular morphology which depends on the metal ion, organic ligand, and/or solvent used in synthesis. By changing any of these precursors, the morphology can be changed. FESEM analysis can be visualized by any change of the surface morphology of NMOFs. For example, ZIF-8 synthesized in dry methanol have almost spherical morphology [25]. But when folic acid (FA) dissolved in DMF is added during synthesis, the morphology changed to cubic structure. This change in structure may be due to the presence of different solvents or presence of different organic ligands. Again, when vancomycin (VAN) and FA both are mixed during the synthesis of ZIF-8, slightly distorted cubic structure is observed. This distortion may also occur due to the presence of VAN.

TEM or HRTEM analysis is another imaging technique to clearly study the crystalline structure of NMOFs and study the presence of any guest nanoparticle into the NMOFs. Principle of TEM is same as SEM or FESEM; here, the only difference is scattered electron beam which passes through the thin section of material and is used in detector to create an interference image. HRTEM provides high-resolution image than TEM. In TEM instrument, only the scattered electron beam is used in detector, whereas both transmitted and scattered electron beams are used in the detector for HRTEM analysis. Wiktor et al. have reviewed and described the importance of the TEM analysis for characterization like crystal structure determination of NMOFs [26].

Selected area electron diffraction (SAED) pattern can be achieved in HRTEM instrument to study the crystallography analysis. SAED pattern for amorphous and crystalline powder is different. Simple diffuse rings are obtained for amorphous material, whereas for crystalline compound ring is formed by using bright spot which is arisen due to Bragg reflection from individual crystal lattice. NMOFs are generally crystalline compound in which characteristic planes exist to produce bright ring spot in SAED pattern.

Lattice fringe analysis can also be performed in HRTEM instrument. It is nothing but a periodic fringe calculated which formed two waves; a transmitted wave exiting from a crystal and a diffracted wave from one lattice plane of the crystal. The spacing of fringe depends upon only the lattice plane which is unique for a crystal lattice. So, the lattice fringe can be used as fingerprint analysis to identify the nanocrystal.

Xu et al. synthesized magnetic Ni-nanoparticles (NP) from the Ni-MOF by in situ hot stage in TEM by continuous enhancement of temperature up to 700°C [27]. They have detected the formation of Ni-NPs by following the TEM image and SAED pattern of the initial Ni-MOFs at every 100°C of rising temperature. At 400°C, Ni-NPs are formed from the Ni-MOFs, confirmed by SAED pattern, and 400–600°C stability of Ni-NPs in carbon units is increasing, confirmed by both TEM image and SAED patterns. At 700°C, some Ni-NPs are coagulated to form a big particle and came out from the carbon moiety. So, the SAED pattern of crystalline Ni-MOFs is gradually broken by following the formation of new crystallinity pattern for Ni-NPs shown in Fig. 13.5. Authors have also analyzed the lattice fringe of Ni-NPC at 600°C to confirm the formation of NPs from the MOFs structure.

Yang et al. synthesized Ag-doped ZnO nanoparticle for photocatalysis where ZnO is derived from ZIF-8 MOFs. The presence of Ag and ZnO is detected from the lattice fringe of 0.235 and 0.256 nm for (111) plane of Ag and (002) plane of ZnO, respectively, which are derived from TEM analysis shown in Fig. 13.6 [28].

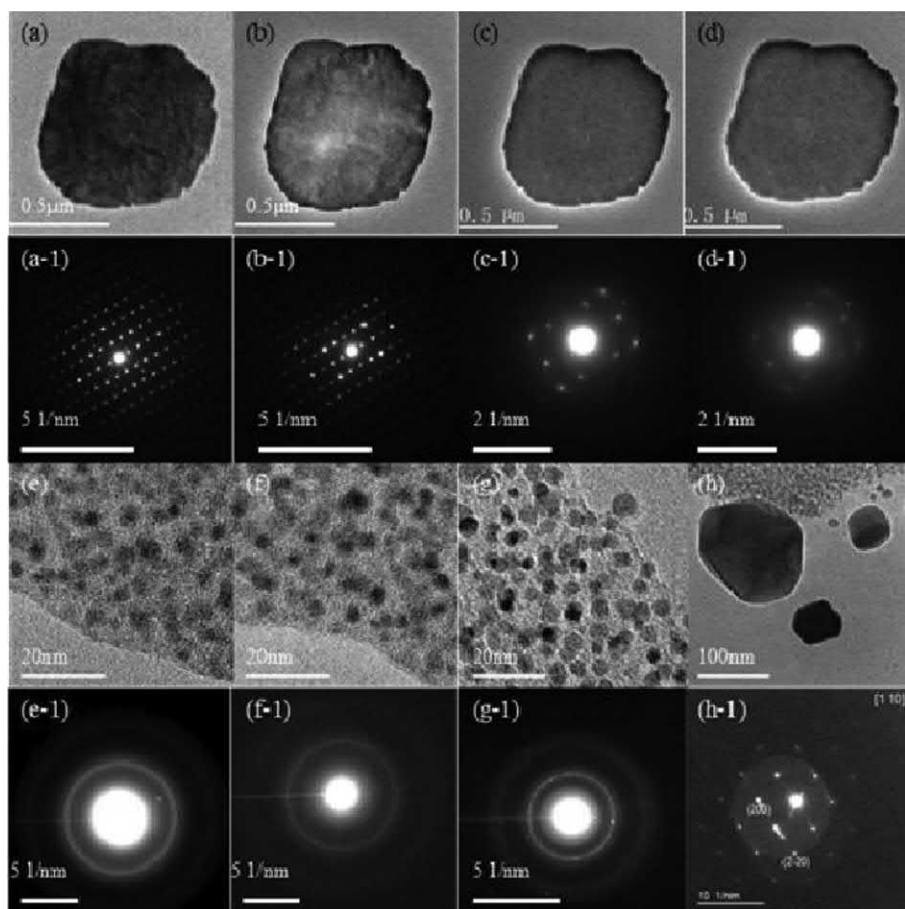
#### 13.2.2.2 Particle size and surface charge analysis

The size distribution of nanoparticle can be measured using dynamic light scattering (DLS) technique. In this analysis, the powder sample is homogeneously suspended in solution, generally water for MOFs, and the hydrodynamic diameter is used to measure the average particle size. DLS instrument can only measure the nanosized particle whose dimension is in the range of 1–1000 nm. Small particles in the suspension undergo random thermal motion known as Brownian motion. Particle size can be measured from this random motion using Stokes-Einstein equation.

$$D_h = \frac{K_B T}{3\pi\eta D_t}$$

Where  $D_h$  is the hydrodynamic diameter,  $D_t$  is the translational diffusion coefficient,  $K_B$  is the Boltzmann's constant,  $T$  is the thermodynamic temperature, and  $\eta$  is the dynamic viscosity. But from DLS analysis, the actual particle size cannot be obtained rather than the hydrodynamic diameter.

In biomedical application of NMOFs, surface charge plays an important role which can be calculated by zeta potential analysis. Generally, the DLS and zeta potential are measured in same instrument, Zetasizer. When the particles are suspended in a solution, a charge is generated on the outer surface of the particle depending upon the surface charge of the particle.

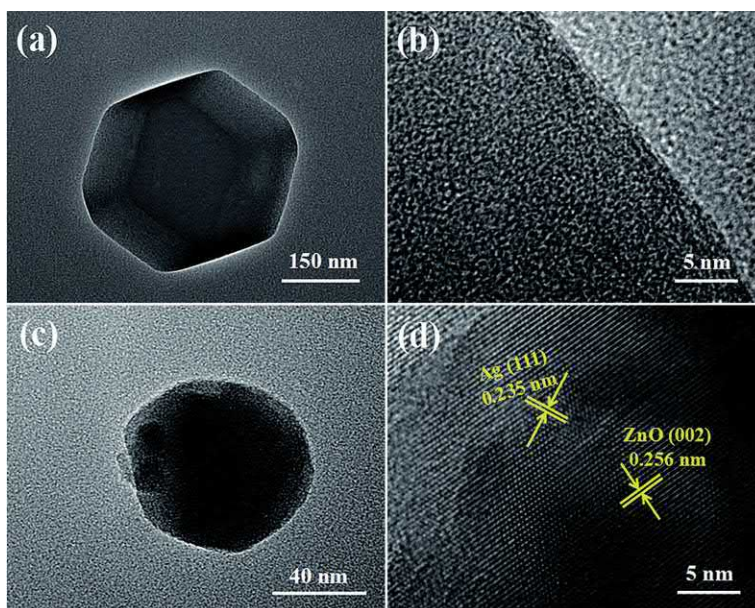


**Fig. 13.5**

The hot stage images of TEM at (A) room temperature, (B) 100°C, (C) 200°C, (D) 300°C, (E) 400°C, (F) 500°C, (G) 600°C, (H) 700°C, and (A-1)–(H-1) the corresponding SAED patterns. *Reproduced from D. Xu, D. Zhang, H. Zou, L. Zhu, M. Xue, Q. Fang, S. Qiu, Guiding by in-situ hot stage in TEM to synthesize magnetic metal nanoparticles from a MOF, Chem. Commun. 52 (2016) 10513–10516, with permission from The Royal Society of Chemistry, Copyright 2019.*

When an electrical potential is applied into the solution, the particles move toward a particular direction with a velocity due to interaction of the charge particle and applied field. The velocity is proportional to the potential charge of the particles' shear plane which is called zeta potential.

Stability of colloidal dispersion can be distinguished by zeta potential measurement. Colloidal dispersion is the necessary condition for biomedical application because in the blood or cell the used particle should be dispersed for long time rather than the coagulation. The zeta potential indicates the surface charge, so large value of zeta potential gives massive repulsion between the particle. So, the particle which has large positive or negative value zeta potential is highly stable in colloidal medium.



**Fig. 13.6**

Low magnification TEM images and HRTEM images of (A and B) ZIF-8 and (C and D) Ag/ZnO. Reproduced from X. Yang, L. Qiu, X. Luo, ZIF-8 derived Ag-doped ZnO photocatalyst with enhanced photocatalytic activity, *RSC Adv.* 8 (2018) 4890–4894, with permission from The Royal Society of Chemistry, Copyright 2019.

For some example, Ranji-Burachaloo et al. studied zeta potential to verify the high dispersity of rMOFs. Reduced MOFs (rMOFs) have higher negative value zeta potential compared to MOFs and prevent the coagulation [29]. Liu et al. synthesized ZrMOF conjugated with DNA aptamer [30]. The aptamer conjugation is confirmed by zeta potential analysis because the positive value of zeta potential of MOFs is converted to negative potential after aptamer conjugation due to the negative value of DNA. Lei et al. developed redox-responsive MOFs for anticancer drug delivery by varying metal with synthesize temperature [31]. They also explain agglomeration in water using the zeta potential value. Zr-MOF has high zeta potential compared to Fe or Al MOFs for which it has high dispersibility in water. The hydrodynamic diameter measured by DLS is also compared to choose the better drug carrier. The hydrodynamic diameter for Zr-MOFs synthesized at 40°C is 125 nm which is most favorable to be used as a drug carrier.

### 13.2.2.3 Surface area analysis

Surface area of NMOFs is an important factor for the biomedical application. Generally, the NMOFs have high surface area with high microporosity. So, they have high loading capability. These surface areas with pore size and pore volume distribution can be analyzed by gas adsorption-desorption isotherm using Brunauer-Emmett-Teller (BET) theory.



The specific surface area can be determined by calculating the amount of physically adsorbed gas on the surface of the solid. The adsorbate gas forms monomolecular layer on the surface of solid adsorbent by weak van der Waal forces. Before the BET analysis, the solid sample is dried at elevated temperature under high vacuum or nitrogen purging. Then the sample is used for gas adsorption (generally nitrogen) at the temperature of liquid nitrogen ( $-196^{\circ}\text{C}$ , i.e., 77.4 K). The amount of adsorbed gas is calculated by volumetric or continuous flow technique. Then the data is treated in Brunauer-Emmett-Teller adsorption isotherm equation:

$$\frac{1}{\left[ V_{\alpha} \left( \frac{P_0}{P} - 1 \right) \right]} = \frac{C - 1}{V_m C} \times \frac{P}{P_0} + \frac{1}{V_m C}$$

Where  $P$  and  $P_0$  are partial vapor pressure of adsorbate gas in equilibrium with the surface at 77.4 K and saturated pressure of adsorbate gas in pascals, respectively.  $V_{\alpha}$  is volume of gas adsorbed at standard temperature and pressure (STP) [273.15 K and atmospheric pressure ( $1.013 \times 10^5$  Pa)], in milliliters,  $V_m$  is volume of gas adsorbed at STP to produce an apparent monolayer on the sample surface, in milliliters.  $C$  is dimensionless constant which associated the enthalpy of adsorption of the adsorbate gas on the powder sample. Using this equation, the adsorption-desorption isotherm can be plotted, and by calculating the value of  $V_m$ , the effective surface area of the solid surface can be measured in  $\text{m}^2 \text{g}^{-1}$  by following the equation:

$$S = \frac{V_m N \alpha}{m \times 22,400}$$

Where  $N$  is the Avogadro constant,  $\alpha$  is effective cross-sectional area of one adsorbate molecule, in square meters,  $m$  is the mass of the solid powder, and 22,400 is the molar volume of adsorbate gas at STP in milliliters.

The surface area determination is highly focused in MOFs to explain the high drug loading capacity. For some example, Uio-66 MOFs possess high surface area with micro-porosity for which it has high drug loading capacity [21,32]. Wang et al. synthesize the core shell MOFs (CS-MOFs), where the core and shell are formed by  $\text{Mn}_3[\text{Co}(\text{CN})_6]_2$  MOFs (C-MOFs) and MIL-100(Fe) MOFs (S-MOFs), respectively. The CS-MOFs has high surface area compared to the C-MOFs, for which the CS-MOFs become an ideal drug carrier [33].

### 13.2.3 Thermal stability analysis

Thermal stability study is not so essential for biomedical application, but necessary to study the stability of NMOFs up to an elevated temperature. This can be performed by Thermogravimetric analysis (TGA), where the amount of weight loss is measured with increasing temperature at a constant heating rate. From the TGA analysis, composition of MOFs that means how many types of molecule present in the MOFs can be confirmed.



By comparing the weight loss percentage, the amount percentage of loading can also be calculated for any biomolecule-loaded NMOFs.

### 13.2.4 Luminescent property analysis

MOFs, having luminescent property, are used in various fields of application including in biomedical field, especially for cell study and/or sensing [34]. Some NMOFs possess inherent fluorescent property due to  $\pi$ -electron enrichment and charge transfer of ligand to metal or metal to ligand [35–38]. In some cases, fluorescent material like upconversion nanoparticle [39–42], gold nanoparticle [43,44], or quantum/carbon dot [45–47] is incorporated into the MOFs during synthesis or by other procedure to make fluorescent MOFs. This luminescent property is determined by measuring the photoluminescence (PL) spectra.

Photoluminescence is the nondestructive powerful optical method of probing the electronic structure of materials. In this process, a light of particular wavelength is directed toward the material, where the light is adsorbed and the electron in the material is excited to higher energy state. After that, the excited electron is returned to the equilibrium state by releasing the excess energy following emission of light (a radiative process) or may not (nonradiative process). When the light is emitted by photo excitation, it is called photoluminescence, as shown in Fig. 13.7. The emitted light is collected and analyzed spectrally, spatially, and also temporally.

The energy of emitted light depends on the difference between excited and equilibrium electron state. The equilibrium electron state is fixed for a material, but the excited electron state depends on the energy of directed light. Generally, different wavelength laser light is used for excitation in PL instrument. So, the PL spectrum is not an adsorption spectrum, whereas it is an

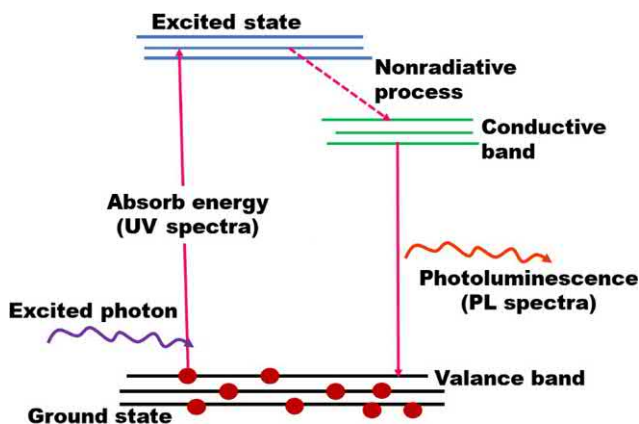


Fig. 13.7  
Principle of UV and PL spectra.

emission spectrum which deals with the transition of electron from excited state to ground state. The value of wavelength at which the molecule adsorbed energy can be used for excitation wavelength and provide the most intense and sometimes red shifted emission spectra.

### 13.2.5 UV-visible spectroscopy

UV-visible spectroscopy study is one of the most important characterizations in biomedical application. Generally, drug molecule or biological macromolecule contains  $\pi$ -electrons with high conjugation. So, they are UV-active which means they can absorb the light of wavelength in the region UV-visible range and give a spectrum in the UV-Vis instrument. So, the content of UV-active drug or any other biomolecule in the NMOFs can be measured calculating and comparing the intensity of the spectrum [48–50]. Again, MOFs are composed of metal and organic linkers. So, they also have an electronic conjugation structure which makes it UV-active and gives an UV-Vis spectrum. The wavelength of light at which maximum absorbance occurs can be found out from the spectrum. This maximum wavelength can be used as excitation energy to obtain the emission spectra in PL instrument for fluorescent MOFs.

UV-Vis spectrophotometer provides the energy of far and near UV and visible region of the electromagnetic spectrum (that means 200–800 nm) to the liquid sample contained in a quartz or glass sample holder. The instrument operates by passing beam of light through the sample and measuring the wavelength and intensity of transmitted light reached in the detector. Generally, tungsten filament, deuterium arc lamp is used as the source of UV-radiation and light emitting diodes (LED) and xenon arc lamps for the visible radiation. The detector is typically a photodiode or a charge couple device (CCD) with monochromators for filtering the light to get single wavelength reach the detector.

The spectrophotometer measures the absorbance or transmittance by following the Lambert-Beer's law. This law is established from the transmittance ( $T$ ) of the transmitted light. If the intensity of transmittance is  $I$  light and  $I_0$  is the intensity of directed light, then transmittance ( $T$ ) is equal to  $I/I_0$  with transmission rate  $I/I_0 \times 100$ . So, the value of absorbance is  $\log(1/T)$ . These values depend proportionally on the concentration and the path length of the beam. Following overall this condition, the Beer-Lambert's equation is as follows:

$$A = \epsilon Cl$$

Where  $A$  is the absorbance,  $C$  is the concentration of solution in  $\text{mol L}^{-1}$ ,  $l$  is the path length of the beam which is the width of the sample holder in cm and  $\epsilon$  is the proportionality constant, which is called molar adsorption coefficient in unit  $\text{L mol}^{-1} \text{cm}^{-1}$ . The value of  $\epsilon$  depends only on the material under certain specific condition. So, the absorbance and transmittance are unitless quantity.

### 13.2.6 Biocompatibility test

Besides the characterization of all these above-discussed techniques, biocompatibility test of NMOFs is essential for biomedical application. NMOFs are composed of metal and organic linkers. All the metals and also the excess quantity of metal are not good for health as well as organic moieties can have some poisonous effect on health. So, before application in biomedical field, one should check the cytotoxicity which can be measured by various methods like dye exclusion, colorimetric assay, fluorometric assay, and luminometric assay. The quantitative cytotoxicity is generally achieved by MTT assay which is a colorimetric method.

MTT is a yellow tetrazole reagent, generally 3-(4,5-dimethylthiazol-2-yl)-2,5-diphenyl tetrazolium bromide, which reduced to purple color formazan, (E,Z)-5-(4,5-dimethylthiazol-2-yl)-1,3-diphenylformazan, by mitochondrial succinate dehydrogenase. As this reaction is only possible in living cell system, using this assay quantitatively measurement of living cell concentration can be possible after addition of a fixed amount of NMOFs.

### 13.3 Conclusion

In this chapter, a brief discussion is presented about various techniques relevant to the characterization of nanosized MOFs for application in biomedical field. MOFs can be of various sizes and shapes like nano- to macro-size MOFs. But for biomedical application, only nanosized MOFs are used; that's why the characterization techniques used for NMOFs are deliberated in this chapter. All these techniques revealed the structural properties like plane detection, atomic modeling, functionality, surface morphology, etc. or physical properties like thermal stability, surface area, photoluminity, etc. of NMOFs. These are common methods to characterize the NMOFs which are used generally in any type of application. For biomedical application, biocompatibility of NMOFs should be studied before application in bio-field for cytotoxicity determination.

### References

- [1] S. Beg, M. Rahman, A. Jain, S. Saini, P. Midoux, C. Pichon, F.J. Ahmad, S. Akhter, Nanoporous metal organic frameworks as hybrid polymer–metal composites for drug delivery and biomedical applications, *Drug Discov. Today* 22 (4) (2017) 625–637.
- [2] J. Liu, L. Chen, H. Cui, J. Zhang, L. Zhang, C.-Y. Su, Applications of metal-organic frameworks in heterogeneous supramolecular catalysis, *Chem. Soc. Rev.* 43 (2014) 6011–6061.
- [3] A.H. Chughtai, N. Ahmad, H.A. Younus, A. Laypkov, F. Verpoort, Metal-organic frameworks: versatile heterogeneous catalysts for efficient catalytic organic transformations, *Chem. Soc. Rev.* 44 (2015) 6804–6849.
- [4] M. Wen, G. Li, H. Liu, J. Chen, T. An, H. Yamashita, Metal–organic framework-based nanomaterials for adsorption and photocatalytic degradation of gaseous pollutants: recent progress and challenges, *Environ. Sci. Nano* 6 (2019) 1006–1025.
- [5] W. Xia, A. Mahmood, R. Zou, Q. Xu, Metal-organic frameworks and their derived nanostructures for electrochemical energy storage and conversion, *Energy Environ. Sci.* 8 (2015) 1837–1866.

- [6] C. Wang, X. Liu, N.K. Demir, J. Paul Chen, K. Li, Applications of water stable metal-organic frameworks, *Chem. Soc. Rev.* 45 (2016) 5107–5134.
- [7] W. Chen, C. Wu, Synthesis, functionalization, and applications of metal-organic frameworks in biomedicine, *Dalton Trans.* 47 (2018) 2114–2133.
- [8] S. Rojas, T. Devic, P. Horcajada, Metal organic frameworks based on bioactive components, *J. Mater. Chem. B* 5 (2017) 2560–2573.
- [9] R. Riccò, W. Liang, S. Li, J.J. Gassensmith, F. Caruso, C. Doonan, P. Falcaro, Metal-organic frameworks for cell and virus biology: a perspective, *ACS Nano* 12 (2018) 13–23.
- [10] S. Keskin, S. Kızılel, Biomedical applications of metal organic frameworks, *Ind. Eng. Chem. Res.* 50 (2011) 1799–1812.
- [11] M. Peller, K. Böll, A. Zimpel, S. Wuttke, Metal-organic framework nanoparticles for magnetic resonance imaging, *Inorg. Chem. Front.* 5 (2018) 1760–1779.
- [12] X. Lian, Y. Fang, E. Joseph, Q. Wang, J. Li, S. Banerjee, C. Lollar, X. Wang, H.-C. Zhou, Enzyme-MOF (metal-organic framework) composites, *Chem. Soc. Rev.* 46 (2017) 3386–3401.
- [13] I.A. Lázaro, R.S. Forgan, Application of zirconium MOFs in drug delivery and biomedicine, *Coord. Chem. Rev.* 380 (2019) 230–259.
- [14] R. Dai, F. Peng, P. Ji, K. Lu, C. Wang, J. Sun, W. Lin, Electron crystallography reveals atomic structures of metal-organic nanoplates with  $M_{12}(\mu_3-O)_8(\mu_3-OH)_8(\mu_2-OH)_6$  ( $M = Zr, Hf$ ) secondary building units, *Inorg. Chem.* 56 (2017) 8128–8134.
- [15] J.M. Chin, E.Y. Chen, A.G. Menon, H.Y. Tan, A.T.S. Hor, M.K. Schreyer, J. Xu, Tuning the aspect ratio of  $NH_2$ -MIL-53(Al) microneedles and nanorods via coordination modulation, *CrystEngComm* 15 (2013) 654–657.
- [16] S. Nandi, H. Reinsch, S. Banesh, N. Stock, V. Trivedi, S. Biswas, Rapid and highly sensitive detection of extracellular and intracellular  $H_2S$  by an azide-functionalized Al(III)-based metalorganic framework, *Dalton Trans.* 46 (2017) 12856–12864.
- [17] X.-Y. Xu, B. Yan, Nanoscale LnMOF-functionalized nonwoven fiber protected by polydimethylsiloxane coating layer as highly sensitive ratiometric oxygen sensor, *J. Mater. Chem. C* 4 (2016) 8514–8521.
- [18] K. Fujii, A.L. Garay, J. Hill, E. Sbircea, Z. Pan, M. Xu, D.C. Apperley, S.L. James, K.D.M. Harris, Direct structure elucidation by powder X-ray diffraction of a metal-organic framework material prepared by solvent-free grinding, *Chem. Commun.* 46 (2010) 7572–7574.
- [19] A.A. Yakovenko, J.H. Reibenspies, N. Bhuvanesh, H.-C. Zhou, Generation and applications of structure envelopes for porous metal-organic frameworks, *J. Appl. Crystallogr.* 46 (2013) 346–353.
- [20] A.A. Yakovenko, Z. Wei, M. Wriedt, J.-R. Li, G.J. Halder, H.-C. Zhou, Study of guest molecules in metal-organic frameworks by powder X-ray diffraction: analysis of difference envelope density, *Cryst. Growth Des.* 14 (2014) 5397–5407.
- [21] A. Ray Chowdhuri, D. Laha, S. Chandra, P. Karmakar, S.K. Sahu, Synthesis of multifunctional upconversion NMOFs for targeted antitumor drug delivery and imaging in triple negative breast cancer cells, *Chem. Eng. J.* 319 (2017) 200–211.
- [22] A. Ray Chowdhuri, D. Bhattacharya, S.k. Sahu, Magnetic nanoscale metal organic frameworks for potential targeted anticancer drug delivery, imaging and MRI contrast agent, *Dalton Trans.* 45 (2016) 2963–2973.
- [23] S.I. Brückner, J. Pallmann, Brunner, Nuclear magnetic resonance of metal-organic frameworks (MOFs), in: S. Kaskel (Ed.), *The Chemistry of Metal-Organic Frameworks: Synthesis, Characterization, and Applications*, vol. 2, Wiley-VCH Verlag GmbH & Co. KGaA, 2016, pp. 607–628.
- [24] F. Ke, C. Peng, T. Zhang, M. Zhang, C. Zhou, H. Cai, J. Zhu, X. Wan, *Sci. Rep.* 8 (2018) 939.
- [25] A. Ray Chowdhuri, B. Das, A. Kumar, S. Tripathy, S. Roy, S.K. Sahu, One-pot synthesis of multifunctional nanoscale metal-organic frameworks as an effective antibacterial agent against multidrug-resistant *Staphylococcus aureus*, *Nanotechnology* 28 (2017) 095102 (13 pp.).
- [26] C. Wiktor, M. Meledina, S. Turner, O.I. Lebedev, R.A. Fischer, Transmission electron microscopy on metal-organic frameworks – a review, *J. Mater. Chem. A* 5 (2017) 14969–14989.
- [27] D. Xu, D. Zhang, H. Zou, L. Zhu, M. Xue, Q. Fang, S. Qiu, Guiding by in-situ hot stage in TEM to synthesize magnetic metal nanoparticles from a MOF, *Chem. Commun.* 52 (2016) 10513–10516.

- [28] X. Yang, L. Qiu, X. Luo, ZIF-8 derived Ag-doped ZnO photocatalyst with enhanced photocatalytic activity, *RSC Adv.* 8 (2018) 4890–4894.
- [29] H. Ranji-Burachaloo, F. Karimi, K. Xie, Q. Fu, P.A. Gurr, D.E. Dunstan, G.G. Qiao, MOF-mediated destruction of cancer using the cell's own hydrogen peroxide, *ACS Appl. Mater. Interfaces* 9 (2017) 33599–33608.
- [30] Y. Liu, W. Hou, L. Xia, C. Cui, S. Wan, Y. Jiang, Y. Yang, Q. Wu, L. Qiu, W. Tan, ZrMOF nanoparticles as quenchers to conjugate DNA aptamers for target-induced bioimaging and photodynamic therapy, *Chem. Sci.* 9 (2018) 7505–7509.
- [31] B. Lei, M. Wang, Z. Jiang, W. Qi, R. Su, Z. He, Constructing redox-responsive metal–organic framework nanocarriers for anticancer drug delivery, *ACS Appl. Mater. Interfaces* 10 (2018) 16698–16706.
- [32] D. Chen, D. Yang, C.A. Dougherty, W. Lu, H. Wu, X. He, T. Cai, M.E. Van Dort, B.D. Ross, H. Hong, *In vivo* targeting and positron emission tomography imaging of tumor with intrinsically radioactive metal–organic frameworks nanomaterials, *ACS Nano* 11 (2017) 4315–4327.
- [33] D. Wang, J. Zhou, R. Chen, R. Shi, C. Wang, J. Lu, G. Zhao, G. Xia, S. Zhou, Z. Liu, H. Wang, Z. Guo, Q. Chen, Core-shell metal-organic frameworks as Fe<sup>2+</sup> suppliers for Fe<sup>2+</sup>-mediated cancer therapy under multimodality imaging, *Chem. Mater.* 29 (2017) 3477–3489.
- [34] Y. Cui, J. Zhang, H. He, G. Qian, Photonic functional metal–organic frameworks, *Chem. Soc. Rev.* 47 (2018) 5740–5785.
- [35] L. Zhang, Z. Kang, X. Xin, D. Sun, Metal-organic frameworks based luminescent materials for nitroaromatics sensing, *CrystEngComm* 18 (2016) 193–206.
- [36] D.J. Wales, J. Grand, V.P. Ting, R.D. Burke, K.J. Edler, C.R. Bowen, S. Mintova, A.D. Burrows, Gas sensing using porous materials for automotive applications, *Chem. Soc. Rev.* 44 (2015) 4290–4321.
- [37] A. Samui, K. Pal, P. Karmakar, S.K. Sahu, In situ synthesized lactobionic acid conjugated NMOFs, a smart material for imaging and targeted drug delivery in hepatocellular carcinoma, *Mater. Sci. Eng. C* 98 (2019) 772–781.
- [38] S.M. Sheta, S.M. El-Sheikh, M.M. Abd-Elzaher, A.R. Wassel, A novel nano-size lanthanum metal–organic framework based on 5-amino-isophthalic acid and phenylenediamine: photoluminescence study and sensing applications, *Appl. Organometal. Chem.* 33 (4) (2019) e4777.
- [39] A. Ray Chowdhuri, D. Laha, S. Pal, P. Karmakar, S.K. Sahu, One-pot synthesis of folic acid encapsulated upconversion nanoscale metal organic frameworks for targeting, imaging and pH responsive drug release, *Dalton Trans.* 45 (2016) 18120–18132.
- [40] M. Li, Z. Zheng, Y. Zheng, C. Cui, C. Li, Z. Li, Controlled growth of metal–organic framework on upconversion nanocrystals for NIR-enhanced photocatalysis, *ACS Appl. Mater. Interfaces* 9 (3) (2017) 2899–2905.
- [41] D. Li, S.-H. Yu, H.-L. Jiang, From UV to near-infrared light-responsive metal–organic framework composites: plasmon and upconversion enhanced photocatalysis, *Adv. Mater.* 30 (2018) 1707377.
- [42] Z. Yuan, L. Zhang, S. Li, W. Zhang, M. Lu, Y. Pan, X. Xie, L. Huang, W. Huang, Paving metal–organic frameworks with upconversion nanoparticles via self-assembly, *J. Am. Chem. Soc.* 140 (2018) 15507–15515.
- [43] F. Cao, E. Ju, C. Liu, W. Li, Y. Zhang, K. Dong, Z. Liu, J. Ren, X. Qu, Encapsulation of aggregated gold nanoclusters in a metal–organic framework for real-time monitoring of drug release, *Nanoscale* 9 (2017) 4128–4134.
- [44] A. Paul, G. Vyas, P. Paul, D.N. Srivastava, Gold-nanoparticle-encapsulated ZIF-8 for a mediator-free enzymatic glucose sensor by amperometry, *ACS Appl. Nano Mater.* 1 (2018) 3600–3607.
- [45] N.A. Travlou, M. Algarra, C. Alcoholado, M. Cifuentes-Rueda, A.M. Labela, J.M. Lázaro-Martínez, E. Rodríguez-Castellón, T.J. Badosz, Carbon quantum dot surface-chemistry-dependent Ag release governs the high antibacterial activity of Ag-metal–organic framework composites, *ACS Appl. Bio Mater.* 1 (2018) 693–707.
- [46] S. Saha, G. Das, J. Thote, R. Banerjee, Photocatalytic metal–organic framework from CdS quantum dot incubated luminescent metallohydrogel, *J. Am. Chem. Soc.* 136 (2014) 14845–14851.

- [47] C. Yao, Y. Xu, Z. Xia, A carbon dot-encapsulated UiO-type metal organic framework as a multifunctional fluorescent sensor for temperature, metal ion and pH detection, *J. Mater. Chem. C* 6 (2018) 4396–4399.
- [48] A. Ray Chowdhuri, T. Singh, S.K. Ghosh, S.K. Sahu, Carbon dots embedded magnetic nanoparticles @chitosan @metal organic framework as a nanoprobe for pH sensitive targeted anticancer drug delivery, *ACS Appl. Mater. Interfaces* 8 (2016) 16573–16583.
- [49] X. Chen, R. Tong, Z. Shi, B. Yang, H. Liu, S. Ding, X. Wang, Q. Lei, J. Wu, W. Fang, MOF nanoparticles with encapsulated autophagy inhibitor in controlled drug delivery system for antitumor, *ACS Appl. Mater. Interfaces* 10 (2018) 2328–2337.
- [50] I.A. Lázaro, S. Haddad, J.M. Rodrigo-Muñoz, R.J. Marshall, B. Sastre, V. del Pozo, D. Fairen-Jimenez, R.S. Forgan, Surface-functionalization of Zr-fumarate MOF for selective cytotoxicity and immune system compatibility in nanoscale drug delivery, *ACS Appl. Mater. Interfaces* 10 (2018) 31146–31157.



# *Adsorption, delivery, and controlled release of therapeutic molecules from MOFs*

Houman Kazemzadeh<sup>a</sup>, Masoud Mozafari<sup>b,c</sup>

<sup>a</sup>Faculty of Pharmacy, Tehran University of Medical Sciences, Tehran, Iran <sup>b</sup>Cellular and Molecular Research Center, Iran University of Medical Sciences (IUMS), Tehran, Iran <sup>c</sup>Department of Tissue Engineering & Regenerative Medicine, Faculty of Advanced Technologies in Medicine, Iran University of Medical Sciences (IUMS), Tehran, Iran

## **14.1 Introduction**

Pharmaceutical applications are always one of the most interesting tasks which can take advantage of other scientific areas such as biomaterials and nanomaterials in order to overcome many obstacles in biology, medicine, etc. [1]. Different genetics, lifestyles, nutrition, enzymes, and biological environments in the body which are not completely known make it hard to underestimate what would happen to therapeutic and other materials that enter the human body [2]. This is where we use biomaterials and nanomaterials to have targeted delivery in order to reduce the interactions between the unknown biological environments and our therapeutic molecules [3]. Different routes have been used such as “organic route” which uses either biocompatible dendritic macromolecules or polymers [4, 5]. The deficiency of this method was the absence of a well-defined porosity which could make it hard to achieve controlled delivery. There is also another route as “inorganic route,” in which the hosts are inorganic porous solids, such as zeolites or mesoporous silicate materials [6]. In this route, the main problem is low drug-loading capacity. To overcome the main problems and have the useful features of both routes, Hybrid inorganic-organic solids with large pores and ability of controlled release and delivery have been proposed [7]. Such characteristics made us able to load various kinds of therapeutic agents through noncovalent or covalent methods with different amounts [8]. One of the most promised hybrids for pharmaceutical applications is metal organic frameworks (MOFs). They are newly developed platforms, which proved themselves as mighty candidates in this matter. These astonishing platforms are constructed from metals (or metal clusters, chains, or layers) which are connected by organic linkers. With this structure, they show some of the highest porosities known

with different range of numbers [9]. This ideal ability makes us able to load and controllably deliver therapeutics and other molecules through the body's complex environments.

## 14.2 Biological concerns for drug delivery development

### 14.2.1 Toxicological study

One of the most important matters in drug delivery development are toxicological studies and biodegradability routes of inserted delivery systems [10]. As mentioned, MOFs are made of metal points which are attached by organic linkers. So these metals and their organic linkers should be nontoxic or results gained from toxicological studies should be used to balance their biological toxic effects. About the metals used in these hybrids, chromium, cadmium, nickel, cobalt, and other metals are not suitable as metal nodes for their high toxicity, but the most appropriate metals are Ca, Cu, Mn, Mg, Zn, Fe, Ti, or Zr. Data on their biological fate and their toxicity are estimated by oral lethal dose 50 (LD50), Ca, 1 g/kg; Cu, 25 µg/kg; Mn, 1.5 g/kg; Mg, 8.1 g/kg; Zn, 350 µg/kg; Fe, 30 g/kg; Ti, 25 g/kg; and Zr. 4.1 g/kg [11].

About the organic linkers in this class of materials, we can divide them into two groups: exogenous linkers and endogenous linkers. Exogenous linkers are the most common ones used in this hybrid which are gained or synthesized from natural compounds without interfering in the body cycles. This group consists of polycarboxylates, imidazolates, pyridyl, amines, etc. The toxicity data (LD50) among few subclass of this group are 5 g/kg (terephthalic acid), 8.4 g/kg (trimesic acid), 5 g/kg (2,6 naphthalenedicarboxylic acid), 1.13 g/kg (1-methylimidazole), 1.4 g/kg (2-methylimidazole), 5 g/kg (isonicotinic acid), and 1.6 g/kg (5-aminoisophthalic acid) [12]. The results indicate that their toxicity is acceptable for biomedical applications.

In an in vivo toxicity test, around 220 mg/kg of MIL-100 and 78 mg/kg of trimesic acid were intravenously injected to rats. The results demonstrated that animal behavior and weight evaluation didn't have any difference between the injected and noninjected ones. So this system is acceptable for drug delivery systems [13].

Considering that most in vivo toxicity tests are mostly investigated in animal physiological state which is almost different from human physiological conditions, more detailed and precise tests in human biological environments are needed. The second group used as linkers are endogenous organic linkers, that is, molecules are constitutive ingredient of body composition. It's mentioned that this group is the most appropriate route for MOF drug delivery because the organic linkers might be reused in the body. This ability could significantly reduce adverse effects. Amino acids MOFs, [Cu(L- or D-glutamic) (H<sub>2</sub>O)]·H<sub>2</sub>O, nucleobases-based 3D

permanently porous MOFs,  $[\text{Zn}_8(\text{adenine})_4(\text{biphenyldicarboxylate})_6\text{O}\cdot 2\text{Me}_2\text{NH}_2]\cdot 8\text{DMF}11\cdot\text{H}_2\text{O}$  (bio-MOF-1) with a BET surface area up to  $1700\text{ m}^2/\text{g}$ , symmetrical cyclic oligosaccharide,  $\alpha$ -cyclodextrin ( $\alpha$ -CD) were employed as a ligand to synthesize two MOFs,  $[(\alpha\text{-CD})(\text{KOH})_2]$  and  $[(\alpha\text{-CD})(\text{RbOH})_2]$  [14].

### 14.2.2 Stability and biodegradability

About the pharmacokinetic of drug delivery systems, a balanced stability and instability (biodegradability) is indeed an important matter. This system should be stable and could efficiently distribute in body and deliver the drug to the targeted site [15]. After targeted delivery, an adequate biodegradability is needed in order to interact well with biological environments and be ejected from the body [16]. Depending on the crystalline structure, composition, particle size, formulation, and external circumstances, the degradation of MOFs can be modified over some days to several weeks [17]. The stabilities of some MOFs have been researched, such as, MIL-100(Cr), MIL-101(Cr), MIL-53(Cr), and Zeolitic Imidazolate Framework-8 (ZIF-8). It should be mentioned that the gathered information are mostly achieved from simulated physiological condition and information about real pharmacokinetic features of these systems are still unknown.

Stability study on MIL-100(Cr), a 3D mesoporous structure, made up of trimeric metal octahedron and 1,3,5-tricarboxybenzene (BTC), demonstrated that this hybrid can degrade after three days in simulated body fluid. MIL-101(Cr) consisting of the identical Cr, trimeric, and terephthalic acid, with a zeotype cubic structure, degraded after 7 days in simulated body fluid (SBF) at  $37^\circ\text{C}$  [18].

A 3D framework constructed from terephthalate (BDC) and trans-chains of Cr octahedron called MIL-53(Cr) degraded after 21 days in SBF [19]. ZIF-8, hybrid composed of  $\text{ZnN}_4$  tetrahedra linked with imidazolate anions, was tested in two different mediums; PBS (phosphate buffered saline, pH 7.4) and acetate buffer (pH is at 5.0, simulated similar to tumor tissue). The results demonstrated degradation after seven days in PBS and degradation after a few minutes in acetate buffer at  $37^\circ\text{C}$ . This significant difference between these two media is related to the boosted protonation of imidazolate linker in acetate buffer which could subsequently lead to the reduction of the complexing power of the linker toward the metals [20].

By controlling the mentioned features (composition, crystalline structure, and external circumstance) and having a brief look at the results demonstrated from each tests and different metals and organic linkers, we can absolutely alter and tune our structures in order to synthesize controllable-degradable hybrids. The main problem is that in vivo information in human body liquid is very little, so further investigations are still needed.

### 14.3 MOFs: Structures and methods of synthesis

Generation of new ideas in pharmaceutical applications is not as hard as transforming it into reality. This transformation needs methods which are called synthesis [21]. In generating ideas, you are free to think and write based on scientific information, but in synthesis there are always unexpected problems. For instance, there are different administration routes such as oral, transdermal, intravenous, etc., but the route which is widely used for biopharmaceutical is IV injection. So we should obey the rules for this route. Firstly, it should have the appropriate particle size to circulate within the smallest capillaries without any aggregation. Particle size should be smaller than 200 nm, so scale down process is needed in order to make nanoscale MOFs [11]. And secondly, preparing homogeneous and stable nanoscale MOFs which could circulate smoothly through vessels is significant. It should be mentioned that scaling down to nanoscale MOFs gave some advantages to us such as: controllable sizes and shapes, tunable surface to volume ratios, and easy surface modifications. These features are used and discussed in following sections [12]. Talking about synthesis of MOFs, four different methods have been used including solvothermal method, reverse microemulsion, ultrasonic synthesis, and microwave irradiation.

**Solvothermal method:** this conventional route is related to several parameters, such as the reaction time, temperature, pressure, stoichiometry, pH, and concentration. By adjusting these parameters, we can alter the kinetic of the reaction or control the rate of nucleation-growth process. Moreover, with the use of blocking agents (acetic acid, hydroxybenzoic acid, pyridine ...), we can effectively gain controllable sized and shaped particle. For instance, the flexible porous iron(III)dicarboxylates MIL-88A (150 nm) [22], MIL-88B\_4CH<sub>3</sub> (40 nm) [22], or the porous zinc terephthalate MOF-5 (100–200 nm) [23] are topical examples obtained by decreasing reaction time or temperature. Furthermore, pyridine was proposed as an inhibitor in the solvothermal synthesis of porous indium terephthalate particles [24].

**Reverse microemulsion:** this route lets us control the nucleation and the growth rate of the nanoscale MOFs. Based on the metal, organic linker, and micelles of cationic cetyltrimethylammonium bromide surfactant (CTAB) in an isooctane/1-hexanol/water mixture, nanometric nonporous Mn-based polycarboxylates MOFs with imaging ability were synthesized [25]. Use of mentioned solutions due to their high toxicity makes it hard to be used in pharmaceutical applications. In another research, Gadolinium BDC nanorods were prepared by stirring a transparent microemulsion of GdCl<sub>3</sub> and [NMeH<sub>3</sub>]<sub>2</sub>[BDC] in the cationic cetyltrimethylammonium bromide (CTAB)/isooctane/1-hexanol/water system for 2 h. The nanorods had different morphologies related to the different  $w$  values ( $w$  = the water/surfactant molar ratio). Under the condition of  $w = 5$ , the obtained nanorods are 100–125 nm in length and 40 nm in diameter, while increasing  $w$  value to 10, nanorods are 1–2  $\mu$ m in length and 100 nm in diameter [26].

Ultrasonic synthesis: this method is a nonharsh, rapid, and high yielding method with low cost and many nanoscale MOFs have been synthesized by this method [27]. The mechanism is acoustic cavitation associated to a collapse of bubbles due to ultrasonic irradiation with localized hot spots and a very large gradient of temperature/pressure and a rapid mobility of the molecules. This could form high energy microreactors which could lead to the rapid crystallization of MOFs. Nanocrystals of microporous MOF,  $Zn_3(BTC)_2 \cdot 12H_2O$ , were synthesized by this method in different duration times. With reaction times of 5 and 10 min, a size range of 50–100 nm nanoparticles and with increasing the reaction time to 30 min, nanocrystals with diameters of 100–200 nm were achieved. Furthermore, increasing the reaction time to 90 min, the diameter of nanocrystals increased to 700–900 nm [28]. In another research, microcrystals of a microporous flexible iron(III) terephthalate MIL-53 and a rigid copper trimesate were successfully prepared. In the end, it should be mentioned that this method is able to control the dimensionality of nanoscale MOFs with tunable size and shape by varying the reaction time [29].

Microwave irradiation: this method has a lot of advantages including rapid crystallization period, adjustable morphology control, and phase selectivity with process parameter evaluation. The mechanism of action is related to high dielectric absorption of polar solvents which could lead to a highly efficient thermal conversion of the energy to local superheated spots, favoring a fast and homogeneous nucleation over the crystal growth process [30]. The zinc terephthalate IRMOF-1, 2, and 3 [31], mesoporous chromium terephthalate MIL-101 [32], flexible microporous iron terephthalate MIL-53 [13], mesoporous iron trimesate MIL-100 [13], iron amino terephthalate MIL-101-NH<sub>2</sub> [13], and the iron fumarate MIL-88A [22] are all synthesized by this method.

#### **14.4 Surface modification of MOFs for delivery purposes**

Designing compatible nanoscale delivery systems like MOFs with human body is always a tough challenge. Always, scientists talk about great potentials of nano-delivery systems like targeted delivery, convenient intracellular and transcellular movement, etc. But to achieve all of these demands, we need good circulation of these systems through human's vascular system. In other words, we have to increase their half-life. So we need a strategy to improve water dispersity, reduce plasma protein binding, bypass reticuloendothelial system, increase the affinity to the targeted tissues and cells, and control the degradation of these systems which could allow us to have delayed-release of therapeutic molecules. In nanoscale MOF delivery system, this strategy is called surface modification [33]. Two main methods have been used to modify this systems surface: silica encapsulation and coating with organic polymers. Other surface functionalization approaches need to be explored to further optimize the in vivo performance of many NMOFs.

Silica encapsulation: this system has some advantages including biocompatibility, increased water dispersibility, and easy functionalization with silyl-derived molecules. Furthermore, this system is mostly used to modify inorganic and polymer nanoparticles. Before silica coating, NMOFs should firstly be coated by hydrophilic polymers such as poly vinyl pyrrolidone to keep them well-dispersed and ignore aggregation in order to have individual particle silica coating. A manganese-based nanoscale MOF which was used for magnetic resonance imaging had a short half-life in water and PBS (3.5 h in water and 18 min in PBS buffer). To delay its degradation, silica-coated Mn nanoscale MOF was prepared by base-catalyzed condensation of tetraethyl ortho silicate on polyvinylpyrrolidone-modified particles of the solid in ethanol. The half-life was successfully increased to 7.5 h in water and 1.44 h in PBS buffer [25].

In another research, iron-BDC MIL-101 was coated with silica and was compared to the uncoated ones: the silica-coated particles had stability of around 14 h in PBS, while the uncoated ones could readily decompose ( $t_{1/2}$  is about 1.2 h). Furthermore, MOF nanoparticles made of a cisplatin derivative and  $Tb^{3+}$  ions with a shell of silica of around 7 nm were synthesized. Its stability and controlled drug release were improved due to controlling thickness of the shell [34].

Organic polymer coating: this method is another way to increase biocompatibility and decrease framework decomposition. The polymers must have an end group which can bind to the NMOF through either vacant metal coordination sites, electrostatic attraction to the particle surface, or covalent attachment to the bridging ligand. These coaters can be added either during the synthesis or postsynthetically. Most polymers used in this method are called hydrophilic stealth polymers such as poly ethylene glycol (PEG) which could efficiently reduce opsonization by blood proteins and uptake by macrophages of the mononuclear phagocyte system [35].

### **14.5 MOFs in pharmaceutical technology**

As previously mentioned, MOFs are built up from nontoxic metals with low toxic organic linkers such as carboxylic or phosphonic acid [9]. Along with their amazing hybrid structure, there are some advantages related to their structure which makes it possible to be used in pharmaceutical and biomedical applications. These advantages include: (1) Use of none or low toxic molecules which makes it easy for the body to handle it. (2) Most of them are biodegradable to some degree especially in aqueous medium. (3) The internal environment made up of hydrophobic-hydrophilic characteristics let us load different therapeutic molecules with different capacities and physicochemical features. (4) The most important feature is that they are highly versatile and different improvement changes can be done on its structure such as changing pore size, boosting drug load, increasing flexibility and interconnectivity, etc. As it was mentioned, in order to use it in body environment, scaling down



to nanostructure is needed [36]. This process is important which could prevent aggregation in body's tight capillaries. We are going to call this nanostructures as nanoscaled MOFs or NMOFs. This class of NMOFs is also advantageous like MOFs including features such as different compositions, shapes, sizes, and chemical properties. They are also biodegradable as a result of labile metal organic bonds which are important for a nanocarrier after targeted drug delivery. With the acknowledgement of all of this amazing features, we are going to summarize some of the recent advances in NMOFs and their targeted and controlled drug delivery.

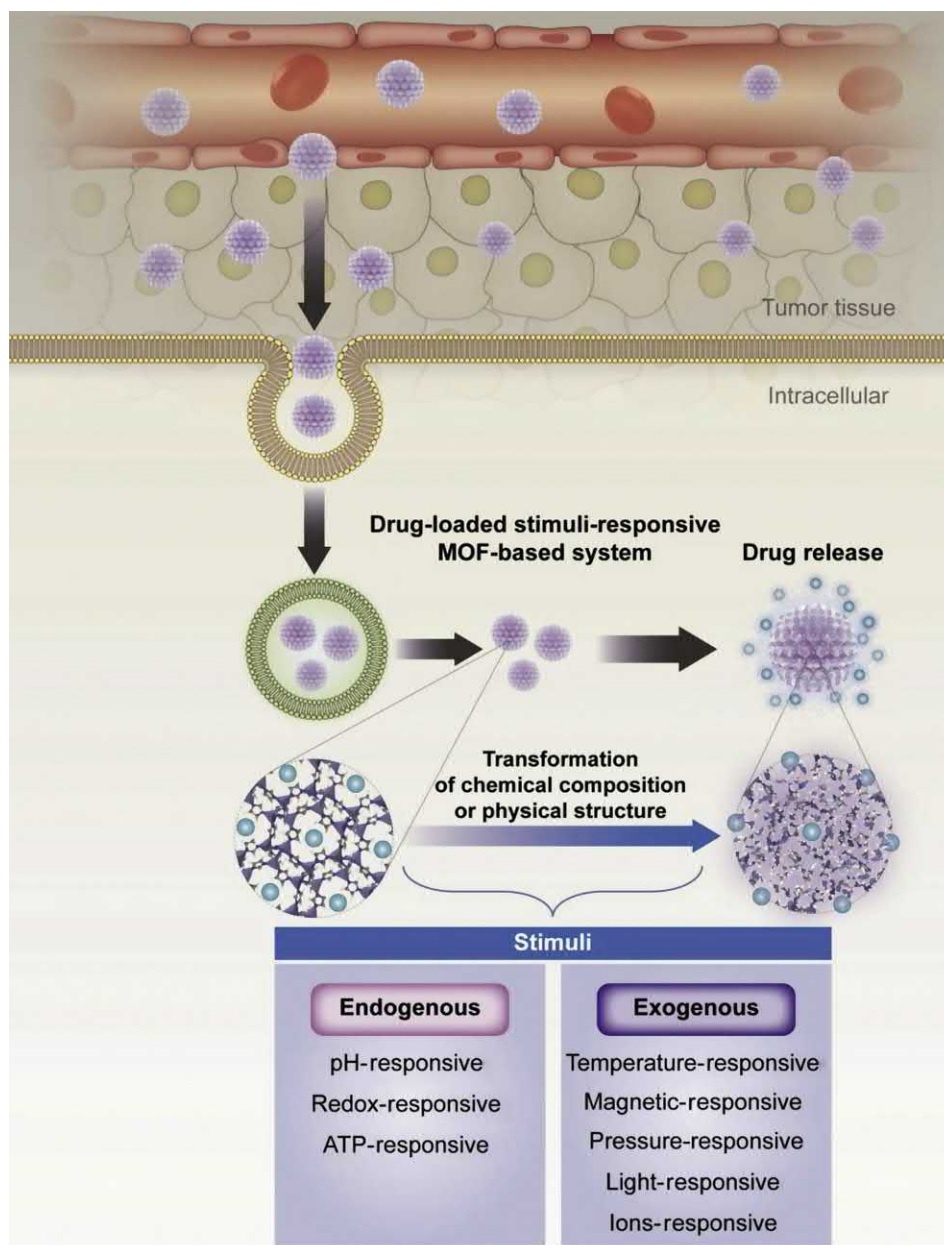
#### **14.5.1 Stimuli-responsive MOFs for drug delivery**

Different pathways have been used to deliver drugs to specific areas of body. Stimuli-responsive pathway is one of the most widely used methods for recent drug delivery systems [37]. Stimuli include many different categories such as pH, magnetic field, ions, temperature, light, and pressure. Between these categories, pH-responsive drug delivery systems are widely used due to the acidic microenvironment of tumors and the high sensitivity of coordination bonds to external pH. Furthermore, these systems can be single stimulus or multiple-stimulus-responsive. NMOFs were no different from other drug delivery systems and used to deliver drugs via stimuli-responsive pathway (Fig. 14.1).

##### **14.5.1.1 pH-sensitive MOFs**

In a recent research, in situ encapsulation of DOX with 1,1'-(1,4-butanediyl) bis (imidazole) (bbi) solution was performed and the surface was coated with silica to prevent rapid decomposition [38]. Furthermore, folic acid was conjugated on the surface of the system to specify the delivery system. The results demonstrated pH-dependent release behavior and good anticancer efficacy. In another research, pH-responsive ZIF-8 was negatively charged and encapsulated with camptothecin (CPT) [39]. The mechanism of drug delivery was driven by the dissociation of the ZIF-8 framework at the acidic target. CPT-ZIF-8 demonstrated increased cell death compared with free CPT-treated cells.

In a novel research, pH-sensitive delivery was used to examine in vitro oral drug delivery. PCN-221 MOF which was prepared from 5,10,15,20-tetrakis (4-carboxyphenyl) porphyrin (TCPP) and  $ZrCl_4$  was conjugated with anticancer drug methotrexate (MTX) and was examined in PBS solution which had a pH varying from 2 to 7.4 [40]. This PBS solution is very similar to the gastrointestinal pH of human body. The results exhibited that about 40% of MTX was released at pH = 2.0 (around the pH of stomach), whereas 100% of MTX was released at pH = 7.4 (close to the intestinal pH) after three days. In a study, CRISPR/Cas9 was conjugated with an engineered single guide RNA and then was encapsulated on zeolitic imidazole framework [41]. This system was further tested and the results revealed knocking down the gene expression of green fluorescent protein by 37% after 4 days. The targeted



**Fig. 14.1**

A general schematic on how a stimuli-dependent metal organic framework is designed and delivered. Reproduced with permission from W. Cai, et al., *Metal-organic framework-based stimuli-responsive systems for drug delivery*, *Adv. Sci.* 6(1) (2019) 1801526.

delivery was due to the sensitivity of ZIF to acidic pH, which resists its structure in other pHs. Furthermore, the designed system overcame the delivery problem due to large protein size and highly charged RNA component.

#### 14.5.1.2 Ion-responsive MOFs

In this method, everything happens via strong electrostatic interactions between the drugs and the frameworks which control the diffusion and release of drugs. Furthermore, after targeted delivery, the ionic exchange happens and the drug will be released in the targeted site. In a recent research, an anionic MOF called bioMOF-1 was explored to test its capability to store, deliver, and release procainamide HCl, a cationic antiarrhythmic drug [42]. The results exhibited adequate drug release in a simulated PBS with pH of 7.4.

In another research, a cationic drug carrier, MOF-74-Fe(III), was conjugated with ibuprofen (an anionic drug) [43]. Because of the special preparation process, the MOF had the ability to be loaded with two distinctive ibuprofen anions. Therefore, two different delivery methods were observed in the simulated PBS solution. At first, sodium ibuprofen and the other coordinated free anions were released because of diffusion or ion exchange between the drug-encapsulated MOF and PBS solution. After that, the further release was triggered by phosphate anions through competitive adsorption.

In a novel research, an NMOF system built up of indium, tris (para-carboxylphenyl) phosphine oxide, and 5-fluorouracil was designed and synthesized [44]. In this system,  $Zn^{2+}$  was used as the competitive binding agent. After conducting several tests in PBS solution with different  $Zn^{2+}$  concentrations, the results revealed that approximately 65% of the 5-FU was released when the  $Zn^{2+}$  concentration was  $500 \times 10^{-9}$  m, with more 5-FU released as the  $Zn^{2+}$  concentration increased. Furthermore, the interaction between 5-FU and in-based MOF was weakened by increasing the temperature.

#### 14.5.1.3 Other stimuli-responsive MOFs

There are some MOFs which have abilities to deliver drugs in temperature and pressure stimuli-response. Switchable UiO-66-PNIPAM nanocarrier conjugated with Resorufin, caffeine, and procainamide [45] and another system [46] consisting ZJU-64 and ZJU-64-CH3 conjugated with methotrexate demonstrated massive drug release due to a slight temperature changes at the physiological temperature of 37 °C. Other systems such as Zr-based MOF built from (2E,2E')-3,3'-(2-fluoro-1,4-phenylene) diacrylic acid (F-H2PDA) and zirconium cluster conjugated with diclofenac were used to prolong the release of the drug in body due to the different pressure of different parts of the body [47].

Humidity was also used as a stimuli for drug delivery. Three novel systems, called HKUST-1 (Cu) (organic linker: 1,3,5-benzene tricarboxylic acid), MOF-74(Zn) (organic linker: 2,5 dihydroxyterephthalate), and RPM6-Zn (linking ligand: biphenyl-4,4'-dicarboxylate; pillar

ligand: 4,4'-azobispyridine), were used for this purpose [48]. After designing the system, an antimicrobial molecule called allyl isothiocyanate (AITC) was loaded into this carrier. After conducting several tests, the results demonstrated that this system is humidity-dependent and, by increasing the humidity, percentage of the drug release increases. Furthermore, the researchers declared that this system can be used for food safety and food industry applications due to AITC excellent antimicrobial characteristics against a broad spectrum of foodborne pathogens and food spoilage-inducing microorganisms.

Reducing agents such as glutathione (GSH) were also a conflict of interest for targeted drug delivery. Cancers' physiological condition has proved that there's a higher concentration of GSH in cancer cells than any other cells. The disulfide bond (S-S), a redox-responsive group that can be cleaved in the presence of GSH, was an attractive group to design an MOF system. The backbone of the system was built up of manganese with dithiodiglycolic acid as the disulfide (SS)-containing organic linker [49]. Then DOX was loaded to the system and was coated with polydopamine. Furthermore, it was modified with PEG in order to achieve spherical structure. After conducting several tests at different pH values, the results revealed that DOX release was quite dramatically accelerated in the presence of GSH. Moreover, protonating the amino group of DOX accelerated drug release at lower pH values.

Insulin and glucose were also investigated to design an MOF system [50]. In this system, Glucose oxidase (GOx) and insulin were efficiently loaded into ZIF-8 in order to design a glucose concentration-dependent MOF system. After conducting several tests at different glucose concentrations, the results revealed that, at 4 mg/mL glucose,  $\approx 420 \mu\text{g/mL}$  of insulin was released in 4 h; however, at either no or 1 mg/mL glucose, only 84 and 145  $\mu\text{g/mL}$  were released in 24 h, respectively. Furthermore, the mechanism of action was mentioned that, at high glucose concentration, GOx produces gluconic acid and  $\text{H}_2\text{O}_2$  from glucose which lowers the pH inside the composite. This event leads to decomposition and thus insulin release.

#### 14.5.1.4 Multiple-stimuli-responsive MOFs

Until now, all of the mentioned drug delivery systems were related to only one stimuli. But our purpose is to deliver drugs to specific targets in human body. So, as it was mentioned humans' body environment is more complex than what we think and there are many unknown objects about it. So, we can use multiple stimuli-responsive MOFs in order to have more control on our delivery system and also overcome unknown obstacles in our delivery pathway.

For warm up, we are going to start with pillararenes. Pillararenes, newly developed supramolecular hosts, proved their ability for host-guest delivery systems due to their special features such as special structure, facile functionalization, and desirable host-guest performance [51].

Multiple-stimuli-responsive drug delivery system (DDS) made up of MOFs and pillararene-based supramolecular nanovalves was synthesized and tested [51]. UMCM-1-NH<sub>2</sub> was used as

the host material and carboxylatopillar [5] arene (CP5) was used as a dual stimuli-responsive gatekeeper which was linked by positively charged pyridinium (Py) stalks (CP5-capped UMCM-1-NH-Py). After testing this system, the result demonstrated that it is dependent on two stimuli: pH and competitive binding. In acidic pH of tumor, the non-covalent binding interaction between cp5 and the stalk weakens, which could lead to unblock the MOF and the drug release occurs. Moreover, adding competitive agents such as methylviologen salts would lead to a desirable drug delivery due to the detachment between cp5 and pyridinium.

Another cp5-mof-based system called CP5-capped UiO-66-NH<sub>2</sub> 5-Fu nanocarrier was synthesized and tested [52]. Before examination, this system was modified by positively charged quaternary ammonium salt as stalks (Q) to thread the negatively charged CP5 rings, to form [2] pseudorotaxanes as stimuli-responsive supramolecular gates which regulate drug release. The results demonstrated that this system was dependent on two stimuli: Zn<sup>2+</sup> which could be a competitive agent and increased temperature which could lead to weakening the interaction between CP5 and stalk.

Another novel system in this category was CP5-gated Zr-MOFs hybrid [53]. This system was also modified by positively charged quaternary ammonium salt stalks. The mechanism of action was due to three reasons: pH, increased temperature, and competitive binding agents. The special thing about this system was that it could be used in bone marrow tumors because of the acidic pH and higher concentration of Ca<sup>2+</sup> in osteoclasts. Furthermore, high temperature could kill tumor cells. So, this triple stimuli-responsive platform can be essential and useful in bone marrow cancers.

Let's switch to another supramolecular macrocycle called  $\beta$ -cyclodextrin ( $\beta$ -CD). This macrocycle has proved its ability for multiple stimuli-responsive platforms in recent investigations.

For instance, a multifunctional MOF platform, from encapsulating DOX, MIL-101-N<sub>3</sub> (Fe), and coating with  $\beta$ -CD derivative ( $\beta$ -CD-SS-BCN), was synthesized [54]. Furthermore, targeted peptide functionalized polymer, Lys (adamantane)-Arg-Gly-Asp-Ser-bi-poly (ethylene glycol) (PEG) 1900 (bi = benzoic imine bond, K(ad)RGDS-PEG1900), was added to the surface of the nanocarrier. This platform was mentioned to work through two mechanisms due to the presence of a benzoic imine bond in K(ad)RGDS-PEG1900 and disulfide bonds linking  $\beta$ -CD on the MOF: pH sensitivity and redox sensitivity. The experiments indicated that tumor cell uptake was increased, toxicity of DOX was decreased, and in overall, the efficacy was increased.

In another experiment in this category, a supramolecular complex consisting of  $\beta$ -CD on the surface of UiO-68-azobenzene was synthesized and tested [55]. Azobenzenes are photosensitive and their isomeration can change between cis and trans. So this light sensitivity

can be used to regulate drug (rhodamine B) delivery. Furthermore, competitive agents such as amantadine could also trigger the dissociation of the gatekeeper from the azobenzene stalks due to its higher binding affinity toward  $\beta$ -CD.

### 14.5.2 MOFs for the induction of antibacterial activities

Bacteria, which are the most important microorganisms that human community had to deal with, have emerged lots of subtypes and subgroups. These subtypes can have good effect like lactobacillus [56], can coexist with human body parts like staphylococci [57], or maybe dangerous for humans like pseudomonas aeruginosa [58]. Through a long time, designing new drugs like beta lactams, cephalosporin, etc. allowed us to control the growth and also the damage of many dangerous subtypes. According to the latest reports, there are several new resistant subtypes which have drawn attention of many scientists [59]. Several attempts have been made to design new bio/nanomaterial-based delivery systems in order to control the growth of some subtypes. NMOFs also revealed its ability against bacteria in several experiments.

A MOF system called Ag@ZIF-8 nanowire with different thickness revealed its antibacterial activity against *Bacillus subtilis* and *Escherichia coli* BL21 [60]. Another MOF system called copper metal organic framework-cotton was strategically fabricated to introduce free amine to tune the physicochemical properties of the material [61]. In this system, MOF  $\text{Cu}_3(\text{NH}_2\text{BTC})_2$  was fabricated between carboxymethyl fiber in order to have a modified copper release. The results demonstrated that this cotton had a massive antibacterial activity against *Escherichia coli* under wet or dry condition. These results allow us to have ideal cottons for clothing, bandages, and other textile applications which limit the growth of bacteria and barely kill most of them [62].

In a recent research, a composite by coating magnesium-mediated metal organic framework (Mg-MOF74) and strontium substituted hydroxyl apatite on the surface of titanium was constructed [63]. This composite was used for local injury treatment with complication like osteosarcoma or bacterial infection. After conducting several tests, the results proved that this system can efficiently kill surrounding *Staphylococcus aureus*, *Escherichia coli*, and Saos-2 cells. The mechanistic study revealed that the superficial Mg-MOF7 rapidly degrades at bacteria or osteosarcoma induces acidic environment and kills the mentioned bacteria. Then the strontium-substituted hydroxyl apatite promoted the proliferation and osteogenic differentiation of osteoblasts.

A MOF system was built in order to improve the obstacles and difficulties of long-term antibacterial therapy like multiple injections for several weeks. This system was constructed from conjugating ceftazidime to ZIF-8 with the purpose of having sustained release over a long period of time [64]. After conducting several tests against *Escherichia coli*, the results



indicated effective antibacterial activity due to the sustained drug release up to a week. Furthermore, this system proved its relevant compatibility with macrophage and lung epithelial cell lines, which allows us to have pulmonary and intracellular infection drug delivery and treatment.

### **14.5.3 Targeted contrast agent delivery via NMOFs**

#### *14.5.3.1 Magnetic resonance imaging*

Cells' physiological condition is the most important issue in designing the treatment protocol [65]. Different diseases have different pathophysiological conditions and could have a massive effect on the biopharmaceutical behavior of drugs. Controlling these conditions demands a tool which could let us know what is happening at any time in the cell. Magnetic resonance imaging (MRI) is a noninvasive imaging technology which gives us a 3D detailed image which could let us know what is happening in the targeted part [66]. Like any other imaging technique, there is a need for contrasting agent in order to achieve adequate 3D image. Gadolinium-based molecules are the most widely used contrast agents in MRI, but its most important side effect is nephrogenic systemic fibrosis, especially in patients with severe renal impairment [67]. By using NMOF system, we can control this fatal side effect and also alter the efficacy of the image by the targeted delivery.

In a recent research, a gadolinium-porphyrin-based NMOF with a spherical structure and good water solubility was synthesized and conjugated with folic acid [68]. In order to identify the capability and biopharmaceutical behavior of the system, several tests were conducted in HepG2 cells, embryonic, and larval zebrafish. The results demonstrated low biotoxicity, excellent magnetic resonance imaging capability, and high tumor eliminating ability.

Regarding gadoliniums' fatal side effect, several other metals were also used as core magnets for MRI. Mn was one of those chosen ones which proved its magnetic ability. In a recent novel research, a NMOF system built up of Zr<sup>4+</sup> and Mn-porphyrin bridging ligand was prepared and then was conjugated with s-nitrosothiol on the surface of the system [69]. Several tests were conducted on a tumor-bearing mouse via an intravenous injection and the results demonstrated acceptable MRI activity, controllable NO release, and synergist photothermal therapy under single near-infrared irradiation. Other than Mn-based NMOF, Fe-based and Au-based NMOFs have also been explored as potential MRI contrast agents.

In a novel recent research, a Fe-based NMOF with bovine serum albumin, sulfonamide, and porphyrin was constructed and tested [70]. Due to the presence of sulfonamide, the NMOF system could actively target the carbonic anhydrase IX of the tumor cells. Furthermore, this system proved its ability in PDT, PTT, and MRI and the results demonstrated that this system can target tumors with hypoxia condition and also increase the fatality rate in 4T1 cancer cell by inducing PTT and PDT together.

In another novel research, a special NMOF system was designed to specifically target triple negative breast cancer (TNBC) which is a fatal and life-threatening cancer [71]. In this system, a TNBC-targeted peptide called ZD2 was engineered and conjugated with a gold nanostar (AuNS) and MIL-101-NH<sub>2</sub> (Fe). After conducting several tests, the results demonstrated good biocompatibility, efficient MRI activity, and stable photothermal ability. Furthermore, this system proved that it could specifically target TNBC cell (MDA-MB-23), but not the other subtype (MDA-MB-435, MDA-MB-468 and MCF-7), which could lead to visualize breast cancer with molecular classification.

#### 14.5.3.2 PDT and PTT therapeutic methods

Along with many applied therapeutic methods for different diseases, there is a need for new routes to overcome the deficiency of those methods [72]. Photodynamic therapy (PDT) and photo thermal therapy (PTT) may be the two new routes for new diseases such as cancer, even though they have been used in several different diseases.

##### PDT

PDT is a new method mainly used for cancer theranostic nowadays. The mechanism of action is due to the activation of photosensitizers by a specific wavelength and generation of ROS system by the activated PS [73]. So, we assume there are three factors for PDT: photosensitizers (PS), light, and tissue O<sub>2</sub> concentration. These three variable factors are in some ways related together. Targeted delivery of PS, depth, wavelength, and extinction coefficient of the irradiated light and the content of oxygen in the tissue in order to activate the ROS system are the important subfactors. Putting these factors together and looking at the mentioned features of NMOF's, it may be concluded that they are the appropriate systems to be synthesized and tested.

At first, porphyrins, which have been used for PDT in different classes under different brand names, were tested. 5,15-di(*p*-benzoato)-porphyrin (H2DBP) was conjugated with Hf<sup>4+</sup> in an NMOF system and was compared with H2DBP alone [74, 75]. The results demonstrated high PS loading, overcoming the aggregation issue, enhanced PDT efficacy, and no dark toxicity in the conjugated system [75]. Another porphyrin class called TCPP (5,10,15,20-tetrakis(4-carboxylphenyl)-porphyrin) was conjugated with Hf<sup>4+</sup> and pegylated in order to overcome low water solubility [76]. After identifying biopharmaceutical features of this system, an in vivo test was exhibited in 4T1 tumor-bearing mice via intravenous injection. The results demonstrated that this system can partially suppress tumor growth via intravenous injection.

The main problem of the H2DBP class was the lowest wavelength absorption of 634 nm, which is near the high energy edge of the tissue-penetrating window (600–900 nm). So, they switched to chlorine-based photosensitizers to modify the absorption at a higher wavelength. 5,15-Di(*p*-benzoato)chlorin (H2DBC) was synthesized and conjugated with Hf<sup>4+</sup> in an

NMOF system [77]. The results demonstrated better ROS generation, induced cellular apoptosis, increased PDT efficacy, and induced immunogenic cell death.

In another novel research, researchers concentrated on the immunogenic cell death caused by chlorine-based NMOF's [78], deficiency of PDT in metastatic cancer therapy, and overexpression of antitumor suppressing molecules such as indoleamine 2,3-dioxygenase (IDO). They synthesized a system built up from 5,10,15,20-tetra (*p*-benzoato) chlorin (H4TBC),  $\text{Hf}^{4+}$ , and an IDO inhibitor (IDOi@TBC-Hf) [79]. This system and TBC-Hf (without IDO inhibitor) were tested for in vivo efficacy and abscopal effect in two colorectal mouse models, CT26 and MC38. The results demonstrated that both systems can reduce primary tumor growth via PDT, but the IDOi@TBC-Hf system could efficiently reduce the sizes of the distant tumors while the other system had a very little effect on it. The mechanistic study suggested that uptake of the antigens from destroyed primary tumor cells and presenting them to specific tumor suppressor T cell plus the IDO inhibitors could systemically activate the immune system against metastatic tumor cell (Fig. 14.2).

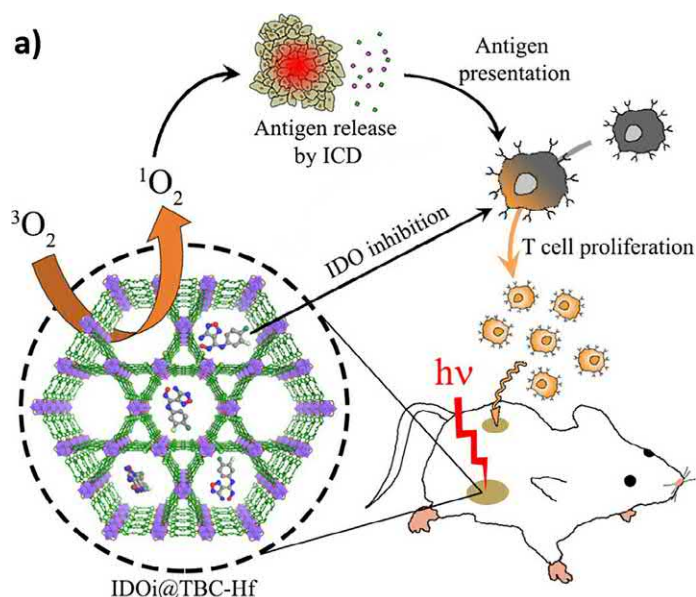


Fig. 14.2

A novel chlorine-based MOF delivery system, which was made up of 5,10,15,20-tetra (*p*-benzoato) chlorin (H4TBC),  $\text{Hf}^{4+}$ , and an IDO inhibitor (IDOi@TBC-Hf), was tested in two colorectal mouse models called CT26 and MC38. The results demonstrated higher abscopal and metastatic inhibitory effect in IDOi@TBC-Hf than TBC-Hf without IDOi. Indoleamine 2,3-dioxygenase (IDO) is an antitumor suppressing molecule that is secreted by tumor cells. So, by inhibiting IDO, tumor suppressing T cells could systemically be activated against metastatic tumor cells. *Reproduced with permission from K. Lu, et al., Chlorin-based nanoscale metal–organic framework systemically rejects colorectal cancers via synergistic photodynamic therapy and checkpoint blockade immunotherapy, J. Am. Chem. Soc. 138(38) (2016) 12502–12510.*

## PTT

Besides all mentioned advantages of PDT, there are also some disadvantages including: (1) Generating ROS system: it's a good ability for PDT, but the reactive oxygen could also harm noncancer cells and increase the side effects. (2) Dependency on tissue oxygen content: hypoxia state is dominant in cancer cells and may cause resistance among PDT. Considering the disadvantages of PDT, another alternative of PDT gained a massive attention in recent years called Photo thermal therapy (PTT). Different from PDT, PTT is oxygen-independent and ROS-free [80]. Mechanistically, it can rise the temperature of the targeted site above 40 degrees and kill targeted cells. Also, it can hyper-sensitize them to chemotherapy and radiotherapy. As for the cancer treatment protocol and the importance of combination therapy, it seems like PTT is a better choice due to its mechanism of action.

In a research, an NMOF system made up of Pd nanocubes, Au nanosheets, ZIF-8, and Doxorubicin (DOX) was designed and synthesized [81]. Pd nanocubes were considered as seeds and Au nanosheets covered them to help the photothermal converting ability of the system. Furthermore, DOX was attached to the system by an acid-sensitive framework, ZIF-8. After an *in vitro* experiment, the results demonstrated enhanced efficacy due to the combined PTT-chemotherapy treatment and also lower toxicity for the combined system than each of them alone.

In another research, a nanocomposite called MCM@PEG-CO-DOX was synthesized and tested [82]. In this system, carbon monoxide was used for combined gas therapy, chemotherapy, and photothermal therapy next to other materials used such as Doxorubicin, pegylated Fe(III)-based nanoMOFs (MIL-100), and modified Mn carbonyl. The results demonstrated efficient antitumor activity and tumor dual-model imaging capability including magnetic resonance imaging (MRI) and photoacoustic imaging (PAI).

In a recent research, a molecularly organic/inorganic hybridized nanocomposite called HMONs-PMOF was synthesized and tested [83]. This system was built upon hollow mesoporous organosilica nanoparticles (HMON) merged with MOF and polydopamine interlayer. After designing the backbone, doxorubicin was loaded to the interior cavity of HMON, while indocyanine green was loaded to the outer porous shell of MOF. Conducting *in vitro* cell experiments demonstrated several different mechanisms of action: (1) Photothermal activity which could lead to lysosomal rupture and facilitating lysosomal escape in order to facilitate doxorubicin diffusion to the cytoplasm. (2) Magnetic resonance and photoacoustic dual-model imaging accomplished by iron ion coordinated on PDA and ICG confined in MOF. (3) Chemotherapeutic effect of doxorubicin. All three mentioned mechanisms had a synergistic effect next to each other and enhanced the antitumor activity of the system.

#### 14.5.3.3 X-ray computed tomography (CT) scan

Different imaging methods provide altered quality images for various purposes. The importance of adequate images in order to achieve exact diagnosis and treatment is undeniable. One of the powerful tools in this matter is X-ray computed tomography scan. In this method, the physician can see anything and everything in your body without cutting it or doing any harmful activity to your body [84]. The device rotates around the body and takes different 2D images which are called slices from each angle. Then the computer takes these different slices and creates cross-sectional pictures. Like other imaging methods, we also need contrast agent to perform all the mentioned procedures. Mostly used contrast agents in this method are iodinated aromatic molecules and barium sulfate. The problem is that they are very small and have rapid clearance which could lead to higher dose administration and higher side effects. That's where we include NMOFs in order to improve bio-distribution and pharmacokinetic features of contrast agents.

In a research, an NMOF system was constructed from iodine-boron-dipyrromethene (BODIPY) and was named UIO-PDT [85]. Several *in vitro* and *in vivo* tests were conducted and the results demonstrated that this system has no obvious severe, acute, or subacute toxicity even at a very high injected dose. Furthermore, the results in rats-bearing hematoma suggested that most of the injected UIO-PDT was accumulated at the tumor site, which gave the best imaging performance after an IV injection for about 24 h.

In another research, gold-based NMOFs were also studied for this matter. In this study, gold nanorod-incorporated nMOF called Au@MIL-88 was synthesized [86]. Low toxicity, high penetration depth, high spatial resolution, and high contrast ability made this system favorable to be tested. The results revealed that, beside the ability for usage in CT scan, this system can also be used in MRI and photoacoustic imaging. Furthermore, this system was modified with poly (ethylene glycol)-carboxyl acid (PEG-COOH) in order to protect MOFs from aggregation during *in vivo* tests and demonstrated high resolution in human glioma models.

In a recent research, a new bismuth NMOF called bismuth-NU-901 was synthesized and tested [87]. This system is made up of eight connected Bi<sub>6</sub> nodes and tetratopic 1, 3, 5, 8-(*p*-benzoate) pyrene linkers. After conducting several *in vitro* tests, the results demonstrated that this new NMOF system has 7 times better contrast intensity than zirconium-based MOFs with same topology 14 times better contrast intensity than commercially available CT contrast agents. With a brief look at the results, bismuth-based MOFs may be the appropriate alternative for commercial CT contrast agent.

#### 14.5.3.4 PET

Cells' different features are related to each other and little change in some parts can make a massive change in other parts. Metabolism is one of the most important tasks in cell which is related to different conditions of the cell. Being healthy or being infected etc. changes

the path of the cells' metabolism. In order to figure out which path is active, we look at the metabolites. In order to specifically identify certain metabolites, there are several different means. Positron-emitting tomography (PET) is a nuclear imaging method which works with positron-emitting radio nucleotides [88]. These radio nucleotides accumulate at the targeted site and generate gamma ray photons. These photons can be captured by sensitive detector panels and the computer makes a 3D image.

In a recent research, an  $^{89}\text{Zr}$ -containing NMOF was designed by attaching Zr to UiO-66 NMOFs and functionalizing it with pyrene-derived PEG. Furthermore, it was conjugated with a peptide ligand called (KDEPQRRSARLSAKPAPPKPEPKPKKAPAKK, F3) in order to have tumor-targeted delivery [89]. After conducting an in vivo test via intravenous injection, this nanoparticle was traced by PET, 2 h after the injection. The results demonstrated that untargeted nanoparticles have lower tumor accumulation than targeted ones. Furthermore, significant uptake by liver and spleen was also observed which needs further investigation. Nonetheless, with a brief look at the results, it seems like Zr-containing NMOFs would be a better choice for the long-term imaging due to its longer half-life than other routine methods used in PET.

#### 14.5.3.5 Optical imaging

Though imaging-guided diagnosis and treatment has been in a lot of attention in bio/Nano medicine therapy, how to specifically deliver the contrast agent to the desired tissue or organ is still a hot topic for researchers to resolve [90]. One of the strongest tools in imaging issue that has proved its ability in recent years is optical imaging [91]. In this method, the device detects the ballistic or diffusive photons in the targeted part and uses the light illumination to design the image of that part [92]. All of these mentioned happenings need to have the contrast agent at the targeted site which could lead us to use NMOF delivery system to achieve it.

In a research, indocyanin green (ICG), an FDA-approved organic dye for clinical applications, was conjugated with metal organic framework called MILL-100 (Fe) and hyaluronic acid in order to increase ICG's water solubility, targeted delivery, and specifically enhance its cancer theranostic sensitivity [93]. After conducting several tests, the results revealed that greater cellular uptake by CD 44-positive MCF-7 occurred, higher tumor accumulations in xenograft tumor were observed, and its ability for image-guided drug delivery and PTT and this system could efficiently inhibit the growth of MCF-7/xenograft tumor cells.

In another study, a novel NMOF system built of Fe-MOF and Eu-MOF was built and tested [94]. In this heterostructure, the spherical Fe-MOF was introduced as the large surface matrix for the growth of rod like Eu-MOF. After designing and synthesizing it, the researchers



announced that this system exhibits excellent magnetic resonance/optical imaging capacity and satisfactory drug delivery behavior.

In a novel recent study, an NMOF system called Fe-MIL-53-NH<sub>2</sub> was used to encapsulate an anticancer drug 5-fluorouracil (5-FU), a fluorescence imaging agent 5-carboxyfluorescein and folic acid [95]. After conducting several tests, the results demonstrated good biocompatibility, strong inhibitory effect on cancer cells, and outstanding magnetic resonance imaging and optical imaging capability. As we can see, the researchers did many tasks only by using one multifunctional nanoplatform. This NMOF system may empower the researchers to design better NMOF platforms with the purpose of aiming new possibilities.

### **14.6 Future perspective**

With the growing interest in the use of NMOF delivery systems and the development of diseases which need new treatment routes, there is still room for many novel NMOF-based delivery systems to be used against these diseases [96].

Alzheimer's is one of the most challenging diseases which human community has been dealing with for many years. In this disease, the main problem is the aggregation of peptides called amyloid beta. This aggregation causes neurotoxicity, and after a while, when many other neurons get involved, Alzheimer's appears. So, an NMOF system called PCN-224 which was constructed from tetra-kis (4-carboxyphenyl) porphyrin (TCPP) and zirconium was used to control amyloid beta's aggregation [97]. After conducting several tests, the results demonstrated the ability of the system to prevent self-assembly aggregation of these peptides and also reduce their toxicity under near-infrared radiation (Fig. 14.3).

Parkinson disease is also one of the most advanced diseases which needs new delivery and treatment routes. In this disease, the dopamine-releasing neurons are damaged at substantia nigra region in the brain, which could lead to Parkinson disease. Conventional routes prefer to use L-3,4-dihydroxyphenylalanine (L-dopa), a carboxylate precursor of dopamine. Although this route has been useful for many years, the side effects like the dysregulation syndrome and the pharmacokinetic problems like competitive absorption forced scientist to design another treatment protocol. In a study, dopamine was loaded into a Fe-based MOF system called MIL-88A and was tested in PC12 cells as the neural cell model. The results proved that this system can be used as long-term delivery tool, protects dopamine from oxidative damage, and enhances targeted delivery [98].

Among many approved administration routes, oral administration is the most widely used route. Several attempts have been made to enhance the ease, absorption, and unwanted happenings like drug decomposition. For instance, acidic pH of the stomach that catalyzes and damages the structure of many drugs, decomposition of the drug before reaching the absorption site, and also the structural damage of drug to the digestive system are all example of



Fig. 14.3

Schematic presentation of the inhibitory effect of porphyrinic metal organic framework called PCN-224 on the aggregation of amyloid beta peptides. The study demonstrates that, via a near-infrared radiation and the high photo-oxygenation efficiency of the nanoparticle, PCN-224 nanoprobe activated by NIR light could successfully inhibit self-assembly of amyloid beta peptides.

Furthermore, the activated nanoprobe could efficiently decrease the amyloid beta-induced cytotoxicity. *Reproduced with permission from J. Wang, et al., Porphyrinic metal–organic framework PCN-224 nanoparticles for near-infrared-induced attenuation of aggregation and neurotoxicity of alzheimer’s amyloid-β peptide, ACS Appl. Mater. Interfaces 10(43) (2018) 36615–36621.*

why we need controlled delivery in oral administration. So, in a study, a copper-based metal organic framework was conjugated with ibuprofen and then was protected with a pH-sensitive biopolymer called carboxymethylcellulose in order to enhance the oral delivery system [99]. The drug release test showed that this system had better protection against stomach’s acidic pH which could help us to have controlled release in the gastrointestinal tract condition. Furthermore, MTT tests revealed that this system has low toxicity against Caco-2 cells (represent the epithelial colorectal cells). With a brief look at the reported results, it seems like this system could have a bright future for controlled oral delivery system.

## References

- [1] R.B. Ramesha Chary, et al., In vitro and in vivo adhesion testing of mucoadhesive drug delivery systems, *Drug Dev. Ind. Pharm.* 25 (5) (1999) 685–690.
- [2] B.B. Spear, M. Heath-Chiozzi, J. Huff, Clinical application of pharmacogenetics, *Trends Mol. Med.* 7 (5) (2001) 201–204.
- [3] H. Kazemzadeh, M. Mozafari, Fullerene-based delivery systems, *Drug Discov. Today* 24 (3) (2019) 898–905.
- [4] D. Peer, et al., Nanocarriers as an emerging platform for cancer therapy, *Nat. Nanotechnol.* 2 (12) (2007) 751.
- [5] M. Rahmati, M. Mozafari, Protein adsorption on polymers, *Mater. Today Commun.* 17 (2018) 527–540.
- [6] M. Manzano, M. Colilla, M. Vallet-Regí, Drug delivery from ordered mesoporous matrices, *Expert Opin. Drug Del.* 6 (12) (2009) 1383–1400.

- [7] H. Nabipour, et al., Mefenamic acid-layered zinc hydroxide nanohybrids: a new platform to elaborate drug delivery systems, *J. Inorg. Organomet. Polym. Mater.* (2018) 1–11.
- [8] M.R. Mohammadi, et al., Nanomaterials engineering for drug delivery: a hybridization approach, *J. Mater. Chem. B* 5 (22) (2017) 3995–4018.
- [9] R.C. Huxford, J. Della Rocca, W. Lin, Metal–organic frameworks as potential drug carriers, *Curr. Opin. Chem. Biol.* 14 (2) (2010) 262–268.
- [10] M. Rahmati, M. Mozafari, Biological response to carbon-family nanomaterials: interactions at the nano-bio interface. *Front. Bioeng. Biotechnol.* 7 (2019) 4, <https://doi.org/10.3389/fbioe.2019.00004>.
- [11] P. Horcajada, et al., Metal–organic frameworks in biomedicine, *Chem. Rev.* 112 (2) (2011) 1232–1268.
- [12] C.-Y. Sun, et al., Metal–organic frameworks as potential drug delivery systems, *Expert Opin. Drug Del.* 10 (1) (2013) 89–101.
- [13] P. Horcajada, et al., Porous metal–organic-framework nanoscale carriers as a potential platform for drug delivery and imaging, *Nat. Mater.* 9 (2) (2010) 172.
- [14] R.A. Smaldone, et al., Metal–organic frameworks from edible natural products, *Angew. Chem. Int. Ed.* 49 (46) (2010) 8630–8634.
- [15] M. Mozafari, A. Organs, The critical impact of controlled drug delivery in the future of tissue engineering, *Trends Biomater. Artif. Organs* 28 (3) (2014) 124–126.
- [16] M. Rahmati, M. Mozafari, Biocompatibility of alumina-based biomaterials—a review, *J. Cell. Physiol.* 234 (4) (2019) 3321–3335.
- [17] S. Kargozar, M. Mozafari, Nanotechnology and nanomedicine: start small, think big, *Mater. Today Proc.* 5 (7) (2018) 15492–15500.
- [18] P. Horcajada, et al., Metal–organic frameworks as efficient materials for drug delivery, *Angew. Chem. Int. Ed.* 118 (36) (2006) 6120–6124.
- [19] P. Horcajada, et al., Flexible porous metal-organic frameworks for a controlled drug delivery, *J. Am. Chem. Soc.* 130 (21) (2008) 6774–6780.
- [20] C.-Y. Sun, et al., Zeolitic imidazolate framework-8 as efficient pH-sensitive drug delivery vehicle, *Dalton Trans.* 41 (23) (2012) 6906–6909.
- [21] I. Amjadi, et al., Synthesis and characterization of doxorubicin-loaded poly (lactide-co-glycolide) nanoparticles as a sustained-release anticancer drug delivery system, *Appl. Biochem. Biotechnol.* 168 (6) (2012) 1434–1447.
- [22] T. Chalati, et al., Optimisation of the synthesis of MOF nanoparticles made of flexible porous iron fumarate MIL-88A, *J. Mater. Chem. B* 21 (7) (2011) 2220–2227.
- [23] S. Hermes, et al., Trapping metal-organic framework nanocrystals: an in-situ time-resolved light scattering study on the crystal growth of MOF-5 in solution, *J. Am. Chem. Soc.* 129 (17) (2007) 5324–5325.
- [24] W. Cho, H.J. Lee, M. Oh, Growth-controlled formation of porous coordination polymer particles, *J. Am. Chem. Soc.* 130 (50) (2008) 16943–16946.
- [25] K.M. Taylor, W.J. Rieter, W. Lin, Manganese-based nanoscale metal–organic frameworks for magnetic resonance imaging, *J. Am. Chem. Soc.* 130 (44) (2008) 14358–14359.
- [26] W.J. Rieter, et al., Nanoscale metal–organic frameworks as potential multimodal contrast enhancing agents, *J. Am. Chem. Soc.* 128 (28) (2006) 9024–9025.
- [27] G. Sargazi, et al., A systematic study on the use of ultrasound energy for the synthesis of nickel–metal organic framework compounds, *Ultrason. Sonochem.* 27 (2015) 395–402.
- [28] L.-G. Qiu, et al., Facile synthesis of nanocrystals of a microporous metal–organic framework by an ultrasonic method and selective sensing of organoamines, *Chem. Commun.* 31 (2008) 3642–3644.
- [29] E. Haque, et al., Synthesis of a metal–organic framework material, iron terephthalate, by ultrasound, microwave, and conventional electric heating: a kinetic study, *Chem. Eur. J.* 16 (3) (2010) 1046–1052.
- [30] G.A. Tompsett, et al., Microwave synthesis of nanoporous materials, *ChemPhysChem* 7 (2) (2006) 296–319.
- [31] Z. Ni, R.I. Masel, Rapid production of metal–organic frameworks via microwave-assisted solvothermal synthesis, *J. Am. Chem. Soc.* 128 (38) (2006) 12394–12395.

- [32] A. Demessence, et al., Elaboration and properties of hierarchically structured optical thin films of MIL-101 (Cr), *Nat. Mater.* 46 (2009) 7149–7151.
- [33] N. Jalali, et al., Surface modification of poly (lactide-co-glycolide) nanoparticles by d- $\alpha$ -tocopheryl polyethylene glycol 1000 succinate as potential carrier for the delivery of drugs to the brain, *Colloids Surf. A* 392 (1) (2011) 335–342.
- [34] K.M. Taylor-Pashow, et al., Postsynthetic modifications of iron-carboxylate nanoscale metal–organic frameworks for imaging and drug delivery, *J. Am. Chem. Soc.* 131 (40) (2009) 14261–14263.
- [35] R. Gref, et al., The controlled intravenous delivery of drugs using PEG-coated sterically stabilized nanospheres, *Adv. Drug Deliv. Rev.* 16 (2–3) (1995) 215–233.
- [36] M. Giménez-Marqués, et al., Nanostructured metal–organic frameworks and their bio-related applications, *Coord. Chem. Rev.* 307 (2016) 342–360.
- [37] P. Zarrintaj, et al., Poloxamer-based stimuli-responsive biomaterials, *Mater. Today Proc.* 5 (7) (2018) 15516–15523.
- [38] P.F. Gao, et al., A new type of pH-responsive coordination polymer sphere as a vehicle for targeted anticancer drug delivery and sustained release, *J. Mater. Chem. B* 1 (25) (2013) 3202–3208.
- [39] J. Zhuang, et al., Optimized metal–organic-framework nanospheres for drug delivery: evaluation of small-molecule encapsulation, *ACS Nano* 8 (3) (2014) 2812–2819.
- [40] W. Lin, et al., A porphyrin-based metal–organic framework as a pH-responsive drug carrier, *J. Solid State Chem.* 237 (2016) 307–312.
- [41] S.K. Alsaiani, et al., Endosomal escape and delivery of CRISPR/Cas9 genome editing machinery enabled by nanoscale zeolitic imidazolate framework, *J. Am. Chem. Soc.* 140 (1) (2017) 143–146.
- [42] J. An, S.J. Geib, N.L. Rosi, Cation-triggered drug release from a porous zinc–adeninate metal–organic framework, *J. Am. Chem. Soc.* 131 (24) (2009) 8376–8377.
- [43] Q. Hu, et al., A low cytotoxic cationic metal–organic framework carrier for controllable drug release, *J. Med. Chem.* 57 (13) (2014) 5679–5685.
- [44] X. Du, et al., Controlled Zn<sup>2+</sup>-triggered drug release by preferred coordination of open active sites within functionalization indium metal organic frameworks, *ACS Appl. Mater. Interfaces* 9 (34) (2017) 28939–28948.
- [45] S. Nagata, K. Kokado, K.J.C.C. Sada, Metal–organic framework tethering PNIPAM for ON–OFF controlled release in solution, *Chem. Commun.* 51 (41) (2015) 8614–8617.
- [46] W. Lin, et al., Low cytotoxic metal–organic frameworks as temperature-responsive drug carriers, *ChemPlusChem* 81 (8) (2016) 804–810.
- [47] K. Jiang, et al., Pressure controlled drug release in a Zr-cluster-based MOF, *J. Mater. Chem. B* 4 (39) (2016) 6398–6401.
- [48] E. Lashkari, et al., Innovative application of metal-organic frameworks for encapsulation and controlled release of allyl isothiocyanate, *Food Chem.* 221 (2017) 926–935.
- [49] J. Zhao, et al., Redox-sensitive nanoscale coordination polymers for drug delivery and cancer theranostics, *ACS Appl. Mater. Interfaces* 9 (28) (2017) 23555–23563.
- [50] Y. Duan, et al., One-pot synthesis of a metal–organic framework-based drug carrier for intelligent glucose-responsive insulin delivery, *Chem. Commun.* 54 (42) (2018) 5377–5380.
- [51] L.-L. Tan, et al., Stimuli-responsive metal–organic frameworks gated by pillar [5] arene supramolecular switches, *Chem. Sci.* 6 (3) (2015) 1640–1644.
- [52] L.L. Tan, et al., Zn<sup>2+</sup>-triggered drug release from biocompatible zirconium MOFs equipped with supramolecular gates, *Small* 11 (31) (2015) 3807–3813.
- [53] L.-L. Tan, et al., Ca<sup>2+</sup>, pH and thermo triple-responsive mechanized Zr-based MOFs for on-command drug release in bone diseases, *J. Mater. Chem. B* 4 (1) (2016) 135–140.
- [54] X.-G. Wang, et al., A multifunctional metal–organic framework based tumor targeting drug delivery system for cancer therapy, *Nanoscale* 7 (38) (2015) 16061–16070.
- [55] X. Meng, et al., Mechanized azobenzene-functionalized zirconium metal-organic framework for on-command cargo release, *Sci. Adv.* 2 (8) (2016) e1600480.
- [56] F. Nagao, et al., Effects of a fermented milk drink containing *Lactobacillus casei* strain Shirota on the immune system in healthy human subjects, *Biosci. Biotechnol. Biochem.* 64 (12) (2000) 2706–2708.

- [57] J.D. Lambris, D. Ricklin, B.V. Geisbrecht, Complement evasion by human pathogens, *Nat. Rev. Microbiol.* 6 (2) (2008) 132.
- [58] H. Budzikiewicz, Siderophores of the human pathogenic fluorescent pseudomonads, *Curr. Top. Med. Chem.* 1 (1) (2001) 1–6.
- [59] R. Zhou, et al., Occurrence of human pathogenic bacteria carrying antibiotic resistance genes revealed by metagenomic approach: a case study from an aquatic environment, *J. Environ. Sci.* 80 (2019) 248–256.
- [60] Y.-F. Guo, et al., Facile synthesis of Ag@ ZIF-8 core-shell heterostructure nanowires for improved antibacterial activities, *Appl. Surf. Sci.* 435 (2018) 149–155.
- [61] H.N. Rubin, et al., Surface-anchored metal–organic framework–cotton material for tunable antibacterial copper delivery, *ACS Appl. Mater. Interfaces* 10 (17) (2018) 15189–15199.
- [62] M.J.M.T. Mozafari, Nanotechnology in wound care: one step closer to the clinic, *Mol. Ther.* 26 (9) (2018) 2085–2086.
- [63] Y. Zhang, et al., Composite coatings of Mg-MOF74 and Sr-substituted hydroxyapatite on titanium substrates for local antibacterial, anti-osteosarcoma and pro-osteogenesis applications, *Mater. Lett.* 241 (2019) 18–22.
- [64] D.G. Sava, et al., Antibacterial countermeasures via MOF-supported sustained therapeutic release, *ACS Appl. Mater. Interfaces* 11 (8) (2019) 7782–7791.
- [65] E.T. Morgan, et al., Physiological regulation of drug metabolism and transport: pregnancy, microbiome, inflammation, infection, and fasting, *Drug Metab. Dispos.* 46 (5) (2018) 503–513.
- [66] P. Caravan, Protein-targeted gadolinium-based magnetic resonance imaging (MRI) contrast agents: design and mechanism of action, *Acc. Chem. Res.* 42 (7) (2009) 851–862.
- [67] P.H. Kuo, et al., Gadolinium-based MR contrast agents and nephrogenic systemic fibrosis, *Radiology* 242 (3) (2007) 647–649.
- [68] Y. Chen, et al., Folic acid-nanoscale gadolinium-porphyrin metal-organic frameworks: fluorescence and magnetic resonance dual-modality imaging and photodynamic therapy in hepatocellular carcinoma, *Int. J. Nanomedicine* 14 (2019) 57.
- [69] H. Zhang, et al., Theranostic Mn-porphyrin metal–organic frameworks for magnetic resonance imaging-guided nitric oxide and photothermal synergistic therapy, *ACS Appl. Mater. Interfaces* 10 (34) (2018) 28390–28398.
- [70] W. Zhu, et al., Albumin/sulfonamide stabilized iron porphyrin metal organic framework nanocomposites: targeting tumor hypoxia by carbonic anhydrase IX inhibition and T1–T2 dual mode MRI guided photodynamic/photothermal therapy, *J. Mater. Chem. B* 6 (2) (2018) 265–276.
- [71] L. Zhang, et al., ZD2-engineered gold nanostar@ metal-organic framework nanoprobe for T1-weighted magnetic resonance imaging and photothermal therapy specifically toward triple-negative breast cancer, *Adv. Healthc. Mater.* 7 (24) (2018) 1801144.
- [72] M. Miola, et al., Glass-ceramics for cancer treatment: so close, or yet so far? *Acta Biomater.* 83 (2019) 55–70.
- [73] T.J. Dougherty, et al., Photodynamic therapy, *J. Natl. Cancer Inst.* 90 (12) (1998) 889–905.
- [74] R. Dai, et al., Electron crystallography reveals atomic structures of metal–organic nanoplates with M12 ( $\mu$ 3-O) 8 ( $\mu$ 3-OH) 8 ( $\mu$ 2-OH) 6 (M = Zr, Hf) secondary building units, *Inorg. Chem.* 56 (14) (2017) 8128–8134.
- [75] K. Lu, C. He, W. Lin, Nanoscale metal–organic framework for highly effective photodynamic therapy of resistant head and neck cancer, *J. Am. Chem. Soc.* 136 (48) (2014) 16712–16715.
- [76] J. Liu, et al., Nanoscale metal–organic frameworks for combined photodynamic & radiation therapy in cancer treatment, *Biomaterials* 97 (2016) 1–9.
- [77] K. Lu, C. He, W. Lin, A chlorin-based nanoscale metal–organic framework for photodynamic therapy of colon cancers, *J. Am. Chem. Soc.* 137 (24) (2015) 7600–7603.
- [78] M. Rahmati, M. Mozafari, Nano-immunoengineering: opportunities and challenges, *Curr. Opin. Biom. Eng.* 10 (2019) 51–59.
- [79] K. Lu, et al., Chlorin-based nanoscale metal–organic framework systemically rejects colorectal cancers via synergistic photodynamic therapy and checkpoint blockade immunotherapy, *J. Am. Chem. Soc.* 138 (38) (2016) 12502–12510.
- [80] J.R. Melamed, R.S. Edelman, E.S. Day, Elucidating the fundamental mechanisms of cell death triggered by photothermal therapy, *ACS Nano* 9 (1) (2015) 6–11.

- [81] X. Yang, et al., A metal–organic framework based nanocomposite with co-encapsulation of Pd@ Au nanoparticles and doxorubicin for pH-and NIR-triggered synergistic chemo-photothermal treatment of cancer cells, *J. Mater. Chem. B* 5 (24) (2017) 4648–4659.
- [82] J. Yao, et al., On-demand CO release for amplification of chemotherapy by MOF functionalized magnetic carbon nanoparticles with NIR irradiation, *Biomaterials* 195 (2019) 51–62.
- [83] L. Chen, et al., Merging metal organic framework with hollow organosilica nanoparticles as a versatile nanoplatform for cancer theranostics, *Acta Biomater.* 86 (2019) 406–415.
- [84] K. Lu, et al., Nanoscale metal–organic frameworks for therapeutic, imaging, and sensing applications, *Adv. Mater.* 30 (37) (2018) 1707634.
- [85] T. Zhang, et al., BODIPY-containing nanoscale metal–organic frameworks as contrast agents for computed tomography, *J. Mater. Chem. B* 5 (12) (2017) 2330–2336.
- [86] W. Shang, et al., Core–shell gold Nanorod@ metal–organic framework nanoprobe for multimodality diagnosis of glioma, *Adv. Mater.* 29 (3) (2017) 1604381.
- [87] L. Robison, et al., A bismuth metal–organic framework as a contrast agent for X-ray computed tomography, *ACS Appl. Biomater.* 2 (3) (2019) 1197–1203.
- [88] S.S.J.N.R.C. Gambhir, Molecular imaging of cancer with positron emission tomography, *Nat. Rev. Cancer* 2 (9) (2002) 683.
- [89] D. Chen, et al., In vivo targeting and positron emission tomography imaging of tumor with intrinsically radioactive metal–organic frameworks nanomaterials, *ACS Nano* 11 (4) (2017) 4315–4327.
- [90] M. Mozafari, et al., Self-assembly of PbS hollow sphere quantum dots via gas–bubble technique for early cancer diagnosis, *J. Luminesc.* 133 (2013) 188–193.
- [91] M. Mozafari, F.J.M. Moztafzadeh, N. Letters, Microstructural and optical properties of spherical lead sulphide quantum dots-based optical sensors, *Micro Nano Lett.* 6 (3) (2011) 161–164.
- [92] J.C. Hebden, et al., Optical imaging in medicine: I. Experimental techniques, *Phys. Med. Biol.* 42 (5) (1997) 825.
- [93] W. Cai, et al., Engineering phototheranostic nanoscale metal–organic frameworks for multimodal imaging-guided cancer therapy, *ACS Appl. Mater. Interfaces* 9 (3) (2017) 2040–2051.
- [94] X. Gao, et al., In situ growth of metal–organic frameworks (MOFs) on the surface of other MOFs: a new strategy for constructing magnetic resonance/optical dual mode imaging materials, *Dalton Trans.* 46 (40) (2017) 13686–13689.
- [95] X. Gao, et al., Controllable synthesis of a smart multifunctional nanoscale metal–organic framework for magnetic resonance/optical imaging and targeted drug delivery, *ACS Appl. Mater. Interfaces* 9 (4) (2017) 3455–3462.
- [96] A.M. Urbanska, S. Ponnazhagan, M. Mozafari, Pathology, chemoprevention, and preclinical models for target validation in barrett esophagus, *Cancer Res.* 78 (14) (2018) 3747–3754.
- [97] J. Wang, et al., Porphyrinic metal–organic framework PCN-224 nanoparticles for near-infrared-induced attenuation of aggregation and neurotoxicity of alzheimer’s amyloid- $\beta$  peptide, *ACS Appl. Mater. Interfaces* 10 (43) (2018) 36615–36621.
- [98] A. Pinna, et al., A MOF-based carrier for in situ dopamine delivery, *RSC Adv.* 8 (45) (2018) 25664–25672.
- [99] S. Javanbakht, et al., Carboxymethylcellulose capsulated Cu-based metal-organic framework-drug nanohybrid as a pH-sensitive nanocomposite for ibuprofen oral delivery, *Int. J. Biol. Macromol.* 119 (2018) 588–596.

## Further reading

- W. Cai, et al., Metal–organic framework-based stimuli-responsive systems for drug delivery, *Adv. Sci.* 6 (1) (2019) 1801526.



# BioMOFs

Hafezeh Nabipour<sup>a</sup>, Masoud Mozafari<sup>b</sup>, Yuan Hu<sup>a</sup>

<sup>a</sup>State Key Laboratory of Fire Science, University of Science and Technology of China, Hefei, PR China

<sup>b</sup>Department of Tissue Engineering & Regenerative Medicine, Faculty of Advanced Technologies in Medicine, Iran University of Medical Sciences (IUMS), Tehran, Iran

## 15.1 Introduction of biomolecules

Evidently, the cell is the fundamental building block of the living systems. These cells or units of life encompass multiple information bioactive molecules. Although there is no certain information on the first formation of the cells, a huge deal of evidence suggests various chemical and physical procedures on the earth or the atmosphere which can guide us to knowledge about simple molecules with cellular status. Upon their entrance into an interacting network, biomolecules got involved in more complex groups and structures. Ultimately, biomolecules expressed themselves in the form of life by giving rise to a robust and organized unit. Living cells comprise various biomolecules including nucleic acids (DNA and RNA), lipids (fats) and carbohydrates, amino acids, proteins, enzymes, fatty acids, nucleotides, nucleic acids, histones, acidic proteins, chlorophyll, and hemoglobin. It is impossible to determine which one of these biomolecules is alive, as none of them can independently express life. As the most primitive manifestation of life, viruses encompass two major biomolecules: protein and RNA or DNA.

## 15.2 Meaning of biomolecules

Biomolecules have been considered as the basis of a living cell. Some of them (i.e., amino acids, nucleotides, and monosaccharides) are the constituents of the more complex ones. The role of biomolecules such as proteins, carbohydrates and fats, enzymes, vitamins, hormones, and nucleic acids is of crucial importance. Some of these biomolecules are in the form of polymers, among which starch, proteins, and nucleic acids can be mentioned which can be considered as the chains of simple sugars, amino acids, and nucleotides, respectively. The structure of the majority of biomolecules is large and highly complicated, making their

reactions mechanisms more sophisticated. Biomolecules' association to the living organisms can be expressed by following sequence:

*Living Cells* → *Organs* → *Tissues* → *Cells* → *Organelles*  
→ *Biomolecules* (*Carbohydrates, proteins, fats, and nucleic acid*)

### 15.3 Types of biomolecules

Among the various types of biomolecules, the nucleotides are of crucial significance as they are the building blocks of DNA and RNA (biomolecules involved in heredity). Lipids are also involved in the formation of biological membranes as well as energy provision. Hormones are another class of biomolecules which are responsible for regulating the metabolism and a myriad of other procedures in living organisms. Carbohydrates also play a key role in supply of energy and its storage. Amino acids, the building blocks of proteins, have an undeniable role in living organisms from the protein synthesis to lipid transport. Although the vitamins are not synthesized by organisms, they are important biomolecules with vital function in the health and survival of the organisms.

There exists a vast spectrum of biomolecules:

**Small molecules:** Lipids, phospholipids, sterols, glycerolipids, glycolipids, vitamins, sugars, carbohydrates, metabolites, hormones, neurotransmitters

**Monomers:** Monosaccharides, nucleotides, amino acids

**Polymers:** Hemoglobin, nucleic acids, DNA, RNA, cellulose, lignin, oligosaccharides, polysaccharides (including cellulose), peptides, oligopeptides, polypeptides, proteins

### 15.4 Applications of biomolecules

In addition to their essential impact on life, biomolecules play a decisive role in industrial purposes, in particular, food and pharmaceutical production. These molecules can be employed as natural catalysts, sensors, or oxidative-reductive agents [1]. Most of the industrial operations occur under nonnatural environments (i.e., at the presence of organic solvents, variable temperatures, and pH values or mechanical processing), while most of the biomolecules can be only applied at mild condition. The delicate nature of biomolecules has given rise to their low operational stability, lack of robustness, and difficult recovery which have challenged their applications. In this content, biomolecules' stabilization will retain their function under industrial condition which is an essential prerequisite for their successful application [2, 3].

## 15.5 Incorporation of biomolecules with inorganic materials and metal-organic frameworks

Biomolecules can be incorporated in a protective matrix which could be an interesting approach for enhancing their stability [2–8]. In comparison to their free counterparts, the biomolecule-matrix composites can show a significant enhancement in their thermal, chemical, and even mechanical stability. Such an approach will drastically extend the operational condition of biomolecules and develop new *in vitro* and *in vivo* potential applications. Known as the nature's catalysts, enzymes exhibit excellent reactivity, selectivity, and specificity at mild conditions [9]. Enzymatic catalysts have been intensively studied for chemical, pharmaceutical, and food purposes [10]. The low operational stability, difficult recovery, and nonreusability at operational conditions have, however, limited the enzymes' application in industry [11]. Enzyme can be immobilized on the solid supports (including sol gels hydrogels, organic microparticles, nonporous and porous inorganic supports) which will dramatically improve their stability and facilitate their separation and recovery simultaneous to protecting their activity and selectivity [12]. Regarding the high surface area and tunable and uniform pores of mesoporous silica materials, a huge deal of studies has been devoted to immobilization of enzymes within them [11, 12]. Mesoporous silica materials do not interact with enzyme molecules; hence, the immobilized enzyme may be leached during the procedure declining the system effectiveness during their reuse [6, 11, 12]. Use of functional organic groups for postsynthetic modification of pore walls can result in their interaction with the immobilized enzyme and preventing from enzyme leaching. This strategy will, however, significantly decline the enzyme loading and/or block the channels [6, 12]. An ideal host matrix should have following features: (1) the hierarchical pore sizes whose larger ones place the enzymes, while smaller pores provide a path for the reactants and products to diffuse, (2) enhanced surface area which will guarantee proper enzyme loading, (3) use of interacting functional organic groups to decorate sufficiently large cages which will prevent from enzyme leaching, and (4) a framework which maintains its integrity under the reaction condition. In this regard, development of innovative porous materials for biomolecules incorporation is of crucial importance. Past decade has witnessed the development of a novel class of porous materials known as porous metal-organic frameworks (MOFs) [13–18]. The reason for such a huge deal of interest on this class of materials lies in their astonishingly large surface areas due to their ultra-micro-porosity and their structural and composition flexibility offering a wide range of pore shapes. In fact, MOFs possess the highest porosity among the available. These two major features have introduced MOFs as a promising candidate for various applications, most of which are attributed to their ultra-high porosity (up to 7000 m<sup>2</sup>/g). Today, MOFs are employed in gas storage/separation procedures [19], sensing [20], magnetism [21], catalysis [22], and several biomedical purposes [23]. Recently, biomolecules have been used as one of the components of biological metal-organic frameworks (bioMOFs).

## 15.6 Definition of BioMOFs

BioMOFs have not been clearly defined yet. A literature survey revealed two different insights [24–28]. While some researchers define bioMOFs as composites comprising at least one biomolecule in the form of an organic ligand, others introduced bioMOFs as a class of high porosity MOFs providing platform for biological and medical applications. The first group emphasizes that MOFs should include nature-derived biomimetic units, whereas the latter are concentrated on MOFs' biological applications. The mandatory standards for biological applications are much more serious than industrial uses. In this regard, the toxicology, stability, efficacy, particle size, and morphology of the bioMOFs have to be extensively assessed before their real application. As a field combining porous crystals with biological field, investigation of bioMOFs not only investigates the structural properties and inner porosity of conventional MOFs, but also addresses their chirality, molecular recognition, and biomolecular catalytic function. Regarding its declined toxicity and proper biocompatibility, bioMOF has been proposed for numerous biological applications. Use of biomolecules in construction of bioMOFs can result in several advantages:

- Simple biomolecules (i.e., amino acids, nucleobases, and sugars) are accessible in large quantities and reasonable prices; hence, bulk quantities of bioMOFs are achievable.
- Incorporation of biomolecules can result in formation of biocompatible MOFs.
- Regarding the structural diversity of biomolecules, they can affect the functional nature of the target bioMOFs giving rise to rigid or flexible bioMOFs.
- Considering the various metal-binding sites offered by biomolecules, they offer several coordination modes which can enhance the structural diversity of bioMOFs.
- The intrinsic self-assembly feature of biomolecules can be exploited for tuning the structure and function of bioMOFs.
- Chirality of biomolecules can facilitate the construction of chiral bioMOFs with interesting recognition, separation, and catalytic attributes [29].

Moreover, the high surface area and porosity of MOFs have made them a promising support for the biomolecules' incorporation in biological applications as they provide more loading sites. Furthermore, the substrates and products can pass through open structure of MOFs; hence, an interaction would occur between the guest biomolecules and its surrounding medium. Also, the metal nodes, ligands, and the topological structures of MOFs are of high diversity; so, the geometrical parameters and other features of bioMOFs can be adjusted for a specific application. Uniformly distributed active groups (both in the pores and on the surface of MOFs) can make the interacting sites to prevent or decrease the leaching of biomolecules. Ultimately, the proper crystallinity of MOFs results in a well-defined network with clear structural information. Such information is vital for investigation of MOFs' interaction/mechanisms with the guest molecules [30].

However, bioMOFs have been in wide attention due to their pretty structures' singular biomimetic features and rich supramolecular chemistry.

### 15.7 Design of BioMOFs with biomolecules

So far, several biomolecules have been incorporated in MOFs. Symmetry defect is, however, an obstacle for synthesis of well-ordered crystalline materials. Besides, the flexibility of most of the biomolecules and labile metal-ligand coordination may result in their mutual penetration and undesirable geometry or stoichiometry, giving rise to nonporous frameworks. These drawbacks have hindered the advancements and applications of bioMOFs. Numerous studies have addressed the synthesis of new bioMOFs which introduced several empirical routes to achieve well-functioning bioMOFs: (i) biomolecules@ MOFs via the covalent coupling structure possessing preexisting MOF linkage or the outer surface obtained by the postsynthetic modification or biomolecules encapsulation inside the MOF porosities by diffusing or permeating; (ii) Formation of a cyclic oligomer through tiny biomolecules with low symmetry; (iii) introduction of an auxiliary ligand with high symmetry (i.e., ZnBTCA) to counterpoise the lower symmetry of the bio-ligand [31]; (iv) application of an asymmetrical bio-ligand resulting in the formation of a secondary unit with high symmetry, i.e., bio-MOF-100 [32].

### 15.8 Nucleobases

The term “nucleobase” refers to five natural compounds known as the differentiating component of nucleotides; three of these bases are common to RNA and DNA (uracil replaces thymine in RNA). Depending on their chemical structures, the bases are divided into two groups: purines and pyrimidines. While purines are larger, double-ring molecules (adenine and guanine), pyrimidines refer to bases possessing only a single ring structure (cytosine and thymine/uracil) [33, 34]. More heteroatoms and hydrogen bond donor or acceptor sites in purine nucleobases have introduced them as a suitable candidate to form coordination bond or interact by other species (compared to the pyrimidines) [35]. Many nucleoside analogues have been employed to treat cancer and viral diseases [36]. Besides these promising applications, nucleobases have been proposed as proper ligands to construct the bioMOFs due to having multiple heteroatoms capable of coordinating cations and forming high strength hydrogen bonds. Adenine (ad) is mostly applied for this purpose as it presents five potential interaction sites: the N6 amino group and N1, N3, N7, and N9 imino nitrogen atoms (Fig. 15.1) [37].

Formation of the MOFs generally involves the nucleobase deprotonation and coordination as well as application of auxiliary polycarboxylate ligands. The majority of studies on nucleobasemetal compounds relies on a 1D or 2D structure and nonbiocompatible metallic element (e.g., Co) [38, 39].

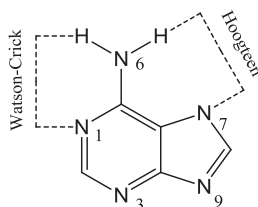


Fig. 15.1

Adenine structure showing the numbering scheme and the Watson-Crick and Hoogsteen faces.

Reproduced with permission from G. Beobide, O. Castillo, J. Cepeda, A. Luque, S. Perez-Yanez, P.

Roman, J. Thomas-Gipson, *Metal-carboxylato-nucleobase systems: from supramolecular assemblies to 3D porous materials*, *Coord. Chem. Rev.* 257 (2013) 2716–2736. Copyright 2013, Elsevier.

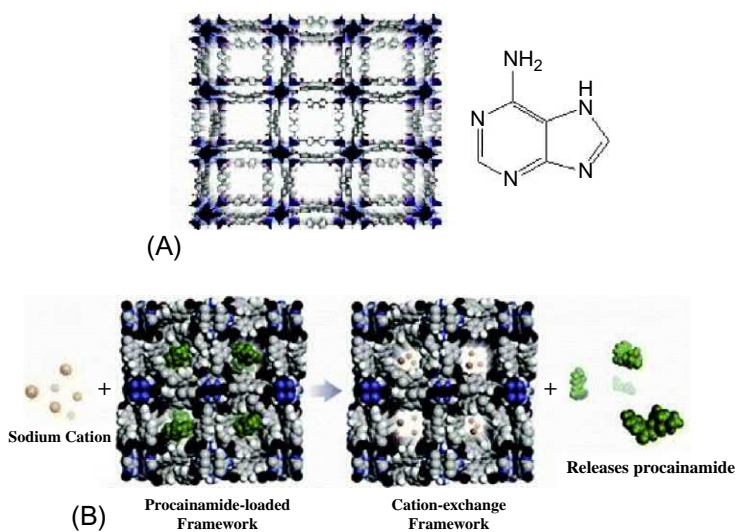


Fig. 15.2

(A) Porous structure of  $[Zn_8(ad)_4(bpdc)_6O \cdot 2Me_2NH_2] \cdot 8DMF \cdot 11H_2O$ ; (B) drug release from bio-MOF-1 through cation exchange. Reproduced with permission from J. An, S.J. Geib, N.L. Rosi, *Cation-triggered drug release from a porous zinc-adeninate metal-organic framework*, *J. Am. Chem. Soc.* 131 (2009)

8376–8377. Copyright 2009, American Chemical Society.

One of the innovative studies on metal-nucleobase synthesis was conducted by Rosi et al.; they entitled their product as “bio-MOFs” [32, 40]. They produced bio-MOF-1 with  $Zn^{2+}$  and adenine (ad), and biphenyldicarboxylate (bpdc) [40].  $[Zn_8(ad)_4(bpdc)_6O \cdot 2Me_2NH_2] \cdot 8DMF \cdot 11H_2O$  (also called bio-MOF-1) was their first three-dimensional permanent porous framework composed of infinite Zn(II)-Ad columns including apex-sharing Zn(II)-Ad octahedral cages. The cages included 8  $Zn^{2+}$  cations surrounded by four Ad ligands through N1, N3, N7, and N9 coordination. According to Fig. 15.2A, the Zn(II)-Ad columns are connected to each other via multiple bpdc linkers, giving rise to large one-dimensional channels which



maintain their stability after elimination of the guest solvent molecules. This sample exhibited the surface area of 1700 m<sup>2</sup>/g for nitrogen adsorption (BET analysis). Owing to its nucleobase content, bio-MOF-1 showed an anionic zeta-potential which could be helpful in drug loading. Encapsulation of a cationic antiarrhythmic drug (procainamide HCl) was achieved through electrostatic interactions which could be easily released via simple cation exchange procedure (Fig. 15.2B).

Lezama et al. developed another porous Ad-derived 3D bioMOF [41]. This framework ([Cu<sub>2</sub>(Ad)<sub>4</sub>(H<sub>2</sub>O)<sub>2</sub>]<sub>2</sub>·[Cu(ox)(H<sub>2</sub>O)]<sub>2</sub>~4H<sub>2</sub>O (where ox is oxalate)) was achieved through paddle-wheel clusters comprising two Cu(II) ions which were bridged by four Ad ligands through N3 and N9 coordination. N7 of each Ad ligand formed a connection to another Cu(II)-ox unit, which is connected to another cluster to lead to a three-dimensional structure. The final structure includes the one-dimensional tube-shaped channels with approximate diameters of 13 Å. The guest waters leave the channels at 95°C with no disturbance to the crystalline structure. A novel adenine-containing bioMOF was introduced by Cai et al. (ZnBTCA (BTC = benzene-1,3,5-tricarboxyl, A = adenine)). In this figure, Zn<sup>II</sup>1 and Zn<sup>II</sup>2 form three bonds with two bidentate carboxyl groups and one adenine (N3 and N9 sites), giving rise to a binuclear-Zn secondary building unit (SBU). This SBU is further expanded along its axial position by connecting 2 monodentate carboxyl groups along the c axis. Further propagation of the mentioned unit could be achieved by coordination with Zn<sup>II</sup>3 which formed the overall framework. One of the distinctive attributes of ZnBTCA is its sinusoidal channels with open Watson-Crick sites which are immobilized on the internal surface in a periodic pattern. These sites provide the conditions required for molecular recognition in host-guest chemistry [31].

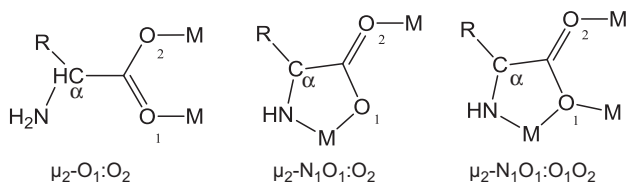
## 15.9 Amino acids

Amino acids (AA) are known with the general formula of H<sub>3</sub>N<sup>+</sup>-(CR<sup>1</sup>R<sup>2</sup>)N-COO<sup>-</sup> in which *n* = 1 and 2 represent α-amino acids and β-amino acids, respectively. Each AA possesses the amino and carboxylic acid groups (H<sub>3</sub>N<sup>+</sup> and -COO<sup>-</sup>, respectively). R also stands for the organic side chain. Amino acids are vital components of life as they are the major constituents of protein and peptide with several undeniably significant biological functions. In terms of coordination, AA possesses two common metal-binding sites: nitrogen of amino and oxygen of carboxylate groups. Some AAs offer other types of metal-binding sites through their side chain residues: for instance, imidazole nitrogen in L-histidine (His) or thiolate and thioether sulfur atom in L-cysteine (Cys) and L-methionine (Met), respectively, as well as β-carboxylic acid groups in aspartic acid (Asp) and glutamic acid (Glu). Basically, amino acids possess an α-carbon. The amino group and α-carboxylic acid groups are bound to this carbon. Metals have tendency toward the typical five-member glycinate (Gly) chelate ring, giving rise to discrete complexes. Extended metal ion-AA frameworks are also achievable through metal ions

coordination by  $\alpha$ -carboxylate groups via bi- or tridentate bridging modes [42]. Amino acids often form metal-AA chelates or discrete polynuclear clusters with prominent biologic actions in nature; i.e., metal ions transport through the blood. Regarding the diverse coordination modes offered by AAs, they can be considered as versatile biomolecules for metal interlinking to bioMOFs.

Incorporation of amino acids in MOFs has gained considerable attention mostly because of the inherent chirality AAs, which may offer enantioselectivity with several possible applications in different processes; i.e., drug enantioselective preparation [43] or release [44]. Presence of a single complexing group (carboxylate) in typical synthesis conditions has made the completely biocompatible 3D AA-based MOFs a rare product as such conditions will lead to 1D or 2D coordination networks [45].

Compared to two or three-dimensional structures, pure AA-based 1D coordination networks are more common. 2D metal ion-AA frameworks were achieved when glycine (Gly) coordinated to metal ions (e.g., Ni(II) [46], Mn(II) [47], and Co(II) [48]) in a 2:1 manner. In such two-dimensional structures, each octahedral metal ion is linked to four other metal ions through glycine ligands with  $\mu_2$ -O<sub>1</sub>:O<sub>2</sub> coordination (Fig. 15.3). Coordination of 2 AA ligands to an octahedral metal ion by typical O,N-chelating mode is another possible connectivity pattern which may result in 2D frameworks. Each AA could also bridge to its neighboring metal ions through its second carboxylate group oxygen ( $\mu_2$ -N<sub>1</sub>O<sub>1</sub>:O<sub>2</sub> coordination mode, Fig. 15.3). Samples with such two-dimensional structures were attained by linking L-phenylamine (Phe) to Mn(II) [49] and Cu(II) [50], L-tryptophan (Trp) to Mn(II) [51], and Ni(II) [52], and L-glutamine (Gln) to Cu(II) [53]. Zhang et al. presented two enantiomeric zeolitic MOFs with zeolite sodalite topology, Ni(L-alanine)<sub>2</sub> and Ni(D-alanine)<sub>2</sub>, on the basis of an enantiopure alanine (Ala) ligand and Ni(II). Each alanine was linked to the Ni(II) ions via the O,N- O,N-chelating mode and the second oxen of its carboxylate groups giving rise to a 3D structure [54]. Despite the scarce reports on three-dimensional metal ion-AA frameworks, some amino acids offer their R side chains for binding metal ions (i.e., the  $\beta$ -carboxylate groups of aspartic and glutamic acids, the imidazole group of histidine, the thiol or thioether groups of cysteine and methionine, respectively, or the phenol ring of tyrosine). Besides offering metal-binding sites, these groups could be employed for bridging the metal ions and even



**Fig. 15.3**

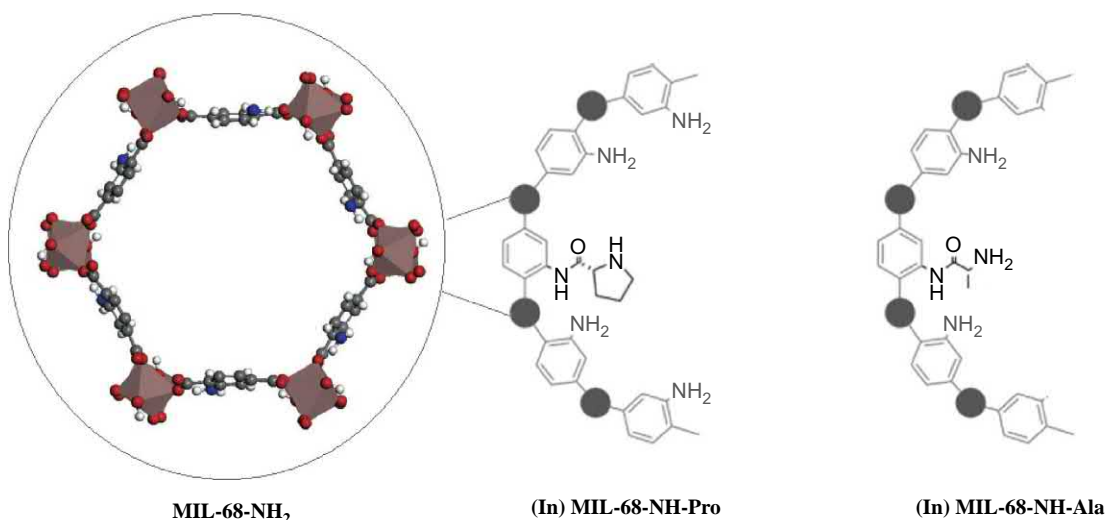
Coordination modes of  $\alpha$ -amino acids, in which NH<sub>2</sub> and COOH represent the amino and carboxylic acid groups, respectively; while R shows the organic side chain.

more enhancement in dimensionality of metal ion-AA networks (Fig. 15.3) [29]. Ma et al. employed the dicarboxylate L-aspartic acid to form a bridge  $Dy_4O_4$  cubane unit. They reported a high porosity framework possessing intersecting channels of ca. 12 Å [55]. A year after, Wang et al. announced the synthesis of a similar structure based on  $[Er_4(\mu_3-OH)_4]^{8+}$  motifs and the dicarboxylate glutamate [56]. Their framework showed approximate parallelogram-shaped pores opening of  $4.4 \times 9.1$  Å. The applicability of the mentioned structure could be only confirmed through biocompatibility assays. Xiao et al. [57] presented two new three-dimensional chiral MOFs possessing chiral amino acid ligands containing *n*-fold interwoven helices composed of the mixed ligands 1,3,5-benzenetricarboxylic acid (BTC) and chiral His and Zn(II). Normal  $\mu_3-N_1O_1:O_1:O_2$  coordination was detected in His and Zn(II) of the system.

The potential chirality of bioMOFs depends on their amino acid nature. Furthermore, the framework porosity could be applied for specific molecular recognition and selective separation, in particular, enantiomers.

### 15.10 Peptides

A short chain of amino acids is called a peptide in which the amino acids are connected to each other through peptide bonds. Peptides differ from proteins by their shorter length; the threshold number of amino acids for definition of a peptide is, however, arbitrary. Peptides generally include two or more amino acids, while the proteins are long arrays of several peptide subunits; that's why they are sometimes called polypeptides. The unique amino acid sequence of each peptides can be determined by its AAs' conformation and stereochemical configuration. Therefore, each peptide will have its specific recognition properties and inherent chirality which can be exploited in various applications, i.e., asymmetric catalysis and enantioselective separation [58]. In humans, peptides can serve as neurotransmitter, hormone, and antibiotic [59]. The increasing attention of pharmacists in these natural compounds lies in their high selectivity combined with their relative safety and well-tolerance. Today, about 140 therapeutic peptides are under investigation in clinical trial studies [60]. Peptides have exhibited proper reactivity toward metal ions, giving rise to various 2D or 3D peptide-based bioMOFs. As the shortest polypeptide, dipeptides have been often applied to construct the peptide-based bioMOFs. Application of peptides as the organic linkers of MOFs could result in several benefits: (i) similar to AAs, peptides offer the same reactive terminal groups ( $-NH_2$  and  $-COOH$ ), however, with an enhanced degree of adaptability due to their double-bond character; this prevents from rotations around the bonds [61]; (ii) infinite number of peptide structures are achievable by changing the peptide length, its AAs' type, and order [62]; (iii) intrinsic chirality of peptides has made them primary candidate for fabrication of chiral MOFs. Rosseinsky group reported the application of carnosine dipeptide (b-alanyl-L-histidine, Car) ligand to form a reaction with Zn(II) ions which led to a ZIF-type three-

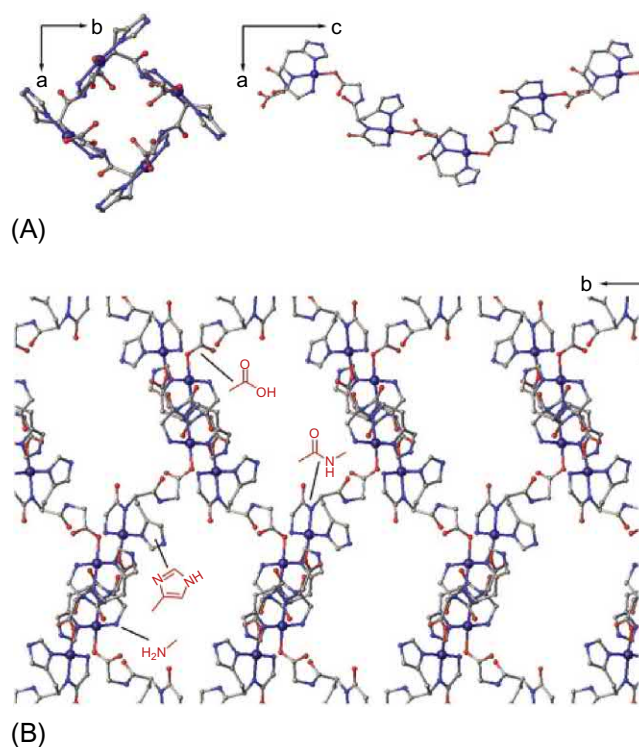


**Fig. 15.4**

Two-step MOF functionalization through peptide coupling. In-atoms are shown as *brown* polyhedra and the bdc-NH<sub>2</sub> linkers in sticks and balls: carbon is *gray*, oxygen is *red*, nitrogen is *blue*, and hydrogen is *white*.

dimensional water-stable MOF, ZnCar; Gly-Ser (GS) was then applied to construct a layered porous framework Zn(GS)<sub>2</sub> with tunable porosity after elimination of the guest [33]. Peptides can also form conjugation with preexisting MOF linkers and frameworks. These molecules can bond with the linkers through a different incorporation method by covalent coupling. Solid-phase peptide synthesis has been widely used for postmodification of the MOFs' linkers. In such cases, the MOF serves as a "bead" to trigger the coupling. The first report on peptide-conjugated MOF using solid-phase peptide synthesis protocol was presented by Canivet et al. who coupled proline and alanine with (In) MIL-68-NH<sub>2</sub> MOFs (Fig. 15.4) [63]. Peptide conjugation to free amines was accomplished through linker by use of bromo-trispyrrolidinophosphonium hexafluorophosphate (PyBroP, coupling agent) and 4-(dimethylamino)pyridine (DMAP, base additive). The MOF retained its crystalline structure after modification. Solid-phase peptide coupling route has opened new horizons to anchor the chiral biomolecules and catalytic species. The mentioned method is also helpful for immobilizing moieties with high activity and/or coordination within the MOF's pores.

Navarro-Sánchez et al. employed a GHG-based (tripeptide Gly-L-His-Gly) chiral Cu(II) 3D MOF to enantioselectively separate the metamphetamine and ephedrine. Based on the MC simulation results, chiral recognition is associated with one of the enantiomers' preferential binding due to additional H-bonds with higher strength in the framework which led to higher stability in diastereomeric adducts (considering energy). Cu(GHG) could be synthesized

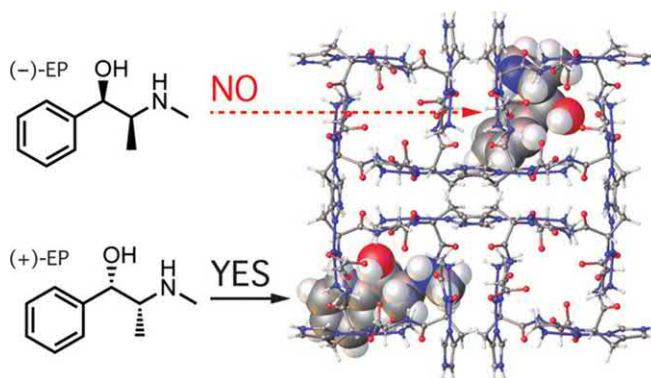


**Fig. 15.5**

(A) Helicoidal chains in Cu(GHG) MOF; (B) functional groups in a peptide backbone used for decoration of the pores surface. *Reproduced with permission from J. Navarro-Sánchez, A.I. Argente-García, Y. Moliner-Martínez, D. Roca-Sanjuán, D. Antypov, P. Campíns-Falcó, M.J. Rosseinsky, C. Martí-Gastaldo, Peptide metal–organic frameworks for enantioselective separation of chiral drugs, J. Am. Chem. Soc. 139(12) (2017) 4294–4297. Copyright 2017, American Chemical Society.*

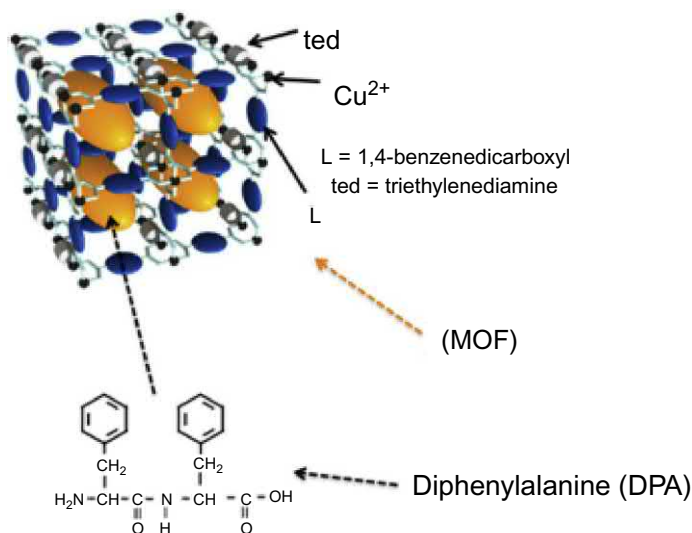
through gradual diffusion of glycyl-L-histidylglycine and Cu(II) acetate. Cu(GHG) produced from 4-fold helicoidal Cu-peptide-Cu chains interconnection with  $\mu_2$ -carboxylate bridged in C-term Gly (Fig. 15.5A). Peptides can serve as metal connectors for inward decoration of the channels' surface with carboxylate, amide, amino, and imidazole groups (Fig. 15.5B). If employed as a chiral SPE cartridge, Cu(GHG) can separate more than 50% of (+)-ephedrine from a racemic within 4 min (Fig. 15.6) [64].

Lei and colleagues synthesized the NP@MOF core-shell nano-probe entitled Au-Cy3P@ZIF-8 in which the pH-sensitive ZIF-8 and cyanine 3 (Cy3)-labeled substrate peptide (Cy3-GRRGKC)-functionalized gold nanoparticle (Au-Cy3P) were the shell and the core responding to acidic environment and CaB activity, respectively. At acidic environments, the mentioned nanostructures could be employed as a dual-recognition switch, hence offering a strategy for lysosomal cathepsin B imaging with high novelty (Fig. 15.7) [65].



**Fig. 15.6**

Chiral polar drugs separation by Cu(GHG). Reproduced with permission from Y. Ikezoe, J. Fang, T.L. Wasik, M. Shi, T. Uemura, S. Kitagawa, H. Matsui, *Peptide–metal organic framework swimmers that direct the motion toward chemical targets*, *Nano Lett.* 15 (2015) 4019–4023. Copyright 2015, American Chemical Society.



**Fig. 15.7**

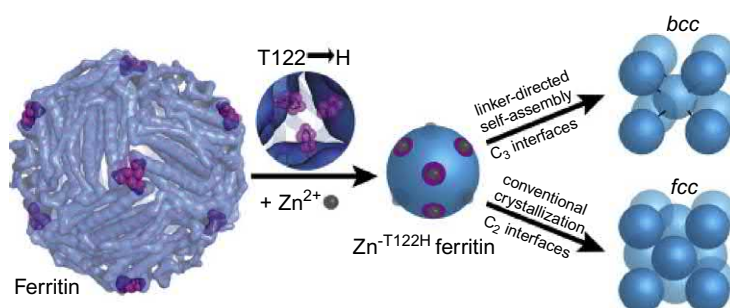
Design of the peptide-MOF motor to swim toward high pH. Reproduced with permission from J. Solà, M. Bolte, I. Alfonso, *Metal-driven assembly of peptidic foldamers: formation of molecular tapes*, *CrystEngComm* 18 (2016) 3793–3798. Copyright 2015, American Chemical Society.

In comparison with dipeptide-MOFs, fewer number of polypeptide-MOFs have been reported which may be attributed to difficulty in constructing a 3D framework due to higher flexibility of longer chains in polypeptides. On the other hand, the peptide's flexibility is the main contributor in adaption and dynamic response of bioMOFs toward guest permeation [66–68]. Peptide-based bioMOFs can be employed as molecular switches as well [24, 28, 69, 70].



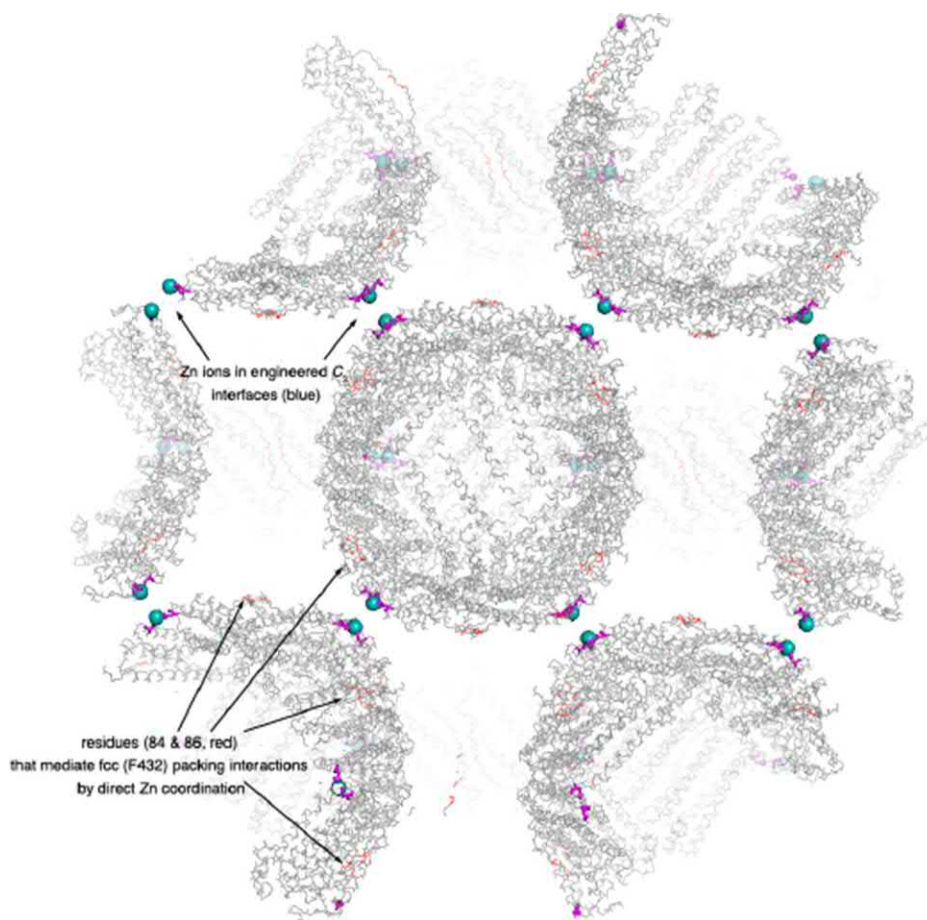
## 15.11 Proteins

Antibodies, enzymes, and structural proteins are basically long chains of amino acids in a sophisticated and flexible 3D structure. These proteins are responsible for highly specific functions within the cells (for instance: cellular dynamics, communication). Owing to their building blocks (AA), proteins can also coordinate metal ions. Indeed, several metal ions are necessary in the function of several proteins (i.e., appropriate protein folding). Although several natural protein complexes have been identified [66], no study has addressed the extended coordination of frameworks associating the metal ions and proteins. The reason can be found in the protein structure whose complexity and flexibility hinder controlling and coordinating metal ions at the protein interface. The covalent conjugation of the protein to MOF linkers is possible through nucleophile sites of proteins (i.e., thiols, amines, and hydroxyls) which form a conjugation with the MOF linkers' carboxylates by nucleophilic substitutions [29]. Tezcan et al. successfully designed a porous three-dimensional protein crystalline framework which was assembled by interactions between metals and organic compounds directed by linkers. As Fig. 15.8 suggests, ferritin (known as the octahedral iron storage enzyme) was adjusted in its  $C_3$  symmetric pores through tripodal Zn coordination site. The bdh-Zn- $T^{122H}$  ferritin system is the first ternary protein-metal-organic crystalline framework in which each constituent can be regarded as an integrated part of the structure. The bcc lattice exhibits an enhanced packing density (packing factor = 0.68) for the spherical building blocks. On the other hand, the ferritin hubs have hollow shape, giving rise to a framework with high porosity and solvent content of 67%. Therefore, the crystals of bdh-Zn- $T^{122H}$  ferritin possess high permeability toward solutes, which lets the ferritin hubs exhibit their intrinsic enzymatic activity inside the lattice (that is soluble  $Fe^{2+}$  oxidation to  $Fe^{3+}$ -oxide mineral crystals) (Fig. 15.9). Generally



**Fig. 15.8**

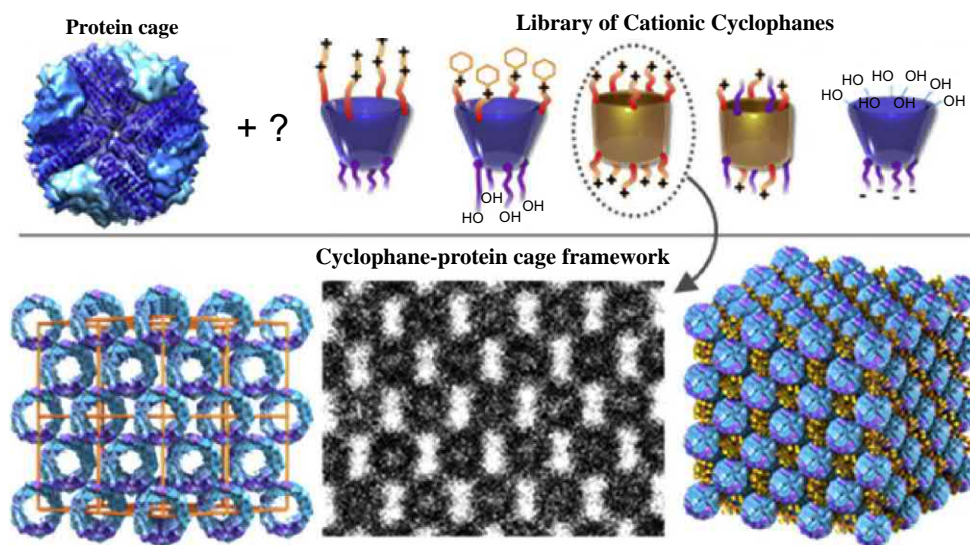
Metal/linker-directed self-assembly of ferritin into 3D crystals; surface-exposed-binding sites for  $Zn^{2+}$  (in gray) were modified at the  $C_3$  pores (magenta) using the T122H mutation. At the presence of ditopic organic linkers, the resulting  $T^{122H}$  ferritin variants formed a bcc lattice. Reproduced with permission from P.A. Sontz, J.B. Bailey, S. Ahn, F.A. Tezcan, A metal organic framework with spherical protein nodes: rational chemical design of 3D protein crystals, *J. Am. Chem. Soc.* 137 (2015) 11598–11601. Copyright 2015, American Chemical Society.



**Fig. 15.9**

Optical micrograph of bdh-Zn-T<sup>122H</sup> ferritin crystals as the result of iron loading/mineralization. bdh-Zn-T<sup>122H</sup> ferritin crystals turned rust-colored after 24 h of soaking in a 10 mM (NH<sub>4</sub>)<sub>2</sub>Fe(SO<sub>4</sub>)<sub>2</sub>·6H<sub>2</sub>O solution which indicates Fe<sup>2+</sup> → Fe<sup>3+</sup> oxidation. *Reproduced with permission from P.A. Sontz, J.B. Bailey, S. Ahn, F.A. Tezcan, A metal organic framework with spherical protein nodes: rational chemical design of 3D protein crystals, J. Am. Chem. Soc. 137 (2015) 11598–11601. Copyright 2015, American Chemical Society.*

speaking, this group of bioMOFs can be considered as the modularly integrated proteins, metal ions, and organic linkers [71]. Two years later, they systematically studied the variations in metal ions in the vertices of the ferritin nodes (Zn<sup>2+</sup>, Ni<sup>2+</sup>, and Co<sup>2+</sup>) and the synthetic dihydroxamate linkers and introduced a comprehensive library including 15 ferritin-MOFs. Results of their research revealed easy modular change of protein-MOFs lattice symmetry and unit cell dimensions like the traditional MOFs synthesis. This has resulted in the ascending development of crystalline protein-MOFs [72].



**Fig. 15.10**

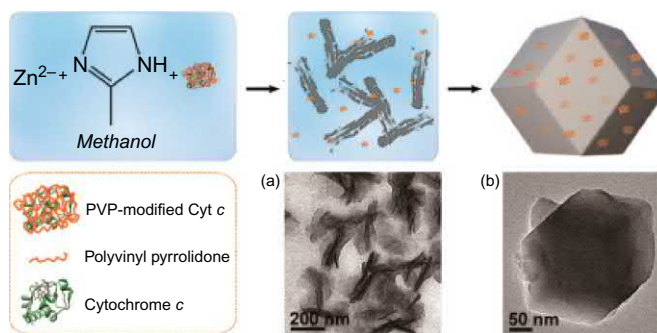
Synthetic cyclophane hosts and native metal-binding protein cages. Reproduced with permission from N.K. Beyeh, Nonappa, V. Liljeström, J. Mikkilä, A. Korpi, D. Bochicchio, G.M. Pavan, O. Ikkala, R.H.A. Ras, M.A. Kostianen, *Crystalline cyclophane–protein cage frameworks*, *ACS Nano* 12 (2018) 8029–8036. Copyright 2018, American Chemical Society.

Encapsulating a series of hemoproteins, microperoxidase-11 (MP-11), myoglobin and cytochrome *c* within a mesoporous MOF, Tb-mesoMOF was achieved. The resulting compound exhibited excellent catalytic activities in the form of the unprecedented size-selective biocatalysis. Based on kinetic studies, encapsulation will result in improved enzyme stability and enhanced enzyme activity in different solvents. Beyeh et al. [73] used synthetic cyclophanes and protein cages to construct a framework (Fig. 15.10). The optimal host was determined as a pillar [5] arene containing 10 protonatable amines with face symmetry which is self-assemble with ferritin cages through electrostatic forces, giving rise to an ordered framework structure. The size of the crystals' interconnected pores between the protein cages varies nano-scales. Cyclophane-protein cage framework is a structure between molecular framework and colloidal crystalline nanoparticle which simultaneously offers the benefits of synthetic supramolecular hosts and the high selectivity of biomolecules. Such advancements will result in development of the versatile heterogeneous catalyst (whose cyclophanes are capable of trapping the guest molecules near the catalytic site of the biomolecule [74]), multipurpose water remedy substances [75], and zeolite-type structures possessing rod-shaped biomolecules [76].

De novo protein encapsulation has been recently proposed for incorporation of proteins into MOFs, regardless of their relatively large size. In this approach, the proteins will be distributed within the MOF synthetic solution during MOF formation. MOF particles prefer to

grow around the proteins; hence, the protein will be finally encapsulated by MOF particles. Study of Lyu et al. involved direct embedding of cytochrome *c* (Cyt *c*) in metal-organic frameworks (MOFs) using a co-precipitation route. The Cyt *c*/ZIF-8 composite was successfully attained independent of PVP; therefore, the coordination interaction between  $Zn^{2+}$  and protein amide bonds probably contributed in the Cyt *c* embedment in the ZIF-8 during crystal growth. PVP-modified Cyt *c* was also distributed in the ZIF-8 synthetic solution which resulted in the formation of Cyt *c*-encapsulated ZIF-8 particles (Fig. 15.11). They declared that the majority of protein molecules were embedded on the surface of ZIF-8 crystals. This approach resulted in 10-fold enhancement in the apparent activity of Cyt *c* in ZIF-8. Cyt *c*-MOF composite succeeded in fast and visible detection of explosive organic peroxides with high sensitivity [77].

The other protein incorporation approach involves application of large-pore MOFs; hence, the proteins can diffuse into the framework. Lykourinou et al. reported the immobilization of MP-11 on mesoporous Tb-TATB MOF (Tb-meso MOF) [78]. They used an MOF with relatively big-sized pore's dimension ( $3.9 \times 4.7$  nm) which enhanced the enzyme diffusion rate. At room temperature, the loading capacity of  $19.1 \mu\text{mol g}$  (enzyme/MOF) was achieved through simple diffusion experiments. Diffusion of MP-11 into the MOF pores was visually verified, although single crystal optical absorption spectroscopy was also employed. Compared to silica supports, this MOF-enzyme support exhibited excellent biocatalytic features. Regarding the strong entrapment of the enzyme inside the MOF cages, enzyme leaching was prevented even after repeated application; such a strong entrapment could be attributed to hydrophobic interactions between enzyme MP-11 and Tb-TATB MOF. After 7 cycles, Tb-TATB MOF managed to maintain  $\sim 47\%$  of its original catalytic activity.



**Fig. 15.11**

Construction of the cytochrome *c*-embedded ZIF-8. Reproduced with permission from F. Lyu, Y. Zhang, R. N. Zare, J. Ge, Z. Liu, *One-pot synthesis of protein-embedded metal-organic frameworks with enhanced biological activities*, *Nano Lett.* 14 (2014) 5761–5765. Copyright 2014, American Chemical Society.

As flexible 3D structures, proteins, such as antibodies and enzymes, could be helpful in construction of soft and biomimetic materials due to their chemically and structurally diverse entities and intrinsic functions (catalysis, electron transfer, and molecular recognition) [79].

### 15.12 Porphyrins and metalloporphyrins

Porphyrins refer to a class of heterocyclic macrocycle organic materials with four modified pyrrole subunits which are mutually connected through their  $\alpha$ -carbons via methine bridges ( $=\text{CH}-$ ). A huge deal of efforts has been devoted to construction of porphyrin/metalloporphyrin-based bioMOFs to be used in gas storage, molecular machines, biomimetic catalysis, and drug delivery purposes [80–90]. Tunable pores of porphyrin-based MOF have increased their drug loading ability, adaptable functionality, and biodegradability. These systems are capable of drug delivery at a controllable rate which made it a versatile therapeutic tool [91]. Use of metalloporphyrin-based drug delivery systems will minimize the complications due to direct drugs administration (i.e., dose quantity and different side effect as the result of nonspecific distribution of drug) [92]. MOF-based substances are stable and compatible inside the physiological environment; hence, they can be considered as an efficient drug carrier. Furthermore, stimuli-responsive, sustained, and adjustable release of drug from metalloporphyrins can be achieved through drug-MOF interactions including hydrophobic interactions, hydrogen bond, and van der Waal's force. Temperature and pH can be employed to control the drug release. MOF has been studied for oral drug delivery [93, 94]. Lin et al. [91] reported a porphyrin-based MOFs PCN-221 which can be applied as an oral drug carrier. For this purpose, they used methotrexate which was adsorbed into the MOF pores through diffusion mechanism. The resulting structure exhibited enhanced drug loading capacity and sustained a controllable pH-responsive drug release [91]. Using hydrogen peroxide, metalloporphyrins-MOFs can be employed for peroxidation of organic substrates. Larsen's and coworkers [95] presented a new class of biomimetic catalysts entitled MOMzyme-1 (metal-organic material enzyme) using selective encapsulation of catalytic metalloporphyrins within one of the three nanoscaled cages of HKUST-1 through application of a "ship-in-a-bottle" method [96]. The mentioned route involved encapsulation of metalloporphyrins within the MOM frameworks, while it was solvothermally synthesized. Interesting result was the selective encapsulation of the metalloporphyrin in the most suitable octahedral cage due to the different sizes and symmetries of the three nanoscale cages of the framework. On the other hand, the benzenesulfonic acid group of the porphyrin ligand was further diffused to neighboring cages, giving rise to an orient-specific proximal and distal heme pocket. This feature plays a vital role in the catalytic functions of the heme enzymes. Furthermore, the hierarchal cages of MOMzyme-1 system will offer several advantages: the large pores can host the metalloporphyrin ingress, while the remained cavities will facilitate the penetration of substrates and products. Based on the porphyrin concentration during

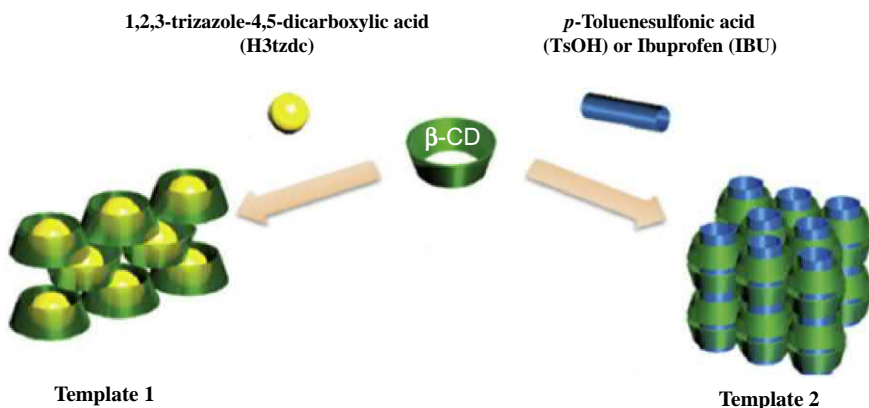


synthesis, up to ~66% (cavity) porphyrin loading was achievable. The catalytic function of the mentioned system was assessed through investigation of the peroxidase activity of Fe4SP@HKUST-1 (one of the MOMzyme-1 catalysts) toward monooxygenation of organic substrates by 2,2'-azinodi(3-ethylbenzthiazoline)-6-sulfonate (ABTS), which was employed as the redox indicator. A comparison was made between the catalytic reaction of this system and that of the homogenous systems (including microperoxidase-11 (MP-11), horse heart myoglobin (hhMb), and Fe4SP). Under solution condition, the maximum yield of the tested systems was comparable with those of MP-11 and Fe4SP. The substrate molecules' diffusion to the HKUST (Cu) frameworks, however, slowed down the formation of the products in this heterogeneous Fe4SP@HKUST-1 systems when compared to their homogeneous counterparts. It must be also noted that ~66% of the initial catalytic activity of Fe4SP@HKUST-1 was recovered after 3 cycles.

### 15.13 Cyclodextrin and other biomolecules

Cyclodextrins refer to cyclic oligosaccharides encompassing 6-cyclodextrin, 7-cyclodextrin, 8-cyclodextrin, or more glucopyranose units which are connected by -(1,4) bonds. These compounds are the product of starch degradation by cyclodextrin glucanotransferase (CGTase) enzyme and are also called cycloamyloses, cyclomaltoses, and Schardinger dextrins [1–3]. The hydrophilic outer edge of cyclodextrin (Rim) combined with its hydrophobic cavity has provided a hydrophobic-binding site. Zhang et al. reported the first successful synthesis of  $\gamma$ -CD-MOFs through microwave-assisted technique which was employed for drug delivery purposes. The size and morphology of  $\gamma$ -CD-MOFs were controlled by use of polyethylene glycol 20000 (PEG 20000) surfactants as well as synthesis process optimization. In comparison with the micron-scale crystals, nano-scale  $\gamma$ -CD-MOFs (100–300 nm) exhibited faster and more Fenbufen adsorption (196 mg/g) reflecting the proper loading properties of  $\gamma$ -CD-MOFs. The crystalline integrity of  $\gamma$ -CD-MOFs was drastically damaged by increasing the reaction time and MeOH ratio. The loading capacity of  $\gamma$ -CD-MOF crystals was assessed using Fenbufen model drug where the nano-sized  $\gamma$ -CD-MOFs (100–300 nm) offered faster and more Fenbufen adsorption (196 mg/g) in EtOH compared with its micron-sized counterpart [97]. Lan et al. synthesized two helical microporous Cs-CD-MOFs, CD-MOF-1 and CD-MOF-2, using  $\beta$ -CD and cesium as building blocks and metal salts, respectively; they also applied 1,2,3-triazole-4,5-dicarboxylic acid (H3tzdc), methyl benzene sulfonic acid (TsOH), or an ibuprofen molecule (IBU) as selective template agents. Single crystal X-ray diffraction analysis confirmed monoclinic *P21* space group of the CD-MOF-1 crystallizes whose asymmetric units only contained one Cs<sup>+</sup> ion and one  $\beta$ -CD molecule. Each Cs<sup>+</sup> ion possessed 6 coordination sites with strongly distorted pentagonal pyramid geometry which were shared by four contiguous  $\beta$ -CD molecules. Its guest-accessible volume could be due to the  $\beta$ -CD molecule's "malposition" stacking effect. CD-MOF-2 showed a monoclinic *C2* space group whose asymmetric unit contained 1.5 crystallographically independent Cs<sup>+</sup> ions and a  $\beta$ -CD molecule





**Fig. 15.12**

The structural formation of CD-MOF-1 (left) and CD-MOF-2 (right) by various templates during the reaction process.

(Fig. 15.12). In CD-MOF-2 framework, the  $\beta$ -CD molecule was simultaneously bound with seven metal ions; it also assembled itself with a three-dimensional bioMOF possessing one-dimensional channels, as vertexes. The filled cage gave rise to a CD-MOF-2, having big “gourd-shaped” cavities offering  $\sim 25.3\%$  volume to the guests. The investigated CD-MOFs are biocompatible and could serve as the drug carrier for high efficacy delivering anticancer drugs [98].

Besides the above-mentioned biomolecules, numerous biomolecules naturally exist in human body, animals, or plants which can be successfully incorporated in MOFs to offer the functionalized bioMOFs with the characteristics of their used biomolecules. Zhu et al. reported incorporation of curcumin into  $\text{Zn}^{2+}$  which resulted in a bioMOF (medi-MOF-1) with escalated porosity and interesting pharmacological behavior under clinical condition. They showed that their bioMOF can serve as both the drug carrier and bioactive ingredient [99].

### 15.14 Conclusion and outlook

Biomolecules (such as amino acids, peptides, nucleobases, and saccharides) contain reactive chemical groups which can coordinate with diverse metallic elements and serve as organic linker in synthesis of MOFs. Explicit application of biomolecules ligands for metal coordination has given rise to a novel class of MOFs known as bio-MOFs, benefiting from improved biocompatibility and specific functionality. Regarding asymmetrical and highly flexible structure of biomolecules, high-quality crystalline bio-MOFs are hardly achievable. Bio-MOFs’ design often requires selection of the biomolecules with high symmetry or introduction of a symmetrical co-ligand. Many of these potential applications can be realized by

addition of biomolecules to MOFs. Given the ideal characteristics of biomolecule, bioMOFs are more biocompatible and easily recyclable. These features will introduce outstanding applications for bioMOFs, including chirality and specific recognition/self-assembly capabilities. BioMOFs could be also exploited for development of micro-scale bio-inspired structures. Numerous issues are still challenging the practical bio-applications of MOFs. The thermal and chemical stabilities of bioMOFs are lower than the traditional biomaterials. For instance, high abundance of phosphate with strong affinity for metal clusters will disturb the metal-ligand coordination equilibrium in favor of the metal-phosphate formation. In this content, enhancing the stability and cell adsorption properties of bioMOFs is vital for development of their biological applications. Moreover, the particle size of MOF has to be closely controlled to obtain a stable formulation adaptable to various administration methods. Nanoparticles agglomeration should be also prevented which requires further studies. Extensive bio-application of bioMOFs requires serious addressing their numerous practical issues. In this context, their toxicity, morphology, machinability, dissolvability, and possibility of preparing their homogeneous nanocrystals need to be closely studied. The biosafety, biodistribution, and in vitro and/or in vivo efficacy of bioMOFs have to meet the standards of real biomedical applications. In addition, for real application of bioMOFs, their stable formulations have to fulfill the standards of a given administration route. Development of organic or inorganic MOFs composites (for example, to be used as patches or creams) could be one solution. Finally, although biomedical use of MOFs is still at its primary stages, studies have indicated several significant superiorities of MOFs compared to the conventional bioorganic or inorganic systems. Despite studying numerous model drug molecules, drug-loaded MOFs have not yet open their way to real applications which may be due to their poor bioavailability; this highlights the urgent need to develop MOFs for further bio-applications.

## References

- [1] S. Prasad, I. Roy, Converting enzymes into tools of industrial importance, *Recent Pat. Biotechnol.* 12 (2018) 33–56.
- [2] Z. Lei, C. Gao, L. Chen, Y. He, W. Ma, Z. Lin, Recent advances in biomolecule immobilization based on self-assembly: organic–inorganic hybrid nanoflowers and metal–organic frameworks as novel substrates, *J. Mater. Chem. B* 6 (2018) 1581–1594.
- [3] H.H. Nguyen, M. Kim, An overview of techniques in enzyme immobilization, *Appl. Sci. Converg. Technol.* 26 (2017) 157–163.
- [4] M. Hartmann, X. Kostrov, Immobilization of enzymes on porous silicas – benefits and challenges, *Chem. Soc. Rev.* 42 (2013) 6277–6289.
- [5] E. Magner, Immobilization of enzymes on porous silicas—benefits and challenges, *Chem. Soc. Rev.* 42 (2013) 6213–6222.
- [6] S. Hudson, J. Cooney, E. Magner, Proteins in mesoporous silicates, *Angew. Chem. Int. Ed.* 47 (2008) 8582–8594.
- [7] S. Kumar, D. Kumar, R. Ahirwar, P. Nahar, Exploring the flexible chemistry of 4-fluoro-3-nitrophenyl azide for biomolecule immobilization and bioconjugation, *Anal. Bioanal. Chem.* 408 (2016) 6945–6956.

- [8] H. Jiang, F.J. Xu, Biomolecule-functionalized polymer brushes, *Chem. Soc. Rev.* 42 (2013) 3394–3426.
- [9] C.J. Reedy, B.R. Gibney, Biomolecule-functionalized polymer brushes, *Chem. Rev.* 104 (2004) 617–650.
- [10] J. Schmid, S. Dordick, B. Hauer, A. Kiener, M. Wubbolts, B. Witholt, Industrial biocatalysis today and tomorrow, *Nature* 409 (2001) 258–268.
- [11] M. Hartmann, D. Jung, Biocatalysis with enzymes immobilized on mesoporous hosts: the status quo and future trends, *J. Mater. Chem.* 20 (2010) 844–857.
- [12] M. Hartmann, Ordered mesoporous materials for bioadsorption and biocatalysis, *Chem. Mater.* 17 (18) (2005) 4577–4593.
- [13] B. Li, H.M. Wen, Y. Cui, W. Zhou, G. Qian, B. Chen, Emerging multifunctional metal-organic framework materials, *Adv. Mater.* 28 (40) (2016) 8819–8860.
- [14] M.I. Nandasiri, S.R. Jambovane, B.P. McGrail, H.T. Schaefer, S.K. Nune, Adsorption, separation, and catalytic properties of densified metal-organic frameworks, *Coord. Chem. Rev.* 311 (2016) 38–52.
- [15] Y. Cui, B. Li, H. He, W. Zhou, B. Chen, G. Qian, Metal-organic frameworks as platforms for functional materials, *Acc. Chem. Res.* 49 (2016) 483–493.
- [16] Q.L. Zhu, Q. Xu, Metal-organic framework composites, *Chem. Soc. Rev.* 43 (2014) 5468–5512.
- [17] S.T. Meek, J.A. Greathouse, M.D. Allendorf, Metal-organic frameworks: a rapidly growing class of versatile nanoporous materials, *Adv. Mater.* 23 (2011) 249–267.
- [18] H.C. Zhou, J.R. Long, O.M. Yaghi, Introduction to metal-organic frameworks, *Chem. Rev.* 112 (2012) 673–674.
- [19] (a) S. Ma, Gas adsorption applications of porous metal-organic frameworks, *Pure Appl. Chem.* 81 (2009) 2235–2251; (b) J.-R. Li, R.J. Kuppler, H.-C. Zhou, Selective gas adsorption and separation in metal-organic frameworks, *Chem. Soc. Rev.* 38 (2009) 1477–1504; (c) L.J. Murray, M. Dinca, J.R. Long, Hydrogen storage in metal-organic frameworks, *Chem. Soc. Rev.* 38 (5) (2009) 1294–1314.
- [20] (a) M.D. Allendorf, C.A. Bauer, R.K. Bhakta, R.J.T. Houk, Luminescent metal-organic frameworks, *Chem. Soc. Rev.* 38 (2009) 1330–1352; (b) A.J. Lan, K.H. Li, H.H. Wu, D.H. Olson, T.J. Emge, W. Ki, M. C. Hong, J. Li, Highly selective catalytic conversion of phenolic bio-oil to alkanes, *Angew. Chem. Int. Ed.* 48 (2009) 2334–2338; (c) B. Chen, S. Xiang, G. Qian, Metal-organic frameworks with functional pores for recognition of small molecules, *Acc. Chem. Res.* 43 (2010) 1115–1124.
- [21] M. Kurmoo, Magnetic metal-organic frameworks, *Chem. Soc. Rev.* 38 (2009) 1353–1379.
- [22] (a) J. Lee, O.K. Farha, J. Roberts, K.A. Scheidt, S.T. Nguyen, J.T. Hupp, Metal-organic framework materials as catalysts, *Chem. Soc. Rev.* 38 (2009) 1450–1459; (b) L. Ma, C. Abney, W. Lin, Enantioselective catalysis with homochiral metal-organic frameworks, *Chem. Soc. Rev.* 38 (2009) 1248–1256; (c) A. Corma, H. Garcia, F.X. Llabrés i Xamena, Engineering metal organic frameworks for heterogeneous catalysis, *Chem. Rev.* 110 (2010) 4606–4655.
- [23] D. Liu, Z.G. Ren, H.X. Li, J.-P. Lang, N.Y. Li, B.F. Abrahams, Single-crystal-to-single-crystal transformations of two three-dimensional coordination polymers through regioselective [2+2] photodimerization reactions, *Angew. Chem. Int. Ed.* 49 (2010) 4767–4770.
- [24] J. Zhuang, A.P. Young, C.-K. Tsung, Integration of biomolecules with metal-organic frameworks, *Small* 13 (32) (2017) 1700880.
- [25] A.C. McKinlay, R.E. Morris, P. Horcajada, G. Férey, R. Gref, P. Couvreur, C. Serre, BioMOFs: metal-organic frameworks for biological and medical applications, *Angew. Chem. Int. Ed.* 49 (2010) 6260–6266.
- [26] P. Horcajada, R. Gref, T. Baati, P.K. Allan, G. Maurin, P. Couvreur, G. Férey, R.E. Morris, C. Serre, Metal-organic frameworks in biomedicine, *Chem. Rev.* 112 (2011) 1232–1268.
- [27] M. Giménez-Marqués, T. Hidalgo, C. Serre, P. Horcajada, Nanostructured metal-organic frameworks and their bio-related applications, *Coord. Chem. Rev.* 307 (2016) 342–360.
- [28] S. Rojas, T. Devic, P. Horcajada, Metal organic frameworks based on bioactive components, *J. Mater. Chem. B* 5 (2017) 2560–2573.
- [29] I. Imaz, M. Rubio-Martínez, J. An, I. Sole-Font, N.L. Rosi, D. Maspoch, Metal-biomolecule frameworks (MBioFs), *Chem. Commun.* 47 (2011) 7287–7302.
- [30] H. Cai, Y.-L. Huang, D. Li, Biological metal-organic frameworks: structures, host-guest chemistry and bio-applications, *Coord. Chem. Rev.* 374 (2019) 207–221.

- [31] H. Cai, M. Li, X.R. Lin, W. Chen, G.H. Chen, X.C. Huang, D. Li, Spatial, hysteretic, and adaptive host-guest chemistry in a metal-organic framework with open Watson-Crick sites, *Angew. Chem. Int. Ed.* 54 (2015) 10454–10459.
- [32] J. An, O.K. Farha, J.T. Hupp, E. Pohl, J.I. Yeh, N.L. Rosi, Metal-adeninate vertices for the construction of an exceptionally porous metal-organic framework, *Nat. Commun.* 3 (2012) 604–610.
- [33] G. Beobide, O. Castillo, A. Luque, S. Pérez-Yáñez, Porous materials based on metal–nucleobase systems sustained by coordination bonds and base pairing interactions, *CrystEngComm* 17 (2015) 3051–3059.
- [34] Z.-J. Lin, J. Lü, M. Hong, R. Cao, Metal–organic frameworks based on flexible ligands (FL-MOFs): structures and applications, *Chem. Soc. Rev.* 43 (2014) 5867–5895.
- [35] F.H. Allen, The Cambridge structural database: a quarter of a million crystal structures and rising, *Acta Crystallogr. Sect. B Struct. Sci.* 58 (2002) 380–388.
- [36] L.P. Jordheim, D. Durantel, F. Zoulim, C. Dumontet, Advances in the development of nucleoside and nucleotide analogues for cancer and viral diseases, *Nat. Rev. Drug Discov.* 12 (2013) 447–464.
- [37] G. Beobide, O. Castillo, J. Cepeda, A. Luque, S. Perez-Yanez, P. Roman, J. Thomas-Gipson, Metal–carboxylato–nucleobase systems: from supramolecular assemblies to 3D porous materials, *Coord. Chem. Rev.* 257 (2013) 2716–2736.
- [38] J. An, S.J. Geib, N.L. Rosi, High and selective CO<sub>2</sub> uptake in a cobalt adeninate metal–organic framework exhibiting pyrimidine- and amino-decorated pores, *J. Am. Chem. Soc.* 132 (1) (2010) 38–39.
- [39] P. Verma, S. Verma, Imine component based modified adenine nucleobase–metal frameworks, *Cryst. Growth Des.* 15 (2015) 510–516.
- [40] J. An, S.J. Geib, N.L. Rosi, Cation-triggered drug release from a porous zinc–adeninate metal–organic framework, *J. Am. Chem. Soc.* 131 (2009) 8376–8377.
- [41] J.P. Garcia-Teran, O. Castillo, A. Luque, U. Garcia-Couceiro, P. Roman, L. Lezama, An unusual 3D coordination polymer based on bridging interactions of the nucleobase adenine, *Inorg. Chem.* 43 (2004) 4549–4551.
- [42] D.B. Linsksay, Amino acids as energy sources, *Proc. Nutr. Soc.* (1980) 53–59.
- [43] E.R. Francotte, Enantioselective chromatography as a powerful alternative for the preparation of drug enantiomers, *J. Chromatogr. A* 906 (1–2) (2001) 379–397.
- [44] A. Suksuwan, L. Lomlim, T. Rungrotmongkol, T. Nakpheng, F.L. Dickert, R. Suedee, The composite nanomaterials containing (R)-thalidomide-molecularly imprinted polymers as a recognition system for enantioselective-controlled release and targeted drug delivery, *J. Appl. Polym. Sci.* 132 (18) (2015) 14368–14373.
- [45] Y. Shimazaki, M. Takani, O. Yamauchi, Metal complexes of amino acids and amino acid side chain groups. Structures and properties, *Dalt. Trans.* (38) (2009) 7854–7869.
- [46] (a) C.D. Ch’ng, S.G. Teoh, S. Chantrapromma, H.K. Fun, S.M. Goh, catena-Poly[[[diaqua-nickel(II)]-di-[mu]-glycine] dichloride], *Acta Crystallogr. Sect. E Struct. Rep. Online* 64 (2008) M865–M866; (b) M. Fleck, L. Bohaty, Two novel glycine metal halogenides: catena-poly[[[diaqua-nickel(II)]-di-[mu]-glycine] dibromide] and catena-poly[[[tetra-aqua-magnesium(II)]-[mu]-glycine] dichloride], *Acta Crystallogr. Sect. C Cryst. Struct. Commun.* 61 (2005) M412–M416.
- [47] (a) R. Mrozek, Z. Rzaczyńska, M. Sikorska-Iwan, T. Glowiak, Crystal structure and vibrational spectra of two complexes of manganese(II) with glycine, *J. Chem. Crystallogr.* 29 (1999) 803–808; (b) T. Glowiak, Z. Ciunik, Two crystal structures of polymorphic bis-(glycine)manganese(II) bromide dehydrate, *Acta Crystallogr. Sect. B: Struct. Crystallogr. Cryst. Chem.* 34 (1978) 1980–1983.
- [48] K. Stenzel, M. Fleck, Poly[[[diaquacobalt(II)]-di-[mu]-glycine] dichloride], *Acta Crystallogr. Sect. E Struct. Rep. Online* 60 (2004) M1470–M1472.
- [49] J.B. Weng, M.C. Hong, R. Cao, Q. Shi, A.S.C. Chan, The paramagnetic 2D chiral-porous polymer of L-phenylalanine and manganese, *Chin. J. Struct. Chem.* 22 (2003) 195–199.
- [50] D. Vanderhe, M.B. Lawson, E.L. Enwall, The crystal structure of bis-(L-phenylalaninato)copper(II), *Acta Crystallogr. Sect. B: Struct. Crystallogr. Cryst. Chem.* B27 (1971) 2411–2418.

- [51] Y. Xie, H.H. Wu, G.P. Yong, Z.Y. Wang, rac-Poly[bis-([mu]-tryptophanato)manganese(II)], *Acta Crystallogr. Sect. E Struct. Rep. Online* 62 (2006) M2089–M2090.
- [52] J. Wang, X. Xu, W. Ma, L. Lu, X. Yang, rac-catena-Poly[nickel(II)-di-[mu]-tryptophanato], *Acta Crystallogr. Sect. E Struct. Rep. Online* 63 (2007) M2867–M2868.
- [53] J.M. Schweigkardt, A.C. Rizzi, O.E. Piro, E.E. Castellano, R.C. de Santana, R. Calvo, C.D. Brondino, Structural and single crystal EPR studies of the complex copper L-glutamine: a weakly exchange-coupled system with syn-anti carboxylate bridges, *Eur. J. Inorg. Chem.* (2002) 2913–2919.
- [54] E. Yang, L. Wang, F. Wang, Q. Lin, Y. Kang, J. Zhang, From cubane to supercubane: the design, synthesis, and structure of a three-dimensional open framework based on a Ln(4)O(4) cluster, *Inorg. Chem.* 53 (2014) 10027–10029.
- [55] B.Q. Ma, D.S. Zhang, S. Gao, T.Z. Jin, C.H. Yan, G.X. Xu, From cubane to supercubane: the design, synthesis, and structure of a three-dimensional open framework based on a Ln<sub>4</sub>O<sub>4</sub> cluster, *Angew. Chem. Int. Ed.* 39 (2000) 3644–3646.
- [56] R. Wang, H. Liu, M.D. Carducci, T. Jin, C. Zheng, Z. Zheng, Lanthanide coordination with  $\alpha$ -amino acids under near physiological pH conditions: polymeric complexes containing the cubane-like [Ln<sub>4</sub>( $\mu_3$ -OH)<sub>4</sub>]<sup>8+</sup> cluster core, *Inorg. Chem.* 40 (2001) 2743–2750.
- [57] J. He, G. Zhang, D. Xiao, H. Chen, S. Yan, X. Wang, J. Yang, E. Wang, Helicity controlled by the chirality of amino acid: two novel enantiopure chiral 3D architectures containing fivefold interwoven helices, *CrystEngComm* 14 (2012) 3609–3614.
- [58] Y. Liu, W. Xuan, Y. Cui, Engineering homochiral metal-organic frameworks for heterogeneous asymmetric catalysis and enantioselective separation, *Adv. Mater.* 22 (2010) 4112–4135.
- [59] L. Huang, L. Massa, K. Jerome, *Quantum Biochemistry*, WILEY-VCH Verlag GmbH & Co. KGaA, Weinheim, 2010, pp. 3–60.
- [60] K. Fosgerau, T. Hoffmann, Peptide therapeutics: current status and future directions, *Drug Discov. Today* 20 (2015) 122–128.
- [61] J.M. Berg, J.L. Tymoczko, L. Stryer, *Biochemistry*, fifth ed., W. H. Freeman, New York, 2002.
- [62] G.L. Patrick, *An Introduction to Drug Synthesis*, Oxford University Press, Oxford, 2015, pp. 227–255.
- [63] J. Canivet, S. Aguado, G. Bergeret, D. Farrusseng, Amino acid functionalized metal-organic frameworks by a soft coupling-deprotection sequence, *Chem. Commun.* 47 (2011) 11650–11652.
- [64] J. Navarro-Sánchez, A.I. Argente-García, Y. Moliner-Martínez, D. Roca-Sanjuán, D. Antypov, P. Campíns-Falcó, M.J. Rosseinsky, C. Martí-Gastaldo, Peptide metal-organic frameworks for enantioselective separation of chiral drugs, *J. Am. Chem. Soc.* 139 (12) (2017) 4294–4297.
- [65] H. Shen, J. Liu, J. Lei, H. Ju, A core-shell nanoparticle-peptide@metal-organic framework as pH and enzyme dual-recognition switch for stepwise-responsive imaging in living cells, *Chem. Commun.* 54 (2018) 9155–9158.
- [66] C. Martí-Gastaldo, J.E. Warren, K.C. Stylianou, N.L. Flack, M.J. Rosseinsky, Enhanced stability in rigid peptide-based porous materials, *Angew. Chem. Int. Ed.* 51 (2012) 11044–11048.
- [67] R. Miyake, C. Kuwata, Y. Masumoto, Selective CO<sub>2</sub> gas adsorption in the narrow crystalline cavities of flexible peptide metallo-macrocycles, *Dalton Trans.* 44 (2015) 2993–2996.
- [68] R. Miyake, M. Shionoya, Concerted ligand exchange and the roles of counter anions in the reversible structural switching of crystalline peptide metallo-macrocycles, *Inorg. Chem.* 53 (11) (2014) 5717–5723.
- [69] Y. Ikezoe, J. Fang, T.L. Wasik, M. Shi, T. Uemura, S. Kitagawa, H. Matsui, Peptide-metal organic framework swimmers that direct the motion toward chemical targets, *Nano Lett.* 15 (2015) 4019–4023.
- [70] J. Solà, M. Bolte, I. Alfonso, Metal-driven assembly of peptidic foldamers: formation of molecular tapes, *CrystEngComm* 18 (2016) 3793–3798.
- [71] P.A. Sontz, J.B. Bailey, S. Ahn, F.A. Tezcan, A metal organic framework with spherical protein nodes: rational chemical design of 3D protein crystals, *J. Am. Chem. Soc.* 137 (2015) 11598–11601.
- [72] J.B. Bailey, L. Zhang, J.A. Chiong, S. Ahn, F.A. Tezcan, Synthetic modularity of protein-metal-organic frameworks, *J. Am. Chem. Soc.* 139 (24) (2017) 8160–8166.

- [73] N.K. Beyeh, V.L. Nonappa, J. Mikkilä, A. Korpi, D. Bochicchio, G.M. Pavan, O. Ikkala, R.H.A. Ras, M. A. Kostiainen, Crystalline cyclophane–protein cage frameworks, *ACS Nano* 12 (2018) 8029–8036.
- [74] H. Zhao, S. Sen, T. Udayabhaskararao, M. Sawczyk, K. Kučanda, D. Manna, P.K. Kundu, J.-W. Lee, P. Král, R. Klajn, Reversible trapping and reaction acceleration within dynamically self-assembling nanoflasks, *Nat. Nanotechnol.* 11 (2015) 82–88.
- [75] A. Alsbaiee, B.J. Smith, L. Xiao, Y. Ling, D.E. Helbling, W.R. Dichtel, Rapid removal of organic micropollutants from water by a porous  $\beta$ -cyclodextrin polymer, *Nature* 529 (2016) 190–194.
- [76] V. Liljeström, A. Ora, J. Hassinen, H.T. Rekola, M.H. Nonappa, V. Hynninen, J.J. Joensuu, R.H. A. Ras, P. Törmä, O. Ikkala, M.A. Kostiainen, Cooperative colloidal self-assembly of metal–protein superlattice wires, *Nat. Commun.* 8 (2017) 671.
- [77] F. Lyu, Y. Zhang, R.N. Zare, J. Ge, Z. Liu, One-pot synthesis of protein-embedded metal–organic frameworks with enhanced biological activities, *Nano Lett.* 14 (2014) 5761–5765.
- [78] V. Lykourinou, Y. Chen, X.-S. Wang, L. Meng, T. Hoang, L.-J. Ming, R.L. Musselman, S. Ma, Immobilization of MP-11 into a mesoporous metal–organic framework, MP-11@mesoMOF: a new platform for enzymatic catalysis, *J. Am. Chem. Soc.* 133 (2011) 10382–10385.
- [79] L.S. Witus, M.B. Francis, Using synthetically modified proteins to make new materials, *Acc. Chem. Res.* 44 (2011) 774–783.
- [80] D. Feng, Z.Y. Gu, J.R. Li, H.L. Jiang, Z. Wei, H.C. Zhou, Symmetry-guided synthesis of highly porous metal–organic frameworks with fluorite topology, *Angew. Chem. Int. Ed.* 124 (2012) 10453–10456.
- [81] H.-L. Jiang, D. Feng, K. Wang, Z.-Y. Gu, Z. Wei, Y.-P. Chen, H.-C. Zhou, An exceptionally stable, porphyrinic Zr metal–organic framework exhibiting pH-dependent fluorescence, *J. Am. Chem. Soc.* 135 (2013) 13934–13938.
- [82] D. Feng, W.-C. Chung, Z. Wei, Z.-Y. Gu, H.-L. Jiang, Y.-P. Chen, D.J. Darensbourg, H.-C. Zhou, Construction of ultrastable porphyrin Zr metal–organic frameworks through linker elimination, *J. Am. Chem. Soc.* 135 (2013) 17105–17110.
- [83] D. Feng, H.-L. Jiang, Y.-P. Chen, Z.-Y. Gu, Z. Wei, H.-C. Zhou, Metal–organic frameworks based on previously unknown  $Zr_8/Hf_8$  cubic clusters, *Inorg. Chem.* 52 (2013) 12661–12667.
- [84] D. Feng, Z.-Y. Gu, Y.-P. Chen, J. Park, Z. Wei, Y. Sun, M. Bosch, S. Yuan, H.-C. Zhou, A highly stable porphyrinic zirconium metal–organic framework with shp-a topology, *J. Am. Chem. Soc.* 136 (2014) 17714–17717.
- [85] T.-F. Liu, D. Feng, Y.-P. Chen, L. Zou, M. Bosch, S. Yuan, Z. Wei, S. Fordham, K. Wang, H.-C. Zhou, Topology-guided design and syntheses of highly stable mesoporous porphyrinic zirconium metal–organic frameworks with high surface area, *J. Am. Chem. Soc.* 137 (2014) 413–419.
- [86] K. Wang, D. Feng, T.-F. Liu, J. Su, S. Yuan, Y.-P. Chen, M. Bosch, X. Zou, H.-C. Zhou, A series of highly stable mesoporous metalloporphyrin Fe-MOFs, *J. Am. Chem. Soc.* 136 (2014) 13983–13986.
- [87] W.-Y. Gao, L. Wojtas, S. Ma, A porous metal–metalloporphyrin framework featuring high-density active sites for chemical fixation of  $CO_2$  under ambient conditions, *Chem. Commun.* 50 (2014) 5316–5318.
- [88] J. Park, D. Feng, H.-C. Zhou, Dual exchange in PCN-333: a facile strategy to chemically robust mesoporous chromium metal–organic framework with functional groups, *J. Am. Chem. Soc.* 137 (2015) 11801–11809.
- [89] J. Park, Q. Jiang, D. Feng, L. Mao, H.-C. Zhou, Size-controlled synthesis of porphyrinic metal–organic framework and functionalization for targeted photodynamic therapy, *J. Am. Chem. Soc.* 138 (2016) 3518–3525.
- [90] K. Wang, X.-L. Lv, D. Feng, J. Li, S. Chen, J. Sun, L. Song, Y. Xie, J.-R. Li, H.-C. Zhou, Pyrazolate-based porphyrinic metal–organic framework with extraordinary base-resistance, *J. Am. Chem. Soc.* 138 (2016) 914–919.
- [91] W. Lin, Q. Hu, K. Jiang, Y. Yang, Y. Cui, G. Qian, A porphyrin-based metal–organic framework as a pH-responsive drug carrier, *J. Solid. State. Chem.* 237 (2016) 307–312.
- [92] R.C. Huxford, J.D. Rocca, W. Lin, Metal–organic frameworks as potential drug carriers, *Curr. Opin. Chem. Biol.* 14 (2010) 262–268.



- 
- [93] Y.N. Xue, Z.Z. Huang, J.T. Zhang, M. Liu, M. Zhang, S.W. Huang, R.X. Zhuo, Synthesis and self-assembly of amphiphilic poly(acrylic acid-*b*-DL-lactide) to form micelles for pH-responsive drug delivery, *Polymer* 50 (2009) 3706–3713.
- [94] S. De Robertis, M.C. Bonferoni, L. Elviri, G. Sandri, C. Caramella, R. Bettini, Advances in oral controlled drug delivery: the role of drug-polymer and interpolymer non-covalent interactions, *Expert Opin. Drug Deliv.* 12 (2015) 441–453.
- [95] R.W. Larsen, L. Wojtas, J. Perman, R.L. Musselman, M.J. Zaworotko, C.M. Vetromile, Mimicking heme enzymes in the solid state: metal–organic materials with selectively encapsulated heme, *J. Am. Chem. Soc.* 133 (2011) 10356–10359.
- [96] P.C. Sahoo, Y.N. Jang, S.W. Lee, Enhanced biomimetic CO<sub>2</sub> sequestration and CaCO<sub>3</sub> crystallization using complex encapsulated metal organic framework, *J. Crystal. Growth.* 373 (2013) 96–101.
- [97] B. Liu, Y. He, L. Han, V. Singh, X. Xu, T. Guo, F. Meng, X. Xu, P. York, Z. Liu, J. Zhang, Microwave-assisted rapid synthesis of  $\gamma$ -cyclodextrin metal–organic frameworks for size control and efficient drug loading, *Cryst. Growth Des.* 17 (2017) 1654–1660.
- [98] J. Liu, T.-Y. Bao, X.-Y. Yang, P.-P. Zhu, L.-H. Wu, J.-Q. Sha, L. Zhang, L.-Z. Dong, X.-L. Cao, Y.-Q. Lan, Controllable porosity conversion of metal-organic frameworks composed of natural ingredients for drug delivery, *Chem. Commun.* 53 (2017) 7804–7807.
- [99] H. Su, F. Sun, J. Jia, H. He, A. Wang, G. Zhu, A highly porous medical metal–organic framework constructed from bioactive curcumin, *Chem. Commun.* 51 (2015) 5774–5777.

# Metal-organic frameworks and exemplified cytotoxicity evaluation

Sajid Bashir<sup>a</sup>, Sai Raghuveer Chava<sup>a,\*</sup>, Daqiang Yuan<sup>b</sup>, Srinath Palakurthi<sup>c</sup>,  
Jingbo Liu<sup>a</sup>

<sup>a</sup>MSC161, 700 University Blvd, Kingsville, TX, United States <sup>b</sup>State Key Laboratory of Structure Chemistry, Fujian Institute of Research on the Structure of Matter, Chinese Academy of Sciences, Fuzhou, PR China <sup>c</sup>Texas A&M Health Science Center, Irma Lerma Rangel, Kingsville, TX, United States

## 16.1 Introduction

Nanotechnology is the science of the “small world,” which unlocks a new research frontier in diversified research fields, such as biomedical application, electronics, catalyst, drug delivery, and construction of sport equipment [1]. Nanoscience has been transformed from benchtop techniques to applied science and technology [2]. Porous materials are named after the amount of empty or void spaces within the material itself. This family of materials has different pore structures and sizes (from nanometer to millimeter), ordered arrangement, several chemical compositions, and several different synthesis methods [3]. Before the 1990s, porous materials were focused on gas separations, absorption, catalysis, and bioengineering, but since then have moved into biological and biomedical applications in addition to industrial uses [4]. Porous materials contain two types: inorganic materials (such as aluminum silicate,  $\text{Al}_2[\text{SiO}_3]_3$ ) and carbonaceous materials. However, crystalline  $\text{Al}_2(\text{SiO}_3)_3$  displays limited porosity, while carbonaceous materials have a distorted structure [5]. Although the materials in the preceding text have a stable structure by a strong Si—O or C—C covalent bond, they lack flexibility in the architecture. As a result, it is important to find flexible and stable materials to further advance porous material research in today’s society.

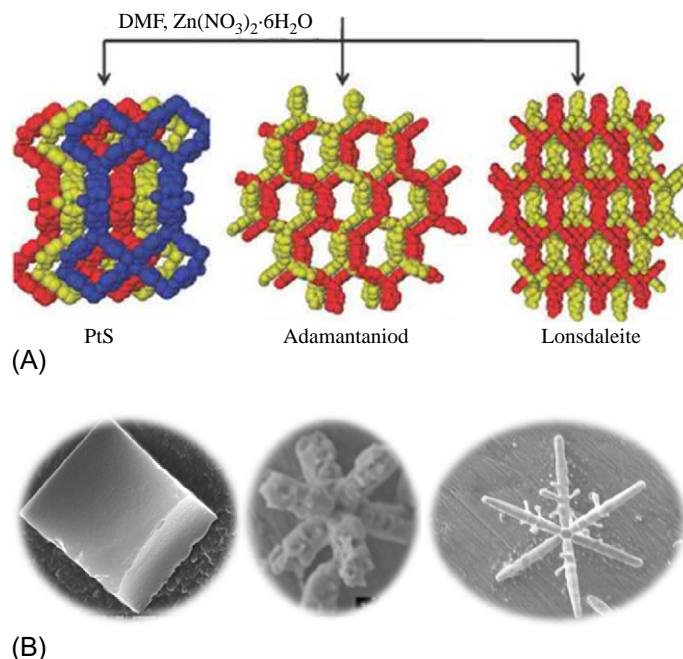
Organometallic compounds are a class of substances containing at least one metal-carbon bond, which the carbon in it is part of an organic group. The metal can be ranging from main group and transition elements. The physical and chemical properties of these organometallic

---

\* Currently working at Emergent BioSolutions.

compounds vary largely according to the difference of organic linkers. They can be available in solid, liquid, and even gaseous form. The properties also depend on the type of carbon-metal bond, which can be a covalent, multicenter covalent bond, and ionic bond [6].

Metal-organic frameworks (MOFs) are an extensive class of complex materials, which are formed by a metal connecting ions and organic bridging ligands [7]. Under comparatively mild fabrication conditions, MOFs can be achieved as either crystalline or amorphous materials [8]. The composition of MOFs, particle size and topology can be easily tuned to improve the properties of MOFs. According to the special extension and atomic arrangement, MOFs can be divided as a one-dimensional (1-D) chain, two-dimensional (2-D) layer, and three-dimensional (3-D) space network structures (cf. Fig. 16.1). Due to MOFs' special structures, their application in multiple fields have already drawn widespread attention from worldwide scientists.



**Fig. 16.1**

(A) Simplified demonstration of different dimensions of MOFs' secondary building blocks and topologies involving triply and doubly interpenetrated PtS (2), hexagonal adamantanoid, and lonsdaleite frameworks synthesized from tetrahedral building block based around 4-methoxy benzene carboxylic acid as a ligand. (B) Scanning electron micrographic images of crystalline metal-organic frameworks for gas capture (center) or catalysis (left or right). (A) Reproduced with permission from M.R. Kishan, J. Tian, P.K. Thallapally, C.A. Fernandez, S.J. Dalgarno, J.E. Warren, B.P. McGrail, J.L. Atwood, *Flexible metal-organic supramolecular isomers for gas separation*, *Chem. Commun.* 46 (4) (2010) 538–540.

Copyright (2010) Royal Society of Chemistry.

The engineered nanomaterials (NMs) present a revolutionary opportunity in cancer and public hygiene research, for example, to attack cancer cells at the cellular and genetic level with much greater precision, or clean water from pathogens [9, 10]. However, the potential toxicity of NMs has hindered their development and commercialization [11]. Studies on the chronic effects of NMs on human health are ongoing, with an expectation of widening the scope and duration of such studies to three decades or more [12]. The reason why this is a concern, based on our past experiences, is how “easily” materials can affect the environment, the food chain, and potentially cause disease [13]. Since the incorporation of NMs is more widespread over the last two decades, the questions of whether NMs have potential side effects due to their use in medicine, or release into the environment, which is more relevant to current needs [14]. This concern has also been raised by governmental agencies, such as the US National Institute for Occupational Safety and Health and Japan’s Ministry of Health [15], particularly related to iron-based NMs, due to their widespread application and usage [16]. This has necessitated systematic studies on iron oxide magnetic nanoparticles ( $\text{Fe}_3\text{O}_4$  MNPs) due to their inherent magnetism and widespread availability [17]. Examples include contrast enhancement agents in magnetic resonance imaging ferrofluids [18], data storage [19], targeted drug delivery [20], and cancer diagnosis and therapy [21], noting that choice of iron species is important [22]. Iron oxide ( $\text{Fe}_3\text{O}_4$ ) with mixed oxidation states has many advantages over single valence state such as low toxicity [23], high biocompatibility [24], and proven biodegradability in the environment [25]. An additional advantage of  $\text{Fe}_3\text{O}_4$  is targeting using the material’s intrinsic magnetic properties. The developed paramagnetic dispersion field is utilized and redispersed after a pulse of an external magnetic field [26]. To generate a precise and responsive field, it is critical to fabricate  $\text{Fe}_3\text{O}_4$  MNPs with a functionalized polymer coating or graft for a proper response with low biotoxicity [27]. Engineering of materials with a defined size, shape, and electrical characteristics to directly inhibit target cell function is challenging and requires a multifold approach (such as selective coatings, core-forming, and micro- to nanoscale integration) for targeted treatment of cancer cells [28]. One practical disadvantage of the coating process is that the magnetism of the generated MNPs decreases due to the unavoidable presence of a magnetically inactive surface layer, such as methyl methacrylate (MMA) [29]. MNPs with functionalized structure and highly magnetic response in the bulk would solve the concerns of coating and field inhomogeneity [30].

In the chapter, MOFs will be introduced in four parts, the first part will consist of background and introduction to the topic (Section 16.2: Introduction of metal-organic frameworks which includes Section 16.2.1: Metal ions, Section 16.2.2: Organic ligands, Section 16.2.3: Solvent, and Section 16.2.4: Secondary building units). The second part will focus on the synthesis of various topologies and includes Section 16.3: Synthetic method of metal-organic frameworks which includes Section 16.3.1: Nanodeposition method, Section 16.3.2: Solvothermal method, Section 16.3.3: Reverse microemulsion method, and Section 16.3.4: Surfactant-temple solvothermal method. The third section covers characterization and begins with Section 16.4: Characterization of metal-organic frameworks which focuses on Section 16.4.1: Transmission

electron microscope and scanning electron microscope. While characterization by ultraviolet-visible spectroscopy and Raman spectroscopy is important, they are not included here, as the focus is on more advanced techniques, nevertheless would constitute an important component. The final section related to the actual application of the MOF and includes [Section 16.5](#): Application of metal-organic frameworks.

The contributions of this chapter focus on one example used in biomedicine in which we demonstrate that (1) grafting  $\text{Fe}_3\text{O}_4$ -MNPs to introduce amphiphilic groups, (2) producing Fe-based nanoscaled metal-organic frameworks (NMOFs) to generate ultrahigh surface area and high activity [31], (3) characterizing magnetic nanoparticles using a number of analytical techniques, and (4) evaluating cell viability by in vitro cytotoxicity analyses. In this study, we present engineered, characterized (e.g., magnetic, biochemical) and evaluated structural properties of two class of NMs, magnetic nanoparticles (MNPs) and nanoscaled metal-organic frameworks (NMOFs). Importantly, the in vitro toxicity was carried out, indicating that the efficacy is in part due to uniform coating of the core, magnetically ordered surface crystallinity, nanoscale size with ultrahigh surface area (current work), and shape for targeted drug delivery and cancer cell diagnostics (future work).

## 16.2 Metal-organic frameworks

Metal-organic frameworks (MOFs), highly porous materials, which embody the beauty of chemical structures and the power of conjoining organic and inorganic chemistry have drawn the increasing importance [32]. Due to the limitless combinations of metal ions and organic ligands, the topology and morphology of MOFs can be tuned for specific applications. However, to obtain MOFs with certain properties and structures, it requires a reasonable choice of reactants and reaction conditions that include the ratio of metal ions and organic ligands, the temperature and pressure during a reaction, and the solvent in the reacting system [33]. Based on a large number of different reacting possibilities, MOFs can be obtained, which have different properties and applications. The general properties and applications are drawn in [Fig. 16.2](#).

During the progression of porous materials, several names and abbreviations were used, such as MOF, PCN, and MIL. The name and examples of MOFs are listed in [Table 16.1](#).

The framework is sensitive to solvent polarity, synthesis temperature, metal center, and ligand type. In the next part, several main factors are introduced including [Section 16.2.1](#): Central metal ions, [Section 16.2.2](#): Organic ligands, [Section 16.2.3](#): Solvents, and [Section 16.2.4](#): Secondary building units.

### 16.2.1 Metal ions

Metal ions play an important role in controlling the properties, pores, and structures of MOFs. The selection of different metal ions can regulate the assembly process, and different coordination geometries of metal ions can result in different network topology structures.

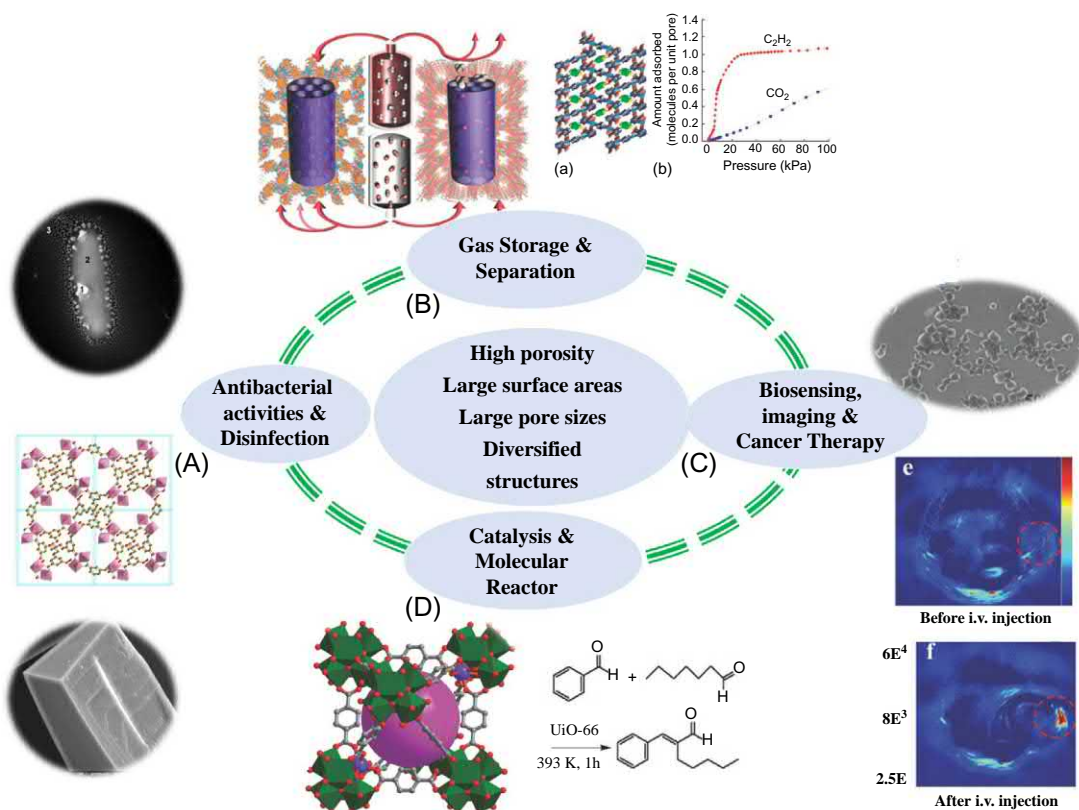


Fig. 16.2

Special properties of MOFs and their applications, (A) MOFs were used for gas capture to mitigate environmental pollution. (B) MOFs were found to increase the potency of antibacterial activities, further enhancing the disinfection and water remediation. (C) Functionalized and gold coshelled MOF high monodispersity and homogeneity were used in cancer imaging to improve biocompatibility and stability. (D) MOFs were used to encapsulate the molecular catalysts into the internal void spaces to fulfill their catalysis. (A) Reproduced with permission from W. Zhuang, D. Yuan, J.R. Li, Z. Luo, H.C. Zhou, S. Bashir, J. Liu, Highly potent bactericidal activity of porous metal-organic frameworks, *Adv. Healthc. Mater.* (2) (2012) 225–238. Copyright (2012) John Wiley and Sons, Inc. (B) Reproduced with permission from J.R. Li, R.J. Kuppler, H.C. Zhou, Selective gas adsorption and separation in metal-organic frameworks, *Chem. Soc. Rev.* 38 (5) (2009) 1477–1504. Copyright (2009) Royal Society of Chemistry. (C) Reproduced with permission from W. Shang, C. Zeng, Y. Du, H. Hui, X. Liang, C. Chi, K. Wang, Z. Wang, J. Tian, Core-shell gold Nanorod@ metal-organic framework nanopores for multimodality diagnosis of glioma, *Adv. Mater.* 29 (3) (2017) 1604381.

Copyright (2017) John Wiley and Sons, Inc. (D) Reproduced with permission from C.D. Wu, M. Zhao, Incorporation of molecular catalysts in metal-organic frameworks for highly efficient heterogeneous catalysis, *Adv. Mater.* 29 (14) (2017) 1605446. Copyright (2017) John Wiley and Sons, Inc.



Table 16.1: Different names of metal-organic frameworks and their examples.

| Abbreviation | Definition                              | Example                                            |
|--------------|-----------------------------------------|----------------------------------------------------|
| MOF          | Metal-organic frameworks                | IR-MOF-15                                          |
| PCN          | Porous coordination networks            | PCN-12                                             |
| MIL          | Materials of Institute Lavoisier        | MIL-HDBK-5                                         |
| ICP          | Infinite coordination polymer particles | ICP-028                                            |
| MZN          | Materials zeolite networks              | MZN-ZSM-E                                          |
| PCP          | Porous coordination polymers            | $n [Zn_2(1, 4\text{-BDC})_2(\text{DABCO})]_n C_6H$ |
| ZIF          | Zeolite imidazole frameworks            | ZIF-8; ZIF-11                                      |

DABCO = 1,4-diazabicyclo [2,2,2] octane.

Until now, the commonly reported metal ions in MOFs are transition metal ions, such as  $Zn^{2+}$ ,  $Cu^{2+}$ ,  $Ni^{2+}$ ,  $Co^{2+}$ ,  $Cr^{3+}$ ,  $Fe^{3+}$ ,  $Ag^+$ , and  $Zr^{4+}$ . The transition metals are elements that have partially filled shells of d-electrons and f-electrons in some of their compounds.

Lanthanide metal ions are relatively new to act as a central element in MOFs [34]. The group of elements with the atomic number increasing from 57 (lanthanum) to 71 (lutetium). Lanthanide elements contain 15 elements—La, Ce, Pr, Nd, Pm, Sm, Eu, Gd, Tb, Dy, Ho, Er, Tm, Yb, and Lu. The lanthanides are f-block elements corresponding to the filling of the 4f electron shell. Compared with other transition metals, lanthanide elements have a larger coordination scope and more flexible coordination geometry [35–38]. As a result, lanthanide MOFs have attracted extensive attention due to their new topologies and special chemical and physical properties arising from the (n-2)f electrons.

Ma et al. had extended 4,4',4''-s-triazine-2, 4,6-triyl-tribenzoic acid ligand for the synthesis of lanthanide MOFs, which includes Dy, Er, and Yb [39]. Due to metal-ligand diversity, different MOFs such as PCN-17 (Dy), PCN-17 (Er), and PCN-17 (Yb) were prepared. PCN-17-type MOFs were used to absorb  $H_2$ ,  $O_2$ ,  $N_2$ , and CO, which showed better selective adsorption of  $H_2$  and  $O_2$  than  $N_2$  and CO (Fig. 16.3).

### 16.2.2 Organic ligands

Organic ligands, also known as an organic linker, play a decisive role in the synthesis of MOFs. A huge diversity of organic ligands has been used for creating MOFs. Different ligands influence the topology structure of MOFs and control the distance of metal ions and the dimension of crystal structures [40]. However, it remains challenges to find methods to well tune the structural characters of MOFs. Organic ligands should contain two or more multidentate functional groups, for example, COOH,  $CS_2H$ ,  $NO_2$ ,  $SO_3H$ , and  $PO_3H$ . Among them, carboxylate ligands are the most common ligands in MOFs due to their strong coordination function and various coordination patterns [41]. For example, (Bpdc2-) 2,2'-bipyridine-5,5'-dicarboxylate is a kind of organic ligands. Based on the different bridging types

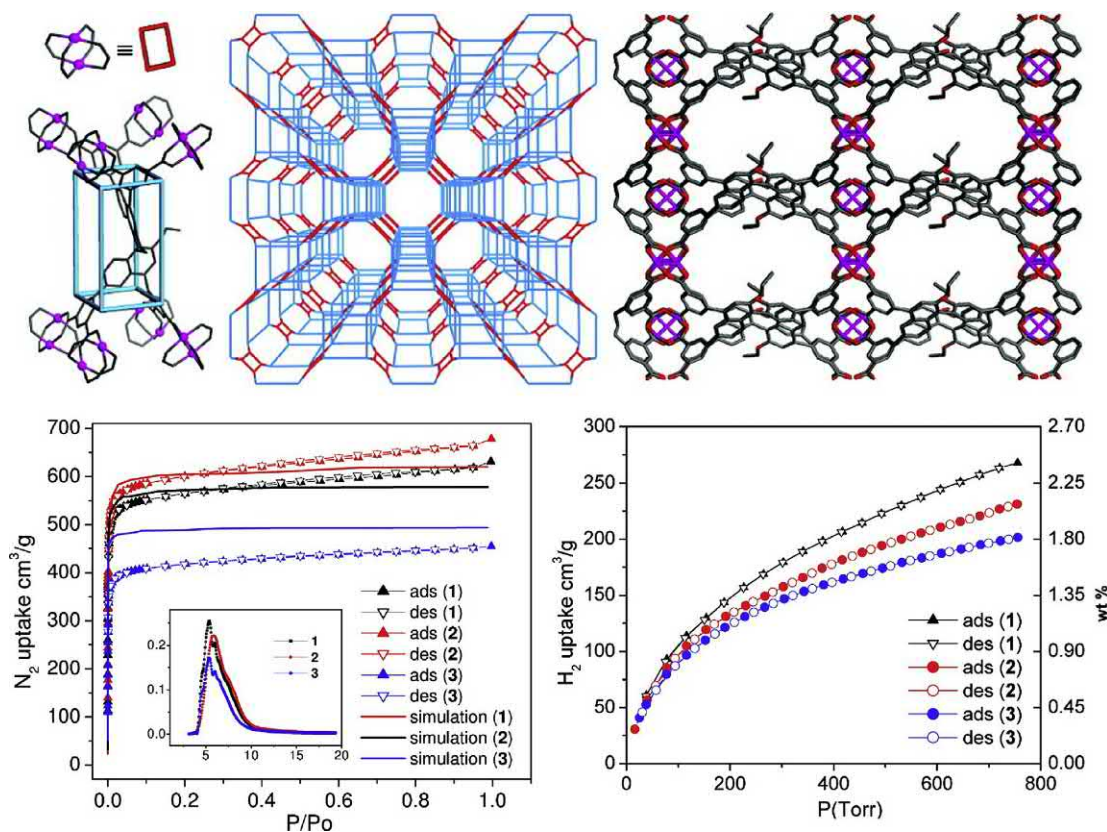
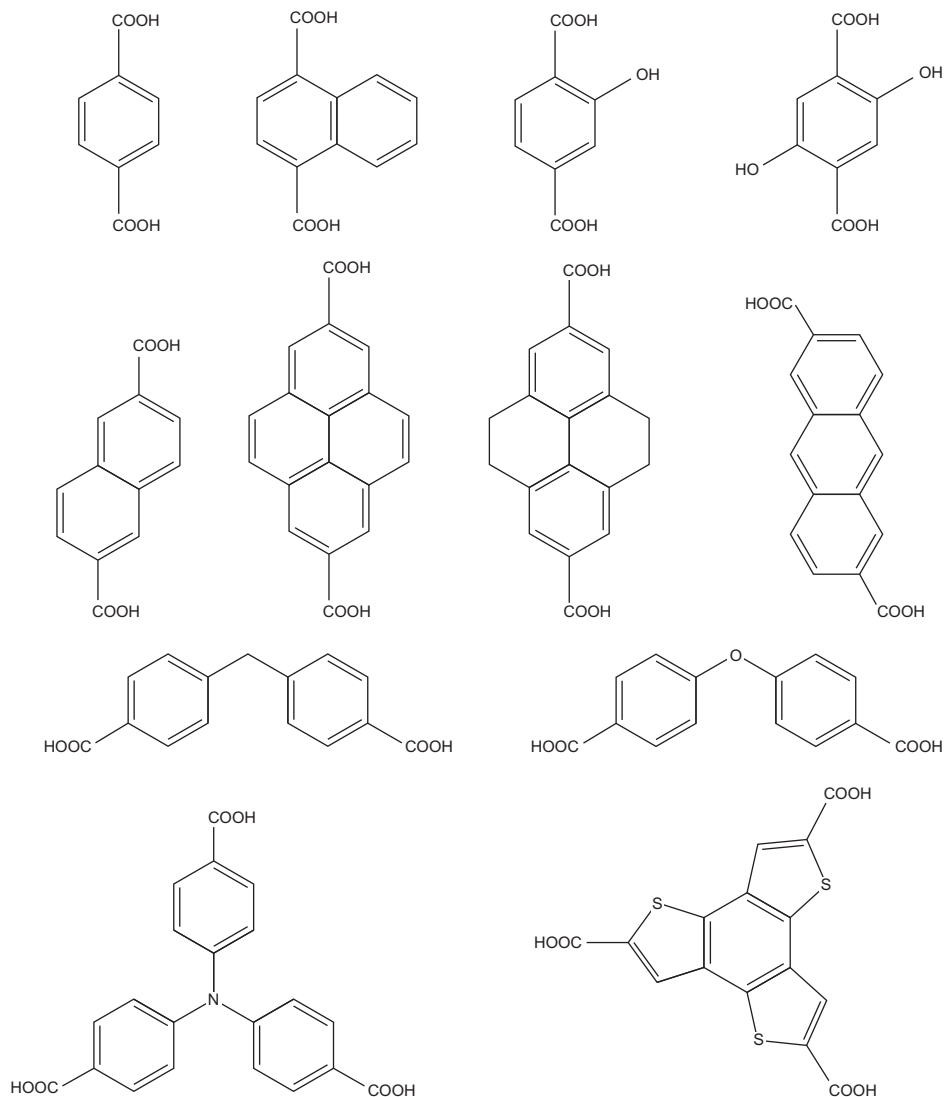


Fig. 16.3

A selected example of copper as the metal center and 1,1'-binaphthyl-derived octacarboxylic acid ligand (L1) primitive cubic network topology with the *top-left* representing a tetragonal distortion of the face-centered cubic structure (P4/mmm or SCU topology) of  $[\text{Cu}_2(\text{O}_2\text{CR})_4]$  paddle wheels (rectangles) and their connectivity with the L1 ligand (prism) in the Cu-MOF1. The *top-middle* is a simplified three-dimensional connectivity scheme of Cu-MOF showing the SCU net-like topology. The *top-right* is a similar image viewed along the horizontal direction, showing 10.6 Å diameter channels. The *lower-left* panel show experimental (main) and calculated  $\text{N}_2$  adsorption isotherms for Cu-MOF1 with ligand L1 (1), Cu-MOF2 with ligand L3 (2), and Cu-MOF3 with ligand L3 (3). Solid triangles (adsorption), open triangles (desorption), and solid lines (GCMC simulation results). Inset shows the pore size distributions (HK method) for 1, 2, and 3 with the x-axis showing pore diameter in Å and the y-axis showing  $Dv(w)$  in  $\text{cm}^3/\text{Å}^3/\text{g}$ , where MOF1, 2 and 3 are  $[\text{Cu}_4(\text{L1})(\text{H}_2\text{O})_4] \cdot 12\text{DEF} \cdot 2\text{H}_2\text{O}$ ;  $[\text{Cu}_4(\text{L2})(\text{H}_2\text{O})_4] \cdot 14\text{DMF} \cdot 2\text{H}_2\text{O}$ ; and  $[\text{Cu}_4(\text{L3})(\text{H}_2\text{O})_4] \cdot 8\text{DMF} \cdot 2\text{H}_2\text{O}$  with L1-H<sub>8</sub>, or L2-H<sub>8</sub>, or L3-H<sub>8</sub> with Cu(II) salts in dimethylformamide (DEF) or dimethylformamide (DMF) at elevated temperatures, respectively with L1 is based around 1,1'-binaphthyl-derived octacarboxylic acid; L2 derived from deprotecting the ethoxy groups of the methyl ester of (R)-L 1 -H<sub>8</sub> and L3 based around 4,4', 6,6'-tetrabromo-2,2'-dibenzyloxy-1,1'-binaphthyl as ligand to form constructing 4,8-connected MOFs of the SCU topology based on copper paddle wheels and aromatics-rich octacarboxylic acid bridging ligands. Reproduced with permission from L. Ma, D.J. Mihalcik, W. Lin, Highly porous and robust 4, 8-connected metal-organic frameworks for hydrogen storage, *J. Am. Chem. Soc.* 131 (13) (2009) 4610–4612. Copyright (2009) American Chemical Society.

**Fig. 16.4**

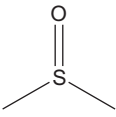
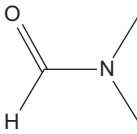
Several different structures of common ligands with different bond angles used in the preparation of MOFs with tunable structures and pore sizes.

ligands can have different angles including 0, 60, 90, 120, and 180 degrees. Some structures of common ligands are listed in Fig. 16.4.

### 16.2.3 Solvent

Most of the metal ions and organic ligands are solid, so both of them need to be dissolved. For the solvent, it needs deprotonating to promote a connection between metal ions and organic ligands. The use of a solvent is an effective method for stabilizing the skeleton of MOFs due to

Table 16.2: Comparison of DMSO and DMF used as a solvent.

| Abbreviation                | DMSO                                                                              | DMF                                                                                 |
|-----------------------------|-----------------------------------------------------------------------------------|-------------------------------------------------------------------------------------|
| Name                        | Dimethyl sulfoxide                                                                | Dimethylformamide                                                                   |
| Chemical formulation        |  |  |
| Molecular weight            | 78.13 g/mol                                                                       | 73.09 g/mol                                                                         |
| Boiling point               | 189°C                                                                             | 153°C                                                                               |
| Density                     | 1.10 g/cm <sup>3</sup>                                                            | 0.94 g/cm <sup>3</sup>                                                              |
| Solubility in diethyl ether | Very soluble                                                                      | Very soluble                                                                        |
| Solubility in water         | Miscible                                                                          | Miscible                                                                            |

the intermolecular interaction between the solvent molecules and the skeleton [42]. The solvent molecules can be used as a guest molecule, which fills in the hole of the compound. And the choice of solvent also affects the structure of MOFs. Recently, the most common solvent is dimethylformamide (DMF) and dimethyl sulfoxide (DMSO). As shown in Table 16.2, the comparison between DMSO and DMF demonstrated their different properties.

#### 16.2.4 Secondary building units

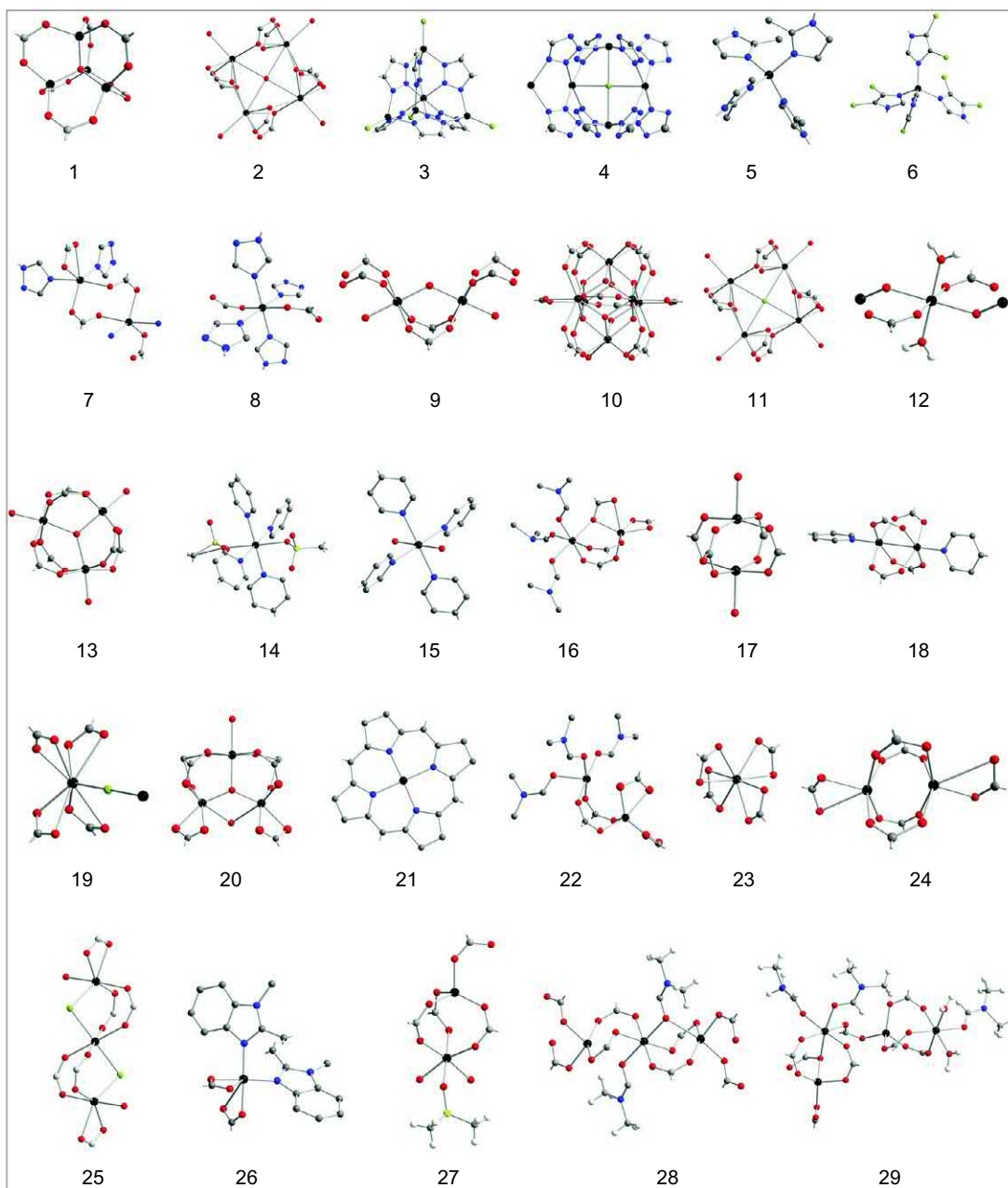
Except for the single metal ion, metal ion clusters are conjunction of metal ions, and organic ligands can be used as inorganic coordination points. And such metal ion clusters are termed as secondary building units (SBUs), which is the basic structure of MOFs. So SBUs play an important role in the study of structures of MOFs [43]. There are 29 types of secondary building units which are shown in Fig. 16.5.

### 16.3 Synthetic method of metal-organic frameworks

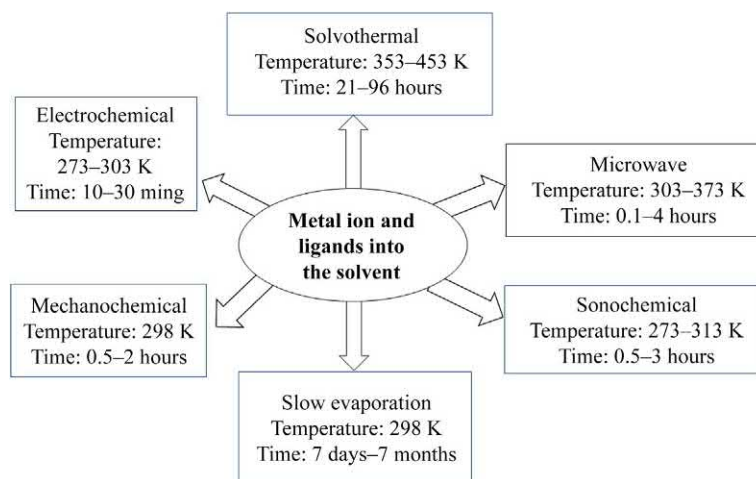
MOFs can be synthesized by some different methods that have been developed for inorganic and organic polymeric nanoparticles [44]. Four general methods can be used to synthesize MOFs: nanodeposition, solvothermal, reverse microemulsion, and surfactant-temple solvothermal methods. Among these four methods, nanoprecipitation is apt to synthesize amorphous materials, while the other three methods can synthesize crystalline materials (Fig. 16.6).

#### 16.3.1 Nanodeposition method

In nanodeposition, which can be used as a typical synthesis method, precursor solutions are mixed at room temperature to allow nanoparticle nucleation and growth. Metal-organic frameworks can be formed due to the particles that are insoluble in the solvent, while the individual metal ions and organic ligands remain soluble.

**Fig. 16.5**

A summary of 29 types of secondary building units (SBUs) involved in cation exchange. *Reproduced with permission from C.K. Brozek, M. Dinca, Cation exchange at the secondary building units of metal-organic frameworks, Chem. Soc. Rev. 43 (16) (2014) 5456–5467. Copyright (2014) Royal Society of Chemistry. Additional MOF symmetry can be found at <https://crystalsymmetry.wordpress.com/nets/mof-nets/>.*



**Fig. 16.6**

A summary of the various MOF synthesis approaches temperatures and time to completion of the crystal [45].

For example, Bilati et al. synthesized nanoparticles in the nanodeposition method. Bilati dissolved the polymer in an organic solvent. Because the polymer was insoluble, then new-formed nanoparticles can be centrifuged to synthesis [34].

### 16.3.2 Solvothermal method

As the requirement for more stable MOFs were accepted, greater problems in crystal nucleation and growth were faced. Under this requirement, the solvothermal method was found as a convenient solution to decrease the synthesis time and to produce more stable metal-organic frameworks. Under the solvothermal method, precursors are always combined with dilute solutions in polar solvents such as water, alcohols, acetone, DMSO, and DMF. While for nanodeposition, nanoparticle nucleation and growth can be achieved at room temperature. The solvothermal method is used at either traditional heating or microwave heating. Due to the high temperature in reaction, more extensive transformations of metal ions and organic ligands occur before MOFs can be obtained. In the solvothermal method, temperatures and heating times provide extra limitations to control the nucleation and growth of MOFs (Fig. 16.7).

For example, indium MOFs were synthesized with 1,4-naphthalene dicarboxylic acid (1,4-NDC) under the solvothermal method (Fig. 16.8) [30, 45].

Both nanodeposition and solvothermal are surfactant-free methods, while reverse microemulsion and surfactant-template solvothermal are surfactant-needed synthesis methods.



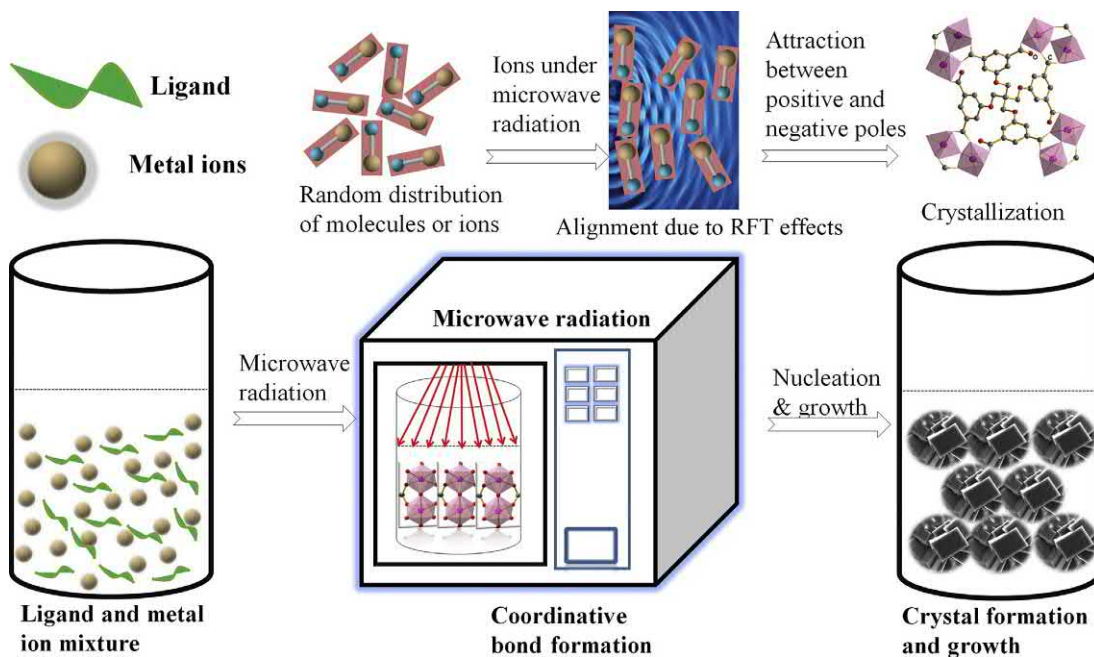


Fig. 16.7

The key procedure of solvothermal method to synthesis MOFs [45].

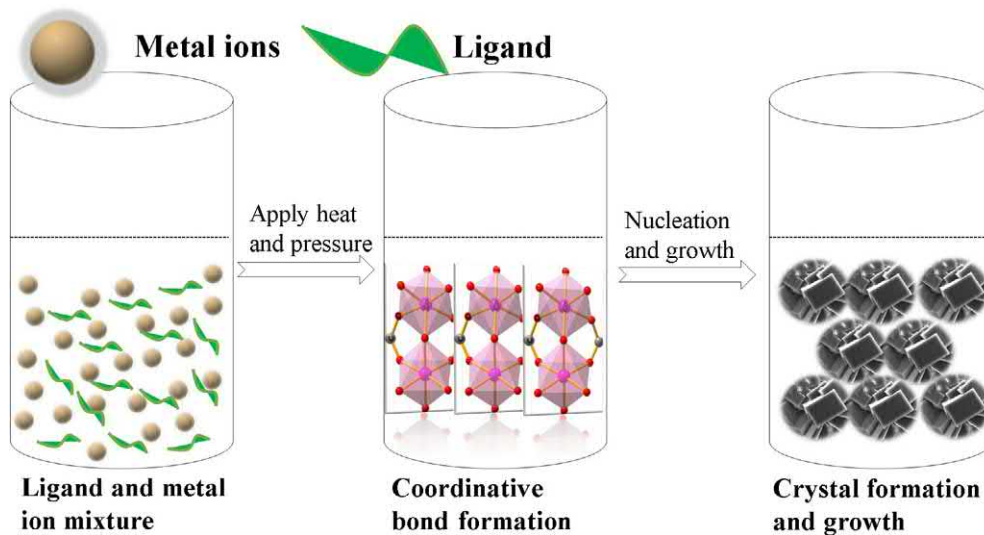


Fig. 16.8

The solvothermal method used to synthesize In-MOFs [45].

### 16.3.3 Reverse microemulsion method

Due to the solubility of metal ions in DMSO, the reverse microemulsion method uses surfactants to stabilize water droplets within a nonpolar organic phase. The addition of a surfactant into the reacting system can promote the kinetic of nano-MOF preparation. This method is found to be user-friendly and cost-effective. Fig. 16.9 shows the procedure of reverse microemulsion method.

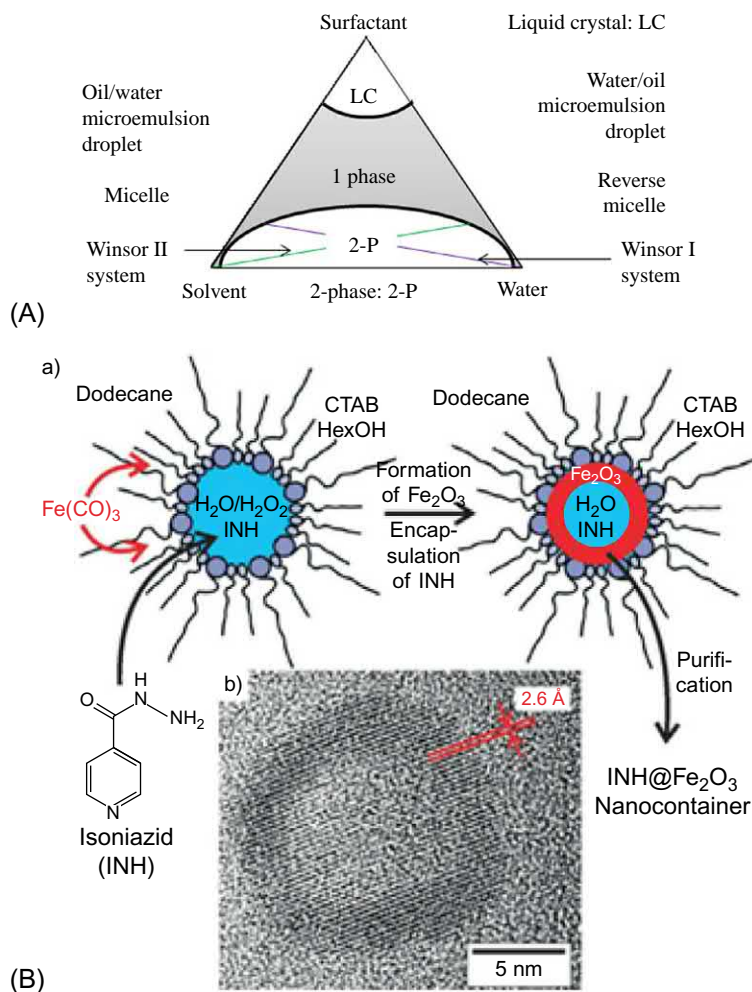


Fig. 16.9

The procedure of reverse microemulsion method used to prepare the nanoparticles, while Liu's group also uses this method to produce Co-MOFs. (A) Summary of microemulsion and reverse emulsion and (B) isoniazid@Fe<sub>2</sub>O<sub>3</sub> hollow nanospheres were synthesized from a standard w/o-ME comprising water, n-dodecane, and HRTEM images. Reproduced with permission from S. Wolf, C. Feldmann, *Microemulsions: options to expand the synthesis of inorganic nanoparticles*, *Angew. Chem. Int. Ed.* 55 (51) (2016) 15728–15752. Copyright (2016). John Wiley and Sons, Inc.

Wang et al. [46] produced aluminum-based porous materials by reverse microemulsion method. The method consists of water-based domains dispersed in an oil phase solvent. As a conclusion, some nanosized MOFs can be synthesized in the water-based domains. So reverse microemulsion is an ideal method to synthesize special functional material, which is not stable at high temperatures and high pressure. Based on this method, Liu's group prepared Co and Cu-based MOFs using BDC as ligands.

#### 16.3.4 Surfactant-template solvothermal method

Surfactant molecules can be used to template the synthesis of MOFs under solvothermal conditions. In a surfactant-template solvothermal method, surfactant molecules show significant influence in defining MOF morphologies.

He et al. [47] synthesized cobalt oxide ( $\text{Co}_3\text{O}_4$ ) nanoparticles by surfactant-template solvothermal method. Both the surfactant and high temperatures made the procedure quickly and stable. As a result, these nanoparticles showed oriented aggregation, which attracted lots of interest. They can be seen as a potential way of creating advanced materials with distinguished topology and structures.

To summarize, the discussion in the preceding text elaborates on four general synthesis methods, and each method has its unique features. Table 16.3 lists the comparison of these four different methods.

### 16.4 Characterization of metal-organic frameworks

To evaluate the morphological and crystalline structure, a series of characterization methods should be used to examine properties and topologies of organometallic compounds [48]. In sample characterization, transmission electron microscope, scanning electron microscope, ultraviolet-visible spectroscopy, and Raman spectroscopy are used as characterization methods.

Table 16.3: Comparison of four different synthesis methods.

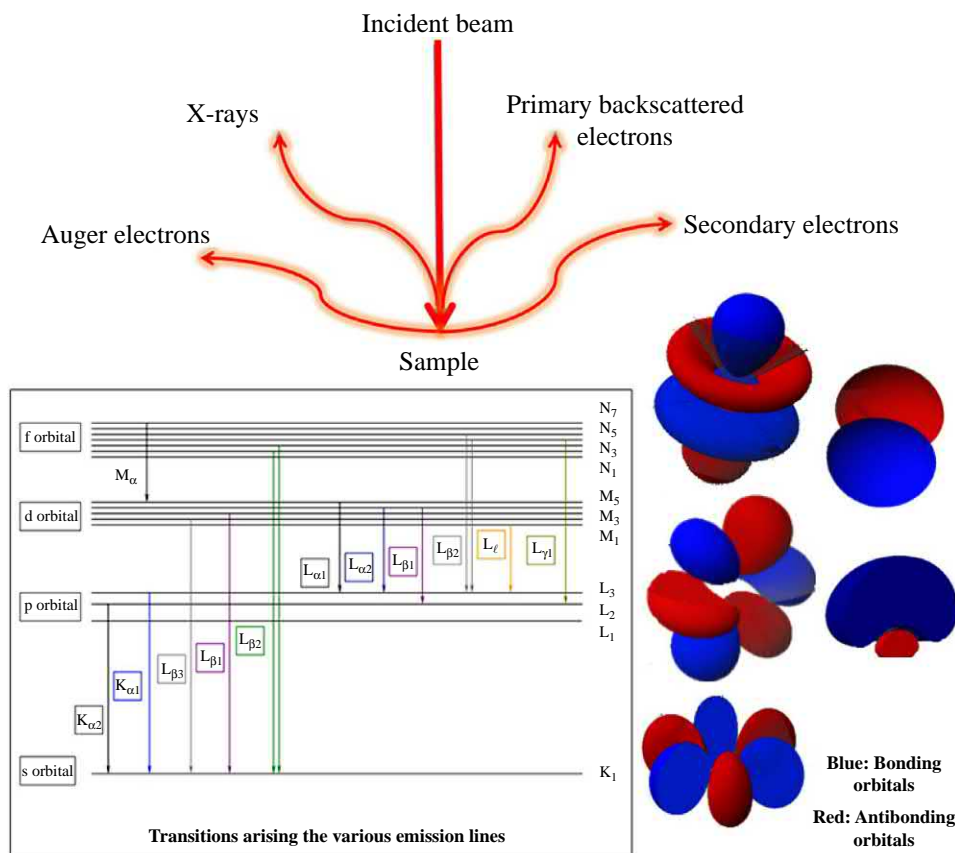
| Synthesis method                 | Temperature          | Surfactant | Crystalline product |
|----------------------------------|----------------------|------------|---------------------|
| Nanodeposition                   | Room temperature     | No         | No                  |
| Solvothermal                     | Heating or microwave | No         | Yes                 |
| Revers microemulsion             | Room temperature     | Yes        | Yes                 |
| Surfactant-template solvothermal | Heating or microwave | Yes        | Yes                 |

### 16.4.1 Transmission electron microscope and scanning electron microscope

Electron microscope (EM) is a microscope using accelerated electrons instead of light for illuminating and using static electrical lenses to focus particles. EM has a much higher resolving power than an optical microscope so it can be used to explain the smaller structure than an optical microscope [49]. In the research, transmission electron microscope (TEM) and scanning electron microscope (SEM) were used to examine the tunable structure of MOFs. In both transmission and scanning electron microscope, the electron gun will emit the electron gun by thermionic, Schottky, or field emission. The generated electrons were monochromatic after being focused into a beam with magnets. The condenser lens systems allow for variations of the illumination aperture and the area of the sample measured. When the electron beam generated via high voltage (120–200 keV), various species are created once the electron beam hits the sample. These species are backscattered electrons, secondary electrons, Auger electrons, x-rays, unscattered electrons, elastically scattered electrons and inelastically scattered electrons [50]. In both SEM and TEM systems, the x-rays are produced when an incident electron causes a secondary electron to leave an atom [51]. A vacancy is produced in an orbital near the nucleus; therefore an electron from an outer shell of the atom will fall to fill the vacancy near the nucleus, creating a surplus of energy (Fig. 16.10). This surplus of energy is released as x-rays, which have unique energies associated with a specific atom. These x-rays are used to determine the elemental composition of the specimens (Figs. 16.11 and 16.12).

The transmission electron microscope (TEM) consists of a high voltage electron beam, electron gun, electrostatic and electromagnetic lenses, objective lens, and fluorescent viewing screen. Fig. 16.11 shows the operational principle of TEM, along with the information collected. The accelerated electrons with high energy can move in a straight line and be transmitted through the thin layer of samples (50–200 nm). These transmitted electrons will be used to generate TEM images. Multiple electromagnetic lenses focus the electrons into a fine beam. The first condenser lens determines the general diameter of the beam (commonly known as spot size) when the electrons hit the sample of interest. The second condenser lens determines the brightness or intensity of the beam on the sample. The beam then passes through an aperture that filters those untightly bound in the beam from traveling through the sample.

A scanning electron microscope (SEM) is another type of electron microscope that produces images of a sample by a focused electrons beam. In the SEM system, the high energy beams of electrons interact with the samples. The secondary and backscattered electrons will be generated and collected to produce scanning electron micrographs [52]. When an incident electron strikes the sample and is bounced back from the sample, backscattered electrons were formed. The elements with higher atomic numbers absorb more incident electrons. Therefore fewer electrons will be backscattered, which will produce higher contrast to different elements. Additionally, when an incident electron strikes the sample, the secondary electrons will be generated. The electron from the sample with surplus energy will be ejected by atoms close (10 nm) to the surface of the sample and are highly influenced by the topography of the sample.



**Fig. 16.10**

The elemental composition analyses using x-ray energy dispersive spectroscopy: the excitation of electrons from a ground state to the excited state, corresponding to the s (K line), p (L line), d (M line), and f (N line) orbitals, and (right-hand side) molecular rendering of the topography of the  $fz_3$ ,  $fxz_2$ , and  $fx$  planes. Orbitals reprinted with permission from Alen Hadzovic, Chapter 2, *Open Inorganic Chemistry*, <https://open-inorganic-chemistry.digitalscholarship.utscc.utoronto.ca/node/41>. Copyright (2018). The University of Toronto Scarborough.

Both backscattered and secondary electrons will be collected to produce SEM images. The secondary electrons are the most used signal to depict the morphology of the sample's surface. Fig. 16.11 shows the key features and simplified operational principles of SEM, as well as the micrographs obtained.

There are numerous similarities between TEM and SEM. Both are types of electron microscopes and provide the images of visualizing, reviewing, and examining small particles or compositions of a sample [53]. Although images produced from both TEM and SEM instruments are at ultrahigh resolution, important differences remain. Firstly, the basic

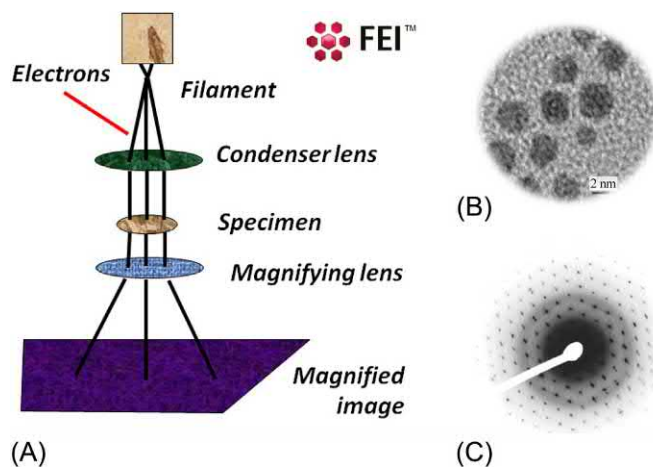


Fig. 16.11

The systematic construction of transmission electron microscope.

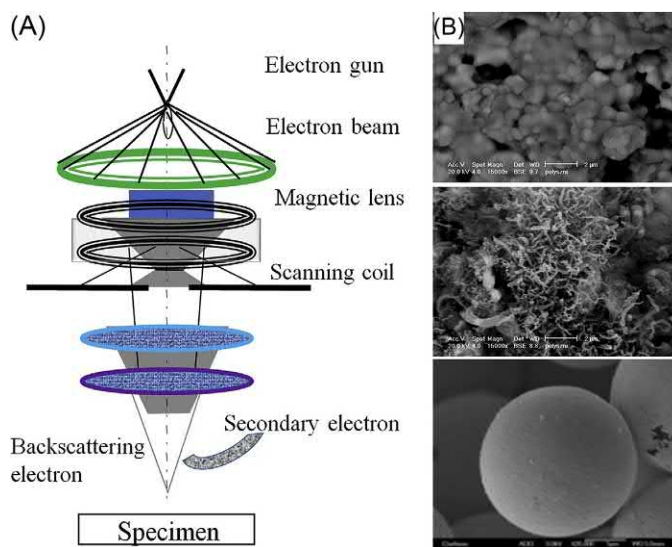


Fig. 16.12

The simplified operational principle of SEM, including an electron gun, a vacuum system, a magnetic lens, and a specimen.

operating principle is different. TEM operates based on transmitted electrons, whereas SEM is based on backscattered and secondary electrons. Secondly, SEM and TEM collect different electrons that are generated upon sample-electron beam interaction. TEM (Fig. 16.12) collected transmitted electrons, allowing for analysis of the internal structure of the samples. SEM collects scattered electrons, leading to surface analysis. Thirdly, SEM and TEM show different types of images. SEM characterizes samples line by line and provides a three-dimensional



(3-D), image while TEM shows samples as a whole and provides a two-dimensional (2-D) image. Fourthly, TEM has an advantage compared with SEM in resolution. TEM can display higher resolution (0.5 Å) than SEM (4 Å). SEM also has its advantage in showing a larger scope of samples than TEM can process.

## 16.5 Application of metal-organic frameworks

MOFs can be used to absorb CO<sub>2</sub> for air cleaning, to store different kinds of energy gas (hydrogen, methane, and acetylene) and catalyst and to separate different gas (carbon dioxide and nitrogen and methane and hydrogen) [54–56]. Additionally, due to the high surface areas with large pore sizes, MOFs can also be used in drug delivery, cancer theragnostic, and antitoxicity application [57–60].

### 16.5.1 Gas storage

The current worldwide concentration of greenhouse gases from energy production has drawn attention to the use of noncarbon or carbon with less generation of waste with gas storage as a primary aim in energy production via hydrogen storage. Gas storage requires a structured storage system, large capacity, low cost, and ease of use. The biggest challenge is how to store hydrogen safely and economically. There are three basic ways to store hydrogen—storing hydrogen in a tank, storing hydrogen as a chemical compound, and storing hydrogen in MOFs. The storing of H<sub>2</sub> in MOFs is based on physioabsorption. MOF scaffolding is of interest due to their high porosity, large internal surface area, diversity of structures, and easily regulated skeleton. PCN-6, a copper porous MOF, was synthesized and confirmed that it can absorb 0.072-kg/kg hydrogen at 77 K, which can be used in hydrogen storage [61–63].

### 16.5.2 Catalyst

MOFs are made of inorganic metal ions and organic ligands, and both of these two components can be used as a catalysis point. Some precedents in recent research have shown that some MOFs with available metal sites can use as a catalyst [64]. Xamena et al. [65] had synthesized Pd-containing MOFs with the molecular formula [Pd(2-pymo)<sub>2</sub>]<sub>n</sub> (2-pymo = 2-hydroxypyrimidinolate). The Pd-based MOF has two different hexagonal windows with a free opening of 4.8 and 8.8 Å and with a fraction of 42% of the crystal volume available to absorbed guests. The research had shown that Pd-MOF exhibits the distinctive behavior of palladium catalysts, promoting the C—C cross coupling, aerobic oxidation, and hydrogenation reactions [65–70].

### 16.5.3 Biological application

The traditional therapeutic molecules are limited since they have important drawbacks such as low stability in biological conditions, poor solubility, and high side effects [71–73]. As a result, a special devotion to the development of structures that satisfy the better control of drug delivery is really important [74]. Since the 1970s, the drug nanocarriers have been sought to find enhanced methods to increase intracellular diffusion and drug's efficiency [75–77]. MOFs as crystalline materials have soon become an unexceptionable alternative due to their combination of a tunable high and systematic porosity [78–84]. MOFs have several advantages over traditional nanomedicines such as chemical diversity, high filling capacity, and essential biodegradability [85–88]. Zhuang et al. prepared Co-TDM MOFs, which exhibited high potency with high ability and long-term stability to inactivate *Escherichia coli* similar to Ag-TiO<sub>2</sub> nanoparticles but at a lesser dose and with faster kinetics [89]. The mechanism for inactivation was found that the lipid membrane was interrupted by reactive oxygen species (ROS), causing cell death. The ROS are chemically reactive molecules containing oxygen. When cell environment changed, ROS can be formed by several mechanisms, including the interaction of ionizing radiation with biological molecules, as an unavoidable by-product of cellular respiration, and synthesized by dedicated enzymes in phagocytic cells like neutrophils and macrophages. Due to their strong oxidability, ROS can damage other molecules and the cell structure of which they are located before. When adding MOFs into a cell, the environment has changed so that it will cause the formation of ROS. In-depth, ROS can lead to apoptosis [90–96].

## 16.6 Materials and methods

The cited example in the succeeding text focuses on synthesis, characterization, and biological application of organometallic compound, especially for transition metal-organic frameworks, unless specified, all chemicals, solvents, and reagents were obtained from VWR International, (West Chester, PA), Sigma-Aldrich (St. Louis, MO), and from Tianjin Chemical Manufacturer, China. Double-distilled and filtered ultrapure water was used (Ultraopure, Barnstead, Dubuque, IA), where the water-based solvent was necessary. All solvents were reagent or high-performance liquid chromatography (HPLC) grade.

A facile reverse microemulsion approach is demonstrated in this review to prepare Fe<sub>3</sub>O<sub>4</sub> MNPs. To prevent Fe<sup>2+</sup> cation from being oxidized, inert gas (Ar) was used. A surfactant as a dispersing agent (C<sub>16</sub>H<sub>26</sub>O<sub>2</sub>) was used to prevent particle agglomeration to achieve monodispersion. The NMOFs were synthesized using a top-down approach via a facile hydrosolvothermal to generate different formulations. Four ligands were used to produce MOFs. Two of them (such as 2'-hydroxy-1,1',3',1''-terphenyl-4,4'',5'-tricarboxylic acid [HTTA, C<sub>21</sub>H<sub>14</sub>O<sub>7</sub>]) and 2'-amino-1,1':3',1''-terphenyl-4,4'',5'-tricarboxylic acid, [ATTA, C<sub>21</sub>H<sub>15</sub>NO<sub>6</sub>]) were produced in two steps: substitution and hydrolysis. The selected ligands

were then mixed with  $\text{Fe}(\text{NO}_3)_3$ , which is a mixed aqueous-dimethyl sulfoxide ( $\text{C}_2\text{H}_6\text{OS}$ , DMSO) solution. The coordinative reaction occurred at  $80^\circ\text{C}$  for about 72 h in a sealed 2-mL vial to allow for crystallization.

The crystalline structure of NMs was investigated by Bruker D8 Advance x-ray diffractometer (XRD) using the copper (Cu)  $\text{K}\alpha_1$  line. The operating conditions were controlled at a voltage of 40 kV and a current of 40 mA, respectively. The scanning range varied from 10 to 100 degrees with a scanning rate of 0.02 degrees/s. The diffraction data were collected at 173 K with a Bruker AXS Smart APEX-II diffractometer using  $\omega$  rotation scans with a scan width of  $0.5^\circ$  and Mo  $\text{K}\alpha$  radiation ( $\lambda = 0.71073 \text{ \AA}$ ). The structures were solved by direct methods and refined by full-matrix least-squares refinements based on F2 using SHELXTL [25]. All nonhydrogen atoms were refined anisotropically with the hydrogen atoms added to their geometrically ideal positions and also refined isotropically. The SQUEEZE routine of PLATON was applied to remove the contributions to the scattering from the disordered solvent molecules in the cavities [26]. The JEM 2010 and FEI G2-F20 transmission electron microscope (TEM) was operated at 200 kV to study the morphology and crystallinity of the NMs. Magnetic properties of a series MNPs were measured using a Lakeshore 7304 vibrating sample magnetometer (VSM) instrument with an applied magnetic field up to 12 kOe at ambient temperature.

Cytotoxicity of NMs was performed against the Chinese hamster ovary (CHO-normal ovarian cell line). A total of  $2 \times 10^4$  cells in 200  $\mu\text{L}$  of medium per well were placed on a 96 well plate. Following overnight incubation (12 h, up to 3 days), the medium was replaced with media containing NMs at different concentrations ( $\mu\text{g}/\text{mL}$ , 1:5, 1:10, 1:50, 1:100, and 1:500) in separate wells. After 24 h of incubation, the medium was removed, and the cells were washed thrice with ice-cold phosphate-buffered saline (PBS) to remove NMs. An aliquot of 50  $\mu\text{L}$  of [3-(4,5-dimethylthiazol-2-yl)]-2,5-diphenyltetrazolium bromide (MTT,  $\text{C}_{18}\text{H}_{16}\text{BrN}_5\text{S}$ , 5 mg/mL) was added in each well. Following incubation for 4 h, formazan crystals formed were dissolved in 150  $\mu\text{L}$  of DMSO, and absorbance at 570 nm was measured using NOVOstar plate reader (BMG lab technologies, Cary, NC, USA). The percentage viability was calculated by comparing the absorbance of treated cells with untreated control cells, which have 100% viability.

## 16.7 Results and discussions

In this review, a reverse microemulsion wet-chemistry approach is shown to prepare  $\text{Fe}_3\text{O}_4$ -MNPs and hydrosolvothermal chemistry to produce Fe-based NMOFs. These NMs were characterized to evaluate their nanostructure and crystallinity. The magnetic properties of metal oxides were also evaluated and discussed in the succeeding text. Importantly, these nanomaterials were tested on Chinese hamster ovary cell (CHO) lines to determine their in vitro toxicity.

## 16.8 Formation and characterization of nanomaterials

As stated previously, two types of NMs were designed and fabricated; magnetic metal oxide nanoparticles (MNPs) and nanoscale metal-organic frameworks (NMOFs), which upon synthesis were characterized. The  $\text{Fe}_3\text{O}_4$ -MNPs ( $6.5 \pm 1.0$  nm) were obtained via an inverse emulsion wet chemistry. The introduction of nitrogen inert gas successfully prevented the  $\text{Fe}^{2+}$  cations from being oxidized, while agglomeration of the MNPs was inhibited using a dispersing agent, polyoxyethylene octylphenol ether (OP-10,  $\text{C}_{16}\text{H}_{26}\text{O}_2$ ). Another key step was grafting the  $\text{Fe}_3\text{O}_4$  core using methyl methacrylate (MMA,  $-\text{[C}_5\text{H}_8\text{O}_2\text{]}_x-$ ) monomer to form a core-shelled structure and to ensure high biocompatibility of MNPs [97]. This hydrophobic-hydrophilic compatibility was achieved using 3-methacryloxy-propyltrimethoxy-silane (KH570,  $-\text{[C}_{10}\text{H}_{20}\text{O}_5\text{Si}]_x-$ ), a silane coupling agent with amphiphilic groups, which introduce chemically active sites. The coupling process introduced hydrophobic groups, surrounded by  $\text{Fe}_3\text{O}_4$  cluster(s) for functionalization (cf. Fig. 16.13A). The process also allowed for facile grafting of MMA monomer onto the surface of  $\text{Fe}_3\text{O}_4$  core. Consequently, the MMA monomers were grafted onto the hydrophobic  $\text{Fe}_3\text{O}_4$  core (cf. Fig. 16.13B). It was found that the grafted  $\text{Fe}_3\text{O}_4$ -MNP polycrystals were composed of face-centered cubic (fcc) obtained from x-ray powder diffraction. The unit cell geometry consisted of stoichiometric iron (Fe) and oxygen (O).

High-resolution transmission electron microscopic (TEM) images of the grafted MNPs (cf. Fig. 16.13C) indicate that the MNPs are near spherical and monodisperse. The ring pattern (insert in Fig. 16.13C) indicated that these grafted  $\text{Fe}_3\text{O}_4$  MNPs are highly crystalline. The ring patterns result intrinsically from the polycrystalline units. From our observation, it can be seen that the crystalline phase of  $\text{Fe}_3\text{O}_4$  MNPs was maintained essentially identical to the pure  $\text{Fe}_3\text{O}_4$  MNPs, regardless of functionalization reported by Yao [97] or grafting by polymer (this study). The XRD studies (Fig. 16.13D and insert) of the grafted MNPs also suggest an ordered crystalline phase of  $\text{Fe}_3\text{O}_4$ -MNPs as a major factor in the determination of their strength of coercivity (discussed later).

Briefly, the iron-based nanoscale metal-organic frameworks (Fe-NMOFs) are generated by a hydrosolvothermal approach to produce a well-defined structure with highly crystallized coordinative compounds (Fig. 16.14A: structural formulae of selected ligands). The selected ligands were composed of amphoteric groups as an organic linker to enhance the biocompatibility. The nucleation of Fe-NMOF crystal units was promoted when the DMSO solvent molecules were evaporated from the solution. One advantage of this synthesis is that diffusion of reactants in the liquid phases is several orders of magnitude faster than in the solid phase, suggesting these synthetic methods can be employed at much lower temperatures. This rapid nucleation favored the formation of Fe-NMOFs along a defined-axis with controllable size and monodispersity. It was also found that the organic linker regulated the size and stability of NMOF crystals, successfully. For example, the combination of Fe(III) with

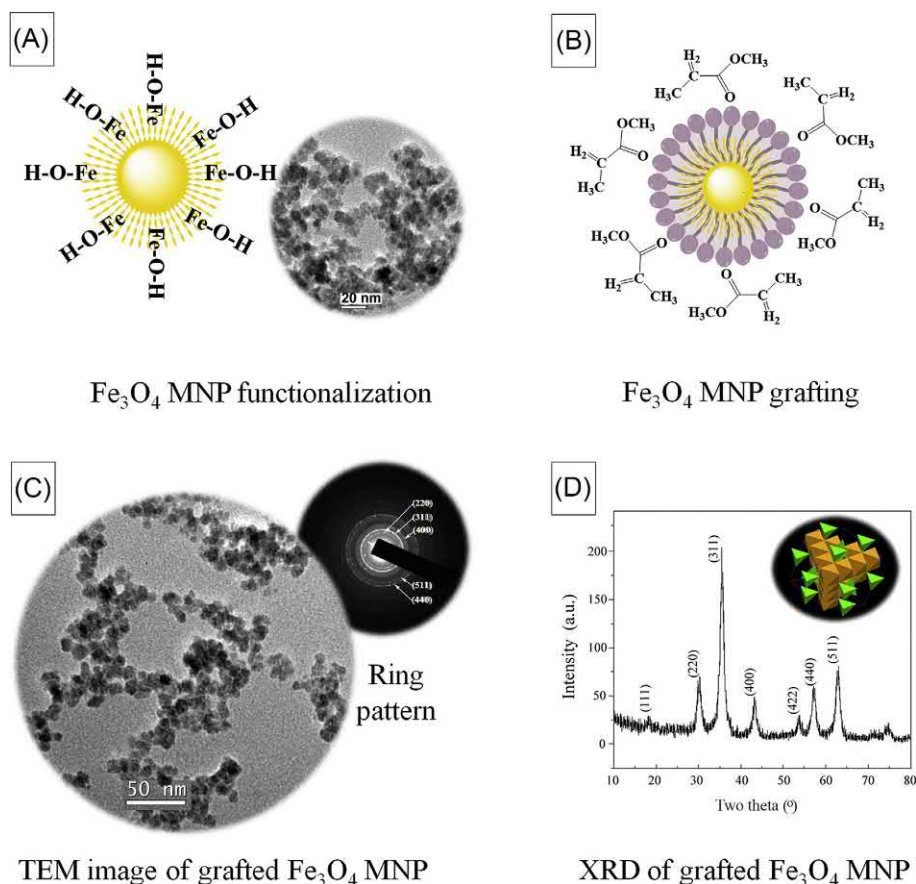


Fig. 16.13

Synthesis, surface grafting, and characterization of  $\text{Fe}_3\text{O}_4$  magnetic nanoparticles (MNPs) to control the particle size, shape, and magnetic property: (A) functionalization of hydrophilic MNPs by reverse microemulsion and modification of these MNPs with silane coupling agent 3-glycidyl-propyl-methoxy silane (KH570), (B) grafting  $\text{Fe}_3\text{O}_4$  MNPs using MAA monomer to increase solubility in water, (C) TEM images and ring pattern of grafted  $\text{Fe}_3\text{O}_4$  MNPs, and (D) x-ray powder diffraction of grafted  $\text{Fe}_3\text{O}_4$  MNPs [45].

benzene-1,4-dicarboxylic acid (BDC) ligand leads to the formation of Fe-NMOFs. x-Ray crystallography (cf. Fig. 16.14B) indicated that the well-crystallized Fe-NMOF has a hexagonal space group  $P63/mmc$  ( $a = 14.278(4)$  Å,  $c = 17.358(6)$  Å, and  $\alpha = 90$  degrees and  $\beta = 120$  degrees). Fe-NMOFs exhibit a porous six connected framework built by linear BDC ligands and six connected oxo-centered trinuclear clusters in which the Fe metal ions are randomly distributed over the crystallographically equivalent metal sites. The ratio of the Fe ions was refined assuming a simultaneous occupation in a 1:1 ratio. The framework topology of Fe-NMOFs is the same as the reported MOFs including Fe-MIL-88 and  $\text{Sc}_3\text{O}(\text{BDC})_6$ , which have a well-defined topology known as the acs net [98, 99]. As expected, the so-prepared

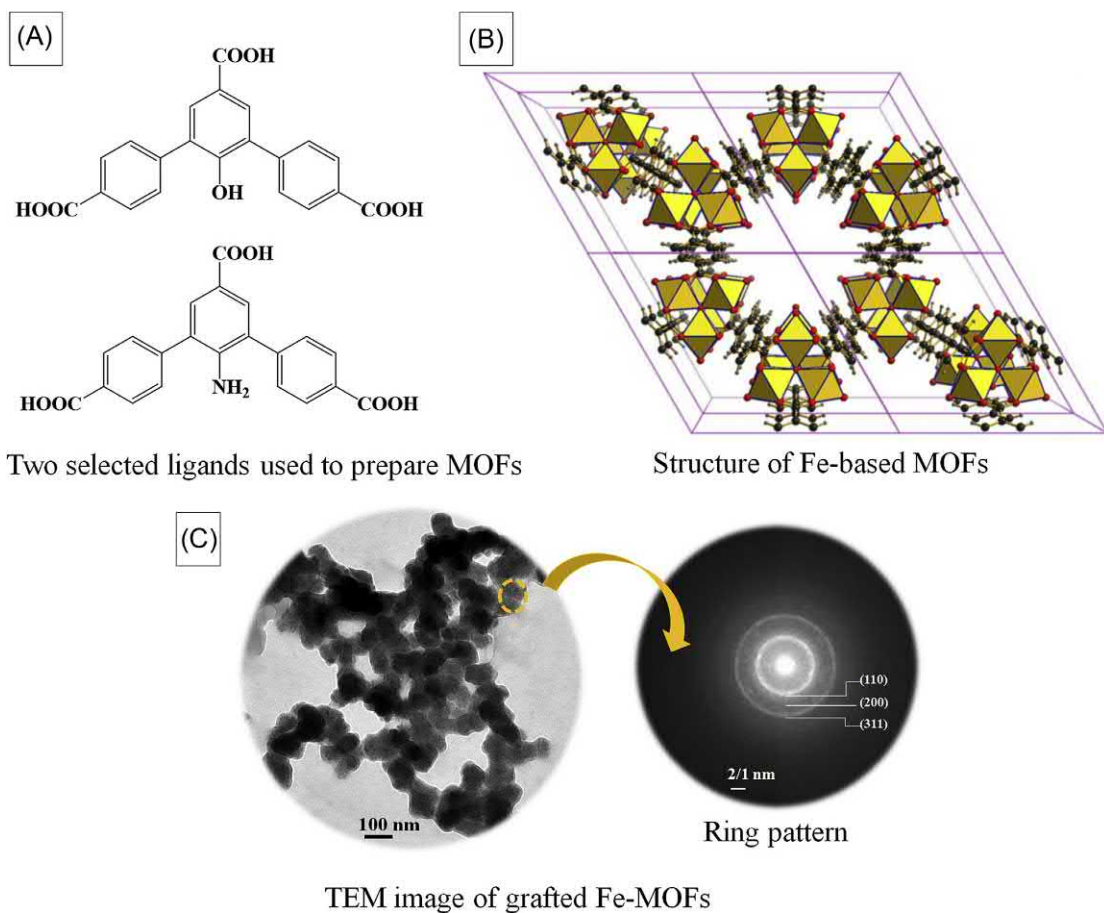


Fig. 16.14

The synthesis and characterization of nano-metal-organic frameworks (NMOFs) using amphiprotic linkers to enhance its biocompatibility: (A) the selected amphiprotic ligands used in this study, (B) the single-crystal x-ray diffraction to elucidate the formation of NMOFs, and (C) the TEM image of a selected Fe-NMOFs and its ring patterns [45].

Fe-NMOFs are highly porous with the theoretical pore volume of  $0.78 \text{ cm}^3/\text{g}$  and an accessible surface area of  $2539 \text{ m}^2/\text{g}$ . TEM images of the Fe-NMOFs (cf. Fig. 16.14C) indicate that near-spherical and monodisperse MOFs were obtained from this solvothermal chemistry. The ring pattern (insert in Fig. 16.14C) also indicated that these MOFs are highly crystalline, corresponding to the single-crystal x-ray analysis.

Our study indicated that the liquid phase of the hydrosolvothermal fabrication is a key process in the fabrication of the precursor film, allowing for rapid diffusion of reactants and growing the precursor to a defined dimension and crystallinity, such as inverse spinel or cubic close-packed lattice(s). Therefore uneven particle growth will be inhibited, resulting in true nanoscaled



homogeneous-coated materials [100]. Our methodology displayed the additional advantage of being cost-effective and flexible, allowing for homogeneous control at the molecular level [101]. Both wet-chemistry approaches also utilize green-synthesis fabrication minimizing generated waste by-products compared with other approaches [102]. In summary, this approach will allow the formulation of monodispersed particles with uniform shapes synthesized under ambient conditions [103].

## 16.9 Magnetic properties of metal oxides

The magnetic property study indicated that the intrinsic coercivity of the  $\text{Fe}_3\text{O}_4$ -MNPs was affected upon modification. The coercivity was determined from the hysteresis loop (magnetization curve). The hysteresis loops of bulk  $\text{Fe}_3\text{O}_4$ -MNPs [97] and four grafted  $\text{Fe}_3\text{O}_4$  MNPs (cf. Fig. 16.15) indicated that both pure  $\text{Fe}_3\text{O}_4$  (cf. Fig. 16.15A) and grafted MNPs

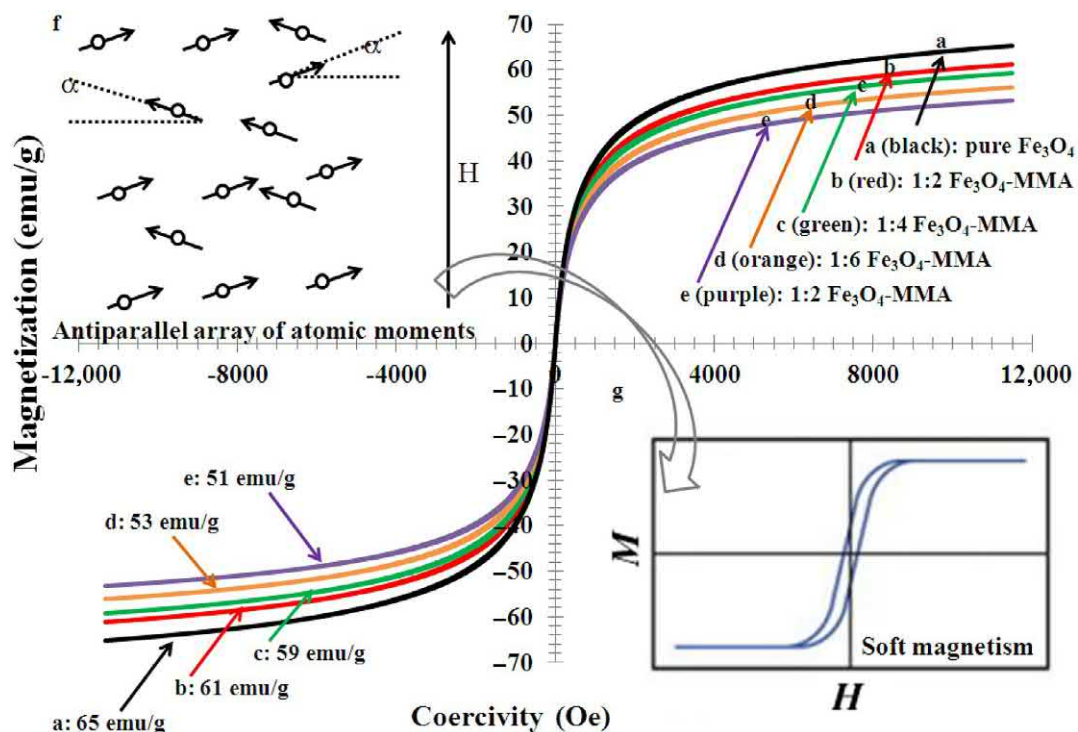


Fig. 16.15

Magnetic property analyses of MNPs derived from a reverse microemulsion. Totally five plots are shown to demonstrate magnetism of one pure  $\text{Fe}_3\text{O}_4$  MNPs and four grafted  $\text{Fe}_3\text{O}_4$  with various stoichiometric amounts of MMA monomer: (A) the magnetization of pure  $\text{Fe}_3\text{O}_4$  MNPs, (B–E) grafted  $\text{Fe}_3\text{O}_4$  MNPs with MMA monomer (molar ratio [mol/L, c/c] of  $\text{Fe}_3\text{O}_4$  MNPs versus MMA = 1:2, 1:4, 1:6, and 1:8 c/c), (F) the schematic of magnetic moment of material, and (G) the generic hysteresis loop of soft magnetic nanomaterials.

(cf. Fig. 16.15B–E) exhibited soft ferromagnetic behavior, due to its near-zero coercivity,  $H_c$  value. The measured magnetic hysteresis loop was attributed to the inverse spinel  $\text{Fe}_3\text{O}_4$  phase. In the bulk phase  $\text{Fe}_3\text{O}_4$ , magnetization mainly arises from electrons occupying the d orbitals, in which the octahedral Fe cations (configuration  $[\text{Ar}]4s^03d^5$ ) are coordinated by O. Five unpaired electrons in the Fe 3d orbitals indicate a high degree of magnetism of  $\text{Fe}_3\text{O}_4$  MNPs. The magnetic properties of these  $\text{Fe}_3\text{O}_4$  MNPs are anticipated to decrease by grafting with nonmagnetic MMA, due to the shielding effect of this nonmagnetic layer (cf. Fig. 16.15F). With the increased amount of addition of MMA, the magnetic intensity was found to be reduced by about 14%, accordingly. The strong ionic bonding between Fe and O also advanced the hybridization of d orbitals of Fe with 2p orbital from oxygen, forming bonding and antibonding orbitals. The occupancy of these orbitals was affected by the degree of MMA incorporation, which determined the bulk magnetic behavior. Therefore it is expected that the fabrication process to produce MNPs with increased surface area and decrease particle size can be achieved through collective control of the contribution of the capped surface magnetization density (cf. Fig. 16.15G).

### 16.10 *In vitro* toxicity evaluations

Cytotoxicity tests of grafted  $\text{Fe}_3\text{O}_4$ -MNPs and Fe-NMOFs were performed in the Chinese hamster ovary (CHO-normal ovarian cell line) model. Low dose particles incubated cells for 24–72 h, under standard conditions. Both classes of MNP and NMOFs exhibited less toxicity (65%–85% cell viability) than iron oxide NPs alone and reveal biocompatibility in the of 0.1–10  $\mu\text{g}/\text{mL}$  (1  $\mu\text{g}/\text{mL}$  = 1 ppm) concentration range. The results suggest that grafted  $\text{Fe}_3\text{O}_4$ -MNPs coated with bipolar MMA and amphiprotic Fe-NMOFs are biocompatible and promising for bioapplications such as drug delivery, magnetic resonance imaging, and magnetic hyperthermia. At concentrations higher than 100  $\mu\text{g}/\text{mL}$  (1:5, 1:10, and 1:50 dilutions volumes (MNP/NMOF): MTT  $v/v$ ), appreciable cytotoxicity was observed for both MNPs and NMOFs (data not shown). Data on the percentage cell viability at different concentrations of MNPs and NMOFs revealed that normal CHO cell lines are  $\sim 100\%$  viable below an NM concentration of 0.002  $\mu\text{g}/\text{mL}$ . Additionally, the hydrophobicities of both MNPs and NMOFs have the advantage of prolonged circulation in the blood, which would facilitate the targeting of tumor cells [104]. The formulation (with KH570/MMA/OP-10) aids enhanced permeability and retention in certain solid tumors, which is often observed and is a beneficial effect on the efficacy and treatment of such cell lines [105]. The efficacy of the formulation can be examined through measurement tumor regression (either by mass or volume or dimension) and increased survival time as compared controls. In the present study, a cell viability assay was conducted, demonstrating the efficacy of both nanoparticles and the nanoframework. The efficacy of the various nanomaterials on the CHO cell line is shown in Fig. 16.16A. For the mixed iron oxide ( $\text{Fe}_3\text{O}_4$ , control system), there appears to be an approximately linear relationship between NMs load and cell viability, with a higher NM load, being more lethal. An approximate effective

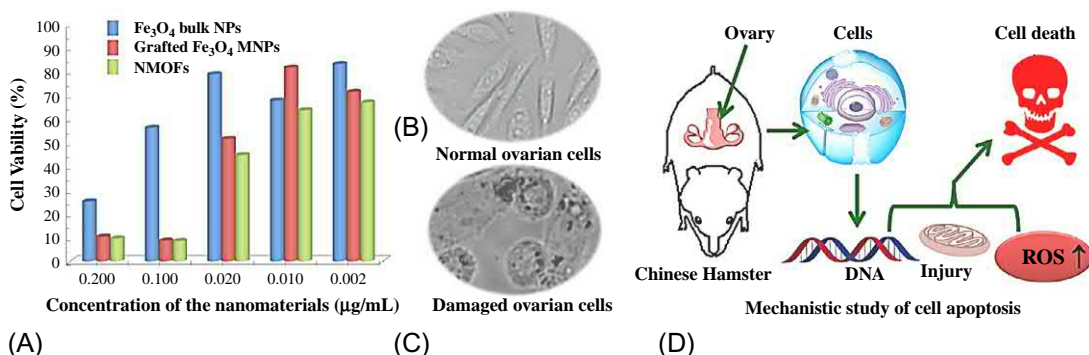


Fig. 16.16

Analyses of cytotoxicity on CHO cell line: (A) cell viability as a function of different concentrations of grafted Fe<sub>3</sub>O<sub>4</sub>-MNPs and NMOFs (Fe<sub>3</sub>O<sub>4</sub> were used as control). Student *t*-test and ANOVA analysis indicate all results are significant ( $P < .05$ ). (B) Selected TEM micrograph of intact CHO cells. (C) TEM micrograph of damaged CHO cells using Fe-NMOFs to understand cell apoptosis. (D) Schematic illustration of mode of inhibition of normal CHO cell lines using NMs [45].

concentration at 50% lethality (EC<sub>50</sub>) is estimated at 0.132 µg/mL. The grafted Fe<sub>3</sub>O<sub>4</sub> MNPs and NMOFs exhibit a log step function ( $\sim$ EC<sub>50</sub> 0.021 µg/mL and 0.018 µg/mL, respectively) with much lower EC<sub>50</sub> values. The relationship between cell viability and NM concentration reflected the nature of particle-cell interactions. With the bulk Fe<sub>3</sub>O<sub>4</sub> (control system, Fig. 16.16B), MNP diffusion appears to be the rate-limiting factor, with greater MNPs “dose” being more lethal. With the grafted MNPs and NMOFs, the ultrahigh surface area and large internal porosity appear to increase the interactions between the NMs and CHO cells, meaning that lower NM “dose” can be effectively delivered (cf. Fig. 16.16C). For example, to kill 50% of the cell population, the NM loading of the grafted and frameworks is 16% and 11% (at  $P < .05$  confidence), respectively, of the NM loading. The results demonstrate that the use of grafted MNPs or NMOFs is viable strategies to inhibit cell growth, including multidrug-resistant cell lines, as an important step to provide effective treatment [106]. A second major advantage of using core-shelled MNPs or MOFs is their flexibility in configuring different surface ligands.

From the micrograms shown in Fig. 16.16B, it is clear that the plasma membrane for the CHO cells is intact, while in Fig. 16.16C, some cytoplasmic membrane peeling has occurred including hypotonic swelling and DNA fragmentation, as the incubation time was increased upon addition of the grafted Fe<sub>3</sub>O<sub>4</sub> MNPs and NMOFs. The mode of inhibition (cf. Fig. 16.16D) is presumably due to the activation of apoptosis factors through binding of NMs with certain cell receptors/surfaces, inducing (extrinsic pathway-based) cell death [107]. The mechanism for apoptosis of cells using MNs is complicated because various cells express different types of surface markers, but cell death would be triggered once NM-cell interaction is initiated [108]. One common mode of inactivation of cells by NMs is through the generation of reactive oxygen species (ROS), which leads to apoptosis. This mechanism results from either direct (due to peroxidation and membrane peeling) or indirect (inhibition of respiration), which result in

death via triggering of certain caspases, that induce the death response [109]. Other modes of cell death include unzipping and fragmentation of DNA (Fig. 16.16C, dark region), inhibition of DNA replication, and degradation of proteins, resulting in apoptosis [110]. Some of our observations are consistent with a study undertaken by Jiang et al. [111] and Huang et al. [112] in which gene activation was related to the degree of reactive oxygen species (ROS)-mediated proliferation or cytotoxicity [113]. The MN-mediated cytotoxicity appears to be via oxidative damage to the plasma membrane (lipid peroxidation followed by lysis), DNA fragmentation (lesions), and degradation of proteins [114]. From a design perspective, MNPs/NMOFs with their large surface-to-volume ratios serve as a link between atomic and biochemical probes, in which ROS induced can be followed, by tracking the topography/topology of the NMs relative to the cell. More specifically, the core-shelled Fe<sub>3</sub>O<sub>4</sub>-NPs served as building blocks of these grafted MNPs composed of polycrystals with mixtures of metallic and polymeric units. The introduction of core-shell Fe<sub>3</sub>O<sub>4</sub> MNPs allows for magnetic core (Fe<sub>3</sub>O<sub>4</sub>) encapsulated in a protective and biocompatible MMA monomer. Within the nanoscaled metal-organic frameworks, various molecular architectures can be achieved, and geometry and cooperative stability can be tuned via modification of ligands. Through the introduction of the amphiphilic organic linker (shown in Fig. 16.14A), Fe-based NMOFs exhibit both biocompatibility [115] and prolonged capacity to circulate in the bloodstream, accordingly to literature reports [116]. This will benefit the targeted drug delivery. Eventually, this nanoscale magnetism tuning approach could be beneficial not only for magnetic hyperthermia but also for other applications that range from the design of magnetic recording media, spintronics, to magnetic resonance imaging (MRI) contrast agent and drug delivery carriers [117].

The use of iron oxides for the treatment of various biological systems is summarized in Table 16.4. Previously reported results from the literature indicate that one area of treatment related to multiple drug resistance (MDR) cells is important because currently there are few successful treatment strategies for patients with MDR cells. The possible reasons for cell tolerance to conventional treatment may be that these cells also express additional biomarkers, such as lung resistance-related protein (LRP), permeability glycoprotein 1 (P-glycoprotein) and B-cell lymphoma 2 (Bcl-2) encoded biomarkers, and deoxyribonucleic acid (DNA) protection. One metric for cell survival is an examination of DNA lesions due to oxidative intracellular processes, which are related to the action of reactive oxygen species at active sites on the NP surface. Systems with greater active sites, such as uncoated nanoparticles would exhibit greater DNA lesions in cells lines, has been observed in the literature.

### **16.11 Conclusions**

The Fe<sub>3</sub>O<sub>4</sub> magnetic nanoparticles and Fe-containing metal-organic frameworks were prepared using a facile wet-chemistry method. It was found that grafted MNPs maintained their reverse spinel crystalline structure and paramagnetism. The MOFs displayed high crystallinity and well-defined topology (known as the acs net [131]). Both nanomaterials displayed EC<sub>50</sub> activity

Table 16.4: Summary of iron-based nanomaterials in the treatment of cancer cell lines.

| Nanoparticles                                                                                                                 | Cells                                                                                                | Outcome                                                                               |
|-------------------------------------------------------------------------------------------------------------------------------|------------------------------------------------------------------------------------------------------|---------------------------------------------------------------------------------------|
| Fe <sub>3</sub> O <sub>4</sub> loaded with adriamycin (ADM) or tetrandrine (Tet) [118]                                        | K562/A02<br>(chronic myelogenous erythroleukemia cell line; adriamycin (ADM) induction K562 clone 2) | 100-fold more decrease in <i>mdr1</i> mRNA level                                      |
| Fe <sub>3</sub> O <sub>4</sub> covered OH <sup>-</sup> incorporated with (CH <sub>3</sub> ) <sub>4</sub> N <sup>+</sup> [119] | COS-7<br>(CV1 in origin carrying SV40 fibroblast-like cells)                                         | No change in cell survival                                                            |
| Doxorubicin (dox) encapsulated in polyisohexylcyanoacrylate nanospheres [120]                                                 | K562 and MCF7<br>(Michigan cancer foundation-breast cancer cell line 7)                              | MRP1 and TOP2 $\alpha$ genes expression was observed                                  |
| Fe <sub>3</sub> O <sub>4</sub> loaded with cisplatin [121]                                                                    | SKOV3/DDP<br>(Sloan-Kettering ovarian adenocarcinoma cell line)                                      | IC <sub>50</sub> 17.4 $\mu$ mol/l for <i>cis</i> -diamminedichloroplatinum (II) (DDP) |
| PEGF-coated nanoparticles [122]                                                                                               | L929<br>(mouse fibroblast cells, strain L, clone 929)                                                | Viability with 27.3 (coated) to 13.6 (uncoated)                                       |
| Silica-coated iron oxide [123]                                                                                                | A549<br>(adenocarcinomic human alveolar basal epithelial cells)                                      | IC <sub>50</sub> = 4 mg/mL                                                            |
| Amine surface-modified iron oxide [124]                                                                                       | HepG2<br>(human hepatocyte cell line glucose deficient)                                              | Cytotoxicity was observed                                                             |
| Tween-coated iron oxide [125]                                                                                                 | J774<br>(murine reticulum cell sarcoma line J, colony 774)                                           | Cytotoxicity related to dose and incubation time                                      |
| Tetraheptylammonium coated iron oxide [126]                                                                                   | K562<br>(erythroleukemia)                                                                            | 60% viability                                                                         |
| Chitosan-coated iron oxide [127]                                                                                              | SMMC-7721<br>(human hepatoma cell line)                                                              | 10% viability                                                                         |
| PEG-coated iron oxide [128]                                                                                                   | L929<br>(adhesive mouse fibroblast cell line)                                                        | 300 $\mu$ g Fe = 50% cell viability                                                   |
| Dextran-coated iron oxide [129]                                                                                               | Human macrophages                                                                                    | 20% cell viability                                                                    |
| Poly(vinyl alcohol) coated iron oxide [130]                                                                                   | L929<br>(adhesive mouse fibroblast cell line)                                                        | Cell viability 27.3 (coated) versus 13.6 (uncoated)                                   |

(11%–16% relative to control Fe<sub>3</sub>O<sub>4</sub> NPs) toward cell apoptosis of Chinese hamster ovary cells, which can be beneficial to the molecule targeting and potentially drug delivery as shown in vitro MTT assay.

## Acknowledgments

The National Science Foundation (NSF-MRI, CBET 0821370), R. Welch Foundation (AC-0006) from the Texas A&M University-Kingsville, are duly acknowledged. Dr. Du from Lanzhou University of Technology and Dr. Zhou

from Texas A&M University are acknowledged for allowing Dr. Liu to use the facility and to evaluate the magnetism and develop ligands and single MOF crystals. The technical support from the Department of Chemistry at Texas A&M University-College Station and Kingsville is also duly acknowledged. The students, Xiangshan Liu from Dr. Liu's group, Kiran Kumar Vangara from Dr. Palakurthi's group, and Ms. Ying Yao from Dr. Du's group, are also acknowledged for their participation in this project to advance their graduate studies.

### **Author contribution**

Dr. Liu conceived the thrust and all nonbiological work, including the first draft and final submission on behalf of all authors. Dr. Palakurthi oversaw and supervised his student (acknowledged) working on the in vitro toxicity and assisted with one figure (Fig. 16A). Dr. Yuan completed the analysis of the single-crystal structure (Fig. 14B). Mr. Sai edited the first draft and completed the data table and reference section. Dr. Bashir contributed to the analyses of toxicity data and mechanism (Fig. 16D) and references and copyright.

### **References**

- [1] R.N. Kostoff, J.A. Stump, D. Johnson, J.S. Murday, C.G. Lau, W.M. Tolles, The structure and infrastructure of the global nanotechnology literature, *J. Nanopart. Res.* 8 (3-4) (2006) 301–321.
- [2] R. Hardman, A toxicologic review of quantum dots: toxicity depends on physicochemical and environmental factors, *Environ. Health Perspect.* 114 (2) (2005) 165–172.
- [3] J.C. Love, L.A. Estroff, J.K. Kriebel, R.G. Nuzzo, G.M. Whitesides, Selfassembled monolayers of thiolates on metals as a form of nanotechnology, *Chem. Rev.* 105 (4) (2005) 1103–1170.
- [4] D. Libaers, M. Meyer, A. Geuna, The role of university spinout companies in an emerging technology: the case of nanotechnology, *J. Technol. Transf.* 31 (4) (2006) 443–450.
- [5] K.W. Powers, M. Palazuelos, B.M. Moudgil, S.M. Roberts, Characterization of the size, shape, and state of dispersion of nanoparticles for toxicological studies, *Nanotoxicology* 1 (1) (2007) 42–51.
- [6] V.L. Colvin, The potential environmental impact of engineered nanomaterials, *Nat. Biotechnol.* 21 (10) (2003) 1166.
- [7] C.W. Lam, J.T. James, R. McCluskey, S. Arepalli, R.L. Hunter, A review of carbon nanotube toxicity and assessment of potential occupational and environmental health risks, *Crit. Rev. Toxicol.* 36 (3) (2006) 189–217.
- [8] J. Curtis, M. Greenberg, J. Kester, S. Phillips, G. Krieger, Nanotechnology and nanotoxicology, *Toxicol. Rev.* 25 (4) (2006) 245–260.
- [9] H.C. Zhou, J.R. Long, O.M. Yaghi, Introduction to metal-organic frameworks, *Chem. Rev.* 112 (2) (2012) 673–674.
- [10] R.M. Dorin, H. Sai, U. Wiesner, Hierarchically porous materials from block copolymers, *Chem. Mater.* 26 (1) (2013) 339–347.
- [11] E.C. Ashby, J.T. Laemmle, Stereochemistry of organometallic compound addition to ketones, *Chem. Rev.* 75 (4) (1975) 521–546.
- [12] S. Keskin, S. Kızılel, Biomedical applications of metal-organic frameworks, *Ind. Eng. Chem. Res.* 50 (4) (2011) 1799–1812.
- [13] J. Rocca, D. Liu, W. Lin, Nanoscale metal-organic frameworks for biomedical imaging and drug delivery, *Acc. Chem. Res.* 44 (2011) 957–968.
- [14] C. Janiak, J. Vieth, MOFs, MILs and more: concepts, properties, and applications for porous coordination networks (PCNs), *New J. Chem.* 34 (2010) 2337–2684.
- [15] J. Rowsell, O. Yaghi, Metal-organic frameworks: a new class porous materials, *Microporous Mesoporous Mater.* 73 (2004) 3–14.
- [16] S. Ma, D. Yuan, X. Wang, H. Zhou, Microporous lanthanide metal-organic frameworks containing coordinatively linked interpenetration: synthesis, gas adsorption studies, thermal stability analysis, and photoluminescence investigation, *Inorg. Chem.* 10 (2009) 1021–1025.



- [17] L. Yang, S. Song, C. Shao, W. Zhang, Z. Bu, T. Ren, Synthesis, structure and luminescent properties of 3D lanthanide (La(III), Ce(III)) coordination polymers possessing 1D nanosized cavities based on pyridine-2,6-dicarboxylic acid, *Synth. Metals* 161 (2011) 1500–1508.
- [18] C. Zhao, Y. Ou, Z. Zhao, X. Yin, Y. Jiang, Crystal structure of bis-aqua(4-pyridine-2,4,6-tricarboxylato-3N,O,O') cerium(III)-water(1:1), {[Ce(PTC)(H<sub>2</sub>O)<sub>2</sub>](H<sub>2</sub>O)<sub>n</sub>}, C<sub>8</sub>H<sub>8</sub>CeNO<sub>9</sub>, NCS 228 (2013) 3–4.
- [19] A. Ebrahim, T. Bando, Ce(III) doped Zr-based MOFs as excellent NO<sub>2</sub> adsorbents at ambient conditions, *ACS Appl. Mater. Interfaces* 5 (2013) 10565–10573.
- [20] T. Prasad, M. Rajasekharan, Cerium(IV)lanthanide(III)-pyridine-2,6-dicarboxylic acid system: coordination salts, chains, and rings, *Inorg. Chem.* 48 (2009) 11543–11550.
- [21] F. Xamena, A. Abad, A. Corma, H. Garcia, MOFs as catalysts: activity, reusability and shape selectivity of a Pd-containing MOF, *J. Catal.* 250 (2007) 294–298.
- [22] Q. Wei, S. Zhang, Q. Yang, S. Chen, W. Gong, Y. Zhang, G. Zhang, C. Zhou, S. Gao, Hydrothermal synthesis, structure, magnetic, and photoluminescent properties of a heterometallic cobalt (II)/cerium(III) coordination compound with the ligand pyrazine 2,3-dicarboxylic acid, *Anorg. Allg. Chem.* 639 (2013) 142–147.
- [23] O. Ayhan, I.L. Malaestean, A. Ellen, J. Leusen, S. Baca, Assembly of cerium(III) 2,2'-bipyridine-5,5'-dicarboxylate-based metal-organic frameworks by solvent tuning, *Cryst. Growth Des.* 14 (2014) 3541–3548.
- [24] M. Kurmoo, Magnetic metal-organic frameworks, *Chem. Soc. Rev.* 38 (5) (2009) 1353–1379.
- [25] F. Sun, G. Zhu, Solvent-directed synthesis of chiral and non-centrosymmetric metal-organic frameworks based on pyridine-3,5-dicarboxylate, *Inorg. Chem. Commun.* 38 (2013) 115–118.
- [26] L. Yang, L. Wu, H. Zhang, S. Song, L. Liu, M. Li, Synthesis, structure and luminescent recognition properties of cerium(IV) coordination polymers based on pyridine-2,6-dicarboxylic acid, *Dyes Pigments* 99 (2013) 257–267.
- [27] N. Stock, S. Biswas, Synthesis of metal-organic frameworks (MOFs): routes to various MOF topologies, morphologies, and composites, *Chem. Rev.* 112 (2012) 933–969.
- [28] D. Tranchemontagne, J. Mendoza-Cortes, M. O'Keeffe, O. Yaghi, Secondary building units, nets and bonding in the chemistry of metal-organic frameworks, *Chem. Soc. Rev.* 38 (2009) 1257–1283.
- [29] P. Horcajada, C. Serre, G. Maurin, N. Ramsahye, F. Balas, M. Vallet-Regi, M. Sebban, F. Taulelle, G. Férey, Flexible porous metal-organic frameworks for a controlled drug delivery, *J. Am. Chem. Soc.* 130 (2008) 6774–6780.
- [30] M. Eddaoudi, D. Moler, H. Li, B. Chen, T. Reineke, M. O'Keeffe, O. Yaghi, Modular chemistry: secondary building units as a basis for the design of highly porous and robust metal-organic carboxylate frameworks, *Acc. Chem. Res.* 34 (2001) 319–330.
- [31] K.M. Taylor-Pashow, J. Della Rocca, Z. Xie, S. Tran, W. Lin, Postsynthetic modifications of iron-carboxylate nanoscale metal-organic frameworks for imaging and drug delivery, *J. Am. Chem. Soc.* 131 (40) (2009) 14261–14263.
- [32] R. Mohammadinasab, M. Tabatabaee, B. Kukovec, H. Aghaie, The cerium(III) coordination polymer with mixed polycarboxylic acids. Preparation of the CeO<sub>2</sub> nanoparticles by thermal decomposition of the polymer, *Inorg. Chim. Acta* 405 (2013) 368–373.
- [33] X. Zheng, L. Li, S. Gao, L. Jin, Hydrothermal synthesis, structures and magnetic properties of two transition metal coordination polymers with a square grid framework, *Polyhedron* 23 (2004) 1257–1262.
- [34] B. Chen, S. Xiang, G. Qian, Metal-organic frameworks with functional pores for recognition of small molecules, *Acc. Chem. Res.* 43 (2010) 1115–1124.
- [35] M. Sindoro, N. Yanai, A. Jee, S. Granick, Colloidal-sized metal-organic frameworks: synthesis and applications, *Acc. Chem. Res.* 10 (2010) 102–112.
- [36] P. Horcajada, R. Gref, T. Baati, P. Allan, G. Maurin, P. Couvreur, G. Férey, R. Morris, C. Serre, Metal-organic frameworks in biomedicine, *Chem. Rev.* 112 (2012) 1232–1268.
- [37] U. Bilati, E. Allemann, E. Doelker, Development of a nanoprecipitation method for the entrapment of hydrophilic drugs into nanoparticles, *Eur. J. Pharm. Sci.* 24 (2005) 67–75.

- [38] L. Wang, L. Zhang, T. Song, C. Li, J. Xu, L. Wang, Solvothermal synthesis, structures and properties of two new in-MOFs based on rigid 1,4-naphthalenedicarboxylate ligand, *Microporous Mesoporous Mater.* 155 (2012) 281–286.
- [39] Y. Chen, S. Ma, Microporous lanthanide metal-organic frameworks, *Rev. Inorg. Chem.* 32 (2–4) (2012) 81–100.
- [40] Y. Liu, J.F. Eubank, A.J. Cairns, J. Eckert, V.C. Kravtsov, R. Luebke, M. Eddaoudi, Assembly of metal-organic frameworks (MOFs) based on indium-trimer building blocks: a porous MOF with soc topology and high hydrogen storage, *Angew. Chem. Int. Ed.* 46 (18) (2007) 3278–3283.
- [41] J. Bae, J.S. Choi, S. Hwang, W.S. Yun, D. Song, J. Lee, N.C. Jeong, Multiple coordination exchanges for room-temperature activation of open-metal sites in metal-organic frameworks, *ACS Appl. Mater. Interfaces* 9 (29) (2017) 24743–24752.
- [42] C.P. Li, M. Du, Role of solvents in coordination supramolecular systems, *Chem. Commun.* 47 (21) (2011) 5958–5972.
- [43] N. Stock, S. Biswas, Synthesis of metal-organic frameworks (MOFs): routes to various MOF topologies, morphologies, and composites, *Chem. Rev.* 112 (2) (2011) 933–969.
- [44] H. Li, M. Eddaoudi, M. O’Keeffe, O.M. Yaghi, Design and synthesis of an exceptionally stable and highly porous metal-organic framework, *Nature* 402 (6759) (1999) 276.
- [45] T. Wang, Synthesis of transition metal-organic frameworks and their application in inhibition of microbial growth, Doctoral dissertation, Texas A&M University-Kingsville, 2014.
- [46] X. Wang, G. Lu, Y. Guo, Y. Wang, Y. Guo, Preparation of high thermal-stable alumina by reverse microemulsion method, *Mater. Chem. Phys.* 90 (2005) 225–229.
- [47] T. He, D. Chen, X. Jiao, Y. Xu, Y. Gu, Surfactant-assisted solvothermal synthesis of Co<sub>3</sub>O<sub>4</sub> hollow spheres with oriented-aggregation nanostructures and tunable particle size, *Langmuir* 20 (2004) 8404–8408.
- [48] A.C. McKinlay, R.E. Morris, P. Horcajada, G. Férey, R. Gref, P. Couvreur, C. Serre, BioMOFs: metal-organic frameworks for biological and medical applications, *Angew. Chem. Int. Ed.* 49 (36) (2010) 6260–6266.
- [49] FEL.com; n.d. An introduction to electron microscopy.
- [50] M.J. Hollenberg, A.M. Erickson, The scanning electron microscope: potential usefulness to biologists a review, *J. Histochem. Cytochem.* 21 (2) (1973) 109–130.
- [51] H. Huxley, Electron microscope studies on the structure of natural and synthetic protein filaments from striated muscle, *J. Mol. Biol.* 7 (1963) 281–308.
- [52] J. Cheng, S. Zheng, G. Yang, A series of lanthanide-transition metal frameworks based on 1-, 2-, and 3D metal-organic motifs linked by different 1D copper(I) halide motifs, *Inorg. Chem.* 46 (2007) 10261–10267.
- [53] O. Ayhan, I. Malaestean, A. Ellern, J. Leusen, S. Baca, P. Kogerler, Assembly of cerium(III) 2,2'-bipyridine-5,5'-dicarboxylate-base metal-organic frameworks by solvent tuning, *Cryst. Growth Des.* 14 (2014) 3541–3548.
- [54] S. Ma, H. Zhou, Gas storage in porous metal-organic frameworks for clean energy applications, *Chem. Commun.* 46 (2010) 44–53.
- [55] A. Torrisi, R. Bell, C. Mellot-Draznieks, Functionalized MOFs for enhanced CO<sub>2</sub> capture, *Cryst. Growth Des.* 10 (2010) 2839–2841.
- [56] S. Henninger, H. Habib, C. Janiak, MOFs as adsorbents for low-temperature heating and cooling applications, *J. Am. Chem. Soc.* 131 (2009) 2776–2777.
- [57] J. Rocca, D. Liu, W. Lin, Nanoscale metal-organic frameworks for biomedical imaging and drug delivery, *Acc. Chem. Res.* 44 (2011) 957–968.
- [58] T. Malinski, Z. Taha, Nitric oxide release from a single cell measured in situ by a porphyrinic-based microsensor, *Nature* 358 (1992) 676–678.
- [59] S. Cohen, Modifying MOFs: new chemistry, new materials, *Chem. Sci.* 1 (2010) 32–36.
- [60] Y. Yan, S. Yang, A. Blake, M. Schroder, Studies on metal-organic frameworks of Cu(II) with isophthalate linkers for hydrogen storage, *Acc. Chem. Res.* 47 (2) (2012) 296–307.

- [61] H. Lin, Y. Shen, D. Chen, L. Lin, B.C. Wilson, B. Li, S. Xie, Feasibility study on quantitative measurements of singlet oxygen generation using singlet oxygen sensor green, *J. Fluoresc.* 23 (1) (2013) 41–47.
- [62] J.C. Wigle, C.C. Castellanos, M.L. Denton, E.A. Holwitt, Nitric oxide measurements in hTERT-RPE cells and subcellular fractions exposed to low levels of red light, in: *International Society for Optics and Photonics*, 2014, p. 89320D.
- [63] E.D. Kerver, I.M. Vogels, K.S. Bosch, H. Vreeling-Sindelarova, R.J. Van Den Munckhof, W.M. Frederiks, In situ detection of spontaneous superoxide anion and singlet oxygen production by mitochondria in rat liver and small intestine, *Histochem. J.* 29 (3) (1997) 229–237.
- [64] W.M. Frederiks, In situ detection of spontaneous superoxide anion and singlet oxygen production by mitochondria in rat liver and small intestine, *Histochem. J.* 29 (3) (1997) 229–237.
- [65] I. Xamena, F.X. Llabrés, O. Casanova, R.G. Tailleux, H. Garcia, A. Corma, Metal-organic frameworks (MOFs) as catalysts: a combination of Cu<sup>2+</sup> and Co<sup>2+</sup> MOFs as an efficient catalyst for tetralin oxidation, *J. Catal.* 255 (2) (2008) 220–227.
- [66] S. Devautour-Vinot, C. Martineau, S. Diaby, M. Ben-Yahia, S. Miller, C. Serre, P. Horcajada, D. Cunha, F. Taulelle, G. Maurin, Caffeine confinement into a series of functionalized porous zirconium MOFs: a joint experimental/modeling exploration, *J. Phys. Chem. C* 117 (2013) 11694–11704.
- [67] W. Zhou, T. Yildirim, Nature and Tunability of enhanced hydrogen binding in METALORGANIC frameworks with exposed transition metal sites, *J. Phys. Chem. C* 112 (2008) 8132–8135.
- [68] C. Oliveira, F. Silva, I. Malvestiti, V. Malta, J. Dutra, N. Costa, R. Freire, S. Junior, Effect of temperature on formation of two new lanthanide metal-organic frameworks: synthesis, characterization and theoretical studies of Tm(III)-succinate, *J. Solid State Chem.* 197 (7–13) (2013).
- [69] P. Pachfule, R. Das, P. Poddar, R. Banerjee, Structural, magnetic, and gas adsorption study of a series of partially fluorinated metal-organic frameworks (HF-MOFs), *Inorg. Chem.* 50 (2011) 3855–3865.
- [70] P. Jain, V. Ramachandran, R. Clark, H. Zhou, B. Toby, N. Dalal, H. Kroto, A. Cheetham, Multiferroic behavior associated with an order-disorder hydrogen bonding transition in metal-organic frameworks (MOFs) with the perovskite ABX<sub>3</sub> architecture, *J. Am. Chem. Soc.* 131 (2009) 13625–13627.
- [71] T. Cook, V. Vajpayee, M. Lee, P. Stang, K. Chi, Biomedical and biochemical applications of self-assembled metallacycles and metallacages, *Acc. Chem. Res.* 46 (2013) 2464–2474.
- [72] S. Moncada, R. Palmer, E. Higgs, Biosynthesis of nitric oxide from L-arginine, *Biochem. Pharmacol.* 38 (1989) 1709–1715.
- [73] J. An, S. Geib, N. Rosi, Cation-triggered drug release from a porous zinc-adeninate metalorganic frameworks, *J. Am. Chem. Soc.* 131 (2009) 8376–8377.
- [74] P. Horcajada, C. Serre, M. Vallet-Regi, M. Sebban, F. Taulelle, G. Férey, Metal-organic frameworks as efficient materials for drug delivery, *Angew. Chem.* 118 (2006) 6120–6124.
- [75] J. Rocca, D. Liu, W. Lin, Nanoscale metal-organic frameworks for biomedical imaging and drug delivery, *Acc. Chem. Res.* 44 (2011) 957–968.
- [76] A. Millward, O. Yaghi, Metal-organic frameworks with exceptionally high capacity for storage of carbon dioxide at room temperature, *J. Am. Chem. Soc.* 127 (2005) 17998–17999.
- [77] T. Glover, G. Peterson, B. Schindler, D. Britt, O. Yaghi, MOF-74 building unit has a direct impact on toxic gas adsorption, *Chem. Eng. Sci.* 66 (2011) 163–170.
- [78] M. Zhao, S. Ou, C. Wu, Porous metal-organic frameworks for heterogeneous biomimetic catalysis, *Acc. Chem. Res.* 47 (4) (2014) 1199–1207.
- [79] S. Ma, D. Yuan, X. Wang, H. Zhou, Microporous lanthanide metal-organic frameworks containing coordinatively linked interpenetration: syntheses, gas adsorption studies, thermal stability analysis, and photoluminescence investigation, *Inorg. Chem.* 47 (2013) 4130–4133.
- [80] M. Kandiah, M. Nilsen, S. Usseglio, S. Jakobsen, U. Olsbye, M. Tilset, C. Larabi, E. Quadrelli, F. Bonino, K. Lillerud, Synthesis and stability of tagged UiO-66 Zr-MOFs, *Chem. Mater.* 22 (2010) 6632–6640.

- [81] Y. Wu, D. Li, W. Xia, S. Guo, W. Dong, Three novel lanthanide metal-organic frameworks (Ln-MOFs) constructed by unsymmetrical aromatic dicarboxylate tectonics: synthesis. Crystal structures and luminescent properties, *Molecules* 19 (2014) 14352–14365.
- [82] Q. Wang, J. Ye, G. Tian, Y. Chen, X. Lu, W. Gong, G. Ning, Three-dimensional Ln(III)-Mn(II) metal-organic frameworks constructed from rod-shaped molecular building blocks: synthesis, structures and magnetic properties, *Inorg. Chem. Commun.* 14 (2011) 889–892.
- [83] X. Yan, L. Qin, L. Yu, L. Han, Synthesis, structure and magnetic properties of a 3D Mn(II)-organic frameworks with ABW-zeolite topology, *J. Mol. Struct.* 1051 (2013) 164–168.
- [84] I. Politzer, G. Griffin, J. Laseter, Singlet oxygen and biological systems, *Chem. Biol. Interact.* 3 (1971) 73–93.
- [85] M. Chen, Z. Wang, C. Sanudo, H. Zhao, C. Liu, Two self-interpenetrating magnetic Mn(II) metalorganic frameworks assembled from rigid or flexible tripodal multicarboxylate ligands, *Inorg. Chem. Commun.* 43 (2014) 121–125.
- [86] F. Nour, J. Eubank, T. Bousquet, L. Wojtas, M. Zaworotko, M. Eddaoudi, Supramolecular building blocks (SBBs) for the design and synthesis of highly porous metal-organic frameworks, *J. Am. Chem. Soc.* 130 (2008) 1833–1835.
- [87] Y. Lv, Y. Feng, J. Cheng, Two new cerium-organic frameworks with unusual network topologies constructed by racemic tartaric acid involving in situ reaction, *Inorg. Chem. Commun.* 15 (2012) 130–135.
- [88] E. Neofotistou, C. Malliakas, P. Trikalitis, Remarkable structural diversity and single-crystal-to single-crystal transformations in sulfone functionalized lanthanide MOFs, *Cryst. Eng. Comm.* 12 (2010) 1034–1037.
- [89] W. Zhuang, D. Yuan, J.R. Li, Z. Luo, H.C. Zhou, S. Bashir, J. Liu, Highly potent bactericidal activity of porous metal-organic frameworks, *Adv. Healthc. Mater.* 1 (2) (2012) 225–238.
- [90] W. Li, Z. Zhang, E. Bithell, A. Batsanov, P. Barton, P. Saines, P. Jain, C. Howard, M. Carpenter, A. Cheetham, Ferroelasticity in a metal-organic frameworks perovskite; towards a new class of multiferroics, *Acta Mater.* 61 (2013) 4928–4938.
- [91] R. Bethel, Enzymes activated by synthetic components, *Nature* 499 (2013) 40–41.
- [92] S. Liu, J. Li, F. Luo, The first transition metal metal-organic frameworks showing cation exchange for highly selectively sensing of aqueous Cu (II) ions, *Inorg. Chem. Commun.* 13 (2010) 870–872.
- [93] S. Moncada, E. Higgs, The discovery of nitric oxide and its role in vascular biology, *Br. J. Pharmacol.* 147 (2006) 193–201.
- [94] X. Zhou, L. Li, A. Li, T. Yang, W. Huang, Three-dimensional lanthanide metal-organic frameworks with the fluorine-based carboxylate ligands: synthesis, structures, and properties, *Inorg. Chem. Acta* 413 (2014) 38–44.
- [95] N. Mckinlay, B. Xiao, P. Morris, Metal-organic frameworks as NO delivery materials for biological applications, *Microporous Mesoporous Mater.* 129 (2010) 330–334.
- [96] H. Wang, R. Wen, T. Hu, Two series of lanthanide metal-organic frameworks constructed from crown-ether-like secondary building units, *Sur. J. Inorg. Chem.* (2014) 1185–1191.
- [97] X. Du, Y. Yao, J. Liu, Structural architecture and magnetism control of metal oxides using surface grafting techniques, *J. Nanopart. Res.* 15 (7) (2013) 1731.
- [98] I.A. Ibarra, X. Lin, S. Yang, A.J. Blake, G.S. Walker, S.A. Barnett, D.R. Allan, N.R. Champness, P. Hubberstey, M. Schröder, Structures and H<sub>2</sub> adsorption properties of porous scandium metal-organic frameworks, *Chem. Eur. J.* 16 (2010) 13671–13679.
- [99] S. Bauer, C. Serre, T. Devic, P. Horcajada, J. Marrot, G. Férey, N. Stock, High-throughput assisted rationalization of the formation of metal-organic frameworks in the Iron(III) aminoterephthalate solvothermal system, *Inorg. Chem.* 47 (2008) 7568–7576.
- [100] J. Xie, S. Peng, N. Brower, N. Pourmand, S.X. Wang, S. Sun, One-pot synthesis of monodisperse iron oxide nanoparticles for potential biomedical applications, *Pure Appl. Chem.* 78 (5) (2006) 1003–1014.
- [101] Y. Sun, X. Ding, Z. Zheng, X. Cheng, X. Hu, Y. Peng, A novel approach to magnetic nano adsorbents with high binding capacity for bovine serum albumin, *Macromol. Rapid Commun.* 28 (3) (2007) 346–351.
- [102] L. Liz, M.A. López Quintela, J. Mira, J. Rivas, *J. Mater. Sci.* 29 (1994) 3797; M. Yamamoto, M. Ohata, *Progr. Org. Coatings* 27 (1996) 277.

- [103] S. Mitra, U. Gaur, P.C. Ghosh, A.N. Maitra, *J. Control Release* 74 (2001) 317; R.Y. Hong, T.T. Pan, Y. P. Han, *J. Appl. Polym. Sci.* 106 (2007) 1439.
- [104] B. Lin, X. Shen, S. Cui, *Biomed. Mater.* 2 (2007) 132. H. Karlsson, P. Cronholm, J. Gustafsson, L. Moller, *Chem. Res. Toxicol.* 21 (2008) 1726.
- [105] R. Weissleder, C. Tung, U. Mahmood, A. Bogdanov, *In vivo* imaging of tumors with protease-activated near-infrared fluorescent probes, *Nat. Biotechnol.* 17 (1999) 375.
- [106] F.Y. Cheng, C.H. Su, Y.S. Yang, C.S. Yeh, C.Y. Tsai, C.L. Wu, ... D.B. Shieh, Characterization of aqueous dispersions of Fe<sub>3</sub>O<sub>4</sub> nanoparticles and their biomedical applications, *Biomaterials* 26 (7) (2005) 729–738.
- [107] A. Tomitaka, T. Yamada, Y. Takemura, Magnetic nanoparticle hyperthermia using pluronic-coated Fe<sub>3</sub>O<sub>4</sub> nanoparticles: an *in vitro* study, *J. Nanomater.* 2012 (2012) 4.
- [108] C. Yu, H. Nakshatri, J. Irudayaraj, Identity profiling of cell surface markers by multiplex gold nanorod probes, *Nano Lett.* 7 (8) (2007) 2300–2306.
- [109] A.S. Arbab, L.A. Bashaw, B.R. Miller, E.K. Jordan, B.K. Lewis, H. Kalish, J.A. Frank, Characterization of biophysical and metabolic properties of cells labeled with superparamagnetic iron oxide nanoparticles and transfection agent for cellular MR imaging, *Radiology* 229 (3) (2003) 838–846.
- [110] A.R. Burke, R.N. Singh, D.L. Carroll, J.C. Wood, R.B. D'Agostino Jr., P.M. Ajayan, ... S.V. Torti, The resistance of breast cancer stem cells to conventional hyperthermia and their sensitivity to nanoparticle-mediated photothermal therapy, *Biomaterials* 33 (10) (2012) 2961–2970.
- [111] Z. Jiang, B.A. Chen, G.H. Xia, Q. Wu, Y. Zhang, T.Y. Hong, ... X.M. Li, The reversal effect of magnetic Fe<sub>3</sub>O<sub>4</sub> nanoparticles loaded with cisplatin on SKOV3/DDP ovarian carcinoma cells, *Int. J. Nanomedicine* 4 (2009) 107.
- [112] Z. Huang, Bcl-2 family proteins as targets for anticancer drug design, *Oncogene* 19 (56) (2000) 6627.
- [113] M. Mahmoudi, S. Laurent, M.A. Shokrgozar, M. Hosseinkhani, Toxicity evaluations of superparamagnetic iron oxide nanoparticles: cell “vision” versus physicochemical properties of nanoparticles, *ACS Nano* 5 (9) (2011) 7263–7276.
- [114] T. Xia, M. Kovoichich, M. Liang, L. Madler, B. Gilbert, H. Shi, ... A.E. Nel, Comparison of the mechanism of toxicity of zinc oxide and cerium oxide nanoparticles based on dissolution and oxidative stress properties, *ACS Nano* 2 (10) (2008) 2121–2134.
- [115] M.M. Song, W.J. Song, H. Bi, J. Wang, W.L. Wu, J. Sun, M. Yu, Cytotoxicity and cellular uptake of iron nanowires, *Biomaterials* 31 (7) (2010) 1509–1517.
- [116] X. Huang, X. Peng, Y. Wang, Y. Wang, D.M. Shin, M.A. El-Sayed, S. Nie, A reexamination of active and passive tumor targeting by using rod-shaped gold nanocrystals and covalently conjugated peptide ligands, *ACS Nano* 4 (10) (2010) 5887–5896.
- [117] G.F. Goya, I. Marcos-Campos, R. Fernandez-Pacheco, B. Saez, J. Godino, L. Asin, ... M.R. Ibarra, Dendritic cell uptake of iron-based magnetic nanoparticles, *Cell Biol. Int.* 32 (8) (2008) 1001–1005.
- [118] B. Chen, Q. Sun, X. Wang, F. Gao, Y. Dai, Y. Yin, ... X. Sun, A reversal in multidrug resistance by magnetic nanoparticle of Fe<sub>3</sub>O<sub>4</sub> loaded with adriamycin and tetrandrine in K562/A02 leukemic cells, *Int. J. Nanomedicine* 3 (2) (2008) 277.
- [119] F.Y. Cheng, C.H. Su, Y.S. Yang, C.S. Yeh, C.Y. Tsai, C.L. Wu, ... D.B. Shieh, Characterization of aqueous dispersions of Fe<sub>3</sub>O<sub>4</sub> nanoparticles and their biomedical applications, *Biomaterials* 26 (7) (2005) 729–738.
- [120] A. Laurand, A. Laroche-Clary, A. Larrue, S. Huet, E. Soma, J. Bonnet, Quantification of the expression of multidrug resistance-related genes in human tumor cell lines grown with free doxorubicin or doxorubicin encapsulated in polyisohexylcyanoacrylate nanospheres, *Anticancer Res.* 24 (6) (2004) 3781–3788.
- [121] Z.H. Li, X.Y. Liu, N. Wang, J.S. Chen, Y.H. Chen, J.T. Huang, ... D.J. Chen, Effects of Deca brominated diphenyl ether (PBDE-209) in the regulation of growth and apoptosis of breast, ovarian, and cervical cancer cells, *Environ. Health Perspect.* 120 (4) (2012) 541–546.
- [122] A. Masoudi, H.R.M. Hosseini, S.M.S. Reyhani, M.A. Shokrgozar, M.A. Oghabian, R. Ahmadi, Long-term investigation on the phase stability, magnetic behavior, toxicity, and MRI characteristics of superparamagnetic Fe/Fe-oxide core/shell nanoparticles, *Int. J. Pharm.* 439 (1–2) (2012) 28–40.

- [123] J.S. Kim, T.J. Yoon, K.N. Yu, M.S. Noh, M. Woo, B.G. Kim, ... M.H. Cho, Cellular uptake of a magnetic nanoparticle is mediated through energy-dependent endocytosis in A549 cells, *J. Vet. Sci.* 7 (4) (2006) 321–326.
- [124] G. Huang, J. Diakur, Z. Xu, L.I. Wiebe, Asialoglycoprotein receptor-targeted superparamagnetic iron oxide nanoparticles, *Int. J. Pharm.* 360 (1-2) (2008) 197–203.
- [125] S. Naqvi, M. Samim, M.Z. Abdin, F.J. Ahmed, A.N. Maitra, C.K. Prashant, A.K. Dinda, Concentration-dependent toxicity of iron oxide nanoparticles mediated by increased oxidative stress, *Int. J. Nanomedicine* 5 (2010) 983.
- [126] G. Lv, F. He, X. Wang, F. Gao, G. Zhang, T. Wang, ... B. Chen, The novel nanocomposite of nano Fe<sub>3</sub>O<sub>4</sub> and polylactide nanofibers for application in drug uptake and induction of cell death of leukemia cancer cells, *Langmuir* 24 (5) (2008) 2151–2156.
- [127] Y. Ge, Y. Zhang, S. He, F. Nie, G. Teng, N. Gu, Fluorescence modified chitosan-coated magnetic nanoparticles for high-efficient cellular imaging, *Nanoscale Res. Lett.* 4 (4) (2009) 287.
- [128] A. Masoudi, H.R.M. Hosseini, M.A. Shokrgozar, R. Ahmadi, M.A. Oghabian, The effect of poly (ethylene glycol) coating on the colloidal stability of superparamagnetic iron oxide nanoparticles as a potential MRI contrast agent, *Int. J. Pharm.* 433 (1–2) (2012) 129–141.
- [129] E. Pawelczyk, A.S. Arbab, A. Chaudhry, A. Balakumaran, P.G. Robey, J.A. Frank, In vitro model of bromodeoxyuridine or iron oxide nanoparticle uptake by activated macrophages from labeled stem cells: implications for cellular therapy, *Stem Cells* 26 (5) (2008) 1366–1375.
- [130] M. Mahmoudi, A. Simchi, M. Imani, A.S. Milani, P. Stroeve, An in vitro study of bare and poly (ethylene glycol)-co-fumarate-coated superparamagnetic iron oxide nanoparticles: a new toxicity identification procedure, *Nanotechnology* 20 (22) (2009) 225104.
- [131] R.C. Huxford, J. Della Rocca, W. Lin, Metal-organic frameworks as potential drug carriers, *Curr. Opin. Chem. Biol.* 14 (2) (2010) 262–268.



# *Toxicity of nanoscale metal-organic frameworks in biological systems*

**Muhammad Sajid, Ihsanullah**

*Center for Environment and Water, Research Institute, King Fahd University of Petroleum and Minerals, Dhahran, Saudi Arabia*

## **17.1 Introduction**

Metal-organic frameworks (MOFs) are a rising class of crystalline porous hybrid materials with extremely high surface areas. They have demonstrated some thrilling applications in gas storage, separation, catalysis, sensing, and drug delivery [1–4]. The research in synthesis and applications of MOFs is developing at an astonishing pace, and it has been stated that at least one article in every new issue of chemistry journals publishes an aspect or application of MOFs [5]. MOFs are synthesized with extremely tunable crystal sizes ranging from few nanometers to micrometers. The applications of MOFs are somehow correlated with their dimensions. For example, MOFs with dimensions in micrometers or above (bulk MOFs) are extensively employed for gas storage, separation, and catalysis. Nanoscale MOFs are generally employed in sensing and drug delivery applications.

Nanoscale MOFs like other nanomaterials cannot be confined to MOFs with dimensions in between 1 to 100 nm because MOFs with dimensions up to 500 nm are also reported as nanoscale MOFs. Nanoscale MOFs basically combine the unique properties of porous materials with that of the nanostructures leading to improved efficiency compared to bulk MOFs [6]. Nanoscale MOFs are more commonly employed in biomedical applications such as drug delivery. It is because of the essential requirement of the particle size that should not exceed 200 nm so that these drug carriers can freely circulate within the smallest capillaries [7].

The synthesis and applications of nanomaterials in different areas are being most widely explored in current research and development activities. It is because nanomaterials exhibit some unique properties compared to the bulk materials such as small size, high surface area, substantial reactivity, excellent mobility, super penetration capacity, etc. Since it is an emerging area of research and new materials are being widely developed and explored, little is known about their toxicity and effects on human and wildlife. Though unique properties

of nanomaterials make them highly functional materials for various applications, at the same time, these properties lay the foundation of their toxicity. Nature, size, shape, mobility, reactivity, surface area, and penetration ability of nanomaterials are the main contributors toward their toxic effects [8].

Since very little is known about the toxicity of the nanomaterials, it is the time to investigate the toxicity of all kinds of nanomaterials and define their maximum allowable limits in the environment, food, and biological samples. Besides, development of sensitive and selective analytical methods for the measurement of nanomaterials in different matrices is not an easy job. Probably, this is the reason that many research groups are now working on analytical method development for determination of nanomaterials in different matrices [9, 10]. Nanoscale MOFs are a subclass of newly emerging nanomaterials and the information about their toxicity in biological systems is scarce.

MOFs have emerged as a promising material for potential applications in bioimaging and biosensing applications. However, there is serious concern about the potentially toxic effects of MOFs in biological systems [11]. The extensive use of MOFs may pose serious health threats to the living organisms exposed to it. This has resulted in a controversial debate on the biocompatibility of MOFs in the biological system. Therefore, it is imperative to understand the potential risks associated with the MOFs' applications in these systems [12–14].

## ***17.2 Factors affecting the toxicity of MOFs in biological systems***

The research in toxicological studies of MOFs is still in its infancy stage. However, some parameters that can induce toxicity in MOFs are well-known. In the literature, the toxic assessment of MOFs is performed mainly based on the types of cross-linkers and metals [15]. In addition to these, some other factors might also contribute to the toxicity such as particle size, ligands, functionalized groups, and the solvent system in which MOF is synthesized [16]. The cellular uptake, biodistribution, translocation, and excretion from the body are profoundly influenced by the shape, degradation rate, nature, and amount of the functional groups over the surface.

### ***17.2.1 Metal ions in the MOFs***

MOFs contain metals and organic binding linkers. The size of metals ions is generally in the nanoscale and they are mostly nonbiodegradable. Some of the commonly used metals used in the synthesis of MOFs are cadmium (II), iron (II/III), nickel (II), zinc(II), cobalt (II), copper (II), and transition metals (e.g. Ni and Co) [16].

The MOFs with well-known toxic metals such as cadmium, arsenic, lead, and chromium may induce serious health complications due to the toxicity of the MOF-forming metals. Thus,

the metals which are generally required as nutrients for the body such as zinc and iron should be employed for the synthesis of the MOFs which are designed for drug delivery or other therapeutic applications.

Generally, the zinc(II) and iron (II) are considered as least toxic, while the cadmium (II) is the most toxic element for applications in a biological system. The possible exposure to these metals may occur via ingestion, inhalation, and dermal penetration. The metal ions may have toxic effects on the environment, as they tend to be oxidized to metal oxide.

### **17.2.2 Organic linkers**

The common organic linkers used in the synthesis of MOFs are carboxylates, amines, phenolates, imidazolates, sulfonates, and phosphonates. Although there is very limited literature on the toxic effects of organic linkers in the MOFs, it is expected that the MOFs can be degraded to these constituent materials and may pose serious health risks due to the characteristics of these linkers [16].

### **17.2.3 Solvent in the MOFs synthesis**

The solvents used in the synthesis of MOFs may also have toxic effects. The most commonly used solvents are diethylene formamide (DEF), ethanol, dimethyl sulfoxide (DMSO), acetone, and dimethylformamide (DMF) [16]. These solvents may be imprisoned in the porous MOFs and might cause various short-term and long-term effects on health and environmental effects.

For example, exposure to DMF causes several adverse health effects such as liver damage, rashes, alcohol intolerance, jaundice, vomiting, nausea, and abdominal pain. Exposure to acetone may cause neurotoxicity, ocular, dermal, and respiratory irritation.

### **17.2.4 Particle size**

The size of the MOF is an essential parameter for toxicity considerations. Many toxicity-related factors, such as cellular uptake, biodistribution, translocation, and excretion from the body, are highly dependent on the size of the material. A reduction in the size of the particle also affects its surface to volume ratio, which in turn increases the reactivity. Many authors have reported that the size of nanoscale materials dictates their translocation and cytotoxicity [8]. This is to emphasize that nanoscale MOFs should be preferably subjected to toxicological studies compared to their bulk counterparts.

Generally, the penetration ability of the particles increases with a decrease in size; however, other parameters such as the charge of the crystal and shape might also play a vital role.

As per one report, the particle size has a negligible effect on the toxicity of MOFs in biological systems. Sava Gallis et al. [17] demonstrated that there is no significant difference in the toxicity between the micron and nano-sized YbNd MOF particles in the human epithelial cell line (A549) exposure. MOF particles of both sizes demonstrated low cytotoxicity to the epithelial cell line when exposed to a dosage of 100  $\mu\text{g/mL}$  for both 24 and 48 h.

### **17.2.5 Solubility and degradation**

With a particular focus on biological systems, the solubility is a critical factor in determining the toxicity of MOFs because it is associated with their degradation. The solubility and degradation depend on the composition of MOFs and the following properties of the biological system:

- (i) pH
- (ii) Ionic strength
- (iii) Peristaltic movements

Under physiological conditions of biological systems, nanoscale organic and inorganic components of the MOFs will not be exclusively soluble, or at least, they will take longer times for complete degradation and excretion from the body. Consequently, they start accumulating in the cells leading to in vivo toxicity. In the case of metallic species, such accumulation will cause high stress within the cells.

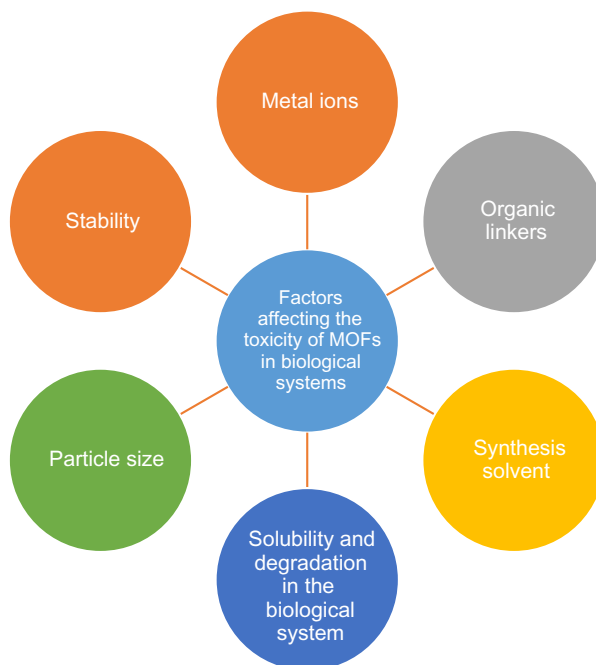
The Fe-based MOFs degrade into iron and organic linkers, where a carboxylate linker is directly excreted from animals via the urine and feces.

Iron ions can cause temporary oxidative stress in the spleen and liver. However, the surplus iron is metabolized and removed in urine and feces.

Apart from the solubility of the MOF in a biological system, its composition can be a major contributing factor toward the toxicity.

### **17.2.6 Stability**

The stability of the MOFs is another critical factor in determining their toxicity in the biological systems. The focus of many researchers is to synthesize the MOFs which are stable both chemically and thermally. The MOFs which are stable up to 500°C have been synthesized [18]. The intent to prepare such MOFs is investigating their potential under a harsh set of conditions. Though such MOFs are not designed for biomedical applications, they may enter into the biological systems through inhalation, ingestion, and dermal intake. The biggest concern is how they will behave under physiological conditions of the body. However, in case of unstable

**Fig. 17.1**

Factors that may affect the toxicity of MOFs in biological systems.

MOFs, their components (metals, linkers, ligands) may leach into cellular apartments, leading to accumulation of metallic and other species. This can result in toxic effects which will highly depend on the nature and concentration of the leached species. The dose of the MOF, the frequency of the treatment, accumulation, and excretion patterns are some other factors which can play a significant role in determining the toxicity of the MOFs in biological systems [19].

This is also true that the toxicities of the individual components may vary from the whole MOF system. Fig. 17.1. shows the major contributing factors toward the toxicities of MOFs in biological systems.

### ***17.3 Why nanoscale metal-organic frameworks in biological systems?***

The ideal drug carriers should have the following features

- (i) Biocompatibility with the targeted biological system
- (ii) Miniaturized dimensions
- (iii) Nontoxicity

As the nanoscale drug carriers have very small dimensions and can easily approach the targeted drug delivery sites in the natural systems, they are highly desired in such applications. However, several parameters that limit the use of most of the existing nanocarriers in drug delivery are their toxicity and poor drug loading and releasing. Thus, MOFs have been emerged as alternative drug carriers due to their exciting properties, tunable structures, and high porosities. They perform better drug loading and discharging in the biological system.

Recently, many authors reported the application of nontoxic metal-based MOFs for drug delivery agents for the diseases like cancer and AIDs. For example, Horcajada et al. employed Fe (III)-based MOFs for this purpose [20]. Although these applications are very encouraging, the issue of the toxicity of MOFs should be evaluated to access their suitability within the biological systems. This evaluation can be performed by *in vitro* and *in vivo* toxicological assays.

The *in vitro* toxicity assays present the following advantages:

- (i) They are fast to perform.
- (ii) They have low cost.
- (iii) They can provide an initial assessment of the toxicity of the materials which are intended for biological applications.
- (iv) Moreover, they are most befitting for high-throughput screening.
- (v) They are supportive in understanding mechanism of toxicity and the way of cellular interaction of drug carriers.

However, this is also important to consider that the results of *in vitro* assays may significantly vary than *in vivo* assays. Therefore, one needs to be very cautious while extrapolating from *in vitro* to *in vivo* considerations.

### ***17.4 In vitro and in vivo toxicity of nanoscale MOFs***

Based on our search on available data on the toxicity of nanoscale MOFs, we observed

- (i) Very limited literature is available on this subject.
- (ii) Toxicity assays have been conducted using different cell lines, thus a comparison of the results is not that meaningful.
- (iii) Several contradictory studies have also been reported.

The nanoZIF-8 (200 nm) was assessed against three human cell lines (mucoepidermoid carcinoma of lung [NCI-H292], colorectal adenocarcinoma [HT-29], and promyelocytic leukemia [HL-60]) and it was found that it does not show any toxicity even at highest tested concentration (109  $\mu\text{M}$ ) [21]. However, in another work, nanoZIF-8 (90 nm) showed some cytotoxicity to HeLa and J774 cell lines; the  $\text{IC}_{50}$  values of 436 and 109  $\mu\text{M}$  were observed against HeLa and J774, respectively [22].



The uncoated nanoscale MOFs were evaluated by in vitro toxicity to HepG2 and MCF7 cells and in vivo against zebrafish embryos. The toxicity of nanoscale MOFs was dependent on

- (i) The nature of the MOF.
- (ii) The solubility of its components in the tested medium.

A strong correlation was observed between in vitro and in vivo toxicity. The major contributing factor was leached metal ions. The other factors that may have significant contribution toward the toxicity of MOFs include the formation of new species upon degradation and nature of crystals (e.g. size, shape, charge, etc.) [23].

However, there are many other factors which should be taken into account, e.g. reactivity, solubility, mobility, penetration ability, nature of functionalized material, type of metal, and organic precursors.

Only few studies talk about in vivo toxicity of nanoscale MOFs. Three different Fe(III) carboxylate nanoMOFs were intravenously injected in rats at high doses for acute in vivo toxicity assays to understand distribution, metabolism, and excretion. This study show that all tested MOFs exhibited low acute toxicity and quickly sequestered by liver and spleen and then further biodegraded and eliminated in urine or feces without metabolization and significant toxicity [24]. In another report, the in vivo toxicity of mechanically downsized Gd(III)-pDBI (pDBI = 1,4-bis(5-carboxy-1H-benzimidazole-2-yl)benzene) NPs was measured by intravenous administration of doses between 0.05 and 0.15 mg/kg using a murine model. This report demonstrated lack of severe toxicity. Nonspecific but minor alterations were found in the liver associated with accumulation of Gd-pDBI NPs [25].

In the literature, numerous MOFs are reportedly tested for biological applications. Till date, MIL (Material Institute Lavoisier) is the most commonly used biomedical materials [26].

In a recent study [26], the toxicological assessment of MIL-100(Fe) was performed using hepatocellular carcinoma (HepG2) and human normal liver cells (HL-7702). It was revealed that MIL-100(Fe) were nontoxic to HL-7702 cells with a concentration of fewer than 80  $\mu\text{g/mL}$ . However, the high concentration of MIL-100(Fe) (i.e. 160  $\mu\text{g/mL}$ ) was found toxic to HL-7702 cells and that could result in the destruction of the cell membranes. It is worthy to mention that HL-7702 cells treated with 160  $\mu\text{g/mL}$  MIL-100(Fe) for 48 h still retain a cell survival rate of  $79.81 \pm 3.01\%$ . Likewise, the toxicological assessment of different concentrations of MIL-100(Fe) on HepG2 cells was reported. It was found that using a high concentration (160  $\mu\text{g/mL}$ ) of MIL-100(Fe), no significant decrease in cellular metabolic activity was observed. This confirms that HepG2 cells had good tolerance to a higher dose of MIL-100(Fe), even at higher doses, and has good biocompatibility with HepG2 cells [26].

Wuttke et al. [12] assessed the nanosafety of different MOF nanoparticles for various medical applications by evaluating their effects on human endothelial and mouse lung cells.

The cytotoxic and inflammatory response of human endothelial cells, alveolar epithelial cells, and alveolar macrophages to MIL (Material of Institute Lavoisier)-101(Cr) and MIL-100(Fe) MOF NPs with and without supported lipid bilayers was examined. A supported lipid bilayer, i.e. 1,2-dioleoyl-sn-glycero-3-phosphocholine (DOPC), is formed around the MIL-100(Fe) and MIL-101(Cr) nanoparticles with the aim to enhance their biocompatibility.

Wang et al. [27] reported low toxicity of zinc-based MOFs and evaluated their drug delivery performance. The prepared MOFs demonstrated promising drug delivery efficiency and displayed low toxicity. In another work, Sun et al. [28] reported a novel low-toxic Ketone Functionalized Gd(III)-MOF having promising anticancer activity against the human liver cancer cells HCC. Another Fe-based MOF, MIL-53(Fe), was found nontoxic and safe (cell viability > 95.27%), when employed as a carrier for the anticancer drug oridonin (Ori) [29]. Zr-based MOFs of UiO-66 containing active silver nanoparticles (AgNPs) with a mild reductant of DMF (AgNPs@UiO-66(DMF)) were employed to evaluate their therapeutic effect against cancer cells [30]. The percentage of cell viability decreased when the concentration of MOFs increased from 10 to 100  $\mu\text{g}/\text{mL}$ . This confirms that the cytotoxicity of the AgNPs@UiO-66(DMF) is in a dose-dependent manner against cancer cells. Li et al. [31] performed *cytotoxicity* test for an UiO-66 MOF which was used as ketoprofen delivery system for treating osteoarthritis (OA). The cytotoxicity test revealed that UiO-66 MOF had no noticeable toxicity and can safely be employed as a delivery vehicle for drugs.

Results indicated that the MIL-100(Fe)@DOPC NPs triggered some apoptotic cell death beyond a minimum dose of 100  $\mu\text{g}/\text{mL}$ . However, both Cr- and Fe-containing MOFs are well-tolerated by endothelial cells. Alveolar epithelial cells tolerate only lipid-coated Cr and Fe-containing MOFs at lower doses of up to 50–100  $\mu\text{g}/\text{mL}$ , respectively. Alveolar macrophages well-tolerated Cr-containing MOFs; however, these cells appear to be sensitive to Fe-containing MOF particles, which cause pronounced induction of a cellular stress response.

The same group also examined the effect of the different MOF NPs, i.e. MIL-101(Cr), MIL-100(Fe), Zr-fumarate (Zr-*fum*) MOF<sub>large</sub>, Zr-*fum* MOF<sub>small</sub>, MIL-100(Cr)@DOPC, and MIL-100(Fe)@DOPC, on gingival fibroblasts, adult human Schwann cells as well as rat neonatal organotypic dorsal root ganglion (DRG) cultures as effector cell systems for dental implants and nerve guidance tubes, respectively [12]. The results exhibited that the MIL-101(Cr), Zr-*fum*, and MIL-100(Fe) were well-tolerated by human gingiva fibroblast which suggests their feasibility for applications in the coating of dental implants. However, Zr-*fum* MOF<sub>large</sub> NPs seem to be the utmost appropriate choice for coating of nerve guidance tubes due to their tolerance in both adult human Schwann cells and rat dorsal root ganglia up to doses of 50  $\mu\text{g}/\text{mL}$  [12].

It is generally assumed that iron and zinc that have been used extensively to build biomolecule-MOF system are safe candidates for applications in biological systems. Numerous available

Fe- and Zn-based MOFs can be used as nanocarriers and they offer many possibilities to achieve an adequate controlled release of various pharmacological molecules [32]. For an instant, less toxic Fe-based MIL-53(Fe) was used for the adsorption of IBU by impregnation of the solids in a hexane IBU-containing solution [33]. Likewise, Zn-based MOFs constructed from 5,5'-5''-(1,3,5-triazine-2,4,6-triyl) tris (azanediyl) triisophthalate (TATAT) and  $Zn^{2+}$  were effectively employed for the delivery of anticancer drug 5-fluorouracil (5-Fu) [34]. Recently, a series of zirconium-based MOFs such as UiO-66 (UiO for Oslo University) has also gained considerable attention due to their nontoxic behavior [35].

Abdelhameed et al. [36] reported that the modified isorecticular metal-organic framework-3 (IRMOF-3) was not toxic to shrimps at a lower concentration of 100  $\mu\text{g}/\text{mL}$ ; however, they were toxic at higher concentration of 200  $\mu\text{g}/\text{mL}$ .

#### 17.4.1 Human exposure to MOFs

The human exposure to MOFs can occur during the occupational activities such as

- (i) Synthesis
- (ii) Characterization
- (iii) Packing
- (iv) Transportation
- (v) During different applications of these materials

The main routes of exposure may include

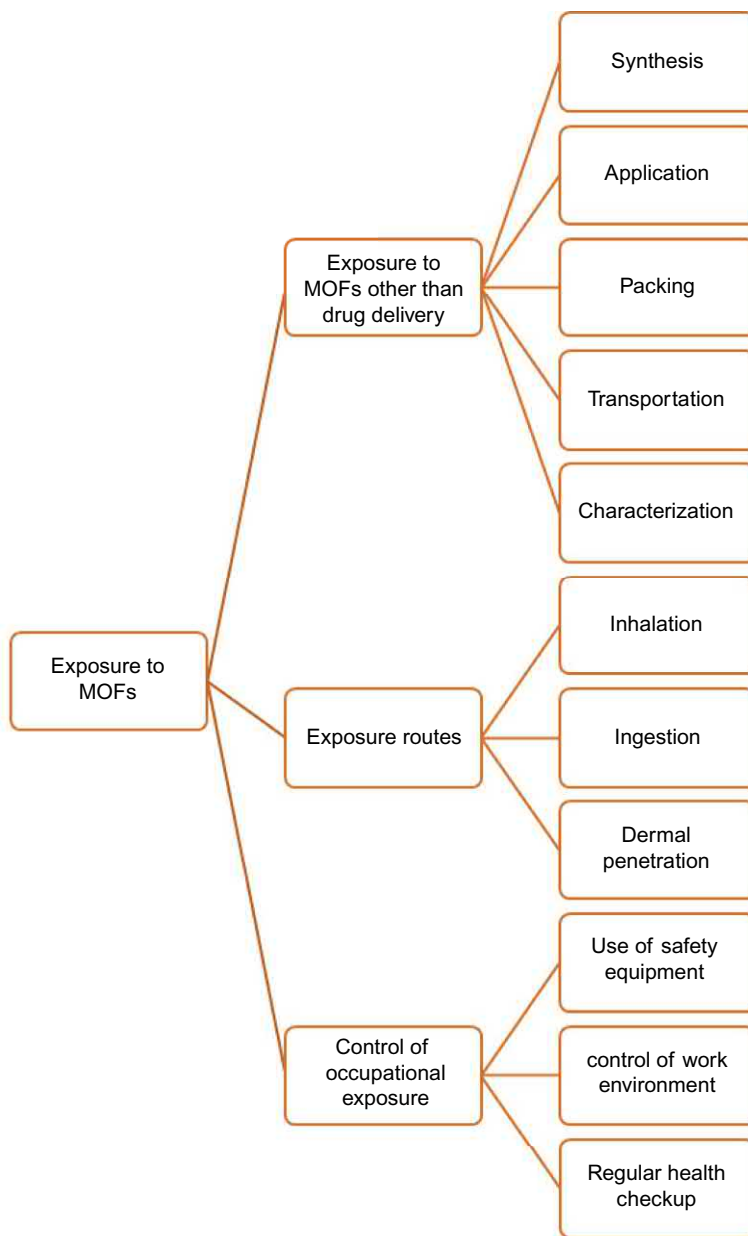
- (i) Dermal penetration
- (ii) Inhalation
- (iii) Ingestion

The occupational exposures can be reduced to certain extent by implementing good lab practices which include

- (i) Use of special personal safety equipment
- (ii) Suitable control of working environment
- (iii) Regular check-up of the working personnel

**Fig. 17.2.** lists the occupational activities which may lead to MOFs' exposure, potential exposure routes, and the steps to reduce occupational exposure at workplace.

The exposure of general public to MOFs in outdoor environment is also a subject which has not been scrutinized yet. Similarly, the presence of nanoscale MOFs in air, soil, and aquatic environments and their succeeding effects on living organisms are not considered so far. The materials which can stay up to temperature of 500°C or above and have extraordinary chemical stability, how will they degrade in natural environment or where will they be disposed of?



**Fig. 17.2**

Occupational activities that may lead to MOFs' exposure, potential exposure routes, and the steps to reduce occupational exposure at workplace.

All these queries need to be responded through extra research studies concentrating on the mechanisms of degradation under ambient conditions. The question of allowable limits of nanoscale MOFs in indoor or outdoor environment could be talked after instituting their toxicity [19].

## 17.5 Conclusion

It can be carefully concluded that more comprehensive studies on the probable environmental and health risks of these emerging materials must be performed before they can be employed for real-world applications. The toxicity of MOFs should be studied in an organized way to safeguard human health and environment. National and International environment protection agencies should develop a methodical way of evaluating all the developed MOFs for their environmental and health impact. In this way, we can reach a stage where we can safely arrange some MOFs based on their toxicity and further regulations can be established. However, all these should not be deferred to the point that one may see MOFs standing with POPs [37], EDCs [38], or other emerging pollutants (USEPA) [39] from the perspective of their toxicity and impact on human health and environment.

## References

- [1] B.M. Connolly, J.P. Mehta, P.Z. Moghadam, A.E.H. Wheatley, D. Fairen-Jimenez, From synthesis to applications: metal–organic frameworks for an environmentally sustainable future, *Curr. Opin. Green Sustain. Chem.* 12 (2018) 47–56, <https://doi.org/10.1016/j.cogsc.2018.06.012>.
- [2] S. Dhaka, R. Kumar, A. Deep, M.B. Kurade, S.-W. Ji, B.-H. Jeon, Metal–organic frameworks (MOFs) for the removal of emerging contaminants from aquatic environments, *Coord. Chem. Rev.* 380 (2019) 330–352, <https://doi.org/10.1016/j.ccr.2018.10.003>.
- [3] T. Faust, MOFs deliver. *Nat. Chem.* 7 (2015) 270, <https://doi.org/10.1038/nchem.2229>.
- [4] Q. Gao, J. Xu, X.-H. Bu, Recent advances about metal–organic frameworks in the removal of pollutants from wastewater, *Coord. Chem. Rev.* 378 (2019) 17–31, <https://doi.org/10.1016/j.ccr.2018.03.015>.
- [5] J.R. Long, O.M. Yaghi, The pervasive chemistry of metal-organic frameworks, *Chem. Soc. Rev.* 38 (2009) 1213–1214, <https://doi.org/10.1039/b903811f>.
- [6] M. Giménez-Marqués, T. Hidalgo, C. Serre, P. Horcajada, Nanostructured metal–organic frameworks and their bio-related applications, *Coord. Chem. Rev.* 307 (2015) 342–360, <https://doi.org/10.1016/j.ccr.2015.08.008>.
- [7] P. Horcajada, R. Gref, T. Baati, P.K. Allan, G. Maurin, P. Couvreur, G. Férey, R.E. Morris, C. Serre, Metal-organic frameworks in biomedicine, *Chem. Rev.* 112 (2012) 1232–1268, <https://doi.org/10.1021/cr200256v>.
- [8] M. Sajid, M. Ilyas, C. Basheer, M. Tariq, M. Daud, N. Baig, F. Shehzad, Impact of nanoparticles on human and environment: review of toxicity factors, exposures, control strategies, and future prospects, *Environ. Sci. Pollut. Res.* 22 (2015) 4122–4143, <https://doi.org/10.1007/s11356-014-3994-1>.
- [9] S.M. Rodrigues, T. Trindade, A.C. Duarte, E. Pereira, G.F. Koopmans, P.F.A.M. Römken, A framework to measure the availability of engineered nanoparticles in soils: trends in soil tests and analytical tools, *TrAC Trends Anal. Chem.* 75 (2015) 129–140, <https://doi.org/10.1016/j.trac.2015.07.003>.
- [10] S.M. Majedi, H.K. Lee, Recent advances in the separation and quantification of metallic nanoparticles and ions in the environment, *TrAC Trends Anal. Chem.* 75 (2016) 183–196, <https://doi.org/10.1016/j.trac.2015.08.009>.
- [11] H.-S. Wang, Metal–organic frameworks for biosensing and bioimaging applications, *Coord. Chem. Rev.* 349 (2017) 139–155, <https://doi.org/10.1016/j.ccr.2017.08.015>.
- [12] S. Wuttke, A. Zimpel, T. Bein, S. Braig, K. Stoiber, A. Vollmar, D. Müller, K. Haastert-Talini, J. Schaeske, M. Stiesch, G. Zahn, A. Mohmeyer, P. Behrens, O. Eickelberg, D.A. Böllükbas, S. Meiners, Validating metal-organic framework nanoparticles for their nanosafety in diverse biomedical applications, *Adv. Healthc. Mater.* 6 (2017) 1600818, <https://doi.org/10.1002/adhm.201600818>.
- [13] T. Simon-Yarza, A. Mielcarek, P. Couvreur, C. Serre, Nanoparticles of metal-organic frameworks: on the road to in vivo efficacy in biomedicine, *Adv. Mater.* 30 (2018) 1707365, <https://doi.org/10.1002/adma.201707365>.

- [14] S.S. Nadar, L. Vaidya, S. Maurya, V.K. Rathod, Polysaccharide based metal organic frameworks (polysaccharide–MOF): a review, *Coord. Chem. Rev.* 396 (2019) 1–21, <https://doi.org/10.1016/j.ccr.2019.05.011>.
- [15] S. Beg, A. Jain, S. Saini, T. Sharma, M.S. Hasnain, S.S. Imam, I. Kazmi, M. Rahman, S. Akhter, B. Singh, Chapter 1. Metal–organic frameworks as expanding hybrid carriers with diverse therapeutic applications, in: A. M. Grumezescu (Ed.), *Organic Materials as Smart Nanocarriers for Drug Delivery*, William Andrew Publishing, Oxford, United Kingdom, 2018, pp. 1–34, <https://doi.org/10.1016/B978-0-12-813663-8.00001-4>.
- [16] P. Kumar, B. Anand, Y.F. Tsang, K. Kim, S. Khullar, Regeneration, degradation, and toxicity effect of MOFs: opportunities and challenges, *Environ. Res.* (2019), <https://doi.org/10.1016/j.envres.2019.05.019>.
- [17] D.F. Sava Gallis, K.S. Butler, L.E.S. Rohwer, A.A. McBride, G. Vincent, C.V. Chong, C.J. Pearce, T.S. Luk, Biocompatible MOFs with high absolute quantum yield for bioimaging in the second near infrared window, *CrystEngComm* 20 (2018) 5919–5924, <https://doi.org/10.1039/C8CE00909K>.
- [18] V. Colombo, S. Galli, H.J. Choi, G.D. Han, A. Maspero, G. Palmisano, N. Masciocchi, J.R. Long, High thermal and chemical stability in pyrazolate-bridged metal–organic frameworks with exposed metal sites, *Chem. Sci.* 2 (2011) 1311, <https://doi.org/10.1039/c1sc00136a>.
- [19] M. Sajid, Toxicity of nanoscale metal organic frameworks: a perspective, *Environ. Sci. Pollut. Res.* 23 (2016) 14805–14807, <https://doi.org/10.1007/s11356-016-7053-y>.
- [20] P. Horcajada, T. Chalati, C. Serre, B. Gillet, C. Sebrie, T. Baati, J.F. Eubank, D. Heurtaux, P. Clayette, C. Kreuz, J.-S. Chang, Y.K. Hwang, V. Marsaud, P.-N. Bories, L. Cynober, S. Gil, G. Férey, P. Couvreur, R. Gref, Porous metal–organic-framework nanoscale carriers as a potential platform for drug delivery and imaging, *Nat. Mater.* 9 (2010) 172–178, <https://doi.org/10.1038/nmat2608>.
- [21] I.B. Vasconcelos, T.G. da Silva, G.C.G. Militão, T.A. Soares, N.M. Rodrigues, M.O. Rodrigues, N.B. da Costa, R.O. Freire, S.A. Junior, Cytotoxicity and slow release of the anti-cancer drug doxorubicin from ZIF-8, *RSC Adv.* 2 (2012) 9437, <https://doi.org/10.1039/c2ra21087h>.
- [22] C. Tamames-Tabar, D. Cunha, E. Imbuluzqueta, F. Ragon, C. Serre, M.J. Blanco-Prieto, P. Horcajada, Cytotoxicity of nanoscaled metal–organic frameworks, *J. Mater. Chem. B* 2 (2014) 262–271, <https://doi.org/10.1039/C3TB20832J>.
- [23] À. Ruyra, A. Yazdi, J. Espín, A. Carné-Sánchez, N. Roher, J. Lorenzo, I. Imaz, D. Maspoch, Synthesis, culture medium stability, and in vitro and in vivo zebrafish embryo toxicity of metal–organic framework nanoparticles, *Chemistry* 21 (2015) 2508–2518, <https://doi.org/10.1002/chem.201405380>.
- [24] T. Baati, L. Njim, F. Neffati, A. Kerkeni, M. Bouttemi, R. Gref, M.F. Najjar, A. Zakhama, P. Couvreur, C. Serre, P. Horcajada, In depth analysis of the in vivo toxicity of nanoparticles of porous iron(III) metal–organic frameworks, *Chem. Sci.* 4 (2013) 1597, <https://doi.org/10.1039/c3sc22116d>.
- [25] T. Kundu, S. Mitra, P. Patra, A. Goswami, D. Díaz Díaz, R. Banerjee, Mechanical downsizing of a gadolinium(III)-based metal–organic framework for anticancer drug delivery, *Chemistry* 20 (2014) 10514–10518, <https://doi.org/10.1002/chem.201402244>.
- [26] G. Chen, X. Leng, J. Luo, L. You, C. Qu, X. Dong, H. Huang, X. Yin, J. Ni, In vitro toxicity study of a porous iron(III) metal–organic framework, *Mol. Ther.* 24 (2019), <https://doi.org/10.3390/molecules24071211>.
- [27] Z.-C. Wang, Y. Zhang, Z.-Y. Li, A low cytotoxic metal–organic framework carrier: pH-responsive 5-fluorouracil delivery and anti-cervical cancer activity evaluation, *J. Clust. Sci.* 29 (2018) 1285–1290, <https://doi.org/10.1007/s10876-018-1446-7>.
- [28] L.-L. Sun, Y.-H. Li, H. Shi, A ketone functionalized Gd(III)-MOF with low cytotoxicity for anti-cancer drug delivery and inhibiting human liver cancer cells, *J. Clust. Sci.* 30 (2019) 251–258, <https://doi.org/10.1007/s10876-018-1482-3>.
- [29] X. Leng, X. Dong, W. Wang, N. Sai, C. Yang, L. You, H. Huang, X. Yin, J. Ni, Biocompatible Fe-based micropore metal–organic frameworks as sustained-release anticancer drug carriers, *Mol. Ther.* 23 (2018), <https://doi.org/10.3390/molecules23102490>.
- [30] C. Han, J. Yang, J. Gu, Immobilization of silver nanoparticles in Zr-based MOFs: induction of apoptosis in cancer cells, *J. Nanopart. Res.* 20 (2018) 77, <https://doi.org/10.1007/s11051-018-4187-5>.



- [31] Z. Li, S. Zhao, H. Wang, Y. Peng, Z. Tan, B. Tang, Functional groups influence and mechanism research of UiO-66-type metal-organic frameworks for ketoprofen delivery, *Colloids Surf. B: Biointerfaces* 178 (2019) 1–7, <https://doi.org/10.1016/j.colsurfb.2019.02.027>.
- [32] M.-X. Wu, Y.-W. Yang, Metal–organic framework (MOF)-based drug/cargo delivery and cancer therapy, *Adv. Mater.* 29 (2017) 1606134, <https://doi.org/10.1002/adma.201606134>.
- [33] P. Horcajada, C. Serre, G. Maurin, N.A. Ramsahye, F. Balas, M. Vallet-Regí, M. Sebban, F. Taulelle, G. Férey, Flexible porous metal-organic frameworks for a controlled drug delivery, *J. Am. Chem. Soc.* 130 (2008) 6774–6780, <https://doi.org/10.1021/ja710973k>.
- [34] C.-Y. Sun, C. Qin, C.-G. Wang, Z.-M. Su, S. Wang, X.-L. Wang, G.-S. Yang, K.-Z. Shao, Y.-Q. Lan, E.-B. Wang, Chiral nanoporous metal-organic frameworks with high porosity as materials for drug delivery, *Adv. Mater.* 23 (2011) 5629–5632, <https://doi.org/10.1002/adma.201102538>.
- [35] Y. Bai, Y. Dou, L.-H. Xie, W. Rutledge, J.-R. Li, H.-C. Zhou, Zr-based metal–organic frameworks: design, synthesis, structure, and applications, *Chem. Soc. Rev.* 45 (2016) 2327–2367, <https://doi.org/10.1039/C5CS00837A>.
- [36] R.M. Abdelhameed, O.M. Darwesh, J. Rocha, A.M.S. Silva, IRMOF-3 biological activity enhancement by post-synthetic modification, *Eur. J. Inorg. Chem.* 2019 (2019) 1243–1249, <https://doi.org/10.1002/ejic.201801442>.
- [37] M. Sajid, C. Basheer, K. Narasimhan, A. Buhmeida, A. Qahtani, M.S. Al-ahwal, Persistent and endocrine disrupting organic pollutants: advancements and challenges in analysis, health concerns and clinical correlates, *Nat. Environ. Pollut. Technol.* 15 (2016) 733–746.
- [38] M. Sajid, C. Basheer, K. Narasimhan, M. Choolani, H.K. Lee, Application of microwave-assisted micro-solid-phase extraction for determination of parabens in human ovarian cancer tissues, *J. Chromatogr. B Anal. Technol. Biomed. Life Sci.* 1000 (2015) 192–198, <https://doi.org/10.1016/j.jchromb.2015.07.020>.
- [39] USEPA, Contaminants of Emerging Concern including Pharmaceuticals and Personal Care Products, <https://www.epa.gov/wqc/contaminants-emerging-concern-including-pharmaceuticals-and-personal-care-products>.

# Functional MOFs as theranostics

Heng Zhao<sup>a</sup>, Christian Serre<sup>a</sup>, Eddy Dumas<sup>b</sup>, Nathalie Steunou<sup>b</sup>

<sup>a</sup>Institut des Matériaux Poreux de Paris, FRE 2000 CNRS, Ecole Normale Supérieure, Ecole Supérieure de Physique et de Chimie Industrielles de Paris, PSL Research University, Paris, France <sup>b</sup>Lavoisier Institute of Versailles, UMR CNRS 8180, UVSQ Paris-Saclay University, Versailles, France

## Abbreviations

|                  |                                       |
|------------------|---------------------------------------|
| <b>3-MA</b>      | 3-methyladenine                       |
| <b>4,4'-DTBA</b> | 4,4'-dithiobisbenzoic acid            |
| <b>5-FAM</b>     | 5-carboxyfluorescein                  |
| <b>5-FU</b>      | 5-fluorouracil                        |
| <b>AS</b>        | artesanate                            |
| <b>BBDC</b>      | 5-boronobenzene-1,3-dicarboxylic acid |
| <b>BSA</b>       | bovine serum albumin                  |
| <b>CO</b>        | carbon monoxide                       |
| <b>Cy</b>        | cyanine                               |
| <b>DOX</b>       | doxorubicin hydrochloride             |
| <b>DDS</b>       | drug delivery systems                 |
| <b>DHA</b>       | dihydroartemisinin                    |
| <b>EPR</b>       | enhanced permeability and retention   |
| <b>ESCP</b>      | ethoxysuccinato-cisplatin             |
| <b>EV</b>        | extracellular vesicle                 |
| <b>FA</b>        | folic acid                            |
| <b>GSH</b>       | glutathione                           |
| <b>HA</b>        | hyaluronic acid                       |
| <b>ICG</b>       | indocyanine green                     |
| <b>LA</b>        | lactobionic acid                      |
| <b>LSS</b>       | liquid-solid-solution                 |
| <b>MDR</b>       | multidrug resistance                  |
| <b>MDT</b>       | microwave dynamic therapy             |
| <b>MIL</b>       | materials of institut lavoisier       |
| <b>MOF</b>       | metal-organic frameworks              |
| <b>MRI</b>       | magnetic resonance imaging            |
| <b>MTT</b>       | microwave thermal therapy             |
| <b>NCPs</b>      | nanoscale coordination polymers       |
| <b>NCs</b>       | nanocubes                             |
| <b>NIR</b>       | near-infrared                         |
| <b>NIRF</b>      | near-infrared fluorescent             |
| <b>nMOF</b>      | nanoMOF                               |
| <b>NPs</b>       | nanoparticles                         |

|             |                                                    |
|-------------|----------------------------------------------------|
| NSF         | nephrogenic systemic fibrosis                      |
| PAI         | photoacoustic imaging                              |
| PB          | Prussian blue                                      |
| PDA         | polydopamine                                       |
| PDT         | photodynamic therapy                               |
| PEG         | polyethylene glycol                                |
| PET         | positron emission tomography                       |
| PPy         | polypyrrole                                        |
| PTT         | photothermal therapy                               |
| QDs         | quantum dots                                       |
| RAFT        | reversible addition-fragmentation chain transfer   |
| RGD         | cyclic arginine-glycine-aspartic acid              |
| ROS         | reactive oxygen species                            |
| SNO         | S-nitrosothiol                                     |
| SPAAC       | strain-promoted [3 + 2] azide-alkyne cycloaddition |
| SPECT       | photon emission computer tomography                |
| TCPP        | tetra(4-carboxyphenyl)porphine                     |
| TNBC        | triple-negative breast cancer                      |
| UCNPs       | upconverting nanoparticles                         |
| USPIO       | ultra-small superparamagnetic iron oxide           |
| VER         | verapamil hydrochloride                            |
| ZGGO        | zinc gallogermanate                                |
| ZIF-8       | zeolitic imidazolate framework-8                   |
| $\beta$ -CD | $\beta$ -cyclodextrin                              |

| <b>Common MOFs</b>          |                                                                        |                                                         |             |
|-----------------------------|------------------------------------------------------------------------|---------------------------------------------------------|-------------|
| MOF                         | Metal cluster/<br>core                                                 | Ligand                                                  | Node        |
| MIL-100(Fe)                 | FeO <sub>6</sub>                                                       | Trimesic acid (BTC)                                     | 6-connected |
| MIL-101(Fe)                 | Fe <sub>3</sub> ( $\mu_3$ -O) <sub>6</sub> ( $\mu_3$ -OH) <sub>3</sub> | Terephthalic acid (BDC)                                 | 6-connected |
| MIL-101(Fe)-NH <sub>2</sub> | Fe <sub>3</sub> ( $\mu_3$ -O) <sub>6</sub> ( $\mu_3$ -OH) <sub>3</sub> | 2-aminobenzene-1,4-dicarboxylate (BDC-NH <sub>2</sub> ) | 6-connected |
| MIL-127                     | Fe <sub>3</sub> ( $\mu_3$ -O) <sub>6</sub> ( $\mu_3$ -OH) <sub>3</sub> | 3,3',5,5'-azobenzene-tetracarboxylate (Tazb)            | 6-connected |
| Fe-MIL-53-NH <sub>2</sub>   | FeO <sub>4</sub> (OH) <sub>2</sub>                                     | Terephthalic acid (BDC)                                 | 6-connected |
| ZIF-8(Zn)                   | Zn <sup>2+</sup>                                                       | 2-methylimidazolate (MeIM)                              | 4-connected |
| Uio-66(Zr)                  | [Zr <sub>6</sub> O <sub>4</sub> (OH) <sub>4</sub> ]                    | Terephthalic acid (BDC)                                 | 6-connected |

## 18.1 Introduction

Theranostics combines therapeutic property and diagnostic imaging to treat disease with high therapeutic effects through a precise and personalized approach together with minimal side effects. In recent years, it has become a hot topic with an increasing interest from chemists or scientists to explore novel theranostic nanoprobes [1, 2].

Biocompatible metal-organic frameworks (MOFs), highly porous crystalline porous solids, have been widely known as drug delivery systems considering their large pore sizes/volumes and ideal drug adsorption capacities. Apart from drug delivery, nanoMOFs also have been considered as imaging agent to diagnose different diseases such as cancer or as therapeutic agent used in preclinic research [3–7]. Most of the nanoMOFs reaching a preclinical in vivo evaluation are based on Fe carboxylates or Zn azolates [8–11]. Until 2010, nanoMOFs have been mainly considered for imaging or therapy, and their use for theranostics gradually attracted researchers' attention particularly since 2015 where it encountered a rapid development [12–16]. Particularly, the construction of hybrid systems associating nanoMOFs with functional organic or inorganic nanoparticles paved the way for the development of multifunctional or multimodal nanoMOF theranostic probe [3, 9, 17].

In this chapter, we mainly discuss the developments of cancer theranostics based on nanoMOFs within the past decade, which includes topical MOFs such as MIL-100(Fe), ZIF-8(Zn) and UiO-66(Zr), etc. This contains the following subchapters: magnetic nanoMOFs, noble metal nanoparticles-encapsulated nanoMOFs, polymer-assisted nanoMOFs, fluorescent nanoMOFs, phototherapeutic nanoMOFs, nuclear medical imaging nanoMOFs, and other stimuli-responsive nanoMOF. Note that a single type of nanoMOF system combines several features and applications at the same time and could match more than one classification.

## ***18.2 MOFs NPs with multitherapy and MR/optical imaging properties***

### ***18.2.1 Magnetic-based MOFs NPs***

Magnetic nanoMOFs is a class of nanomaterials combining the magnetic properties of the metal or metal-oxides nanoparticle with the drug-loading ability of the nanoMOF. These systems are able to carry and deliver specific drugs in biological systems whose release is triggered on a controlled manner under the application of a magnetic field [18, 19]. Magnetic resonance imaging (MRI) is a powerful imaging technique due to its ability to provide high spatial resolution and tissue penetration. In the present case, the magnetic nanoparticles affect the relaxivity of the protons from water. High spin paramagnetic gadolinium (Gd) or iron (Fe) oxides superparamagnetic nanoparticles are typically integrated or coupled with nanoMOFs as MRI contrast agents.

#### ***18.2.1.1 Gd-based MOF NPs***

As positive contrast agents, Gd-based nanoMOFs produce a large shortening of the longitudinal relaxation time (T1) and high longitudinal relaxivity ( $r_1$ ). Boyes's et al. have prepared polymer-modified Gd nanoMOFs via a reversible addition-fragmentation chain transfer (RAFT) polymerization for targeted imaging and treatment of cancer [20]. However, bimodal imaging (magnetic resonance and fluorescence microscopy) and cell growth inhibition were only considered at the in vitro level.

Yin's group also developed a Gd-carboxylate nanoMOFs theranostic platform for MRI-guided pH-responsive chemotherapy in vivo based on a 5-boronobenzene-1,3-dicarboxylic acid (BBDC) as a versatile ligand, leading to an enhanced permeability and retention (EPR) effect and glucose-mediated glucose-transported protein (GLUT1) tumor targeting; this led to: (i) an improved biocompatibility, (ii) efficient active targeting of tumors, and (iii) a pH-responsive switch for leakage-free DOX delivery as three birds with one stone [21].

Via utilizing photodynamic porphyrin carboxylate as Gd MOFs ligand, Li's group developed a FA-conjugated Gd-porphyrin MOF for fluorescence imaging and MRI dual-modality imaging and photodynamic therapy using zebrafish to develop tumor model of Hepatocellular carcinoma [22]. The relaxivities of the resulting Gd-based nanoMOFs were significantly higher than typical Gd chelates and the EPR effect took advantage of their higher molecular weights. Such a multimodal imaging approach is attractive to guide cancer therapy clinically.

#### 18.2.1.2 Fe-carboxylate MOFs NPs

Considering the potential leaching of highly toxic  $Gd^{3+}$  ions from the in vivo degradation of Gd-carboxylate-based nanoMOFs, which may lead to nephrogenic systemic fibrosis (NSF) in patients, highly porous nontoxic iron(III)-carboxylate nanoMOFs have attracted so far a great deal of attention as drug nanocarriers.

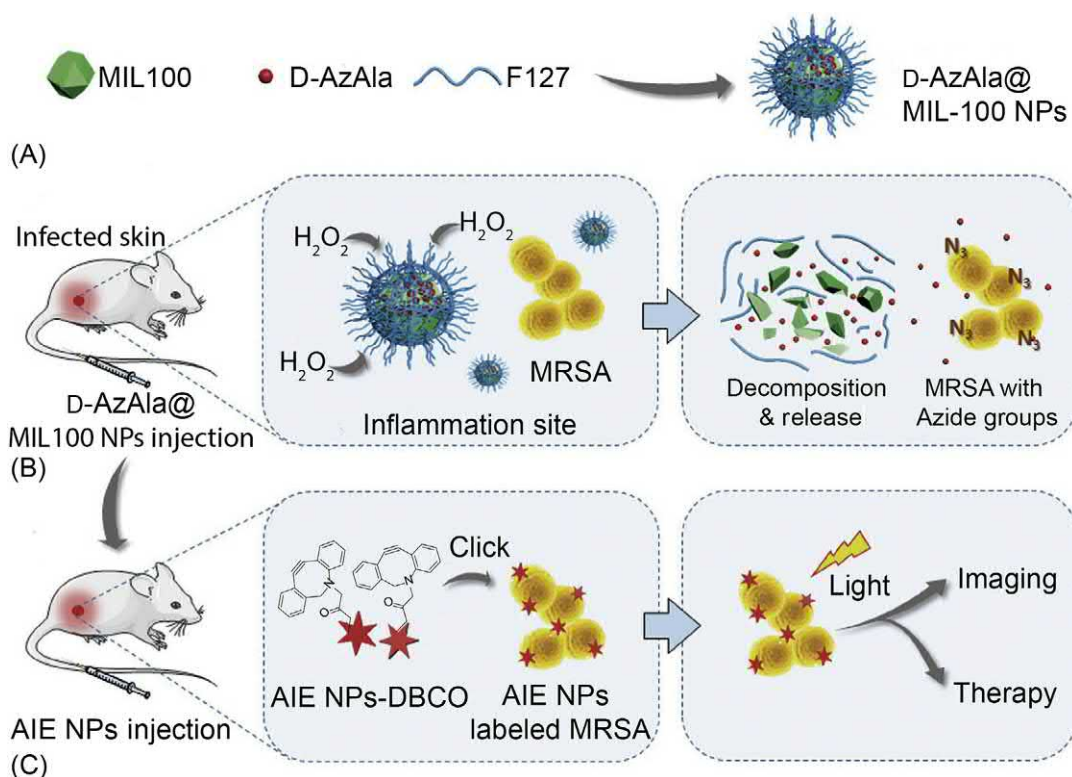
To make nanoMOFs efficient theranostic systems, it is necessary to synthesize nanoparticles of several hundred nanometers with a narrow polydispersity. Among the large number of existing Fe-carboxylate MOFs, MIL-n materials combine several features of interest: a good chemical stability, a large porosity suitable for high drug payloads, a low toxicity, and intrinsic imaging properties. Horcajada et al. have shown that MIL nanoMOFs with engineered cores and surfaces are a class of nanocarriers for the controlled delivery of series of challenging antitumoral and retroviral drugs, which also possess interesting in vivo imaging properties and opens the way for theranostics, or personalized patient treatments [23].

Lin's group also reported a strategy of delivering an imaging contrast agent organic fluorophore together with an anticancer drug ethoxysuccinato-cisplatin (ESCP) prodrug by postsynthetic grafting of the outer surface of the MIL-101(Fe) nanoMOF (MIL stands for Materials of Institut Lavoisier) [24].

To overcome the poor biodistribution of drugs with frequent dose-related side effects, Zhang's group reported a biocompatible nanoMOF-based tumor targeting Drug Delivery Systems (DDS) developed through a one-pot organic solvent-free "green" postsynthetic surface modification procedure. Authors started from the preformed MIL-101(Fe)- $N_3$  nanoMOF, then functionalized by a bicyclononyne functionalized  $\beta$ -cyclodextrin ( $\beta$ -CD) derivative (through strain-promoted [3 + 2] azide-alkyne cycloaddition (SPAAC)) further combined with an adamantane functionalized PEG polymer and targeting peptide cyclic arginine-glycine-aspartic

acid (RGD) through host-guest interactions [25]. Due to the covalently linked pH-responsive benzoic imine bond and the redox-responsive disulfide bond, this multifunctional DDS showed an acidic environment-enhanced tumor cell uptake and tumor intracellular GSH-triggered drug release, which inhibited tumor growth effectively with minimal side effects.

Based on MIL-100(Fe) nanoparticles and through SPAAC reaction, Liu et al. designed a novel two-steps strategy for specific in vivo imaging of bacteria based on the metabolic labeling technique for image-guided antibacterial therapy (Fig. 18.1) [26]. Herein, 3-azido-d-alanine (d-AzAla) was first labeled on MIL-100 (Fe) NPs and after intravenous injection and d-AzAla was selectively integrated into the cell walls of bacteria, which was then confirmed by fluorescence imaging from DBCO-Cy5.



**Fig. 18.1**

The proposed strategy of bacteria diagnosis and therapy by the  $H_2O_2$ -responsive MOFs assisted in vivo metabolic labeling of bacteria (methicillin-resistant *Staphylococcus aureus* (MRSA)). (A) The synthesis of azido-labeled D-AzAla@MIL-100 (Fe) NPs (d-AzAla = 3-azido-D-alanine). (B) The accumulation and decomposition of D-AzAla@MIL-100 (Fe) NPs in the presence of  $H_2O_2$  at the site of the infected tissue, followed by internalization of invading bacteria. (C) Ultra-small AIE (aggregation-induced emission) NPs with dibenzocyclooctyne (DBCO) group bind with bacteria through click reaction for tracking and effective photodynamic therapy (PDT) of bacteria [26].



In another study, Liu et al. synthesized under ambient conditions pH-responsive nanoparticles of coordination polymers (denoted Fe-CPNDs) via a simple and scalable method based on the reaction among  $\text{Fe}^{3+}$  ions, gallic acid, and poly(vinylpyrrolidone) [27]. As a class of renal clearable nanomedicine, these ultra-small nanoparticles of Fe-CPNDs (5.3 nm) were used for pH-sensitive MRI-guided photothermal therapy which completely suppressed tumor growth. In short, one can consider that based on the very low toxicity and the interesting photothermal/photodynamic properties of these nanoMOFs, solely Fe(III) carboxylate nanoMOFs could be considered as safe and efficient candidates for theranostics in nanomedicine. However, the potential challenges for clinical translation may still be limited by their current lack of commercialization.

### 18.2.1.3 Composite nano-objects based on Fe-carboxylate MOFs

The association of MOFs and functional nanoparticles has led to the creation of new multifunctional composite hybrid systems. However, until recently, these hybrid materials have been mainly considered for other applications such as hydrogen storage or heterogeneous catalysis [28–31]. In nanomedicine, series of hybrid nanostructures were recently constructed from nanoMOFs to form multifunctional drug delivery systems.

Chen's group developed core-shell Prussian Blue (PB) nanocube@Fe-BTC MOF for pH-responsive artemisinin delivery, MRI, and fluorescence optical imaging (FOI)-guided chemo/photothermal combinational cancer therapy [32]. Interestingly, dual nanoMOFs integrated the T1/T2 MRI, photothermal ability, and photoluminescence properties of PB. Furthermore, this strategy was applied for the construction of PB@ZIF-8 nanoparticle system, and the endogenous degradation of ZIF-8 in acid tumor microenvironment was combined with exogenous NIR stimuli to realize efficient drug delivery [33].

Ultra-small superparamagnetic magnetite ( $\text{Fe}_3\text{O}_4$ ) nanoparticles have generated a widespread interest due to their potential applications in magnetic separation, magnetic hyperthermia, magnetic targeting, and MRI. Sahu's group incorporated  $\text{Fe}_3\text{O}_4$  nanoparticles into a degradable zinc carboxylate metal-organic framework (IRMOF-3) and the cancer chemotherapy drug paclitaxel was conjugated to the magnetic NMOFs through hydrophobic interactions for targeted anticancer drug delivery and MR imaging [34]. The targeting nanoparticles killed the cancer cells effectively, but only an in vitro model was considered so far. To some extent, these folic acid-conjugated magnetic NMOFs also showed a stronger  $T_2$ -weighted MRI contrast.

Chen's group developed  $\text{Fe}_3\text{O}_4$ @C@Fe-BTC MOF nanoparticles through a layer-by-layer formation of Fe-BTC MOF at the surface of particles combining  $\text{Fe}_3\text{O}_4$  and carbon dots. While  $\text{Fe}_3\text{O}_4$ @C imparts multimodal imaging properties (photoluminescence and MR) and magnetic targeting ability, Fe-BTC MOF was used for the co-delivery of the anticancer Dihydroartemisinin (DHA), the toxicity of which is increased in the presence of Fe(II) [35].

Through the pH-responsive degradation of Fe-BTC, MOF Fe(III) was released in the tumor followed by its reduction into ferrous ions. The interaction of Fe(II) with DHA led to the production of reactive oxygen species (ROS). A similar strategy was applied by using preformed PB nanocubes  $\text{Mn}_3[\text{Co}(\text{CN})_6]_2$ . Similar core-shell  $\text{Fe}_3\text{O}_4$ @nanoMOF composites were also obtained with UiO-66 and Bio-MOF for simultaneous drug delivery and tumor visualization via MRI [36, 37].

As an ultra-small superparamagnetic iron oxide (USPIO) NP, maghemite ( $\gamma\text{-Fe}_2\text{O}_3$ ) is of great interest. Steunou et al. designed through a postsynthetic strategy a maghemite-nanoMIL-100 (Fe) bimodal nanovector as a platform for image-guided therapy [38]; when the maghemite content was of 10 wt%, this led to relaxivity values reaching those of the commercial USPIO systems, while keeping the drug delivery properties of the bare nanoMOF paving the way for their use in theranostics.

#### 18.2.1.4 Mn-based MOFs NPs

Manganese(II) ( $\text{Mn}^{2+}$ ), although with a higher toxicity and lower daily dose compared to iron ions, has been demonstrated with its five unpaired 3d electrons to be an effective T1 contrast agent in MRI. Recently, Mn-based MOFs have, therefore, been considered for theranostics.

Lin's group reported the self-assembly of a Mn-bisphosphonate nanoscale coordination polymers (NCPs) with a lipid and PEG coating; this theranostic NCP platform was capable of delivering a chemotherapeutic drug to cancer cells and behaved as an MRI contrast agent simultaneously to cancer cells with high cargo loadings [39].

Considering the toxic adverse effects and resistance to drugs of chemotherapy, Yin's group developed theranostic Mn-porphyrin Zr(IV) carboxylate nanoMOFs; the bridging Mn-porphyrin ligand was used for a MRI-guided nitric oxide and photothermal synergistic therapy [40]. Interestingly, free-radical NO treatment was introduced to overcome the disadvantages of singlet oxygen ( $^1\text{O}_2$ )-based PDT due to the local hypoxia of tumor and through the formation of heat-sensitive NO donor S-Nitrosothiol (SNO). NO release and PTT were obtained simultaneously under near-infrared (NIR) light irradiation.

#### 18.2.2 MOFs NPs for photodynamic and photothermal therapy

Phototherapeutic therapy, including photothermal therapy (PTT) and photodynamic therapy (PDT), is an highly effective, noninvasive, selective method for cancer treatment [41].

Meng's group prepared flexible Mn-doped UiO-66 nanocubes (NCs) with a small particle size ( $\sim 60$  nm) through a one-pot hydrothermal route. This led to a nanosystem combining microwave dynamic (MDT) and microwave thermal (MTT) therapies well suited to suppress

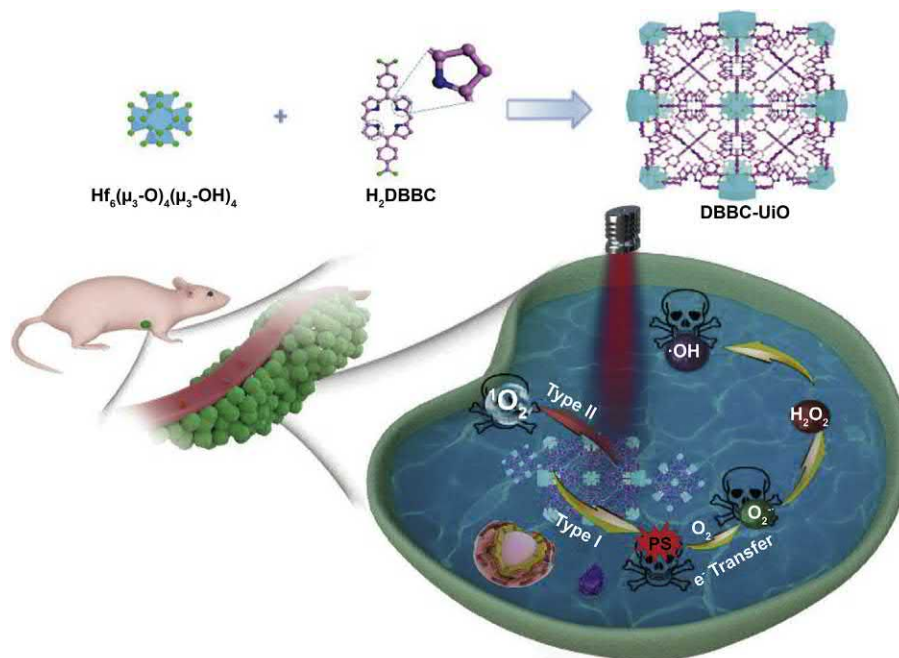
the tumor cell growth in vivo and in vitro under mild microwave irradiation [42], highlighting the synergic effect between MTT and MDT.

Porphyrin ligands are interesting for photodynamic therapy, but their use is limited by their poor solubility, self-quenching, and aggregation issues. Porphyrin carboxylate-based MOFs are a recent subclass of MOFs with a good biocompatibility, although they are still produced using toxic solvents, emitting bright red fluorescence for fluorescence imaging; they exhibit also photosensitizing properties suitable for photodynamic therapy. Ju's group designed multifunctional porphyrin-based MOFs NPs by assembling porphyrin, folate targeting-motif, and dye-labeled peptide into MOF cages [43]. After folate receptor-mediated uptake, the nanoprobe could efficiently generate  $^1\text{O}_2$  in mitochondria to induce cell apoptosis.

Zr(IV)-based porphyrinic MOF nanoparticles PCN-224 also attracted attention for tumor-targeted photodynamic therapy and hypoxia-amplified bioreductive therapy [44, 45]. Through cancer cell membrane coating, another novel cancer cell membrane@Pt(II) porphyrinic MOF (mPPt) was also developed as a biomimetic theranostic  $\text{O}_2$ -meter for cancer-targeted photodynamic therapy and phosphorescence imaging [46]. In type II mechanism of photodynamic therapy (PDT), the ground triplet-state molecular oxygen ( $^3\text{O}_2$ ) is transformed to the reactive singlet oxygen ( $^1\text{O}_2$ ). However, the process is extremely dependent on oxygen ( $\text{O}_2$ ), and the lack of  $\text{O}_2$  will directly suppress the PDT efficacy. In the type I mechanism,  $\text{O}_2^- \bullet$  molecule could be further converted to partially recyclable  $\text{O}_2$  under the effects of intracellular superoxide dismutase (SOD) and part of them could be transformed to high toxic hydroxyl radical ( $\text{OH} \bullet$ ). To overcome a hypoxia microenvironment, Dong's group developed bacteriochlorin-based Hf MOFs termed DBBC-UiO as a NIR laser-induced  $\text{O}_2^- \bullet$  generator for photoacoustic imaging (PAI)-guided PDT through synergistic type I ( $\text{O}_2$ -independent) and type II mechanism for hypoxia tumor ablation (Fig. 18.2) [47]. Tumor-specific PAI and highly efficient hypoxic solid tumor ablation were shown in the experiment.

### ***18.2.3 Nano-objects based on MOFs and inorganic NPs for optical imaging, photodynamic/photothermal therapy***

Noble metal nanoparticles (NPs), especially anisotropic gold NPs (AuNPs), are broadly recognized as candidates for cancer theranostics because of their good biocompatibility, high light-to-heat conversion efficiency, and unique near-infrared (NIR) light absorption feature. Note, however, that the elimination pathways of such nanoparticles are highly questionable particularly when the nanoparticles are nondegradable. In general, nanoparticles with a size of  $<5$  nm will undergo in vivo renal elimination via the kidneys and finally through urine. In the case of nanoparticles  $>5$  nm, the biodegradable ones can be disassembled first and then return to the metabolic circulation, while most nondegradable nanoparticles ( $>5$  nm) will be retained in long term in liver nonparenchymal cells such as Kupffer cells, which act as barriers of hepatobiliary elimination [48].



**Fig. 18.2**

The synthetic procedure and photo-induced PDT mechanism of DBBC-UiO.

### 18.2.3.1 Core-shell Au NRs@MOFs

Tang's group combined anisotropic gold nanorods (AuNR) and ZIF-8 into core-shell nanostructures AuNRs@ZIF-8 as a multifunctional nanoplatform for near-infrared-induced synergistic chemo-photothermal therapy (Fig. 18.3) [49]. Gold nanorods with high NIR-light-triggered photothermal properties are good candidates for photothermal therapy, and its drug-loading capacity was improved through the ZIF-8 shell. However, this work was mainly focused on photothermal therapy and more work needs to be done considering the questionable elimination of nondegradable Au NPs.

Through similar strategy, Li's group developed biocompatible Au@Ag nanorod@ZIF-8 core-shell nanoparticles for surface-enhanced Raman scattering (SERS) imaging and doxorubicin (DOX) delivery. For a better SERS signal, 4-aminothiophenol (4-ATP) was adsorbed on the surface of Au@Ag nanorod and the ZIF-8 shell played the role of the drug carrier and also improved the stability and biocompatibility of the SERS tag. A targeting drug therapy and imaging was shown in vitro [50].

Zhang's group used functionalized gold nanorods to construct through a solvothermal method porphyrinic nanoMOFs-coated gold nanorods (AuNR@MOFs) for combined photodynamic/photothermal/ chemotherapy of tumor. Camptothecin (CPT) was chosen as a

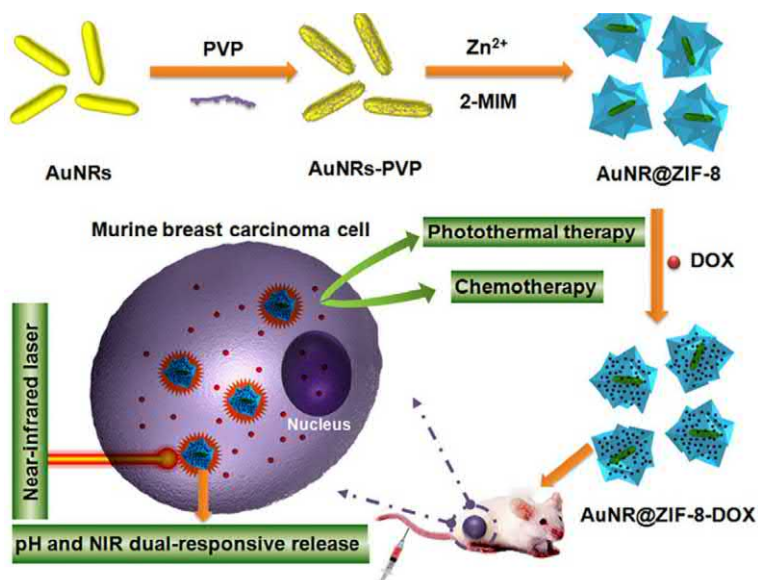


Fig. 18.3

The fabrication of AuNR@ZIF-8 core-shell nanostructures as a novel multifunctional nanoplatform for synergistic chemo-photothermal cancer therapy both in vitro and in vivo.

model drug, and through the triple synergistic therapy, the tumor cells were damaged efficiently both in vitro and in vivo [51].

Janus nanoparticles have shown also to have a great potential as theranostic platform in tumor treatment, but were mainly limited to oxides and metals. Interestingly, Han's group prepared a unique lactobionic acid (LA)-modified AuNR/ZIF-8 Janus nanoplatform via a selective growth of ZIF-8 on the polyacrylic acid (PAA) side of preformed Janus Au NR/ PAA nanoparticles. These original nano-objects were used for CT imaging-guided liver cancer therapy by the combined effect of chemotherapy and PTT [52].

#### 18.2.3.2 Nano-objects based on MOFs and Au nanospheres/nanoclusters

The Au nanosphere with a size of tens of nanometers could not only act as photothermal agents to kill cancer cells and promote drug release, but also enhanced Raman signal. Meanwhile, considering nanoscale metal-organic frameworks (NMOFs) with high porosities and high internal surface areas as drug delivery system, Hu's group designed Raman tag-bridged core-shell Au@Cu<sub>3</sub>(BTC)<sub>2</sub> nanoparticles for Raman imaging and synergistic chemo-photothermal therapy [53]. Theranostic applications for cell tracking and in vivo synergistic chemo-photothermal therapy of tumor were conducted, but the tumors were partially retained. Moreover, the toxicity of Cu ion and the elimination of Au nanosphere with large particle size may be a potential problem.

Gold quantum dots are very small nanoparticles (a few nm) which exhibit distinctive optical and magnetic behaviors compared with larger gold nanoparticles. Au nanoclusters (AuNCs) have been extensively applied as fluorescent probes for various biomedical applications due to their unique chemical and physical properties [54–56], especially for cell imaging or detection [57–59] and even for *in vivo* theranostics [60]. There is also an interest in biomedicine for hybrid Au nanoclusters, such as Au<sub>25</sub> nanoclusters [61–63].

Yang's group has developed an inorganic-organic Fe<sub>3</sub>O<sub>4</sub>/ZIF-8-Au<sub>25</sub> nanocomposite for magnetically targeted photodynamic/photothermal therapy. Briefly, upon 808 nm NIR light irradiation, the attached Au<sub>25</sub> clusters can generate hyperthermia to produce a unique photothermal therapy modality, while an efficient singlet oxygen can also be produced for PDT. Furthermore, the encapsulated Fe<sub>3</sub>O<sub>4</sub> nanocrystals could also serve as a PTT agent [64]. The introduction of small Au nanoclusters, when designing hybrid theranostic nanoMOFs, is quite advantageous not only due to their ability to produce ROS for photodynamic therapy, but also as a result of their easier renal clearance in comparison to larger inorganic nanoparticles.

Wang's group designed a multifunctional Fe<sub>3</sub>O<sub>4</sub>@PAA/AuNCs/ZIF-8 NPs nanoplatform with a 130 nm size that combines MR, CT, and fluorescence tri-modal imaging, ultrahigh anticancer drug-loading, and dual pH-responsive drug release properties (Fig. 18.4) [65]. In this work, Fe<sub>3</sub>O<sub>4</sub>@PAA core-shell NPs and GSH-capped AuNCs were prepared, respectively,

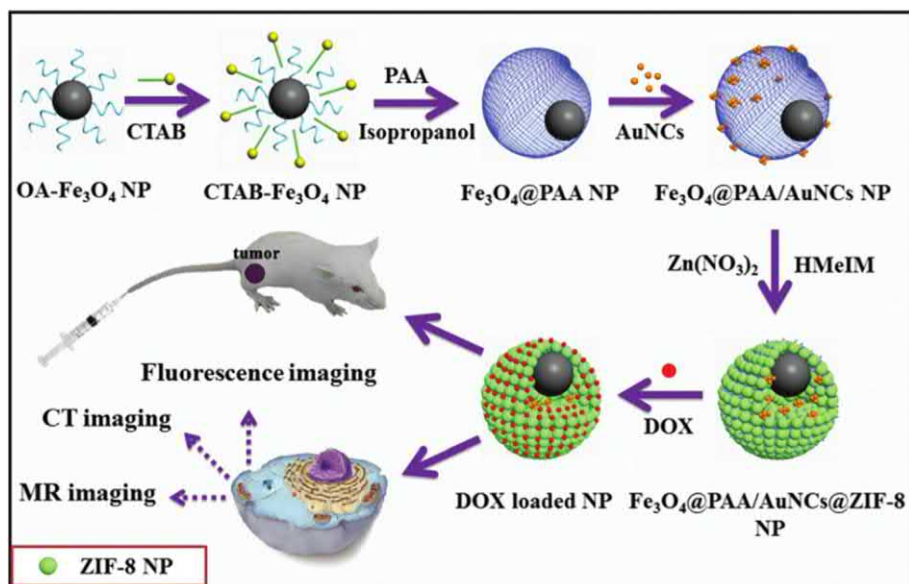


Fig. 18.4

The preparation of Fe<sub>3</sub>O<sub>4</sub>@PAA/AuNCs/ZIF-8 composite NPs for simultaneous tri-modal cancer imaging and chemotherapy.



and then ZIF-8 was formed at the surface of  $\text{Fe}_3\text{O}_4\text{@PAA/AuNCs}$ . Such multifunctional NPs are of interest for their multimodal cancer diagnostics and visualized-synergistic therapy.

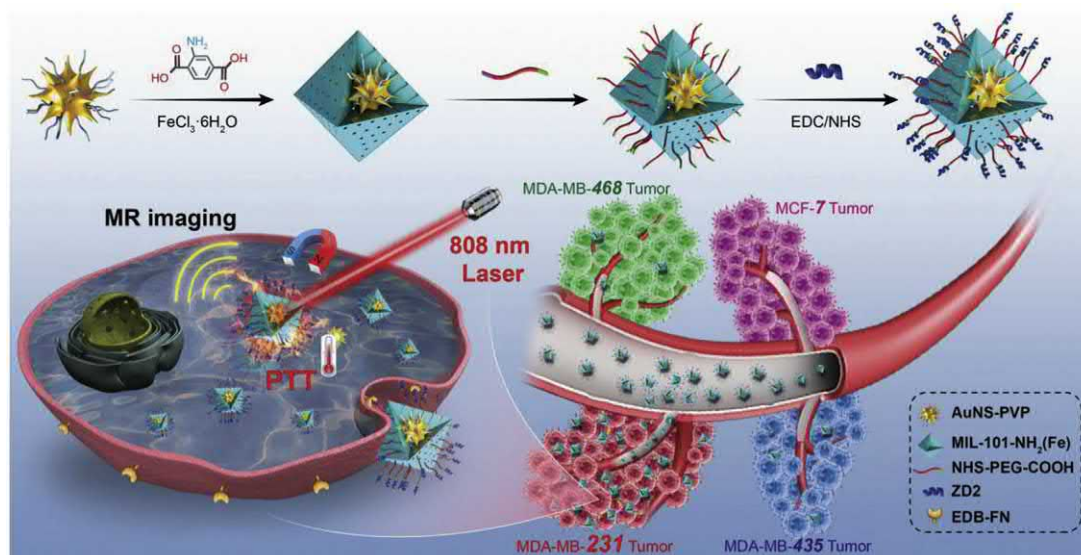
In another approach, the attachment of BSA-modified AuNCs at the surface of MIL-101(Fe) was performed to build multifunctional theranostic nanoMOFs. MIL-101(Fe) $\text{@BSA-AuNCs}$  presented MRI and fluorescence properties and was used as microwave-sensitive reagent for microwave thermal therapy, MRI, and fluorescence imaging (FI) [66].

### 18.2.3.3 Core-shell Au nanostar@ nanoMOF

To cure the triple-negative breast cancer (TNBC), one of the most dangerous subtypes among breast cancers, Zeng's group prepared core-shell gold nanostar@ MIL-101- $\text{NH}_2(\text{Fe})$  whose surface is covalently modified by a short peptide ZD2 able to target the TNBC. This nano-object was used for T1-weighted MRI and photothermal therapy specifically targeting TNBC (Fig. 18.5) [67]. MIL-101- $\text{NH}_2(\text{Fe})$  is a biocompatible and biodegradable MOF-bearing amino groups that could be further functionalized by ZD2 to achieve an active-targeted ability. MIL-101- $\text{NH}_2(\text{Fe})$  through its very large pores is able to upload record amounts of drugs which is of interest for further synergistic cancer therapy.

### 18.2.3.4 Nano-objects based on MOFs and upconversion NPs (UCNPs)

Upconversion nanoparticles (UCNPs), capable of converting near-infrared radiation to visible light, were chosen as optical probe in biological assays and medical imaging. Deng's group



**Fig. 18.5**

The synthesis of AuNS@MOF-ZD2 nanoprobes and application of T1-weighted MRI and photothermal therapy specifically toward MDA-MB-231 tumor (TNBC) [67].

developed an aptamer-modified core-shell nano-objects composed of upconversion luminescent  $\text{NaYF}_4:\text{Yb}^{3+}/\text{Er}^{3+}$  nanoparticles-based core and Fe-BTC MOF shell. These UCNPs@MOF nanocomposites exhibit upconverting green emission under laser excitation at 980 nm, thereby providing the possible optical imaging for in vivo bioprobes. This hybrid system showed great promises for simultaneous in vitro upconverting imaging and chemotherapy of cancer cells [68]. Apart from MIL100(Fe), ZIF-8 was also developed to encapsulate UCNPs with the modification of folic acid, which demonstrated in vitro its efficient pH-responsive drug delivery properties [69].

Cha's group used DNA-mediated assembly of core-satellite structures composed of Zr (IV)-based porphyrinic MOF (PCN-224) and UCNPs for photodynamic therapy (PDT) [70]. Herein, singlet oxygen ( $^1\text{O}_2$ ) was generated by Zr porphyrinic MOF NPs upon photo-irradiation in NIR. By assembling UCNPs with MOFs, it was possible to take advantage of the increased penetration of NIR light. UCNP NPs were used to excite the porphyrinic ligand due to their ability to absorb in the NIR and emit visible light. A high singlet oxygen production was observed under 980 nm irradiation by using the core-satellite UCNP-PCN-224 and this amount was significantly higher than what can be produced from simply mixing UCNPs and MOF NPs.

#### 18.2.3.5 Nano-objects based on CuS and MOF NPs

CuS NPs is one of the most common PTT agents used for the design of nanocomposites suitable for chemo-PTT. ZIF-8 was used by Luan's group to co-encapsulate the anticancer quercetin, CuS nanoparticles, in order to reach a synergy between chemotherapy and PTT [71]. Moreover, folic acid-bovine serum albumin (FA-BSA) conjugates were grafted to stabilize the CuS@ZIF-8-QT and design an active-targeting drug delivery system. As a result, in vivo and in vitro anticancer PTT/chemotherapy was demonstrated under NIR irradiation.

Yin's group developed an "all-in-one" antitumor and antirecurrence/metastasis nanocarrier by combining CuS nanoparticles, protoporphyrin IX, and Doxorubicin during the synthesis of ZIF-8 to obtain a chemo-, photothermal-, and photodynamic-nanosystem able to eliminate solid tumors under the guidance of MRI and infrared thermal imaging [72].

### 18.2.4 Hybrid nanoparticles by combining MOFs with organic molecules and materials

#### 18.2.4.1 Photothermal MOFs-polymer nanocomposites

Polymers are commonly combined to MOF nanovectors not only to process and stabilize MOFs NPs, but also to enhance their blood circulation and enable specific cell targeting. In addition, polymers were also used to impart physical properties such as PTT ability. In the following, we will discuss recent examples in which polymers were used as photothermal agents.

As a type of photothermal agent, polypyrrole (PPy) has shown great potential for the photothermal treatment of cancer *in vitro* and *in vivo*. Fan's group fabricated multifunctional core-shell PPy@MIL-100(Fe) nanoparticles with PPy NPs acting as cores and the MIL-100(Fe) as the outer shell. Doxorubicin (DOX) was encapsulated in the MOF for a simultaneous photothermal therapy and chemotherapy of cancer cells. Herein, the introduction of PVP was used to facilitate the nucleation and growth of MIL-100(Fe) on the surface of PPy [73]. This resulted finally into an outstanding *in vivo* synergistic anticancer ability. Following a similar strategy, Wang's group further conducted Photoacoustic(PA) and MR dual-mode imaging and synergistic chemo-photothermal killing effects *in vitro* based on PPy@MIL-100 nanoparticles [74]. The strong NIR absorbance and T<sub>2</sub> relaxation signal of PPy@MIL-100(Fe) NCs were utilized for PAI and MRI and synergistic chemo-photothermal killing effects were achieved. However, these two studies were limited to *in vitro* theranostics.

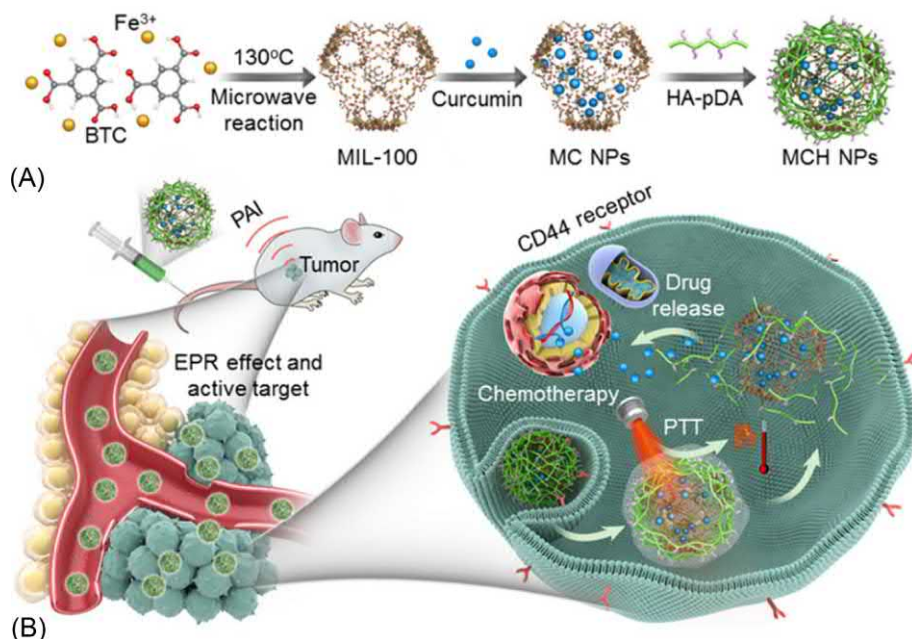
PPy was also formed *in situ* in the presence of preformed MIL-53(Fe) particles which provide Fe<sup>3+</sup> ions able to oxidize Py to PPy. PPy-MIL-53(Fe) nanocomposites with strong NIR absorbance can be applied for PPT to destroy cancerous cells, while anticancer drug DOX could be loaded in the composite particles. These multifunctional nanocomposites can be of interest for tumor theranostics through a combined photothermal-chemotherapy [75, 76].

Polydopamine was also combined to MOFs due to its facile synthesis, biocompatibility, and high photothermal conversion efficiency.

Zhao's group fabricated hybrid particles by coating ZIF-8 nanoparticles with polydopamine (PDA), followed by a surface modification with hyaluronic acid (HA) and Fe<sup>3+</sup> for targeted drug delivery and MRI [77]. Prior to the surface modification, DOX was encapsulated in the porosity of ZIF-8. In order to realize a pH-responsive drug release system, ZIF-8 was selected considering its intrinsic pH-dependent stability. HA was used to target the prostate cancer line PC-3, while Fe<sup>3+</sup> cations impart T1 MRI properties. The targeting ability of DOX@ZIF-8-HA was confirmed and the *in vitro* chemotherapeutic efficacy was shown, but no further *in vivo* study was performed.

Based on MIL-100(Fe), Zhang et al. prepared hybrid particles by coating curcumin-loaded MIL-100(Fe) NPs with PDA-modified HA and studied them for photoacoustic imaging-guided chemo-/photothermal cancer therapy (Fig. 18.6) [78]. A high photothermal conversion ability was achieved in these hybrid particles through the introduction of both curcumin and PDA-HA. The coating of HA-PDA resulted in a tumor-targeting ability as well as improved the stability of the nanoMOF in the blood, resulting in a significant antitumor effect after intravenous injection into tumor-bearing mice.

Polyaniline (PAN) exhibits strong absorption coefficients, excellent photostability, but a poor water solubility. Wang et al. synthesized nanoscale polymer-MOF UiO-66@polyaniline with



**Fig. 18.6**

(A) The preparation of MCH NPs through the formation of MIL-100(Fe), curcumin loading, and HA-PDA surface coating; (B) Under the guidance of PAI in vivo, efficient chemo-/photothermal combinational tumor therapy of MCH NPs was conducted via combinational-enhanced penetration and retention (EPR) and tumor-targeting effects [78].

an appropriate particle size, good water-dispersibility, strong NIR absorbance, high photostability, and photothermal conversion efficiency suitable for PTT-based cancer treatment in vitro and in vivo under guidance of photothermal imaging [79]. Due to its negatively charged surface, UiO-66 could adsorb aniline through electrostatic interaction that was further polymerized using ammonium persulfate as an oxidizing agent.

MOFs@polymer composites based on Zr dicarboxylate nanoMOFs, such as UiO-66@CyP (CyP represents cyanine polymer), were obtained for NIR fluorescence imaging-guided PTT-based cancer treatment by utilizing multicomponent passerini reaction to realize the polymerization of NIR dye cyanine (Cy) on the surface of UiO-66 nanocrystals [80]. UiO-66 nanocrystals were used as templates for the polymerization, and the resulting UiO-66@CyP exhibited high PTT performance in cancer treatment. Note that the utilization of Zr for biomedical applications is highly questionable due to the exogenous nature of Zr as well as the very low solubility in body fluids of the biodegradation products (Zr oxides/phosphates).

#### 18.2.4.2 C dots

Compared with toxic metal-based quantum dots (QDs), fluorescent carbon nanodots (C-dots) display strong fluorescence intensity and are harmless to the environment. This makes them appealing candidates for diagnostic analysis, bio-imaging, etc. Wang's group reported a two-step room temperature synthesis of green fluorescent C-dots incorporated into ZIF-8 as a simultaneous pH-responsive drug delivery and fluorescence imaging system [81]. These hybrid nanocomposites showed remarkable properties depending on the incorporated C-dots with versatile shapes and functions.

#### 18.2.4.3 Graphitic carbon nitride ( $g\text{-C}_3\text{N}_4$ ) nanosheets

The  $g\text{-C}_3\text{N}_4$  nanosheets are efficient visible-light photosensitizer for PDT. Lee's group first designed a nanoscale core-shell platform based on DOX-loaded  $g\text{-C}_3\text{N}_4\text{@ZIF-8}$  nanoparticles for photo-chemotherapy under dual-color imaging (the red fluorescence of DOX and the blue fluorescence of  $g\text{-C}_3\text{N}_4$  nanosheets) [82]. The combination of the chemotherapeutic effects of DOX and the PDT effect of  $g\text{-C}_3\text{N}_4$  nanosheets led to a high therapeutic efficacy.

#### 18.2.4.4 Fluorescent dyes

Most near-infrared region (NIR) organic dyes such as Indocyanine green (ICG) are ideal imaging and photodynamic/photothermal therapy agents. However, their poor aqueous solubility, low cancer specificity, and low sensitivity in cancer theranostics have limited so far their clinic translation. To overcome these issues, Liu's group developed hyaluronic acid (HA) and ICG-engineered MIL-100(Fe) nanoparticles (MOF@HA@ICG NPs) for imaging-guided, anticancer photothermal therapy (PTT) [83].

Apart from MIL-100(Fe), NIR dyes were also combined to ZIF-8, MIL-53, or Fe(III) tetracarboxylate "socMOF" (or MIL-127), and the dye-MOF NPs inhibited tumor growth through photothermal or photodynamic therapy, while exhibited outstanding NIR or fluorescence imaging capacity both in vitro and in vivo [84–86].

Through postsynthetic surface modification process, one can also design fluorescent nanoMOFs denoted "NMOF." Damirin's group synthesized a smart multifunctional NMOF for MR/optical imaging and targeted drug delivery [87]. First, Fe-MIL-53-NH<sub>2</sub> was used for encapsulating the drug 5-fluorouracil (5-FU) and served as a MR contrast agent. Subsequently, the fluorescence imaging agent 5-carboxyfluorescein (5-FAM) and the targeting reagent folic acid (FA) were conjugated to the 5-FU-loaded Fe-MIL-53-NH<sub>2</sub>. The obtained drug delivery system (DDS) showed both a good biocompatibility, tumor-enhanced cellular uptake, strong cancer cell growth inhibitory effect, excellent fluorescence imaging, and finally an outstanding MRI capability.



## 18.2.5 MOF NPs for nuclear medical imaging

### 18.2.5.1 Positron emission tomography (PET)

Compared to other imaging techniques, positron emission tomography (PET) imaging has superior detection sensitivity, deeper signal penetration, and better quantitative capacity, thus gaining more widespread use in both preclinical and clinical scenarios. Hong's group developed a biocompatible isotope zirconium-89 ( $^{89}\text{Zr}$ ,  $t_{1/2} = 78.4$  h)-labeled UiO-66 nanoMOF platform for PET imaging and tumor targeting DOX delivery to treat tumor-bearing mice [88]. These functionalized  $^{89}\text{Zr}$ -UiO-66 nanoMOFs with strong radiochemical and material stability are of interest as an image-guidable, tumor-selective cargo delivery nanoplatform.

Liu's group developed a chelator-free  $^{64}\text{Cu}$ -labeled method that can precisely tune the size of drug-loaded amorphous ZIF MOF particles at room temperature and analyze in vivo the impact between the particle size and the cancer theranostics [89] to trace MOFs through PET imaging. These 60 nm radiolabeled nanoMOFs exhibited a longer blood circulation with over than 50% higher tumor accumulation compared with larger particles of 130 nm. Although ZIF MOF is specifically promising for drug carrier, the toxicity of ZIF-8 nanoparticles cannot be ignored, which may severely limit its further clinical application. Meng's group developed biocompatible ZIF-8 nanoparticles by coating  $\text{ZrO}_2$  onto the surface for chemo-microwave thermal tumor synergistic therapy [90]. Ionic liquid (IL) was loaded into the pore for enhanced microwave thermal therapy and  $\text{ZrO}_2$  could also act as an excellent CT contrast agent. Meaningfully, the toxicity problem of ZIF-8 nanoparticles successfully was solved, which is helpful for further research.

Chen's group fabricated a PEGylated Zr/porphyrinic MOF-Au nanohybrid, in which AuNPs were grown in situ on the MOF NPs for  $\text{O}_2$ -Evolving Synergistic Chemoradiotherapy (Fig. 18.7) [91]. The biodistribution of the nanomedicine was investigated by PET imaging through Cu-64 radiolabeling method. Herein, AuNPs as radiosensitizers were decorated on the surface of MOF to stabilize the nanocomposite, whereas the MOF scaffold acts as a container for loading chemotherapeutic drug doxorubicin, achieving an enhanced synergistic radiochemotherapy.

### 18.2.5.2 Single photon emission computer tomography (SPECT)

Liu's group fabricated PEG functionalized 2D-NMOFs composed of  $\text{Zn}^{2+}$  and tetra (4-carboxyphenyl) porphyrin (TCPP) labeled with the diagnostic radioisotope  $^{99\text{m}}\text{Tc}$  for single photon emission computer tomography (SPECT) imaging and chemo-photodynamic cancer therapy [92]. Through SPECT, efficient tumor homing of those  $^{99\text{m}}\text{Tc}$ -labeled 2D-NMOFs was observed upon intravenous injection.



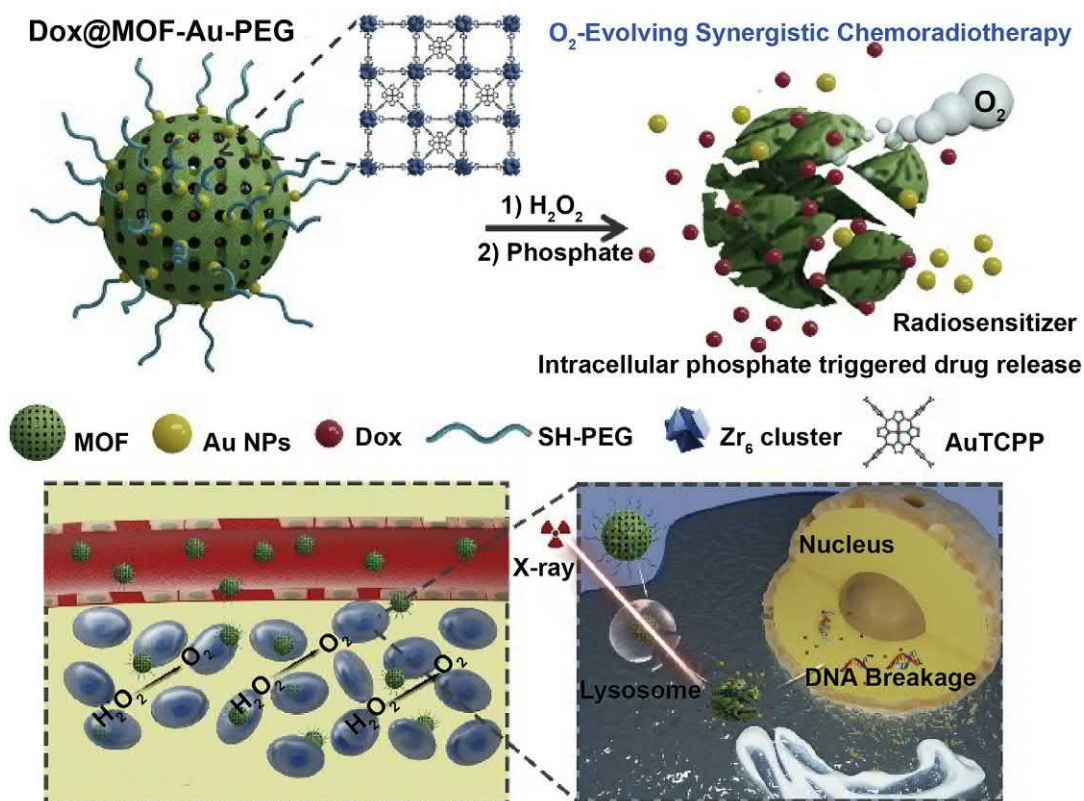


Fig. 18.7

The main components of Dox@MOF-Au-PEG and the mechanism of  $\text{O}_2$  self-supplying synergistic chemoradiotherapy.

### 18.2.5.3 Computed tomography (CT)

Meanwhile, considering strong X-ray attenuating ability of the Hf element, Xie's group developed a multifunctional Hf-porphyrin NMOF platform [Hf/TCPP] with a high TPZ loading for Computed Tomography (CT) imaging that combined PDT and hypoxia-activated chemotherapy [93]. Hf/TCPP nanoparticles could efficiently produce ROS for PDT upon irradiation, while the depletion of the oxygen did further enhance the hypoxic environment of tumors to induce the activation of TPZ associated with better in vivo efficacy. Via a mixed-component strategy, photoactive chlorin was incorporated into the Hf-UiO-66 archetype structure, named TCPC-UiO, in a view of multimodal CT/thermal/photoacoustic imaging, photodynamic, and photothermal therapy (Fig. 18.8) [94]. TCPC-UiO showed an impressive anticancer activity against tumor-bearing mice in vivo, with a tumor inhibition rate above 90%.

Tumor hypoxia is a typical feature of solid tumors, which limits the applications in radiotherapy because of radiation resistance. Based on the upregulated expression of CA IX by hypoxia in

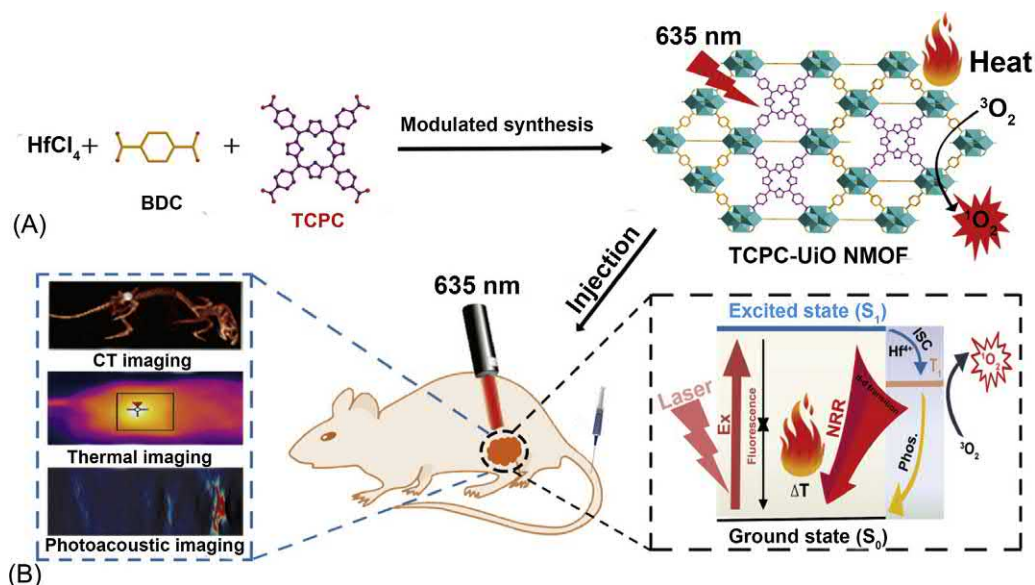


Fig. 18.8

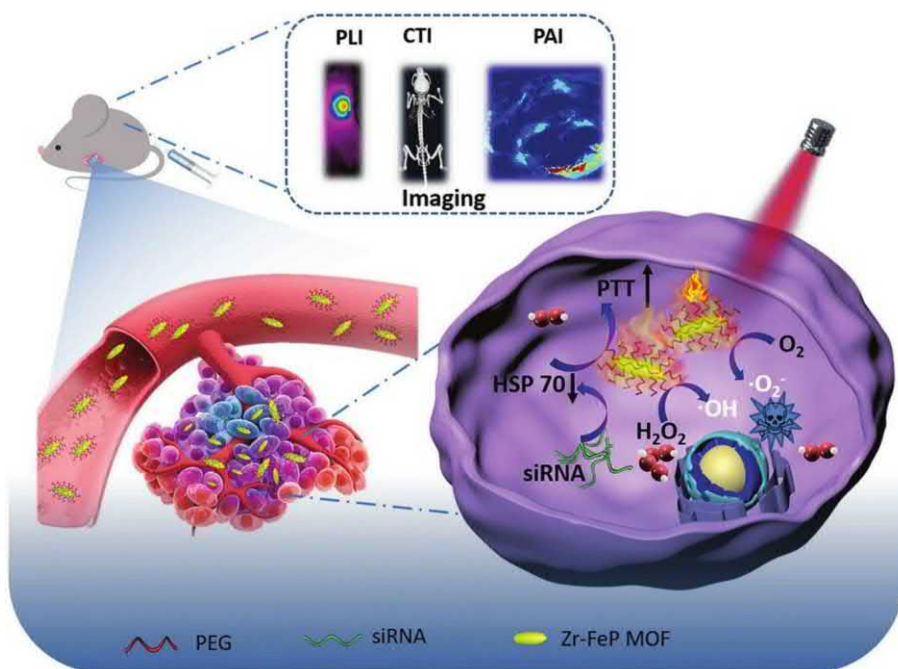
The synthesis and mechanism for cancer therapy of TCPC-UiO by light activation. (A) Synthesis of TCPC-UiO NMOF and schematic description of heat and singlet oxygen generation under laser irradiation. (B) Photophysical mechanism for cancer therapy under light activation of a combination therapy guided by CT/thermal/photoacoustic imaging.

tumor, Meng's group developed quercetin-modified Zr MOFs for simultaneously enhancing RT therapeutic effects and CT imaging [95]. The 1,4-benzenedicarboxylic acid produced from Zr-MOF biodegradation can strongly bind to the  $\text{Zn}^{2+}$  of CA IX, which can inhibit the catalytic activity of CA IX and result in downregulating tumor hypoxia and quercetin (QU) acts as a radiosensitizer. The as-prepared Zr-MOF-QU as CA IX inhibitor exhibited improved radiation-mediated apoptosis.

Following again an "all-in-one" strategy, Dong's group developed zirconium-ferriporphyrin MOF (Zr-FeP MOF) nanoshuttles for multimodal imaging diagnosis, PDT, and low-temperature PTT synergistic treatments (Fig. 18.9) [96].

### 18.2.6 Other stimuli-responsive nanoMOF

New responsive MOFs nanocarriers sensitive to tumor microenvironment such as low pH and/or a high glutathione (GSH) concentration have been developed [97, 98]. Encapsulation of stimuli-responsive molecules into MOFs paves the way for constructing novel stimuli-responsive systems able to trigger drug release at tumor site. Qi's group developed an intrinsic GSH-responsive MOFs carrier, denoted as MOF-Zr(DTBA), using 4,4'-dithiobisbenzoic acid (4,4'-DTBA) able to release drugs in vivo [99]. Curcumin (CCM) was further incorporated



**Fig. 18.9**

Multimode imaging diagnosis and combination of low-temperature PTT and PDT for cancer treatment based on siRNA/Zr-FeP MOF nanoshuttles.

into MOF-Zr(DTBA) to construct CCM@MOF-Zr(DTBA). Its superior anticancer efficacy was verified through *in vitro* and *in vivo* experiments.

Fang's group-encapsulated autophagy inhibitor 3-methyladenine (3-MA) into ZIF-8 to build a pH-sensitive and tumor-targeting controlled drug delivery system denoted 3-MA@ZIF-8 NPs for antitumor application [100]. ZIF-8 framework was shown to be effective in terms of drug control release and controlling autophagy by encapsulating autophagy inhibitors. Based on ZIF-8 MOF, pH-responsive theranostic nanoMOFs have been developed for imaging, tumor suppression, and multidrug resistance (MDR), etc. [101, 102].

Oxidative stress can also affect the therapy of cancer cells, and therefore, Ning's group developed a liposomal formulation of dichloroacetic acid (DCA) and metal-organic framework (MOF)-Fe<sup>2+</sup> (MD@Lip) for synergistic amplification of oxidative stress-mediated antitumor activity [103]. DCA can stimulate intracellular H<sub>2</sub>O<sub>2</sub> generation and promote MOF-Fe<sup>2+</sup> to convert H<sub>2</sub>O<sub>2</sub> to cytotoxic •OH, inducing cancer cell apoptosis. MD@Lip showed selective accumulation in tumors and effective inhibition to tumor growth in *in vivo* studies.

For a better drug delivery, it is critical to pass biological barriers *in vivo*; biomimetic membrane camouflage of MOF strategy has been developed for the inhibition of tumor growth

considering its advantageous homotypic targeting ability, prolonged circulation, and phagocytosis prevention [104]. Li's group constructed a biomimetic cascade nanoreactor (designated as Mem@GOx@ZIF-8@BDOX) for tumor-targeted starvation therapy-amplified chemotherapy by assembling tumor cell membrane cloak and glucose oxidase (GOx) onto zeolitic imidazolate framework (ZIF-8) with the loading prodrug of hydrogen peroxide ( $H_2O_2$ )-sensitive BDOX [105]. The biomimetic cascade nanoreactor could be for fluorescent imaging, and meanwhile, remarkably improve the therapeutic efficacy through the synergistic therapy.

Considering that MOFs have emerged as promising delivery vehicles, the construction of stimuli-responsive nanoMOFs is critical for the development of cancer theranostics, and Liu's group designed a general approach for the preparation of stimuli-responsive multifunctional MOFs [106]. Different types of MOFs including ZIF-8, MIL101, and UiO-66 were synthesized first and then functionalized with polydopamine (PDA) after DOX loading, followed by the conjugation with targeting molecules for targeted drug delivery. Importantly, the stimuli-responsive multifunctional MOFs showed great potential in combined chemo-photothermal therapy.

For the purpose of precise therapy and reducing side effects, more smart targeting molecules-modified stimuli-responsive nanotheranostic probe with the ability of affording immune evasion shall be developed, and it is very meaningful to explore series of facile and general synthesis methods of stimuli-responsive nanoMOF hybrid composites based on tumor microenvironment.

### 18.3 Challenges

So far many new hybrid nanoMOFs systems have been constructed and have demonstrated, in most cases in vitro, a potential benefit that combines the DDS properties of the nanoMOFs and the imaging or stimuli-responsive behavior of the functional nanoparticles (organic or inorganic). However, when dealing with biomedical applications, this is necessary to consider the potential toxic effects of the system in play. In the case of such nanoMOFs hybrid systems, one should ideally demonstrate the biocompatibility, biodegradability, and lack of accumulation into the body of the nanoparticles such as done previously with the bare porous iron(III) carboxylate materials [15]. Before constructing theranostic probe, in vitro and in vivo toxicity experiments should be considered for each nanocarrier. Besides, these nanosystems shall ideally be produced following green, environmentally friendly, and energy-efficient routes using water or nontoxic organic solvents such as alcohols [107, 108]. Another very important parameter is to control the physical and chemical properties of the nanoparticles such as the particle size that should be smaller than 200 nm with an excellent control of the dispersity. This is likely that most of hybrid nanoMOFs candidates considered so far for bioapplications fail to meet these demanding criteria.

In addition, the colloidal stability of the hybrid nanoMOFs in different biological media shall strongly affect the biodistribution and pharmacokinetics in vivo [109]. If a considerable effort has been devoted to surface modification [110–113], such as conjugating targeting molecule, coating with PEG or polymer, the stability of these systems could be improved, leading to a longer blood circulation half-life, better drug delivery abilities, and therapeutic efficiencies.

## 18.4 Conclusion/perspectives

This paper gives a detailed description on the recent developments of hybrid nanoMOFs concerning theranostics. MOFs themselves are promising candidates for drug delivery and a large array of strategies to produce hybrid nanoMOFs combined with various active molecules or nanoparticles have been produced that bear magnetic, fluorescent, or thermal properties suitable for imaging-guided therapy. In a view of future MOFs' clinical use, one shall now focus on the development of optimal nontoxic multifunctional stimuli-responsive nanoMOFs formulations with a suitable stability in body fluids.

## References

- [1] S.M. Janib, A.S. Moses, J.A. MacKay, Imaging and drug delivery using theranostic nanoparticles, *Adv. Drug Deliv. Rev.* 62 (11) (2010) 1052–1063.
- [2] J.H. Ryu, et al., Theranostic nanoparticles for future personalized medicine, *J. Control. Release* 190 (2014) 477–484.
- [3] M.X. Wu, Y.W. Yang, Metal-organic framework (MOF)-based drug/cargo delivery and cancer therapy, *Adv. Mater.* 29 (23) (2017).
- [4] K. Lu, et al., Nanoscale metal-organic frameworks for therapeutic, imaging, and sensing applications, *Adv. Mater.* 30 (37) (2018) e1707634.
- [5] H.-S. Wang, Metal-organic frameworks for biosensing and bioimaging applications, *Coord. Chem. Rev.* 349 (2017) 139–155.
- [6] P. Horcajada, et al., Metal-organic frameworks as efficient materials for drug delivery, *Angew. Chem. Int. Ed. Engl.* 118 (36) (2006) 6120–6124.
- [7] D. Cunha, et al., Rationale of drug encapsulation and release from biocompatible porous metal-organic frameworks, *Chem. Mater.* 25 (14) (2013) 2767–2776.
- [8] T. Simon-Yarza, et al., Nanoparticles of metal-organic frameworks: on the road to in vivo efficacy in biomedicine, *Adv. Mater.* 30 (37) (2018) e1707365.
- [9] C. He, D. Liu, W. Lin, Nanomedicine applications of hybrid nanomaterials built from metal-ligand coordination bonds: nanoscale metal-organic frameworks and nanoscale coordination polymers, *Chem. Rev.* 115 (19) (2015) 11079–11108.
- [10] P. Horcajada, et al., Metal-organic frameworks in biomedicine, *Chem. Rev.* 112 (2) (2012) 1232–1268.
- [11] A.C. McKinlay, et al., BioMOFs: metal-organic frameworks for biological and medical applications, *Angew. Chem. Int. Ed. Engl.* 49 (36) (2010) 6260–6266.
- [12] J. Della Rocca, W. Lin, Nanoscale metal-organic frameworks: magnetic resonance imaging contrast agents and beyond, *Eur. J. Inorg. Chem.* 2010 (24) (2010) 3725–3734.
- [13] R.C. Huxford, J. Della Rocca, W. Lin, Metal-organic frameworks as potential drug carriers, *Curr. Opin. Chem. Biol.* 14 (2) (2010) 262–268.



- [14] J. Della Rocca, D. Liu, W. Lin, Nanoscale metal-organic frameworks for biomedical imaging and drug delivery, *Acc. Chem. Res.* 44 (10) (2011) 957–968.
- [15] W. Cai, et al., Metal-organic framework-based nanomedicine platforms for drug delivery and molecular imaging, *Small* 11 (37) (2015) 4806–4822.
- [16] M. Giménez-Marqués, et al., Nanostructured metal-organic frameworks and their bio-related applications, *Coord. Chem. Rev.* 307 (2016) 342–360.
- [17] S. Beg, et al., Nanoporous metal organic frameworks as hybrid polymer-metal composites for drug delivery and biomedical applications, *Drug Discov. Today* 22 (4) (2017) 625–637.
- [18] R. Ricco, et al., Applications of magnetic metal-organic framework composites, *J. Mater. Chem. A: Mater.* 1 (42) (2013) 13033.
- [19] P. Falcaro, et al., Application of metal and metal oxide nanoparticles@MOFs, *Coord. Chem. Rev.* 307 (2016) 237–254.
- [20] M.D. Rowe, et al., Polymer-modified gadolinium metal-organic framework nanoparticles used as multifunctional nanomedicines for the targeted imaging and treatment of cancer, *Biomacromolecules* 10 (4) (2009) 983–993.
- [21] H. Zhang, et al., Smart metal-organic frameworks-based nanoplatforms for imaging-guided precise chemotherapy, *ACS Appl. Mater. Interfaces* 11 (2019) 1886–1895.
- [22] Y. Chen, et al., Folic acid-nanoscale gadolinium-porphyrin metal-organic frameworks: fluorescence and magnetic resonance dual-modality imaging and photodynamic therapy in hepatocellular carcinoma, *Int. J. Nanomedicine* 14 (2019) 57–74.
- [23] P. Horcajada, et al., Porous metal-organic-framework nanoscale carriers as a potential platform for drug delivery and imaging, *Nat. Mater.* 9 (2) (2010) 172–178.
- [24] K.M. Taylor-Pashow, et al., Postsynthetic modifications of iron-carboxylate nanoscale metal-organic frameworks for imaging and drug delivery, *J. Am. Chem. Soc.* 131 (40) (2009) 14261–14263.
- [25] X.G. Wang, et al., A multifunctional metal-organic framework based tumor targeting drug delivery system for cancer therapy, *Nanoscale* 7 (38) (2015) 16061–16070.
- [26] D. Mao, et al., Metal-organic-framework-assisted in vivo bacterial metabolic labeling and precise antibacterial therapy, *Adv. Mater.* 30 (18) (2018) e1706831.
- [27] F. Liu, et al., Gram-scale synthesis of coordination polymer nanodots with renal clearance properties for cancer theranostic applications, *Nat. Commun.* 6 (2015) 8003.
- [28] M. Meilikhov, et al., Metals@MOFs – loading MOFs with metal nanoparticles for hybrid functions, *Eur. J. Inorg. Chem.* 2010 (24) (2010) 3701–3714.
- [29] J. Juan-Alcañiz, J. Gascon, F. Kapteijn, Metal-organic frameworks as scaffolds for the encapsulation of active species: state of the art and future perspectives, *J. Mater. Chem.* 22 (20) (2012) 10102.
- [30] H.R. Moon, D.W. Lim, M.P. Suh, Fabrication of metal nanoparticles in metal-organic frameworks, *Chem. Soc. Rev.* 42 (4) (2013) 1807–1824.
- [31] C. Rösler, R.A. Fischer, Metal-organic frameworks as hosts for nanoparticles, *CrystEngComm* 17 (2) (2015) 199–217.
- [32] D. Wang, et al., Controllable synthesis of dual-MOFs nanostructures for pH-responsive artemisinin delivery, magnetic resonance and optical dual-modal imaging-guided chemo/photothermal combinational cancer therapy, *Biomaterials* 100 (2016) 27–40.
- [33] D. Wang, et al., Biodegradable core-shell dual-metal-organic-frameworks nanotheranostic agent for multiple imaging guided combination cancer therapy, *Theranostics* 7 (18) (2017) 4605–4617.
- [34] A. Ray Chowdhuri, D. Bhattacharya, S.K. Sahu, Magnetic nanoscale metal organic frameworks for potential targeted anticancer drug delivery, imaging and as an MRI contrast agent, *Dalton Trans.* 45 (7) (2016) 2963–2973.
- [35] D. Wang, et al., Magnetically guided delivery of DHA and Fe ions for enhanced cancer therapy based on pH-responsive degradation of DHA-loaded Fe<sub>3</sub>O<sub>4</sub>@C@MIL-100(Fe) nanoparticles, *Biomaterials* 107 (2016) 88–101.



- [36] H.X. Zhao, et al., Theranostic metal-organic framework core-shell composites for magnetic resonance imaging and drug delivery, *Chem. Sci.* 7 (8) (2016) 5294–5301.
- [37] V. Nejadshafiee, et al., Magnetic bio-metal-organic framework nanocomposites decorated with folic acid conjugated chitosan as a promising biocompatible targeted theranostic system for cancer treatment, *Mater. Sci. Eng. C Mater. Biol. Appl.* 99 (2019) 805–815.
- [38] S. Sene, et al., Maghemite-nanoMIL-100(Fe) bimodal nanovector as a platform for image-guided therapy, *Chem* 3 (2) (2017) 303–322.
- [39] D. Liu, et al., Theranostic nanoscale coordination polymers for magnetic resonance imaging and bisphosphonate delivery, *J. Mater. Chem. B* 2 (46) (2014) 8249–8255.
- [40] H. Zhang, et al., Theranostic Mn-porphyrin metal-organic frameworks for magnetic resonance imaging-guided nitric oxide and photothermal synergistic therapy, *ACS Appl. Mater. Interfaces* 10 (34) (2018) 28390–28398.
- [41] Q. Guan, et al., Photodynamic therapy based on nanoscale metal-organic frameworks: from material design to cancer nanotherapeutics, *Chem. Asian J.* 13 (21) (2018) 3122–3149.
- [42] C. Fu, et al., Microwave-activated Mn-doped zirconium metal-organic framework nanocubes for highly effective combination of microwave dynamic and thermal therapies against cancer, *ACS Nano* 12 (3) (2018) 2201–2210.
- [43] L. Zhang, et al., A porphyrin photosensitized metal-organic framework for cancer cell apoptosis and caspase responsive theranostics, *Chem. Commun. (Camb)* 51 (54) (2015) 10831–10834.
- [44] J. Park, et al., Size-controlled synthesis of porphyrinic metal-organic framework and functionalization for targeted photodynamic therapy, *J. Am. Chem. Soc.* 138 (10) (2016) 3518–3525.
- [45] S.Y. Li, et al., Cancer cell membrane-coated biomimetic platform for tumor targeted photodynamic therapy and hypoxia-amplified bioreductive therapy, *Biomaterials* 142 (2017) 149–161.
- [46] L. An, et al., In situ sulfidation of Cu<sub>2</sub>O by endogenous H<sub>2</sub>S for colon cancer theranostics, *Angew. Chem. Int. Ed. Engl.* (2018).
- [47] K. Zhang, et al., A bacteriochlorin-based metal-organic framework nanosheet superoxide radical generator for photoacoustic imaging-guided highly efficient photodynamic therapy, *Adv. Sci.* (2019) 1900530.
- [48] W. Poon, et al., Elimination pathways of nanoparticles, *ACS Nano* 13 (5) (2019) 5785–5798.
- [49] Y. Li, et al., Coordination-responsive drug release inside gold nanorod@metal-organic framework core-shell nanostructures for near-infrared-induced synergistic chemo-photothermal therapy, *Nano Res.* 11 (6) (2018) 3294–3305.
- [50] P. Jiang, Y. Hu, G. Li, Biocompatible Au@Ag nanorod@ZIF-8 core-shell nanoparticles for surface-enhanced Raman scattering imaging and drug delivery, *Talanta* 200 (2019) 212–217.
- [51] J.-Y. Zeng, et al., Porphyrinic metal-organic frameworks coated gold nanorods as a versatile nanoplatform for combined photodynamic/photothermal/chemotherapy of tumor, *Adv. Funct. Mater.* 28 (8) (2018) 1705451.
- [52] H. Zhang, et al., Preparation of one dimensional nanorod/metal organic framework Janus nanoplatform via side-specific growth for synergistic cancer therapy, *Biomater. Sci.* (2019).
- [53] J. He, et al., Design of Raman tag-bridged core-shell Au@Cu<sub>3</sub>(BTC)<sub>2</sub> nanoparticles for Raman imaging and synergistic chemo-photothermal therapy, *Nanoscale* 11 (13) (2019) 6089–6100.
- [54] D. Li, Z. Chen, X. Mei, Fluorescence enhancement for noble metal nanoclusters, *Adv. Colloid Interf. Sci.* 250 (2017) 25–39.
- [55] X. Jiang, et al., Ultrasmall noble metal nanoparticles: breakthroughs and biomedical implications, *Nano Today* 21 (2018) 106–125.
- [56] N. Kaur, et al., Biomedical applications for gold nanoclusters: Recent developments and future perspectives, *Nanoscale Res. Lett.* 13 (1) (2018) 302.
- [57] X. Bai, S. Xu, L. Wang, Full-range pH stable au-clusters in nanogel for confinement-enhanced emission and improved sulfide sensing in living cells, *Anal. Chem.* 90 (5) (2018) 3270–3275.
- [58] Y. Li, et al., Multifunctional gold nanoclusters-based nanosurface energy transfer probe for real-time monitoring of cell apoptosis and self-evaluating of pro-apoptotic theranostics, *Anal. Chem.* 88 (22) (2016) 11184–11192.

- [59] X. Wang, et al., Preparation of novel fluorescent nanocomposites based on Au nanoclusters and their application in targeted detection of cancer cells, *ACS Appl. Mater. Interfaces* 9 (51) (2017) 44856–44863.
- [60] C. Zhang, et al., Gold nanoclusters-based nanoprobes for simultaneous fluorescence imaging and targeted photodynamic therapy with superior penetration and retention behavior in tumors, *Adv. Funct. Mater.* 25 (8) (2015) 1314–1325.
- [61] S.K. Katla, et al., Atomically precise Au<sub>25</sub>(SG)<sub>18</sub> nanoclusters: rapid single-step synthesis and application in photothermal therapy, *ACS Appl. Mater. Interfaces* 10 (1) (2018) 75–82.
- [62] S. Miyata, et al., Antimicrobial photodynamic activity and cytocompatibility of Au<sub>25</sub>(Capt)<sub>18</sub> clusters photoexcited by blue LED light irradiation, *Int. J. Nanomedicine* 12 (2017) 2703–2716.
- [63] X.D. Zhang, et al., Enhanced tumor accumulation of sub-2 nm gold nanoclusters for cancer radiation therapy, *Adv. Healthc. Mater.* 3 (1) (2014) 133–141.
- [64] D. Yang, et al., Au<sub>25</sub> cluster functionalized metal-organic nanostructures for magnetically targeted photodynamic/photothermal therapy triggered by single wavelength 808 nm near-infrared light, *Nanoscale* 7 (46) (2015) 19568–19578.
- [65] R. Bian, et al., A combination of tri-modal cancer imaging and in vivo drug delivery by metal-organic framework based composite nanoparticles, *Biomater. Sci.* 3 (9) (2015) 1270–1278.
- [66] X. Ma, et al., Multifunctional iron-based metal-organic framework as biodegradable nanozyme for microwave enhancing dynamic therapy, *Biomaterials* 214 (2019) 119223.
- [67] L. Zhang, et al., ZD2-engineered gold nanostar@metal-organic framework nanoprobes for T1-weighted magnetic resonance imaging and photothermal therapy specifically toward triple-negative breast cancer, *Adv. Healthc. Mater.* 7 (24) (2018) e1801144.
- [68] K. Deng, et al., Aptamer-mediated up-conversion core/MOF shell nanocomposites for targeted drug delivery and cell imaging, *Sci. Rep.* 5 (2015) 7851.
- [69] A.R. Chowdhuri, et al., One-pot synthesis of folic acid encapsulated upconversion nanoscale metal organic frameworks for targeting, imaging and pH responsive drug release, *Dalton Trans.* 45 (45) (2016) 18120–18132.
- [70] L. He, et al., DNA-assembled core-satellite upconverting-metal-organic framework nanoparticle superstructures for efficient photodynamic therapy, *Small* 13 (24) (2017).
- [71] W. Jiang, et al., CuS@MOF-based well-designed quercetin delivery system for chemo-photothermal therapy, *ACS Appl. Mater. Interfaces* 10 (40) (2018) 34513–34523.
- [72] J.C. Yang, et al., An “all-in-one” antitumor and anti-recurrence/metastasis nanomedicine with multi-drug co-loading and burst drug release for multi-modality therapy, *Chem. Sci.* 9 (36) (2018) 7210–7217.
- [73] Y.D. Zhu, et al., PPy@MIL-100 nanoparticles as a pH- and near-IR-irradiation-responsive drug carrier for simultaneous photothermal therapy and chemotherapy of cancer cells, *ACS Appl. Mater. Interfaces* 8 (50) (2016) 34209–34217.
- [74] X. Chen, et al., Facile synthesis of polypyrrole@metal-organic framework core-shell nanocomposites for dual-mode imaging and synergistic chemo-photothermal therapy of cancer cells, *J. Mater. Chem. B* 5 (9) (2017) 1772–1778.
- [75] J. Huang, et al., Metal-organic framework as a microreactor for in situ fabrication of multifunctional nanocomposites for photothermal-chemotherapy of tumors in vivo, *ACS Appl. Mater. Interfaces* 10 (45) (2018) 38729–38738.
- [76] X. Cai, et al., Controllable synthesis of highly monodispersed nanoscale Fe-soc-MOF and the construction of Fe-soc-MOF@polypyrrole core-shell nanohybrids for cancer therapy, *Chem. Eng. J.* 358 (2019) 369–378.
- [77] F. Shu, et al., Fabrication of a hyaluronic acid conjugated metal organic framework for targeted drug delivery and magnetic resonance imaging, *RSC Adv.* 8 (12) (2018) 6581–6589.
- [78] Y. Zhang, et al., Engineering metal-organic frameworks for photoacoustic imaging-guided chemo-/photothermal combinational tumor therapy, *ACS Appl. Mater. Interfaces* (2018).
- [79] W. Wang, et al., Nanoscale polymer metal-organic framework hybrids for effective photothermal therapy of Colon cancers, *Adv. Mater.* 28 (42) (2016) 9320–9325.

- [80] L. Yan, et al., Size controllable and surface tunable zeolitic imidazolate framework-8-poly(acrylic acid sodium salt) nanocomposites for pH responsive drug release and enhanced in vivo cancer treatment, *ACS Appl. Mater. Interfaces* 9 (38) (2017) 32990–33000.
- [81] L. He, et al., Carbon nanodots@zeolitic imidazolate framework-8 nanoparticles for simultaneous pH-responsive drug delivery and fluorescence imaging, *CrystEngComm* 16 (16) (2014) 3259.
- [82] R. Chen, et al., Graphitic carbon nitride nanosheet@metal-organic framework core-shell nanoparticles for photo-chemo combination therapy, *Nanoscale* 7 (41) (2015) 17299–17305.
- [83] W. Cai, et al., Engineering phototheranostic nanoscale metal-organic frameworks for multimodal imaging-guided cancer therapy, *ACS Appl. Mater. Interfaces* 9 (3) (2017) 2040–2051.
- [84] Y. Li, et al., Facile synthesis of a metal-organic framework nanocarrier for NIR imaging-guided photothermal therapy, *Biomater. Sci.* 6 (11) (2018) 2918–2924.
- [85] P. Yang, et al., Metal-organic framework nanoparticles with near-infrared dye for multimodal imaging and guided phototherapy, *ACS Appl. Mater. Interfaces* 11 (12) (2019) 11209–11219.
- [86] X. Cai, et al., Interfacially synthesized Fe-soc-MOF nanoparticles combined with ICG for photothermal/photodynamic therapy, *Dalton Trans.* 47 (45) (2018) 16329–16336.
- [87] X. Gao, et al., Controllable synthesis of a smart multifunctional nanoscale metal-organic framework for magnetic resonance/optical imaging and targeted drug delivery, *ACS Appl. Mater. Interfaces* 9 (4) (2017) 3455–3462.
- [88] D. Chen, et al., In vivo targeting and positron emission tomography imaging of tumor with intrinsically radioactive metal-organic frameworks nanomaterials, *ACS Nano* 11 (4) (2017) 4315–4327.
- [89] D. Duan, et al., Size-controlled synthesis of drug-loaded zeolitic imidazolate framework in aqueous solution and size effect on their cancer theranostics in vivo, *ACS Appl. Mater. Interfaces* (2018).
- [90] L. Su, et al., High biocompatible ZIF-8 coated by ZrO<sub>2</sub> for chemo-microwave thermal tumor synergistic therapy, *ACS Appl. Mater. Interfaces* 11 (11) (2019) 10520–10531.
- [91] Z. He, et al., A catalase-like metal-organic framework nanohybrid for O<sub>2</sub>-evolving synergistic chemoradiotherapy, *Angew. Chem. Int. Ed. Engl.* 58 (26) (2019) 8752–8756.
- [92] W. Zhu, et al., Two-dimensional metal-organic-framework as a unique theranostic nano-platform for nuclear imaging and chemo-photodynamic cancer therapy, *Nano Res.* (2018).
- [93] M. Liu, et al., Hypoxia-triggered nanoscale metal-organic frameworks for enhanced anticancer activity, *ACS Appl. Mater. Interfaces* 10 (29) (2018) 24638–24647.
- [94] X. Zheng, et al., Nanoscale mixed-component metal-organic frameworks with photosensitizer spatial-arrangement-dependent photochemistry for multimodal-imaging-guided photothermal therapy, *Chem. Mater.* 30 (19) (2018) 6867–6876.
- [95] T. Ma, et al., Quercetin-modified metal-organic frameworks for dual sensitization of radiotherapy in tumor tissues by inhibiting the carbonic anhydrase IX, *ACS Nano* 13 (4) (2019) 4209–4219.
- [96] K. Zhang, et al., Metal-organic framework nanoshuttle for synergistic photodynamic and low-temperature photothermal therapy, *Adv. Funct. Mater.* 28 (42) (2018) 1804634.
- [97] S.Z. Ren, et al., Nanoscale metal-organic-frameworks coated by biodegradable organosilica for pH and redox dual responsive drug release and high-performance anticancer therapy, *ACS Appl. Mater. Interfaces* (2019).
- [98] J. Zhao, et al., Redox-sensitive nanoscale coordination polymers for drug delivery and cancer theranostics, *ACS Appl. Mater. Interfaces* 9 (28) (2017) 23555–23563.
- [99] B. Lei, et al., Constructing redox-responsive metal-organic framework nanocarriers for anticancer drug delivery, *ACS Appl. Mater. Interfaces* 10 (19) (2018) 16698–16706.
- [100] W. Cai, et al., Gold nanorods@metal-organic framework core-shell nanostructure as contrast agent for photoacoustic imaging and its biocompatibility, *J. Alloys Compd.* 748 (2018) 193–198.
- [101] Y. Lv, et al., Chromium-doped zinc gallogermanate@zeolitic imidazolate framework-8: a multifunctional NAnoplatform for rechargeable in vivo persistent luminescence imaging and pH-responsive drug release, *ACS Appl. Mater. Interfaces* (2018).

- 
- [102] H. Zhang, et al., Rational design of metal organic framework nanocarrier-based codelivery system of doxorubicin hydrochloride/verapamil hydrochloride for overcoming multidrug resistance with efficient targeted cancer therapy, *ACS Appl. Mater. Interfaces* 9 (23) (2017) 19687–19697.
- [103] L. Sun, et al., Synergistic amplification of oxidative stress-mediated antitumor activity via liposomal dichloroacetic acid and MOF-Fe<sup>2+</sup>, *Small* 15 (2019) e1901156.
- [104] G. Cheng, et al., Self-assembly of extracellular vesicle-like metal-organic framework nanoparticles for protection and intracellular delivery of biofunctional proteins, *J. Am. Chem. Soc.* 140 (23) (2018) 7282–7291.
- [105] H. Cheng, et al., A biomimetic cascade nanoreactor for tumor targeted starvation therapy-amplified chemotherapy, *Biomaterials* 195 (2019) 75–85.
- [106] J. Feng, et al., Stimuli-responsive multifunctional metal–organic framework nanoparticles for enhanced chemo-photothermal therapy, *J. Mater. Chem. B* 7 (6) (2019) 994–1004.
- [107] A. García Márquez, et al., Green microwave synthesis of MIL-100(Al, Cr, Fe) nanoparticles for thin-film elaboration, *Eur. J. Inorg. Chem.* 2012 (32) (2012) 5165–5174.
- [108] V. Agostoni, et al., A “green” strategy to construct non-covalent, stable and bioactive coatings on porous MOF nanoparticles, *Sci. Rep.* 5 (2015) 7925.
- [109] E. Bellido, et al., Understanding the colloidal stability of the mesoporous MIL-100(Fe) nanoparticles in physiological media, *Langmuir* 30 (20) (2014) 5911–5920.
- [110] E. Bellido, et al., Heparin-engineered mesoporous iron metal-organic framework nanoparticles: toward stealth drug nanocarriers, *Adv. Healthc. Mater.* 4 (8) (2015) 1246–1257.
- [111] A.G. Márquez, et al., Biocompatible polymer–metal–organic framework composite patches for cutaneous administration of cosmetic molecules, *J. Mater. Chem. B* 4 (43) (2016) 7031–7040.
- [112] A. Zimpel, et al., Imparting functionality to MOF nanoparticles by external surface selective covalent attachment of polymers, *Chem. Mater.* 28 (10) (2016) 3318–3326.
- [113] M. Gimenez-Marques, et al., GraftFast surface engineering to improve MOF nanoparticles furtiveness, *Small* 14 (40) (2018) e1801900.

# Functional MOFs as molecular imaging probes and theranostics

Rajasekharreddy Pala<sup>a,b,c</sup>, Subhaswaraj Pattnaik<sup>d</sup>, Yun Zeng<sup>e</sup>, Siddhardha Busi<sup>d</sup>, Surya M. Nauli<sup>a,b</sup>, Gang Liu<sup>c</sup>

<sup>a</sup>Department of Biomedical & Pharmaceutical Sciences, Chapman University School of Pharmacy (CUSP), Harry and Diane Rinker Health Science Campus, Chapman University, Irvine, CA, United States

<sup>b</sup>Department of Medicine, University of California Irvine, Irvine, CA, United States

<sup>c</sup>State Key Laboratory of Molecular Vaccinology and Molecular Diagnostics & Center for Molecular Imaging and Translational Medicine, School of Public Health, Xiamen University, Xiamen, China

<sup>d</sup>Department of Microbiology, School of Life Sciences, Pondicherry University, Puducherry, India

<sup>e</sup>Department of Pharmacology, Xiamen Medical College, Xiamen, China

## 19.1 Introduction

From last few decades, a significant resurgence of several chronic microbial infections, life-threatening diseases, disorders, and related infectious diseases has happened, though there is a significant and emerging technological development in the field of biotechnological and biomedical sectors [1]. In last few decades, a broad spectrum of infectious diseases, disorders, and microbial infections such as cancer, diabetes, cardiovascular diseases, cystic fibrosis, tuberculosis, AIDS, and several other life-threatening complications has generated serious public health concern with high rate of mortality and morbidity [2, 3]. The discovery of antibiotics and novel drugs to control progression of chronic microbial infections, life-threatening diseases, and disorders in the 20th century critically improved the conventional biomedical practices by strictly minimizing the risks associated with complicated operations and invasive recitations [4]. However, the indiscriminate and irrational use of antibiotics has led to the emergence of multidrug resistance (MDR) which significantly affected the growth and development of conventional antibiotics. Besides, the increasing gap between the emergence antibiotic resistance and development of new class of antibiotics has further aggravated the health risks to human beings [5]. In this context, it is imperative to search for the alternative therapeutic approaches which critically complement the proper utilization of conventional therapeutic strategies in the post-antibiotic era.

### **19.1.1 Nanostructures as next-generation therapeutics**

The emergence of nanotechnological platforms into the field of biomedicines and pharmaceutical sectors has revolutionized the current understanding of therapeutic strategies, smart and early diagnosis of infectious diseases, targeted delivery of the therapeutic drug candidates, and complementing the therapeutic efficacy of conventional therapy [6, 7]. The nanotechnological intervention has provided a multifaceted platform for development of promising biosensing, bioimaging, and therapeutic agents, thereby providing ample research opportunities for early diagnosis of diseases and thus enhancing the therapeutic efficacy of the conventional therapeutic strategies [7]. The advent of multifaceted nanomedicine in the treatment of cancer has created considerable attention among the scientific community to develop novel nanomedicines to treat life-threatening diseases such as diabetes, cardiovascular diseases, Alzheimer's disease, and Parkinson's disease [8]. The introduction of nanotechnology into the field of biotechnology also found to be influential in tissue engineering, drug delivery, food safety and processing, waste water treatment, agricultural sustainability, and new product development [9]. The unique physicochemical characteristics such as high surface to volume ratio, biocompatibility, optical stability, and tunable size of novel nanomaterials resulted in widespread applications. For example, unique surface plasmon resonance (SPR) characteristic and strong optical absorptivity of metal nanoparticles strongly stimulated its applications in biosensing and diagnosis [10].

The concept of green nanotechnology also provides a new paradigm in developing eco-friendly, nontoxic, and efficient nanomaterials as an alternative and effective therapeutics against microbial infections, drug resistance-associated health risks, and other life-threatening diseases [11]. From the inception of nanotechnology towards biomedical applications, design and development of smart nanomaterials for targeted drug delivery systems and localized therapeutics have gained considerable attention. In this context, stimuli-responsive drug delivery systems have been considered as promising approach in biotherapeutics, especially cancer therapeutics as the release of drug moieties is stringently coordinated by intrinsic and external stimuli [12, 13]. The intrinsic or endogenous stimuli are generally pH-, redox-, and ATP-responsive, whereas the external or exogenous stimuli are generally temperature-, light-, pressure-, ion-, and magnetic-responsive.

### **19.1.2 Concept of metal-organic frameworks (MOFs)**

Metal-organic frameworks (MOFs) are next-generation hybrid nanomaterials, basically composed of metal ions or metal clusters which are linked by organic compounds/ligands. The diversity of different chemical moieties and different metal ions is involved in the design of MOFs greatly improving the physicochemical properties. The unique physicochemical characteristics such as large surface area, high porosity, and highly improved tunability of MOFs enable its candidature for widespread biomedical, pharmaceutical, and biotechnological

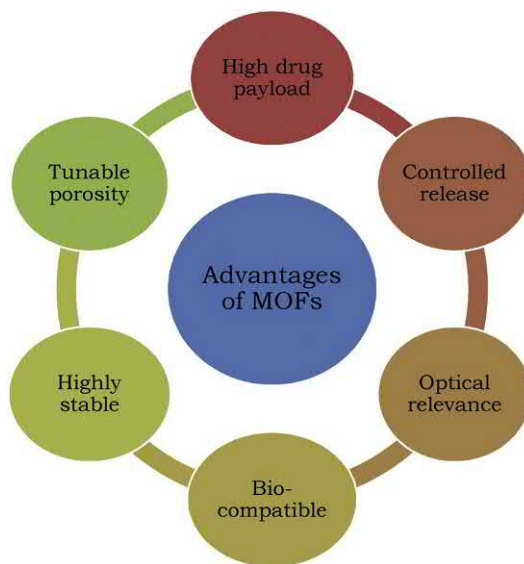


applications [14, 15]. MOFs are also popularly known as porous coordination polymers (PCPs) owing to their tunable porosity and involvement of coordination chemistry in the design and synthesis of hybrid nanomaterial, MOFs [16]. The concept of supramolecular chemistry provided a new paradigm to the material science sectors for development of novel and biomedically relevant nanomaterials such as covalent organic frameworks (COFs) and MOFs [17]. The advent of next-generation hybrid nanomaterial, MOFs, has also showed tremendous potential in chemical sensing, diagnostics, and theranostic applications [18, 19]. The concept of MOFs emerged in the pursuit of synthesizing novel nanomaterials with improved physicochemical characteristics and widespread applications. It is evident from the rich lineage of different organic nanomaterials such as liposomes, micelles, and dendromeric nanoparticles which showed promising therapeutic properties, but got limited by varied drug payload. Meanwhile, the inorganic nanomaterials, especially metal-based nanoparticles, possess large surface area with high drug load capacity and stimuli-controlled drug release profile. However, biodegradability issues and limitations in post-synthetic modulations limit their widespread applications.

In this context, designing and synthesizing novel hybrid materials combining the advantageous characteristics of both inorganic and organic nanomaterials could be of promising importance. In this regard, MOFs as self-assembled hybrid nanomaterials constituting metal ion clusters and organic ligands are found to be influential in the biomedical and pharmaceutical applications [20]. The organic subunits in MOFs' architecture usually comprised of carboxylates, phosphonate, sulfonate, and heterocyclic compounds which generally formed the bridging ligands. Meanwhile, the inorganic setup in MOFs' architecture is represented by variety of metal ions or metal clusters together known as secondary-binding units (SBUs). In principle, a bridging ligand (ditopic, tritopic, tetratopic, or multitopic linkers) reacts with a metal ion with more than one vacant or labile site. The final framework topology of MOF is governed by both SBU connectors and organic ligand linkers [21].

### **19.1.3 Advantages of MOFs**

The design and development of MOFs as an advanced nano-formulation exhibit characteristic advantages such as low therapeutic doses, improved therapeutic persistence, characteristic tunability, and fast inactivation. In addition, MOFs also do not have certain limitations which are generally associated with other nano-formulations. MOFs are also able to oxidize and depolarize the outer membranes of microbes and cause the inhibition of protein synthesis and provided new horizon in combating chronic microbial infections [15]. In addition, MOFs showed remarkable properties such as enhanced flexibility and low density, tunable porosity, and rich diversity in metal ions and linkers involved [17] (Fig. 19.1). The design and development of MOFs provided a uniform platform to combine multiple functionalities such as inorganic and organic moieties in a single framework, thereby providing an ideal system for



**Fig. 19.1**

Schematic representation of the advantageous properties of metal-organic frameworks (MOFs).

designing a periodic arrangement of functional molecular subunits. The tunable porosity associated with multidimensional MOFs also provided the credibility within the framework for post-synthetic modification [22]. The wide range of adjustment of the framework's functional groups and pore size makes MOFs advantageous over their other counterparts such as rigid nanoparticle carriers in the form of controlled drug release profile, high drug payload, and biocompatibility which critically improved their widespread biomedical applications [23]. The use of metal ions or metal clusters into the MOFs' architecture characteristically improved the structural and colloidal stability of the hybrid nanomaterials, suggesting their efficacy in solving the limitations associated with solubility, biocompatibility, bioavailability, controlled release profile, and drug payload in the conventional nanomaterials [24]. The drug delivery potential of MOFs is generally coordinated in response to certain intrinsic or extrinsic stimuli such as pH, magnetic field, ions, temperature, and pressure [25].

## **19.2 Synthesis and characterization of MOFs**

MOFs are generally synthesized by the self-assembly of polydentate bridging organic ligands and metal cations under mild conditions. MOFs can be synthesized through variety of methods such as conventional solvothermal/hydrothermal synthesis performed in an autoclave with high temperature and pressure and with the use of an organic solvent at its boiling point (typically dialkyl formamides, alcohols, and pyridine). Apart from conventional methods, the synthesis of MOFs could also be synthesized through other synthetic methods such as microwave-assisted, sonochemical, electrochemical, mechanochemical and ionothermal

processes, ultrasonic synthesis, microfluidic syntheses or dry gel conversion, and high-throughput syntheses [14, 26]. The building blocks of MOFs can be held together by several types of bonding and this diversity can be present in a single MOF crystal. Such bonding types include metal coordination, hydrogen bonding, electrostatic interactions, and  $\pi$ - $\pi$  stacking. The synthesis of MOFs includes three basic strategies such as rapid nucleation (i.e., fast precipitation followed by accelerated heating), nanoreactor confinement (using reverse phase microemulsion systems), and coordination modulation (by chemically modulating the interactions between the metal and organic ligand). One of the most important characteristics of synthesizing highly advanced MOFs is the ability and platform provided by MOF materials for improved surface functionalization using the extensive conjugation chemistry approach and surface ligand chemistry during the post-synthetic phase [27]. Based on synthesis, MOFs could be categorized into (i) Simple MOFs (1st generation), (ii) functionalized MOFs (2nd generation), and (iii) Smart MOFs (3rd generation). The 1st generation MOF has the basic architecture of two basic components such as metal ion clusters and organic moiety. The 2nd generation MOFs lead to functionalization for target-oriented delivery of bioactive moieties. Meanwhile, the 3rd generation MOFs contain biomolecules such as cations, drugs, bioactives, toxins, and gases within their framework for targeted delivery [28].

During the synthesis of MOFs, the multidentate linkers (dicarboxylates or tricarboxylates) allow the formation of rigid frameworks by inducing aggregation of metal ions into the M-O-C clusters, where the metal ions are locked into their position of the network vertex by the carboxylates. These organic links play an important role in defining the pore sizes and organic adsorptive sites of MOFs, which eventually determine the extent of biomedical applications [29]. Owing to the unique physicochemical characteristics and tenability of MOFs, they are regarded as promising nanocarriers for the uptake of bioactive drug candidates, high molecular weight proteins, and low molecular weight peptides. Nevertheless, the preparation of traditional MOFs sometimes leads to undesirable products with decreased efficacy in biomedical targeting and other pharmacological applications. In this context, combining the superior properties of MOFs and the rapid magnetic responsivity of magnetic material to build magnetic MOF composites could be of promising importance in enhancing the efficacy of encapsulated drug moieties, protein, and peptide moieties for widespread applications in the field of biomedicines, pharmaceutical sectors, environmental management, and different technological fields [30].

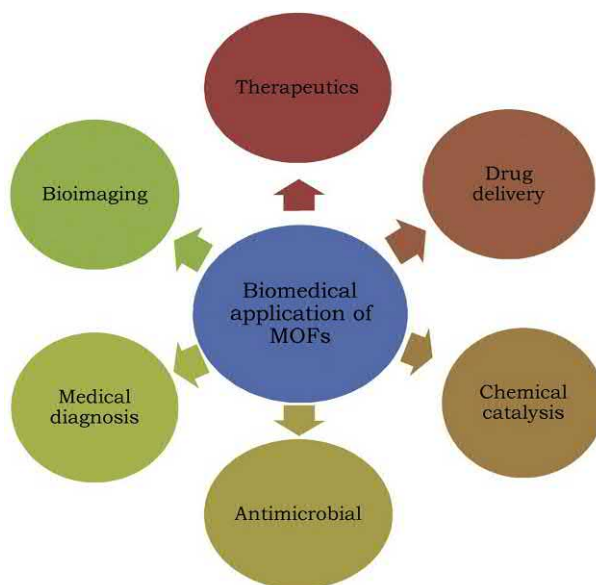
In the last few years, the concept of MOFs is considered to be influential in early diagnostics and therapeutic applications owing to their multifaceted functional modalities and unique physicochemical properties. The widespread applications of multimodal MOFs include drug uptake, controlled drug release, targeted drug delivery, early diagnosis, bioimaging, biosensing, and environmental management [31]. The unique physicochemical properties of MOFs could be assigned due to the inherent structural feature associated with organic ligands

in combination with diversified metal ion clusters. These characteristic features such as chemical tenability and ease in post-synthetic modification in the hybrid nanomaterials have provided new dimension for widespread applications [32]. In recent times, hybridizing the conventional MOFs with external selected components could give rise to novel MOF Hybrid materials with improved physicochemical characteristics and enhanced biomedical, pharmaceutical, and therapeutic applications as compared to parent MOFs. The hybrid MOFs have been found to be promising strategies for targeted drug delivery and therapeutics [33]. The synthesis/preparation of MOF hybrids could be implemented through either covalent modification or noncovalent interactions. The covalent mode of preparation focused upon the incorporation of external materials into the MOFs at the metal nodes or organic ligands without hampering the parental characteristics of MOFs.

Apart from covalent modification, noncovalent interactions such as encapsulation, layer-by-layer deposition, and in situ growth function by trapping the species within the MOF pores, layering them on top of the parent MOF, or growing MOFs crystals in situ with the species. Noncovalent modification mode of synthesis is comparatively easier owing to their promising aspect of allowing the individual characteristics of the participating materials, MOFs, and hybridizing materials to work synergistically in the resultant MOF hybrids, while requiring fewer synthetic efforts than covalent modifications. This method eliminates the metal node and/or the organic linker, leaving behind only the newly synthesized materials with the inherited uniform nanoframe of the template/precursor [33]. On the basis of crystal structure arrangement, MOFs can be categorized into two types: crystalline and amorphous. The crystalline MOFs possess infinite arrangement of highly regular and frequently reproducing solid porous framework with improved physicochemical sorption characteristics as well as long-range order. The amorphous MOFs contain analogous building blocks and retain their connectivity like the crystalline MOFs. However, the amorphous MOFs lack long-range periodic order. The amorphous MOFs gained considerable attention owing to their drug delivery applications [34].

### ***19.3 Biomedical and pharmaceutical applications of MOFs***

The advent of highly porous hybrid nanomaterials, i.e., MOFs, has been found to be of considerable importance in gas storage, alkane/alkene separation, biosensing, water remediation, and catalysis process during organic reactions [35, 36]. In particular, functionalized MOFs are found to have potential adsorption capacity which enables its role in the efficient removal of toxic dyes and pollutants from the environment, thereby playing crucial role in environmental management [37]. The development of MOFs as promising nanocarriers has given new dimensions to the current understanding of therapeutic strategies. The advent of MOFs could be tuned and designed for cell- or tissue-specific targeted drug



**Fig. 19.2**

Schematic illustration of biomedical application of metal-organic frameworks (MOFs).

delivery, transport of drugs across different cellular barriers, early diagnostics by acting as promising bioimaging agent, and improved therapeutic strategy [17] (Fig. 19.2).

### 19.3.1 Antimicrobial properties of MOFs

From historical perspectives of the use of nanomaterials in biomedical and pharmaceutical applications, silver nanoparticles (AgNPs) have gained considerable interest owing to their unique physicochemical properties and widespread antimicrobial potential against various pathogenic microorganisms. The extent of antimicrobial properties of AgNPs could be improved by specifically designing novel nanocomposites comprising of silver-based MOFs and organic graphene oxide nanomaterials (GO-Ag-MOFs). The promising antimicrobial properties shown by GO-Ag-MOFs nanocomposites could be attributed to species-specific physicochemical properties, varied mechanism of actions, and the ability for postsynthetic functionalization [38]. Recently, the antibacterial efficacies of three Zn-based MOFs such as IRMOF-3, MOF-5, and Zn-BTC were determined against pathogenic bacteria, *Escherichia coli*, *Staphylococcus aureus*, *S. lentus*, and *Listeria monocytogenes*. When the designed MOFs were used in combination with conventional antibiotics such as ampicillin and kanamycin, the hybrid nanomaterials exhibited promising bactericidal properties owing to the synergistic or additive effects of the participating materials. The antibiotics containing hybrid MOFs showed promising antibacterial potential as compared to MOFs or antibiotics when used alone. The promising antibacterial efficacy of antibiotics-loaded Zn-based MOFs suggested their

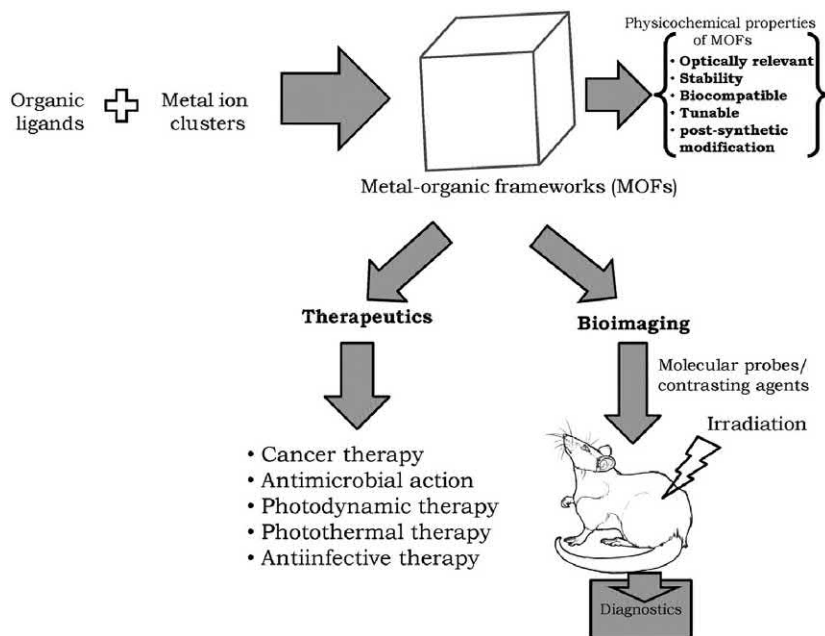
functional role in critically enhancing the potency of conventional antibiotics, thereby reducing the burden of the new discovery of antimicrobial pharmaceuticals in the postantibiotic era [39].

The use of hydrazinebenzoate as linking moieties in the development of Zn-based MOFs was also explored to target the growth and metabolic activities of highly resistant *S. aureus*, thereby suggesting its efficacy in controlling the nosocomial infections [40]. Earlier, cobalt-based MOFs have also been reported for their efficacy as promising bactericidal agents against Gram-negative pathogenic bacteria owing to their high drug payload and controlled release profile [41]. The silver nanoparticles are classically known for their bactericidal properties. In order to enhance the efficacy of silver-based nanomaterials, novel Ag-based MOFs were designed. The enhanced stability profile, optical characteristics, slow and sustained release profile, and the ability of the hybrid nanomaterials in disrupting the bacterial membrane dynamics characteristically improved the bactericidal properties against *E. coli* and *S. aureus* [18]. The unique physicochemical properties, in particular the sustained release profile of MOFs, specifically improved the bactericidal properties of encapsulated silver ions against microbial pathogens [42]. The antibacterial efficacy of zirconium-based MOFs could be correlated with the generation of highly reactive oxygen species (ROS), leading to microbial death, and could be of promising importance in next-generation antimicrobials [43].

The antimicrobial efficacy of copper-based benzene tricarboxylate (Cu-BTC)-based MOFs was reported in recent times against bacterial pathogens, *E. coli* and *S. aureus*, and fungal pathogen, *Candida albicans* [44]. The important characteristic of Cu-BTC-based MOFs is their nontoxicity which enables the production of biocidal synthetic fabrics in the textile industries. Earlier, the antifungal properties of Cu-BTC MOFs were reported against *Aspergillus niger*, *A. oryzae*, *Fusarium oxysporum*, and *C. albicans* [45]. The synergistic effect of broccoli extract (*Brassica oleracea*) in combination with MOF nanocubes (MOF-5-NC) controls the growth and metabolic activity of clinically relevant *Pseudomonas aeruginosa*. The immense antibacterial activity of these nanohybrids against bacterial pathogens suggested could be correlated with their unique physicochemical properties, controlled release profile, and bacterial membrane disruption by ROS generation [46].

Antibacterial action has been observed with MOFs belonging to the M-CPO-27 family containing Mg, Cu, Fe, Mn, Co, Ni, or Zn as metals and 2,5-dihydroxyterephthalate as the organic linker. Among these metals, MOFs containing Ni and Zn have shown promising antimicrobial activity [47]. The antibacterial properties of MOFs are attributed to the presence of metal ions, which easily internalize inside the bacterial cell wall and alter the synthesis of proteins. For instance, HKUST-1, MOF-199, and CuBTC MOFs have shown promising antibacterial action against *Escherichia coli*. The literature reports have also demonstrated that Ag-containing MOFs have proved to be the better antibacterial agents compared with conventional disinfecting agents with wide-spectrum action and lack of resistance over the





**Fig. 19.3**

Schematic overview of the synthesis of metal-organic frameworks (MOFs), their unique physicochemical properties, and theranostic applications.

plain Ag ions [18]. Moreover, the potential for delivering the antibacterial agent metronidazole has been illustrated in Fig. 19.3, where the Ni-CPO-27 MOF indicated drastic augmentation in the antibacterial activity of the drug against *Pseudomonas aeruginosa* and *Staphylococcus aureus* [48].

### 19.3.2 Antiinfective properties of MOFs

*Pseudomonas aeruginosa* is an opportunistic pathogenic Gram-negative bacterium causing severe pulmonary infections and other hospital-acquired infections in immunocompromised individuals. In 2017, *P. aeruginosa* was rated as critically acclaimed pathogen as per the WHO's guidelines owing to its resistance profile against available conventional antibiotics. In this context, it is important to design and develop novel therapeutic strategies to combat microbial infections and associated multidrug resistance (MDR) phenomenon. Recently, guanine-embedded copper-based MOFs were designed and developed to target the resistance profile of *P. aeruginosa* PAO1 by significantly modulating the expression of *oprD*, which plays crucial role as antibiotic-resistant factors. The regulation of *oprD* expression by copper-based MOFs suggested their promising efficacy in controlling the drug resistance profile of pathogenic bacteria, thereby improving the functional modalities of conventional antibiotics [49]. The development of biofilm dynamics is considered as an important factor in

the progression of microbial infection, and most importantly, the emergence of drug resistance profile. In this context, it is imperative to design next-generation antibiofilm agents targeting the disruption of biofilm architecture, thereby downregulating the resurgence of antibiotic resistance [50, 51]. In recent times, the nanotechnological intervention has provided new dimension to explore novel antibiofilm agents and their smart incorporation into nanocarriers for effective biofilm inhibition. The advent of antibiofilm agent, aminoimidazole coated into highly porous, tunable MOFs, greatly improved the biofilm disruption by localized delivery of loaded drug moieties by disrupting the biofilm matrix of *Salmonella typhimurium* [52].

### **19.3.3 Phototherapy properties of MOFs**

In recent years, the advent of photodynamic therapy targeting the progression of diseases gained considerable interest owing to its characteristic ability to use photosensitizers which, on activation, generate reactive oxygen species (ROS). In this regard, MOFs could be used to encapsulate species-specific photosensitizers which on activation significantly modulated the progression of cancer cells by generating ROS [17]. Similarly, photothermal therapy constitutes a novel therapeutic strategy where the targeted radiation excites a photosensitizer, which in turn specifically targeted killing of cancerous cell by generating enormous heat energy. The efficacy of thermal ablation technique in killing cancerous cells lies in the fact of proper utilization of specific photosensitizers. In this context, the unique physicochemical properties, high drug payload, and controlled release profile of MOFs could be used as multifaceted platform for the efficient incorporation of photosensitizers, thereby providing an improved suppression of cancer cells progression [17].

### **19.4 MOFs as next-generation bioimaging tools**

The unique physicochemical characteristics such as diverse chemical functionalities, tunable porosity, and architectural surface properties of MOFs have given new dimensions to be used in chemical sensing, as molecular probing agents, diagnostic tools, and most importantly, as drug delivery agents [27]. As MOFs represent the combinatorial assembly of metal ion clusters, organic-binding ligands, and structural motifs, they possess unique physicochemical properties which correspond to widespread applications. The functional attributes such as biodegradability, ease of postsynthetic modification, high drug payload, and tunable characteristics have proved the MOFs as promising bioimaging agents and could substantiate the conventional magnetic resonance imaging (MRI), optical imaging, and X-ray computed tomography (CT) technologies in early diagnosis of several chronic diseases and disorders and other clinical setup [53]. As per the current trends, a variety of nanomaterials such as silver nanoparticles (AgNPs), polymeric nanoparticles, and mesoporous silica nanoparticles (MSNs)

are regarded as promising contrasting agents for bioimaging purposes. Apart from these nanomaterials, recently MOFs have created a buzz among the scientific community owing to their multimodal drug delivery applications as well as efficient contrast agents.

MOFs could be used as  $T_1$ - (spin-lattice relaxation time) or  $T_2$ - (spin-spin relaxation time) or combined  $T_1$ - and  $T_2$ -contrast agents for MRI image enhancement [29, 54, 55]. Apart from normal MOFs, paramagnetic metal ions-containing MOFs also exhibited its candidature as promising contrasting agents for MR imaging. The importance of paramagnetic MOFs as efficient contrasting agents as compared to clinical small molecule contrast agents is the availability of large number of paramagnetic metal centers in the framework architecture and their enhanced per-metal-based relativity [56]. The recent development in the design and synthesis of gadolinium-based MOFs and manganese-based MOFs has attracted considerable attention as promising molecular probes for MRI purpose, thereby replacing the conventional contrasting agents [57].

In the development of stable, reliable, and reproducible molecular probes for bioimaging applications, nanotechnological intervention has provided new dimension in the proper utilization of dye molecules/contrasting agents. The unique optical and other physicochemical characteristics of MOFs such as photoluminescence, high crystallinity, and extended stability have gained considerable attention for the incorporation of resorufin and rhodamine-6G into the MOFs architecture. The hybrid nanomaterials critically improved the stability and reliability of the encapsulated dyes and could be utilized as promising molecular probes in imaging the progression of human hepatocyte cell (FL83B) and human hepatocellular carcinoma (HepG2). The lack of cytotoxicity in using MOFs as promising bioimaging tools could be explored towards the early diagnosis of disease progression [58]. The biocompatibility and CT imaging of iodine-boron-dipyrrromethene (BODIPY)-containing MOF nanocrystals, named UiO-PDT, have been studied. The *in vivo* CT imaging suggested the enhanced efficacy of synthesized MOFs, UiO-PDT nanocrystals, in targeting the tumor sites without affecting the surrounding connective tissues and organs, thereby providing the best imaging performance. The aforementioned findings suggest that the MOFs-based nanohybrids could have the potential for use as promising CT contrast agents [59].

### **19.5 MOFs as phototheranostics**

Owing to the unique physicochemical properties, optical characteristics, biocompatibility, drug release efficacy, and improved drug payload, MOFs have gained considerable attention in designing and developing novel theranostic probes for disease diagnosis and therapy [56]. The advent of MOFs has created a multifunctional platform for targeted bioimaging and localized drug delivery, which has already been in demand for early diagnosis and cancer therapeutics. The MOFs based on conversion nanoparticles (UCNPs) could be prescribed as

promising contrasting agents for optical imaging and other biomedical applications owing to their unique optical properties. The introduction of highly specific aptamers in combination with MOFs-based UCNPs could be targeted in cancer therapy owing to their species-specific target of interest [60].

The advent of multifunctional nanoplateforms based on hyaluronic acid and indocyanine green-engineered MOFs significantly attributed to its drug payload capacity, near-infra red (NIR) absorbance, and enhanced photostability. The unique photostability and high NIR absorptibility resulted in enhanced imaging-guided photothermal therapy against cancer progression, thereby providing a unique theranostic platform to fight against cancer [61]. The unique characteristics such as low toxicity profile, enhanced biocompatibility, and tunable photostability significantly enhanced the photothermal ability of MOFs-based multidimensional nanoplateforms in combination with different functional moieties against cancer cells [12, 13]. The highly versatile, programmable stimuli-responsive MOFs have the unique ability to work in combination with an array of diverse functional moieties, which enable its multifaceted applications in photothermal therapy [62]. The drug delivery efficacy of MOFs is generally controlled by three basic cargo-delivery strategies such as encapsulation strategy, direct assembly strategy, and postsynthetic modulation strategy [63].

### ***19.6 MOFs as magnetic theranostics***

The characteristic features such as size tunability, ease in surface functionalization, colloidal stability, biocompatibility, and high drug payload have proven the efficacy of magnetic nanoparticles in targeted drug delivery and theranostics [64]. The magnetic properties like saturation magnetization, coercivity, and magneto-crystalline anisotropy are found to be highly relevant in effective bioimaging and therapeutics [65]. Recently, MOFs get considerable attention in theranostic platforms owing to their unique magnetic properties and unique accessibility for surface modification. Recently, magnetically active MOFs nanocomposites comprising ferric oxide ( $\text{Fe}_3\text{O}_4$ ) nanorods and nanocrystals of  $\text{Cu}_3$  (Benzene-1,3,5-tricarboxylate)<sub>2</sub> were developed for localized targeting of nimesulide, an anticancer drug to treat pancreatic cancer [66]. Arsenic trioxide is served as potent antagonistic agent against a variety of solid tumors and cancer progression. However, their cytotoxic profile and therapeutic inefficacy limit their widespread applications in cancer therapy. In this context, it is imperative to develop novel nanocarriers such as MOFs which constitutively improved the pharmacokinetic profile, high drug payload, drug release profile, and therapeutic processes for localized and targeted delivery of arsenic trioxide [67].

In cancer therapeutic process, doxorubicin has been used as promising anticancer agent. However, its biocompatibility and bioavailability issues have urged the scientific community to quest for novel carrier system for localized and efficient delivery of doxorubicin at the

target sites targeting the cancer progression. In this context, recently, doxorubicin was encapsulated into the hyaluronic acid-conjugated MOFs which critically improved the early diagnosis and efficient therapeutics in the treatment of cancer. The obtained hybrid nanoplatform could not only deliver DOX into cancer cells, but also could be applied for magnetic resonance (MR) imaging and fluorescence imaging, thereby achieving simultaneous therapeutic and diagnostic functions. Considering the relatively complicated process of the above design, it is highly desirable to develop a facile strategy to construct a multifunctional theranostic nanoplatform [68]. In the development of cancer therapy, three important functional modalities such as magnetic/fluorescence imaging, cell targeting, and drug storage delivery are crucial in the management of cancer progression. Each of the above-mentioned functional modalities has their own advantages and disadvantages. In this context, designing a suitable platform by taking consideration of the three functional modalities could be of promising aspect in cancer therapeutics. The advent of MOFs has provided a unique platform to carry these functional modalities to target the tumor cells by integrating the multimodal imaging capability [69].

Recently, the nanoporous MOFs composed of iron metal and organic ligand, amino terephthalate (MIL-101-NH<sub>2</sub>-Fe), were utilized as promising nanocarrier for targeted delivery of anticancer drug, i.e., 5-fluorouracil in the treatment of breast cancer. The specifically designed MOFs characteristically improved the therapeutic efficacy of 5-fluorouracil by improving the stability of 5-fluorouracil and also enhanced the controlled release profile, thereby suggesting the efficacy in controlling cancer progression [70]. In the treatment of ovarian cancer, cisplatin was regularly used. However, indiscriminate uses of cisplatin lead to resistance by ovarian cancer cells. In this context, it is important to design hybrid nanomaterials basically composed of MOFs for the co-delivery of cisplatin and pooled small interfering RNAs (siRNAs) to enhance the therapeutic index of cisplatin with sustained release profile at the target sites. The advent of MOFs in combination with cisplatin also characteristically silenced the MDR genes and improved the sensitivity of ovarian cancer cells to cisplatin. In addition, the use of MOFs also protects siRNAs from nuclease degradation, enhances siRNA cellular uptake, and promotes siRNA escape from endosomes to silence MDR genes in cisplatin-resistant ovarian cancer cells [71].

Apart from cancer therapy, the feasibility of MOFs and MOF hybrids could also engage towards controlling the progression of other infectious as well as noninfectious diseases. Recently, antitubercular drug, i.e., isoniazid, was successfully encapsulated into MOFs (Fe-MIL-101-NH<sub>2</sub>), which characteristically improved the therapeutic efficiency of isoniazid by improving the drug payload, extended release profile, and targeted delivery at the target sites. In addition, the role of MOFs as typical contrast MRI agents has provided new scope to scientific community for early diagnosis of life-threatening diseases and disorders by replacing the conventional MRI agents for bioimaging applications [72].

## 19.7 Current trends and future perspectives

From last few decades, the advent of interdisciplinary nanotechnology into the field of biology has provided a new dimension to the biomedical and pharmaceutical research modalities exponentially. The design and development of various nanomaterials with specific physicochemical properties served as multifaceted platforms for widespread applications. The advent of nanotechnological intervention has shown promising aspects to be used as diagnostic imaging agents, contrast agents for bioimaging modalities, and targeted drug delivery platforms for localized and species-specific therapeutics by characteristically improving the drug payload and its therapeutic efficacy. In recent times, the concept of nanocomposites by combining the characteristic materials with dual function achieves improved efficacy in drug delivery and therapeutics. The design and development of these dual or multimodal nanocomposites have given new dimension to the current knowledge on biomedical diagnostics and targeted therapeutics in particular in the treatment of cancer and other infectious diseases [72].

From the historical perspectives, recently, MOFs have been emerged as potential nanocarriers for targeted delivery of drug moieties to control various diseases and disorders owing to their characteristic features such as porosity, tenability, and ease of synthesis. In addition, the unique physicochemical properties of MOFs also provided its candidature as promising contrasting agent for bioimaging applications with widespread functional modalities [73]. Although the unique physicochemical properties of MOFs have provided an array of potential biomedical and pharmaceutical applications, certain limitations associated with MOFs limit their further clinical applications. The foremost limitation associated with MOFs is basically the hydrophobic nature of MOFs which lead to agglomeration, thereby inhibiting the passive targeting of the so-called enhanced permeability and retention (EPR) effect. In addition, poor biocompatibility issues associated with majority of MOFs significantly affected the stability and therapeutic index of the loaded drug moieties due to the quick removal of the drug moieties by the reticuloendothelial system (RES) during blood circulation. Apart from these limitations, MOFs lack active auto-targeting ability resulting in decreased therapeutic efficacy. In order to counteract the limitations associated with MOFs, attempts are being carried out in terms of postsynthetic modifications or complexation, thereby improving the drug release profile and also therapeutic index [50, 51]. Although the characteristic properties such as micropore volumes and large surface areas improved the functional modalities of MOFs for widespread and desirable applications, the uptake of large objects remains hindered due to narrow pores, thereby limiting their applications in the field of biology and pharmaceuticals [74].

Among the different drug delivery systems (DDS) for drug administration, MOFs emerged as promising carrier system for the targeted delivery therapeutic drug moieties and therapeutic enzymes by critically controlling the release profile as well as enhancing drug payload [75].



Cyclodextrins (CDs) are biodegradable cyclic oligosaccharides and are considered to enhance the solubility index of drug moieties and greatly improved the bioavailability of drug candidates owing to their low toxicity, flexible structure, and high drug payload. Recently, the characteristic features of CDs are employed as promising ligand components in the design and synthesis of MOFs (CD-MOFs). The CD-based MOFs have all the desirable characteristic features such as porous features of MOFs and the encapsulation efficacy of CDs for drug molecules for improved drug delivery applications [76]. Interestingly, the advent of multidimensional MOFs is also found to be of promising importance in protein-based theranostics for effective and efficient delivery and controlled release of native active protein moieties in living cells [77].

## **19.8 Conclusion**

In recent times, the unique physicochemical properties and practical feasibility of MOFs have gained considerable attention for widespread applications in the field of material science, biology, nanotechnology, and drug delivery. The advantageous features such as biodegradability, biocompatibility, bioavailability, tunable porosity, high drug payload, controlled release profile, and ease of surface modification are considered for its diverse applications in diagnosis, bioimaging modules, drug delivery, and theranostics. As per the recent trends in designing and developing novel nanomaterials as promising drug delivery platforms, the advent of MOFs could be of strategic and smart nanomaterials for early diagnosis of diseases owing to their reliable efficacy as molecular probes in bioimaging applications. Apart from bioimaging, the theranostic applications of MOFs also considerably attracted the scientific community for development of next-generation therapeutics. The limitations associated with MOFs such as poor selectivity, low capacity, and high cost could be taken into consideration for improving the efficacy of MOFs as promising diagnostic tools and drug delivery platforms.

## **Acknowledgments**

This work was supported by the Major State Basic Research Development Program of China (2017YFA0205201 and 2018YFA0107301), the National Natural Science Foundation of China (81422023, 81801817, U1705281, and U1505221), the Fundamental Research Funds for the Central Universities (20720160065 and 20720150141), and the Program for New Century Excellent Talents in University, China (NCET-13-0502).

## **References**

- [1] D.M. Morens, A.S. Fauci, Emerging infectious diseases: threat to human health and global stability, *PLoS Pathog.* 9 (7) (2013) e1003467.
- [2] C. Dye, After 2015: infectious diseases in a new era of health and development, *Phil. Trans. R. Soc. B* 369 (2014) 20130426.

- [3] C.A. Michael, D. Dominey-Howes, M. Labbate, The antimicrobial resistance crisis: causes, consequences, and management, *Front. Public Health* 2 (2014) 145.
- [4] S. Ashkenazi, Beginning and possibly the end of the antibiotic era, *J. Paediatr. Child Health* 49 (2013) E179–E182.
- [5] A. Rangel-Vega, L.R. Bernstein, E.A. Mandujano-Tinoco, S.J. Garcia-Contreras, R. Garcia-Contreras, Drug repurposing as an alternative for the treatment of recalcitrant bacterial infections, *Front. Microbiol.* 6 (2015) 282.
- [6] S. Zaidi, L. Misba, A.U. Khan, Nano-therapeutics: a revolution in infection control in post antibiotic era, *Nanomed. Nanotechnol. Biol. Med.* 13 (7) (2017) 2281–2301.
- [7] X. Zhu, A.F. Radovic-Moreno, J. Wu, R. Langer, J. Shi, Nanomedicine in the management of microbial infection – overview and perspectives, *Nano Today* 9 (2014) 478–498.
- [8] A.P. Nikalje, Nanotechnology and its applications in medicine, *Med. Chem.* 5 (2015) 2.
- [9] N. Dasgupta, S. Ranjan, C. Ramalingam, Applications of nanotechnology in agriculture and water quality management, *Environ. Chem. Lett.* 15 (4) (2017) 591–605.
- [10] A.P. Ramos, M.A.E. Cruz, C.B. Tovani, P. Ciancaglini, Biomedical applications of nanotechnology, *Biophys. Rev.* 9 (2) (2017) 79–89.
- [11] B. Das, S.K. Dash, D. Mandal, T. Ghosh, S. Chattopadhyay, S. Tripathy, S. Das, S. K. Dey, D. Das, S. Roy, Green synthesized silver nanoparticles destroy multidrug resistant bacteria via reactive oxygen species mediated membrane damage, *Arab. J. Chem.* 10 (2017) 862–876.
- [12] X. Cai, B. Liu, M. Pang, J. Lin, Interfacially synthesized Fe-soc-MOF nanoparticles combined with ICG for photothermal/photodynamic therapy, *Dalton Trans.* 47 (45) (2018) 16329–16336.
- [13] W. Cai, J. Wang, C. Chu, W. Chen, C. Wu, G. Liu, Metal-organic framework-based stimuli-responsive systems for drug delivery, *Adv. Sci.* 6 (2018) 1801526.
- [14] G. Wyszgrodzka, B. Marszalek, B. Gil, P. Dorozynski, Metal-organic frameworks: mechanisms of antibacterial action and potential applications, *Drug. Disc. Today* 21 (6) (2016) 1009–1018.
- [15] R.K. Alevijeh, S. Beheshti, K. Akhbari, A. Morsali, Investigation of reasons for metal-organic framework's antibacterial activities, *Polyhedron* 156 (2018) 257–278.
- [16] Z. Liao, T. Xia, E. Yu, Y. Cui, Luminescent metal-organic framework thin films: from preparation to biomedical sensing applications, *Crystals* 8 (2018) 338.
- [17] G. Chedid, A. Yassin, Recent trends in covalent and metal organic frameworks for biomedical applications, *Nano* 8 (2018) 916.
- [18] X. Lu, J. Ye, D. Zhang, R. Xie, R.F. Bogale, Y. Sun, L. Zhao, Q. Zhao, G. Ning, Silver carboxylate metal-organic frameworks with highly antibacterial activity and biocompatibility, *J. Inorg. Biochem.* 138 (2014) 114–121.
- [19] C. Pettinari, F. Marchetti, N. Mosca, G. Tosi, A. Drozdov, Application of metal-organic frameworks, *Polym. Int.* 66 (2017) 731–744.
- [20] R. Liu, T. Yu, Z. Shi, Z. Wang, The preparation of metal-organic frameworks and their biomedical applications, *Int. J. Nanomedicine* 11 (2016) 1187–1200.
- [21] E. Sharmin, M. Zafar, Introductory Chapter: Metal Organic Frameworks (MOFs), InTech, 2016. <https://doi.org/10.5772/64797>.
- [22] W. Zhou, S. Begum, Z. Wang, P. Krolla, D. Wagner, S. Brase, C. Woll, M. Tsotsalas, High antimicrobial activity of metal-organic framework-templated porphyrin polymer thin films, *ACS Appl. Mater. Interface* 10 (2018) 1528–1533.
- [23] M.A. Haydar, H.R. Abid, B. Sunderland, S. Wang, Metal organic frameworks as a drug delivery system for flurbiprofen, *Drug. Des. Dev. Ther.* 11 (2017) 2685–2695.
- [24] S. Rojas, F.J. Carmona, C.R. Maldonado, P. Horcajada, T. Hidalgo, C. Serre, J.A. R. Navarro, E. Barea, Nanoscale zinc pyrazolate metal-organic frameworks as drug-delivery systems, *Inorg. Chem.* 55 (2016) 2650–2663.
- [25] M.X. Wu, Y.W. Yang, Metal-organic framework (MOF)-based drug/cargo delivery and cancer therapy, *Adv. Mater.* 29 (2017) 1606134.

- [26] N. Manousi, G.A. Zachariadis, E.A. Deliyanni, V.F. Samanidou, Applications of metal-organic frameworks in food sample preparation, *Molecules* 23 (2018) 2896.
- [27] S. Wang, C.M. McGuirk, A. d'Aquino, J.A. Mason, C.A. Mirkin, Metal-organic framework nanoparticles, *Adv. Mater.* 30 (2018), 1800202. <https://doi.org/10.1002/adma.201800202>.
- [28] M.H. Akhter, Nanocomposite Hybrid Metal-Organic Framework in Drug Delivery and Theranostic Application, *Pharmafocusasia*, 2018.
- [29] M.A. Chowdhury, Metal-organic-frameworks as contrast agents in magnetic resonance imaging, *Chem. Bioeng. Rev.* 4 (4) (2017) 225–239.
- [30] A.K. Ebrahimi, M. Barani, I. Sheikhshoae, Fabrication of a new superparamagnetic metal-organic framework with core-shell nanocomposite structures: Characterization, biocompatibility, and drug release study, *Mater. Sci. Eng. C.* 92 (2018) 349–355.
- [31] M.A. Chowdhury, The applications of metal-organic-frameworks in controlled release of drugs, *Rev. J. Chem.* 7 (1) (2017) 1–22.
- [32] P.Z. Li, J. Su, J. Liang, J. Liu, Y. Zhang, H. Chen, Y. Zhao, A highly porous metal-organic framework for large organic molecule capture and chromatographic separation, *Chem. Commun.* 53 (2017) 3434.
- [33] J.D. Sosa, T.F. Benett, K.J. Nelms, B.M. Liu, R.C. Tovar, Y. Liu, Metal-organic framework hybrid materials and their applications, *Crystals* 8 (2018) 325.
- [34] S. Beg, M. Rahman, A. Jain, S. Saini, P. Midoux, C. Pichon, F.J. Ahmad, S. Akhter, Nanoporous metal organic frameworks as hybrid polymer-metal composites for drug delivery and biomedical applications, *Drug Disc. Today* 22 (4) (2017) 625–637.
- [35] X.M. Quan, Y.D. Liu, H.J. Choi, Magnetorheology of iron associated magnetic metal-organic framework nanoparticle, *J. Appl. Phys.* 117 (2015)17C732.
- [36] X. Yao, X. Ma, X. Gao, L. Jia, Preparation of magnetic metal organic framework nanocomposites for efficient and selective adsorption of hemoglobin from bovine blood, *RSC Adv.* 7 (2017) 29330–29338.
- [37] E.N. Augustus, A. Nimibofa, I.A. Kesiye, W. Donbebe, Metal-organic frameworks as novel adsorbents: a preview, *Am. J. Environ. Protect.* 5 (2) (2017) 61–67.
- [38] M.D. Firouzjaei, A.A. Shamssabadi, G.M. Sharifian, A. Rahimpour, M. Soroush, A novel nanocomposite with superior antibacterial activity: a silver-based metal organic framework embellished with graphene oxide, *Adv. Mater. Interface* 5 (2018) 1701365.
- [39] N. Bhardwaj, S.K. Pandey, J. Mehta, S.K. Bhardwaj, K.H. Kim, A. Deep, Bioactive nano-metal-organic frameworks as antimicrobials against Gram-positive and Gram-negative bacteria, *Toxicol. Res.* 7 (2018) 931–941.
- [40] J. Restrepo, Z. Serroukh, J. Santiago-Morales, S. Aguado, P. Gomez-Sal, M.E.G. Mosquera, R. Rosal, An antibacterial Zn-MOF with hydrazinebenzoate linkers, *Eur. J. Inorg. Chem.* 2017 (2017) 574–580.
- [41] S. Aguado, J. Quiros, J. Canivet, D. Farrusseng, K. Boltes, R. Rosal, Antimicrobial activity of cobalt imidazolate metal-organic frameworks, *Chemosphere* 113 (2014) 188–192.
- [42] M. Berchel, T.L. Gall, C. Denis, S.L. Hir, F. Quentel, C. Elleouet, T. Montier, J.M. Rueff, J.Y. Salaun, J. P. Haelters, G.B. Hix, P. Lehn, P.A. Jaffres, A silver-based metal-organic framework material as a 'reservoir' of bactericidal metal ions, *New J. Chem.* 35 (2011) 1000–1003.
- [43] M. Liu, L. Wang, X. Zheng, Z. Xie, Zirconium-based nanoscale metal-organic framework/poly (ε-caprolactone) mixed-matrix membranes as effective antimicrobials, *ACS. Appl. Mater. Interface* 9 (47) (2017) 41512–41520.
- [44] H.E. Emam, O.M. Darwesh, R.M. Abdelhameed, In-growth metal organic framework/synthetic hybrids as antimicrobial fabrics and its toxicity, *Colloid. Surf. B. Biointerface* 165 (2018) 219–228.
- [45] S. Bouson, A. Krittayavathananon, N. Phaththarasupakun, P. Siwayaprahm, M. Sawangphruk, Antifungal activity of water-stable copper-containing metal-organic frameworks, *R. Soc. Open Sci.* 4 (2017) 170654.
- [46] V. Pezeshkpour, S.A. Khosravani, M. Ghaedi, K. Dashtian, F. Zare, A. Sharifi, R. Jannesar, M. Zoladl, Ultrasound assisted extraction of phenolic acids from broccoli vegetable and using sonochemistry for preparation of MOF-5 nanocubes: comparative study based on micro-dilution broth and plate count method for synergism antibacterial effect, *Ultrason. Sonochem.* 40 (2018) 1031–1038.

- [47] A.C. McKinlay, P.K. Allan, C.L. Renouf, M.J. Duncan, P.S. Wheatley, S.J. Warrender, D. Dawson, S. E. Ashbrook, B. Gil, B. Marszalek, T. Duren, J.J. Williams, C. Charrier, D.K. Mercer, S.J. Teat, R. E. Morris, Multirate delivery of multiple therapeutic agents from metal-organic frameworks, *APL Mater.* 2 (2014) 124108.
- [48] A.C. McKinlay, et al., Multirate delivery of multiple therapeutic agents from metal-organic frameworks, *APL Mater.* 2 (2014) 5199–5217.
- [49] F. Abbasloo, S.A. Khosravani, M. Ghaedi, K. Dashtian, E. Hosseini, L. Manzouri, S. S. Khorramrooz, A. Sharifi, R. Jannesar, F. Sadri, Sonochemical-solvothermal synthesis of guanine embedded copper based metal-organic framework (MOF) and its effect on oprD gene expression in clinical and standard strains of *Pseudomonas aeruginosa*, *Ultrason. Sonochem.* 42 (2018) 237–243.
- [50] X. Li, B. Wu, H. Chen, K. Nan, Y. Jin, L. Sun, B. Wang, Recent developments in smart antibacterial surfaces to inhibit biofilm formation and bacterial infections, *J. Mater. Chem. B* 6 (2018) 4274–4292.
- [51] Y. Li, Y. Zheng, X. Lai, Y. Chu, Y. Chen, Biocompatible surface modification of nano-scale zeolitic imidazolate frameworks for enhanced drug delivery, *RSC Adv.* 8 (2018) 23623.
- [52] B. Claes, T. Boudewijns, L. Muchez, G. Hooyberghs, E.V. Van der Eycken, J. Vanderleyden, H. P. Steenackers, D.E. De Vos, Smart metal–organic framework coatings: triggered antibiofilm compound release, *ACS Appl. Mater. Interfac.* 9 (5) (2017) 4440–4449.
- [53] D. Liu, K. Lu, C. Poon, W. Lin, Metal-organic frameworks as sensory materials and imaging agents, *Inorg. Chem.* 53 (4) (2014) 1916–1924.
- [54] M.A. Chowdhury, Metal-organic-frameworks for biomedical applications in drug delivery, and as MRI contrast agents, *J. Biomed. Mater. Res. Part A* 105A (2017) 1184–1194.
- [55] R. Pala, Y. Zeng, S. Pattnaik, S. Busi, N. Alomari, S.M. Nauli, G. Liu, Functionalized silver nanoparticles for sensing, molecular imaging and therapeutic applications, *Curr. Nanomed.* 8 (2018) 1–17.
- [56] H.X. Zhao, Q. Zou, S.K. Sun, C. Yu, X. Zhang, R.J. Li, Y.Y. Fu, Theranostic metal–organic framework core–shell composites for magnetic resonance imaging and drug delivery, *Chem. Sci.* 7 (2016) 5294–5301, <https://doi.org/10.1039/c6sc01359g>.
- [57] B.S. Barros, O.J. de Lima Neto, A.C. de Oliveira Fros, J. Kulesza, Metal-organic framework nanocrystals, *Chem. Select.* 3 (2018) 7459–7471.
- [58] U. Ryu, J. Yoo, W. Kwon, K.M. Choi, Tailoring nanocrystalline metal-organic frameworks as fluorescent dye carriers for bioimaging, *Inorg. Chem.* 56 (2017) 12859–12865.
- [59] T. Zhang, L. Wang, C. Ma, W. Wang, J. Ding, S. Liu, X. Zhang, Z. Xie, BODIPY-containing nanoscale metal–organic frameworks as contrast agents for computed tomography, *J. Mater. Chem. B* 5 (2017) 2330–2336.
- [60] K. Deng, Z. Hou, X. Li, C. Li, Y. Zhang, X. Deng, Z. Cheng, J. Lin, Aptamer mediated up-conversion Core/MOF shell nanocomposites for targeted drug delivery and cell imaging, *Sci. Rep.* 5 (2015) 7851.
- [61] W. Cai, H. Gao, C. Chu, X. Wang, J. Wang, P. Zhang, G. Lin, W. Li, G. Liu, X. Chen, Engineering phototheranostic nanoscale metal-organic frameworks for multimodal imaging-guided cancer therapy, *ACS Appl. Mater. Interfac.* 9 (3) (2017) 2040–2051.
- [62] J. Feng, Z. Xu, P. Dong, W. Yu, F. Liu, Q. Jiang, F. Wang, X. Liu, Stimuli-responsive multifunctional metal-organic framework nanoparticles for enhanced chemo-photothermal therapy, *J. Mater. Chem. B* 7 (2019) 994–1004.
- [63] L. Wang, M. Zheng, Z. Xie, Nanoscale metal–organic frameworks for drug delivery: a conventional platform with new promise, *J. Mater. Chem. B* 6 (2017) 707–717, <https://doi.org/10.1039/c7tb02970e>.
- [64] O.L. Gobbo, K. Sjaastad, M.W. Radomski, Y. Volkov, A. Prina-Mello, Magnetic nanoparticles in cancer theranostics, *Theranostic* 5 (11) (2015) 1249–1263.
- [65] D. Yoo, J.H. Lee, T.H. Shin, J. Cheon, Theranostic magnetic nanoparticles, *Acc. Chem. Res.* 44 (10) (2011) 863–874.
- [66] F. Ke, Y.P. Yuan, L.G. Qiu, Y.H. Shen, A.J. Xie, J.F. Zhu, X.Y. Tian, L.D. Zhang, Facile fabrication of magnetic metal–organic framework nanocomposites for potential targeted drug delivery, *J. Mater. Chem.* 21 (2010) 3843–3848.

- [67] R. Ettliger, M. Sonksen, M. Graf, N. Moreno, D. Denysenko, D. Volkmer, K. Kerl, H. Bunzen, Metal-organic framework nanoparticles for arsenic trioxide drug delivery, *J. Mater. Chem. B* 6 (2018) 6481.
- [68] F. Shu, D. Lv, X.L. Song, B. Huang, C. Wang, Y. Yu, S.C. Zhao, Fabrication of a hyaluronic acid conjugated metal organic framework for targeted drug delivery and magnetic resonance imaging, *RSC Adv.* 8 (2018) 6581.
- [69] X. Gao, M. Zhai, W. Guan, J. Liu, Z. Liu, A. Damirin, Controllable synthesis of a smart multifunctional nanoscale metal – organic framework for magnetic resonance/optical imaging and targeted drug delivery, *ACS Appl. Mater. Interface* 9 (2017) 3455–3462.
- [70] M. Miri, N. Motakef-Kazemi, S.A. Shojaosadati, A. Morsali, Application of a nanoporous metal organic framework based on iron carboxylate as drug delivery system, *Iran. J. Pharmaceut. Res.* 17 (4) (2018) 1164–1171.
- [71] C. He, K. Lu, D. Liu, W. Lin, Nanoscale metal–organic frameworks for the co-delivery of cisplatin and pooled siRNAs to enhance therapeutic efficacy in drug-resistant ovarian cancer cells, *J. Am. Chem. Soc.* 136 (14) (2014) 5181–5184.
- [72] G. Wyszogrodka, P. Dorozynski, B. Gil, W.J. Roth, M. Strzempek, B. Marszalek, W. P. Weglarz, E. Menaszek, W. Strzempek, P. Kulinowski, Iron-based metal-organic frameworks as a theranostic carrier for local tuberculosis therapy, *Pharm. Res.* 35 (2018) 144.
- [73] L. Tang, J. Shi, X. Wang, S. Zhang, H. Wu, H. Sun, Z. Jiang, Coordination polymer nanocapsules prepared using metal–organic framework templates for pH-responsive drug delivery, *Nanotechnology* 28 (2017) 275601.
- [74] W. Xuan, C. Zhu, Y. Liu, Y. Cui, Mesoporous metal-organic framework materials, *Chem. Soc. Rev.* 41 (2012) 1677–1695, <https://doi.org/10.1039/c1cs15196g>.
- [75] S. Rojas, I. Colinet, D. Cunha, T. Hidalgo, F. Salles, C. Serre, N. Guillou, P. Horcajada, Toward understanding drug incorporation and delivery from biocompatible metal-organic frameworks in view of cutaneous administration, *ACS Omega* 3 (2018) 2994–3003.
- [76] Y. Han, W. Liu, J. Huang, S. Qiu, H. Zhong, D. Liu, J. Liu, Cyclodextrin-based metal-organic frameworks (CD-MOFs) in pharmaceuticals and biomedicine, *Pharmaceutics* 10 (2018) 271.
- [77] T.T. Chen, J.T. Yi, Y.Y. Zhao, X. Chu, Biomineralized metal-organic framework nanoparticles enable intracellular delivery and endo-lysosomal release of native active proteins, *J. Am. Chem. Soc.* 140 (31) (2018) 9912–9920.

# ***Carbohydrates in metal organic frameworks: Supramolecular assembly and surface modification for biomedical applications***

Jingwen Qiu<sup>a</sup>, Xue Li<sup>a</sup>, Ruxandra Gref<sup>a</sup>, Antonio Vargas-Berenguel<sup>b</sup>

<sup>a</sup>National Center for Scientific Research (CNRS), Institute of Molecular Sciences, Paris-Sud University, Paris-Saclay University, Orsay, France <sup>b</sup>Department of Chemistry and Physics, University of Almeria, Almería, Spain

## **20.1 Introduction**

Nanotechnology revolutionizes drug delivery by achieving drug transcytosis, drug targeting, and theranostics. Biocompatible and biodegradable metal organic frameworks (MOFs) [1, 2] have been designed and synthesized for biomedical application. Recently, nanoscale MOFs (nanoMOFs) emerge as an attracting class of hybrid nanomaterials for biomedical application. MOFs are formed by the self-assembly of metal centers and bridging organic ligands, leading to the formation of crystalline architectures with regular and high porosities. They have been increasingly used for biomedical applications in the last decade, taking advantage of their high drug loading capability, biodegradability, and high versatility in terms of architecture and physico-chemical properties [1, 3–6]. However, the vast majority of MOFs described were composed of metallic ions or clusters and synthetic organic ligands. Recently, more and more attention was dedicated to the use of natural materials for the fabrication of MOFs, which are inherently compatible with the metabolic system [7, 8].

Carbohydrates (oligosaccharides and/or polysaccharides) have been well-recognized as edible materials. Together with lipids, proteins, and nucleic acids, they are one of the four major classes of biomolecules. Carbohydrates are unique candidates for drug-carrier preparation since they possess several advantages, such as biocompatibility and biodegradability. A variety of nanocarriers composed of carbohydrates have been reported [9, 10], including covalently/ ionically cross-linked polysaccharide-based nanosponges [11], self-assemblies [12], dendrimers [10], nanocapsules [13], hydrogels [14], micelles [15], and multilayered polysaccharide vesicles [10]. However, the challenge in synthesizing MOFs from



carbohydrates lies in the inherent asymmetry of the building units, which are not easily amenable to the formation of highly porous crystallized frameworks. A strategy was reported to overcome this problem by the adoption of the cyclic oligosaccharide cyclodextrin (CD), which is comprised of six to eight asymmetric  $\alpha$ -1,4-linked D-glucopyranosyl residues. CDs are naturally available oligosaccharides enzymatically produced from starch. In contrast to other linear carbohydrates, CDs are typical “cage” molecules of a truncated cone shape with a hydrophobic cavity and a hydrophilic surface [16]. The most common natural CDs are  $\alpha$ ,  $\beta$ , and  $\gamma$ -CDs, containing 6, 7, and 8 glucopyranose units, respectively. Their ability to coordinate with metal ions makes possible the formation of CD-based MOFs. The CD building units could be linked by metal ions, such as  $K^+$ ,  $Na^+$ ,  $Rb^+$ ,  $Cs^+$ ,  $Sr^+$ ,  $Pb^{2+}$ ,  $Fe^{3+}$ , to form a body-centered porous crystallized MOF structure [17,18]. CDs remain the only type of carbohydrate being able to form MOF crystals.

In addition to their ability to form supramolecular constructs, the hydrophilicity and versatility of carbohydrate materials make them attractive materials for surface modification of preformed drug nanocarriers. For instance, several polysaccharides [19] are currently investigated as potential alternatives for poly(ethylene glycol) (PEG) coatings, which is one of the most popular strategies to decorate NPs’ surface to increase the blood circulation time [20–22]. It has been reported that some modified dextrans, heparin (hep), low molecular weight chitosan, and starch derivatives have similar “stealth effects” by forming a hydrated layer, which allows the NPs to evade opsonization and subsequently phagocytosis, therefore prolonging NPs’ circulation time in the blood stream [23]. Moreover, carbohydrates are of high interest for targeting. The surface of the cell is rich in carbohydrate moieties which constitute potential recognition sites for carbohydrate-mediated interactions between cells and drug carriers coated with suitable site-directing molecules. This ability to be specifically recognized by receptors on the cell-surface indicates their potential utility as targeting ligands for therapeutic applications. For example, mannose [24, 25], chitosan, hyaluronic acid, and chondroitin sulfate [26] have been used as targeting ligands to macrophages for intracellular infection treatment. In addition, surface modification with carbohydrates may offer NPs with higher stability and controlled release.

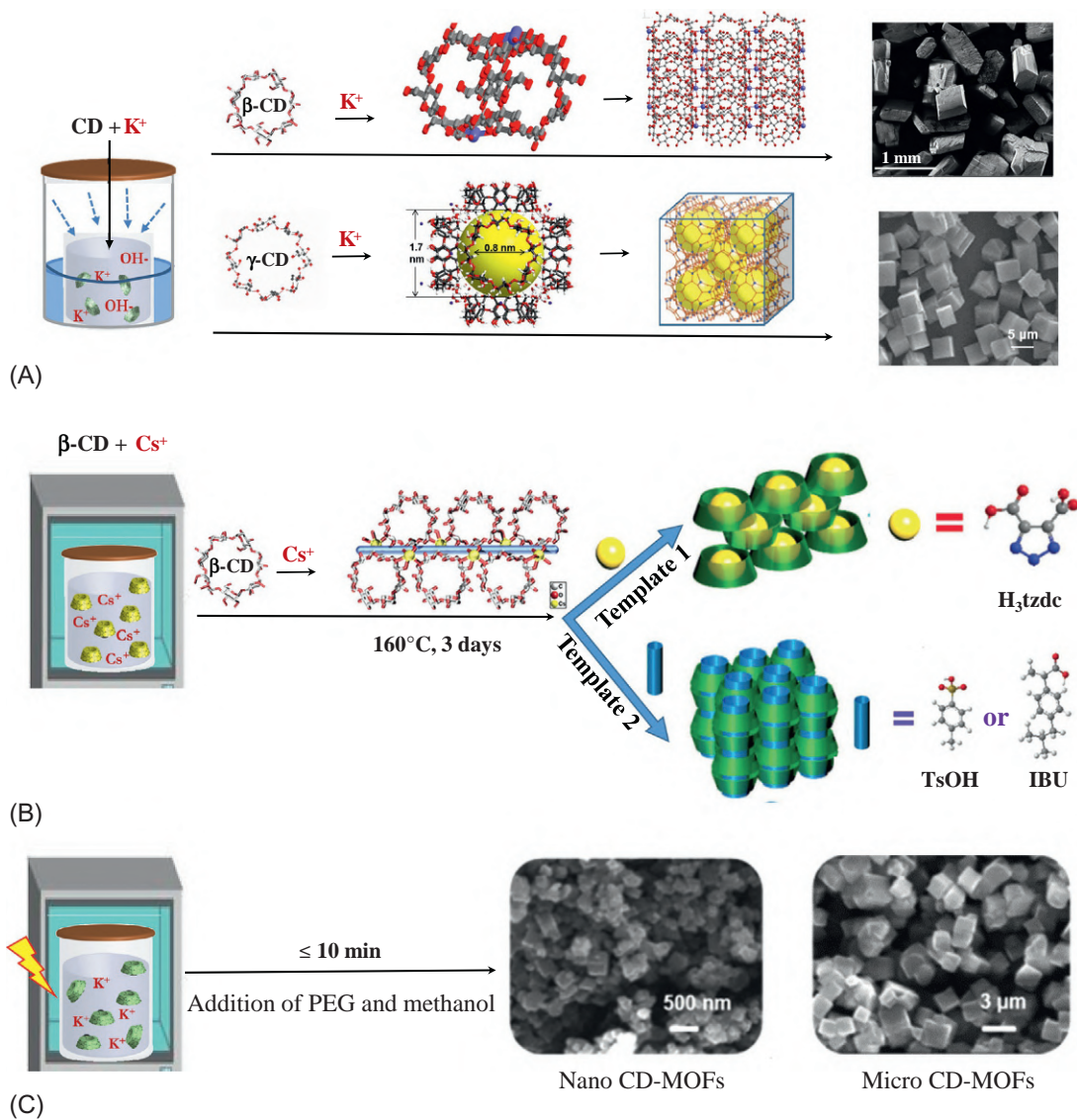
A variety of carbohydrates are used for surface functionalization of nanocarriers, including CDs, dextrin, chitosan, starch, galactose, fucose, sialic acid, glucose, rhamnose, mannose, etc. [23]. Various nanomaterials have been modified with different carbohydrates, including poly(lactic-co-glycolic) acid (PLGA), NPs, liposomes, metallic NPs, magnetic NPs, quantum dots, micelles, etc. [23, 25, 27, 28]. However, surface modification of the porous MOFs is challenging since it requires specific coating materials and methods to avoid penetration of the coating materials inside the porous structure of MOFs, thus altering their drug loading capability. Carbohydrates are among the most versatile materials to functionalize MOFs since they present the advantages of: (i) lack of toxicity; (ii) they could mediate the cell

internalization; and (iii) they are easily further modified with other functional moieties. Recently, carbohydrate-based materials such as CDs [29], hep [30], hyaluronic acid (HA) [31], and chitosan [32, 33], which have larger molecular size than the diameter of the MOF pores, have been studied as coating materials. Interestingly, carbohydrate materials (such as CDs) can be easily functionalized with ligands (targeting, fluorescent imaging, etc.), which paves the way for a versatile surface modification of MOFs for multifunctional targeted drug delivery. The MOFs currently used for these investigations are iron polycarboxylate MOFs, which have emerged as a new class of versatile, biodegradable, and nontoxic drug carriers. Because of their high pore volumes and surface areas, MOFs were shown to load unprecedented amounts (within the 20–70 wt% range) of a series of drugs able to efficiently penetrate within the porous 3D structures [1, 2].

Both carbohydrate-based MOFs (CD-MOFs) and the surface modification of preformed MOFs (iron polycarboxylate MOFs) with carbohydrate materials will be described in this chapter. Control of particle size is a key parameter for drug delivery because this dictates the physicochemical properties of particles to obtain well-defined, reproducible, and stable formulations. Different strategies to synthesize CD-MOFs with controlled dimensions as well as their capability to incorporate drugs will be summarized. Recently, significant progress has been made in engineering CD-MOFs for drug delivery. Indeed, these particles were initially used for other potential applications in separation, sensing, gas storage, catalysis, and template synthesis [18]. CD-MOFs with controlled sizes have shown excellent capacity to incorporate a series of drugs [17, 18]. The use of CD-MOFs as drug carriers will be discussed, including the different strategies employed for drug incorporation, particle characterization, and the efforts to stabilize the drug-loaded particles. The second part of the chapter will address the use of carbohydrates for the surface-functionalization of iron polycarboxylate MOFs. A series of issues involved in this procedure will be discussed, including: (i) different methods to coat the MOF; (ii) various techniques to characterize the MOFs before and after surface modification; and (iii) biological evaluation of the coated MOFs.

## **20.2 MOFs synthesized from edible building blocks of CDs**

The first reported CD-MOF [34] is composed of  $\gamma$ -CD and  $K^+$ , which has regular cubic morphology and controllable size distribution. The spontaneous coordination of metal ions and  $\gamma$ -CDs generates cubic  $(\gamma\text{-CD})_6$  units which further assemble, by regular repetition, into a body-centered packed architecture with interconnected pores (Fig. 20.1A, *yellow*) with a diameter of 17 Å delimited by a window of 7.8 Å (diameter of  $\gamma$ -CDs). In addition to  $\gamma$ -CD,  $\alpha$ -CD and  $\beta$ -CD were shown to be able to form CD-MOFs with diverse structures as shown in Fig. 20.1 [35, 41–43].



**Fig. 20.1**

Overview of CD-MOF synthesis methods. (A) Vapor diffusion methods were widely used for synthesis of different CD-MOFs. Examples were given for  $\alpha$ CD-MOF(K) [35] and  $\gamma$ CD-MOF(K) [36, 37]. (B) Hydrosolvothermal method [38] employed for  $\beta$ CD-MOF(Cs) synthesis using  $H_3tzdc$ ,  $TsOH$ , or  $IBU$  as templates.  $H_3tzdc$ , 1,2,3-triazole-4,5-dicarboxylic acid;  $TsOH$ , methyl benzene sulfonic acid;  $IBU$ , ibuprofen. (C) Microwave-assisted method [39, 40] applied to optimize the synthesis of  $\gamma$ CD-MOF(K) within 10 min. Modified with permission from X. Li, et al., Cyclodextrin-based metal-organic frameworks particles as efficient carriers for lansoprazole: study of morphology and chemical composition of individual particles, *Int. J. Pharm.* 531(2) (2017) 424–432; A. Yang, et al., Green synthesis of  $\beta$ -cyclodextrin metal-organic frameworks and the adsorption of quercetin and emodin, *Polyhedron* 159 (2018) 116–126, copyright 2017 and 2018, Elsevier; J. Liu, et al., Controllable porosity conversion of metal-organic drug delivery, *Chem. Commun.* 53 (2017) 7804–7807, copyright 2017, Royal society of Chemistry; B. Liu, et al., Microwave-assisted rapid synthesis of gamma-cyclodextrin metal-organic frameworks for size control and efficient drug loading, *Cryst. Growth Des.* 17 (4) (2017) 1654–1660, copyright 2017, American Chemical Society.

### 20.2.1 Synthesis methods for CD-MOFs

Abundant efforts have been made to synthesize CD-MOFs with homogeneous size distribution during the last few years. The main synthetic strategies used to develop CD-MOFs are summarized in Fig. 20.1.

*Vapor diffusion method.* The vapor diffusion method is the earliest synthetic pathway to produce CD-MOFs [34]. Essentially,  $\gamma$ CD-MOF were prepared by reacting  $\gamma$ -CD with potassium hydroxide (KOH) in aqueous solution, followed by vapor diffusion of methanol into the solution during 2–7 days (Fig. 20.1A). A variety of CD-MOFs were first prepared combining  $\gamma$ -CD and  $K^+$ ,  $Rb^+$ ,  $Cs^+$ ,  $Na^+$ ,  $Sr^+$  by Stoddart's group [34, 44]. This methodology requires only ambient temperature and pressure; however, the obtained crystals had diameter in the range of 200–400  $\mu$ m. Furukawa et al. [45] modified this method by adding cetyltrimethyl ammonium bromide (CTAB) to control the growth of  $\gamma$ CD-MOF crystals. When CTAB was added to the crystallization medium, it covered the surface of  $\gamma$ CD-MOF crystals, and thus, slowed down the growth rate and reduced the final crystal size [45]. Homogeneous and monodisperse  $\gamma$ CD-MOFs were generated in the diameter range of 1–10  $\mu$ m. More interestingly, Furukawa et al. successfully achieved the nanoscaled  $\gamma$ CD-MOFs (200–300 nm) by the addition of both methanol and CTAB in the crystallization medium. However, it still took several days for the synthesis. Liu et al. [46] developed an effective solvent evaporation approach to synthesize this type of  $\gamma$ CD-MOFs by setting reaction temperature at 50°C. Remarkably, the reaction time was significantly reduced to 6 h. The size of the resulting CD-MOFs was well-controlled by addition of CTAB or/and methanol (in the range of 1–10  $\mu$ m with CTAB and around 600 nm with CTAB and methanol) [36, 37]. Recently, a “green” seed-mediated method was designed to rapidly produce  $\gamma$ CD-MOFs [47]. Instead of the surfactant CTAB which is potentially toxic and difficult to remove, short-chain starch NPs were employed as the seed to control the nucleation and growth of  $\gamma$ CD-MOFs. The results demonstrated that the crystal structure and cubic morphology were preserved, while the size of the particles was monodisperse with mean diameter around 2  $\mu$ m when the seed was added. However, this method could not be scaled-down CD-MOFs to the nano-regime.

In addition to  $\gamma$ -CD,  $\alpha$ -CD and  $\beta$ -CD were shown to be able to form CD-MOFs [35, 41–43]. As shown in Fig. 20.1A, Sha et al. obtained the  $\alpha$ CD-MOF by vapor diffusion method in one month using  $\alpha$ -CD and KOH, where tetramethylammonium hydroxide solution was employed as a new additive [35]. The resulting  $\alpha$ CD-MOF consists of the secondary units of  $[K_6(CD)_2]$  dimer torus, which are further linked with adjacent six  $[K_6(CD)_2]$  dimer forming 2D layer with both large pores with a diameter of 11.5 Å and small pores with a diameter of 7.3 Å. Similarly,  $\alpha$ CD-MOF could be synthesized with NaOH as metal source. Modified vapor diffusion methods were adopted to synthesize  $\beta$ CD-MOF by dissolving  $\beta$ -CD and NaOH in ethanol/water in a sealed vessel. After two weeks reaction,  $\beta$ CD-MOFs were formed, with each  $K^+$  ion coordinating with six oxygen atoms from the surrounding four  $\beta$ -CDs. Two adjacent  $\beta$ -CDs were connected by a  $K^+$  to form the pores. Due to the structural

features of  $\alpha$ CD-MOF and  $\beta$ CD-MOF which don't have regular cubic 3D structures as  $\gamma$ CD-MOFs, observed morphologies of  $\alpha$ CD-MOF and  $\beta$ CD-MOF exhibited relatively nonregular shapes compared to the cubic  $\gamma$ CD-MOFs (Fig. 20.1A). It was found that the size of the particles was difficult to be controlled and inhomogeneous morphologies contrary to the regular cubic  $\gamma$ CD-MOFs were observed.

*Hydrosolvothermal method.* Hydrosolvothermal method has been widely employed in MOFs synthesis [48]. Typically, the reaction took place under high-pressure and high-temperature conditions. Synthetic process was influenced by several parameters, such as the reaction time, temperature, stoichiometry, dilution pH, and additives. A  $\beta$ CD-MOF was successfully prepared from  $\beta$ -CD and sodium oxalate ( $\text{Na}_2\text{C}_2\text{O}_4$ ) using a mixture of methanol and water and heating it at  $160^\circ\text{C}$  for 3 days [38]. Liu et al. designed a novel template-induced strategy to produce different  $\beta$ CD-MOFs (Cs) using 1,2,3-triazole-4,5-dicarboxylic acid ( $\text{H}_3\text{tzdc}$ ), methyl benzene sulfonic acid (TsOH), or ibuprofen (IBU) molecules as templating agents [40]. As shown in Fig. 20.1B, different structures of  $\beta$ CD-MOFs were obtained when employing different templates. Sha et al. obtained a novel type of  $\alpha$ CD-MOF by a solvothermal method at  $160^\circ\text{C}$  with a reaction time of 4 days starting with a mixture of  $\alpha$ -CD and KOH. Moreover, metal-organic nanotubes built from  $\beta$  or  $\gamma$ CD and  $\text{Pb}^{2+}$  were also synthesized through a solvothermal reaction [49].

*Microwave-assisted hydro/solvothermal methods.* As a classical synthetic protocol, the microwave-assisted method has also been employed in the synthesis of MOFs. This synthetic method offers the advantages of simple, rapid, inexpensive, environment-friendly, and efficient nonconventional heating with high yields. Liu et al. obtained  $\gamma$ CD-MOFs using the microwave-assisted method within 10 min as shown in Fig. 20.1C [39]. Both size and morphology of  $\gamma$ CD-MOF were systematically investigated by altering the reaction time, temperature, and solvent ratio, in order to obtain micro- and nanometer-sized crystals. Polyethylene glycol with a molecular weight of 20,000 g/mole (PEG 20,000) was used for the first time to control the size and morphology of  $\gamma$ CD-MOFs. Monodispersed  $\gamma$ CD-MOF were obtained with different sizes (200 nm to 300  $\mu\text{m}$ ) and were further used for drug encapsulation.

The three general methods described above have been the most employed strategies for CD-MOF synthesis. The best method to both obtain a rapid reaction and control the particle size was the microwave-assisted hydro/solvothermal synthesis. The mean diameter of synthesized CD-MOF was in the range of 200 nm to centimeter scale. There are still some other synthetic routes (e.g., ultrasonic, mechano-chemical, electrochemical) employed for MOF synthesis possibly worthy to try for CD-MOF aiming to further reduce the particle size. Regardless of the method used to synthesize CD-MOFs, the choice of the additives (CTAB, menthol, PEG, etc.) is obviously crucial for both size control and their biomedical applications. Up to date, PEG could be considered among the best additive, considering its low toxicity and great capabilities to control the mean diameter of the synthesized CD-MOF.



### 20.2.2 Drug entrapment

A variety of active molecules, including anticancer drugs (doxorubicin (DOX), fluorouracil (5-FU), methotrexate, quercetin), antiinflammatory drugs (IBU, furbiprofen, fenbufen, ketoprofen, and piroxicam), antihypertensive drug (azilsartan), angiotensin-converting enzyme inhibitors (captopril), various pharmaceutical ingredients (salicylic acid, ferulic acid, folic acid, and pseudolaric acid B), and food additives (curcumin and sucralose) have been successfully incorporated in CD-MOFs using three main strategies, which are the impregnation method, the co-crystallization method, and the grinding method.

*Impregnation method.* This is a conventional method which generally involves three steps: (1) synthesis of CD-MOFs, (2) activating MOFs by removing solvents/ligands from the pores, and (3) incorporation of drugs within CD-MOFs in suitable solvents. It is noteworthy that the nature of solvents, pH of CD-MOF (alkaline or neutral), and the encapsulation materials play an important role on the drug loading properties. For example, when relatively nonpolar solvents were used, the uptake of IBU into CD-MOFs was low (<5 wt%). In contrast, the encapsulation of IBU in ethanol increased dramatically to 26 wt%, which was close to the theoretical value calculated by Monte Carlo simulations [50]. The hypothesis is that the IBU encapsulation is related to an anion exchange process, which means that the hydroxyl group present in CD-MOFs was able to take away the protons from IBU. This process could take place easily in ethanol rather than in nonpolar solvents. Considering the pH of CD-MOFs, it was reported that the neutralized CD-MOFs were more effective than alkaline CD-MOFs to protect sucralose, possibly due to the fast hydrolysis of sucralose in alkaline condition [51]. As shown in Table 20.1, a large variety of active molecules have been successfully loaded into CD-MOFs by this method.

*Co-crystallization method.* In addition to impregnation, co-crystallization emerged as a promising strategy for drug encapsulation. To do so, the drugs were added in the crystallization medium before the formation of CD-MOFs. In the case of lansoprazole (LPZ), co-crystallization significantly improved the drug loading capacity in  $\gamma$ CD-MOF (K), as compared to impregnation (9.4 wt% for impregnation and 23 wt% for co-crystallization) [37]. Indeed, in the impregnation process, drug molecules have to cross their way through the preformed tight CD-MOF channels. In contrast, in the co-crystallization process,  $\gamma$ -CD:drug complexes are directly formed and assembled into drug-loaded CD-MOF particles, still preserving their crystallinity. In a nutshell, co-crystallization was shown to offer more probability for the drugs to interact with the CDs in the crystalline matrix.

The LPZ-loaded  $\gamma$ CD-MOF particles were characterized in terms of morphology, sizes, and crystallinity, showing almost perfect cubic structures with monodispersed size distributions (Fig. 20.2). Moreover, Raman spectra of randomly chosen particles were recorded, indicating that each individual cube had practically the same chemical composition, i.e., drug content [37]. Thus, it was shown that the LPZ-loaded particles



Table 20.1 Overview of drug encapsulation in CD-MOFs.

| Loading methods    | CD-MOFs         |                      | Drug                     | Drug payload<br>(%, w/w) | Refs.        |    |          |
|--------------------|-----------------|----------------------|--------------------------|--------------------------|--------------|----|----------|
|                    | CDs             | Metal                |                          |                          |              |    |          |
| Impregnation       | $\gamma$ -CD    | $K^+$                | Azilsartan               | 23                       | [52]         |    |          |
|                    |                 | $K^+$                | Budesonide               | 25                       | [53]         |    |          |
|                    |                 | $K^+$                | Captopril                | 19                       | [46]         |    |          |
|                    |                 | $K^+$                | Coenzyme Q10             | 31                       | [54]         |    |          |
|                    |                 | $K^+$                | Curcumin                 | n.i. <sup>a</sup>        | [55]         |    |          |
|                    |                 | $K^+$                | Doxorubicin              | 6~8                      | [56]         |    |          |
|                    |                 | $K^+$                | Doxorubicin              | 6~8                      | [57]         |    |          |
|                    |                 | $K^+$                | Doxorubicin              | 7                        | [58]         |    |          |
|                    |                 | $K^+$                | Epigallocatechin gallate | 21                       | [59]         |    |          |
|                    |                 | $K^+$                | Fenbufen                 | 20                       | [46]         |    |          |
|                    |                 | $K^+$                | Fenbufen                 | 20                       | [39]         |    |          |
|                    |                 | $K^+$                | Fenbufen                 | 6                        | [60]         |    |          |
|                    |                 | $K^+$                | Flurbiprofen             | 12                       | [46]         |    |          |
|                    |                 | $K^+$                | Folic acid               | 60                       | [61]         |    |          |
|                    |                 | $K^+$                | Ibuprofen                | 26                       | [50]         |    |          |
|                    |                 | $K^+$                | Ibuprofen                | 13                       | [36, 37]     |    |          |
|                    |                 | $K^+$                | Ketoprofen               | 4                        | [60]         |    |          |
|                    |                 | $K^+$                | Lansoprazole             | 9/2                      | [36, 37]     |    |          |
|                    |                 | $K^+$                | Leflunomide              | 14                       | [62]         |    |          |
|                    |                 | $K^+$                | Sodium diclofenac        | 50                       | [63]         |    |          |
|                    |                 | $Na^+$               | Sodium diclofenac        | 49                       | [63]         |    |          |
|                    |                 | $Fe^{3+}$            | Sodium diclofenac        | 55                       | [63]         |    |          |
|                    |                 | $K^+$                | Sucralose                | 28                       | [51]         |    |          |
|                    |                 | $K^+$                | Vitamin A palmitate      | 10                       | [64]         |    |          |
|                    |                 |                      | $\alpha$ -CD             | $Na^+$                   | Ferulic acid | 11 | [35, 42] |
|                    |                 |                      |                          | $Na^+$                   | 5-FU         | 9  | [35, 42] |
| $K^+$              | 5-FU            |                      |                          | 26                       | [35, 42]     |    |          |
| $Na^+$             | Methotrexate    |                      |                          | 38                       | [35, 42]     |    |          |
| $Na^+$             | Quercetin       |                      |                          | 32                       | [35, 42]     |    |          |
| $Na^+$             | Silybummarianum |                      |                          | 13                       | [35, 42]     |    |          |
|                    | $\beta$ -CD     | $Cs^+$ ( $H_3tzdc$ ) | 5-FU/methotrexate        | 138/69                   | [39, 40]     |    |          |
|                    |                 | $Cs^+$ ( $TsOH$ )    | FU/methotrexate          | 151/122                  | [39, 40]     |    |          |
| Grinding           | $\beta$ -CD     | $K^+$                | Quercetin/emodin         | 15/20                    | [43]         |    |          |
|                    |                 | $K^+$                | Azithromycin             | 34                       | [65]         |    |          |
|                    |                 | $Na^+$               | 5-FU                     | 23                       | [38]         |    |          |
|                    |                 | $Na^+$               | 5-FU/quercetin           | n.i. <sup>a</sup>        | [41]         |    |          |
| Co-crystallization | $\gamma$ -CD    | $K^+$                | 5-FU/quercetin           | n.i. <sup>a</sup>        | [41]         |    |          |
|                    |                 | $K^+$                | Ferulic acid             | 13                       | [66]         |    |          |
|                    |                 | $K^+$                | Ibuprofen                | 23                       | [50]         |    |          |
|                    |                 | $K^+$                | Ibuprofen                | 13                       | [36, 37]     |    |          |
|                    |                 |                      | Lansoprazole             | 23                       | [36, 37]     |    |          |

<sup>a</sup>n.i., not indicated.

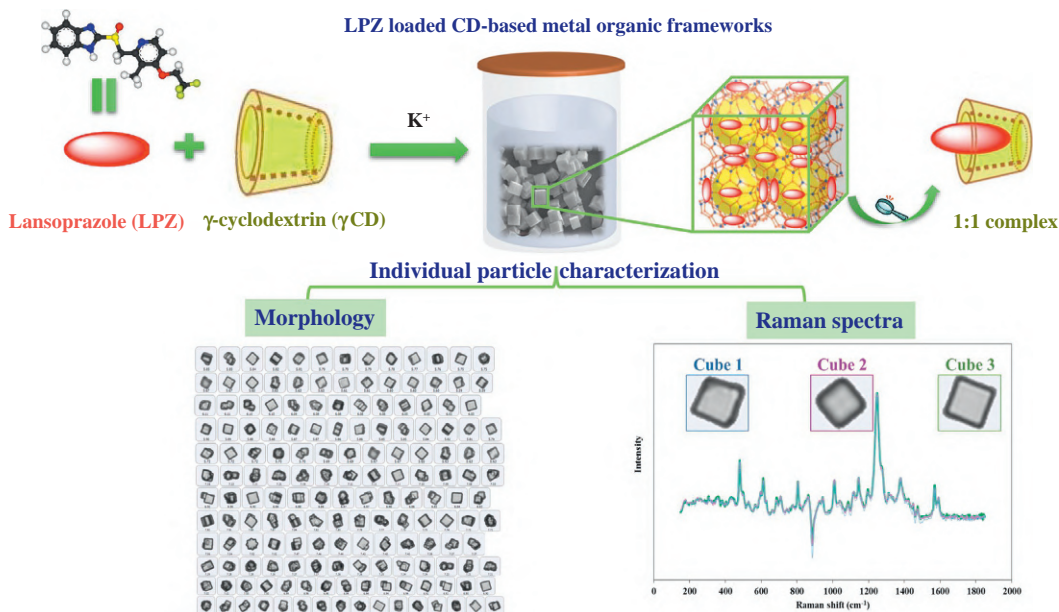


Fig. 20.2

Drug loading and characterization. LPZ was successfully loaded in CD-MOF by co-crystallization method, achieving high drug loadings up to 23 wt%, corresponding to LPZ:CD molar ratio of 1:1. The obtained LP-loaded particles were monodisperse with cubic morphologies and homogenous chemical compositions, as indicated by Raman spectra of randomly chosen individual particles. *Reproduced with permission from H. Li, et al., Composite CD-MOF nanocrystals-containing microspheres for sustained drug delivery, Nanoscale, 9 (2017a) 7454–7463; X. Li, et al., Cyclodextrin-based metal-organic frameworks particles as efficient carriers for lansoprazole: Study of morphology and chemical composition of individual particles, Int. J. Pharm., 531(2) (2017b) 424–432. Copyright 2017, Elsevier.*

had a remarkable homogeneity in terms of both drug loading and size. Advantageously, the one-pot co-crystallization simplifies the drug loading process together with avoiding the use of potentially toxic organic solvents sometimes needed for impregnation.

However, the co-crystallization method is highly dependent on the structure of the drug molecules and sensitive to the pH value of the crystallization medium. For instance, the inclusion of ferulic acid (FA) in  $\gamma$ CD-MOF (K) was found to be strongly pH-dependent in a range of 6.8 to 13.1 [66]. The reaction yield dramatically decreased from 59.3% to 19.0% at low pH. Interestingly, the molar ratio of FA to  $\gamma$ -CD in FA/CD-MOF increased from 0.15 (pH 13.1) to 1.06 (pH 6.8), indicating that the drug loading capacity was improved at low pH. It is worth noting that when FA: $\gamma$ -CD inclusions were prepared in a first step, followed by addition of KOH, FA was not encapsulated in CD-MOF, suggesting that FA: $\gamma$ -CD complex was destabilized by KOH and that the free FA could not be adsorbed on the resulting CD-MOF in aqueous solution.

Another study reported the successful IBU loading in nanoscale  $\gamma$ CD-MOF (K) by co-crystallization, showing similar drug payloads with impregnation methods (13.0 wt% for

impregnation and 12.7 wt% for co-crystallization) [36]. The drug payload achieved by this method is dependent on the drug molecules. Further investigation is still needed to comprehensively understand the mechanism of this drug-dependent phenomena. Possibly, the affinity between the drug and the cavity of  $\gamma$ -CD and/or CD-MOF, the drug:  $\gamma$ -CD ratio, and pH play important roles on the drug payloads.

The reported studies show that drug loadings obtained by co-crystallization and impregnation are highly dependent on drug structure and experimental conditions. Few data are available in the literature so far making it difficult to draw a general trend.

*Grinding method.* Mechanical grinding is one of the methods typically applied to prepare guest molecules/CD inclusion complexes. Recently, it has also been used to encapsulate the guest molecules into CD-MOFs [38,65]. Drug-loaded CD-MOFs could be prepared by simply grinding the guests with preformed CD-MOFs. Several parameters were shown to impact drug inclusion during grinding, such as the molar ratio between the guest drug and CD in CD-MOF, the grinding time, and the temperature [41]. For the first time, the 5-FU and quercetin drug combination could be successfully co-encapsulated in CD-MOFs using the grinding method. In brief, 5-FU, quercetin, and  $\beta$ CD-MOFs were milled at a molar ratio of 1:1:1 using ethanol as wetter at room temperature. The drug-loaded CD-MOF were obtained after grinding for 1 h. This study demonstrated that two drugs with different molecular structures and dimensions could be simultaneously incorporated into CD-MOFs; however, the drug payloads were not indicated. As reported by Lu et al. [38], when 5-FU was loaded individually, the obtained payload reached 23 wt%. The highest drug payload achieved by grinding method is 34 wt% in the case of azithromycin [65].

*Benefits of drug incorporation in CD-MOFs.* Once incorporated in CD-MOF via different strategies, the active molecules were shown to gain beneficial properties, including improved stability, enhanced water solubility, and bioavailability. For example, in reason of the protective effect of the CD-MOF matrix, the stability of incorporated vitamin A palmitate (VAP) was significantly improved [64]. It was hypothesized that the VAP molecules were curled inside the chambers formed by dual  $\gamma$ -CDs pairs in  $\gamma$ CD-MOF(K). This in turn led to an enhanced stability upon storage, comparable or even better than other products in the market, with around 1.6-fold elongated half-life. Similarly, the stability of encapsulated curcumin was enhanced by at least 3 orders of magnitude as compared to free curcumin or to curcumin: $\gamma$ -CD complexes [55]. In this latter case, the enhanced drug stability was attributed to the strong interaction between curcumin and CD-MOFs through hydrogen bond interaction between the OH group of CDs and the phenolic hydroxyl group of the curcumin.

Taking advantage of the unique structure of CDs, “cage” molecules with proven abilities to increase the apparent water solubility of many drugs, CD-MOFs were engineered to release supersaturated drug solutions upon their disassembly [52]. It was shown recently that the solubility of azilsartan could be improved by 340-fold as compared to free drug. This dramatic increase was attributed to drug nanoclusters formation in the confined nano-cages of CD-MOFs

followed by their release upon matrix dissolution in water [52]. Moreover, this strategy allowed to improve the bioavailability of azilsartan in Sprague-Dawley rats by 9.7-fold after loading into CD-MOF, as compared to free drug. These investigations indicate that CD-MOFs are efficient drug delivery carriers enabling to enhance drug bioavailability.

*Surface coating.* CD-MOFs demonstrated high drug loading capabilities together with several other advantages for drug delivery as compared with more traditional drug carriers based on other materials. However, due to their physical frailness and degradability in aqueous media, which may lead to their disassembly before reaching the target tissues or organs, CD-MOFs were considered inappropriate for some routes of administration, such as the intravenous one. In this context, considerable efforts have been made to improve the stability of CD-MOFs in aqueous media. Firstly, ethylene glycol diglycidyl ether was employed to cross-link the hydroxyl groups in adjacent CDs in the CD-MOF supramolecular assemblies, thus generating cubic gel particles stable towards dissolution in aqueous media [45]. However, the resulting particles were not biodegradable in biological media, which is another important requirement for biomedical applications. To address the challenges related to CD-MOF instability in aqueous solutions, another approach was carried on by Li et al. [36]. CD-MOF nanocrystals were incorporated into a biocompatible polymer (polyacrylic acid, PAA) matrix by a solid in oil-in-oil (s/o/o) emulsification-solvent evaporation method. The resulting composite microspheres showed enhanced stabilities in water and sustained drug release. However, this approach led to large particles, beyond the micrometer size.

In order to maintain the size of the CD-MOFs in the nanometric range, efforts have been made to coat directly CD-MOF nanoparticles. For example,  $\gamma$ CD-MOFs with improved water stability were successfully achieved by incorporating hydrophobic  $C_{60}$  in their matrices through host-guest interactions between  $\gamma$ CD and  $C_{60}$  [58]. Interestingly, neither the structural integrity nor the BET (Brunauer-Emmett-Teller) surface area was affected after surface modification. DOX was successfully incorporated reaching a payload of 6.5 wt%. Moreover, DOX was released in a sustained manner after CD-MOF incubation in phosphate buffer saline. When tetrakis(4-hydroxyphenyl) porphyrin (TCPP)-conjugated  $C_{60}$  was used instead of  $C_{60}$ , the resulting CD-MOFs were shown to have fluorescent properties, enabling their detection *in vitro* and *in vivo* [67]. More recently, CD-MOFs were surface-modified with cholesterol [56], thus exhibiting good stabilities in aqueous media. It was thus possible to administer the resulting cholesterol-shielded and DOX-loaded nanoparticles by intravenous route, and results showed a significantly increased blood half-life of DOX up to 0.5 h, which was four times higher than the one of free DOX. Moreover, the nanoparticles were well-tolerated also *in vivo*. However, this strategy involved the covalent grafting of cholesterol to the CDs at the CD-MOF surface. This might potentially lead to the release of modified CDs and the degradation process of the coated CD-MOFs still needs to be unraveled.

*Further prospective of CD-MOFs.* In a nutshell, CD-MOFs advantageously combined CD's proven biocompatibility for medical applications and CD's capacity to assemble in regular

porous structures which were further shown to be beneficial for drug incorporation. Among the three strategies for drug incorporation, co-crystallization method seems to be the most promising one, due to its simplicity and ability to enhance drug loadings. However, the most common method to load drugs remains the impregnation technique. All drug loading methods were shown to be strongly dependent upon drug physicochemical characteristics and abilities to form inclusion complexes with CDs.

When incorporated inside CD-MOF, the drugs were efficiently stabilized against degradations. Moreover, in the case of poorly soluble drugs, drug solubility in water was significantly increased due to the formation of drug:CD complexes, once the drug-loaded CD-MOFs disassemble in water. The poor stability in aqueous media remains the main drawback of CD-MOFs, which hampers their biomedical applications, especially for intravenous administration. Although versatile strategies have been deployed to improve their stability, they are limited by complex procedures and/or necessity to covalently graft the coating material.

In terms of stability, other MOFs made using different metal and linkers were shown to be more stable in aqueous environment. For instance, iron polycarboxylate MOFs are intrinsically stable, which widens their biomedical application as compared to CD-MOFs. The following section will be focused on the surface modification of iron polycarboxylates MOFs with carbohydrate-based materials.

### ***20.3 Carbohydrates as functional surface coatings for MOFs***

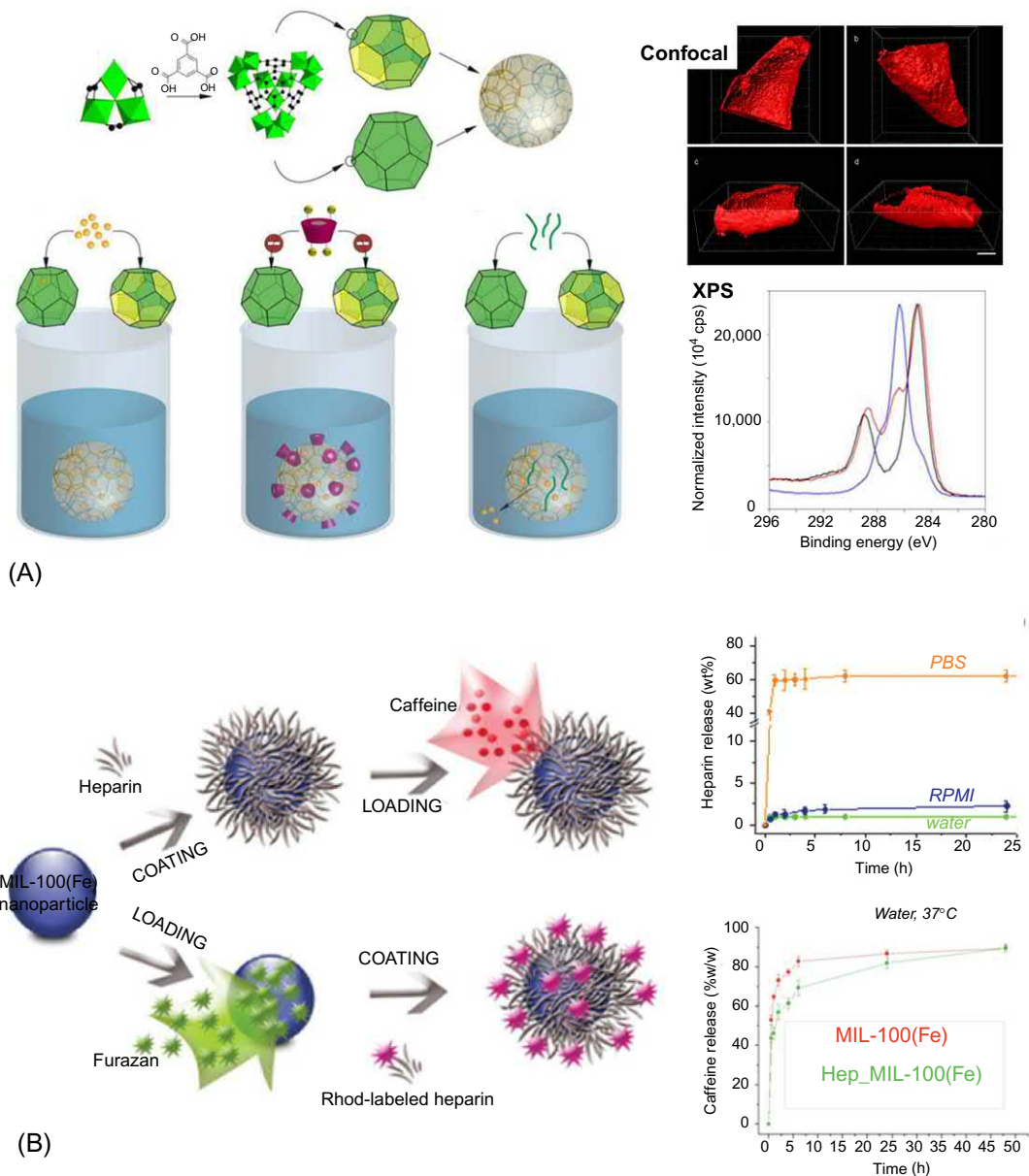
MOFs made of iron carboxylates, and especially iron (III) trimesate MIL-100(Fe), have emerged as an important class of porous, biodegradable, and multifunctional nanomaterials of main interest for biomedical applications (MIL, stands for Materials from Institut Lavoisier). Indeed, their high surface area allowed loading high amounts of a large variety of drugs able to penetrate within the porous MOF structures [2]. The porous MIL-100(Fe) solids are built up from Fe(III) octahedra trimers and trimesate linkers (1,3,5-benzene tricarboxylate) which self-assemble forming a porous architecture delimiting large (29 Å) and small (24 Å) mesoporous cages. In MIL-100(Fe) nanoMOFs, two types of cages are accessible for drug adsorption inside the open 3D-porosity. To access these cages, drugs penetrate through pentagonal (5.6 Å) and/or hexagonal windows (8.6 Å). Advantageously, due to the presence of Fe and free water molecules in their structure, the nanoMOFs acted as efficient T<sub>2</sub>-weighted contrast agents for Magnetic Resonance Imaging (MRI), of interest for theranostics applications [68]. These nanoMOFs, loaded or not with drugs, were well-tolerated in vivo [69–71].

Like other types of nanoparticles, nanoMOFs need to be further functionalized with engineered coatings to control their in vivo fate. Surface modification is commonly used to

control drug release, reduce plasma protein binding, prolong blood circulation, and attach functional moieties for imaging and targeting. However, the surface modification of nanoMOFs is challenging because many coating materials such as PEG chains could penetrate inside the pores, which disturb drug loading. As stated in the introduction, carbohydrate-based materials are among the most versatile ones for surface modification. The first noncovalent nanoMOF coating study was reported by the group of Dr. Gref [29], where phosphorylated CD (CD-P) derivatives were used to modify iron trimesate nanoMOFs MIL-100(Fe) in aqueous media, employing a fast, one-step, and completely “green” (organic solvent-free) procedure (Fig. 20.3A). Briefly, the nanoMOFs were surface-modified by impregnation with CD-P aqueous solution at room temperature. The success of this strategy lies on the fact that the phosphate groups conjugated on the CD-P could efficiently coordinate with the available iron trimer sites on the surface of nanoMOFs. They played a cooperative role to ensure the stability of the coatings. Besides, CD-P were too bulky to cross the microporous windows of the nanoMOFs, leaving CD-P located only on the external MOF surface. The resulting coated nanoMOFs have been comprehensively characterized by a set of complementary techniques, including transmission electron microscopy (TEM), X-ray powder diffraction (XPRD), dynamic light scattering (DLS), solid state NMR, and X-ray photoelectron spectroscopy (XPS), among others.

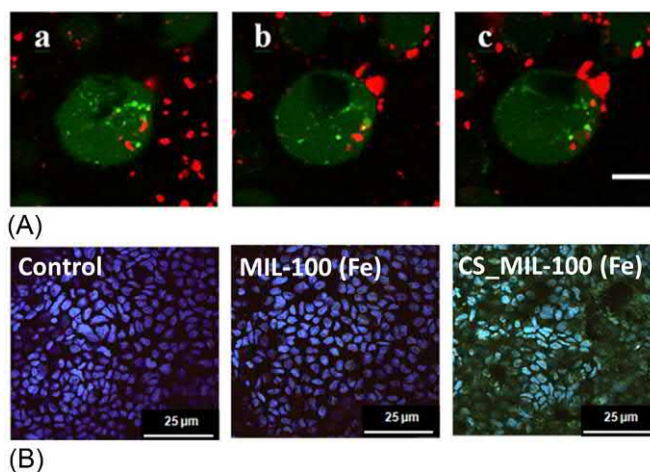
As shown in Fig. 20.3A, the presence of CD-P within the nanoMOF top layers was visualized by confocal microscopy in the particular case of larger MOF particles ( $>10\ \mu\text{m}$ ) which were modified with Rhodamine (Rh)-labeled CD-P. XPS confirmed that CD-P was located on the nanoMOF top layers (5–10 nm depth) by showing both carbon C1s “fingerprints” of the carbon skeleton of MIL-100(Fe) (284.8 and 289 eV, C-C or C-OOH, respectively) and CD-P “fingerprint” (main contribution at 286.3 eV) in the CD-P-coated nanoMOFs. The phosphate-iron coordination was evidenced as the principal binding mechanism by Isothermal titration calorimetry (ITC), showing the absence of interaction between nonphosphated CD and nanoMOFs. On the contrary, the binding isotherm for the CD-P/nanoMOFs interaction displayed a strong interplay. Elemental analysis and spectrofluorimetry were used to quantify the amount of CD-P attached on the surface of nanoMOFs, exhibiting maximal adsorbed values around 20 wt%. The stability of the coating under physiological simulated conditions was also investigated, showing that less than 10% of the total CD-P coating was detached after 24 h incubation, whatever the incubation media (phosphate buffer saline or cell culture media). Moreover, it was illustrated that the CD coating did not impact the supramolecular architecture nor the porosity of the nanoMOFs, as confirmed by constant BET surface area before and after coating. The nanoMOF morphology, crystallinity, drug loading, and release properties were not affected after the coating procedure. Remarkably, CD-P-coated nanoMOFs were devoid of toxicity *in vitro* in different cell lines, as the uncoated ones. Finally, confocal microscopy investigations (Fig. 20.4A) showed that nanoMOFs readily internalized in J774 macrophages, maintaining their CD-based coating.





**Fig. 20.3**

Overview of surface modification strategies and characterization of nanoMOFs coated with carbohydrates. (A) CD-P was used to functionalize iron trimesate nanoMOF [29]. The methodology of characterization was set up using a series of complementary techniques including: (i) confocal images of the Rh-labeled CD-P located only on the surface of nanoMOFs; (ii) XPS showing C1s binding energy spectra for nanoMOFs (black), CD-P (blue) and CD-P-modified nanoMOFs (red). (B) When nanoMOFs were modified with hep [30], the hep release was investigated in different media and it allowed to sustain the release of the incorporated caffeine. *Reproduced with permission from V. Agostoni, et al., A “green” strategy to construct non-covalent, stable and bioactive coatings on porous MOF nanoparticles, Sci. Rep. 5 (2015) 7925–7931; E. Bellido, et al., Heparin-engineered mesoporous iron metal-organic framework nanoparticles: toward stealth drug nanocarriers, Adv. Healthc. Mater. 4(8) (2015) 1246–1257. Copyright 2015, Nature; 2015, Wiley Online Library.*



**Fig. 20.4**

Surface modification plays an important role on cell internalization. (A) Interaction between J774 macrophages and CD-P-coated MOFs studied by confocal microscopy. Cells were stained in *green* with calcein, whereas the *red* signal comes from Rh-labelled CD-P-coated nanoMOFs. Images represent three distinct optical sections inside cells at different heights above the glass slide:

(a) 2.3  $\mu\text{m}$ ; (b) 4.9  $\mu\text{m}$ , and (c) 7.6  $\mu\text{m}$ . Cell nucleus appears in *black*. Bar represents 5  $\mu\text{m}$ .

(B) Coating with chitosan leads to an increased intestinal permeability with respect to the noncoated material [32]. Confocal microscopy images of Caco-2 cells containing uncoated and chitosan-coated MIL-100(Fe) NPs observed by iron self-reflection signal (*green channel*) and the nucleus stained by DAPI (*blue channel*). The images were taken after 2.5 h incubation. (A) Reproduced with permission from V. Agostoni, et al., A “green” strategy to construct non-covalent, stable and bioactive coatings on porous MOF nanoparticles, *Sci. Rep.* 5 (2015) 7925–7931. Copyright 2015, Nature; (B) T. Hidalgo, et al., Chitosan-coated mesoporous MIL-100 (Fe) nanoparticles as improved bio-compatible oral nanocarriers, *Sci. Rep.* 100 (2017) 1–14. Copyright 2017, Nature.

Further studies were performed taking advantage of the versatility of CD coatings in terms of chemical modification. First, mannose was grafted onto CD-P previously to coat the nanoMOFs [29]. The CD-P-mannose derivative could be adsorbed readily onto the nanoMOF surfaces, allowing a better recognition by human retinoblastoma Y79 cells hyperexpressing the mannose receptor. The amounts of CD-P-mannose-modified nanoMOFs able to penetrate inside the cells were twice higher than using the uncoated nanoMOFs.

Another study was based on the strong host-guest interaction between adamantyl (Ad) and  $\beta$ -CD. Ad-conjugated PEG chains (Ad-PEG) were used to further functionalize the surface of the CD-P-coated nanoMOFs. By this way, CD-P: Ad-PEG inclusion complexes were bound strongly to the nanoMOFs and were firmly anchored [29]. PEGylation has been since many years an effective strategy to reduce premature clearance of NPs from the circulation by hindering adhesion of proteins on nanoMOFs’ surface, avoiding their recognition and removal by macrophages. Another strategy for nanoMOF PEGylation was to employ GraftFast surface engineering using PEG or hyaluronic acid (HA) acrylates, which were polymerized [31]. In this study, HA-PEG was covalently linked by a single step GraftFast

reaction on the surface of nanoMOFs. A maximal polymer amount of  $32.9 \pm 0.3$  wt% was reached in the case of PEG<sub>5kDa</sub>-Rh. The resulting PEGyated nanoMOFs exhibited improved colloidal and chemical stabilities in different biological media as compared to uncoated nanoMOFs, while conserving their porosity which allowed the adsorption of bioactive molecules. Moreover, it was shown that the PEG coating could reduce macrophage uptake *in vitro*.

The study of CD-P surface modification was further extended by synthesizing a series of randomly phosphorylated  $\beta$ -CD monomers and polymers appended with mannose or Rh [72]. In all cases, the amount of CD-based materials attached to the nanoMOFs reached 20–26 wt%, which is similar to the CD-P one [29]. It was further demonstrated that the coating stability was directly related to the density of the grafted phosphate groups, further confirming that the interaction between the phosphate groups and the iron sites at the nanoMOFs' surface was crucial for the coating process. Recently, native  $\beta$ -CD was also used to functionalize the iron terephthalate nanoMOF (MOF-235) [73], taking advantage of the coordination interaction between the hydroxyl groups of  $\beta$ -CD and the unsaturated Fe(III) metal ions of MOF-235. The supramolecular assemblies further displayed properties as effective catalysts in H<sub>2</sub>O<sub>2</sub>-luminol chemiluminescence reaction due to the synergistic effect between  $\beta$ -CD and MOF-235. However, the stability of the CD coating was not evaluated.

In addition to CDs, hep was employed as an efficient coating material to decorate the surface of MIL-100(Fe) nanoMOFs by a similar impregnation method [30], whereas nanoMOFs were dispersed in ethanol instead of aqueous solution (Fig. 20.3B). The amount of hep attached to the nanoMOFs was  $12.5 \pm 1.8$  wt%. The stability of hep coating was also investigated in three different biological media (water, cell culture medium, and PBS). In water or cell culture medium, the release of a small quantity of hep (2 wt%) was observed after 24 h incubation. However, up to 50 wt% of hep was released in PBS within 1 h, which was much higher than the CD-P release from CD-P-coated MOFs in the same conditions [29], suggesting a lower stability of the hep coatings. Caffeine was selected as molecule of interest to investigate drug loading and release capacity. The payloads for the uncoated and hep-coated nanoMOFs were similar:  $43 \pm 2$  and  $42 \pm 6$  wt%, respectively. Interestingly, hep-coated nanoMOFs exhibited an ability to better control the drug release, as compared with uncoated nanoMOFs, especially during the first hours. As shown in Fig. 20.3B,  $46 \pm 3$  and  $56 \pm 4$  wt% were released from the uncoated nanoMOFs after 1 h in water and PBS, while only 20 wt% of caffeine was released during the same period for the coated nanoMOFs. The hypothesis was that the dispersive interaction of caffeine molecules with hep slowed down their diffusion outwards the nanoMOFs. Furthermore, *in vitro* investigations were performed with the murine macrophage cell line J774 in order to assess the potential stealth properties of fluorescent hep-coated nanoMOFs. It was reported that the hep coating significantly slowed down the internalization process, but this was the case only at early stages of incubation. It was hypothesized that this might be related to the removal of hep from the nanoMOFs' surfaces in the biological media.

Recently, chitosan was also employed to modify the same iron trimesate MIL-100(Fe) nanoMOFs [32] by similar methods. The amount of chitosan attached to the nanoMOFs reached  $49.1 \pm 0.3$  wt % and was estimated by fluorescence spectrometry after impregnation of the nanoMOFs with Rh-labeled chitosan. In addition to the conventional techniques, a combination of high-resolution X-ray Absorption Near-Edge Structure (XANES) and computing simulation techniques was employed to investigate the specific interactions between the chitosan coating and the nanoMOFs. It was thus demonstrated that both Fe<sup>II</sup> and Fe<sup>III</sup> sites were able to interact with the chitosan macromolecules. No significant toxic effects on human colorectal carcinoma cells (Caco-2) were detected before or after chitosan coating. Interestingly, chitosan-coated nanoMOFs exhibited a significantly higher cell uptake as compared with the uncoated NPs after only 2.5 h incubation (Fig. 20.4B). Moreover, chitosan-coated nanoMOFs reduced the immune response, which might be related to a lower recognition by the immune system. The chitosan-coated nanoMOFs appeared promising for oral administration to improve intestinal barrier bypass of entrapped drugs.

To summarize, a variety of carbohydrate-based biocompatible materials were used for nanoMOF surface modification, improving colloidal stability, controlling drug release, and mediating cell penetration. It paves the way for a versatile surface modification of nanoMOFs for targeted multifunctional drug delivery and other applications.

## 20.4 Conclusions and future outlook

The development of carbohydrate-based MOFs or carbohydrate-coated MOFs for drug delivery is still in its infancy when compared to other nanocarriers. Nonetheless, these supramolecular porous architectures emerged as a promising platform owing to the combined advantages of both carbohydrates (biodegradability, biocompatibility, hydrophilicity, and the ability to mediate cell penetration of the nanocarriers) and MOFs (structural and chemical diversity, biodegradability, and the capacity to adsorb a series of drugs which could penetrate inside their pores reaching high loadings). Beside CD, hep, chitosan, and HA described here, we foresee that many other carbohydrate-based materials will be employed for MOF synthesis and/or surface modification in the future. There is a plethora of drugs which could benefit from incorporation in (CD) MOFs. The presence in some cases of different types of pores in (CD) MOFs could be used to load different drugs in each type of pore. Moreover, it was possible to form drug clusters in the pores, dramatically increasing the loadings. Moreover, pores could be used as microreactors to synthesize metal nanoparticles, which is another important recent trend. It was also demonstrated that MOFs could release supersaturated drug solutions.

Moreover, together with the drugs, the incorporation of contrast agents for MRI has not been investigated so far in the case of CD-MOFs. Together with drug insertion in the matrices, this approach could be of interest for the development of theranostic platforms.

Although several in vitro efficacy studies have been carried on with both carbohydrates-based MOFs and carbohydrates-coated MOFs, up to date, there still are only very few in vivo investigations with these new systems. To deeper assess the clinical relevance of these formulations, systematic in vivo toxicological studies are required to bring the concept from lab-scale to patient bedside. With more efforts for their design and optimization, these versatile supramolecular assemblies are expected to have a bright future in drug delivery.

## Acknowledgments

Financial support for this work was provided by the French National Research Agency (ANR-14-CE08-0017, ANR-16-CE18-0018 and PCInano) and the Spanish Ministry of Economy and Competitiveness (Grants CTQ2017-90050-R).

## References

- [1] G. Férey, et al., A chromium terephthalate-based solid with unusually large pore volumes and surface area, *Science* 309 (5743) (2005) 2040–2042.
- [2] P. Horcajada, et al., Metal-organic frameworks as efficient materials for drug delivery, *Angew. Chem. Int. Ed.* 45 (36) (2006) 5974–5978.
- [3] M. Eddaoudi, et al., Modular chemistry: secondary building units as a basis for the design of highly porous and robust metal-organic carboxylate frameworks, *Acc. Chem. Res.* 34 (4) (2001) 319–330.
- [4] G. Férey, Hybrid porous solids: past, present, future, *Chem. Soc. Rev.* 37 (1) (2008) 191–214.
- [5] S. Kitagawa, R. Kitaura, S. Noro, Functional porous coordination polymers, *Angew. Chem. Int. Ed.* 43 (2004) 2334–2375.
- [6] O.M. Yaghi, et al., Reticular synthesis and the design of new materials, *Nature* 423 (6941) (2003) 705–714.
- [7] H. An, et al., Incorporation of biomolecules in metal-organic frameworks for advanced applications, *Coord. Chem. Rev.* 384 (2019) 90–106.
- [8] J. Zhuang, A.P. Young, C.K. Tsung, Integration of biomolecules with metal-organic frameworks, *Small* 13 (32) (2017) 1–14.
- [9] H.P.S. Abdul Khalil, et al., Biodegradable polymer films from seaweed polysaccharides: a review on cellulose as a reinforcement material, *Express Polym. Lett.* 11 (4) (2017) 244–265.
- [10] B. Kang, et al., Carbohydrate nanocarriers in biomedical applications: functionalization and construction, *Chem. Soc. Rev.* 44 (22) (2015) 8301–8325.
- [11] G. Tejashri, B. Amrita, J. Darshana, Cyclodextrin based nanosponges for pharmaceutical use: a review, *Acta Pharma.* 63 (3) (2013) 335–358.
- [12] Y. Yang, et al., Advances in self-assembled chitosan nanomaterials for drug delivery, *Biotechnol. Adv.* 32 (7) (2014) 1301–1316.
- [13] M. Swierczewska, et al., Polysaccharide-based nanoparticles for theranostic nanomedicine, *Adv. Drug Deliv. Rev.* 99 (2016) 70–84.
- [14] S. Uthaman, et al., Carbohydrate-based nanogels as drug and gene delivery systems, *J. Nanosci. Nanotechnol.* 14 (1) (2014) 694–704.
- [15] N. Zhang, P.R. Wardwell, R.A. Bader, Polysaccharide-based micelles for drug delivery, *Pharmaceutics* 5 (2) (2013) 329–352.
- [16] D. Duchêne, et al., Cyclodextrin-based polymeric nanoparticles as efficient carriers for anticancer drugs, *Curr. Pharm. Biotechnol.* 17 (3) (2016) 248–255.
- [17] Y. Han, et al., Cyclodextrin-based metal-organic frameworks (CD-MOFs) in pharmaceutics and biomedicine, *Pharmaceutics* 10 (2018) 1–21.



- [18] T. Rajkumar, et al., Cyclodextrin-metal-organic framework (CD-MOF): from synthesis to applications, *J. Ind. Eng. Chem.* 72 (2019) 50–66.
- [19] J. Simon, et al., Protein corona mediated stealth properties of biocompatible carbohydrate-based nanocarriers, *Isr. J. Chem.* 58 (2018) 1363–1372.
- [20] A.L. Klibanov, et al., Amphipathic polyethyleneglycols effectively prolong the circulation time of liposomes, *FEBS Lett.* 268 (1) (1990) 235–237.
- [21] R. Gref, et al., Biodegradable long-circulating polymeric nanospheres, *Science* 263 (5153) (1994) 1600–1603.
- [22] R. Gref, et al., The controlled intravenous delivery of drugs using PEG-coated sterically stabilized nanospheres, *Adv. Drug Deliv. Rev.* 16 (2–3) (1995) 215–233.
- [23] C. Lemarchand, R. Gref, P. Couvreur, Polysaccharide-decorated nanoparticles, *Eur. J. Pharm. Biopharm.* 58 (2) (2004) 327–341.
- [24] L.Y. Filatova, N.L. Klyachko, E.V. Kudryashova, Targeted delivery of anti-tuberculosis drugs to macrophages: targeting mannose receptors, *Russ. Chem. Rev.* 87 (4) (2018) 374–391.
- [25] B. Kang, et al., Carbohydrate-based nanocarriers exhibiting specific cell targeting with minimum influence from the protein corona, *Angew. Chem. Int. Ed. Engl.* 54 (2015) 7436–7440.
- [26] V. Sihorkar, S.P. Vyas, Potential of polysaccharide anchored liposomes in drug delivery, targeting and immunization, *J. Pharm. Pharm. Sci.* 4 (2) (2001) 138–158.
- [27] G. Cutrone, J.M. Casas-Solvas, A. Vargas-Berenguel, Cyclodextrin-modified inorganic materials for the construction of nanocarriers, *Int. J. Pharm.* 531 (2017) 621–639.
- [28] K. Jain, et al., A review of glycosylated carriers for drug delivery, *Biomaterials* 33 (16) (2012) 4166–4186.
- [29] V. Agostoni, et al., A “green” strategy to construct non-covalent, stable and bioactive coatings on porous MOF nanoparticles, *Sci. Rep.* 5 (2015) 7925–7931.
- [30] E. Bellido, et al., Heparin-engineered mesoporous iron metal-organic framework nanoparticles: toward stealth drug nanocarriers, *Adv. Healthc. Mater.* 4 (8) (2015) 1246–1257.
- [31] M. Giménez-Marqués, et al., GraftFast surface engineering to improve MOF nanoparticles furtiveness, *Small* 14 (40) (2018) 1–11.
- [32] T. Hidalgo, et al., Chitosan-coated mesoporous MIL-100 (Fe) nanoparticles as improved bio-compatible oral nanocarriers, *Sci. Rep.* 100 (2017) 1–14.
- [33] X. Liang, et al., Facile preparation of metal-organic framework (MIL-125)/chitosan beads for adsorption of Pb(II) from aqueous solutions, *Molecules* 23 (7) (2018) 1–14.
- [34] R.A. Smaldone, et al., Metal-organic frameworks from edible natural products, *Angew. Chem.* 49 (46) (2010) 8630–8634.
- [35] J. Sha, et al., Nontoxic and renewable metal-organic framework based on alpha-cyclodextrin with efficient drug delivery, *RSC Adv.* 6 (2) (2016) 82977–82983.
- [36] H. Li, et al., Composite CD-MOF nanocrystals-containing microspheres for sustained drug delivery, *Nanoscale* 9 (2017) 7454–7463.
- [37] X. Li, et al., Cyclodextrin-based metal-organic frameworks particles as efficient carriers for lansoprazole: study of morphology and chemical composition of individual particles, *Int. J. Pharm.* 531 (2) (2017) 424–432.
- [38] H. Lu, et al., Study on a new cyclodextrin based metal-organic framework with chiral helices, *Inorg. Chem. Commun.* 61 (2015) 48–52.
- [39] B. Liu, et al., Microwave-assisted rapid synthesis of gamma-cyclodextrin metal-organic frameworks for size control and efficient drug loading, *Cryst. Growth Des.* 17 (4) (2017) 1654–1660.
- [40] J. Liu, et al., Controllable porosity conversion of metal-organic drug delivery, *Chem. Commun.* 53 (2017) 7804–7807.
- [41] J. Sha, et al., Synthesis and structure of new carbohydrate metal-organic frameworks and inclusion complexes, *J. Mol. Struct.* 1101 (2015) 14–20.
- [42] J. Sha, et al., Unprecedented  $\alpha$ -cyclodextrin metal-organic frameworks with chirality: structure and drug adsorptions, *Polyhedron* 127 (2016) 396–402.
- [43] A. Yang, et al., Green synthesis of  $\beta$ -cyclodextrin metal-organic frameworks and the adsorption of quercetin and emodin, *Polyhedron* 159 (2018) 116–126.



- [44] R.S. Forgan, et al., Nanoporous carbohydrate metal-organic frameworks, *J. Am. Chem. Soc.* 134 (1) (2012) 406–417.
- [45] Y. Furukawa, et al., Nano- and micro-sized cubic gel particles from cyclodextrin metal-organic frameworks, *Angew. Chem. Int. Ed.* 51 (42) (2012) 10566–10569.
- [46] B. Liu, et al., Optimized synthesis and crystalline stability of  $\gamma$ -cyclodextrin metal-organic frameworks for drug adsorption, *Int. J. Pharm.* 514 (1) (2016) 212–219.
- [47] C. Qiu, et al., Green synthesis of cyclodextrin-based metal-organic frameworks through the seed-mediated method for the encapsulation of hydrophobic molecules, *J. Agric. Food Chem.* 66 (2018) 4244–4250.
- [48] C. He, et al., Nanomedicine applications of hybrid nanomaterials built from metal-ligand coordination bonds: nanoscale metal-organic frameworks and nanoscale coordination polymers, *Chem. Rev.* 115 (19) (2015) 11079–11108.
- [49] Y. Wei, et al., Pb(II) metal-organic nanotubes based on cyclodextrins: biphasic synthesis, structures and properties, *Chem. Sci.* 3 (7) (2012) 2282–2287.
- [50] K.J. Hartlieb, et al., Encapsulation of ibuprofen in CD-MOF and related bioavailability studies, *Mol. Pharm.* 14 (1) (2017) 1831–1839.
- [51] N. Lv, et al., Improvement in thermal stability of sucralose by  $\gamma$ -cyclodextrin metal-organic frameworks, *Pharm. Res.* 34 (2) (2016) 269–278.
- [52] Y. He, et al., Drug nanoclusters formed in confined nano-cages of CD-MOF: dramatic enhancement of solubility, *Acta Pharm. Sin.* B 9 (1) (2018) 97–106.
- [53] X. Hu, et al., Nanoporous CD-MOF particles with uniform and inhalable size for pulmonary delivery of budesonide, *Int. J. Pharm.* 564 (2019) 153–161.
- [54] Y. Inoue, et al., Characterization of inclusion complex of coenzyme Q10 with the new carrier CD-MOF-1 prepared by solvent evaporation, *AAPS PharmSciTech* 19 (7) (2018) 3048–3056.
- [55] Z. Moussa, et al., Encapsulation of curcumin in cyclodextrin-metal-organic frameworks: dissociation of loaded CD-MOFs enhances stability of curcumin, *Food Chem.* 212 (2016) 485–494.
- [56] V. Singh, et al., Moisture resistant and biofriendly CD-MOF nanoparticles obtained via cholesterol shielding, *Chem. Commun.* 53 (2017) 9246–9249.
- [57] V. Singh, et al., Template-directed synthesis of a cubic cyclodextrin polymer with aligned channels and enhanced drug payload, *RSC Adv.* 7 (2017) 20789–20794.
- [58] H. Li, et al., Facile stabilization of cyclodextrin metal-organic frameworks under aqueous conditions via the incorporation of C<sub>60</sub> in their matrices, *Chem. Commun.* 52 (35) (2016) 5973–5976.
- [59] F. Ke, et al., Synergistic antioxidant activity and anticancer effect of green tea catechin stabilized on nanoscale cyclodextrin-based metal-organic frameworks, *J. Mater. Sci.* (2019). Available at: <http://link.springer.com/10.1007/s10853-019-03604-7>.
- [60] X. Xu, et al., Evaluation of drug loading capabilities of  $\gamma$ -cyclodextrin-metal-organic frameworks by high performance liquid chromatography, *J. Chromatogr. A* 1488 (2017) 37–44.
- [61] J. Xu, et al., A “Ship-in-a-Bottle” strategy to create folic acid nanoclusters inside the nanocages of  $\gamma$ -cyclodextrin metal-organic frameworks, *Int. J. Pharm.* 556 (2019) 89–96.
- [62] I. Kritskiy, et al.,  $\gamma$ -Cyclodextrin-metal organic frameworks as efficient microcontainers for encapsulation of leflunomide and acceleration of its transformation into teriflunomide, *Carbohydr. Polym.* 216 (2019) 224–230.
- [63] M.P. Abuçafy, et al., Supramolecular cyclodextrin-based metal-organic frameworks as efficient carrier for anti-inflammatory drugs, *Eur. J. Pharm. Biopharm.* 127 (2018) 112–119.
- [64] G. Zhang, Enhanced stability of vitamin A palmitate microencapsulated by  $\gamma$ -cyclodextrin metal-organic frameworks, *J. Microencapsul.* 35 (3) (2018) 249–258.
- [65] H. Arima, et al., Recent advances in cyclodextrin delivery techniques, *Expert Opin. Drug Deliv.* 12 (9) (2015) 1425–1441.
- [66] W. Michida, et al., Crystal growth of cyclodextrin-based metal-organic framework with inclusion of ferulic acid, *Cryst. Res. Technol.* 50 (7) (2015) 556–559.
- [67] A. Nagai, et al., Encapsulation of isolated C<sub>60</sub> molecules in a cyclodextrin-based metal-organic framework, *J. Chem. Eng. Jpn* 51 (7) (2018) 615–619.

- [68] P. Horcajada, et al., Metal-organic frameworks in biomedicine, *Chem. Rev.* 112 (2012) 1232–1268.
- [69] T. Baati, et al., In depth analysis of the in vivo toxicity of nanoparticles of porous iron(III) metal-organic frameworks, *Chem. Sci.* 4 (2013) 1597–1607.
- [70] T. Simon-Yarza, et al., Smart metal-organic-framework nanoparticles for lung targeting, *Angew. Chem. Int. Ed.* 56 (49) (2017) 15565–15569.
- [71] T. Simon-Yarza, et al., Nanoparticles of metal-organic frameworks: on the road to in vivo efficacy in biomedicine, *Adv. Mater.* 30 (37) (2018) 1–15.
- [72] A. Aykaç, et al., A non-covalent “click chemistry” strategy to efficiently coat highly porous MOF nanoparticles with a stable polymeric shell, *Biochim. Biophys. Acta Gen. Subj.* 1861 (4) (2017) 1606–1616.
- [73] X. Mao, et al., Talanta  $\beta$ -cyclodextrin functionalization of metal-organic framework MOF-235 with excellent chemiluminescence activity for sensitive glucose biosensing, *Talanta* 188 (2018) 161–167.

### ***Further reading***

- Z. Amoozgar, Y. Yeo, Recent advances in stealth coating of nanoparticle drug delivery systems, *Wiley Interdiscip. Rev. Nanomed. Nanobiotechnol.* 4 (2) (2012) 219–233.
- L. Han, et al., Molecular mechanism of loading sulfur hexafluoride in  $\gamma$ -cyclodextrin metal-organic framework, *J. Phys. Chem. B* 122 (2018) 5225–5233.
- D. Ko, Y. Yeo, Application of polysaccharides for surface modification of nanomedicines, *Ther. Deliv.* 3 (12) (2012) 1447–1456.
- X. Li, et al., Compartmentalized encapsulation of two antibiotics in porous nanoparticles: an efficient strategy to treat intracellular infections, *Part. Part. Syst. Char.* 36 (3) (2019) 1800360.
- J. Liu, S. Willför, C. Xu, A review of bioactive plant polysaccharides: biological activities, functionalization, and biomedical applications, *Bioact. Carbohydr. Diet. Fibre* 5 (1) (2015) 31–61.
- L. Lumholdt, T.T. Nielsen, K.L. Larsen, Surface modification using self-assembled layers of amphiphilic cyclodextrins, *J. Appl. Polym. Sci.* 41047 (2014) 1–8.
- G. Wenz, Cyclodextrins as building blocks for supramolecular structures and functional units, *Angew. Chem.* 33 (1994) 803–822.

# *Metal-organic frameworks for drug delivery: Degradation mechanism and in vivo fate*

Ioanna Christodoulou<sup>a,b</sup>, Christian Serre<sup>b</sup>, Ruxandra Gref<sup>a</sup>

<sup>a</sup>National Center for Scientific Research (CNRS), Institute of Molecular Sciences, Paris-Sud University, Paris-Saclay University, Orsay, France <sup>b</sup>Institut des Matériaux Poreux de Paris, FRE 2000 CNRS, Ecole Normale Supérieure, Ecole Supérieure de Physique et de Chimie Industrielles de Paris, PSL Research University, Paris, France

## **21.1 Introduction**

More than 100 years ago, Paul Ehrlich, a Nobel Prize winner, was dreaming about “magic bullets”, or chemical compounds that could bind to specific pathogens in order to selectively destroy them. Inspired by this concept, scientists nowadays focus their efforts on engineering nanoscale drug carriers that could load drugs and transport them specifically to diseased tissues, thus acting as “magic bullets”.

However, to be used as nanocarrier, a particulate system has to fulfill a series of requirements:

- Biodegradability to avoid accumulation in the living organism
- Lack of toxicity and excretion of the degradation products
- High drug payloads and good incorporation yields of the active molecules
- Controlled release of the cargo
- Selective targeting of diseased cells or organs
- Possibilities of surface modifications to control in vivo fate and ensure stability
- Good detection by imaging techniques
- “Green”, reproducible, and scalable synthesis

A wide variety of drug nanocarriers has been developed in the field of nanomedicine, including liposomes, polymeric micelles, dendrimers, and nanoparticles. Each system presents advantages and disadvantages, in terms of stability, toxicity, and capacity to incorporate drugs with specific properties. For instance, organic carriers such as liposomes discovered in the mid-1960s attracted high interest because of their composition based on natural phospholipids [1]. On the other hand, drug payloads were often low, especially for hydrophobic

molecules, and the vesicular structures were fragile in complex media. While liposomes were adapted to incorporate hydrophilic drugs into their inner aqueous compartment, polymeric micelles were mainly used for the delivery of lipophilic drugs and they could readily disassemble, depending on their critical micellar concentration [2]. Dendrimers have also been studied as drug carriers, but the cost of their synthesis is relatively elevated [3]. Polymeric nanoparticles are generally endowed with good shelf stability, but due to the hydrophobic nature of the biocompatible materials, most hydrophilic drugs were difficult to be incorporated [4].

In this context, recently, a new family of hybrid porous particles, named metal-organic frameworks (MOFs), was discovered and proposed for drug delivery. Contrary to the organic particles described above, MOFs are hybrid porous materials, consisting of metal nodes connected to organic bridging ligands [5–7]. Traditionally, they are used in applications such as gas storage, adsorption, and catalysis [8–10]. MOFs are also used as molecular sieves for the separation of gases or larger molecules. In 2006, Férey and coworkers presented for the first time the use of a Cr-based MOF, as a potential system for drug delivery, by successfully encapsulating the analgesic and antiinflammatory drug ibuprofen into its pores [11]. Later on, the first nanoscale biocompatible Fe-based MOF was used to incorporate a series of drugs with either hydrophilic or hydrophobic character [12].

MOFs appeared as ideal candidates for biomedical applications. Their open porosity was expressed by unprecedented surface areas (they can reach 7839 m<sup>2</sup>/g) [13]. Drug payloads reached 25% wt or more [12, 14–16]. MOFs' intrinsic amphiphilic microenvironment was adapted to host both hydrophilic and hydrophobic active molecules. Finally, the possibility to produce MOFs using a practically unlimited variety of metals and organic ligands ends up to a boundless combination of them, which in turn generates new structures of MOFs.

On the other hand, as always, there are two sides to every coin. To begin with, MOFs were first used in the domains of energy and storage, where a significant stability is required. However, in the domain of biomedicine, the carriers should be stable during the loading and the coating procedures and also during their circulation in the living organism, until they reach their target. However, they should eventually degrade and release their cargo. In a nutshell, a subtle balance between stability and degradation is needed to design effective MOFs for drug targeting purposes.

It should also be kept in mind that MOFs should possess engineered shells to reach their biological targets and that these coatings may in turn play a role in the degradation processes. Moreover, drugs in the MOF pores can either stabilize or destabilize the matrices, as they can interfere with the fluxes of water and ions from the outside media and with the diffusion of the degradation products.

At this point, it is worth to mention that MOFs are coordination polymers, and contrary to organic nanocarriers with strong chemical bonds (nanoparticles, micelles, dendrimers, etc.), they show peculiar features related to their degradation in various media.

It is, therefore, extremely challenging to control the chemical stability of the MOFs and simultaneously maintain their biodegradable character intact. Herein, we discuss these challenges based on recent literature on MOFs for biomedical applications.

## 21.2 Synthesis of biodegradable MOFs

To design biodegradable MOFs carriers, first metals and ligands with minimal toxicities should be chosen.  $\text{Fe}^{2,3+}$ ,  $\text{Ca}^{2+}$ ,  $\text{Zr}^{2+}$ ,  $\text{Co}^{2+}$ ,  $\text{Mn}^{2+}$ , and  $\text{Zn}^{2+}$  are some of the elements which are included already, in traces, in the composition of the human body.

Concerning the ligand compositions, two families are particularly appealing, the carboxylates and the imidazolates, because of their high polarity and their easy elimination from the human body [17]. The method and the reaction conditions are important factors to be taken into account in the design of MOFs. A wide variety of synthetic pathways has been developed, including hydrothermal/solvothermal, electrochemical, and microwave-assisted methods [18, 19]. Among them, one of the most appealing synthesis routes was the microwave irradiation one, as it leads to homogenous nanoparticles within short reaction times [20].

Independently of the synthesis procedure, it is highly recommended that nontoxic solvents and mild conditions (“green” synthesis) should be used. Whenever this is not possible, the organic solvents need to be totally removed from the final product. It is finally crucial to mention the possibility of scaling up the synthesis of the particles in an industrial level. BASF has already developed synthesis techniques and produces in ton scale a variety of MOFs named Basolite for energy applications and catalysis [21].

Named as MIL-family (Materials of Institute Lavoisier), the iron-carboxylate MOFs are considered as one of the most adapted groups of MOFs for bioapplications. Zinc-imidazolate MOFs and mainly ZIF-8 are also interesting candidates. Some other systems, UiO-66(Zr) (UiO stands for University of Oslo) or HKUST-1 (Hong Kong University of Science and Technology), are also used extensively in bioapplications. Last but not the least, a new group was developed, called bioMOFs, in which biomolecules were used as constitutive linkers. For example, BioMIL-5 synthesized from  $\text{Zn}^{2+}$  and azelaic acid was stable in aqueous solutions and, after degradation, azelaic acid was released [22]. All these materials are gathered in Table 21.1, showing the large variety of ligands and possibility to reach pore sizes up to 34 Å.

Obviously, the unlimited combination of different metals and ligands leads to the formation of new porous materials with different sizes and properties, some of which are suitable for bioapplications. However, the stability of these materials remains still an important issue and the most studied one, MIL-100(Fe), was considered one of the most promising candidates [23]. MIL-100 is a mesoporous MOF consisting of iron trimers connected by trimesic acid ligands, which reproduce a crystalline structure with two different types of cages (25 and 29 Å),

Table 21.1 Overview of biodegradable MOFs.

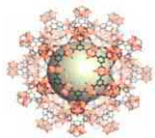

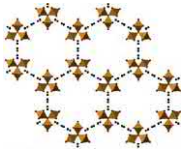

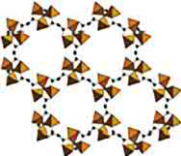


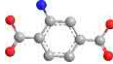
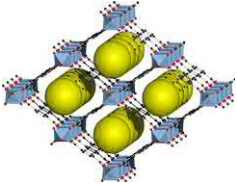

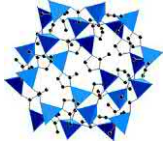
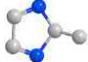
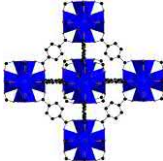

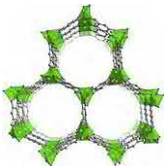

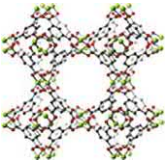

| MOF name    | Structure                                                                           | Organic ligand                                                                                               | Pore size (Å) | References |
|-------------|-------------------------------------------------------------------------------------|--------------------------------------------------------------------------------------------------------------|---------------|------------|
| MIL-100(Fe) |    | Trimesic acid<br>           | 25<br>29      | [12]       |
| MIL-89(Fe)  |    | Muconic acid<br>            | 11            | [12]       |
| MIL-88A(Fe) |    | Fumaric acid<br>            | 13.9          | [12]       |
| MIL-101_NH2 |   | Aminoterephthalic acid<br> | 29<br>34      | [12]       |
| MIL-53      |  | Terephthalic acid<br>     | 8.5           | [12]       |
| ZIF-8       |  | 2-Methyl imidazolate<br>  | 11.6          | [63]       |
| UiO-66(Zr)  |  | Terephthalic acid<br>     | 12            | [64]       |



Table 21.1 Overview of biodegradable MOFs—cont'd

| MOF name     | Structure                                                                         | Organic ligand                                                                                                      | Pore size (Å) | References |
|--------------|-----------------------------------------------------------------------------------|---------------------------------------------------------------------------------------------------------------------|---------------|------------|
| CPO-27-Co/Ni |  | 2,5-Dihydroxyterephthalic acid<br> | 11            | [65]       |
| HKUST-1      |  | Trimesic acid<br>                  | 9             | [66]       |

accessible through pentagonal (5.6 Å) and hexagonal windows (8.6 Å) [24]. MIL-100(Fe) advantageously presented high drug loadings and good stability by maintaining simultaneously its biodegradable character [25].

### 21.3 Drug loading and release

A wide variety of active molecules have been incorporated in the pores of MOFs, such as anticancer, antiviral and antiinflammatory drugs, or antibiotics. Recently, oligopeptides, nucleic acids, and proteins were also encapsulated inside the MOFs' pores [26] and even hydrogen for cancer therapy [27]. Ibuprofen was successfully encapsulated into the pores of MIL-100(Cr) and MIL-101(Cr) [24]. However, the toxicity issues of the chromium metal was an important issue and this metal could be successfully replaced by iron leading to the formation of MIL-53(Fe), a flexible MOF structure that by the effect of its “breathing” phenomenon could adsorb into its pores the drug ibuprofen [28]. In 2010, a wide range of nanosized iron-carboxylate MOFs, adapted for intravenous administration, was described [12]. By this way, it was demonstrated that the loading capacity was related to the pore and window sizes, as well as the nature of the constitutive ligands. Of note, a variety of drugs, hydrophobic, hydrophilic, and amphiphilic, were successfully incorporated [14, 29].

In another example, M-CPO-27 (where M = Ni or Co) adsorbed significant amounts of NO, a biological active gas, of interest for its antibacterial, antithrombotic, and wound healing applications [30]. HKUST-1 was the guest of different molecules (ibuprofen, anethole, and guaiaicol) with a loading of more than 30 wt% [32]. Lin et al. synthesized a Tb<sup>3+</sup>-based MOF coated with Silica for platinum-based anticancer drug delivery [33]. Moreover, Gd<sup>3+</sup>-based MOFs were developed as contrast agents for MRI [34, 35]. In another study, Mn<sup>2+</sup> nanorods

were proposed for the same imaging purpose, in order to avoid the toxicity issues raised from the use of  $Gd^{3+}$  [34, 35]. In conclusion, increasing interest is dedicated to the use of MOFs for drug incorporation and/or imaging purposes. Table 21.2 summarizes the different families of active molecules incorporated in nanoscale MOFs.

**Table 21.2 Loadings of different active molecules.**




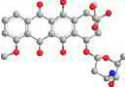
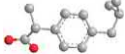

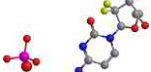
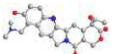
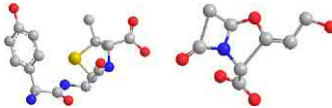




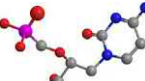


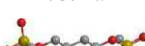



| MOF         | Active molecule                                                                                                  | Drug loading (wt%) | References |
|-------------|------------------------------------------------------------------------------------------------------------------|--------------------|------------|
| MIL-100(Fe) | Busulfan<br>                    | 25.5               | [12]       |
|             | AZT-TP<br>                      | 21.2               | [12]       |
|             | Cidofovir<br>                   | 16.1               | [12]       |
|             | Doxorubicin<br>                 | 9.1                | [12]       |
|             | Ibuprofen<br>                 | 33                 | [12]       |
|             | Caffeine<br>                  | 24.2               | [12]       |
|             | Gemcitabine monophosphate<br> | 30                 | [36]       |
|             | Topotecan<br>                 | 11.6               | [41]       |
|             | Amoxicillin/clavulanate<br>   | 13/22              | [42]       |

Table 21.2 Loadings of different active molecules—cont'd

| MOF          | Active molecule                                                                                  | Drug loading (wt%) | References |
|--------------|--------------------------------------------------------------------------------------------------|--------------------|------------|
| MIL-89(Fe)   | Busulfan<br>    | 9.8                | [12]       |
|              | Cidofovir<br>   | 14                 | [12]       |
| MIL-88A (Fe) | Busulfan<br>    | 8.0                | [12]       |
|              | AZT-TP<br>      | 0.6                | [12]       |
|              | Cidofovir<br>   | 2.6                | [12]       |
| MIL-101_NH2  | AZT-TP<br>      | 42.0               | [12]       |
|              | Cidofovir<br> | 41.9               | [12]       |
|              | Busulfan<br>  | 14.3               | [12]       |
| MIL-53       | AZT-TP<br>    | 0.24               | [12]       |
|              | Ibuprofen<br> | 22                 | [12]       |
|              | Caffeine<br>  | 23.1               | [12]       |

Continued

Table 21.2 Loadings of different active molecules—cont'd

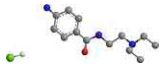

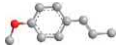

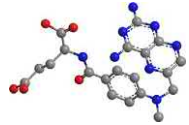


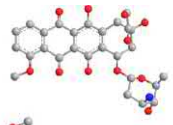
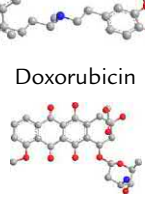
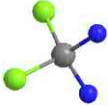
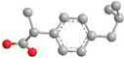

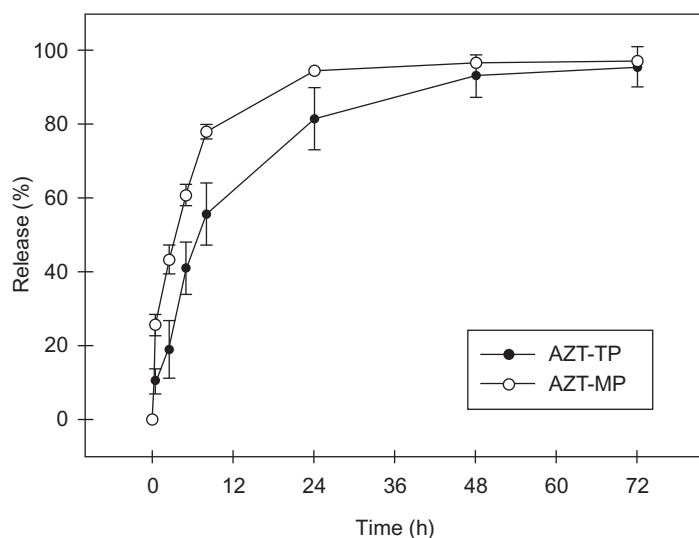
| MOF          | Active molecule                                                                                                 | Drug loading (wt%)                                                             | References |
|--------------|-----------------------------------------------------------------------------------------------------------------|--------------------------------------------------------------------------------|------------|
| bio-MOF-1    | Procainamide hydrochloride<br> | 22                                                                             | [42a]      |
| HKUST-1      | Ibuprofen<br>                  | 34                                                                             | [31, 32]   |
|              | Anethole<br>                   | 38                                                                             | [31, 32]   |
|              | Guaicaol<br>                   | 40                                                                             | [31, 32]   |
| PCN-221      | MTX<br>                        | 40                                                                             | [42b]      |
| CPO-27-Ni/Co | RAPTA-C<br>                   | 100                                                                            | [67]       |
| ZIF-8        | 5-Fluorouracil<br>           | 45.4                                                                           | [16]       |
|              | Doxorubicin/verapamil<br>    | 8.9/32                                                                         | [68]       |
| UiO-66(Zr)   | Doxorubicin<br>              | The amount of DOX loadable into UiO-66 was calculated to be 1 mg DOX/mg UiO-66 | [31, 32]   |

Table 21.2 Loadings of different active molecules—cont'd

| MOF | Active molecule                                                                                | Drug loading (wt%) | References |
|-----|------------------------------------------------------------------------------------------------|--------------------|------------|
|     | Cisplatin<br> | 29.8               | [68a]      |
|     | Ibuprofen<br> | 35.5               | [68b]      |
|     | Aspirin<br>   | 25.5               | [68b]      |

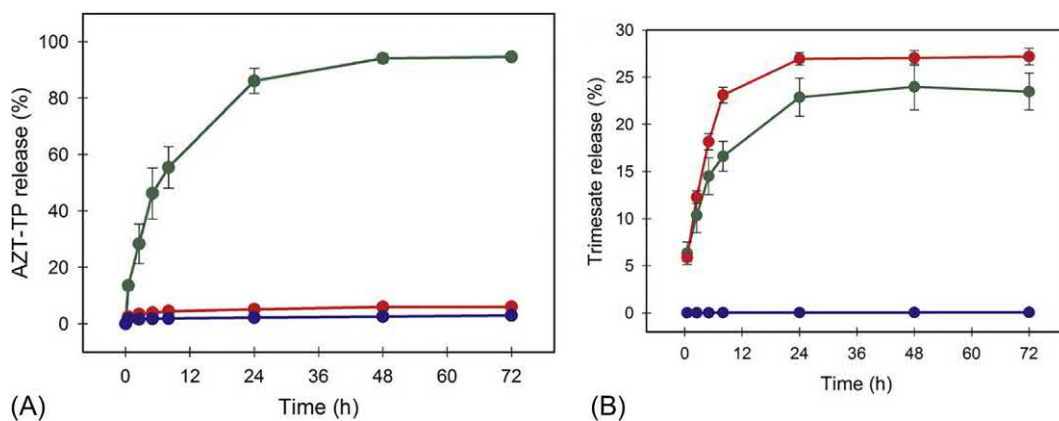
It is of main importance that the MOF carrier doesn't alter its properties during and after the drug loading procedure and also that the loading efficiency is high enough. The most common loading procedures consist of impregnations of MOF particles in aqueous or ethanolic drug solutions, during which the active molecules are incorporated into the pores of the MOFs by diffusion and coordinate with the metal sites and/or organic ligands. Some of the most studied active molecules are the phosphorylated drugs, such as the anticancer drug Gemcitabine monophosphate or the azidothymidine triphosphate (AZT-TP), which were incorporated in MIL-100(Fe) with yields close to 100% [36, 37]. It was found that azidothymidine monophosphate (AZT-MP) was released faster from the MOFs as compared to AZT-TP, as a result of its weaker interaction with the nanoparticles [37] (Fig. 21.1).

After drug loading, the release of the cargo was typically studied in different media, such as PBS (phosphate buffer saline), Tris (containing sulfates), and biological mediums with or without serum [38]. In PBS, the most investigated release medium, a competition for the metal sites of the framework, was observed between the phosphates, the linker, and the active molecule. As shown in Fig. 21.2, the phosphates in the release media triggered both drug and ligand releases, whereas no drug release was observed in Tris buffer or in water [39]. In another study, the degradation mechanism of MOF particles loaded with the antibiotic gentamicin was investigated in different media [40]. The release of the constitutive ligand was both influenced by the presence of the incorporated drug and the nature of the release media.



**Fig. 21.1**

Degradation of loaded MOFs with two different phosphorylated drugs: release of AZT-MP and AZT-TP in PBS at 37°C. Reproduced with permission from V. Agostoni, et al., *Impact of phosphorylation on the encapsulation of nucleoside analogues within porous iron(III) metal-organic framework MIL-100(Fe) nanoparticles*, *J. Mater. Chem. B* 1 (34) (2013) 4231–4242, copyright 2013, *J. Mater. Chem. B*.



**Fig. 21.2**

Release of the drug and the constitutive ligand in different media: (A) release of AZT-TP in PBS (green line), Triss buffer (red line), and H<sub>2</sub>O (blue line). (B) Release of trimesic acid in PBS (green line), Triss buffer (red line), and H<sub>2</sub>O (blue line). Reproduced with permission from V. Agostoni, et al., *Towards an improved anti-HIV activity of NRTI via metal-organic frameworks nanoparticles*, *Adv. Healthc. Mater.* 2 (12) (2013) 1630–1637, copyright 2013, *Advanced Healthcare Materials*.



As a consequence, it is logic to assume that the presence and the nature of molecules entrapped into the pores of the MOFs affect the degradation kinetics, either by accelerating or by slowing it down. This has been demonstrated in the case of the topotecan, an anticancer drug entrapped in MIL-100(Fe) nanoparticles [41].

Topotecan has the particularity of forming aggregates in solution and  $\pi$ - $\pi$  stacking interactions in solid state. It could be efficiently loaded inside the MOF pores after step by step impregnations (“ship in a bottle” method). By this way, impregnation took place in diluted drug solution, where the molecules were not aggregated and could pass through the MOF windows (Fig. 21.1). However, once in the pores, topotecan molecules aggregated forming clusters and the final loading reached 12 wt%. In this case, around 14 topotecan molecules were packed inside each cage of the framework. Interestingly, this clustering effect dramatically reduced the degradation of the MOFs, possibly by avoiding the penetration of the outer medium in the pores (Fig. 21.3).

More recently, it was shown that two different molecules could be co-incorporated inside MIL-100(Fe) nanoparticles [42]. The antibiotics amoxicillin (AMOX) and potassium clavulanate (CL) were co-encapsulated reaching a total drug loading close to 35 wt%. As already mentioned, MIL-100(Fe) is a mesoporous material with two different types of cages (25 and 29 Å) accessible through pentagonal and hexagonal windows (5.5 and 8.6 Å). CL was preferentially packed inside the small cages, whereas AMOX was located in the large ones. Of interest, the loaded nanoparticles penetrated inside infected macrophages releasing their drug cargo in the vicinity of the intracellular pathogen. It was demonstrated that the MOFs degraded inside the cells, within a few hours. However, the mechanism of intracellular degradation was not investigated.

In a nutshell, the degradation mechanism of the MOF carriers was found to be related to the amount and nature of the incorporated active molecules, their location (large and/or small cages), capacity to form aggregates inside the pores, as well as nature of the degradation medium and concentration of ion species. Therefore, it would be of great interest to perform a systematic study of the degradation mechanism of the loaded particles in different media.

## 21.4 Degradation

The stability of the MOF particles depends on several parameters, such as their constitutive ligands and metal ions, the medium, the temperature, and the pH. In addition, the presence of loaded molecules in the cores or an outer coating shell also affects MOF suspensions' stabilities and degradation.

As an example, a series of zirconium-based MOFs were studied after modifications of their constitutive ligands in different media and their chemical and thermal stability was reported [43].

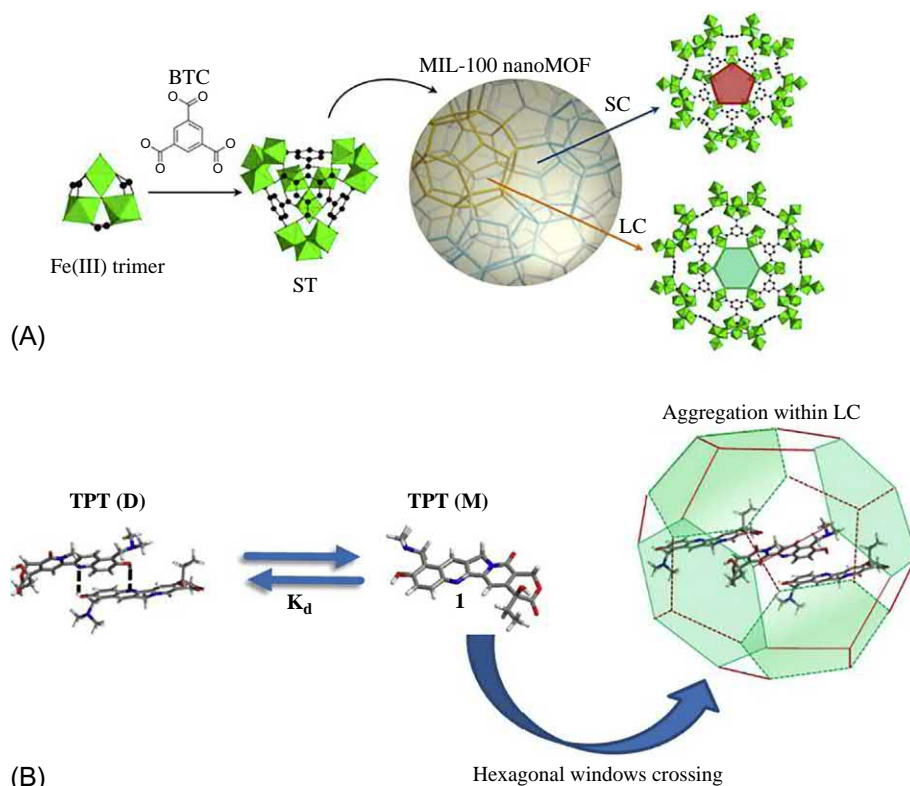


Fig. 21.3

Self-assembly of MIL-100(Fe) and loading of Topotecan: (A) Schematic representation of the synthesis of MIL-100(Fe). Formation of supertetrahedra by the ligand (trimesic acid) and the metal (iron) and self-assembly into the final mesoporous MOF, MIL-100(Fe). MIL-100 consists of two cages, small and large ones, which can be accessed by hexagonal and/or pentagonal windows. (B) Dissociation of the dimers of topotecan into monomers and their entrapment selectively in the large cages (LC) of the MIL-100. Once the monomers are entrapped, they are prone to aggregate by  $\pi$ - $\pi$  interactions inside the pores. *Reproduced with permission from M.R. Di Nunzio, et al., A “ship in a bottle” strategy to load a hydrophilic anticancer drug in porous metal organic framework nanoparticles: efficient encapsulation, matrix stabilization, and photodelivery, J. Med. Chem. 57 (2) (2014) 411–420, copyright 2014, Journal of Medicinal Chemistry.*

The length of the ligand chain, as well as the attachment of functional groups (amino and nitrogen atoms) and finally their impregnation in various chemical solvents altered the stability of the MOFs, as it was proven by a series of complementary techniques (PXRD, FTIR, TGA, etc.).

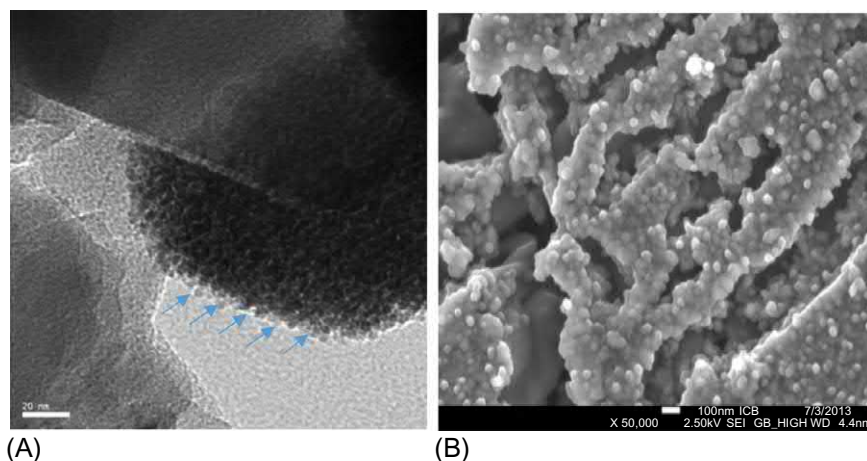
In other studies, the influence of the medium on the degradation mechanism of a Mg-gallate MOF was investigated [44]. The constitutive ligand of this MOF is a natural active molecule (gallic acid) with a remarkable antioxidant activity once it is released inside the organism. It was shown that the release of the ligand was provoked by the degradation of the framework

itself, but the kinetics of the release were influenced by the medium. More precisely, the stability of the particles was tested in water and in RPMI and a lower stability was observed in RPMI, probably due to the presence of phosphates in this medium.

Recently, the degradation mechanism of two different iron-carboxylate MOFs, MIL-100(Fe) and MIL-53(Fe), was deeply studied under two different conditions [45]. The behavior of both particles was investigated in boiling water (100°C) and after the adjustment of the pH to 7 by addition of NaOH. Interestingly, it was shown that during degradation in boiling water, the XRD patterns remained unchanged, whereas microscopic techniques revealed the formation of small aggregates of 3–4 nm consisting of  $\alpha$ -Fe<sub>2</sub>O<sub>3</sub> in the case of MIL-100(Fe) together with a well-crystallized product (goethite), or hematite in the case of MIL-53(Fe). In contrast, at pH 7, both studied material became amorphous and partially degraded into an iron (oxo)hydroxide material, ferrihydrite (Fig. 21.4).

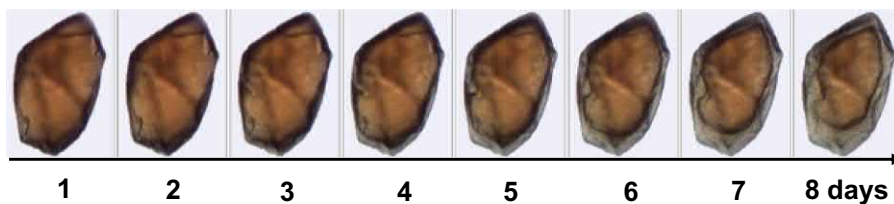
The above study revealed the partial degradation of the MOFs and the formation of different products at elevated temperatures or after pH modifications. However, these studies referred only to the degradation of the particles in water and not in a buffer, nor a biological media.

Another study investigated the degradation mechanism of large MIL-100(Fe) crystals and the effect of incorporated anticancer drugs after 8 days of incubation in PBS by using Raman microscopy [46]. Advantageously, the method enabled studying the morphological features of thousands of particles during their degradation and to take Raman spectra on selected ones.



**Fig. 21.4**

Morphology of MIL-100(Fe) and MIL-53(Fe) after reflux in water 100°C: (A) TEM image of MIL-100(Fe) sample after reflux in water at 100°C for 48 h. (B) SEM image of MIL-53(Fe) after reflux in water at 100°C for 8 h. Reproduced with permission from I. Bezverkhyy, et al., *Degradation of fluoride-free MIL-100(Fe) and MIL-53(Fe) in water: effect of temperature and pH*, *Microporous Mesoporous Mater.* 219 (2016) 117–124, copyright 2015, *Microporous and Mesoporous Materials*.



**Fig. 21.5**

Incubation in PBS of a micron-sized MIL-100(Fe) crystal. Taken by Raman microscopy of a micron-sized MIL-100(Fe) crystal during 8 days. Reproduced with permission from X. Li, et al., *New insights into the degradation mechanism of metal-organic frameworks drug carriers*, *Sci. Rep.* 7 (1) (2017) 13142, copyright 2017, *Scientific Reports*.

Even after 8 days of incubation in PBS, the global morphology and the size of the particles remained unaffected. However, an eroded amorphous shell around a practically intact crystalline core could be clearly visualized when following an individual MOF crystal over several days (Fig. 21.5).

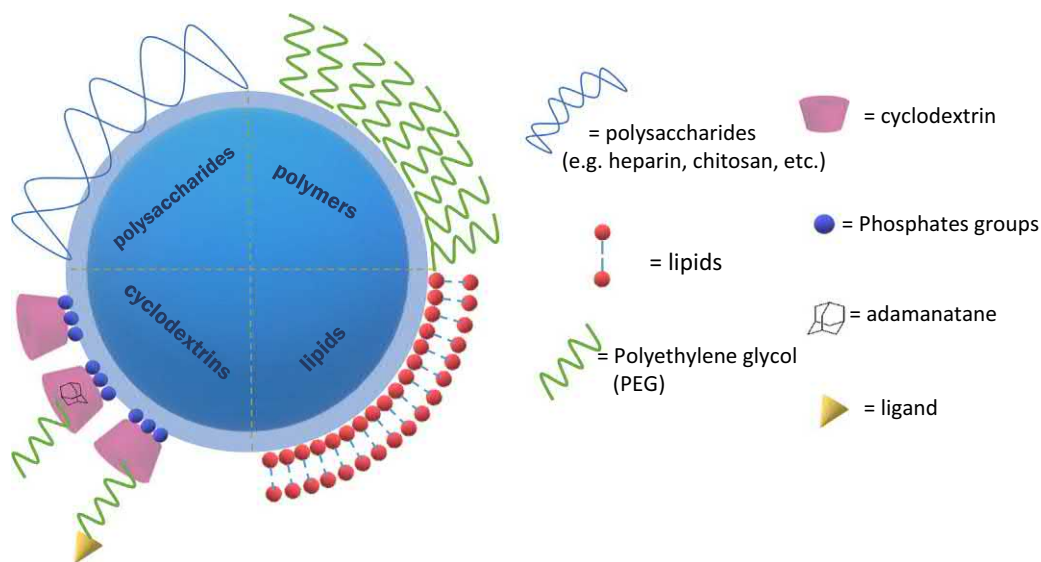
On the contrary, neither drug loading nor coating did affect the integrity of the MOF crystals. These findings are in agreement with studies performed with nanoscale MIL-100(Fe) particles, for which neither loading with the anticancer drug Gemcitabine monophosphate nor the coating with phosphated cyclodextrins induced degradation [36, 47].

Of interest, Mossbauer spectroscopy and Energy Dispersive X-Ray Analysis revealed that, upon degradation in phosphate buffer saline, the final degradation product of MOFs presumably contained iron phosphate [46]. Indeed, phosphates from the degradation media could coordinate with iron sites, leading to the release of the trimesate constitutive ligands and thus to the amorphization of the material.

It can be expected that the composition of the degraded material is related to the nature of the complexing molecules in the degradation medium. This would need further investigations. Indeed, when a biodegradable polymer such as poly (lactic-*co*-glycolic) acid (PLGA) degrades, the final products are always lactic acid and glycolic acid. In the particular case of MOFs, the nature of the degraded products would depend strongly on the degradation medium and its ability to complex iron sites to release trimesate linkers. This highlights the importance of studying in depth the degradation of each type of MOF in different experimental conditions.

## 21.5 Surface engineering

Surface engineering is generally performed to improve nanoparticle colloidal stability and for targeting diseased organs and tissues. Appropriate surface modification of highly porous MOFs should



**Fig. 21.6**  
Surface modifications.

- Not degrade the carrier during the coating procedure
- Be anchored on the external surface of the particles and not affect the internal porosity of the particles
- Have a biodegradable character without side toxic effects
- Undergo an easy and “green” procedure

Several approaches, schematically represented in Fig. 21.5, were described to modify the surface of nanoscale MOFs (Fig. 21.6).

First attempts of MOF surface modification consisted in grafting silica shells in order to avoid rapid dissolution [34, 35]. Interestingly, the drug release was controlled by varying the silica thickness. The silica coating stabilized the particles against degradation ( $t_{1/2}$  = 1.2h for the uncoated ones and  $t_{1/2}$  = 16 h for the silica-coated MOFs).

As mentioned, surface modification should not alter the internal porosity of the particles. Polyethylene glycol (PEG) is a hydrophilic polymer used in biochemistry for modifying a variety of biomolecules and it is one of the most common used polymers, approved by the US Food and Drug Administration (FDA). PEGylation is the process of grafting PEG on the surface of the nanocarriers, in order to improve their pharmacokinetics and to avoid their aggregation. Gupta et al. studied the influence of the coating with PEG chains on the drug release of drug-conjugated MIL-101(Fe) particles [48]. Firstly, the particles were functionalized with amino groups, followed by ibuprofen loading and surface coating by PEG chains. The surface-modified particles were incubated in PBS at different pHs and their degradation mechanism was explored. It was shown that the release of the drug cargo was strongly dependent on the pH.

The acidic pH provoked a faster release of the drug as compared to neutral pH. It was also discovered that the release was slowed down after surface modifications, mainly because of the protection of the particles by the PEG corona, which prohibited the penetration of the phosphates from the release media into the core to erode it.

In another study, Zr-based MOFs were considered for surface modifications [49]. Because of a lower pK<sub>a</sub> of fumaric acid as compared to terephthalic acid, the fumarate analog was more stable than the terephthalate one during incubation in PBS 10 mM at pH=7.4. Moreover, after PEGylation, the stability of the Zr-fumarate particles was further increased, indicating that the coating plays an important role on the stability.

An innovative system was engineered for Positron Emission Tomography (PET) imaging coupled with tumor targeting [31]. UiO-66 (Zr) MOFs loaded with Doxorubicin and the isotope <sup>89</sup>Zr were coated by a series of molecules in a “Lego” manner and they were studied both in vitro and in vivo as drug carriers and theragnostic agents. It was shown that the release of DOX in simulated physiological conditions was pH-dependent. The released drug amounts were higher in acidic conditions. Here again, surface modification significantly improved the stability of the MOF particles, by establishing strong  $\pi$ - $\pi$  interactions with the bridging organic ligands of the MOFs.

However, in the case of MIL-100 (Fe) nanoparticles, it was shown that PEG coating can easily penetrate inside the open MOF porosity, which makes the coating of these materials particularly challenging [47]. Indeed, PEG is able to fill the pores leading to a dramatic loss of the incorporated drugs. To address this issue, a strategy was to coat the outer surface of the MOFs with bulky materials, by keeping their porosity unaffected [47]. Thus, MIL-100(Fe) nanoparticles were covered by phosphated cyclodextrins, biocompatible molecules that efficiently coordinated to the CUS sites at the surface of the nanoMOFs, leading to stable coatings in biological media, despite their noncovalent nature.

Bulky enough, cyclodextrins were anchored only on the MOFs' external surface. By a simple incubation with aqueous nanoMOF suspensions, an efficient coating was achieved by coordination of phosphates with iron sites at the surface, and it could be further functionalized with PEG chains and targeting moieties, such as mannose by a Lego-type methodology. To do so, PEG chains were grafted with adamantane which formed inclusion complexes with cyclodextrins, maintaining PEG at the surface and avoiding its penetration inside the MOF pores. Of note, the coating procedure did not degrade the MOFs nor induce drug leakage.

More recently, three different phosphated cyclodextrins (CD-P) were used to coat MIL-100(Fe) nanoparticles and their influence on the release of AZT-TP was studied [50]. Moreover, polymeric cyclodextrins were used and it was demonstrated that the drug release was better controlled in this case, as compared to monomeric cyclodextrins. Indeed, the thicker shell could afford better interactions with the drug, slowing down its release. This study is an evidence that



the nature of the coating material and the encapsulated active molecule can both affect the degradation of the MOF particles and the release patterns.

$\beta$ -CD was also used to coat an iron-based MOF (MOF-235), significantly increasing their stability, because of the external shell [51]. Another versatile method for MOF surface modifications was the noncovalent bonding of biomolecules such as chitosan and heparin [52, 53]. Both macromolecules were used for the coating of MIL-100(Fe) nanoparticles. Heparin is a polysaccharide large enough ( $8.2 \times 8.9 \text{ \AA}$ ) not to penetrate within the MIL-100(Fe) porosity. It also has various functional groups (i.e., sulfate, carboxylic, and hydroxyl) prone to interact with MOF surface. As for cyclodextrins [47, 50], MOF coating was performed in aqueous solutions by simple impregnation. The degradation of the nanoparticles was not influenced by the presence of the heparin coating.

In a similar manner, MIL-100(Fe) nanoparticles were coated with chitosan, a biocompatible polysaccharide. The stability of the coating was evaluated using chitosan grafted with a fluorescent dye. In parallel, the degradation profile of coated and uncoated nanoparticles was investigated by quantifying the release of the organic ligand trimesate at  $37^\circ\text{C}$  in different media. Interestingly, in the case of PBS the release of the ligand was around 30 wt% for the uncoated and less than 7 wt% for the coated particles, indicating that chitosan hinders the degradation of the nanoparticles and improved their chemical stability, probably because of the slower penetration inside the cores of the degrading phosphates from the suspension media due to the presence of the shell.

Lipid coating is also another convenient method for MOF coating and stabilization. Nanoscale coordination polymers (NCPs) based on  $\text{Zn}^{2+}$ ,  $\text{Zr}^{4+}$ , and  $\text{Gd}^{3+}$  ions and containing methotrexate (MTX) as bridging ligand were synthesized and they were further encapsulated in a functionalized lipid bilayer for the delivery of MTX into cancer cells.  $\text{Zn}^{2+}$  metal ions were first chosen because of their biocompatibility. However, the nanoparticles were not stable enough to be coated by the lipid layer. Therefore, the more stable tetravalent metal ion  $\text{Zr}^{4+}$  was chosen and the lipid coating was successfully achieved. However, the resulting nanoparticles were unstable in PBS and in simulated body fluid (SBF). Finally,  $\text{Gd}^{3+}$ -based MOFs were most stable during and after coating. In the same context, Wuttke et al. successfully synthesized MOFs lipid nanocarriers, using as a lipid layer DOPC (1,2-dioleoyl-sn-glycero-3-phosphocholine) for the hostage of dye molecules [53a]. According to the *in vitro* studies performed by these authors, it was proved that the coating of the particles by lipid layer prevented the fast release of their cargo.

More recently, a GraftFast polymerization procedure was developed to coat MIL-100 nanoparticles with a PEG or a polysaccharide shell [54]. Specifically, MIL-100(Fe) and MIL-100(Al) were coated with different polymers (480 Da, 2 and 5 kDa acryl-PEGs and acryl-hyaluronic acid grafted with PEG). Acrylate polymerization occurred at the outer MOF surface preserving its porosity and without degradation. Of note, degradation of the coated particles was reduced as

compared to uncoated ones. More precisely, 50 wt% of the trimesate was released in PBS after 24 h incubation for the uncoated particles and 43 and 38 wt% for the particles coated with PEG<sub>2kDa</sub> and PEG<sub>5kDa</sub>, respectively. This result shows not only that the chemical stability of the nanoparticles was improved by coating, but also that it depends on the molecular weight of the coating polymer.

From the above studies, it can be concluded that after coating, MOF degradation can either be unaffected or be significantly reduced. Indeed, some coating procedures and materials can protect MOFs against degradation. It would be of high interest to establish a relationship between the nature of the coating and the degradation patterns. This would pave the way toward the design of engineered coatings that will not alter the MOF physico-chemical properties, but improve their colloidal stability and control the degradation in biological media.

## ***21.6 Toxicity and in vivo fate***

One of the major concerns with in vivo administration of the nanocarriers is their potential toxicity after degradation/metabolism inside the body. The degradation mechanism of the MOF particles is difficult to be mimicked in vitro, as body fluids contain thousands of different ions, proteins, and cells. Moreover, depending on their administration route, the MOFs get in contact with different media.

There is still a lot of research to be performed to unravel the in vivo degradation mechanism of MOFs as only scarce studies mention the biodegradability of these relatively novel drug carriers inside the body. Some of these studies were mainly focused on biodistribution of nanoMOFs after intravenous administration and their lack of toxicity [55].

In one of the first attempts to investigate the in vivo fate of MOF nanoparticles in a living organism, Baati et al. performed in vivo toxicity tests in Wistar rats using three different Fe-based nanocarriers: MIL-88A, MIL-88B-CH<sub>3</sub>, and MIL-100 [25]. All of the particles were neither loaded nor coated, and one month after intravenous administration of 220 mg/kg of MOFs, no evident sign of toxicity was detected. In another study, nanoscale MOFs were loaded with the antineoplastic drug busulfan, leading to dramatic pharmacokinetic changes as compared with unloaded nanoparticles [56]. The degradation profile of the particles appeared to be affected by drug loading and the loaded particles were eliminated faster from the organism than the unloaded ones [56]. In a more recent study, MIL-89 nanosized MOFs were evaluated in vivo for their ability to treat pulmonary arterial hypertension (PAH) [57]. Uncoated and PEGylated particles were investigated and none of them induced toxicity after intravenous administration. Interestingly, it was shown that the coated particles were more stable than the uncoated ones.

More recently, MIL-100 particles loaded with the anticancer drug Gemcitabine-monophosphate were intravenously administered to treat lung cancer in a mice model [58]. Interestingly, the nanoparticles immediately aggregated after injection and contact with blood, and the

aggregates were sequestered into the lungs. This strategy enabled delivering locally their active anticancer drug cargo to kill cancer cells. Interestingly, aggregates rapidly disassembled and the animals tolerated the treatment. It was shown that this aggregation/disaggregation mechanism was related to the nanoparticles' surface charge and to the pH of the suspension media. Moreover, it was hypothesized that the fast degradation of the particles in the presence of phosphates from blood could trigger the disassembly of the aggregates.

In a complementary study, the behavior in vitro and in vivo of a large series of MOFs was studied by using as model Zebrafish embryos [59]. A strong correlation between in vitro and in vivo studies was found. Interestingly, a lower toxicity was observed for the particles that were degraded slower. After cell internalization or in vivo administration, each nanoMOF was degraded showing different degradation products and patterns.

In different fields than drug delivery, a copper-based MOF used as a catalyst was synthesized, in order to perform localized drug synthesis in mitochondria [60]. The catalytic activity and stability of this complex were indicated by using the localized synthesized resveratrol-derived drug, and most importantly, the in vivo tests performed in *C. elegans* and mice models proved the biocompatibility of the catalyst.

In another study, MOFs were used as radio-sensitizers to improve the performance of radiotherapy [61]. MOF nanoparticles synthesized from the heavy metal hafnium ( $\text{Hf}^{4+}$ ) and a porphyrin ligand were coated by PEG chains and studied in vitro and in vivo as potential candidates for radiotherapy treatments. After 30 days of exposure in mice models, their biocompatibility was proved, mainly because of the successful excretion of the nanoparticles from the organism. Even further, a new treatment strategy combining local Photodynamic Therapy Treatment and Immunotherapy by using MOF nanoparticles was introduced [62]. A chlorin-based nanoMOF loaded with the immunotherapy agent that inhibits indoleamine 2,3-dioxygenase (IDO) was studied in vivo showing that both primary-treated and distant-untreated tumors were shrunk, because of the synergistic effect of the therapy.

After taking into consideration the previously reported pharmacokinetics and biodistribution data, it can be concluded that the presence and the nature of a drug molecule inside the MOF framework affect their degradation behavior. Each MOF shows a different degradation mechanism, which is strongly related to the composition of the release media. This is one of the main reasons that each drug-loaded MOF material designed for biomedical applications should be examined individually in terms of stability and consequently of biodegradability

## 21.7 Conclusions and future outlook

In reason of their versatility in terms of sizes, composition and surface modification, biodegradability, and biocompatibility, MOFs engineered for biomedical applications demonstrated their usefulness for drug delivery applications. They were able to load

unprecedented amounts of drugs with various physico-chemical properties. However, the stability of nanoscale MOFs in vitro (biological media) and in vivo (after intravenous administration) remains still challenging to be controlled.

Furthermore, the intriguing effects of drug clustering in cages on the stability of MOFs are another interesting observation to be exploited. Shells were shown to stabilize MOFs against degradation and aggregation and this research field is expected to be in constant growth.

While polymeric nanoparticles typically degrade forming oligomers and further monomers of well-known chemical structures, MOF end-degradation products are dependent on the degradation media. This peculiar behavior incites to perform exhaustive studies to unravel the MOF degradation behavior as well as to identify the nature of the degraded material in relation with its elimination from the body. One strategy reviewed here was the investigation of the degradation of individual large MOF particles, with focus on the chemical composition of different regions on a same particle as a function of degradation time. Such studies could be carried on with a series of particles with different compositions and sizes.

With a deep knowledge on the degradation mechanism of MOFs, their peculiar aggregation/disaggregation behavior in complex media could be further exploited to engineer novel MOFs for biomedical applications.

## References

- [1] G. Gregoriadis, Liposomes in drug delivery: how it all happened, *Pharmaceutics* 8 (2) (2016) 19.
- [2] A.P. Clark, et al., Liposomes as drug delivery systems, *Cancer Pract.* 6 (4) (1998) 251–253.
- [3] E. Kahraman, et al., Potential enhancement and targeting strategies of polymeric and lipid-based nanocarriers in dermal drug delivery, *Ther. Deliv.* 8 (11) (2017) 967–985.
- [4] B.L. Banik, P. Fattahi, J.L. Brown, Polymeric nanoparticles: the future of nanomedicine, *Wiley Interdiscip. Rev. Nanomed. Nanobiotechnol.* 8 (2) (2016) 271–299.
- [5] M. Eddaoudi, et al., Modular chemistry: secondary building units as a basis for building units as a basis for robust metal-organic carboxylate frameworks, *Acc. Chem. Res.* 34 (4) (2001) 319–330.
- [6] G. Férey, Hybrid porous solids: past, present, future, *Chem. Soc. Rev.* 37 (1) (2008) 191–214.
- [7] S. Kitagawa, et al., Functional porous coordination polymers, *Angew. Chem. Int. Ed.* 43 (18) (2004) 2334–2375.
- [8] A.G. Wong-foy, et al., Exceptional H<sub>2</sub> saturation uptake in microporous metal-organic frameworks, *JACS Commun.* 128 (11) (2006) 3494–3495.
- [9] T. Grant Glover, et al., MOF-74 building unit has a direct impact on toxic gas adsorption, *Chem. Eng. Sci.* 66 (2) (2011) 163–170.
- [10] E. Soubeyrand-Lenoir, et al., How water fosters a remarkable 5-fold increase in low-pressure CO<sub>2</sub> uptake within mesoporous MIL-100(Fe), *J. Am. Chem. Soc.* 134 (24) (2012) 10174–10181.
- [11] P. Horcajada, et al., Metal-organic frameworks as efficient materials for drug delivery, *Angew. Chem. Int. Ed.* 45 (36) (2006) 5974–5978.
- [12] P. Horcajada, et al., Porous metal-organic-framework nanoscale carriers as a potential platform for drug delivery and imaging, *Nat. Mater.* 9 (2) (2010) 172–178.
- [13] S. Raschke, et al., Balancing mechanical stability and ultrahigh porosity in crystalline framework materials, *Angew. Chem. Int. Ed.* 57 (42) (2018) 13780–13783.

- [14] M. Giménez-Marqués, et al., Nanostructured metal-organic frameworks and their bio-related applications, *Coord. Chem. Rev.* 307 (2016) 342–360.
- [15] F.R.S. Lucena, et al., Induction of cancer cell death by apoptosis and slow release of 5-fluoracil from metal-organic frameworks Cu-BTC, *Biomed. Pharmacother.* 67 (8) (2013) 707–713.
- [16] C.Y. Sun, et al., Zeolitic imidazolate framework-8 as efficient pH-sensitive drug delivery vehicle, *Dalton Trans.* 41 (23) (2012) 6906–6909.
- [17] P. Horcajada, et al., Metal-organic frameworks in biomedicine, *Chem. Rev.* 112 (2012) 1232–1268.
- [18] Y. Lee, et al., Synthesis of metal-organic frameworks: a mini review, *Korean J. Chem. Eng.* 30 (9) (2013) 1667–1680.
- [19] N. Stock, et al., Synthesis of metal-organic frameworks (MOFs): routes to various MOF topologies, morphologies, and composites, *Chem. Rev.* 112 (2) (2012) 933–969.
- [20] J. Klinowski, et al., Microwave-assisted synthesis of metal-organic frameworks, *Dalton Trans.* 40 (2) (2011) 321–330.
- [21] P. Silva, et al., Multifunctional metal-organic frameworks: From academia to industrial applications, *Chem. Soc. Rev.* 44 (19) (2015) 6774–6803.
- [22] C. Tamames-Tabar, et al., A Zn azelate MOF: combining antibacterial effect, *CrystEngComm* 17 (2) (2014) 456–462.
- [23] E. Bellido, et al., Understanding the colloidal stability of the mesoporous MIL-100(Fe) nanoparticles in physiological media, *Langmuir* 30 (20) (2014) 5911–5920.
- [24] P. Horcajada, et al., Synthesis and catalytic properties of MIL-100(Fe), an iron(III) carboxylate with large pores, *Chem. Commun.* 100 (27) (2007) 2820–2822.
- [25] T. Baati, et al., In depth analysis of the in vivo toxicity of nanoparticles of porous iron(III) metal-organic frameworks, *Chem. Sci.* 4 (4) (2013) 1597–1607.
- [26] J. Zhuang, A.P. Young, C.K. Tsung, Integration of biomolecules with metal-organic frameworks, *Small* 13 (32) (2017) 1–14.
- [27] G. Zhou, et al., Porphyrin-palladium hydride MOF nanoparticles for tumor-targeting photoacoustic imaging-guided hydrogenothermal cancer therapy, *Nanoscale Horiz.* 4 (2019) 1185–1193.
- [28] P. Horcajada, et al., Flexible porous metal-organic frameworks for a controlled drug delivery, *J. Am. Chem. Soc.* 130 (21) (2008) 6774–6780.
- [29] C. He, et al., Nanomedicine applications of hybrid nanomaterials built from metal-ligand coordination bonds: nanoscale metal-organic frameworks and nanoscale coordination polymers, *Chem. Rev.* 115 (19) (2015) 11079–11108.
- [30] A.C. McKinlay, et al., Multirate delivery of multiple therapeutic agents from metal-organic frameworks, *APL Mater.* 2 (12) (2014) 124108-1–124108-8.
- [31] D. Chen, et al., In vivo targeting and positron emission tomography imaging of tumor with intrinsically radioactive metal-organic frameworks nanomaterials, *ACS Nano* 11 (4) (2017) 4315–4327.
- [32] Q. Chen, et al., Controlled release of drug molecules in metal-organic framework material HKUST-1, *Inorg. Chem. Commun.* 79 (2017) 78–81.
- [33] W.J. Rieter, et al., Nanoscale coordination polymers for platinum-based anticancer drug delivery, *J. Am. Chem. Soc.* 130 (35) (2008) 11584–11585.
- [34] K.M.L. Taylor, et al., Surfactant-assisted synthesis of nanoscale gadolinium metal-organic frameworks for potential multimodal imaging, *Angew. Chem. Int. Ed.* 47 (40) (2008) 7722–7725.
- [35] K.M.L. Taylor, et al., Manganese-based nanoscale metal-organic frameworks for magnetic resonance imaging, *J. Am. Chem. Soc.* 130 (44) (2008) 14358–14359.
- [36] V. Rodriguez-Ruiz, et al., Efficient “green” encapsulation of a highly hydrophilic anticancer drug in metal-organic framework nanoparticles, *J. Drug Target.* 23 (7–8) (2015) 759–767.
- [37] V. Agostoni, et al., Impact of phosphorylation on the encapsulation of nucleoside analogues within porous iron(III) metal-organic framework MIL-100(Fe) nanoparticles, *J. Mater. Chem. B* 1 (34) (2013) 4231–4242.
- [38] S. Rojas, et al., Nanoscaled zinc pyrazolate metal-organic frameworks as drug-delivery systems, *Inorg. Chem.* 55 (5) (2016) 2650–2663.

- [39] V. Agostoni, et al., Towards an improved anti-HIV activity of NRTI via metal-organic frameworks nanoparticles, *Adv. Healthc. Mater.* 2 (12) (2013) 1630–1637.
- [40] X. Unamuno, et al., Biocompatible porous metal-organic framework nanoparticles based on Fe or Zr for gentamicin vectorization, *Eur. J. Pharm. Biopharm.* 132 (2018) 11–18.
- [41] M.R. Di Nunzio, et al., A “ship in a bottle” strategy to load a hydrophilic anticancer drug in porous metal organic framework nanoparticles: efficient encapsulation, matrix stabilization, and photodelivery, *J. Med. Chem.* 57 (2) (2014) 411–420.
- [42] X. Li, et al., Compartmentalized encapsulation of two antibiotics in porous nanoparticles: an efficient strategy to treat intracellular infections, *Part. Part. Syst. Charact.* 36 (3) (2019) 1800360.
- [42a] J. An, S.J. Geib, N.L. Rosi, Cation-triggered drug release from a porous zinc-adeninate metal-organic framework, *J. Am. Chem. Soc.* 131 (2009) 8376–8377, <https://doi.org/10.1021/ja902972w>.
- [42b] W. Lin, et al., A porphyrin-based metal-organic framework as a pH-responsive drug carrier, *J. Solid State Chem.* 237 (2016) 307–312, <https://doi.org/10.1016/j.jssc.2016.02.040>.
- [43] J.B. Decoste, et al., Stability and degradation mechanisms of metal-organic frameworks containing the  $Zr_6O_4(OH)_4$  secondary building unit, *J. Mater. Chem. A* 1 (18) (2013) 5642–5650.
- [44] L. Cooper, et al., A biocompatible porous Mg-gallate metal-organic framework as an antioxidant carrier, *Chem. Commun.* 51 (27) (2015) 5848–5851.
- [45] I. Bezverkhyy, et al., Degradation of fluoride-free MIL-100(Fe) and MIL-53(Fe) in water: effect of temperature and pH, *Microporous Mesoporous Mater.* 219 (2016) 117–124.
- [46] X. Li, et al., New insights into the degradation mechanism of metal-organic frameworks drug carriers, *Sci. Rep.* 7 (1) (2017) 13142.
- [47] V. Agostoni, et al., A “green” strategy to construct non-covalent, stable and bioactive coatings on porous MOF nanoparticles, *Sci. Rep.* 5 (2015) 1–7.
- [48] V. Gupta, et al., Development of biocompatible iron-carboxylate metal organic frameworks for pH-responsive drug delivery application, *J. Nanosci. Nanotechnol.* 19 (2) (2018) 646–654.
- [49] I. Abánades Lázaro, et al., Surface-functionalization of Zr-fumarate MOF for selective cytotoxicity and immune system compatibility in nanoscale drug delivery, *ACS Appl. Mater. Interfaces* 10 (37) (2018) 31146–31157.
- [50] A. Aykaç, et al., A non-covalent “click chemistry” strategy to efficiently coat highly porous MOF nanoparticles with a stable polymeric shell, *Biochim. Biophys. Acta Gen. Subj.* 1861 (4) (2017) 1606–1616.
- [51] X. Mao, et al.,  $\beta$ -Cyclodextrin functionalization of metal-organic framework MOF-235 with excellent chemiluminescence activity for sensitive glucose biosensing, *Talanta* 188 (April) (2018) 161–167.
- [52] E. Bellido, et al., Heparin-engineered mesoporous iron metal-organic framework nanoparticles: toward stealth drug nanocarriers, *Adv. Healthc. Mater.* 4 (8) (2015) 1246–1257.
- [53] T. Hidalgo, et al., Chitosan-coated mesoporous MIL-100(Fe) nanoparticles as improved bio-compatible oral nanocarriers, *Sci. Rep.* 7 (January) (2017) 1–14.
- [53a] A. Zimpel, T. Preiß, R. Röder, H. Engelke, M. Ingrisch, M. Peller, J.O. Rädler, E. Wagner, T. Bein, U. Lächelt, S. Wuttke, Imparting functionality to MOF nanoparticles by external surface selective covalent attachment of polymers, *Chem. Mater.* 28 (10) (2016) 3318–3326, <https://doi.org/10.1021/acs.chemmater.6b00180>.
- [54] M. Giménez-Marqués, et al., GraftFast surface engineering to improve MOF nanoparticles furtiveness, *Small* 14 (40) (2018) 1–11.
- [55] T. Simon-Yarza, et al., Nanoparticles of metal-organic frameworks: on the road to in vivo efficacy in biomedicine, *Adv. Mater.* 30 (37) (2018) 1–15.
- [56] M.T. Simon-Yarza, et al., Antineoplastic busulfan encapsulated in a metal organic framework nanocarrier: first in vivo results, *J. Mater. Chem. B* 4 (4) (2016) 585–588.
- [57] N.A. Mohamed, et al., Chemical and biological assessment of metal organic frameworks (MOFs) in pulmonary cells and in an acute in vivo model: relevance to pulmonary arterial hypertension therapy, *Pulm. Circ.* 7 (3) (2017) 643–653.



- [58] T. Simon-Yarza, et al., A smart metal–organic framework nanomaterial for lung targeting, *Angew. Chem. Int. Ed.* 56 (49) (2017) 15565–15569.
- [59] A. Ruyra, et al., Synthesis, culture medium stability, and in vitro and in vivo zebrafish embryo toxicity of metal-organic framework nanoparticles, *Chem. Eur. J.* 21 (6) (2015) 2508–2518.
- [60] F. Wang, et al., A biocompatible heterogeneous MOF–Cu catalyst for in vivo drug synthesis in targeted subcellular organelles, *Angew. Chem. Int. Ed.* 58 (21) (2019) 6987–6992.
- [61] J. Liu, et al., Nanoscale metal-organic frameworks for combined photodynamic & radiation therapy in cancer treatment, *Biomaterials* 97 (2016) 1–9.
- [62] K. Lu, et al., Chlorin-based nanoscale metal-organic framework systemically rejects colorectal cancers via synergistic photodynamic therapy and checkpoint blockade immunotherapy, *J. Am. Chem. Soc.* 138 (38) (2016) 12502–12510.
- [63] K.S. Park, et al., ZIFs - first synthesis, *Proc. Natl. Acad. Sci. USA* 103 (27) (2006) 10186–10191.
- [64] K.P. Lillerud, et al., A new zirconium inorganic building brick forming metal organic frameworks with exceptional stability, *J. Am. Chem. Soc.* 130 (42) (2008) 13850–13851.
- [65] P.D.C. Dietzel, et al., An in situ high-temperature single-crystal investigation of a dehydrated metal-organic framework compound and field-induced magnetization of one-dimensional metal-oxygen chains, *Angew. Chem. Int. Ed.* 44 (39) (2005) 6354–6358.
- [66] S.S.-Y. Chui, et al., A chemically functionalizable nanoporous material  $[\text{Cu}_3(\text{TMA})_2(\text{H}_2\text{O})_3]_n$ , *Science* 283 (1999) 1148–1150.
- [67] E. Quartapelle Procopio, et al., Study of the incorporation and release of the non-conventional half-sandwich ruthenium(ii) metallodrug RAPTA-C on a robust MOF, *Chem. Commun.* 47 (42) (2011) 11751–11753.
- [68] H. Zhang, et al., Rational design of metal organic framework nanocarrier-based codelivery system of doxorubicin hydrochloride/verapamil hydrochloride for overcoming multidrug resistance with efficient targeted cancer therapy, *ACS Appl. Mater. Interfaces* 9 (23) (2017) 19687–19697.
- [68a] K.A. Mocniak, I. Kubajewska, D.E.M. Spillane, G.R. Williams, R.E. Morris, Incorporation of cisplatin into the metal-organic frameworks UiO66-NH<sub>2</sub> and UiO66-encapsulation vs. conjugation, *RSC Adv.* 5 (102) (2015) 83648–83656.
- [68b] S. Rojas, I. Colinet, D. Cunha, T. Hidalgo, F. Salles, C. Serre, N. Guillou, P. Horcajada, Toward understanding drug incorporation and delivery from biocompatible metal-organic frameworks in view of cutaneous administration, *ACS Omega* 3 (3) (2018) 2994–3003, <https://doi.org/10.1021/acsomega.8b00185>.

### ***Further reading***

- S. Braig, et al., MOF nanoparticles coated by lipid bilayers and their uptake by cancer cells, *Chem. Commun.* 51 (87) (2015) 15752–15755.
- H. Zheng, et al., One-pot synthesis of metal-organic frameworks with encapsulated target molecules and their applications for controlled drug delivery, *J. Am. Chem. Soc.* 138 (3) (2016) 962–968.

# *Metal-organic frameworks (MOFs) for enzyme immobilization*

Leena B. Vaidya, Shamraja S. Nadar, Virendra K. Rathod

*Department of Chemical Engineering, Institute of Chemical Technology, Mumbai, India*

## **22.1 Introduction**

Enzyme, a natural green catalyst, can speed up biotransformation by minimizing the activation energy without actually being participated in the reaction [1]. Enzymes catalysis has been thoroughly explored in various applications, production of chemicals, and pharmaceuticals by both industry and research academics [2–4]. Generally, practical application of enzyme has been hampered due to small range of pH, less stability at a higher temperature, low chemical stability, self-aggregation, etc. [5, 6].

Immobilization has been developed as an extensive tool for the stabilization and repetitive continuous utilization of enzymes [7, 8]. It was found that operational stability (such as thermal stability, chemical stability as well as their storage stability) of enzymes has profoundly increased after their immobilization, which helps in overcoming [9]. Immobilization makes easy separation and continuous utilization of enzymes by lowering the contamination in reaction process medium, which causes a magnificent decrease in the cost of purification process for enzymes, and therefore, can be used in continuous as well as fixed bed industrial applications [10, 11]. Enzyme immobilization with different matrices takes place through physical forces as well as covalent interactions. The selection of immobilization strategy and choice of immobilization matrix are extremely important to prevent the loss of enzyme activity [12]. There are various physical and chemical methods for enzyme immobilization such as surface adsorption, entrapment, microencapsulation, covalent attachment, and cross-linking [13].

Enzyme immobilization on solid matrices has been extensively studied by a different group of researchers [14–16]. Over the decades, porous nano-based materials (such as sol-gel matrices, hydrogels, organic micro-sized particles, and mesoporous silica) have been adapted as the favorable alternative matrix for enzyme immobilization due to high surface area, tailored pore-size distribution, and controllable pore geometry [6]. However, immobilization of

enzymes carried out during sol-gel reaction synthesis may lead to complete denaturation of enzyme. Additionally, immobilization of enzyme in hydrogels/microparticles suffers from leaching, enzyme denaturation, and mass transfer limitation [17]. Among various porous nano-based carrier for immobilization, mesoporous silica has been most rigorously explored. However, the leaching of enzyme during reaction processes is a major disadvantage. Also, it shows significantly lower recovery and reuse due to nonspecific interaction of enzyme molecules and silica [18].

Recently, organic-inorganic hybrid materials (such as metal-organic frameworks (MOFs) and nanoflowers) have gained considerable attention as an immobilization platform [19]. For the last few decades, MOF has gained prodigious appreciation from all over the world as tailored porous material. It has distinctive attributes such as structural ability, surface topology, low densities, crystallographic structure, designable organic ligand, and high pore volume [20–22]. They have been employed in various sectors such as catalysis, separation, luminescent sensors, drug/enzyme carriers, and energy conversion/storage application areas due to structural and functional tenability [23, 24]. MOFs are fabricated using metal and tunable organic linker which was linked together through strong metal-ligand bonding ( $\pi$ - $\pi$  interactions and hydrogen bonding), resulting in the framing of two-dimensional or three-dimensional extended structures [20]. Various studies investigated MOFs such as MOF-5, MIL-101, and zeolitic imidazole frameworks (ZIFs) as a model MOF in the field of gas separation, catalysis, and drug delivery [25]. MOF has a great potential as a support material for enzyme immobilization platform due to unique characteristics such as high pore volume and area of surface, tunable pore size, and easy modification on metal and ligands with moderate synthetic conditions [26, 27].

This book chapter consists of different strategies of preparation of enzyme-MOF composites such as surface immobilization, pore encapsulation, covalent binding, and de novo approach. Further, it highlights the benefits of MOFs brought to the immobilized enzyme with respect to their various characteristics such as catalytic activity, thermal kinetics, chemical stability, Michaelis-Menten kinetics, recyclability, and storage stability. We anticipate that this book chapter will motivate researchers to investigate in the field of the MOF composites as an immobilization platform and their practical applications beyond proof-of-concept studies.

## ***22.2 Design of MOF as a platform***

A synthesis process of MOF includes metal ion and organic ligands, which form coordination bonds to form a highly crystalline structure with extremely high surface area with versatile 3D extended structures [28]. The attachment of various biomolecules such as proteins and enzymes is expedited by this exceptional functionality of MOFs through covalent and noncovalent interactions. Currently, MOFs with large pore size such as HKUST-MOF, Tb-TATB, Mn-MOF, and PCN-333 have been extensively studied by researchers [26]. Tunable porosity and enormous functional groups of MOFs on the surface are required for immobilization of

enzyme [29]. Nowadays, there has been some rigorous research ongoing to synthesize zeolitic imidazolate frameworks (ZIFs), Tb-BDC, MIL-88, and HKUST-1 under desired conditions to acknowledge the leading problem of preservation of enzyme activity. In recent years, MOFs have emerged as a major area of enzyme immobilization [30–32].

### 22.3 Enzyme-MOF composite

Free enzymes can be immobilized with different types of solid support via various types of bonding interactions. These immobilization strategies can be classified into four categories: surface immobilization, pore encapsulation, covalent binding, and de novo approach (Fig. 22.1) [33]. The selection of methodologies should be based on the properties of enzymes, type of solid support, and targeted applications [21].

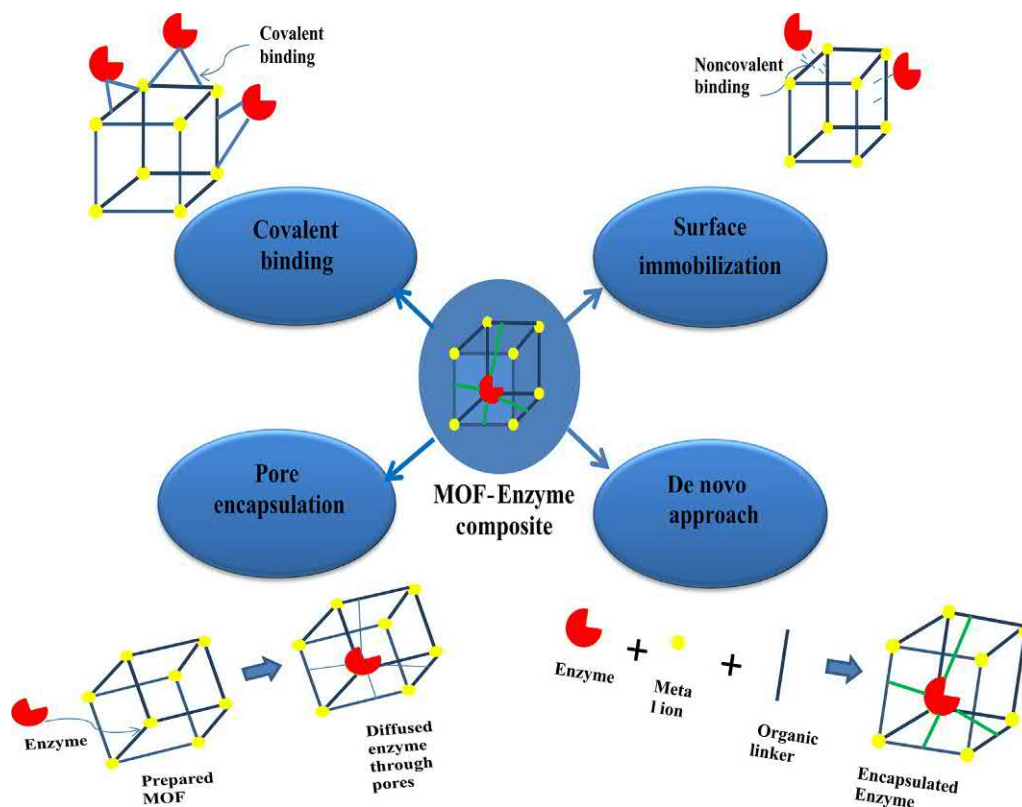


Fig. 22.1

Schematic of the various immobilization methodologies for MOF-enzyme composites.

### 22.3.1 Surface immobilization

Surface immobilization is the easiest method for enzyme immobilization which involved the physical adsorption of enzyme on the surface of MOF matrix. Adsorption of enzymes via physical weak interactions involves  $\pi$ - $\pi$  interactions, molecular interactions, and charge interactions [34]. The summary of enzyme immobilization onto MOF by surface immobilization technique is listed in Table 22.1. Tagging of enzymes with dye is one of the representations of surface attachment of enzyme by physical forces [43]. Lin and coworkers proposed a simple method for the development of trypsin-FITC immobilized MOFs (MOF bioreactor) by combining trypsin with CYCU-4 and MIL-101 (Fig. 22.2). This was the first enzyme dye tagging mechanism study which demonstrated that the enzyme molecules could first combine with dyes and able to enter into the defined MOF pores. It was observed that dye could easily penetrate into the pores and enzyme molecules remain anchored on the surface of MOFs by half an hour of mixing which acts as a driving force with 72% peptide sequence

**Table 22.1: MOF-enzyme composites formed by surface immobilization.**

| MOF                                     | Enzyme                       | Enzyme loading and activity                                                  | Application                                       | Improvement over free enzyme                                                  | Refs. |
|-----------------------------------------|------------------------------|------------------------------------------------------------------------------|---------------------------------------------------|-------------------------------------------------------------------------------|-------|
| CYCU-4                                  | Trypsin                      | 55.2 mg mg <sup>-1</sup>                                                     | BSA digestion                                     | High catalytic activity than free enzymes<br>Improved reusability             | [35]  |
| UiO-66                                  | Trypsin                      | 80 mg g <sup>-1</sup>                                                        | Enhanced industrial catalysis                     | –                                                                             | [36]  |
| Cu-BTC                                  | Lipase (BSL2)                | 50 mg mg <sup>-1</sup>                                                       | Esterification                                    | Modification of BSL2 increased stability and showed 90.7% of initial activity | [37]  |
| UiO-66                                  | PPL                          | 202.4, 196.7, 196.1, 198.9, 194.2 $\mu$ mol PPL g <sup>-1</sup>              | Warfarin synthesis                                | Retained most activity after storing at 4°C for 35 days                       | [38]  |
| ZIF-7, ZIF-8, ZIF-67, ZIF-68 and ZIF-70 | Glucose dehydrogenases (GDH) | 584.9 mg g <sup>-1</sup>                                                     | Electrochemical biosensing of glucose             | Sensor that was reusable 50 times                                             | [39]  |
| Cu-MOF                                  | Laccase                      | 502 mg g <sup>-1</sup>                                                       | Biodegradation of reactive textile dye pollutants | –                                                                             | [40]  |
| Zr                                      | Laccase                      | 0.157 mmol L <sup>-1</sup><br>221.83 mg g <sup>-1</sup><br>95.90 $\pm$ 0.28% | –                                                 | Activity remains 50% (10 cycles), 55.4% at end of 3 week of storage           | [41]  |
| MIL-100-Fe                              | GOx                          | –                                                                            | Glucose sensor                                    | Limit of detection is 5 mM                                                    | [42]  |

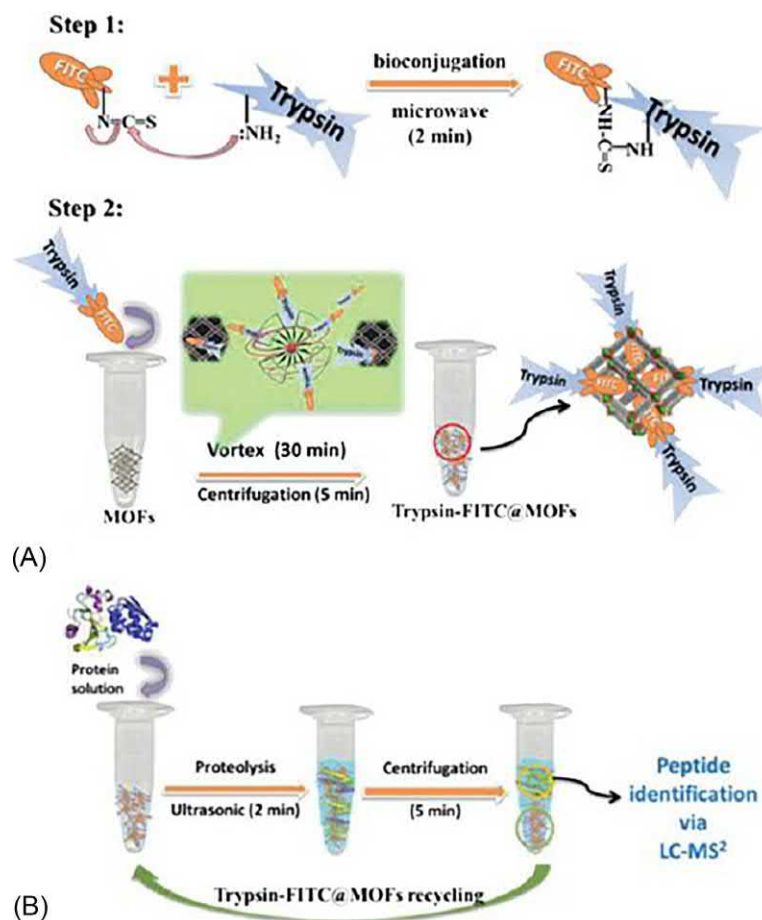


Fig. 22.2

Schematic representation of (A) trypsin tagging and immobilized onto the surface of MOFs and (B) protein digestion. Reproduced with permission from W. Liu, S. Lo, B. Singco, C. Yang, H. Huang, C. Lin, *Novel trypsin-FITC@MOF bioreactor efficiently catalyzes protein digestion*, *J. Mater.* 1 (2013) 928–932, <https://doi.org/10.1039/c3tb00257h>. The Royal Society of Chemistry.

coverage. This novel trypsin-based MOF bioreactor demonstrated high protein digestion, exhibiting high proteolytic activity that was stable over several cycles. Further, they fabricated a novel fast multipoint bioreactor by trypsin as molecule using a dye, 4-chloro-7-nitrobenzofurazan (NBD), which helps in binding of trypsin molecules to the MOFs such as MIL-101(Cr), MIL-100(Cr), UiO-66(Zr), and CYCU-4(Al). Results indicated that MOFs such as MIL-53(Al) and MIL-53(Cr) (channel size around 0.8–1.1 nm) showed poor adsorption capacities, while the other two types of MOFs (MIL-101(Cr) and DUT-4(Al)) (with window and channel size around 1.2 nm) provided exhaustive adsorption abilities (>99%), and almost 92% adsorption capacity was obtained from DUT-5(Al) and CYCU-4. The above



observations supported the high correlation between the FITC adsorption and the window (or channel) size carried by the MOFs [35]. Liu et al. immobilized *Bacillus subtilis* lipase (BSL2) on Cu-BTC porous MOF via adsorption and used it for the esterification of lauric acid and benzyl alcohol. Template-free synthesized hierarchically porous Cu-BTC MOF with anchored BSL2-Surfactant exhibited the great enzyme activity even after 10 cycles of recycling [36]. Furthermore, simple physical adsorption approach was explored for the porcine pancreatic lipase (PPL) as a biocatalyst on different crystalline MOFs such as UiO-66, UiO-66-NH<sub>2</sub>, MIL-53(Al), and carbonized MIL-53(Al) with dimensions of 4.6 × 2.6 × 1.1 nm by Hung et al. In this study, PPL large molecules only could anchor to the exterior surface of MOFs. The immobilized PPL was used for the first time to catalyze Micheal addition reaction to produce anticoagulant warfarin. In another study, Mao et al. studied the adsorption of glucose dehydrogenase (GDH) through electrostatic and hydrophobic interactions onto the array of ZIFs series of MOFs. Characterization techniques such as FTIR, XRD, and SEM were adopted to confirm the adsorption of GDH onto MOFs [39]. Various researchers carried out similar work for numerous enzymes such as laccase on MIL-100(Fe) [44], β-Glu (β-glucosidase) on MIL-53(Al), NH<sub>2</sub>-MIL-53(Al), and Mg-MOF 74 [45].

The remarkable characteristic of MOF such as large pore size has enabled small protein incorporation (3–4 nm in diameter). However, incorporation of large size of bulky enzymes is possible only by incorporation of long chain cross-linker as one of the counterparts of MOF.

### 22.3.2 Pore encapsulation methods

Forgoing studies of enzyme-MOFs attributed that the physical adsorption of enzyme mainly manifests the major shortcoming which is a leaking of enzyme [46]. To overcome this, the enzyme was encapsulated within the pore of MOF which was done by soaking MOF crystals in a solution of the desired enzyme for certain time depending on the system. Pore encapsulation method is regarded as a better method because of the confinement of enzyme within MOF through diffusion. Catalytic properties (selectivity of enzyme and substrate diffusion for specific applications) can be balanced by selection of counterparts of MOF [47]. A novel class of mesoporous MOFs showed the intrinsic advantages over microporous MOFs by providing confide protective covering for enzyme and preventing aggregation enzyme molecules. Pore encapsulation can be classified into two types [48]: (i) unmodified MOF known as a cage inclusion in which pore size of MOF is larger than window size and (ii) channel-type porogen unmodified MOF where pore size of MOF is as small as window size through which pore is accessible. A typical example of enzyme encapsulation within MOF cage was reported by Pisklak et al. In this example, microperoxide-11(MP-11) was encapsulated in nanocrystalline of Cu-MOF via diffusion. The hierarchically porous Cu-MOF showed a Langmuir surface area of 1260 m<sup>2</sup> g<sup>-1</sup> and average pore size of 1.78 nm, which was suited for immobilization of

MP-11. It showed 63% higher catalytic activity than native form and even after seven recycles MP-11 retained its catalytic activity of 48.9% [49].

Hierarchical channel type of mesoporous MOF was first time reported by Li et al. in 2016 for encapsulation of nerve detoxifying enzyme organophosphorus acid anhydrolase (OPAA) into mesoporous zirconium MOF (PCN-128y). The prepared PCN-128y showed 4.4 nm hexagonal channels and 1.7 nm of triangular channels (Fig. 22.3). OPAA/PCN-128y was used to detoxify diisopropyl fluorophosphate (DFP), a less toxic nerve agent simulant, and an extremely toxic nerve agent. Encapsulation of OPAA in PCN-128y MOF gives higher temperature stability (over 70°C) than free enzymes [50]. Further, researchers have investigated the effect of porogen, which helps in enlargement of pore size of MOF. Ding et al. investigated the utilization of surfactant CTAB to develop microporous UiO-66. The enormous surface area of UiO-66 was used for immobilization of laccase. Laccase/UiO-66 has shown higher phenol degradation in just 12 h. On the same ground, lysozyme was adsorbed on mesoporous zeolitic imidazole frameworks (ZIFs) with mesopores around 35.6 nm [41].

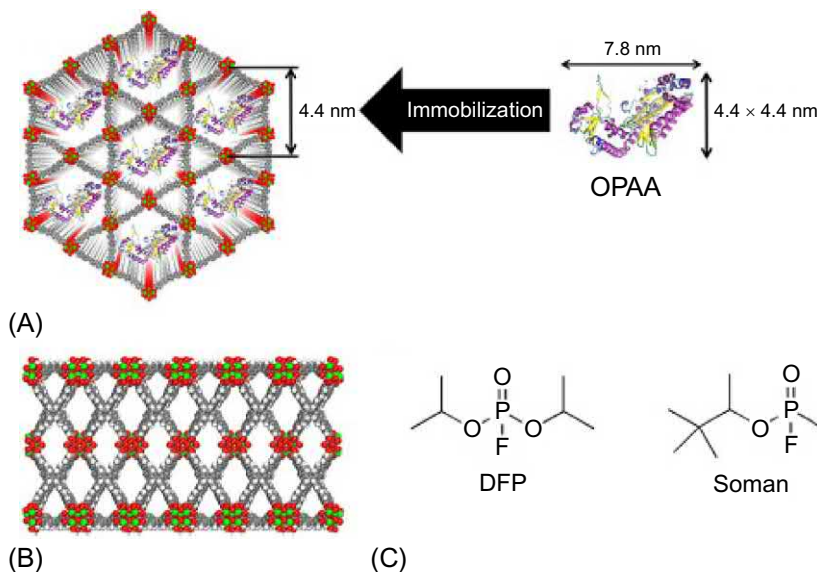


Fig. 22.3

Schematic representation (A) immobilization of OPAA in the mesoporous PCN-128y. (B) Side view of PCN-128y showing mesoporous and microporous channels (C) structure of nerve agents. *Reproduced with permission from P. Li, S.Y. Moon, M.A. Guelta, S.P. Harvey, J.T. Hupp, O.K. Farha, Encapsulation of a nerve agent detoxifying enzyme by a mesoporous zirconium metal-organic framework engenders thermal and long-term stability, J. Am. Chem. Soc. 138 (2016) 8052–8055, <https://doi.org/10.1021/jacs.6b03673>. Copyright 2016.*

*The American Chemical Society and Division of Chemical Education, Inc.*

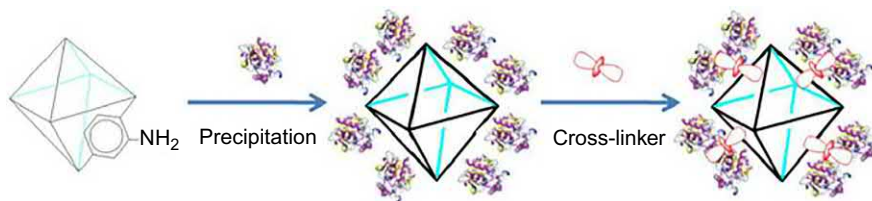
However a denser MOF framework may limit the accessibility of substrate to encapsulate enzyme molecules, which ultimately suffers from mass transfer limitation. MOF is a fascinating topic for host matrices, but it is not feasible for bulky enzymes due to size limitations [51]. Jiang et al. established the novel facile approach for controllable construction of ZIFs-MOF hollow composite via protein-induced under mild conditions through soft-template strategy. Hollow ZIF-8 with 3.4 nm pore size was utilized for encapsulation of *Burkholderia cepacia* lipase (BCL). Enhanced solvent stability and activity recovery of BCL/H-ZIF-8 were showed over free and BCL/ZIF-8 due to reduced mass transfer limitation.

### 22.3.3 Covalent binding

Surface of different MOFs has a wide variety of functional groups (amino, hydroxyl, carboxyl groups, etc.). Covalently bounded enzyme on the surface of MOFs provides enhanced stability and recyclability. This method outmatched the recyclability of the immobilized enzymes with diverse type of MOFs support and lesser enzyme leakage as compared to their noncovalent interactions [52]. The summary of enzyme immobilization onto MOF by covalent bonding is given in Table 22.2. Immobilization of enzyme through covalent binding was thoroughly discussed in work study of Park et al. In this study, surface anchoring of enhanced green fluorescent protein (EGFP) and *Candida antarctica* (CAL-B) onto an array of MOFs such as 1D-MOF, 2D-MOF, and IRMOF-3 was also discussed. The 1D-MOF, 2D-MOF, and 3D-MOF groups of carboxylate were activated by ethyl-3-(3-dimethylaminopropyl) carbodiimide (EDC) and dicyclohexyl carbodiimide (DCC). The pendant carboxylate groups of the organic linker were used for the enzyme interaction and activated carboxylate groups of the MOF were

Table 22.2: MOF-enzyme composites formed by covalent binding.

| MOF                                                        | Enzyme      | Enzyme loading and activity      | Application           | Improvement over free enzyme                                    | Refs. |
|------------------------------------------------------------|-------------|----------------------------------|-----------------------|-----------------------------------------------------------------|-------|
| IRMOF-3                                                    | GFP, lipase | 0.18 mg g <sup>-1</sup>          | Trans-esterification  | 103-fold higher activity                                        | [53]  |
| UiO-66-NH <sub>2</sub>                                     | SEH         | 87.3 mg g <sup>-1</sup><br>17.6U | Asymmetric hydrolysis | Higher yield and higher enantiomeric excess                     | [54]  |
| ZIF monolith                                               | Typsin      | 0.42 mg typsin cm <sup>-1</sup>  | BSA digestion         | –                                                               | [55]  |
| MIL-88B(Cr)-NH <sub>2</sub><br>MIL-88B(Cr),<br>MIL-101(Cr) | Trypsin     | –20%–50%                         | Proteolysis           | Similar activity as free enzymes; activity was decrease to half | [56]  |



**Fig. 22.4**

Schematic representation of synthesis of immobilization of SEH onto UiO-66-NH<sub>2</sub>. *Reproduced with permission from C. Zhang, X. Wang, M. Hou, X. Li, X. Wu, J. Ge, Immobilization on metal-organic framework engenders high sensitivity for enzymatic electrochemical detection, ACS Appl. Mater. Interfaces 9 (2017) 13831–13836, <https://doi.org/10.1021/acsami.7b02803>. Copyright 2016. The American Chemical Society and Division of Chemical Education, Inc.*

interacted with amino groups of protein (EGFP) and formed the covalent amide bonds with formation of enzyme-MOF complex [56]. Shih et al. carried out experiment involving MIL-88B(Cr)-NH<sub>2</sub>, MIL-88B(Cr), and MIL-101(Cr) for the immobilization of trypsin. MOFs were treated with dicyclohexyl carbodiimide, which allowed them to interact with amino groups of trypsin and formed conjugate. It was observed that Try-MIL-88B-NH<sub>2</sub>(Cr) showed similar activity as free enzyme but after immobilization Try-MIL-88B(Cr) and Try-MIL-101(Cr) showed half of the initial activity. Research work was done in a similar area of the immobilization of lipase (EDC activated) on Fe<sub>3</sub>O<sub>4</sub>@MIL-100(Fe) and Fe<sub>3</sub>O<sub>4</sub>@Bio-MOF(ZnGlu) [56].

Cao et al. immobilized soybean epoxide hydrolase (SEH) onto functionalized UiO-66-NH<sub>2</sub> via cross-linking method (Fig. 22.4). Immobilized SEH showed effective operational parameter stability than native form. The activities of immobilized form and free enzyme at 45°C showed more than 17.6 U and 10.1 U activities, respectively. In storage stability studies, SEH/UiO-66-NH<sub>2</sub> showed 97.5% of its original activity after 4 weeks [57].

### 22.3.4 De novo encapsulation method

Generally, the presynthesized MOF-based immobilization methods always suffer from low immobilization yield, enzymes leaching, and low stability (in terms of temperature and chemical stability) [26]. Therefore, it demands extensive research for the development of a strategy, which increases the area of MOF as an immobilization platform. In this approach, organic linker and inorganic metal ions were combined to encapsulate enzyme as protective covering under biocompatible conditions. During the process of synthesis, enzyme induces the formation of MOF and facilitates crystallization of biomolecules around enzyme which resulted in entrapment of enzyme. This approach categorized into the encapsulation in the presence of stabilizing agent (surfactants) named as coprecipitation (Table 22.3) and direct facile encapsulation without any stabilizing agent known as biomineralization (Table 22.4) [33, 73].

Table 22.3: MOF-enzyme composites formed by co-precipitation.

| MOF             | Enzyme                             | Enzyme loading or activity | Application                         | Improvement over free enzyme                                         | Refs. |
|-----------------|------------------------------------|----------------------------|-------------------------------------|----------------------------------------------------------------------|-------|
| ZIF-90          | Catalase                           | 5% (w/w)                   | Peroxidase degradation              | Increases tolerance to proteinase K                                  | [58]  |
| ZIF-8           | Cyt <i>c</i>                       | –                          | Oxidation of Amplex red             | 10-fold increase in the activity                                     | [59]  |
| ZIF-90<br>ZIF-8 | Catalase                           | –                          | Stability over urea and temperature | 6 M urea and 80°C was the highest concentration with 3-fold increase | [60]  |
| ZIF-8           | HRP                                | –                          | Peroxidase activity                 | ~2–5 folds higher activity than free HRP in solution                 | [61]  |
| ZIF-8           | $\alpha$ -Amylase and glucoamylase | Activity 73.3U per mg      | Starch hydrolysis                   | 52% of residual activity even after five cycles                      | [62]  |
| Cu-MOF          | Glucosidase                        | 81.89%                     | Cellulose hydrolysis                | 98% glucose yield, 70% productivity in the eight cycles              | [63]  |

A pioneered work de novo approach was introduced by the Lyu and coworkers for the first time. They synthesized Cyt *c*/ZIF-8 (zeolitic imidazolate frameworks) crystals by adding Cyt *c*, zinc nitrate, and 2-methylimidazole in assistance of polyvinylpyrrolidone (PVP). The presence of PVP stabilized the Cyt *c* in methanol and maintained its dispersion (Fig. 22.5). The small pore size of ZIF prevents leaching of enzyme as compared to other techniques. It also showed an enhancement in the activity of Cyt *c* by 10-fold as compared to free enzyme [59]. In another example, Ge et al. demonstrated the synthesis of novel horseradish peroxidase (HRP)/ZIF-8 crystals with an average size of 30 nm. In this work, reverse micelles were prepared from water, Brij C10 and cyclohexane for the coprecipitation of enzyme, and Zn<sup>2+</sup> and organic linker to synthesize enzyme-MOF nanocrystal (Fig. 22.6) [61]. Similarly, Wang et al. carried out the facile encapsulation of glucosidase into Cu-MOF through simple mixing of enzyme solution and *para*-aminobenzoic acid. Encapsulation of  $\beta$ -G in Cu-MOF exhibited enhanced reusability, and even after 10 cycles of reusability, 90% of catalytic activity was retained [63].

Biomimetic is another strategy for encapsulation of biologically active compounds under protective exterior. Remarkable features of MOF including crystal size, morphology, and compositional specificity can significantly be controlled by facile self-assemble one-pot biomineralization method. Mechanism of biomineralization involves the mixing of enzyme and

Table 22.4: MOF-enzyme composites formed by biomineralization.

| MOF              | Enzyme                                      | Application                                          | Improvement over free enzyme                                                                                                                            | Refs. |
|------------------|---------------------------------------------|------------------------------------------------------|---------------------------------------------------------------------------------------------------------------------------------------------------------|-------|
| ZIF              | HRP, GOx                                    | Glucose detection                                    | Detection of low concentration of glucose (0.4 $\mu$ M) with excellent selectivity                                                                      | [64]  |
| ZIF-8            | Catalase                                    | –                                                    | 400% higher activity by catalase@ZIF composites with cruciate flower-like structure (12.24) nm as compared to rhombic dodecahedral morphology (3.28) nm | [65]  |
| ZIF-8            | (R)-1-phenylethanol dehydrogenase ((R)-PEDH |                                                      |                                                                                                                                                         | [66]  |
| ZIF-8            | HRP, trypsin, lipase, urease                | Bio-storage, chemical processing and pharmaceuticals | 80% of catalytic activity vs 20% catalytic activity of free HRP                                                                                         | [67]  |
| ZIF-8            | Lipase                                      | Kinetic resolution of R,S-2 octanol                  | Enhanced tolerance to trypsin digestion and 91% of catalytic activity retained                                                                          | [68]  |
| ZIF-8            | Glucoamylase                                | Investigation of reusability and storage capacity    | 57% of activity over 6 cycles<br>91% of activity retained till 25 days of storage                                                                       | [69]  |
| ZIF-8            | Lipase                                      | Investigation of reusability and storage capacity    | 3.2-folds increment as against free lipase                                                                                                              | [70]  |
| ZIF-8            | Urease                                      | –                                                    | Enhanced stability over large temperature range                                                                                                         | [71]  |
| ZIF-8 and ZIF-10 | HRP<br>Lipase<br>Cyt c                      | Protein engineering                                  | Enhanced tolerance against organic solvents                                                                                                             | [72]  |

MOF precursors (ligands and metal ions) as a solution, and in turn, the enzymes concentrate the MOF basic building blocks, which leads to nucleation of porous crystal and rapid crystallization of MOF particles with encapsulated enzymes [32, 46]. This green synthesis of enzyme-MOF composite attributed an establishing step for extensive study of this concept.



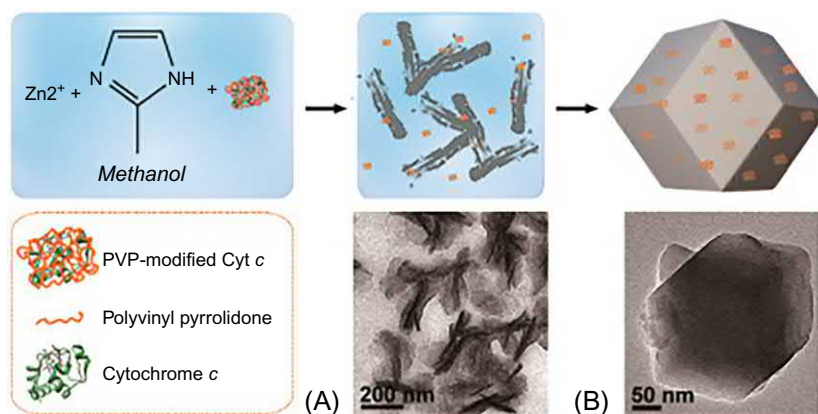


Fig. 22.5

Schematic representation of preparation of the cytochrome *c*-embedded ZIF-8. TEM Images of cyt *c*/ZIF-8 composite for reaction time of (a) 5 h (b) 24 h. Reproduced with permission from F. Lyu, Y. Zhang, R.N. Zare, J. Ge, Z. Liu, *One-pot synthesis of protein-embedded metal-organic frameworks with enhanced biological activities—supporting Information*, *Nano Lett.* 14 (2014) 5761–5765, <https://doi.org/10.1021/nl5026419>. Copyright 2014. The American Chemical Society and Division of Chemical Education, Inc.

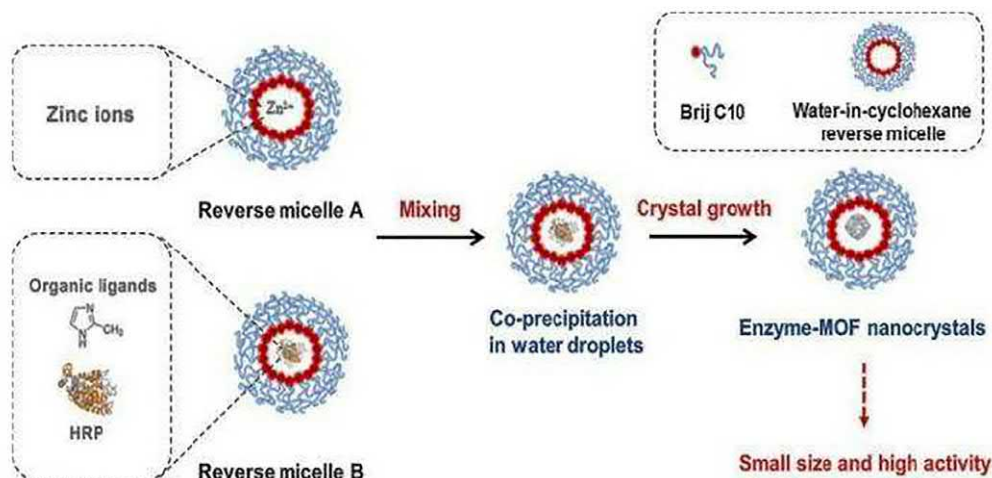
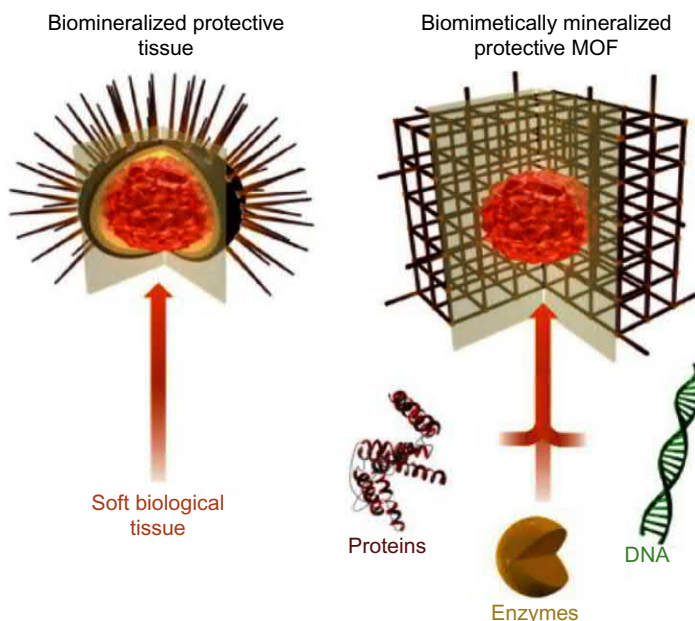


Fig. 22.6

Schematic illustration of synthesis of HRP-MOF nanocrystals in reverse micelles. Reproduced with permission from P. Chulkaivalsucharit, X. Wu, J. Ge, *Synthesis of enzyme-embedded metal-organic framework nanocrystals in reverse micelles*, *RSC Adv.* 5 (2015) 101293–101296, <https://doi.org/10.1039/c5ra21069k>. The Royal Society of Chemistry.

Taking advantage of mild synthetic conditions of ZIFs, metal frameworks have been profoundly investigated in situ synthetic processes for enzyme immobilization. Pioneered work of Liang and coworkers demonstrated the development of immobilization system which could be universally adopted for encapsulation of biomolecules such as enzymes (lipase, HRP, trypsin, and urease), DNA, and oligonucleotides into ZIFs metal framework



**Fig. 22.7**

Schematic illustration of biomimetically mineralized MOF. *Reproduced with permission from K. Liang, R. Ricco, C.M. Doherty, M.J. Styles, S. Bell, N. Kirby, S. Mudie, D. Haylock, A.J. Hill, C.J. Doonan, P. Falcaro, Biomimetic mineralization of metal-organic frameworks as protective coatings for biomacromolecules, Nat. Commun. 6 (2015) 1–8, <https://doi.org/10.1038/ncomms8240>. Copyright © 2015. Macmillan Publishers Limited. All rights reserved.*

(Fig. 22.7). The encapsulation is simply done by addition of enzyme into 2-methylimidazole solution and zinc acetate at ambient room temperature [67]. He et al. successfully prepared a biocomposite where a thermophilic lipase encapsulated in ZIF-8 via self-assembly method improved its operational parameters such as chemical stability and catalytic activity. Lipase/ZIF-8 showed 1.5-fold improved conversion in transesterification reaction as compared to free form [68].

In the encapsulation method, the concentration of metal ions, organic linker, and enzyme plays an important role in its morphology, crystallinity, and activity recovery. Liang et al. (2016) studied the difference between two efficient strategies of enzyme encapsulation of such composite materials: biomimetic mineralization (in the absence of PVP) and controlled coprecipitation using PVP. The enzyme biocomposite prepared by coprecipitation exhibited a profound increase in activity due to smaller crystal size (120 nm) and uniform enzyme distribution on the surface of MOF, allowing ease of reactants diffusion. However, biocomposite prepared by biomimetalization showed higher thermal stability in the temperature range of 23–70°C [71].

In the preparation experiment, the parameters like metal ion, organic linker concentration, additives, and preparation media play a crucial role. These parameters directly affect the morphology, crystallinity, enzyme loading, and activity. To understand the effect of

concentration of metal ions and organic linker, Cui et al. studied the morphology of prepared catalase@ZIF by varying  $\text{Zn}^{2+}$  ion concentration (0.05–0.8 M) and 2-methylimidazole concentrations (0.05–1 M). It has been reported that catalase@ZIF did not form in the absence of organic cross-linker. Nanosheets began to form when 0.3 M of 2-methylimidazole has been used. Further, as the concentration increased, nanosheets aggregate to form uniform cruciate flower-like nanostructures (Fig. 22.8). In the next experiment, the authors

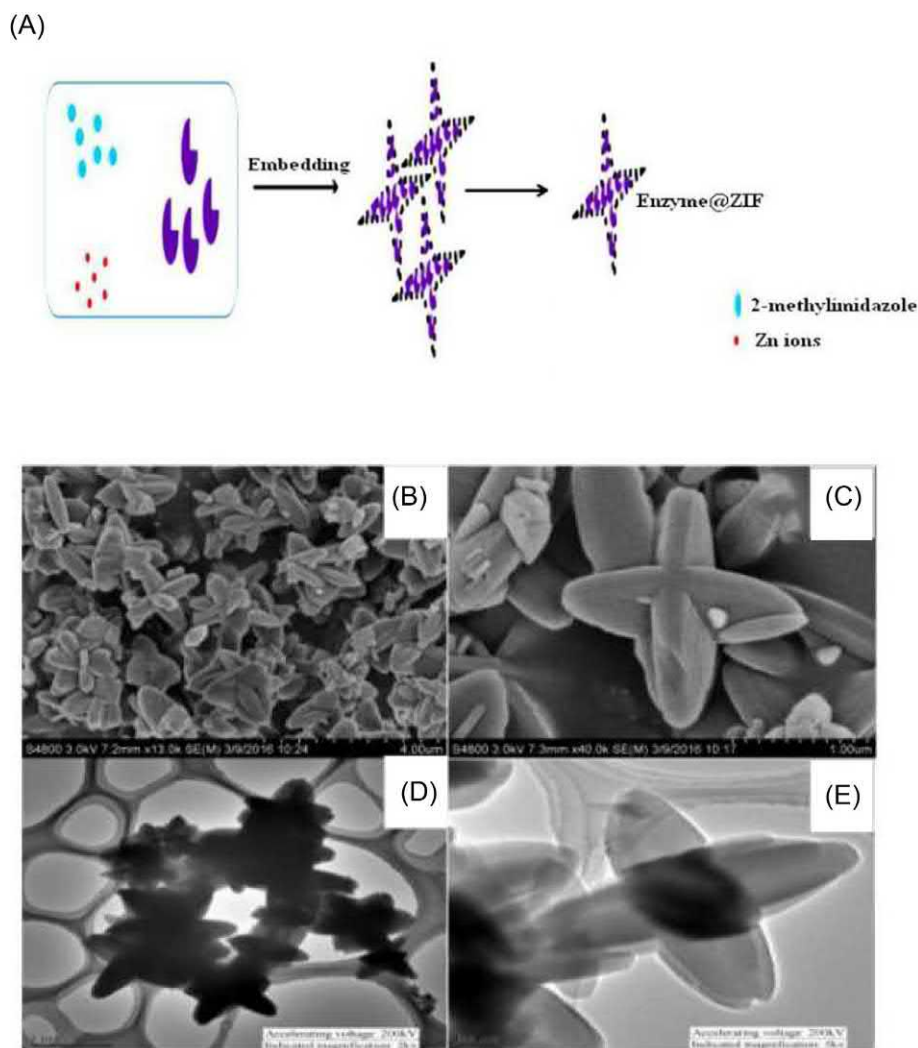
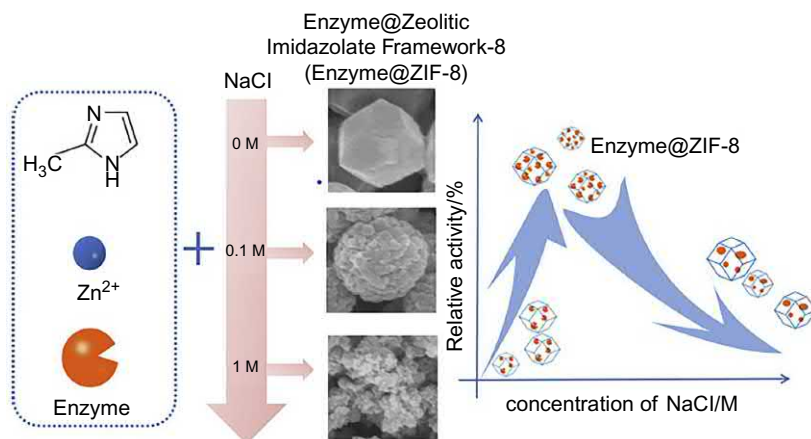


Fig. 22.8

Schematic illustration of the synthesis of the catalase@ZIF composites and SEM images (A–C), TEM images (D, E) of catalase@ZIF composites with cruciate flower-like shape. *Reproduced with permission from J. Cui, Y. Feng, T. Lin, Z. Tan, C. Zhong, S. Jia, Mesoporous metal-organic framework with well-defined cruciate flower-like morphology for enzyme immobilization, ACS Appl. Mater. Interfaces (2017), <https://doi.org/10.1021/acsami.7b00512>. Copyright 2017. The American Chemical Society and Division of Chemical Education, Inc.*

varied the metal ion concentration to get ZIF particles with the shape of standard rhombic dodecahedra, cubes, sphere, flowerlike polyhedra, and cruciate flower-like. The ZIFs with various structural morphologies could be formed due to strong coordination interaction between organic cross-linker and metal ions [65]. These results demonstrated that the concentration of metal ions, cross-linker, and stabilizer has crucial role in the morphology of enzyme-MOF composites. Usually, the enzyme solution contained small molecules such as buffer components, salts, and so on, which affect the morphology as well as the crystallinity. In this context, Pu et al. determined the effect of NaCl on the preparation of enzyme-MOF as well as other catalytic properties. They observed that PEDH/ZIF-8 exhibited a profound increase in activity by 2.5 folds in the presence of NaCl as compared to plain PEDH/ZIF-8 (Fig. 22.9). Further, they observed 38% residual activity after 7 cycles of reusability, which was 20% higher than plain PEDH/ZIF-8. Authors claimed that the improvement in catalytic properties was due to flower ball structured enzyme-MOF composite prepared by NaCl, which may protect enzyme molecules from damage during reaction [66]. The surface amino acids and charge on the protein molecules determine the nucleation sites and growth of MOF. Maddigan et al. investigated the efficacious method for systematic control of biomimetic mineralization by chemically modifying functional groups of amino acid onto surface of proteins. In the experimental process, they introduced two different model proteins, i.e., bovine serum albumin (BSA) and hemoglobin. The synthesis of ZIF-8 was observed within seconds which was induced by BSA, while hemoglobin yielded a low quantity ZIF-8 MOF. They found that biomimetically mineralized ZIF-8 precipitate was not formed with proteins that have a higher isoelectric point (pI) due to negative charge under the basic synthetic condition. In order to form

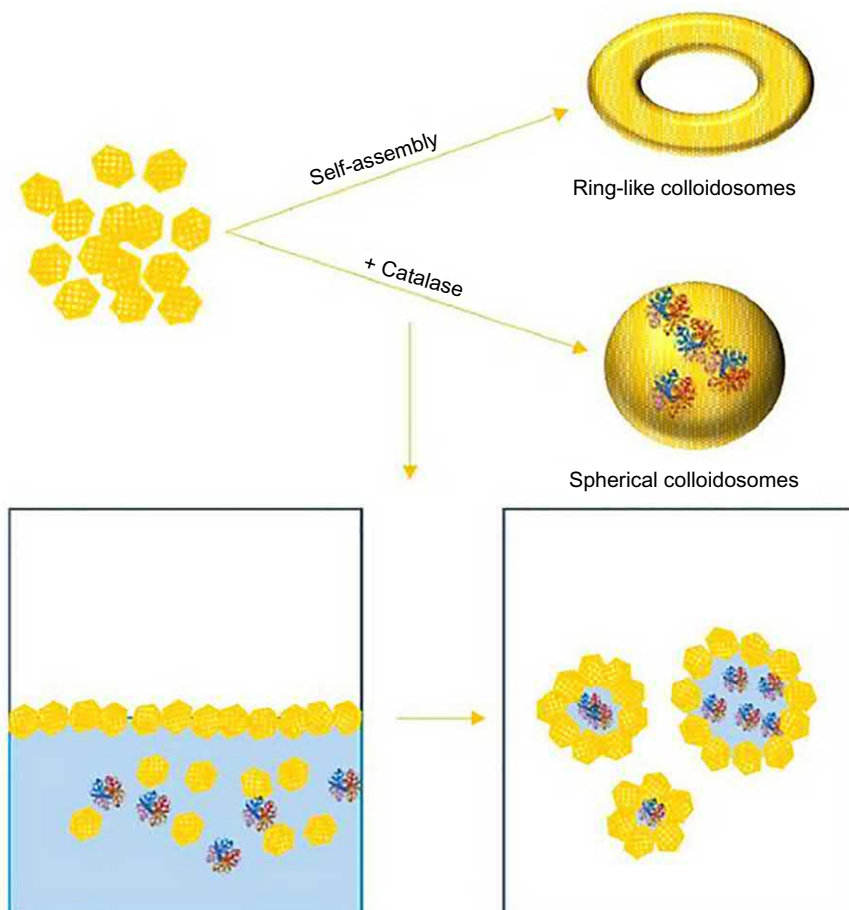


**Fig. 22.9**

Effects of NaCl on the shape and enzyme activity of enzyme@ZIF-8. Reproduced with permission from S. Pu, X. Zhang, C. Yang, S. Naseer, X. Zhang, J. Ouyang, D. Li, J. Yang, *The effects of NaCl on enzyme encapsulation by zeolitic imidazolate frameworks-8*, *Enzym. Microb. Technol.* 122 (2019) 1–6, <https://doi.org/10.1016/j.enzmictec.2018.12.003>. Copyright 2018. Elsevier B.V. All rights reserved.

ZIF-8 with protein with lower pI protein, authors came up with a certain chemical modification of protein to change pI values and surface modification. Therefore, significant detail knowledge regarding interface chemistry of the metal-organic framework is very much required for the development of this area [74].

Apart from the conventional de novo enzyme encapsulation methods, different novel approaches have been proposed by a few scientists to get highly stable hierarchically porous MOF platform for enzymes. Zhu et al. successfully synthesized the facile ring-shaped three-dimensional colloidosomes composed of MOFs via one-step emulsion-based technique for the immobilization of catalase (Fig. 22.10). This ZIF-8 colloidosome was



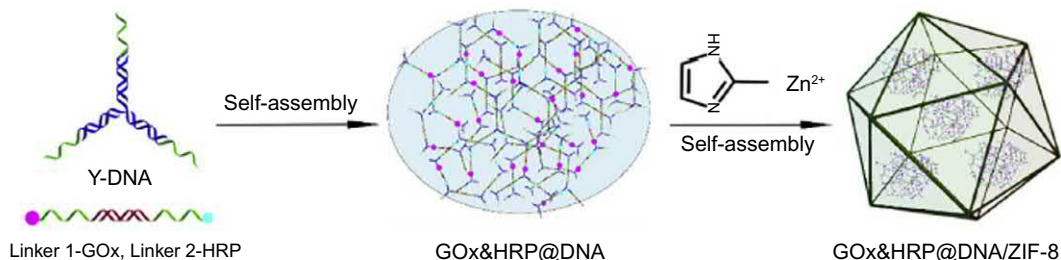
**Fig. 22.10**

Schematic of self-assembly of ring-like ZIF-8 colloidosomes and spherical colloidosomes with encapsulated catalase. *Reproduced with permission from G. Zhu, M. Zhang, Y. Bu, L. Lu, X. Lou, L. Zhu, Enzyme-embedded metal-organic framework colloidosomes via an emulsion-based approach, Chem. Asian J. 13 (2018) 2891–2896, <https://doi.org/10.1002/asia.201800976>. © 2018 WILEY-VCH Verlag GmbH & Co. KGaA, Weinheim.*



used for encapsulating catalase. The catalytic activity, thermal stability, and reusability were determined for immobilized enzyme and compared with the free enzyme. The ZIF-8 colloidosome with embedded catalase retained 44.2% of catalytic activity even after incubation of composite at 65°C for one hour, while free catalase sustained its 6.6% residual of activity. Recyclability study of three-dimensional composite showed 80% of retention in enzyme activity after five cycles [75]. In another strategy, Song et al. [76] introduced DNA as a cross-linker to improve enzymatic activity and overall catalytic efficiency. The cross-linked multienzyme HRP and GOx had been successfully encapsulated into ZIF-8 (Fig. 22.11). The  $K_M$  of encapsulated multienzyme was 0.27-fold lower than those of free enzymes. The immobilized multienzyme exhibited enhanced performance to detect low concentration of glucose (LOD 0.4  $\mu\text{M}$ ) with excellent selectivity [76]. In another example, researchers introduced a novel approach of core-shell nanoparticle (NP)@MOF nanocomposites for enzyme immobilization. NP@MOF nanocomposite was formed by self-organizing lysozyme by coating the surface with various functional groups. Wide variety of functional groups such as  $-\text{COOH}$  and  $-\text{NH}_2$  of enzyme induced the heterogeneous nucleation to form a shell around enzyme molecules. The newly investigated method exhibited profound merits such as easy and mild synthetic conditions, facile interfacial functionalizations, and structural tuning for construction of nanoparticle@MOF nanocomposites [76].

This method allows the enzyme encapsulation which preserves enzyme activity from inhospitable environmental conditions (such as high temperature, wide pH range, and exposure to organic solvents). However, in some of the cases, there is possibility of reduction in biocatalytic activity after immobilization of enzyme due to mass transfer limitation caused by rigid MOF structures and conformational changes of enzyme.



**Fig. 22.11**

Schematic for cross-linking multiple enzymes by Y-scaffold and entrapment in (ZIF-8). Reproduced with permission from J. Song, W. He, H. Shen, Z. Zhou, M. Li, P. Su, Y. Yang, *Construction of multiple enzyme metal-organic frameworks biocatalyst via DNA scaffold: a promising strategy for enzyme encapsulation*, *Chem. Eng. J.* (2019) 174–182, <https://doi.org/10.1016/j.cej.2019.01.138>. Copyright 2019. Elsevier B.V.

All rights reserved.



## 22.4 Characteristics of MOF

### 22.4.1 Catalytic activity

Usually, the enzymes-MOF composites showed profound improvements in catalytic characteristics such as thermal, pH, and chemical stability. Besides, the catalytic activity of enzymes-MOF composites is lower than the free form. The researchers found that the lowering of enzyme activity after immobilization might be due to following two reasons: (i) the conformational changes occurred during process immobilization of enzymes and (ii) the mass transfer restriction resistance by the framework around the enzyme molecules [77].

The researchers have developed a few novel strategies to enhance the enzyme activities after immobilization onto/into MOFs. Gascón et al. prepared GOx-embedded Fe-based MOF under mild conditions. The authors observed that the activity of GOx@MOF was 2.4-folds higher than that of the free form. This enhancement in activity might be due to the presence of Fe<sup>++</sup> ions during the immobilization process [78]. In another example, Shi et al. conjugated lipase onto dopamine surface-modified ZIF-8. The presence of hydrophilic surface led to enhanced catalytic activity as a result of lower diffusion resistances. In another strategy, the low-frequency ultrasound was induced to activate enzyme molecules by changing 3D structure before immobilization [79]. Nadar and Rathod reported a two-step enzyme immobilization strategy. The first step involved activation of lipase enzyme (referred as sonicated lipase), while the second step consisted of the encapsulation of hyperactive lipase within ZIF-8. The secondary structural analysis of lipase before and after immobilization was carried out by FTIR data tools. It was seen that secondary structure of lipase-MOF were retained as same as the sonicated lipase. This result concludes that MOFs with fixed enzyme molecules retain their flexibility within MOF [80].

### 22.4.2 Thermal stability

The free enzymes lose their biocatalytic activity after getting exposed to elevated temperature due to disruption of nonbonding interactions and conformational changes. MOF stabilizes the immobilized enzyme at higher temperatures by providing a protective environment, forming new chemical bonds between enzyme and support. Usually, thermal stability is calculated in terms of inactivation rate constant ( $K_d$ ), half-life ( $t_{1/2}$ ), and deactivation energy ( $E_d$ ) [81]. Salgaonkar et al. investigated encapsulation of the orange peel peroxidase (OPP) in MOF for dye degradation. It was observed that OPP-MOF showed twofold increase in the temperature range of 40–60°C as compared to native form [82].

### 22.4.3 Michealis-Menton kinetics

Affinity of enzymes toward substrate and rate of catalysis determined by kinetic parameters ( $K_m$  and  $V_{max}$ ) of free and immobilized enzymes were recorded [19, 22]. In the enzymatic electrochemical detection, Cyt *c* was embedded within mesoporous and microporous channels

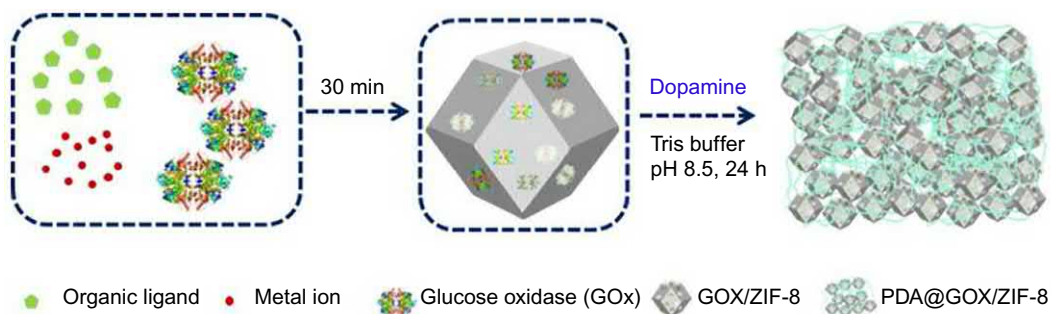
of ZIF. It showed Michealis-Menton ( $K_M$ ) reduced by 50% as compared to native Cyt *c*. The lower value of  $K_M$  is responsible for the higher affinity of substrates and this was the most suitable immobilization strategy for the fabrication of enzyme electrode with high sensitivity. In another example, encapsulation of  $\beta$ -glucosidase in Cu(PABA) showed higher  $K_M$  and  $V_{max}$  values (3.86 mM and 1.48 mM min<sup>-1</sup>) as compared to free  $\beta$ -glucosidase ( $K_M$  2.46 mM and  $V_{max}$  0.64 mM min<sup>-1</sup>). The lowering in  $K_m$  signifies that the affinity toward substrate has been increased. However, due to mass transfer limitations, it showed a decrease in  $V_{max}$  value [63]. Nadar and Rathod investigated that affinity of enzymes for substrates might decrease after immobilization due to localization of enzyme within MOF compartments. This might be due to steric hindrance created by metal framework, which resulted in restriction on the access of substrates [69]. Further, the same researcher group co-immobilized  $\alpha$ -amylase and glucoamylase in ZIF metal-organic framework. They found the same scenario in case of  $K_M$  and  $V_{max}$ . Some of the researchers showed an improved affinity for substrates by enzymes after immobilization such as laccase/Zr MOF, CA/ZIF-8 [62].

#### 22.4.4 Chemical stability

Enzymes undergo denaturation when it exposed to extreme conditions such as higher pH and exposed to organic solvents. A stressful surrounding alters the conformation and active site, which results in obliterated enzymatic activity. Liang et al. investigated the protective environment provided for horseradish peroxidase (HRP) by ZIF-MOF and other porous materials (CaCO<sub>3</sub> and SiO<sub>2</sub>). When ZIF/HRP, CaCO<sub>3</sub>/HRP, and SiO<sub>2</sub>/HRP were incubated at 80°C in a water bath, ZIF/HRP retained 88% activity, while CaCO<sub>3</sub>/HRP and SiO<sub>2</sub>(7 nm)/HRP showed 39% and 65% activity. In another example, covalently immobilized SEH-MOF biocomposite, SEH/UiO-66-NH<sub>2</sub>, maintained their activity up to 60% under extreme pH condition (in the range of 8.5–10.5) compared with free SEH. Also, in the recent study, a PCN-888 mesoporous MOF also showed an enhanced protective effect against trypsin digestion after treating with trypsin for 60 min [67]. Also, hyperhalophilic alcohol dehydrogenase (ADH) enzyme improved its activity against 5 and 10% of organic solvents in the immobilized form. The activity of HvADH2@MOF was highest activity in methanol and acetonitrile solutions [83].

#### 22.4.5 Reusability

For the industrial applications, reusability of enzymes holds prodigious importance. Many researchers have made rigorous effort to improve the recyclability of enzymes for industrial applications [84]. Nadar and Rathod investigated the recyclability of the glucoamylase-embedded MOF. After six cycles, the glucoamylase-MOF retained 57% residual activity. However, enzyme leaching did not occur for the six recycles, which was confirmed by Bradford protein assay [69]. The authors claimed that reduction in activity might be due to loss of low-density MOFs during centrifugation and washing step. In order to overcome the separation of



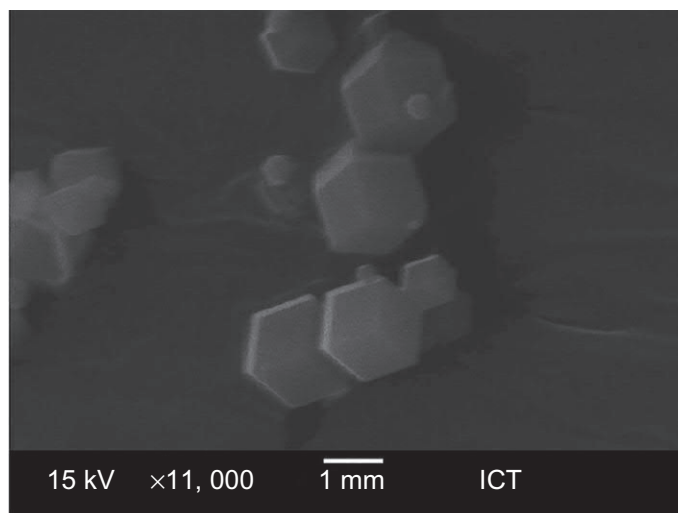
**Fig. 22.12**

Schematic preparation of PDA@GOx/ZIF-8. *Reproduced with permission from X. Wu, C. Yang, J. Ge, Z. Liu, Polydopamine tethered enzyme/metal-organic framework composites with high stability and reusability, Nanoscale 7 (2015) 18883–18886, <https://doi.org/10.1039/c5nr05190h>. The Royal Society of Chemistry.*

enzyme-MOF composite, polymerized dopamine (DPA) was used as adhesive nature to stick organic and inorganic surfaces via covalent bond and noncovalent bonds. Wu et al. proposed polydopamine as a cross-linker to tethered GOx/ZIF MOF. The GOx/ZIF was synthesized by adding dopamine and kept for 24 h. The polymerization of dopamine led to formation of micro-sized agglomeration (Fig. 22.12). Larger size of PDA@GOx/ZIF had shown a prodigious effect on reusability of enzyme-MOF. Over the 10 cycles of reuse, PDA@GOx/ZIF showed almost the same activity as that of original activity, while conventional GOx/ZIF showed 70% reduction in activity over 2 cycles of use [35, 85].

#### 22.4.6 Storage stability

Over the course of study of enzyme, it was followed that the long-term stability had been a major issue in case of free native enzymes. Researchers have developed reliable biocatalysts, which overcome this issue by localization of enzyme in the protective microenvironment [86]. Salgaonkar et al. studied the storage stability of peroxidase by immobilizing orange peel peroxidase; OPP-MOF showed better chemical and conformational stability even after 18 days of storage, which was confirmed by the SEM image of OPP-embedded MOF (Fig. 22.13). They have illustrated no distortion of the active sites of OPP-embedded MOF after a long duration of storage. Residual activity of OPP-MOF (88%) was higher as compared to free native (47%) [82]. In similar studies, Pang et al. (2016) carried out an experiment in which laccase was immobilized on mesoporous Zr-MOF. Laccase@Zr-MOF showed 50% retention of its activity even after continuous use up to 10 times and observed efficient storage stability till 3 weeks in aqueous phase by maintaining its activity to 55.4% of its initial enzyme activity [41].



**Fig. 22.13**

SEM images of OPP-MOF after 18 days of storage. *Reproduced with permission from M. Salgaonkar, S.S. Nadar, V.K. Rathod, Biomineralization of orange peel peroxidase within metal organic frameworks (OPP-MOFs) for dye degradation, J. Environ. Chem. Eng. 7 (2019) 102969, <https://doi.org/10.1016/J.JECE.2019.102969>. Copyright 2019. Elsevier B.V. All rights reserved.*

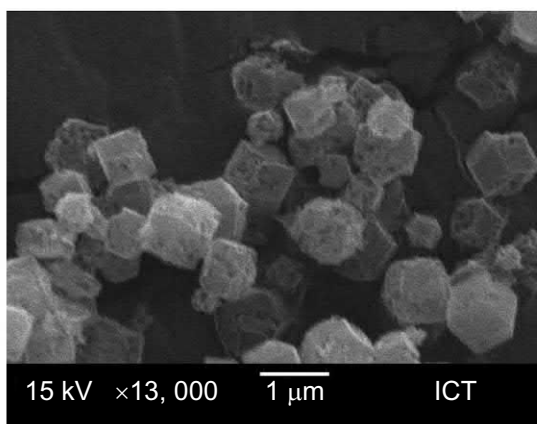
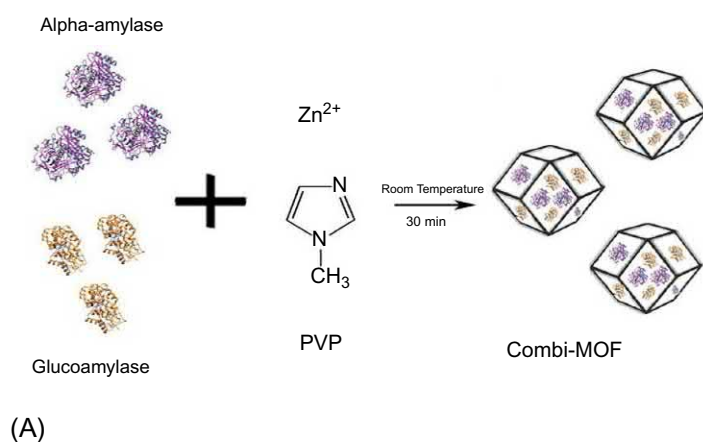
## 22.5 Multienzyme MOF composites

Recently, extensive research has been conducted on biocatalytic techniques for the synthesis of a large range of good chemicals. In the traditional approach, multistep fine chemical reactions are carried out in separate stages [87]. In this process, the intermediate product acts as a substrate for the next step of reactions; thus, the product has been purified. Such conventional synthetic approach requires a high cost of operation with low-value products and low yield with large use of hazardous chemicals. These synthetic processes can be efficiently modified by combining multistep reaction processes into a single step with the help of co-immobilized catalytic system [19, 88]. The intermediate product of reaction rapidly goes to the next available active site of multienzyme system to the next reaction. This helps in the formation of single step facile reaction instead of multistage reaction with eliminating the issue of separation of intermediate. These cascading enzymatic reactions have several merits such as less use of solvent, small time of reaction, less volume of the reactor, space time yields with the huge advantage of less generation of hazardous waste concerning green environmental practices as well as human benefits [86].

In pioneered work, Lian et al. employed MOF with different pore sizes for immobilization of horse radish peroxidase (HRP) and glucose oxidase (GOx). Authors have prepared PCN-888 with cages size of 2.0, 5.0, and 6.2 nm. It showed that large cavity (6.2 nm) was accommodated by

GOx, while intermediate cavity (5.0 nm) was occupied by HRP. It also showed that the coupling of two enzymes could only be achieved by the unique sequential coupling GOx followed by HRP. It showed high catalytic activity with minimum leaching of enzymes. Also, the multienzyme system maintained their activity over four cycles without significant loss in activity [89].

In another approach, multienzyme-embedded MOF readily prepared through a biomineralization process in aqueous solution with mild reaction conditions. Nadar et al. investigated the combi-MOF encapsulated with  $\alpha$ -amylase and glucoamylase for the hydrolysis of starch. In the experimental procedure, two enzyme solutions were mixed with zinc acetate and 2-methylimidazole in the presence of PVP as stabilizing agent (Fig. 22.14A). In comparison with the free native form of enzyme, the thermal stability was calculated as a



**Fig. 22.14**

Schematic representation of (A) Combi-metal organic frameworks (combi-MOF) of  $\alpha$ -amylase and glucoamylase (B) scanning electron microscopic (SEM) image of combi-MOF calcinated at 420°C for 2 h. Reproduced with permission from M. Salgaonkar, S.S. Nadar, V.K. Rathod, Combi-metal organic framework (Combi-MOF) of  $\alpha$ -amylase and glucoamylase for one pot starch hydrolysis, *Int. J. Biol. Macromol.* 113 (2018) 464–475, <https://doi.org/10.1016/j.IJBIOMAC.2018.02.092>. Copyright 2018. Elsevier B.V. All rights reserved.

half-life, which showed approx. three-fold enhanced thermal stability in the temperature range of 55–75°C. The surface structure of combi-MOF after calcination was characterized by SEM (Fig. 22.14B). Interestingly, it was observed that the surface of combi-MOF possessed small pore size (5 to 20 nm), which was evident in the presence of enzyme molecule on the surface of combi-MOF [62]. Similarly, Wu et al. reported the one-step aqueous preparation of multiple enzymes containing ZIF-8 as a protective structure containing HRP and GOx. This enzyme-MOF matrix was used for the selective and quantitative analysis of glucose. The facile synthetic process of biomineralization is appealing for fabricating various types of multienzyme MOF system for applications in industrial biocatalysis, biosensors, and biomedical engineering [64].

## **22.6 Magnetic MOF-enzyme composite**

Although MOF platform improves catalytic properties such as activity and thermal and chemical stability of immobilized enzyme, its nanometric size makes the separation of enzyme-MOF composite very complex which hurdles the reusability of biocatalyst. Considering this barrier, the researchers came up with a novel strategy in which magnetic nanoparticles were embedded within enzyme-MOF composite (magnetic-enzyme MOF). The incorporation of magnetic nanoparticle makes these composites magnetically active without changing its intrinsic properties of MOF. These multifunctional magnetic-MOFs exhibit some distinctive properties such as large surface area, high enzyme loading, and easy separation [90].

The enzyme can be immobilized either by one-pot in situ immobilization technique or by chemical/physical binding onto presynthesized magnetic-MOF. There are three immobilization strategies: (i) physical binding, (ii) covalent/coordination bonding, and (iii) de novo encapsulation method. The list of different enzymes immobilized onto magnetic-MOF is summarized in Table 22.5.

Physical adsorption of enzyme onto/into magnetic-MOF is cost-efficient, facile, and comprehensively used for immobilization. The surface area, pore volume/size, and surface functional groups play an important role for enzyme immobilization onto MOF. Also, various forces such as hydrophilic/hydrophobic and electrostatic interactions between magnetic MOF and enzyme hinder the leaching of enzyme during reaction [67]. Considering this fact, Huo and group developed Zn-based magnetic-MOFs made up of PDA-ZIF-90 incorporated with magnetic nanoparticles for immobilization of trypsin. Magnetic ZIF-90 was synthesized in two steps: (i) Functionalization of magnetic nanoparticle by polydopamine (PDA) as a hydrophilic medium to preserve the enzyme activity and (ii) The outer shell of 2-methylimidazole build around pickering-stabilized hydrogel magnetic core (Fig. 22.15). Further, the activity of the immobilized trypsin was determined by using BSA protein. It was observed that the activity of trypsin was enhanced due to allosteric effect, which efficiently digests BSA within a minute. In contrast, the free enzyme showed slower digestion as compared to immobilized trypsin [95].



Table 22.5: Enzyme immobilization by using various magnetic-MOFs.

| Metal            | Ligand               | Coating agent | Enzyme                       | Mode of immobilization | Refs. |
|------------------|----------------------|---------------|------------------------------|------------------------|-------|
| Zn <sup>2+</sup> | 2-methylimidazole    | Citric acid   | GOx                          | Biomineralization      | [91]  |
| Fe <sup>3+</sup> | H <sub>3</sub> BTC   | EDTA-2Na      | Lipase                       | Metal-ion affinity     | [92]  |
| Fe <sup>3+</sup> | H <sub>3</sub> BTC   | EDTA-2Na      | Lipase                       | Covalent binding       | [92]  |
| Fe <sup>3+</sup> | NH <sub>2</sub> -BDC | –             | <i>Candida rugosa</i> lipase | Physical adsorption    | [93]  |
| Zr <sup>4+</sup> | H <sub>2</sub> BDC   | Agarose       | CalB lipase and trypsin      | Physical adsorption    | [94]  |
| Cu <sup>2+</sup> | H <sub>3</sub> BTC   | Dopamine      | Trypsin                      | Physical adsorption    | [95]  |
| Fe <sup>3+</sup> | H <sub>3</sub> BTC   | Citric acid   | Cholesterol oxidase          | Physical adsorption    | [96]  |

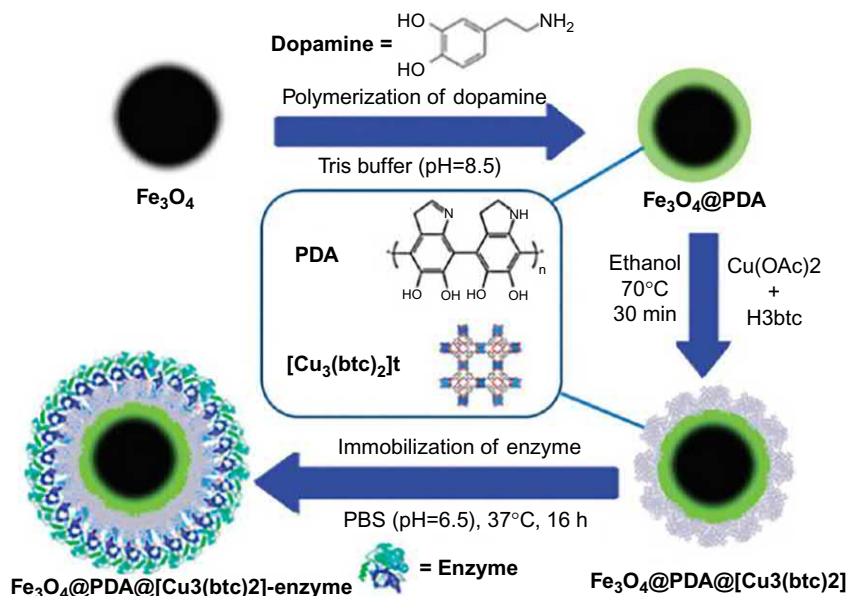


Fig. 22.15

The synthetic route to Fe<sub>3</sub>O<sub>4</sub>@PDA on Cu-based microspheres and the procedure for enzyme immobilization. Reproduced with permission from M. Zhao, X. Zhang, C. Deng, *Rational synthesis of novel recyclable Fe<sub>3</sub>O<sub>4</sub>@MOF nanocomposites for enzymatic digestion*, *Chem. Commun.* 51 (2015) 8116–8119, <https://doi.org/10.1039/c5cc01908g>. Copyright 2015. The Royal Society of Chemistry.

Generally, in physical adsorption-based immobilization technique, there is a high possibility of enzyme leaching out due to weak interaction between the support material and enzyme molecules. It causes not only loss of enzyme in reaction mixture, but also increases the cost of product purification. This can be overcome by covalent binding of enzyme molecules with MOF supports, which can improve the catalytic efficiency attributed to multipoint stabilization [32]. Also, this methodology improves reusability performance due to chemical bonding with support [97]. Mostly, MOF surface is functionalized with reactive groups (for example  $-\text{COOH}$ ,  $-\text{NH}_2$ ,  $-\text{OH}$  groups, etc.), which can be easily coupled with amino/carboxyl group on the enzyme's surface [98].

Recently, Samui and coresearchers prepared functionalized magnetically active  $\text{NH}_2\text{-MIL-88B}$  by solvothermal method. The surface functional groups were further chemically activated by *N*-(3-dimethylaminopropyl)-*N*-ethylcarbodiimide hydrochloride (EDC). The chemically functionalized magnetic-MOF allows lipase molecules to bind via covalent bonds (Fig. 22.16). The immobilization yield of lipase on magnetic-MOFs was  $280 \text{ mg g}^{-1}$  with the activity recovery of 86%. The morphology of magnetic MOF was found to be bipyramidal hexagonal prism-like

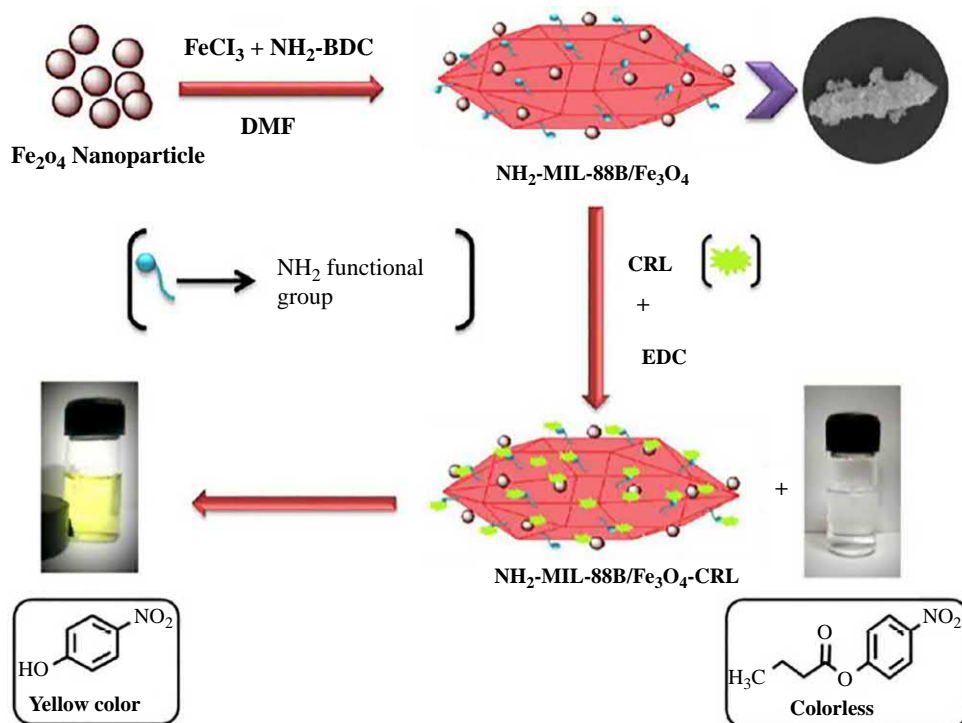


Fig. 22.16

The schematic representation of immobilization of lipase onto  $\text{NH}_2\text{-MIL-88B/Fe}_3\text{O}_4$ . Reproduced with permission from A. Samui, A.R. Chowdhuri, T.K. Mahto, S.K. Sahu, Fabrication of a magnetic nanoparticle embedded  $\text{NH}_2\text{-MIL-88B}$  MOF hybrid for highly efficient covalent immobilization of lipase, *RSC Adv.* 6 (2016) 66385–66393, <https://doi.org/10.1039/c6ra10885g>. Copyright 2016. The Royal Society of Chemistry.

structure with the average size of 80 nm. Further, pH (6–9) and thermal (30–60°C) stability of immobilized lipase was found to be enhanced as compared to free form. At the end, immobilized lipase retains nearly 84% residual activity after 5th cycle of reuse in batch mode [93].

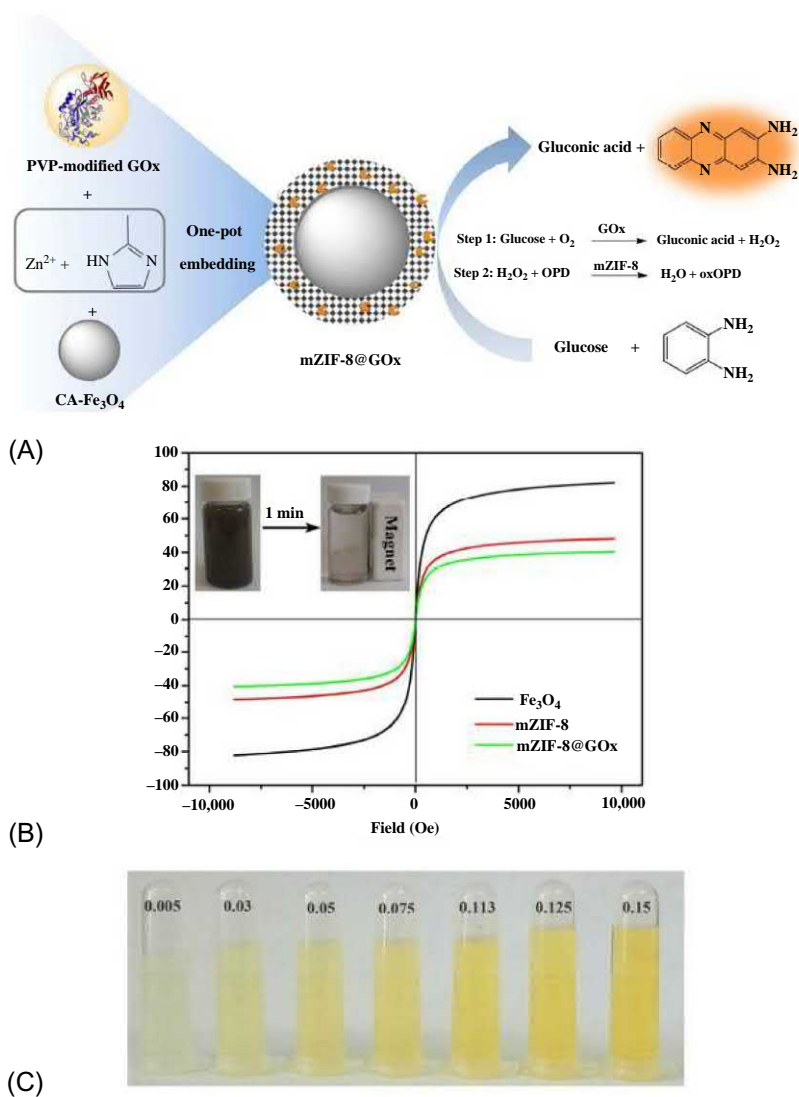


Fig. 22.17

Schematic illustration of mechanism of glucose detection by GOx-embedded mZIF-8 (A), (B) hysteresis loops of Fe<sub>3</sub>O<sub>4</sub>, mZIF-8, and mZIF-8@GOx and magnetic separation of magnetic-MOF biocatalyst (inset). (C) Colorimetric change of OPD solutions containing mZIF-8@GOx with respect to glucose concentration. Reproduced with permission from C. Hou, Y. Wang, Q. Ding, L. Jiang, M. Li, W. Zhu, D. Pan, H. Zhu, M. Liu, Facile synthesis of enzyme-embedded magnetic metal-organic frameworks as a reusable mimic multi-enzyme system: mimetic peroxidase properties and colorimetric sensor, *Nanoscale* 7 (2015) 18770–18779, <https://doi.org/10.1039/c5nr04994f>.

The postsynthetic immobilization approaches, i.e., physical adsorption or covalent binding, require the presynthesized magnetic-MOF. During immobilization, enzyme molecules directly bind into MOF pores, where they prevent the immobilization due to vast size of enzyme compared to the much smaller pore size of MOFs. Sometimes, enzyme may undergo structural changes which would suffer from lower catalytic activity [99]. Hence, Hou and his colleague developed a novel strategy based on the biomineralization. They have entrapped enzyme molecules within the MOF by a simple de novo approach without affecting the intrinsic properties of MOF. In this protocol, enzyme and MOF precursors along with carboxy functionalized magnetic nanoparticles were stirred together in solution, which resulted in the formation of magnetic-enzyme MOF composite. The mild synthetic condition is the major advantage of de novo method to conserve catalytically active structure of enzyme [89, 100].

Hou and coworkers introduced the novel de novo encapsulation strategy for enzyme immobilization along with magnetic nanoparticles within MOF. In this method, simultaneous immobilization of glucose oxidase (GOx) and magnetic nanoparticles (as an artificial peroxidase enzyme) into MOF was performed in a single step. The immobilization process is illustrated in Fig. 22.17. The prepared magnetic biocatalyst exhibited excellent pH and thermal stability. Further, it was used for rapid colorimetric detection of glucose. It showed linear correlation of glucose in the range of 5.0 to 150.0  $\mu\text{M}$  with a limit of detection (LOD) of 1.9  $\mu\text{M}$ . Finally, the residual activity remained unchanged even after twelve successive cycles, which emphasized its robustness. Hierarchical channel-type MOFs with pores can protect the enzyme even under harsh conditions [91]. An excellent and magnificent improvement in catalytic efficacy, exceptional chemical/thermal stability, facile accessibility to active sites, encouraging recyclability, and high enzyme loading are fascinating features of enzyme-MOF composites.

## References

- [1] A.A. Homaei, R. Sariri, F. Vianello, R. Stevanato, Enzyme immobilization: an update, *J. Chem. Biol.* 6 (2013) 185–205, <https://doi.org/10.1007/s12154-013-0102-9>.
- [2] M.B. Anson-Schumacher, O. Thum, Immobilised lipases in the cosmetics industry, *Chem. Soc. Rev.* 42 (2013) 6475–6490, <https://doi.org/10.1039/c3cs35484a>.
- [3] P. Adlercreutz, Immobilisation and application of lipases in organic media, *Chem. Soc. Rev.* 42 (2013) 6406–6436, <https://doi.org/10.1039/c3cs35446f>.
- [4] O. Kirk, T.V. Borchert, C.C. Fuglsang, Industrial enzyme applications, *Curr. Opin. Biotechnol.* 13 (2002) 345–351, [https://doi.org/10.1016/S0958-1669\(02\)00328-2](https://doi.org/10.1016/S0958-1669(02)00328-2).
- [5] S.S. Nadar, N.V. O, S. Suresh, P. Rao, D.J. Ahirrao, S. Adsare, Recent progress in nanostructured magnetic framework composites (MFCs): synthesis and applications, *J. Taiwan Inst. Chem. Eng.* 91 (2018) 653–677, <https://doi.org/10.1016/J.JTICE.2018.06.029>.
- [6] E. Magner, Immobilisation of enzymes on mesoporous silicate materials, *Chem. Soc. Rev.* 42 (2013) 6213–6222, <https://doi.org/10.1039/c2cs35450k>.
- [7] N. Miletić, A. Nastasović, K. Loos, Immobilization of biocatalysts for enzymatic polymerizations: possibilities, advantages, applications, *Bioresour. Technol.* 115 (2012) 126–135, <https://doi.org/10.1016/j.biortech.2011.11.054>.

- [8] D.N. Tran, K.J. Balkus, Perspective of recent progress in immobilization of enzymes, *ACS Catal.* 1 (2011) 956–968, <https://doi.org/10.1021/cs200124a>.
- [9] A.S. Bommarius, M.F. Paye, Stabilizing biocatalysts, *Chem. Soc. Rev.* 42 (2013) 6534–6565, <https://doi.org/10.1039/c3cs60137d>.
- [10] T. Xie, A. Wang, L. Huang, H. Li, Z. Chen, Q. Wang, Recent advance in the support and technology used in enzyme immobilization, *Afr. J. Biotechnol.* 8 (2009) 4724–4733.
- [11] Z. Zhou, M. Hartmann, Recent progress in biocatalysis with enzymes immobilized on mesoporous hosts, *Top. Catal.* 55 (2012) 1081–1100, <https://doi.org/10.1007/s11244-012-9905-0>.
- [12] R.A. Sheldon, Enzyme immobilization: the quest for optimum performance, *Adv. Synth. Catal.* 349 (2007) 1289–1307, <https://doi.org/10.1002/adsc.200700082>.
- [13] R.A. Sheldon, S. Van Pelt, Enzyme immobilisation in biocatalysis: why, what and how, *Chem. Soc. Rev.* 42 (2013) 6223–6235, <https://doi.org/10.1039/c3cs60075k>.
- [14] J. Zdarta, A. Meyer, T. Jesionowski, M. Pinelo, A general overview of support materials for enzyme immobilization: characteristics, properties, practical utility, *Catalysts* 8 (2018) 92, <https://doi.org/10.3390/catal8020092>.
- [15] D. Brady, J. Jordaan, Advances in enzyme immobilisation, *Biotechnol. Lett.* 31 (2009) 1639–1650, <https://doi.org/10.1007/s10529-009-0076-4>.
- [16] S. Cao, P. Xu, Y. Ma, X. Yao, Y. Yao, M. Zong, X. Li, W. Lou, Recent advances in immobilized enzymes on nanocarriers, *Cuihua Xuebao/Chinese J. Catal.* 37 (2016) 1814–1823, [https://doi.org/10.1016/S1872-2067\(16\)62528-7](https://doi.org/10.1016/S1872-2067(16)62528-7).
- [17] M. Hartmann, X. Kostrov, Immobilization of enzymes on porous silicas—benefits and challenges, *Chem. Soc. Rev.* 42 (2013) 6277–6289, <https://doi.org/10.1039/c3cs60021a>.
- [18] S.S. Nadar, V.K. Rathod, A co-immobilization of pectinase and cellulase onto magnetic nanoparticles for antioxidant extraction from waste fruit peels, *Biocatal. Agric. Biotechnol.* 17 (2019) 470–479, <https://doi.org/10.1016/j.cbab.2018.12.015>.
- [19] S. Talekar, V. Ghodake, T. Ghotage, P. Rathod, P. Deshmukh, S. Nadar, M. Mulla, M. Ladole, Novel magnetic cross-linked enzyme aggregates (magnetic CLEAs) of alpha amylase, *Bioresour. Technol.* 123 (2012) 542–547, <https://doi.org/10.1016/j.biortech.2012.07.044>.
- [20] H.L. Jiang, Q. Xu, Porous metal-organic frameworks as platforms for functional applications, *Chem. Commun.* 47 (2011) 3351–3370, <https://doi.org/10.1039/c0cc05419d>.
- [21] J. Mehta, N. Bhardwaj, S.K. Bhardwaj, K.H. Kim, A. Deep, Recent advances in enzyme immobilization techniques: metal-organic frameworks as novel substrates, *Coord. Chem. Rev.* 322 (2016) 30–40, <https://doi.org/10.1016/j.ccr.2016.05.007>.
- [22] S.S. Nadar, R.G. Pawar, V.K. Rathod, Recent advances in enzyme extraction strategies: a comprehensive review, *Int. J. Biol. Macromol.* 101 (2017) 931–957, <https://doi.org/10.1016/j.ijbiomac.2017.03.055>.
- [23] H. Cai, Y.L. Huang, D. Li, Biological metal-organic frameworks: structures, host-guest chemistry and bio-applications, *Coord. Chem. Rev.* 378 (2019) 207–221, <https://doi.org/10.1016/j.ccr.2017.12.003>.
- [24] P. Falcaro, R. Ricco, A. Yazdi, I. Imaz, S. Furukawa, D. MasPOCH, R. Ameloot, J.D. Evans, C. J. Doonan, Application of metal and metal oxide nanoparticles at MOFs, *Coord. Chem. Rev.* 307 (2016) 237–254, <https://doi.org/10.1016/j.ccr.2015.08.002>.
- [25] J.C. Lloyd, E.M. Masko, C. Wu, M.M. Keenan, D.M. Pilla, W.J. Aronson, J.T. Chi, S.J. Freedland, Fish oil slows prostate cancer xenograft growth relative to other dietary fats and is associated with decreased mitochondrial and insulin pathway gene expression, *Prostate Cancer Prostatic Dis.* 16 (2013) 285–291, <https://doi.org/10.1038/pcan.2013.19>.
- [26] M. Eddaoudi, D.F. Sava, J.F. Eubank, K. Adil, V. Guillerme, Zeolite-like metal-organic frameworks (ZMOFs): design, synthesis, and properties, *Chem. Soc. Rev.* 44 (2015) 228–249, <https://doi.org/10.1039/c4cs00230j>.
- [27] B. Chen, Z. Yang, Y. Zhu, Y. Xia, Zeolitic imidazolate framework materials: recent progress in synthesis and applications, *J. Mater. Chem. A* 2 (2014) 16811–16831, <https://doi.org/10.1039/c4ta02984d>.
- [28] Y.R. Lee, J. Kim, W.S. Ahn, Synthesis of metal-organic frameworks: a mini review, *Korean J. Chem. Eng.* 30 (2013) 1667–1680, <https://doi.org/10.1007/s11814-013-0140-6>.

- [29] X. Lian, Y. Fang, E. Joseph, Q. Wang, J. Li, S. Banerjee, C. Lollar, X. Wang, H.-C. Zhou, Enzyme–MOF (metal–organic framework) composites, *Chem. Soc. Rev.* 46 (2017) 3386–3401, <https://doi.org/10.1039/C7CS00058H>.
- [30] S. Kempahanumakkagari, V. Kumar, P. Samaddar, P. Kumar, T. Ramakrishnappa, K.H. Kim, Biomolecule-embedded metal-organic frameworks as an innovative sensing platform, *Biotechnol. Adv.* 36 (2018) 467–481, <https://doi.org/10.1016/j.biotechadv.2018.01.014>.
- [31] M.B. Majewski, A.J. Howarth, P. Li, M.R. Wasielewski, J.T. Hupp, O.K. Farha, Enzyme encapsulation in metal–organic frameworks for applications in catalysis, *CrystEngComm* 19 (2017) 4082–4091, <https://doi.org/10.1039/C7CE00022G>.
- [32] D.S. Raja, W.L. Liu, H.Y. Huang, C.H. Lin, Immobilization of protein on nanoporous metal-organic framework materials, *Comments Inorg. Chem.* 35 (2015) 332–350, <https://doi.org/10.1080/02603594.2015.1059827>.
- [33] Y. Hu, L. Dai, D. Liu, W. Du, Y. Wang, Progress & prospect of metal-organic frameworks (MOFs) for enzyme immobilization (enzyme/MOFs), *Renew. Sust. Energ. Rev.* 91 (2018) 793–801, <https://doi.org/10.1016/j.rser.2018.04.103>.
- [34] P. Li, J.A. Modica, A.J. Howarth, E. Vargas L, P.Z. Moghadam, R.Q. Snurr, M. Mrksich, J.T. Hupp, O.K. Farha, Toward design rules for enzyme immobilization in hierarchical mesoporous metal-organic frameworks, *Chem* 1 (2016) 154–169, <https://doi.org/10.1016/j.chempr.2016.05.001>.
- [35] W. Liu, S. Lo, B. Singco, C. Yang, H. Huang, C. Lin, Novel trypsin–FITC@ MOF bioreactor efficiently catalyzes protein digestion, *J. Mater.* 1 (2013) 928–932, <https://doi.org/10.1039/c3tb00257h>.
- [36] W.L. Liu, C.Y. Wu, C.Y. Chen, B. Singco, C.H. Lin, H.Y. Huang, Fast multipoint immobilized MOF bioreactor, *Chem. Eur. J.* 20 (2014) 8923–8928, <https://doi.org/10.1002/chem.201400270>.
- [37] N. Nobakht, M.A. Faramarzi, A. Shafiee, M. Khoobi, E. Rafiee, Polyoxometalate-metal organic framework-lipase: an efficient green catalyst for synthesis of benzyl cinnamate by enzymatic esterification of cinnamic acid, *Int. J. Biol. Macromol.* 113 (2018) 8–19, <https://doi.org/10.1016/j.ijbiomac.2018.02.023>.
- [38] Y. Cao, Z. Wu, T. Wang, Y. Xiao, Q. Huo, Y. Liu, Immobilization of: *Bacillus subtilis* lipase on a Cu-BTC based hierarchically porous metal-organic framework material: a biocatalyst for esterification, *Dalton Trans.* 45 (2016) 6998–7003, <https://doi.org/10.1039/c6dt00677a>.
- [39] W. Ma, Q. Jiang, P. Yu, L. Yang, L. Mao, Zeolitic imidazolate framework-based electrochemical biosensor for in vivo electrochemical measurements, *Anal. Chem.* 85 (2013) 7550–7557, <https://doi.org/10.1021/ac401576u>.
- [40] Z. Zhong, S. Pang, Y. Wu, S. Jiang, J. Ouyang, Synthesis and characterization of mesoporous Cu–MOF for laccase immobilization, *J. Chem. Technol. Biotechnol.* 92 (2017) 1841–1847, <https://doi.org/10.1002/jctb.5189>.
- [41] S. Pang, Y. Wu, X. Zhang, B. Li, J. Ouyang, M. Ding, Immobilization of laccase via adsorption onto bimodal mesoporous Zr-MOF, *Process Biochem.* 51 (2016) 229–239, <https://doi.org/10.1016/j.procbio.2015.11.033>.
- [42] S. Patra, T. Hidalgo Crespo, A. Permyakova, C. Sicard, C. Serre, A. Chaussé, N. Steunou, L. Legrand, Design of metal organic framework-enzyme based bioelectrodes as a novel and highly sensitive biosensing platform, *J. Mater. Chem. B* 3 (2015) 8983–8992, <https://doi.org/10.1039/c5tb01412c>.
- [43] Q. Qiu, H. Chen, Y. Wang, Y. Ying, Recent advances in the rational synthesis and sensing applications of metal-organic framework biocomposites, *Coord. Chem. Rev.* 387 (2019) 60–78, <https://doi.org/10.1016/j.ccr.2019.02.009>.
- [44] S. Patra, S. Sene, C. Mousty, C. Serre, A. Chaussé, L. Legrand, N. Steunou, Design of laccase-metal organic framework-based bioelectrodes for biocatalytic oxygen reduction reaction, *ACS Appl. Mater. Interfaces* 8 (2016) 20012–20022, <https://doi.org/10.1021/acsami.6b05289>.
- [45] V. Gascón, E. Castro-Miguel, M. Díaz-García, R.M. Blanco, M. Sanchez-Sanchez, *In situ* and post-synthesis immobilization of enzymes on nanocrystalline MOF platforms to yield active biocatalysts, *J. Chem. Technol. Biotechnol.* 92 (2017) 2583–2593, <https://doi.org/10.1002/jctb.5274>.



- [46] S.S. Nadar, S.D. Gawas, V.K. Rathod, Self-assembled organic–inorganic hybrid glucoamylase nanoflowers with enhanced activity and stability, *Int. J. Biol. Macromol.* 92 (2016) 660–669, <https://doi.org/10.1016/j.ijbiomac.2016.06.071>.
- [47] G. Liu, Y. Xu, Y. Han, J. Wu, J. Xu, H. Meng, X. Zhang, Immobilization of lysozyme proteins on a hierarchical zeolitic imidazolate framework (ZIF-8), *Dalton Trans.* 46 (2017) 2114–2121, <https://doi.org/10.1039/c6dt04582k>.
- [48] J. Cui, S. Ren, B. Sun, S. Jia, Optimization protocols and improved strategies for metal-organic frameworks for immobilizing enzymes: current development and future challenges, *Coord. Chem. Rev.* 370 (2018) 22–41, <https://doi.org/10.1016/j.ccr.2018.05.004>.
- [49] T.J. Pisklak, M. Macías, D.H. Coutinho, R.S. Huang, K.J. Balkus, Hybrid materials for immobilization of MP-11 catalyst, *Top. Catal.* 38 (2006) 269–278, <https://doi.org/10.1007/s11244-006-0025-6>.
- [50] P. Li, S.Y. Moon, M.A. Guelta, S.P. Harvey, J.T. Hupp, O.K. Farha, Encapsulation of a nerve agent detoxifying enzyme by a mesoporous zirconium metal-organic framework engenders thermal and long-term stability, *J. Am. Chem. Soc.* 138 (2016) 8052–8055, <https://doi.org/10.1021/jacs.6b03673>.
- [51] K. Wang, N. Li, X. Hai, F. Dang, Lysozyme-mediated fabrication of well-defined core-shell nanoparticle@metal-organic framework nanocomposites, *J. Mater. Chem. A* 5 (2017) 20765–20770, <https://doi.org/10.1039/c7ta06419e>.
- [52] Y. Du, J. Gao, L. Zhou, L. Ma, Y. He, X. Zheng, Z. Huang, Y. Jiang, MOF-based nanotubes to hollow nanospheres through protein-induced soft-templating pathways, *Adv. Sci.* 6 (2019) 6–11, <https://doi.org/10.1002/advs.201801684>.
- [53] S. Jung, Y. Kim, S.J. Kim, T.H. Kwon, S. Huh, S. Park, Bio-functionalization of metal-organic frameworks by covalent protein conjugation, *Chem. Commun.* 47 (2011) 2904–2906, <https://doi.org/10.1039/c0cc03288c>.
- [54] S.L. Cao, D.M. Yue, X.H. Li, T.J. Smith, N. Li, M.H. Zong, H. Wu, Y.Z. Ma, W.Y. Lou, Novel nano-/micro-biocatalyst: soybean epoxide hydrolase immobilized on UiO-66-NH<sub>2</sub> MOF for efficient biosynthesis of enantiopure (R)-1, 2-octanediol in deep eutectic solvents, *ACS Sustain. Chem. Eng.* 4 (2016) 3586–3595, <https://doi.org/10.1021/acssuschemeng.6b00777>.
- [55] L. Wen, A. Gao, Y. Cao, F. Svec, T. Tan, Y. Lv, Layer-by-layer assembly of metal-organic frameworks in macroporous polymer monolith and their use for enzyme immobilization, *Macromol. Rapid Commun.* 37 (2016) 551–557, <https://doi.org/10.1002/marc.201500705>.
- [56] Y.H. Shih, S.H. Lo, N.S. Yang, B. Singco, Y.J. Cheng, C.Y. Wu, I.H. Chang, H.Y. Huang, C.H. Lin, Trypsin-immobilized metal-organic framework as a biocatalyst in proteomics analysis, *ChemPlusChem* 77 (2012) 982–986, <https://doi.org/10.1002/cplu.201200186>.
- [57] C. Zhang, X. Wang, M. Hou, X. Li, X. Wu, J. Ge, Immobilization on metal-organic framework engenders high sensitivity for enzymatic electrochemical detection, *ACS Appl. Mater. Interfaces* 9 (2017) 13831–13836, <https://doi.org/10.1021/acsami.7b02803>.
- [58] F.K. Shieh, S.C. Wang, C.I. Yen, C.C. Wu, S. Dutta, L.Y. Chou, J.V. Morabito, P. Hu, M.H. Hsu, K.C. W. Wu, C.K. Tsung, Imparting functionality to biocatalysts via embedding enzymes into nanoporous materials by a de novo approach: size-selective sheltering of catalase in metal-organic framework microcrystals, *J. Am. Chem. Soc.* 137 (2015) 4276–4279, <https://doi.org/10.1021/ja513058h>.
- [59] F. Lyu, Y. Zhang, R.N. Zare, J. Ge, Z. Liu, One-pot synthesis of protein-embedded metal-organic frameworks with enhanced biological activities—supporting information, *Nano Lett.* 14 (2014) 5761–5765, <https://doi.org/10.1021/nl5026419>.
- [60] F.S. Liao, W.S. Lo, Y.S. Hsu, C.C. Wu, S.C. Wang, F.K. Shieh, J.V. Morabito, L.Y. Chou, K.C.W. Wu, C. K. Tsung, Shielding against unfolding by embedding enzymes in metal-organic frameworks via a de novo approach, *J. Am. Chem. Soc.* 139 (2017) 6530–6533, <https://doi.org/10.1021/jacs.7b01794>.
- [61] P. Chulkaivalsucharit, X. Wu, J. Ge, Synthesis of enzyme-embedded metal-organic framework nanocrystals in reverse micelles, *RSC Adv.* 5 (2015) 101293–101296, <https://doi.org/10.1039/c5ra21069k>.
- [62] M. Salgaonkar, S.S. Nadar, V.K. Rathod, Combi-metal organic framework (Combi-MOF) of  $\alpha$ -amylase and glucoamylase for one pot starch hydrolysis, *Int. J. Biol. Macromol.* 113 (2018) 464–475, <https://doi.org/10.1016/j.IJBIOMAC.2018.02.092>.

- [63] L. Wang, W. Zhi, J. Wan, J. Han, C. Li, Y. Wang, Recyclable  $\beta$ -glucosidase by one-pot encapsulation with Cu-MOFs for enhanced hydrolysis of cellulose to glucose, *ACS Sustain. Chem. Eng.* 7 (2019) 3339–3348, <https://doi.org/10.1021/acssuschemeng.8b05489>.
- [64] X. Wu, J. Ge, C. Yang, M. Hou, Z. Liu, Facile synthesis of multiple enzyme-containing metal-organic frameworks in a biomolecule-friendly environment, *Chem. Commun.* 51 (2015) 13408–13411, <https://doi.org/10.1039/c5cc05136c>.
- [65] J. Cui, Y. Feng, T. Lin, Z. Tan, C. Zhong, S. Jia, Mesoporous metal-organic framework with well-defined cruciate flower-like morphology for enzyme immobilization, *ACS Appl. Mater. Interfaces* (2017), <https://doi.org/10.1021/acscami.7b00512>.
- [66] S. Pu, X. Zhang, C. Yang, S. Naseer, X. Zhang, J. Ouyang, D. Li, J. Yang, The effects of NaCl on enzyme encapsulation by zeolitic imidazolate frameworks-8, *Enzym. Microb. Technol.* 122 (2019) 1–6, <https://doi.org/10.1016/j.enzmictec.2018.12.003>.
- [67] K. Liang, R. Ricco, C.M. Doherty, M.J. Styles, S. Bell, N. Kirby, S. Mudie, D. Haylock, A.J. Hill, C. J. Doonan, P. Falcaro, Biomimetic mineralization of metal-organic frameworks as protective coatings for biomacromolecules, *Nat. Commun.* 6 (2015) 1–8, <https://doi.org/10.1038/ncomms8240>.
- [68] H. He, H. Han, H. Shi, Y. Tian, F. Sun, Y. Song, Q. Li, G. Zhu, Construction of thermophilic lipase-embedded metal-organic frameworks via biomimetic mineralization: a biocatalyst for ester hydrolysis and kinetic resolution, *ACS Appl. Mater. Interfaces* 8 (2016) 24517–24524, <https://doi.org/10.1021/acscami.6b05538>.
- [69] S.S. Nadar, V.K. Rathod, Facile synthesis of glucoamylase embedded metal-organic frameworks (glucoamylase-MOF) with enhanced stability, *Int. J. Biol. Macromol.* 95 (2017) 511–519, <https://doi.org/10.1016/j.ijbiomac.2016.11.084>.
- [70] F. Pitzalis, C. Carucci, M. Naseri, L. Fotouhi, E. Magner, A. Salis, Lipase encapsulation onto ZIF-8: a comparison between biocatalysts obtained at low and high zinc/2-methylimidazole molar ratio in aqueous medium, *ChemCatChem* 10 (2018) 1578–1585, <https://doi.org/10.1002/cctc.201701984>.
- [71] K. Liang, C.J. Coghlan, S.G. Bell, C. Doonan, P. Falcaro, Enzyme encapsulation in zeolitic imidazolate frameworks: a comparison between controlled co-precipitation and biomimetic mineralisation, *Chem. Commun.* 52 (2016) 473–476, <https://doi.org/10.1039/c5cc07577g>.
- [72] X. Wu, C. Yang, J. Ge, Green synthesis of enzyme/metal-organic framework composites with high stability in protein denaturing solvents, *Bioresour. Bioprocess.* 4 (2017) 24, <https://doi.org/10.1186/s40643-017-0154-8>.
- [73] M. Jian, B. Liu, R. Liu, J. Qu, H. Wang, X. Zhang, Water-based synthesis of zeolitic imidazolate framework-8 with high morphology level at room temperature, *RSC Adv.* 5 (2015) 48433–48441, <https://doi.org/10.1039/C5RA04033G>.
- [74] N.K. Maddigan, A. Tarzia, D.M. Huang, C.J. Sumby, S.G. Bell, P. Falcaro, C.J. Doonan, Protein surface functionalisation as a general strategy for facilitating biomimetic mineralisation of ZIF-8, *Chem. Sci.* 9 (2018) 4217–4223, <https://doi.org/10.1039/c8sc00825f>.
- [75] G. Zhu, M. Zhang, Y. Bu, L. Lu, X. Lou, L. Zhu, Enzyme-embedded metal-organic framework colloidosomes via an emulsion-based approach, *Chem. Asian J.* 13 (2018) 2891–2896, <https://doi.org/10.1002/asia.201800976>.
- [76] J. Song, W. He, H. Shen, Z. Zhou, M. Li, P. Su, Y. Yang, Construction of multiple enzyme metal-organic frameworks biocatalyst via DNA scaffold: a promising strategy for enzyme encapsulation, *Chem. Eng. J.* (2019) 174–182, <https://doi.org/10.1016/j.cej.2019.01.138>.
- [77] W. Liang, R. Ricco, N.K. Maddigan, R.P. Dickinson, H. Xu, Q. Li, C.J. Sumby, S.G. Bell, P. Falcaro, C. J. Doonan, Control of structure topology and spatial distribution of biomacromolecules in protein@ZIF-8 biocomposites, *Chem. Mater.* 30 (2018) 1069–1077, <https://doi.org/10.1021/acs.chemmater.7b04977>.
- [78] V. Gascón, C. Carucci, M.B. Jiménez, R.M. Blanco, M. Sánchez-Sánchez, E. Magner, Rapid in situ immobilization of enzymes in metal-organic framework supports under mild conditions, *ChemCatChem* 9 (2017) 1182–1186, <https://doi.org/10.1002/cctc.201601342>.
- [79] S.S. Nadar, V.K. Rathod, Ultrasound assisted intensification of enzyme activity and its properties: a mini-review, *World J. Microbiol. Biotechnol.* 33 (2017), <https://doi.org/10.1007/s11274-017-2322-6>.

- [80] S.S. Nadar, V.K. Rathod, Encapsulation of lipase within metal-organic framework (MOF) with enhanced activity intensified under ultrasound, *Enzym. Microb. Technol.* 108 (2018), <https://doi.org/10.1016/j.enzmictec.2017.08.008>.
- [81] S.S. Nadar, A.B. Muley, M.R. Ladole, P.U. Joshi, Macromolecular cross-linked enzyme aggregates (M-CLEAs) of  $\alpha$ -amylase, *Int. J. Biol. Macromol.* 84 (2016) 69–78, <https://doi.org/10.1016/j.ijbiomac.2015.11.082>.
- [82] M. Salgaonkar, S.S. Nadar, V.K. Rathod, Biomineralization of orange peel peroxidase within metal organic frameworks (OPP–MOFs) for dye degradation, *J. Environ. Chem. Eng.* 7 (2019) 102969, <https://doi.org/10.1016/J.JECE.2019.102969>.
- [83] C. Carucci, L. Bruen, V. Gascón, F. Paradisi, E. Magner, Significant enhancement of structural stability of the hyperhalophilic ADH from *Haloferax volcanii* via entrapment on metal organic framework support, *Langmuir* 34 (2018) 8274–8280, <https://doi.org/10.1021/acs.langmuir.8b01037>.
- [84] U.V. Sojitra, S.S. Nadar, V.K. Rathod, Immobilization of pectinase onto chitosan magnetic nanoparticles by macromolecular cross-linker, *Carbohydr. Polym.* 157 (2017) 677–685, <https://doi.org/10.1016/j.carbpol.2016.10.018>.
- [85] X. Wu, C. Yang, J. Ge, Z. Liu, Polydopamine tethered enzyme/metal-organic framework composites with high stability and reusability, *Nanoscale* 7 (2015) 18883–18886, <https://doi.org/10.1039/c5nr05190h>.
- [86] U.V. Sojitra, S.S. Nadar, V.K. Rathod, A magnetic tri-enzyme nanobiocatalyst for fruit juice clarification, *Food Chem.* 213 (2016) 296–305, <https://doi.org/10.1016/j.foodchem.2016.06.074>.
- [87] S. Talekar, S. Desai, M. Pillai, N. Nagavekar, S. Ambarkar, S. Surnis, M. Ladole, S. Nadar, M. Mulla, Carrier free co-immobilization of glucoamylase and pullulanase as combi-cross linked enzyme aggregates (combi-CLEAs), *RSC Adv.* 3 (2013) 2265–2271, <https://doi.org/10.1039/c2ra22657j>.
- [88] S. Talekar, G. Joshi, R. Chougale, B. Nainegali, S. Desai, A. Joshi, S. Kambale, P. Kamat, R. Haripurkar, S. Jadhav, S. Nadar, Preparation of stable cross-linked enzyme aggregates (CLEAs) of NADH-dependent nitrate reductase and its use for silver nanoparticle synthesis from silver nitrate, *Catal. Commun.* 53 (2014) 62–66, <https://doi.org/10.1016/j.catcom.2014.05.003>.
- [89] X. Lian, Y.P. Chen, T.F. Liu, H.C. Zhou, Coupling two enzymes into a tandem nanoreactor utilizing a hierarchically structured MOF, *Chem. Sci.* 7 (2016) 6969–6973, <https://doi.org/10.1039/c6sc01438k>.
- [90] S.S. Nadar, V.K. Rathod, Magnetic-metal organic framework (magnetic-MOF): a novel platform for enzyme immobilization and nanozyme applications, *Int. J. Biol. Macromol.* 120 (2018) 2293–2302, <https://doi.org/10.1016/J.IJBIOMAC.2018.08.126>.
- [91] C. Hou, Y. Wang, Q. Ding, L. Jiang, M. Li, W. Zhu, D. Pan, H. Zhu, M. Liu, Facile synthesis of enzyme-embedded magnetic metal-organic frameworks as a reusable mimic multi-enzyme system: mimetic peroxidase properties and colorimetric sensor, *Nanoscale* 7 (2015) 18770–18779, <https://doi.org/10.1039/c5nr04994f>.
- [92] J. Wang, G. Zhao, F. Yu, Facile preparation of Fe<sub>3</sub>O<sub>4</sub>@MOF core-shell microspheres for lipase immobilization, *J. Taiwan Inst. Chem. Eng.* 69 (2016) 139–145, <https://doi.org/10.1016/j.jtice.2016.10.004>.
- [93] A. Samui, A.R. Chowdhuri, T.K. Mahto, S.K. Sahu, Fabrication of a magnetic nanoparticle embedded NH<sub>2</sub>-MIL-88B MOF hybrid for highly efficient covalent immobilization of lipase, *RSC Adv.* 6 (2016) 66385–66393, <https://doi.org/10.1039/c6ra10885g>.
- [94] J. Huo, J. Aguilera-Sigalat, S. El-Hankari, D. Bradshaw, Magnetic MOF microreactors for recyclable size-selective biocatalysis, *Chem. Sci.* 6 (2015) 1938–1943, <https://doi.org/10.1039/c4sc03367a>.
- [95] M. Zhao, X. Zhang, C. Deng, Rational synthesis of novel recyclable Fe<sub>3</sub>O<sub>4</sub>@MOF nanocomposites for enzymatic digestion, *Chem. Commun.* 51 (2015) 8116–8119, <https://doi.org/10.1039/c5cc01908g>.
- [96] Y. Wu, Y. Ma, G. Xu, F. Wei, Y. Ma, Q. Song, X. Wang, T. Tang, Y. Song, M. Shi, X. Xu, Q. Hu, Metal-organic framework coated Fe<sub>3</sub>O<sub>4</sub> magnetic nanoparticles with peroxidase-like activity for colorimetric sensing of cholesterol, *Sensors Actuators B Chem.* 249 (2017) 195–202, <https://doi.org/10.1016/j.snb.2017.03.145>.

- [97] O. Barbosa, C. Ortiz, Á. Berenguer-Murcia, R. Torres, R.C. Rodrigues, R. Fernandez-Lafuente, Glutaraldehyde in bio-catalysts design: a useful crosslinker and a versatile tool in enzyme immobilization, *RSC Adv.* 4 (2014) 1583–1600, <https://doi.org/10.1039/C3RA45991H>.
- [98] K.K. Tanabe, S.M. Cohen, Postsynthetic modification of metal-organic frameworks—a progress report, *Chem. Soc. Rev.* 40 (2011) 498–519, <https://doi.org/10.1039/c0cs00031k>.
- [99] E. Gkaniatsou, C. Sicard, R. Ricoux, J.-P. Mahy, N. Steunou, C. Serre, Metal–organic frameworks: a novel host platform for enzymatic catalysis and detection, *Mater. Horiz.* (2017), <https://doi.org/10.1039/C6MH00312E>.
- [100] Y. Chen, S. Han, X. Li, Z. Zhang, S. Ma, Why does enzyme not leach from metal-organic frameworks (MOFs)? Unveiling the interactions between an enzyme molecule and a MOF, *Inorg. Chem.* 53 (2014) 10006–10008, <https://doi.org/10.1021/ic501062r>.

### ***Further reading***

- C. Tudisco, G. Zolubas, B. Seoane, H.R. Zafarani, M. Kazemzad, J. Gascon, P.L. Hagedoorn, L. Rassaei, Covalent immobilization of glucose oxidase on amino MOFs via post-synthetic modification, *RSC Adv.* 6 (2016) 108051–108055, <https://doi.org/10.1039/c6ra19976c>.

# *State-of-the-art and future perspectives of MOFs in medicine*

**Sergio Carrasco**

*Department of Organic Chemistry, Stockholm University, Stockholm, Sweden*

Throughout the previous chapters, we have explored different key aspects of the MOF technology: basic concepts, structure and properties, characterization techniques, a broad variety of synthetic procedures, some limiting issues concerning their use in (bio)medical applications, and the current strategies to improve the biocompatibility of these materials to achieve the desired purpose. Here, in this last chapter, we pretend to offer a brief overview of the state of the art focusing the attention of the reader on those details that, although possibly unnoticed, have paved the way for the next generation of metal-organic framework materials and are behind the reasons of the changing trends in terms of applicability.

As it has been discussed previously, in a simple and a concise manner, MOFs are hybrid polymeric materials comprised of metal ions/clusters and an organic linker resulting in highly porous materials. Indeed, IUPAC includes in the definition for these materials the presence of potential voids [1]. Although, in general, it is widely accepted that MOFs crystallize in well-defined space groups, no further difference between crystalline and amorphous networks should be considered as temperature, pressure, and/or external stimuli, among other parameters, may considerably impact the structure and, as a result, their potential porosity. The amount of solvent or other guest molecules filling the pores is extremely dependent on both the synthetic routes followed to prepare the materials and the washing/activation procedures. In other words, the presence of fully or partially loaded pores with different molecules may lead to different diffraction patterns as those expected from the corresponding empty raw MOFs [2]. Furthermore, the long-range periodic order may be affected, resulting in amorphous-like diffraction patterns, but maintaining the porosity, basic building blocks, and connectivity upon using different synthetic conditions or postsynthetic modifications such as ball milling, pressurization, heating, and melt quenching [3]. Although nowadays this discussion between crystalline and amorphous MOFs can be considered overpassed and it is far from the scope of this chapter, the reader is referred to the literature for further information [4]. Similar controversies have been overcome regarding, for example, the exclusive use of carboxylate-based organic linkers [5] as other organic molecules bearing

different moieties, such as —SH [6], —OH [7], or —N(R)(H) [8], have been successfully used for MOFs development.

Nowadays, the difference between MOFs and porous organic frameworks (POFs) seems clear [9]. However, it is worth to mention that as the research and the development of these materials can be considered relatively novel, distinctions were not so evident during the early 1990s. Indeed, due to the first vague definitions, concepts were all cross-linked and some common mistakes still can be found in some manuscripts regarding that aspect. POFs are those polymers purely fabricated upon combination of organic building blocks [10] and can be classified according to either their crystallinity, being usually known as covalent organic frameworks (COFs) showing in general reversible covalent bonds [11], or amorphous porous organic polymers (POPs) [12], if the covalent bonds are irreversible and the resulting material lack of a diffraction pattern. In general, POPs are more stable than COFs and show a broader variety of possibilities in terms of connections and porosity ranges. On the other hand, the advances in MOF technology and characterization techniques have paved the way for reticular chemistry as an emerging science [13, 14], trying to explain the differences between interconnected and noninterconnected networks that conventional crystallography is not able to cover, although sometimes the terminology can be considered complex for nonexperts.

MOFs have widespread use in different fields between 1994 and 2019, including catalysis [15], gas storage [16], purification [17], separation [18], energy [19], or sensors [20], but undoubtedly their application in medicine has outstand over them during the period 2014–18 due to the impact in human health-related issues. Within this chapter, the reader will find a comprehensive data analysis of the manuscripts published in the literature regarding the areas commented before paying special attention to medicine, the reasons and the driving forces behind of and responsible for the change in the trends in terms of applicability, the evolution and the state of the art of this field according to the maturation of the MOF technology, some relevant and pioneer examples, and a critical discussion focused on the main advantages and drawbacks of using MOFs in the field of medicine.

### ***23.1 A brief story of MOFs, applications, and recent trends***

Considering MOFs as hybrid polymers themselves, in the borderline between organic and inorganic materials, is essential for the understanding of their rapid evolution and establishing a convenient contextualization. Different from other hybrid materials or advanced composites, MOFs show both characteristics after being obtained in one single step through solvothermal, sonochemical, microwave-assisted, electrochemical, or mechanochemical syntheses by simply mixing the convenient components, under singular reaction conditions (temperature, pressure, solvent nature and polarity, concentration and ratio of metal salts/organic linkers, presence or absence of additives or modulators, among others). They belong to a diffuse barrier covering a few but critical aspects from a multitude of disciplines such as Materials Science, Physical



Chemistry, Organic and Inorganic Chemistry, and Engineering. More than 70,000 structures were officially reported in the Cambridge Crystallographic Data Centre (CCDC) in 2017 [21], regardless those amorphous or liquid MOFs. The multiple connections between a broad variety of secondary building units (SBUs) and on-demand-synthesized organic linkers have broadened the scope of these materials up to practically infinite possibilities. Thus, it is reasonable to explain the interest of the scientific community in such materials as, in order to achieve the same properties using composite materials, a limited range of options are available in terms of fabrication procedures, functionalization methodologies, and compatibility between materials showing different natures. However, it is worth to mention that some MOFs show a relevant lack of properties in several fields, limitations that have been overcome thanks to the application of the same technologies used to prepare composites [22]. One can conclude that the evolution of MOF publications receives the constant feedback from both the abovementioned fields and the arising of new synthetic procedures, improving the overall properties of these polymeric hybrids and contributing to their maturation.

Yaghi should be undoubtedly known as the pioneer of the development of MOFs as we know nowadays. Together with Michael O’Keeffe, they are considered the fathers of the reticular chemistry [13, 14, 23]. Although the concept “metal-organic framework” was introduced for the first time in 1994 [24], the fabrication of extended metal-organic materials was demonstrated more than a century ago, in 1897, when an open structure consisting of  $\text{Ni}^{2+}$  ions, cyanide molecules, ammonia, and benzene molecules was successfully prepared by Hofmann and Küspert [25]. However, when new characterization techniques such as X-ray diffraction (XRD) came into scene, this polymer, originally claimed as an extended 2D network, demonstrated to be crystal aggregations in a sheet-like fashion where the benzene molecules were encapsulated favoring the stability of the structure through  $\pi$ - $\pi$  interactions [26]. MOFs can be characterized using a broad amount of characterization techniques available nowadays. However, until the second half of the twentieth century, when techniques that are considered of routine today appeared, the presence of large voids within crystalline matrices could not be confirmed. This fact led to prominent research to achieve these 2D and 3D polymers during the following years. More information about this fascinating process can be found elsewhere, remarking the milestones and the challenging routes followed [27]. The end of the road can be located in 1989, when Hoskins et al. prepared a copper-based network from a copper-acetonitrile complex by replacing the ligands with the linker 4,4',4'',4'''-tetracyanotetraphenylmethane [28].

Since 1994, the number of publications regarding MOFs has been increasing exponentially (Fig. 23.1A), resulting in 4081 scientific documents including articles and reviews in 2018, and almost 3000 by August 2019. This may be considered a result of the maturing of MOF technology and its combination with the novel micro/nano-structuration techniques for establishing novel robust and reproducible methods for the synthesis of new polymeric materials, as commented above. If the trends are being constant, it is expected to achieve around

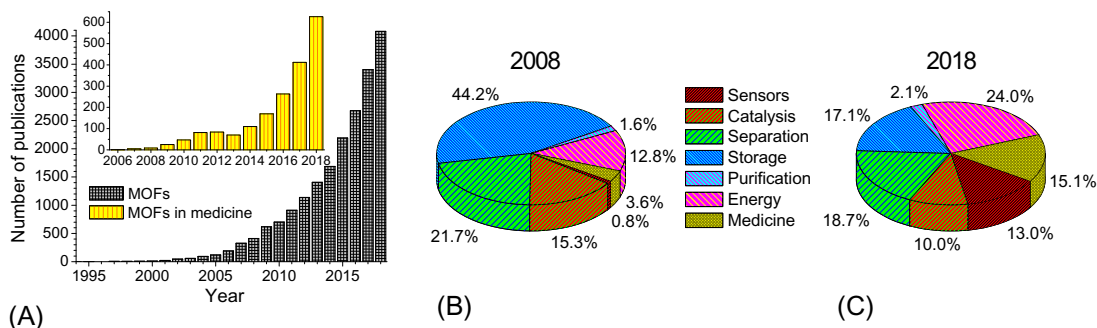


Fig. 23.1

(A) Number of publications of MOFs in the period 1994–2018. Inset: use of MOFs in medical areas from 2006 to 2018. Distribution of the use of MOFs in seven different fields in (B) 2008 (249 works selected over the overall amount of papers published, 413) and (C) 2018 (3138 over 4081). *Data from Web of Science.*

5100 publications during this year, which represents a general increase of 25% over 2018. Remarkably, it was necessarily almost a decade to find practical applications for these materials, probing their efficiency as the zeolites, their pure inorganic counterparts, in a more efficient way. In 2001, the first work probing the use of MOFs as efficient gas separation/adsorption systems was reported by Fletcher et al. [29] The authors studied the adsorption of different gases in a  $\text{Ni}^{2+}/4,4'$ -bipyridine MOF, claiming for the first evidence of specific interactions between guests and functional groups within the pores in this flexible network. They evaluated the effect of the temperature on the adsorption isotherms, observing structural changes and different loading efficiencies when alcohols were used, concluding that the expansion of the MOF itself is not necessarily related to the way the gases permeate throughout the matrix, but highly dependent on the functional groups located in the internal walls of the pores and the corresponding gas interactions.

One year later, the group of Prof. Yaghi reported the first MOF-based gas storage system based on isorecticular Zn polymers [30]. Starting from the well-known MOF-5, the authors performed several linker modifications in an elegant fashion to expand the pore size keeping constant the raw topology. This strategy has been a recurrent topic in MOF technology within the last years and several authors have evaluated the influence of using both metals showing similar electronics and oxidation states and modified organic linkers, retaining the original structure but improving the inherent properties [31–35]. This work constituted as well the first evidence of the critical effect of reaction conditions like the concentration of the starting materials, as the authors were able to fabricate both interpenetrating and noninterpenetrating networks, with a critical impact over the pore volume of the final material, just by diluting the concentration of metals and linkers. Interestingly, although the use of functionalized linkers with convenient organic moieties, like terephthalic acid derivatives including  $-\text{Br}$  or  $-\text{NH}_2$ , could be of relevance for their future application, resulting MOFs showed smaller pore

sizes compared to the original polymer, as expected from these moieties allocated inside them. Finally, they evaluated the storage capacity for methane of the new materials, finding for IRMOF-6 the highest loading efficiencies compared to previously reported zeolites and other isorecticular MOFs due to the hydrophobic nature of  $C_2H_4$  units.

Also in 2002, the first potential sensor system was proposed based on trivalent lanthanide cations (Eu, Tb, Ce) and 2,6-naphthalenedicarboxylic acid [36]. The emission of the polymers in the visible range upon irradiation with UV-light demonstrated for the first time the applicability of these materials for sensor development. If the previous work demonstrated the possibility to obtain isorecticular MOFs by changing the nature of the ligand, this example constituted the first work where isostructural MOFs were obtained by replacing the metal cation. Despite the interesting work performed herein, the system was not applied to the quantification of molecular species in real samples. It was not until 2007 when Chen et al. applied other lanthanide-based MOF using trimesic acid for the quantification of small molecules such as ethanol, acetone, and DMF, depending on the quenched/enhanced fluorescence of the polymer [37]. Several works for sensing humidity [38], pH [39], metal cations [40], volatile organic compounds [41], gases [42], or explosives [43] have been described afterwards and, more interestingly, the first MOF-based biosensor for larger molecules was proposed in 2012 [44]. Authors developed a glucose sensor based on ZIF-8, a MOF consisting of Zn and 2-methylimidazole, being successfully applied in human blood serum samples.

All these first examples illustrate that years 2001 and 2002 can be considered the transition of the MOF technology from the prehistory, where publications were indistinctly released based on mere new structures and topologies, to the ancient and the middle age, where real applications were found for these materials. This analogy with historic periods is not casual and perfectly fits with the different MOF generations produced since 1994 [45]. The changes in the trends to ensure the applicability of these polymers seem to match the transition between the first and the second generation of MOFs. While the former comprise those structures showing nonpermanent porosity due to the host-guest dependence, the later correspond to MOFs showing robust and stable pores. It is thus reasonable to think that this transition boosted and enabled their use in real-life applications as recyclability and reusability are the key aspects for the applications considered herein [46]. On the other hand, the modern and contemporary ages can be assimilated to the third and the fourth generations, respectively. It is a nonnegligible fact that some potential applications were still hindered as a consequence of the poor properties of MOFs from the second generation. In fact, applications described above were limited to the storage, sensing, and separation of small molecules showing relatively poor interactions or medium to low selectivities [47]. Interactions with linkers (through hydrogen bonding, hydrophobic  $\pi$ - $\pi$  interactions, electron donor/acceptor interactions, or the formation of a dative covalent bonding) and structural metals (through open metal sites, either via reversible bonds or electrostatically) constitute the basis of the applicability of MOFs [48, 49].

The third generation enabled the preparation of external stimuli-responsive materials showing flexible and dynamic frameworks depending on temperature, pressure, and/or environmental conditions [50]. The so-called “breathing” MOFs can be included in the definition of the third generation as, after an external stimuli is applied, the total pore volume and size dramatically change. The chromium-terephthalate MIL-88B(Cr) can be considered by far the canonic MOF showing this ability due to the broad-related scientific production [51]. First published by Serre et al., this polymer was able to experiment a unit cell expansion of even a 135% compared to the as-synthesized raw material depending on the guests inside the pores. However, similar MOFs were described before by the group of Prof. Fujita [52]. On the other hand, the fourth generation comprised different postsynthetic modifications, including chemical modifications maintaining or improving the MOF structure and porosity to introduce new functionalities and postprocessing procedures resulting in new MOF-derived or carbon-based materials, such as pyrolysis or thermal annealing [53]. This milestone was the answer to the limitations found for the previous generations and implied a truly revolution in MOF technology. Further details concerning MOF limitations will be deeply discussed in the following section, particularly focused on the field of biomedicine. Since then, a significant bloom was observed in fields such as catalysis, energy, sensors, or medicine. The transition between the second and the third/fourth generations is not as clear as the corresponding between the first and the second, as different applications started to appear within a 6-years period (2004–09)

Although suspected in a theoretical manner, it was not until 2004 when the first evidence of catalytic applications based on MOFs appeared for the selective cyanosilylation of benzaldehyde using a 2D Cu-trimesic acid MOF. The use of these polymers for energy applications was already predicted using computational models [54], but the first evidence arose in 2008 [55], regardless their hydrogen storage capacity. Combelles et al. suggested an iron-terephthalate MOF (MIL-53) as cathode in Li-ion batteries. One year later, the system was successfully developed showing a remarkable electrochemical enhancement compared to conventional Li batteries [56].

In this context, the first work concerning biomedical applications appeared in 2006 by Horcajada et al. [57]. She is considered the pioneer of the use of MOFs in medicine nowadays and demonstrated for the first time the potential of these materials for drug delivery. A comparison between MOFs and other well-established delivery system is presented for the first time, introducing the “hybrid” methodology versus pure organic and inorganic materials. Ibuprofen adsorption was studied in Cr-terephthalate MOFs MIL-100 and MIL-101. Due to their different pore sizes, each polymer was able to adsorb different amounts of this drug, MIL-101 being able to uptake even four times more ibuprofen (1.4 g/MOF) than its terephthalate counterpart as a consequence of the larger pore sizes and volumes. Despite the toxicity of Cr(III) ions compared to Fe(III), they demonstrated that small amounts of polymer were required to achieve high dosages, achieving the most relevant requirements of porous materials for drug delivery, i.e., the necessity of large pores, a selective occupation

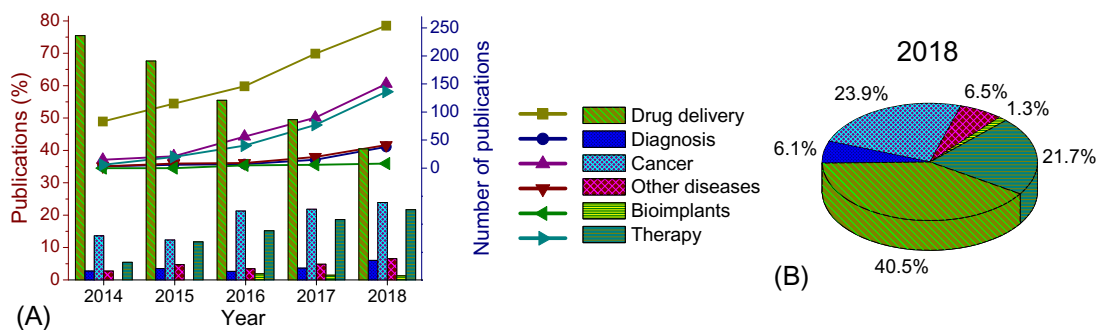
of mesopores, and interassembly of organic compounds, these three factors being accomplished by large when considering MOFs for this goal. Delivery kinetics were tested in vitro in simulated body fluids, finding different regimes according to the interactions of ibuprofen onto/within MIL-101. Initially, the drug showed some diffusion processes through the cages' windows, while the final drug fraction was delivered slowly due to the pore size and ionic interactions, as the drug was loaded as an anion and  $\pi$ - $\pi$  interactions, taking 6 days to ensure a complete release. Comparison with other mesoporous inorganic materials, such as MCM-41 (2 days), demonstrated higher loading capacities and longer delivery times, which is of importance for a persistent and more efficient administration.

A convenient and critical comparison is required considering the fields of application of MOFs from 2008 to 2018. If we neglect all the manuscripts regarding the fabrication of new structures where applications are not demonstrated, i.e., just concerning the synthesis and the characterization of new MOFs or the improvements over the syntheses already described, seven main fields can be distinguished. In 2008, storage-related applications were by large the vastest field where MOFs played an important role, particularly concerning gases (Fig. 23.1B). Hundred and ten publications, representing a remarkable 44.2% over the total applications, were released, while medicine only represented a discreet 3.6% (9 works). This behavior can be explained as discussed before, as a consequence of the limited properties of these materials belonging to the first generations for real medical applications. Separation (21.7%, 54 publications) and catalysis (15.3%, 38) were the other fields where MOF technology was focused on the applicability in 2008. Only purification (1.6%, 4) and sensors (0.8%, 2) resulted in less articles than medicine at that time. A constant and significant improvement over the fabrication methodologies and the releasing of new MOF generations resulted in an equitable distribution of publications in 2018 within the abovementioned fields (Fig. 23.1C). Although the amount of publications related to storage raised up to 713, the percentage value decreased to 17.1%, favoring the research and efforts in other areas. As expected, the same trend was found for the other two broadest areas in 2008, separation and catalysis that decreased to 18.7% (780) and 10.0% (416), respectively. These three areas together represented more than an 80% in 2008, but in 2018 were less than 50%. This detriment favored indistinctly energy (24.0%, 998), medicine (15.1%, 627), and sensors (13.0%, 539). A remarkable 10-years average increase of 60%, taking into consideration the increase of the number of publications of one year compared to the previous, was found in medicine, followed by energy (42%) and sensors (28%). If these trends are constant, ca. 1000 manuscripts may be expected by the end of 2019, although during the first 7 months, only 372 manuscripts in the field of medicine have been already published. Despite some of the works are not still indexed in databases, it is not very likely to cover the expectations, being more reasonable to attend the in-year behavior of 90 manuscripts/month, which would result in approximately 800 papers.

At this point, it is worth to mention a main drawback when comparing these values with databases. Even using boolean operations to discard reiterative manuscripts appearing in

different areas at the same time, the reality is that every field considered herein as independent is interconnected to each other, resulting in impossibility to discard between applications in some cases. For example, point-of-care devices can be included as sensors due to their function and operation procedure. However, these systems are designed for the in/ex situ monitorization of different biological analytes in presumably nonhealthy patients, thus considering them as medical-related publications. In other words, the convergence trends nowadays are unavoidable, and the new systems proposed are a result of multidisciplinary collaborations, as the MOF technology itself. On the other hand, data showed here are obtained from Web of Science. If the reader crosses the terms “metal-organic frameworks” and “medicine” in other databases such as Scopus, similar trends can be found, although the values offered for the number of publications may slightly differ. Scopus, additionally including conference papers and book chapters, offers 4802 publications compared to WOS (4081) in 2018, and more than 4000 works already published during 2019. From those, regarding medical applications, the former database includes 345 publications versus 372 in the latter to date.

Another interesting analysis arises from the study of data regarding the final use of MOFs within biomedicine. Fig. 23.2A shows both the number of publications and the percentage over the total amount of manuscripts published for selected specialized-related medicine fields. The 5-years period, 2014–18, was selected for comparison purposes, when the growth of MOF publications in medicine can be considered constant (increase of ca. 60% per year) and the number of publications was larger than 100 in order to ensure a significant analysis of the data batch. Drug delivery was not only the first area where MOFs were applied in medicine, but also the application that experienced the highest 5-years average growth, by large (58%) compared to cancer (19%), and far from the practically negligible increase of bioimplants (< 1%). Although the situation for drug delivery is similar to that described for storage or separation as a decrease in the overall percentage with years is observed (from a 75.4% in 2014 to a 40.5% in 2018, Fig. 23.2B), the increase in the number of publications compensated by far the reported



**Fig. 23.2**

- (A) Number of publications of MOFs in different medical applications in the period 2014–18 (*straight lines*, right axis) and the relative percentage per year for each application (*bars*, left axis).  
 (B) Distribution of the use of MOFs in six different medical applications in 2018. Data from *Web of Science*.



values for other areas (from 83 publications in 2014 to 254 in 2018). However, further comparisons in relative terms similar to the ones established for the previous applications cannot be performed as the competing areas have not surpassed the amount of 100 publications yet, thus resulting in nonreliable increments. Only cancer-related applications, showing 150 publications in 2018 (increment of 67% compared to 2017) compared to 254 works for drug delivery (increase of 25% in 2018), seem to surpass them under this relative analysis, demonstrating the evidence that the fields where MOFs are recently finding a new applicability experience larger growths in detriment of the first areas. Two main aspects can be concluded from these trends. The first and more evident is that MOF systems for drug delivery seem to be the most promising application in medicine and where the scientific community has focused its attention in the last years. The second, and maybe not so obvious, is that this application is experiencing a faster maturing effect compared to other areas and materials, highlighting the relevance of MOFs as biocompatible carriers. However, areas like cancer treatment are experiencing larger relative growths due to their social impact.

Although the relative studies are hampered in terms of application fields, one can compare MOFs with well-known mature materials used for the same purpose. Mesoporous silica nanoparticles for drug delivery have experienced an average increase of 14% during the last five years, while organic polymers only a 6%. These values can be compared with the 35% of these hybrid materials in the period 2014–18. Furthermore, checking the corresponding individual relative growths per year, it is surprising to observe that the previous inorganic nanoparticles showed a 26%, 7%, and 5% growth in 2016, 2017, and 2018 and organic materials a 1%, 8%, and –1% in the last 3 years, respectively. One may speculate that these decreases, even negatives, can be attributed to the presence of improved materials surpassing them for drug delivery. This is a key evidence of how MOFs have strongly erupted within the field of medicine, replacing these old-fashioned and limited materials by better and improved polymers showing larger drug loading efficiencies and longer releases in terms of time.

Coming back to the utility of MOFs in medicine, here it is even more complicated to establish a clear barrier between each use than considering general applications. Although considered in a separate manner, the concepts “cancer” and “therapy” totally overlap. For this reason, the values given in [Fig. 23.2B](#) for therapy treatments include those manuscripts where MOFs are used as labels or markers for specific targets excluding carcinogenic cells or related proteins expressed by them. The trends in both areas ([Fig. 23.2A](#)) are similar, thus confirming the intimate relationship between them. Similarly, “diagnosis” applications match other areas such as point-of-care devices and sensors and are related to cancer and other diseases caused by microbes, bacteria, or viruses, as some MOFs are used not only for the early detection, but also for the treatment/therapy itself. Diagnosis represents here a wide definition, mainly including imaging procedures using MOFs as contrast agents or fluorescent labels. Before moving forward, a few words on the rest of applications should be mentioned.

In 2007, Rieter et al. prepared a hybrid composite based on nanoscaled MOFs used as cores and a silica coating as shell [58]. The support material consisted of lanthanide (Eu, Gd, Tb) terephthalates prepared through reverse microemulsion polymerization in the form of nanorods, being possible to modulate the aspect ratio by adding different amounts of cetyltrimethylammonium bromide (CTAB) as surfactant and water during the synthesis. Polymers were further functionalized with polyvinylpyrrolidone (PVP) and a sol-gel methodology was finally applied to cover the PVP-functionalized nanoMOF rods with controlled-thickness mesoporous silica layers. Importantly, this work was one of the first demonstrations of how MOFs could be protected to avoid dissolution and thus limiting the potential release of metal cations to the external media that, as will be discussed briefly, is a key aspect for biomedical fields. This work constitutes a paradigmatic example of the use of MOFs in multidisciplinary areas such as sensors, functionalizing the silica layer with a Tb complex for the detection of bacterial spores as a consequence of its coordination ability to dipicolinic acid present in these pathogens. But, in addition, authors proposed this material as a potential candidate for future imaging. However, one of the first evidences of MOFs used for diagnosis appeared the next year, when the group of Lin prepared a Gd-mellitic acid nanoMOF using a similar surfactant-assisted method as described before, with potential use in magnetic resonance imaging due to the paramagnetic nature of the metal ion [59]. Since then, the number of publications of MOFs used for diagnosis, following both luminescent or contrast strategies, increased considerably.

As expected, MOFs for cancer treatment started as drug delivery systems [60]. In 2010, Horcajada et al. reported on the synthesis of the first biocompatible Fe-carboxylate MOFs for the encapsulation of drugs typically used for cancer and HIV treatment, such as cidofovir, busulfan, azidothymidine triphosphate, and doxorubicin, none of them previously encapsulated in already available carriers with the exception of the last drug. The use of different organic linkers, i.e., muconic acid, fumaric acid, trimesic acid, 2-aminoterephthalic acid, and terephthalic acid, resulted in different structures like MIL-89, MIL-88A, MIL-100, MIL-101, and MIL-53, respectively, in the nanometric range (<200 nm). In order to improve the biocompatibility of these materials and avoid potential aggregation of the nanoparticles, they were covered with different organic polymers such as PEG, dextran or chitosan, and proved that the efficiency of these functionalized MOFs did not statistically differ from those corresponding to the raw materials. Some of them showed limited stability during *in vitro* experiments, like MIL-88A, but this could be considered as an advantage due to the endogenous nature of the structural components (Fe and fumarate ions). *In vivo* toxicity was also tested in rats and no differences in several indicators were found compared to the control population, lacking of immune or inflammatory reactions after administration, and being easily excreted. Seventy-five percent of pediatric cancer patients were cured upon the administration these materials, demonstrating the real applicability of MOFs in medicine. Furthermore, they successfully tested the Fe-MOFs as contrast agents in imaging.

Later, in 2014, Lu et al. reported the first work concerning the use of MOFs in photodynamic therapy [61]. They prepared a Hf-porphyrin MOF and used it as an effective photosensitizer for the treatment of resistant neck and head cancers. The UiO-like structure avoided aggregation of photosensitizer units and potential self-quenching, enhanced the generation of reactive oxygen species such as singlet oxygen, and facilitated their diffusion out of the nanoMOF in contact with cancer cells. The stability of the material was proven after its incubation in physiological media, followed by *in vitro* experiments in carcinogenic human cells, demonstrating a fast incorporation of the nanoMOFs inside them and finally tested *in vivo* in mice, showing tumor shrinking even after the first treatment day and, more relevantly, no damage was observed in tissues or skin after the photodynamic therapy treatment, being able to totally remove 50% of treated tumors after only 8 days.

The potential use of MOF for the treatment of other issues includes, for example, the encapsulation of procainamide as an antiarrhythmic drug [62]. Here, authors prepare the bio-MOF-1 consisting of Zn-adeninate units capable to maintain its crystalline structure even after several weeks in biological buffers. Moreover, this article represents the importance of the use of biocompatible organic linkers in the preparation of such polymers to improve the biocompatibility of MOFs, as even if the material is decomposed and degraded inside patients, components can be easily excreted or incorporated as exogenous components. The drug selected for this study shows a lack of stability *in vivo*, thus requiring be administrated every 3–4 h to patients. Using this material, procainamide is released during 72 h, triggered by the presence of buffer cations, and showing the largest releasing profile within the first 20 h in biological media.

Recently, MOFs have been proposed and used in osteogenic implants [63]. Chen et al. prepared ZIF-8 nano- and microMOF films, consisting of Zn-imidazolate arranged units, on porous titanium showing excellent cell adhesion. The later polymer films showed a lower proliferation of MG63 human osteosarcoma cells compared to blanks and the former material. The biodegradation study demonstrated that Zn ions were slowly released without a significant burst-release effect and a relevant *in vitro* antibacterial activity was found compared to raw titanium, the MOF being responsible for the partial decomposition of bacterial membranes. All these aspects studied in this work have contributed to the successful preparation of such composites for osteogenic implants in bones (Fig. 23.3) and, more recently, in teeth [64].

This book covers, reunited for the first time, all the vast aspects concerning the use of MOFs in (bio)medicine, from the synthesis to the application in a thorough manner. However, several critical reviews and book chapters have been published to date which should be considered by the reader in order to check in detail the evolution of the MOF technology as it is briefly showed in this chapter. The first review reporting these aspects appeared in 2010 [65] and, as could not be otherwise, Horcajada published in 2012 the most cited review [66], with 2108 citations in August 2019, discussing the most relevant and key aspects

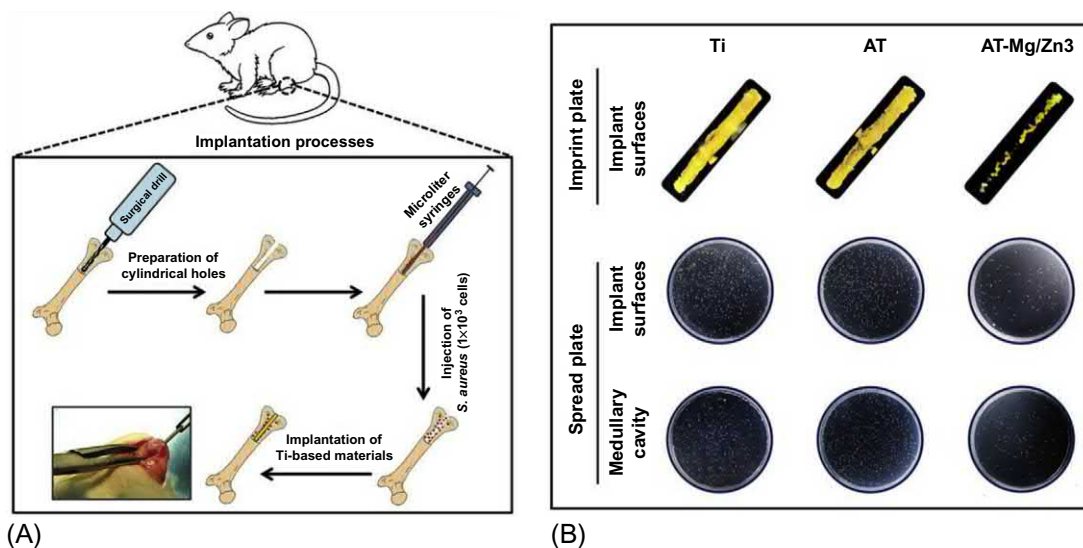


Fig. 23.3

Osteogenic medical implants based on Mg/Zn-MOF74 layers over titanium pieces, inserted after femur drilling in mice (A), showing a remarkable antibacterial activity compared to the titanium support (Ti) or the alkali-heat-treated titanium (AT) after implantation for 3 days with bacterial infection (B). *Reproduced with permission from X. Shen, Y. Zhang, P. Ma, L. Sutrisno, Z. Luo, Y. Hu, Y. Yu, B. Tao, C. Li, K. Cai, Fabrication of magnesium/zinc-metal organic framework on titanium implants to inhibit bacterial infection and promote bone regeneration, Biomaterials 212 (2019) 1–16.*

that should be observed in MOF development to enhance their biocompatibility, focusing on the composition, the formulation, and the most relevant real-life medical applications to date, including at that time mainly drug delivery and storage and delivery of gasotransmitter gases. A deep discussion on the main drawbacks of using these polymers in biomedicine was presented in terms of toxicity and biodegradability. Since then, and considering the exponential growth of publications in this field, new and updated works have appeared summarizing the most relevant advances, broadening the application scope according to the new technologies, fabrication methodologies, and the on-demand design of new structures to circumvent the most relevant issues finding new fascinating properties. The reader is referred to the literature for further information [67–72]. Among these general revisions, interesting overviews on the use of MOFs in drug delivery [73–76], photodynamic therapy [77–79], or in vivo imaging and diagnosis [80–82] can be found in the literature. The amount of reviews considering the first application surpasses considerably the others, highlighting the fact that drug delivery has been the most exploited area within the last years. Remarkably, any review concerning the use of MOFs in medical implants has been released to date as a consequence of the lower scientific production compared to other medical applications, but considering the recent bloom in this field, it is expected that such publications appear during 2020–21.

## ***23.2 Toward the golden age of MOF technology in medicine***

Scientific community working on MOFs has agreed about relevant aspects and requirements that should be observed for their use in medical applications. Compared to other well-known and defined materials, such as biopolymers, inorganic nanoparticles, or biological elements used in medicine, which can be considered as mature technologies, MOFs are still in diapers. Regarding purely inorganic nanoparticles, which usually require organic coatings to avoid aggregation, MOFs show an inherent ability to avoid this issue in biological fluids due to their hybrid nature [83]. Parak et al. presented a very interesting review where they compare MOFs with other widely applied nanomaterials in biomedicine such as mesoporous silica nanoparticles and dendrimers [74]. Hybrid polymers exploit both their inner and outer surface properties in contrast with those classic materials, showing some other interesting advantages and challenging limitations that will be commented in this section for each particular application and from a general point of view.

Since the very beginning, it was clear that the “size” requirement is the barrier established in nanoMOFs of <200 nm to allow a free circulation even in the smallest capillaries [66]. Nanoparticles not only show remarkable and different properties and larger surface areas compared to their bulk counterparts, but also show higher biocompatibility for in vivo applications. Their ease of functionalization to include different specific moieties, biomolecules, or biocompatible polymers, among others, for binding specific targets and enhance their selectivity emphasizes on the idea that every material should be specifically designed for each application depending on the desired activity and properties. Particle size determines the biodistribution, translocation, cellular uptake, and excretion [84]. On the other hand, each administration method needs its own formulation. In that sense, the size matters not only to avoid tissue damage, but also to prepare stable, reproducible, and convenient administration formats, such as aerosols, tablets, pellets, etc. [66]

Independently on the application, nowadays, the major concerns of MOFs in biomedicine are nanosafety and toxicity. Materials based on both biocompatible metals and organic linkers, those known as bioMOFs [85], can still be toxic due to the nature of the final particle itself or, in other words, the high reactivity of the atoms in the surface of nanoMOFs as a consequence of the large surface-to-volume ratio allows them to penetrate in healthy cells or attack undesired targets regardless the original components. In contrast, mesoporous silica nanoparticles and organic polymers are known to be extremely biocompatible and their effects in vivo have been well-established. Initial in vitro studies have demonstrated the low cytotoxicity of different MOF formulations [84, 86]. The first systematic in vitro study of the effect of a battery of Zr, Fe, Cr-MOFs in both healthy and damaged cells was performed in 2017 for their potential use as drug carriers and medical implants [87]. However, although several MOFs have been proven to be useful for in vivo applications, some improvements are still required. Serre et al. published in 2018 a relevant review highlighting these

challenges [88], such as the scarce data availability for in vivo human toxicity of organic ligands, criticizing that the vast majority of in vivo examples are only applied to cancer instead of healthy cell lines to certainly prove the lack of toxicity of the MOF.

On the other hand, MOFs are, in general, less stable than their pure inorganic or organic counterparts. Although this could be considered as an advantage, as the structural components may be excreted easily from living organisms, termed as biodegradability, the rapid dissolution of some of them under physiological conditions and different pH values and ionic strengths may lead to uncontrolled releases of the guest, in the case of drug delivery, or disintegration before reaching and labeling abnormal cells/tissues, in imaging [89]. Nevertheless, bioMOFs are an interesting alternative to avoid this limitation due to the easy excretion of the constituent components, showing a high-efficient releasing effect while degrading even if the material shows a poor porosity [65]. Apart from that, also the potential accumulation of metals in target tissues or organs, such as the liver, may lead to new diseases and toxic effects. Nowadays, efforts are focused on the development of new high-stable and biocompatible nanoMOFs, using pharmaceutical compounds as organic linkers, or by coating the surface with polymers already used for medical purposes, among others [90].

Some other relevant but not less important issues that MOF technology has still to confront include their regulation, selectivity, and economics. In other words, MOFs have to demonstrate their potential use during in vivo experiments lacking of toxicity. As concluded elsewhere [87], practically each target will require not only the study of a MOF system for different healthy and damaged cells, but also successfully surpass the severe and strict medical legislations that depend on each country. Ethical issues may arise if, for example, a MOF-based treatment is approved, but demonstrates that, with time, it may lead to another disease [91]. On the other hand, not only the administration formula and location matter, but also the ability to reach the specific target discriminate between different physiological environments [72]. Finally, scale-up could be a major concern as MOF formulations have to be prepared in a reproducible manner [92], showing similar properties and/or loading capacities per synthesized batch, and integrated into the specific administration form.

Focusing on individual applications, other advantages and limitations should be taken into account. For drug delivery, MOFs should be able to specifically target damaged tissues, irregular cells, or stranger pathogens showing a lack of fragmentation, degradation, and/or aggregation. A desirable control of dosage and spatial and temporal release of the drug based on stimuli-triggered mechanisms is needed [76]. Thus, biodegradability, bioavailability, and toxicity are the major concerns in drug delivery. In that sense, size, shape, and composition rule the physicochemical properties of MOF materials. But other aspects should be taken into account, such as the fabrication of these materials that should be performed following reproducible straightforward methodologies and enabling industrial scaling-up procedures [65]. Further, MOFs allow for noncovalent encapsulation of drugs inside the cages, showing higher loading capacities than other mesoporous materials, although some limitations regarding



the pore aperture should be considered [72]. Nevertheless, new findings in MOF technology, such as the isoreticular expansion commented before or the use of polymers showing the so-called “breathing” capacity, have partially circumvented this critical issue [66]. In addition, biomolecules such as DNA, enzymes, or other proteins are able to mineralize MOFs and control their size, activity, morphology, and crystallinity upon encapsulation [93]. The large loading capacity and the long-term temporal release of the drugs, in part as a consequence of the window aperture, compensate by large the use of MOFs over old-fashioned materials such as mesoporous silica nanoparticles. Moreover, these hybrid polymers can be both externally and internally functionalized to improve the biocompatibility and allow hydrophilic and hydrophobic environments inside the pores for the encapsulation of different drugs on demand, respectively [70]. Different drug loading approaches have been successfully applied for the preparation of active MOFs, including those based on simple electrostatic interactions or hydrogen bonds, prefunctionalization of organic ligands, postsynthetic modifications, and ligand exchange or metal metathesis [69]. This broad variety of possibilities, together with their loading and releasing efficiencies, have confirmed MOFs as a superior opponent due to the poor postfunctionalization chemistry involving silica, practically based on silanol chemistry, or the low adsorption showed by conventional organic polymers [68].

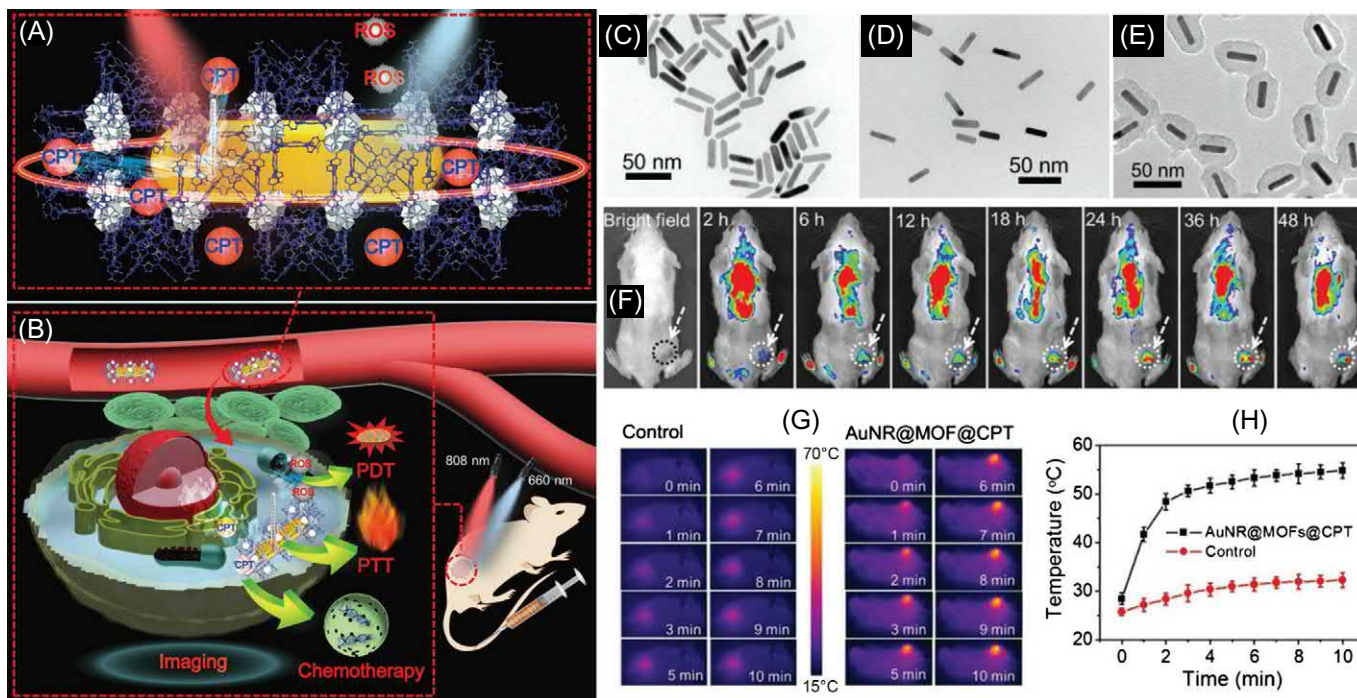
In terms of imaging, MOFs themselves can be used as biomarkers, for example in magnetic resonance imaging [94], due to the presence of paramagnetic meta ions. However, when desired structures cannot be obtained or are not suitable for such imaging modalities, postsynthetic modifications enable the possibility of introducing fluorescent labels or contrast agents within the polymeric network [95]. Thus, a dual behavior is shown: not only drug delivery can be achieved, but also the *in vivo* localization of the nanocarrier and the evaluation of the efficiency of the therapeutic process, enabling the use of MOFs in the field of theranostics. It is worth to mention that this second approach is not as usual as the former, mainly because (1) larger and time-consuming synthetic steps are required, and (2) if the final application combines both imaging and drug delivery, then the drug loading efficiency decreases to allow the label be incorporated. MOFs show relevant advantages in this field, such as a high rate of margination to escape from the blood flow through vessel walls, can be surface-functionalized to show a strong affinity for damaged or carcinogenic instead of healthy cells, and can easily and rapidly penetrate cells and tissues [96].

Regarding the photodynamic therapy, due to their incredible loading efficiencies, MOFs have risen as candidates to encapsulate photosensitizers, usually showing poor stability and high cytotoxicity while using other carriers [72]. Furthermore, their encapsulation within the framework minimizes the aggregation of the photosensitizers, improving the solubility and increasing the cellular uptake, and enabling their combination with other treatments [77]. Porphyrinic-based MOFs have proven to be an optimal platform for this application as the matrix allows the free diffusion of both triple and singlet oxygen throughout the polymer network, and they were the first MOFs tested [67]. Some other relevant examples concern the use of MOFs from the fourth generation [78].

### 23.3 Future trends and conclusions

We are currently knocking the fifth generation's door of MOFs and two new tendencies seem to support this transition: surface modifications through polymer coatings or surface grafting, using biomolecules like lipids, enzymes, or proteins, and the use of composite materials in the form of core-shell nanoparticles in order to improve the selectivity and the biostability [65, 67]. It is particularly interesting to note the efforts made during the last years on the fabrication of composite-based MOFs where synergetic effects are expected upon the combination of different materials, conferring MOFs new properties they use to lack, such as magnetism using ferromagnetic nanoparticles or luminescence coming from quantum dots or, more interestingly, upconversion nanoparticles in nonlinear optical processes for imaging, among others [20]. In addition, a recent and a promising technique based on pore-space partitioning MOFs has been published which may allow for the encapsulation of different drugs simultaneously for broader scopes and improved treatments according to the differentiation between pores [97]. The comprehension of all the available possibilities is essential for unraveling the future advances and discoveries, not only in medicine but also in other relevant fields such as catalysis or energy. New fabrication methodologies and the application of different procedures adapted from the plastic and metal industries seem to be crucial and constitute the straightforward steps toward a practically infinite palette of possibilities. The use of nanoMOFs is important not only because of their extraordinary chemical reactivity, which can be exploited to functionalize them with a multitude of molecules, but also due to the lower melting points compared to larger micron-sized particles [98]. In that sense, liquid MOFs have been already proposed as potential candidates for medical applications [99], and amorphous MOFs have already demonstrated their applicability in drug delivery [100], although no further evidences can still be found in other biomedical areas.

Relevant examples of the aspects commented before can be recently found in the literature, constituting a full evidence of the importance of using both biological coatings and core-shell technology. For instance, the field of theranostics is rapidly awakening as new core-shell MOF-based composites are now well-understood and being studied in a deep detail to avoid synthetic reproducibility issues. Lanthanide-doped upconversion nanoparticles in combination with porphyrinic PCN-222 MOFs in a Janus-like morphology have been used elsewhere [101]. A Förster resonance energy transfer (FRET)-based mechanism was followed upon near infrared light irradiation to produce singlet oxygen and, although the penetration and the absorption of these wavelengths throughout the tissues are limited, this nanoMOF has demonstrated excellent properties to efficiently absorb this light avoiding the typical use of intense UV or visible radiations that can seriously damage healthy cells. They successfully tested the cytotoxicity of the material, being able to suppress breast tumors in mice while loading the MOF with doxorubicin by combining chemotherapy and photodynamic therapies. A combination of both photodynamic and photothermal therapies has been demonstrated by Zeng et al., based



**Fig. 23.4**

PCN-222-covered gold nanorods (AuNRs@PCN-222) used as multifunctional theranostic system for cancer combined therapy by loading the drug camptothecin. (A) Schematic structure of the composite. (B) Combined photodynamic/photothermal/chemotherapy of tumor. Transmission electron microscopy images of: (C) as-synthesized AuNRs, (D) PEG-functionalized AuNRs, and (E) AuNRs@PCN-222, (F) The in vivo fluorescence images of the mice after intravenous injection of the composite, (G) The in vivo thermal images of the mice after intravenous injection of PBS as a control (left) and the composite (right) with 808 nm laser irradiation, and (H) temperature change curve of tumor tissues as a function of irradiation time. Reproduced with permission from J.-Y. Zeng, M.-K. Zhang, M.-Y. Peng, D. Gong, X.-Z. Zhang, *Porphyritic metal-organic frameworks coated gold nanorods as a versatile nanoplatfor for combined photodynamic/photothermal/chemotherapy of tumor*, *Adv. Funct. Mater.* 28(8) (2018) 1705451.

on gold nanorods as cores, showing a relevant absorption of the infrared light due to their localized surface plasmon resonance properties, and PCN-222 as shell for singlet oxygen generation [102] (Fig. 23.4). In this case, camptothecin is encapsulated within the MOF and the system, after *in vitro* and *in vivo* experiments showing the lack of toxicity, was used to image the tumors, release the drug in a triggered fashion upon infrared radiation, and increase the localized temperature of the tumor killing unhealthy cells. More recently, Liu et al. have demonstrated the use of MIL-101(Fe)-NH<sub>2</sub>-coated black phosphorus photosensitizers for the tandem catalysis of H<sub>2</sub>O<sub>2</sub> generated intracellularly in excess to O<sub>2</sub> and its further conversion into reactive oxygen species [103]. This hybrid composite, showing two differentiated and confined zones, demonstrated a 8.7-fold higher efficiency for photodynamic therapy than other previously reported materials, and subcutaneous HeLa tumors in mice were successfully removed after 14 days due to the efficiency of singlet oxygen generation and the hyperthermia. Some other relevant advances have been made in radiotherapy, using Hf-based porphyrinic MOFs [104] and immunotherapy, by decorating their surface with specific antibodies [105].

Chedid and Yassin proposed in a review from 2018 the use of MOFs as potential antidotes for human metal-poisoning according to their coordination ability and their widespread application in different fields for the similar goal such as water and environmental remediation [72]. However, to date, this hypothesis has not been further developed from an experimental point of view. In the later application, MOFs are generally embedded within hydrophilic polymeric matrices or membranes. One should envision how to reproduce similar performances in a biocompatible manner, trapping the desired metals, ensuring a full integrity of the nanoMOFs circulating through capillaries and avoiding the leaching of the already captured metal ions close to another organs and tissues that might result in lethal consequences. If the idea is to excrete those nanoparticles out of the organism, then smaller particle sizes than 200 nm and extremely hydrophilic materials are required to avoid their collapse and aggregation within the urinary system, particularly in kidneys, and facilitating their diffusion through different barriers to be efficiently removed. Another nontested but interesting and promising application is the use of nanoMOFs as nerve guidance tube substituents for medical implants in order to bridge peripheral nerves in reconstruction surgeries [87] (Fig. 23.5). Although not used yet, authors demonstrate the potential applicability of Zr-fumarate MOFs for that purpose without significant *in vitro* toxicity when using adult Schwann cells in a low dose range, being a convenient formulation for coating nerves. An interesting new kind of MOF-based composites consisting of magnetic helical microstructures, called artificial bacterial flagella, covered by Zn-imidazolite ZIF-8 layers has been proposed for single-cell targeting and the pH-triggered drug release in a precise manner through a complex microfluidic channel network [106] (Fig. 23.6). Authors gave them the name of MOFBOTS and it is the first evidence of providing artificial locomotion to these polymers that can be guided under weak rotational magnetic fields in contrast with other reported magnetic MOFs, which require higher magnetic fields. The material described herein has successfully circumvented the selectivity issue, being able to



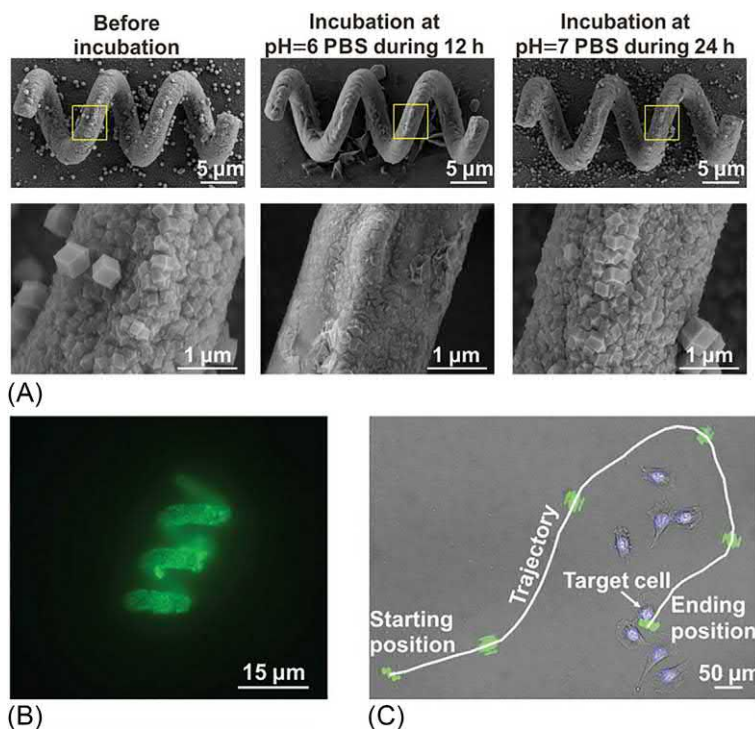
**Fig. 23.5**

Different possible applications of nanoMOF for diagnosis (left), therapy (right), and for the creation of smart surfaces (bottom). Particularly, Wuttke et al. proposed the use of these polymers as nerve guidance tube substituents, probing for the first time their biocompatibility in vitro in a systematic manner. Reproduced with permission from S. Wuttke, A. Zimpel, T. Bein, S. Braig, K. Stoiber, A. Vollmar, D. Müller, K. Haastert-Talini, J. Schaeske, M. Stiesch, G. Zahn, A. Mohmeyer, P. Behrens, O. Eickelberg, D.A. Bölükbas, S. Meiners, *Validating metal-organic framework nanoparticles for their nanosafety in diverse biomedical applications*, *Adv. Healthc. Mater.* 6(2) (2017) 1600818.

target the desired tumor in a motion-controlled fashion. To date, this system has been only used to deliver rhodamine B as a drug model, merely applied to in vitro experiments and some aspects, such as the controlled directionality, and should be addressed prior to perform in vivo assays. Nevertheless, it is expected that these drawbacks may be overcome soon and the use of MOFBOTS would be extended in the near future for real-life applications.

On the other hand, although it is not the main focus of this book, reproducible syntheses at the large-scale and commercialization of MOFs require special attention as their contribution to the field of biomedicine should be considered as the last relevant steps, after in vivo experiments had shown a lack of toxicity of MOFs for humans and safe regulations had been overcome,





**Fig. 23.6**

(A) Scanning electron microscopy images of magnetic helical artificial flagella covered with ZIF-8 crystals, as-synthesized and after being treated at different pH and buffered media. The material showed stability at physiological pH, but degradation at pH 6 that could be used as an advantage for controlled drug delivery due to the acidic environment of cancer cells. (B) Fluorescence image of one MOFBOT after being loaded with rhodamine B. (C) Microscopy image showing the movement of one rhodamine B-loaded MOFBOT structure along a complex trajectory, targeting a single cell. Reproduced with permission from X. Wang, X.-Z. Chen, C.C.J. Alcântara, S. Sevim, M. Hoop, A. Terzopoulou, C. de Marco, C. Hu, A.J. de Mello, P. Falcaro, S. Furukawa, B.J. Nelson, J. Puigmartí-Luis, S. Pané, MOFBOTS: metal–organic-framework-based biomedical microrobots, *Adv. Mater.* 31 (27) (2019) 1901592.

throughout the complex route to successful real applications. BASF was the first company commercializing these materials in different formats as pellets and extrudates upon the use of binders in small volumes [66, 107–109], and Merck has recently included in his catalog an interesting tool, the metal-organic framework constructor, to identify potential organic linkers, metal precursors, and a broad variety of secondary building units for commercial purchasing [110]. In 2016, the first company dedicated entirely to large-scale MOF production appeared, MOF Technologies, as a spin-off of Queen’s University (Belfast) [111]. The company is able to prepare 10 MOFs at production runs of up to 100 kg and 15 in the range mg-g following solvent-free, scalable, and continuous processes [112]. The reader is referred to the literature for further information [113–115]. Interestingly, in 2018, the University of St Andrews’



spin-out MOFgen Ltd. pioneered the fabrication of these polymers for biomedical applications at industrial level, emphasizing on MOF-based drug delivery systems, novel antimicrobial formulations, infection control, and preventing vasoconstriction and thrombus [116].

Are MOFs the most suitable candidates for medical applications in the future? Attending the trends commented in this chapter and regarding other materials, the amount of publications, and the relative growths of each, one may expect an affirmative answer. The use of nanoMOFs in biomedicine regarding the works published within 2008–18 has shown the largest relative increase compared to other well-established areas such as catalysis, gas storage, or separation in the same period. Drug delivery has been the most extended application, but the use of new strategies, such as coating with biological elements and the fabrication of core-shell composite materials surpassing the fascinating but limited properties of the first MOF generations, and the practically infinity of synthetic methodologies resulting in materials showing breathing capacities and tunable pore sizes through approaches like isoreticular expansion, have paved the way for their application in different medical fields. In addition, MOFs have emerged as promising carriers for encapsulating photosensitizers in photodynamic/thermal therapies for cancer treatment. Remarkably, the synergy of using MOFs for simultaneous purposes such as drug delivery/imaging, drug delivery/photodynamic therapy, among other combinations, has made complicated to establish a solid barrier between each individual application, if not senseless.

Preliminary poorly characterized *in vitro* cytotoxic experiments have been continuously supported by new *in vivo* biocompatibility studies, demonstrating the suitability of these materials in biomedicine, and that every developed system must be designed and tested according to the final target and purpose, being harmless for healthy patients and organisms/tissues/cells. Still some aspects should be solved, particularly those concerning legislations, regulations, and ethical considerations, before they can be fully and safely applied in some of these new potential applications, but, although related, these issues can be considered out of the scope of the MOF technology itself. Pharmaceutical formulations have been considerably improved, enabling the possibility of large-scale productions in different formats, even in the kg range, in a reproducible manner, and new companies have emerged according to the interest of this field to satisfy the on-growing demand.

In summary, the privilege position of MOFs in medicine arises from their hybrid nature, structural diversity, porosity and, more importantly, because of their tunability. They show the largest pore volumes described to date for this purpose and can undergo almost infinite chemical modifications. Although classical inorganic and organic materials show larger stability, MOFs surpass them in every other aspect such as loading efficiencies or low cytotoxicity *in vitro* and, furthermore, different synthetic strategies can be followed to improve the previous drawback, their biocompatibility, enabling even the most challenging drugs to be encapsulated playing with the hydrophilic/hydrophobic behavior of the pores, and the possibility of using endogenous components to improve the biodegradability. Stimuli-triggered

nanoMOFs resulting from the new fabrication methodologies have enabled a precise control over the kinetic delivery profiles, allowing a persistent action of the drugs even after weeks of administration, thus lacking of the “burst effect” showed by the pure organic and inorganic counterparts. Every approach discussed herein yields hybrid materials with significant pharmacological effects, a careful control over kinetic release profiles upon modulating host-guest interactions and reproducible loading capacities with potential scaling-up features in the pharmaceutical industry.

This book is entirely dedicated to the importance of MOFs in (bio)medicine and every single application described within this field until August 2019. We hope that, as the first full book published in this area, it will be considered as a guide for the researchers in the near future. Undoubtedly, and somehow hopefully, it will be old-fashioned soon due to the new upcoming MOF generation based on the abovementioned strategies to address the current limitations. After all, this is the consequence of continuous and constant efforts to improve the novel on-demand technologies.

## References

- [1] S.R. Batten, N.R. Champness, X.-M. Chen, J. Garcia-Martinez, S. Kitagawa, L. Öhrström, M. O’Keeffe, M. Paik Suh, J. Reedijk, Terminology of metal–organic frameworks and coordination polymers, *Pure Appl. Chem.* 85 (8) (2013) 1715–1724.
- [2] A.A. Yakovenko, Z. Wei, M. Wriedt, J.-R. Li, G.J. Halder, H.-C. Zhou, Study of guest molecules in metal–organic frameworks by powder X-ray diffraction: analysis of difference envelope density, *Cryst. Growth Des.* 14 (11) (2014) 5397–5407.
- [3] T.D. Bennett, A.K. Cheetham, Amorphous metal–organic frameworks, *Acc. Chem. Res.* 47 (5) (2014) 1555–1562.
- [4] T.D. Bennett, S. Horike, Liquid, glass and amorphous solid states of coordination polymers and metal–organic frameworks, *Nat. Rev. Mater.* 3 (11) (2018) 431–440.
- [5] S.R. Batten, N.R. Champness, X.-M. Chen, J. Garcia-Martinez, S. Kitagawa, L. Öhrström, M. O’Keeffe, M.P. Suh, J. Reedijk, Coordination polymers, metal–organic frameworks and the need for terminology guidelines, *CrystEngComm* 14 (9) (2012) 3001–3004.
- [6] S. Iram, M. Imran, F. Kanwal, Z. Iqbal, F. Deeba, Q.J. Iqbal, Bismuth(III) based metal organic frameworks: luminescence, gas adsorption, and antibacterial studies, *Z. Anorg. Allg. Chem.* 645 (1) (2019) 50–56.
- [7] S. Sharma, D. Mittal, A.K. Verma, I. Roy, Copper-gallic acid nanoscale metal–organic framework for combined drug delivery and photodynamic therapy, *ACS Appl. Bio Mater.* 2 (5) (2019) 2092–2101.
- [8] S. Wang, M. Wahiduzzaman, L. Davis, A. Tissot, W. Shepard, J. Marrot, C. Martineau-Corcus, D. Hamdane, G. Maurin, S. Devautour-Vinot, C. Serre, A robust zirconium amino acid metal–organic framework for proton conduction, *Nat. Commun.* 9 (1) (2018) 4937.
- [9] S.M.J. Rogge, A. Bavykina, J. Hajek, H. Garcia, A.I. Olivos-Suarez, A. Sepúlveda-Escribano, A. Vimont, G. Clet, P. Bazin, F. Kapteijn, M. Daturi, E.V. Ramos-Fernandez, F.X. Llabrés i Xamena, V. Van Speybroeck, J. Gascon, Metal–organic and covalent organic frameworks as single-site catalysts, *Chem. Soc. Rev.* 46 (11) (2017) 3134–3184.
- [10] S. Das, P. Heasman, T. Ben, S. Qiu, Porous organic materials: strategic design and structure–function correlation, *Chem. Rev.* 117 (3) (2017) 1515–1563.
- [11] S.J. Lyle, P.J. Waller, O.M. Yaghi, Covalent organic frameworks: organic chemistry extended into two and three dimensions, *Trends Chem.* 1 (2) (2019) 172–184.

- [12] C.J. Jansen, E. Esposito, A. Fuoco, M. Carta, Microporous organic polymers: synthesis, characterization, and applications, *Polymers* 11 (5) (2019) 844.
- [13] O.M. Yaghi, Reticular chemistry—construction, properties, and precision reactions of frameworks, *J. Am. Chem. Soc.* 138 (48) (2016) 15507–15509.
- [14] O.M. Yaghi, Reticular chemistry in all dimensions, *ACS Cent. Sci.* 5 (8) (2019) 1295–1300.
- [15] L. Jiao, Y. Wang, H.-L. Jiang, Q. Xu, Metal–organic frameworks as platforms for catalytic applications, *Adv. Mater.* 30 (37) (2017) 1703663.
- [16] H. Li, K. Wang, Y. Sun, C.T. Lollar, J. Li, H.-C. Zhou, Recent advances in gas storage and separation using metal–organic frameworks, *Mater. Today* 21 (2) (2018) 108–121.
- [17] R.-B. Lin, S. Xiang, H. Xing, W. Zhou, B. Chen, Exploration of porous metal–organic frameworks for gas separation and purification, *Coord. Chem. Rev.* 378 (2019) 87–103.
- [18] X. Zhao, Y. Wang, D.-S. Li, X. Bu, P. Feng, Metal–organic frameworks for separation, *Adv. Mater.* 30 (37) (2018) 1705189.
- [19] C.-C. Hou, Q. Xu, Metal–organic frameworks for energy, *Adv. Energy Mater.* 9 (23) (2019) 1801307.
- [20] S. Carrasco, Metal-organic frameworks for the development of biosensors: a current overview, *Biosensors* 8 (4) (2018) 92.
- [21] P.Z. Moghadam, A. Li, S.B. Wiggin, A. Tao, A.G.P. Maloney, P.A. Wood, S.C. Ward, D. Fairen-Jimenez, Development of a Cambridge structural database subset: a collection of metal–organic frameworks for past, present, and future, *Chem. Mater.* 29 (7) (2017) 2618–2625.
- [22] Q.-L. Zhu, Q. Xu, Metal–organic framework composites, *Chem. Soc. Rev.* 43 (16) (2014) 5468–5512.
- [23] O. Delgado Friedrichs, M. O’Keeffe, O.M. Yaghi, Three-periodic nets and tilings: semiregular nets, *Acta Crystallogr. A* 59 (6) (2003) 515–525.
- [24] O.M. Yaghi, D.A. Richardson, G. Li, C.E. Davis, T.L. Groy, Open-framework solids with diamond-like structures prepared from clusters and metal-organic building blocks, *MRS Proc.* 371 (2011) 15–19.
- [25] K.A. Hofmann, F. Küspert, Verbindungen von Kohlenwasserstoffen mit Metallsalzen, *Z. Anorg. Chem.* 15 (1) (1897) 204–207.
- [26] J.H. Rayner, H.M. Powell, 67. Structure of molecular compounds. Part X. Crystal structure of the compound of benzene with an ammonia–nickel cyanide complex, *J. Chem. Soc.* (1952) 319–328.
- [27] M. Fujita, From Hofmann complexes to organic coordination networks, in: L.R. MacGillivray (Ed.), *Metal-Organic Frameworks: Design and Application*, John Wiley & Sons, Hoboken, NJ, 2010, pp. 1–36.
- [28] B.F. Hoskins, R. Robson, Infinite polymeric frameworks consisting of three dimensionally linked rod-like segments, *J. Am. Chem. Soc.* 111 (15) (1989) 5962–5964.
- [29] A.J. Fletcher, E.J. Cussen, T.J. Prior, M.J. Rosseinsky, C.J. Kepert, K.M. Thomas, Adsorption dynamics of gases and vapors on the nanoporous metal organic framework material Ni<sub>2</sub>(4,4’-bipyridine)<sub>3</sub>(NO<sub>3</sub>)<sub>4</sub>: guest modification of host sorption behavior, *J. Am. Chem. Soc.* 123 (41) (2001) 10001–10011.
- [30] M. Eddaoudi, J. Kim, N. Rosi, D. Vodak, J. Wachter, M. Keffe, O.M. Yaghi, Systematic design of pore size and functionality in isorecticular MOFs and their application in methane storage, *Science* 295 (5554) (2002) 469.
- [31] J. Bitzer, W. Kleist, Synthetic strategies and structural arrangements of isorecticular mixed-component metal–organic frameworks, *Chem. Eur. J.* 25 (8) (2019) 1866–1882.
- [32] L. Feng, S. Yuan, J.-S. Qin, Y. Wang, A. Kirchon, D. Qiu, L. Cheng, S.T. Madrahimov, H.-C. Zhou, Lattice expansion and contraction in metal-organic frameworks by sequential linker reinstallation, *Matter* 1 (1) (2019) 156–167.
- [33] B. Tahmouresilerd, M. Moody, L. Agogo, A.F. Cozzolino, The impact of an isorecticular expansion strategy on the performance of iodine catalysts supported in multivariate zirconium and aluminum metal–organic frameworks, *Dalton Trans.* 48 (19) (2019) 6445–6454.
- [34] G.E.M. Schukraft, S. Ayala, B.L. Dick, S.M. Cohen, Isorecticular expansion of polyMOFs achieves high surface area materials, *Chem. Commun.* 53 (77) (2017) 10684–10687.
- [35] H. Furukawa, Y.B. Go, N. Ko, Y.K. Park, F.J. Uribe-Romo, J. Kim, M. O’Keeffe, O.M. Yaghi, Isorecticular expansion of metal–organic frameworks with triangular and square building units and the lowest calculated density for porous crystals, *Inorg. Chem.* 50 (18) (2011) 9147–9152.

- [36] Z. Wang, C.-M. Jin, T. Shao, Y.-Z. Li, K.-L. Zhang, H.-T. Zhang, X.-Z. You, Syntheses, structures, and luminescence properties of a new family of three-dimensional open-framework lanthanide coordination polymers, *Inorg. Chem. Commun.* 5 (9) (2002) 642–648.
- [37] B. Chen, Y. Yang, F. Zapata, G. Lin, G. Qian, E.B. Lobkovsky, Luminescent open metal sites within a metal–organic framework for sensing small molecules, *Adv. Mater.* 19 (13) (2007) 1693–1696.
- [38] J. Liu, F. Sun, F. Zhang, Z. Wang, R. Zhang, C. Wang, S. Qiu, In situ growth of continuous thin metal–organic framework film for capacitive humidity sensing, *J. Mater. Chem.* 21 (11) (2011) 3775–3778.
- [39] B.V. Harbuzaru, A. Corma, F. Rey, J.L. Jordá, D. Ananias, L.D. Carlos, J. Rocha, A miniaturized linear pH sensor based on a highly photoluminescent self-assembled europium(III) metal–organic framework, *Angew. Chem. Int. Ed.* 48 (35) (2009) 6476–6479.
- [40] B. Chen, L. Wang, Y. Xiao, F.R. Fronczek, M. Xue, Y. Cui, G. Qian, A luminescent metal–organic framework with Lewis basic pyridyl sites for the sensing of metal ions. *Angew. Chem. Int. Ed.* 48 (3) (2009) 500–503.
- [41] A.H. Khoshaman, B. Bahreyni, Application of metal organic framework crystals for sensing of volatile organic gases, *Sensors Actuators B Chem.* 162 (1) (2012) 114–119.
- [42] S. Achmann, G. Hagen, J. Kita, M.I. Malkowsky, C. Kiener, R. Moos, Metal-organic frameworks for sensing applications in the gas phase, *Sensors* 9 (3) (2009) 1574–1589.
- [43] A. Lan, K. Li, H. Wu, D.H. Olson, T.J. Emge, W. Ki, M. Hong, J. Li, A luminescent microporous metal–organic framework for the fast and reversible detection of high explosives, *Angew. Chem. Int. Ed.* 48 (13) (2009) 2334–2338.
- [44] C. Hou, Q. Xu, L. Yin, X. Hu, Metal–organic framework templated synthesis of Co<sub>3</sub>O<sub>4</sub> nanoparticles for direct glucose and H<sub>2</sub>O<sub>2</sub> detection, *Analyst* 137 (24) (2012) 5803–5808.
- [45] J. Liu, L. Chen, H. Cui, J. Zhang, L. Zhang, C.-Y. Su, Applications of metal–organic frameworks in heterogeneous supramolecular catalysis, *Chem. Soc. Rev.* 43 (16) (2014) 6011–6061.
- [46] H.-C. Zhou, J.R. Long, O.M. Yaghi, Introduction to metal–organic frameworks, *Chem. Rev.* 112 (2) (2012) 673–674.
- [47] H. Wang, Q. Wang, S.J. Teat, D.H. Olson, J. Li, Synthesis, structure, and selective gas adsorption of a single-crystalline zirconium based microporous metal–organic framework, *Cryst. Growth Des.* 17 (4) (2017) 2034–2040.
- [48] J.V. Alegre-Requena, E. Marqués-López, R.P. Herrera, D.D. Díaz, Metal–organic frameworks (MOFs) bring new life to hydrogen-bonding organocatalysts in confined spaces, *CrystEngComm* 18 (22) (2016) 3985–3995.
- [49] A. Karmakar, P. Samanta, A.V. Desai, S.K. Ghosh, Guest-responsive metal–organic frameworks as scaffolds for separation and sensing applications, *Acc. Chem. Res.* 50 (10) (2017) 2457–2469.
- [50] F.-X. Coudert, Responsive metal–organic frameworks and framework materials: under pressure, taking the heat, in the spotlight, with friends, *Chem. Mater.* 27 (6) (2015) 1905–1916.
- [51] C. Serre, C. Mellot-Draznieks, S. Surblé, N. Audebrand, Y. Filinchuk, G. Férey, Role of solvent-host interactions that lead to very large swelling of hybrid frameworks, *Science* 315 (5820) (2007) 1828.
- [52] K. Biradha, M. Fujita, A springlike 3D-coordination network that shrinks or swells in a crystal-to-crystal manner upon guest removal or readsorption, *Angew. Chem. Int. Ed.* 41 (18) (2002) 3392–3395.
- [53] Z. Yin, S. Wan, J. Yang, M. Kurmoo, M.-H. Zeng, Recent advances in post-synthetic modification of metal–organic frameworks: new types and tandem reactions, *Coord. Chem. Rev.* 378 (2019) 500–512.
- [54] T. Sagara, J. Klassen, E. Ganz, Computational study of hydrogen binding by metal-organic framework-5, *J. Chem. Phys.* 121 (24) (2004) 12543–12547.
- [55] C. Combelles, M.L. Doublet, Structural, magnetic and redox properties of a new cathode material for Li-ion batteries: the iron-based metal organic framework, *Ionics* 14 (4) (2008) 279–283.
- [56] G. de Combarieu, M. Morcrette, F. Millange, N. Guillou, J. Cabana, C.P. Grey, I. Margiolaki, G. Férey, J.M. Tarascon, Influence of the benzoquinone sorption on the structure and electrochemical performance of the MIL-53(Fe) hybrid porous material in a lithium-ion battery, *Chem. Mater.* 21 (8) (2009) 1602–1611.
- [57] P. Horcajada, C. Serre, M. Vallet-Regí, M. Sebban, F. Taulelle, G. Férey, Metal–organic frameworks as efficient materials for drug delivery, *Angew. Chem. Int. Ed.* 45 (36) (2006) 5974–5978.
- [58] W.J. Rieter, K.M.L. Taylor, W. Lin, Surface modification and functionalization of nanoscale metal-organic frameworks for controlled release and luminescence sensing, *J. Am. Chem. Soc.* 129 (32) (2007) 9852–9853.

- [59] K.M.L. Taylor, A. Jin, W. Lin, Surfactant-assisted synthesis of nanoscale gadolinium metal–organic frameworks for potential multimodal imaging, *Angew. Chem. Int. Ed.* 47 (40) (2008) 7722–7725.
- [60] P. Horcajada, T. Chalati, C. Serre, B. Gillet, C. Sebrie, T. Baati, J.F. Eubank, D. Heurtaux, P. Clayette, C. Kreuz, J.-S. Chang, Y.K. Hwang, V. Marsaud, P.-N. Bories, L. Cynober, S. Gil, G. Férey, P. Couvreur, R. Gref, Porous metal–organic-framework nanoscale carriers as a potential platform for drug delivery and imaging, *Nat. Mater.* 9 (2009) 172.
- [61] K. Lu, C. He, W. Lin, Nanoscale metal–organic framework for highly effective photodynamic therapy of resistant head and neck cancer, *J. Am. Chem. Soc.* 136 (48) (2014) 16712–16715.
- [62] J. An, S.J. Geib, N.L. Rosi, Cation-triggered drug release from a porous zinc–adeninate metal–organic framework, *J. Am. Chem. Soc.* 131 (24) (2009) 8376–8377.
- [63] J. Chen, X. Zhang, C. Huang, H. Cai, S. Hu, Q. Wan, X. Pei, J. Wang, Osteogenic activity and antibacterial effect of porous titanium modified with metal-organic framework films, *J. Biomed. Mater. Res. A* 105 (3) (2017) 834–846.
- [64] X. Shen, Y. Zhang, P. Ma, L. Sutrisno, Z. Luo, Y. Hu, Y. Yu, B. Tao, C. Li, K. Cai, Fabrication of magnesium/zinc-metal organic framework on titanium implants to inhibit bacterial infection and promote bone regeneration, *Biomaterials* 212 (2019) 1–16.
- [65] A.C. McKinlay, R.E. Morris, P. Horcajada, G. Férey, R. Gref, P. Couvreur, C. Serre, BioMOFs: metal–organic frameworks for biological and medical applications, *Angew. Chem. Int. Ed.* 49 (36) (2010) 6260–6266.
- [66] P. Horcajada, R. Gref, T. Baati, P.K. Allan, G. Maurin, P. Couvreur, G. Férey, R.E. Morris, C. Serre, Metal–organic frameworks in biomedicine, *Chem. Rev.* 112 (2) (2012) 1232–1268.
- [67] Y. Liu, Y. Zhao, X. Chen, Bioengineering of metal-organic frameworks for nanomedicine, *Theranostics* 9 (11) (2019) 3122–3133.
- [68] S. Keskin, S. Kızılel, Biomedical applications of metal organic frameworks, *Ind. Eng. Chem. Res.* 50 (4) (2011) 1799–1812.
- [69] V. André, S. Quaresma, Bio-inspired metal-organic frameworks in the pharmaceutical world: a brief review, in: F. Zafar, E. Sharmin (Eds.), *Metal-Organic Frameworks*, IntechOpen, 2016, pp. 135–156.
- [70] W. Chen, C. Wu, Synthesis, functionalization, and applications of metal–organic frameworks in biomedicine, *Dalton Trans.* 47 (7) (2018) 2114–2133.
- [71] A. Cabrera-García, Z. Díaz-Betancor, E. Rivero-Buceta, Zeolites and metal-organic frameworks as biomedical nanodevices, in: V. Blay, L.F. Bobadilla, A.C. García (Eds.), *Zeolites and Metal-Organic Frameworks*, Amsterdam University Press, Amsterdam, 2018, pp. 265–288.
- [72] G. Chedid, A. Yassin, Recent trends in covalent and metal organic frameworks for biomedical applications, *Nanomaterials* 8 (11) (2018) 916.
- [73] I. Mihad, S. Rana, A.H. Ghaleb, Anti-cancer drug delivery using metal organic frameworks (MOFs), *Curr. Med. Chem.* 24 (2) (2017) 193–214.
- [74] S. Wuttke, M. Lismont, A. Escudero, B. Rungtaweeworant, W.J. Parak, Positioning metal-organic framework nanoparticles within the context of drug delivery—a comparison with mesoporous silica nanoparticles and dendrimers, *Biomaterials* 123 (2017) 172–183.
- [75] M.-X. Wu, Y.-W. Yang, Metal–organic framework (MOF)-based drug/cargo delivery and cancer therapy, *Adv. Mater.* 29 (23) (2017) 1606134.
- [76] L. Wang, M. Zheng, Z. Xie, Nanoscale metal–organic frameworks for drug delivery: a conventional platform with new promise, *J. Mater. Chem. B* 6 (5) (2018) 707–717.
- [77] Q. Guan, Y.-A. Li, W.-Y. Li, Y.-B. Dong, Photodynamic therapy based on nanoscale metal–organic frameworks: from material design to cancer nanotherapeutics, *Chem. Asian J.* 13 (21) (2018) 3122–3149.
- [78] M. Lismont, L. Dreesen, S. Wuttke, Metal-organic framework nanoparticles in photodynamic therapy: current status and perspectives, *Adv. Funct. Mater.* 27 (14) (2017) 1606314.
- [79] Y. Sakamaki, J. Ozdemir, Z. Heidrick, O. Watson, H.R. Shahsavari, M. Fereidoonzhad, A.R. Khosropour, M.H. Beyzavi, Metal–organic frameworks and covalent organic frameworks as platforms for photodynamic therapy, *Comments Inorg. Chem.* 38 (6) (2018) 238–293.
- [80] M.A. Chowdhury, Metal-organic-frameworks as contrast agents in magnetic resonance imaging, *ChemBioEng Rev.* 4 (4) (2017) 225–239.

- [81] H.-S. Wang, Metal–organic frameworks for biosensing and bioimaging applications, *Coord. Chem. Rev.* 349 (2017) 139–155.
- [82] S.E. Miller, M.H. Teplensky, P.Z. Moghadam, D. Fairen-Jimenez, Metal-organic frameworks as biosensors for luminescence-based detection and imaging, *Interface Focus* 6 (4) (2016).
- [83] P. Rivera-Gil, D. Jimenez De Aberasturi, V. Wulf, B. Pelaz, P. Del Pino, Y. Zhao, J.M. De La Fuente, I. Ruiz De Larramendi, T. Rojo, X.-J. Liang, W.J. Parak, The challenge to relate the physicochemical properties of colloidal nanoparticles to their cytotoxicity, *Acc. Chem. Res.* 46 (3) (2013) 743–749.
- [84] M. Sajid, Toxicity of nanoscale metal organic frameworks: a perspective, *Environ. Sci. Pollut. Res.* 23 (15) (2016) 14805–14807.
- [85] H. Cai, Y.-L. Huang, D. Li, Biological metal–organic frameworks: structures, host–guest chemistry and bio-applications, *Coord. Chem. Rev.* 378 (2019) 207–221.
- [86] C. Tamames-Tabar, D. Cunha, E. Imbuluzqueta, F. Ragon, C. Serre, M.J. Blanco-Prieto, P. Horcajada, Cytotoxicity of nanoscaled metal–organic frameworks, *J. Mater. Chem. B* 2 (3) (2014) 262–271.
- [87] S. Wuttke, A. Zimpel, T. Bein, S. Braig, K. Stoiber, A. Vollmar, D. Müller, K. Haastert-Talini, J. Schaeske, M. Stiesch, G. Zahn, A. Mohmeyer, P. Behrens, O. Eickelberg, D.A. Bölükbas, S. Meiners, Validating metal-organic framework nanoparticles for their nanosafety in diverse biomedical applications, *Adv. Healthc. Mater.* 6 (2) (2017) 1600818.
- [88] T. Simon-Yarza, A. Mielcarek, P. Couvreur, C. Serre, Nanoparticles of metal-organic frameworks: on the road to in vivo efficacy in biomedicine, *Adv. Mater.* 30 (37) (2018) 1707365.
- [89] M. Bosch, M. Zhang, H.-C. Zhou, Increasing the stability of metal-organic frameworks, *Adv. Chem.* 2014 (2014) 8.
- [90] X. Li, L. Lachmanski, S. Safi, S. Sene, C. Serre, J.M. Grenèche, J. Zhang, R. Gref, New insights into the degradation mechanism of metal-organic frameworks drug carriers, *Sci. Rep.* 7 (1) (2017) 13142.
- [91] T. Simon-Yarza, S. Rojas, P. Horcajada, C. Serre, The situation of metal-organic frameworks in biomedicine, *Compr. Biomater. II* 4 (2017) 719–749.
- [92] P. Silva, S.M.F. Vilela, J.P.C. Tomé, F.A. Almeida Paz, Multifunctional metal–organic frameworks: from academia to industrial applications, *Chem. Soc. Rev.* 44 (19) (2015) 6774–6803.
- [93] K. Liang, R. Ricco, C.M. Doherty, M.J. Styles, S. Bell, N. Kirby, S. Mudie, D. Haylock, A.J. Hill, C. J. Doonan, P. Falcaro, Biomimetic mineralization of metal-organic frameworks as protective coatings for biomacromolecules, *Nat. Commun.* 6 (2015) 7240.
- [94] M. Peller, K. Böll, A. Zimpel, S. Wuttke, Metal–organic framework nanoparticles for magnetic resonance imaging, *Inorg. Chem. Front.* 5 (8) (2018) 1760–1779.
- [95] K. Lu, T. Aung, N. Guo, R. Weichselbaum, W. Lin, Nanoscale metal–organic frameworks for therapeutic, imaging, and sensing applications, *Adv. Mater.* 30 (37) (2018) 1707634.
- [96] D. Liu, K. Lu, C. Poon, W. Lin, Metal–organic frameworks as sensory materials and imaging agents, *Inorg. Chem.* 53 (4) (2014) 1916–1924.
- [97] Y. Wang, X. Zhao, H. Yang, X. Bu, Y. Wang, X. Jia, J. Li, P. Feng, A tale of two trimers from two different worlds: a COF-inspired synthetic strategy for pore-space partitioning of MOFs, *Angew. Chem. Int. Ed.* 58 (19) (2019) 6316–6320.
- [98] H. Goesmann, C. Feldmann, Nanoparticulate functional materials, *Angew. Chem. Int. Ed.* 49 (8) (2010) 1362–1395.
- [99] R. Gaillac, P. Pullumbi, K.A. Beyer, K.W. Chapman, D.A. Keen, T.D. Bennett, F.-X. Coudert, Liquid metal–organic frameworks, *Nat. Mater.* 16 (2017) 1149.
- [100] C. Orellana-Tavra, E.F. Baxter, T. Tian, T.D. Bennett, N.K.H. Slater, A.K. Cheetham, D. Fairen-Jimenez, Amorphous metal–organic frameworks for drug delivery, *Chem. Commun.* 51 (73) (2015) 13878–13881.
- [101] Y. Li, Z. Di, J. Gao, P. Cheng, C. Di, G. Zhang, B. Liu, X. Shi, L.-D. Sun, L. Li, C.-H. Yan, Heterodimers made of upconversion nanoparticles and metal–organic frameworks, *J. Am. Chem. Soc.* 139 (39) (2017) 13804–13810.



- [102] J.-Y. Zeng, M.-K. Zhang, M.-Y. Peng, D. Gong, X.-Z. Zhang, Porphyrinic metal–organic frameworks coated gold nanorods as a versatile nanoplatform for combined photodynamic/photothermal/chemotherapy of tumor, *Adv. Funct. Mater.* 28 (8) (2018) 1705451.
- [103] J. Liu, T. Liu, P. Du, L. Zhang, J. Lei, Metal–organic framework (MOF) hybrid as a tandem catalyst for enhanced therapy against hypoxic tumor cells, *Angew. Chem.* 131 (23) (2019) 7890–7894.
- [104] J. Deng, K. Wang, M. Wang, P. Yu, L. Mao, Mitochondria targeted nanoscale zeolitic imidazole framework-90 for ATP imaging in live cells, *J. Am. Chem. Soc.* 139 (16) (2017) 5877–5882.
- [105] X. Duan, C. Chan, W. Lin, Nanoparticle-mediated immunogenic cell death enables and potentiates cancer immunotherapy, *Angew. Chem. Int. Ed.* 58 (3) (2019) 670–680.
- [106] X. Wang, X.-Z. Chen, C.C.J. Alcántara, S. Sevim, M. Hoop, A. Terzopoulou, C. de Marco, C. Hu, A.J. de Mello, P. Falcaro, S. Furukawa, B.J. Nelson, J. Puigmartí-Luis, S. Pané, MOFBOTS: metal–organic-framework-based biomedical microrobots, *Adv. Mater.* 31 (27) (2019) 1901592.
- [107] Commercially Available MOFs in Sigma Aldrich-Merck, <https://www.sigmaaldrich.com/materials-science/material-science-products.html?TablePage=103996366> (Accessed 15 August 2019).
- [108] S. Cavenati, C.A. Grande, A.E. Rodrigues, C. Kiener, U. Müller, Metal organic framework adsorbent for biogas upgrading, *Ind. Eng. Chem. Res.* 47 (16) (2008) 6333–6335.
- [109] A.F.P. Ferreira, J.C. Santos, M.G. Plaza, N. Lamia, J.M. Loureiro, A.E. Rodrigues, Suitability of Cu-BTC extrudates for propane–propylene separation by adsorption processes, *Chem. Eng. J.* 167 (1) (2011) 1–12.
- [110] Merck Metal-Organic Framework Constructor Tool, <https://www.sigmaaldrich.com/materials-science/learning-center/mof-constructor.html> (Accessed 15 August 2019).
- [111] MOF Technologies, <https://www.moftechnologies.com/> (Accessed 15 August 2019).
- [112] A. Scott, Round two for MOF commercialization, *Chem. Eng. News* 95 (24) (2017) 18–19.
- [113] Editorial, Frameworks for commercial success, *Nat. Chem.* 8 (2016) 987.
- [114] B. Yilmaz, N. Trukhan, U. Müller, Industrial outlook on zeolites and metal organic frameworks, *Chin. J. Catal.* 33 (1) (2012) 3–10.
- [115] Global Metal-organic Frameworks (MOF) Market Growth 2019–2024, 2019, LP Information Inc, <https://www.fiormarkets.com/report/global-metal-organic-frameworks-mof-market-growth-2019-2024-375203.html> (Accessed 14 October 2019).
- [116] MOFgen Ltd., <http://www.mofgen.com/> (Accessed 15 August 2019).

# Index

Note: Page numbers followed by *f* indicate figures and *t* indicate tables.

## A

- Acetic acid, 119, 147, 207, 209–211, 236
- Acrylate polymerization, 483–484
- ACSYNAM, 213–215
- Active pharmaceutical ingredients (APIs), 72, 83–87
- Acute toxicity, 76–78, 389
- Adenine-based bioMOFs, 76–78, 77*f*
- Adsorption
- based immobilization technique, 515
  - of enzymes, 494–497, 513
  - of glucose dehydrogenase (GDH), 494–496
  - ibuprofen, 530–531
  - isotherms, 527–528
- Alcohol dehydrogenase (ADH) enzyme, 509
- Alendronate, 81–82, 82*f*
- Alkaline earth metals, 49–51
- Alkyne-functionalized poly(ethylene) glycol (PEG) chains, 246–248
- Allyl isothiocyanate (AITC), 305–306
- Amino acids (AA), 327–329, 328*f*
- Amino-functionalized linkers, 125
- 3-Aminopropyltriethoxysilane (APTES), 172, 172*f*
- 4-Aminothiophenol (4-ATP), 405
- Amorphization, 207
- on drug release, 256
  - mechanochemical, 208*f*
  - thermal, 99
  - of zeolite crystals, 206–207
- Amorphous MOFs, 256, 277, 430, 525–527
- Amorphous porous organic polymers, 526
- Anisotropic gold nanoparticles, 404
- Anisotropic gold nanorods (AuNR), 405
- Anodic dissolution/electrosynthesis, 179–183
- Antibacterial activity, MOFs for induction of, 308–309
- Antibacterial therapy, 308–309, 401, 401*f*
- Antibiotics amoxicillin (AMOX), 477
- Antibiotics-loaded Zn-based MOFs, 431–432
- Anticancer drugs, 145–147, 149, 199–201, 236, 254, 256, 303–305
- Antiinfective properties, MOFs, 433–434
- Antimicrobial properties, MOFs, 431–433
- Antitubercular drug, 437
- Antiviral drugs, 79, 145–147
- Anton Paar Monowave, 162, 162*f*
- APIs. *See* Active pharmaceutical ingredients (APIs)
- Applications, MOFs, 351*f*, 364–365
- bio-applications, 199–201, 365
  - biomedical applications, 102–106, 430–434, 431*f*
  - catalyst, 364
  - gas storage, 364
  - pharmaceutical applications, 297–298, 430–434
- Aptamer conjugation, 288
- Aptamer-functionalized NMOFs (Apt-NMOFs), 254–256
- Arrhenius equation, 225–228
- Arsenic trioxide, 436
- Aryl halides, Pd-catalyzed alkynylation of, 130–131
- Attenuated total reflection (ATR) mode, 283
- Au nanoclusters (AuNCs), 406–408
- Au nanospheres, 406–408
- AuNS@MOF-ZD2 nanopores synthesis, 408*f*
- Auxiliary MOFs, 170
- Azelaic (1,7-heptanedicarboxylic) acid, 85
- Azidothymidine monophosphate (AZT-MP), 475, 476*f*
- Azidothymidine triphosphate (AZT-TP), 79, 145–147, 475
- Azobenzene, 97–98, 307–308

## B

- Bacillus subtilis* lipase (BSL2), 494–496
- Bacterial spores, detection of, 534
- BASF, 469, 543–545
- bdh-Zn-<sup>1122</sup>Hferritin system, 333–334
- Beer-Lambert's equation, 291
- Benzaldehyde, 116–117
- cyanosilylation of, 530
- 1,3,5-Benzenetricarboxylate (BTC), 179–182, 253–254
- BET. *See* Brunauer-Emmett-Teller (BET)
- Bioactive molecules, 72, 85, 88, 198*t*, 321

- Biocompatibility test, 292  
Biocompatible Fe-carboxylate MOFs, 534  
Biocompatible MOFs, 384, 399, 535  
  physical and chemical characteristics, 70  
Biocompatible MOFs, organic ligands  
  active pharmaceutical ingredients and dietary supplements, 83–87  
  amino acids and peptides, 73–75  
  carboxylate ligands, 71  
  carboxylic acids, 78–81  
  intrinsic biological properties and therapeutic action, 71  
  nucleobases, 76–78  
  phosphonic acids, 81–83  
  schematic representation of composition, 71, 71*f*  
  simulated physiological conditions, 72  
  toxicological safety, 71  
Biodegradability, 538  
Biodegradable MOFs, 470–471*t*  
  synthesis, 469–471  
Bioimaging tools, MOFs as next-generation, 434–435  
Bioligands, 102–103  
Biological applications, MOFs, 199–201, 365  
Biological metal-organic frameworks (bioMOFs), 323, 469, 537–538  
  adenine-based, 76–78, 77*f*  
  BioMOF-1, 305  
  definition of, 324–325  
  design with biomolecules, 325  
  potential chirality of, 329  
  synthesis of, 325  
Biological system  
  nanoscale metal-organic frameworks in, 387–388  
  toxicity of MOFs in, 384–387  
Biomedical applications, MOFs, 430–434, 431*f*  
BioMIL-1, 83–84, 84*f*  
BioMIL-2, 104–105  
BioMIL-3, 79  
BioMIL-5, 85  
Biomimetically mineralized MOFs, 503–506, 503*f*  
Biomimetic strategy, 500–503  
Biomineralization, 499–503, 512–513  
  MOF-enzyme composites formed by, 501*t*  
bioMOFs. *See* Biological metal-organic frameworks (bioMOFs)  
Biomolecules, 265–268, 321–322  
  applications of, 322  
  chirality of, 324  
  incorporation of, 323  
  meaning of, 321–322  
  nature of, 322  
  spectrum of, 322  
  types of, 322  
Bioreactors, 21, 494–496  
Biotage initiator, 162, 162*f*  
Biotransformation, 491  
Bipolar electrosynthesis (BPES), 184  
Bisphosphonic acids (BPOs), 81, 82*f*  
Bond formation  
  C-C bond formation, 125, 133  
  covalent, 246–248  
Boolean operations, 529  
Bowen's Reaction Principle, 141–142  
BPES. *See* Bipolar electrosynthesis (BPES)  
Bragg reflection, 285  
Bragg's law, 280  
Breast cancer cell lines, 254  
Breast carcinoma, 262–265  
Broccoli extract (*Brassica oleracea*), synergistic effect of, 432  
Brownian motion, 286  
Brunauer-Emmett-Teller (BET) adsorption isotherm equation, 289  
  analysis, 284  
  surface area, 115, 261–262, 455  
  theory, 288  
*Burkholderia cepacia* lipase (BCL), 498  
**C**  
Cadmium (Cd) ion, 99  
Cage-within-cage network, 48–49, 48*f*  
Calcein-loaded MOFs, 250–251  
  nanoparticles, endocytosis, 256–257  
  particles, 256  
Calcium zoledronate (Ca-Zol), 82–83  
Camptothecin (CPT), 303, 405–406, 540–542  
Cancer cell lines  
  breast, 254  
  iron-based nanomaterials in treatment of, 374*t*  
Cancer therapy, 436–437  
  MOFs for, 534  
  of TCPC-UiO by light activation, 415*f*  
Carbamazepine (CBZ), 102  
Carbohydrate-based materials, 446–447, 456–457, 461  
Carbohydrate-based MOFs (CD-MOFs), 447, 461  
Carbohydrates, 445–447  
  as functional surface coatings for MOFs, 456–461  
Carbonaceous substrates, deposition of MOF on, 189  
Carboxylate-based organic linkers, 525–526  
Carboxymethylcellulose, 315–316  
Carcinoma  
  breast, 262–265  
  hepatocellular, 269–271, 389, 400, 435  
  of human lung, 199–201, 388  
Carriers  
  degradation mechanism of, 477  
  drug, 258, 387–388, 467–468, 482, 484  
  nanocarrier, 467–468  
  organic, 467–468  
Catalase@ZIF composites  
  synthesis, 504*f*  
Catalysts, 364  
  enzymatic, 323  
  heterogeneous solid, 111–112

- Catalytic activity, 508  
 CD. *See* Cyclodextrin (CD)  
 C dots, 412  
 Cell Counting Kit-8 (CCK-8) assay, 254  
 Cell tracking, theranostic applications for, 406  
 Cetyltrimethylammonium bromide (CTAB), 144–145, 449, 534  
 surfactant, 300  
 Characterizations, MOFs, 278–292, 360–364  
 catalytic activity, 508  
 chemical stability, 509  
 elemental and functionality analysis, 281–284  
 Michealis-Menton kinetics, 508–509  
 particle size and surface charge analysis, 286–288  
 phase purity and structure modeling, 279–280  
 reusability, 509–510  
 storage stability, 510  
 structural characterization, 278–284  
 surface area analysis, 288–289  
 surface characterization, 284–289  
 thermal stability, 508  
 Charged particles, 184–185  
 Chinese hamster ovary cell (CHO) lines, 366, 373–374  
 Chiral polar drugs separation, 332f  
 Chiral three-dimensional MOFs, 74, 75f  
 Chitosan, 446, 461, 483  
 Chlorine-based MOF delivery system, 311f  
 4-Chloro-7-nitrobenzofurazan (NBD), 494–496  
 Chromium metal, toxicity issues of, 471  
 Chromium-terephthalate MIL-88B(Cr), 530  
 Click modulation protocol, 149f, 248f  
 Clofibrac acid (CA), 102  
 Co-crystallization method, drug entrapment, 451, 453  
 COFs. *See* Covalent organic frameworks (COFs)  
 Colloidal dispersion, stability of, 258, 287  
 Colloidal particles, 184–185  
 Combi-metal organic frameworks (combi-MOF), 512f  
 Commercialization of MOFs developments, 213–215, 214f  
 world's first commercial use, 213  
 Composite, MOFs, 237–239  
 fabrication, 540  
 multienzyme, 511–513  
 Composite, phototoxicity of, 269–271  
 Conductive glass substrates, deposition of MOFs on, 188–189  
 Construction of metal-organic frameworks, 13, 14–15f  
 Conventional organic solvents, 232  
 Coordination polymers (CPs), 11, 277, 468  
 definition, 3–4  
 IUPAC, 2–4  
 macromolecules, 4  
 MOFs vs., 7–8  
 nonmolecular crystals, 3–4  
 organometallic polymers, 3–4  
 straight-chain polymers (1D) compound, 2–3  
 Coordinative postsynthetic modification, 248–250  
 Copper-based benzene tricarboxylate (Cu-BTC), 229, 231–232  
 based MOFs, 432  
 Copper catalyzed azide-alkyne cycloaddition (CuAAC), 246–248, 248f  
 Core-shell Au nanostar@ nanoMOF, 408  
 Core-shell Au NRs@MOFs, 405–406  
 Core-shell nanoparticles, 238–239, 506–507  
 Covalent binding, 498–499, 498t  
 Covalent bond formation, 246–248  
 reversible, 531–532  
 Covalent electrografting, 186  
 Covalent organic frameworks (COFs), 426–427, 526  
 Covalent postsynthetic modification, 246–248  
 CpG ONDs. *See* Cytosine-guanine oligonucleotides (CpG ONDs)  
 cp5-mof-based system, 307  
 CPO-27, sonochemical synthesis of, 228, 228f  
 CPs. *See* Coordination polymers (CPs)  
 CRISPR/Cas9, 303–305  
 Crystal conversion, porosification associated with, 206–207  
 Crystalline, 347  
 materials, 197  
 MOFs, 525–526  
 solid MOFs, 492  
 Crystals  
 metal-organic, 11  
 micrometric-sized, 182–183  
 size of MOFs, 166  
 structure of MOFs, 281f  
 Cu-BTC. *See* Copper-based benzene tricarboxylate (Cu-BTC)  
 Cu(GHG) MOF, helicoidal chains in, 331f  
 Cu-MOFs synthesis, 150–152, 151f  
 Curcumin (CCM), 415–416  
 CuS nanoparticles, nano-objects based on, 408–409  
 Cu<sub>3</sub>(BTC)<sub>2</sub> with palladium complexes, 132f  
 α-Cyano-4-hydroxycinnamic acid (α-CHC), 256  
 Cyanosilylation of benzaldehyde, 530  
 Cyclodextrin (CD), 338–339, 438–439, 445–446, 482  
 polymeric, 482–483  
 β-Cyclodextrin (β-CD), 307, 400–401  
 Cyclodextrin-MOFs (CD-MOFs), 455–456  
 drug encapsulation in, 452t  
 drug incorporation in, 454  
 surface coating, 455  
 synthesis, 447–456, 448f

- Cyclophane-protein cage framework, 335, 335f
- Cyt *c*/ZIF-8 (zeolitic imidazolate frameworks) crystals, 500
- Cytochrome *c*-embedded ZIF-8, 336f  
preparation, 502f
- Cytosine-guanine oligonucleotides (CpG ONDs), 254–256
- Cytotoxic experiment, *in vitro*, 545
- Cytotoxicity  
on CHO cell line, 372f  
of nanomaterials (NMs), 366  
test, 371–372
- D**
- D-camphoric acids, 58–59
- DDS. *See* Drug delivery system (DDS)
- Deep eutectic solvents (DES), 232
- Deferiprone, 84–85
- Degradation, *in vitro*, 145–147
- Degradation of MOFs, 386, 477–480  
carriers, 477  
Mg-gallate MOF, 478–479  
particles, 475, 476f
- Dendrimers, 467–468, 537
- De novo encapsulation method, 499–507
- De novo protein encapsulation, 335–336
- Deoxyribonucleic acid (DNA), 76
- Deposition of MOFs  
carbonaceous substrates, 189  
conductive glass substrates, 188–189  
metallic substrates, 186–188
- DES. *See* Deep eutectic solvents (DES)
- Design of MOFs, 492–493
- Detoxify diisopropyl fluorophosphate (DFP), 497
- 1,4-Diazabicyclo [2.2.2]octane framework (DABCO), 98
- 5,15-Di(p-benzoato)chlorin (H2DBC), 310–311
- Dichloroacetic acid (DCA), 147–148, 416
- Difference envelope density (DED), 280, 282f
- Diffuse reflectance (DRIFTS) mode, 283
- Dihydroartemisinin (DHA), 402–403
- Dimensions of MOFs, 348f
- Dimethylammonium cations, 76–78
- Dimethylformamide (DMF), 232, 385
- 3-(4,5-dimethylthiazol-2-yl)-2,5-diphenyltetrazolium bromide (MTT), 292  
metabolic assays, 261
- Dispersive spectroscopy, X-ray energy, 362f
- DLS. *See* Dynamic light scattering (DLS)
- DNA probes, 267–268
- Dopamine (DPA)  
polymerized, 509–510  
releasing neurons, 315
- Dox@MOF-Au-PEG, 414f
- Doxorubicin (DOX), 254, 312, 410, 436–437  
loaded nanoparticles, 254
- Doxorubicin-loaded ZIF-8 complex, 199–201
- Drug  
antitubercular, 437  
entrapment, 451–456  
incorporation in CD-MOFs, 454  
nanocarriers, 467–468  
noncovalent encapsulation of, 538–539
- Drug administration, drug delivery systems (DDS) for, 438–439
- Drug carriers, 258, 387–388, 467–468, 482, 484  
nanoscale, 388
- Drug delivery, 532–533  
efficacy of MOFs, 436  
mesoporous silica nanoparticles for, 533  
porous materials for, 530–531  
potential of MOFs, 427–428  
stimuli-responsive MOFs for, 303–308
- Drug delivery development  
stability and biodegradability, 299  
toxicological study, 298–299
- Drug delivery system (DDS), 258, 400–401  
for drug administration, 438–439  
multiple-stimuli-responsive, 306–307  
pharmacokinetic of, 299  
stimuli-responsive, 426
- Drug-loaded nanoparticles, 251–253, 259
- Drug-loaded Zr-based MOFs, mechanical amorphization of, 256
- Drug loading  
and characterization, 453f  
and release, 471–477, 476f
- Drug release, amorphization on, 256
- Dyes  
fluorescent, 412  
near-infrared region (NIR) organic, 412
- Dynamic light scattering (DLS), 284, 286–287
- E**
- Electrochemical synthesis of MOFs, conductive substrates, 186–189
- Electrochemical synthesis routes of thin films of MOFs, 179–186, 180–181f  
anodic dissolution, 179–183, 182f  
bipolar electrosynthesis (BPES), 184  
electrophoretic deposition, 184–185  
galvanic displacement, 185  
reductive electrosynthesis, 183–184
- Electrodeposited MOF thin film, 189
- Electromagnetic radiations, 160
- Electron microscope (EM), 361
- Electrons, photo-ejected, 284
- Electrophoretic deposition method, 184–185
- Electrosynthesis, 178  
anodic, 179–182  
reductive, 183–184

- EM. *See* Electron microscope (EM)
- Encapsulation, De novo protein, 335–336
- Endocytosis of calcein-loaded nanoparticles, 256–257
- Energy dispersive X-ray (EDX) analysis, 281
- Engineered nanomaterials (NMs), 349
- Enhanced green fluorescent protein (EGFP), 498–499
- Enhanced permeability and retention (EPR) effect, 400, 438
- Enzymatic catalysts, 323
- Enzymes, 491 *See also specific types of enzyme*  
 adsorption of, 494–497, 513  
 affinity of, 508–509  
 alcohol dehydrogenase (ADH), 509  
 biocomposite, 503  
 catalysis, 491  
 catalytic properties of, 496–497  
 immobilization, 491–492, 494–496  
 leaching, 491–492, 509–510  
 lipase, 508  
 MOF composites, 508  
 multiple, cross-linking, 507f  
 physical adsorption of, 513  
 reusability of, 509–510
- Enzyme@ZIF-8, shape and enzyme activity of, 505f
- Ethoxysuccinato-cisplatin (ESCP) prodrug, 251–253
- 1-Ethyl-3-(3-dimethylaminopropyl) carbodiimide (EDC), 261
- Ethylene glycol diglycidyl ether, 455
- Exosomes, 250–251, 250f
- External stimuli-responsive materials, 530
- F**
- Fabrication, 245  
 hydrosolvothermal, 369–370  
 methodology, 540
- Fe-based MOFs, 315, 386, 390, 468, 508
- Fe-based NMOF, 309, 366, 372–373
- Fe-carboxylate MOFs  
 composite nano-objects based on, 402–403  
 nanoparticles, 400–402
- Fe-MIL-53, 95f, 197–199, 228f, 239
- Fe-MOFs synthesis, 145–147, 146f, 148f
- Fe-NMOF crystal units, nucleation of, 367–369
- Ferritin  
 crystals, 334f  
 metal/linker-directed self-assembly of, 333f
- Ferromagnetic nanoparticles, 540
- Field emission scanning electron microscopy (FESEM), 172f
- Film/membrane preparation, MOFs, 171–173
- Films, MOF, 171–173, 187
- FITC-tagged trypsin@MOF, 509–510
- Flexibility modes of MOFs, 198f
- Flexible metal-organic frameworks  
 1,4-benzenedicarboxylate (BTC), 95  
 Cr-MIL-53 hybrid solid, dehydration-hydration, 94–95, 95f  
 drug delivery materials, 93–94, 94f  
 HKUST-16, 95  
 ibuprofen, 94–95  
 nanobiotechnology, 93  
 nontoxic nanocarriers, 93–94  
 stress-induced chemical detection, 95  
 structure of, 93–95  
 toxicology, 93–94
- Flexible metal-organic frameworks, aspects of  
 breathing phenomenon, 96–97  
 linker rotation, 97  
 photoinduction, 97–98  
 subnetwork displacement, 97  
 swelling mode, 97  
 thermal-induction, 98–99
- Flexible metal-organic frameworks, origins of  
 biomedical applications, 102–106  
 flexible ligands (FL-MOFs), 100–102  
 secondary building units (SBUs), 99–100
- FlexiWAVE microwave system, 163
- Fluctuations, pressure, 223
- Fluorescence microscopy, 261
- Fluorescent dyes, 412
- Folate receptors (FR), 82–83
- Folic acid, 265, 303
- Formation of MOFs, 187, 325
- Förster resonance energy transfer (FRET)-based mechanism, 540–542
- Fourier-transform infrared spectroscopy (FTIR), 283
- Free enzymes, 493
- Free fatty acids (FFA), 74–75
- Free functional organic sites (FOSs), 125–126
- G**
- Gadolinium (Gd), 309  
 based MOF nanoparticles, 399–400  
 molecules, 309
- Gadolinium-porphyrin-based NMOF, 309
- Galvanic displacement method, 189
- Gas sorption isotherms, 4–5
- Gas storage, 364  
 MOF-based, 528–529
- GCE. *See* Glassy carbon electrode (GCE)
- Gemcitabine-monophosphate, 484–485
- Glass substrates, deposition of MOFs on conductive, 188–189
- Glassy carbon electrode (GCE), 189
- Glucose dehydrogenase (GDH), adsorption of, 494–496
- Glucose detection, 516f
- Glucose-mediated glucose-transported protein (GLUT1) tumor targeting, 400
- Glucose oxidase (GOx), 306
- Glucose sensor, 529
- Glutathione (GSH), 306



- Gold nanoparticles (AuNPs), 413  
 anisotropic, 404  
 Gold nanorods, 405  
 Gold quantum dots, 407  
 GO-Ni-BTC, 237  
 GQD. *See* Graphene quantum dots (GQD)  
 GrafiFast  
 polymerization, 483–484  
 reaction, 145–147  
 Graphene quantum dots (GQD), 254  
 Graphite, 237  
 Graphitic carbon nitride nanosheets, 412  
 Green chemistry, 124–125, 211  
 Green nanotechnology, 426  
 Grinding method, drug entrapment, 454
- H**
- Heck reaction, 112–113  
 modified MOFs for, 121–125, 124*f*  
 HeLa cells, 250–251, 259  
 Helium, 284  
 Henry coefficients, 104–105  
 Heparin-coated material, 261–262  
 Hepatocellular carcinoma, 269–271, 389, 400, 435  
 Heterogeneous catalysts, 112  
 Heterogeneous solid catalysts, 111–112  
 Hf-porphyrin MOF, 535  
 synthesis, 264*f*  
 Highly coordinated carboxylate-based (metal oxide) secondary-binding units, 25–32, 26*f*, 28–31*f*  
 Hinged metal organic framework (HMOF), 99  
 HKUST-1, 178–179, 229–231  
 films, 187  
 Hollow mesoporous organosilica nanoparticles (HMON), 312  
 Homogeneous catalysis, 111  
 Horseradish peroxidase (HRP), 509  
 MOF nanocrystals synthesis, 502*f*  
 Horseradish peroxidase (HRP)/ZIF-8 crystals synthesis, 500
- HRTEM, 285, 288*f*  
 Human colorectal adenocarcinoma (HT-29), 199–201  
 Human exposure to MOFs, 391–392, 392*f*  
 Human promyelocytic leukemia (HL-60), 199–201  
 Hybrid inorganic-organic solids, 297–298  
 Hybrid materials, organic-inorganic, 492  
 Hybrid MOFs, 429–430  
 Hybrid nanomaterials, 426–427, 435  
 self-assembled, 427  
 Hybrid nanoMOFs systems, 417  
 Hybrid nanoparticles, 409–412  
 Hybrid polymeric materials, 525–526  
 Hybrid polymers, 537–539  
 MOFs as, 526–527  
 Hybrid porous particles, 468  
 Hydrogels, 491–492  
 Hydrogen, 284  
 Hydrophilic polymeric matrices/membranes, 542–543  
 Hydrophobic environment surrounding metallic sites, 151–152  
 Hydrophobic molecules, 467–468  
 Hydrosolvothermal fabrication, 369–370  
 Hydrosolvothermal method, 450  
 Hydrothermal, defined, 141–142  
 Hydrothermal materials synthesis, 142–143  
 Hydrothermal synthesis of MOFs, 141–143, 178  
 hydrothermal approach, 145–153  
 mechanism and general protocols, 143–145  
 Hydrothermal technique, 142–143  
 Hyperhalophilic alcohol dehydrogenase (ADH) enzyme, 509  
 Hypoxia, tumor, 414–415
- I**
- Ibuprofen adsorption, 530–531  
 ICG. *See* Indocyanine green (ICG)  
 Immobilization, 491  
 enzyme, 491–492, 494–496  
 of glucose oxidase (GOx), 511–512  
 of horse radish peroxidase (HRP), 511–512  
 of palladium ions, 121–122  
 porous nano-based carrier for, 491–492  
 of soybean epoxide hydrolase (SEH), 499  
 Immobilized enzymes, 509–510  
 Immobilized porcine pancreatic lipase, 494–496  
 Impregnation method, drug entrapment, 451  
 Indocyanine green (ICG), 314, 412  
 Indoleamine 2,3-dioxygenase (IDO), 311, 485  
 Infinite rod like SBUs, 38–40, 38–39*f*  
 Inorganic nanoparticles, 537  
 for optical imaging, photodynamic/photothermal therapy, 404–409  
 Inorganic route, 297–298  
 In situ immobilization technique, 513  
 In situ polymerization, 149  
 Insulin, 306  
 International Union for Pure and Applied Chemistry (IUPAC), 2–4  
 In vitro cytotoxic experiments, 545  
 In vitro degradation, 145–147  
 In vitro toxicity assays, 388  
 evaluations, 371–373  
 of nanoscale MOFs, 388–392  
 In vivo fate, toxicity and, 484–485  
 In vivo toxicity, 534  
 of nanoscale MOFs, 388–392  
 tests, 298–299  
 Iodine doping of MOFs, 150  
 Ion- and liquid-assisted grinding, 204  
 Ion-exchange process, 120–121  
 Ionic liquids (IL), 232  
 Ion-responsive MOFs, 305  
 ION-X, 213–215, 214*f*  
 Iron-based MOF, 483

- Iron-based nanomaterials, 374*t*  
 Iron-based nanoscale metal-organic frameworks (Fe-NMOFs), 367–369  
 Iron-carboxylate MOFs, MIL-100(Fe) and MIL-53(Fe) degradation mechanism of, 479  
 Iron ions, 386  
 Iron oxide magnetic nanoparticles, 349  
 Iron polycarboxylate MOFs, surface-functionalization of, 447  
 Irradiation, microwave, 161*f*, 301  
 Isorecticular metal-organic frameworks (IRMOF-1), 5–7  
 Isostructural MOFs, 529  
 Isothermal titration calorimetry (ITC), 457  
 Isotherms, adsorption, 527–528
- J**  
 Janus nanoparticles, 406
- K**  
 Kneecap-like rotational axis, 100  
 Knoevenagel condensation, 112–113  
   modified MOFs for, 113–121, 114*f*, 116*f*  
 Krebs cycle, 78  
 Krypton (Kr), 103–105
- L**  
 Lactate dehydrogenase (LDH) generation assay, 262–265  
 Lambert-Beer's law, 291  
 Lansoprazole (LPZ), 451–453, 453*f*  
 Lanthanide-based MOF, 529  
 Lanthanide metal ions, 352  
 Layer-by-layer (LBL) technique, 150  
 Leaching, enzyme, 491–492, 509–510  
 LFSE. *See* Ligand field stabilization energy (LFSE)  
 Ligand field stabilization energy (LFSE), 228  
 Ligands, 354*f*  
   organic, 352–354  
   porphyrin, 404  
 Linkers, MOF, 333–334  
 Lipase enzyme, 508  
 Lipid coating, 483  
 Liposomes, 467–468  
 Liquid MOFs, 526–527, 540  
 Living cells, 321  
 LPZ-loaded particles, 451–453  
 Luminescence, 540  
 Luminescent MOFs, 277  
 Luminescent property analysis, 290–291
- M**  
 Magic bullets, 467  
 Magnetically active MOFs nanocomposites, 436  
 Magnetic-based MOFs nanoparticles, 399–403  
 Magnetic bio-MOF (MBMOF), 238  
 Magnetic metal oxide nanoparticles (MNPs), 367  
 Magnetic MOF-enzyme composite, 513–517, 514*t*  
 Magnetic nanoMOFs, 399  
 Magnetic nanoparticles (MNPs), 349  
   iron oxide, 349  
 Magnetic properties of metal oxides, 370–371  
 Magnetic property analyses of MNPs, 370*f*  
 Magnetic resonance imaging (MRI), 309–310  
 Magnetic theranostics, 436–437  
 Magnetism, 349, 370–373, 370*f*  
 Manganese-based nanoscale MOF, 302  
 MARS 6, 163  
 MCH nanoparticles preparation, 411*f*  
 MDR. *See* Multidrug resistance (MDR)  
 Mechanochemical MOF (M-MOF), 228–229  
 Mechanochemical reaction, acceleration of, 207–211, 208–211*f*  
 Mechanochemical synthesis, 203–211  
   acceleration of mechanochemical reaction, 207–211, 208–211*f*  
   challenges to the mainstream adoption of, 215–216, 216*t*  
   classifications of mechanochemical method, 204  
   mechanochemical dry conversion of metal source, 205–206  
   porosification associated with crystal conversion, 206–207  
 Mechanochemistry, 216  
 Mechanosynthesis, MOFs, 204  
   continuous flow system of, 211, 211*f*  
 Medical implants, osteogenic, 536*f*  
 Medicine, MOFs in, 525–536  
   golden age of MOF technology in, 537–539  
 Mesoporous MOFs, 497  
 Mesoporous silica materials, 323  
 Mesoporous silica nanoparticles, 538–539  
   for drug delivery, 533  
 Meso-tetra(4-pyridyl)porphine linker (MTPP), 99  
 Metabolism, 313–314  
 Metal-carboxylate MOFs, 13  
 Metal-cluster secondary building units, 38–39  
 Metal complexes, transition, 122  
 Metal ions, 145, 152–153, 155, 188, 350–352  
   lanthanide, 352  
   in MOFs, 384–385  
   solubility of, 359  
 Metallic substrates, deposition of MOFs on, 186–188  
 Metalloligands, 50  
 Metalloporphyrin, 337–338  
 Metalloporphyrin-based drug delivery systems, 337–338  
 Metal-organic crystals, 11  
 Metal-organic frameworks (MOFs) advantages, 427–428, 428*f*  
   concept, 426–427, 429–430  
   design and development, 427–428

- Metal-organic frameworks (MOFs)  
(Continued)  
development, 430–431  
functions, 2  
importance of, 2–3  
manufacturer, 212*t*  
nanoscale MOFs, 2  
organic in, 5  
structures and methods of  
synthesis, 300–301
- Metal-organic frameworks-enzyme  
composite, 493–507  
covalent binding, 498–499, 498*t*  
De novo encapsulation method,  
499–507  
formed by biomineralization,  
501*t*  
formed by co-precipitation, 500*t*  
immobilization methodologies  
for, 493*f*  
magnetic, 513–517, 514*t*  
pore encapsulation methods,  
496–498  
surface immobilization, 494–496,  
494*t*, 495*f*
- Metal-organic frameworks  
nanoparticles  
Fe-carboxylate, 400–402  
gadolinium (Gd)-based, 399–400  
magnetic-based, 399–403  
Mn-based, 403  
nano-objects based on, 408–409  
for photodynamic and  
photothermal therapy,  
403–404
- Metal-organic frameworks  
nanoparticles for nuclear  
medical imaging, 413–415  
computed tomography (CT),  
414–415  
positron emission tomography  
(PET), 413  
single photon emission computer  
tomography (SPECT), 413
- Metal-organic frameworks particles  
degradation mechanism of, 475,  
476*f*  
stability of, 477
- Metal-organic frameworks  
synthesis, 153, 201, 433*f*  
and characterization, 428–430  
and evaluation processes, 202*f*  
solvent in, 385
- Metal organic linker, 492
- Metal-organic polyhedra (MOPs),  
12–13, 36–38, 36–37*f*
- Metal oxides, magnetic properties  
of, 370–371
- Metal-poisoning, potential antidotes  
for human, 542–543
- Metal, transition, 112
- Mg-gallate MOF, degradation  
mechanism of, 478–479
- Mg-MOF-74 synthesis, 215*f*
- Mg-Olsalazine bioMOF, 86*f*, 87
- Michealis-Menton kinetics,  
508–509
- Microemulsion, 230  
reverse, 359–360, 359*f*
- Micrometric-sized crystals,  
182–183
- Microparticles, 491–492
- Microporous MOFs, 496–497  
nanocrystals of, 301
- Microporous NMOFs, 278
- Microscopic cavitations bubbles,  
223
- Microwave-assisted hydro/  
solvothermal method, 450
- Microwave-assisted seeding  
process, 171*f*
- Microwave-assisted synthesis  
(MWAS), 160–161, 166–169,  
167–168*f*
- Microwave dynamic (MDT)  
therapy, 403–404
- Microwave-induced thermal  
deposition, 171–172
- Microwave irradiation, 161*f*, 301
- Microwave radiation, 169–172
- Microwave synthesis of MOFs,  
160–161, 161*f*, 164–173, 165*t*,  
225–228  
commercial microwave  
equipment, 161–164,  
162–163*f*  
influence of reaction conditions,  
165–169  
postsynthetic modifications,  
169–171
- Microwave thermal (MTT) therapy,  
403–404
- MIL-100(Fe) nanoparticles,  
261–262  
postsynthetic functionalization  
of, 262*f*  
postsynthetic modification and  
cargo loading of, 263*f*
- MIL-53 system, 99–102
- Mixed linker, 125
- Mixed linker MOF (MIXMOF),  
122–123
- Mixed-metal-organic frameworks  
(MM-MOFs)  
advantages, 45  
alkali metals, 47–49  
alkaline earth metals, 49–51  
crystalline porous materials, 45  
d<sup>10</sup> metals, 51–56  
heterometallic-organic  
frameworks, 45–47, 46*f*  
ion exchange, charged  
frameworks, 46–47  
metal cations, 46–47  
N-donor and O-donor coligand,  
46–47  
postsynthetic metalation  
(PSMet), 46–47, 46*f*  
rare earth metals, 61–63  
transition metals, 56–61
- Mn-based MOFs nanoparticles, 403
- Modulators, 246–248
- MOFBOTS, 542–543
- MOF-74, sonochemical synthesis  
of, 228, 228*f*
- MOFs@polymer composites, 411
- MOFs-supported phospholipid  
bilayers formation, 150*f*
- MOMzyme-1 system, 337–338
- Monte Carlo simulations, 78
- MOPs. *See* Metal-organic polyhedra  
(MOPs)
- MRI. *See* Magnetic resonance  
imaging (MRI)
- Multiatomic secondary-binding  
units, 12
- Multidimensional MOFs, 427–428
- Multidrug resistance (MDR), 425
- Multienzyme MOF composites,  
511–513

- Multifaceted nanomedicine, 426  
 Multimodal MOFs, 429–430  
 Multiple drug resistance (MDR) cells, 373  
 Multiple enzymes, cross-linking, 507*f*  
 Multiple-stimuli-responsive drug delivery system (DDS), 306–307  
 Multiple-stimuli-responsive MOFs, 306–308  
 MWAS. *See* Microwave-assisted synthesis (MWAS)
- N**
- Nanocarriers, 467–468  
 Nanoclusters, Au, 406–408  
 Nanocomposites, 438  
   magnetically active MOFs, 436  
   photothermal MOFs-polymer, 409–411  
 Nanocrystals of microporous MOF, 301  
 Nanodeposition method, 355–357  
 Nanomaterials (NMs), 446–447  
   chronic effects of, 349  
   crystalline structure of, 366  
   cytotoxicity of, 366  
   engineered, 349  
   formation and characterization of, 367–370  
   potential toxicity of, 349  
   synthesis and applications of, 383–384  
   toxicity of, 384  
 Nanomedicine  
   biodistribution of, 413  
   multifaceted, 426  
 Nano-MOFs (NMOFs), 145–147, 277, 399, 456–457, 535, 538, 540, 542–543, 543*f*, 545  
   cell internalization, 459*f*  
   Gd-carboxylate, 400  
   hybrid, 417  
   magnetic, 399  
   stimuli-responsive, 415–417  
   surface modification, 459*f*  
   surface modification strategies and characterization of, 458*f*  
   synthesis and characterization of, 369*f*  
 Nano-objects  
   based on CuS and MOF nanoparticles, 408–409  
   based on MOFs, 404–409  
 Nanoparticles (NPs), 239, 537 *See also specific types of nanoparticles*  
   core-shell, 238–239  
   doxorubicin-loaded, 254  
   Fe-carboxylate MOFs, 400–402  
   ferromagnetic, 540  
   gadolinium (Gd)-based MOF, 399–400  
   hybrid, 409–412  
   inorganic, 404–409, 537  
   iron oxide magnetic, 349  
   magnetic-based MOFs, 399–403  
   mesoporous silica, 538–539  
   Mn-based MOFs, 403  
   nano-objects based on CuS, 408–409  
   nano-objects based on MOF, 408–409  
   polymeric, 467–468  
   size distribution of, 286  
   ultra-small superparamagnetic iron oxide (USPIO), 403  
 Nanoporous materials, 197  
 Nanoporous MOFs, 437  
 Nanoporous carbons (NPCs), 129  
 Nanoscale  
   drug carriers, 388  
   MOFs in biological systems, 387–388  
 Nanoscale coordination polymers (NCPs), 403, 483  
 Nanoscale metal-organic frameworks (NMOFs), 2, 367, 383–384, 406, 445  
   delivery system, 301  
   surface area of, 288  
   targeted contrast agent delivery via, 309–315  
   in vitro toxicity of, 388–392  
   in vivo toxicity of, 388–392  
 Nanosheets, graphitic carbon nitride, 412  
 Nanospheres, Au, 406–408  
 Nanostructured Co(II) MOF, 119–120  
 Nanostructures, as next-generation therapeutics, 426  
 Nanotechnological intervention, 426  
 Nanotechnology, 445  
 2,6-Naphthalenedicarboxylic acid (NDC), 117  
 Natural green catalyst, 491  
 NBD. *See* 4-Chloro-7-nitrobenzofurazan (NBD)  
 NCPs. *See* Nanoscale coordination polymers (NCPs)  
 Near-infrared region (NIR) organic dyes, 412  
 Negative thermal expansion (NTE), 98  
 Nephrogenic systemic fibrosis (NSF), 400  
 Next-generation bioimaging tools, MOFs as, 434–435  
 Next-generation therapeutics, nanostructures as, 426  
*N*-Heterocyclic carbene (NHC), 131–132  
 Niacin, 83–84  
 Ni-BTC synthesis, 231–233  
 Nitrogen-containing secondary building units, 32–36, 32–35*f*  
 NMOFs. *See* Nanoscale metal-organic frameworks (NMOFs)  
 Nomenclature of MOFs, 5–7  
 NPCs. *See* Nanoporous carbons (NPCs)  
 NPs. *See* Nanoparticles (NPs)  
 NSF. *See* Nephrogenic systemic fibrosis (NSF)  
 Nuclear magnetic resonance (NMR) spectroscopy, 283  
 Nucleation, 225–228  
   of Fe-NMOF crystal units, 367–369  
 Nucleic Acid Database, 106  
 Nucleobases, 325–327  
 Nucleolin, 254–256

## O

OMSs. *See* Open metal sites (OMSs)  
 On-demand-synthesized organic linkers, 526–527  
 One metal-carbon bond, 347–348  
 OPAA. *See* Organophosphorus acid anhydrolase (OPAA)  
 Open metal sites (OMSs), 125–126  
 Optical imaging, 314–315  
 Ordered nanoporous materials, 197  
 Organic carriers, 467–468  
 Organic dyes, near-infrared region (NIR), 412  
 Organic-inorganic hybrid materials, 492  
 Organic ligands, 245, 385, 534  
 Organic linkers. *See* Organic ligands  
 Organic polymers, 534  
   coating, 302  
   porous, 269–271  
 Organic route, 297–298  
 Organic structure-directing agent (OSDA), 197  
 Organometallic compounds, 347–348  
 Organophosphorus acid anhydrolase (OPAA), 497  
   encapsulation of, 497  
   immobilization of, 497f  
 Osteogenic medical implants, 536f  
 Oxidative stress, 416

## P

PAH. *See* Pulmonary arterial hypertension (PAH)  
 Palladium ions, immobilization of, 121–122  
 Pamidronate (pam), 82  
 PAN. *See* Polyaniline (PAN)  
 Paramagnetic MOFs, 435  
 Parkinson disease, 315  
 Particle size, MOFs, 385–386  
 PCN-222-covered gold nanorods (AuNRs@PCN-222), 541f  
 PCPs. *See* Porous coordination polymers (PCPs)  
 PDA. *See* Polydopamine (PDA)

Pd-catalyzed alkynylation, of aryl halides, 130–131  
 Pd-HoMOF catalyst, synthetic route for, 123f  
 Pd nanocubes, 312  
 Pd nanoparticles, 122, 126–127  
 Pd(II) Schiff base complex, 127f  
 PDT. *See* Photodynamic therapy (PDT)  
 PEG. *See* Poly(ethylene glycol) (PEG)  
 PEGylation, 481–482  
   of UiO-66, 149f, 259  
 Peptides, 329–332, 330f, 332f  
 PET. *See* Positron emission tomography (PET)  
 Pharmaceutical applications, MOFs, 297–298, 430–434  
 Pharmaceutical technology, MOFs in, 302–315  
 Phenethylamine, 87  
 Phosphate buffer saline (PBS), 475  
 Phosphated cyclodextrins (CD-P), 482–483  
 Phosphonic acids, 81–83  
 Phosphotungstic acid (PTA), 239  
 Photodynamic porphyrin carboxylate, 400  
 Photodynamic therapy (PDT), 310–311, 409, 434, 535, 539–542  
   and imaging units, 268–272  
   MOFs nanoparticles for, 403–404  
 Photo-ejected electrons, 284  
 Photoinduction, 97–98  
 Photoluminescence (PL), 290  
 Photosensitizers, 268–269, 535, 539  
 Phototheranostics, MOFs as, 435–436  
 Phototherapeutic therapy, 403–404  
 Phototherapy properties, MOFs, 434  
 Photothermal activity, 312  
 Photothermal MOFs-polymer nanocomposites, 409–411  
 Photothermal therapy (PTT), 312, 540–542  
   MOFs nanoparticles for, 403–404  
 Phototoxicity of composites, 269–271

pH-responsive drug delivery systems, 303  
 pH-sensitive MOFs, 303–305  
 Physical postsynthetic modification, 256–257, 257f  
 Physicochemical properties, MOFs, 429–430  
 Pillararens, 306  
 Pillared square grids, 16–18  
 PNIPAM. *See* Poly-*N*-isopropylacrylamide (PNIPAM)  
 POE. *See* Points of extension (POE)  
 POFs. *See* Porous organic frameworks (POFs)  
 Point-of-care devices, 531–532  
 Points of extension (POE), 12, 16f  
 Polymers  
   emission of, 529  
   hybrid, 537–539  
 Poly(ethylene glycol) (PEG), 258–259  
 Polyaniline (PAN), 410–411  
 Polydopamine (PDA), 410  
   PDA@GOx/ZIF-8, 510f  
 Polyethylene glycol (PEG), 302, 450, 481–482  
 Polyhedra, metal-organic, 36–38, 36–37f  
 Polymeric cyclodextrins, 482–483  
 Polymeric nanoparticles, 467–468, 486  
 Polymerization  
   acrylate, 483–484  
   GraftFast, 483–484  
   reversible addition-fragmentation chain transfer (RAFT), 399  
 Polymerized dopamine (DPA), 509–510  
 Polymers, 258–265, 409  
   coordination, 11  
   organic, 534  
   porous coordination, 245  
   porous organic, 269–271  
 Poly-*N*-isopropylacrylamide (PNIPAM), 259–260  
 Polypeptides, 329–330  
 Polypyrrole (PPy), 410

- Polysaccharide-based metal-organic frameworks (Polysaccharide-MOFs), 102–103
- Polysaccharides, 446
- Polyvinylpyrrolidone (PVP), 534
- POPs. *See* Porous organic polymers (POPs)
- Porcine pancreatic lipase (PPL), 494–496  
immobilized, 494–496
- Pore encapsulation method, 496–498
- Pore walls, postsynthetic modification of, 323
- Porosification, associated with crystal conversion, 206–207
- Porosity of MOFs, 324
- Porous coordination polymers (PCPs), 245, 426–427
- Porous hybrid nanomaterials, 430–431
- Porous materials, 112, 347
- Porous nano-based carrier, for immobilization, 491–492
- Porous nano-based materials, 491–492
- Porous organic frameworks (POFs), 526
- Porous organic polymers (POPs), 269–271  
amorphous, 526
- Porphyrin-based MOF, 337–338, 539
- Porphyrin carboxylate, photodynamic, 400
- Porphyritic metal organic framework, inhibitory effect of, 316*f*
- Porphyritic MOF nanoparticles, Zr(IV)-based, 404
- Porphyritic PCN-222 MOFs, 540–542
- Porphyrin ligands, 404
- Porphyrins, 310, 337–338
- Positive thermal expansion (PTE), 98
- Positron emission tomography (PET), 313–314, 413, 482
- Postsynthetic encapsulation, noncovalent, 250–251
- Postsynthetic metalation (PSMet), 46–47, 46*f*
- Postsynthetic modification (PSM), 245–246  
coordinative, 248–250  
covalent, 246–248  
hybridization with materials, 251–256, 252*f*, 255*f*  
noncovalent, 250–251  
physical, 256–257, 257*f*  
types, 246–257
- Potassium clavulanate (CL), 477
- Potential sensor system, 529
- Powder X-ray diffraction (PXRD), path1, 251–253, 279–280, 279*f*
- Pressure fluctuations, 223
- Pressure swing adsorption (PSA), 104–105
- Production of MOFs, 201–203  
large-scale production, 201, 203, 205–206
- Protein, 333–337  
encapsulation, *De novo*, 335–336  
*Pseudomonas aeruginosa*, 433–434
- Pseudorotaxanes, 307
- PSM. *See* Postsynthetic modification (PSM)
- PTT. *See* Photothermal therapy (PTT)
- Publications of MOFs, 527–528, 528*f*, 532*f*, 534
- Pulmonary arterial hypertension (PAH), 484
- Pure-phase MOFs, 166–167
- PXRD. *See* Powder X-ray diffraction (PXRD)
- Pyridine-3-carboxylic acid, 83–84
- Q**
- Quality of bare MOFs, 131–132
- R**
- Radiation  
electromagnetic, 160  
microwave, 169–172
- Reactive oxygen species (ROS), 80–81, 365, 372–373, 434  
generation assay, 262–265
- Recommended Dietary Allowance (RDA), 76–78
- Reduced MOFs (rMOFs), 288
- Reductive electrosynthesis, 183–184
- RES. *See* Reticuloendothelial system (RES)
- Reticular chemistry, 11–12, 38–40
- Reticuloendothelial system (RES), 438
- Reverse microemulsion, 300, 359–360, 359*f*
- Reversible addition-fragmentation chain transfer (RAFT) polymerization, 399
- Reversible covalent bonds, 531–532
- Ribonucleic acid (RNA), 76
- rMOFs. *See* Reduced MOFs (rMOFs)
- Rod MOFs, 39–40
- ROS. *See* Reactive oxygen species (ROS)
- S**
- SBUs. *See* Secondary-binding units (SBUs); Secondary building units (SBUs)
- Scanning electronmicroscope (SEM), 361–364, 363*f*
- Secondary-binding units (SBUs), 427
- Secondary building units (SBUs), 11, 99–100, 327, 355, 356*f*, 526–527  
concept, 11–15  
designed synthesis, 11–12  
highly coordinated carboxylate-based (metal oxide), 25–32, 26*f*, 28–31*f*  
infinite rod like, 38–40, 38–39*f*  
metal-cluster, 38–39  
nitrogen-containing, 32–36, 32–35*f*  
traditional carboxylate based (metal-oxide), 19–25, 20–22*f*, 24*f*
- Selected area electron diffraction (SAED), 285
- Self-assembled hybrid nanomaterials, 427



- SEM. *See* Scanning electronmicroscope (SEM)
- Sensor  
 glucose, 529  
 potential, 529
- Sigma-Aldrich provides MOF  
 Constructor Tool, 211–212
- Silica encapsulation, 302
- Silica materials, mesoporous, 323
- Silver nanoparticles (AgNPs),  
 431–432
- Simulated body fluid (SBF), 81–82,  
 483
- Single crystal XRD (SC-XRD), 11,  
 279
- Single lipid bilayers (SLBs), 82
- Single metal nodes, 16–18
- Single photon emission computer  
 tomography (SPECT), 413
- Single-stranded DNA (ssDNA),  
 253–254
- Small interfering RNAs (siRNAs),  
 437
- Small-scale microwave units,  
 163*f*  
 WAVE unit, 163, 164*f*
- SNAs. *See* Spherical nucleic acids  
 (SNAs)
- S-nitrosothiols (RSNOs), 105
- Solid catalysts, heterogeneous,  
 111
- Solid-phase peptide synthesis,  
 329–330
- Solid-solid reaction, 203
- Solubility, MOFs, 386
- Solvent, 354–355
- Solvent-free synthesis, 203
- Solvothermal, defined, 141–142
- Solvothermal method, 300,  
 357–358, 358*f*  
 surfactant-template, 360
- Sonicated lipase, 508
- Sonochemical reactions, 223–224
- Sonochemical synthesis, 231
- Sonochemistry, 223–225
- Sonogashira reaction, 112–113  
 modified MOFs for, 125–132
- Soybean epoxide hydrolase (SEH),  
 499  
 immobilization of, 499
- SPECT. *See* Single photon emission  
 computer tomography  
 (SPECT)
- Spectrophotometer, UV-Vis, 291
- Spectroscopy, X-ray energy  
 dispersive, 362*f*
- ssDNA. *See* Single-stranded DNA  
 (ssDNA)
- Stability, MOFs, 386–387
- Stealth effects, 446
- Stimuli-dependent metal organic  
 framework, 304*f*
- Stimuli-responsive drug delivery  
 systems, 426
- Stimuli-responsive MOFs, 305–306  
 for drug delivery, 303–308
- Stimuli-responsive nanoMOF,  
 415–417
- Stokes-Einstein equation, 286
- Stress, oxidative, 416
- Structured illumination microscopy  
 (SIM), 256–257
- Surface adsorption, 491,  
 509–510
- Surface amino acids, 503–506
- Surface characterization, MOFs,  
 284–289
- Surface coating  
 carbohydrate-based MOFs  
 (CD-MOFs), 455  
 for MOFs, 456–461
- Surface engineering, 480–484,  
 480–481*f*
- Surface enzyme immobilization,  
 494–496, 494*t*, 495*f*
- Surface-functionalization, of iron  
 polycarboxylate MOFs, 447
- Surface modification, 301  
 phosphated cyclodextrins  
 (CD-P), 460
- Surface modification of MOFs,  
 480–483, 481*f*  
 for delivery purposes, 301–302  
 nanoMOFs, 459*f*
- Surface morphology analysis,  
 284–286
- Surface plasmon resonance (SPR),  
 426
- Surfactant-template solvothermal  
 method, 360
- Suzuki-Miyaura reaction, modified  
 MOFs for, 125–132, 126*f*
- Suzuki reaction, 112–113  
 Suzuki coupling reaction,  
 129–130, 129*f*
- Synthesis process approach of  
 MOF, 492–493
- Synthetic cyclophane, hosts and  
 native metal-binding protein  
 cages, 335*f*
- Synthetic method of metal-organic  
 frameworks, 355–360  
 nanodeposition method,  
 355–357
- SynthWAVE microwave system,  
 163
- T**
- Targeted delivery, 297–299
- TEM. *See* Transmission electron  
 microscope (TEM)
- Tetra-kis (4-carboxyphenyl)  
 porphyrin (TCPP), 315
- 3,3,5,5-Tetramethylbenzidine  
 (TMB), 145–147
- Thalassemia syndrome, 84–85
- Theranostics, 398, 540–542  
 magnetic, MOFs as, 436–437
- Thermal ablation technique, 434
- Thermal amorphization, 99
- Thermal deposition, microwave-  
 induced, 171–172
- Thermal-induction, 98–99
- Thermal stability, 289–290, 508
- Thermogravimetric analysis (TGA),  
 289–290
- Thin films of MOFs,  
 electrochemical synthesis  
 routes of, 179–186, 180–181*t*
- Three-dimensional composite,  
 recyclability of, 506–507
- TNBC. *See* Triple-negative breast  
 cancer (TNBC)
- Topology of MOFs, 11–12
- Topotecan, 477, 478*f*
- Total antioxidant capacity (TAC)  
 test, 74–75
- Toxicity. *See also specific types  
 of toxicity*  
 acute, 76–78, 389

- factors, 385  
of nanomaterials, 384  
and in vivo fate, 484–485  
Toxicity of MOFs, 145, 387*f*,  
543–545  
in biological systems, 384–387  
Traditional carboxylate based  
(metal-oxide) secondary  
building units, 19–25, 20–22*f*,  
24*f*  
Traditional therapeutic molecules,  
365  
Transformation of MOFs, 112–113  
Transition metals, 112  
complexes, 122  
Transmission electron microscope  
(TEM), 361–364, 363*f*  
Triazine molecules, 113  
Triethylamine, 235  
Triple-negative breast cancer  
(TNBC), 408  
Tritopic BTC linker, 12  
TruPick, 213  
Trypsin-FITC immobilized MOFs,  
494–496  
Trypsin-FITC@MOF bioreactor,  
509–510  
Tumor hypoxia, 414–415  
Tunable organic linker, 492  
2D Cu-trimesic acid MOF, 530  
Two-dimensional metal-organic  
framework (2D-MOF), 113
- U**  
UCNPs. *See* Upconversion  
nanoparticles (UCNPs)  
UCT. *See* Ultrasonic computed  
tomography (UCT)  
UiO-66-BODIPY, 271  
UiO-66-NH<sub>2</sub> nanoparticles, 260*f*,  
266*f*, 268*f*  
UiO-66-N<sub>3</sub> nanoparticles, surface  
functionalization of, 249*f*  
UiO-PDT synthesis, 272*f*  
UiO-66-TPP-SH synthesis, 270*f*
- Ultra-small superparamagnetic iron  
oxide (USPIO) nanoparticles,  
403  
Ultra-small superparamagnetic  
magnetite nanoparticles, 402  
Ultrasonic computed tomography  
(UCT), 223  
Ultrasonic intensity, 224  
Ultrasonic synthesis, 301  
Ultrasound-assisted ball milling  
technique, 237  
Ultrasounds in MOFs, 225–239  
alternative methods, 230–231  
conventional studies, 225–230,  
226–227*t*  
effect of concentration, 234–235,  
234–235*f*  
effect of modulators and  
additives, 235–236  
effect of reaction time,  
233–234  
effect of solvents, 231–232  
effect of ultrasound power and  
temperature, 233  
effects of synthesis parameters,  
231–236  
 $\alpha,\beta$ -Unsaturated compounds, 113  
Upconversion nanoparticles  
(UCNPs), 282, 408–409  
UV-visible spectroscopy, 291  
UV-Vis spectrophotometer, 291
- V**  
Vacuum swing adsorption (VSA),  
104–105  
Vancomycin (VAN), 285  
van der Waal forces, 289  
Vapor diffusion method, 449–450  
Vitamin A palmitate (VAP), 454  
Vitamin B3 deficiency, 83–84
- W**  
Watson-Crick and Hoogsteen  
faces, 326*f*
- X**  
Xenon (Xe), 103–105  
X-ray computed tomography (CT)  
scan, 313  
X-ray diffraction (XRD), 527  
single-crystal, 11  
X-ray energy dispersive  
spectroscopy, 362*f*  
X-ray photoelectron spectroscopy  
(XPS), 283–284
- Z**  
Zebrafish embryos, 485  
Zeolite imidazolate framework  
(ZIF), 5–7  
Zeolite-like metal-organic  
frameworks (ZMOFs), 18  
Zeolites  
crystal size of, 199  
vs. MOFs, 197–199, 198*t*  
synthesis, 197–198  
Zeolitic imidazole frameworks (ZIFs),  
16–18, 199–201, 230–231, 469,  
492–493, 497  
synthetic conditions of, 500–503  
ZIF-8, 97, 99  
Zeta potential, 287  
ZIF-8 colloidosomes, 506–507  
self-assembly of ring-like, 506*f*  
Zinc-based MOFs, 390  
Zirconium-based MOFs, 477–478  
antibacterial efficacy of, 432  
ZMOFs. *See* Zeolite-like metal-  
organic frameworks (ZMOFs)  
Zn-based MOFs development, 432  
Zn-imidazolate ZIF-8 layers,  
542–543  
Zn ions, 535  
Zn-MOFs synthesis, 152–153  
Zoledronate (zol), 82  
Zr-based MOFs, 150*f*, 482  
Zr(IV)-based porphyrinic MOF  
nanoparticles, 404  
<sup>89</sup>Zr-containing NMOF, 314  
Zr-fumarate MOFs, 542–543

# METAL-ORGANIC FRAMEWORKS FOR BIOMEDICAL APPLICATIONS

A growing number of metal-organic frameworks with biomedical engineering applications are being reported. Increasing attention is being paid to metal-organic frameworks due to their several advantages over conventional materials. *Metal-Organic Frameworks for Biomedical Applications* is a comprehensive, authoritative reference for the biomedical application of metal-organic frameworks, offering a substantial and complete treatment of published results that have yet to be critically reviewed. It offers a summary of current research and provides in-depth understanding of the role of metal-organic frameworks in biomedical engineering.

The title consists of twenty-two chapters on the state-of-the-art, from leading international researchers in the field. Chapters are arranged by target-application in biomedical engineering, allowing medical and pharmaceutical specialists to translate current materials and engineering science on metal-organic frameworks into their work

- Presents the state-of-the art in metal-organic frameworks for biomedical application
- Offers comprehensive treatment of metal-organic frameworks useful to pharmaceutical and medical experts who are non-specialists in materials science
- Helps materials scientists and engineers understand the needs of biomedical engineering

**Masoud Mozafari** is a Fellow of The Lunenfeld-Tanenbaum Research Institute, Mount Sinai Hospital, University of Toronto. He has been previously the Head of the Bioengineering Research Group, Cellular and Molecular Research Center, Faculty of Advanced Technologies in Medicine at Iran University of Medical Sciences (IUMS). He is known for the development of strategies for the regeneration of damaged tissues/organs. Dr. Mozafari is one of the recipients of “WIPO Medal for Inventors” from the World Intellectual Property Organization (WIPO) – the United Nations (UN), for inventions that significantly contribute to the economic and technological development in the field of biomaterials.



**WP**

WOODHEAD  
PUBLISHING

An imprint of Elsevier  
[elsevier.com/books-and-journals](http://elsevier.com/books-and-journals)

ISBN 978-0-12-816984-1



9 780128 169841